Schriftenreihe Baustoffe und Massivbau
Structural Materials and Engineering Series

Heft 10
No. 10

Ultra High Performance Concrete (UHPC)

Proceedings of the

Second International Symposium on Ultra High Performance Concrete

Kassel, Germany
March 05-07, 2008

kassel university press

Edited by
E. Fehling, M. Schmidt, S. Stürwald
University of Kassel, Germany

Bibliographic information published by Die Deutsche Bibliothek

Die Deutsche Bibliothek lists this publication in the Deutsche Nationabibliografie;
detailed bibliographic data are available on the Internet at http://dnb.d-nb.de

ISBN: 978-3-89958-376-2
URN urn:nbn:de:0002-3765

2008, kassel university press GmbH, Kassel
www.upress.uni-kassel.de

Printed by Unidruckerei, University of Kassel

Series Editors

Prof. Dr.-Ing. E. Fehling
Universität Kassel
Fachbereich Bauingenieurwesen
Fachgebiet Massivbau
Kurt-Wolter-Str. 3
34125 Kassel
Tel. +49 (561) 804 2656
Fax. +49 (561) 804 2803
bauing.massivbau@uni-kassel.de
www.uni-kassel.de/fb14/massivbau

Prof. Dr.-Ing. habil. M. Schmidt
Universität Kassel
Fachbereich Bauingenieurwesen
Fachgebiet Werkstoffe des Bauwesens und Bauchemie
Mönchebergstr. 7
34125 Kassel
Tel. +49 (561) 804 2601
Fax. +49 (561) 804 2662
baustk@uni-kassel.de
www.uni-kassel.de/fb14/baustoffkunde

Editor

Dipl.-Ing. Simone Stürwald
Universität Kassel
Fachbereich Bauingenieurwesen
Fachgebiet Massivbau
Kurt-Wolter-Str. 3
34125 Kassel
Tel. +49 (561) 804 2683
Fax. +49 (561) 804 2803
stuerwald@uni-kassel.de
www.uni-kassel.de/fb14/massivbau

Preface

Ultra High Performance Concrete (UHPC) not only offers superior compressive strength but also extraordinary ductility and far more durability than ordinary concrete. It enables to build structures which are sustainable and economical and come with light and filigree appearance at the same time.

During the last four years, since the First International Symposium on Ultra High Performance Concrete held in Kassel in 2004, UHPC has gained much more attendance all over the world, being it by different types of applications for interesting structures or by research on the material itself and the optimization of its production and behaviour. Much of this work has been presented and discussed at the

Second International Symposium on Ultra High Performance Concrete in Kassel in 2008

in more than 100 lectures. The presentations have given a broad survey of all aspects of UHPC including raw materials, micro- and macro-structures, mechanical behaviour, durability as well as of construction and design specifications appropriate for this material. Exciting architectural concepts and many examples of interesting engineering applications have been presented at the symposium.

The symposium was organized by the Institute of Structural Engineering, Faculty of Civil Engineering of the University of Kassel, Germany.

The Conference Proceedings contain the conference papers and presentations. We hope that the conference and the excellent papers will promote further development and exploitation of Ultra High Performance Concrete – one of the most challenging construction material for the 21st century.

Kassel, March 2008

Prof. Dr.-Ing. Ekkehard Fehling Prof. Dr.-Ing. habil. Michael Schmidt

Contents

Scientific Committee

Chairmen

Prof. Ekkehard Fehling
University of Kassel, D

Prof. Michael Schmidt
University of Kassel, D

Members

Dr. Mouloud Behloul
Lafarge Company, F

Prof. Klaas van Breugel
Delft University of Technology, NL

Prof. Eugen Brühwiler
École Polytechnique Fédérale de Lausanne, CH

Prof. Harald Budelmann
University of Braunschweig, D

Prof. Manfred Curbach
Dresden University of Technology, D

Prof. Robert Day
University of Calgary, CA

Prof. Lennart Elfgren
Lulea University of Technology, S

Prof. Pietro Gambarova
Politecnico di Milano, I

Dr. Benjamin A. Graybeal
Federal Highway Administration, USA

Prof. Jürgen Grünberg
University of Hannover, D

Prof. Petr Hájek
Czech Technical University in Prague, CZ

Prof. Josef Hegger
RWTH Aachen University, D

Prof. Detlef Heinz
Technische Universität Münschen, D

Steve Kosmatka
Portland Cement Association, USA

Dr. Ralf Krelaus
University of Kassel, D

Prof. Christian Meyer
Columbia University, USA

Prof. Bernhard Middendorf
University Dortmund, D

Dr. Christoph Müller
German Cement Works Association (VDZ), D

Prof. Harald S. Müller
Karlsruhe University of Technology, D

Prof. Aurelio Muttoni
École Polytechnique Fédérale de Lausanne, CH

Prof.Johann Plank
Technische Universität München, D

Prof. Marco di Prisco
Politecnico di Milano, I

Jacques Resplendino
DIRMED, F

Dr. Henry G. Russell
Engineering Consultant, USA

Prof. Mohammed Shekarchizadeh
University of Tehran, IR

Prof. Lutz Sparowitz
Graz University of Technology, A

Dr. Dietmar Stephan
University of Kassel, D

Thierry Thibaux
Eiffage TP, F

Prof. Nguyen Tue
University of Leipzig, D

Prof. Franz-Josef Ulm
Massachusetts Institute of Technology, USA

Prof. Joost C. Walraven
Delft University of Technology, NL

Organizing Committee

Symposium's Secretary

Mrs. Simone Stürwald
University of Kassel, D

Chairman of the Organizing Committee

Mr. Kai Bunje
IBB Fehling + Jungmann GmbH, Structural and Material Consulting Engineers, Kassel, D

Members

Prof. Ekkehard Fehling

Prof. Michael Schmidt

Mrs. Ute Müller

Mrs. Bianca Böhmer

Mrs. Elvira Berndt

Sponsors and Supporters

The University of Kassel provided essential support in infrastructure and administration for the Symposium. Special thanks go to the following sponsors and supporters:

fédération internationale du béton
Case Postale 88
CH-1015 Lausanne
Switzerland

American Concrete Institute
ACI International
PO Box 9094
Farmington Hills, MI 48333
USA

Portland Cement Association
5420 Old Orchrad Road
Skokie, IL 60077
USA

Verein Deutscher Zementwerke e.V.
Tannenstr. 2
40476 Düsseldorf
Germany

Deutscher Beton- und Bautechnik-Verein e.V.
Kurfürstenstraße 129
10785 Berlin
Germany

Deutscher Aussuss für Stahlbeton (DAfStb)
im DIN Deutsches Institut für Normung e.V.
Burggrafenstraße 6
10787 Berlin Tiergarten
Germany

Deutsche
Forschungsgemeinschaft

DFG

Deutsche Forschungsgemeinschaft
Kennedyallee 40
53175 Bonn
Germany

Exhibitors

Further thanks go to the following companies, which have taken part in the technical exhibition:

Dyckerhoff AG
Biebricher Straße 69
65203 Wiesbaden
Germany

STRATEC
Strahl- und Fasertechnik GmbH
An der Schleuse 3
58675 Hemer
Germany

QUANTACHROME
Rudolf-Diesel-Str. 12
85235 Odelzhausen
Germany

Maschinenfabrik
Gustav Eirich GmbH & Co. KG
Walldürner Str. 50
74736 Hardheim
Germany

Densit ApS
Rørdalsvej 44
9220 Aalborg SØ
Denmark

Elkem AS, Materials
P.O. Box 8126 Vaagsbygd
4675 Kristiansand
Norway

PANalytical GmbH
Nürnbergerstr. 113
34123 Kassel
Germany

Part 1:

Worldwide Experience

Franz-Josef Ulm
Prof.
Massachusetts Institute of Technology
Cambridge, MA, USA

Paul Acker
Dr., Res. Dir.
Lafarge
France

Nanoengineering UHPC Materials and Structures

Summary

In this contribution, we present some elements of nanoengineering of UHPC materials and structures. At the nanoscale, we show that Ultra High Performance Concrete (UHPC) is a nanogranular material, whose superior macroscopic properties derive from an ultra-high dense packing of nano-sized C-S-H particles. This ultra-high dense packing is achieved by means of a refined mix-design involving the water-to-cement ratio, the silica-fume content and heat-treatment. Based on this fundamental knowledge, it is possible to translate progress in nanoscience and nanoengineering into day-to-day UHPC engineering applications. This is illustrated for the prototype development of highway bridge girders, which is currently under consideration in the United States for the next generation of high performance sustainable infrastructure.

Keywords: *Nanoengineering; Packing; Ultra High Performance Concrete; Highway Bridge Girders.*

1 Introduction

Recent progress in nanoscience and technology makes it possible to assess the mechanical properties of cement-based materials at the nanoscale [1-2], and to identify universal material properties [3-4]. In particular, it has been shown, for classical cement-based materials of normal water-to-cement based materials, that the smallest elementary solid component of cement-based materials, that is the Calcium-Silica-Hydrates (C-S-H), exists in at least two forms, low and high density [3]. Both forms are built up by the same fundamental unit of material invariant properties, while they assert their difference by two distinct limit packing densities at the nanoscale. The low-density C-S-H comes close to the so-called random packing limit of mono-sized spheres (64%), which is the highest packing density a particulate material can achieve in an unordered fashion. In contrast, the packing of the high-density C-S-H comes very close to the so-called face-centered-cubic packing, which is the densest packing spheres can achieve in an ordered fashion (74%), similar to the packing of oranges in a grocery shop or the stacking of cannon balls. In this way the high-density C-S-H achieves a nano-strength and stiffness roughly twice that of the low-density form [4].

The focus of this contribution is two-fold: (1) to confirm these findings for Ultra-High Performance Concrete (UHPC), and (2) to apply this finding for the nanoengineering of UHPC materials and structures.

2 Nano-Phase Properties and Structure of UHPC Materials

2.1 Results from Statistical Nanoindentation Technique

The backbone of the identification of core properties and structural arrangement of the nanoscale phases which form within the unique chemical environment of pores and which cannot be adequately recapitulated ex situ in bulk form, is the nanoindentation test.

Briefly we recall that nanoindentation consists of making contact between a sample and an indenter tip of known geometry and mechanical properties, followed by a continuously applied and recorded change in load, *P*, and depth, *h*. Typical tests consist of a constantly increasing load, followed by a short hold and then a constant unloading; a *P-h* curve is reported. The analysis of the P-h curve proceeds by applying a continuum scale model to derive an indentation modulus, *M*, and a hardness, *H*:

$$M = \frac{\sqrt{\pi}}{2}\frac{S}{\sqrt{A_c}}; \qquad H = \frac{P}{A_c} \tag{1}$$

where $S = \left(dP/dh\right)|_{h=h_{\max}}$ is the (measured) initial slope of the unloading branch of the *P-h* curve, *P* is the (measured) maximum indentation load, and A_c is the projected contact area of the indenter on the sample surface.

Recognizing the high heterogeneity of cement paste at the nano- and micro-scale, applying the indentation technique is a challenge, as it is difficult to choose to indent on a specific material phase with sufficient repeatability. To address this challenge, it is advantageous to perform large grids of indentations on heterogeneous samples. Then, if the grid size and indentation depth are chosen properly, each indentation test may be treated as an independent statistical event; and a subsequent statistical deconvolution of the indentation results can be applied [2,4]. Typical results of the deconvolution are displayed in Figure 1 (a-b), in terms of probability density functions (PDF) of a w/c=0.5 cement paste. The PDFs show that there are two major and two minor hydration products present in the hydrated material system, which are sensed by nanoindentation: the Low-Density Calcium-Silica Hydrate phase (LD C-S-H), and the High-Density C-S-H phase (HD C-S-H), with the LD C-S-H largely dominating over the HD C-S-H in the nanomechanical response.

For comparison, Figures 1(d-e) display the PDFs for a w/c=0.2 materials, that is the typical binding phase of UHPC materials like Ductal®. A comparison of the nano-contact mechanics response readily reveals the differences between normal w/c-materials and this low w/c-material:

1. While the mechanical phase properties remain almost unchanged, the LD C-S-H phase almost disappears, in favor of the HD C-S-H phase which becomes the dominating phase in the material.
2. An additional ultra-high density C-S-H phase of statistically significant volume proportions is recognized, which is characterized by mechanical phase properties much above the values previously known for the hydration products in cement-based materials.

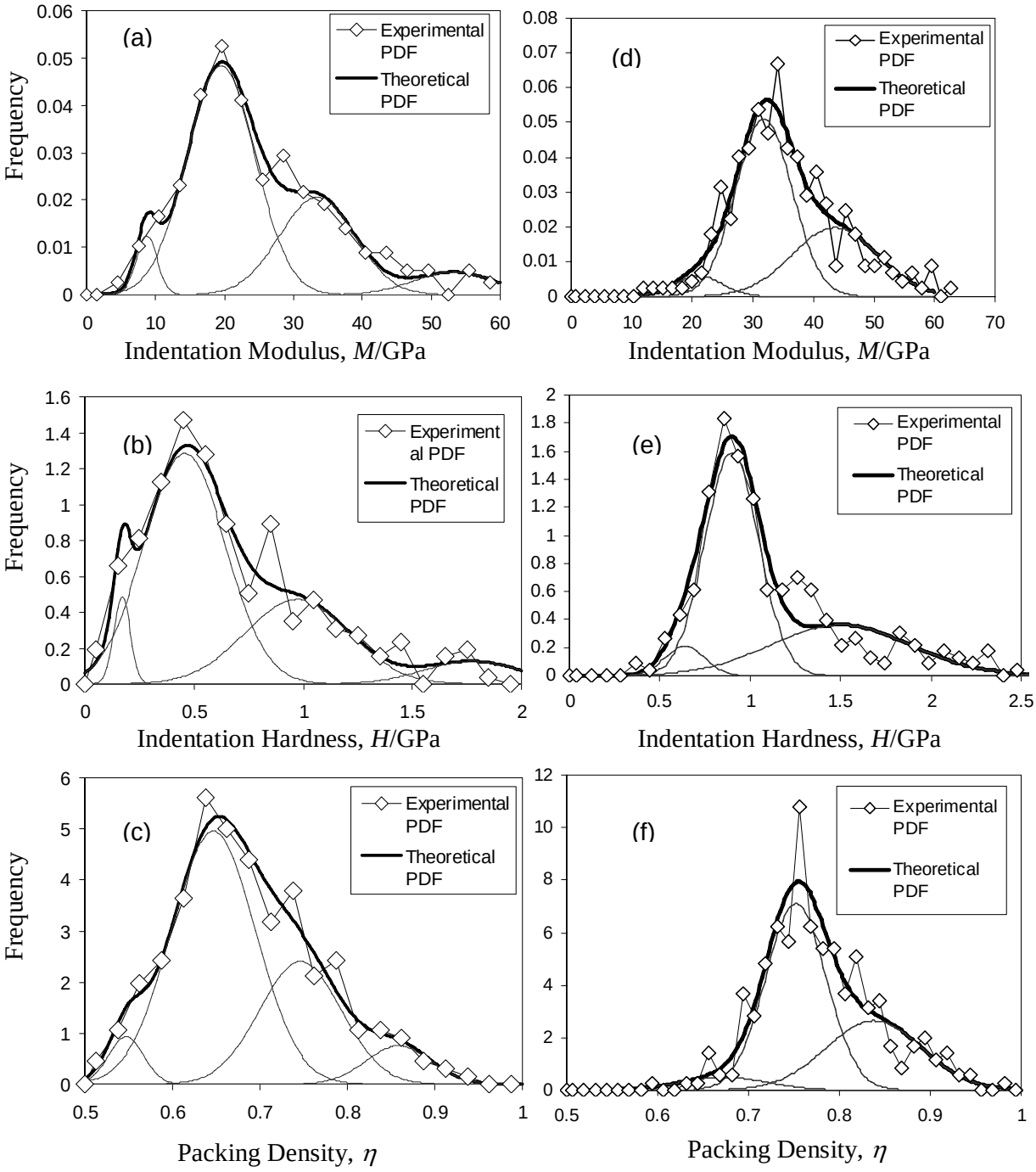

Figure 1: Probability Density Functions of nannoindentation results of indentation modulus, indentation hardness and packing density: (a-c) w/c=0.5; (d-f) w/c=0.2.

2.2 Packing Density Distributions

It is important to note that the indentation modulus and the indentation hardness are a priori two independent quantities: M relates to the elasticity content, while H relates to the strength. On the other hand, for a heterogeneous material like cement paste, if the solid phase of all hydration phases is the same, M and H have one thing in common; that is the nanostructure.

Indeed, a straight forward dimensional analysis of the indentation quantities readily reveals [2,4]:

$$\left.\begin{aligned}\frac{M}{m_s} &= \Pi_M\left(\nu_s,\eta,\eta_0\right)\\ \frac{H}{h_s} &= \Pi_H\left(\alpha_s,\eta,\eta_0\right)\end{aligned}\right\} \tag{2}$$

where $m_s = \lim_{\eta=1} M$ and $h_s = \lim_{\eta=1} H$ are the particle-to-particle contact stiffness and contact hardness, while ν_s and α_s represent the Poisson's ratio and the friction coefficient of the solid C-S-H phase. In return, Π_M and Π_H are scaling relations of M and H, that depend primarily on the solid's packing density η ("one minus porosity"), and the morphology of the solid, represented by the percolation threshold η_0 in Eqs. (2); that is the solid fraction required to provide a continuous force path through the system. Consider then *N* indentation tests on a material surface of a heterogeneous material. There are 2 x *N* measured (M,H) values, while there are 5+N unknowns: the four particle properties ($m_s, h_s, \nu_s, \alpha_s$) and the percolation threshold η_0; and *N* packing densities η for each location of the indentation grid. Therefore, provided the existence of a unique solid phase present in the porous microstructure, the scaling relations (2) are a versatile tool to identify the C-S-H particle properties and to probe the microstructure sensed by the large array of grid indentation tests, if *N*>>5. Figure 2 which displays these scaling relations for the w/c=0.5 and w/c=0.2 materials, clearly shows that the scaling is independent of the mix proportions, meaning that both materials, normal concrete and UHPC, have the same elementary C-S-H solid phase, characterized by $m_s = 63.5$ GPa, $h_s = 3.2$ GPa, $\nu_s = 0.2$ and $\alpha_s = 0.2$ (friction angle 10-15 degree). Thus, all what differs between hydrated cement paste of different mix proportions are the volume proportions of the following characteristic C-S-H phases (Fig. 1(c) and 1(f)):

1. The lowest packing of C-S-H particle one may detect in cement pastes is a C-S-H packing close to the random-loose packing fraction of uniform spheres of 0.555±0.005, which corresponds to a sphere packing at its rigidity-percolation threshold. We found such a random-loose packed phase in a very small volume fraction (5%) in the w/c=0.5 white cement paste, while it is absent in the w/c=0.2 cement paste.
2. The Low-Density C-S-H phase (LD) has a characteristic mean packing density of 64-65%, which comes remarkably close to the random limit packing density of spheres of η≈0.64, which corresponds to the maximum packing density in the random close-packed limit (known as RCP). The LD C-S-H phase is the dominating hydration phase in high water: cement ratio materials, and can be strongly reduced by reducing the water: cement ratio.
3. The High-Density C-S-H phase (HD) has a characteristic mean packing density of 74-75%, which comes remarkably close to the densest possible spherical packing in three-dimensions of η=π/√(18)≈0.74, which is the ordered face-centered cubic (fcc) or

hexagonal close-packed (hcp) packing. One could argue that this limit packing could also be achieved by mono-sized ellipsoids; yet an ellipsoidal packing is associated with a percolation threshold below 0.5, which is not consistent with the statistical indentation results. The HD C-S-H phase is a minor phase in high water: cement materials, and becomes the dominant in UHPC low water: cement ratio materials.

4. An Ultra-High Density C-S-H phase (UHD) seems also achievable in cement-based materials, having a characteristic mean packing density of 85-86%. Clearly, such a high packing density cannot be achieved with mono-sized spheres, but hints to packing of particles of different size. Indeed, the found packing density comes remarkably close to a two-scale random limit packing of $\eta=2\times0.64-0.64^2= 0.87$.

Finally, if we remind ourselves that the packing density is the solid complement of the porosity, it is possible to estimate the average C-S-H porosity from the technique. It amounts to 31.4% for the w/c=0.5 material, and to 24% for the highly packed w/c=0.2 UHPC material.

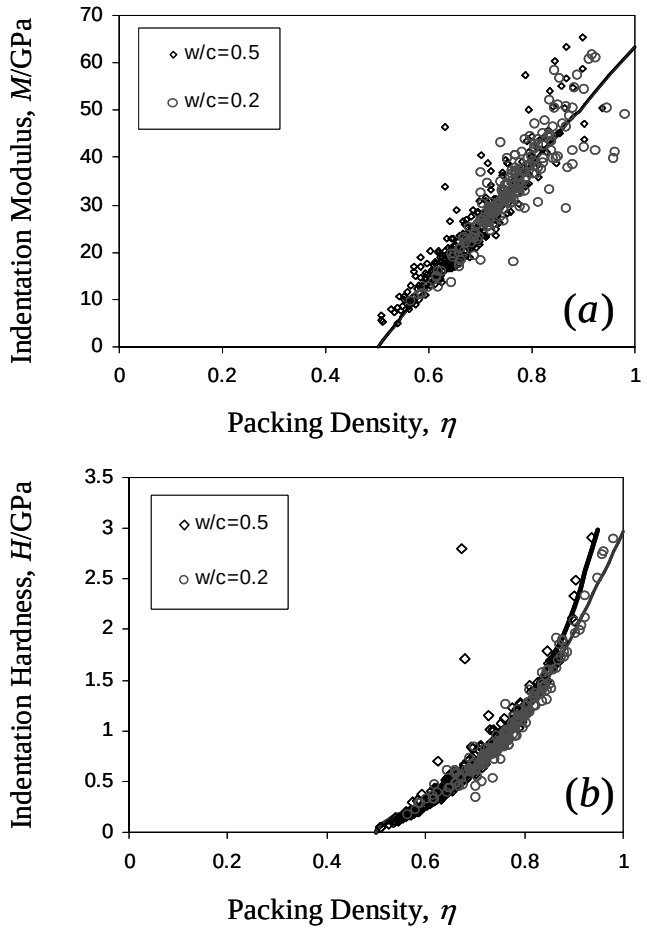

Figure 2: Packing density scaling relations of (a) indentation modulus, and (b) indentation hardness, for w/c=0.5 and w/c=0.2 materials.

3 Closure: Nanoenginnering UHPC Materials and Structures

By far, the key design parameter for UHPC materials and structures is the packing density of elementary C-S-H particles of a characteristic size of roughly 5nm [5-6]. Thus inverting the

classical top-down approach of concrete engineering, it becomes possible to translate the progress in nanoscience of cement-based materials into day-to-day material-structural engineering applications. This is illustrated in Figure 3, showing the prototype development of a UHPC highway bridge girder [7-8]. Made out of Ductal®, the prestressed bridge girder is designed for US highway bridges with a span of 20-35 meters, which make up roughly 85% of the total US bridge inventory. With a deck of only 3in (~7.8 cm) thick, this prototype girder achieves a maximum span-to-height ratio of L/H~30, and an overall weight reduction of approximately 30% compared to current standard, allowing rapid construction; thus avoiding extended traffic interruptions. Thanks to low porosity due to ultra-high dense C-S-H packing, achieved by Ductal®'s mix formulation (w/c ratio, silica fumes) and fabrication process (heat treatment), the bridge has a high durability performance requiring low maintenance. The prototype has been successfully tested in 2006 by the US Federal High Way Administration; and is currently under consideration by the FHWA as an attractive material-structural solution for rejuvenating the US highway bridge inventory.

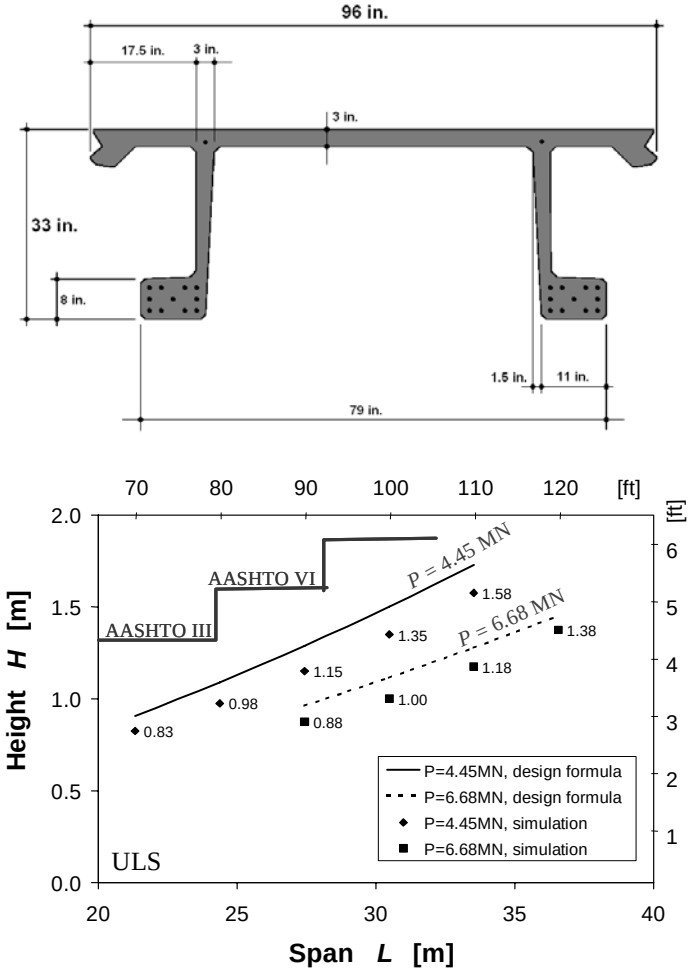

Figure 3: Prototype development of UHPC highway bridge girder: Section dimensions (Top), Height vs. span for different prestress level [7].

4 References

[1] Constantinides, G., Ulm, F.-J., Van Vliet, K. (2003) “On the use of nanoindentation for cementitious materials”, Concrete Science & Engineering, Materials & Structures, RILEM, Vol. 36, 191–196.

[2] Ulm, F.-J., Vandamme, M., Bobko, C., Ortega, J.A., Tai, K. Ortiz, C. (2007). “Statistical Indentation Techniques for Hydrated Nanocomposites: Concrete, Bone and Shale”, J. American Ceramic Society, 90(9), 2677–2692.

[3] Constantinides, G., Ulm, F.-J. (2004). “The effect of two types of C-S-H on the elasticity of cement-based materials: results from nanoindentation and micromechanical modeling”, Cement & Concrete Research, Vol. 34 (1), 67-80.

[4] Constantinides, G., Ulm, F.-J. (2007) “The nanogranular nature of C-S-H“, J. Mech. Physics of Solids, 55 (1), 64-90.

[5] Jennings, H.M. (2004) “Colloid model of C-S-H and implications to the problem of creep and shrinkage”, Materials and Structures, 37(265), 59-70.

[6] Jennings H.M, Thomas J.J, Gevrenov J.S, Constantinides G, Ulm F.-J. (2007). “A multi-technique investigation of the nanoporosity of cement paste”, Cement & Concrete Research, Vol. 37 (3), 329-336.

[7] Park H., Ulm F.-J., and Chuang E. (2003). "Model-based optimization of ultra high performance concrete highway bridge girders," CEE Report R03-01, Massachusetts Institute of Technology, March.

[8] Shim, J.M., and Ulm, F.J. (2004). "Prediction of Early-Age Cracking of UHPC Materials and Structures: A Thermo-Chemo-Mechanics Approach," MIT-CEE Report R04-03 to Lafarge, M.I.T., Cambridge, MA.

Benjamin Graybeal
Research Structural Engineer
U.S. Federal Highway Administration
Washington D.C., U.S.A.

UHPC in the U.S. Highway Transportation System

Summary

Progress toward greater implementation of ultra-high performance concrete in the U.S. highway transportation system is continuing. Since the initiation of the Federal Highway Administration's UHPC research program in 2001, major strides have been made toward introducing the concrete and transportation industries to this next generation of concrete technology. As of late 2007, one UHPC I-girder highway bridge was open to traffic, one UHPC superstructure bridge was under construction, and other UHPC components were in design. However, the challenges facing widespread implementation of UHPC are still significant. The lack of design code provisions, industry unfamiliarity with the product, and high initial costs are limiting the projects that include UHPC. Addressing these issues will require significant knowledge transfer, industry willingness to accept incremental transformations, and a greater reliance on life cycle costing.

Keywords: *prestressed girder, structural testing, flexure, shear, design provisions, challenges to implementation, deployment status report, highway infrastructure*

1 Introduction

Ultra-High Performance Concrete (UHPC) is an emerging technology that has the potential to significantly impact the U.S. highway transportation system. As is the case in most of the developed world, the U.S. highway infrastructure is heavily dependent on concrete and steel. The infrastructure construction that occurred in the mid-20th century, followed by the successive decades-long deterioration of this infrastructure, has focused a great deal of attention on the creation of durable, long-lasting structures. New materials that display enhanced mechanical and durability properties make it possible to construct new infrastructure and rebuild aging infrastructure in new forms and with longer lives. Significant advancement in cementitious materials research in the last two decades has led to the coalescing of knowledge and the creation of a new class of materials, namely UHPCs. Although similar to conventional cementitious products in their constituents, scientific advances have allowed for the creation of market-ready materials with multiple times the strength and durability of conventional concretes.

However, the implementation of UHPCs is progressing slowly. The lack of design code provisions relevant to these concretes presents a challenge, effectively requiring that all structural design either make limited use of the advanced properties of UHPC or be based on

directly applicable research results and first principles of engineering. Industry unfamiliarity is also driving up the cost of UHPC with precasters charging a premium to cover the perceived risk and showing an unwillness to modify their operations to efficiently fabricate UHPC components until they see a clear market for the products. Finally the high per unit volume cost of the concrete necessitates a life cycle costing approach to determining best value for an owner, but this concept has encountered slow implementation in the United States.

2 Research Efforts

Research related to the development, properties, and application of UHPC within the United States is progressing. Many university researchers have secured industry and/or government funding for UHPC-related research. In particular, the most recent federal transportation legislation contained designated research funding specifically for UHPC. However, when compared to the research funding mechanisms in place in Europe and East Asia, UHPC research in the United States is more constrained.

The U.S. Federal Highway Administration began its UHPC research program in 2001. The intent of this program is to 1) determine the properties of UHPC as would be expressed when used in the highway system, 2) determine the best applications for UHPC in the highway system, and 3) aid in the initial deployment of UHPC into the highway system. The initial phases of this research effort have been completed and the results are detailed in [1,2]. These phases focused on determining the basic mechanical and durability behaviors of UHPC and on determining how UHPC would behave when used in common prestressed concrete superstructure elements.

There are currently four research efforts underway within FHWA's UHPC program. The first is a program to develop a modular precast/prestressed concrete superstructure/deck element applicable to average highway bridges around the United States. The intent of the concept is to combine the increased strength and the enhanced durability of UHPC into a packaged bridge that can be fabricated offsite then quickly and efficiently assembled onsite. In the U.S. highway transportation system the majority of bridges span 20 to 35 m and are composed of superstructures and decks that are nearing the end of their design life. The replacement of these bridges will likely exacerbate traffic congestion on the highways. The development of modular components that allows for the replacement of the superstructure and deck of a bridge overnight will be a major leap forward for our transportation system. A first generation superstructure/deck modular component was designed, constructed, and tested between 2004 and 2006 [3]. A second generation is currently being designed to address the shortcomings that the first generation was intended to demonstrate. Figure 1 shows the proposed second generation component designed to span up to 30 m while allowing for overnight bridge construction/reconstruction.

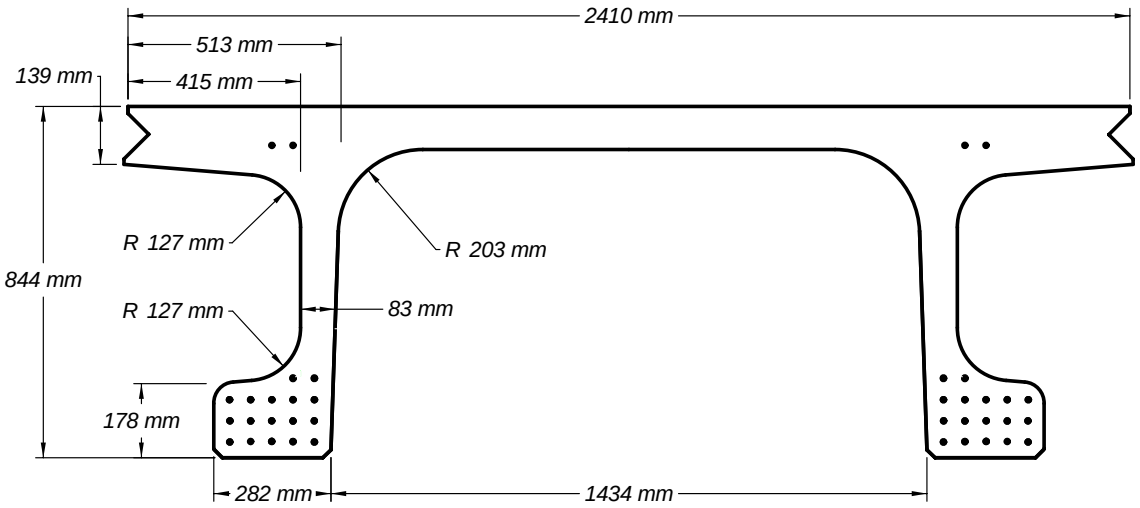

Figure 1: Proposed UHPC Deck-Bulb-Double-Tee Girder Cross Section

The second research effort is focused on providing a remedy for the need to replace deteriorated bridge decks which reside on viable superstructures. Deterioration of bridge decks, especially in northern climates which experience freezing temperatures, is the most significant maintenance and bridge rehabilitation issue facing the U.S. highway system. In recent years there has been a major push in the United States to develop modular deck components that can be assembled onsite during a brief period of bridge and/or bridge lane closure. The advanced properties of UHPC open the possibility of designing a component that is as strong and robust as existing cast-in-place concrete decks while also being of significantly greater durability. The first phase of this effort has been completed and is reported in [4]. The component that has been developed is a two-way ribbed precast deck element with dimensions as shown in Figure 2.

The third research effort is focused on quantifying advanced structural and durability properties of UHPC. For instance, the existing body of knowledge related to the tensile fatigue behaviour of UHPC after initial tensile cracking is limited. In order for U.S. design codes to allow general use of the advanced tensile mechanical properties of UHPC in transportation structures, those properties will need to be demonstrated to be applicable over a wide range of environmental and mechanical stressors. One phase of this research effort is investigating the post-cracking tensile fatigue of UHPC subjected to multiple stress (strain) ranges. Another phase is planned to investigate the combined influence of chloride-laden water on steel fiber reinforcement bridging cyclically stressed cracks. Within this overall research effort another part of the program is planned to investigate the durability and structural response of a full-scale UHPC modular deck component stressed both environmentally and structurally and then to compare these results to a similarly stressed conventional concrete component.

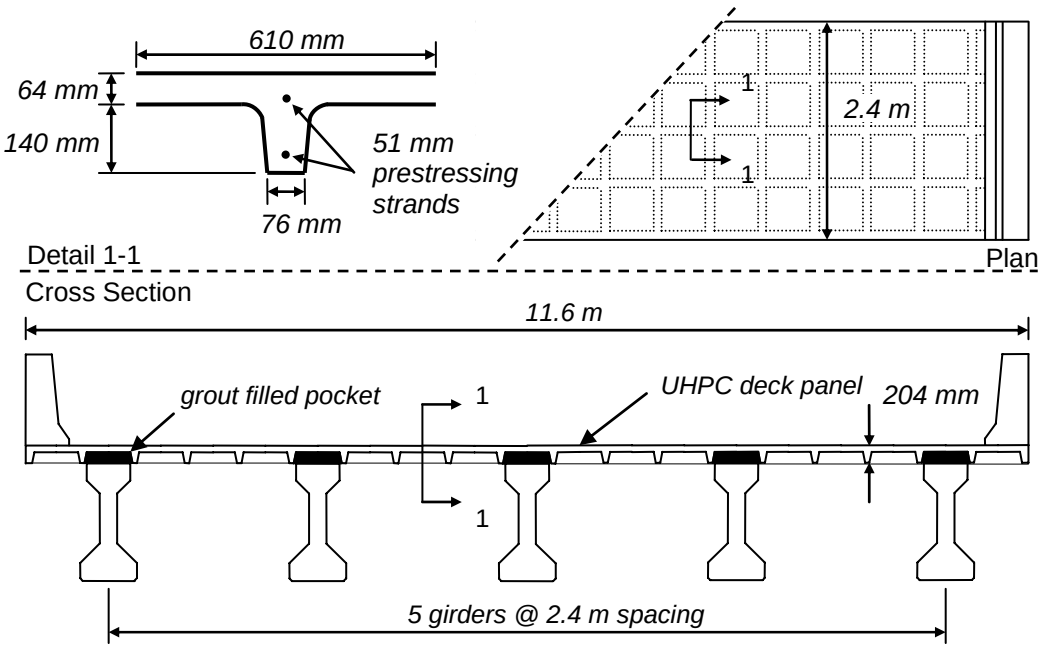

Figure 2: Proposed UHPC Two-Way Ribbed Precast Bridge Deck Element

The fourth research effort is focused of addressing issues of immediate importance to the industry tasked with fabricating UHPC components. One topic currently being investigated is the use of cubes instead of cylinders for the determination of compressive strength. Another topic is the potential use of ultrasonic inspection techniques to determine the setting state of UHPC within a closed, restraint-inducing form.

3 Deployment Status

The Mars Hill Bridge in Wapello County Iowa is the first UHPC superstructure bridge on a public road in the United States. This three-girder bridge spans 33 m with 1.07-m deep prestressed girders. The girders were modified from the standard Iowa Bulb-Tee design through the use of shallower top and bottom flanges and a narrower web. The normal discrete mild steel shear reinforcement was also eliminated as testing demonstrated that the UHPC with its steel fiber reinforcement was sufficient to carry the design loads. This bridge opened to traffic in early 2006. A photo of this bridge is shown in Figure 3 and futher details can be found in [5].

The Cat Point Creek Bridge in Richmond County Virginia is currently under construction and will be the second UHPC superstructure bridge in the United States. This ten span bridge will contain one UHPC span that covers 24.8 m and contains five 1.14-m deep girders. This bridge is expected to open to traffic in early 2008.

A third bridge is currently under design with this structure likely using the second generation UHPC modular superstructure/deck component that was mentioned previously. This bridge will be constructed in Buchanan County Iowa in late 2008.

Figure 3: UHPC I-girder Bridge in Wapello County, Iowa

Many other State Departments of Transportation are considering using UHPC in their bridge inventories. Superstructures are one potential application with longer and lighter prestressed girders both being a possibility. Decks are also being considered, with UHPC potentially being used for precast modular deck components and as a cast-in-place cementitious material in joints and pour-backs. DOTs are also considering using UHPC in specific areas where high durability is required such as the transition slab between the pavement and the bridge deck.

4 Challenges to Widespread Deployment in the U.S. Highway System

The implementation of UHPC in the U.S. highway transportation system is progressing slowly. As is always the case with established industries primarily serving the government sector, implementation of innovations occurs methodically. Five specific reasons for the slow pace are described below.

First, unless an industry sees a clear financial benefit, it is unlikely to invest in innovative technologies. This leads to a situation wherein the industry perceives a risk to using a new material and is hesitant to modify their current operations such that they can efficiently use the new material. As would be expected, the costs of fabricating UHPC components are thus significantly higher than for fabricating similar conventional concrete components.

Second, owners (in this case government agencies) are traditionally risk averse and tend to take measured responses when presented with innovative solutions to existing problems. Any single piece of the transportation infrastructure is expected to last for decades. Limited

budgets and fear of a slightly reduced likelihood of success as compared to conventional practice reduce the opportunity for implementing creative solutions.

Third, the lack of design code provisions relevant to the advanced properties of these concretes is a clear hinderance. This effectively requires that all structural design proceed along one of two paths. The designer could choose to make limited use of the advance properties of UHPC effectively using the advanced properties of UHPC as an added safety factor. Alternatively, the designer could rely on research results, effectively requiring some level of demonstration testing prior to implementation.

Fourth, the limited number of applications of UHPC to date necessarily means that limited experience exists with regard to inspection, maintenance, and repair of UHPC structures. Although it is anticipated that UHPC structures will perform well once deployed into the highway system, UHPC is not immune to damage caused by impacts from overheight or wayward vehicles or from unanticipated structural loadings. Methods for inspection of UHPC for damage and for repairing UHPC components will need to be further developed prior to widespread acceptance of UHPC in the highway industry.

Finally, the constituent materials in UHPC necessarily mean that it will have a higher per unit volume cost that conventional and high performance concretes. It is unlikely that this increase in cost can be offset entirely through the use of more efficient structural designs. In order to offset this increased cost, the enhanced durability properties of UHPC must be explicitly considered through a life cycle costing approach. This concept has encountered slow implementation within the United States. largely due to tight budgets for infrastructure construction/reconstruction.

5 Conclusion

The use of UHPC in the highway industry is progressing in the United States just as it is around the world. Advanced cementitious materials exhibiting increased strength and enhanced durability clearly have a role to play in the construction/reconstruction bridges. Research to date has demonstrated that the properties of UHPC will open many new avenues for engineers and architects. However, challenges exist that can be expected to continue to hinder the deployment of UHPC into the civil infrastructure. Most significantly, the risk aversion of government entities and industry partners, the high cost of UHPCs, and the lack of codified design provisions related to UHPC will likely all contribute to slow progress in UHPC deployment.

6 References

[1] Graybeal, B.: Material Property Characterization of Ultra-High Performance Concrete. Federal Highway Administration Report No. FHWA-HRT-06-103. August 2006. McLean, Virginia, USA.

[2] Graybeal, B.: Structural Behavior of Ultra-High Performance Concrete Prestressed I-Girders. Federal Highway Administration Report No. FHWA-HRT-06-115. August 2006. McLean, Virginia, USA.

[3] Graybeal, B.; Hartmann, J.: Experimental Testing of UHPC Optimized Bridge Girders: Early Results. In: Proc. Precast/Prestressed Concrete Institute National Bridge Conference, Palm Springs, California, 2005.

[4] Garcia, H.; Graybeal, B.: Anaylsis of an Ultra-High Performance Two-Way Ribbed Bridge Deck Slab. National Techncial Information Service Report No. PB2007-112112. August 2007. Springfield, Virginia, USA.

[5] Bierwagen, D.; McDonald, N.: Ultra High Performance Concrete Highway Bridge. In: Proc. Precast/Prestressed Concrete Institute National Bridge Conference, Palm Springs, California, 2005.

Dr Mark Rebentrost
General Manager - Ductal®
VSL Australia Pty Ltd
Sydney, Australia

Dr Gavin Wight
Technical Manager - Ductal®
VSL Australia Pty Ltd
Sydney, Australia

Experience and Applications of Ultra-high Performance Concrete in Asia

Summary

Ultra-high performance concretes (UHPC) exhibits exceptional mechanical and durability properties. RPC is a cementitious material consisting of cement, sand, silica fume, silica flour, admixture and water. It is almost self-placing, has a compressive strength of 150-200 MPa and a flexural strength of 30-40 MPa. This paper presents examples of UHPC structures that have been designed and constructed in Asia from the perspective of an Australian construction specialist. Applications in Australia and New Zealand include the first road bridge built using UHPC and completed in October 2004, a series of footbridges in New Zealand providing ramp access to train stations, panels at a power station that are subjected to continuous salt water spray, and panels for blast protection. Project examples from Korea and Japan are also described.

Keywords: *reactive powder concrete, bridges, pedestrian, durability, project examples*

1 Introduction

The Ultra-high performance concrete (UHPC) described in this paper is of the reactive powder concrete (RPC) type known under the brand name of Ductal® and originally developed by Rhodia, Lafarge and Bouygues [1]. The constituents of RPC are cement, fine sand, silica fume, silica flour, superplasticiser, water with a low water-cement ratio, and may include either high-strength steel fibres or non-metallic fibres.

The extremely good durability properties of UHPCs are well documented [2, 3, 4]. The compression strength of Ductal® fabricated in Australia is in the order of 200 MPa, flexural strength of up to 45 MPa and a Young's modulus of 47 GPa. The behavior in compression can be described as having a ductile softening plateau. UHPCs are often heat treated to limit the residual shrinkage, normally shrinkage is up to 500microns, and improve mechanical performance. The design and general properties of Ductal® are described in detail in [5]

The ultra-high strength of UHPCs put them outside the direct provisions of the Australian design standards and therefore a specific design guide was required [6]. Research was undertaken at the University of NSW in view of developing a design guide complying with the intent of AS 3600 [7]. This research included beam tests to evaluate shear strength parameters and mechanical strength tests to determine characteristic design strengths [8].

The development of this guide took into account the extensive material research undertaken in France [9].

UHPC has been used around the world predominantly in the construction of pedestrian and road bridges [10], protective panels [11], and architectural applications [12]. This paper provides a summary of the applications in Asia in recent years from an Australian perspective. VSL Australia has been fabricating UHPC solutions for more than five (5) years and the team in Sydney is the Knowledge Centre for UHPC applications in the VSL Group.

2 Australia and New Zealand

2.1 Shepherds Creek Road Bridge: NSW, Australia

Secondary transport roads in Australia are dominated by short span highway bridges, many of which are approaching design life and carrying capacity limits. The Shepherd's Creek Bridge replaced an ageing timber bridge. It comprises four traffic lanes and a footway, Fig 1(a). The bridge is a single span of 15m with a 16° skew. The superstructure, shown during construction in Fig 1(b), comprises 16 precast pre-tensioned RPC beams and an in-situ 170mm thick RC deck slab. The concrete slab is cast on 25mm thin permanent precast RPC formwork panels that span between the beams. The I-section beams have a depth of 600mm and are spaced at 1.3m centres.

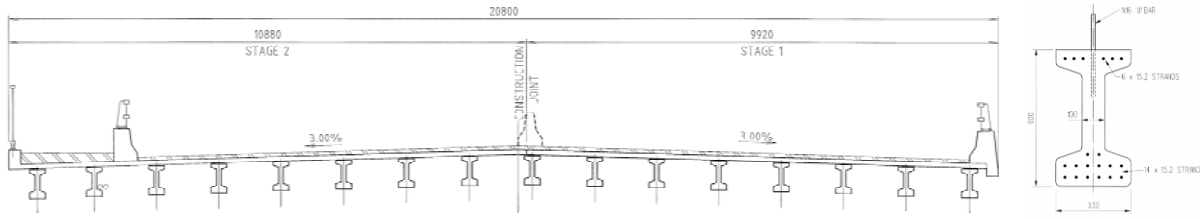

a. Cross section and beam details

b. Installed beams and formwork slabs

c. Bridge open to traffic

Figure 1: Shepherds Creek Road Bridge: Australia

As part of the RTA (Road Traffic Authority) certification programme for RPC in Australia, the Shepherds creek bridge was load tested on completion of the first two lanes, and again one year later. The tests confirmed that the behaviour of the bridge conformed to the design. Fig 1(c) shows the bridge open to highway traffic. In September 2005, the RTA issued a policy

statement giving approval for RPC to be used on RTA bridges and structures. Additional project information can be found in [13].

2.2 A Series of Pedestrian Bridges: Auckland, New Zealand

An important part of the station redevelopment being undertaken by the Auckland Regional Transport Network Ltd is a series of new footbridges, providing ramp access for pedestrians to cross the railway tracks. To-date, five (5) stations have had the footbridges replaced, the first being Papatoetoe Station which is described in the following paragraphs. A second footbridge at Penrose Station also in Auckland has recently been completed using the same Ductal® bridge element utilised on the Papatoetoe Station footbridge. The bridge has a total length of 265m consisting of 15 spans of mostly 20m, and was opened to the public in March 2006. The third major upgrade was completed at Papakura station in August of 2007.

The station at Papatoetoe was the first station to have the new footbridges. The conforming design for the Papatoetoe pedestrian bridge was a conventional prestressed concrete structure until a New Zealand contractor saw an opportunity to reduce the weight and cost by using a UHPC (Ductal®) solution proposed by VSL Australia. The main advantage of the alternative solution is the significant weight reduction, resulting in reduced design earthquake actions imposed by the New Zealand design code and cost savings in the substructure and erection.

The Papatoetoe Footbridge has a total length of 175m consisting of ten simply supported spans, with the majority of spans being 20m long. There are two shorter spans of 8.2 and 10.2m. The bridge spans are formed using two precast Ductal® segments. The deck is 50mm thick, contains no ordinary reinforcement, and has two symmetrical legs with large circular holes that provide architectural interest and reduce weight; Fig 2a and 2b give details. Ribs protrude 350mm below the top of the deck slab at 2.7m centres along the beam to add torsional rigidity. The tension steel is provided by ten (10) ∅12.7mm post-tensioned strands in the bottom of each leg and six (6) strands at the top to balance stresses. Both tendon profiles are straight and anchored directly against the RPC without the need for further anchorage reinforcement.

Production of the Papatoetoe bridge beams (Fig 2c) commenced in December 2004 and was completed over a ten week period. To achieve the required architectural shape and surface finish, a special steel formwork was utilised, comprised of a fixed internal form and two side forms that shape the exterior surface and web penetrations. The larger elements were match cast in two segments to allow later transportation on standard 40-foot containers (Fig 2d).

The RPC beams were post-tensioned on site after delivery to New Zealand. Prior to erection a topping surface made of ordinary concrete was applied to the Ductal® superstructure. This surface was graded in accordance with accessibility guidelines and has a varying thickness.

Steel hand rails were secured directly to the RPC superstructure (Fig 2e). A more detailed account of the design is given in [5] and of the construction account in [14].

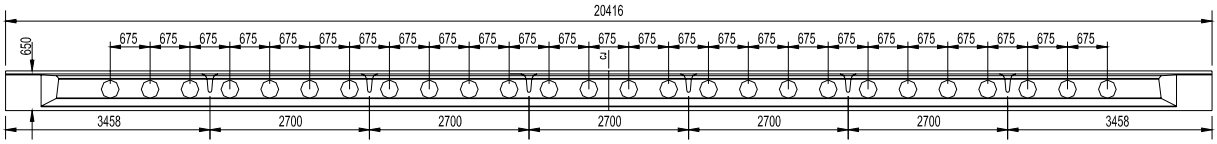

a. Typical elevation of a 20.4 m π-shaped UHPC(Ductal®) beam

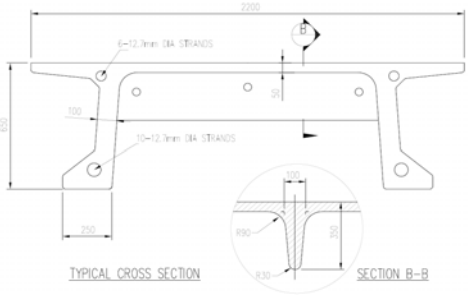

b. Cross section of UHPC beam element

c. Demoulding of match-cast segments

d. Segments in transpor

e. UHPC span with railing attached being lifted

f. Completed Papatoetoe Footbridge

g. Penrose Footbridge during construction

Figure 2: Papatoetoe and Penrose Footbridge: Auckland, New Zealand

2.3 Infrastructure Protection Applications

UHPC such as reactive powder concrete (RPC) exhibit exceptional energy absorption capacity and resistance to fragmentation, making it ideal for panels and components that need to perform under explosive, impact or shock loads. The flexural toughness of RPCs enhanced with fine steel fibres is greater than 200 times that of conventional fibre reinforced

concrete. Furthermore, under very high strain rates (>250/sec), ultimate compressive and tensile capacities can increase up to 1.5 times [15, 16].

In Australia, VSL has undertaken tests where panels are subjected to large-scale blast effects at various distances, close-charge effects, projectile impacts from armour piercing bullets and fragment simulated projectiles as well as special weapons effects mitigation. Further details of these tests using UHPC is provided in a another paper presented at this conference.

Panels for the first structure incorporating blast resistant optimised RPC panels were manufactured in March 2005 at the VSL plant in Melbourne. The client was the Department of Foreign Affairs and Trade of the Australian Government. Panels are up to 4.5m long x 2.0m wide x 100mm thick. They are being used to provide blast resistance to an existing building in a high risk international location. The panels were installed on site in July 2005. Photos of the panels prior to shipment from the VSL factory and as installed on site are shown in Fig 3.

a. UHPC blast resisting panels b. Installed UHPC panels

Figure 3: Optimised UHPC panels for protection of government facility

2.4 Durability Application: Eraring Power Station Covers

The attemperating weir at Eraring power station is used to take salt water from Lake Macquarie in New South Wales (Australia), which is combined with warm water from the power station and then discharged back into the lake over large boulders, which generates continuous spray of salt water that needs to be contained to avoid severe corrosion to the power station facilities.

The weir consists of three cells that are 11m wide. A cover consisting of conventional precast pre-tensioned concrete planks had contained the spray for only 14 years before a number of planks started to collapse due to corrosion, see Fig 4(a). The owner required a replacement cover that had a design life of at least 100 years. Using reactive powder concrete, with its extraordinary durability properties such as low chloride ion diffusion rate, VSL Australia

engineered a structural solution with an estimated design life in excess of 5 times that required.

(a) Weir prior to upgrade showing failed planks

(b) Typical UHPC panel

(c) Installation of new UHPC panels

(d) Weir in operation, August 2004

Figure 4: Photos of Eraring power station weir covers

The UHPC panels have typical dimensions of 11.0 × 2.3m, a nominal thickness of only 25mm, and are supported by two integral 250mm deep beams, as illustrated in Fig 4(b). The panels were precast and pre-tensioned and are extremely light compared to other systems weighing only 3.5 tonnes each. A total of 920m^2 of UHPC panels were supplied and installed in August 2004. Fig 4(c) and 4(d) show the installation and completed weir respectively.

2.4.1 Seating Plats for a Stadia

Following repeated interest from construction clients, VSL Australia has investigated the feasibility of an optimised UHPC precast element for stadia seating plats. These plats support stadia seating and are usually fabricated from ordinary concrete, the design of which is governed by vibration comfort requirements and self-weight. In modern stadia, multi-level seating is often levered out to provide maximum capacity, and therefore the weight of the seating plats is a significant factor in the supporting structure design.

For this comparison a typical span of 13m was taken, for which the standard concrete plat is L-shaped. The optimised UHPC plat is designed to maximise vibration comfort, minimise self-weight and provide superior durability ensuring lower maintenance costs and a long design life. The reduced self-weight provides a reduction in direct costs in the supporting structure and erection including faster crane movements, multiple unit lifting for faster installation and fewer truck movements on site and. Fig 5 shows the optimised UHPC plat

section and 3-unit assembly, with Table 1 listing the primary performance advantages. While no UHPC plats have been fabricated to-date, the concept is being explored for application in new and for the upgrade of existing stadia in Australia, New Zealand, Switzerland and the UK.

Table 1: Performance advantages of optimised UHPC stadia seating plats

Performance Criteria	**Typical Concrete Plank**	**UHPC Optimised Plank**
Weight	8.6 t	4.2 t
Deflection (Dead & Dynamic Live Load)	6.5mm	4.0mm
Vibration (1st Mode, higher is better)	7.6 Hz	12.5 Hz
Durability	Acceptable by Design	Significantly better

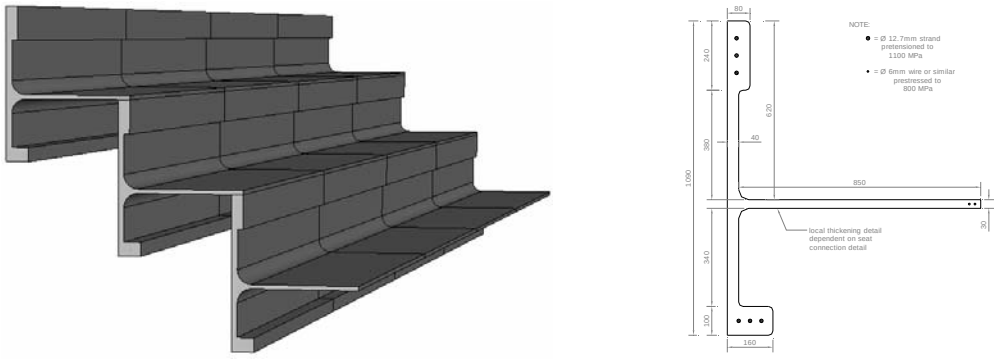

Figure 5: Concept for optimised UHPC stadia seating plats

3 Japan

One of the major contributors in furthering UHPC applications in Japan is the Taisei Corporation and Taiheiyo Cement under licence of Lafarge. There are also other precasters in Japan that specialise in UHPC.

3.1 Sakata-Mirai Footbridge: Sakata, Japan

Sakata-Mirai Bridge was designed to fit into the graceful and monotone local environment [17]. The bridge takes full advantage of the characteristics of Ductal® and does not use any passive reinforcement, instead achieving strength through external prestressing. The bridge is extremely light with a dead weight of only 56 tonnes; approximately a fifth of the dead load of an equivalent ordinary PC structure, resulting in an economic advantage of around 10% [17]. Fig 6 shows the bridge, which consists of a single 50.2m span, and a typical cross section at mid-span showing the two external prestressing tendons consisting of 31-∅15.2mm strands. The section height varies from 550mm at the supports to a maximum of 1650mm at mid-span (Fig 6) to satisfy deflection limits of span/600. A 3-D non-linear FEM analysis taking into account the holes was utilised to carry out detailed design verification. The bridge consists of six (6) precast segments that were erected onto temporary steel girders on piled abutments. An in-situ joint was used to connect the segments prior to post.

Figure 6: Sakata-Mirai Footbridge: Japan

3.1.1 Other Bridges Applications

Bridge and related applications of UHPC in Japan have been predominantly in the form of box girders with very thin webs often similar to the ideas of the Sakata-Mirai Footbridge described above; the Table below lists known projects utilising UHPC supplied kindly by Hiroshi Shiratani of the Taisei Corporation.

Table 2: List of UHPC Bridge Applications in Japan

Name [Location]	Type	Span [m]	Width [m]	Completion Date	Notes
Horikoshi Ramp [Fukuoka]	Highway	16	8.5	11-2005	Composite I-girder
Torisaki River [Hokkaido]	Highway	45	11.3	12-2006	Launching nose
DNP Tokai Factory	Motorway	2.9	6.5		
Akakura [Yamagata]	Footbridge	35	3.5	01-2004	Box girder
Tahara Bridge [Aichi]	Footbridge	12	2.6	04-2004	Box girder
Toyota Gym [Aichi]	Footbridge	28	4.5	02-2007	Box girder
Sanken-ike [Fukuoka]	Footbridge	2-40	3.5	06-2007	Box girder
Keio Uni [Tokyo]	Footbridge	11	2.0	03-2005	
Hikita [Tottori]	Footbridge	63.3	3.0	Construction	Box girder (web & flange only)

Fig 7 on the right, shows the unique application of UHPC for the Torisaki River Bridge. Here a corrugated steel web girder, erected by incremental launching, uses UHPC for the lower chords of the launching nose portion. The bridge has a maximum span of 54.5m, and a launching nose length of 45m. After completion of launching, the nose portion is transformed to the permanent girder.

Figure 7: Other UHPC Bridges in Japan; Left: Akakura Footbridge, Right: Torisaki River Bridge

3.1.2 Haneda Airport Slabs

The expansion of Haneda Airport Runway D will utilise the world's largest single project application of UHPC (Ductal®) in the world to date; work on the project started in July of 2007, with initial experimental works conducted two years prior. In addition to supplying the preblend Ductal® material, Taiheiyo Cement (under licence from Lafarge) is also responsible for the mixing operation for the UHPC slabs. The project is an excellent example of how weight savings and durability make for an overall economical UHPC solution. Fig 8 shows the runway extension over water that is supported by a complex steel jacketed structure.

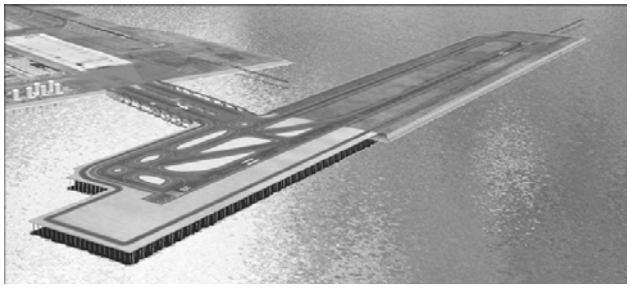

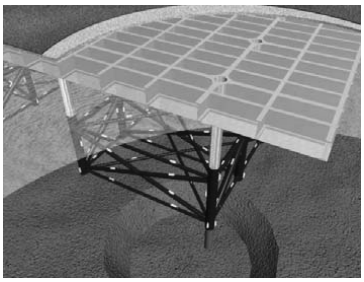

Figure 8: Haneda Airport Runway D; Left: Panoramic View, Right: Pier Section

The cost reduction in the required steel jacket fabrication for the supporting structure yields an overall construction cost saving for the project, a direct function of the weight savings achieved through the use of the UHPC slabs. The high level of mechanical performance, good fatigue, freeze and thaw performance, and excellent durability further enhances the whole-life costing of the project.

Table 3: Testing of UHPC slab

	Prestressed Concrete Slab	**UHPC Slab**
Weight per Slab	221 kN (100%)	97 kN (44%)
Average Dead Load including Fillers	7.84 kN/mm^2	3.83 kN/mm^2
Average Slab Depth	320mm	135mm

The plan dimensions of the UHPC precast slabs for the piers of the Haneda Airport Runway D are 7.8 x 3.6m. There are approximately 7,000 slab units that provide an area of 200,000m^2; equivalent to 24,000m^3. The UHPC slabs are ribbed, pre-tensioned with high-strength strand and have an effective depth of only 135mm. The slabs were designed for ultimate wheel loads of 320kN. Prototype testing of the slabs, shown in Fig 9, yielded an ultimate carrying capacity of 600kN/wheel. Table 3 gives a comparison between the UHPC slab weights and prestressed concrete slab. A low carbonation rate, water permeability and good salt damage resistance helped in achieving the 100 year design life in the aggressive environment.

Figure 9: Testing of UHPC slab

4 Korea

Since the introduction of UHPC, Ductal® licensed by Lafarge and utilised on the Sunyudo Bridge, VSL Korea has been actively seeking projects to utilise these UHPC materials again.

4.1.1 Sunyudo Footbridge: Seoul, Korea

To date, the Sunyudo (Peace) Footbridge in Seoul (Fig 10a) is the largest RPC bridge in the world with a single span of 120m. It is comprised of six (6) precast and post-tensioned segments of PI-shaped section. The section developed for the Sunyundo Footbridge, consists of a transversally ribbed upper slab and two girders. The width of the arch is 4.3m, has a section depthof 1.3m and a thin (30mm) slab supported by transversal ribs at 1.225m, and two longitudinal ribs at the extremities of the transversal section. This ribbed slab is supported by two 160m thick webs. The transversal ribs are prestressed by ∅12.7mm sheathed and greased monostrands. Small specially adapted anchors similar to those used in the construction of the Sherbrooke footbridge (17) were used to transfer the prestressing forces. In the longitudinal direction, the structure is prestressed by three (3) tendons in each leg. The arch is supported at each end by two reinforced concrete foundations 9m deep resisting the horizontal thrust of the arch. Further design and construction details have been described in other publications [12, 19].

Figure 10: Sunyudo Footbridge: Seoul, Korea

4.1.2 Realization of a Hanging Walkway

VSL has had numerous enquiries in Asia for light-weight, highly durable walkway attachments to existing or new road bridges. In the past these types of structures have often been constructed from steel, with ordinary concrete solutions being too heavy, but recent whole-of-life and other durability considerations have steered engineers to look into UHPC solutions; one of these is a hanging walkway for the proposed Gyeomjae Bridge in Korea. A typical cross-section of the hanging walkway solution is shown in Figure 11. The concept significantly reduces the size of the concrete box girder and separates pedestrian and road traffic . At the time of writing, the project is undergoing final design consideration.

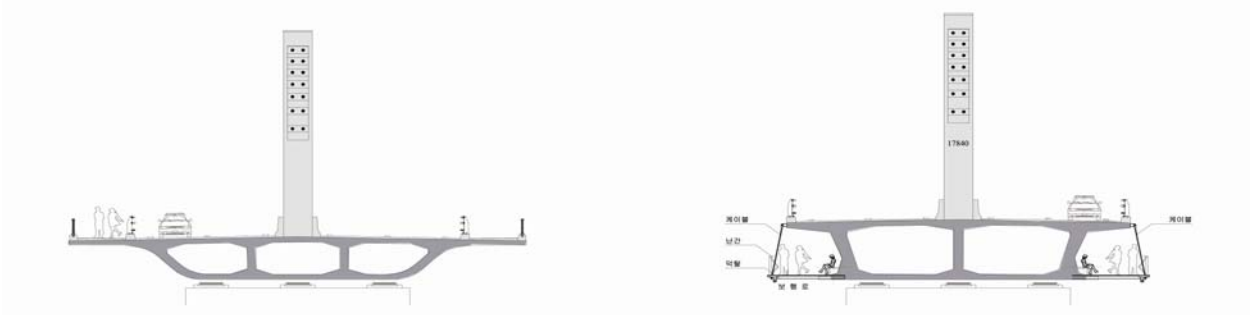

Figure 11: Gyeomjae Bridge; Left: Conforming Design, Right: Design with UHPC hanging walkway

The proposed UHPC walkway consists of thin plank type segments (as shown on the right), post-tensioned through a longitudinal rib to form modules that can be lifted into place as a single unit. The planks are further ribbed transversely to provide torsional rigidity and bending strength. The UHPC modules are suspended off the concrete box girder using hanger bars and a steel pin joint on the inside. Each UHPC module with a width of 4m and 6m length weighs only 4.5t.

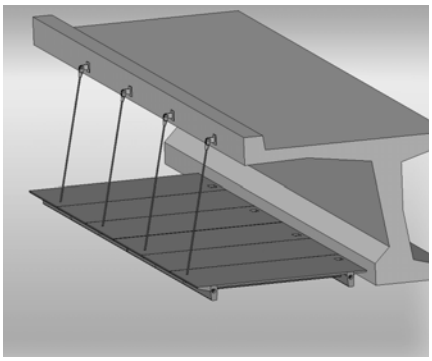

5 Concluding Remarks

The paper has provided an overview of the application of an UHPC, mainly named Ductal® throughout Asia from an Australian perspective. While UHPC is not a replacement for conventional concrete, it can create opportunities and provide economical and innovative solutions in areas where normal concrete struggles to form a solution. In Asia, VSL and other Lafarge licensees have successfully developed and shown the benefits of UHPC as an alternative to conventional road bridge construction, for footbridge applications in earthquake prone areas, and in applications requiring durability or blast effects damage mitigation.

6 References

[1] Richard, P.; Cheyrezy, M.: Composition of reactive powder concrete. Cement and Concrete Research, Vol. 25, No. 7, S.1501-1511, 1995.

[2] Roux, N., Andrade, C., Sanjuan, M. A. Experimental Study of Durability of Reactive Powder Concretes. Journal of Materials in Civil Engineering, Vol. 8, No. 1, S. 1-6, 1996.

[3] Schmidt, M. Ultra-Hochleistungsbeton – Ausgangsstoffe, Eigenschaften und Leistungsfaehigkeit, Ultra-Hochfeter Beton, Plannung und Bau der ersten Bruecke mit UHPC in Europa, Kassel Univ. Press, 2003, pp 5-20.

[4] Pimienta, P. Chanvillard, G. Durability of UHPFRC specimens kept in various aggressive environments, 10 DBMC International Conference on Durability of Building Materials and Components, Lyon, France, April 2005.

[5] Wight, G., Rebentrost, M., Cavill, B., Designing Bridges with Ductal® Reactive Powder Concrete, 23rd Biennial Conference, Concrete Institute, Adelaide, Australia, 18-20 October 2007, pp. 249-258.

[6] Gowripalan, N.; Gilbert, R. I.: Design Guidelines for Ductal® Prestressed Concrete Beams. Design Guide, School of Civil and Environmental Engineering, The University of New South Wales, Sydney, Australia, 2000.

[7] AS 3600-2001: Concrete Structures. Standards Australia, Sydney, Australia, 2001.

[8] Gowripalan, N.; Watters, R.; Gilbert, I.; Cavill, B.: Reactive Powder Concrete (Ductal®) for Precast Structural Concrete – Research and Development in Australia. 21st Biennial Conference of the Concrete Institute of Australia, Brisbane, Australia, 2003.

[9] AFGC / SETRA Working Group: Ultra High Performance Fibre-Reinforced Concrete – Interim Recommendations. Report, Association Française de Génie Civil, Paris, France, 2002.

[10] Rebentrost, M; Cavill, B.: Reactive Powder Concrete Bridges. AustRoads 6th Bridge Conference, Perth, Australia, 2006.

[11] Cavill, B.; Rebentrost, M.: Ductal® - a high-performance material for resistance to blasts and impacts. In: Australian Journal of Structural Engineering, Vol. 7, No. 1, S. 37-45, 2006.

[12] Acker, P.; Behloul, M.: Ductal® Technology: A Large Spectrum of Properties, A Wide Range of Applications. fib Symposium, Avignon, France, 2004.

[13] Gilbert I, Gowripalan N and Cavill B. On the Design of Precast, Prestressed Reactive Powder Concrete (Ductal®) Girders, Austroads 4th Bridge Conference, Adelaide, Australia, November 2000.

[14] Rebentrost M. Design and Construction of the First Ductal® Bridge in New Zealand, New Zealand Concrete Industry Conference, Auckland, New Zealand, September 2005

[15] Ngo, T., Mendis, P., Lam, N. and Cavill, B. Performance of Ultra-High Strength Concrete Panels subjected to Blast Loading, The 2005 Science, Engineering and Technology Summit, Canberra, July 2005.

[16] Fujikake, K., Senga, T., Udea, N., Ohno, T. And Katagiri, M. Effects of Strain Rate on Tensile Behaviour of Reactive Powder Concrete, Journal of Advanced Concrete Technology, Vol. 4, No. 1pp 79-84, Feb 2005.

[17] Tanaka Y, Musya H, Ootake A, Shimoyama Y and Kaneko A. Design and Construction of Skata-Mirai Footbridge Using Reactive Powder Concrete, Proceedings of the 1st fib Congress, Osaka, Japan, October 2002.

[18] Blais, P.Y. and Couture, M. Precast, Prestressed Pedestrian Bridge - World's First Reactive Powder Concrete Structure. PCI Journal, Sept.-Oct. 1999, pp. 61-71.

[19] Ricciotti, Bridge to the Future. ASCE Civil Engineering Magazine, Vol 71 No 1, November 2001.

Jacques Resplendino
Chief engineer
Chairman of the AFGC-SETRA working group on UHPFRC
Official representative
Bridges and structures coordinator
Direction Interdépartementale des Routes Méditerranée
Marseille, France

Ultra-High Performance Concretes – recent realizations and research programs on UHPFRC bridges in France

Summary

This paper provides a review of the realization of two road bridges made of UHPFRC, and two research programs on UHPFRC bridge application recently carried out in France. The first structure presented is the n°34 overpass (PS34) on the A51 motorway. It is a single span road bridge 47m40 long made of a prestressed UHPFRC box beam. It was built in 2005 in BCV® by Campenon Bernard Regions (Vinci group). The second road bridge is the Saint Pierre La Cour Bridge which has a composite deck made of UHPFRC precast prestressed I-girders beams connected to a traditional reinforced concrete slab. It was built in 2005 in Ductal® by Quilles (Bouygues TP group). The third part of this paper presents a research program concerning the design of a ribbed UHPFRC slab for a composite steel concrete bridge. The last part of the paper deals with a research concerning bridge deck solutions using UHPFRC, composites (glassfibre) and active and/or passive steel reinforcements. It was conducted within the European project NR2C (New Road Conception Concepts).

Keywords: *ultra high performance concrete ; fibre ; precast ; composite structure ; durability ; design methods ; placement methods ; composite materials*

1 Introduction

The AFGC-SETRA UHPFRC Recommendations published in 2002 [1] explain in detail the way to characterize UHPFRC performances and to calculate structures. These recommendations were written while the first world UHPFRC road bridges (Bourg Lès Valence overpasses) were realized. From then on, several structures and bridges haven been built using the recommandations. Some further remarkable realizations and design projects have led to increased knowledge and gains of experience about UHPFRC application.

2 The n°34 Overpass (PS34) on the A51 motorway

The n°34 overpass on the A51 motorway is built in BCV®, the UHPFRC developed by the ciment factory Vicat, and the Vinci group. It was built in 2005 by Campenon Bernard Regions

(Vinci group) for AREA society, the owner, with the assistance in works contracts by Scetauroute company [2].
The checking of final design and the supervision of the excecution is made by CETE de Lyon.

2.1 General description of the structure

The structure is a single span road bridge 47.4 m long made of a prestressed box girder (fig 1). It supports a third class, three meters wide road.
The box beam has a constant height equal to 1m60. The upper slab has a constant thickness equal to 14cm. The webs and the lower slab have a constant thickness equal to 12 cm (fig 2).

Figure 1: General view of the PS34 bridge

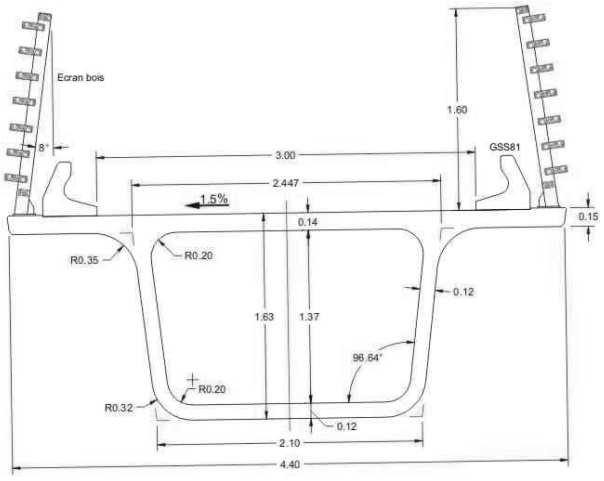

Figure 2: Cross section of the PS34 bridge

No global traditional steel reinforcement has been implemented in the typical segments, which are longitudinaly prestressed by six 19T15S external câbles. The deck is made of 22 UHPFRC match-cast pasted prefabricated segments. Using BCV® durability remarkable performances, and the fact that the match cast pasted joints stay under high compression, there is neither watertight nor paving layer on the structure, which is a première for a road bridge in France. The upper surface of the slab is made using a special formwork surface which gives high rugosity for vehicule adhesion.

2.2 BCV® characteristics

2.2.1 BCV® general characteristics

Béton Composite Vicat (BCV®) has a 28 days characteristic compressive strength from 130 MPa to 150 MPa, and a direct tensile strength about 12 MPa.
The BCV formula used for PS34 has a 2% volume fibre content with two sizes of fibres : 2/3 of 20 mm length fibres, 1/3 of 12 mm length fibres. No polymer fibre has been used.

2.2.2 Tensile strength of the BCV®

The characterisation of the BCV® strength was made in accordance to the AFGC/SETRA recommendations considering thick elements :

- three cylindric specimens Ø11x22 for compressive strength,
- six 10x10x40 specimens for third-point flexural tests on un-notched prisms for cement matrix tensile strengh,
- six 10x10x40 specimens for centre-point flexural tests on notched prisms for post cracking tensile strength.

BCV® has a characteristic direct tensile strength of about 8 MPa for the elastic stage, and 8 MPa for the post cracking strength (8 MPa correspond to the characteristic tensile strength for a crack width of about 0,3mm). These values have been corrected to take into account dispersion effects due to the placement method by K coefficients determined by suitability tests as described below.

2.3 Final design of the bridge

The structure has been designed with normal road loads of a third class road bridge.
With respect to longitudinal bending, full compression is required, to avoid any decompression at serviceability limit state, according to the presence of match-cast pasted joints. At the Ultimate limit state, the structure has a very small decompression so that shear capacity is always ensured by the compressed residual part of the cross-section. Transverse bending forces are carried only by the tensile strength capacity of the UHPFRC.

2.4 Suitability tests

For suitabiliy tests, the company engaged an important testing program to validate several mix-proportioning alternatives, to validate several formwork surface finishings for the different concrete surfaces, to examine concrete placement methods (with a moving or fixed pipe, with a puomp), in order to determine the fibre orientation coefficient K. The concrete surfaces of PS 34 segments are innovative because of their texture. Wood imitation has been chosen for the external surface of the webs and the lower slab, and a granular aspect for the upper slab which directly serves as carriageway without any watertightness, or other asphalt layer (Fig 3).

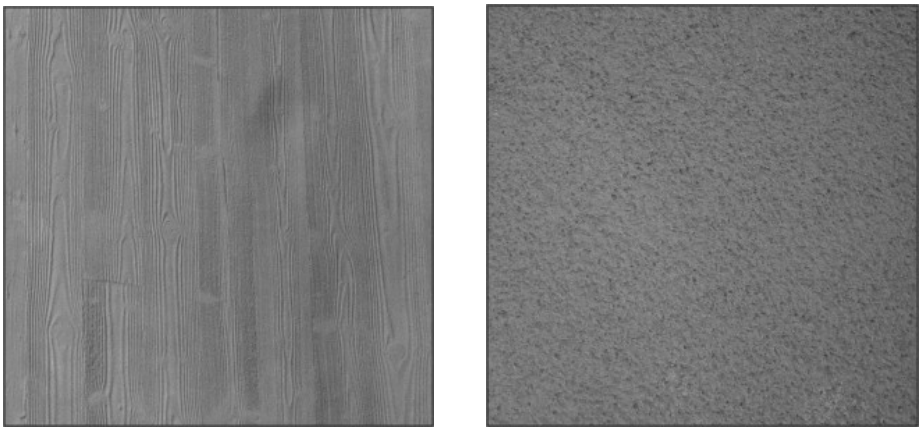

Figure 3: Wood and upper slab granular formwork surface

Two test segments with actual size have been built to validate the K coefficient value taken into account for the design. (Fig 4).

The traditional method consists in placing concrete with a moving pipe in order to avoid any UHPFRC flow, and provide isotropic fibre orientation. The disadvantage of this method is to be dependent on the operator and requires important controle procedures. In order to develop a more systematic and reproductive method for regular segments, the company wanted to introduce concrete in a single point (in the middle of the upper slab), testing several methods to inject concrete (with a pump, with a pipe,..). This method presents the disadvantage to orient fibres according to the flow, and to provoke a front of the flux at the opposite of the injection point (middle of the lower slab). Considering this special placement method a value of K = 1,5 has been taken into account for the preliminary design. The results of the suitabiliy test showed that 1,5 was a safe value except at the level of the flux front in the middle of the lower slab. Several methods to mix flux in that zone have been tested but not retained, because of insufficient results and difficulties to operate. Locally, traditional reinforcement was added in that zone to solve the problem.

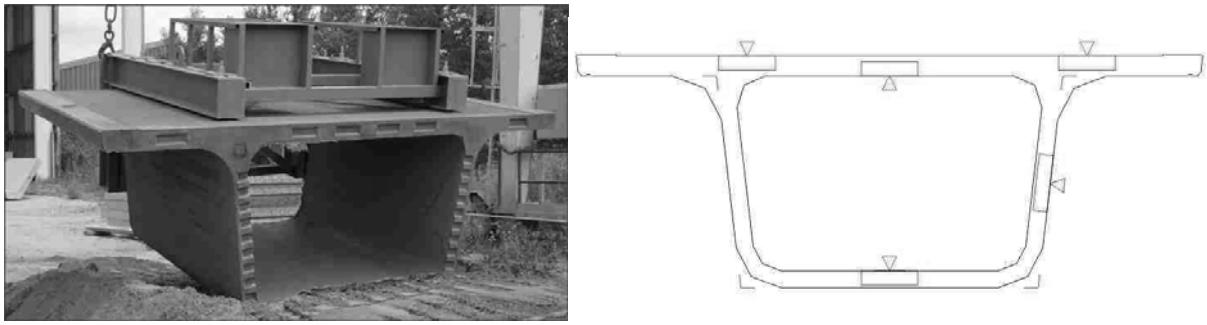

Figure 4: Actual size test segment

2.5 Segment precasting and bridge erection

The 22 segments were built in Romagnieu (Isère – Southeastern France), in the Campenon Bernard company precasting factory, which is equipped with a powerful mixing plant especially adapted for UHPFRC. Each segment was vertically manufactured above the adjacent segment. Manufacture begins by the segment in the middle of the structure which allows to progress towards the extremities with two distinct casting areas. After the

precasting stage, the segments were transported on site, onto an assembling platform prepared along the motorway platform. They were pasted and joined together by a temporary prestressing. At that time, some snow covered the deck and we observed local defects of the watertightness which were resolved by local joint injections. When all the segments were gathered together, final prestressing (six 19T15S cables) was implemented and caused the deck unsticking from its assembling area.Afterwards the deck (less than 200 tonnes total weight) was placed with a crane directly on its final bearings.

2.6 Conclusion – lessons from this realization

This project has shown that it was possible to avoid any watertight or pavement layer on an UHPFRC structure, under the condition to use a special formwork surface which gives high roughness for vehicle adhesion. To obtain perfect watertight of the upper slab it is also necessary to have significant compression in the joint, and to realize match-cast pasted joints with a lot of care.

Compared to a classical overpass, this UHPFRC solution provides an important profit on material quantites (80 m^3 of UHPFRC instead of 200 m^3 of C35/45 concrete). This solution allows to eliminate any intermediate piers which caused a real esthetic problem considering the breach geometry.

The structure realization also offers more security by the removal of pops and all the classical security problems during assembling and striking.

As for the economical approach, this solution is interesting if the formwork equipment coste is balanced with realization of two or three identical structures, which can allow to lower the price of the material when employed in a strategy of industrialized output.

Another interest is also of course the execution delay which is reduced more than one month as compared to an ordinary solution, and the durability of the structure which is highly increased due to the material performances of UHPFRC.

3 The Bridge of St Pierre La Cour

This bridge is located at a railway overpass by the Saint Pierre La Cour bypass in Mayenne region (Northwestern France). It has been built during spring 2005 by the contractor Quille (Bouygues TP group) for the owner Lafarge Cements [3][4]. Conceptual and final design have been done by the Design Office of Bouygues T.P. and checked by the CETE of Lyon. Precast elements have been constructed in CPC workshop in Brive.

3.1 General description

The deck of the bridge is made of ten precast prestressed I-girder beams made of Ductal® , connected to a traditional reinforced concrete slab (Fig 5).

The bridge has a simple span of 19m, the total width is 12.909m. The structure is crossing at an angle of 54° and carries two 7.5m wide lanes and two lateral footpaths of 2.5 and 1.5 m wide respectively.

The traditional concrete slab (200mm thick) is poured in a second stage on precast panels in Ductal® of 25 mm thickness.

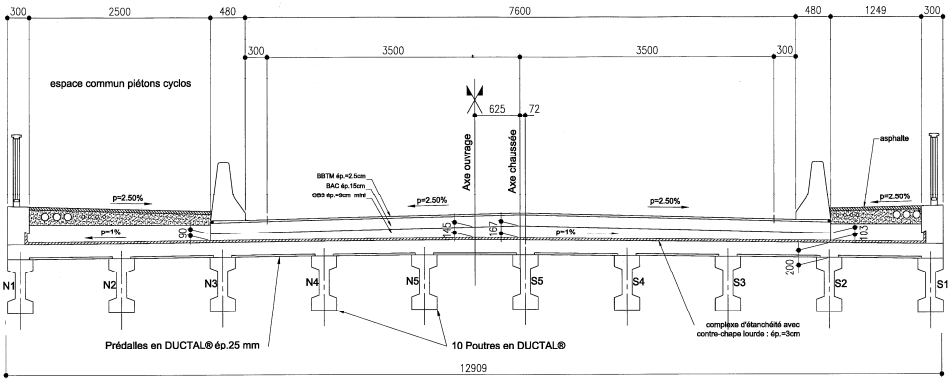

Figure 5: Cross section of Saint Pierre La Cour Bridge

3.2 The Material

Ductal® is an an UHPC reinforced with fibres which can be made of steel 12mm length (Ductal®-FM), made of organic material (Ductal®-FO) or combination of both steel and organic material (Ductal® AF). For structural applications as Saint Pierre La Cour Bridge, one use Ductal®-FM (or Ductal® AF if fire resistance is required).

Main characteristics of the material are obtained by tests carried out following the AFGC and SETRA recommendations as explained above. Compression strength is was controlled on cylindrical samples (reduced dimensions (dia. 70 x 140 mm). A characteristic value greater than 180 MPa was obtained. The precast panels were tested under 4 points-bending using un-notched specimens, obtained from a real panel (same thickness) with dimensions 640x360x25 mm.

For beams two different tests were performed on 70x70x280 mm samples :

- Four point bending tests on un-notched specimens : these tests allowed to determine the first cracking strength in bending from which the direct tensile strength was deduced using the *Fib* scale effect model. In the case of this project, the characteristic value of the direct tensile strength equals 9.7 MPa,
- Three point bending tests on notched specimens : these tests allowed to determine the tensile stress versus crack opening using a reverse analysis method [1]. In this project, the tensile strength for a crack opening of 0.3 mm equals 7.5 MPa.

The suitability tests are then performed on a prototype fabricated using the same casting procedure as for the full scale elements. A 3 mlong prototype of the beam was fabricated using the same casting procedure as for the full scale girders (fig 6). The prototype was heat treated and then several 70x70x280 mm samples were taken out from this prototype in different orientations. Mechanical tests have been then performed on these specimens in order to determine the fiber orientation factors K. The obtained orientation factor was equal to 1.34 for the global effects (e.g. shear, bending, …) and 1.81 for the local effects (e.g. zone of prestressing introduction, punching shear verifications…).

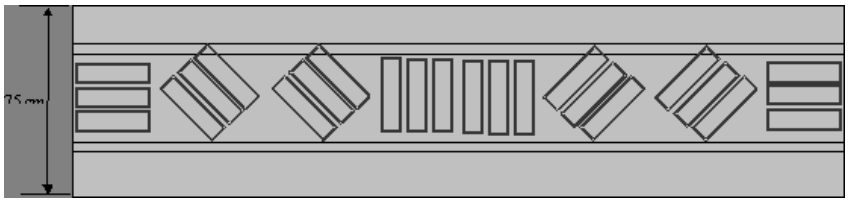

Figure 6: Prototype for suitability tests with the position of the taken out specimens

For thin panels, AFGC-SETRA recommendations propose a value of K equal to 1 considering that characterization of the concrete is made with a representative element of the actual structure (same size and thickness). One can note that this assertion is true only if the method used for casting the test specimens is the same as the actual placement method. In the case of Saint Pierre La Cour bridge placement methods were different and give quite different tensile strengths corresponding to a K coefficient equal to 1.5.

3.3 Prefabrication of the Ductal® elements and erection of the bridge

The girders and panels were prefabricated at CPC precast plant, next to Brive (Southwestern France). The Ductal® was mixed in batches of 1.9 m^3 in a traditional mixer with a capacity of 2.5m^3. The flat panels were demoulded 18 hours after casting and were then heat treated at 90°C and HR>90% during 48 hours. Adapted curing conditions were applied for the fabrication of the girders. The formworks were heated at a temperature of 40°C until the setting time. This curing conditions allowed to reach a compressive strength of 80 MPa at 18 hours needed for the prestressing de-tensioning. After complete demoulding, the girders were covered and heat treated with a humidity saturated atmosphere with a temperature between 70°C and 90°C. Conventional construction method was used for the erection of the bridge. The 20 m long girders have the significant advantage of being light and with a weight not exceeding 9.5 tons. This lightness allows to reduce the size of the crane.

After installation of the girders and the panels, the ordinary concrete deck was poured using traditional method. The design allows a quick installation of the deck and therefore reduces the traffic disturbance under the bridge.

3.4 Conclusion – lessons from this realization

A mistake in the application of part 2.4 of the Recommendations [1] concerning verification of general equilibrum of pure distribution contribute led to cracking at the end of the first precast beam a few hours after detensioning. This phenomenon disappeared after a modification of the design in order to meet Recommendations which are quite relevant for this topic.

Suitability tests showed that for thin panels with the same size and the same thickness as the actual structure, a value of K equal to 1 is valid only if the method used for casting test specimens is the same as the actual placement method.

A comparison with a traditional concrete deck solution shows that the concrete volume reduction factor equals 2.2. This solution is directly in competition with composite steel and concrete bridge. It is economically interesting in case of railway or motorway overpass with important traffic constraints.

This structure is also very efficient for durability: all concrete surfaces are either in UHPFRC or protected by a watertight layer. It could be also a very good solution in case of a structure with severe fire performance requirement, provided using Ductal® AF.

4 Experimental validation of a ribbed UHPFRC slab for a composite steel concrete bridge

4.1 General description of the structure

The studied bridge is an innovative steel-concrete composite bridge made of two longitudinal steel beams connected to an UHPFRC ribbed slab. It was studied within the French R & D project MIKTI focusing on innovative steel-concrete composite bridges [5], [6]. The UHPFRC slab has a width of 12m. Distance between beams is equal to 6,5 m (fig 7). The slab thickness is 0.05 m, the total thickness with the ribs is 0.38 m, and the rib spacing is 0.6 m from axis to axis in both directions. The average thickness of the slab is equal to 0.15 m.

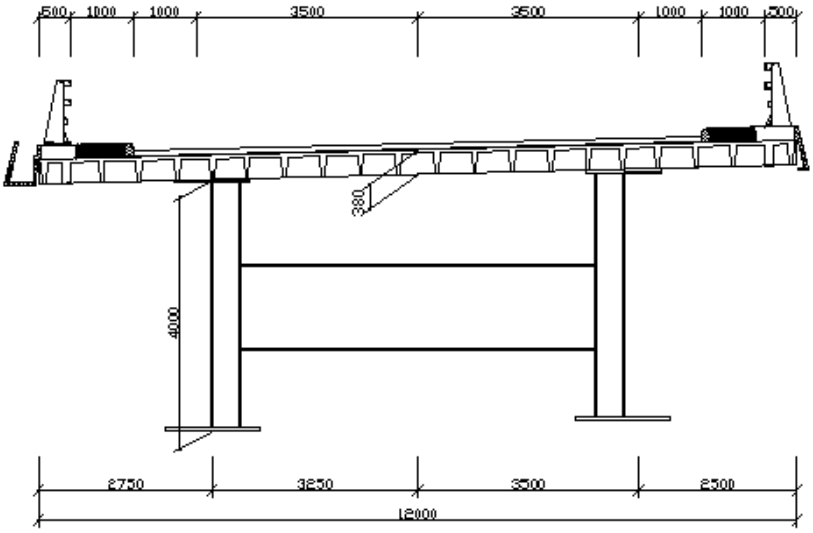

Figure 7: Cross section of the bridge

The slab is made of precast segments 2.5 m long, 12 m wide, prestressed in both directions. Transverse pre-stressing is realized by two rectilinear T15S tendons in each rib. The lower tendon is sheathed all along negative bending moment zones.

The design in order to keep a minimum residual longitudinal compression in the slab at the SLS equal to 4 MPa gives a longitudinal prestressing made of seventeen 7T15S cables. These cables are external, placed between longitudinal ribs.

Bridge erection follows the steps below :

- all precast segments are placed on steel beams,
- they are gathered by cast in place UHPFRC joints,
- the slab is prestressed by longitudinal cables,
- it is connected to the steel girders,
- jacking of supports is applied to add compression in the slab.

Conversely to what we note for ordinary concrete, very reduced creep and shrinkage and high modulus of UHPFRC make longitudinal prestressing in the slab very efficient especially when applied before the connexion to the steel beams. It is the same efficiency for jacking of supports realized after the connexion of the slab to the steel girders.

An important problem for the slab design is the safety barrier anchorage. To keep a conception conforming to regulations, a “type P” prestressed anchorage was chosen, which is a regular French anchorage for trucks barrier added on existing slab. This type of anchorage allows to dissociate the lateral longitudinal anchorage beam made of ordinary reinforced concrete from the UHPFRC slab in which the longitudinal beam is anchored by prestressed bars (fig 8).

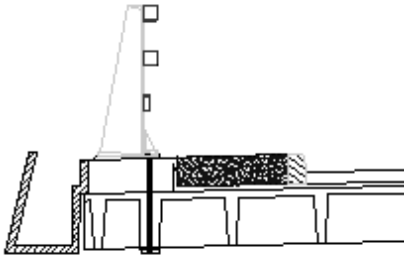

Fig. 8: Anchorage of the safety barrier

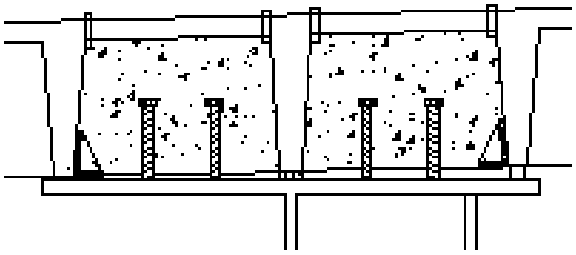

Fig. 9: Connexion of the slab to the girder

The connexion between the ribbed deck and the steel beams is realized in filling box cells on upper flange by a self-compacting C80/95 concrete, encasing 2, 3 or 4 traditionnal studs 22 mm in diameter (Fig 9). A high performance concrete C80/95 is sufficient to guarantee that the less resistant part of the connexion are the steel studs and not any other HPC or UHPFRC part.

4.2 Experimental program carried out at Laboratoire Central des Ponts et Chaussées (LCPC)

An exhaustive experimental program was carried out at LCPC Structures Laboratory [7][8] in order to validate :

- the fatigue performance of the structure,
- the local bending strength and punching shear resistance of the slab,
- the global bending strength of the slab,
- the safety barrier anchorage strength,
- the connection of the ribbed deck to the steel girders (push-out test),

Although longitudinal cable anchorages at the end of the slab did not need special requirement, we add to this program local compression tests in order to validate innovative design of UHPFRC anchor blocks for post-tensioning tendons in order to reduce the size of traditional anchorage and to justify the possibility to avoid any traditional reinforcement behind anchorage. Experimental validation for fatigue, bending and punching strength, and resistance of barrier anchorage was performed on a 6.1 m-wide model slab made of two ribbed segments, one made of Ductal®-FM and the other of BSI®, at scale 1 for length and thickness, with a transverse span reduced to 4 m (fig 10).

Figure 10: Test specimen for fatigue, bending and pushing strength, barrier anchorage

The results of this important research program are detailed in references [7] to [11].

4.2.1 Fatigue resistance

Loads refer to Eurocode 1 part 2 models 1 and 3 with two wheels corresponding to 0.4 x 0.4 m or 0.19 x 0.26 m impacts applied on a plate made of 90 mm-thick polymer material representing 90 mm-thick bituminous concrete pavement layer. These results provide a safety margin in terms of load applied without fatigue initiation over 100 years larger than 1.25.

4.2.2 Local bending strength and punching resistance of the slab

The reference load was derived from Eurocode standard wheel with a 0.4 x 0.4 m impact and 150 kN service life value applied at the centre of a box cell on the 90 mm-thick polymer plate representing the pavement layer. It was impossible to obtain any failure with that load until a force greater than 700kN, even without any polymer plate corresponding to a deck without any pavement layer. To obtain failure, the size of the impact was reduced to 0.19 x 0.26 m. With the polymer plate, it was still impossible to obtain any failure. With the reduced impact size directly applied on the concrete (no pavement layer), failure was obtained for a load value ranging from 350 kN to 417 KN corresponding to a safety factor greater than 2.3.

4.2.3 Safety barrier anchorage strength

Two quasi-static horizontal tests were performed to break posts supporting the barrier. Failure by yielding the fuse screws fixing the post to the bridge edge beam effectively took place twice with several cracks in the longitudinal anchorage beam made of ordinary reinforced concrete. No damage appeared in the UHPFRC slab.

4.2.4 Global bending strength of the slab

The safety factors identified experimentally corresponding to a bending failure with yielding of the lower prestressing steels were equal to 1.9 at the SLS, 2 for ULS.

4.2.5 Connexion of the ribbed deck to the steel girders (push-out test)

A push-out test was performed to control the design of the connexion between the slab and the steel beam. French and Eurocode provisions give ULS resistance of the specimen equal to 700 or 900 kN, corresponding to steel studs yielding. Yielding took place without any failure until the force reached 1800 kN (safety factor higher than 2).

4.3 Conclusion – lessons from this research program

All performed tests showed that the structure provides an important security with respect to fatigue, bending or punching shear. Tests performed on posts showed that it is possible to anchor a truck barrier without any passive reinforcement in UHPFRC slab.

Very few creep and shrinkage and high modulus of UHPFRC make longitudinal prestressing in the slab very efficient especially when applied before connexion to the steel beams. Il is the same efficiency for jacking of supports realized after connexion.

For maintenance, the main interest of this type of structure is to obtain a slab without any crack, made of a material with high durability performances.

Reduction of steel weight is about 15% to 20% so that the price of the deck for a long bridge is equivalent to a traditional composite steel – concrete bridge. The important reduction of the deck weight provides complementary saving on bearings.The low weight of the deck is very interesting in case of bad soil or seismic environment. It also allows lauching the frame with the slab ; that provides a good solution for erection under severe traffic constraints.

5 Solutions for bridge decks made of UHPFRC and composite materials (glass fibres reinforced polymer)

This research was conducted within the frame of the European project NR2C (New Road Conception Concepts). The studies concerned bridge deck solutions using Ultra-High Performance Fibre-Reinforced Concrete, composites (glass fibres reinforced polymer) and active and/or passive steel reinforcements. Two types of bridges have been studied : those with a 10 metre span for small crossings, and those with a 25 metre span which corresponds to half the length of a motorway overpass [12].

5.1 Studied structures

For 10 m span we studied UHPFRC prestressed ribbed slab, UHPFRC ribbed slab with notched longitudinal rib and glass fibre reinforcement, UHPFRC ribbed slab with notched longitudinal rib and passive steel reinforcement.

For 25 m span we studied quite the same solutions (UHPFRC prestressed ribbed slab, UHPFRC ribbed slab with notched longitudinal rib and glass fibre reinforcement) and complementary structures : UHPFRC ribbed slab with notched longitudinal rib reinforced by glass fibre and prestressing, UHPFRC ribbed slab with lattice longitudinal rib and glass fibre

reinforcement, UHPFRC ribbed slab with lattice longitudinal rib and passive steel reinforcement.

5.2 Lessons from this research

This research showed that the most advantageous solutions in terms of materials savings are fully prestressed UHPFRC decks. For 10 metre span structures, these solutions lead to financially viable structures under current economic conditions.

Mixed UHPFRC/glassfibre solutions are penalised by the poor ratio of the Young's modulus to the connection strength of the two materials which means that they have to be overdimensioned in order to meet the deflection requirements of the decks. If bridges are to be built with fulfilment of strain conditions while loading both materials sufficiently, slender structures will have to be eliminated; the section height will be unattractive and cause problems in terms of the web design and the shear force transfer areas.

For 10 metre span bridges, notched web girders and steel footings are interesting alternatives to fully prestressed solutions. Similarly, for 25 metre span bridges, the combination of UHPFRC and composite materials can become advantageous in the case of partially prestressed UHPFRC prefabricated lattice beams.

6 Conclusion

Recent examples of UHPFRC bridges in France and projects studied within the frame of recent joint R&D programs have helped to gain experience in the safe application of UHPFRC Recommendations [1] and valuable application to bridge design. Lightweight 10 to 25 metre span overpasses may get interesting application in the case of severe traffic or geometric constraints, and become economic in comparison with traditionnel structures such encased steel girders within a concrete slab. Longer span steel-concrete composite bridges may also take benefit of these recent studies. A constant growing number of projects on the making tends to confirm interest of these materials of future.

7 References

[1] Resplendino, Petitjean et al : Ultra-Hign Performance Fibre-Reinforced Concretes, Interim recommandations, AFGC-SETRA, Bagneux, Fance (152p, both in French and English), January, 2002.

[2] Resplendino, Bouteille, Delauzun, Maleco, Dumont, Cantrelle, Chanliaud, Clergue, Lingard, Capra, Linger, Martin, Marc Guilloud : Construction of an overpass on the A51 Motorway, made of a prestressed box beam built with UHPFRC, in the French technology of concrete, AFGC, The second fib congress, Neaples (2006)

[3] Hanoteau, Behloul, Bayard, Resplendino, Bouteille, Boutonnet, Vildaer, Radiguet, Bernhard, Padovan : Ductal : a new material, the bridge of St Pierre La Cour, in the French technology of concrete, AFGC, The second fib congress, Neaples (2006)

[4] Behloul, Bayard, Resplendino : Ductal® prestressed girders for a traffic bridge in Mayenne, France, 7th international Conference on Short and Medium span Bridges, Montreal, Canada, 2006.

[5] Resplendino, Bouteille : PN MIKTI. Etude d'un pont mixte à dalle BFUP nervurée, CETE de Lyon, technical report, 46p., 2003

[6] Resplendino., Bouteille : Derniers développements dans l'utilisation des bétons fibrés ultra performants en France. In : Proc. GC'2005, Paris (France), 2005.

[7] Toutlemonde, Resplendino, Sorelli, Bouteille, Brisard : Innovative design of Ultra-high Performance Fiber-reinforced concrete ribbed slab : experimental validation and preliminary detailed analyses, 7th International Symposium on Utilization of High Strength / High Performance Concrete, Washington D.C. (USA), june 20-22, 2005.

[8] Toutlemonde et al. : Experimental validation of a ribbed UHPFRC bridge deck, Second International Symposium on Ultra High Performance Concrete, Kassel (Germany), March 05-07, 2008

[9] Toutlemonde et al. : Local bending tests and punching failure of a ribbed UHPFRC bridge deck. In: Proc. FRAMCOS-6, Catania (Italy), 2007.

[10] Toutlemonde et al. : Local compression tests and analysis validating innovative design of UHPFRC anchor blocks for post-tensioning tendons, In: Proc. FRAMCOS-6, Catania (Italy), 2007.

[11] Toutlemonde et al. : Fatigue performance of UHPFRC ribbed slab applied as a road bridge deck verified according to eurocodes, In: Proc. CONSEC'07, Tours (France), 2007.

[12] Resplendino., Bouteille : Étude de solutions de tabliers de ponts réalisés en Béton Fibré Ultra Performant (BFUP) et en Matériau Composite (Fibre de verre). In : Proc. GC'2007, Paris (France), 2007.

Joost Walraven
Prof. Dr.-Ing.
Delft University of Technology
The Netherlands

On the way to design recommendations for UHPFRC

Summary

Ultra High Performance Fibre reinforced Concrete (UHPFRC) is a material with a great potential. It combines high strength with high ductility and high durability. First appealing applications have been carried out, showing the possibilities. Like for every material that is in the state of development, a number of uncertainties and open questions exist. At many places research is being carried out in order to optimize our knowledge. Large scale applications are only possible if generally accepted design recommendations are available. At the time the fib Task Group 8.6 is working with the aim to generate a first international set of design rules for UHPFRC.

Keywords: *high performance concrete, design recommendations, code rules*

1 Introduction

Parallel to the development of structural materials and their application, the way in which we build is subject to evolution as well. It is logic that building recommendations should not only keep up with actual developments, but preferable go in front and anticipate on new concepts. If the development of codes during the last decades is regarded, obvious changes can be noted. In the past emphasis was put on achieving structures with adequate safety against collapse and suitable behaviour in service (user friendliness). The problems occurring with large scale degeneration of structures learned that an important design aspect had been disregarded: structures should be designed for durability as well. In forthcoming codes, design for durability will have the same value as design for safety and serviceability. Already now it is realized that, in order to achieve “durability” of structures, not only the physical aspects of our structural materials should be regarded. Lack of durability may also occur because structures do not any more meet the demands of functionality. This holds true for instance for apartment buildings where the demands of today differ substantially from those of a number of decades ago. This is not only a matter of changing demography, but also of economy and culture. In a reaction on this tendency new concepts are developed, based on flexibility and adaptability. This holds also true for bridges, which have to cope with a significant increase of traffic loads and traffic intensity. Moreover, it should not be forgotten that elegance and beauty are as well important conditions for a long service life. Another important change with regard to the daily work of structural engineers is that we, more and more, have to deal with retrofitting and upgrading of structures. Protection of older structures against ongoing deterioration is an important new task. Finally an important change in

design is the introduction of defined performance concepts. For materials this means that we will not only design for strength, like in the past, but as well for other properties like resistance against chloride penetration, frost-thaw cycles, abrasion and even for colour and texture. This means that in future design codes “design by testing” will show up as a new important element.

Looking to UHPFRC it can be concluded that this material fits very well in future-oriented thinking. Since it offers the properties high strength, high toughness and high durability, it is a very challenging material to realize structures with large spans, which are at the same time light, elegant and durable. Moreover it is a material with the potential to be applied for retrofitting of structures. Examples are the thousand of bridge decks which have to be repaired. A thin overlay of UHPFRC does not increase the dead weight very much, but can substantially contribute to durability and bearing capacity. Moreover the light weight of structural components of UHPFRC can be a favourable precondition for adaptability of structures. Finally UHPFRC can contribute to the wish to get away from the historical coupling of concrete qualifications “rude”, “heavy” und ugly.

Figure 1: Providing an old bridge with a new HPFRC bridge deck

Figure 2: Elegant staircase of UHPFRC in combination with traditional reinforcement (Courtesy B. Aarup, Denmark)

Providing a new code for UHPFRC means that such applications should be supported by new rules. Therefore not only the mechanical properties should be given, but also physical properties should be regarded, in order to honour the suitability of UHPFRC for service life design. With regard to the mechanical properties adequate attention should be given to aspects like fatigue, since light, large span structures could be prone to the effects of dynamic loading more than in the past.

At this moment there are three national recommendations covering UHPFRC:

- French recommendations covering high performance concretes (BFUP rules), edited in January 2002.These recommendations were prepared by AFGC (French Association for Civil Engineers) and SETRA (French Road and Traffic Governmental Agency)
- RILEM method for fibre reinforced concrete. This recommendation is more directed to classic fibre reinforced concretes
- JSCE (Japanese Society of Civil Engineers) Recommendation for UHPFRC edited in September 2004)

In Germany a national recommendation is now in the finalizing stage.

2 Basic considerations

2.1 Scope

One of the first actions a new Task Group should take care of is defining the scope of the work. Already here a basic question can be raised. At this moment fib Task Group 8.3 concentrates on what could be denoted with the term “Conventional Fibre Reinforced Concrete”, whereas Task Group 8.6 should concentrate on “Ultra High Performance Fibre Reinforced Concrete”.
So, logically the first question is where the work of the first Task Group ends and that of the second Task Group starts. At first sight this looks quite obvious: one could simply define a compressive strength limit, like B120. However, giving this further consideration, it is found that such a limit is too simple. Concrete’s with strengths higher than B120 could behave like conventional concrete and contrary. This depends essentially on the effectiveness of the fibres and its interaction with the mixture.

Another possibility is to distinguish “hardening” and “softening” fibre concrete’s. From a scientific point of view this is a sound solution. The stress – strain relation of a hardening material loaded in tension shows four branches: at first an increasing elastic branch, followed after cracking by a branch which increases with a smaller inclination. After passing the top an unstable falling branch is observed, followed by a stable, less steep, branch (Fig. 3a). A softening material is characterized by the absence of the second branch (Fig. 3b). This has an important consequence: a fibre concrete with a hardening behaviour will show a distributed crack pattern if subjected to centric tension, whereas a fibre concrete with a softening behaviour is characterized by single crack formation. In the second case the strain is non-uniform. It can be defined as the average value of the crack width and the elastic deformation of the uncracked parts aside the crack. However, also such a subdivision of fibre concrete in two types on the basis of “hardening” versus “softening” can be ambiguous: a material which is softening in centric tension may surely be hardening in bending. So, the transition between softening and hardening does not only depend on the fibre type and volume, in combination with the mixture, but as well on the type of load.

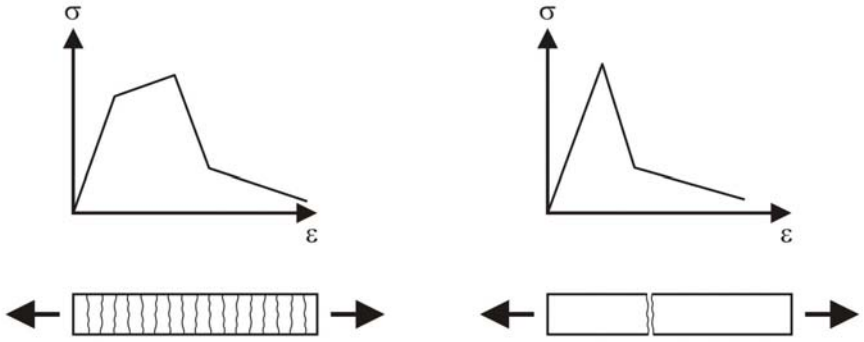

Figure 3: a. (left) Stress strain relation for a hardening type of fibre concrete and its consequence for the cracking behaviour under centric tension
b. (right) Stress –strain relation for a softening type of fibre concrete and it consequence for the cracking behaviour under centric tension

2.2 How to regard the effect of fibres

Another basic question for the derivation of design recommendations is whether the fibres in the concrete should be regarded as being an integral part of a composite material or as reinforcement, with an effect comparable to reinforcement by steel bars. If the fibres could be regarded as an alternative to conventional steel bar reinforcement, this would simplify the task of the codewriter very much: generally the same formulations could be used. For a fibre concrete with a softening behaviour this is certainly an option, although fibre concrete at crack opening does not show a real yielding plateau like a steel bar. The stable branch in tension (third part of the relation, Fig. 3b) declines under a relatively low angle, which is mainly due to gradually pulling out of individual fibres. High and ultra high performance fibre concretes mostly contain a large volume of short, small diameter, fibres without mechanical anchorages. They are activated immediately upon micro cracking. So, the material apparently stays longer in the elastic stage. If macro cracks appear, they still are active but in a less efficient way than long fibres with mechanical anchorages. Certainly an interesting material in this respect is hybrid fibre concrete, where short and long fibres are combined, see e.g. Markovic [1].

2.3 Representativity of stress – strain relations

A very important aspect to be noted before speaking about the question how a representative stress – strain relation for UHSFRC should be obtained is the phenomenon of fibre orientation. Fig. 4 shows a collection of curves, obtained on test specimens with the same dimensions, all made with fibre reinforced concrete B35, with 40 kg/m^3 fibres Dramix 80/60 [2]. Although the
test specimens and the concrete composition are exactly the same, the scatter in results is enormous. Deriving a design stress-strain relation from such a series of tests would inevitably lead to an overconservative design.

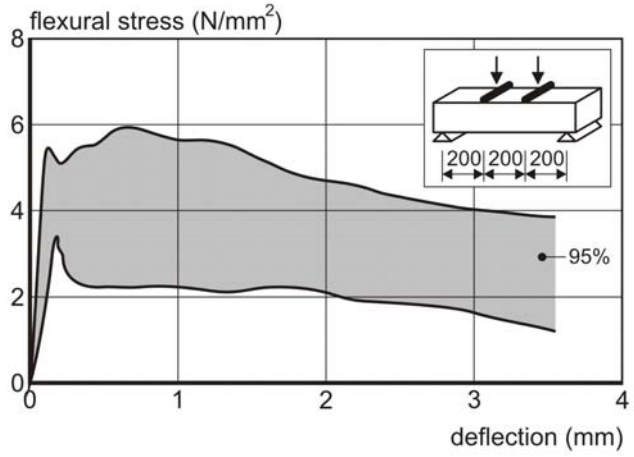

Figure 4: Flexural stress – deflection relations obtained from 71 bending tests on steel fibre reinforced concrete, Gossla [2]

Meanwhile it is realised that the way of manufacturing the specimen is governing for the load deflection relation obtained. Various ways of filling the mould and mechanical compaction lead to large differences in fibre orientation and concentration. Recognizing this, RILEM defined a standard test beam with a notch and prescribed exactly how to fill the mould and how, and how long, to carry out mechanical compaction, and how to measure the load deflection relation and load crack opening relation. Finally it is described how stress – strain relations can be derived, on the basis of reversed analysis, from the test results Fig. 5 shows the test beam as defined by RILEM. Indeed the scatter of results, for the prescribed number of 6 tests, is decreased significantly by the procedure described. On the other hand it is not clear how representative those results are for practical FRC structures, which are not cast according to accurately defined rules. Moreover the manufacturing procedure, as described in Fig. 6a, is suitable for relatively dry concretes, but not for self compacting concretes, which are gaining popularity. If a self-compacting fibre concrete is concerned, it is not possible to fill the mould in the prescribed way.

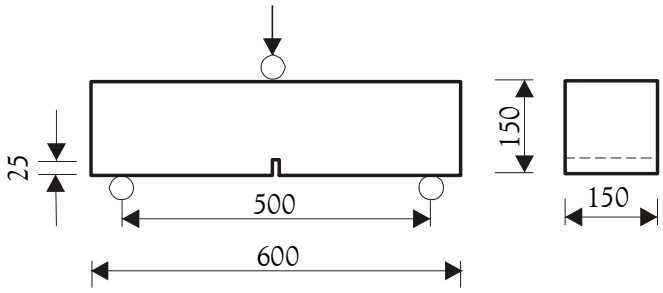

Figure 5: RILEM Standard test

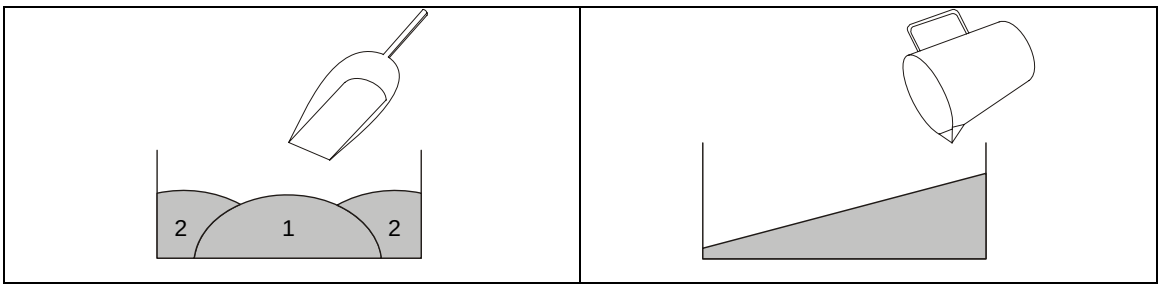

Figure 6: a. (left) Prescribed way of filling the mould for the RILEM test beam
b. (right) Filling the mould with self compacting fibre reinforced concrete

Due to the effects described the load deflection relations for concrete with the same strength and amount of similar fibres but different consistency, can differ by a factor 2 (Grünewald [2]). The differences are predominantly due to the effect of fibre orientation, which is strongly influenced by the method of casting and compacting. Fig. 7 shows X-ray photographs taken from a tunnel lining element cast with self compacting fibre concrete. The pictures show large deviations from homogeneity. It is clear that the stress – strain relations obtained by the standard test are not reflecting the real behaviour in the structure, at least not in this case. It is therefore understandable, that there are still discussions on how to link the results of the

standard test to the actual situation of a structural element, cast in-situ or at a precast concrete plant.

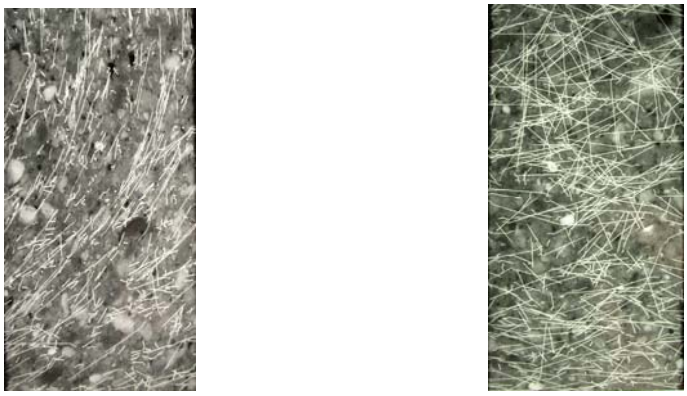

Figure 7: X-ray photographies from the same tunnel lining element cast with self compacting fibre concrete [3].

In the French regulations for UHPFRC [4] the influence of fibre orientation in the standard test specimens and the structural elements is recognized. The solution offered is based in the introduction of two types of tests. Here thin and thick elements are distinguished, in order to reflect as much as possible the structural behaviour of thin and thick structural members in practice.

a. If the bending behaviour of a thin element is concerned, the standard test should be carried out on a specimen where the cross-sectional height is smaller than $3L_f$, where L_f is the fibre length. By choosing a standard bending tests with such a small thickness, Fig. 8, the stress – strain relation includes already somehow the effect of alignment by the boundary conditions, which is expected to occur in thin structural elements as well.

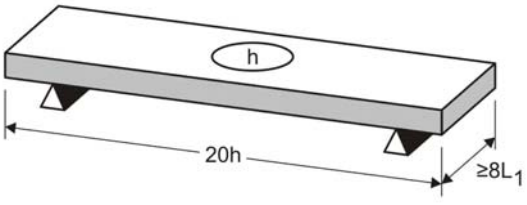

Figure 8: Standard test for thin UHPFRC members [5]

Anyhow this test is not considered as the absolute truth, since it is advised to apply a correction factor 1/K to the results obtained from specimens taken from the actual structural element.

b. For the design of thicker elements ($h \geq L_f$) the following procedure is advised:
"Cast and notch a prism. Perform a flexural test with it. Conduct inverse analysis to determine a post-cracking stress crack width (σ-w) relation. Correct this relation derived from this test so as to integrate scale and boundary effects associated with

the specimen shape and casting method. Weight this law with a reduction coefficient 1/K representing the difference between a flexural test result for a cast prism and what would have been obtained on prisms sawn from an actual structural element. To determine an exact factor K for the particular application considered, make components that are representative for the actual geometry and manufacturing method used for the structure, and take specimens along the directions of principal stress"

A disadvantage is that in both cases (thin and thick) the standard test does not pretend to give a basic relation. The stress – crack opening curve is rather arbitrary and has only a value as a general reference in relation to more detailed tests on area's of the structural element. For various types of structural elements advisory values for 1/k could be given, but this needs a lot of further effort. In fact this method comes very near to "type testing" of complete elements.

It may be wondered if it is not possible to get a more reliable basic stress – strain relation which fulfills the two most important demands:

- it reflects the fundamental behaviour of fibre reinforced concrete
- the test displays a minimum scatter

In this respect a suggestion made in [6] is worth to consider (Fig. 9). It regards a circular slab as the standard tensile test specimen, which has a circular line support at its edge. If the specimen is loaded by a load in the centre, failure will occur by the formation of a number of yield lines. The bearing capacity at yielding follows from the relation $P_u = 2\pi\ R\ m_u$ where R is the radius of the circular slab and m_u is the "yield moment" per unit length of the crack. Since many yield lines are involved in the failure mechanism, the influence of manufacturing fades away. Indeed it was shown by tests, that the scatter in results was very low (Fig 9, right)

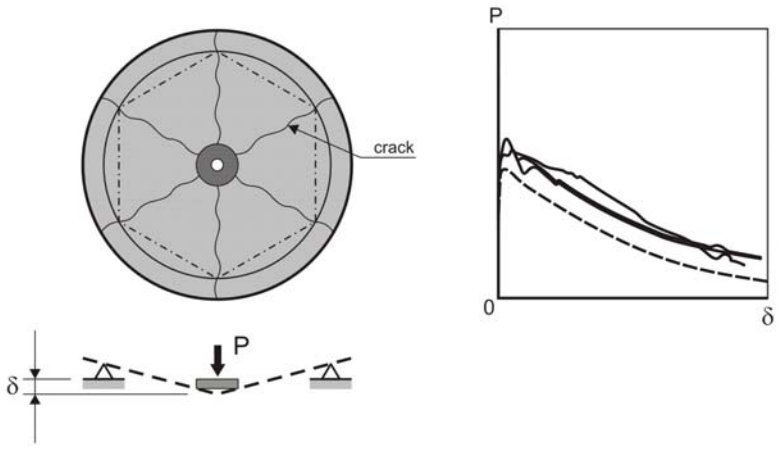

Figure 9: Circular slab as a standard test to determine the basic mechanical properties [6]

If the results obtained in this way are used as a basis for practical design, also here conversion factors have to be introduced. In this respect the volume of the decisive area of the element for design is of importance. If the bearing capacity of a member depends on a small area, the possibility that in the governing section a low amount of fibres with an unfavourable orientation applies should be regarded for reliability. In such a case a higher safety coefficient should apply than in the case that there is adequate redistribution. In fact such an approach would go back to the theory of Weibull, (weakest link model). The concept of working with an RVE (representative volume element) regarding the volume with the highest stresses (over a certain threshold value, e.g. 95%) might be a good option.

2.4 Simplicity versus accuracy

During years attempts have been made to derive stress-strain relations from tests. In case of a softening behaviour a stress – crack width relation is obtained, which is subsequently converted into a stress – strain relation (a well-known tool for structural engineers) by introducing an artificial length, along which the crack width is smeared out. It may be wondered if it is realistic, taking as well into account the other arguments given before, to aim at the highest accuracy in deriving stress – strain relations for fibre concrete.

This is illustrated for the case of a short slab element with a thickness of 50 mm, a width of 200 mm and a span of 600 mm. The concrete is provided with 1,6 Vol.% fibres and has a strength of about 140 MPa. The casting direction was a variable in the research project. Some specimens were cast in X direction, others in Y-direction. The response was simulated with a layer model where two stress strain relations were used as basic input with different degrees of simplification. The results are shown in Fig. 10. The experimental curves show considerable differences, due to the different direction of casting (x-direction versus y-direction). The most simplified stress-strain curve gives a result that is not very different from that obtained with the less simplified stress –strain relation. Both lines fall between the limits of scatter due to different casting directions. For more information on this analysis reference is made to [7] and [8].

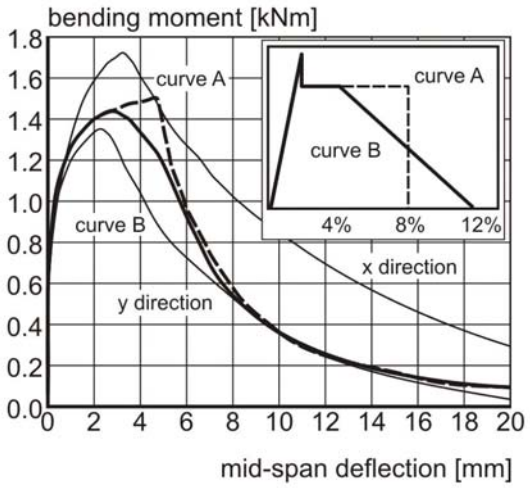

Figure 10: Results of bending tests and simulations with two simplified relations [7,8].

Formulations with a reasonable degree of simplification can serve well for extending existing models for structural design to fibre reinforced concrete. An example is the crack width control of fibre concrete in combination with traditional reinforcement. Tests were carried out on concrete tensile ties with a cross section of 50 x 50 mm and a centric steel reinforcing bar d_s = 10mm. The concrete cylinder strengths were 130 and 180 MPa respectively. The concrete was reinforced with 0, 0.8 and 1.6Vol.% short steel fibres. The cracking patterns for 3 bars with f_c = 130 MPa and the three fibre volumes are given in Fig. 12. The model for crack width control as found in the Model Code for Concrete Structures 1990 can be easily extended for this case if a stress - strain relation for the fibre reinforced concrete as shown in Fig. 11 is used.

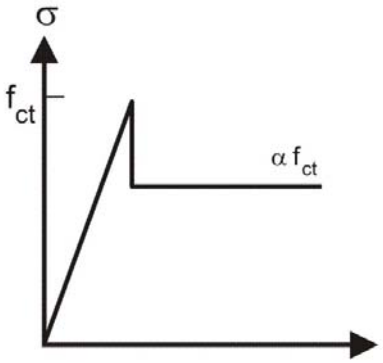

Figure 11: Simplified stress strain relation for UHPFRC in centric tension

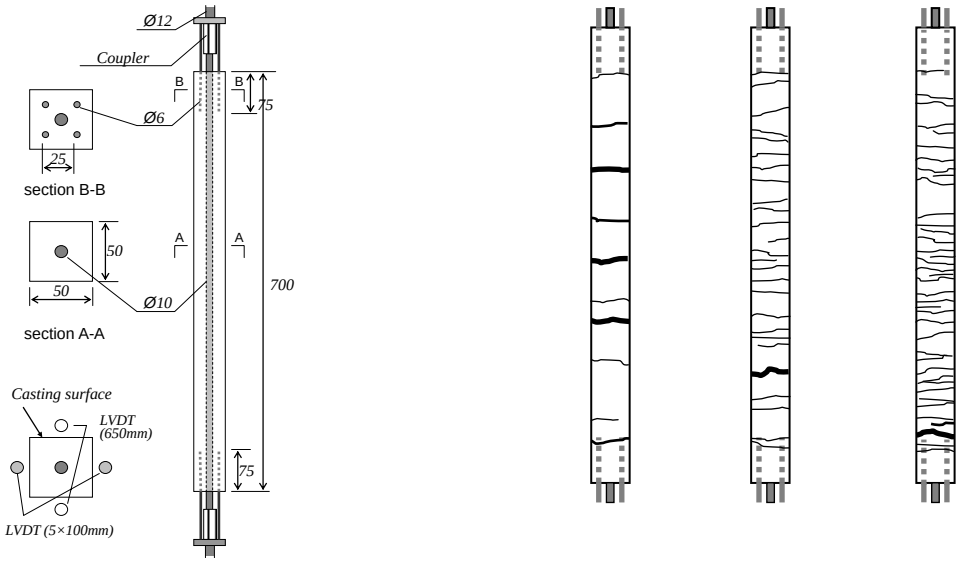

Figure 12: Test set-up for study of crack formation in concrete tensile tie, reinforced with longitudinal steel and fibres (left). Cracking patterns for tensile ties reinforced with 0, 0.8 and 1.6 Vol.% of steel fibres, steel bar d_s = 10mm concrete strength f_c = 130 MPa (Shionaga [9]).

From centric tensile tests on dog-bone shaped specimens for the concrete with a compressive strength of 130 MPa a centric tensile strength f_{ct} = 5.5 N/mm^2 and a post cracking reduction factor α = 0.72 was found. For the concrete with a strength 180 N/mm^2 a

centric tensile strength f_{ct} = 9.0 N/mm^2 and a post cracking reduction factor α = 0.88 was found. For extending the crack formation theory to reinforced UHPFRC especially the difference between the centric tensile strength and the post cracking "plastic" strength is relevant, because this difference determines the length of the disturbed region at both sides of the crack due to crack formation and as such the crack distance. Table 1 gives for a number of tests the crack spacing as observed in the test and the calculated spacing. The agreement is seen to be good.

Table 1: Observed and predicted crack spacing

Comp. strength	**V_f Vol.%**	**Mean crack spacing (mm)**	**Predicted crack spacing (mm)**
130	0	56	43
	0.8	23	21
	1.6	14	17
180	0	44	57
	0.8	27	28
	1.6	26	22

3 On the way to an international recommendation

At the time fib Task Group 8.6 "Ultra High Performance Fibre Concrete" works on an international recommendation for UHPFRC. It is tried to take profit of the existing experience and combine this with new knowledge from recent research programs. As UHPFRC is a quickly developing material, the code should be future oriented. On the other hand it should be operational immediately after appearance as well. So, there will be links to the concept of the new Model Code for Concrete Structures and to the content of Eurocode-2. The content of the new recommendation for UHPFRC will be:

1. Scope
2. Terminology
3. Basic principles
4. Material properties
5. Design
6. Material properties and design for special actions
7. Design, mixing and placement
8. Conservation

The most important chapters are 4 and 5. Chapter 4 "Materials" has subchapters on compressive strength, tensile strength, flexural tensile strength, stress-strain relations, stress – crack opening relations, E-modulus, Poisson's ratio, strain rate effects, time dependant effects, fatigue effects, temperature effects, transport of liquids and gazes, multi-axial behaviour, fracture mechanics aspects, chloride penetration, porosity and permeability, oxygen permeability, carbonation, portlandite content, fibre orientation. Chapter 5 "Design"

will regard bending, shear, torsion, strut and tie action. Detailing, deformation, crack width control, tightness, vibration and service life design.
The members of the committee are:

Germany:	M. Schmidt, E. Fehling, K. Bunje, S. Greiner, K.H. Reineck, T. Leutbecher, D. Weisse, N.G. Tue, F. Dehn, Ma
France:	J. Resplendino, M. Behloul, P. Rossi, A. Simon, T. Thibaux
Netherlands:	J. Walraven (chairman), S. Grünewald, E. Lappa
Italy:	M. di Prisco, P. Bamonte, P. Gambarova,
Denmark:	B. Aarup
Croatia:	M. Skazlic

The commission plans to have a full recommendation in about a year from now.

4 Conclusions

1. For UHPFRC a future oriented code has to be written, which is operational at the same time. So, the code should not only regard design for ULS and SLS, but also take into account aspects like service life design and performance based design.
2. An important task is to get a code which is not a “stand alone” code, but is consistent with the codes for “classic” fiber reinforced concrete. The best would be to have finally a integral code for all fibre reinforced materials
3. An important point of discussion is how to unambiguously characterize the material by a standard test, in combination with conversion factors for practical situations.
4. Stress – strain, or stress crack width relations my have a different level of sophistication.
   For daily use the relations should be as simple as possible, with due regard to the expected accuracy.

5 References

[1] Markovic, I., “High Performance Hybrid-Fibre Concrete – Development and Utilisation” PhD-Thesis, Delft University of Technology, Jan. 2006

[2] Gossla, U., “Bearing capacity and safety of steel fibre reinforced elements”, German Association for Structural Concrete (DAfStb), Issue 501, ISBN 30410-65701-0 (in German)

[3] Grünewald, S., Walraven, J.C., “Sensitivity of the bending behaviour of self-compacting fibre reinforced concrete to then method of casting”, Proc. 5th Int. Symposium on Cement and Concrete”, Shanghai, October 2002, pp. 1160 – 1165

[4] Grünewald, S., Walraven, J.C., Obladen, B., Zegwaard, J.W., Langbroek, M., Nemegeer, D. “Tunnel segments of self-compacting steel fibre reinforced concrete”, 3rd Symposium on SCC, August 2003, Reykjavic, Proceedings, pp. 715-724.

[5] SETRA/AFGC, “Ultra High Performance Fibre-Reinforced Concretes: Interim recommendations”, January 2002.

[6] Marti, P., Pfyl, Th., Sigrist, V., Ulaga, T., “Harmonized test procedures for steel fibre reinforced concrete:, ACI _Materials Journal, Vol. 96, No. 6, Nov.-Dec. 1999, pp. 676-685.

[7] Yang, Y., Walraven, J.C., den Uijl. J.A., “Study on bending behaviour of an UHPC overlay on a steel orthotropic deck”, paper, this conference

[8] Yang, Y., “Bending behaviour of a high performance concrete overlay on an orthotropic steel deck”, Master thesis, TU Delft, 2007.

[9] Shionaga, R., Walraven, J.C., den Uijl, J.A., Sato, Y., “Combined effect of steel fibres and reinforcing bars in high performance fibre concrete”, Proceedings ibausil, Weimar, 20-23 September 2006, Part 2, pp. 207-214

Part 2:

Raw Materials

Josef Strunge
Dr.rer.nat, Dipl.-Min.; Director WDI
Dyckerhoff AG
Wiesbaden, Germany

Thomas Deuse
Dipl.-Ing.; Productmanger
Dyckerhoff AG
Wiesbaden, Germany

Special cements for ultra high performance concrete

Summary

High performance concrete mixtures usually are designed of ordinary portland cement OPC in combination with silica fume SF. Dense packing of the particles in combination with the pozzolanic reaction realise benefits in concrete like improved early and high strengths and a dense cement paste with high durability. Similar properties can be achieved by using OPC and microfine cements of the Mikrodur® technology. In case of UHPC the very important dense packing has to be achieved by very coarse OPC and nanoscale SF at very low w/c ratios, so that the binder components can't hydrate completely and even work as fillers! A better way might be a dense packing of reactive binder components like OPC, microfine cements and nanoscale synthetic silicas. Similar concrete properties in combination with easy handling can be achieved by these new binders, which fulfil the requirements of the German cement standards.

1 Dense packing and pozzolanic reaction

The development of high performance concrete started many years ago by using silica fume, a by-product of ferro silicon metal industries. High amounts of silicon dioxide (88-95%) combined with extraordinary fine particle sizes let silica fume become the most important reactive filler for concrete mixtures. The mode of action is firstly a dense packing of the particles and secondly a reaction with the hydration products of the cement. After 6 to 8 hours of the formation of tricalciumsilicate C_3S remarkable amounts of $Ca(OH)_2$ are formed, which react with the SiO_2 of the silica fume. The so called 'pozzolanic reaction' was determined first at roman concrete mixtures containing volcanic ashes of Pozzuoli, a small village near Naples in Italy.

1.1 High strength concrete with extended durability

Examples for concrete mixtures with silica fume are the cooling tower of the power station Neurath and precast elements for a high strength bridge in Pfungstadt.

Table 1: Mix design of high strength concrete with Sulfadur® and silica fume

Table 1		**Neurath**	**Pfungstadt**
Sulfadur CEM I 42.5 R-HS/NA	kg/m³	250	360
Silica fume slurry	kg/m³	52	32
Fly ash	kg/m³	75	60
Aggregates 0/16	kg/m³	1934	1884

1.1.1 Cooling tower Neurath with ready mixed concrete

In cooling towers the hot water is sprayed from round about a third of the height to the bottom. The cooling is realized by the chimney effect of the ambient air going through the tower. The steam is mixed with smoke containing small amounts of sulphur, which produce sulphuric acid in the wet stage. For this reason the surface of the tower must be coated or consist of a very resistant concrete. Due to good practical experiences at the power station Niederaußem in 1999 the RWE Power decided to use the same mixture to reach a very dense concrete C60/75, which does not need to be coated [2].

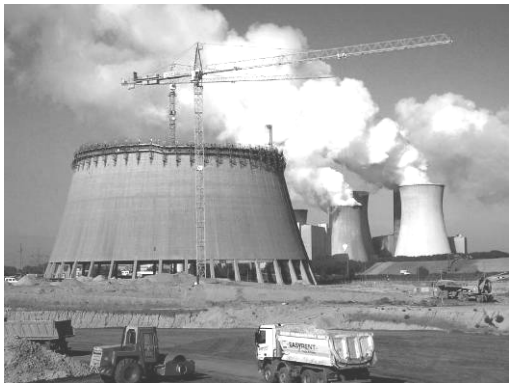

Figure 1: Cooling tower at power station Neurath

1.1.2 High strength bridge with precast elements in Pfungstadt

In 1934 the first bridge in Pfungstadt near Darmstadt was built to cross the motorway Frankfurt-Basel. Increased traffic demanded for an additional lane in 2007. Due to the situation of the crossing road and to achieve a maximum height for traffic on the motorway a construction with high strength precast elements was chosen. With special allowance of the authority the beams were made of high strength concrete C70/85 and fitted during a night closing [3].

Figure 2: Assembly of the high strength beams for the bridge in Pfungstadt

2 Premium cements with Mikrodur technology

High performance concrete can also be designed without silica fume with modified cements. Since more than 15 years Dyckerhoff has produced the microfine cements (Mikrodur) in a special production process. Portland cement clinkers and blast furnace slags are milled and separated individually. The final product guarantees a constant grain size distribution, because it is produced in an individual mixing process according to the requirements. The initial field of application of these microfine cements was geotechnical injection for sealing and strengthening. 3 different types are currently available: F d_{95} < 16 µm, U d_{95}< 9.5 µm and X d_{95}< 6 µm. Using this technique it is possible to influence properties of OPC in different ways. Microfine clinker particles accelerate the hydration process whereas microfine particles of blast furnace slag lead to higher strength in the end and extend the concrete's durability. By mixing one or more types of the microfine particles with OPC, the specific properties can be precisely created. The resulting cements are special products, which fulfil all requirements of the German cement standards.

Figure 3: Comparison d95 of CEM I 52.5 R and microfine cement

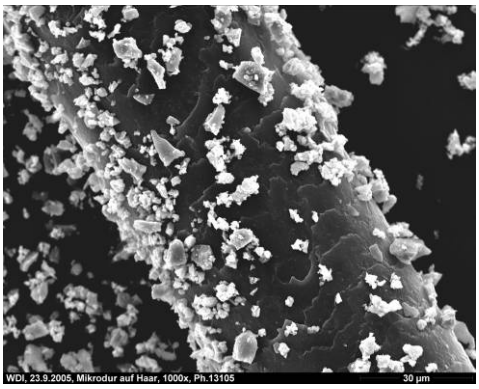

Figure 4: SEM of Mikrodur particles on a human hair

Examples for application of premium cements with microfine cements (Mikrodur technology) are the building of high strength columns in bright fair faced concrete at the Lufthansa Aviation Center in Frankfurt and a high strength mass concrete for the base of Kranhaus^{Plus} in Cologne.

Table 2: Examples for mix designs of concretes with Dyckerhoff premium-cements

Table 2		**LAC Frankfurt**	**Kranhaus^{PLUS} Cologne**
		Veridur® CEM II/A-S 52.5 R	Variodur® CEM III/A 52.5 N
Cement content	kg/m³	470	280
Fly ash	kg/m³	70	100
Aggregates 0/16	kg/m³	1889	1879
w/c ratio	[-]	0,28	0,45
Compressive strenght $ß_{D28}$	[MPa]	110	85

2.1 Fair faced high strength concrete at Lufthansa Aviation Center Frankfurt

The construction of the Lufthansa Aviation Center is characterised by columns with a small diameter, which are covered by large glass windows. In the edges of different parts of the building the columns needed to be made of high strength concrete. Due to the architect's requirement all columns should have bright appearance in fair faced concrete quality [4].

Figure 5:

Lufthansa Aviation Center Frankfurt left column: C80/95 (Veridur Cem II/A-S 52.5 R) right column: C45/55 (CEM I 42.5 R)

Table 3: Comparison of concrete mixtures with CEM I 42.5 R and silica fume slurry and with premium-cement Veridur CEM II/A-S 52.5 R:

Table 3		**High strength concrete C80/95**	
Concrete mix design		Veridur	Silica fume
Veridur CEM II/A-S 52.5 R	[kg/m³]	470	-
CEM I 42.5 R	[kg/m³]	-	400
Silica fume slurry	[kg/m³]	-	70
Fly ash	[kg/m³	70	80
water	[kg/m³]	130	155
Additive on cement weight	[%]	1.5	3.0
Slump a_{10}	[mm]	620	640
a_{45}	[mm]	610	580
Compressive strenght $ß_{D1}$	[MPa]	73	28
$ß_{D7}$	[MPa]	90	85
$ß_{D28}$	[MPa]	110	108

2.2 High strength bulk concrete at the base of Kranhaus^{Plus} Cologne

Near the Cologne Rhine harbour new achitecture is celebrated at the construction of the so-called Crane-houses. The name is derived from the shape, which should be similar to the appearance of the old cranes in the harbour. The base had to be made of high strength concrete with a moderate hydration heat. The best values were measured in a concrete mixture C60/75 with Variodur CEM III/A 52.5 N.

Figure 6:

Design model of the "crane-Houses"

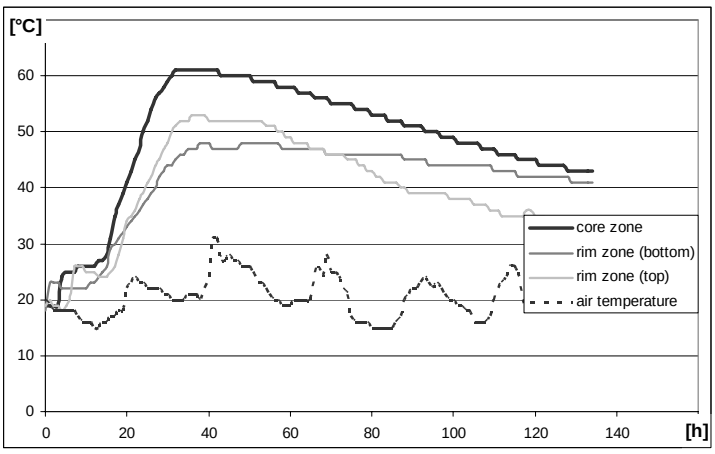

Figure 7:

Measurement of the concrete's hydration heat during the building of the base of Kranhaus^{Plus}, Cologne [6]

3 New cement with nanoscale synthetic pozzolans

Apart from the cement the most important component to achieve dense packing and strength improvement is silica fume by producing additional calcium silicate hydrates C-S-H (pozzolanic reaction).

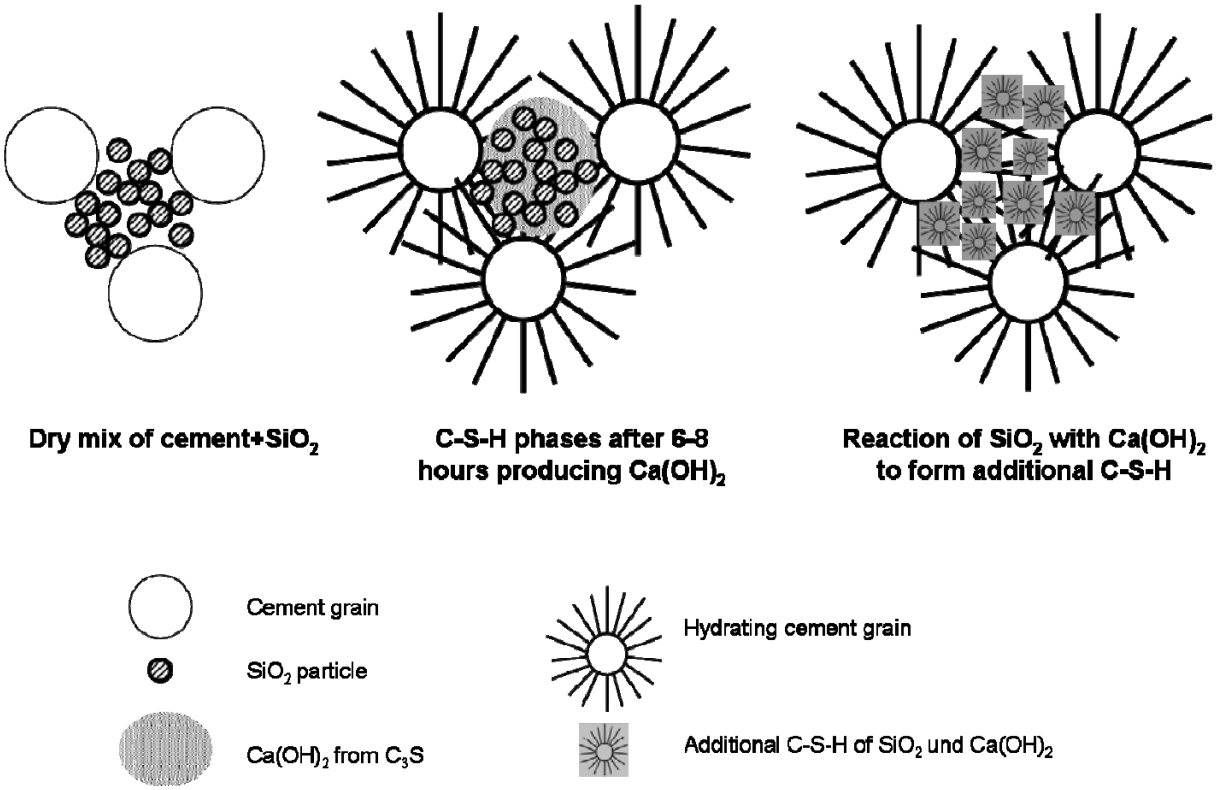

Figure 8: Pozzolanic reaction

Following this mode of action the Mikrodur technology can be improved for the use in UHPC by adding silicon dioxide. The main SiO_2 product in common UHPC mixtures is silica fume, which is formed as by-produkt in the ferro silicon metal industries. The particle distribution is not continuously graded and the particle size ranges between 100 and 1.000 nm. There is a big difference in the size compared to the coarse cement grains!

Figure 9: reactive binder components of common UHPC mixtures

A nearly continuous grain size distribution even in the reactive binder components can be achieved using OPC, microfine cements and industrially produced nanoscale synthetic silicas. These products are well known for many years for example in the rubber and plastic industries as reinforcing fillers. Synthetic silicas are formed by precipitation or a pyrogenic

process based on quartz sand as raw material. Synthetic silicas are pure white powders, which are produced worldwide for example by Evonik Degussa. The products are x-ray amorphous and do not cause silicosis. Due to the controlled industrial production, the physical and chemical properties of the synthetic silicas are much more constant than those of silica fume.

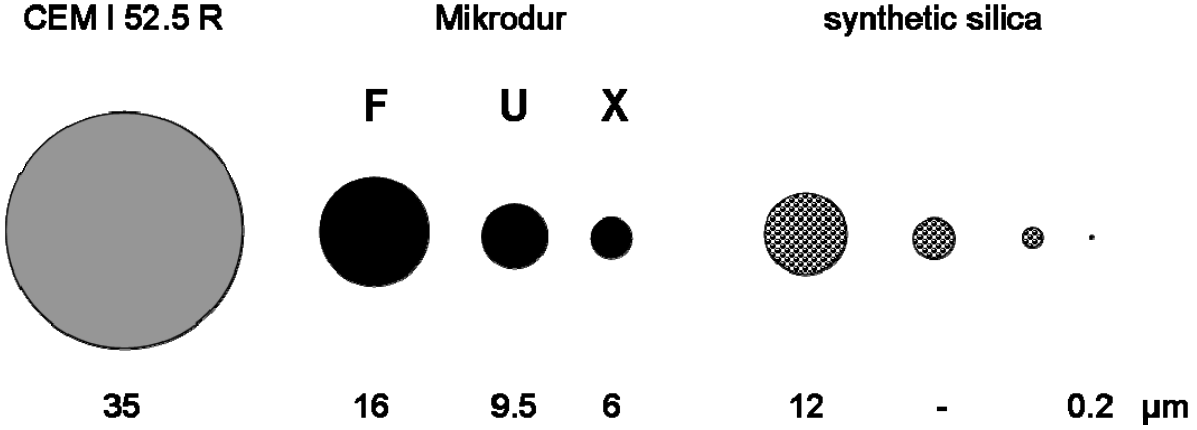

Figure 10: reactive binder components with microfine cements and synthetic silicas

The reaction of the synthetic SiO_2 particles with the cement runs much faster compared to silica fume. Korpa and Trettin [7] tested the pozzolanic reactivity by measuring the pH value in mixtures of $Ca(OH)_2$ and silica fume resp. Aerosil (pyrogenic synthetic silica):

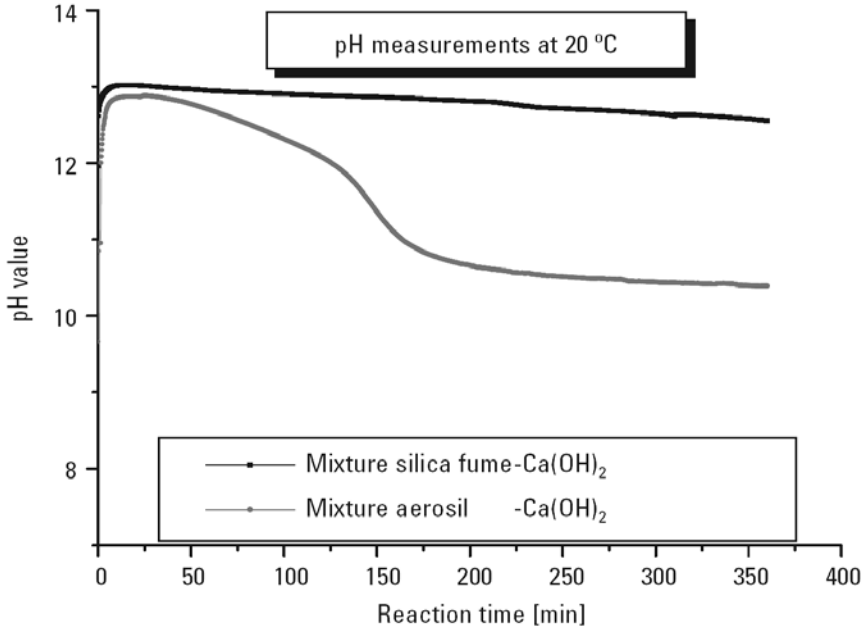

Figure 11:

Pozzolanic reactivity of pyrogenic nanoscale oxides [7]

Continuous dense packing of different reactive components instead of coarse cement and microfine silica fume offers new chances for the microstructure. For example cements mixtures containing microfine clinker particles in combination with nanoscale synthetic silicas can accelerate the hydration process. Microfine grains of blast furnace slag together with nanoscale synthetic silicas extend the durability of concrete. Dense packing of the reactive components is the first step.

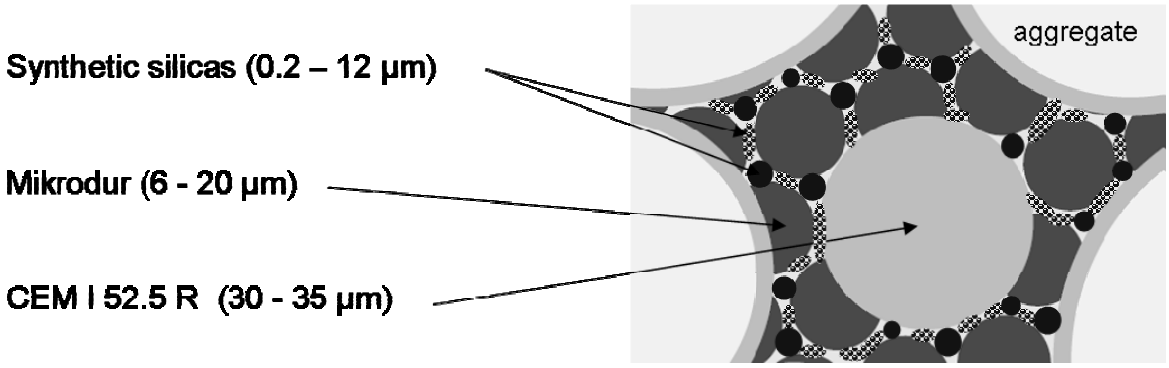

Figure 12: Dense packing of reactive binder components

3.1 Mortar tests in laboratory

In laboratory tests different mix designs of the new cement (Nanodur®) were tested in a very simple composition. It started with a ratio Nanodur : Sand (90 µm) = 40 : 60. The mortar was produced according to DIN EN 196-1, except the water/cement ratio, which was 0.28. To achieve a slump of 125 mm ± 3 mm on Hägermann table, a PCE Superplastizer was added. The temperature of all ingredients was 20°C ± 2°C. For the strength testing prisms 16 cm x 4 cm x 4 cm were used. Flexural strengths of more than 20 MPa and compressive strength values of 150 MPa were achieved with different types of the new cement.

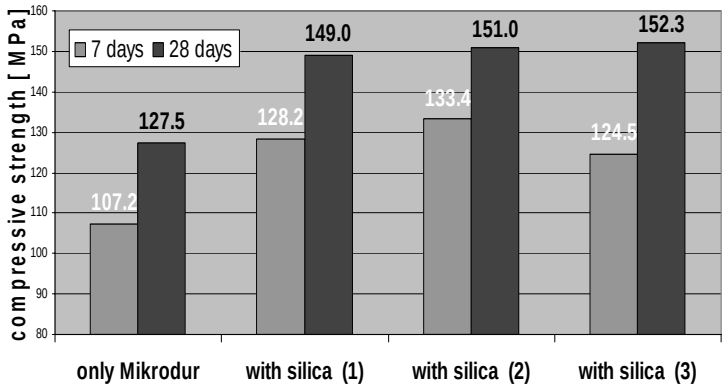

Figure 13: Strength of mortar

3.2 UHPC with the new cement

The next step was to use the new cement in an UHPC mixture without any silica fume.

Figure 14: UHPC board 120cm x 40cm x 1cm, Span: 100 cm

Table 4: Mix design of the UHPC board for demonstration

Table 4	**Mix design and strength**								(prism 16 cm x 4 cm x 4 cm)	
Nanodur cement [kg/m³]	Sand <125 µm [kg/m³]	Sand < 0,5 mm [kg/m³]	crushed basalt 2/5 mm [kg/m³]	steel fibre long [kg/m³]	steel fibre short [kg/m³]	Water [kg/m³]	PCE [% of cement weight]	w/c-ratio	Compressive strength 28 d, 20°C [MPa]	Flexural strength 28 d, 20°C [MPa]
609	**402**	**442**	**873**	**41**	**61**	**158**	**3**	**0,26**	**190**	**23**

Following the style of the mix designs described in [8], the aim was to work without silica fume and to generally reduce the amount of binder. Firstly, the cement was premixed in a special powder mixer and then added to the dry aggregates. After the dosage of water and PCE the singularized steel fibres were added. The total time for dosage and mixing was in the range of five minutes. Then the pasty material was filled into a formwork and the air was removed by a spiked roller. The picture (Fig. 14) was taken after the board was stored at 40°C for 7 days.

3.3 Conclusions

One of the main handicaps for the application of UHPC is the handling of large quantities of silica fume and cement, which only allows specialized companies to work on this subject. A premixed cement consisting of an OPC comprising microfine portland cement clinker, blast furnace slag grains and different synthetic silicas ensures easy handling, dosage and homogeneity even with short mixing times. That also means a really dense packing of reactive binder components. The pozzolanic reaction is accelerated by the very reactive synthetic silicas. Thus it is possible to create binders for UHPC with respect to certain requirements. It is possible to produce these binders according to the German cement standards and so they can be used without special allowance. Also very important is the fact, that the handling of the new cement is nearly comparable to the one of fine OPCs. Altogether the development of a cement like Nanodur® may improve the quality and will make the UHPC production - perhaps also in ready mix plants - much easier.

4 References

[1] Deuse, T.; Schultz, W.; Strunge, J.: Special cements for high performance concrete, CPI-worldwide, 1-2007, Object reports Dyckerhoff: http://www.dyckerhoff.com/_produkte/prod10.htm

[2] Naturzugkühler Neurath

[3] Hochleistungsbetonfertigteile Brücke Pfungstadt (see also CPI-wordwide 4-2007)

[4] Lufthansa Aviation Center, Flughafen Frankfurt am Main

[5] Kranhaus, Köln

[6] Temperature measurements on site, TPA Gesellschaft für Qualitätssicherung und Innovation GmbH,
Köln, 2007 (not published)

[7] Korpa, A.; Trettin, R.: Nanoscale puzzolans for improving ultra high performance cementitious binders, Cement International 1/2007

[8] Forschungsbericht DFG FE 497/1-1, Kassel, 2005

Jennifer C. Scheydt
Dipl.-Ing.
University of Karlsruhe
Karlsruhe, Germany

Gunther Herold
Dr.-Ing. Dr. rer. nat.
University of Karlsruhe
Karlsruhe, Germany

Harald S. Müller
Prof. Dr.-Ing.
University of Karlsruhe
Karlsruhe, Germany

Mathias Kuhnt
Dipl.-Ing.
Gebrüder Dorfner GmbH & Co.
Hirschau, Germany

Development and Application of UHPC Convenience Blends

Summary

Two ultra high strength concrete convenience blends have been developed by the authors. The blends are characterised by their self-compacting like properties and their good workability. The mixtures were fluidised by a pulverised superplasticizer (SP). It could be shown that the flowability of the mortar improves with increasing SP dosage up to a limit value beyond which adverse effects could be observed. Furthermore, the influence of different types of cements on the fresh as well as the hardened concrete properties was investigated.

Keywords: *UHPC convenience blend, precast elements plant, application of UHPC*

1 Introduction

A big drawback of ultra high performance concrete (UHPC) is its demanding handling. Even a slight change in the quality of the mixture components can cause a significant rise of the water demand of the mixture and thus a loss of workability of the concrete. Therefore, a strict quality control of all composition materials is required. Furthermore, the storage of the high number of constituents for the production of UHPC in a precast elements or ready-mix plant is an economic problem.

Taking this into account, the Institute of Concrete Structures and Building Materials (IfMB), in cooperation with Gebrüder Dorfner GmbH & Co. has developed an UHPC convenience blend called DORSICEM (abbrev.: D). It is available as a coarse aggregate mixture (D_{coarse}, d_{max} = 8 mm) and as a fine aggregate mixture (D_{fine}, d_{max} = 0.5 mm). Further, the mixtures are also available as a pure mineral blend without cement, so the cement can be chosen appropriate to the requirements of the manufactured element.

In the following, the development of the convenience blends by the IfMB is presented. The substitution of the liquid superplasticizer (SP) by a pulverised one was mainly performed by means of rheological investigations. The performance of the developed mixtures is

extensively described in the fresh and the hardened state. Furthermore, first experiences concerning the use of the convenience blends in the precast elements plant and a first application of the material in the GeoPark in Hirschau, Bavaria, are presented.

2 Characterisation of the convenience blends

Ultra high performance concretes are characterised by their high number of mixing components. As can be seen from Table 1, the developed mixtures also consist of 8 different dry mixing components. To provide easy handling of the mixtures and to ensure constant quality of the mixing components, the dry components are premixed and delivered as a convenience blend. Only water has to be added to fluidise the mixtures. Also, depending on the application, fibres can be added to increase the ductility and the fire resistance, respectively. As a coarse aggregate, a high quality quartz gravel is used in the UHPC mixture D_{coarse}. Both mixtures show the same mortar composition.

Table 1: Mixing compositions [kg/m³] of the developed mixtures and mean particle size d50 [mm] of the quartz sand and powders

Mixture	Quartz gravel (3 - 8 mm)	Quartz sand (d_{50} ≈ 0,30 mm)	Quartz powder A (d_{50} ≈ 0,10 mm)	Quartz powder B (d_{50} ≈ 0,03 mm)	Quartz powder C (d_{50} ≈ 0,02 mm)	CEM I 42,5 R-HS	Microsilica	Superplasticizer[1)]	Mixing water	Steel fibres[2)]
D_{fine}	-	472	270	160	175	772	236	17	208	196
D_{coarse}	635	355	203	120	131	582	178	13	157	196

[1)] pulverised
[2)] 2.5 % by volume; optional

Table 2: Properties of the mixtures in the fresh state

Mixture	Slump flow [mm]	Flow time t_{500} [sec]	V-funnel flow time [sec]
D_{fine}	840	6	11
D_{coarse}	770	12	16
SCC	600 ÷ 800	≈ 2	< 6

Table 2 shows the behaviour of the mixtures in the fresh state. From the comparison of the mixtures to a self-compacting concrete (SCC), their self-compacting like properties become apparent. Thus, the mixtures were assessed according to the DAfStb code of practice on self-compacting concrete [1]. The compressive strength of the investigated mixtures was tested on cubes with a length of 150 mm ($f_{cm,cube}$) at the age of 7 and 28 days, respectively after water storage at 20 °C. Furthermore, the compressive strength after heat treatment at 90 °C was investigated at a concrete age of 7 days ($f_{cm,cube,90°C}$). All tested concretes were

fibre reinforced (steel fibres, l/d = 45, 2.5 % by volume). The compressive strength of the tested mixtures ranged between 122 MPa and 224 MPa depending on the maximum aggregate size and the curing treatment (see Table 3). The flexural tensile strength f_{cf} was tested on beams (100/100/570 mm) at the age of 28 days after water storage at 20 °C.

Table 3: Strength values [MPa] of the developed mixtures

Mixture	$\mathbf{f_{cm,cube,7}}$ [1) 2)]	$\mathbf{f_{cm,cube,28}}$ [1) 2)]	$\mathbf{f_{cm,cube,90°C,7}}$ [2) 3)]	$\mathbf{f_{cf,28}}$ [1)2)]
D_{fine}	122	157	206	26
D_{coarse}	124	166	224	20

[1)] water storage (20 °C)
[2)] reinforced with steel fibres, l/d = 45 (2.5 % by volume)
[3)] heat treatment (3 days at 90 °C)

In general, the compressive strength of the coarse aggregate mixture is slightly higher than that of the ultra high strength mortar.

3 Development of the convenience blends

The development of the convenience blends started from a mixture developed at the IfMB. In order to optimise the particle size distribution and thus the packing of the powder mix, quartz powders and quartz sand with different particle size distributions were used within the mixture development. The respective distributions are characterised by their mean particle size d_{50} (see Table 1). To assure a simple handling of the product, the liquid SP was substituted by a pulverised product based on polyacrylate. The most important steps within the concrete development are presented below.

3.1 Investigations on the variation of cement

Usually, cements with a low C_3A-content are used within UHPC due to their low water demand, see e. g. [2]. The only cement with a strength class of 52.5 as well as with a low C_3A-content available on the German market was the CEM I 52.5 R-HS/NA used within the experiments (see Table 4). Because of the restricted availability of this cement, also a CEM I 42.5 R-HS was investigated. The cements differed mainly in the Blaine-value (see Table 4).

The properties of the mixture in the fresh state (plastic viscosity and yield stress) were investigated by means of a rotational rheometer on the basis of a flow-curve regression according to the Bingham-model. For the methodology applied in these measurements refer to [3]. The flexural tensile strength and the compressive strength were tested on prisms at the mortar age of 7 days after heat treatment at 90 °C ($f_{cf,90°C,7}$ and $f_{cm,90°C,7}$). Table 4 shows that the mortar containing the cement CEM I 42.5 R-HS exhibited a lower plastic viscosity than the mortar containing the cement CEM I 52.5 R-HS/NA and this exhibited a superior workability. While a low plastic viscosity implies a better flowability, an adequate yield stress means a higher resistance to sedimentation of the coarse aggregate.

Table 4: Strength values and properties in the fresh state of the mixture Dfine depending on the cement type used

Cement type [-]	**Blaine value** [cm²/g]	**Plastic viscosity μ** [10^{-6}Nm·min] [1)]	**Yield stress τ_0** [10^{-6}Nm] [1)]	$f_{cf,90°C,7}$ [MPa] [2)]	$f_{cm,90°C,7}$ [MPa] [2)]
CEM I 52.5 R-HS/NA	4590	1976	4467	27	201
CEM I 42.5 R-HS	3815	1738	4943	27	191

[1)] properties in the fresh state (liquid superplasticizer)
[2)] prisms, 40/40/160 mm, heat treated (3 days at 90 °C)

As can also be seen from Table 4, the mechanical behaviour is not distinctively influenced by the strength class of the cement, which can mainly be traced back to the high amount of non-hydrated cement within UHPC.

3.2 Investigations on the use of a pulverised superplasticizer

The primary objective during the development of the convenience blend was to assure an easy handling, adapted particularly for the use in the ready-mix or precast elements plant. This was achieved by introducing a pulverised superplasticizer (SP). Thus, during concrete production, only water has to be added to fluidise the mixture.

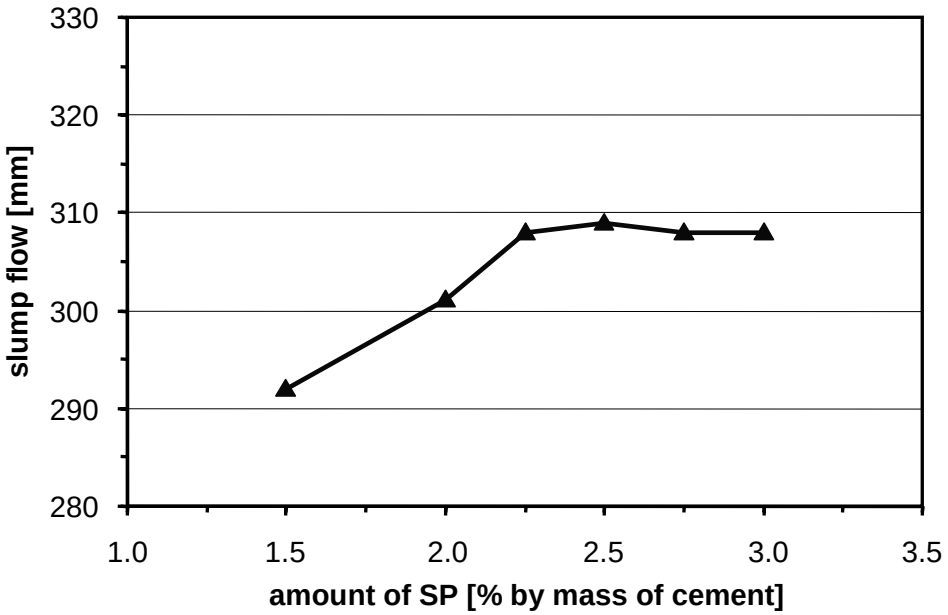

Figure 1: Slump flow of the Dfine mixture depending on the amount of pulverised SP added

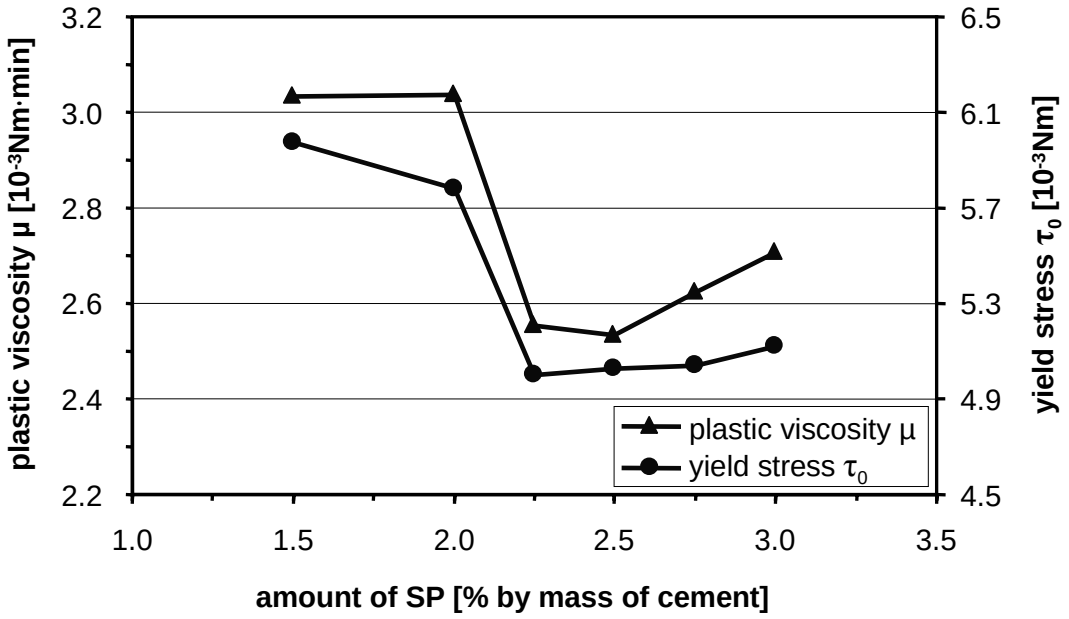

Figure 2: Plastic viscosity μ and yield stress τ0 of the mixture Dfine depending on the amount of pulverised SP added

Figure 1 shows the slump flow of the ultra high strength mortar D_{fine} tested according to DIN EN 1015-3 (without shock) [4]. It can be seen that the slump flow increases by approx. 5 % after increasing the amount of SP from 1.50 to 2.25 % by mass of cement. Beyond that, an increase of the SP dosage does not lead to a further improvement of the consistency.

These experimental results are proved by the results of the plastic viscosity and the yield stress of the mixture (see Figure 2). The specific values decline by 16 % and 14 %, respectively due to a rise of the SP amount from 1.50 to 2.25 % by mass of cement. A further increase of the SP dosage up to 2.75 % however results in a slight increase of the plastic viscosity and the yield stress. This can be ascribed to an excess of the saturation point of the SP. Beyond this point, the excess SP leads to a loss of the flowability of the mortar.

Thus, for the final mixture, an amount of 2.20 % SP by mass of cement was chosen (see Table 1), which guarantees self-compacting properties and a good workability in the precast plant.

3.3 Relevance of intensive quality control

Within the framework of the experimental program, the need for intensive quality control measures both of the mixtures themselves and of the mixing components became apparent. In particular, the cement and the pulverised SP showed distinct fluctuations concerning important material parameters such as the water demand or the Blaine-value. Because of the low water-cement-ratio of UHPC, a rise in the water demand of the mixing components is directly related to a loss of the flowability of the fresh concrete. Thus, the self-compacting properties of the concrete also disappear and the strength declines due to entrapped air.

Table 5 shows the properties of the fine aggregate mixture in the fresh state containing different batches of the same cement CEM I 52.5 R-HS/NA. As can be seen, the fluctuations in the fineness of the cement distinctly afflects in the fresh mortar properties.

Table 5: Properties in the fresh state of the mixture Dfine containing CEM I 52.5 R-HS/NA depending on the batch of the cement used

Cement batch [-]	**Blaine value** [cm²/g]	**Plastic viscosity μ** [10^{-6}Nm·min]	**Yield stress τ_0** [10^{-6}Nm]	**Slump flow** [mm]
A	4590	1976	4467	315
B	4880	3318	7286	257

Due to this change in the Blaine value, a rise of 68 % of the plastic viscosity and 63 % of the yield stress respectively was observed (see Table 5). The slump flow tested according to [4] decreased by 18 %. As ascertained by the cement producer, there were also distinct variations concerning the setting of the cement paste. While the initial set of batch A started after 315 minutes, the setting of batch B already started 44 minutes earlier after 271 minutes.

This indicates that UHPC is highly susceptible to changes in the quality of the raw materials. Hence, a strict quality control is necessary during all stages of production.

4 First applications of the developed convenience blends

Especially due to an increasing demand on durability and sustainability, UHPC is increasingly gaining interest for the construction industry. In view of the prefabrication of thin components for structural engineering, construction of bridges or multi-storey buildings, plenty of new construction possibilities arise due to the favourable properties of this new material. Further, its steel-like properties also offer interesting options in machine or steel construction. In the following, a current application of the UHPC convenience blends is described: the construction of concrete houses for the GeoPark in Hirschau, Bavaria.

The „Industriepfad GeoPark“ is a discovery trail dealing with the digging for the raw materials kaolin, quartz and feldspar. In a number of stations, information related to these minerals is exhibited, each station being protected by a concrete house made from UHPC.

For demonstration purposes, some of the houses were built with the UHPC convenience blends (see Figure 4).

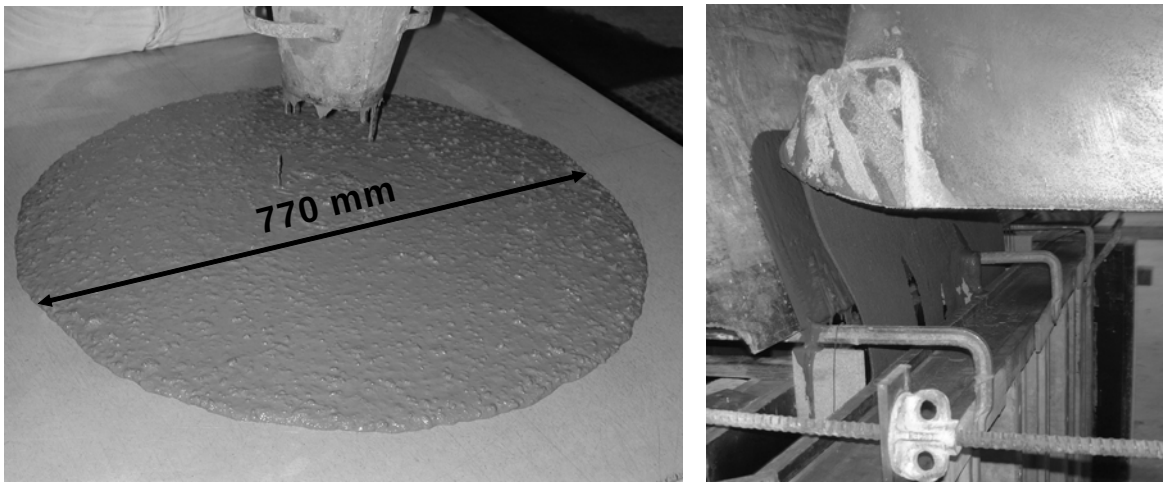

Figure 3: Slump flow according to [1] of the mixture Dcoarse (left) and filling of the formwork with Dfine (right)

Figure 4: UHPC-house (height 3 m, width 2 m, wall thickness 80 mm) after demoulding (left) and in the GeoPark (right)

The mixtures were produced in the precast elements plant using a conventional plate mixer. The resulting fresh concretes possess self-compacting properties (see Figure 3 and Table 2), a necessary precondition for the easy handling of the fresh concrete and the filling of the moulds.

5 Conclusion and outlook

The use of UHPC within the precast plant is complicated due to the high number of mixing components. Furthermore, much time and effort has to be invested concerning quality management of the components and thus of the fresh and hardened concrete.

For this reason, two types of UHPC convenience blends were developed. Easy handling and constant quality are guaranteed by the consistent control of the mixing components carried

out by the producer. Thus, the developed blends permit an enlargement of the precast products in terms of slim profiles and highly durable structures.

6 References

[1] DAfStb-Richtlinie „Selbstverdichtender Beton“. Ausgabe 11, Beuth Verlag, Berlin, 2003.

[2] Siebel, E.; Müller, C.: Geeignete Zemente für die Herstellung von UHFB. In: Ultrahochfester Beton. Innovationen im Bauwesen. Beiträge aus Praxis und Wissenschaft. S. 13-204. König, G.; Holschemacher, K.; Dehn, F. (Eds.), Bauwerk Verlag, Berlin, 2003.

[3] Scheydt, J. C.: Dauerhaftigkeitskenngrößen von ultrahochfestem Beton. Diploma thesis, Institute of Concrete Structures and Building Materials, University of Karlsruhe (TH), November 2004.

[4] DIN EN 1015-3:2007-05. Prüfverfahren für Mörtel für Mauerwerk - Teil 3: Bestimmung der Konsistenz von Frischmörtel (mit Ausbreittisch). Beuth Verlag, Berlin, 2007.

Thomas Hirschi
Dipl Ing. HTL
Head Marketing / Technique
Sika Services AG
Zürich, Switzerland

Franz Wombacher
Dr. Sc. Nat.
TC Manager CC&M
Sika Technology AG
Zürich, Switzerland

Influence of different superplasticizers on UHPC

Summary

Superplasticizers have a big influence on the fresh and hardened concrete properties and this is even more pronounced in high performance and ultra high performance concrete. Additionally it has to be considered that a direct correlation to the behaviour in standard concrete applications is not appropriate. The comprehension of the superplasticizer into a mix design is essential. Big differences occur mainly in setting time and early strength development, whereas the influence on final strength is not significantly influenced. Regarding slump life, some variations are obvious and could be essential for special applications.

Keywords: *superplasticizer, polymer, water reduction, slump life, strength, adsorption, setting*

1 General function of superplasticizers in ultra high performance concrete

The development of superplasticizers for concrete is strongly influenced by the requirements. On the one hand there are demands regarding the durability. The owners interests are focused on the durability because long life cycles and low cots for rehabilitation and protection are the main tasks. On the other hand the contractors are interested in an easy to handle concrete in order to save resources and time.

With the development of superplasticizers based on polycarboxylates, a new field of application could be opened. After the development of high strength and high flowable concrete, Self Compacting Concrete (SCC) showed the new possibilities of this new superplasticizer generation.

The main characteristics of the polycarboxylate based superplasticizers are the following:

- High water reduction (up to 40%)
- High flowability
- Polymer-design allows to control the main characteristics (setting time and workability)
- Blending of different polymers is possible: formulation of customized solutions

With these main characteristics it is possible to adapt the polymer to the cement conditions and to achieve a perfect optimization of the cement paste.

The binder content of ultra high performance concrete is 4 times higher compared to a standard concrete, which leads to an increased admixture content of up to 15 times. This shows the importance of the choice of the right superplasticizer type.

2 Criteria for a suitable superplasticizer for ultra high performance concrete

The criteria to describe the influence of different superplasticizers on the fresh- and hardened properties of UHPC are more or less the same as in a standard concrete or SCC mix.

2.1 Fresh concrete

To quantify the fresh concrete behaviour, the following parameters were tested:

- Initial slump: The initial slump was checked with the flow table spread (Hägermann) according to EN 459-2 but without compacting, lifting and dropping the base-plate.
  The initial slump gives an indication of the flowability achieved by the superplasticizer type.
- Slump life: Describes the behaviour of the UHPC over time. According the slump life an estimation of polymer for a special application is possible. For example a polymer with a shorter slump life and a high early strength development could be suitable for precast elements.
  The slump was checked initially, 20, 40 and 60 minutes after mixing
- Visual check: The visual check is a subjective test but very important for the differentiation of the different superplasticizers. Homogeneity, thixotropy, bleeding and much more can be judged by a visual check.

2.2 Hardened concrete

The hardened concrete properties are manly checked to ensure the durability and mechanical behaviour of the concrete. To compare the influence of different superplasticizers on its hardened concrete performance, the following tests were done:

- Strength: Compressive- and flexural strength were measured to quantify the influence of the superplasticizers on early and final strength. The compressive and flexural strength were measured according to EN 191-1 with prism (4x4x16 cm)
- Temperature: The temperature is a central indicator for the heat development and the setting behaviour in the UHPC. The temperatures were recorded with a data logger under semi diabatic conditions: temperature 20°, relative humidity 65%.

Further fresh and hardened concrete tests are possible and useful for general issues. For a practical selection of a suitable superplasticizer for a UHPC-mix the above mentioned investigations are sufficient.

3 Testing of the influence of different superplasticizers for UHPC

The evaluation process is structured in 3 parts. The first step is based on polymer experience out of standard mix designs followed by a screening in small scale UHPC mixes and ends with standard laboratory trials.

3.1 First indication based on polymer know-how

For the design of a UHPC mix, the know-how of the basic behaviour of a polymer type is essential. This first step is based on general experience with such polymers in standard concrete mix designs. In the following figure a summary of such an indication is shown:

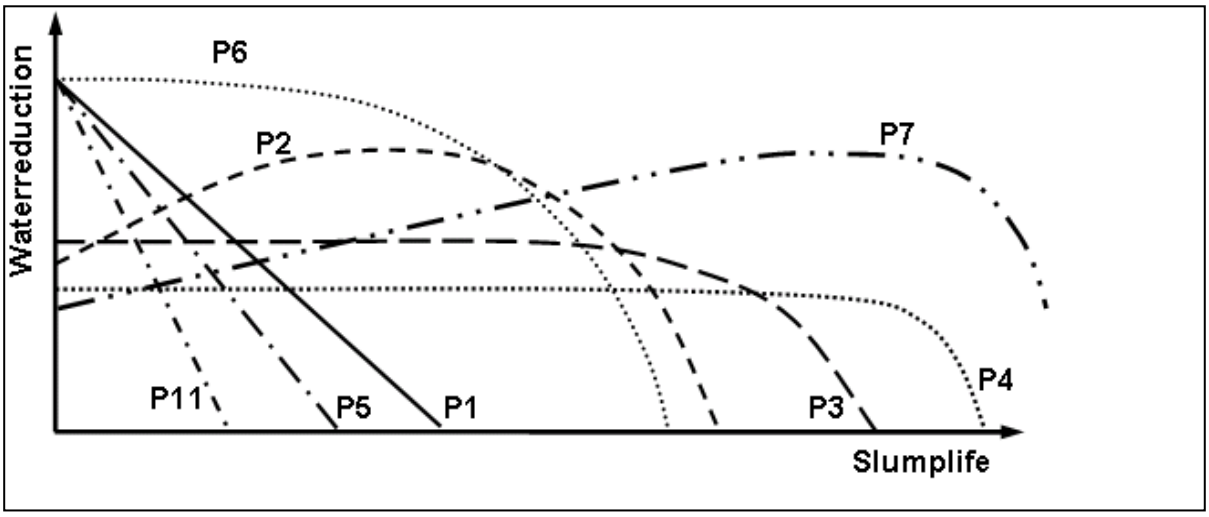

Figure 1: Workability behaviour of different polymers

In the whole testing procedure the following polymer were used:

- P1: Poly-methacrylic acid based with medium side chain length
- P2: Poly-acrylic acid based with medium side chain length
- P3: Poly-methacrylic acid based with medium side chain length
- P4: Amine modified poly-methacrylic acid based with medium side chain length, (reduced C/E)
- P5: Poly-Acrylic acid based with long side chain length
- P6: Poly-Methacrylic acid based with long side chain length
- P7: Amine modified poly methacrylic backbone with medium side chain length
- P11: Poly-Acrylic acid based with long side chain length

Important requirements for an ultra high performance concrete are generally high water reduction and a fast adsorbing time. The demanded workability (slump life) is depending on the project requirements. As you can see in figure 1, polymers P1, P5 and P6 could be a good solution and P2, P3 or P11 are probably suitable too. The water reduction of P4 and P7 is obviously to low.

Concerning the mixing time, different polymers have different a behaviour. As polymers adsorb on positively charged cement hydrates their eagerness or speed of adsorption is

mainly depending on how much negatively charged sites (e.g. carboxylic groups) the polymer contains. The eagerness is chemically expressed by the C/E-ratio of the polymer (free carboxylic groups vs. esterified carboxylic groups of the backbone). Additionally the adsorption is also influenced by the confirmation of the polymer in solution and this is depending on one hand on the backbone (acrylic vs. methacrylic type) and o the other hand on the side chain length. A fast adsorbing polymer can reduce the mixing time in a standard concrete mix. The different adsorption behaviour of the tested polymers is mentioned below:

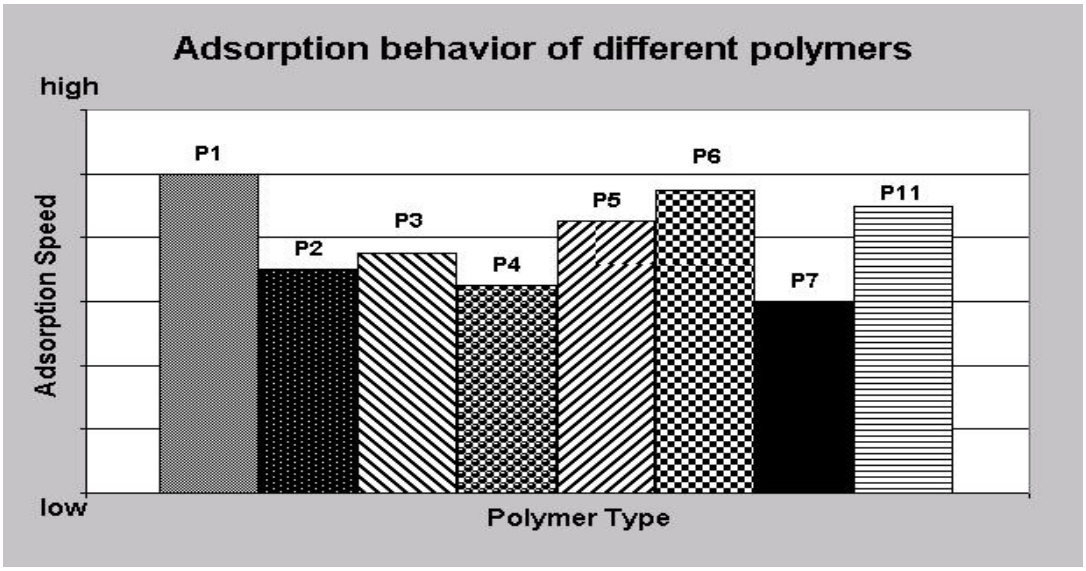

Figure 2: Adsorption behaviour of different polymers

The impression of this first screening has to be confirmed in the next test-series with a suitable UHPC-mix design in Hobart-mixer.

3.2 Screening based on small scale lab. trials

In this phase of the selection, the idea of the first part has to be confirmed. Additionally differences in strength, setting behaviour and visual impression should give a clear picture for possible applications.

For the test series, the following mix design was chosen due to experience of previous studies:

Table 1: Mix design used in the laboratory tests.

Cement	CEM I 52.5 R	1050 kg/m3
Micro silica		250 kg/m3
Quartz sand	0.08 - 1.2 mm	827 kg/m3
Steel fibres	Dramix OL 13/.16	195 kg/m3
Water		205 kg/m3
Superplasticizer	Sika® ViscoCrete®	45 kg/m3

Another important factor for the laboratory trials was the mixing sequence. The test series were produced according to the following mixing sequence:
For the test series, the following mixing sequence was chosen due to experience of previous studies:

Table 2: Mixing sequence

Dry mixing	1 min
water dosage	3 min
Admixture dosage	5 min
Fibre dosage	1 min
Final mixing	2 min

3.2.1 Slump life / water reduction

The loss of the slump can give some indication about required application. For prefabricated elements, a shorter slump life is needed than in ready mix application. The results of the laboratory trials show some variation compared to the polymer behaviour described in figure 1. The variation is not as big as in standard concrete applications. This behaviour is due to the high content of superplasticizer in an UHPC mix. Figure 3 shows, that polymer P4 has a very short slump life in a UHPC mix contrary to standard concrete applications. All the other polymers show a slump life of over one hour.
Regarding the water reduction, the laboratory tests indicate some variations between 135 mm and 187 mm. The best results were achieved with polymer P11 whereas the lowest water reduction results from the mix with P4. These findings correspond mostly qualitative with the estimations of figure 1, which are based on a standard concrete mix.

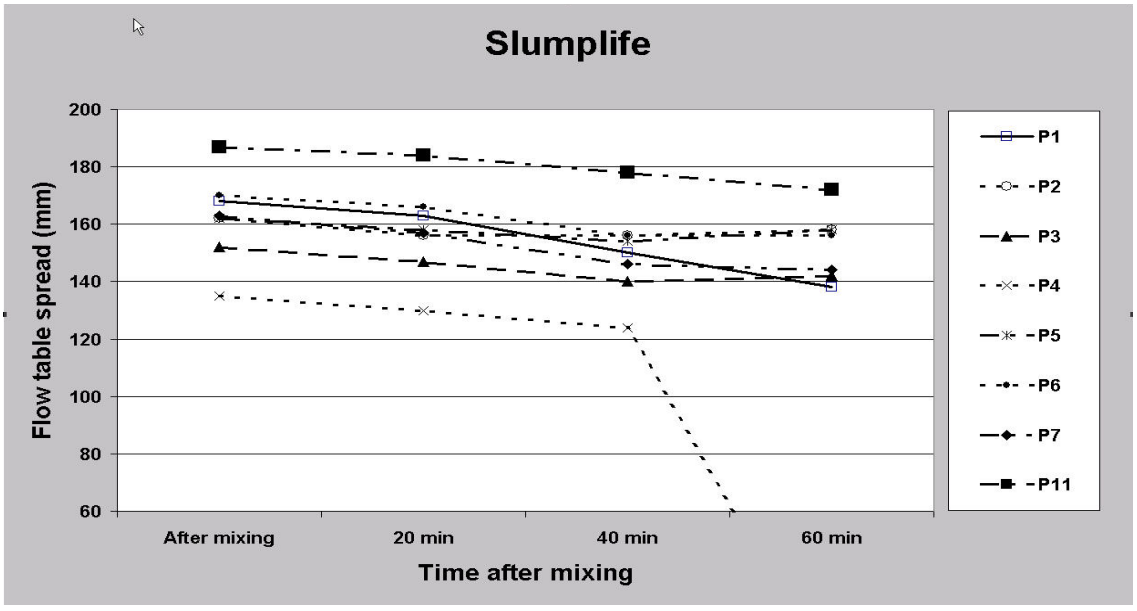

Figure 3: Slump life of different polymers

3.2.2 Setting behaviour

The setting time was determined on the basis of the records of temperatures described under 2.2. The setting times show big variations and give a good indication for the early strength development. In spite of the short slump life, polymer P4 does not have the shortest setting time. Beside the highest water reduction, polymer P11 also has the shortest setting time.

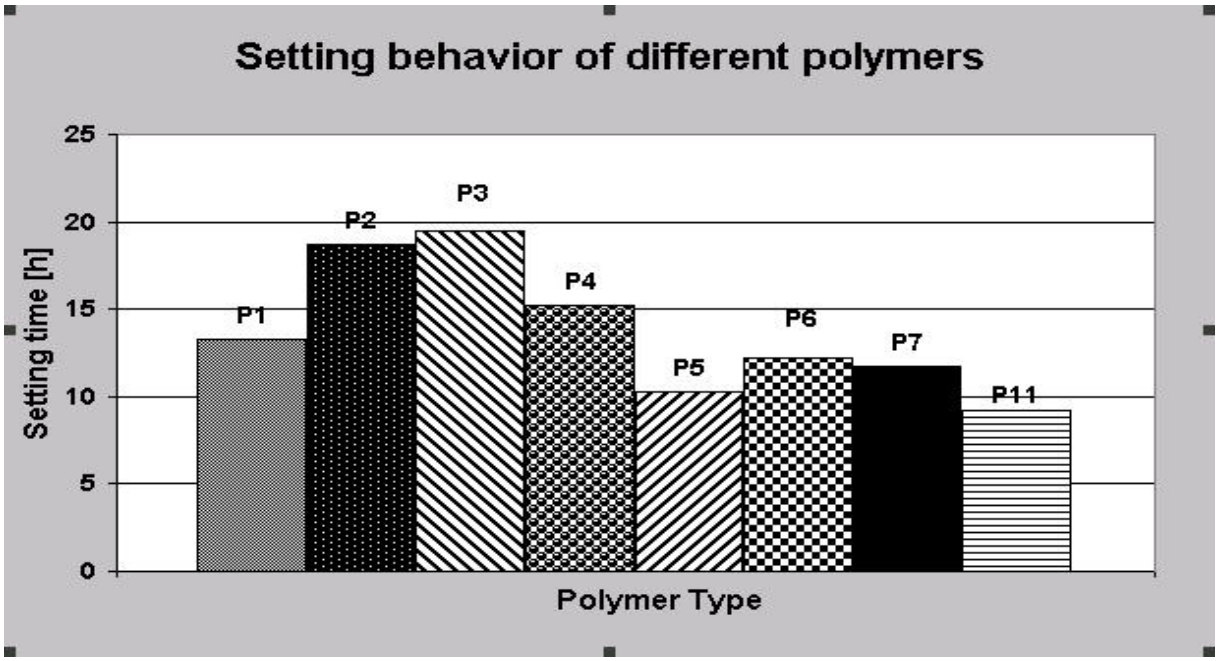

Figure 4: Setting behaviour of different polymers

3.2.3 Strength development

To evaluate some variations in strength and strength development, the following strength were measured:

- Compressive strength: 1, 7 and 28 days
- Flexural strength: 1, 7 and 28 days

According to the setting behaviour (figure 4), the early strength after one day show big variations. The mixes with polymer P5, P7 and P11 have the highest early strength. The compressive strength corresponds very well with the flexural strength. After 7 and 28 days, the strengths reach the same level. In this phase of the hydration, the binder system is crucial for the strength development. The influence of the superplasticizer is negligible.

Due to the early strength development, only some types of superplasticizers are suitable for early strength applications like prefabricated elements. For example Polymer P5 and P11 are good opportunities for such an application because of their good early strengths.

Because of the slightly better flexural strengths, Polymer P1 and P3 can be used for applications, were a high flexural strength is needed.

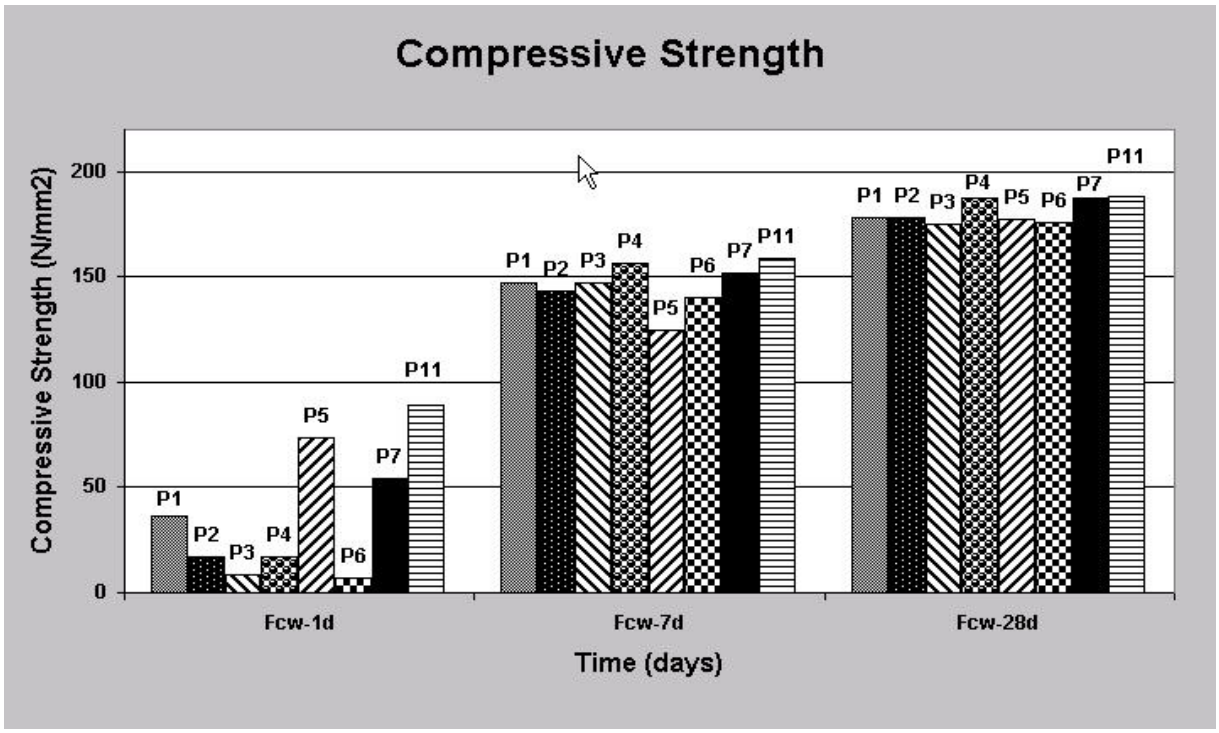

Figure 5: Compressive strength development

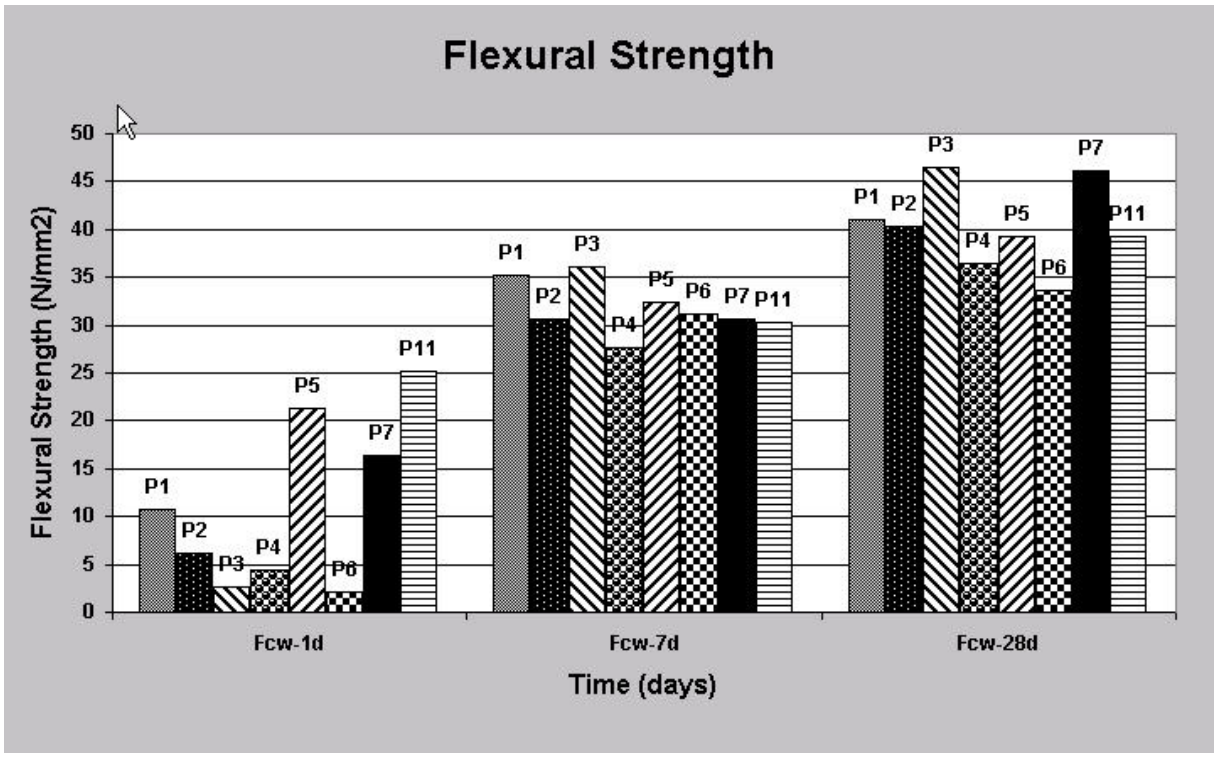

Figure 6: Flexural strength development

3.2.4 Mixing behaviour / Visual check

According to the different adsorption behaviours, the behaviour during the mixing sequences was slightly different from polymer to polymer. The main differences occurred in the time between 5.5 and 6 minutes after beginning of mixing. Polymers 1, 6 and 11 showed a slightly better dispersion. An optimisation of the mixing sequence should be part of field trials, because the mixer type has a big influence.

In these laboratory trials the rating of the homogeneity and handling are based on a visual check. The Impression of these small variations is below-mentioned.

Table 3: Rating of homogeneity based on a visual check

	P1	**P2**	**P3**	**P4**	**P5**	**P6**	**P7**	**P11**
homogeneity	good	very good	on average	bad	on average	on average	bad	good
handling	on average	on average	on average	on average	on average	on average	on average	on average

4 Conclusions

The selection of a suitable superplasticizer is mainly defined by the application. After a first screening like the laboratory trials with the Hobart mixer, the range of products can be reduced. With this concept, it's possible to start very quickly with field trials and save time and resources. During the field trials it is essential to focus on other topics than the selection of superplasticizers like mixing sequence, variations and local conditions.

The goal of mix design should be always a good team work. It's useless to test numbers of diverent admixtures, if some basic data are available. The main focus in the selection of the superplasticizer should be always on the slump life and the early strength. If a suitable polymer is available for the needed application a fine tuning by the admixture supplier is possible to fulfil other parameters like homogeneity or handling.

5 References

[1] Mäder U.; Lallemant-Gamboa I.; Chaigon J. ; Lombard J-P. : Ceracem, a new high performance concrete : characterisations and applications

[2] Lallemant-Gamboa I.; Chanut S. ; Lombard J-P. ; Chaigon J. ; Thibaux T. : Formulation, characterizations and applications of an ultra high performance concrete

Etsuo Sakai
Tokyo Institute of Technology
Graduate School of Science and Engineering
Tokyo , Japan

Keisuke Aizawa
Tokyo Institute of Technology
Graduate School of Science and Engineering
Tokyo , Japan

Akinori Nakamura
Tokuyama Corparation
Develop Dept. Cement Bisiness Div.Yamaguchi,
Japan

Hiroyoshi Kato
Tokuyama Corparation
Develop Dept. Cement Bisiness Div.Yamaguchi,
Japan

Masaki Daimon
Tokyo Institute of Technology
Graduate School of Science and Engineering
Tokyo , Japan

Influence of superplasticizers on the fluidity of cements with different amount of aluminate phase

Summary

This paper discusses the effective factors on the fluidity and the early hydration of preproduction cement with different amount of C_3A produced in the real plant. Napthalene based and polycarboxylate based superplasticizers are used. It was clarified that C_3A contents and the amount of the soluble alkali in cement influenced on the fluidity of cement. This is related to the increasing of specific surface area of cement by early hydration and the adsorption inhibition of superplasticizes by the contens of soluble alkali of cement. The heat liberation of cement at early stage is influenced by the C_3A and the soluble alkali contents, and free lime (F-CaO) is related to the soluble alkali in the same plant. There is good correlation between the apparent viscosity of cement pastes and the heat liberation of early hydration in each of three proposed ranges of ranges of F-CaO content

Keywords: *Aluminate phase, Real plant, Fluidity, Heat liberation, Superplasticizer*

1 Introduction

Portland cement wiht C_3A content in the less than 5% such as low heat Protland cement and moderate heat Portland cement is very usful for the production of high performance concrete. However, raw materials originating from waste have recently come to be used as ingredients in cement. The waste in common use contains a higher proportion of Al_2O_3 (the aluminate phase) than ordinary Portland cement (OPC). With little prospect of major increases in conventional cement production in the future and with pressure on the cement industry to

contribute to sustainability, it is very likely that cements with more of this aluminate phase will have to be used[1]. Many researchers have studied and reported on the effects of cement properties on the fluidity of superplasticized cement pastes[2,3]. The C_3A, SO_3, gypsum hemihydrate and soluble alkali content as well as fineness and the specific surface area of the hydrated cement paste have all been cited as cement qualities that affect the performance of the superplasticizer. Taking as an example Eco-Cement, which has the highest aluminate phase content of any cement in the world, it has been reported that the quantity of polycarboxylate-based superplasticizer added is substantially greater than with ordinary cement and that cement paste fluidity is determined by the quantity of adsorbed superplasticizer per specific surface area[4]. However, there have been a paucity of studies on superplasticizer interactions as the content of the aluminate phase changes. Yamada et al. studied cement with a C_3A content of 5.3-7.3% and an alkali content, K_2O in particular, of not less than 1%. The results of this study showed that alkalis, particularly K_2O, in C_3A increase the reactivity and decrease the fluidity of cement pastes and that the ratio of the SO_3 content to that of Na_2O in the clinker is an important factor[1]. Given the likely increase in the quantity of waste being treated in the future, it is necessary to develop a quality control method for use at commercial plants based on a quantitative evaluation of the effects aluminate content on the fluidity of cement pastes. To that end, the accumulation of data from numerous cement plants is necessary. This paper describes the effects of C_3A on the fluidity and the very early hydration of cement pastes prepared for the purpose from clinker materials manufactured at commercial plants, varying in C_3A content from 3.7% to 10%. This paper presents the important information to propose a performance evaluation method for the fluidity of cement pastes based on measured the heat liberation of cement early hydration.

2 Test method

2.1 Materials used

The cement samples in the research were prepared by adding gypsum to the clinker materials having the chemical compositions shows in Table 1. Finess of these cements is ajusted about 3300 cm^2/g. These clinkers were manufactured at commercial plants for the purposes of this research. Chemical compositions were measured in accordance with JIS R5204: "Chemical analysis method for cement by X-ray fluorescence". The content of free lime (F-CaO) was measured in accordance with the Japan Cement Association Standard Testing Method JCASI-01-1997. The soluble alkali content was measured in accordance with ASTM C114. The weight of each test sample was 3.5 g. Alkalis were analyzed by inductively coupled plasma (ICP) spectrometry.

In order to evaluate the effects of cement chemical composition and the constituent compounds of the cement, the particle size and the method of adding gypsum were standardized.

Table 1: Chemical and mineral composition of cement

No	Chemical composition (%)											Bouge(%)			
	igloss	SiO_2	Al_2O_3	Fe_2O_3	CaO	MgO	SO_3	Na_2O	K_2O	Cl^-	F-CaO	C_3S	C_2S	C_3A	C_4AF
1	0.64	24.9	3.53	3.36	62.8	1.53	1.90	0.15	0.42	0.0011	0.24	31.5	47.7	3.7	10.2
2	0.99	23.8	3.20	2.77	65.1	1.56	1.93	0.13	0.34	0.0016	0.51	50.7	30.2	3.8	8.4
3	0.85	25.0	3.53	2.83	64.1	1.63	1.90	0.15	0.35	0.0054	0.31	36.4	44.3	4.6	8.6
4	0.78	23.6	3.97	2.89	64.4	1.73	1.98	0.20	0.44	0.0082	0.37	44.6	34.1	5.6	8.8
5	0.76	21.3	4.94	3.16	65.8	1.61	1.92	0.20	0.38	0.0070	0.37	61.5	14.7	7.8	9.6
6	0.70	21.8	4.97	2.96	65.4	1.73	1.87	0.21	0.24	0.0045	0.17	56.6	19.9	8.2	9.0
7	0.78	20.2	4.87	2.76	66.4	2.05	1.92	0.24	0.47	0.0097	0.95	70.5	4.82	8.2	8.4
8	0.81	20.7	5.30	3.22	65.4	1.61	1.94	0.30	0.47	0.0034	0.42	61.5	12.9	8.6	9.8
9	0.75	20.6	5.20	2.86	66.0	1.97	1.80	0.22	0.40	0.0035	0.43	66.0	9.44	8.9	8.7
10	0.85	20.2	5.09	2.62	67.0	1.95	1.98	0.22	0.35	0.0175	0.63	72.7	3.23	9.1	8.0
11	0.67	20.1	5.50	3.12	65.9	1.73	1.89	0.28	0.29	0.0050	0.25	67.4	6.86	9.3	9.5
12	0.90	20.4	5.64	3.07	65.9	1.54	1.87	0.28	0.48	0.0271	0.40	63.9	10.4	9.8	9.3
13	0.93	19.9	5.39	2.51	66.6	1.95	2.02	0.26	0.51	0.0191	0.76	71.7	2.93	10.0	7.6

Fineness: Blaine method

Gypsum (with a ratio of 50-to-50 hemihydrate-to-dihydrate) was mixed with a coarsely pulverized clinker and the mixture was pulverized. Comparing the C_3A content determined by the Rietveld method (software: RIETAN 2000) with that estimated using the Bogue calculation, the Bogue value was found to be smaller than the Rietveld by 2-3%. However, the two methods indicated a similar trend so the latter is used in this paper. Cement with a C_3A content in the 3.7% to 10.0% range (as estimated using the Bogue calculation) and an F-CaO content in the 0.17% to 0.95% range was used.

2.2 Test method

A polycarboxylate-based superplasticizer (PC34)[5] was added at 0.2% and 0.4% by mass and a naphthalene-base superplasticizer (BNS) was added at 0.6% and 1.0% by mass of cement. Superplasticizer contents are given as a dry mass as a percentage of the mass of cement. The apparent viscosity of a cement paste with a water-to-cement ratio of 0.32 and mixed using a spatula for 10 minutes was measured using a stress-control rotating double-cylindrical viscosity meter (Model: RT20 Z41 TI by HAAKE). The measuring program was set so that the shear stress increased from 0 Pa to 200 Pa and then decreased from 200 Pa to 0 Pa (cycle time: 5 minutes) and the apparent viscosity of the cement paste under a shear stress of 200 Pa was measured. Hydration of the cement paste prepared by the method described above was brought to a stop by the use of a large quantity of acetone. The paste was dried using an aspirator under reduced pressure (2.33×10^3Pa)for 24 hours and the BET specific surface area of the paste was measured with a continuous-flow surface area analyzer (Model: SA-6200 by Horiba, Ltd.). The heat liberation in the first 60 minutes of cement hydration at a water-to-cement ratio of 0.40 was measured using a conduction calorimeter.

3 Test results and discussion

3.1 Effects of cement properties on the fluidity of cement pastes

Figure 1 shows the relationship between the C_3A content of the cement and the apparent viscosity of the cement paste. The apparent viscosity varied greatly for C_3A contents greater than about 8%, irrespective of the type of superplasticizer, PC34 or BNS. Particularly noticeable was the large variation in apparent viscosity when dosage of BNS was smaller. In contrast, for C_3A contents below about 8%, the apparent viscosity was constant regardless of the type and dosage of superplasticizer.

Table 2 shows the results of a multiple regression analysis on the data given in Figure 1 (that is, on the relationship between apparent viscosity of the cement paste and the C_3A and F-CaO content of the cement). The multiple correlation coefficients were very large, 0.94 for PC34 and 0.90 for BNS, suggesting that cement paste fluidity is controlled by the content of these two components. For example, a variation of 1% in the C_3A content results in the apparent viscosity changing by 14.3 MPa-s and 15.1 MPa-s at the 0.4% PC34 content and the 1.0% BNS content, respectively; similarly, a variation of 1% in the F-CaO content results in the apparent viscosity changing by 298 MPa-s and 310 MPa-s at the 0.4% PC34 content and 1.0% BNS content, respectively.

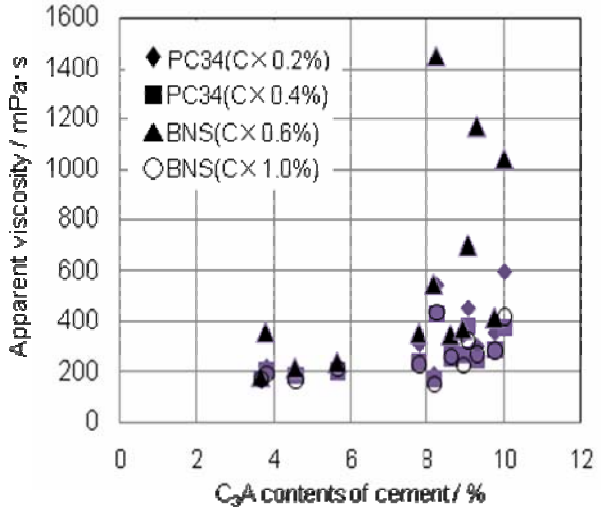

Figure 1: Influence of C3A contents for cement on the fluidity of cement paste with superplasticizers (the brackets indicates the dosage of superplasticizer to cement)

Table 2: Multiple regression analysis for apparent viscosity of cement paste

Factor \ Superplasticizer	PC34 (C×0.4%)	BNS (C×1.0%)
C_3A	14.3	15.1
F-CaO	298	310
intercept	22	2
R^2	0.94	0.90

R^2: multiple correlation coefficients

Figure 2 shows the influence of C_3A content or F-CaO content on the specific surface area of the cement 10 minutes after hydration began. The specific surface area increased with C_3A content for a similar F-CaO content regardless of the type of superplasticizer. Further, the specific surface area increases with increasing F-CaO content for a constant C_3A content. The fact that cement paste fluidity is dominated by C_3A and F-CaO is related to an increase in specific surface area as hydration proceeds. It is presumed that the quantity of small hydrate powder particles increases and the quantity of adsorbed superplasticizer per specific surface area decreases. When F-CaO is added to synthesized pure C_3A, hydration is restrained immediately upon addition of water[6], a result that differs from the results shown in Figure 2.

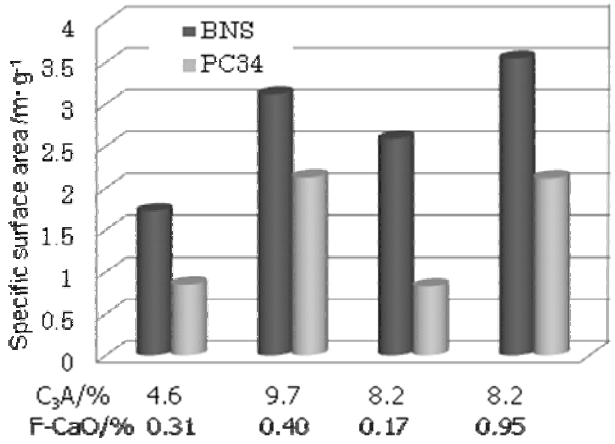

Figure 2: Specific surface area of hydrated cement (measured by BET)

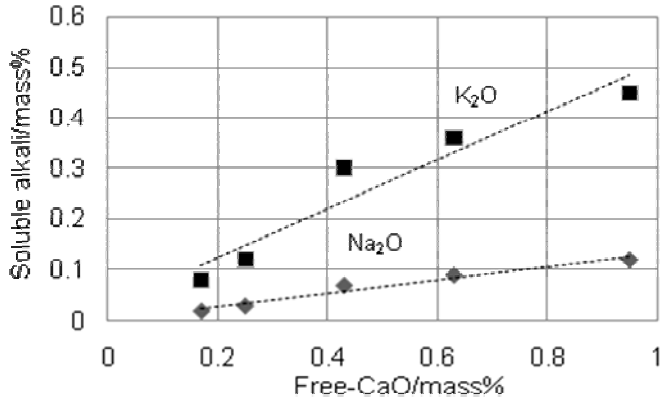

Figure 3: Relation between F-CaO and soluble alkali

Figure 3 shows the relation between F-CaO content at similar C_3A contents and soluble alkali content. For cement manufactured commercially, the soluble alkali content increases with increasing F-CaO content. It is presumed that residual F-CaO is associated with alkalis in the cement and the activity of C_3A increases as a result of alkali action. Accordingly, a method of adding F-CaO after burning of cement is likely to restrain the reaction of C_3A, but this remains a topic for further study.

From the results of the relationship between the absorption of superplasticizer per unit surface area, for superplasticizers PC34 and BNS added at 0.4% and 1.0% by mass of cement, and apparent viscosity of the cement paste, the apparent viscosity decreased, meaning fluidity was higher, with increasing superplasticizer adsorption. That is, as already reported, the fluidity of cement paste is dominated by the quantity of superplasticizer adsorbed per unit surface area[4]. To achieve a given apparent viscosity, the quantity of adsorbed BNS per unit surface area was about four times greater than the amount of PC34. This is the same tendency as with Eco Cement and is related to relative ease with which the superplasticizer is taken into the hydrates, a characteristic of superplasticizer molecule size. Variations in the amount of superplasticizer adsorbed even with the same superplasticizer content are associated with the cement's soluble alkali content, as already revealed in many reports. The higher the soluble alkali contents in the cement, the lower the quantity of adsorbed superplasticizer; as a result the apparent viscosity is higher and the fluidity of the cement paste is lower. As regards the adsorption inhibiting effect of soluble alkalis and their tendency to cause contraction of polymer molecules, the mechanism of this behavior has already been elucidated through much research[7]. In this study, the quantity of both PC34 and BNS adsorbed decreased with increasing soluble alkali content.

3.2 Early heat of hydration and fluidity

Figure 4 shows the relationship between heat of hydration one hour after the addition of water and apparent viscosity of the cement paste for cases with PC34 added. The apparent viscosity tends to increase with increasing heat of hydration and the change is rapid when the heat of hydration exceeds 14J-g^{-1}. It suggests also that heat of hydration could be used for quality control. Heat of hydration is related to the C_3A content: as the C_3A content increases, the heat of hydration also increases. However, the effects of soluble alkalis on the reaction of C_3A are also included in the heat of hydration. As already noted, heat of hydration is also associated with both soluble alkali content and F-CaO content.

To demonstrate this, the F-CaO content is divided into three ranges: 0.3% and below, 0.3% to 0.5%, and over 0.5%. The relationship between heat of hydration and apparent viscosity for cement paste made with PC-34, as shown in Figure 4, can be represented by a regression line for each range. The apparent viscosity, or conversely the fluidity, of the cement paste can then be estimated from the heat of hydration based on the dosage of superplasticizer and the F-CaO content.

In a similar way, the relationship between heat of hydration and apparent viscosity for cement paste with BNS can be organized by superplasticizer content and F-CaO content. For the polycarboxylate-based superplasticizer, the coefficients of correlation are large, except below 0.3% where the number of test samples is insufficient, suggesting that it is possible to estimate cement paste fluidity from the heat of hydration. The coefficients of correlation for BNS tend to be lower than for PC34. This might be acceptable if more test samples are taken and the range below 0.3% (where the number of test samples was insufficient) is ignored, but also the fluidity of the cement paste made with BNS sometimes changes suddenly. This phenomenon will need to be taken into account.

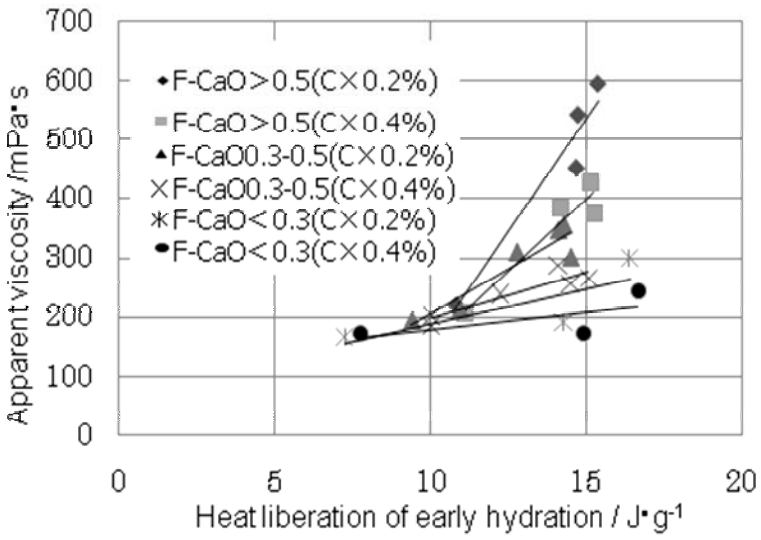

Figure 4: Relation between apparent viscosity of paste and the heat liberation of cement hydration with PC34

Finally, the effect factors for the early hydration and the fluidity of cement pastes are summarized. Heat is released when C_3A hydrates. The amount of heat released depends on the C_3A content and the soluble alkali content. The F-CaO content is related to the soluble alkali content as already noted. The fluidity of the cement paste decreases as the heat of hydration increases, a phenomenon associated with the increased specific surface area of the formed hydrates. To obtain a given fluidity, extra superplasticizer needs to be adsorbed. If the superplasticizer is added at a fixed dosage, the adsorption of superplasticizers per specific surface area decreases and the fluidity drops. Early heat of hydration is dominated by the C_3A content and the F-CaO (soluble alkali) content. As hydrates form, the quantity of ultra-fine particles rises. This then influences the fluidity in addition to superplasticizer adsorption.

4 Conclusions

The authors studied the effects of the properties of cement with varying C_3A contents, prepared for research purposes from clinker manufactured at commercial plants, on the fluidity of cement paste containing a polycarboxylate or naphthalene superplasticizer. The results of the study are summarized below.

(1) The C_3A and F-CaO content of cement affects the fluidity of the cement paste. The domination of cement paste fluidity by C_3A and F-CaO is related to an increase in specific surface area that occurs with hydration.

(2) Appropriate cement paste fluidity can be ensured regardless of the type of superplasticizer by maintaining the C_3A content below about 8%.

(3) For cement manufactured at commercial plants, the soluble alkali content is related to the F-CaO content. The reactions of C_3A are accelerated in the presence of soluble alkalis.

(4) The early heat of hydration is determined by the C_3A content and the F-CaO (soluble alkali) content.

(5) The F-CaO content is related to the soluble alkali content. The inhibition of superplasticizer adsorption by soluble alkalis can be evaluated from the F-CaO content.
(6) There is good correlation between the apparent viscosity of cement pastes and the early heat of hydration in each of three proposed ranges of F-CaO content. Measurement of the early heat of hydration therefore one method of evaluating the fluidity of cement pastes.

This research, focusing on a possible method of quality control that might ensure the fluidity of cement pastes, should prove very significant.

5 Acknowledgment

The work was carried out with a Grant for Encouragement of Research from the Japan Cement Association and Grant-in-Aid for Scientific Research (C) from the Japan Society for the Promotion of Science. The authors wish to thank these two organizations for supporting their work.

6 References

[1] Yamada, K.; Kim, C.B.; Ichitsubo, K. and Ichikawa, M.: Combined Effect of Cement Characteristics on the Performance of Superplasticizers - An Investigation in Real Cement Plants, Proc. 8th CANMET/ACI Int'l Conf. On Superplasticizers and Other Chemical Admixtures in Concrete, Supplementary Papers, 159-174 ,2006.
[2] Japan Cement Association: Report of the Fluidity Research Committee(in Japanese) , 2003.
[3] Japan Concrete Institute: Report of the Cementitious Materials and Aggregates Research Committee(in Japanese),2005.
[4] Sakai, E.; Nozaki, T.; Atarshi, D. and Daimon, M.: Proc. 8th CANMET/ACI Int'l Conf. On Superplasticizers and Other Chemical Admixtures in Concrete, Supplementary Papers, pp.227-237(2006).
[5] Sakai, E.; Kawakami, A. and Daimon, M.: Dispersion mechanisms of comb-type superplasticizers containing grafted poly(ethylen oxide) chains, Macromol. Symp.,Vol.175,367-376,2001.
[6] Sakai, E.; Kang, J.K. and Daimon, M.: Influence of superplasticizers on the very early hydration of Ca3Al2O6 in the presence of gypsum,CaSO4 0.5H2O and CaO, Cement Sci.& Concrete tech.,No.56,36-41,2002.
[7] Sakai, E.; Yamada, K. and Ohta, A.: Molecular structure and dispersion-adsorption mechanisms of comb-type superplasticizers used in Japan,Vol1(1)16-25(2003).

´

Nguyen Viet Tue
Prof. Dr. -Ing.
University Leipzig
Leipzig, Germany

Jianxin Ma
Dipl. -Ing.
University Leipzig
Leipzig, Germany

Marko Orgass
Dipl. -Ing.
MFPA Leipzig
Leipzig, Germany

Influence of addition method of suplerplasticizer on the properties of fresh UHPC

Summary

This paper deals with the influence of superplasticizer addition time on the properties of fresh UHPC. Superplasticizer was added in UHPC by two addition methods, i.e., direct addition and stepwise addition. The results showed that the stepwise addition remarkably enhanced the dispersing effect of the superplasticizer and increased the flowability of UHPC. To explain these results more experiments were carried out on cementitious pastes with 3 cements and 2 superplasticizers. Besides the addition methods used in UHPC the delayed addition was also involved. Same results were obtained as in UHPC. The enhancing effect of stepwise and delayed addition is related to the cement/superplasticizer interaction in the initial cement hydration period and affected by the cement activity as well as by the adsorption behaviour of superplasticizer. The cement activity was evaluated with isothermal calorimetry. At last a favoured cement/superplasticizer combination was suggested to simplify the UHPC mixing procedure.

Keywords: *UHPC, direct addition, stepwise addition, delayed addition*

1 Introduction

Ultrahigh Performance Concrete (UHPC) is characterized with high packing density of fine powder composed of cement, microsilica and inert fine filler, i.e. quartz powder. The volumetric water to powder ration (V_w/V_p) in the cementitious matrix in UHPC is extreme low. To ensure the desired self-compacting properties polycarboxlateeher-based-superplasticizer is used and the mixing procedure, especially the addition method of the superplasticizer, should be optimized. Superplasticizer can be added in three methods. In the direct addition it is added together with mixing water, while in stepwise addition it is separated in 2 parts. The first part is added together with or direct after water addition. The second part is dosed in different time intervals after wet mixing. In delayed addition all superplasticizer is added at a specified time after water addition. Experiences in conventional high performance concrete using SNF or SMF- based superplasticizer show that the delayed addition can remarkably

improve the dispersing performance of the superplasticizer [1-3]. For polycarboxylateether-based superplasticizers the results in literatures are confused. In [5] an enhanced dispersing effect was noted, if the superplasticizer was delayed added in concrete, while in [4] no influence of the addition time of the superplasticizer was observed. The author's own experiments showed that the addition time has large influence on the rheological properties of UHPC [6]. It can be assumed that the influence of the addition time on the dispersing performance of a certain superplasticizer is affected not only by the superplasticizer itself, but also by its combination with cement. In the present paper the influence of addition time of superplasticizer on the properties of fresh UHPC was studied. Extra experiments were carried out on cementitious pastes whose composition were similar as the matrix in UHPC. The purpose was to find a cement/superplasticizer combination, at which the properties of fresh UHPC are less sensitive to the addition method of the superplasticizer.

2 Materials

The composition of experimented UHPC containing coarse aggregates and cementitious pastes (abbr.: P1, P2, …, P6) are listed in Table 1. The superplasticizer dosages in the pastes are the saturation dosages for corresponding cement-superplasticizer combination. They were detected by means of the Marsh-cone. All cements are ordinary Portland cements with high early strength. The cements C1 and C3 have high sulphate resistance. The superplasticizers are polycarboxylateether based.

Table 1: Composition of UHPC and cementitious pastes

Materials	denote	UHPC	P1	P2	P3	P4	P5	P6
CEM I 42,5 R HS	C1	1	1			1		
CEM I 52,5 R	C2			1			1	
CEM I 42,5 R HS/NA	C3				1			1
Superplasticizer 1	SP1	3.6%						
Superplasticizer 2	SP2	2.1%	4.1%	4.8%	2.7%			
Superplasticizer 3	SP3					4.1%	4.8%	2.7%
Microsilica		0.18	0.18	0.18	0.18	0.18	0.18	0.18
Quartz powder		0.54	0.54	0.54	0.54	0.54	0.54	0.54
Water (incl. water in SPs)		0.29	0.27	0.28	0.25	0.27	0.28	0.25
Quartz sand (0.3 - 0.8 mm)		0.82						
Basalt split (2 - 5 mm)		1.96						

3 Experiments on UHPC

The UHPC was mixed in an intensive mixer. Mixing intensity and mixing time for each mixing step can be programmed prior mixing and automatically recorded during mixing. superplasticizers were added with two sequences, i.e. direct addition and stepwise addition. In the direct addition all superplasticizer was dissolved in mixing water and added in concrete after 30 seconds dry mixing. Then all components were mixed continually for 5 minutes with

higher mixing intensity. In stepwise addition the superplasticizers were added separately. After 30 seconds dry mixing water was added during ca. 15 seconds, direct followed by the addition of SP1 within 5 seconds. Then the mixing lasted with lower mixing intensity till to the addition of SP2. SP2 was added at different time after water had been added. Just before the addition of SP2 the mixing intensity was adjusted to the higher one . The mixing from water addition to the end of the mixing lasted 240 seconds.

The properties of the fresh UHPC were evaluated with slump flow, air content and the sedimentation. These parameters were determined immediately after the end of mixing according to the guideline for self-compacting concrete (SCC) recommended by DAfStb [9]. The sedimentation was investigated according to the wash out method in this guideline. The mesh width of the sieve was 2 mm instead of 8 mm for SCC in the guideline.

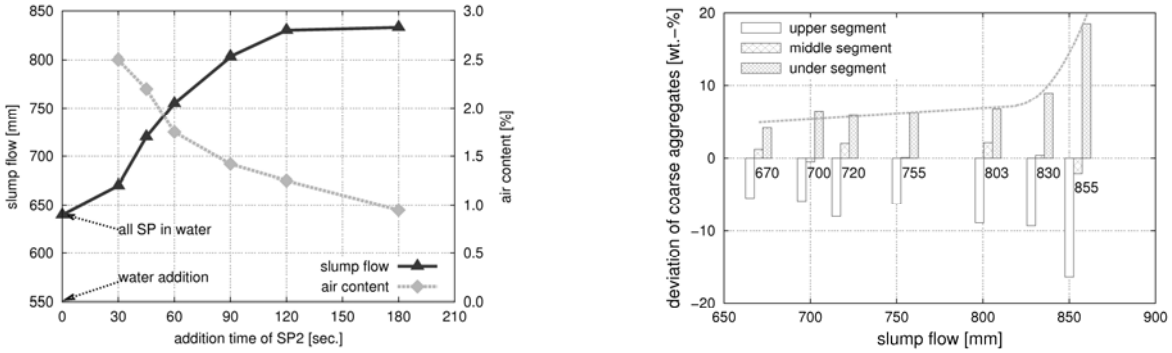

(a) slump flow and air content (b) sedimentation of UHPC

Figure 1: properties of fresh UHPC in dependence of SP addition time

It is obviously to see that the addition time of the superplasticizer has large influence on the fluidity of UHPC. The later the SP2 in UHPC added, the higher the fluidity (Fig. 1a). Meanwhile, the viscosity of UHPC was significantly reduced. As result the air content in the fresh UHPC decreased from 2.5% to 1%. On the other hand UHPC tends to sediment. In Fig. 1b it can be seen that the slump flow of UHPC containing coarse aggregates should not exceed 830 mm. Otherwise the sediment increases dramatically.

In fact, the high sensitivity of the fresh UHPC properties to the superplasticizer addition time, as described above, is disadvantage for the production of UHPC in practice. If the superplasticizer was somewhat earlier or later added during the mixing process, the properties of UHPC would strongly fluctuate. Furthermore, to achieve the desired self-compacting properties SP2 should be added at least 60 seconds later after water addition. This makes the mixing procedure somewhat complicated. To simplify the mixing procedure it is necessary to find a new cement/superplasticizer combination, at which the properties of fresh UHPC are less sensitive to the addition time of the superplasticizer. For this purpose more experiments were performed on pastes with different cement/superplasticizer combinations (P1 – P6 in Table 1).

4 Experiments on cementitious pastes

The fluidity of the pastes was measured using a flow cone with an upper diameter of 70 mm, a lower diameter of 100 mm and a height of 60 mm. The viscosity of the pastes was indirectly evaluated with a Marsh Cone. The testing procedure is described in [7]. The time needed for a certain volume of paste to flow out of the cone with a small opening was recorded. The longer the flow time, the higher is the viscosity. The paste volume to flow out in the present experiments was 1.1 Litre. As the viscosity of the cementitious paste in UHPC is higher than that in normal or high strength concretes, the diameter of the opening was 25 mm, while for the pastes in normal and high strength concrete a 10 mm diameter is preferred.

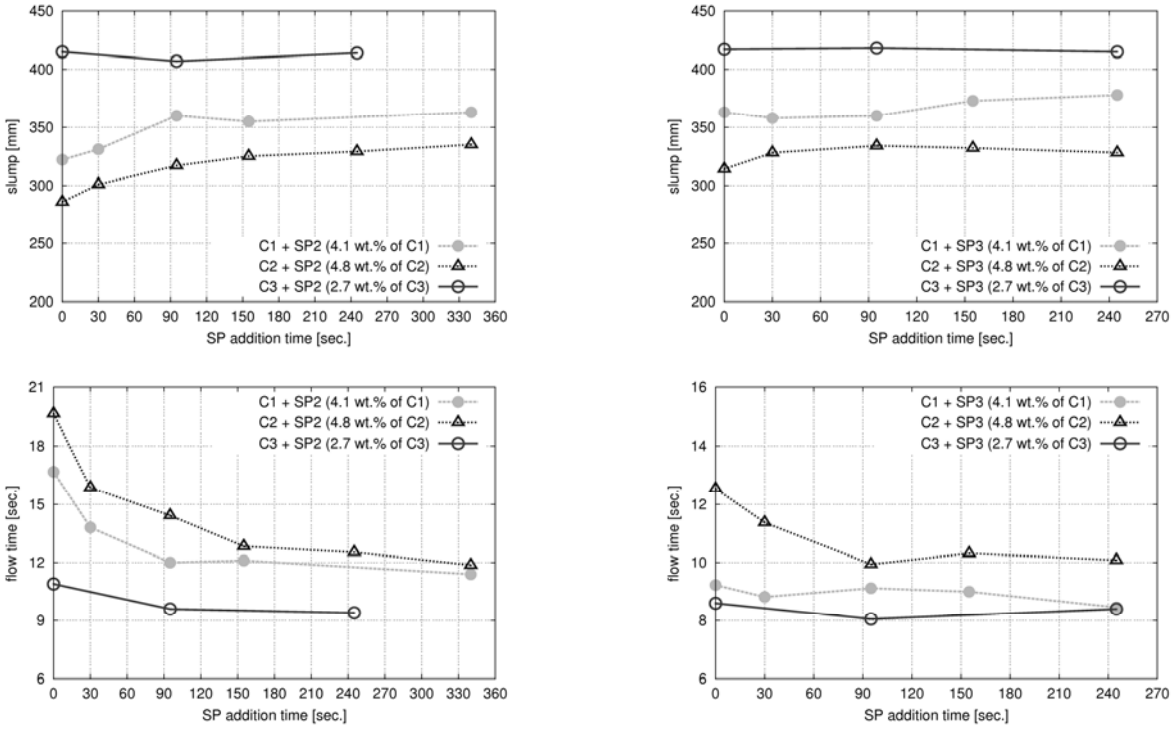

(a) pastes containing SP2 (b) pastes containing SP3

Figure 2: slump and flow time in dependence on the SP addition time (delayed addition)

For the determination of the influence of superplasticizer addition time on the fluidity cementitious pastes (P1 – P6) were mixed in a mortar mixer. The mixing time for each step was recorded using a stop watch. Pastes were mixed in 3 sequences, i.e. direct addition, stepwise addition, and delayed addition. The stepwise addition simulates the mixing sequence for UHPC. Superplasticizer was separated in 2 parts. The first part was 2/3 of the total superplasticizer dosage and was added 30 seconds after the beginning of water addition which lasted ca. 15 seconds. The rest 1/3 superplasticizer was added in different time after water addition. In the delayed addition all superplasticizer was added at different time after water addition.

As same as observed in the experiments on UHPC, stepwise addition of superplasticizer results in higher fluidity and lower viscosity of the pastes than the direct addition. The later

the second part superplasticizer added, the larger this effect. The delayed addition is slightly more effective than the stepwise addition. Fig. 2 shows the results for the delayed addition.
Additionally, the aptitude of the change in the paste rheological properties caused by the addition time of the superplasticizer is affected by cement and superplasticizer type. As can be seen in Fig. 2 the rheological properties, especially the viscosity, of pastes (P2 and P5) composed of CEM I 52.5 R (C2) were strongly affected by the addition method of superplasticizer, while pastes (P3 and P6) containing CEM I 42.5 R HS/NA (C3) were hardly affected. The influence of the addition time of superplasticizer on pastes containing CEM I 42. R HS (C1) is depended on the superplasticizer used. Regarding the superplasticizer, pastes with SP2 show higher sensitivity to the addition time of superplasticizer than pastes with SP3 (P1 vs. P4, P2 vs. P5).

5 Discussion

As described above the stepwise and delayed addition of superplasticizer reduce the viscosity and improve, at least do not decrease, the fluidity of the pastes and thus also that of the UHPC. The enhancing effect on the rheological properties is depended on the cements and superplasticizers used as well as their combinations. In the case of SNF- and SMF-superplasticizers this is explained by the intercalation of superplasticizer molecule into the hydration products formed in the initial cement hydration. The later the superplasticizer added, the less it would be intercalated into the initial hydration products. More superplasticizer will be adsorbed on the surface of fine particles and disperse the agglomerates. The dispersing effect of the superplasticizer is therefore improved [8].
However, the superplasticizer used in UHPC is based on polycarboxylateether (PC). The molecule is much larger because of their side chains. This could make their intercalation more difficult. There is no definite evidence for the intercalation of PC-based superplasticizer into the hydration products. In [10,11] and [12] the intercalation of PC-based superplasticizer with long side chains of 45 and 90 ethyleneoxide (EO) in layered hydration products C_4AH_{19} and C_2AH_8 from synthesized pure C_3A was observed. However, in these experiments the conditions were different from that in real cement hydration, as no gypsum was added in the reaction system. The strong competitive intercalation of SO_4^{2-} was thus eliminated.

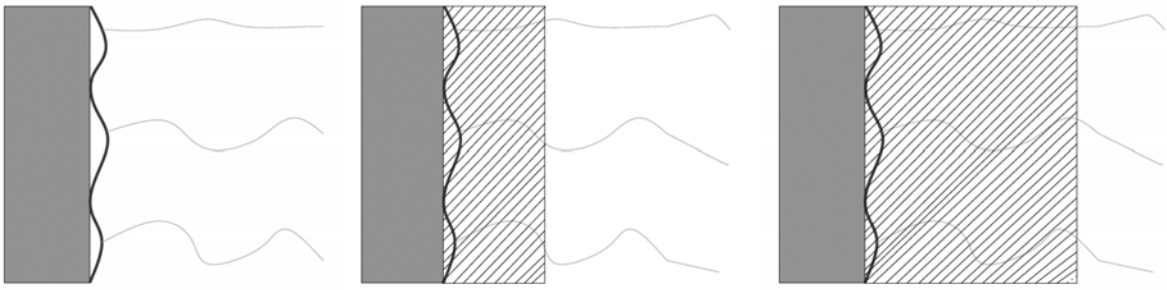

(a) just after contact-with (water+SP) (b) few minutes after contact with (water+SP) (c) few minutes after contact with (water+SP)

Figure 3: illustration of the direct addition, cement with lower (b) and higher (c) activity

In [13] a model was proposed to explain the long time dispersing effect of comb copoplymer, such as PC-superplasticizer. The dispersing effect of PC-based superplasticizer is related to its steric repulsive force. The main chain of the molecular adsorbs on the surface of cement particle, while the polyethylene oxide side chains extend into the aqueous solution among solid particles (Fig. 3a). During the cement hydration the front of the hydrate products progress from cement surface towards the space occupied by the aqueous solutions. The side chain of the superplasticizer will be partially buried in the hydration products (Fig. 3b and Fig. 3c). Only the part which is sticking out from the hydrate products is active for dispersion. The longer the out sticking chain, the better is the dispersing effect. The length of the side chain sticking out from the hydrate products can be affected by many factors, such as the original side chain length, the cement activity, the addition time of the superplasticizer, the adsorption velocity of the superplasticizer, and the ion concentration, e.g. SO_4^{2-}, as the side chain would be shrunk by it [14]. The adsorption velocity is not only defined by the molecular structure of the superplasticizer. It is also affected by the combination with cement.

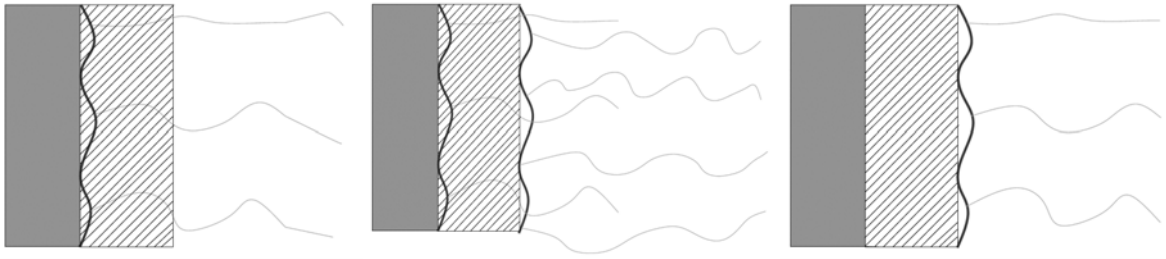

(a) direct addition (b) stepwise addition (c) delayed addition

Figure 4: illustration of the direct addition (a), stepwise addition (b) and delayed addition (c)

The enhancing effect of stepwise and delayed addition on the fluidity of paste can be illustrated in Fig.4. If superplasticizer is dosed in paste together with or direct after the water addition, it adsorbs on the surface of cement or on the thin layer of hydration products formed in the prior few seconds. In the next several minutes the hydrate products extend outwards and bury the side chain in it. The sticking out side chain, which is responsible for dispersing, will be shortened (Fig. 4a). In the case of stepwise addition the second part superplasticizer is later added and adsorbs on hydrate products formed prior. This part of superplasticizer would be less buried and more effective for dispersing than the first part (Fig. 4b). It is imaginable that the later the second part superplasticizer added, the less it would be buried and the more effective it would be. This is verified by the experimental results on UHPC (Fig. 1). In the case of delayed addition the same tendency can be imagined (Fig. 4c).
As mentioned in section 4, the aptitude of the enhancing effect through stepwise and delayed addition of the superplasticizer is affect by cement activity and superplasticizer used. The activities of the 3 cements were evaluated by the heat evolution rate measured by isothermal calorimetry (Fig. 5). The hydrations in the first 30 minutes are shown in Fig. 5b. The w/c-ratio in the calorimetry tests was 0.4, as cement could not totally immerse in water at lower w/c-ratio. It can be seen that C2 has the high activity, while C1 and C3 have medium and low one, respectively. In the first 15 minutes, which correspond to the period from water addition through mixing to the measurement of the slump flow of the pastes, the hydration heat

released by C2, C1 and C3 are 19.7, 11.1 and 2.2 J/g, respectively. The C3 behaves almost inert in this period. Therefore pastes P3 and P6 containing C3 are hardly affected by the addition time of superplasticizer, while the P2 and P5 containing C2 were strongly affected. The influence of addition time of superplasticizer on pastes containing CEM I 42. R HS (C1) is depended on the superplasticizer used.

Due to the lack of information about the molecular structure of the superplasticizers it is difficult to analyze why the fluidity of the pastes with the SP3 is relative less insensitive to the addition time than the pastes with SP2 (P4 vs. P1 and P5 vs. P2). One can suppose that the dispersing effect of superplasticizer with high adsorption velocity would be more affected by its addition time. Superplasticizer with very long side chain would be less affected.

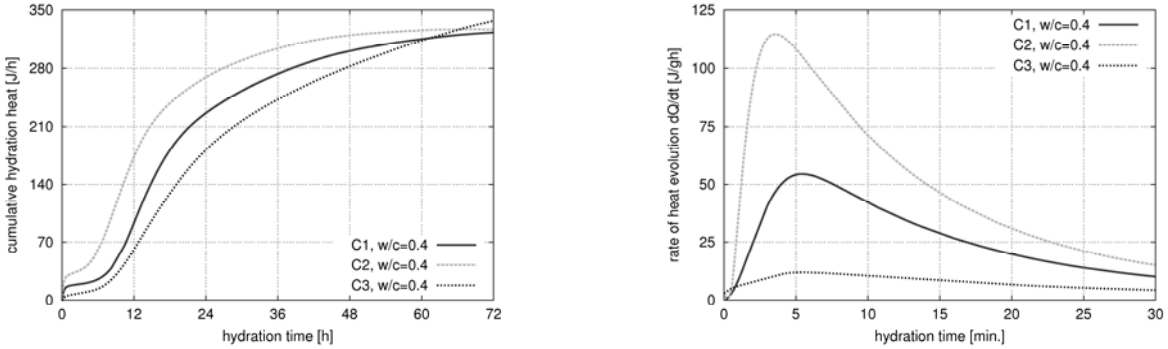

(a) hydration in 3 days (b) initial hydration

Figure 5: hydration of tested cements

6 Conclusions

In the present paper the influence of addition time of superplasticizer on the properties of fresh UHPC has been studied. In order to explain the results obtained on UHPC the rheological properties of cementitious pastes with similar composition as the matrix in UHPC were investigated. The experiments on cementitious pastes involved different cement/superplasticizer combinations and 3 addition methods of superplasticizers, i.e. direct addition, stepwise addition and delayed addition. Based on the results following conclusions can be drawn:

- The fluidity of UHPC can be improved by stepwise addition of the superplsticizer. The later the second part superplasticizer added after water, the higher was the fluidity. Meanwhile the viscosity of fresh UHPC was decreased. This significantly lowered the air content in fresh UHPC. The same tendency has been also obtained on cemeitious pastes.
- The aptitude the fluidity being improved or the viscosity being decreased by stepwise and delayed addition of superplasticizer is depended on the cement activity and the superplasticizer adsorption behaviour. The higher the cement activity, the more effective the stepwise and delayed addition. On the contrary the rheological properties of paste containing the cement which hydrates extremely slow in the initial period are hardly affected by the addition method of superplasticizer.

- To simplify the mixing procedure a cement/superplasticizer combination at which the properties of fresh UHPC will be less affected by the addition time of superplasticizer is favoured. Cement with slow initial hydration would be preferred.

7 References

[1] Aiad, I.; El-Aleem, S. A.; El-Didamony, H.: Effect of delayng additin of some concrete admixtures on the rheological properties of cement pastes. In: Cement and Concrete Research 32, No. 11, S.1839-1843, 2002

[2] Aiad, I.: Influence of time addition of superplasticizers on the theological properties of fresh cement pastes. In: Cement and Concrete Research 33, No. 8, S.1229-1234, 2003

[3] Uchikawa, H.; Sawaki, D.; Hanehara, S.: Influence of kind and added timing of organic admmixture on the composition, structure and property of fresh cement paste. In: Cement and Concrete Research 25, No. 2, S.353-364, 1995

[4] Hirsch, C.M.: Untersuchungen zur Wechselwirkung zwischen polymeren Fliessmitteln und Zementen bzw. Mineralphasen der frühen Zementhydratation. Dissertation, Technische Universität München, 2005

[5] Fernandez-Altable, V.; Casanova, I.: Influence of mixing sequence and superplasticizer dosage on the rheological response of cement pastes at different temperatures. In: Cement and Concrete Research 36, No. 7, S.1222-1230, 2006

[6] Tue, N. V.; Dehn, F.; Schneider, H.; Ma, J.; Orgass, M.; Schenk, G.; Küchler, M.: Das Verbundrohr als Innovationsmotor für hybrides Bauen. Report, Institute of Structural Concrete and Building Materials, University Leipzig, 2004

[7] Roy, R. Le; Roussel, N.: The Marsh Cone as a viscometer: theoretical analysis and practical limits. In: Materials and Structures 38, No. 1, S.25-30, 2005

[8] Flatt, R.J.; Houst, Y.F.: A simplified view on chemical effects perturbing the action of superplasticizers. In: Cement and Concrete Research 31, No. 8, S.1169-1176, 2001

[9] Deutscher Ausschuss fuer Stahlbeton: DAfStb-Richtlinie selbstverdichtender Beton, November 2003

[10] Plank, J.; Dai, Z.; Andres, P. R.: Preparation and characterization of new Ca-Al-polycarboxylate layered double hydroxides. In: Materials Letters 60, No. 29-30, S.3614-3617, 2006

[11] Plank, J.; Dai, Z.; Zouaoui, N.; Vlad, D.: Intercalation of polycarboxylate superplasticizers into C3A hydration phases. In: Proc. of 8th CANMET/ACI International Conference on Superplasticizers and Other Admixtures in Concrete, Sorrento, Italy, Oct. 29 - Nov. 1, 2006

[12] Plank, J.; Keller, H.; Andres, P.R.: Novel organo-mineral phases obtained by intercalation of maleic anhydride-allyl ether copolymers into layered calcium aluminium hydrates. In: Inoganica Chimica Acta 359, No. 15, S.4901-4908, 2006

[13] Sakai, E.; Daimon, M.: Mechanisms of superplasticizer. In: Materials Science of Concrete IV. American Cement Society, Westville, OH, S.91-111, 1995, edited by J. Skalny, S. Mindess

[14] Yamada, K.; Ogawa, S.; Hanehara, S.: Controlling of the adsorption and dispersing force of polycarboxylate-type superplasticizer by sulfate ion concentration in aqueous phase. In: Cement and Concrete Research 31, No.3 S.375-383, 2001

Part 3:

Mixture

Park, Jung Jun
Mr., Researcher
Korea Institute of Construction Technology
Goyang, Korea

Kang, Su Tae
Mr., Researcher
Korea Institute of Construction Technology
Goyang, Korea

Koh, Kyung Taek
Dr., Researcher fellow
Korea Institute of Construction Technology
Goyang, Korea

Kim, Sung Wook
Dr., Researcher fellow
Korea Institute of Construction Technology
Goyang, Korea

Influence of the Ingredients on the Compressive Strength of UHPC as a Fundamental Study to Optimize the Mixing Proportion

Summary

In this paper, to make Ultra-High Performance Concrete(UHPC) with the range of compressive strength 180MPa, it was investigated how each ingredient of UHPC influenced on the compressive strength. The variables considered in this test were water-binder ratio, replacement of silica fume, size and proportion of sand, type and replacement of filling powder, and whether using of steel fiber UHPC or not. As a result, in water-binder ratio 0.20, we could make UHPC with compressive strength of over 180MPa through using of silica fume, quartz sand with the particle size of under 0.5mm, filling powder and steel fiber.

Keywords: *Ultra-High Performance Concrete(UHPC), steel fiber, compressive strength of 180MPa*

1 Introduction

The concrete is economic and durable construction material and is most widely used with steel materials. However, the concrete has intrinsic defects of low tensile strength and flexural strength, which causes it to crack easily. In addition, the brittle failure of concrete has been a problem due to increased compressive strength after high strength concrete has been commercialized. In order to overcome the defects and problems, various types of fiber reinforced cementitious composites with improved toughness are being used[1,2]. In particular, Ultra-High Performance Concrete(UHPC) is being noticed, which are made by mixing steel fibers with ultra-high strength cementitious matrix with compressive strength of more than 100MPa to give high toughness[2].

UHPC has improved compressive strength compared with existing normal concretes and fiber reinforced concretes, increased toughness in case of failure of bending, tension, and compression, and high durability through densification of cementitious matrix due to ultra-high strength. Mechanical performance as well as durability will step forward when UHPC

with these performance is applied to concrete structures instead of normal concretes. In Korea, RPC (Reactive Powder Concrete) was applied in constructing foot bridge in Sunyoo-do, which has increased the interests in UHPC, but the research in this field is almost absent domestically.

Therefore, to make UHPC with the range of compressive strength 180MPa, it was investigated how each ingredient of UHPC influenced on the compressive strength. First of all the experimental variables were water-binder ratio, replacement of silica fume, size and proportion of sand, type and replacement of filling powder, and whether using of steel fiber in UHPC or not.

2 Experimental Design

2.1 experimental variables

The experimental variables considered in this paper are shown in Table 1. “O“ and “X“ in a row means if the corresponding material was used or not in the mixture to estimate the effect of each variable.

Table 1: Test variable

Variable	W/B (%)	Material						
		OPC	Silica fume	Sand		Filling powder		Steel fiber
		C	SF	S		F		STF
				A	B	A	B	
W/B	0.16~0.24	○	○	×	○	×	×	×
Mineral admixture	0.20	○	○	×	○	×	×	×
Sand	0.20	○	○	○	○	×	×	×
Filling powder	0.20~0.24	○	○	○	○	○	○	×
Steel fiber	0.20~0.24	○	○	○	○	×	○	○

2.2 Materials used

Domestic ordinary portland cement and silica fume as an admixture are used in the experiment. Their physical and chemical properties are shown in Table 2. Domestic sand with grain size of 0.5mm and below was used for fine aggregate, and coarse aggregate is not used. Two types of fine aggregate used are A(density: 2.62g/cm^3, average grain size: 0.3~0.5mm, SiO_2 93%) and B(density: 2.62g/cm3, average grain size: 0.17~0.3mm, SiO2 93%). Polycarboxylic ether-type superplasticizers with density of 1.01g/cm^3 and 30% of solid ingredient in dark brown liquid were used. Domestically processed filling powders with average grain size of 100μm and 13μm were used and their physical and chemical properties are shown in Table 3.

High elastic steel fibers, which has density of 7.8g/cm^3, length of 13mm, diameter of 0.2mm, and yield strength of 2500 Mpa, used to increase toughness at 2% concrete volume friction ratio.

Table 2: Physical and chemical properties of cement and mineral admixture

Item	Surface area (cm^2/g)	Density (g/cm^3)	Ig.loss (%)	Chemical composition (%)		
				MgO	SO_3	SiO_2
C	3,333	3.14	1.40	2.8	2.3	-
SF	200,000	2.10	1.50	0.1	-	96.0

Table 3: Physical and chemical properties of filling powders

Item		Size(μm)	Ig.loss (%)	Chemical composition (%)				
				Al2O3	MgO	CaO	Fe2O3	SiO2
Filling powder	A	100	0.01	0.15	0.003	0.004	0.01	99.3
	B	13	0.01	0.15	0.004	0.03	0.01	99.3

2.3 Mix

The table 4 below shows relative mix compositions of materials used in this experiment written by weight ratio. The mix design of UHPC used in this experiment is not configured on such a mix of unit volume as in normal concretes, instead it is configured on relative ratio of materials based on the quantity of cement.

Table 4: Mix compositions of UHPC (by weight)

Item	W/B	B		S	FP	SP	STF (V_f)
		OPC	SF				
Optimum mix design	0.16~0.24	1	0~0.35	1~1.3	0~0.4	0.016	2%

2.4 Curing Procedure

Moist curing was performed for one day, thereafter the forms of specimen were removed, and water curing with high temperature at the temperature of 90±2°C for 3 days was carried out[3,4].

2.5 Mixing Method

UHPC was mixed using mixer with the volume of $50m^3$ based on the sequence, time and speed listed in Fig. 1.

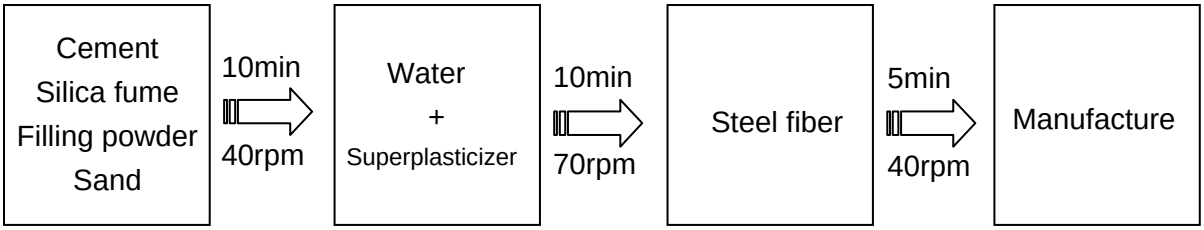

Figure 1: Mixing method

2.6 Tests of Compressive Strength

The compressive strength of UHPC were estimated with 50mm cubic specimen in an experiment of developing an optimum mix design, and the compressive strength values were calculated by averaging the values of 5 specimens.

3 Experimental Results and Discussion

3.1 Development for the optimum mix design of UHPC

(1) Effects of Water-Cementitious Materials Ratio

Figure 2 shows the change of compressive strengths with various water-cementitious materials ratios. The ratio of silica fume is fixed at 0.25. The result of experiment showed that the compressive strength increased as water-cementitious materials ratio thought decreased, which was far below the targeted compressive strength of 180MPa. It was estimated that the strength of UHPC did not depend on failures of cement paste instead it depended on interface failures between the cement paste and fine aggregates.

According to the experimental results about the effects of water-cementitious materials ratio on compressive strengths, we concluded that lowering water-cementitious materials ratio had limitation in manufacturing UHPC target compressive strength of 180MPa, therefore other methods such as using filling powders had to be considered.

(2) Effects of Silica fume

Figure 3 shows the changes in compressive strengths with the ratio of silica fume. The result showed that the compressive strength was the highest when the ratio of silica fume reached 0.25 and decreased at higher ratios. The effect of silica fume in UHPC is considered in three aspects, Which is physical and chemical aspect. The first and second are related to chemical aspect and third to physical aspect. First, in order for silica fume to undergo a pozzolanic reaction, calcium hydroxide is required, which is generated when the cement undergo hydration. In this experiment, we assumed that the quantity of calcium hydroxide required for pozzolanic reaction of silica fume was sufficient until the ratio of silica fume reached 0.25. Second, since the amount of cement decreased when the ratio of silica fume exceeded 0.25, the calcium hydroxide required for pozzolanic reaction was relatively deficient, therefore it would cause the decrease of the compressive strength[5]. The third is concerned with physical effect of silica fume. The particle size of silica fume is very small compared with cement and it can increase the packing density of composites when it is used as a substitute of cement. The results show that the increase of compressive strength up to 0.25 of silica fume/cement ratio may somewhat related to packing effect.

After studying the effect of silica fume on the strengths, the most optimum ratio of silica fume is suggested to be 0.2~0.3. In the future, fly ash or blast furnace slag will be considered in manufacturing more economic UHPC.

(3) Effects of Aggregate

In this paper, we used fine aggregates with the size below 5mm instead of coarse aggregates in developing UHPC in order to ensure homogeneity of concrete and improve the strengths.

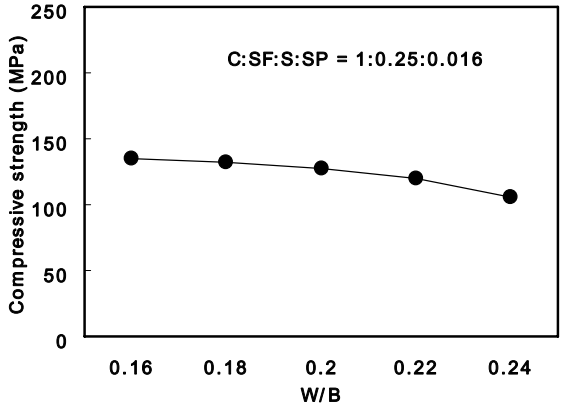

Figure 2: Compressive cementitious material ratio

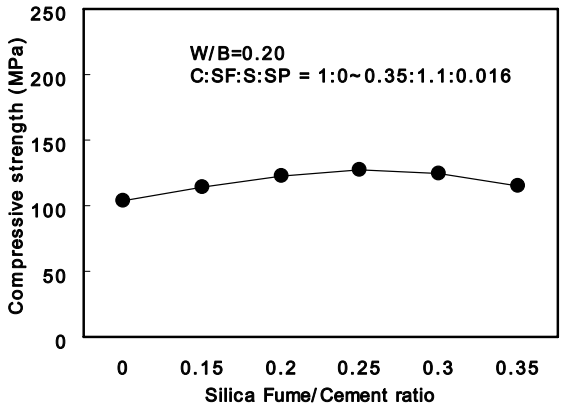

Figure 3: Compressive strengths according to content of silica fume

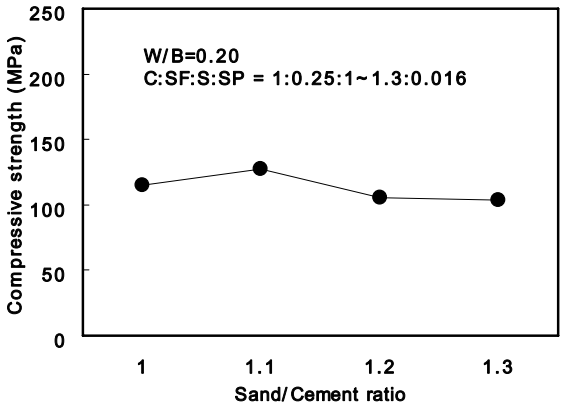

Figure 4: Compressive strengths according to ratio of sand and cement

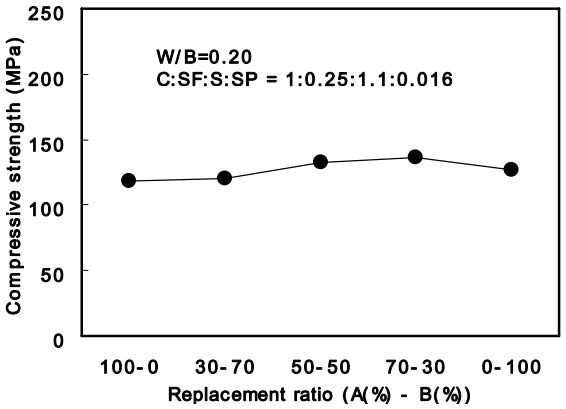

Figure 5: Compressive strengths according to sand size

Figure 4 shows the effects of ratio of sand on the compressive strengths. The result showed that the compressive strengths were the highest when the ratio of aggregate to cement was 1.1. Figure 5 shows the relationship of the size of aggregate to the compressive strengths.

We concluded that combining aggregates of different sizes were more advantageous to in increase strengths than using aggregate of unified size. In particular, the compressive strengths were the highest when 70% of aggregate A and 30% of aggregate B was combined.

(4) Effects of Filling powder

In this study, we examined the use of filling powder that could act as filler which can enhance the density of composites, between cement paste and aggregates to prevent interface

failures and improve strength of UHPC. Figure 6 shows the experimental result of compressive strength by the size of filling power. The filling powder A with grain size of 100μm had few effects on increase of strength, but filling powder B with grain size of 13μm increased the compressive strength by 55MPa(31%) compared to ' Non' specimen without filling powder. The result showed that filling powder increased the strength by acting as filler in interface between the cement and aggregate. The size of filling powder most effective in increasing the strength was 13μm. Figure 7 shows the experimental result that measured compressive strengths at filling powder-cement ratios of 0, 0.1, 0.2, 0.3, and 0.4 when the grain size of filling powder B was 13μm. It was concluded that 0.3 of filling powder-cement ratio was the most appropriate mix ratio to improve the compressive strength. It was concluded that 0.3 of filling powder-cement ratio was the most appropriate mix ratio to density the composites and therefore improve the compressive strength.
Figure 8 shows the compressive strengths as water-cementitious materials ratio changes when filling powder is used or not. If filling powder was used, the strength increased irrespective of water-cementitious materials ratio, and if water-binder ratio decreased, the compressive strength increased. For the ultra-high strength cementitious composites with low water-cementitious materials ratio, the strength was not determined by cement paste failures but by adhesive failures between cement paste and aggregate[3,5]. If we try to reduce water-binder ratio or use the filling powder smaller than 13μm, the compressive strength of UHPC seems to be increased.

(5) Effects of Steel fiber
In this experiment, we added steel fibers of 2% in volume friction ratio in manufacturing UHPC, and measured compressive strengths by changing water-cementitious materials ratio. Figure 10 shows the effect of steel fiber on the compressive strengths of UHPC. The result of test shows that adding steel fiber increases compressive strengths by 13% irrespective of water-cementitious materials ratio. In particular, adding steel fiber when water-cementitious materials ratio was 0.20 increased the compressive strength to 200MPa, which indicated the possibility of manufacturing UHPC.

(6) Example of Optimum Composition
As shown above, we obtained the composition of UHPC with compressive strength of 180MPa in the experiment by examining how the ingredients affect the compressive stregth in UHPC manufactured with actively available domestic materials except silica fume and steel fiber.

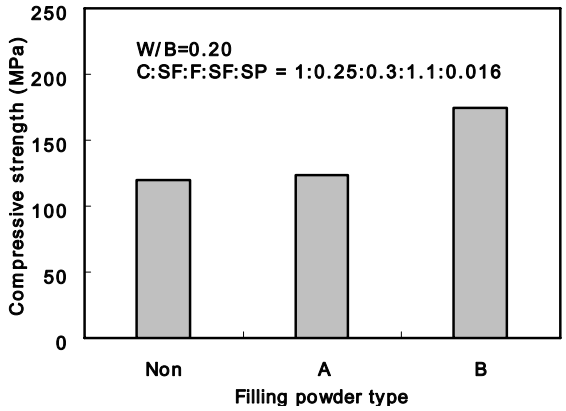

Figure 6: Compressive strengths according to filling powder type

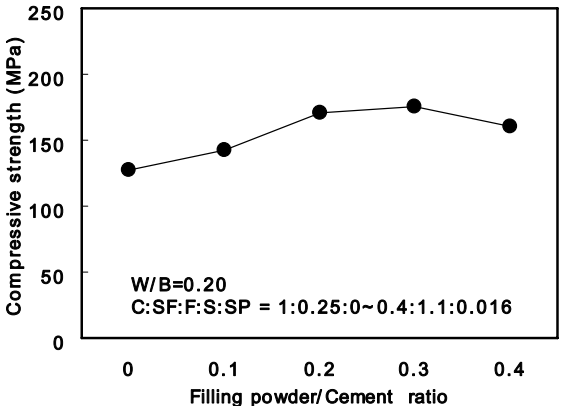

Figure 7: Compressive strengths according to ratio of filling powder and cement

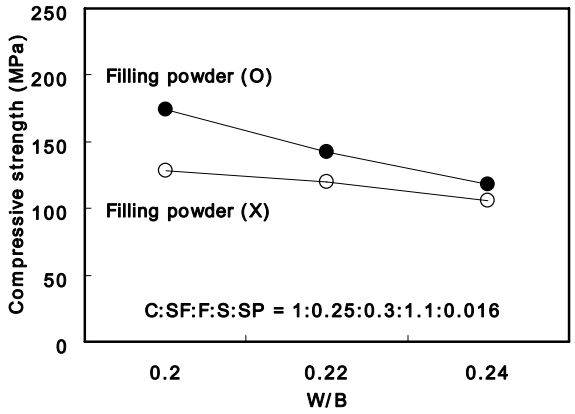

Figure 8: Compressive strengths with and without filling powder

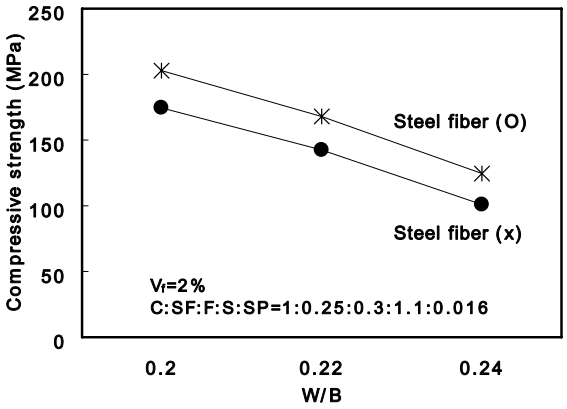

Figure 9: Compressive strength with and without steel fiber

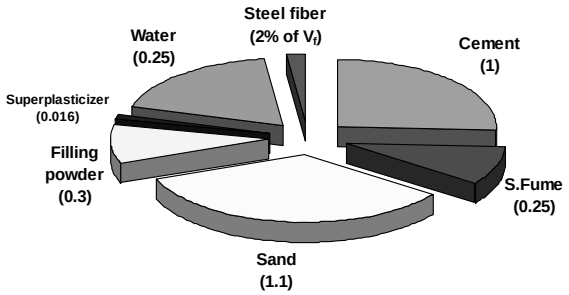

Figure 10: Example of optimum mix proportion of UHPC

Based on the result obtained so far in this test, the example of composition for UHPC with compressive strength of 180MPa can be summarized in Figure 10. If thre are substitutes for

silica fume or steel fibers can be produced domestically, UHPC can be manufactured more economically without expensive imported materials.

4 Conclusion

From this study, we can draw conclusions as follows :

Through studying the effect of silica fume on the strengths, the most optimum ratio of silica fume is suggested to be 0.2~0.3.

The compressive strengths were the highest when the ratio of aggregate to cement was 1.1 and In particular, the compressive strengths were the highest when 70% of aggregate size of 0.3~0.5mm and 30% of aggregate size of 0.17~0.3mm was combined.

If we use filling powder with grain size of about 13μm, interface failure of cement paste and aggregate will be prevented and compressive strength of UHPC will be incresed, and the compressive strength was the highest at filling power/cement ratio of 0.3.

Under water-cementitious material ratio 0.2, we could make UHPC with compressive strengths of 180MPa by properly using silica fume, quartz sand in below with a diameter of under 0.5mm, filling powder with particle size of below 13μm, superplasticizer and steel fiber.

If we try to reduce water-binder ratio or use the filling powder smaller than 13μm, the compressive strength of UHPC may be increased.

5 Acknowledement

This study was carried out as one of the research on Hybrid Cable-Stayed Bridge 2020(HYCAB 2020) in the Korea Institute of Construction Technology(KICT). The authors would like to gratefully acknowledge financial support from HYCAB 2020 of KICT.

6 References

[1] Vivek Bindiganavile; Nemkumar Banthia; Bandt Aarup: ACI Material Journal, Vol.99, No.6, November-December pp.543-548, 2002.

[2] Pierre Richard; Marcel Cheyrezy: COMPOSITION OF REACTIVE POWDER CONCRETES, Cement and Concrete Research, Vol.25, No.7, pp.1501-1511, 1995.

[3] KICT: Development of the advanced technology of durability in concrete bridges, 2006.

[4] Kim, S.W.; Park, J.J.; Koh, K.T.; Kang, S.T.; Lee, J.H.: The effect of curing method on compressive strength properties of UHPCC, Proceedings of the Korean Society of Civil Engineers, 2003.

[5] Park, J.J.; Koh, K.T.; Kang, S.T.; Ryu, G.S.; Kim, S.W.; Lee, J.H.: The effect of material factors on the compressive strength of ultra-high strength Steel Fiber Reinforced Cementitious Composites, Procee-dings of the Korean Concrete of Institude, Vol.16, No.1, S.288-291, 2004.

Ludger Lohaus
Univ.-Prof. Dr.-Ing.
Leibniz Universität Hannover
Hanover, Germany

Peter Ramge
Dipl.-Ing.
Leibniz Universität Hannover
Hanover, Germany

Robustness of UHPC - A New Approach for Mixture Proportioning

Summary

Experiences with UHPC have clearly shown the problem of the unsatisfactory robustness concerning variations in the material properties of its components. Solving these problems is a precondition for establishing the new material in building praxis. For design of a robust mixture the knowledge of the “optimal mixture” is necessary; however the robust mixture proportioning will differ thereto. The robust mixture will not achieve the maximum possible performance in the relevant concrete properties (for example the compressive strength). But for the robust mixture it is required to reproduce the aimed properties with a satisfactory assurance despite any unfavourable influences. In this paper a new approach for the proportioning of robust UHPC mixtures is suggested. Further the influence of the fresh concrete properties on the robustness of the hardened concrete is pointed out by means of laboratory tests.

Keywords: *robustness, superplasticizer, mixture proportioning, packing density, water demand*

1 Introduction

Robustness is the ability, of a concrete mixture to satisfy its defined requirement profile despite any unfavourable influences they may be predictable or unpredictable. For UHPC the main requirements are the hardened concrete properties strength and durability. In general the fresh concrete properties are of lower interest; however proper placement is a crucial condition for consistent hardened concrete properties. That makes also the consistency and the workability time to key properties that have to be considerer for a robust mix design. One crucial condition for a robust mixture proportioning for UHPC as well as for ordinary concrete is a surplus of fines. Therefore it is important to know the actual packing conditions in the mix.

Based on extensive experiences in the development of high performance concrete mixtures including UHPC [1-4] and investigations on their robustness, a new approach for the mix design of robust concrete mixtures with high powder contents is suggested. One key point of this approach is to include the superplasticizers (SP) when determining the water demand of the materials that are used for the mixture. Caused by the high deflocculating potential, the presence of PCE-based superplasticizers leads to a lower water demand respectively a higher packing density of the powder solids than without superplasticizers. These values are

more convenient to describe the actual conditions in an UHPC mix than conventional water demand values.

2 The Superplasticizer Based Approach

In general the water demand of any granular mix depends on the specific surface and the packing density. For coarse aggregates the packing density is the dominant parameter. However in [5] it is confirmed that also for fine powders in the particle size range of cement still the measurable value of the water demand is mainly influenced by the packing density and not the specific surface

Amongst the various methods to determine the water demand the most common ones are the β_p value according to Okamura [6], the water demand at standard consistency according to DIN EN 196-3 [6] and the water demand according to Puntke [5,6]. They have all in common that they do not include the effects of superplasticizers.

As high performance concretes (UHPC in particular) are always made with superplasticizers it seems necessary to include these effects in the determination of the characteristic "water demand" respectively the characteristic attainable packing density. For each granular mixture a certain consolidation point exists where just enough water is present to fill all the voids but no additional water to enable flowing of the paste or mortar. For mixtures without superplasticizers this point corresponds with the βp value according to Okamura, expressed as the volumetric water/powder ratio (V_f/V_p-value) or more general as the fluid/solid ratio (V_f/V_s), including also the coarser particles like sand if present. Already small contents of PCE-based superplasticizers cause a significant increase in the slump flow compared with the mixture without superplasticizer whereas the consolidation point drops significantly.

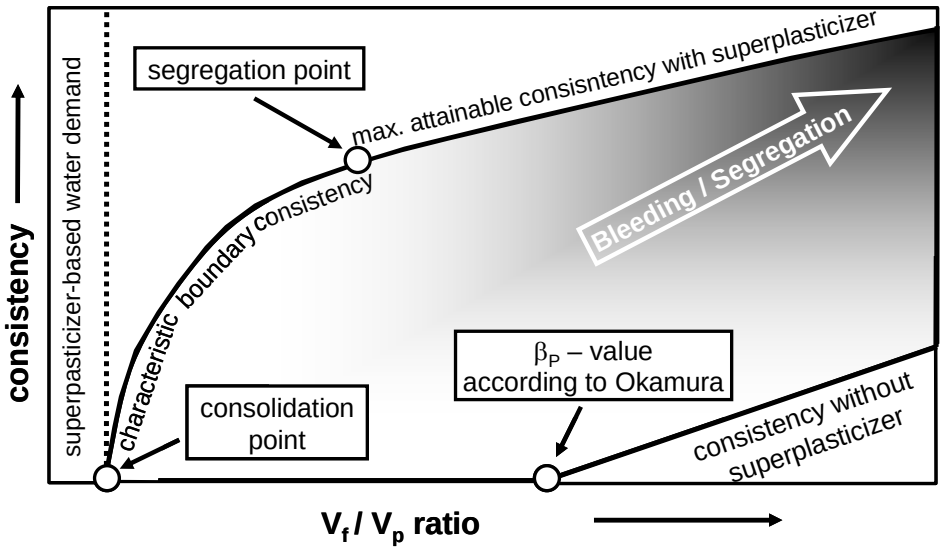

Figure 1: Model of the superplasticizer-based approach

The superplasticizer based approach [7] describes the attainable consistency of paste including superplasticizer in dependence of the V_f/V_p ratio. The model conception is illustrated in fig. 1.

Tests without superplasticizers are the basis of the model (consistency without superplasticizer). With decreasing V_f/V_p ratios the consistency of the paste decreases linearly, until no flowability is to be observed any longer. This point corresponds with the β_p-value according to Okamura. With increasing V_f/V_p ratios the point of segregation is reached. Above this point the paste is no longer stable, the solids tend to separate.
Adding superplasticizers, the consistency can be increased to a specific maximum value for each V_f/V_p ratio. At that point the so called saturation point is reached [8]. Now the paste shows almost no yield stress, so that an additional superplasticizer dosage cannot lower the yield stress any further, therefore no larger slump flow can be observed.
The maximum consistency decreases with low V_f/V_p ratios, whereby the needed superplasticizer content strongly rises. With high V_f/V_p ratios above the segregation point it is possible to obtain large slump flow values with relatively moderate superplasticizer dosages. Because of strong separation features in this range, a practical application is not reasonable. This behaviour changes with lower V_f/V_p ratios below the segregation point. Here it is possible to design concretes with high superplasticizer contents, even beyond the saturation point. These pastes are extremely flowable and at the same time stable against any segregation. If the V_f/V_p ratio is decreased further, the maximum attainable slump flow value decreases. Due to the dispersion and the related reduction of the agglomerates, a very high packing density can be obtained, significantly higher than without superplasticizer. The minimum consolidation point is called “Superplasticizer-based Water Demand”. This characteristic value is significantly lower than the β_p-value according to Okamura. It is likewise lower than the water demand according to Puntke or DIN EN 196-3. It is noteworthy that near this point the maximum attainable consistency is limited by the V_f/V_p value. For a given powder mix this so called boundary consistency can not be exceeded by means of higher SP dosage, only by changing the V_f/V_p ratio.
The model is valid for all powders or powder mixtures that would be adequate for the determination of the β_p value according to Okamura these are mainly cements and fine inert powders. As for the β_p value the experiments do not give satisfying results, if the material is too coarse (e.g. sand only), because the fluid’s viscosity is to low to carry the particles. The determination of the maximum possible packing density respectively the minimum water demand with a modified Okamura test method as described above (water + SP, with SP dosage above the saturation point) seems reasonable for the appliance in high performance concrete technology, because the test conditions represent the conditions in a real concrete mix much better than with the other testing methods.

3 Experiments

In a recent research project [9], investigations on the robustness of UHPC mixtures were carried out. Based on a given UHPC mixture that is successfully used in the German DFG research program SPP 1182, the mixture proportioning was systematically varied. The materials that were used were a quartz sand (0,125-0,5 mm) (QS), a quartz powder (QP), a CEM I 52,5R HS/NA cement (CEM), silica fume (in dry powder form) (SF) and a fine fly ash (FA). As fluid a mix of a PCE-based superplasticizer and water in the mixing ratio 1/6 was

used. In a first step the various materials were characterized concerning their superplasticizer based water demand. Than the superplasticizer based water demand values of mixtures of two components at a time were systematically determined. This was done to find the mixing ratio with the highest attainable packing density but also to find mixtures where the fines are dominant. Figure 2 shows an example for a mixture consisting of sand on the one hand and a powder mix on the other hand. The proportioning of the powder was chosen in a separate test row, and is kept for this test, whereas the sand content is systematically varied. Left of the minimum water demand is the range where the coarse particles (sand) are dominant, whereas right of the minimum the fines are dominant. For each measurement point in fig. 2 the characteristic boundary consistency curves were determined. Those values that are marked with circles represent mixing ratios that are also used for the later hardened concrete investigations.

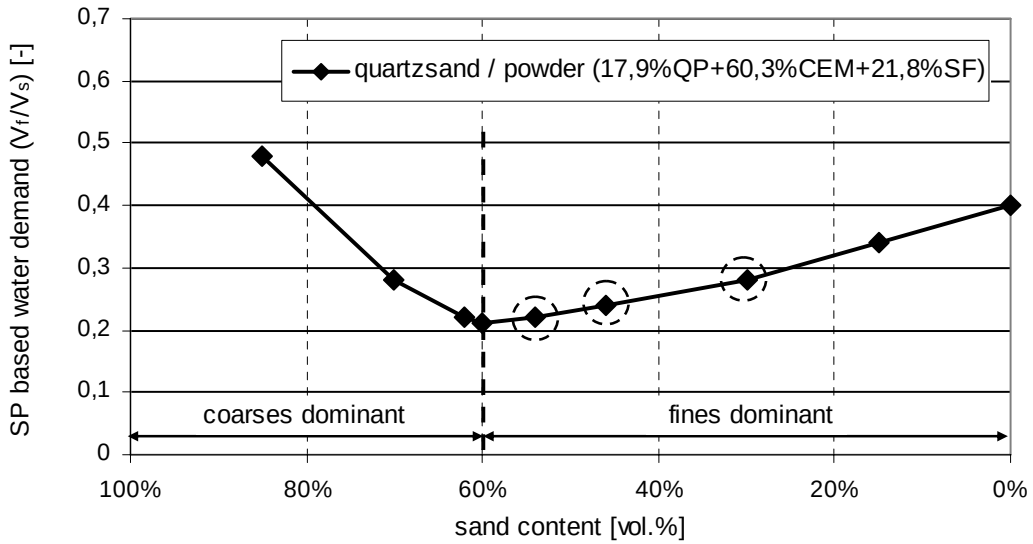

Figure 2: superplasticizer based water demand for certain mixing ratios of a sand/powder mix

The boundary consistency curves are shown in figure 3. For the sake of a better overview they are spited in two pictures. On the left hand side all those curves with coarse particles being dominant are shown, on the right hand side are those with fines being dominant. For a better orientation the curve for “past only” is shown in both pictures. It can be seen that in the range of the packing optimum (60-46% sand) the curves look similar and run close to each other. They start with an almost linear slope but between 30 and 40 cm slump flow they show a distinct bend. In the range before this bend the mixtures are stable and can be adjusted relatively freely by adding fluid. If the sand is dominant the curves start to bend much earlier (70% and 85%) and it is not possible to adjust stable mixtures with a reasonable slump flow. The high necessary amount of fluid to fill the voids in conjunction with the low powder content leads to a very thin past which itself is not stable enough to keep the whole mortar together, segregation occurs. For low sand contents the linear area in the first part of the curve gets longer, whereas the gradient degreases. For paste only the whole curve is linear (in the shown range) almost like it is known from the β_p value according to Okamura. In this case it

is caused by the relatively high silica fume content of 21.8 vol.% in the paste. The silica fume does not disperse fully and can thus act as a stabilizer. In a next step hardened concrete properties were investigated on selected mixtures. Table 1 gives an overview of the mixture variations.

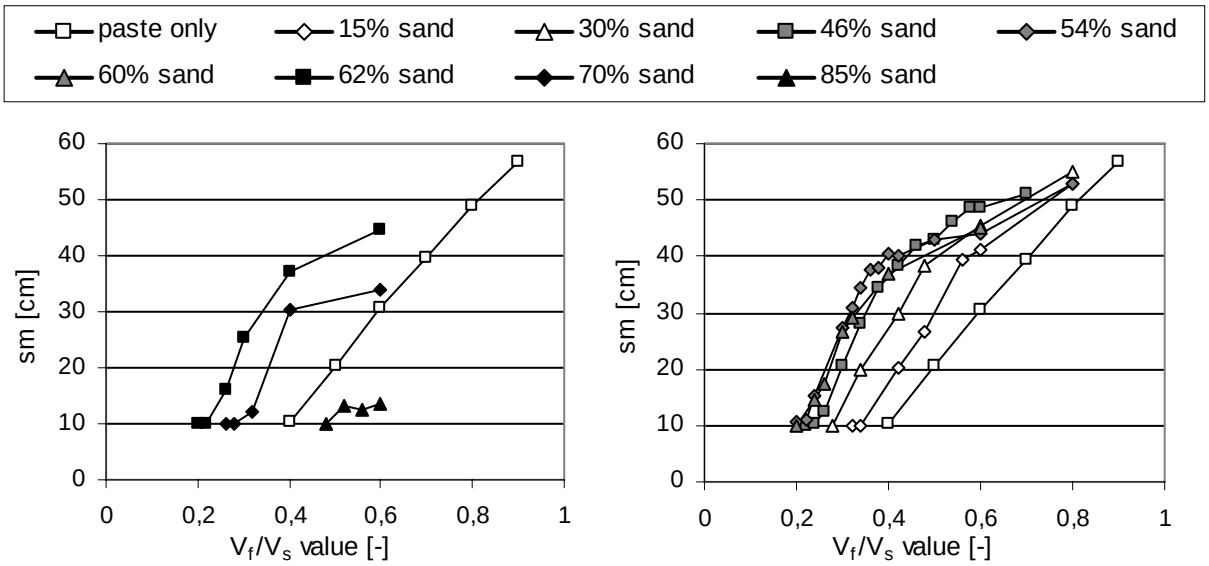

Figure 3: boundary consistency curves for the mixing ratios shown in figure 3

In the test row each mixture was produced twice, but each time adjusted to a different slump flow value. For the investigations the slump flow values (Haegermann cone) of 20 cm and of 30 cm were used. For the examination of the hardened concrete properties prismatic samples (4 x 4 x 16 cm³) were produce. The compressive strength as well as the flexural strength was determined after 2, 7 and 28 days.

Table 1: mixture variations for hardened concrete tests

Mix-No.	**total solid fraction[Vol.%]**					**powder fraction [Vol.%]**			
	QS	**QP**	**CEM**	**FA**	**SF**	**QP**	**CEM**	**FA**	**SF**
M1, M2	54,0	8,3	27,8	-	10,0	17,9	60,3	-	21,8
M3, M4	46,0	9,7	32,6	-	11,7	17,9	60,3	-	21,8
M5, M6	30,0	12,6	42,2	-	15,2	17,9	60,3	-	21,8
M7, M8	54,0	9,5	31,9	-	4,6	20,6	69,4	-	10
M9, M10	46,0	11,1	37,5	-	5,4	20,6	69,4	-	10
M11, M12	54,0	10,5	35,5	-	-	22,9	77,1	-	-
M13, M14	46,0	12,4	41,6	-	-	22,9	77,1	-	-
M15, M16	46,0	9,7	32,6	5,9	5,9	17,9	60,3	10,9	10,9
M17, M18	46,0	9,7	32,6	11,7	-	17,9	60,3	21,8	-

Table 2 shows the actual mixture proportioning for each mixture as well as the slump flow values and v-funnel times. The actual fluid to solid volume ratio (V_f/V_s) is also listed. In figure 4 to 6 the compressive strength is shown versus the w/c ratio respectively the water binder ratio (w/b). In this case silica fume and fly ash are counted 100% to the binder fraction.

4 Results

The experiments show that a dominance of fine particles in a mixture is necessary to be able to adjust high slump flow values. As soon as the coarse materials are dominant a disproportionate high amount of fluid is necessary to allow flowing, and with further addition of fluid the mixture segregates before a useful slump flow value can be reached. Whereas with a high surplus of fines it is possible to adjust mixtures to slump flow values up to 40 cm without any segregation.

Table 2: mixture proportioning and fresh concrete properties

Mix-No.	Components [kg/m³]						V_f/V_s	sm	t_v
	QS	QP	CEM	FA	SF	Fluid	[-]	[cm]	[s]
M1	1139	174	699	-	179	213	0,266	21,3	83
M2	1103	169	678	-	173	238	0,306	29,5	14
M3	973	205	824	-	210	210	0,262	20,5	128
M4	931	196	788	-	201	245	0,320	29,5	-
M5	613	257	1032		263	237	0,306	21,5	146-
M6	576	241	970		247	284	0,390	30,5	10
M7	1149	202	811	-	83	206	0,255	20,8	89
M8	1118	196	790	-	81	227	0,289	31,0	13
M9	965	234	939	-	96	217	0,273	19,8	143
M10	947	229	921	-	94	232	0,298	29,0	20
M11	1138	222	893	-	-	213	0,267	21,5	91
M12	1100	215	863	-	-	240	0,311	31,8	31
M13	948	255	1025		-	231	0,295	21,5	99
M14	931	250	1007		-	245	0,319	31,0	21
M15	971	204	822	119	105	213	0,265	21,5	99
M16	943	199	799	116	102	235	0,302	30,5	11
M17	960	202	812	235	-	222	0,280	18,8	-
M18	940	198	796	230	-	238	0,307	30,0	10

It is well known that the ruling parameter of the hardened concrete properties is the w/c ratio. However it could be shown that the proper flowability and filling ability is at least as important to secure reproducible high strength. In many cases the viscosity of the mixture that was adjusted to a slump flow of 20cm was so high, that large air pockets formed and imperfections in the form filling accrued. For those badly cast samples lower strength values were achieved as for the corresponding mixtures with the higher fluid content and thus the higher w/c ratio. With actual w/c ratios varying from 0,21 up to 0,33 compressive strength values (28 days) were achieved mainly in a range between 120 and 160 MPa. However due to the above mentioned circumstances the data shows no systematic dependencies between w/c ratio and 28 days compressive strength. This again shows that those mixtures that allows the adjustment of the consistency by adjusting the fluid content bear advantages concerning the robustness, because proper flowability and filling ability are the condition for satisfying hardened concrete properties.

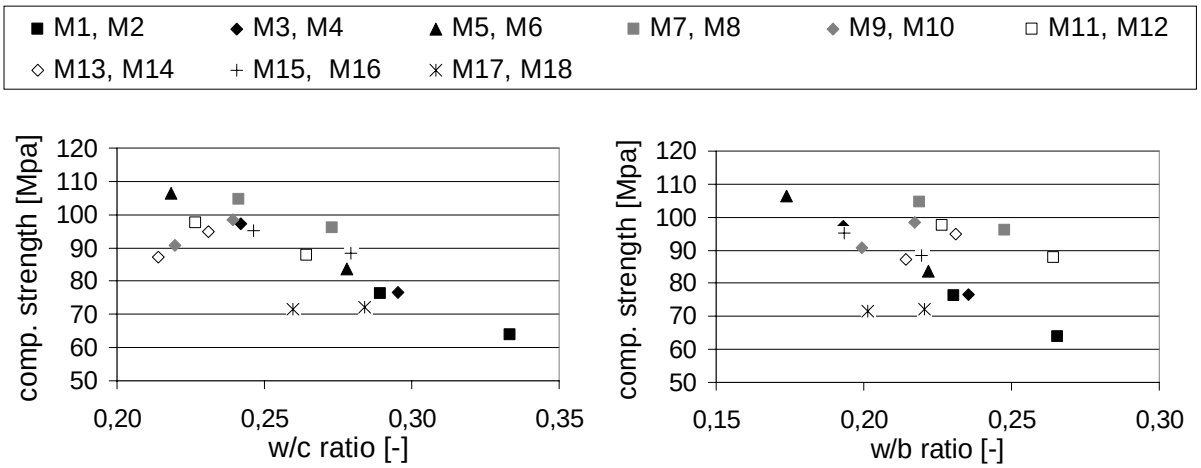

Figure 4: 2 days compressive strength versus w/c ratio (left) resp. w/b ratio (right)

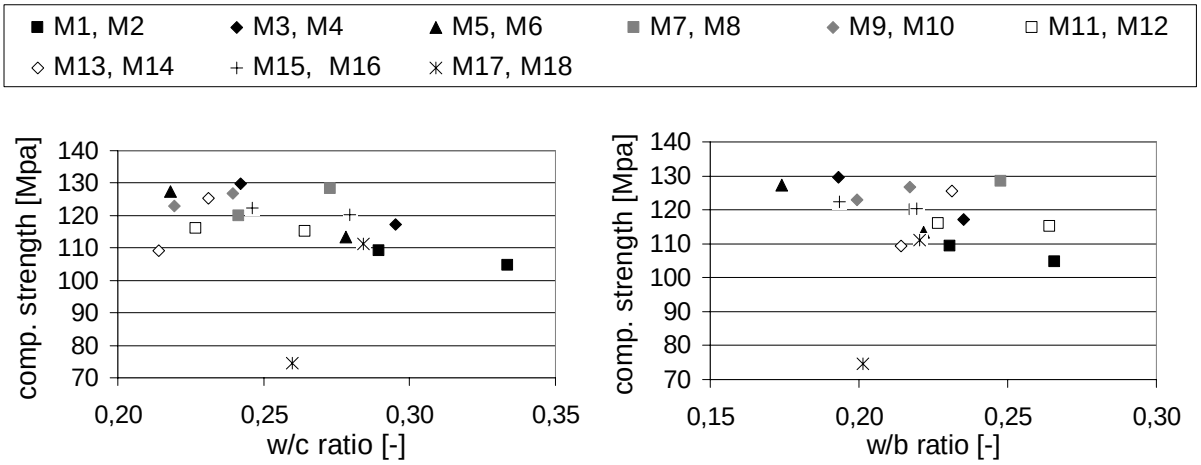

Figure 5: 7 days compressive strength versus w/c ratio (left) resp. w/b ratio (right)

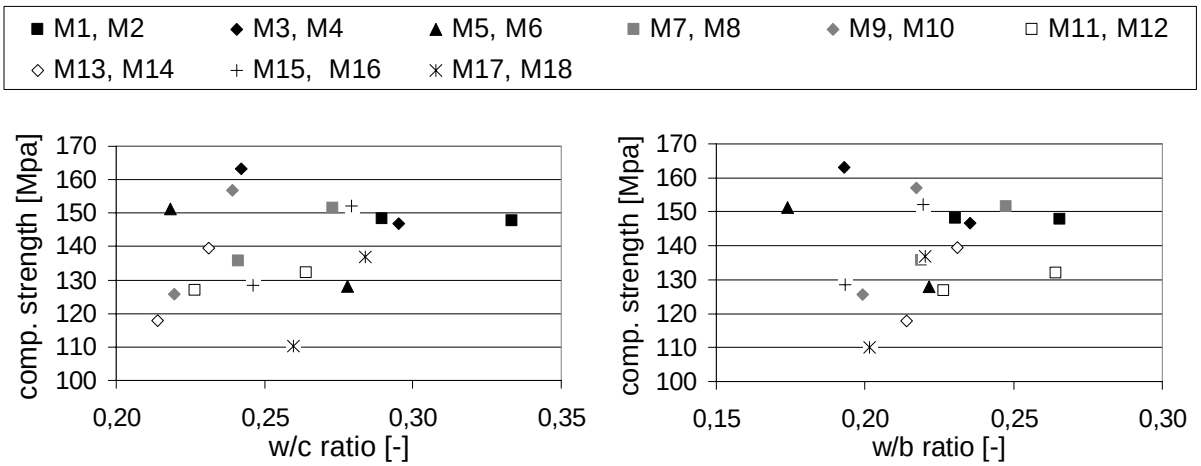

Figure 6: 28 days compressive strength versus w/c ratio (left) resp. w/b ratio (right)

5 Conclusion and Outlook

With the Superplasticizer-based Water Demand a useful value to characterize cementitious powder mixtures is presented. Not only a boundary value for the maximum attainable packing density can be found but also a curve describing the boundary consistency of a paste or mortar composition can be generated. This is valuable information for mixture proportioning.

For the enhancement of the robustness of UHPC a mix design is suggested that secures a surplus of fines for each grain size level. This surplus will lead to an overall packing density, that is lower than the maximum achievable packing density, but it will assure that for each grain size level the coarse particles will not become dominant despite any unfavourable influences (changes in the dosage, changes in the characteristic properties of the materials). Through this mixture proportioning voids, caused by the granular setup of the coarser particles can be avoided successfully. Therefore an adjustment of the consistency is possibly which guarantees proper flowability and filling ability of the mixture, which in turn is the condition for reproducible hardened concrete properties.

Further research should be done to study the influence of boundary conditions like changes in the temperature or the mixing process on the robustness and how these negative effects can be avoided respectively minimised by means of mixture proportioning. Special attention should be paid the interaction of silica fume (or other nano-scaled mineral stabilizers) and superplasticizers including the newest superplasticizer developments. The long term aim is to develop of a general concept for the mix design of high performance concretes with increased robustness.

6 References

[1] Höveling, H.: Robustheit von Selbstverdichtendem Beton, PhD thesis Universität Hannover, Institut für Baustoffe, (Hannover, 2006).

[2] Lohaus, L.; Petersen, L.; Höveling, H.: Verbundstützen am Lehrter Bahnhof -Ausbetonieren von Stahlverbundstützen, ein effizienter Einsatzbereich für hochfließfähigen Beton, beton 55 (4) (2006) pp. 158 - 163.

[3] Höveling, H.: Frischbetontechnologie für SVB und andere Hochleistungsbetone, 45. Forschungskolloquium des DAfStb, (Wien, 06. / 07. October 2005).

[4] Lohaus, L.; Höveling, H.: Robustimprovement für Selbstverdichtenden Beton (SVB), 15. Internationale Baustofftagung ibausil, Bauhaus-Universität Weimar, procedings – Vol. 2 pp. 177-187, (Weimar, September 2003).

[5] Puntke, W. Wasseranspruch von feinen Kornhaufenwerken, beton 51 (5) (2002) pp. 242-248.

[6] European Committee for Standardization: EN 196 – Methods of testing cement, (2005).

[7] Lohaus, L.; Ramge, P.; Höveling, H.; Anders, S.: Superplasticizer-Based Approach for Optimized Pastecomposition and Robustness of SCC, 5th Int. RILEM Symposium SCC2007, (Ghent, 3.-5. Sept 2007).

[8] Spanka, G.; Grube, H.; Thielen, G.: Wirkungsmechanismen verflüssigender Betonzusatzmittel. beton 44 (11) (1995) pp. 802-808 and beton 44 (12) (1995) pp. 876-881.

[9] Lagos, C.: Untersuchungen zur Robustheit von UHPC-Mischungen, master's thesis Universität Hannover, Institut für Baustoffe, (Hannover, 2007).

Ursula Stark
Dr.-Ing., Senior scientist
Bauhaus-University Weimar
Weimar, Germany

Anette Mueller
Prof. Dr.-Ing. habil.
Bauhaus-University Weimar
Weimar, Germany

Optimization of packing density of aggregates

Summary

The results of particle shape and particle size measurements carried out with the photo-optical method show a significant relationship between the packing density and the width of particle size distribution, characterized with the Fuller-exponent n. The particle shape, described with the descriptor sphericity SPHT, is the parameter of the different curves. The packing density increases with the increase of the width of particle size distribution to the maximum of these curves and otherwise also, when the particle shape will be changed from angular and rough to rounded and smooth. So the same packing density of aggregates is achieved with a broad distribution and an angular and rough particle shape or with a narrow distribution and a well-rounded particle shape. The workability properties, for instance of a self compacting mortar, depends therefore on the packing density and additionally on the particle roughness.

Keywords: *packing density, particle shape, particle size distribution, self compacting concrete, workability, rheology*

1 Introduction

Very recent developments in concrete technology, such as self compacting concrete or ultra high performance concrete but also the development of new generations of photo-optical measuring methods, make it necessary and possible to broaden the understanding of, in particular, the action of fine aggregates in the concrete. The packing density, which represents the connecting link between the properties of fresh and hardened concrete like the workability or strength on the one hand and the particle size distribution as well as the particle shape on the other hand, has thereby the central importance. The new generation of measuring techniques offers the possibility to measure simultaneously both the particle size distribution and the particle shape with one measurement. The basic concept is the combination of using the quick digital photography against the light and the image analysis. The statistical analyses of measuring results allow to describe the total bulk with characteristically values for size and shape in difference to the traditionally methods. The results can give very much information's due to the narrow sized particle size fractions and the possibility to measure a high amount of particles by using the dynamic image analysis principle.

Both the SCC and the UHPC have a higher content of sand and powder compared to the regular concrete, combined with the use of highly effective plasticizers. Therefore greater

importance attaches to the properties of the basic mortar of these concretes and especially to the properties of the type of used sand like natural or crushed sand or a mixture of both. This paper examines at first the fundamental correlations between the properties of the fine aggregates, that means between the particle size distribution and the particle shape on the one hand and the packing density on the other hand. At second the influence of the packing density and additionally of the particle roughness on the rheological behaviour was investigated. These investigations was carried out with a SCC mortar. The basic results of investigations, published in this paper, can be transfer to the UHPC mortars, because both mortars have a similar granulometric composition. Therefore it can be expected, that a comparable rheological behaviour could be obtained with the same properties of aggregates.

2 Properties of fine aggregates and workability properties of SCC mortars

The properties of fine aggregates like sand are characterised with the particle size distribution, the particle shape and morphology as well as the different densities. The investigation results are generated by using the measuring device HAVER CPA 4 2MB real time with a line camera and against the continuous back-light of a halogen-fed light strip. The particles are moving by free falling in a random orientation through the measuring plane. The particle shape can be analysed in a total range from 100 µm up to 63 mm.

The particle shape is characterized with the descriptors length to width ratio L/W for elongation and the ratio of measured perimeter to circumference of circle with the same area $P/2 \cdot \sqrt{\pi \cdot A}$ for sphericity SPHT (in [1] also named with circularity). The roughness is characterized with ratio sphericity to L/W.

The particle size distribution was described with the function according to Fuller [2] $Q_3(x) = (x/x_{max})^n$. The value x_{max} is in this context the maximum particle size of the distribution. Exponent n, also frequently referred as the Fuller-exponent, provides information on the width of the distribution.

The packing density is defined as the portion of the total space occupied by the solid particles in a poured volume. A compacted “bulk volume”, the vibrating density, is generally taken as the basis for packing density. Packing density is therefore calculated from the quotient of vibrating density and bulk density.

With reference to the working practice, the equivalent characteristics slump flow and funnel flow time were used for assessment of rheological properties of the SCC mortars in the own tests. In an initial step, mortars of a constant formulation and a constant slump flow of 240 mm were prepared with variation of the sand type. The corresponding quantity of plasticizer determined as a function of the type of sand. In a second stage, mortars were prepared with the quantities of plasticizer determined for selected sands and the funnel flow time was measured. Both the plasticizer requirement and the funnel flow time were used to describe the workability behaviour of SCC-mortar.

3 Results of investigations

The range of values for the particle shape descriptors of fine and coarse aggregates examined and the width of particle size distribution n is shown in Figure 1 and Table 1.

Table 1: Value range for particle shape descriptors and Fuller exponent n

	Natural aggregates		**Crushed aggregates**	
Parameters	Min. value	Max. value	Min. value	Max. value
L/W	1.34	1.57	1.46	1.78
SPHT	1.05	1.16	1.11	1.36
n (for sands only)	0.68	2.06	0.50	0.86

All the numerical values stated are volume-referred arithmetical means for the analyzed part of the fine aggregate (> 100 µm).

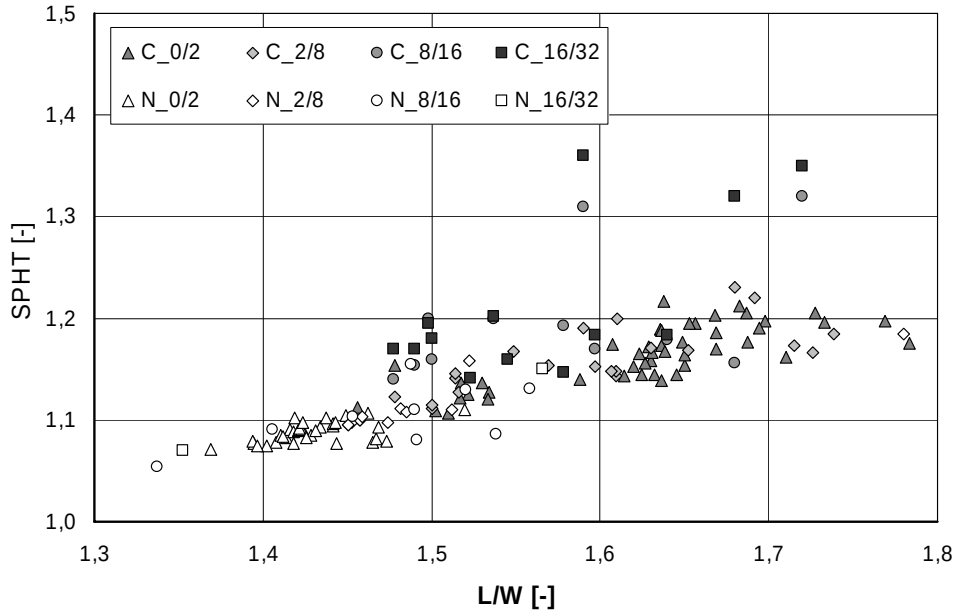

Figure 1: Sphericity and L/W values for the fine and coarse aggregates examined

It is clearly apparent from Figure 1 that the shape parameters for natural sands and gravels (N=natural) are in the lower numerical value range, whereas the crushed fine and coarse aggregates (C=crushed) are in the larger numerical range for L/W and SPHT. The width of the particle size distribution (see Table 1) also differs significantly. Natural sands primarily have narrow distributions with high values of n. Crushed sands have predominately broad distributions with low values of n. Typical plots for particle size distributions are shown in Table 2.

The evaluation of all tests up to now for determination of the correlation between the granulometric factors with the resulting bulk material properties, characterized by packing density, is summarized in Figure 2. As in Figure 1, the results obtained with coarse aggregates are also included here in addition to these correlations. The results by Liebezeit [3] and Bollert [4] on natural and crushed sands, by Stein [5] on model mixtures of fine aggregates and by

Daburger [6] on model mixtures of coarse aggregates, which are included in the graphic, made it possible to show that the width of particle size distribution and the particle shape of aggregates influence their packing density. The maximum particle size of the distribution has no influence in this context. The diagram indicates good agreement at the measured data with the curves calculated in accordance with Peronius and Sweeting [7].

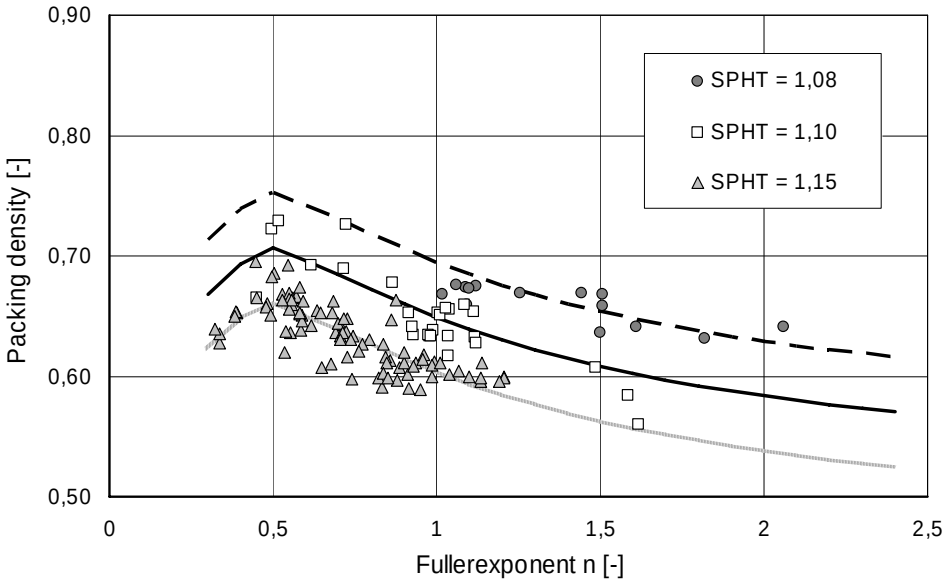

Figure 2: Packing density as a function of particle size and particle shape.

The diagram also shows, on the one hand, that for a constant particle shape the packing density rises up to a maximum as the exponent n falls, of whether natural or crushed and fine or coarse aggregates are examined. On the other hand, the packing density rises at a constant n as sphericity values decline that means, if the particles become rounder and / or the surface smoother.

The most important result of this diagram is, that the same packing densities can be obtained either for sands with rounded particles and a narrow size distribution (natural sands) or for sands with angular and rough particles and a broad distribution (crushed sands). This is shown in Table 2 for sands with the same packing density of 0.66. This value was achieved by natural sand NS 09 and also by crushed sand CS14.

The results of the tests to determine the required quantity of plasticizer permitted the conclusion that there is a significant correlation between the packing density of the sands and the quantity of plasticizer, as shown in Figure 3. As expected, the plasticizer requirement is low in the case of high packing densities and increases as packing densities fall until, in an extreme case, no flow anywhere is achieved. This was the case with 8 (2 natural and 6 crushed sands) of 53 sands examined.

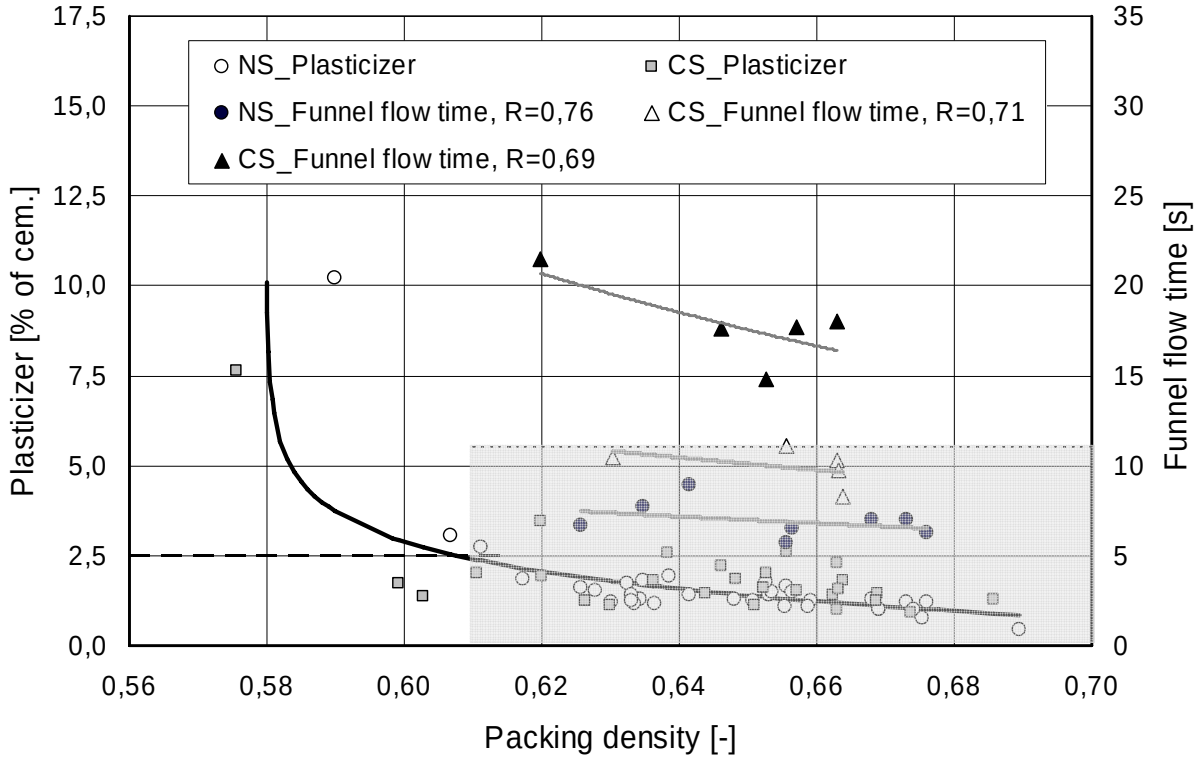

Figure 3: Workability properties of natural and crushed sands

The funnel flow time was analysed with 18 sands (8 natural sands and 10 crushed sands) by Bollert [4], by Ostheeren [8] and by a student's project work [9]. In Figure 3 you can see the results of these flow tests. The differences between the natural and crushed sands in terms of plasticizer requirement are apparent only in scatter-width of the results, whereas the results of the flow tests exhibit significant differences. As the packing density declines, the flow times increase more strongly when using crushed sands than is the case with natural sands. Furthermore the flow time becomes higher, if the particle shape will be more angular or the surface will be rougher. The parameter of the three curves of flow time is therefore the value of roughness R.

If a quantity of about 2.5 %, referring to the cement content, is set as a limit for plasticizer quantity and the flow time must be lower than 11 s [10], then good workability behaviour will be achieved in the grey marked range of the diagram in Figure 3 under the conditions selected for testing of the SCC mortars.

Table 2 shows the characterisation of two different sands in correlation with the workability behaviour of SCC mortars produced of these two sands.

Table 2: Characterisation of two sands with the same packing density

	Natural sand NS 09	**Crushed sand CS 14**
Rock type	Natural sand from the Quaternary / Pleistocene	Greywacke
Particle size as supplied	0/2 mm	0/2 mm
Particle size distribution	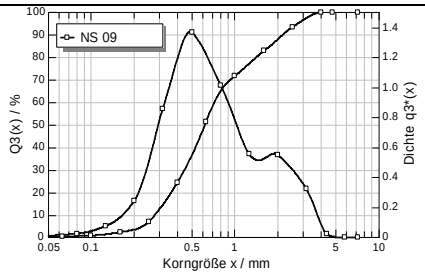	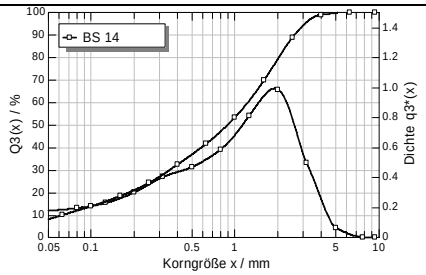
Stereomicroscope image	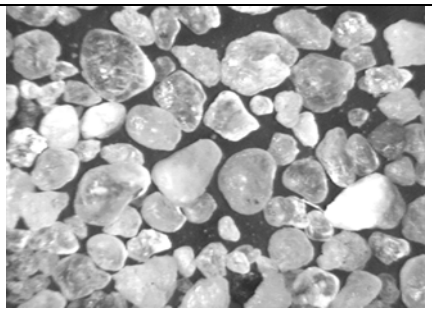	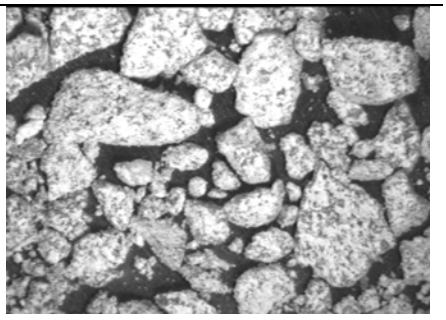
Image of CPA analysis		
Sphericity SPHT [-]	1,08	1,18
Fuller exponent n [-]	1,03	0,56
Roughness = SPHT / L/W	0,77	0,70
Packing density [-]	0,66	0,66
Plasticizer demand [% of cement quantity]	1,50	1,55
Funnel flow time [s]	6,5	9,7

4 Conclusions

In summery the results currently available permit the conclusion that the workability properties of SSC mortars depends on the packing densities of the used sands and the roughness of these sands. The packing density is influenced again of the width of the particle size distribution and the particle shape, characterized with the descriptor SPHT. Under the conditions selected for the tests it can be concluded, that all sands, which values of packing densities and roughness are laying in the marked range in Figure 3, can be used as component in SCC mortar solitary or as mixture of natural and crushed sands. The last statement, the using of defined mixtures of natural and crushed sands, as well as transferability to UHPC mortars must be confirmed in further works.

5 References

[1] Representation of results of particle size analysis – Part 6: The descriptive and quantitative representation of particle shape and morphology. Working draft. ISO/WD 9276-6.2, ISO 2004, Verantwortlicher Bearbeiter: Stintz, M.

[2] Fuller, W. B. and Thomson, S. E.: The Laws of Proportioning Concrete. Transactions of American Society of Civil Engineers, Vol. LIX, New York, Dec. 1907.

[3] Liebezeit, St.: Brechsand für Selbstverdichtenden Beton. Diplomarbeit, 2005, Bauhaus-Universität Weimar, Reg.-Nr.: B/2004/138, Fak. Bauingenieurwesen, Lehrstuhl ABW, Betreuer: Dr.-Ing. U. Stark.

[4] Bollert, Ch.: Einfluss der Kornform und der Korngröße der feinen Gesteinskörnungen auf die Verarbeitungseigenschaften und die Festigkeit von SVB-Mörteln. Diplomarbeit, 2007, Bauhaus-Universität Weimar, Reg.-Nr.: WW/2006/04, Fak. Bauingenieurwesen, Lehrstuhl ABW, Betreuer: Dr.-Ing. U. Stark.

[5] Stein, D.: Optimale Packungsdichte von feinen Gesteinskörnungen für Selbstverdichtende Betone. Diplomarbeit, 2006, Bauhaus-Universität Weimar, Reg.-Nr.: B/2005/83, Lehrstuhl ABW, Betreuer: Dr.-Ing. U. Stark.

[6] Daburger, H.: Einfluss der Kornform von Gesteinskörnungen auf Packungsdichte und Frischbetoneigenschaften. Diplomarbeit, 2006, Bauhaus-Universität Weimar, Reg.-Nr.: B/2006/03, Lehrstuhl ABW, Betreuer: Dr.-Ing. U. Stark.

[7] Peronius, N. Sweeting, T.J.: On the correlation of minimum porosity with particle size distribution. Powder Technology 42 (1985) 113 – 121.

[8] Ostheeren, K.: Rheologische Untersuchungen an Basismörteln Selbstverdichtender Betone mit Sanden unterschiedlicher Kornformen, Diplomarbeit, 2007, Bauhaus-Universität Weimar, in Bearbeitung, Lehrstuhl ABW, Betreuer: Dr.-Ing. U. Stark.

[9] Grau, M., Harz, Ph., Pflantz, K., Niebel, S., Kaiser, M. Rothhagen, B.: Projektarbeitarbeit zum Thema „Charakterisierung von Rest- und Abfallstoffen und deren Verwertung“, Betreuer: Dr.-Ing. U. Stark.

[10] Deutscher Ausschuss für Stahlbeton; DAfStb-Richtlinie Selbstverdichtender Beton (SVB–Richtlinie); DIN e.V., Berlin, November 2003.

Torsten Kowald
Dipl.-Min.; PhD student
University of Siegen
Siegen, Germany

Reinhard Trettin
Prof. Dr. rer. nat. habil.
University of Siegen
Siegen, Germany

Nils Dörbaum
student
University of Siegen
Siegen, Germany

Torsten Städler
Dr. rer. nat., chief engineer
University of Siegen
Siegen, Germany

Xin Jiang
Prof. Dr. rer. nat. habil.
University of Siegen
Siegen, Germany

Influence of Carbon Nanotubes on the micromechanical properties of a model system for ultra-high performance concrete

Summary

Carbon nanotubes (CNTs) are well known for their extraordinary mechanical properties. Their high aspect ratio, high resistance to corrosion and low specific weight make them a very promising reinforcement material for modern building materials. So far carbon nanotubes were incorporated into normal concretes, high and ultra-high performance concretes as well as model systems leading to improved mechanical properties. The further improvement of the UHPC´s properties by use of CNTs is only possible if the interaction between the CNTs and the binder is understood. To show the influence of carbon nanotubes on the micromechanical properties of the hydration products of a tricalcium silicate model system were examined by the nanoindentation method. For a reduction of the hydrations complexity a model system with mechanical properties of UHPC was chosen. The results show that the CNTs influence the proportions of the hydration products. The presentation will show specialties in the application of the carbon-based nanostructures and their influence on the composite.

Keywords: *carbon nanotubes, tricalcium silicate, C-S-H, nanoindentation, UHPC*

1 Introduction

To enhance the performance of modern building materials like ultra-high performance concrete (UHPC) fibres are very often used to overcome certain weaknesses of this material. The fibres are utilized to improve the flexural strength, the ductility or the fire-resistance. Due to their mechanical properties, high aspect ratio and their stability against corrosion carbon

nanotubes (CNTs) are very promising reinforcements for a new generation of building materials.

To advance the mechanical properties of the nano-composites the dispersion of the CNTs and the linkage between the CNTs and the binder matrix has to be optimized. In addition, detailed information about the influence of the CNTs on the hydration and the mechanical properties of the binder´s reaction products is necessary to further improve the composite.

Within plain cement pastes multi-walled carbon nanotubes (MWNTs) respectively single-walled carbon nanotubes (SWNTs) led to an increase in the compressive strength by 30% in case of the MWNTs and 6% when the SWNTs had been used [1]. When properly used the CNTs lead to improved mechanical properties of the nanocomposite [2–4]. The flexural strength of model systems with pure tricalcium silicate (C_3S) as binder and 0.5 ma.% of different carbon nanostructures improved up to 45% [4]. The nanostructures not only act as a reinforcement material but also have influence on the hydration and the resulting microstructure of the binder. *In situ* x-ray powder diffraction measurements showed a huge influence on the crystallization of portlandite showing less and smaller crystals compared to a sample without MWNTs. Isothermal calorimetric measurements showed an acceleration of the hydration by the MWNTs so that the effect was not due to a retarding effect [4]. The influence on the portlandite crystallization shows that the used MWNTs have a clear influence on the hydration of C_3S and showed an accelerated reaction with very fine portlandite. The effect of getting finer crystallisation products when using MWNTs could also been seen by SEM-investigations. Another team [5] mentioned a reaction of the COOH-groups at the CNTs surface with the solution so that a chemical link between the hydration products and the CNTs is possible. This means that the functional groups can act as crystal seeds resulting in an increased number of finer hydration products.

Recently the nanoindentation method was used on cement-based composites to study the micromechanical properties of hydration products on the micro- and nanoscale [6, 7]. This method has proven to be very useful by studying mechanical properties and fractions of hydration products.

We used pure tricalcium silicate as a simplified model system to study the influence of untreated and oxidized MWNTs on the micromechanical properties of the hydration products.

2 Experimental Part

1 ma.% of untreated (Mu) or oxidized MWNTs (Mo) were incorporated into pressure-compacted C_3S-prisms to see how they are influencing the mechanical properties of the hydration products by use of the nanoindentation method. The results were compared with a reference system without CNTs (R).

2.1 Sample Preparation

As binder pure triclinic C_3S with a free lime content of 0.18 ma.%, a specific density of 3.12 g/cm³ and a particle size of d_{50}=4 µm at a water to binder ratio of 0.22 had been used. The tricalcium silicate was synthesized from a stoichiometrical mixture of calcium carbonate and silicon dioxide at 1450°C. After the synthesis and grinding the C_3S was controlled by XRD for purity and presence of C_2S and CaO. When the CaO amount calculated by the

rietveld method was below 0.5 ma.% the amount was additionally controlled by the Franke method. Two types of commercial MWNTs were used during the experiments. The untreated MWNTs were purchased from Sun Nanotech Co. Ltd. and the oxidized MWNTs from Bayer. MaterialScience AG. The properties of the MWNTs are listed in table 1. The MWNTs (1 ma.% by binder content) were dispersed by sonification for 28 minutes within the mixing water than a polycarboxylate-based superplasticizer (2 ma.% by binder content) was added and the dispersion sonificated for additional 2 minutes.

Table 1: Product specifications for MWNTs

Manufacturer	**Sun Nanotech Co. Ltd**	**Bayer MaterialScience AG**
Purity	> 80 %	> 95 %
Free amorphous content	< 10 %	not detectable
Diameter	10 – 30 nm	5 – 20 nm
Length	1 – 10 µm	1 - >10 µm
Treatment	---	Refluxed in HNO_3

After the mixing process the pastes were moulded into prism-shaped forms and compacted by applying a pressure of 125 N/mm² for 30 minutes. The prisms were demoulded after 2 days of storage at a relative humidity of >90 % and 20 °C. Afterwards the prisms were cured 5 d under water at 20 °C. Than the samples were stored in a cabinet dryer for 2 d at 70 °C and stored in a desiccator until the polishing took place. Prior to the polishing the prisms were embedded into epoxy resin. At the last step the samples had been polished by use of a diamond spray with a particle size of 1 µm. The average roughness of the polished surfaces as examined by AFM was below 70 nm.

2.2 Experimental details for nanoindentation

The indentation tests were performed under quasi-static conditions using a scanning nanoindenter [8] (TriboIndenter, Hysitron Inc., Minneapolis, MN) equipped with a Berkovich diamond indenter in a load-controlled set-up. Three times a hundred indents (grids of ten times ten indents with 10 µm spacing) were positioned in each sample, respectively. Each indent followed a simple loading/holding/unloading scheme featuring a loading/unloading rate of 200 µN/s, 10 s hold time under maximum load, and a maximum load of 4 µN.

Finally, the standard Oliver-Pharr method [9] was used to calculate the indentation modulus E_i and the hardness H from the unloading portion (65-95%) of the load-displacement data recorded during each test. These quantities are defined as

$$E_i = \frac{E_s}{1-\nu_s^2} = \left[\frac{2\sqrt{A_c}}{\sqrt{\pi}S} - \frac{1-\nu_t^2}{E_t} \right]^{-1} \quad \text{and} \quad H = \frac{P_{max}}{A_c} \ , \tag{1}$$

where A_c and S are the contact area and contact stiffness at maximum load, P_{max}, respectively, E is Young's modulus, ν is Poisson's ratio, and the subscripts s and t refer to the sample and indenter tip materials, respectively.

3 Results

3.1 Elastic Modulus

The distributions of the reduced elastic modulus (E_r) for the three different samples are shown in figures 1 – 3. By inspecting the distribution curves four different phases could be identified at 47 GPa, 60 GPa, 95 GPa and 130 GPa. These phases are marked as I, II, III and IV. The phases I and IV can be attributed to portlandite and tricalcium silicate. The values found are in good agreement with those mentioned in the literature (CH: 36±3 – 40±4 GPa; C_3S: 135±7 GPa) [6, 10, 11, 12]. The phases II and III can be attributed to the LD and HD C-S-H. Compared to the data found in the literature (~20 GPa for LD / ~30 GPa for HD C-S-H) [6, 10, 11] the results for the elastic modulus are much higher. This can be explained by the fact that we were using pressure compacted samples

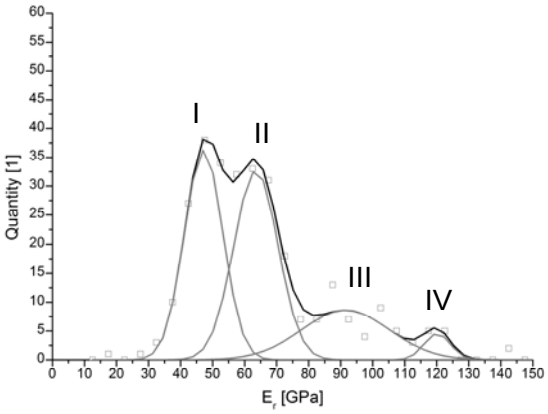

Figure 1: (upper left) Distribution for the reduced elastic modulus of the reference sample (R)

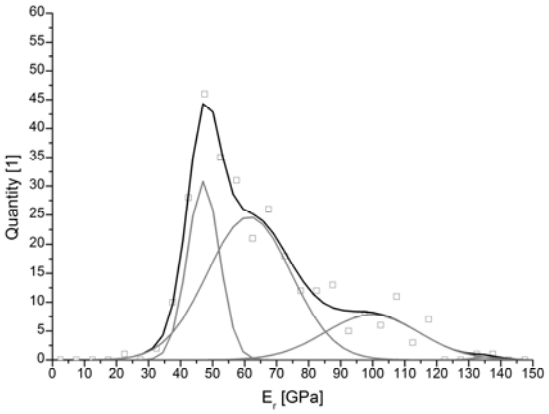

Figure 2: (upper right) Distribution for the reduced elastic modulus of the sample containing 1 ma.% untreated CNTs (Mu)

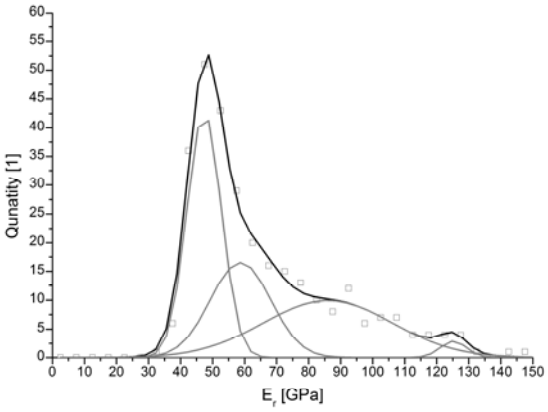

Figure 3: (left) Distribution for the reduced elastic modulus of the sample containing 1 ma.% oxidized CNTs (Mo)

To quantify the phases four Gaussian-shaped curves (gray) were fitted to the observed data (grey boxes). The median Young´s modulus for every phase and sample and their relative intensities can be found in table 2.

Table 2: Comparison of the Young´s modulus for samples R, Mu and Mo

Sample	**I**	**II**	**III**	**IV**
	E [GPa]	**E [GPa]**	**E [GPa]**	**E [GPa]**
R	47±1 (38%)	63±1 (39%)	93±3 (20%)	124±2 (3%)
Mu	47±1 (26%)	61±3 (55%)	102±6 (19%)	---
Mo	47±1 (38%)	58±8 (26%)	87±13 (34%)	130±2 (2%)

The values in brackets are showing the relative intensities.

The relative intensities for each phase are also plotted in figure 4. It can be seen that the incorporation of the CNTs are mainly influencing the amount of the two types of C-S-H (II, III). While the unmodified MWNTs led to an increase in the amount of the LD C-S-H the oxidized MWNTs increased the amount of the HD C-S-H. The LD/C-S-H ratio of 66% is in good agreement with the one (65%) found in [6]. In the case of the sample Mu this ratio is 74% and 43% for Mo.

There is nearly no influence on the median values for the Young´s modulus but on the distribution of the C-S-H phases especially in the case of sample Mo.

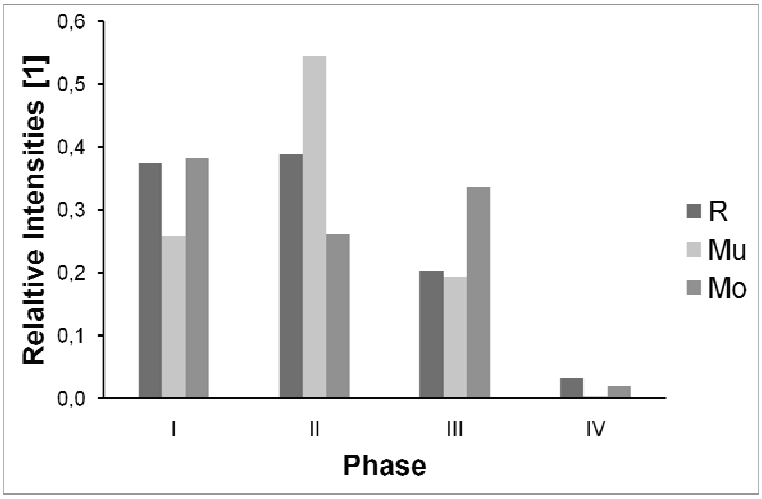

Figure 4: Comparison of the relative intensities

4 Conclusions

Depending on their field of application modern building materials like UHPC have to fulfil certain requirements. These are beside their good compressive strength mainly their flexural and tensile strength, ductility, corrosion-resistance, fire-resistance and weight. Some of these properties can be achieved or improved by the use of fibres. Mechanical properties, high aspect ratio, low specific weight and stability against corrosion make carbon nanotubes (CNTs) very promising reinforcement materials to advance modern building materials. It is known that the CNTs improve the mechanical properties of building materials [1–4]. Additionally the CNTs seem to influence the hydration [4, 5]. By the nanoindentation measurements we studied if there is also an influence on the C-S-H.

In this work the nanoindentation method was used to study the influence of untreated and oxidized multi-walled nanotubes on the micromechanical properties as well the proportions of the hydration products. To reduce the complexity of a real ultra-high performance system and the resulting hydration products we used a model system consisting of the main cement phase tricalcium silicate and a water to binder ratio of 0.22. Like already shown in [4] and [5] the MWNTs have an influence on the hydration and the resulting microstructure of the binder. The analysis of the distribution of the elastic modulus (figures 1 – 3) within the composite material showed that especially the oxidized multi-walled nanotubes influenced the ratio of the LD and HD C-S-H (see table 2 and figure 4) shifting it from 66% to 43%. The untreated nanostructures led to an increased amount of the LD C-S-H and the oxidized ones to an increase in the amount of the HD C-S-H. Also a broader distribution for the C-S-H had

been found. The increased number of COOH-groups on the surface of the oxidized multi-walled nanotubes seems to lead to C-S-H with a HD character.
The results show that the MWNTs can be used for a regulation of the hydration products to further improve the properties of ultra-high performance concretes. Systematic investigations have to be done to fully understand the interaction between the carbon nanotubes and the hydration products and therefore being able further improve the performance of UHPC.

5 Acknowledgement

The authors like to thank the DFG for financially supporting this work.

6 References

[1] Campillo, I., Dolado, J.S. and Porro, A.: High-Performance Nanostructured Materials For Construction. In: Proceedings of the 1st International Symposium on Nanotechnology in Construction, Paisley, 2003, pp. 110-121

[2] Kowald, T. and Trettin, R.: Kohlenstoffbasierte Nanostrukturen in modernen anorganischen Bindemitteln. In: Tagung Bauchemie, GDCh-Fachgruppe Bauchemie, 2004, pp. 162-165

[3] Kowald, T. and Trettin, R. H. F.: Influence of surface-modified Carbon Nanotubes on Ultra-High Performance Concrete. In: Proceedings of the International Symposium on Ultra High Performance Concrete, kassel university press GmbH, 2004, pp. 195-202

[4] Jiang, X., Kowald, T.L., Staedler, T. and Trettin, R.H.F.: Carbon Nanotubes As A new Reinforcement Material For Modern Cement-Based Materials. In: Proceedings of the 2nd International Symposium on Nanotechnology in Construction, RILEM Publications s.a.r.l, 2005, p. 26

[5] Li, G.Y., Wang, P.M. and Zhao, X.: Mechanical behaviour and microstructure of cement composites incorporating surface-treated multi-walled carbon nanotubes. In: Carbon (43) (2005), pp. 1239-1245

[6] Constandinides, G. and Ulm, F.-J.: The nanogranular nature of C-S-H. In: Journal of the Mechanics and Physics of Solids, 55 (2007), pp. 64-90

[7] Sáez de Ibarra, Y., Gaitero, J. J, Erkizia, E. and Campillo, I.: Atomic force microscopy and nanoindention of cement pastes with nanotube dispersions. In: physika status solidi, (a) 203, No. 6 (2006), pp. 1076-1081

[8] Baker, S.P.: Mechanical properties and fracture toughness of multilayer hard coatings using nanoindentation. In: Thin Solid Films 308-309, 289 (1997)

[9] Oliver, W.C. and Pharr, G.M.: An improved technique for determining hardness and elastic modulus using load and displacement sensing indentation experiments. In: Journal of Materials Research 7, (1992) 1564

[10] Constantinides, G. and Ulm, F.-J.: The effect of two types of C-S-H on the elasticity of cement-based materials: Results from nanoindentation and micromechanical modeling. In: Cement Concrete Research 34, (2004) pp. 67–80

[11] Acker, P.: Micromechanical analysis of creep and shrinkage mechanisms, In: F.-J. Ulm, Z. Bazant, F. Wittman (Eds.), Creep, Shrinkage and Durability Mechanics of Concrete and other Quasi-Brittle Materials, Elsevier, Oxford, UK, 2001, pp. 15–25

[12] Velez, K., Maximilien, S., Damidot, D., Fantozzi, G. and Sorrentino F.: Determination by nanoindentation of elastic modulus and hardness of pure constituents of Portland cement clinker. In: Cement Concrete Research 31, (2001) pp. 555–561

Stephanie Márquez
Graduate Student
University of Utah
Salt Lake City, USA

Shannon Hanson
Undergraduate Student
University of Utah
Salt Lake City, USA

Paul J. Tikalsky
Prof.
University of Utah
Salt Lake City, USA

Environmental Advantages of Ternary Cement Combinations

Summary

Ternary and binary blended cementitious combinations provide advanced technical and environmental performance in concrete structures. These cementitious blends are being developed to meet both increasing detailed technical performance specifications and the requirement to reduce CO_2 emissions related to concrete materials and construction. CO_2 emissions related to portland cement are high because the production of portland cements requires both the reduction of limestone ($CaCO_3$) to calcium oxide (CaO) and the burning of fuels for high temperature combustion and grinding. The blending of cement with pozzolans such as fly ash and ground granulated blast furnace slag (GGBFS) allow for a decrease in the amount of cement required for a concrete mixture.

Current research at the University of Utah is developing UHPC mixtures with ternary cementitious blends to meet multiple technical performance characteristics and meet sustainability performance criteria for low emission concrete production. Some engineers confuse high strength or “ultra-high strength” concrete as essential for UHPC. Strength is only one of many performance characteristics in concrete and often times not the controlling element of long life performance. With the use of UHPC mixtures the sustainability of a structure is increased by meeting technical requirements to lengthen its life-cycle and reduce the CO_2 emissions related with its construction.

This paper analyzes the CO_2 emissions resulting from the building of UHPC structures, where performance is measured both in technical characteristics and environmental impact. The analysis will use data provided by US Department of Energy (USDOE) and other sources to estimate the total CO_2 emissions for a standard structure with and without ternary and binary concrete mixtures.

Sustainability is becoming a major selection criteria in new construction as businesses worldwide are attempting to build structures in a more eco-friendly manner. Currently Leadership in Energy and Environmental Design (LEED) provides minimal energy credit toward the reduction of CO_2 in concrete structures using UHPC concrete mixtures. Analysis of the emissions involved in concrete production for performance based concrete will provide

a means of determining CO_2 emissions for comparison and future consideration of larger environmental credit.

Keywords: *ternary cement, sustainability, ground granulated blast furnace slag, pozzolans*

1 Background

The environmental impact of infrastructure projects is increasingly becoming important in engineering design. Buildings and structures strive to be more sustainable. In order to be sustainable, a design needs to take into account the consequences of the structure on human health, the future of flora and fauna and the impact on the availability of resources. LEED strives to award structures through a rating system that jugdes the amount of sustainability considered.

1.1 Importance of Sustainability

For structures, measures can be taken to decrease the impact of construction materials and to efficiently allocate natural resources. There are two means to greatly enhance the sustainablity of newly constructed building and infrastructure projects; 1) use lower energy and CO_2 materials or reuse previously allocated energy and CO_2 materials, or 2) design longer life projects to ammortise the energy and CO_2 over a greater period of time. Currently, the manufacture of portland cement is energy and CO_2 intensive and concrete is the second most used resource on Earth next to water [2].

A primary concern of many sustainability projects is the amount of CO_2 released into the atmosphere. CO_2 and other greenhouse gases in large enough quantities decrease the quality of air for many forms of life. The heat trapping properties of CO_2 contribute to the greenhouse effect and to climate change. The calcination process from which cement is made from burning limestone emits nearly 1kg of CO_2 for every 1kg of portland cement produced [5]. It is an aim for structures to have long life expectancies to reduce the frequency replacement of structures; this reduces the materials needed for the infrastructure and reduces the amount of CO_2 that would be emitted for these additional materials needed for a more short-lived version of a structure.

1.2 Current LEED Ratings for Ternary Mixture Designs

The ternary blend mixtures of concrete that reduce CO_2 emissions by replacing some percent of the cement with other cementious materials such as GGBFS, silica fume or fly ash help buildings attain points for sustainability through the LEED ratings system. Currently, version 2.2 of the rating system for new construction and major renovations states that if the value of the post consumer products plus half of the pre-consumer products adds to 10% of the total value of the material cost for the project, then one point shall be awarded [4]. If 20% of the total value of material cost for a structure is comprised of post consumer and half pre-consumer products, another point is added [4].

LEED points are awarded for many energy saving criteria to rate a building as either LEED Certified, Silver, Gold, or Platinum. The points are scaled as: Certified is 26-32 points; Silver is 33-38 points; Gold is 39-51 points; and Platinum is 52-69 points [4].

2 Research Methods

The University of Utah is currently studying ternary blends of cementious materials to develop concrete to last one hundred years. 120 mixtures and about 6,000 mortar and concrete specimens were studied over three years to find the top 25 mixtures. Data regarding the CO_2 output of the processes used to create ternary blend mixtures of concrete is applied to seven of the 120 mixtures of this study. These seven mixtures conform to the at least five specified performance characteristics at a superior level. This is well beyond the expectations of "normal" portland cement concrete that is produced for engineered projects. This means that the mixtures satisfy requirements in the ASTM standards for 28-day strength, 28:7-day strength ratios, drying shrinkage, salt scaling, chloride ion penetration. In addition these mixtures have a reduction in CO_2.

The seven mixture designs are described in Table 1 [7]. With the use of Table 1 CO_2 emissions for a cementitious materials were developed. The CO_2 emmissions of the mixtures take into account the CO_2 related to transportation, aggregate production, and cementious materials production. These are compared to the CO_2 levels for a concrete mixture using solely portland cement as the cementious material. This analysis is then applied to the CO_2 emissions related to the building of a five km highway and the sustainability achieved when using ternary cementitious materials. These calculations were also applied to a building at the University of Utah to show its environmental impact related to CO_2 emissions.

3 Results

In Table 1 below, the mixture designs are listed with the respective percentages of cementitious materials used; each of the listed mixtures use a reduced amount of portland cement with other materials such as GGBFS, fly ash, and silica fume [7].

Table 1: Summary of Mixtures

Mixture Number	w/cm	Cementitious Materials Content (kg/m³)	Portland Cement (%)	GGBFS (Grade 100) (%)	Class F Fly Ash (%)	Silica Fume (%)
102	0.43	348.8	70		30	
103	0.43	334.6	55	40		5
101	0.43	334.6	50	50		
105	0.43	348.8	55	42		3
108	0.43	349.4	70		27	3
109	0.43	348.8	65		30	5
110	0.43	334.6	95			5

Table 2 includes the cost of the concrete mixtures in Euros per cubic meter, CO_2 emissions from the concrete mixtures in a five kilometer highway, and the percent of CO_2 emissions reduction of the concrete mixtures compared to a solely portland cement concrete mixture (PCC). A 100% portland cement mixture is not mentioned in the list of mixtures considered since it is not typically used. This highway is five kilometers long, two lanes (each three and a half meters wide), and a quarter of a meter thick; the emissions are shown for the different mixtures.

Table 2: Cost and CO_2 Emissions

Mixture Number	Concrete Cost (€/m³)	CO_2 Emissions (kg CO_2/m³ material)	CO_2 Emissions for 5 km highway (Mg)	% CO_2 Emissions Reduced
102	77.99	230.65	2018.21	27.1
103	128.45	178.90	1565.37	41.1
101	82.58	164.43	1438.74	45.8
105	110.10	186.27	1629.85	41.1
108	105.51	231.03	2021.51	27.1
109	123.86	214.83	1879.78	32.1
110	128.45	297.48	2602.99	2.0

The emissions are taken from data that added the emissions exhausted burning limestone to portland cement and the processes required to manufacture GGBFS [5]. GGBFS requires regrinding to be the appropriate size for concrete mixtures and therefore has an associated CO_2 emission for the equipment required for the process [5]. Both silica fume and fly ash do not have any CO_2 emissions associated in these calculations since there is no grinding or processing, and that both of these cementious materials are byproducts of another process [5]. The cost analysis is taken from data related in U.S. dollars and the U.S. market and were directly converted to Euros [8].The equivalent of this highway built using solely portland cement in its mixture has more CO_2 emissions associated with it than the UHPC ternary blend mixture highways. Mixture number 101 is found to have the most significant reduction of CO_2 emissions with 45.8% less CO_2 than a PCC mixture; the smallest amount of portland cement is used in this mixture design and therefore is expected to have the least contribution of CO_2. The most economical mixture design is number 102 with €77.99 per cubic meter. This mixture design replaced 30% of the portland cement with class F fly ash.

The average design life of a bridge deck prior to the use of any performance specifications in the North-eastern United States is 27 years [3]. The design life of a UHPC bridge deck is estimated to have a design life of 100 years [1]. If the costs are amortized over the life of the bridge based on its technical performance, the cementitious material cost for a non-UHPC bridge will be approximately €5 per year per cubic meter versus an average cost of €1.5 per year per cubic meter for a UHPC bridge [8].

The performance categories for the mixture designs are listed in Table 3. When mixtures are required to meet 4 or more high performance grades, the mixtures become substantially more engineered to a point where UHPC is a more appropriate title [6]. The level of concrete

performance as follows: compressive strength ratios of 28:7 day strengths of Grade 2 greater than 1.3, shrinkage for Grade 1 with less than 600 microstrain at 56 day period, and scaling according to ASTM C672 between 1 and 3 on a scale of 5 [6]. The concrete was also designed to limit chloride ion penetration to Grade 2 which is less than 1500 Coulombs at 56 days in AASHTO T277 [6]. A mixture of pure portland cement has high permeability, a scaling value of three, and 3500 coulombs of chloride ion penetration, and a strength ratio of about 1.15 [6].

Table 3: UHPC Characteristics

Mixture Number	**Mixture**	**Compressive Strength (MPa)**			**Shrinkage (ASTM C 157) (με)**	**Scaling (ASTM C 672)**	**Chloride Ion Penetrability AASHTO T-277 (Coulombs)**	
		7 day	**28 day**	**28:7 day**	**28 day**	**50 cycles**	**28 days**	**56 days**
102	30% FA	30.75	40.33	1.31	430	1.5	850	820
103	40% GGBFS 5%SF	43.92	63.09	1.44	370	3	830	810
101	50% GGBFS	31.85	46.68	1.47	550	1.5	680	690
105	42% GGBFS 3%SF	46.47	50.26	1.95	330	3	500	360
108	27%FA 3%SF	34.61	49.23	1.42	520	NA	600	440
109	30% FA 5% SF	35.16	46.40	1.32	420	NA	700	580
110	5% SF	45.30	59.29	1.31	500	NA	1100	1260

Figure 1 summarizes the CO_2 emissions versus the percent portland cement used in the different types of mixtures [5]. This verifies the direct relationship between the amount of portland cement and the amount of CO_2 emissions; the higher the amount of cement used in a mixture, the higher the amount of CO_2 emissions involved in production.

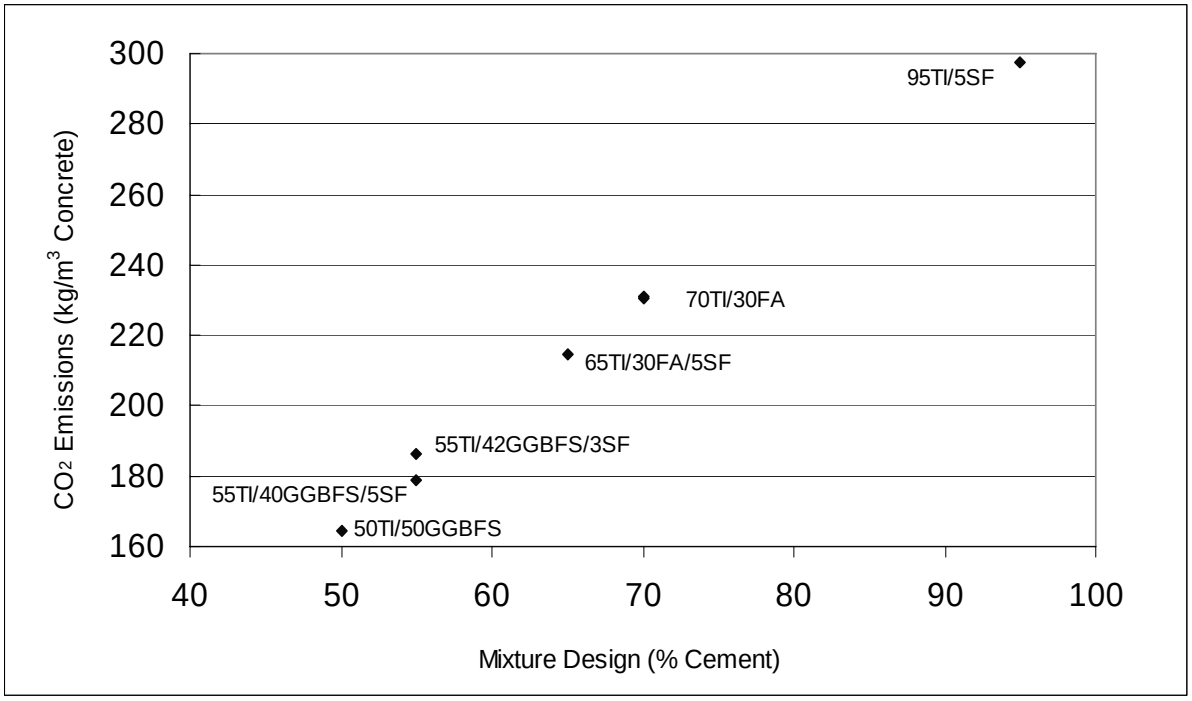

Figure 1: CO_2 Emissions versus percent portland cement

To see the CO_2 savings in a concrete structure, the volume of concrete needed for a four story steel building with concrete foundation and floors is analyzed using UHPC ternary blend concrete versus a mostly PCC mixture of concrete. The total volume of concrete in the building is 2850 cubic meters. Table 4 shows the different amounts of CO_2 associated with the different concrete mixtures for the building [5].

Table 4: CO2 Emissions in Given Concrete Building

Mixture Number	**Concrete Cost (€/m³)**	**CO_2 Emissions (kg CO_2/m³ material)**	**CO_2 Emissions for Concrete Building (Mg)**	**% CO_2 Emissions Reduced**
102	77.99	230.65	657.36	27.1
103	128.45	178.90	509.86	41.1
101	82.58	164.43	468.62	45.8
105	110.10	186.27	530.86	41.1
108	105.51	231.03	658.43	27.1
109	123.86	214.83	612.27	32.1
110	128.45	297.48	847.83	2.0

4 Conclusions and Recommendations

The demand of meeting multiple performance requirement for both techncial and environmental performance creates a unique challenge for engineers. However, through comparing the top UHPC mixture designs in 28-day strength, 28:7-day strength ratios, shrinkage, scaling, chloride ion penetration, cost and CO_2 emission reductions, the design that best addresses all of these issues is mixture number 105. Mixture number 105 is the most economical for the amount of reduction while still maintaining significantly high strength, and relatively low amount of shrinkage, scaling and chloride ion penetration. Mixture number 105 uses 55% portland cement, 42% slag and 3% silica fume.

There are significant savings in CO_2 emissions and material cost when designing long-lasting structures. For this reason, there is growing effort to increase the credit attributed to UHPC concrete for structure designs that utilize ternary blend mixtures than what is currently stated in the LEED rating system.

5 References

[1] Bentz, E.; Thomas, M.; D.,A.: Life-365 Service Life Prediction Model, Computer Program for Predicting the Service Life and Life-Cycle Costs of Reinforced Concrete Exposed to Chlorides, 2001.

[2] International Emissions Trading Association:, Financing Response to Climate Change, In: Greenhouse Gas Market 2006, Page 129, 2006.

[3] Konečný, P.; Tikalsky, P. J.; D.G. Tepke: Performance Assessment of Concrete Bridge deck Applying SBRA Approach and FEM model.

[4] Leadership in Energy and Environmental Design: Green Building Rating System For New Construction & Major Renovations, Version 2.2. In: Materials and Resources, Sections 4.1-4.2, Pages 55-56, October 2005.

[5] Marceau, M.L., Nisbet, M.A., VanGeem, M.G.: Life Cycle Inventory of Portland Cement Concrete PCA.

[6] Tepke, D.G.; Tikalsky, P.J.: Best Construction Practices For Concrete Bridge Decks. In: Penndot Research, February 2007.

[7] Tikalsky, P. J.; Scheetz, B.E.; Tepke, D. G.: Task 6 Final Report Statewide High Performance Concrete Initiative. In: Penndot Research, January 2007.

[8] Tikalsky, P. J.; Suresh, S.: Summary of Evaluation of AAA Concrete Mixtures, Task 5 Special Study 2 Report. In: Penndot Research, December 2005.

Part 4:

Fiber Reinforcement

Jürgen Schnell
Prof. Dr.-Ing.
TU Kaiserslautern
Fachgebiet Massivbau und Baukonstruktion
Kaiserslautern, Germany

Florian P. Ackermann
Dipl.-Ing.
TU Kaiserslautern
Fachgebiet Massivbau und Baukonstruktion
Kaiserslautern, Germany

Ronald Rösch
Dr. rer. nat.
Fraunhofer-Institut für Techno- und Wirtschaftsmathematik ITWM
Kaiserslautern, Germany

Tetyana Sych
Dipl.-Math. Tech.
Fraunhofer-Institut für Techno- und Wirtschaftsmathematik ITWM
Kaiserslautern, Germany

Statistical analysis of fibre distribution in ultra high performance concrete using computer tomography

Summary

In a joint research project of the Kaiserslautern University of Technology and the Fraunhofer ITWM Kaiserslautern fibre reinforced concrete was analysed using the computer tomography method. Particular attention should be paid to the evaluation and analysis of the distribution and the orientation of the fibres. In primary test series the applicability of the method becomes apparent.

Keywords: *fibre distribution, fibre orientation, computer tomography*

1 Introduction

Concerning its compressive strength, concrete is classified in normal-, high performance- and ultra-high performance concrete (UHPC). UHPC are concretes with a compressive strength over 150 MPa. The ductility decreases with increasing compressive strength. Therefore, UHPC shows very brittle fracture behaviour with an abrupt breakdown under compression. In order to accomplish a more ductile behaviour and a good crack control, steel fibres can be admixed. They will not only improve the ductility in compression but also in tension.

For the function as load bearing element, the ductility has to be guaranteed. Therefore a uniform distribution of fibres is aimed at. To some extent the geometry of the structural system and the fresh concrete characteristic effect the orientation of fibres. Self compacting concretes with their capability of flow behaviour exhibit an orographical direction of fibres, too.

In case the fibres are lined up matching the tension trajectories, the optimal tension bearing capacity is effected. Normally, the fibres are spatially distributed at random. So, it is quite reasonable that the determination of the distribution of fibres is very important in order to verify the realistic tension bearing capacity.

Aim of the research project of the Kaiserslautern University of Technology in collaboration with the Fraunhofer ITWM is the generation and evaluation of tomography pictures from fibre reinforced specimens. The focus of such research work has been put on the analysis of the fibre arrangement in relation to volume ratio, specific fibre length and directional distribution. Thereby, steel fibres as well as synthetic fibres should be looked on.

2 Existing methods

The application of fibre reinforced concrete mixes necessitates the random control of fibre ratio and fibre distribution. This requirement arises in research work as well as in quality controls at the building site and in giving expertises in cases of damage. Until now, the determination of fibre ratio of fresh and hardened concrete is very labour-intensive (elutriation of the fibres or destruction of a specimen and afterwards disentanglement and weighing of the fibres).

The Institute for Building Material, Solid Construction and Fire Control (iBMB) of the Braunschweig Technical University has developed a process in order to evaluate the steel fibre volume ratio of cube specimens. Using magnetic induction of ferromagnetic materials, the apparatus provides certain results of the volume ratio (see http://www.hertznet.de/messtechnik.html).

Tue et. al. [1] have demonstrated that the optoanalytical method provides practical results. The orientation of fibres can be rated with a sufficient accuracy. Actually, the method has to be achieved on separated intersections which -in terms of labour- is very costly.

In [2] initial researches for the determination of fibre distribution using computer tomography are described. At this time, it was possible to gather tomographic pictures but not to analyse the fibre distribution and orientation. The computer programs did not cope to solve this problem yet.

Investigations using the computer tomography in analysing structures of concrete specimen (e.g. microporous structure) were also arranged by the Federal Institute for Materials Research and Testing (BAM, Berlin) [3].

Today, the computer programs show a higher development status. Within the research project, the existing programs should be enhanced with further details in order to get the possibility of an easier determination.

Supplementary to the magnetic and optoanalytical systems the computer tomography provides the opportunity to evaluate the volume ratio and furthermore the exact orientation and direction of any fibre reinforced concrete.

3 Fundamentals of computer tomography

A computer tomographic image is created by directing X-rays through an object from multiple orientations and measuring their resultant decrease in intensity (see [4]).

The simplest common elements of X-ray radiography are an X-ray source, an object to be imaged through which the X-rays pass, and a series of detectors that measure the extent to which the X-ray signal has been weakened by the object (Figure 1). A single set of X-ray

intensity measurements on all detectors for a given object position and scanner geometry is termed a radiograph.

The fundamental principle behind computer tomography is to acquire multiple radiographs of an object over a range of angular orientations. By this means, additional dimensional data are obtained in comparison to conventional X-radiography, in which there is only one view. These data and a specialized algorithm [5] are then used to reconstruct the distribution of X-ray attenuation in the slice plane. Next step is to create two-dimensional images called slices, because they correspond to what would be seen, if the object were sliced along the scan plane.

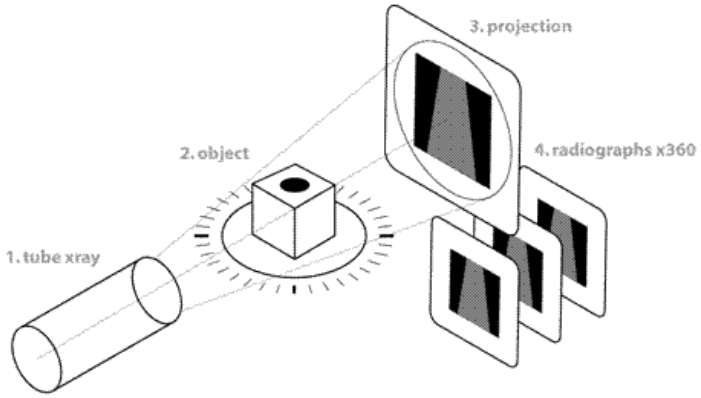

Figure 1: Schematic illustration of an X-ray scanning process

The gray levels in a CT slice correspond to X-ray attenuation, which reflects the proportion of X-rays scattered or absorbed as they pass through each voxel. X-ray attenuation is primarily a function of X-ray energy and the density and the atomic number of the material being imaged.

By acquiring a stacked, contiguous series of CT images, data describing an entire volume can be obtained.

4 Tests

4.1 First test series

In the first test series, a small specimen of an UHPC beam was investigated. The UHPC was provided with fibre volume ratio of 144 kg/m³, which is equivalent to 1.83 Vol.-% having used the straight DM 0.15/6.0 microfibre from Krampe-Harex. Table 1 gives a detailed description of the specimen.

Table 1: Description of the sample, series #1

Concrete	Dimensions	Type of fibres	Fibre length	Fibre diameter
UHPC_A	5×5×10 mm	DM 0.15/6.0	6 mm	0.15 mm

The sample was scanned using a µCT-System at RJL Micro and Analytic, Bernhard E. Heneka GmbH. The effective pixel size is 9.77 µm. It becomes apparent that already the

small samples of series #1 show good results. In a third series, bigger sized samples of UHPC are being examined in order to get a better accuracy.

4.2 Second test series

Two portions, cut from conventional steel fibre-reinforced concrete beams made with different mix design, were used for the second series. The concrete was provided with fibre volume ratio of 60 kg/m³, what is equivalent to 0.76 Vol.-% having used the straight endhooked HE+ 1.0/60 fibre from Arcelor-Bissen. Table 2 gives a detailed description of each piece.

Table 2: Description of the samples, series #2

Concrete	Dimensions	Type of fibres	Fibre length	Fibre diameter
SFHE_A	50×50×50 mm	HE+ 1.0/60	60 mm	1 mm
SFHE_B	47×50×52 mm	HE+ 1.0/60	60 mm	1 mm

Both samples were scanned using a µCT-System at Fraunhofer IZRT, Fürth. In both cases the effective pixel size is 75.81 µm. The size of the samples ensures that the X-rays come through the entire body of the volume. Due to the high density of the concrete matrix and the high energy absorption rate of steel fibres, for the time being this is the maximum possible sample size allowing to achieve complete 3D scans as exactly as possible. In the following, however, it will be shown that in order to obtain good statistical results for the bigger sized fibres (macro fibres) one needs 3D images produced at bigger samples. The search for a possibility to scan larger volumes is currently in progress.

4.3 Third series

A third series objecting studies on bigger sized UHPC samples with the dimensions 50x50x50 mm is in progress now. So the orientation analysis of UHPC could be determined with a smaller scatter band.

5 Mathematical algorithms for orientation analysis and test results

5.1 Image processing and analysis

The computer aided image processing and analysis was performed using MAVI software developed at Fraunhofer ITWM, which includes a set of dedicated algorithms.

The reconstructed 3D images were cropped in order to remove the empty space around the volumes. After the crop procedure they contain 456x474x932 (respectively, in x, y and z directions) pixels for the UHPC_A sample, 620×625×570 pixels for the SFHE_A sample and 580×610×640 pixels for the SFHE_B one and are coded on 8 bits (the pixels are labelled from 0 (black) to 255 (white)).

5.2 Segmentation of the fibres

A first step of the segmentation process consists in obtaining threshold images to separate fibres and concrete matrix. The threshold level is set in such way as to minimize the number of isolated voxels in each phase. Pixels having higher gray value than the threshold level are interpreted as belonging to fibre phase. Figure 2 shows the two dimensional slices of

reconstructed 3D images of UHPC_A (top), SFHE_A (middle) and SFHE_B (bottom) prior to (left) and after (right) the fibres were segmented. The slices were taken perpendicular to the x-direction.

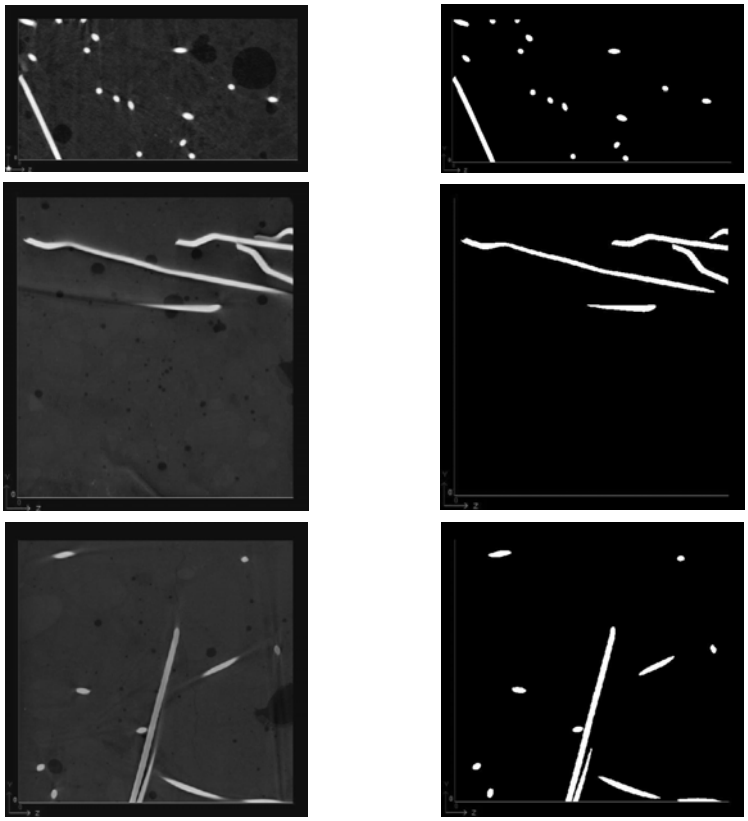

Figure 2: Two dimensional slices of 3D images prior to and after the segmentation.

5.3 Test results

After the segmentation process has been done, it is possible to compute the geometric characteristics of the fibre phase. The method is based on measuring the Minkowski functionals (or intrinsic volumes) [6]. In 3D these are volume V, surface S, integral of mean curvature M, and integral of total curvature K. For convex particles, M and K are the surface integrals of the mean and total curvatures, respectively. In addition, they can be extended to finite clusters of convex particles by use of an inclusion-exclusion principle (see [7, Section 2.2.1] for details).

For macroscopic homogeneous random structures, the densities of the Minkowski functionals are considered. That means, instead of the total values, one considers the expected values of the functionals per unit volume. Thus the analysis starts with computing the volume fraction (1-porosity) V_V, the specific surface area S_V, the density of the integral of mean curvature M_V, and the density of the integral of total curvature K_V.

Based on these results, other characteristics can be deduced. For fibre structures, the specific fibre length $L_V = M_V / \pi(1-V_V)$ is of particular interest.

Table 3 contains the measured values of fibre volume fraction and specific fibre length for the considered concrete samples.

Table 3: Measured values

Specimen	Fibre volume fraction	Specific fibre length
UHPC_A	1.6 Vol.-%	7868.97 m/m³
SFHE_A	0.5 Vol.-%	7256.71 m/m³
SFHE_B	0.7 Vol.-%	7941.48 m/m³

It can be seen that the measured fibre volumes of the samples UHPC_A (effective: 1.83; measured: 1.6) and SFHE_B (effective: 0.76; measured: 0.7) correspond approximately to the used fibre ratio. In specimen SFHE_A the fibre volume ratio is undercut. Furthermore, the fibres are not distributed spatially at random in this specimen. They are oriented in one direction primarily.

5.4 Fibre orientation analysis

Estimated distribution of fibre orientation in a typical point of a fibre was obtained by use of the “Field Features”–Module of the image analysis software MAVI. The estimator is based on a discrete version of the Crofton formulae from integral geometry and uses measurements of lengths of projection onto lines. Due to discretisation, the orientations of the lines are limited to the following, given by the grid: three coordinate axes, six face diagonals and four space diagonals. A thorough description of this method can be found in [6].

Figures 3, 4 and 5 compare 3D renderings of steel fibres and estimated fibre orientation distribution for the concrete samples. The results of fibre orientation analysis have been mapped onto the sphere by the method described in [8].

The steel fibres in the UHPC_A sample on Figure 3 show an orientation towards the diagonal direction in the x-z-plane as well as in the x-y-plane, which also can be seen in the rendered image. The steel fibres in the SFHE_A sample on Figure 4 show a concentration around the z- axis with some scatter in x-direction, which correlates well with visual information on the rendered volume image. The fibres in the SFHE_B sample (Figure 5), however, tend to isotropy with light accent in the z-direction, which again corresponds to what can be seen on the rendered image.

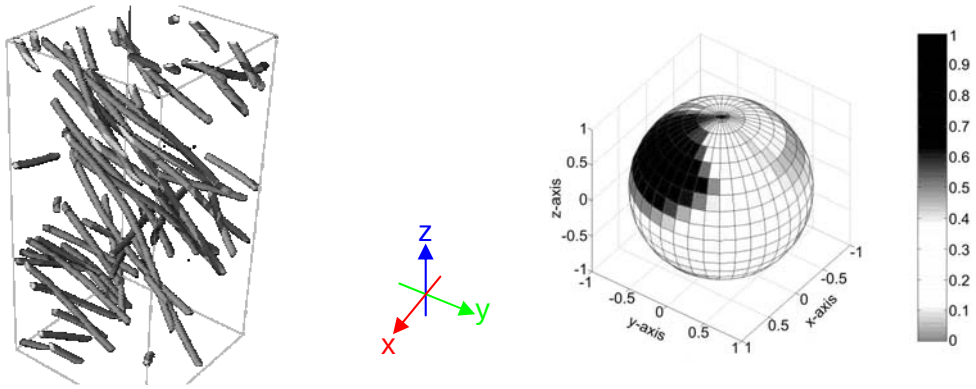

Figure 3: 3D rendering of steel fibres (left) and estimated fibre orientation (right) of UHPC_A

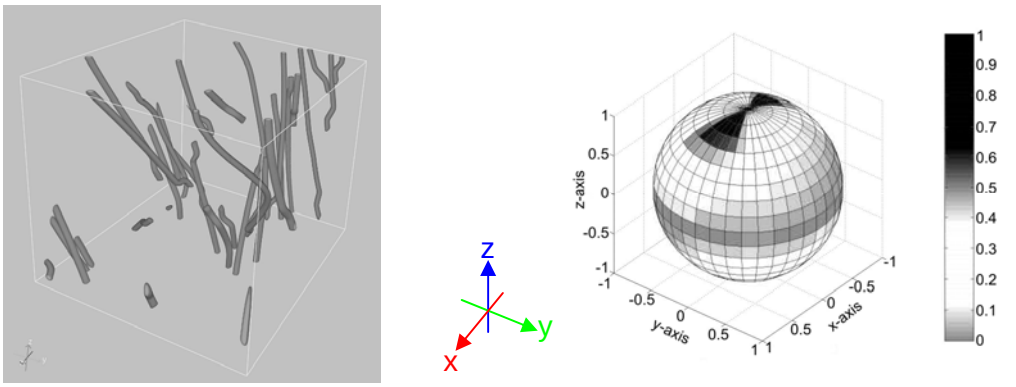

Figure 4: 3D rendering of steel fibres (left) and estimated fibre orientation (right) of SFHE_A

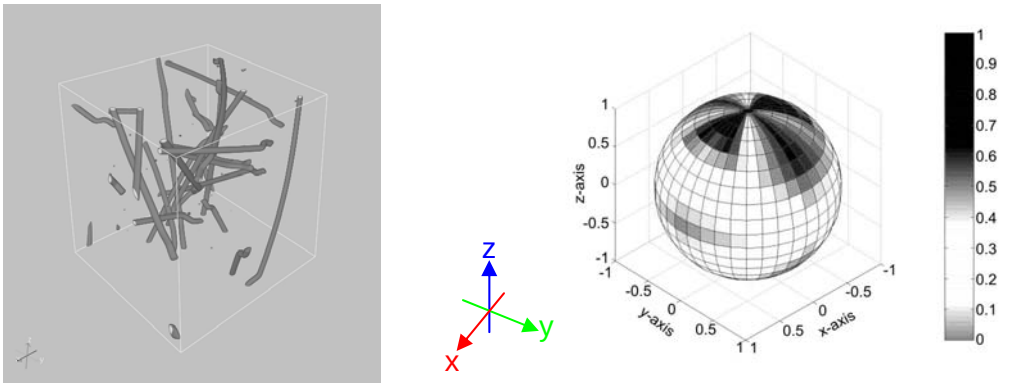

Figure 5: 3D rendering of steel fibres (left) and estimated fibre orientation (right) of SFHE_B

Table 4: Orientation values

UHPC_A		SFHE_A		SFHE_B	
(x,y,z)	**%**	**(x,y,z)**	**%**	**(x,y,z)**	**%**
[1 0 0]	6.11 %	[1 0 0]	0.00 %	[1 0 0]	1.92 %
[0 1 0]	2.80 %	[0 1 0]	0.00 %	[0 1 0]	10.15 %
[0 0 1]	4.93 %	[0 0 1]	39.72 %	[0 0 1]	19.31 %
[1 1 0]	8.23 %	[1 1 0]	5.10 %	[1 1 0]	6.47 %
[-1 1 0]	3.68 %	[-1 1 0]	1.21 %	[-1 1 0]	5.90 %
[1 0 1]	28.13 %	[1 0 1]	15.29 %	[1 0 1]	6.62 %
[-1 0 1]	0.00 %	[-1 0 1]	4.46 %	[-1 0 1]	8.18 %
[0 1 1]	0.84 %	[0 1 1]	0.00 %	[0 1 1]	11.61 %
[0 -1 1]	17.25 %	[0 -1 1]	18.29 %	[0 -1 1]	11.43 %
[1 1 1]	1.03 %	[1 1 1]	3.53 %	[1 1 1]	6.41 %
[-1 1 1]	5.59 %	[-1 1 1]	4.42 %	[-1 1 1]	4.92 %
[1 -1 1]	19.57 %	[1 -1 1]	5.12 %	[1 -1 1]	2.91 %
[-1 -1 1]	1.83 %	[-1 -1 1]	2.86 %	[-1 -1 1]	4.16 %

In Table 4 the results of the orientation analysis are summarised. In addition to the principal axis directions the 45° rotated directions were determined. So altogether there are 13 possible directions. If the fibres are directed parallel to the tension trajectories the full load bearing capacity can be reached. A deviating orientation from the tension direction results in

a lower bearing capacity. In the technical literature this effect is considered by the fibre orientation value η (e.g. see [9]). Due to the precision division into 13 directions the load bearing capacity of the fibres can be considered concerning the related orientation.

6 Conclusions and outlook

A procedure for estimating fibre orientation in fibre-reinforced concretes using 3D tomographic images was accomplished. Applications to three different samples demonstrate the use of this approach for assessing fibre orientations.

It should be noted, that the number of fibres within the tested samples is too small in order to speak about reliable statistical analysis. Increasing of the volume dimensions, however, will lead to the lower pixel resolution and, consequently, to more complicated segmentation and analysis procedures.

Obtaining volume images of larger concrete samples and application of new practical approach to fibre orientation estimation by use of anisotropic Gaussian filtering described in [8] is the objective of our future work.

7 Acknowledgements

We would like to thank B. E. Heneka and Vitali Weizel for image acquisition, H. Riedel for 3D rendering, and M. Godehardt for fibre orientation plots. Furthermore we are grateful to the German Society for Concrete and Construction Technology DBV for financial support.

8 References

[1] Tue, N. V. et. al.: Ein optoanalytisches Verfahren zur Bestimmung der Faserverteilung und –orientierung in stahlfaserverstärktem UHFB, Beton- und Stahlbetonbau 102 (2007), Heft 10, S. 674-680

[2] Linsel, S.; Dehn, F.: Determination of fibre distribution in self-compacting steel fibre concrete (SCSFC) by computer tomography (CT), Proceedings of the 6. International Symposium on utilization of High-Strength/High-Performance Concrete, Leipzig 2002, S. 1129-1137

[3] F. Weise, B. Meng: Identifikation von Schädigungsprozessen in Beton mit innovativen Prüftechniken, DAfStb-Fachtagung 2007

[4] Ketcham, R.A.; Carlson, W.D.: Acquisition, optimization and interpretation of X-ray computed tomographic imagery: Applications to the geosciences. Computers and Geosciences, 27, 381-400, 2001.

[5] Herman, G.T.: Image reconstruction from projections. AcademicPress, New York, 1980.

[6] Schladitz, K.; Ohser, J.; Nagel, W.: Measuring intrinsic volumes in digital 3D images. DGGI, 247-258, 2006

[7] Ohser, J.; Mücklich, F.: Statistical Analysis of Microstructures in Materials Science. J. Wiley & Sons, Chichester, New York, 2000

[8] Robb, K.; Wirjadi, O.; Schladitz, K.: Fiber orientation estimation from 3D image data: Practical algorithms, visualization, and interpretation. Proc. 7th International Conference on Hybrid Intelligent Systems (HIS 2007), Kaiserslautern, Germany, 2007.

[9] Lin, Y.: Tragverhalten von Stahlfaserbeton. Deutscher Ausschuss für Stahlbeton, Heft 494, Berlin 1999.

John Wuest
Dr., Civil Engineer EPF
MCS - Ecole Polytechnique Fédérale (EPFL)
Lausanne, Switzerland

Emmanuel Denarié
Senior Scientist, Dr. Civil Engineer EPF
MCS – Ecole Polytechnique Fédérale (EPFL)
Lausanne, Switzerland

Eugen Brühwiler
Professor, Dr. Civil Engineer ETH
MCS - Ecole Polytechnique Fédérale (EPFL)
Lausanne, Switzerland

Model for predicting the UHPFRC tensile hardening response

Summary

Ultra High Performances Fibre Reinforced Concretes (UHPFRC) are characterised by an extremely low permeability and outstanding mechanical properties. These characteristics make UHPFRC suitable to locally “harden” reinforced concrete structures subjected to aggressive environments and/or mechanical stresses. Results from uni-axial tensile tests on different UHPFRC materials and cast in different directions have shown a variety of mechanical behaviours. In particular, the tensile strain-hardening behaviour ranges from 0.1-0.4 % but, in some cases, completely vanishes. A meso-mechanical model is developed to predict the UHPFRC tensile response as a function of the volume, aspect-ratio, distribution and orientation of the fibres and the mechanical properties of the matrix. The model allows the determination of the effect of two parameters, the coefficient of orientation and the volume of fibre, on the tensile strain hardening behaviour.

Keywords: *UHPFRC, strain hardening, fibre orientation, simulation model*

1 Introduction

More and more durability and load carrying capacity problems emerge from aging existing civil structures. In order to solve these problems, UHPFRC materials are being employed because of their easy on-site casting combined with their excellent strength and durability properties. The tensile performances of these materials are dependent on various factors such as the quality of the matrix, the orientation and distribution of the fibres, the aspect-ratio and the volume of fibres.

In [1], the fibre orientation and distribution in two specimens constituted from different fibrous mixes, which showed dissimilar hardening behaviour, were investigated through image analysis. Unfortunately, even if a difference was observed, it was not directly possible to determine if the fibre orientation was responsible of the increase of the hardening domain. Moreover, [1] tested also two specimens (same mix) cast in different directions. The results showed two very dissimilar behaviours in tension (hardening-softening and only softening). In

this case the fibre orientation analysis showed a significant difference in the coefficient of orientation which explained the different tensile responses observed. Moreover, the different models developed by [2], [3], [4], [5] to determine the response of fibre reinforced composite are not sufficient for predicting the extent of the hardening domain in UHPFRC.
These two remarks emphasize the need of the development of a novel meso-mechanical model that allows predicting the hardening domain in tension based on the factors mentioned above.

2 Materials and experimental results

2.1 Materials properties

The tensile behaviour of three materials is studied in this paper. The first two UHPFRC (UHPFRC-1 and 2) investigated contain a high amount of cement (>1000 kg/m^3), a relatively high quantity of steel fibres (4-6%) and has a low water/cement ratio (<0.15). A higher aspect ratio of the fibres was used for UHPFRC 2 compared to UHPFRC 1 leading to a decrease in fibre volume in order to obtain sufficient workability. The third material is an ECC developed and tested by [6] and had 2% by volume of PVA fibres.

2.2 Experimental results

UHPFRC-1 and 2 were tested using dogbone specimens with a total length of 700 mm, with a constant cross-section of 5000 mm^2 (100x50 mm) over a length of 300 mm. The measurements were done over a 350 mm distance (figure 2). The ECC was also studied with a dogbone specimen with a constant cross-section of 968 mm^2 over a length of 185 mm. All specimens were cast horizontally.
UHPFRC-2 and ECC had a significant hardening domain, i. e. 0.24% and 1% respectively. Contrary to this, UHPFRC-1 had a more limited hardening domain (0.1%). The fibre orientation and distribution were investigated in [1] on one specimen of each UHPFRC group (Table 1). The results show that the UHPFRC-2 has highly oriented fibres parallel to the principle stress compared to UHPFRC-1, which helps increasing the hardening domain.

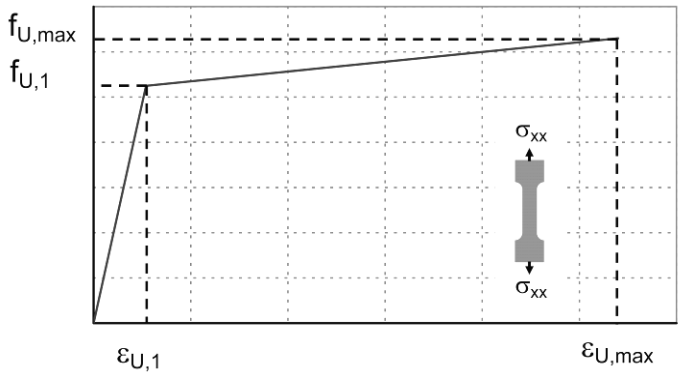

Figure 1: Description of the parameters of a tensile test response mentionned in table 1

Table 1: Tensile test results for the three groups of tested specimens

		Group specimen results				Selected specimen results			
		$\varepsilon_{U,1}$ [%]	$f_{U,1}$ [MPa]	$\varepsilon_{U,max}$ [%]	$f_{U,max}$ [MPa]	$\varepsilon_{U,1}$ [%]	$f_{U,1}$ [MPa]	$\varepsilon_{U,max}$ [%]	$f_{U,max}$ [MPa]
UHPFRC-1	Average	0.018	9.0	0.07	9.65	0.021	10	0.1	10.7
	Std. Dev.	0.002	0.9	0.02	0.7				
UHPFRC-2	Average	0.027	10.5	0.27	12.6	0.032	11.5	0.24	13
	Std. Dev.	0.006	1.0	0.06	1.4				
ECC	Average	-	3.11	0.99	4.89	Not mentionned			
	Std. Dev.		0.23	0.57	0.07				

3 Mechanical model of random micro cracking

The model for predicting the response in tension of hardening-softening cementitious materials is explained in details in [7] and consists of two parts:

- Sectional model of one micro-crack

This part of the model was adapted from the approach developed by [9]. It consists in the superposition of the matrix softening behaviour (σ_m), the pre-stress already present in the fibre before cracking (σ_{fps}) and the fibre bridging (σ_{fb}) to predict the sectional response.

$$\sigma_U(w) = \sigma_{fps}(w) + \sigma_{fb}(w) + \sigma_m(w) \quad (1)$$

The fibre bridging is considered by equation 2 which corresponds to the summation of the contribution of all the fibres depending of their out of plane angle f(θ).

$$F_{fb} = \sum_{i=0}^{n_f} F_{fb,i} \cdot f(\theta) \quad (2)$$

The force bridged by each fibre ($F_{fb,i}$) for a crack opening (w) can be calculated using equations 3 and 4 depending on the crack opening.

$$F_{fb,i} = \sqrt{\frac{\pi^2 \tau_0 E_f {d_f}^3 (1+\eta)}{4} w} \qquad 0 < w < w_{db} \quad (3)$$

$$F_{fb,i} = \pi d_f \tau (L_e - w + w_{db}) \qquad w_{db} < w < w_{db} + L_e \quad (4)$$

$$w_{db} = \frac{4\tau_0 {L_e}^2}{E_f d_f (1+\eta)} \qquad \eta = V_f E_f / (V_m E_m) \quad (5)$$

$$\tau = \tau_0((L_e + w_{db}) - w_{db})w + \tau_0\left(1 + \frac{w_{db}}{(L_e + w_{db} - w_{db})}\right) \quad (6)$$

With w_{db}: crack opening at which full debonding is complete; d_f : fibre diameter; V_f: fibre volume; V_m: Matrix volume; E_f: Fibre module of elasticity; E_m: Matrix module of elasticity.

The hypotheses considered are a constant frictional stress τ_0 during the debonding process, a uniform distribution of the fibre embedment length (L_e) and the decay of the frictional stress with increasing crack opening (equation 6).

- Combination of discretely distributed micro-cracks

Potential cracks spaced every 0.02 mm are created on all the tensile specimen length. They are activated if the stress exceeds the first cracking resistance ($f_{U,1}$). The first cracking resistance is randomly distributed over the specimen length following a normal distribution. The average and standard-deviation are deduced from the experimental results.
The stress releases in the neighbourhood of propagating micro-cracks locally prevent creating a further micro-crack. Moreover, in the model, the stress increases until one of the sections can no more withstand it and enters into the softening behaviour.
The total displacement is calculated using equation 7 which takes into account the elastic displacement of the un-cracked part and the contribution of all the opening cracks. A similar approach has been suggested in [10].

$$\Delta l = \sum_{i=0}^{N} w_i(\sigma_u) + \frac{\sigma_u}{E_u} L_R \qquad (7)$$

The hypothesis considered in this part of the model is that only the resistance of the matrix varies.

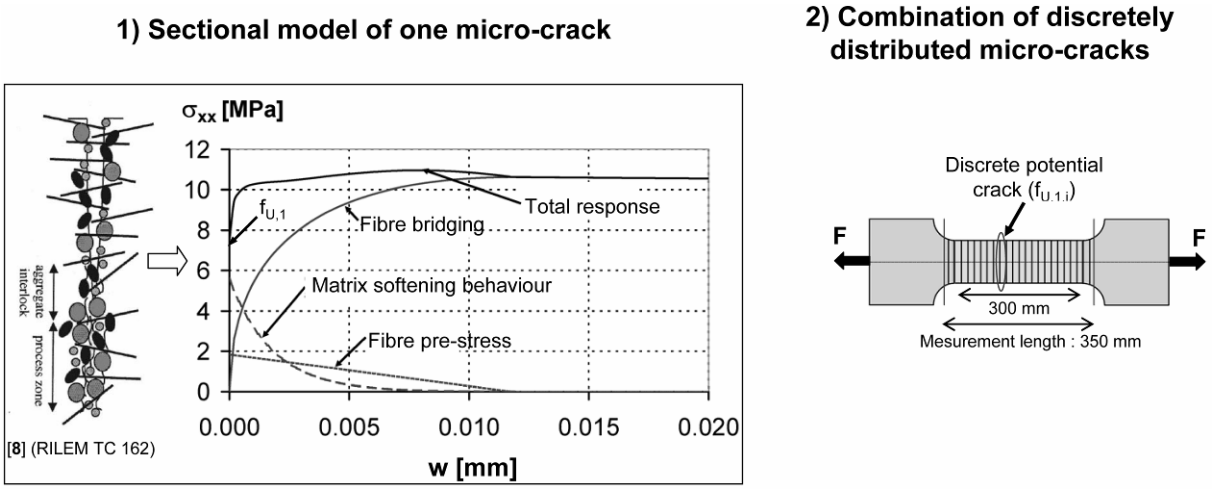

Figure 2: Description of the two parts of the model

4 Validation

The model is validated using the results of the three tensile tests described in section 2.2.
The parameters used in the simulation are given in table 2. For UHPFRC-1 all the properties are directly obtained from the experimental results.

Table 1: Description of the parameter used in the simulation (GF is the matrix fracture energy, Ff,R is the fibre maximum resistance in tension and Gd is the chemical bond between the fibre and the matrix)

		UHPFRC-1	UHPFRC-2	ECC
Sectional model of a micro-crack	τ_0 [MPa]	6.9	6.5	2.44
	G_d [J/m^2]	-	-	4.71
	C_{OR} [-]	0.24	0.66	0.43
	V_f [%]	6.39	4.27	2.00
	E_f [MPa]	210'000	210'000	48'000
	E_m [MPa]	40'000	40'000	15'900
	L_f [mm]	10	13	12
	d_f [mm]	0.2	0.16	0.039
	G_F [J/m^2]	10	10	50
	$F_{f,R}$ [MPa]	3200	2500	1000
Combination of discretly distributed mico-cracks	E_U [J/m^2]	49'000	52'000	16'438
	$f_{U,1,sim}$ (Average) [MPa]	10.1	13.5	4.6
	$f_{U,1,sim}$ (Std. Dev.) [MPa]	0.7	1.2	0.6

For UHPFRC-2, the frictional stress (τ_0) is obtained by back analysis of the ultimate resistance of the specimen ([7]). For the ECC, the parameters were found in [6] and [11]. Only the coefficient of orientation is determined by back analysis of the ultimate tensile resistance.

a) b)

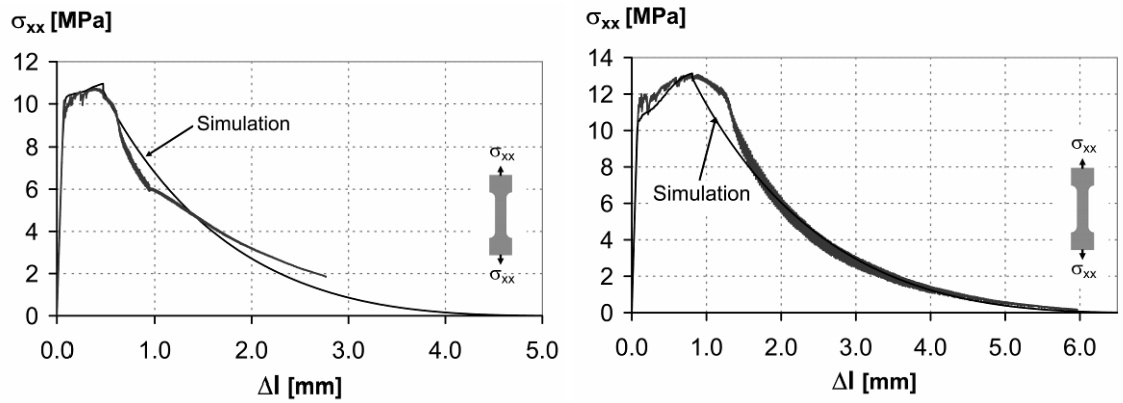

Figure 3: Comparing experimental and simulation results: a) UHPFRC-1; b) UHPFRC-2

For the two UHPFRC materials tested, a good correspondence between the simulations and the tensile test response is obtained in terms of the shape of the curves and the extent of the hardening domain. The model does however not perfectly follow the experimentally measured softening curves; this is due to the configuration of the test used. Dogbone specimens, which are less adapted for measuring the softening domain ([7]), were employed and explain the obtained difference in shape.

The last validation is done using the ECC. In this situation, the equation for the fibre pull-out has to be modified to take into account the chemical bond (G_d).

$$P = \sqrt{\frac{\pi^2 \tau_0 E_f {d_f}^3 (1+\eta)}{4} w + \frac{\pi^2 G_d E_f {d_f}^3}{2}} \tag{8}$$

We can observe on figure 4 that the model is able to reproduce the extent, the shape of the hardening domain and the drop after the peak resistance due to fibre rupture.

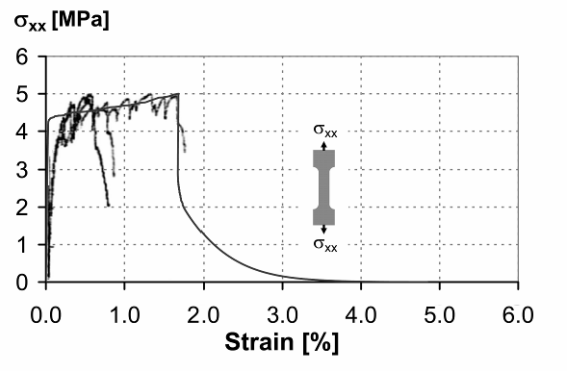

Figure 4: Comparing experimental and simulation results for the ECC

On the other side, the model gives a more rigid response in the elastic domain than the experimentally measured one; this is mostly due to the lack of information on this material, particularly the modulus of elasticity.

5 Parametric study

Two parameters will be investigated in this study: the effect of the coefficient of orientation and the fibre volume.

a) Coefficient of orientation

The effect of the coefficient of orientation is investigated using the same parameters as in table 1 for the specimens UHPFRC-1 and 2 but varying the coefficient of orientation from 0.56 to 1.

As can be seen on figure 5 a), the use of a coefficient of orientation of 0.56 for Mix 2, leads to a response which is similar to the smallest tensile test of the group. Thus, all the tested specimens should present a coefficient of orientation higher than 0.56 if we consider the hypothesis of a constant volume of fibre. Moreover, the development of cracks is increased with the use of a higher coefficient of orientation, leading to an extended hardening domain. As can be seen on figure 5 b), the Mix 2, which has fibres with a higher aspect ratio has always an increased hardening domain compared to Mix 1 for the same coefficient of orientation. This is mainly due to the fact that the fibre of Mix 2 requires a higher force before being pulled-out.

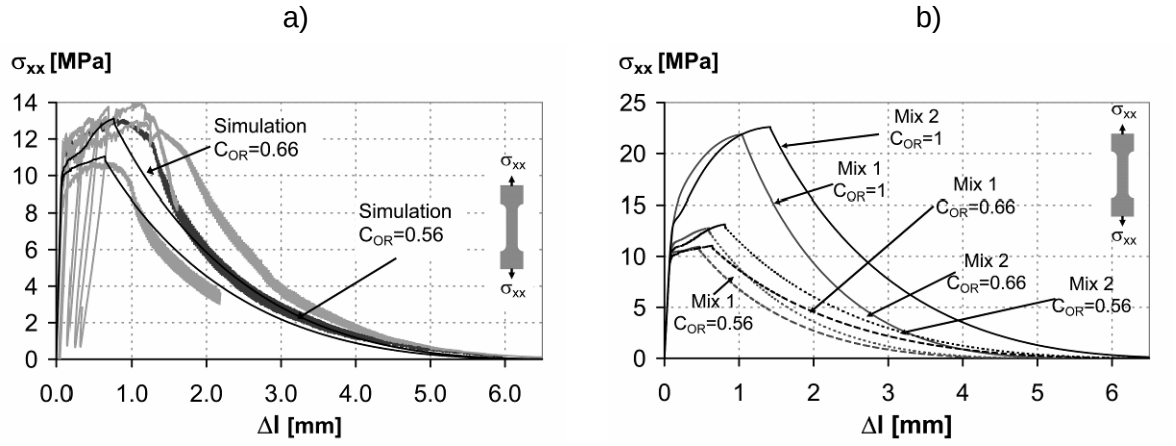

Figure 5: a) Comparison between the simulation with a COR of 0.56 and the experimental resullts for UHPFRC-2; b) Effect of the COR on the tensile response for Mix 1 and 2

Also, these fibres are more effective at bridging a crack. In other words, they allow withstanding a larger crack opening with the same force compared to those used in Mix 1.

b) Volume of fibre

The effect of the volume of fibre is investigated on the two same mixes than in the previous study. The volume of fibre is varied between 5 and 9 % and between 3 and 6 % for Mix 1 and Mix 2 respectively.

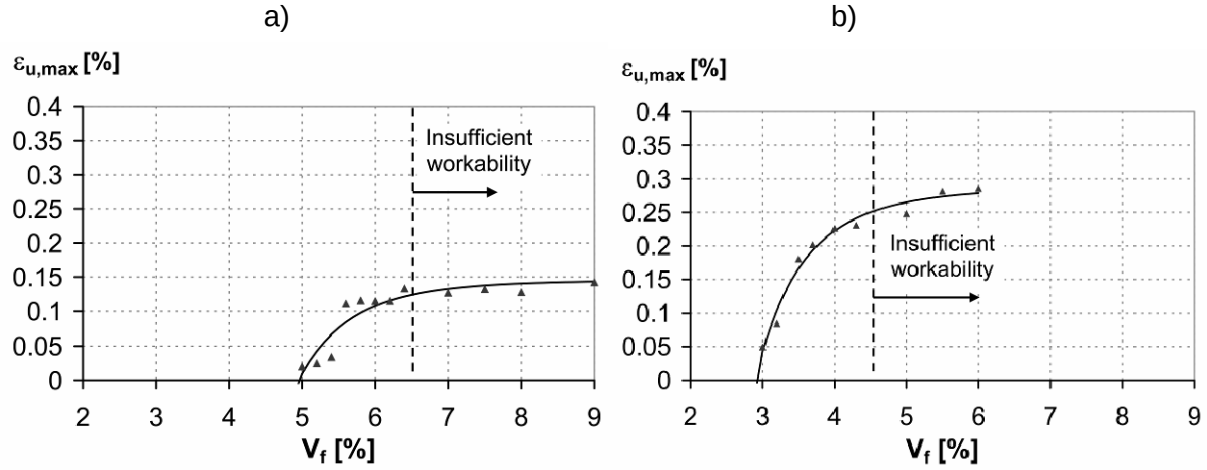

Figure 6: Extent of the hardening domain as a function of Volume of fibre: a) Mix 1; b) Mix 2

The extent of the hardening domain does not increase linearly with increasing volume of fibre but tends to an asymptotic value (figure 6); i. e. with Mixes 1 and 2 a maximum hardening domain of about 0.15 and 0.3 % respectively may be reached. It is important to point out that the slope of the hardening domain versus volume of fibre is more important for Mix 2. A decrease of the fibre volume has thus a more significant effect on the hardening behaviour for Mix 2. Moreover, Mix 1 seems to be more effective with respect to the use of the hardening domain. Assuming that the mix is still applicable with high volume of fibre, Mix 1

(V_f=6%) has already attained it's asymptotic value while in Mix 2 (V_f=4%) it is still necessary to increase the volume of fibre before attaining the asymptotic value.

6 Conclusions

- A novel meso-mechanical model was developed and validated with experimental results in order to predict the extent of the hardening domain for different cementitious materials.
- The orientation of the fibres in the specimen has a significant impact on the hardening response. A coefficient of orientation smaller than 0.64 does not allow creating an extended hardening behaviour.
- The tensile hardening response of mixes with a high fibre aspect-ratio and lower dosages are more sensitive to a variation of the fibre dosage.

7 Acknowledgments

The Swiss State Secretariat for Education and Research (SER) in the context of the European project Sustainable and Advanced Materials for Roads Infrastructures (SAMARIS) has financially supported this research.

8 References

[1] Wuest J., Denarié E., Brühwiler E.: Measurement and modelling of fibre distribution and orientation in UHPFRC. In: Proc. HPFRCC5, Proceedings PRO 53, Mainz, pp. 259-266, 2007.

[2] Naaman A.: Strain hardening and deflection hardening fiber reinforced cement composites. In: Proc. HPFRCC4, Proceedings Pro 30, Ann Arbor, pp.95-113.

[3] Li V. C., Leung C. K. Y.: Steady-State and Multiple Cracking of Short Random Fiber Composites. In: ASCE Journal of Engineering Mechanics 188, No 11, pp. 2246-2264, 1992.

[4] Pfyl T.: Tragverhalten von Stahlfaserbeton. PhD Thesis ETH, N°15005, Zürich, 2003. (in German).

[5] Markovic I.: High-Performance hybrid-Fibre Concrete : Developpement and Utilisation. PhD Thesis, TU Delft, Delft, 2006.

[6] Li V. C., Wu C., Wang S., Ogawa A., Saito T.: Interface tailoring for Strain-hardening Polyvinyl Alcohol- Engineered Cementitious Composites (PVA-ECC). In: ACI Materials Journal 99, No 5, pp. 463-472, 2002.

[7] Wuest J.: Comportement structural des Bétons de Fibres Ultra Performants en traction dans des éléments composes. PhD Thesis, N° 3987, EPFL, Lausanne, 2007. (In French, submitted).

[8] RILEM TC 162-TDF: Test and Design Methods for Steel Fibre Reinforced Concrete. In: Materials and Structures 35, pp.579-582, 2002.

[9] Li V. C., Stang H., Krenchel H.: Micromechanics of crack bridging in fibre-reinforced concrete. In: Materials and Structures 26, pp.486-494, 1993.

[10] Yang J., Fischer G.: Simulation of the tensile stress-strain behaviour of strain hardening cementitious composites. In: Proc. Measuring, Monitoring and Modelling Concrete Properties, Alexandroupolis, pp. 25-31, 2006.

[11] Kanda T., LI V. C.: Practical Design Criteria for Satured Pseudo Strain Hardening Behavior in ECC. In: Journal of Advanced Concrete Technology 4, No 1, pp. 59-72, 2006.

Withit Pansuk
Dr., Researcher
Hokkaido University
Sapporo, Japan

Hideki Sato
System Engineer
Xincor miXell Co., Ltd.
Tokyo, Japan

Yasuhiko Sato
Dr., Associate Professor
Hokkaido University
Sapporo, Japan

Ryosuke Shionaga
Researcher
IHI Corporation
Yokohama, Japan

Tensile Behaviors and Fiber Orientation of UHPC

Summary

Ultra High Performance Concrete (UHPC), which combines the benefit of self compacting concrete and fiber reinforced concrete, was originally developed in this study. As is well known, the properties of fiber reinforced concrete strongly depend on the actual fiber characteristic in the mixture. The main parameters in this study were assigned as the fiber length and their orientation by the direction and distance of flow at casting. In order to investigate the tensile behavior of UHPC specimens, the direct tensile test on concentrically fiber reinforced prisms with the originally proposed test method was applied. Crack widths were measured by the image analysis of photos taken by the high-quality digital camera during the loading test. Moreover, the actual fiber distribution in test specimens was shown by the image analysis of pictures taken by the microscope. The number of steel fiber on the slides was counted separately from the matrix by the computer program. Finally, the effects of test parameters on tensile behaviors of developed UHPC mixture were shown by the stress-crack width relationship and measured fiber orientation number.

Keywords: *UHPC, steel fibers, tensile, fiber orientation, image analysis*

1 Introduction

The attempt to increase the strength of matrix in concrete has exacerbated the weakness of concrete because increasing strength is accompanied by increased brittleness. To try overcoming this weakness by increasing the ability of the composite to absorb energy after the matrix has cracked, fibers have been included into the concrete matrix to produce Ultra High Performance Concrete (UHPC). As is well known, the structural performance of UHPC members reinforced with steel fiber strongly depends on the actual tensile behaviors and fiber orientation. However, the existing test method for the tensile behaviors of fiber reinforced concrete such as the direct tensile test with strain gages/linear variable displacement transducers (LVDT's) or the bending test with an inverse analysis cannot provide the tensile characteristic of a single crack and the relationship with the actual fiber orientation on cracked plane. To predict the tensile behaviors of UHPC more precisely, the test method must be developed. The production of the specimens and the wall-effect highly

affect the test response so larger specimens compared with plain concrete have to be prepared in order to limit the effect of the walls on the test response as much as possible. For example, test cylinders can be drilled from larger specimens [1]. To show the post-cracking performance of steel fiber reinforced concrete correlated with the number of fibers crossing the crack, Kooiman [2] reported on counting fibers in the cracked cross-sections of beams tested in bending. Alternatively, fibers can be distinguished and counted with appropriate image analysis of picture of a beam cross-section since the concrete absorbed the flashlight while the fibers reflected it [3]. In this study, original mixture of UHPC was derived from the properties at the fresh state such as slump flow and funnel time and compressive strength at the hardening state. The main parameters in this study were assigned as the fiber length and their orientation by the direction and distance of flow at casting. Crack widths were measured by the image analysis of photos taken by the high-quality digital camera during the direct tensile test. Moreover, the actual fiber distribution in test specimens was shown by the image analysis of pictures taken by the microscope. Finally, the effects of test parameters on tensile behaviors of developed UHPC mixture were shown by the stress-crack width relationship and measured fiber orientation number.

2 Experimental program

2.1 Materials and mixture compositions

The appropriate mixture was derived from the properties at the fresh state such as the slump flow and the funnel time following the requirement of the self-compacting concrete [4]. The slump flow was measured with a 60 mm high slump cone for mortar with 70 mm diameter at the top and 100 mm diameter at the bottom. The diameter of the slump spread measured after the removal of the cone was approximately 300 mm. The funnel time was measured with 300 mm high V-shaped funnel for mortar with 30×30 mm^2 outlet size at the bottom. The controlled funnel time was approximately 10 seconds. Finally, the concrete mixture consists of 665 kg/m^3 of ordinary Portland cement, 1033 kg/m^3 of sand, 214 kg/m^3 of water, 443 kg/m^3 of 396 m^2/kg Blaine fineness of fly ash and 33 kg/m^3 of superplasticizer RHEOBUILD SP8LS. To adjust the mixture composition for the addition of the fibers, the content of the steel fibers was replaced against the same volume of the aggregates. Two types of straight steel fibers, 0.16 mm diameter with 6 and 13 mm long, were applied in the experiments. Their tensile strength is above 2000 MPa. For each batch of concrete, the mean value of compressive strength tested at an age of 28 days on three cylinder specimens was 62 MPa.

2.2 Mixing and casting procedures

A 60-liter Omni concrete mixer was used in this study. After powder materials, aggregate, admixture and water had been mixed, fibers were gradually added into the mixing matrix. The production process has a prominent influence on the quality of conventional fiber reinforced concrete [2]. Also, the method and intensity of compaction affect the orientation and the distribution of the steel fibers and the variation of the result [2]. Thus, the “flow-method” (Figure 1 [5]) consisted of filling the concrete from one side into the mold and allowed the concrete to level itself was applied in the casting of large specimens (Figure 2).

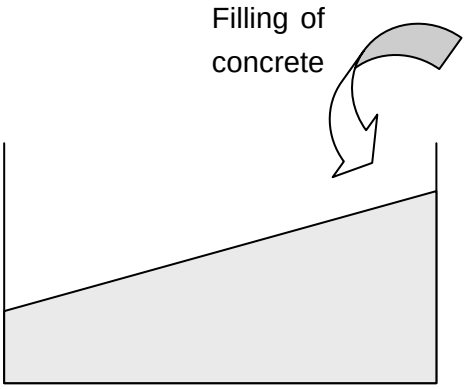

Figure 1: Filling method “Flow”

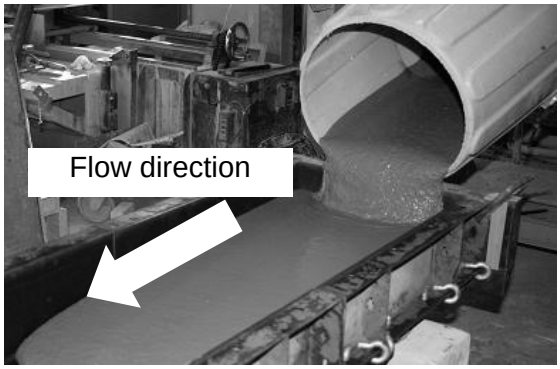

Figure 2: Filling the concrete into steel mold

2.3 Detail of specimens and parameters

The main parameters in this study were assigned as the fiber length and their orientation by the direction and distance of flow at casting. After mixing, the concrete was directly poured from the mixer into the wide steel mold in one direction as shown in Figure 2. The molds were 1200 and 1800 mm in total length having a width of 400 mm and a total depth of 100 mm as shown in Figure 3. After the poured concrete leveled itself in the mold, thin steel plate and frame were installed into the fresh concrete to select and separate the test zone that actual fiber orientation may be influenced by the flow distance, flow direction and the wall-effect as shown in Figures 3 and 4. Specimens were demolded one day after casting and only the concrete in the steel frame were cured in the room-temperature water until the age of 28 days. Then, each cured concrete specimens were cut into small test specimens for direct tensile test with the size of 150 × 50 × 40 mm as shown in Figure 6. The main parameters studied in the experimental program, the total numbers of specimens and reference pictures are summarized in Table 1 and Figure 5.

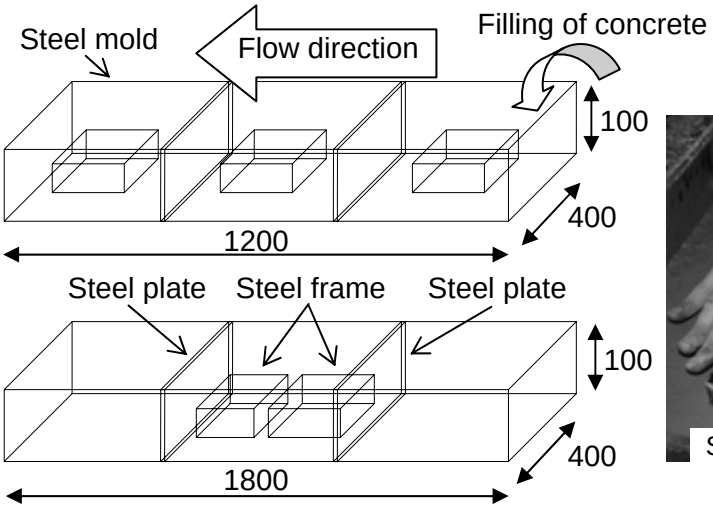

Figure 3: Size and arrangement of molds

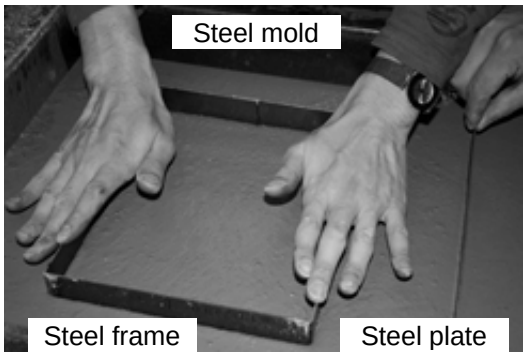

Figure 4: Installation of steel plate and frame

Table 1: Summary of parameters and numbers of specimens

Specimens	Fiber length	Direction to flow direction	Selected zone
Series A			
A-1	6 mm	Parallel	Center
A-2			
A-3		Perpendicular	
Series B			
B-1	13 mm	Parallel	Center
B-2		Perpendicular	
Series C			
C-1	6 mm	Parallel	Filling
C-2			Center
C-3			End

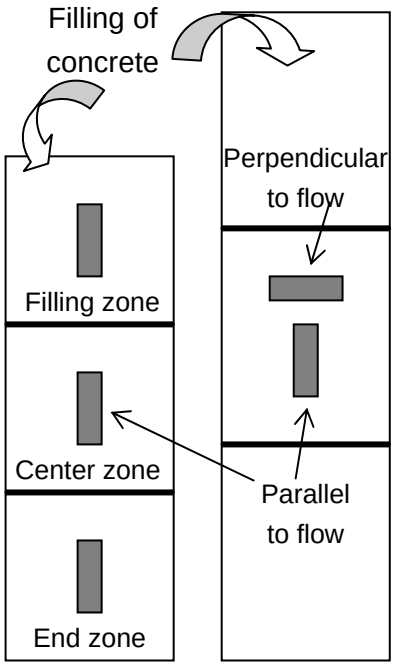

Figure 5: Selected zone for tensile test

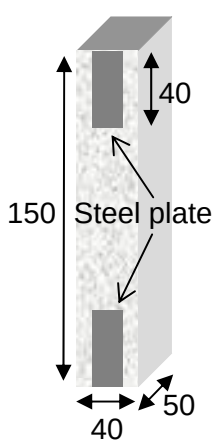

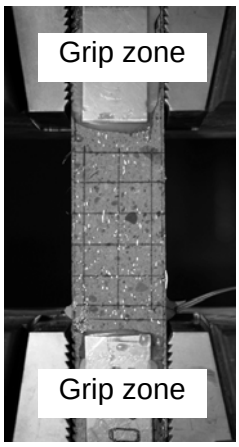

Figure 6: Specimens for the tensile test

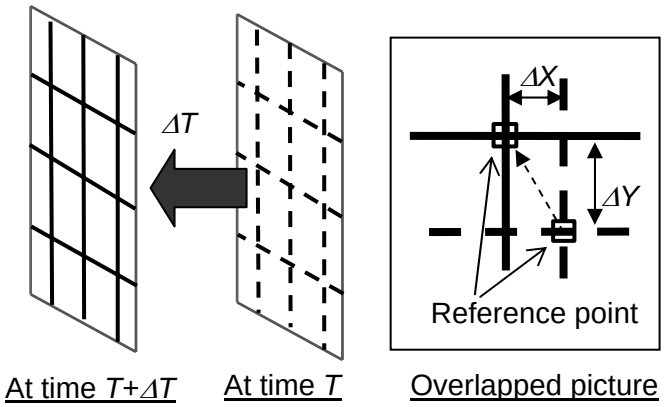

Figure 7: Displacement by the image analysis

2.4 Test method and measurement

To obtain the tensile properties of the material, the direct tensile test was conducted. In order to get the homogeneous distribution of fiber throughout the whole tensile specimen, the final specimens for testing were obtained by cutting off the initial specimen from steel frame. The full details of the final specimens are shown in Figure 6. The steel plates were used to strengthen the grip zones to prevent the local failure due to the high compressive stress (Figure 6). In stead of strain gages or LVDT's, crack widths were measured by the image analysis of photos taken by the high-quality digital camera during the 0.1-mm/min loading test. The camera with a resolution of 10.1 mega pixels was used to capture the movement of the reference points on the specimen during photo-taking time interval (ΔT). Two taken pictures were overlapped to each other by the computer program and the displacement in the horizontal (ΔX) and vertical (ΔY) direction was measured (Figure 7). The measured displacement represented the crack width when the reference points were set at the opening

of each crack. The measure process for displacement was repeated until the completed tensile stress-crack opening relationships can be obtained.

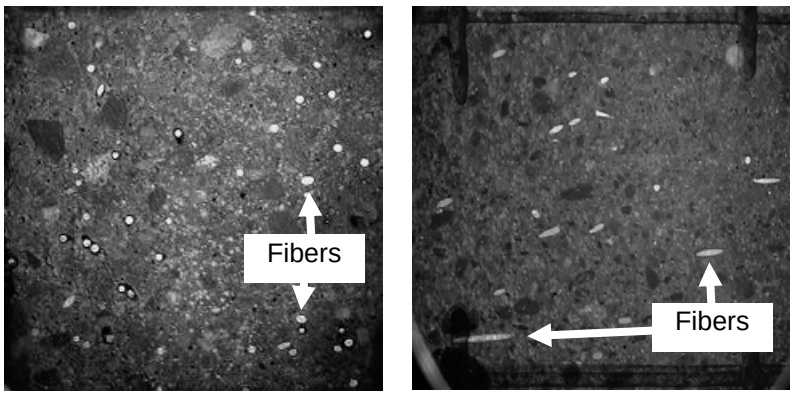

Specimen A-1 Specimen A-3

Figure 8: Slid planes taken by a microscope

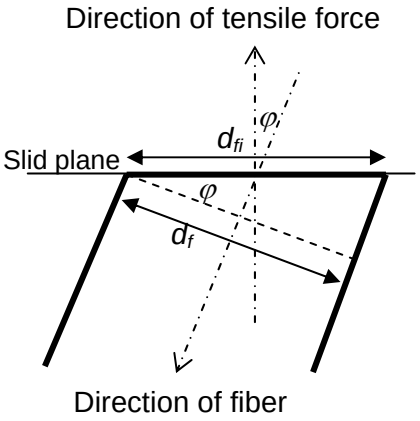

Figure 9: Diameter of fiber on slid plane

To obtain the actual fiber orientation of the tensile specimens, all specimens were slid perpendicularly to the direction of the applied tensile force at the sections without crack after the tensile test was done. The slid specimens were neutralized by phenolphthalein to turn the color of matrix into pink. By using pictures taken by a microscope, the area of fibers could be easily distinguished from the matrix by the difference in the color as shown in Figure 8. The shape of the fibers on the taken pictures will only be a full circle when it is oriented at an angle of 90 degrees to the slid surface [3]. At any other angle, the fiber will be seen as an ellipse. The value of the fiber diameter divided by the length of the longer major axis of an ellipse indicates the angle φ of each fiber orientated in the slid surface. A total orientation number η_φ that gives a general impression about the overall orientation of all fibers in the tensile specimens was determined with the following equation [3]:

$$\eta_\varphi = \frac{1}{N} \cdot \sum_i^N \cos\varphi = \frac{1}{N} \cdot \sum_i^N d_f / d_{fi} \tag{1}$$

Where *N* = the number of fibers in the slid section, φ = the angle between the direction of the applied tensile force and the steel fiber (Figure 9).

3 Results and discussion

3.1 Tensile behaviors

The observed tensile behaviors of all test specimens by a digital camera are shown in Figure 10. Because of the variation in the compressive strength of each batch of concrete, measured tensile stresses were normalized by the tensile strength of the plain concrete calculated from the concrete strength of each batch as shown in Figure 10. Apparently, UHPC reinforced with steel fiber has an improved tensile strength compared to the reference plain concrete. The same tendency has been reported in previous study [6].

The tensile behaviors of specimens in series A show the effect of the flow direction on short steel fiber (6 mm). It can be seen that the tensile strength and post-peak behavior can be improved if the tensile stress is applied at the direction of the concrete flow. In the same way, from the results of series B, the tensile strength and post-peak behavior are also improved when the tensile stress is applied at the direction of the concrete flow for 13-mm fiber. It can be considered that the direction of steel fibers in the self-compacting matrix tries to arrange itself into the direction of concrete flow which can be proved by the actual fiber orientation later. Moreover, the effect of the length of fiber can be shown by the comparison of results of series A and B (Figure 10). It can be said that the normalized tensile strength and the fracture energy are higher for the longer fiber in both parallel and perpendicular direction to concrete flow. However, the effect of the fiber length on the maximum crack opening cannot be seen from the relationship. Results of series C show the effect of the flow distance and wall on the tensile behaviors of specimens. The steel mold was shortened into 1200 mm to increase the effect of the wall at the end zone (Figure 5). It can be seen that specimen from center zone (C-2) has the higher normalized tensile strength and fracture energy than specimens from the filling and end zones. It can be considered that the orientation of fibers in the filling zone is disturbed by the filling of concrete and fibers can arrange itself into the direction of concrete flow after flowed into the center zone. However, the orientation of fibers is disturbed again by the obstruction of the concrete flow by the wall at the end zone. The actual fiber orientation of all specimens can be shown by the image analysis later.

3.2 Fiber orientation

Image analysis was used to count the fibers in the cross-section of the tensile specimens. The measured average angle φ, number of fibers and fiber orientation number are summarized in Table 2. Corresponding to the measured tensile behaviors (Figure 10), the higher fiber orientation number can be observed from the specimens that the tensile strength and/or post-peak behavior are improved. It can be said from the results of series A and B that fibers try to arrange itself into the direction of concrete flow because the orientation numbers in the direction parallel to concrete flow are higher than that in the perpendicular direction. However, it can be observed that the effect of flow direction is larger for the longer fibers because the orientation number of B-1 is higher than that of A-1 and A-2. From the comparison of the orientation number of series C, it can be concluded that the filling of concrete and the obstruction of the concrete flow have an influence on the orientation of fibers. On the other hand, the flow distance can improve the arrangement of fibers in the direction of concrete flow as shown by the higher value of the orientation number of C-2 compared with specimens C-1 and C-3.

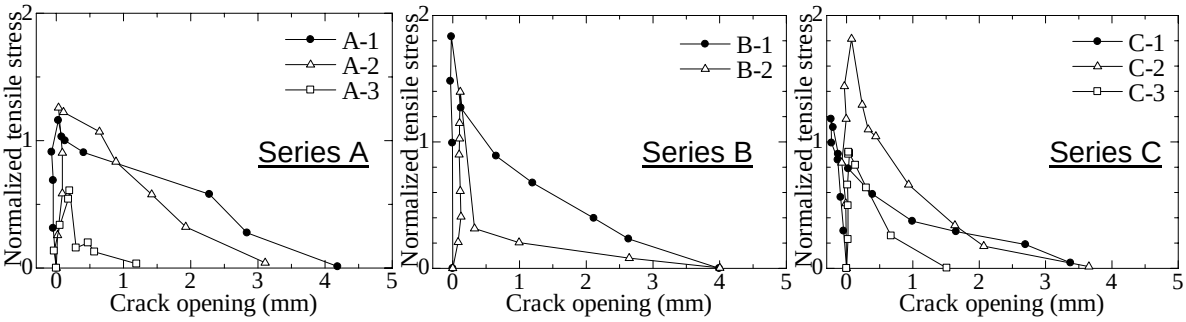

Figure 10: Tensile stress-crack opening relationships

Table 2: Summary of results from the image analysis

Series		A			B		C	
Specimens	A-1	A-2	A-3	B-1	B-2	C-1	C-2	C-3
Average angle φ	47.2	46.3	55.4	39.4	59.5	45.9	37.8	46.9
Number of fibers	425	419	103	305	147	258	170	376
Fiber orientation	0.65	0.66	0.53	0.74	0.48	0.66	0.76	0.65

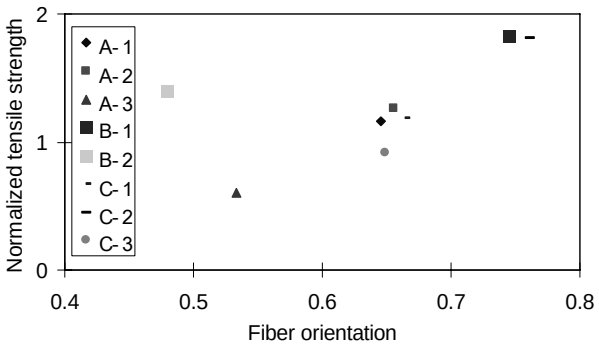

Figure 11: Tensile strength - fiber orientation

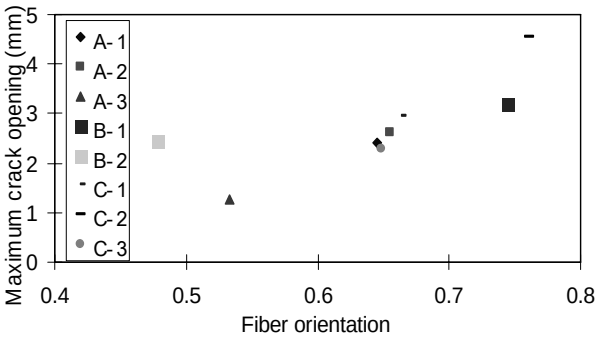

Figure 12: Crack opening - fiber orientation

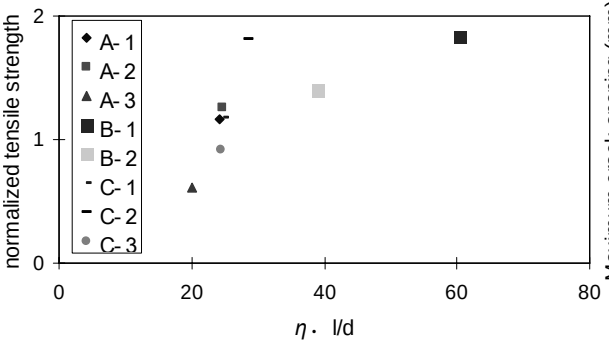

Figure 13: Tensile strength - η·l/d relationship

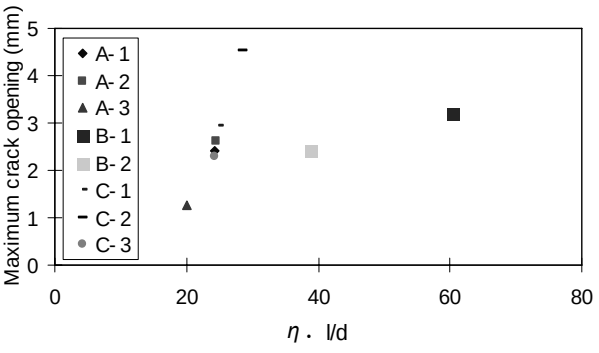

Figure 14: Crack opening - η·l/d relationship

In this study, the normalized tensile strength (the maximum value of the normalized tensile stress from Figure 10) and maximum crack opening are selected to show the effectiveness of UHPC reinforced with fibers. Figures 11 and 12 show the normalized tensile strength-fiber orientation relationship and the maximum crack opening-fiber orientation relationship, respectively. It is clearly seen from Figures 11 and 12 that the normalized tensile strength and the maximum crack opening increase proportionally with the increase in fiber orientation.

To normalize the relationship in Figures 11 and 12 with fiber length and diameter, the fiber orientation is replaced by η·l/d factor (η = orientation number, l = fiber length and d = fiber diameter) as shown in Figures 13 and 14. Similarly, it is clearly seen from Figures 13 and 14 that the normalized tensile strength and the maximum crack opening increase with the increase in η·l/d factor. Because of only limited number of data, the concrete relation could not be derived for the relationship in Figures 11, 12, 13 and 14.

It can be concluded that the actual fiber orientation in UHPC member are varied with the locations due to the main parameters in this study such as the filling location, the angle of flow direction to direction of tensile stress, the flow distance and the obstruction of the flow. And, the actual fiber orientation has a strong relation with the tensile characteristic of UHPC such as the tensile strength and the maximum crack opening. As a result, the actual fiber orientation at different locations in UHPC member should be considered in the prediction of the structural performance of member.

4 Conclusions

The following conclusions can be drawn based on the findings of this study:

(1) In stead of strain gages or LVDT's, the direct tensile test method that the displacement or crack widths are measured by the image analysis of photos taken by the digital camera are introduced. With this proposed method, the measurement of post-peak behavior of a single crack can be obtained.

(2) Flow distance and fiber length have a positive effect on the orientation of fiber in the flow direction. However, the filling of concrete and the obstruction of the concrete flow have a negative effect. The effects on the orientation of fiber can be shown by the fiber orientation number by the image analysis.

(3) The actual fiber orientation has a strong effect on the tensile characteristic of UHPC. As a result, in the prediction of the structural performance of UHPC members, the varied actual fiber orientation at the different locations in member should be considered.

5 References

[1] Grunewald, S.: Performance-based design of self-compacting fibre reinforced concrete. PhD-thesis, Department of Structural and Building Engineering, Delft University of Technology, 2004.

[2] Kooiman, A.G.: Modelling steel fibre reinforced concrete for structural design. PhD-thesis, Department of Structural and Building Engineering, Delft University of Technology, 2000.

[3] Lappa, E. S.; Braam, C. R.; Walraven, J. C.: Static and fatigue bending tests of UHPC. In: Proceedings of the International Symposium on Ultra High Performance Concrete, Kassel, 449-458, 2004.

[4] Okamura, H.; Ouchi, M.: Self-compacting concrete. In: Journal of Advanced Concrete Technology 1, No. 1, S.5-15, 2003.

[5] RILEM TC 162-TDF: Test and design methods for steel fibre reinforced concrete, Draft recommendation. In: Materials and Structures 33, S.3-5, 2000.

[6] Markovic, I.: High-performance hybrid-fibre concrete: Development and utilisation. PhD-thesis, Department of Structural and Building Engineering, Delft University of Technology, 2006.

Dong Joo Kim
Ph. D. Candidate
University of Michigan
Ann Arbor, USA

Antoine E. Naaman
Professor Emeritus
University of Michigan
Ann Arbor, USA

Sherif El-Tawil
Associate Professor
University of Michigan
Ann Arbor, USA

High Tensile Strength Strain-Hardening FRC Composites with less than 2% Fiber Content

Summary

Tensile strain hardening FRC composite with a tensile strength exceeding 10 MPa and a tensile strain capacity close to 0.5% was developed using only 2% fiber volume fraction in high strength matrix (84 MPa). Two high strength steel fibers, Hooked and Torex fiber, of tensile strength exceeding 2000 MPa were selected. In single fiber pullout tests, both fibers showed slip-hardening behavior without fiber failure, and the Torex fiber showed high slip capacity before bond decay generating large amount of pullout work or energy. In direct tensile tests of bell-shaped specimens, the use of both high strength steel Hooked and Torex fiber led to strain hardening-behavior. In some cases, strain-hardening was achieved with a fiber volume fraction of only 1%. However, there were clear differences in the cracking behavior of the composite depending on the type of fiber. With Torex fibers at 2% fiber content, the crack spacing was less than 4.5 mm and crack width prior to maximum load was less than 21 microns; the corresponding values for the high strength hooked fiber were 6.5 mm and 29 microns respectively.

Keywords: *high strength steel fiber, strain hardening, slip hardening, multiple cracking*

1 Introduction

Many researches have worked to increase the strength and ductility of concrete and cementitious composites. As a result, high performance concretes (HPC) and ultra-high performance concretes (UHPC) were developed with the aid of water reducing agents, chemical admixtures, and the addition of very fine fillers. HPC and UHPC are usually first characterized by their compressive strength. Initially HPC had compressive strengths ranging between 40 and 70 MPa. For UHPC, strengths in excess of 200 MPa have been attained. Such high strength is expected to reduce the required section size of reinforced and prestressed concrete structural members such as bridge girders, beams and columns. However UHPCs are extremely brittle in both tension and compression. Adding fibers to such matrices improves their ductility and fracture properties. So far, ultra high performance

tension without using high fiber contents (ranging from 5% to 11% by volume) such as in the examples of SIFCON (slurry infiltrated fiber concrete), SIMCON (slurry infiltrated mat concrete) and $CEMTEC_{multiscale}$ (Multiscale Cement Technical Composites). The properties and applications of SIFCON were first reported by Lankard (1985). The tensile and compressive behavior of SIMCON were reported by Krstulovic and Al-Shannag (1997) and Krstulovic and Malak (1999). Naaman and Homrich (1989) described experimental studies on the tensile behavior of SIFCON and proposed a model predicting the ascending branch of its tensile stress-strain curve. Naaman et al. (1992) also investigated the flexural behavior of reinforced concrete beams in a SIFCON matrix. Rossi (2005) introduced new cement composites called $CEMTEC_{multiscale}$ by using three different types of steel fibers with 11% total fiber volume fraction; Rossi et al (2005) reported that $CEMTEC_{multiscale}$ can achieve 50-58 MPa modulus of rupture in bending and more than 200 MPa compressive strength. Recently, several researchers reported on the mechanical, compressive and time dependent behavior of UHPFRC (Habel et al. (2006), Graybeal (2007), and Habel et al. (2006)). Behloul (2007) described many applications of Ductal, a type of UHPFRC with moderate fiber content, in bridges and footbridges and showed that Ductal technology can achieve 200 MPa compressive strength, 45 flexural strength and 11 MPa tensile strength**.**

Since each 1% of steel fibers usually cost more than the entire cement matrix, there is urgent need to minimize the cost of the composite for practical applications. The main objective of this study was to develop a tensile strain hardening Fiber Reinforced Cementitious (SH-FRC) composites with a tensile strength exceeding 10 MPa, a corresponding tensile strain capacity close to 0.5%, and a fiber content less than 2% by volume. The compressive strength of the matrix described in this study was about 84 MPa. While higher compressive strengths could have been used, they would generate significantly higher fiber bond strengths (adhesive, frictional and mechanical) which lead in some cases to failure of the fibers upon matrix cracking and during fiber pull-out. To minimize fiber failure, two steel fibers of tensile strength exceeding 2000 MPa were selected; one fiber was circular in cross-section and hooked at its ends, and the other was triangular in cross-section and twisted along its longitudinal axis (here called Torex). Pull-out tests of single fibers were carried out as well as direct tensile tests on cement matrices containing 1% and 2% fibers by volume.

2 Slip hardening and strain hardening

Strong correlation between single fiber pull-out behavior and tensile behavior of FRC composites was reported by Kim et al in 2007. Used two types of high strength deformed steel fibers, high strength Hooked and Torex fiber, they showed that slip hardening pullout behavior with large slip capacity before bond decay helps achieve strain-hardening FRC composites with high strain capacity in tension accompanied by multiple micro cracks.

Figs. 1a and 1b show typical single fiber pullout behavior of Hooked and Twisted fiber, respectively. Although both deformed Hooked and Twisted fibers, show slip hardening behavior, the slip capacity of Twisted fiber is much higher than that of Hooked fiber as illustrated in Fig. 1. The higher slip capacity of Twisted (Torex) fiber originates from the unique untwisting pullout mechanism which engages the whole embedded length of fiber

during fiber pullout, while only a small portion of the fiber length is engaged in hooked fibers (Naaman 1999, Alwan et al 1999, Sujiravorakul 2001).

The amount of pullout work (or energy) during the pullout described in Fig. 1 depends on slip capacity and can be interpreted to derive an equivalent bond strength with the assumption that bond strength remains constant along the fiber embedded length for the selected slip. For any given slip capacity, a different equivalent bond strength can be determined, including the case where the slip is the maximum observed in a typical pull-out test. Kim et al (2007) suggested equation (1) to calculate the equivalent bond strength assuming the maximum slip is equal to the fiber embedded length.

$$\tau_{equivalent} = \frac{8E_{PULLOUT}}{\pi d_f L_f^{\,2}} \qquad (1)$$

Where, $E_{PULLOUT}$ is Pullout energy, d_f : Fiber diameter and L_f : Fiber length.

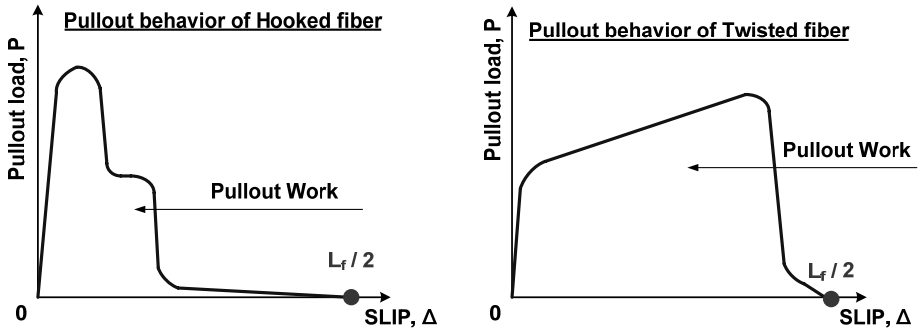

Figure 1: Typical pullout behavior of Hooked and Twisted fiber

Fig. 2 shows typical tensile behavior of an FRC composite using Twisted (Torex) fiber with 2% fiber content by volume. Clear strain hardening behavior is observed; the tensile load resistance after first cracking strength σ_{cc} steadily increases up to post cracking strength σ_{pc} and is accompanied with multiple micro-cracks. It is clear that the slip hardening behavior in fiber pullout helps achieve strain hardening behavior in tension.

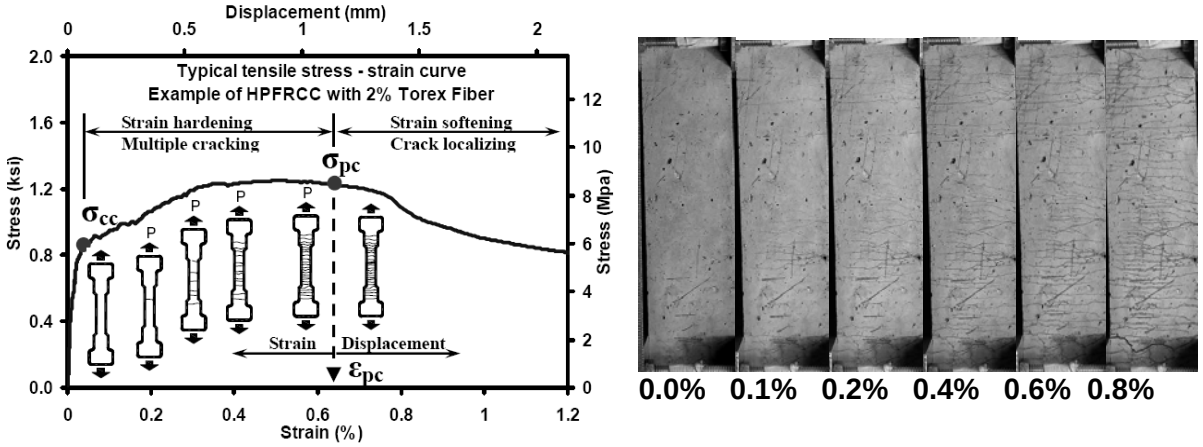

Figure 2: Typical tensile behavior of Twisted (Torex) fiber reinforced composites. a) Tensile stress-strain response up to peak stress. b) Cracking behavior at different strain levels

3 Experimental Program

As mentioned above, two types of high strength steel fibers (Hooked and Twisted) with slip hardening pull-out behavior, were used in a high strength cementitious matrix (84MPa) with 1% and 2% fiber by volume. Single fiber pullout tests and direct tensile tests were carried out using a servo-controlled hydraulic testing machine (MTS810).

3.1 Materials and specimen preparation

The matrix mix composition and proportions are shown in Table 1, and the properties of fibers are shown in Table 2. It should be noted that VMA (Viscosity Modifying Agent) was added to the matrix to increase viscosity and ensure uniform fiber distribution in the matrix. The compressive strength of the matrix was measured from 100x200 mm cylinders and this matrix composition is self-consolidating mixture.

Table 1: Composition of Matrix Mixtures by weight ratio and compressive strength

Cement (Type III)	Fly ash	Sand (Flint)	Silica Fume	Super - Plasticizer	VMA	Water	$f_c^{'}$ (MPa)
0.80	0.20	1.00	0.07	0.04	0.012	0.26	84

Table 2: Properties of Fibers used in this study

Fiber Type	Diameter (mm)	Length (mm)	Density, g/cc	Tensile strength, (MPa)	Elastic Modulus, (GPa)
Hooked	0.38	30	7.9	2300	200
Twisted	0.3*	30	7.9	2760**	200

* Equivalent diameter ** Tensile strength of the fiber after twisting

3.2 Test setups and procedure

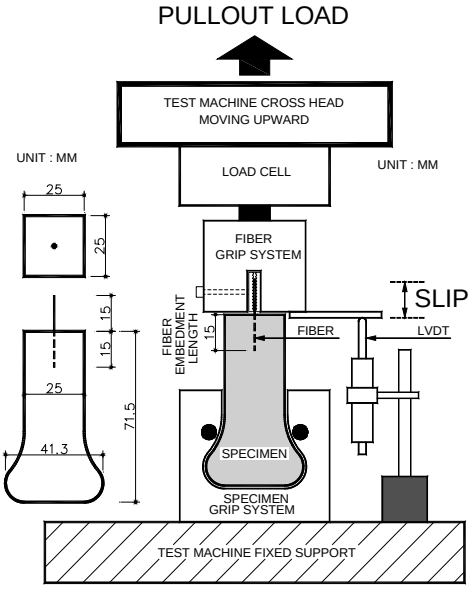

Figure 4: Tensile test specimen and setup

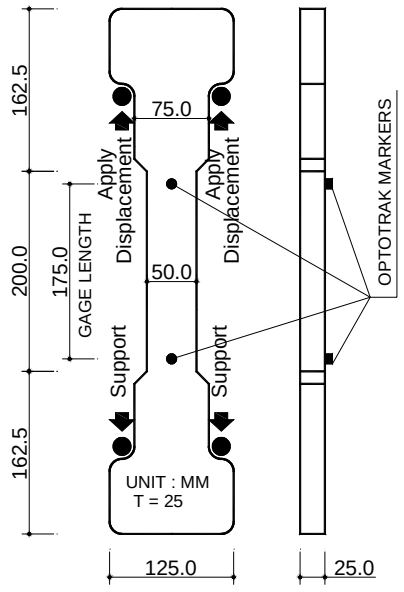

Figure 3: Pull out test specimen and setup

The geometry of pullout test specimen and test set-up is shown in Fig. 3. The embedment length of the fiber was 15mm (= 0.59 inch) and the fiber was placed at the center of the specimen. The specimen's axis was located along the loading axis and the fiber axis; the fiber was gripped firmly to prevent any slip in the gripping device. The geometry of the double bell end-shaped tensile test specimen and test set up are shown in Fig. 4 (Naaman et al. 2007). Two layers of steel wire mesh were used to reinforce the bell shaped ends to minimize failure at the grips and out of the gage length. The gage length was selected to be 175mm (=7 inch), between two infrared markers; displacement between the markers was measured using a non-contacting motion measuring instrument (OPTOTRAK System) placed at about one meter from the specimen; the measurement accuracy was 0.001 mm.

3.3 Test results

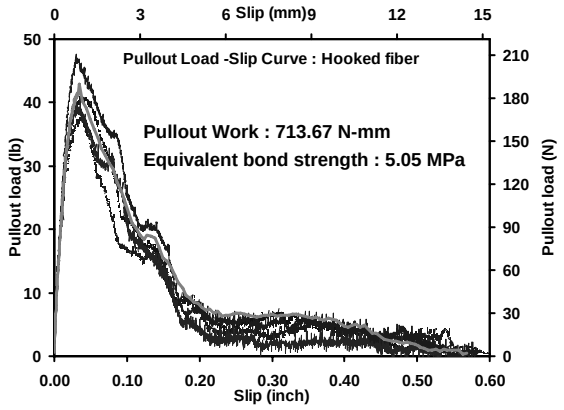

(a) Pullout Load - Slip curve, Hooked fiber

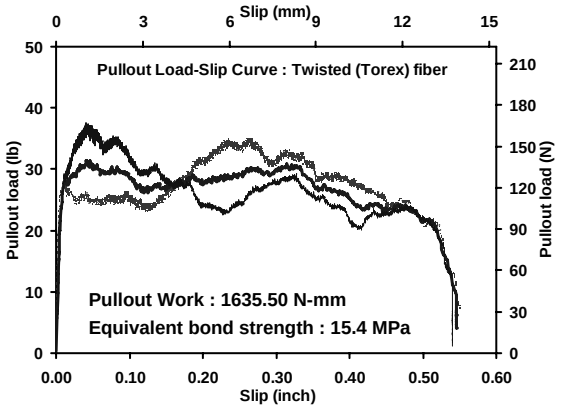

(b) Pullout Load - Slip curve, Twisted fiber

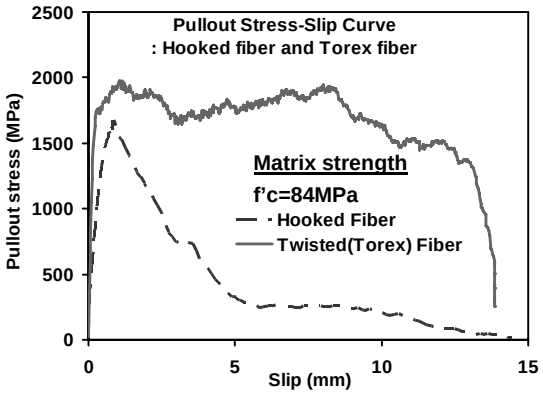

(c) Average Pullout Stress - Slip curve for both Hooked and Twisted fiber

Figure 5: Pullout behavior of both Hooked and Twisted fiber

Pullout load - slip response curves of the high strength steel Hooked and Twisted fiber are shown in Figs. 5a and 5b, respectively. Note that while the pull-out load axis has the same scale for both fibers, the tensile stress induced in the fiber is different because they have different cross-sections. Figure 5c compares the average curve derived for each fiber, plotted as tensile stress in the fiber versus slip. It can be observed that the twisted fiber, in which the tensile stress reaches 2000 MPa, is significantly more efficient than the hooked fiber for which the maximum tensile stress reaches 1600 MPa. The average pullout energy (area under the pull-out curve) was determined and the equivalent bond strength for each

fiber was calculated from Eq. (1). The pullout energy of the Torex fiber was 1635.50 N-mm while that of the Hooked fiber was 713.67 N-mm. The corresponding equivalent bond strength was 15.4 MPa for Torex fiber and 5.05 MPa for high strength Hooked fiber, respectively.

Tensile stress – strain curves and photos illustrating the number of cracks and crack spacing in each test series are given in Fig. 6. Average numerical values of several parameters describing tensile response such as first cracking strength, maximum post cracking strength, strain capacity at maximum post cracking strength and number of cracks (and related crack spacing) are shown in Table 3. These values are averaged from at least three specimens. Figure 7 illustrates and compares graphically some of the parameters of Table 3.

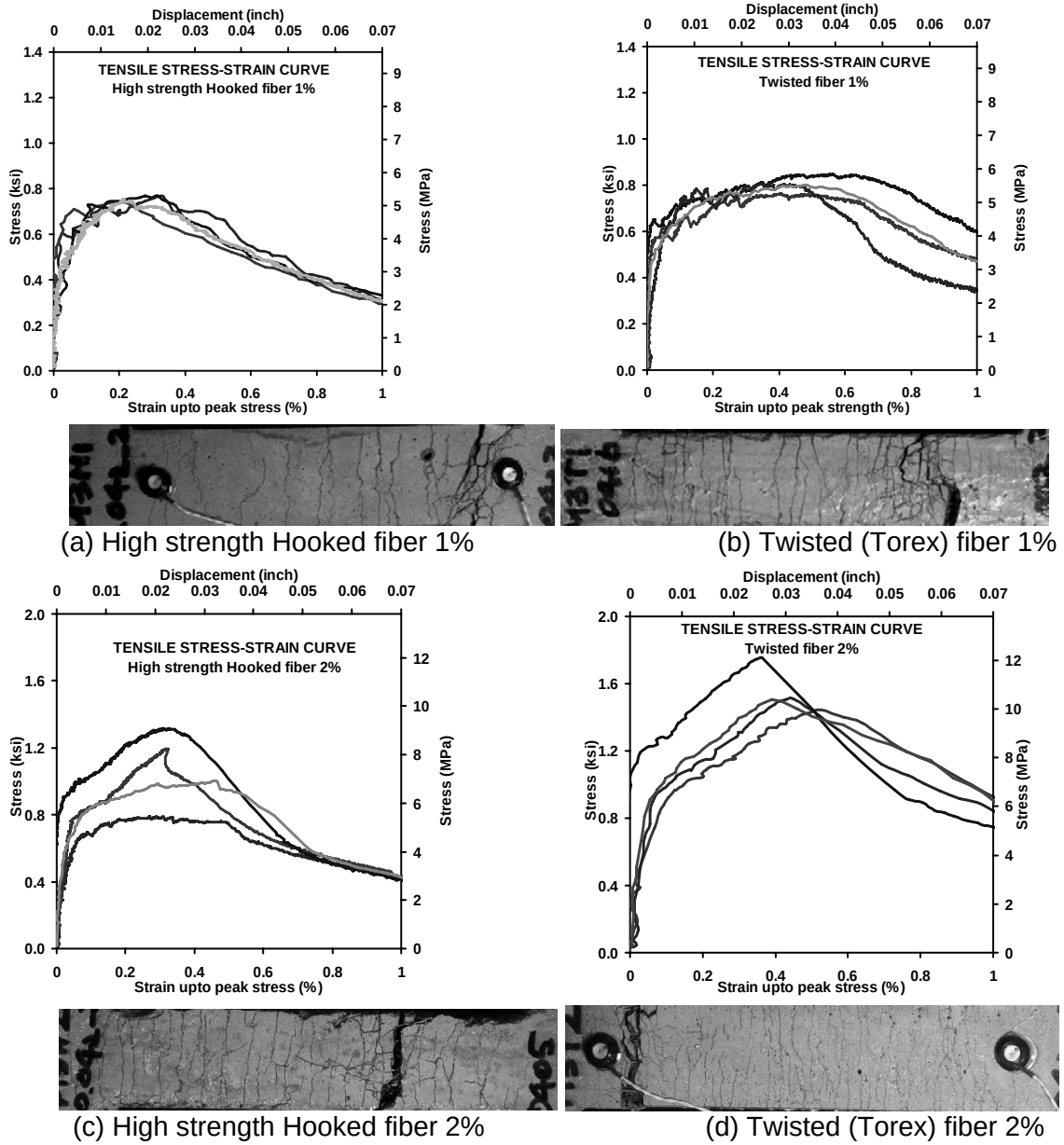

(a) High strength Hooked fiber 1% (b) Twisted (Torex) fiber 1%

(c) High strength Hooked fiber 2% (d) Twisted (Torex) fiber 2%

Figure 6: Tensile stress – strain curve and cracking behaviour

Table 3: Average experimental results obtained from the tensile tests

Fiber type & Volume fraction	First cracking strength	Post Cracking Strength	Strain Capacity	Number of cracks	Crack Spacing	Average Crack Width
	MPa	MPa	%	EA	mm	micrometer
Hooked 1%	4.299	5.207	0.301	15	11.85	37
Hooked 2%	5.143	7.562	0.387	27	6.56	29
Twisted 1%	4.264	5.499	0.616	23	7.74	49
Twisted 2%	6.997	10.778	0.452	39	4.56	21

4 Evaluation of the experimental results

The tensile stress – strain curves observed for all test series showed strain hardening behavior and multiple cracking characteristics, for both 1% and 2% fiber content by volume. While both fibers were effective in developing tensile strain hardening response of the composite, the twisted fiber was much more effective than the hooked fiber (Table 3 and Fig. 7). For a volume fraction of 2%, the test series with Twisted (Torex) fibers achieved a maximum post-cracking stress of 10.8 MPa, at a strain of about 0.45%, with an average crack spacing of 4.5 mm and an average crack width of 21 micrometer.

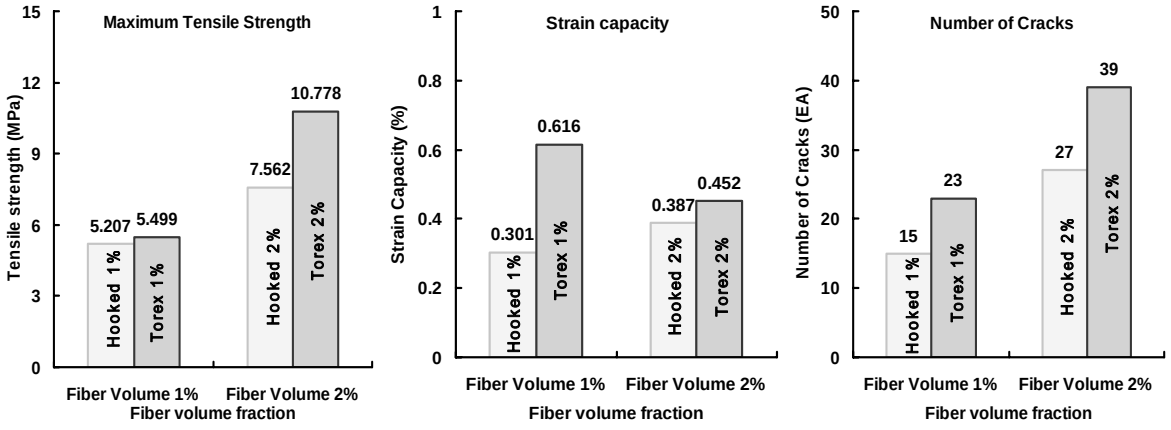

(a) Maximum Tensile strength (b) Strain capacity (c) Number of cracks

Figure 7: Effect of fiber type and volume fraction

5 Conclusions

This study investigated the performance of high strength Hooked and Twisted (Torex) fiber in a high strength cementitious matrix (84 MPa) in both pullout and tensile test.

- Although both Hooked and Twisted (Torex) fibers show slip-hardening behavior under pull-out due to their mechanical bond, Twisted (Torex) fiber led to an equivalent bond strength about 3 times that of the Hooked fiber.
- In tensile tests, the use of both Hooked and Twisted (Torex) fiber reinforced specimens led to strain hardening behavior. However, Twisted (Torex) fiber was much more effective than the hooked fiber in terms of maximum tensile strength, strain capacity and number of cracks within gage length.

Finally, with Twisted (Torex) fibers at 2% fiber content by volume in a high strength cementitious matrix (84MPa), the objective of achieving SH-FRC composites with post-

cracking direct tensile strength of about 10 MPa and strain capacity close to 0.5% was attained. At time of this writing a new level of 17 MPa has also been achieved in a SIFCON strain-hardening FRC composite with a fiber volume fraction of 4%, and is being used as a reference base for the next level.

6 References

[1] Alwan, J. M. Naaman, A. E., and Guerrero, P., “Effect of Mechanical Clamping on the Pull-out Response of Hooked Steel Fibers Embedded in Cementitious Matrices.,” Concrete Science and Engineering, Vol. 1, Mar. 1999, pp. 15-25

[2] Graybeal, B. A., “Compressive behavior of Ultra-High-Performance Fiber-Reinforced Concrete,” ACI Materials Journal, Vol. 104, No. 2, Mar.-April 2007, pp. 146-152.

[3] Habel, K., Denarie, E. And Brühwiller, E., ”Time dependent behavior of elements combing ultra-high performance fiber reinforced concretes (UHPFRC) and reinforced concrete,” Materials and Structures, Vol. 39, No. 5, June 2006, pp. 557-569.

[4] Habel, K., Viviani, M., Denarie, E. And Brühwiller, E., ”Development of the mechanical properties of an Ultra-High Performance Fiber Reinforced Concrete (UHPFRC),” Cement and Concrete Research, Vol. 36, Issue 7, July 2006, pp. 1362-1370.

[5] Kim, D., El-Tawil, S. and Naaman, A.E, “Correlation between single fiber pullout behavior and tensile response of FRC composites with high strength steel fiber”, in Prints, HPFRCC5, Mainz, Germany, July 10-13, 2007, pp. 67-76.

[6] Krstulovic-Opara, N. and Al-shannag M. J., “Compressive behaviour of Slurry Infiltrated Mat Concrete,” ACI Materials Journal, Vol. 96, No. 3, May-June 1999, pp. 367-378.

[7] Krstulovic-Opara, N. and Malak, S., “Micromechanical Tensile behaviour of Slurry Infiltrated Continuous-Fiber-Mat Reinforced Concrete (SIMCON),” ACI Mat. Journal, 94(5), Sep.-Oct. 1997, pp. 373-384.

[8] Lankard., D. R., “Slurry Infiltrated Fiber Concrete (SIFCON) : Properties and Applications,” Very high strength cement based materials, Vol. 42, Materials Res. Society, Pittsburgh, 1985, pp. 277-286.

[9] Naaman, A. E. and Homrich, J. R., “Tensile Stress-Strain Properties of SIFCON,“ ACI Material Journal, Vol. 86, No. 3, May-June 1989. pp. 244-251.

[10] Naaman, A. E., “Fibers with slip-hardening Bond,” in High Performance Fiber Reinforced Cement Composites – HPFRCC 3,” H.W. Reinhardt and A.E. Naaman, Editers, RILEM Pro 6, RILEM Publications S.A.R.L., Cachan, France, May 1999, pp. 371-385.

[11] Naaman, A. E., Fischer, G. and Krstulovic-Opara, N., “Measurement of Tensile properties of fiber reinforced concrete : Draft submitted to ACI Committee 544,” HPFRCC5, Mainz, Germany, July 10-13, 2007, pp. 3-12. Give here the exact proceedings. You have them.

[12] Naaman, A. E., Reinhardt, H. W. and Fritz, C., “Reinforced Concrete Beams with SIFCON Matrix,” ACI Structural Journal, Vol. 89, No. 1, Jan.-Feb. 1992, pp. 79-88.

[13] Rossi, P., “Development of new cement composite materials for construction,” Proceedings of the Institution of Mech. Engineers, Part L, Jnl. of Materials: Design and Applications, 219(1), 2005, pp. 67-74.

[14] Rossi, P., Arca, A., Parant, E. And Fakhri, P., “Bending and Compressive behaviors of a new cement composites,” Cement and Concrete Research, 35(1), Jan. 2005, pp. 27-33.

[15] Sujiravorakul, C., “Development of High Performance Fiber Reinforced Cement Composites Using Twisted Polygonal Steel Fibers,” Ph.D. thesis, University of Michigan, Ann Arbor, Feb. 2001.pp.230.

Martin Empelmann
Prof. Dr.-Ing.
Technical University Brunswick, (iBMB)
Brunswick, Germany

Manfred Teutsch
Dr.-Ing. Academic Director
Technical University Brunswick, (iBMB)
Brunswick, Germany

Guido Steven
Dipl.-Ing. Research Assistant
Technical University Brunswick, (iBMB)
Brunswick, Germany

Improvement of the Post Fracture Behaviour of UHPC by Fibres

Summary

The development of Ultra-High Performance Concrete (UHPC) now offers a complete new range of application for RC-constructions. But due to the brittle material behaviour of UHPC at the ultimate compressive and tensile strength, it is advisable to add steel fibres (UHPFRC) to the concrete mix, in order to obtain a more ductile material behaviour. Research work has been carried out at the iBMB of the Technical University Brunswick, Germany, with the aim to improve the cost-effectiveness and sustainability of these UHPFRC mixes [7]. The following paper summarises the results of these three test series (tensile, compressive and fire tests) and gives recommendations for the addition of fibres, with regard to the type of steel fibres, the steel fibre aspect ratio (fibre length l_f / diameter d_f), as well as the steel fibre and polypropylene fibre content.

Keywords: *material properties UHPC and UHPFRC, fibre type, fibre content, stress-strain-relationship, fire resistance*

1 Introduction

Ultra-High Performance Concrete (UHPC) is a new material with a very high compression strength and excellent durability. However, if the ultimate compressive and tensile strength is reached, UHPC shows an extremely brittle material behaviour, with a nearly complete loss of load carrying capacity after the maximum load is exceeded. The addition of steel fibres, leading to Ultra High Performance Fibre Reinforced Concrete (UHPFRC) improves the post fracture behaviour significantly. As, on the other hand, the required high-strength steel fibres are expensive and reduce the workability of the concrete, a test series with nine concrete mixes variations of the reference mix (UHPFRC-B4Q) was carried out at the iBMB, in order to find the optimum fibre content in connection with an optimal mechanical performance. This benchmark test was part of the DFG Priority Program (SPP) 1182 [7].
Furthermore some preliminary fire tests with nine different versions of the reference concrete mix (UHPFRC-B4Q) were carried out in order to investigate the behaviour of UHPFRC at

high temperatures, with regard to the spalling phenomenon known from other concretes with a dense microstructure, such as SCC and HPC.

2 Investigated Concrete Mixes

Based on the reference concrete mix (UHPFRC-B4Q) given in Table 1, eight variants of UHPFRC-B4Q were investigated. These mixes are based on the same concrete mix as given in Table 1, but differ with regard to the steel fibre type and content. Details (fibre type and volumetric ratio v_f) are given in Table 2. As a benchmark, the behaviour of a concrete mix without steel fibres (UHPC-B4Q) was studied too, which means that in total the results of ten different concrete mixes are presented here.

Table 1: UHPFRC-B4Q (B4Q-0) concrete mix

UHPFRC 160 (B4Q-0)	[kg/m³]	[kg/dm³]	[dm³]		[kg/m³]	[kg/dm³]	[dm³]
CEM-I 52.5 R HS-NA	650.0	3.10	209.7	Basalt 2/5	298.5	3.06	97.5
ELKEM Microsilica Grade 983	177.0	2.20	80.5	Basalt 5/8	298.5	3.06	97.5
Quartz sand 0.125/0.50 mm	354.0	2.65	133.6	Water	158.0	1.00	158.0
Quartz flour I	325.0	2.65	122.6	Superplasticizer Glenium 51	30.4	1.11	27.4
Quartz flour II	131.0	2.65	49.4	SF l_f/d_f = 9/0.15 mm (2.47 Vol.-%)	193.9	7.85	24.7

Table 2: Investigated mix variants of B4Q

Steel fibre l_f / d_f	B4Q-0 (SPP-ref.)	B4Q-1	B4Q-2	B4Q-3	B4Q-4	B4Q-5	B4Q-6	B4Q-7	B4Q-8	B4Q w/o SF
9 / 0.15 mm	2.47 Vol.-%						0.25 Vol.-%			
17 / 0.15 mm									1.50 Vol.-%	
15 / 0.15 mm		0.50 Vol.-%				0.25 Vol.-%	0.25 Vol.-%			
30 / 0.38 mm		1.50 Vol.-%	1.50 Vol.-%	1.25 Vol.-%	1.00 Vol.-%	1.00 Vol.-%	1.00 Vol.-%	0.75 Vol.-%		
PP-microfibre	0.0 kg/m³	1.0 kg/m³	0.0 kg/m³	0.5 kg/m³	0.0 kg/m³	0.0 kg/m³	1.5 kg/m³	0.0 kg/m³	2.0 kg/m³	0.0 kg/m³

From each concrete mix a series of test specimens was produced, i.e. five cylinders Ø 150 mm x 300 mm for the compression strength tests, three 100 mm cubes for additional compression tests, three beams with b/h/l = 150 mm x 150 mm x 700 mm for bending tests, and one test specimen with the dimensions of 200 mm x 200 mm x 500 mm for the fire test. The test specimens were poured carefully and compacted on a vibration table. The beams and the test specimens for the fire test were additionally compacted with internal vibrators.
After two days at 20 °C and 65 % relative humidity the tests specimens were demoulded and stored under water until they were tested at the age of 28 days. Only the test specimens for the fire tests were stored at 20 °C and 65 % relative humidity for 56 days.

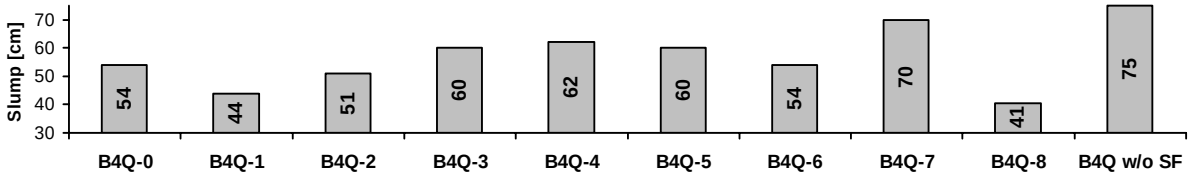

Figure 1: Slump spread diameter of the different concrete mixes

The difference in workability is documented by the measured slump spread diameter given in Figure 1. In relation to the reference mix B4Q-0 it can be seen that the mix B4Q-1 shows a slump spread reduction of almost 20 %, whereas B4Q-7 shows an increase of the slump

spread by nearly 30 %, indicating the considerable influence of the steel fibre type and content on the concrete workability.

3 Tensile Load Bearing Behaviour of UHPFRC

In order to investigate the load bearing behaviour of UHPFRC under tension, bending tests according to [1] were carried out. The test set-up for the 4-point-bending test is shown in Figure 2.

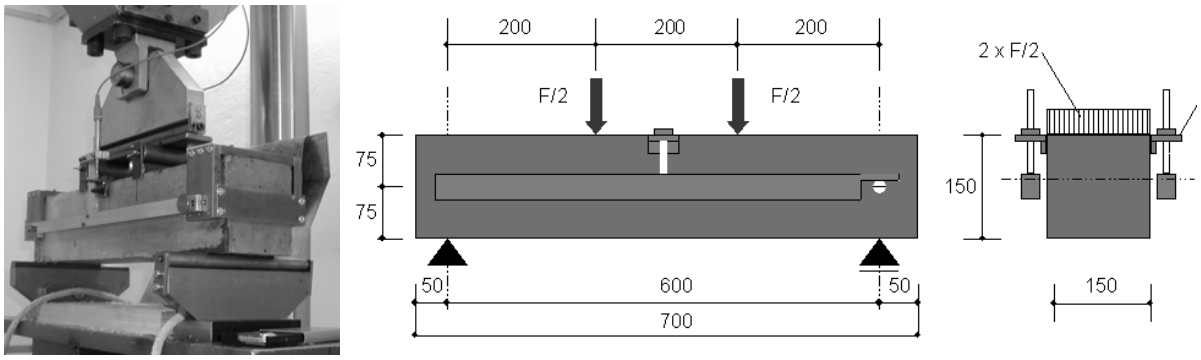

Figure 2: Test set-up according to [1] for the determination of the stress-strain relationship of UHPFRC in tension (all dimensions in mm)

The load-mid-span deflection relationship for all concrete mixes are given in Figure 3.

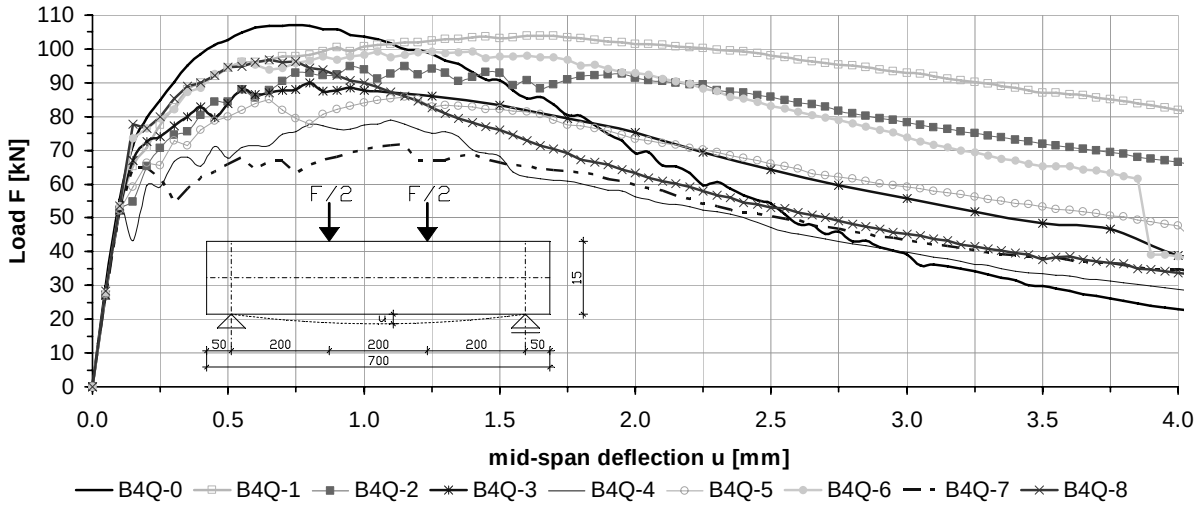

Figure 3: Load-mid-span deflection relationship for all concrete mixes (B4Q)

The different curves given here already represent the mean value obtained from the three specimens tested for each concrete mix. It can be seen, that the reference mix B4Q-0 shows the highest tensile strength value and that the values obtained from the other mixes differ up to 35 %.

For the classification of the post cracking tensile load bearing behaviour of steel fibre concrete it is useful to introduce so called “performance classes” [1]. For the classification of steel fibre concrete, the post-cracking flexural tensile strength obtained in the 4-point bending

tests at a mid-span deflection of 0.5 mm and 3.5 mm is used. These values are derived according to equation (1) and (2) [1].

$$f^{f}_{cflk,0.5} = 0.7 \cdot \frac{1}{n} \cdot \sum_{i=1}^{n} \frac{F_{0.5,i} \cdot \ell}{b_i \cdot h_i^{2}} \qquad \textbf{(1)}$$

$$f^{f}_{cflk,3.5} = 0.7 \cdot \frac{1}{n} \cdot \sum_{i=1}^{n} \frac{F_{3.5,i} \cdot \ell}{b_i \cdot h_i^{2}} \qquad \textbf{(2)}$$

Figure 4 gives the post-cracking flexural tensile strength values for the concrete mixes. It can be seen that the reference mix B4Q-0 shows the largest decrease of approx. 70 % of the flexural tensile strength values at 0.5 mm and 3.5 mm mid-span deflection of all concrete mixes. Except B4Q-8, with a decrease of 60 %, all the other concrete mixes show a decrease of 50 % or less, which indicates that concrete mixes with longer steel fibres (l_f / d_f = 30 / 0.38 mm) might be more favourable for higher strains in contrast to mixes with shorter steel fibres (l_f = 9 mm and 17 mm). It can be noted as a further result, that for a characteristic post-cracking flexural tensile strength value $f^{f}_{cflk,0.5}$ larger than 10 MPa, a steel fibre content of more than v_f = 1.25 Vol.-% is necessary. The same applies for a value $f^{f}_{cflk,3.5}$ larger than 6 MPa, where, in addition to a steel fibre content of more than v_f = 1.25 Vol.-%, the longer steel fibres with a length l_f = 30 mm have to be used.

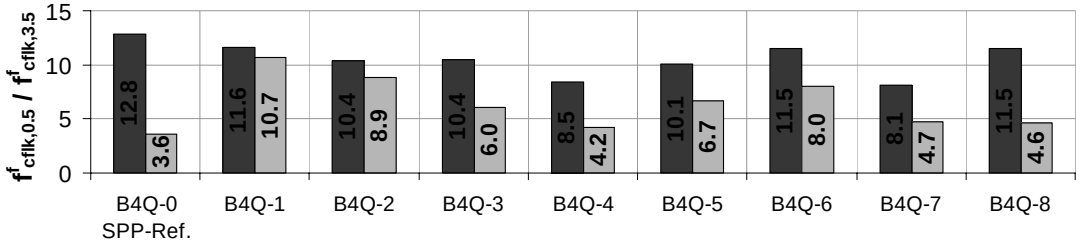

Figure 4: Characteristic post-cracking flexural tensile strength $f^{f}_{cflk,0.5}$ and $f^{f}_{cflk,3.5}$ [1]

4 Compressive Load Carrying Behaviour of UHPFRC

Figure 5 shows the principle test set-up and one of the test specimens prior to testing. The Ø 150 mm x 300 mm cylinders were placed directly between the loading plates of the 10 MN testing machine and no further additional measures for the load transfer (e.g. steel brushes) were applied. To ensure an even load transfer into the test specimen, the end surfaces, i.e. the loading areas were face-grinded two days prior to the test.

The lateral strain was measured with two strain gauges in the middle of the cylinders (see Figure 5, right). The longitudinal deformation was derived from the piston lift of the testing machine and two linear variable differential transducers (LVDT), arranged at the opposite sides of the test specimens. The longitudinal strains were measured by two vertical strain gauges, placed at opposite sides of the cylinder (see Figure 5, left).

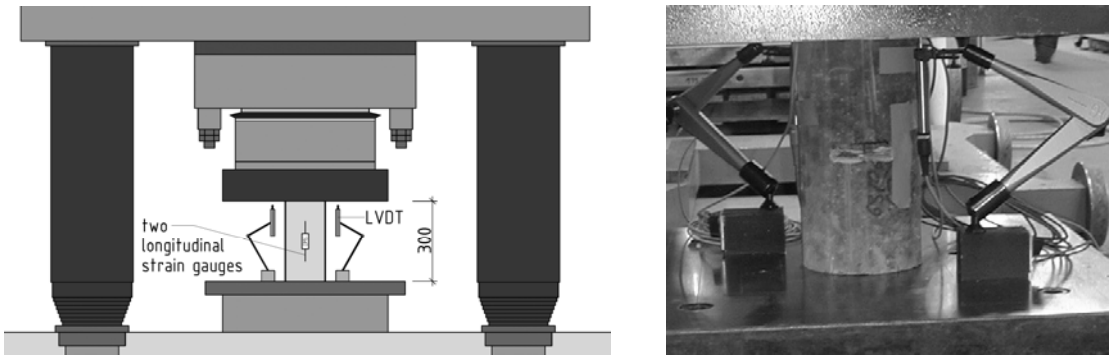

Figure 5: Test set-up for the determination of the compressive stress-strain relationship

The compressive strength f_{ck} values derived from these tests according to [3], the compressive strain ε_{cu} at the maximum load level and the modulus of elasticity E_{cm} (secant elastic modulus taken at 0.4 f_{ck}) are given in Table 3.

Table 3: Compressive strength f_{ck} results of B4Q-0 to B4Q-8

	B4Q-0 (SPP-ref.)	B4Q-1	B4Q-2	B4Q-3	B4Q-4	B4Q-5	B4Q-6	B4Q-7	B4Q-8	B4Q w/o SF
grade:	UHPFRC 160	UHPFRC 145	UHPFRC 140	UHPFRC 145	UHPFRC 145	UHPFRC 145	UHPFRC 145	UHPFRC 145	UHPFRC 150	UHPC 145
f_{ck}: [3]	-160.8	-146.0	-144.6	-146.1	-148.8	-148.4	-146.8	-146.6	-152.7	-145.5
ε_{cu}:	-3.31 ‰	-3.37 ‰	-3.25 ‰	-3.18 ‰	-3.31 ‰	-3.35 ‰	-3.43 ‰	-3.34 ‰	-3.42 ‰	-3.05 ‰
E_{cm}: [3]	52.2 GPa	49.3 GPa	50.5 GPa	51.7 GPa	51.7 GPa	50.2 GPa	49.1 GPa	48.5 GPa	51.2 GPa	47.6 GPa

Similar to the tensile tests the B4Q-0 mix shows the highest compressive strength compared to the other mixes, which show a compressive strength decrease of 5 % (for the l_f / d_f = 17 / 0.15 mm fibres) up to 8 % (for the l_f / d_f = 30 / 0.38 mm fibres), which indicates a certain influence of the fibre type on the compressive strength. The strain at the ultimate loading ε_{cu} is in the range of 3.2 to 3.4 ‰ and only the non-reinforced B4Q shows a smaller value of 3.05 ‰. The modulus of elasticity is in the range of 48 to 52 GPa.

Figure 6 shows the stress-strain relationship of the mono-fibre-mixes, with a typical load decrease between 3.5 and 4.0 ‰ and a more or less similar curve progression for larger strain values.

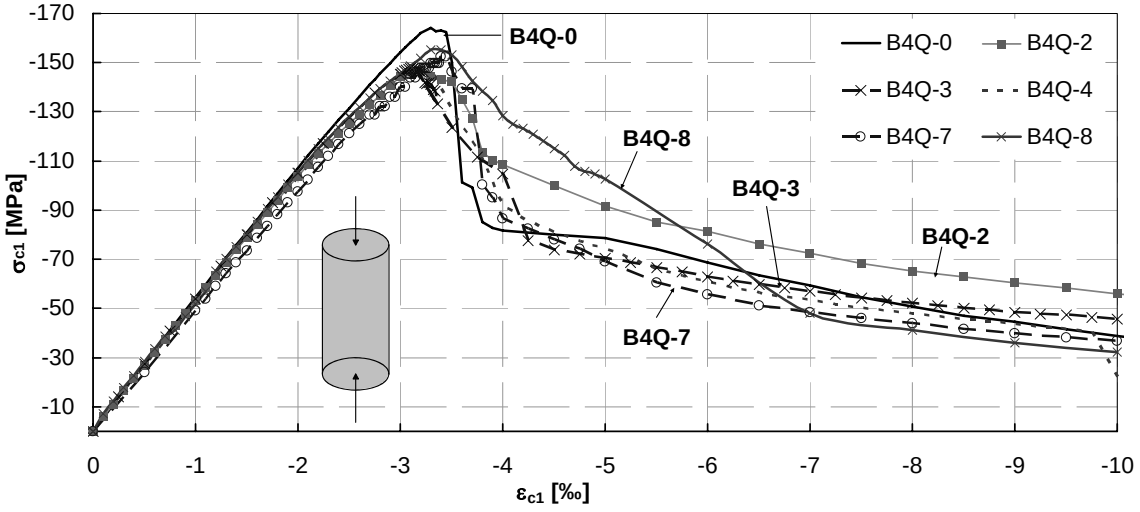

Figure 6: Compression stress-strain-curve of UHPFRC for mono-fibre-mixes

It can be noted that the UHPFRC with longer steel fibres (l_f ≥ 17 mm) show a similar performance as the B4Q-0 with shorter fibres (l_f = 9 mm), but with a considerably reduced steel fibre content.

Figure 7 shows the stress-strain relationship of UHPFRC with fibre-cocktails. In relation to the reference mix B4Q-0, for 2 mixtures a considerable improvement can be noted in the strain range between 3.5 and 5 ‰. For higher strains than 5 ‰ only the mix B4Q-1 shows a significant difference, which means an improvement in robustness. It should be also noted here, that the stress-strain curve of the B4Q without steel fibres (B4Q w/o SF) shows a nearly vertical decrease after maximum loading level is reached. These test specimens collapse explosively and without any prior warning.

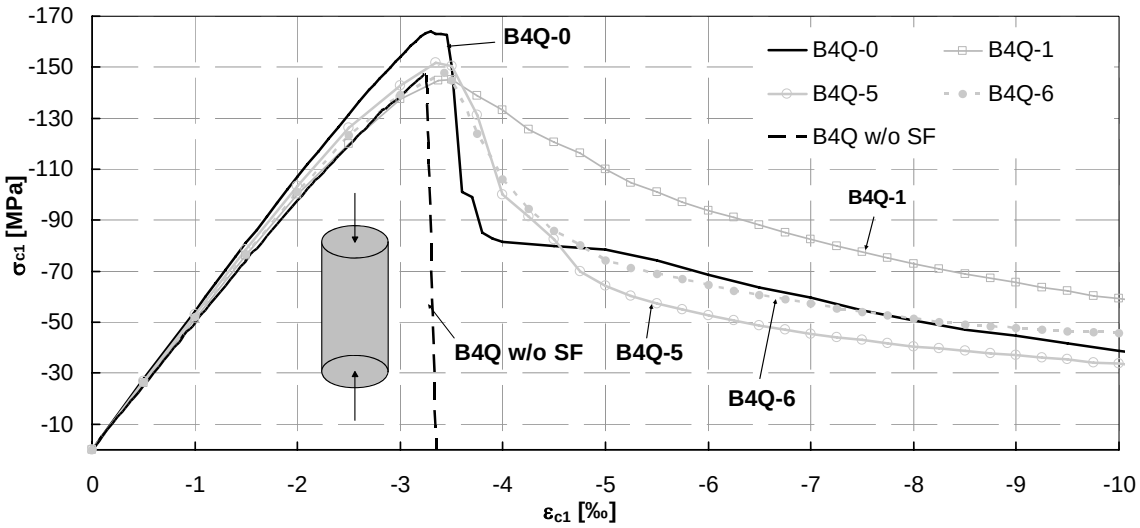

Figure 7: Compression stress-strain-curve of UHPC and UHPFRC for fibre-cocktail-mixes

In order to describe the compressive stress-strain relationship, an analytical approach would be useful. If one compares the analytical approaches given in [3-6], it appears that the adaptation of HPC models given there is suitable for the ascending part of the stress-strain relationship of UHPFRC, as shown in Figure 8 for concrete B4Q-0. However, the descending part of the stress-strain-curve of UHPFRC cannot be described with the currently available approaches.

A more suitable approach („own approach“) is developed at the iBMB, which is able to describe the compression stress-strain relationship with a quad-linear model and allows a better description of the descending branch. The ascending branch of the curve is described by the approach given in [6] and the descending branch based on empirically determined values. As can be seen in Figure 8, there is a satisfactory correlation between this approach and the test results.

Table 4 show the own approach for the compression stress-strain-curve of UHPFRC (left) and B4Q-0 (filling degree: α_{in} = 0,91 [7], f_{ck} = 160 MPa, E_{cm} = 52.2 GPa, ε_{cu} = 3.31 ‰, right).

B4Q-0 is made with v_f = 2.47 Vol.-% of high-strength steel fibres with l_f / d_f = 9 / 0.15 mm (Σ v_f x l_f / d_f = 2.47 % x 9 / 0.15 mm= 1.482).

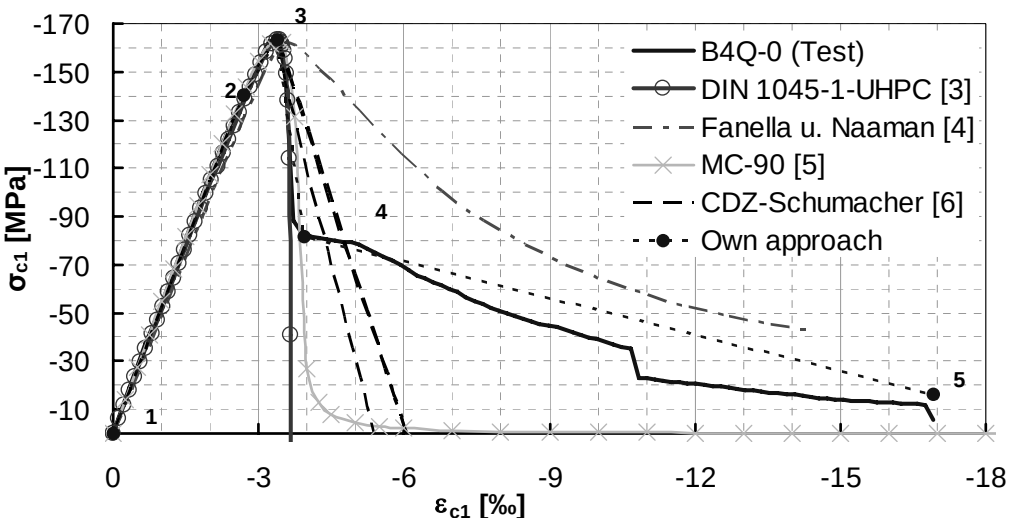

Figure 8: Comparison of test results of B4Q-0 with different approaches

Table 4: Approach for the stress-strain-curve of UHPFRC (left) and B4Q-0 (right)

Point i	ε_{ci} / ε_{cu}	f_{ci} / f_{ck}	ε_{ci}	f_{ci}
1	0.0	0.0	0.0	0.0
2	$(2\alpha_{in} - 1)\ f_{ck} / E_{cm}$	$(2\alpha_{in} - 1)$	(2 x 0.91 - 1) x 160 MPa / 52.2 GPa x -3.31 ‰ = -2.50 ‰	(2 x 0.91 - 1) x -160 MPa = -131.2 MPa
3	1.0	1.0	-3.31 ‰	-160 MPa
4	1.25	$0.35\ \Sigma\ v_f\ l_f/d_f$	1.25 x -3.31 ‰ = -4.13 ‰	0.35 x 1.482 x -160 MPa = -83.0 MPa
5	5.0	$0.1\ \Sigma\ v_f\ l_f/d_f$	5.0 x -3.31 ‰ = -16.55 ‰	0.1 x 1.482 x -160 MPa = -23.7 MPa

5 Spalling Behaviour at High Temperatures

The spalling behaviour of UHPC and UHPFRC at high temperatures is – as known from HPC – much more unfavourable than common normal-strength concretes (NSC). As a preliminary investigation fire tests of the concrete mixes B4Q-0 to B4Q-8 were carried out at the iBMB with the aim to determine the necessity, efficiency and necessary steel fibre and PP-microfibre content of this concrete to avoid spalling [7]. Figure 9 show six unloaded specimens with the dimensions of 200 mm x 200 mm x 500 mm made of UHPFRC before and after a 90 minute fire test. The moisture content before test was between 2.8 to 3.4 %. It can be seen that only the concrete mixes with PP-microfibres addition shows a sufficient spalling behaviour. The concrete mixes without PP-microfibres deteriorated more or less completely. Further on, it should also be noted that the specimen with B4Q-0 (2.47 Vol.-% short steel fibres with l_f = 9 mm and no PP-fibre addition) shows a better spalling behaviour than the test specimens B4Q-2, B4Q-4 and B4Q-5 (with long steel fibres with l_f = 30 mm and no PP-fibre addition). Additional tests carried out in this context show, that for this UHPFRC with a moisture content smaller 3.4 % a PP-fibre content of up to 2.0 kg/m³ PP-microfibres is needed to avoid spalling.

In general the fire behaviour of UHPC has to be investigated more deeply. Especially the material properties for the fire design and construction and design rules are not available at the moment. Further research work has to be carried out urgently in this field.

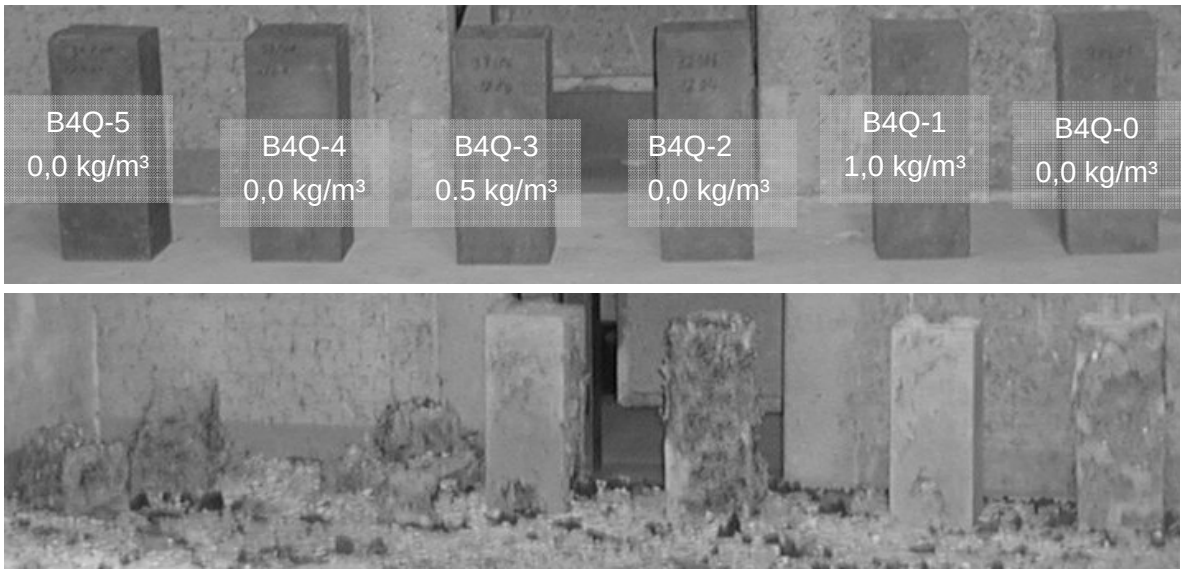

Figure 9: Test specimens with B4Q-0 to B4Q-5 (from right to left) before and after a 90 minute fire test, PP-fibre content given in upper picture

6 Conclusion

A series of tests was carried out in order to determine the tensile and compressive load bearing behaviour of different UHPFRC mixes. The test results can be summarised as follows:

- The post-peak behaviour of UHPFRC can be improved by the addition of steel fibres. The main parameters to describe the influence are the type of steel fibres, the aspect ratio (l_f/d_f) and the amount of fibres within the mixes.
- By the use of longer steel fibres (fibre length $l_f \geq 17$ mm instead of 9 mm) the required amount of steel fibres can be reduced significantly.
- Spalling of the concrete surface of this UHPFRC at high temperatures can be avoided by the addition of approximately 2.0 kg/m³ PP-microfibres.

7 Acknowledgement

The authors thank the “Deutsche Forschungsgemeinschaft (DFG)“ for their financial support in the context DFG Priority Program (SPP) 1182 “Sustainable Construction with Ultra-High-Performance Concrete (UHPC)”.

8 References

[1] DAfStb: 21. Entwurf der Richtlinie für „Stahlfaserbeton“. February 2005. (Not published).
[2] DAfStb: Sachstandsbericht Ultrahochfester Beton, May 2007. (Not published).
[3] DIN 1045-1-3: Tragwerke aus Beton, Stahlbeton und Spannbeton, Part 1-3. July 2001.
[4] Fanella, A.P., Naaman, A.E.: Stress-strain properties of fibre reinforced mortar in compression. ASI Journal, Vol. 82, July-Aug. 1985, pp. 475-483
[5] High performance concrete: Recommended extensions to the Model Code 90, CEB, 1995
[6] Schumacher, P.; Rotation Capacity of self-compacting SFRC. TU Delft, Diss. 2006.
[7] Teutsch, M.; Steven, G.: DFG-SPP 1182-Arbeitsbericht UHPFRC-Druckglieder. (Not published)

Sung Wook Kim
Research fellow
Korea Institute of Construction Technology
Goyang-Si, Korea

Su Tae Kang
Researcher
Korea Institute of Construction Technology
Goyang-Si, Korea

Jung Jun Park
Researcher
Korea Institute of Construction Technology
Goyang-Si, Korea

Gum Sung Ryu
Researcher
Korea Institute of Construction Technology
Goyang-Si, Korea

Effect of Filling Method on Fibre Orientation & Dispersion and Mechanical Properties of UHPC

Summary

The increase of tensile strength and improvement of toughness stand as the most remarkable advantages promoting the exploitation of Ultra High Strength Concrete (UHPC). Since such improvements are realized through the addition of steel fibres, the orientation and dispersion of the fibres in the matrix have naturally significant influence on the mechanical properties of UHPC. Fibre-reinforced concrete being manufactured by means various kinds of specimen shape and diversified filling methods and directions, these variables are likely to produce effect on the dispersion and orientation of fibres in UHPC leading to large differences in its mechanical properties. Accordingly, need is for a thorough investigation on the effect of filling method. This study intends to evaluate the effect of placing and flow direction not only on the orientation and dispersion of fibres but also on the tensile behavior of UHPC. Section analysis using photographic shooting is adopted to investigate the fibre alignment and reveals considerable difference in the fibre alignment according to the placing and flow direction. The best alignment appears to be achieved when placing is done in the direction of the flexural tensile stress. Such placing and flow direction produce little difference in the first cracking strength but significant discrepancy up to 50% in the ultimate tensile strength.

Keywords: *ultra high performance concrete, fibre, orientation, dispersion, filling, flow*

1 Introduction

The evolution of concrete technology has attained a level dealing with ultra high strength features going beyond the classic concept of high strength and has even permit the development of Ultra High Performance Concrete (UHPC) solving also the problem of brittleness that was the most critical one for the high strengthenization of concrete[1]. The matrix based on RPC (Reactive Powder Concrete) commonly called as cement is composed of an adequate proportion of particles with diameter below 1mm and is characterized by a brittle behavior. In order to supplement such brittleness, UHPC uses steel fibres which allows it to develop extremely high strength together with remarkable performance regard to

toughness and durability aspects[2]. The mechanical characteristics of UHPC are its compressive strength ranging from about 180 to 200MPa, its splitting tensile strength averaging 10 to 12MPa and its flexural tensile strength running on the mean from 30 to 35MPa. The most important advantages of fibre reinforced concrete are the increase of tensile strength and improvement of toughness. The improvement of such mechanical properties can be optimized through an arrangement of the fibres suited to the orientation of the stress. This can be achieved through the control of the orientation and dispersion of continuous long fibres in the matrix. Short fibres with length of 15 to 30mm are generally adopted in fibre reinforced concrete. These fibres are dispersed randomly in all directions so as to exhibit isotropy. However, since UHPC are not using coarse aggregates and show high fluidity, the orientation and dispersion of the fibres may rely on the flow direction owing to the casting sequence or shape of the structure. So many studies were carried out with the orientation and dispersion in fiber-reinforced concrete since the early seventies[3-5]. However the studies were focused on the material mechanics but did not deal with the flow characteristics. Recently, Ozyurt et al.[6], Stähli et al.[7] did this kind of studies, which were still restricted in specimen scale. Accordingly, this study examines the orientation and dispersion of the fibres according to placing and flow directions in order to evaluate the corresponding effects on the cracking strength and flexural strength.

2 Test setup and method

2.1 Specimen level

The composition of matrix used is given in Table 1 and 2% vol. steel fibers were used. The flow test showed the flowabiliy of about 230mm. This study performed at first specimen level tests using rectangular specimens with dimensions of 100mm× 100mm×400mm to evaluate the orientation and dispersion of the fibres according to the placing and flow directions of UHPC in fresh state. The specimens were tested by four point bending test. Two cases were considered for the placing and flow directions: casting in the longitudinal direction and guided flow, and casting in the vertical direction. This study being limited to flexural members and particularly to plates, placing direction for specimens standing vertically to present height of 400mm has not been considered. Figure 1 illustrates each of the placing and flow directions adopted during the manufacture of the specimens.

Table 1: The composition (by Vol. ratio)

OPC	1
Water	0.25
Silica fume	0.25
Sand	1.1
Filling powder	0.3
Superplasticizer.	0.018

(a) Placing direction parallel to flexural tension (b) Placing direction perpendicular to flexural tension

Figure 1: Placing and flow directions of concrete

Survey was done by cutting the specimens in the 3 directions to evaluate the characteristics of the fibres' arrangement within the specimens according to the orientation. The specimens were cut in 4 equal sections along their 400mm length of which the 2 median sections were cut longitudinally, vertically and transversally into 4 equal portions as shown in Figure 2. High resolution photographs were taken at each of the cutting planes to investigate the orientation and dispersion of the fibres. Thereafter, 4-point bending tests were conducted to examine the relationship between the orientation and dispersion of the fibres and the tensile characteristics of UHPC. The tests were carried out through displacement control using an actuation system with capacity of 250kN. The deflection at the center of the flexural members was measured by means of LVDT installed at the center of the specimens.

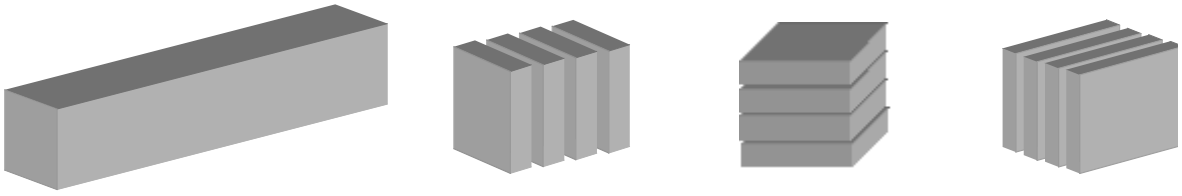

(a) Shape of specimen (b) Longitudinal direction (c) Vertical direction (d) Transverse direction

Figure 2: Section cutting directions of specimens

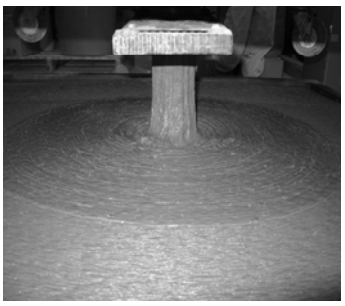

Figure 3: Placing and flow directions

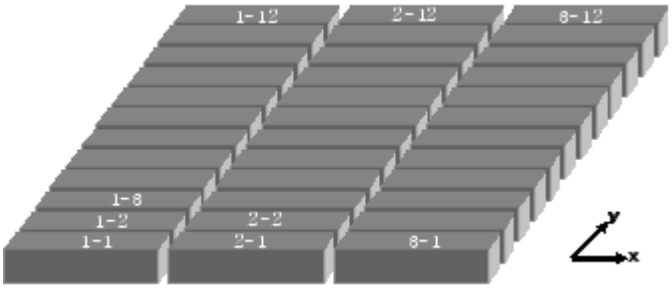

Figure 4: Label and shape of plate pieces

2.2 Structure level

In the precedent section, tests were carried out at the specimen level regard to the orientation and dispersion of the fibres according to the placing and flow directions. However, the flow in rectangular specimens of 100mm×100mm×400mm is disturbed by the small dimensions of the members, which is likely to produce differences in the flow characteristics and the corresponding orientation of the fibres in real structures. Chao et al.[8] reported that the tensile strength and behaviour was different according to the scale in the direct tensile test. More realistic orientation and dispersion of the fibres can be evaluated for specimens presenting dimensions closer to those of real structures. Accordingly, this section investigates these effects at a level comparable to actual structures. Plate with dimensions of 1320mm×1320mm×100mm was thus manufactured and cut into rectangular pieces of about 100mm×100mm×440mm to evaluate the cracking strength and flexural tensile strength with respect to the position by four point bending test. Placing was done by free fall from a height of about 200mm at the centre of the plate. The fresh UHPC was let to flow radially by itself. Since UHPC exhibits fluidity reaching its self-filling possibility, complete filling was realized

without additional finishing work except surface finishing. Figure 3 depicts the placing and flow directions during the manufacture of the plate structure. Figure 4 illustrates the cutting directions of the manufactured plate and the designation of each of the resulting pieces.

3 Test results and analysis

3.1 Specimen level

Figure 5 presents the results at the specimen level related to the orientation and dispersion of the fibres according to the placing and flow directions of UHPC. Figure 5 shows the alignment of the fibres at the cutting planes in each direction. In the case of placing parallel to the flexural tension, the fibres are seen to be evenly dispersed in the longitudinal direction with most of them being oriented vertically whereas their alignment appears to be inconsistent in the vertical and transversal directions. On the other hand, when placing is done perpendicularly to the flexural tension, the alignment of the fibres in the longitudinal direction becomes improper while satisfactory in the transversal direction. Moreover, the fibres are seen to be distributed more densely at the edges than at the centre in the vertical direction. These results can be attributed to the rolling flow of the fluid due to the restraint of the flow in the transverse direction when placing is done vertically.

	Longitudinal cutting plane	Vertical cutting plane	Transverse cutting plane
[CASE 1] Placing parallel to flexural tensile stress			
[CASE 2] Placing perpendicular to flexural tensile stress	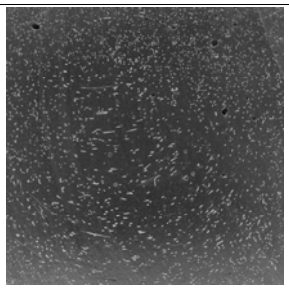	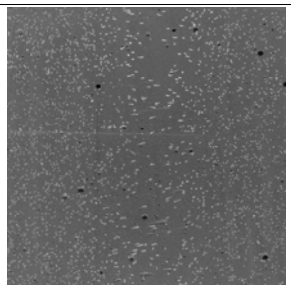	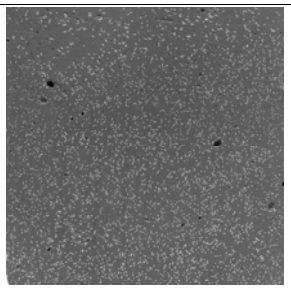

Figure 5: Orientation and dispersion of fibers according to the placing and flow directions

Figure 6(a) illustrates the behavior until the initiation of crack and Figure 6(b) represents the whole flexural tensile behavior. Even if CASE 1 presents a first cracking load slightly larger than CASE 2, the corresponding maximum tensile load is seen to be larger by about 50%. This means that, even if the initial cracking strength is relatively less influenced by the effect of the orientation and dispersion of the fibres, this effect becomes considerable on the maximum tensile strength. These results can be explained by the dependency of the initial cracking strength to the strength of the matrix and the large influence of the pullout strength of the fibres acting per unit area on the maximum tensile strength.

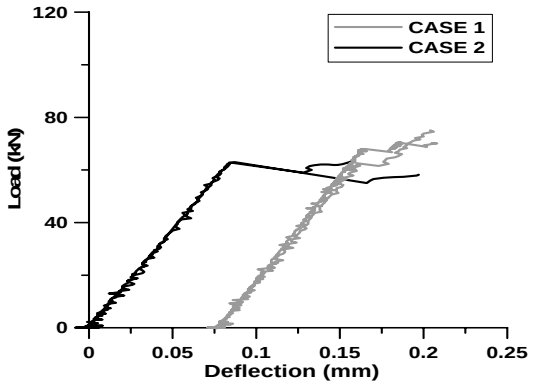

(a) Load-deflection curve regard to crack initiation

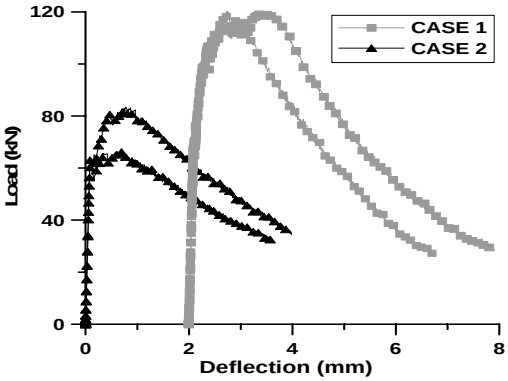

(b) Load-deflection curve regard to flexural tensile behavior

Figure 6: Bending test results at specimen level according to the placing and flow directions

3.2 Structure level

Table 2 summarizes the test results at the structure level. The deflection at the centre during the first cracking for the 36 pieces is seen to remain in a very narrow range running from about 0.06mm to 0.08mm. The corresponding flexural tensile stress is showing values between approximately 13 and 20MPa. Even if the initial crack stress presents slightly different values according to the position, no sensitive difference is observed when comparing series “1” to series “2”. However, considering the different initial crack stresses developed in the symmetrical series “1” and series “3”, the flexural stress occurring at first cracking appears to have no particular tendency according to the position.

However, it was verified that the maximum flexural stress exhibits significant difference with respect to the position. Figures 7(a) and 7(b) plot respectively the flexural behaviours of series “1” and series “2” according to the position. It can be seen that both series develop flexural strength increasing from the centre toward the edges. In the case of series “1”, pieces 7, 8, 9, and 10 are seen to have nearly no or very short hardening region whereas pieces 11 and 12 are presenting large increase of the flexural strength and also hardening after cracking. On the other hand, a comparison of series “2” with series “1” reveals the occurrence of relatively larger flexural strength for identical y coordinates as well as hardening.

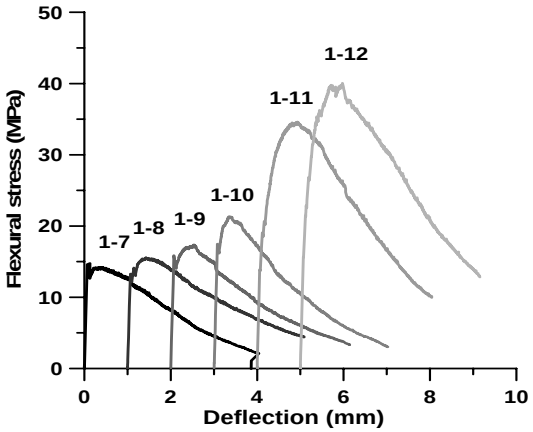

(a) Flexural behavior of series “1” by position

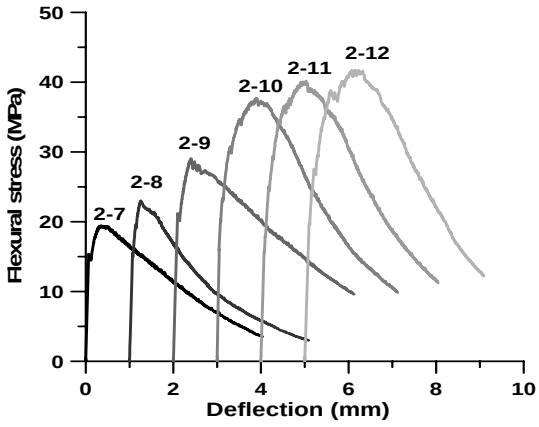

(b) Flexural behavior of series “2” by position

Figure 7: Bending test results at structure level according to the placing and flow directions

Table 2: Test results at structure level

Piece No.	Dimension			At first cracking			Ultimate state				
	Width (mm)	Height (mm)	Length (mm)	Load (kN)	Flexural stress (MPa)	Deflection (mm)	Load (kN)	Flexural strength (MPa)	Deflection (mm)	$\cos^2\theta$	θ
1-1	97	100	428	54	16.7	0.07	120	37.1	0.80	0.87	21.05
1-2	97	101	427	54	16.4	0.08	95	28.8	0.80	0.68	34.70
1-3	98	102	428	55	16.2	0.06	84	24.7	0.50	0.58	40.39
1-4	96	103	427	58	17.3	0.08	76	22.6	0.70	0.53	43.25
1-5	102	104	427	48	13.1	0.07	57	15.5	0.40	0.36	52.91
1-6	97	104	427	58	16.8	0.07	58	16.8	0.07	0.39	51.18
1-7	99	104	428	52	14.6	0.07	52	14.6	0.07	0.34	54.11
1-8	98	105	427	50	13.9	0.06	50	13.9	0.06	0.33	55.19
1-9	94	104	427	54	15.9	0.07	58	17.1	0.50	0.40	50.67
1-10	94	104	427	58	17.1	0.08	72	21.3	0.35	0.50	45.08
1-11	95	103	428	46	13.7	0.06	116	34.5	0.90	0.81	25.82
1-12	96	103	428	53	15.6	0.06	136	40.1	1.00	0.94	14.16
2-1	96	102	437	59	18.0	0.08	134	40.9	1.20	0.96	11.69
2-2	98	101	437	53	15.9	0.07	126	37.8	1.00	0.89	19.61
2-3	98	103	436	49	14.1	0.06	132	38.1	1.20	0.89	19.01
2-4	98	104	436	52	14.9	0.07	121	34.6	0.80	0.81	25.73
2-5	101	105	436	55	14.8	0.07	130	35.0	1.20	0.82	24.96
2-6	98	105	437	51	14.2	0.06	92	25.5	0.70	0.60	39.26
2-7	99	105	437	56	15.4	0.07	70	19.2	0.50	0.45	47.78
2-8	100	105	437	57	15.5	0.07	85	23.1	0.25	0.54	42.54
2-9	99	104	436	72	20.3	0.09	105	29.6	0.40	0.69	33.59
2-10	99	104	436	57	16.1	0.05	135	38.0	0.90	0.89	19.17
2-11	100	104	434	58	16.1	0.08	145	40.2	1.00	0.94	13.70
2-12	98	105	438	71	19.9	0.09	152	42.6	1.30	1.00	0.00
3-1	96	102	434	67	19.9	0.08	130	38.7	1.35	0.91	17.71
3-2	102	103	433	54	15.0	0.08	102	28.4	0.80	0.67	35.25
3-3	97	102	434	47	13.9	0.07	90	26.6	0.70	0.63	37.76
3-4	101	102	433	64	18.1	0.08	70	19.8	0.40	0.46	47.04
3-5	91	102	433	62	19.8	0.08	62	19.8	0.08	0.46	47.09
3-6	90	103	434	60	19.1	0.08	60	19.1	0.08	0.45	47.91
3-7	92	102	434	60	18.8	0.08	60	18.8	0.08	0.44	48.37
3-8	91	103	435	64	19.7	0.08	64	19.7	0.08	0.46	47.17
3-9	104	110	435	71	17.9	0.08	71	17.9	0.08	0.42	49.59
3-10	105	110	435	71	17.7	0.09	79	19.7	0.31	0.46	47.12
3-11	104	110	435	73	18.4	0.08	104	26.2	0.40	0.62	38.33
3-12	105	110	435	71	17.6	0.08	152	37.6	1.50	0.88	20.05

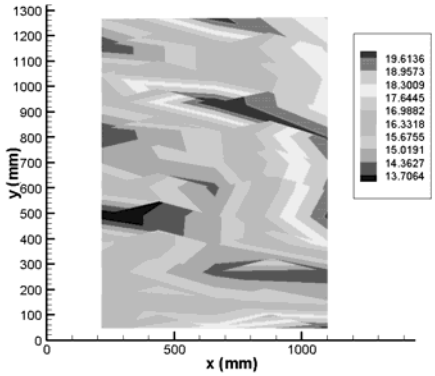

(a) Comparison of stress at first cracking

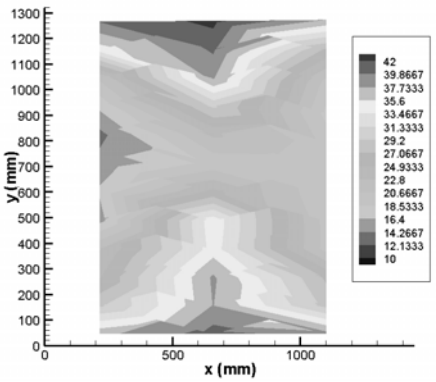

(b) Comparison of maximum flexural stress

Figure 8: Comparison of the initial crack and maximum flexural stresses by position in the plate

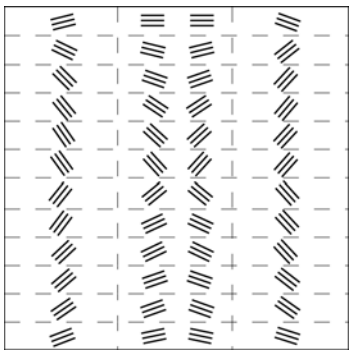

Figure 9: Evaluation of the relative orientation of the fibres by position in the plate

Figure 8(a) and 8(b) display the contour of the initial crack stress and maximum flexural stress by position. In Figure 8(b), the edges are developing larger flexural strength than the centre and, assuming that UHPC is flowing radially from the centre, it is verified that the flexural strength of the specimens subjected to flexural stress in a direction perpendicular to the flow are larger. In other words, most of the median pieces of series “1” and series “3” subjected to flexural stresses parallel to the flow direction develop small strength, while most of the pieces of series “2” subjected to flexural stresses normal to the flow as well as the outer pieces of series “1” and series “3” exhibit large strength at the whole.

Based on these results, the orientation of the fibres was evaluated by means of a two-dimensional approach. Letting σ_0 be the maximum tensile stress acting on the fibre disposed perpendicularly to the flexural stress, the maximum tensile stress of the composite due to the bridging effect of the fibre inclined by an angle θ to the flexural stress becomes $\sigma_0 \cos^2\theta$. Assuming that the maximum flexural stress occurs when $\theta = 0°$ in the experimental results of this study, the relative value θ of each piece can be determined. The corresponding results are arranged in Table 1 and are drawn for each of the so-obtained positions in Figure 9. An observation of the figure makes it possible to presume that the fibres are characterized by an alignement perpendicular to the radial flow expanding from the position where UHPC was poured.

4 Conclusions

The changes in the orientation and dispersion of fibres according to the placing and flow directions of ultra high performance concrete (UHPC) have been evaluated at the specimen and structure levels. Investigation of the effect of these results on the flexural behavior of UHPC has been conducted.

(1) The orientation of fibres according to the placing and flow directions of UHPC has been evaluated both at the specimen and structure level through the evaluation of the flexural strength.
(2) The first cracking strength was seen to be relatively indifferent to the placing and flow directions. However, the maximum tensile strength exhibited difference of about 50% at the specimen level and up to about 2 times at the structure level.
(3) Large differences in the alignment of the fibers were verified according to the placing and flow directions. The best orientation and dispersion of fibres were obtained when placing and flow occurred in the flexural tension direction.
(4) The evaluation of the effects of the placing and flow characteristics at the structure level revealed that the flexural strength increased when the flow of UHPC is oriented perpendicularly to the direction of the principal tensile stress. It was verified that the alignement of the fibres approaches the normal to the flow for larger flow distance from the pouring site.
(5) Accordingly, the evaluation of the tensile strength of UHPC shall imperatively consider the effects of the placing and flow directions. During the design of the structure, the design tensile strength shall be determined with sufficient consideration of the placing conditions on field and the flow characteristics according to the shape of the relevant member.

5 Acknowledement

The work presented in this paper was funded by Center for Concrete Corea(05-CCT-D11), supported by Korea Institute of Construction and Transportation Technology Evaluation and Planning (KICTTEP) under the Ministry of Construction and Transportation (MOCT).

6 References

[1] P. Richard and M. Cheyrezy, "Composition of Reactive Powder Concrete", Cement and Concrete Research, Vol. 25, No. 7, 1995, pp. 1501-1511.
[2] O. Bonneau et al., "Mechanical Properties and Durability of Two Industrial Reactive Powder Concretes", ACI Materials Journal, Vol. 94, No. 4, 1997, pp. 286-290.
[3] A. E. Naaman, and H. W. Reinhardt, "Characterization of High Performance Fiber Reinforced Cement Composites-HPFRCC", Proceedings of the Second International Workshop 'HPFRCD2', pp. 3-6, 1995.
[4] S. P. Shah and C. Ouyang, "Mechanical Behavior of Fiber-reinforced Cement-based Composites", Journal of American Ceramic Society, Vol. 74, No. 11, 1991, pp. 2727-2738.
[5] Y. Akkaya, J. Picka, and S. P. Shah, "Spatial Distribution of Aligned Short Fibers in Cement Composites", ASCE Materials in Civil Engineering, Vol. 12, No. 3, 2000, pp. 272-279.
[6] N. Ozyurt, T. O. Mason, S. P. Shah, "Correlation of Fiber Dispersion, Rheology and Mechanical Performance of FRCs", Cement and Concrete Composites, Vol. 29, 2007, pp. 70-79.
[7] P. Stähli, M. Sutter and J. G. M. van Mier, "Improving the Mechanical Properties of HFC by Adjusting the Filling Method", Proceedings of the Fifth International RILEM Workshop 'HPFRCC5', 2007, pp. 23-30.
[8] S. Chao, W. Liao, T. Wongtanakitcharoen, and A. E. Naaman, "Large Scale Tensile Tests of High Performance Fiber Reinforced Cement Composites", Proceedings of the Fifth International RILEM Workshop 'HPFRCC5', 2007, pp. 77-86.

Part 5:

Curing and Durability

Theresa M. Ahlborn
Ph.D., P.E., Associate Professor and Director, Center of Structural Durability
Michigan Technological University
Houghton, Michigan

Donald Li Misson
Graduate Research Assistant
Michigan Technological University
Houghton, Michigan

Erron J. Peuse
Structural/Geotechnical Engineer
Wilcox Professional Services, LLC
Cadillac, Michigan

Christopher G. Gilbertson
P.E., Research Engineer
Michigan Technological University
Houghton, Michigan

Durability and Strength Characterization of Ultra-High Performance Concrete under Variable Curing Regimes

Summary

The effects of curing regimes and specimen age on the strength and durability properties of a fiber-reinforced ultra-high performance concrete (UHPC) have been investigated. Regardless of when the thermal treatment was applied, UHPC consistently attained compressive stresses above 207 MPa, a modulus of elasticity of approximately 55 GPa, and a Poisson's ratio of 0.21. UHPC also demonstrated an extremely high resistance to freeze-thaw cycling (durability factor of over 100), coefficient of thermal expansion values only slightly higher than that of normal strength concretes, and negligible chloride ion penetration. Furthermore, ASTM and AASHTO standard methods were employed, yet modified, to aid in developing draft standards for testing some UHPC material properties in the United States.

Keywords: *ultra-high performance concrete, UHPC, durability, freeze-thaw, rapid chloride, coefficient of thermal expansion, modulus of elasticity, Poisson's ratio, compressive stress, curing*

1 Introduction

Ultra-high performance concrete (UHPC), a family of concretes with compressive strengths typically exceeding 150 MPa, is relatively new in the United States. Other countries have already begun to take advantage of the unique material characteristics of UHPC for exciting and innovative systems, but U.S. engineers and designers are currently interested in properties validated by ASTM (American Society for Testing and Materials) and AASHTO (American Association of State Highway and Transportation Officials) testing standards. Precasters and engineers are also seeking information on mechanical behavior variations for structural elements that are thermally treated at different concrete ages and more representative of conditions similar to a precaster's plant. All UHPC specimens in this study were cast and cured at Michigan Tech's Cement & Concrete Research Facilities using one UHPC blend. The pre-mix, steel fibers, superplasticizer, and water were mixed in accordance

with manufacturer's recommendations. Details of the materials, mixing process and testing standards may be found in Ahlborn et. al [1].

2 Mechanical Property Testing

Four different curing regimes: (a) 48-hour thermal steam treatment, (b) ambient air curing, (c) delayed thermal steam treatment (10-day delay before curing applied) and (d) double-delayed thermal steam treatment (24-day delay before curing applied) were used to determine the impact of the thermal cure timing on the compressive strength (ASTM C 39), modulus of elasticity and Poisson's ratio (ASTM C 469), and flexural cracking strength (ASTM C 1018) of an ultra-high performance concrete. While these standards are intended for use with normal strength concrete, they were modified slightly to facilitate their applicability to UHPC.

All specimens were demolded at 70 hours, and stored at room teperature until a curing regime was applied. Thermally steam treated (TT) specimens were subjected to a 90°C and 100 percent relative humidity steam bath for a total cure time of 48-hours (not including 6 hour ramp up and 6 hour ramp down times) immediately after demolding. For ambient air curing (Air), the specimens were allowed to cure in the air at ambient temperatures after demolding. Delayed (DTT) and double-delayed (DDTT) thermal steam treatment followed the same procedure as the thermal steam treatment except that there was a 10-day and 24-day delay before curing, respectively.

2.1 Compressive Strength

Compressive testing on 76 x 152 mm cylinders showed that the compressive stress was independent of the age at which thermal treatment was applied and the age at which the specimen was tested (Table 1). The mean compressive stress for 28-day TT, DTT, and DDTT cylinders were 214, 206, and 203 MPa, respectively. The air cured specimens gained strength with age and recorded a 28-day compressive strength of 165 MPa. Sample coefficent of variations (COV) are also listed and shows the data tightness.

Table 1: Specimen mean compressive stress results

Curing Regime	Age	Sample Size	Sample Mean Compressive Stress (MPa)	Sample COV
Air	3	6	99.6	3.8
	7	6	137.3	1.8
	14	6	153.7	3.2
	28	6	165.0	2.2
TT	7	6	208.8	2.9
	14	6	207.4	4.6
	28	6	214.4	1.3
DTT	14	5	205.0	3.5
	28	6	206.3	2.2
DDTT	28	5	202.9	3.2

As shown in Table 1, the mean compressive stresses of the air cured specimens increased as they continue to cure, much like traditional concrete. However, TT and DTT cured specimens show almost no compressive strength gain after the steam curing. Even when thermal treatment is delayed and applied to older specimens (such as DTT and DDTT specimens) there is not a statistical difference when compared to compressive strengths of UHPC thermally treated after demolding.

2.2 Modulus of Elasticity and Poisson's Ratio

Modulus of elasticity testing was performed on 76 x 152 mm cylinders from each of the four curing regimes following ASTM C 469. The modulus of elasticity of UHPC specimens 14 days and older was only slightly impacted by the thermal treatment (Figure 1.a). Air cured specimens at 14 and 28 days had a mean modulus of elasticity of 54,100 MPa. All of the thermally treated specimens (TT, DTT, and DDTT) had a population mean modulus of elasticity of 56,200 MPa. Therefore, the thermally cured specimens had a modulus of elasticity value only 4 percent greater than the 28-day Air cured specimens. The same curing increased the compressive stress by 26 percent. Figure 1.a also shows that the modulus of elasticity value increased for the Air cured specimens until 14 days, as was expected from the increase in compressive stress shown in Table 1.

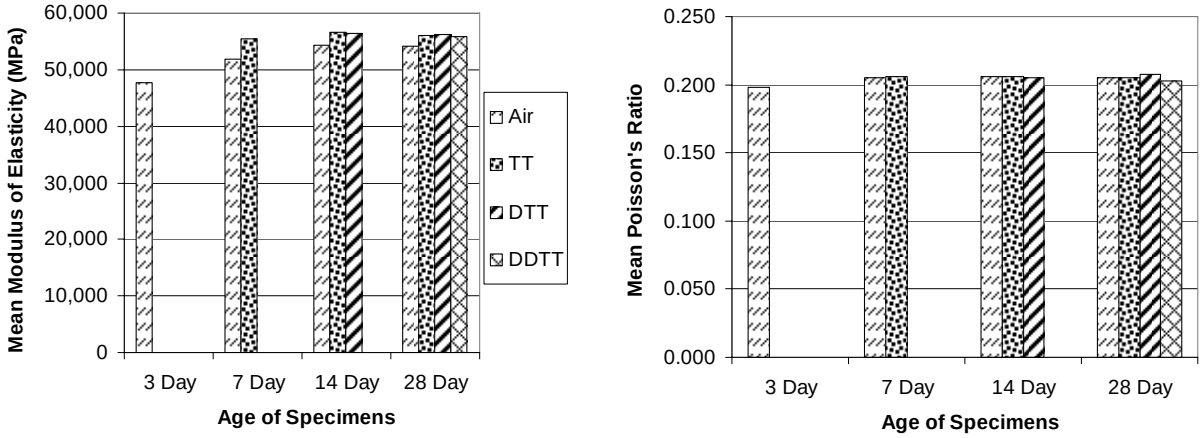

Figure 1: (a) Specimen mean Modulus of Elasticity results for all ages and curing regimes, (b) Specimen mean Poisson's ratio results for all ages and curing regimes

Differing from the modulus of elasticity, the four curing regimes had no impact on Poisson's ratio. Instead, all specimens, independent of age or curing regime, statistically had the same population mean (see Figure 1.b). The mean value for all samples, 0.21, is comparable with SETRA recommendations [2], and is slightly greater than the commonly accepted Poisson's ratio value for normal strength concrete of 0.20.

2.3 Modulus of Rupture in Bending

For flexural third point testing following ASTM C 1018 on 51 x 51 x 286 mm beams, only three curing regimes were compared (Air, TT, and DTT). Contrary to the compression and modulus results, all curing regimes had different population means for first crack stress. The sample means for first crack stress are shown in Table 2.

Table 2: UHPC first flexural crack stress

Curing Regime	Age	Sample Size	Corrected Mean First Crack Flexural Stress (MPa)	COV
Air	28	12	5.13	10.9
TT	28	12	7.31	8.0
DTT	28	12	8.10	9.1

3 Durability Testing

Durability testing considered rapid chloride penetration, freeze-thaw, and coefficient of thermal expansion and compared two curing regimes: ambient air curing (Air) and thermal treatment (TT) following manufacturer's recommended curing practices. Some modifications of ASTM and AASHTO standards were employed to maintain the integrity of these curing regimes.

3.1 Rapid Chloride Penetration

Electric Indication of Concrete's Ability to Resist Chloride Ion Penetration, ASTM C 1202, was followed for both specimen preparation and testing. The test involves applying a 60V electric potential across a saturated 51 mm thick by 102 mm diameter cylinder for 6 hours and measuring the total charge passing. Initially, the creation of a "electric short" circuit due to the steel fiber reinforcement was a concern [3], but because of the random fiber distribution and short fiber length no such "electric short" was ever created. Specimens were tested for each of the following curing regimes: 7-day thermally treated, 28-day air-treated, and 28-day thermally treated. Results are summarized in Table 3.

Table 3: Rapid Chloride Penetration Summary Data

Curing regime	Age at testing (days)	Sample Size	Charge passed (coulombs)		Chloride ion penetrability
			Mean	Standard deviation	
Air	28	4	75	15	Negligible
TT	7	2	11	2.1	Negligible
TT	28	4	15	3.5	Negligible

All of the specimens exhibited chloride ion penetrations in the negligible range (< 100 Coulombs passed), with lower total charge passing through the TT specimens than through Air cured specimens. In addition, the ionic movement in the TT specimens was independent of the age at testing (7-days or 28-days), which is congruent with other research data [3]. Furthermore, the low standard deviations also show consistency between batches, as samples were randomly selected from four batches. Finally, it should be noted that in materials such as UHPC that contain a high amount of silica fume, the ASTM C 1202 test method tends to indicate a lower chloride movement rate than would normally be expected from concretes without silica fume [4].

3.2 Freeze-Thaw

Freeze-thaw durability is a necessary attribute for concretes in the mid-northern climates. To study the effect of freezing and thawing on the relative dynamic modulus (RDM), mass, and

length of UHPC specimens, six 75 x 100 x 406 mm UHPC beams were tested in an 80-beam freeze-thaw chamber following ASTM C 666 Procedure B: rapid freezing in air, and thawing in water. In addition to the beams tested in the freeze-thaw chamber (FT), 6 side-study (SS) beams (2 from each batch - one TT sample and one Air sample) were cycled in and out of a separate water bath at ambient temperature to compare their mass change and RDM values (equivalent to durability factor when specimens reach 300+ cycles) to the specimens undergoing freeze-thaw cycling. Table 4 summarizes the data obtained from this testing. UHPC evidenced a high resistance to freeze-thaw cycling as there were no signs of distress recorded as RDM decrease, mass loss, or length change. Comparatively, Graybeal showed that specimens submerged in a water bath after curing experience mass gain, RDM increase, and an increased compressive strength [3].

Table 4: Freeze Thaw Summary Data

Curing Regime	Testing regime-specimen age (days)	Sample Size	Freeze-thaw cycles	RDM at end of cycling (%)	Length Change (%)	Mass Change (%)
Air	FT-28	6	300+	101.57	0.0004	+0.54
TT	FT-28	6	300+	100.29	0.00004	+0.08
Air	SS-28	6	None	101.91	N.A.	+0.22
TT	SS-28	6	None	100.10	N.A.	+0.06

N.A. – no data acquired

Figure 2 shows the RDM over number of cycles (with eight cycles completed per day). The RDM values increased independent of curing, however, the Air cured specimens increased much more dramatically. Additionally, the RDM of the Air cured specimens increased similarly regardless of testing regime (FT or SS). Therefore, the increase is closely tied to the effect of cycling the specimens in and out of water, and not necessarily the effect of freeze damage

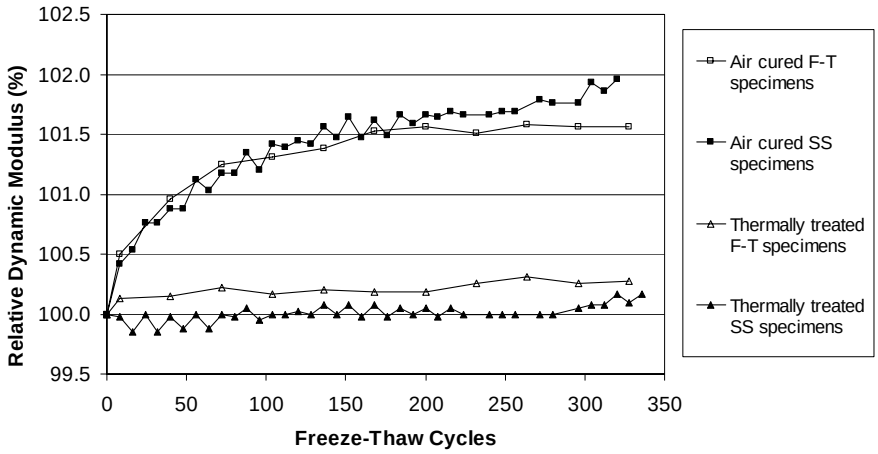

Figure 2: Mean relative dynamic modulus of air cured and thermally treated UHPC specimens

3.3 Coefficient of Thermal Expansion

Coefficient of thermal expansion (CTE) testing was performed on 3, 7, 14, and 28-day Air cured specimens and on 7-day and 28-day TT specimens following the FHWA Procurement Specification [5] which closely follows AASHTO-TP 60-00 [6]. However, following previous research [3] and to avoid any reaction between water and unhydrated cement particles in the cement matrix, all of the UHPC specimens were kept unsaturated during testing through the use of an epoxy coating. A summary of the CTE values for the specimens is presented in Table 5.

Table 5: Coefficient of thermal expansion summary

Curing regime	Specimen Age (days)	Sample Size	Mean CTE value (mm/mm/ºC)	Standard deviation (mm/mm/ºC)
Air	3	3	13.6 x10^{-6}	0.1 x10^{-6}
Air	7	4	13.7 x10^{-6}	0.1 x10^{-6}
Air	14	3	13.8 x10^{-6}	0.2 x10^{-6}
Air	28	3	13.9 x10^{-6}	0.3 x10^{-6}
TT	7	3	14.8 x10^{-6}	0.1 x10^{-6}
TT	28	3	14.7 x10^{-6}	0.3 x10^{-6}

The unsaturated 28-day TT specimen's mean CTE was 14.7 x 10^{-6} mm/mm/°C, and was higher than the CTE value for unsaturated 28-day Air specimens (13.9 x 10^{-6} mm/mm/°C). The results also demonstrate that the age of a specimen at testing plays a more significant role in Air-cured UHPC specimens than in thermally-treated UHPC specimens. The mean data in Table 5 indicate little change from the 7-day thermally treated specimens to the 28-day specimens, but Figure 3 shows an increasing CTE value as the air cured specimens age.

Figure 3: Mean and one standard deviation values for CTE of air-cured UHPC specimens

Measured CTE values of UHPC during testing were slightly higher than typical normal and high strength concrete CTE values of approximately 7.4-13 x 10^{-6} mm/mm/°C [7]. This is expected because the CTE of a concrete is most greatly influenced by the CTE of its aggregate and UHPC consists mostly of fine sand (41 percent) and portland cement (29 percent). Therefore, the CTE value for UHPC would be expected to fall between the range of

a 1:6 cement/natural silica sand mortar (12 x 10^{-6} mm/mm/°C) [8] and saturated portland cement pastes (18-20 x 10^{-6} mm/mm/°C).

4 Conclusions

UHPC mechanical and durability properties compared well with others [3] and showed repeatability between laboratories. The ASTM and AASHTO standards used in this study generally apply to UHPC with a few minor modifications to some test procedures. Draft recommendations for procedures are being developed.

4.1 Mechanical Properties

Independent of age at curing and the age at which the specimen was tested, thermally treated specimens reached average compressive stresses greater than 200 MPa, while Air cured specimens at 28 days had a compressive stress of 165 MPa. Modulus of elasticity was not greatly affected by various curing regimes, and thermally treating only increased the modulus of elasticity by 3.8 percent. Furthermore, modulus of elasticity data compared well with the SETRA relationship [2] when Air cured specimens are removed from the analysis. The mean Poisson's Ratio value was 0.21 and was not affected by any of the curing regimes. However, first crack stress was affected by changes in the curing regime and increased from 5.1 MPa for Air cured specimens, to 7.3 MPa for TT specimens, and 8.1 MPa for DTT specimens.

4.2 Durability Properties

Thermal treatment increased UHPC's resistance to ionic movement, and both thermally treated specimens and air cured specimens showed negligible chloride ion penetrability. Also, UHPC can be considered a frost-resistant concrete that does not become sufficiently saturated to be damaged by freezing according to ASTM C 666. Freeze-thaw specimens showed no sign of deterioration even though UHPC does not include air entrainment. The coefficient of thermal expansion of UHPC was slightly higher than that of normal-strength or high-strength concrete. Average CTE values for UHPC at 28-days were 14.7 x 10-6 mm/mm/°C and 13.9 x 10-6 mm/mm/°C for thermally treated and Air cured specimens, respectively. The air-treated specimens exhibited increasing CTE values as UHPC aged up to 14-days. However, CTE values for thermally treated UHPC did not significantly change with age.

5 Impacts

The compressive strength, modulus of elasticity, and Poisson's Ratio did not significantly vary once UHPC was thermally treated, and therefore could have a large impact on how ultra-high performance concretes are used in the United States. This may allow a precaster to make several elements over a short period of time and cure them at a later time, thus providing more flexibility in the casting and curing sequence. However, design considerations need to consider strength reductions for air-cured specimens, as well as other material properties (such as creep and shrinkage) that are not studied herein.

6 Acknowledgements

The authors would like to thank the Michigan Department of Transportation (MDOT) and Michigan Tech's University Transportation Center: Materials in Sustainable Transportation Infrastructure (MiSTI) for their support and guidance throughout this project.

7 References

[1] Ahlborn, T.M.; Misson, D.L.; Peuse, E.J.; Gilbertson, C.G.: Ultra-High Performance Concrete for Michigan Bridges – Material Performance. MDOT RC#-X, Michigan Department of Transportation, June 2008 pending; CSD-2008-11 Report, Center for Structural Durability, Michigan Technological University.

[2] SETRA (Service d'études techniques des routes et autoroutes), and AFGC (Association Française de Génie Civil): Ultra High Performance Fibre-Reinforced Concretes - Interim Recommendations, (Bétons Fibrés à Ultra-Hautes Performacnes – Recommandations Provisoires). France, January 2002.

[3] Graybeal, B.A.: Material Property Characterization of Ultra-High Perfomance Concrete. In: FHWA-HRT-06-103, Federal Highway Administration, August 2006.

[4] Mindess, S.; Young, J.F.; Darwin, D.: Concrete 2nd Edition, Pearson Education, Inc., Upper Saddle River, New Jersey, 2003.

[5] Federal Highway Administration: Development and Manufacture of Equipment for Measuring the Coefficient of Thermal Expansion (CTE) of Concrete. Contract No. - DTFH61-05-C-00010. Received Nov. 15, 2007.

[6] AASHTO TP60-00, Standard Method of Test for Coefficient of Thermal Expansion of Hydraulic Cement Concrete, American Association of State Highway and Transportation Officials. In: Standard Specifications for Transportation Materials and Methods of Sampling and Testing, Washington, D.C., 2000.

[7] Federal Highway Administration: Thermal Coefficient of Portland Cement Concrete. Retrieved October 30, 2007 from http://www.fhwa.dot.gov/pavement/pccp/thermal.cfm. Published 06/09/06.

[8] Mehta, P.K,; Monteiro, P.J.: Concrete Microstructure, Properties, and Materials 3rd Edition, The McGraw-Hill Companies, Inc., New York, New York, 2006.

Ingo Schachinger
Dr.-Ing.
beton-team
Augsburg, Germany

Harald Hilbig
Dr. rer. nat.
cbm, TU München
Munich, Germany

Thorsten Stengel
Dipl.-Ing.
cbm, TU München
Munich, Germany

Effect of Curing Temperature at an Early Age on the Long-Term Strength Development of UHPC

Summary

In order to achieve compressive strengths above 200 MPa, UHPC is normally heat treated at an early age (2 days) for 24 to 48 hours at 90°C. Essentially, this accelerates the pozzolanic reaction of silica fume with $Ca(OH)_2$. Contrary to expectation, this long-term study shows that the strength development of UHPC after heat treatment has not ceased. The compressive strength of a heat treated UHPC was observed to increase from 220 to 280 MPa over 8 years' storage in water. ^{29}Si MAS NMR spectroscopy revealed that the chain length of the C-S-H phases increased from values between 5 and 6 to 9 during this period. A distinct increase in compressive strength of UHPC not subjected to heat treatment (20°C) was also observed at high ages. The compressive strength was 250 MPa at an age of six years which was 58% more than the 28 day strength of 160 MPa. This is due to the slow, but continuous, pozzolanic reaction of the silica fume and the increase in C-S-H phase chain length.

Keywords: *UHPC, silica fume, heat treatment, ^{29}Si MAS NMR, C-S-H chain length*

1 Introduction

Between 1990 and 1995 in France and Canada progress was made in the development of a type of concrete called Poudres Réactives (BPR) or Reactive Powder Concrete (RPC). In the mean time the term ultra high performance concrete (UHPC) has become established as the international designation for this type of concrete. Since the end of the 1990s several UHPC demonstration structures have been built such as filigree footbridges with wide spans in Sherbrooke (Canada, 1997), Seoul (South Korea, 2002) and Kassel (Germany, 2007). In Cattenom (France, 1997), a UHPC substructure of a cooling tower may be found which is very durable despite exposure to an aggressive environment. Other examples of UHPC realization include several aesthetically ambitious demonstration objects like the toll station in Millau (France, 2004). These structures are all less than ten years old and therefore the concrete still relatively young. The design of the structures was usually based on test results for concrete specimens with an age of at most 28 days. The experience gained during the

design and realization of some of these structures influenced the French guidelines for UHPC which appeared in 2002. The results of this study on the long-term development of compressive strength at high ages of up to eight years should increase the level of trust and acceptance for the novel cementitious material UHPC. Since it is not possible to extract cores from the highly stressed UHPC structural components, the development of compressive strength at high ages is of particular interest with regard to the assessment of safety margins.

In the present investigations, not only specimens stored under normal conditions (20°C, enclosed in polyester foil or submerged in water) were considered, but also specimens subjected to heat treatment for 24 hours at 50, 65 or 90°C at an early age. Besides measurements of compressive strength, ^{29}Si MAS NMR spectroscopy was used to determine the degree of hydration of cement and silica fume as well as the chain length of the C-S-H phases.

2 Experimental

2.1 Materials and Compositions

The present investigations were performed using four different UHPC compositions and a model binder paste mix which were produced between 1999 and 2001. The same cement and silica fume were used for three of the UHPC mixes stored at 20°C and the model mix (made in 2001). The heat treated UHPC1 (produced in 1999) contained different binder materials. The 28 day compressive strengths after storage at 20°C were between 155 and 171 MPa, see Table 1. The composition of the UHPC and the curing method are in Table 1.

Table 1: Composition and curing of the UHPC mixes

Mix	**UHPC1 (1999)**		**UHPC2 (2001)**		**UHPC3 (2001)**		**UHPC4 (2001)**	
28 d compressive strength* **	160 MPa		171 MPa		165 MPa		155 MPa	
Temperature, storage and heat treatment	20°C 50, 65 and 90°C		20°C		20°C		20°C	
Cement	CEM I 42.5 R		CEM I 42.5 R-HS		CEM I 42.5 R-HS		CEM I 42.5 R-HS	
w/c	0.23		0.27		0.33		0.27	
Silica fume content [wt.%] w.r.t . cement	28		30		30		18	
	Quantity		**Quantity**		**Quantity**		**Quantity**	
Material	**kg/m³**	**l/m³**	**kg/m³**	**kg/m³**	**kg/m³**	**l/m³**	**kg/m³**	**l/m³**
Quartz sand (< 0.5 mm)	872	329	943	356	943	356	943	356
Stone flour (< 0.063 mm)	153*	56	458**	149	458**	149	458**	149
Cement	889	287	683	212	636	198	736	229
Silica fume	248	105	205	87	189	80	132	56
Superplasicizer	57	52	44	41	28	25	43	39
Water	171	171	155	155	192	192	171	171
Total	2390	1000	2488	1000	2446	1000	2483	1000

* Quartz flour, ** Basalt flour, *** Stored at 20 °C

2.2 NMR Spectroscopy

Solid state NMR experiments were performed with a Bruker Avance 300 spectrometer (magnetic field strength 7.0455 T, resonance frequency of ^{29}Si is 59.63 MHz). To measure the ^{29}Si MAS NMR spectra, the samples were packed in 7 mm zirconia rotors and spun at 5 kHz at an angle of 54°44' (MAS). The chemical shifts were recorded relative to external tetramethylsilane (TMS). The single pulse technique was applied with a pulse width of 6 µs. Owing to the slow relaxation of the silica fume, a repetition time of 45 s was chosen and a typical number of scans was 2000. Thirty Hertz line broadening was applied to all spectra prior to deconvolution. The signal patterns of the spectra were deconvoluted with the Bruker WINNMR software using a Lorentz curve which led to the best result. The interpretation of the ^{29}Si NMR spectra was performed according to the Q^n-Quotation, Figure 1.

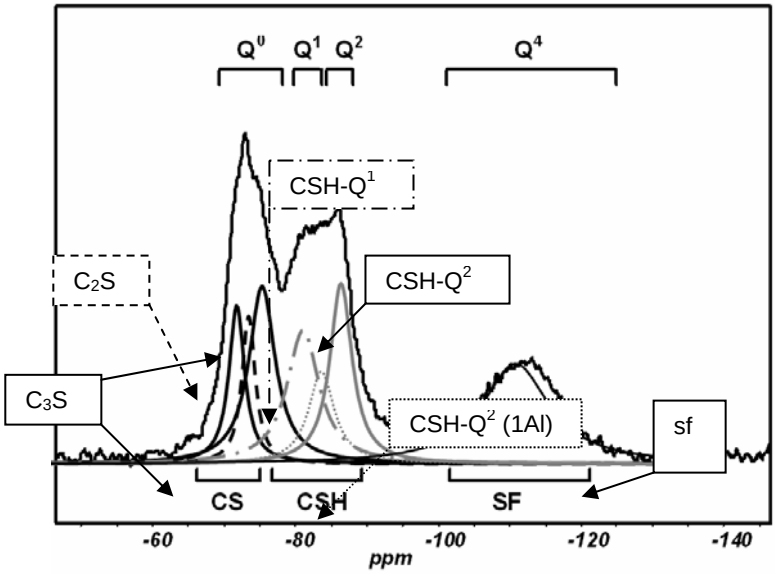

Figure 1: ^{29}Si MAS NMR spectrum for the model binder mix Portland cement and 20 wt.% silica fume (w/c = 0.27) at an age of 28 days

By combining the integrated intensity of the different NMR signals, it is possible to calculate the degree of hydration of cement *Z* and silica fume *sf* with respect to Si as well as the mean chain length of the C-S-H phases, equations 1 to 3 [4].

$$H_{Si,Z}, = \frac{I(Q^1) + I(Q^2) + I(Q^4) - {sf}/{Z} \cdot I(Q^0)}{I(Q^0) + I(Q^1) + I(Q^2) + I(Q^4)} \quad \textbf{Eq. 1}$$

$$H_{Si,sf} = \frac{I(Q^1) + I(Q^2) + I(Q^0) - {sf}/{Z} \cdot I(Q^4)}{I(Q^0) + I(Q^1) + I(Q^2) + I(Q^4)} \quad \textbf{Eq. 2}$$

$$\overline{C} = \frac{2\left(I(Q^1) + I(Q^2)\right)}{I(Q^1)} \quad \textbf{Eq. 3}$$

3 Experimental Results

3.1 Investigation of Hydration Using ^{29}Si NMR Spectroscopy

The slow pozzolanic reaction of silica fume at 20°C which led to a change in the structure of the C-S-H phases (see Figure 2) was responsible for the increase in compressive strength at high ages. Parallel strength and ^{29}Si MAS NMR measurements performed with hardened binder specimens at an age of 28 days (w/c = 0.27, 20 wt.% silica fume) and UHPC at an age of one year (w/c = 0.27, 18 wt.% silica fume) and eight years (w/c = 0.23, 28 wt.% silica fume) confirm this relationship, cf. Table 2.

Using ^{29}Si MAS NMR Zanni et al. [5] proved that at 20°C quartz flour in concrete is absolutely inert - even after long storage times. Moreover, silica fume has a larger specific surface than quartz flour. Thus the model mix, which is almost identical in composition to the binder paste matrix of one of the UHPC mixes, is comparable to UHPC.

Table 2: Degree of hydration of cement and silica fume it dependence of age, heat treatment and composition

Specimen	**Age**	**Degree of hydration**		**Mean chain length**	**Compressive strength**
		CEM	**SF**		
Specimens stored at 20°C	[days]	[%]	[%]	[-]	[MPa]
Model mix (0.27 – 20)	1	30.6	10.2	3.5	92
Model mix (0.27 – 20)	7	38.5	26.2	4.4	135
Model mix (0.27 – 20)	28	37.8	47.1	5.7	156
	[years]	[%]	[%]	[-]	[MPa]
UHPC2 (0.27 – 30)	1.123	39.1	51.3	7.6	199
UHPC3 (0.33 – 30)	1.123	47.2	66.3	6.0	175
UHPC4 (0.27 – 18)	1.123	35.2	72.8	5.8	172
UHPC1 (0.23 – 28)	8.370	30.7	76.4	8.4	252
Heat treated specimens **UHPC1 (0.23 – 28)** **Temperature / Prestorage time**	[years]	[%]	[%]	[-]	[MPa]
50°C / 1 d	8.438	25.2	85.0	7.7	263
90°C / 1 d	8.553	30.9	90.4	9.1	247
50°C / 5 d	8.427	35.4	78.8	8.3	* ≥ 256
65°C / 5 d	8.427	34.6	81.3	7.6	* ≥ 272
90°C / 5 d	8.543	35.6	83.3	8.1	249

* these compressive strengths were already determined at an age of 6.041 years

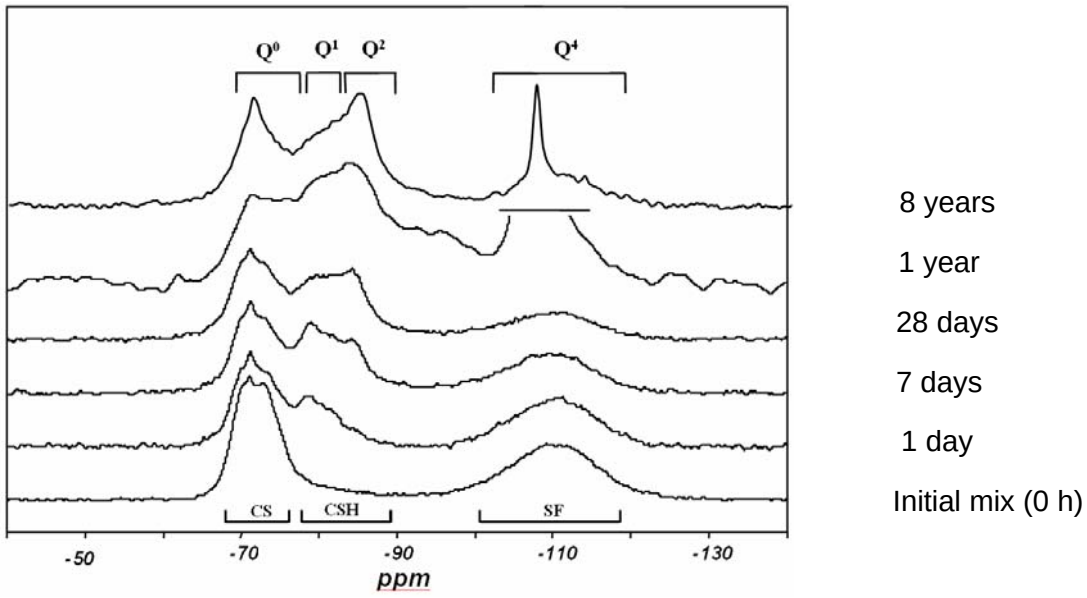

Figure 2: ^{29}Si MAS NMR spectra for the model mix (0.27-20) up to 28 days (bottom) and UHPC mixes after 1 year (0.27-18) and 8 years (0.23-28)

At an age of 28 days, the proportion of hydrated silica phases of the cement in the model mix was approximately 38%. The hydration reaction of the cement was completed after, at latest, seven days, see Figure 3. The proportion of reacted silica fume increased during normal storage from 47%, at an age of 28 days, to 76% after eight years. During this period the amount of C-S-H formed clearly increased and the Q^2 signal for bridging silicate tetrahedra at -85 ppm increased indicating a growth in mean chain length of the C-S-H phases from 5.7 to 8.4. In the case of the heat treated specimens, the proportion of reacted silica fume (80 to 90%) was much larger. The degrees of hydration of cement and silica fume determined by ^{29}Si NMR spectroscopy and the chain lengths of the C-S-H phases are shown in Table 2.

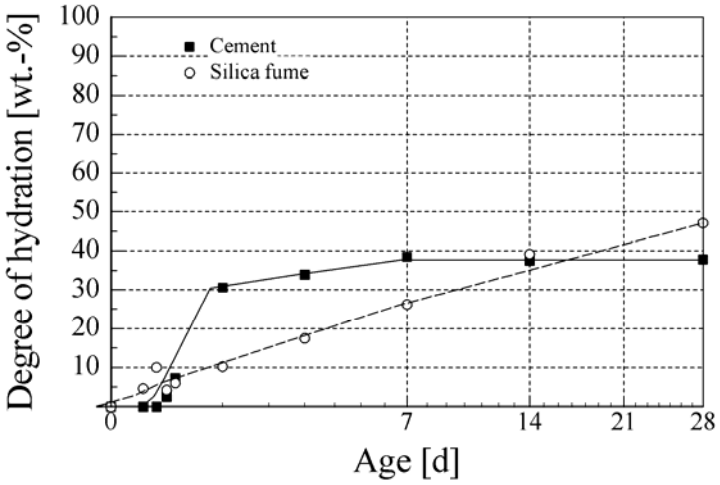

Figure 3: Hydration of the silicate phases of cement and silica fume measured with ^{29}Si MAS NMR for the model mix (w/c= 0.27, CEMI, 20% sf)

3.2 Long-Term Development of Compressive Strength at 20°C

The results for the compressive strength measurements for very different UHPC compositions at the high ages of 1, 3.5, 6 and 8 years are shown in Figure 4. At an age of 3.5 years the strength is 40% above the 28 day value indicating a considerable increase in hardening at high ages. Since all the UHPC mixes were produced without fibres, the specimens were extremely brittle - especially at high ages. Because of this, specimen preparation and mounting in the testing machine led to a large scatter of the measured values: It was up to 50 MPa within a test series. This explains the lower compressive strength of the eight year old compared with the six year old specimens in Figure 4; 225 as opposed to 250 MPa, respectively.

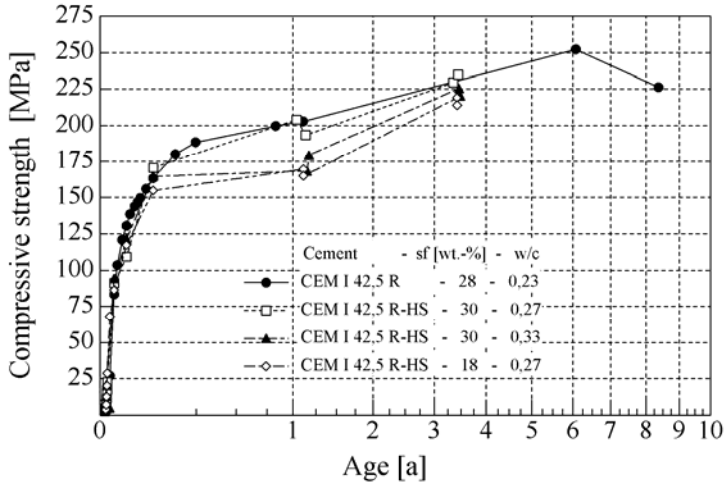

Figure 4: Long-term compressive strength of different UHPC compositions stored at 20°C (enclosed in a polyester sheet or submerged in water). Values are plotted versus time on a square root scale.

The results of the ^{29}SI MAS NMR investigations showed a distinct increase in mean chain length of the C-S-H phases at high ages. Obviously, strength increases with the mean chain length of the C-S-H phases. This relationship confirms the results of Zanni et al.

4 Effect of Age at Heat Treatment and Temperature on Compressive Strength at Ages up to 28 Days

Beginning the 24 hour heat treatment at an age of five days was found to be most favourable for the achievement of high strengths at ages up to 28 days, Figure 5. This was valid for heat treatments at 50, 65 and 90°C, Figure 5. After five days, the maximum possible hydration of the Portland cement is reached which is below 100% owing to the low w/c ratio. The effect of the storage time before heat treatment is confirmed by the results of Ma who recommended commencing heat treatment on reaching a UHPC compressive strength of 90 MPa. The present UHPC compositions reached this strength in just under three days. Depending on the type and dosage of superplasticizer, strength development can be delayed by up to two days under certain conditions.

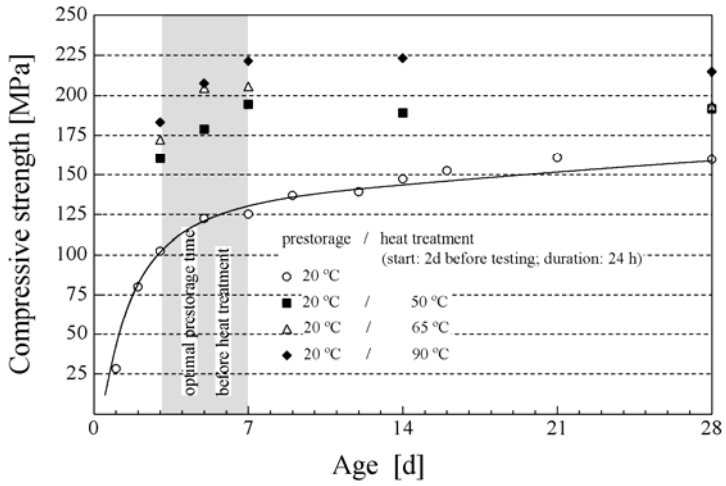

Figure 5: Effect of age at the beginning of heat treatment and heat treatment temperature on the compressive strength of UHPC 1 at ages up to 28 days.

A high compressive strength of 225 MPa, obtained by optimal heat treatment (beginning at an age of five days, 90°C) and reached after only seven days, was equalled only after a very long storage period (roughly 3.5 years) at 20°C, cf. Figure 4.

5 Long-Term Development of Compressive Strength after Heat Treatment at an Early Age

The results of these investigations contradict statements in the literature where the development of shrinkage and strength as well as the chemical reactions causing them are terminated by heat treatment at an early age. All the heat treated specimens with ages up to eight years exhibited a further gain in strength of as much as 30%, see Figure 6.

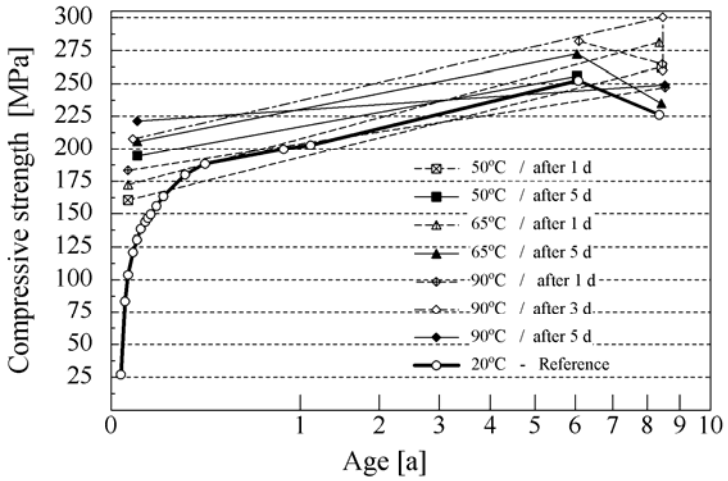

Figure 6: Long-term evolution of compressive strength of UHPC 1 during storage under normal conditions and after heat treatment at early ages

Irrespective of treatment history, the specimens between six and eight years old all had high compressive strengths of 250 to 300 MPa which corresponds to values measured for natural stone, e.g. granite. If UHPC is not heat treated at an early age or only at temperatures up to

90°C then it may be assumed that a final strength of 250 to 300 MPa will be reached after six years. Significantly higher strengths are only possible through the more complicated process of heat treating at temperatures around 250°C. By adding steel fibres to the mix, typically 3 vol.%, ductility increases and the statistical scatter of strength values is reduced. It must therefore not be expected that fibres increase strength.

6 Conclusions

- To obtain high compressive strengths at early ages it is expedient to heat treat UHPC for at least 24 hours following storage for five days at 20°C. After five days, the hydration of the cement, which is 35 to 40% due to the low w/c ratio, is essentially complete.
- Heat treatment at 50 to 65°C at an early age results in high compressive strengths of 200 MPa. At 90°C the pozzolanic reaction of silica fume is greatly accelerated so that compressive strengths of 225 MPa are reached at an age of only seven days.
- Irrespective of previous treatment, all specimens exhibited very high compressive strengths ranging from 250 to 300 MPa at high ages of six to eight years. This corresponds to values measured for natural stone, e.g. granite. The ongoing increase in strength at high ages is due to the pozzolanic reaction of silica fume and growth of C-S-H phase chains to lengths between eight and nine SiO_4 tetrahedra.
- Since the design of structural components made of UHPC is based on compressive strength measured at an age of 28 days or following heat treatment, a safety margin of 20 to 50% is valid for concrete strength at an age of 6 years.

7 References

[1] Interim Recommendations for Ultra High Performance Fibre-Reinforced Concretes. Association Francaise de Genie Civil (AFGC) / Service d´ètudes techniques des routes et autoroutes (SETRA), working group on Ultra-High Performance Fibre-Reinforced Concrete, Januar 2002.

[2] H. Hilbig, F.H. Köhler, P. Schießl: Quantitative 29Si MAS NMR spectroscopy of cement and silica fume containing paramagnetic impurities, Cem. Concr. Res. 36 (2006) 326-329

[3] H. Hilbig, F.H. Köhler, P. Schießl: Hydratation von Hochleistungs-Feinkorn-Betonen, NMR-spektroskopische Untersuchungen, 15. Internationale Baustofftagung, Tagungsband, 2003, Weimar, 1-0489 – 1-0496.

[4] Zanni, Hélène; Cheyrezy, Marcel; Maret, Vincent; Philippot, Samuel; Nieto, Pedro: Investigation of Hydration and Pozzolanic Reaction in Reactive Powder Concrete (RPC) Using 29Si NMR. Cement and Concrete Research, (1996) Vol. 26, No. 1, S. 93-100.

[5] Ma, Jianxin: Experimental Investigations for the Production of Ultra-High Strength Concrete. Lacer No. 6, 2001, S. 215-228.

Urs Müller
PhD., Researcher
Federal Institute for Materials Research and Testing (BAM),
Division VII.1 - Building Materials,
Berlin, Germany

Birgit Meng
Prof. PhD., Division Leader
Federal Institute for Materials Research and Testing (BAM),
Division VII.1 - Building Materials,
Berlin, Germany

Hans-Carsten Kühne
PhD., Researcher
Federal Institute for Materials Research and Testing (BAM),
Division VII.1 - Building Materials,
Berlin, Germany

Jiri Nemecek
PhD., Assistant Professor
Czech Technical University
Department of Mechanics
Prague, Czech Republic

Patrick Fontana
PhD., Researcher
Federal Institute for Materials Research and Testing (BAM),
Division VII.1 - Building Materials,
Berlin, Germany

Micro texture and mechanical properties of heat treated and autoclaved Ultra High Performance Concrete (UHPC)

Summary

The goal of the presented study was to evaluate the effects of thermal treatment on the curing of UHPC with the intention of reducing curing times and enhance the mechanical properties of UHPC. Two different mix designs were used. The heat treatment conditions consisted of simple heating in an oven and autoclaving under steam pressure. Mechanical properties were enhanced with heat treatment and autoclaving but autoclaved samples showed a considerable higher flexural strength. The micro texture of samples cured at elevated temperatures was different to those cured under ambient conditions. TEM studies showed that quartz filler reacted with the cement matrix in the heat cured samples. The results showed that in particular autoclaving of UHPC shows a promising positive influence on the micro texture and phase assemblage of the materials in conjunction with secondary cementitious materials.

Keywords: *ultra high performance concrete, micro texture, mechanical strength, secondary cementitious materials*

1 Introduction

The developments in concrete technology show a significant trend towards the application of hybrid and multifunctional materials and structural parts. The major motivations of these developments aim usually in an improvement of the concrete properties in the fresh and hardened state as well as in an extension of material durability and the lifetime of concrete structures. One of the more recent research topics in the field of improving the concrete composition is ultra high performance concrete, a development which resulted in a material with considerable different properties compared to standard concrete. These properties are best highlighted by their high mechanical strength in conjunction with a ductility not found in standard concrete formulations. Heat treatment of concrete has a long standing tradition in the pre-cast concrete industry and is mainly used in order to reduce curing time and increase early strength. Heat curing was also considered for UHPC and reactive powder concrete (RPC), respectively, from the very beginning [1,2]. Applied were different temperatures up to 400 °C. Usual effects of heat treatment consists in the development of a more dense micro texture with the formation of crystalline calcium silicate phases, in the temperature range over 200 °C predominantly xonotlite (C_6S_6H). Pure heat treatment results usually in a reduction of pores in the nanometer range and an increased compressive strength, compared to the same specimen cured under ambient conditions [3].

However, steam pressure curing is mainly applied to pure calcium silicate systems, such as autoclaved aerated concrete (AAC) and has been applied to these systems since the 20's of the last century. Early studies on the phase stability and the mechanical properties of these steam cured calcium silicate systems can be found in Assarsson [4], Taylor [5]. In this system curing with a defined steam pressure seems to stimulate the formation of crystalline calcium silicate phases much earlier than in a purely temperature controlled curing regime. Mitsuda & Taylor [6] reported the formation of the crystalline phase tobermorite already at 90 °C under a H_2O saturation pressure. The compressive strength of sample specimen seems to be strongly controlled by the steam pressure in the autoclave, as reported in their study by Gerstner & Henning [7]. Higher steam pressure caused higher strength in their sample specimens but over a certain time period (usually 10 to 24 h) compressive strength passed through a maximum and was slightly decreased afterwards. Micro structural analysis showed that this effect was combined with an increase in crystal size of the hydrous reaction products. Besides the effect of accelerating curing and increasing early strength, heat treatment and autoclaving could be useful for cementitious systems containing secondary cementitious materials, i.e. granulated blast furnace slag or fly ash. In particular maintaining a controlled steam pressure at elevated temperatures as a curing regime could possibly be influential on the reaction rate of these mineral additions compared to the same system cured at ambient conditions. This is indicated in the study of Beaudoin & Feldman [8] who investigated autoclaved cement pastes with variable amounts of quartz powder and fly ash.

The goal of the study was therefore to investigate the influence of autoclave (steam) curing on the mechanical properties and micro texture of UHPC. The study included also heat treatment under atmospheric pressure and curing under ambient conditions (23 °C, 1 bar) in order to compare the effects of the different curing regimes on the properties of the UHPC's.

As secondary cementitious materials fly ash and silica fume was used. In particular the use of fly ash was envisioned to considerably reduce the high amount of cement and micro silica usually used for UHPC without loss of strength properties and performance.

2 Starting Materials and Methods

In total two different UHPC formulations were used for the study. The mix designs are shown in Table 1. One mix contained only silica fume as addition, the other mix additionally fly ash with a lower amount of cement and silica fume. Steel fibers were not used in this study because of interference with the micro textural analysis. The starting materials were thoroughly mixed in a high shear mixer and then casted to prisms of 160 x 40 x 40 mm^3. After 1 day the prisms were demoulded and cured: 1. under water at 23 °C for 6 days (reference), 2. at 250 °C for 2 days and 3. at 200 °C and 14 bar steam pressure for 8 h.

Table 1: Mix design of the two UHPC formulation (in kg/m^3).

	Mix 1	**Mix 2**
Cement	850	650
Quartz sand	1000	860
Quarz filler	210	150
Silica fume	140	70
Fly ash	-	140
Water	170	110
Plasticizer	used	used

The specimens were then stored at 23 °C and 50 % r.h. until the 7^{th} day and 28^{th} day, respectively. Afterwards mechanical strength testing was performed. Samples for micro textural analysis were taken from additional specimens. After 7 days the hydration was stopped by drying the samples under vacuum at 40 °C. The samples were split into small pieces of ca. 5 mm size and then embedded in epoxy resin. Afterwards the embedded samples were ground and polished without water in order to avoid leaching of soluble components. The analytical methods consisted in scanning electron microscopy (SEM) studies (LEO Gemini 1530 VP) including textural and micro chemical analysis and transmission electron microscopy (TEM) studies (Jeol STEM JEM 2200FS) on one heat treated sample of mix 2. On all samples mechanical tests were performed consisting of compressive strength and flexural strength measurements. Additionally analysis was performed on mix 1 paste samples: thermal gravimetry in order to evaluate the pozzulanic consumption of portlandite, the determination of the modulus of elasticity on macro samples and nano indentation (CSM Indentation Tester) for analyzing micro mechanical properties (modulus of elasticity, hardness). The latter is in particular useful to get information about the mechanical properties of the hydrous reaction products only.

3 Results

3.1 Mechanical Properties

The results of the uniaxial compressive and flexural strength testings shows in general a clear influence of the different curing regimes. The 7 day compressive strength of the heat cured sample series of both mixes were higher compared to the one cured at 23 °C (Fig. 1a). Mix 2 showed for the 23 °C series a considerable lower and for the steam cured samples a slightly lower value. The series of mix 1 and 2 cured at 250 °C showed almost the same results for compressive strength. Interestingly the compressive strength of the mix 1 samples cured at 250 °C/1 bar was slightly higher when tested after 7 days compared to the samples tested after 28 days. This might be due to a different state of moisture after 7 and 28 days.
The flexural strength, however, exhibited a more unusual behavior. Here, the autoclaved series of both mix designs furnished the highest values (Fig. 1b) and was more than double as high as the one cured at 23 °C. In contrast the series cured at 250 °C/1 bar showed the lowest values (Fig. 1b). This could be due to the presence of micro cracks in the material texture as a consequence of induced stress during the cooling of the specimens. The results were also confirmed by the measurements of the modulus of elasticity of paste samples of mix 1. Here a similar pattern was observed with the highest values for autoclaved and lowest for samples cured at 250 °C/1 bar, though not as distinctive compared to the results of flexural strength.

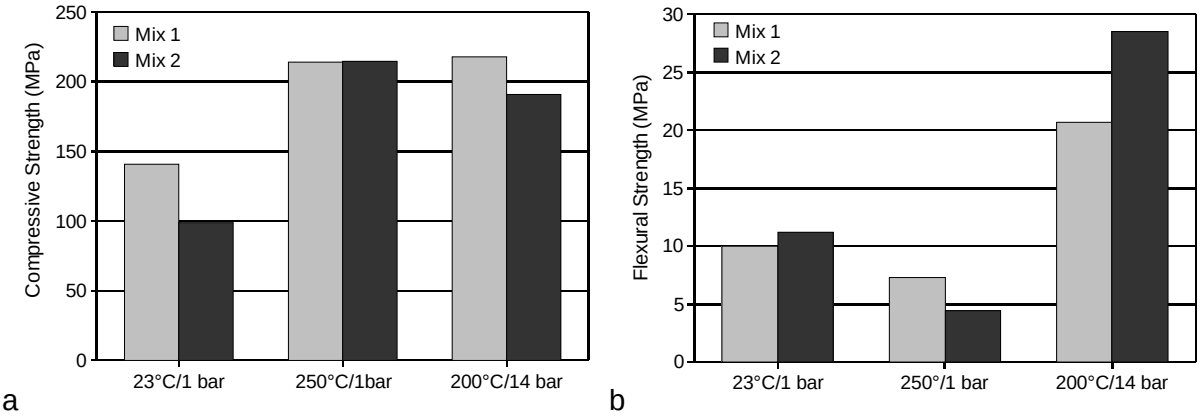

Figure 1: Seven day (a) Compressive strength and (b) flexural strength of mortar samples of the two mix designs.

The results of nano indentation show almost no influence of the curing regime on the modulus of elasticity of the hydration products (between 36.7 and 34.5 GPa), though the statistical variation in the results was fairly high. The hardness of the paste was more distinctive. Autoclaved samples furnished the highest results (1175 MPa) followed by at 250 °C/1 bar cured samples (1107 MPa) and the samples cured at 23 °C (901 MPa).

3.2 Micro Texture and Micro Chemistry

Macroscopically the reference samples and the autoclaved specimens showed no difference in appearance. However, the 250 °C/1 bar cured sample exhibited color differences in the sample cross sections indicating a heat and probably also a moisture profile during the heat curing and subsequent cooling. Figure 2 gives a overview of the micro texture of the samples

in form of polished cross sections. The mix 1 samples (upper row in Fig. 2) exhibit a much higher content of remnant clinker indicating a lower hydration degree. The texture of heat cured mix 1 samples show a denser cement paste compared to the 23 °C cured set. The texture of autoclaved and 250 °C/1 bar cured specimens is very similar. The 250 °C/1 bar cured samples shows a very dense micro texture with visible portlandite. Notable is the often etched appearance of the borders of quartz filler, indicating a reaction of quartz with the cement paste (Fig. 3a).

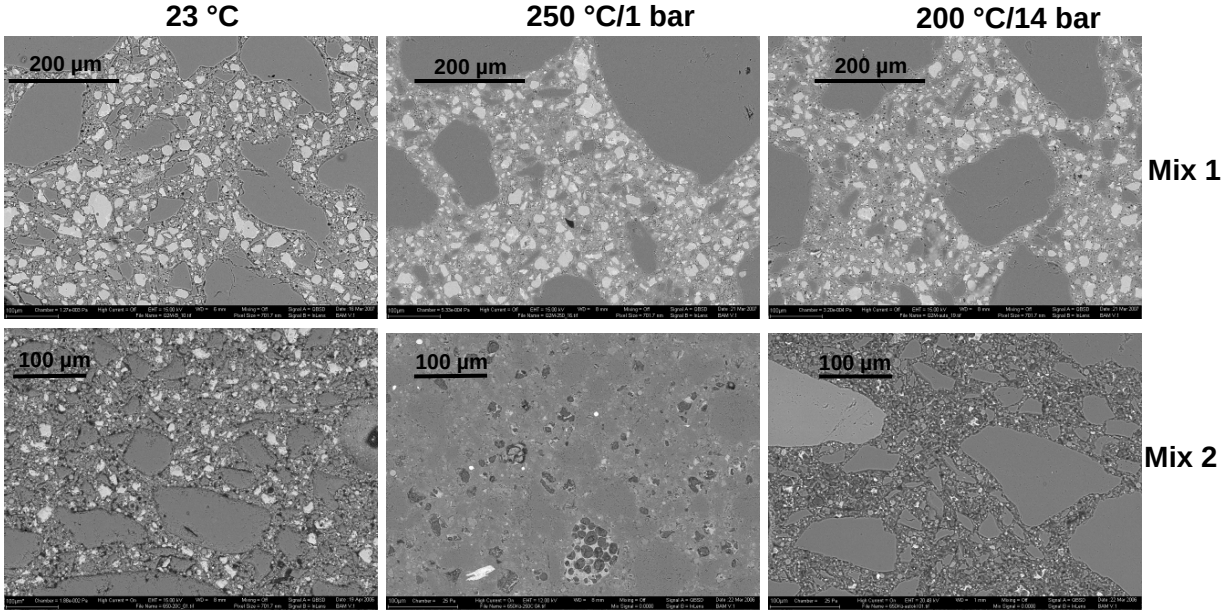

Figure 2: Micro texture of the UHPC samples (SEM-BSE images). The mix 2 samples show a distinctive difference in micro texture between heat treated and autoclaved samples (see text)

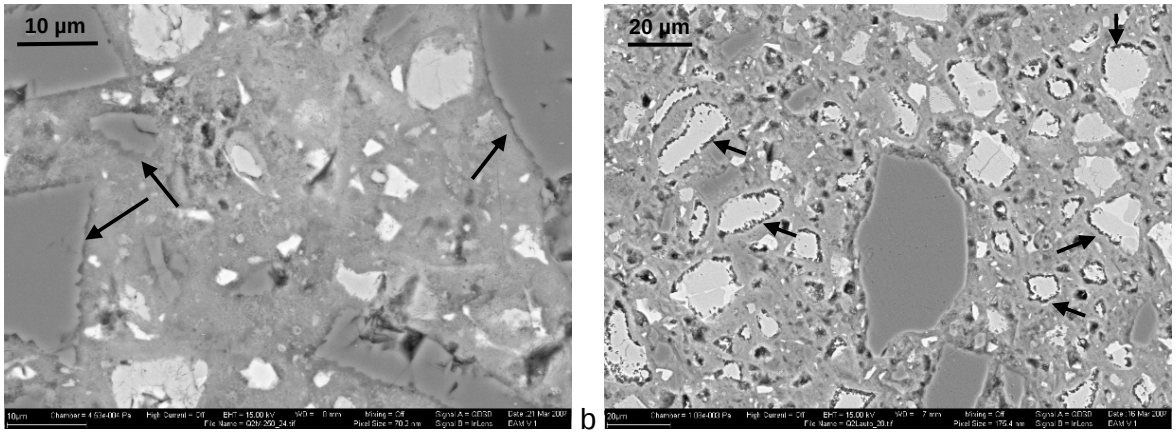

a b

Figure 3: a. SEM-BSE images of mix 1, 250 °C/1 bar cured sample. Note the dense micro texture and the etched borders of the quartz grains (arrows). b. Mix 1, autoclaved. The clinker in the paste show separated hydration shells and distinctively etched clinker borders (arrows).

Autoclaved samples show a slightly more porous micro texture with pores concentrated mostly between clinker grains and inner CSH (Fig. 3b) in form of separated hydration shells [9]. Larger portlandite crystals were not found in the micro texture anymore. This could also

be confirmed by thermo gravimetry were the amount of portlandite disappeared in the autoclaved specimens, showing that steam curing caused a total consumption of portlandite during the hardening in the mix 1 samples. The mix 2 samples (lower row of Fig. 2) showed a lower amount of remnant clinker, suggesting a higher degree of hydration. The samples cured at 250 °C/1 bar exhibited similar etched grains of quartz filler as the corresponding one of mix 1. They showed also a much denser micro structure as the autoclaved samples. The latter one did not exhibit separated hydration shells around clinker grains, as observed in mix 1. In order to evaluate if quartz is reactive during heat treatment of UHPC one sample cured at 250 °C/1 bar of mix 2 was in detail investigated by TEM. Figure 4 shows a quartz grain with a reaction rim of CSH inside a lamella, which was prepared by focussed ion beam (FIB) technique. In Figure 4a the original boundaries of the quartz grain can faintly be recognized (arrow). Inside the boundaries predominately very long fibers of CSH with length of up to 500 nm occur (Fig. 4b). Outside the boundaries average fiber lengths is below 50 nm (Fig. 4c). The elemental maps in Figure 4d indicate that CSH surrounding the grain has a lower Ca/Si ratio than farther away from the grain.

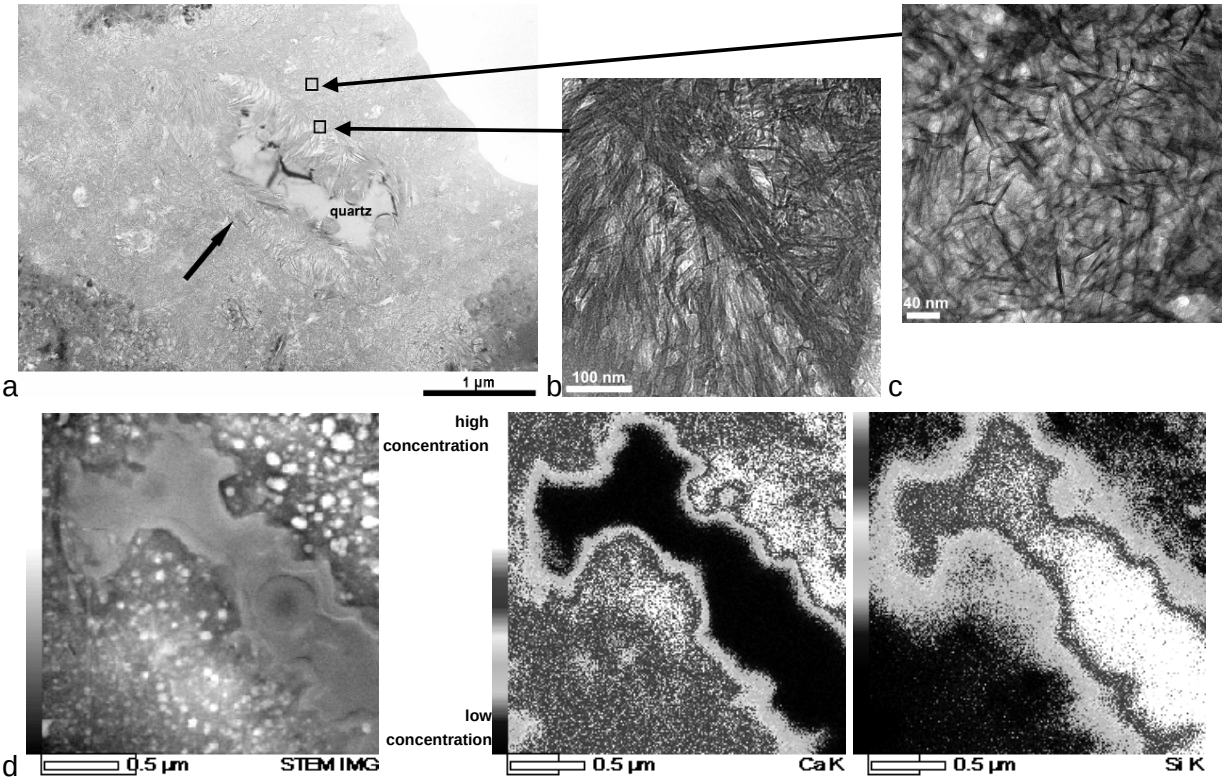

Figure 4: Bright field images from TEM depicting a quartz filler grain and CSH fibers (a). Longer CSH fibers around the grain boundary (b). Shorter fibers in the cement paste (c). d. Elemental mapping of calcium and silicon of the same quartz grain and surrounding CSH (EDX).

The influence of fly ash on the micro texture of mix 2 samples could be seen by micro chemical analysis of the cement paste by SEM-EDX. Figure 5 shows the results of the spot analysis in form of atom ratios of Si/Ca vs. Al/Ca. The aluminum of the fly ash seems to have generally raised the Al/Ca ratio of the mix 2 samples. Since aluminum and silicon seem to increase proportional, possibly the aluminum is incorporated into the CSH-phase. Autoclaved

samples of mix 2 seem to have reacted stronger with the fly ash resulting in higher silicon and aluminum content of the hydrate phase. Interestingly autoclaved and at 250 °C/1 bar cured samples of mix 1 showed identical elemental ratios, which indicates equal consumption of silica fume in the system. If there are any crystalline phases present in the cement paste of the heat treated UHPC's the Si/Ca ratios suggest tobermorite and/or truscottite ($C_6S_{10}H_3$) as main crystalline phases for the mix 2 autoclaved samples and xonotlite and/or tobermorite for the other samples. So far, only xonotlite could be confirmed in mix 2 specimens cured at 250° C/1 bar by electron diffraction on a TEM.

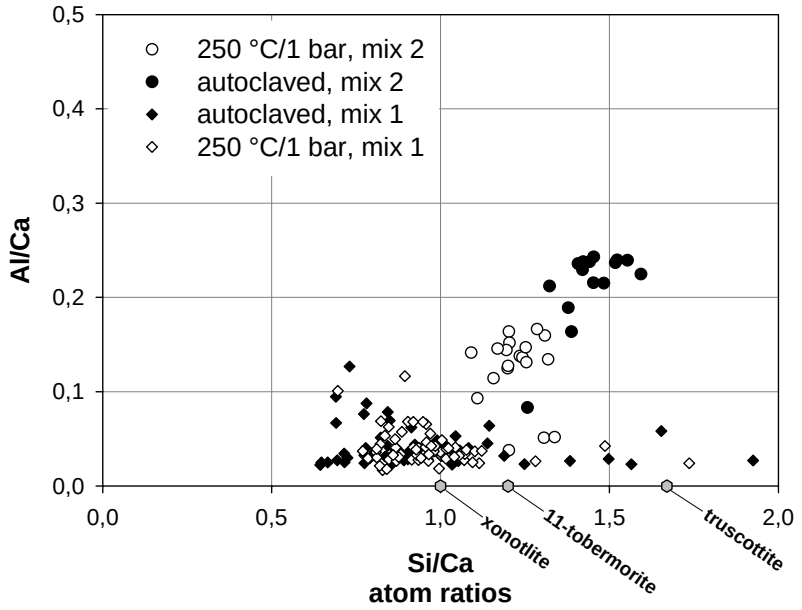

Figure 5: Atom ratios from micro chemical analysis of the autoclaved and at 250 °C/1 bar cured samples of mix 1 (diamonds) and mix 2 (circles). The results of the 23 °C cured samples are not shown here. The Si/Ca ratios of three crystalline phases observed in heat treated CaO-SiO_2-H_2O – systems are marked as well.

4 Conclusions

The results of the study showed clearly a strong influence of the thermal or hydrothermal curing regime on the mechanical properties and micro texture of UHPC. The different mechanical properties are at least partly controlled by the micro texture of the cement paste. Compared to UHPC cured under ambient conditions heat treated and autoclaved specimens show generally a denser micro structure, which explains the increase in compressive strength. The differences in flexural strength is certainly influenced by the different conditions of heating in an oven and autoclaving under a H_2O pressure. Simple heating at high temperature (250 °C) certainly causes a strong temperature gradient inside the UHPC samples in the initial heating phase and during cooling. This may lead to stress and micro cracking in the cement paste [10]. In particular the escape of moisture from the subsurface zone during the heating might be a major problem in all temperature intervals causing additionally a moisture profile. This effect is mitigated by the steam curing were the steam pressure in the autoclave maintains a stable moisture content inside the specimens, thus

minimizing stress due to a combined moisture/temperature gradient. The addition of quartz powder has to be seen from a different viewpoint. Under ambient curing conditions quartz filler is non-reactive. Heat treated concrete, however, causes reaction of quartz with the cement paste. If it is only with portlandite or also with other hydrate phases has to be investigated in future studies. The addition of fly ash in mix 2 seems to have no negative impact on the micro texture or mechanical properties. The data acquired showed that fly ash reacts strongly when the concrete were heat cured or autoclaved. This could be an important factor for the reduction in amount of cement and the quite expensive silica fume by the replacement with alternative more cost effective secondary cementitious materials.

5 Acknowledgements

The authors would like to thank our BAM colleagues Andre Gardei, Wolfram Schmidt, Romeo Saliwan-Neumann, Wolfgang Gesatzke and Ilona Dörfel for their support and help in performing the tests and analysis. Especially we want to thank Professor Frank Dehn for his discussion about the topic of heat and steam curing of UHPC and for providing the initial idea for this study.

6 References

[1] Cheyrezy, M.; Maret, V.; Frouin, L.: Microstructural analysis of RPC (Reactive Powder Concrete). In: Cement and Concrete Research, 25, No. 7, 1491-1500, 1995.

[2] Sauzeat, E.; Feylessoufi, A.; Villieras, F.; Yvon, J.; Cases, J.M.; Richard, P.: Textural analysis of Reactive Powder Concretes. Proc. 4th International Symposium on Utilization of High-Strength/High-Performance Concrete, Paris, 1996.

[3] Dehn, F.: Ultrahochfeste Betone. In: König, G.; Tue, N. V.; Zink, M.: Hochleistungsbeton-Bemessung, Herstellung und Anwendung. Verlag Ernst & Sohn, Berlin, 2001.

[4] Assarsson, G. O.: Hydrothermal reactions of calcium hydroxide-quartz at 120-220°C. In: Journal of Physical Chemistry, 64, 328-331, 1958.

[5] H.F.W. Taylor: Hydrothermal reactions in the system $CaO–SiO_2–H_2O$ and the steam curing of cement and cement-silica products. In: Proc. The Fourth International Symposium on the Chemistry of Cement, Washington D.C., 167–190, 1960.

[6] Mitsuda, T.; Taylor, H. F. W.: Influence of aluminium on the conversion of calcium silicate hydrate gels into 11 A tobermorite at 90 °C and 120 °C. In: Cement and Concrete Research, 5, No. 3, 203-209, 1975.

[7] Gerstner, B.; Henning, O.: Phasenbildung und Festigkeitsentwicklung bei der Kalksandsteinbildung. In: TIZ - Fachberichte Rohstoff-Engeneering, 105, No. 3, 148-151, 1981.

[8] Beaudoin, J. J.; Feldman, R. F.: A study of mechanical properties of autoclaved calcium silicate systems. In: Cement and Concrete Research, 5, No. 2, 103-118, 1975.

[9] Scrivener, K. L.: Backscattered electron imaging of cementitious microstructures: understanding and quantification. In: Cement and Concrete Composites - Special Issue: Scanning electron microscopy of cements and concretes, 26, No. 8, 935-945, 2004.

[10] Dehn, F.: Temperature behaviour of ultra high-performance concrete (UHPC) - A micro analytical reflect. In: Proc. International Symposium on Ultra High Performance Concrete, Kassel, 731-742, 2004.

Andrzej Cwirzen
Dr. research scientist
Helsinki University of Technology
Espoo, Finland

Karin Habemehl-Cwirzen
Dr. senior research scientist
Helsinki University of Technology
Espoo, Finland

Vesa Penttala
Professor, D.Sc.
Helsinki University of Technology
Espoo, Finland

The effect of heat treatment on the salt freeze-thaw durability of UHSC

Summary

Salt freeze-thaw durability of ultra high strength concretes (UHSC) was studied. The ultra high performance concretes contained coarse granite and diabase aggregates and in one case short steel fibers. The water to cement ratio varied from 0.22 to 0.26. Amorphous silica fume (25% by the cement weight) was used as additional binder in all mixes. The obtained compressive strength values varied from 150 to 200 MPa. The specimens were either cured in water or were heat-treated at 90 ºC for two days prior to the water curing. Freeze-thaw durability was determined in accordance with the CDF test procedure with the number of cycles increased to 200 in the case of the specimens with coarse aggregate particles. The test results showed low surface scaling values after 56 freeze-thaw cycles in all test specimens. After 150 freeze-thaw cycles the heat-treated specimens showed an increase in the surface scaling values, which eventually reached 500 g/m^2 at the end of the test. The measurements of the internal damage determined by ultrasonic transit time showed a similar tendency. The relative dynamic modulus dropped below 50% after 200 freeze-thaw cycles in the case of the heat-treated specimens while the non-heat-treated specimens showed a very small change. The addition of short steel fibers decreased significantly the internal damage of the heat-treated specimens but, at the same time, these specimens obtained higher surface scaling values. The presence of the coarse aggregates did not significantly alter the microstructure of the binder matrix. No internal transition zone characterized by increased porosity, higher amount of Portlandite or AFt phases was visible during SEM (Scanning Electron Microscopy) investigation. MIP-tests (Mercury Intrusion Porosimetry) revealed a fine microstructure in all of the studied concretes. The specimens in which short steel fibers were introduced revealed crack formation originating from the fiber/binder interface already at 28 days after casting. The subsequent freeze-thaw cycles caused further propagation of the cracks. Nearly no microcracking of the binder matrix was observed in any of the non-heat-treated samples before or after 200 freeze-thaw cycles.

Keywords: *UHSC, coarse aggregates, salt freeze-thaw durability, SEM, MIP*

1 Introduction

The first ultra high strength concretes (UHSC) were developed back in the 70's and 80's; Brunaer et al. [1], Bache et al [2], Brichall et al. [3]. The main target was to obtain as an dense as possible microstructure of the binder matrix. In all cases, except of the so-called MDF concrete developed by Birchall which incorporated a polyvinyl alcohol (PVA) polymer, a very low water to binder ratio in combination with high addition of secondary binders and micro fillers was used. Furthermore, the coarse aggregates were made of hard rock e.g. diabase, basalt or coarse aggregates were excluded. Nowadays, the most widely used UHSC is the Reactive Powder Concrete (RPC) and its derivatives. The roots of this material go back to France and Canada where in the 90's the theoretical bases were formulated by DeLarrard et al. [4, 5, 6] who developed the so called linear packing density model (LPDM), solid suspension model (SSM) and more recently the compressive packing model (CPM). The basic RPC mix consists of cement, silica fume, fine sand, quartz and often short steel fibers [7]. The high dosage of cement which varies between 800 to 1000 kg/m^3 is indicated as one of the major disadvantages of RPC. In many cases the produced mixes showed a rapid loss of workability and high amount of entrapped air, [8, 9]. It is also common to use heat treatment to further enhance the microstructure and mechanical properties of RPC. Specimens are heated to temperatures ranging from 90 to 450 ^{o}C usually 24 or 48 hours after casting. The duration varies between 24 hours to 1 week. The main effect of the heat treatment is the acceleration of the hydration processes by enhancement of the pozzolanic reaction of SF and fine fillers. Since application of heat treatment can cause certain unfavorable processes several scientists studied its effect on the physical and mechanical properties of concrete. One of the most comprehensive investigations was done by Zanni et al. [10] who used the NMR technique. The obtained results revealed that the consumption of silica fume strongly depends on the temperature and duration of the treatment. An increase in the temperature from 90 to 250 ^{o}C enhanced the pozzolanic activity from 15 to 70%. In the case of crushed quartz an engagement into the pozzolanic activity was observed above 200 ^{o}C and after 48 hours of heat treatment. The pozzolanic activity of quartz was not clearly observed at 90 ^{o}C. The hydration ratio increased from 10% to 55% between 90 ^{o}C and 250 ^{o}C. Furthermore, the CSH average chain length was increasing. In temperatures above 200 ^{o}C the formation of xonotlite was observed too. In general, silica fume appeared to be more active which is caused by its smaller particle size. A longer heat treatment duration appeared to increase the pozzolanic activity of SF and quartz filler. For instance after 8 hours at 90 ^{o}C there was no pozzolanic activity detected in the case of quartz filler but after 40 hours the activity index was increased to 40%. The hydration degree appeared to increase from 10 to 25% between 8 and 48 hours which is more than hydration degree after 28 days curing at 20 ^{o}C. Similar research was done by Cheyrez et al. [11] who used mercury intrusion porosimetry, thermogravimetric analysis and x-ray diffraction instead of NMR. The results showed similar trends of increasing pozzolanic activity of quartz and silica fume with temperature and time. Furthermore, it was shown that according to the thermogravimetric analysis the hydration degree for RPC varied from 40 to 60% and heat treatment enhanced the proportion of bound water. Specimens heat treated at 200 ^{o}C showed a residual

expansion after cooling down to 20 ^{o}C. The authors attributed this to the formation of low density tobermorite and not to microcracking. The results by Cheyrez et al. revealed also that heat treatment affects the porosity. MIP porosity threshold was lowered with increased temperature. The results revealed that within the temperature range from 20 to 65 ^{o}C the setting pressures did not affect the amount of pores having a diameter smaller than 100 μm. This result, according to the authors, showed that the main role of pressure is the elimination of entrapped air voids and removal of part of the free water. At temperatures between 80 and 200 ^{o}C the porosity appeared to be lower for the pressed specimens. Application of temperatures higher than 250 ^{o}C caused an increase of porosity which was attributed to formation of xonotlite accompanied with water release. The final conclusion was that the RPC characterized by the smallest porosity should be heat treated at 150 to 200 ^{o}C and pressure should be applied. The influence of the curing regime on the mechanical properties and microstructure of ultra high strength mortar was studied by Cwirzen [12]. The microstructure and microchemistry were investigated by scanning electron microscopy and mercury intrusion porosimetry. The results revealed that longer heating times increased the hydration degree, refined the microstructure and resulted in higher ultimate compressive strength. Very late and very early application of the heat treatment caused a lower hydration degree and a smaller long-term increase of compressive strength. The scanning electron microscope investigation revealed the formation of one hydration rim around anhydrous cement particles and presence of hollow shell in all specimens. Heinz and Ludwig [13] studied possible delayed ettringite formation in UHPC subjected to heat treatment. The commercially available “Duracret” concrete from Schewenk was used in this research. Five different types of cements were used. Addition of SF varied from 12 to 25 % by the cement weight. The water to cement ratio was 0.22. The heat treatment included application of temperatures between 65 and 180 ^{o}C. The obtained results showed an increase of the 28-day compressive strength from around 180 to 280 MPa, depending on the cement type, with temperature increase from 20 to 180 ^{o}C. Similarly to the results described earlier, a refinement of the porosity could be observed with increasing heat treatment temperature. The phase composition was studied using XRD, thermal analysis (DSC/TG) and SEM. The results showed formation of ettringite in specimens cured at 20 and 65 ^{o}C but not at higher temperatures. The main reason is the lack of portlandite in cement paste after heat treatment in temperatures above 65 ^{o}C which can be attributed to higher pozzolanic activity of SF and quartz. In order to determine secondary ettringite formation tests were performed by Duggan [14]. The results showed no expansion due to secondary ettringite formation in any of the UHPC concretes. In accordance with the authors’ knowledge there are no results available concerning the effect of the heat treatment on the long-term freeze-thaw durability of UHSC. Therefore, the main objective of this research was to study the effect of the heat treatment on the frost de-icing salts durability of UHSC with and without coarse aggregates.

Experimental

Two types of ultrahigh strength concretes were investigated within this study. The first type had a typical RPC mix composition while the second was RPC incorporating coarse diabase

or granite aggregates. All of the test concretes were produced using a sulfate resistant cement CEM I 42.5 N (SR). The fine quartz which was used as micro filler had the mean particle diameter of 16 μm. The used quarry sand had a maximum particle diameter of 600 μm. The amorphous undensified silica fume (SF) grade 983U was delivered by Elkem-Norway. The RPC mix composition was optimized by using the method based on the determination of the minimum water demand. The optimization procedure is described elsewhere [15].

The proportions of silica fume, quartz, sand and cement were constant while the amounts of coarse aggregates are given in Table 1. The content of the used polycarboxylate superplasticizer and water depended on the mix. Two types of curing procedures were used. The first procedure included heat treatment consisting of 48 hours of steam curing at 90°C followed by storage at 95% of the relative humidity. In the second procedure all specimens were stored at 95% R.H. until the testing and no heat treatment was applied. This curing procedure was chosen in accordance with the results obtained from the previous research, see elsewhere [12]. The rheological properties were determined by means of concrete flow measured by the mini cone method and the flow table. The compressive strength was measured by 10x10x10 cm^3 cubes after 7, 28 and 180 days.

Table 1 : Mix design. Proportions are given in accordance with the cement weight which equals 1.

Test concrete	Silica fume	Sand (160-600um)	Coarse aggregates					W/C
			Diabase (3-6 mm)	Granite (2-5 mm)	Granite (5-8 mm)	Steel fibers	Quartz fillers	
F26/022/N	0.25	0.8					0.2	0.22
F26/022/H	0.25	0.8					0.2	0.22
F26/024/G/F/H	0.25	0.8		1		0.1	0.2	0.24
F26/024/G/3/H	0.25	0.8			2		0.2	0.238
F26/024/G/3/N	0.25	0.8			2		0.2	0.238
F26/026/D/H	0.25	0.8	2				0.2	0.259
F26/026/D/N	0.25	0.8	2				0.2	0.259

The frost durability was determined in accordance with the CDF test procedure [16]. The concrete specimens were cast separately and had dimensions of 70x110x150 mm^3. The test surface was cast against a teflon plate and no release oil was applied on the moulds. 3% sodium chloride solution was used as the freezing medium. One freeze-thaw cycle lasted 12 hours with a temperature change $\pm 20^0$C. The tests were continued for 56 and 200 freeze-thaw cycles. Surface scaling, internal damage and water uptake were measured. The internal damage was determined in accordance with the measured relative ultrasonic transit time.

The microstructure was studied by environmental scanning electron microscopy (ESEM) and mercury intrusion porosimetry (MIP). The specimens for the ESEM investigation were impregnated with resin and polished using a diamond spray (9 to 0.25 μm). All images were

taken in the backscattered electron mode which allowed to identify the particular phases according to the procedure described by Scrivener [17]. MIP specimens were 25 mm high and had a diameter of 20 mm. The cores were cut from concrete cubes at the age of 28 days and were vacuum dried for 6 weeks.

2 Test results

2.1 Mechanical and fresh concrete properties of the test concretes

The fresh concrete properties were determined by measuring the maximum flow value which are shown in Table 2. The test method was a modified slump test which is described in EN 12350-2 and Cwirzen et al. [18]. All of the test concrete revealed a flow-like consistency and had an average flow value between 650 and 860 mm. The 28-day compressive strength of non- heat-treated concretes varied between 132 and 137 MPa. The heat-treated concrete reached values around 180 MPa. The flexural strength varied between 12 and 15 MPa. The presence of steel fibres did neither improve the compressive strength nor the flexural strength.

Table 2: Mechanical and fresh concrete properties.

Test concrete	Flow [mm]	28-day compressive strength	28-day flexural strength
F26/022/N	785	137	14.8
F26/022/H	860	183	13.3
F26/024/G/F/H	650	181	14.3
F26/024/G/3/H	740	171	13
F26/024/G/3/N	730	132	11.9
F26/026/D/H	825	187	15.1
F26/026/D/N	845	138	13.5

2.2 Microstructure

The microstructure of all test concretes appeared to be very similar. The two images shown in figure 1 represent the areas in the vicinity of granite aggregate and sand particle. The examination revealed increased porosity in some areas in the vicinity of the coarse aggregate particles. However, since this was a random phenomenon a local microbleeding could be indicated as the main cause. Otherwise no visible interfacial transition zone was found in any of the studied specimens. The BSE images did not reveal a generally higher porosity, more portlandite nor less anhydrous cement in the vicinity of the aggregates.

The MIP test results are shown in figure 2. The highest total porosity and the coarsest pores were detected in the non heat-treated specimens without coarse aggregates. The application of the heat treatment appeared to refine the porosity in the entire measuring range. The incorporation of coarse aggregates resulted in a slightly higher amount of pores having a radius smaller than 10 nm which could be caused by the earlier described local

micro bleeding. A similar effect, although to a higher extend was observed in concretes with coarse aggregates and steel fibers.

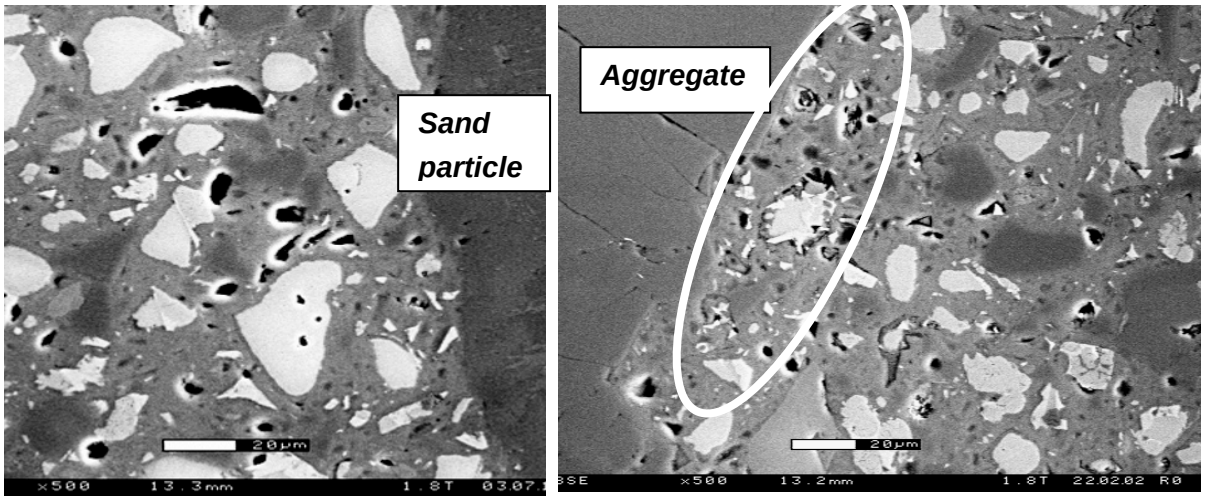

Figure 1: Backscattered electron image of polished specimens with and without coarse aggregates. The visible higher porosity is marked by an ellipse.

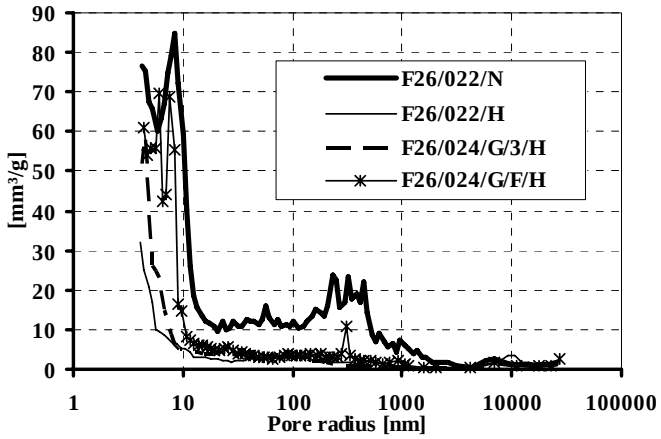

Figure 2: MIP test results.

2.3 Freeze-thaw durability

The freeze-thaw test results and the measured water uptake values are shown in figures 3-5. As expected, the measured water uptake during the test was slightly higher in the specimens incorporating coarser aggregates. After approximately 70 cycles a rapid increase of the water uptake was noticed in specimens F26/026/D/H and F26/024/H. The measured surface scaling values are shown in figure 4. The lowest amount of the scaled material after 200 cycles was collected from the non heat-treated concretes incorporating coarse aggregates; F26/026/D/N and F26/024/G/3/N. The heat treated specimens; F26/026/D/H, which contained diabase aggregates had surface scaling values of ~150 g/m^2 after 56 freeze-thaw cycles and 500 g/m^2 after 200 cycles. The concretes without coarse aggregates revealed lower surface scaling values in comparison with the heat treated specimens incorporating coarse aggregates up to 56 cycles. The presence of short steel fibers appeared to increase the surface scaling. The visual examination of the deteriorated surfaces revealed that most of

the scaled material originated from the vicinity of the steel fibers located close to the exposed surface.

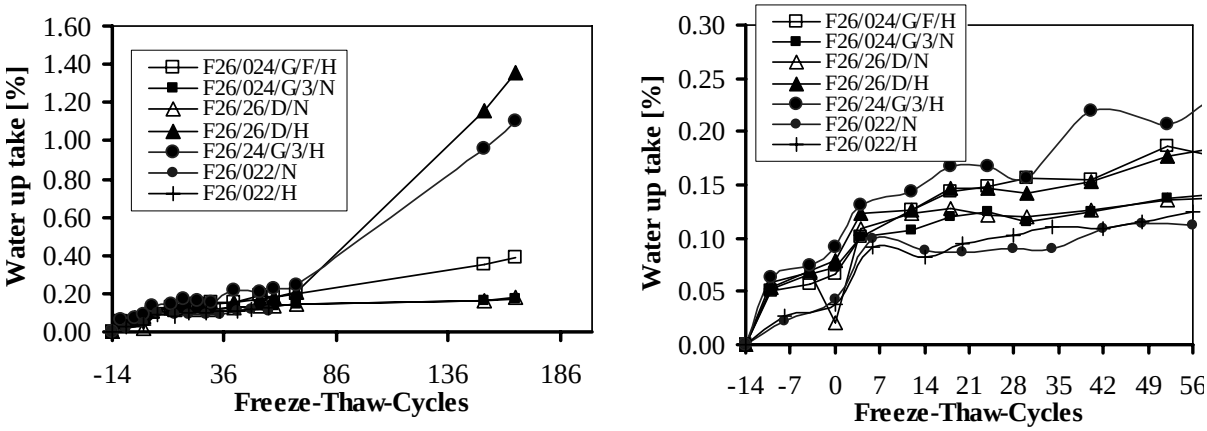

Figure 3: Water uptake measured during freeze-thaw testing. Negative number on the horizontal scale denotes the measurements done before the start of the first freeze-thaw cycle.

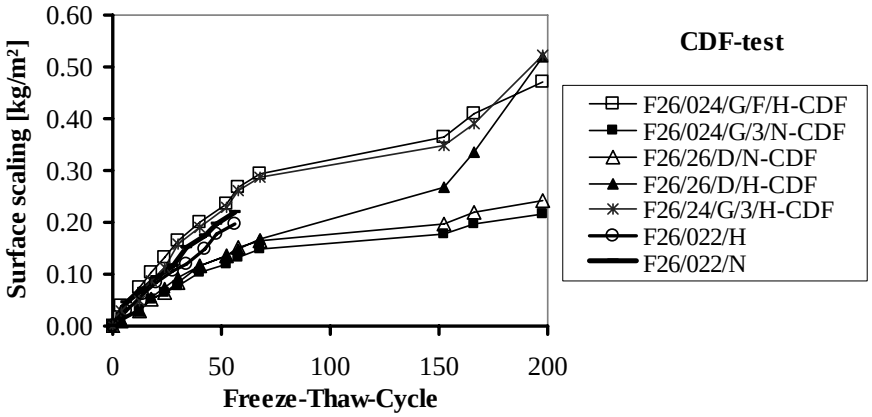

Figure 4: Surface scaling of test concretes determined in accordance with CDF test procedure.

The development of the internal damage is shown in figure 5. The test revealed that after 56 freeze-thaw cycles none of the studied specimens showed a significant internal damage. However, higher number of freeze-thaw cycles caused an increase of the internal damage. Eventually, after 200 cycles the heat treated specimens incorporating granite and diabase aggregates were completely disintegrated. The presence of short steel fibers appeared to decrease the degree of the internal damage and no extensive internal damage was observed until ~170 freeze-thaw cycles.

ESEM investigation of some of the specimens after freeze-thaw cycles was done. The BSE images of concrete with and without coarse aggregates and one with coarse aggregates and steel fibers are shown in figure 6.

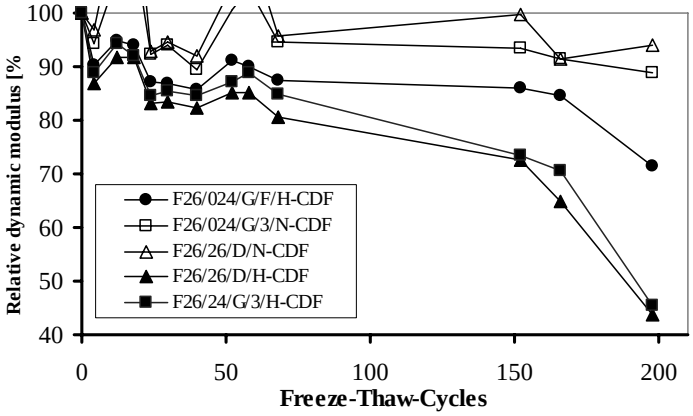

Figure 5: Internal damage expressed as change of the dynamic relative modulus of elasticity determined by measurements of the ultrasonic transit time.

ESEM examination confirmed the CDF test results. No significant cracking of the binder matrix of concrete F26/022/H (heat treated without coarse aggregates), figure 6a and F26/024/G/3/N (non-heat-treated with coarse aggregates) was observed. On the contrary, the heat-treated concrete incorporating coarse aggregates and steel fibers revealed extensive cracking of the bulk binder matrix and in the interfacial zone between steel fibers and matrix, figure 6b.

a) b)

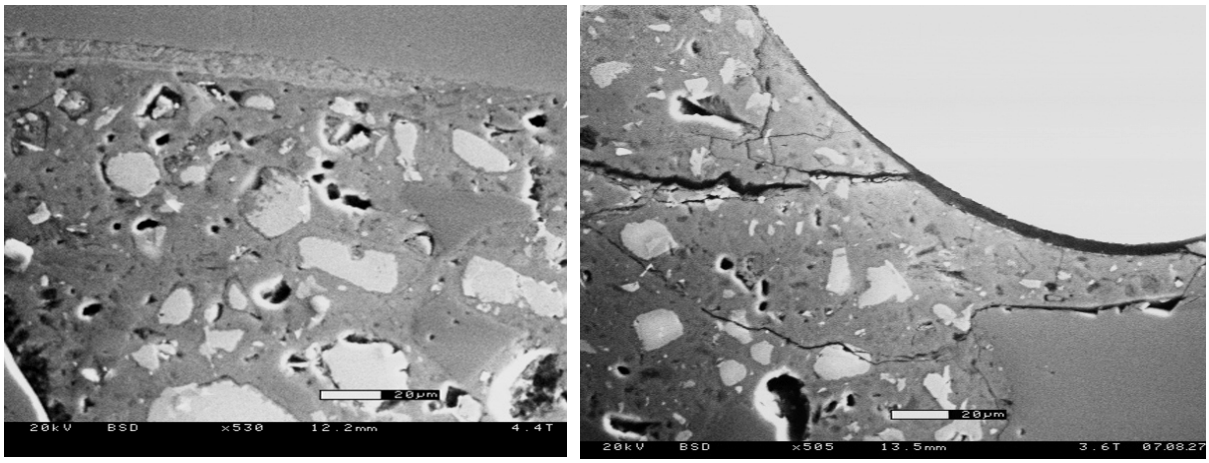

Figure 6: SEM images of concrete specimens a) F26/022/H subjected to 56 freeze thaw cycles and b) to 200 freeze thaw cycles in the case of concrete F26/024/G/F/H.

3 Discussion

The results showed that in general the heat treated concretes incorporating coarse aggregates revealed more extensive deterioration when subjected to 200 freeze-thaw cycles compared to the non-heat-treated samples. In the case of the surface scaling, a higher increase of the surface scaling rate could be observed until around 70 freeze-thaw cycles in all test concretes. Subsequently, in the following 90 cycles the accumulated amount of the scaled material was very low. After around 150 cycles a sudden increase of the scaling could

be observed in the case of the heat treated specimens. This increase related to a rapidly developing internal damage, figure 5. Also the water uptake increased significantly after around 70 cycles in the case of the heat treated concretes. These concretes revealed also finer porosity. However, this did not result in lower water uptake as expected; instead it tended to be slightly higher until the internal damage and excessive surface scaling started to develop. The damage mechanism could be directly attributed to the variation of the relative humidity within the specimen, Penttala [19]. Obviously, the heat treatment and extensive self desiccation caused by a very low water to binder ratio and 25% addition of silica fume resulted in a very low internal relative humidity. The progressive water uptake into the external layer of concrete specimens and freezing of capillary water caused increase of the relative humidity in these layers. Consequently, the ultimate difference of the relative humidity values resulted in increasing tensional stresses which at some point exceed the strength capacity of the binder matrix and resulted in microcracking. The specimens incorporating steel fibers revealed very high surface scaling especially in the vicinity of the fibers located near the test surface. Presumably, the ITZ present between the fiber surface and binder matrix enhanced the water ingress during freeze-thaw cycles. At the same time the presence of steel fibers lowered the internal damage. The relative dynamic modulus of elasticity increased from 45% to 75%. In the authors' opinion the fibers stopped the crack propagation following the mechanism described by Cwirzen and Penttala [18]. According to this mechanism the fibers bridge the cracks formation and hinder their further propagation.

4 Conclusions

The effect of the heat treatment of UHSC on the frost deicing salts durability was studied. The test concretes had water to binder ratio from 0.22 to 0.59. All mixes included silica fume and fine quartz fillers. Some of the mixes incorporated also coarse granite or diabase aggregates. Additionally, short steel fibers were added to one mix. The curing included storage in water at 20^{o}C followed in some cases by 48 hours of heat treatment at 90^{o}C. The test results revealed that the mixes incorporating coarse aggregates were characterized by a flow-like consistency and a 28-day compressive strength of around 180 MPa. The incorporation of coarse aggregates increased the capillary porosity and probably caused the formation of a narrow transition zone between cement matrix and coarse aggregates. The water uptake recorded before the freeze-thaw cycle was higher in the heat treated concretes containing coarse aggregates. The lowest surface scaling and the less extensive internal damage were recorded in the non-heat-treated concretes incorporating coarse aggregates. The presence of steel fibers appeared to lower the internal damage by restraining the crack formation. At the same time they caused higher surface scaling.

5 References

[1] Brunauer, S.; Ydenfreund, M.M.; Odler, I.; Skalny, J.: Hardened portland cement pasted pf low porosity, VI mechanism of the hydration processes, Cement and Concrete Research, Vol.3(2), pp. 129-147, 1973.

[2] Bache, H.H.: Densified Cement/Ultra-Fine Particle-Based Materials, In Proc. International Conference on Superplasticizers in Concrete, Ottawa, pp.12, 1981.
[3] Birchall, J.D.; Howard, A.J.; Kendall, K.: Flexural strength and porosity of cement, Nature, Vol.289, (5796), pp. 388-390, 1981.
[4] De Larrard, F.;Concrete mix proportioning- a scientific approach, E&FN SPON, 200 p, 1999
[5] De Larrard, F.; Sedran, T.; Mixture proportioning of high-performance concrete, Cement and Concrete Research, Vol. 32(11), pp. 1699-1704, 2002.
[6] De Larrard, F.; Gorse, J.F.; Puch, C.; Comparative studies of various silica fumes as additives in high-performance cementitious materials, Materials and Structures, Vol.25(149), pp. 265-272, 1992.
[7] Richard, P.; Cheyrezy, M.; Composition of reactive powder Concrete, Cement and Concrete Research, Vol.25, No.7, pp.1505-1511, 1995.
[8] Cwirzen, A.; Penttala, V.; Vornanen, C.; Junna, K.; Self-compacting ultra-high-strength concrete containing coarse aggregates, Helsinki University of Technology, Report 20, 129p. , 2006,
[9] Bonneau, O; Vernet, C; Moranville, Optimization of the rheological behavior of reactive powder concrete, In Proc. 1st Int. Symp. On HPC and RPC, Sherbrooke, Canada, Vol.3, pp. 99-118, 1998.
[10] Zanni H.; Cheyrezy M.; Maret V.; Philippot S.; Nieto P: Investigation of hydration and pozzolanic reaction in Reactive Powder Concrete (RPC) using Si NMR, Cement and Concrete Research, Vol.26, No.1, 93-100, 1996.
[11] Cheyrezy M.; Maret V; Frouni L: Microstructural analysis of RPC (Reactive Powder Concrete), Cement and Concrete Research, Vol. 25, No.7, 1491-1500, 1995.
[12] Cwirzen, A., The effect of the heat treatment regime on the properties of RPC, Advances in Cement Research, Vol.19, No.1, pp.25-33, 2007.
[13] Heinz, D.; Ludwig, H.M.: Heat treatment and the risk of DEF Delayed ettringite formation in UHPC, Proc. Int. Symposium on Ultrahigh Performance Concrete, Kassel, Germany, pp.717-730, 2004.
[14] Duggan, C.C.: Rapid test of concrete expansivity due to internal sulfate attack, ACI Materials, Vol.89(5), pp. 469-480, 1992.
[15] Cwirzen, A.; Penttala V.;RPC mix optimization by determination of the minimum water requirement of binary and polydisperse mixtures, Proc. ISISS 2005 Conference, Nanjing, China, 2005.
[16] EN 12390-9, 2002, “Testing hardened concrete – Part 9: Freeze-thaw resistance – Scaling”, p. 23. (including CDF and slab test with de-icing salts)
[17] Scrivener, K.L.; Pratt, P.L.: The characterization and quantification of cement and concretes microstructures, In: Proceedings of the First International RILEM Congress on Pores structure and Materials Properties, Versailles, France, pp. 61-68, 1987.
[18] Cwirzen, A., Penttala, V.; Effect of increased aggregate size on the mechanical and rheological properties of RPC, Proceedings of Second International Symposium on Advances in Concrete through Science and Engineering, Quebec, Canada, 2006.
[19] Penttala, V.: Mechanical and physical responses, volumetric changes in pore phases, and the effects of tension and entropy paradox in pore water of freezing mortar and concrete (submitted to Cement and Concrete Research)

Jennifer C. Scheydt
Dipl.-Ing.
University of Karlsruhe
Karlsruhe, Germany

Gunther Herold
Dr.-Ing. Dr. rer. nat.
University of Karlsruhe
Karlsruhe, Germany

Harald S. Müller
Prof. Dr.-Ing.
University of Karlsruhe
Karlsruhe, Germany

Long Term Behaviour of Ultra High Performance Concrete under the Attack of Chlorides and Aggressive Waters

Summary

Within the framework of long term investigations, several ultra high performance concretes were exposed to a one-dimensional attack of acid water and the relevant corrosion depth at the border zone of the concretes was calculated on the basis of the dissolved calcium mass. Furthermore, the corroded border zone was characterised by means of infrared spectroscopy and a scanning electron microscope (SEM). For the examination of the chloride penetration resistance, concrete samples were immersed in a NaCl solution for several months and the interactions between chloride and concrete were recorded. The obtained results allow a quantification of the very high durability of ultra high performance concrete.

Keywords: *long term behaviour, chloride attack, aggressive waters, infrared spectroscopy, SEM*

1 Introduction

So far only little experience has been gathered concerning the application of ultra high performance concrete in practice. Hence, its long term behaviour is still largely unknown, also due to limited research on this subject. Within the framework of a research project supported by the Deutsche Forschungsgemeinschaft (DFG), the microstructure and durability of UHPC was extensively investigated. Subsequently, the mixing composition and the mechanical properties of the investigated concretes were determined. Furthermore, the results of the experiments concerned with the attack of aggressive waters and the attack of chlorides are presented.

2 Mixing composition and mechanical properties of the investigated UHPC

The investigations on durability were carried out on a coarse aggregate mixture (UHPC) and on a fine aggregate mixture (RPC) that were developed at the Institute of Concrete Structures and Building Materials (IfMB). The mixing compositions of the investigated mixtures are given in Table 1.

Table 1: Mixing compositions [kg/m³], water-cement-ratio (w/c) and water-binder-ratio (w/b) of the investigated concretes UHPC and RPC

Concrete	CEM I 52,5 R-HS/NA	Microsilica	Basalt 2/8	Quartz sand	Quartz powder A	Quartz powder B	Steel fibres (l/d = 8/0.175 mm)	Superplasticizer	Mixing water	w/c	w/b
UHPC	582	178	714	355	326	132	196	29	137	0,27	0,21
RPC	774	236	-	472	434	175	196	38	184	0,27	0,21

Table 2: Strength values and modulus of elasticity [MPa] of the investigated concretes UHPC and RPC

Concrete	$f_{cm,cube}$ [1)]	$f_{cm,cube,90°C}$ [2)]	f_{cf} [1)]	$E_{c,28}$ [1)]
UHPC	190	251	24.2	52 500
RPC	177	222	25.3	45 700

[1)] water storage
[2)] heat treatment

The mechanical properties of the steel fibre reinforced (2.5 % by volume) concretes UHPC and RPC were tested at a concrete age of 28 days and can be seen in Table 2. The compressive strength $f_{cm,cube}$ was determined on cubes with an edge length of 150 mm. Due to heat treatment (3 days at 90 °C), the compressive strength increased by 32 % (UHPC) and 25 % (RPC) respectively compared to the compressive strength after water storage. The modulus of elasticity $E_{c,28}$ was determined on cylinders (d/h = 150/300 mm).

3 Attack of aggressive waters

The attack of aggressive waters containing hydrochloric acid (pH 1, pH 3, pH 5) was investigated on a defined concrete surface (150 x 150 mm²) under dynamic, non-abrasive conditions. By a frequent exchange of the attacking medium, the repression of the solution reaction was prevented. The pH-value of the aggressive waters was kept constant by means of titrators. Besides the influence of the pH-value, also the maximum aggregate size and the influence of thermal treatment of the hardened concrete were taken into account.

3.1 Development of the corrosion front

The relevant corrosion depth at the border zone of the concrete was calculated on the basis of the calcium mass dissolved in the attacking medium. Thus the calculated corrosion depth indicates an averaged value for the surface attacked.

Figure 1 illustrates the development of the corrosion depth of the ultra high performance concretes UHPC and RPC compared to the corrosive behaviour of a normal strength concrete C30/37 that was investigated in previous studies [1].

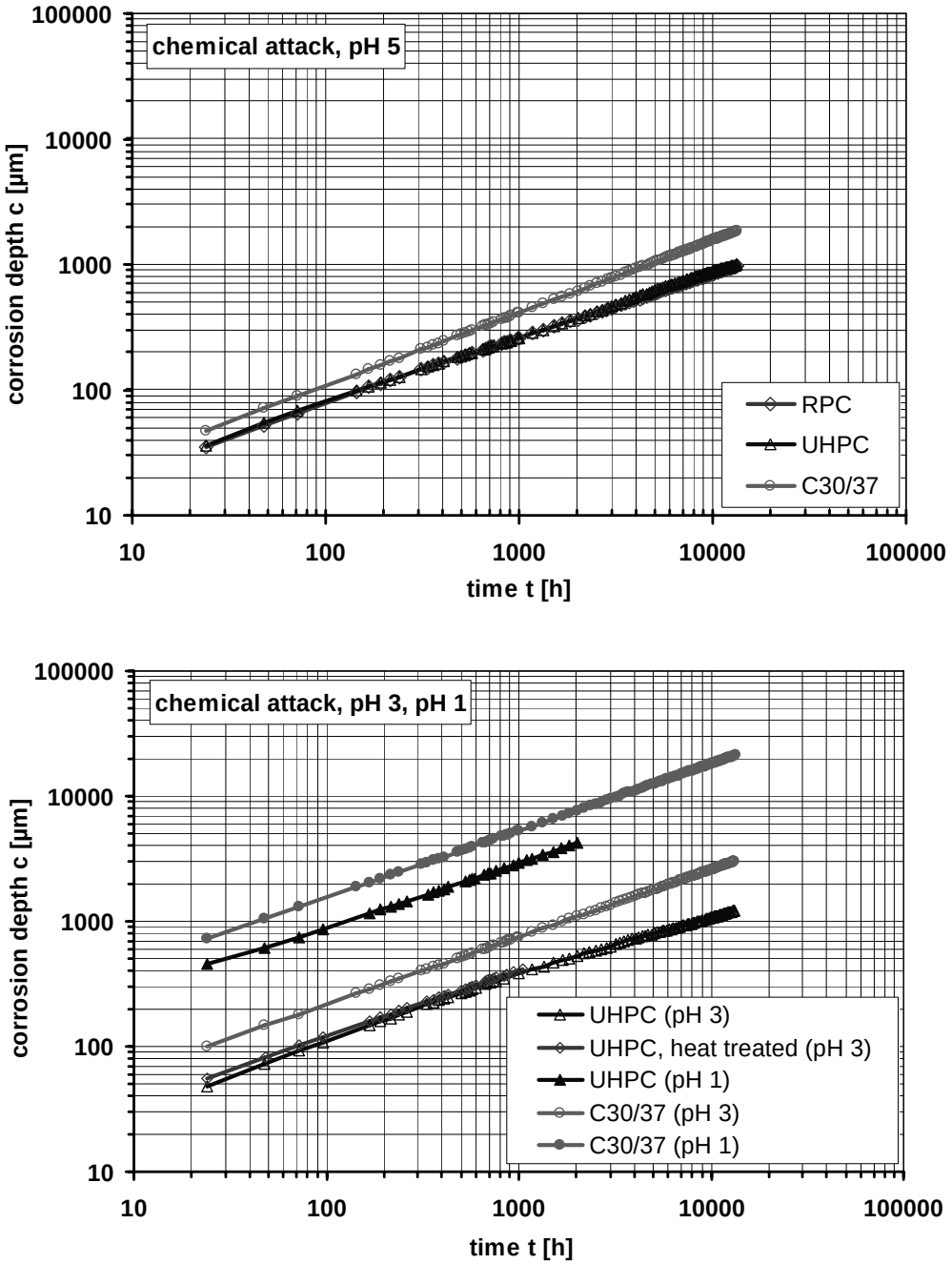

Figure 1: Development with time of the corrosion depth c of the mixtures UHPC and RPC due to the attack at pH 5 (above), pH 3 and pH 1 (below) compared to the behaviour of a normal strength concrete C30/37

Table 3 shows the regression functions associated with the experiments. The determination coefficient R^2 is nearly 1.0 for all regression functions. Within a double logarithmic scale, an increasing factor of the regression function means a parallel translation of the straight line towards a higher corrosion depth. An increasing exponent means an increasing gradient and so an acceleration of the corrosion process over time.

Table 3: Regression functions c(t) and corrosion depth after 6 and 80 weeks of attack for the investigated concretes

pH-value	Concrete	Regression function c(t)	Corrosion depth after x weeks of attack [µm]	
			x = 6	x = 80
pH 5	RPC	$7.51 \cdot t^{0.51}$	261	970
	UHPC	$7.61 \cdot t^{0.52}$	261	993
	C30/37	$7.57 \cdot t^{0.58}$	413	1845
pH 3	UHPC	$16.74 \cdot t^{0.45}$	381	1217
	UHPC, heat treated	$10.61 \cdot t^{0.53}$	418	-
	C30/37	$18.25 \cdot t^{0.54}$	751	3023
pH 1	UHPC	$78.38 \cdot t^{0.52}$	2916	-
	C30/37	$133.05 \cdot t^{0.53}$	5308	-

As can be seen from Table 3, both UHPC and RPC show nearly the same regression function and thus a very similar corrosion depth for an attack at pH 5, while the normal strength concrete C30/37 differs mainly in the exponent. The corrosion depth of the UHPC and RPC respectively is approx. 50 % lower than for the C30/37 after 80 weeks of attack. However, for an attack at pH 3 the functions for UHPC and C30/37 differ both in factor and exponent and the corrosion depth is 60 % lower for UHPC after a corrosion period of 80 weeks. After 80 weeks of attack, the corrosion depth of UHPC increased by approx. 20 % when the intensification of the attack increased from pH 5 to pH 3 (see Table 3).

The experiments on the attack at pH 1 as well as the investigations on the influence of the heat treatment of the UHPC have been under way for a shorter period so far. Due to heat treatment, a slight reduction of the resistance against the attack of aggressive waters could be observed (see Table 3). One explanation for this effect is a possible development of microcracks due to the thermal treatment, which leads to an increase in the attacked surface. In the case of the attack at pH 1, the corrosion depth of the UHPC was 45 % lower than that for the normal strength concrete after 6 weeks of attack. This lies in the same range as an attack at pH 3 (cp. Table 3). Compared to the attack at pH 3, the corrosion depth of the UHPC attacked at pH 1 is more than 7 times higher after 6 weeks of leaching.

Besides the experiments presented above, further investigations on the influence of the attacking medium (water containing sulphuric acid) are in progress.

3.2 Change in microstructure due to the attack of aggressive waters

The border zone of the corroded concrete was characterised by means of infrared spectroscopy and a scanning electron microscope (SEM). In Figure 2 the corroded border zone of the ultra high performance concretes RPC and UHPC can be seen after the attack of aggressive waters at pH 5 and pH 3.

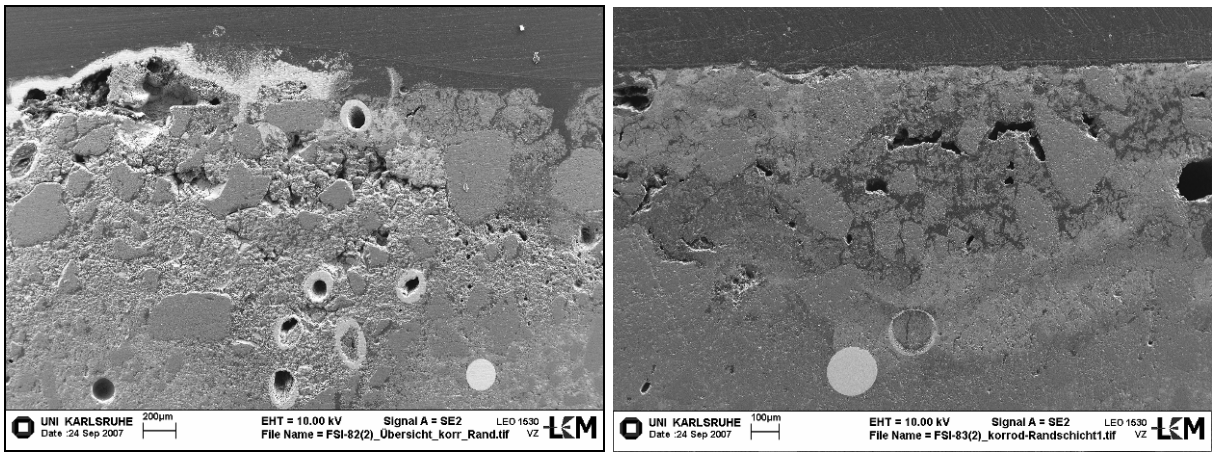

Figure 2: Corroded border zone of the mixture RPC after the attack at pH 5 (left) and of the mixture UHPC after the attack at pH 3 (right)

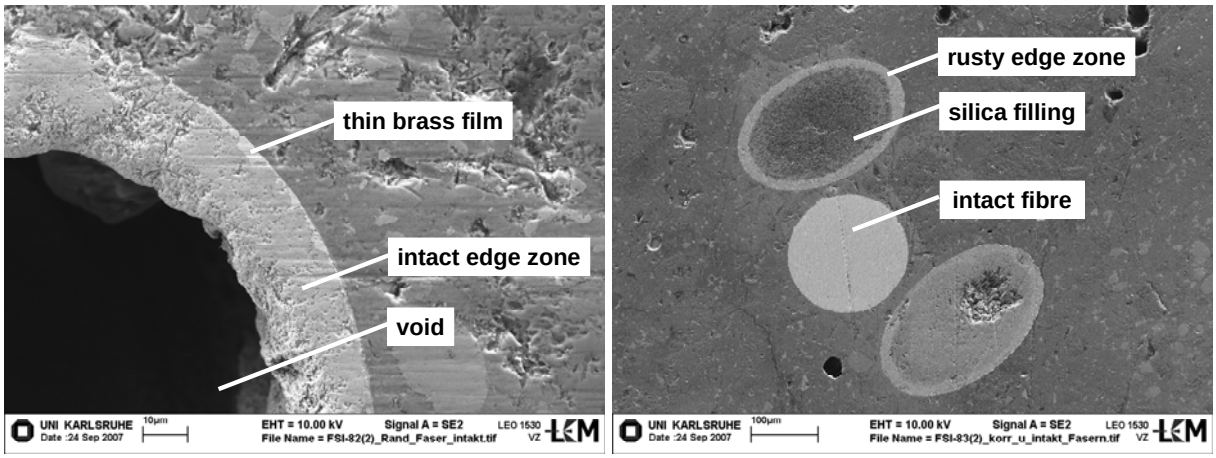

Figure 3: Detail of a corroded fibre after the attack at pH 5 (left) and after the attack at pH 3 (right)

As a typical characteristic for the attack at pH 5, the fibres were corroded and only a thin intact steel zone was left (see Figures 2 and 3, left). A reason for this effect might be that the porous rust filling of the fibres is removed by the grinding process within the specimen preparation. Differing from this appearance, the fibres attacked at pH 3 show a rusty border zone and the void is filled with silica (see Figures 2 and 3, right).

Independent from the intensity of the attack, the fibres seem to corrode from the inside. Depending on manufacture, the fibres are covered with a brass film that could be detected by means of SEM. It is possible that the brass generates a kind of protective cover, so that the border zone of the fibres is protected from corrosion and the corrosion is initiated from the cut cross section of the fibres. On the other hand, the steel corrosion is accelerated by the brass due to the potential difference.

It was frequently observed that highly corroded and intact fibres were situated in direct proximity, see Figure 3 (right). This effect is still under investigation.

A thin bay-coloured surface coating resulted from the attack of the aggressive waters that was investigated by infrared spectroscopy (Figure 4). Therefore, the thin coating was locally removed by spatula.

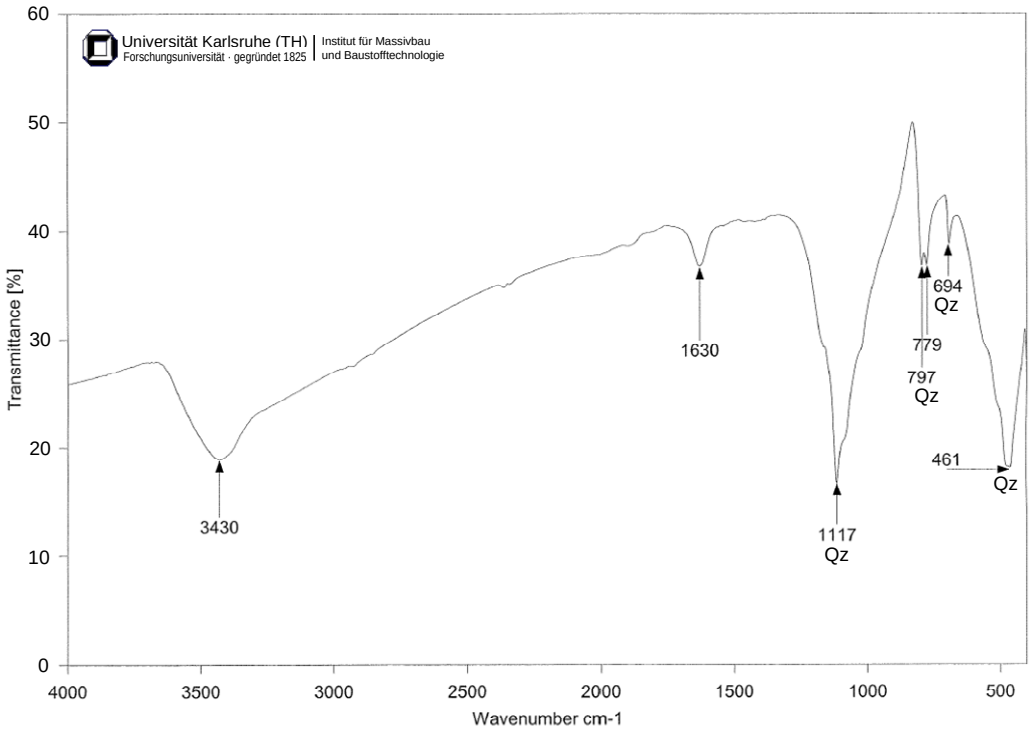

Figure 4: Infrared spectrum of the bay-coloured surface coating of the ultra high performance concrete after the attack of aggressive waters (pH 5)

For increasing wave numbers (> 2000 cm^{-1}), the infrared spectrum is affected by increasing absorption. The high absorption is caused by the formation of a secondary phase (Fe_2O_3/FeOOH) on the surface of the specimen. The band at 1117 cm^{-1}, the double band at 797 and 779 cm^{-1} and the bands at 694 and 461 cm^{-1} can be attributed to the quartz (Qz) that was added to the mixture as quartz sand and powder (see Table 1). Because this mineral is resistant to acids within these low-acid environments, it remains on the surface of the corroded specimen in addition to the ferrous secondary product. Hence, a corrosion product consisting of quartz powder and ferrous oxide hydroxide (FeOOH) is built up on the surface attacked.

4 Chloride attack

The resistance of ultra high performance concretes to chloride intrusion was investigated by placing the specimens into an NaCl solution (3 %) with an intrusion depth of 2 to 3 mm. After “suction” of the NaCl solution for different periods, the surface attacked was removed in different layers by grinding and was investigated by means of potentiometric titration of halogen. The resulting chloride profiles related to the chloride content of the concretes before attack (blank value) are shown in the Figures 5 and 6 for the ultra high performance concretes UHPC and RPC. The curves for RPC and UHPC are obtained from 2 experimental series.

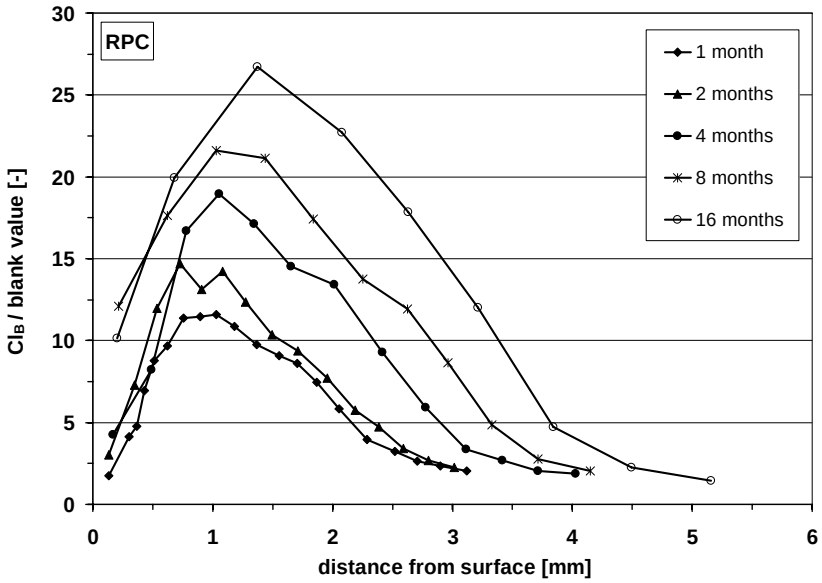

Figure 5: Chloride profiles of the mixture RPC after different periods of attack (1, 2, 4, 8 and 16 months)

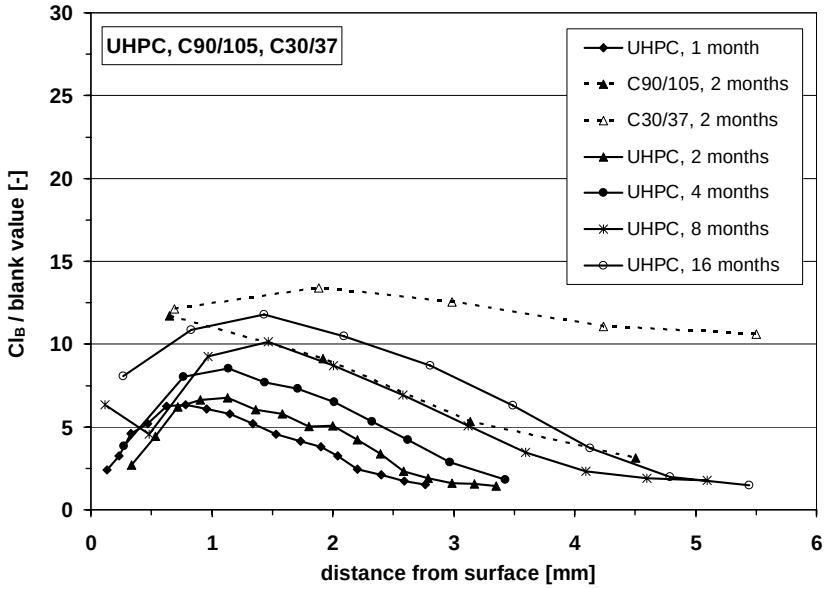

Figure 6: Chloride profile of the mixture UHPC after different periods of attack (1, 2, 4, 8 and 16 months) compared to a normal strength concrete C30/37 and a high strength concrete C90/105 (2 months of attack)

It can be seen that the chloride content increases up to a maximum value. Thereafter, the chloride concentration decreases to the blank value. Furthermore, the maximum moves towards the inside of the specimen and the intrusion depth increases.

The intrusion depths are similar both for the RPC and the UHPC and lie between approx. 3 mm after 1 month of attack and 5 mm after 16 months of attack. However, the maximum chloride concentration is nearly twice as high for the RPC. The RPC contains a much higher amount of matrix than the UHPC (see Table 1). It may be assumed that the chloride ions can better be adsorbed by the microstructure of the matrix of the RPC than by that of the UHPC.

In addition, Figure 6 shows the chloride profiles of a normal strength concrete C30/37 and a high strength concrete C90/105 after 2 months of chloride attack. The maximum chloride content both of the C30/37 and of the C90/105 is considerably higher than that of the ultra high performance concretes after 2 months of suction. Furthermore, the C30/37 especially shows a significantly lower decrease of the chloride concentration which indicates a much higher absorption of chloride solution and thus a significantly higher intrusion depth of chlorides.

Due to a permanent exposure to the attacking solution it was expected that the maximum chloride content occurs on the exposed surface of the specimen. Therefore, it has to be investigated, to wich extend this phenomenon is influenced by the test method. However, the shifting of the maximum with increasing exposure time indicates that the phenomenon can be ascribed to the concrete structure or the phase composition of the material.

Further experiments on the resistance against chloride attack after 32 months of attack are in progress. Moreover, the influence of heat treatment and fibre reinforcement is being investigated, see e. g. [2].

Additional experiments on normal and high strength concretes will be carried out to enhance the understanding of the material behaviour of ultra high performance concrete.

5 Conclusion and outlook

An essential basis for the practical application of ultra high performance concretes is the knowledge of its long term behaviour. Because only limited conclusions can be drawn by accelerated experiments, real-time examinations in particular are carried out within the introduced research project. Most of the investigations mentioned above are still in progress.

Besides the experiments dealt with above, an extended research is being carried out concerning the microstructure of ultra high performance concrete. The investigations cover porosity, transport characteristics and other aspects of durability, e. g. carbonation, see [2] or [3].

6 References

[1] Herold, G.: Korrosion zementgebundener Werkstoffe in mineralsauren Wässern. Dissertation, Institute of Concrete Structures and Building Materials, University of Karlsruhe (TH), Karlsruhe, 1999.

[2] Scheydt, J. C., Herold, G., Müller, H. S.: Dauerhaftigkeit ultrahochfester Grob- und Feinkornbetone. In: Proceedings of the 16. Internationale Baustofftagung ibausil 2006, volume 2, Weimar, September 2006, pp. 51-60.

[3] Herold, G., Scheydt, J. C., Müller, H. S.: Development and durability of ultra high performance concretes. In: Concrete Plant + Precast Technology, Volume 72, 10/2006, pp. 4-14.

Part 6:

Structural Bond

Hiroyuki Obata
M. Eng.
Taiheiyo Cement Corporation
Tokyo, Japan

Tatsuo Nishizawa
Prof.
Ishikawa National College of Technology
Ishikawa, Japan

Iwao Sasaki
Dr. Eng.
Public Works Research Institute
Ibaraki, Japan

Makoto Katagiri
Dr. Eng.
Taiheiyo Cement Corporation
Chiba, Japan

Effect of Improved Interfacial Bond on Whitetopping Using Ultra High Strength Fiber Reinforced Concrete

Summary

This study examined methods to improve the bonding strength between UFC panels and grout, which is very important in ensuring good performance of ultra-thin whitetopping with high strength concrete (HSC-WT). For that, several methods with combinations of forming macro textures on the panel surface and special surface treatment with chemical ingredients on the interface were examined using shear tests and direct tension tests in the laboratory. After the examinations, some candidate methods were selected and applied to full scale pavement load tests, and the effects on pavement behavior were investigated. Positive effects of the methods were confirmed from the tests. Also, the possibility of early opening to traffic of the pavement was examined by increasing the early age of strength of the grout.

Keywords: *ultra high strength fiber reinforced concrete, precast panel, whitetopping, bond strength test, shear strength test, full-scale pavement test, grout*

1 Introduction

Recommendations for the Design and Construction of Ultra High Strength Fiber Reinforced Concrete Structure (Draft)[1] were published and application of UFC in the actual structure is expected. Because UFC has a very dense matrix and contains short fibers, it has excellent mechanical properties and durability compared with conventional concrete[2]. When UFC, with such mechanical properties, is used as pavement material, it is expected that thinner but tougher concrete pavement will be possible.

Asphalt is the most common road pavement material in Japan but becomes mastic deformation from the wheel load at high temperature, and wheel tracks will form under heavy traffic. This type of damage in asphalt pavement is generally limited to the surface layer, and the whitetopping repair technique[3] was developed where a concrete overlay is applied on the surface of the damaged asphalt. However, there are problems associated with the conventional white topping technique, such as limits to the thickness of the concrete layer due to the small bending strength of concrete and long road closure to cure concrete. High

strength concrete whitetopping (HSC-WT) was developed for our study using ultra-thin thickness precast UFC for fast construction in order to solve the existing problems.

HSC-WT consists of a UFC panel (t = 30 mm) and a bonding layer (grout, t = 20 mm) as shown in Figure 1, and after placement of the UFC panel, grout is injected underneath the panel to integrate with the existing pavement.

According to the numerical analysis on dynamics[4],[5] the development of interfacial bonding technique of the UFC panel with the grout was the key to this technique. Accordingly, element tests for the bonding characteristics of the UFC panel and the grout were conducted in addition to the existing studies[6],[7]. Some of the methods, by which satisfactory bond strength was achieved, were applied to the load test on full-scale pavement to confirm the effect.

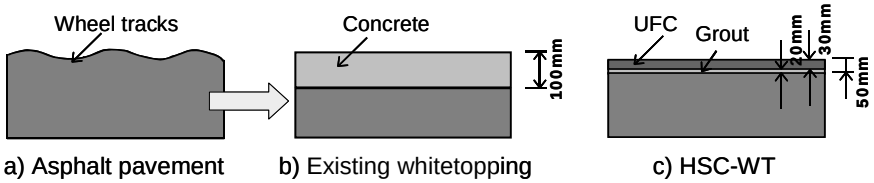

Figure 1: Whitetopping using UFC Panel

2 Study of the bonding layer specification of UFC panels

The effect of irregularities in the UFC panel surface and surface treatment by primer as means to enhance interfacial bond strength were investigated by elemental tests.

2.1 Outline of the tests

(1) Material used

UFC was prepared by mixing 180 kg/m^3 of water, 2254 kg/m^3 of UFC Premix (Ductal(R) Premix manufactured by Taiheiyo Cement Corporation) with 2 vol. % of steel fiber. The UFC was cured for 24 hours after placement at a temperature of 20°C, and after demould, it was further cured with 90°C steam for 48 hours.

Two fast curing type grouts I and II (hauynite cement) with different strength levels and cement grout (ordinary cement) were used as the grout material. The compressive strength of each grout material at 20°C according to JSCE-G-505 is as shown in Figure 2. The figure indicates that bond strength will stabilize in 7 days. Accordingly, the bond strength test and shear strength test were conducted after 7 days curing at 20°C from placement of the grout.

Fifty percent solid concentration SBR emulsion was used as a primer and applied to the surface of UFC test piece with a brush. The amount of SBR applied was 300 g/m^2 for the surface with irregularities and 150 g/m^2 for smooth surfaces.

(2) Test piece

The back surface of the UFC panel was provided with irregularities in order to achieve bond strength and shear strength. The convex forming type (d = 19 mm, h = 5 mm) and aggregate dispersion type (size 1310 crushed stone dispersed at 7 kg/m^2) were used as described in

our previous study[7] (Figure 3). Test pieces used for the bond strength test were the UFC panels, 400 x 400 x 50 mm in size cured as described above and 20 mm thick grout material. Test pieces for the two-interface shear strength test were prepared by setting up two UFC panels (100 x 100 x 100 mm) that were cured as described above at a 100 mm distance in the form with grout material between the two panels (Figure 4). The test pieces were used in the tests after curing at 20°C for 7 days from placement of the grout.

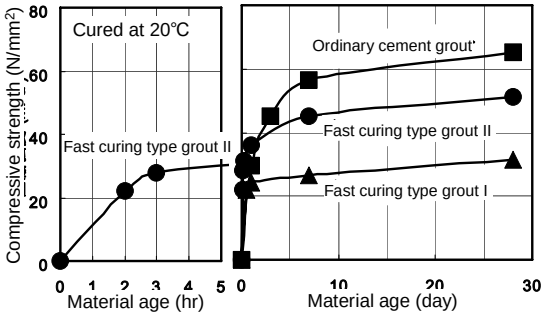

Figure 2: Strength Achievement of the Grout

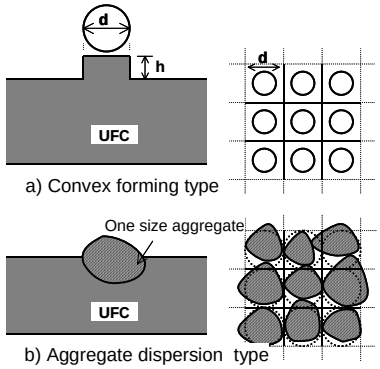

Figure 3: Irregularity provided on the surface of UFC panel

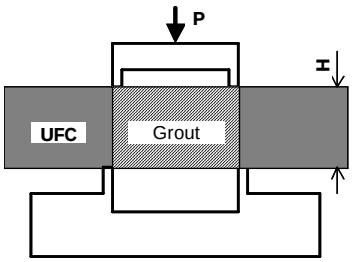

Figure 4: Dual Face Shear Strength Test

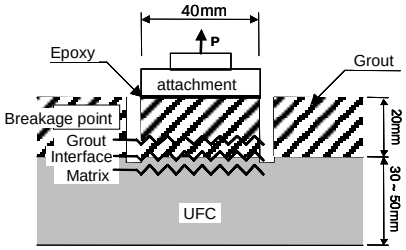

Figure 5: Bond Strength Test

(3) Test method

In the bond strength test, maximum tensile load was measured by application of a vertical tensile load on the test piece using steel attachments bonded to the test piece using the Building Research Institute type bond strength tester (capacity: 30 kN) as shown in Figure 4, and bond strength was obtained by dividing the maximum tensile load with the bonded area. Number of tests for each level was nine locations. The two-interface shear strength test was conducted following the procedure for the shear strength test for steel fiber reinforced concrete (JSCE-G 553-1999) as shown in Figure 5.

2.2 Test results

Figure 6 shows the results of bond and shear strength tests for a total of 12 levels in combination of surface irregularity pattern, use or non-use of primer, and grout material. Compression strength of the grout material in the tests was 28.6 N/ mm^2 for fast curing grout I, 57.2 N/ mm^2 for fast curing grout II, and 63.3 N/ mm^2 for conventional grout. In this study, 1N/ mm^2 or more of the control value is used for both bond and shear strength referencing the results of the previous study[8].

(1) Effect of the primer

As shown in Figure 6, an increase in the bond and shear strength was observed at any test level due to application of the primer. While the effect of the primer on bond strength was generally large, it was especially significant for the test levels without irregularities in the surface (smooth surface) as shown in Figure 6 (1) and (2). Although the mechanism for the effect of the primer was not fully understood, it was considered primarily due to the anchoring effect of the primer penetrating into microscopic cavities.

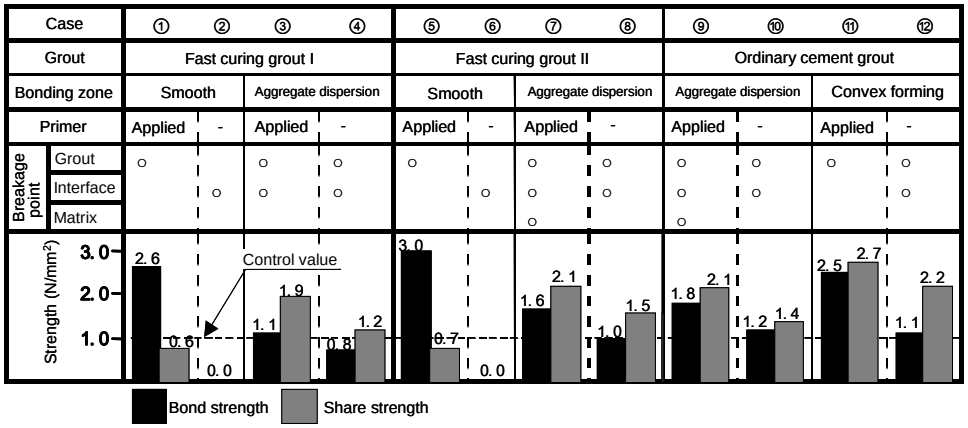

Figure 6: Results of Shear and Two-Interface Shear Strength Test

(2) Effect of surface irregularity

In the bond and shear strength test, shear strength was improved by providing surface irregularities by convex forming and aggregate dispersion. As shown in Figure 6 (3), (9), and (11), bond and shear strength was effectively improved by combined use of primer.

(3) Effect of grout material

Specifications to achieve 1N/ mm^2 of the control value from the combined effect of primer and surface irregularities can be found for all grout materials tested.

3 Full scale load test on the pavement

A method to increase the bond strength of the UFC panel with grout was shown from the element tests conducted. Verification as to whether such a method effectively functions under the behavior of actual pavement was conducted using a full scale load test.

3.1 Outline of the test

(1) Test pavement

About 48 m^2 of test pavement was constructed at the test track of the Public Works Research Institute for the full-scale load test as shown in Figure 7. Six levels of test pavement were constructed in Sections A to F with the conditions satisfying the criterion of 1N/ mm^2 or more in the above bond and shear strength tests. The effect of the specification of bonding surface, effect of dimensions of the UFC panel, and capability for early opening to traffic for different types of grout material were investigated.

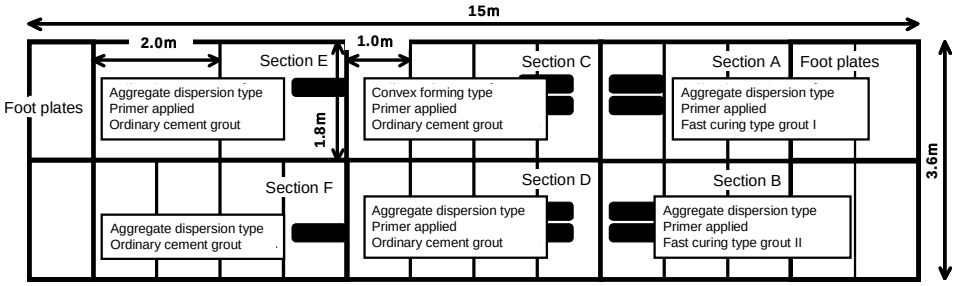

Figure 7: Test Pavement Outline

(2) Construction procedure

The procedure for constructing the test pavement was as follows. First, 50 mm in thickness of asphalt pavement was removed. Next, a UFC panel was placed, unevenness was adjusted, and then grout material was placed using a mortar pump. Finally, joints were filled with elastic material to complete the test pavement.

(3) Load test

A running load was applied with the test carriage (wheel load of 50 kN) until the total number of wheel passes reached 150,000 at the speed of 10 km/hr. The test started two weeks after construction of the test pavement, and it took six months to complete the load test from the start.

(4) Method to investigate behavior of the test pavement

Visual and hammering inspections of crack and delamination of the UFC panel was conducted to monitor the behavior of the test pavement due to the process of the load test when the total number of wheel passes was between 0 to 150,000. Furthermore, in order to inspect the status of damage of the pavement structure after the load test in detail, a core sample (diameter: 100 mm, depth: 200 mm) was taken from the test pavement at each section, and an appearance check and bond strength test of core samples were conducted.

3.2 Test results and discussion

(1) Crack and delamination

Survey results of cracks and delamination at the start of the load test and after 150,000 wheel passes are shown in Figure 8. The shaded area indicated the spot of a cavity underneath the UFC panel from hammering. While no cracks in the UFC panel were observed before 150,000 wheel passes, delamination occurred and expanded with the number of wheel passes. Delamination that occurred before the start of the load test was due to poor filling of grout during construction (Figure 8 before load test) and delamination tended to expand from this position. It was also observed that delamination tended to occur from the joint between panels, and it was considered due to steps between panels at the joint.

To examine the inside of the test pavement, a core sample with 100 mm diameter and about 150 mm in depth was taken. (a) Sound portion (No. 1), (b) and (c) delaminated portion in construction (No. 2 and No. 3), and (d) delaminated portion occurred in the load test (No. 4) from core samples as shown in Figure 9 as the representative portion. From the appearance

examination of the core samples, it was found that delamination occurred at the interface between the UFC panel and grout (No. 2, 3, and 4), delamination during construction was either the section where delamination occurred after filling with grout or a section with poor filling of grout (No. 2 and 3), and that delamination expanded due to loading from a small section of poorly filled grout that could not be detected by hammering after construction. The delamination in No. 2 that occurred during construction was believed due to separation in construction of the UFC panel with lower flexural rigidity. Care should be taken during construction when fast curing grout is used, and filling of grout should be adequate in order to increase the durability of HSC-WT.

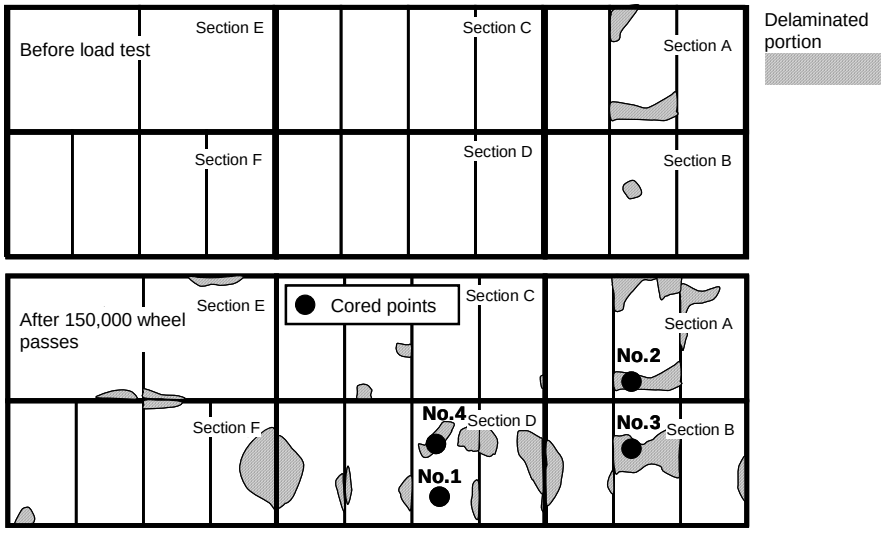

Figure 8: Observation Results of Crack and Delamination

(a) Sound portion (b) Delaminated portion in construction (c) Portion of poor grout filling (d) Delaminated portion in loading test

Figure 9: Status of Crack and Delamination

(2) Possibility for early opening to traffic

Possibility for early opening to traffic was investigated using grout material with comparable temporal and long-age strength (fast curing grout I for Section A and fast curing grout II for Section B). Compression strength of the grout after 28 days of curing under field conditions was 30.2 N/mm^2 for fast curing grout I and 59.8 N/mm^2 for fast curing grout II, and the relationship between temporal strength and long-age strength shown in Figure 2 was successfully demonstrated under field conditions.

At Sections A and B, delamination expanded from a section of poorly filled grout during construction, but delamination did not expand to other panels, and no cracks were observed

in the panel. The results indirectly indicated that a certain level of durability was reached by the specification for Section B after 2-3 hours from construction.

(3) Specification of bonding surface

Convex forming for Section C, aggregate dispersion for Section D, and no application of primer for Section F were used to investigate the effects of the bonding surface specification of the UFC panel. While delamination in Section C was less frequent than in Sections D and F, no cracks in the UFC panel were observed in any sections, and no significant differences in durability were detected. The difference due to the specification was not significant within the range of the specification that was selected for each section to satisfy 1 N/mm^2 or more of bond and shear strength.

(4) Effect of dimensions of the panel

To investigate the effect of UFC panel dimensions, the panel area in Section E was enlarged twice compared to the others. The results of the load test showed that the occurrence of delamination was less compared with other sections, and no cracks in the UFC panel were observed. This indicated, within the dimensions tested in this study, that enlarging the panel area and reducing the joints was effective for improving durability.

(5) Bonding strength of the test pavement

The relationship between bond strength in the laboratory test (Figure 6) and bond strength in the field test using core samples is shown in Figure 10. Bond strength for all sections of the field test satisfied the control value for bond and shear strength of 1 N/mm^2, and although direct comparison was impossible due to differences in the test conditions, it was confirmed that specifications established by the laboratory test satisfied the criterion in the field test.

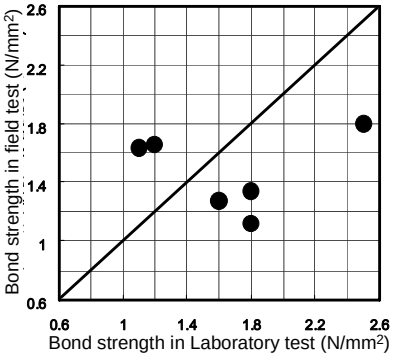

Figure 10: Relation of Bond Strength in Laboratory Test and Field Test

4 Conclusion

The following findings were obtained from a full scale load test for investigation of specifications to improve interfacial bonding characteristics between the UFC panel and grout, which is important in determining the behavior of HSC-WT and its effect on the behavior of the overall pavement.

(1) Bond strength can be effectively improved by application of the primer, and shear strength can be effectively improved by increasing the irregularity of the surface. Specifications that satisfy the criterion of 1 N/mm^2 can be established with a combination of

bonding surface specifications, such as primer application, and providing irregularities to the surface.

(2) Durability can be enhanced by improving accuracy in placement of the panel and grout because the step between panels and poor filling of grout can cause delamination.

(3) Early opening to traffic is possible using high strength fast curing grout.

(4) The effect of the bonding surface specification to durability such as pattern of surface irregularity and use of primer is not significant, exceeding the control value of bond and shear strength of 1 N/mm^2.

(5) Durability can be increased by enlarging the dimensions of the UFC panel.

(6) The specification of the bonding surface established in the laboratory test was confirmed by the field test, and no cracks in the UFC panel were detected in the load test up to 150,000 wheel passes, and durability of HSC-WT was confirmed.

5 Acknowledgement

We express special appreciation for funding for this study from the 2006 Grant-in-Aid for Scientific Research of the Japan Society for the Promotion of Science (Representative Researcher: Prof. Tatsuo Nishizawa, Ishikawa National College of Technology)

6 References

[1] Recommendations for Design and Construction of Ultra High Strength Fiber Reinforced Concrete Structure (Draft), Concrete Library 113, JSCE, 2004.

[2] Shimoyama, Y.; Uzawa, M.: Characteristic and Application of Ductal®, Journal of Research of the Taiheyo Cement Corporation, No. 142, pp. 55-62, 2002.

[3] Noda, E.; About Whitetopping, Doro Kensetsu (bimonthly Road Construction), No.576, 1996.

[4] Nishizawa, T.; Obata, H.; Sasaki, I.; Kokubu, K.: Dynamic Behavior of Ultra-thin Whitetopping Structure with High Strength Concrete under Traffic Load, International Conference on Best Practices for ULTRATHIN and THIN Whitetoppings, 5, 2005.

[5] Taketsu, H.; Nishizawa, T.; Obata, H.; Sasaki, I.; Kokubu, K.: Dynamic Behavior of Whitetopping Pavement using High Strength Concrete, Journal of Pavement Engineering, JSCE, Vol.11, pp. 123-130, 2006.

[6] Obata, H.; Nishizawa, T.; Sasaki, I.; Kokubu, K.: Shear Characteristic at Interface between UFRC Concrete Composite Material, Proceedings of 60th Annual Meeting, JSCE, 5-109, pp. 217-218, 2005.

[7] Obata, H.; Nishizawa, T.; Sasaki, I.; Kokubu, K.: Bonding Characteristic of Ultra High Strength Fiber Reinforced Concrete with Inorganic Grout Material, Proceedings of 61st Annual Meeting, JSCE, 5-117, pp. 233-234, 2006.

[8] Nishizawa, T.; Obata, H.; Sasaki, I.; Kokubu, K.: Viscoelastic Behavior of Ultra-thin Layer Whitetopping using Ultra High Strength Fiber Reinforced Concrete, Proceedings of 60th Annual Meeting, JSCE, 5-107, pp. 213-214, 2005.

Steffen Anders
Dr.-Ing.
Bilfinger Berger AG
Mannheim, Germany

Ludger Lohaus
Prof. Dr.-Ing.
University of Hannover
Institute of Building Materials
Hannover, Germany

Ultra-High Performance Concrete in Grouted Connections - Potential and Design Aspects

Summary

Grouted Connections are a well-known means of fixing offshore structures to the seabed. In the last decade this technology was transferred from the oil- and gas industry to Offshore Wind Energy Converters. In contrast to the oil- and gas industry Ultra-High Performance grouts are planned in these connections. Therefore this paper deals with the specifics of connections grouted using UHPC. Apart from significant increases in the load-bearing capacity the fatigue strength is shown to be increased either. In addition UHPC leads to higher stresses in the confining steel tubes as well as in the shear keys. Approaches for their design are briefly outlined.

Keywords: *Grouted Connections, Load-Deformation curve, Design, Fatigue*

1 Introduction

Grouted connections, or Grouted Joints as they are often called in the offshore industry, are a well-known method of fixing offshore structures to the seabed. For fixed offshore platforms usually shear connectors so called “shear keys” are used to increase the load-bearing capacity. In addition, the technology is used for strengthening and repair of aged offshore structures.

In the last decade, the technology of Grouted Connections was transferred to foundations of Offshore Wind Energy Converters (OWEC). Therefore extensive experiments on the static and fatigue performance of Ultra-High Performance Concrete (UHPC) in Grouted Joints were performed with focus on the effects of the compressive strength of the grout and the fibre reinforcement of the grout as well as the height of the shear keys on the load-deformation behaviour.

2 Basics of Grouted Connections

For the design and construction of axially loaded Grouted Joints in offshore applications three major recommendations exist, given by the American Petroleum Institute (API) [1], the Health and Safety Executives (HSE) [2] as well as Det Norske Veritas (DNV) [3,4]. [4] is the only code especially developed for OWECs.

According to figure 1 Grouted Joints are made of two steel tubes with different diameters that are connected using grout. The tube with the larger diameter is called the sleeve, the smaller

tube is called the pile. Generally, the connection can be constructed with or without shear keys. The basic parameters characterizing the load-deformation behaviour and the maximum load are the ratio of diameter to thickness of pile, sleeve and grout (D/t), the compressive strength of the grout and the ratio of height to spacing (h/s) of the shear keys. The diameter to thickness ratio characterizes the confinement of the grout provided by the steel tubes. Concerning the shear keys a maximum h/s-ratio of 0.1 is given in the recommendations, but has rarely been used in experiments or offshore.

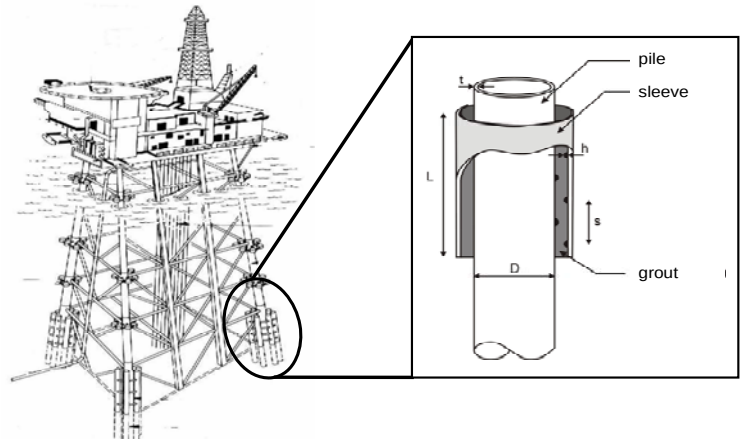

Figure 1: Grouted Joints in fixed offshore platforms, characteristic properties and design with and without shear keys

Regarding connections with shear keys, three load bearing mechanisms are distinguished: adhesion and friction in the interfaces between grout and steel tubes and the load-bearing capacity of compression struts which develop between the shear keys on the pile and the sleeve. The main failure modes of connections with shear keys are shear failure along the shear connectors for closely spaced shear keys and crushing of the grout on the stressed side of the shear keys for Grouted Joints with an appropriate spacing of the shear keys. In this case, diagonal cracks occur in the grout. Finally the pile is pushed through the grout in either case. More detailed information on the characteristic properties and the failure mechanisms can be found in references [5,6,7,8].

The fatigue performance of Grouted Connections depends on the loading regime. According to Hordyk [9] the slope of the S/N-curve increases with a decreasing stress ratio (R), especially in reverse loading. In case of compression-compression loading the slope of the S/N-curve is small, but exhibits large scatter in the number of cycles to failure.

3 Grouted Connections with UHPC – Experiments and Results

3.1 Specimens and Experimental Programme

The specimens used were designed according to Det Norske Veritas [4]. Important limiting conditions were the application of standard steel profiles and compressive loading of pile and sleeve without the danger of yielding. Figure 2 displays the resulting geometry and a specimen of a grouted connection subjected to static loading. It can easily be seen that the steel tubes provide a strong confinement due to the thickness of the tubes resulting in stiff

specimens. Compared to the limits given in the regulations the specimens are stiffer than covered by the recommendations.

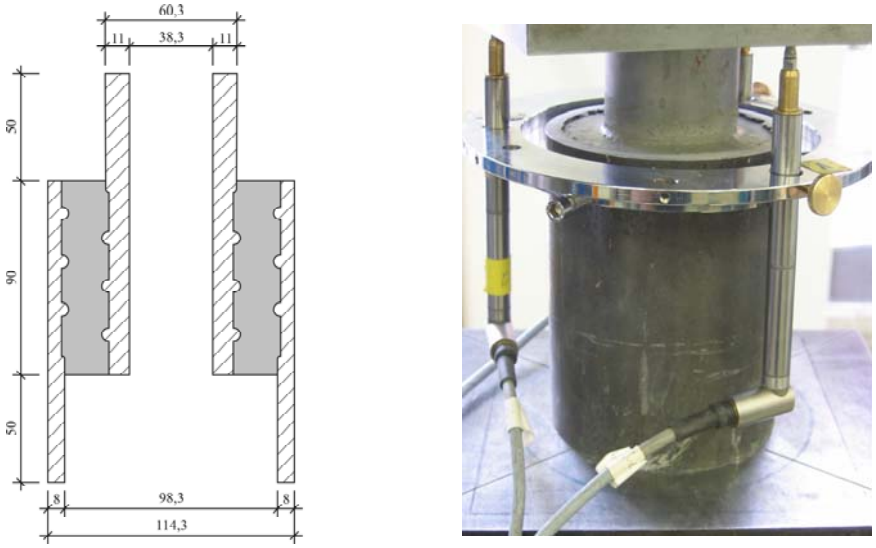

a) longitudinal section b) picture of a specimen

Figure 2: a) longitudinal section (lengths in mm) and b) picture of a specimen

In the case of static loading the compressive strengths of the grout were about 60 MPa (C60), 110 MPa (C110), 150 MPa (C150) and 170 MPa (C170). All grouts were tested with and without fibre reinforcement of 2 vol.-% short, high-strength steel fibres, as well as shear keys with h/s ratios of 0.013 (h = 0.3 mm) and 0.056 (h = 1.25 mm). Detailed information concerning the tested materials and the testing conditions can be found in reference [11].

3.2 Quasi-static Loading

In figure 3 the marked effect of shear keys is demonstrated. The maximum pile shear strength of a specimen without shear keys is about 0.75 MPa. The load-bearing capacity is increased to about 16 MPa at an h/s-ratio of 0.013. If shear keys with h/s = 0.056 are applied, the pile shear strength can be increased up to 28 MPa. All displayed tests were performed using a C150 without fibre reinforcement.

Concerning the stress-slip curve, Grouted Connections show a behaviour that can be divided into two parts. A first linear-elastic part, which is terminated by the first slip. The second part is characterized by non-linear behaviour. This part ends with the pile shear strength. As stated by Lamport [8], the first part is characterized by the development of diagonal cracks in the grout. The non-linear second part of the curve is driven by gradual crushing of the grout in front of the shear keys. In this case, wedges of crushed grout develop which nevertheless transfer the load from the shear keys into the compression struts until the ultimate capacity is reached. The confining steel tubes cause the marked ductility of the connection, even if the UHPC itself is known for a distinct brittle mode of failure. In figure 3 the pile shear stress is calculated by dividing the load by the surface area of the pile.

If steel fibres are used, the stress at first slip and the pile shear strength can be significantly increased. Generally the ultimate stress can be increased using a higher compressive strength of the grout, higher shear keys or fibre reinforcement.

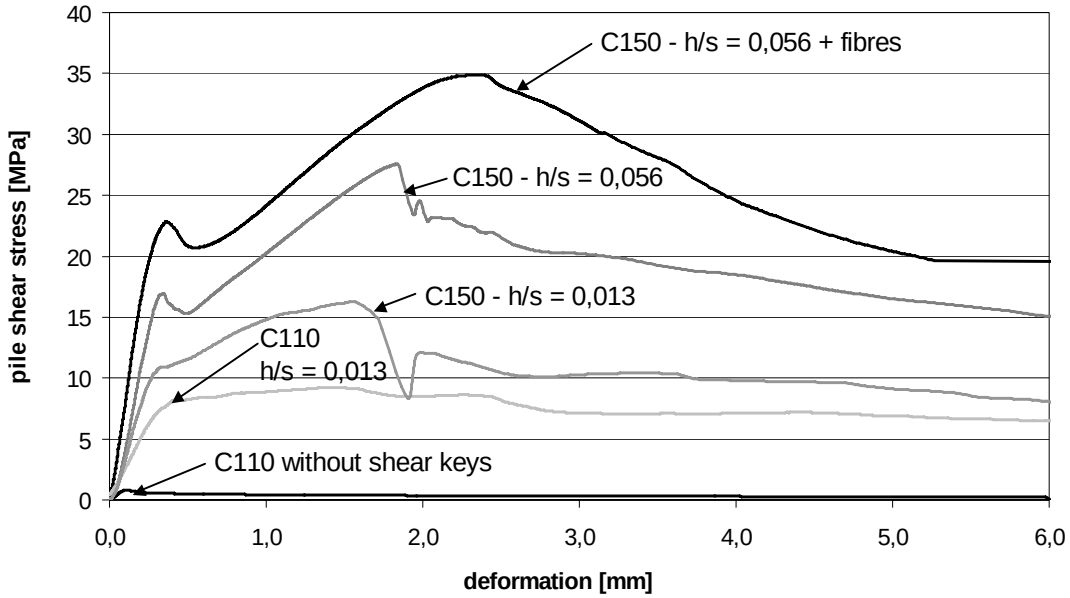

Figure 3: Effects of shear keys, the h/s-ratio, grout-compressive strength and fibre reinforcement on the load-deformation behaviour of Grouted Joints

The effect of steel fibre reinforcement on the stress at first slip and the pile shear strength is an increase of about 25 % in the load bearing capacity compared to the grout without fibres independent of the compressive strength of the grout and the h/s-ratio. In addition, it seems as if the three possibilities to enhance the load-bearing capacity namely the compressive strength of the grout, the fibre reinforcement and the h/s-ratio are independent and can be used additively.

3.3 Fatigue Loading

In figure 4, the results of the performed fatigue tests are displayed. The ultimate number of cycles to failure is given in logarithmic scale. The stress range is normalized using the static pile shear strength at the first slip. The lower load limit is kept constant at 5 % of the static stress at first slip. It is found that the ultimate numbers of cycles show a significant scatter as already reported by Hordyk [9] for tests in compression-compression. Except for the C110 with h/s=0.056 and fibres, all specimens show comparable ultimate numbers of cycles to failure. Consequently the increases stated for the static pile shear strength can be transferred to fatigue loading. Conclusive reasons for the inferior results of the C110, h/s=0.056 with fibres could not be found.

If defined values for the deformation of the connections are used as failure criteria instead of final failure, S/N-curves with a steeper slope were found, which limit the number of cycles until a specific deformation is reached. In this case the safety margins could possibly be reduced. In cases of stress reversals the slope of the S/N-curves increases anyway.

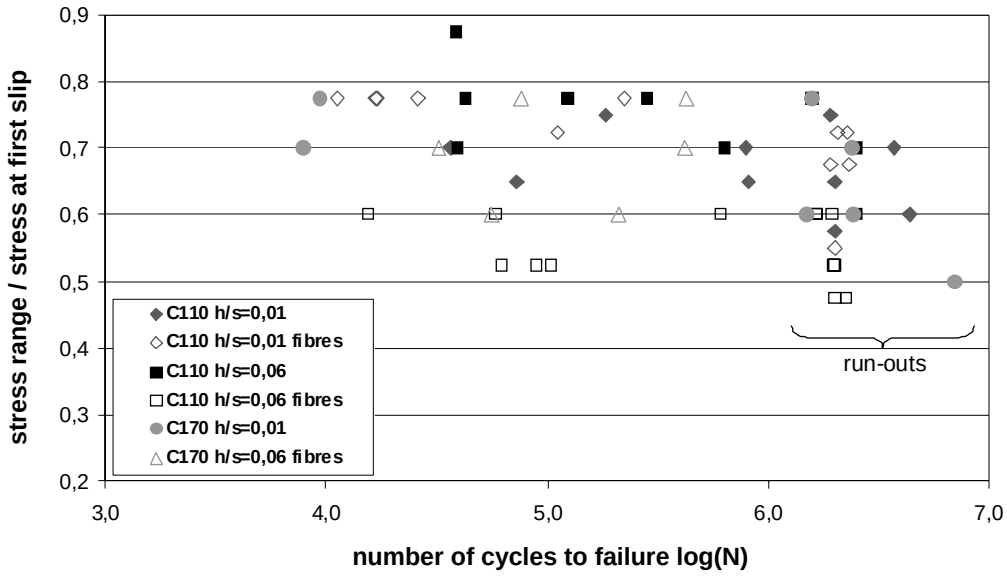

Figure 4: Ultimate number of cycles of Grouted Joints with different UHPCs, the stress range is normalized using the static pile shear strength at first slip

4 Design Aspects

Figure 5 displays that in some cases the shear keys shear off if the grout has a sufficient compressive strength. In addition it can be seen that the shear keys are subjected to different stresses at different heights. Therefore the shear keys, as well as the pile and the sleeve have to be considered separately in design to resist the stresses induced by the Ultra-High Performance grout. Obviously these stresses increase with an increasing strength of the grout. According to an approach given by the American Petroleum Institute [1] the shear keys can be designed by applying a stress of 2.5 times the compressive strength of the grout on the stressed side of the shear key. Based on this approach, the minimum ratio of shear key width (w) to shear key height (h) can be calculated for the failure of the shear keys:

$$\min(w/h) = \frac{2.5 \cdot \sqrt{3} \cdot A_{SR,P}}{\pi \cdot D_P \cdot f_{y,k} \cdot h} \cdot f_{cu} \qquad (1)$$

In this equation $A_{SR,P}$ equals the stressed area of the shear keys, D_P the outer diameter of the pile, $f_{y,k}$ the yield stress of the steel, h the shear key height and f_{cu} the unconfined compressive strength of the grout.

In the experiments described above the w/h-ratio was chosen to be 2.0. The shear keys are estimated to fail at a compressive strength of about 180 MPa. This value was also found in the experiments. The shear keys failed if a compressive strength of about 190 MPa (C170 with fibre reinforcement) was applied, whereas no failure was found for a compressive strength of 150 MPa. In fatigue tests, the shear keys failed even earlier at a stress range of about 65 % of the static pile shear strength. Therefore the approach by the API is supposed to be transferable to Grouted Connections with UHPC.

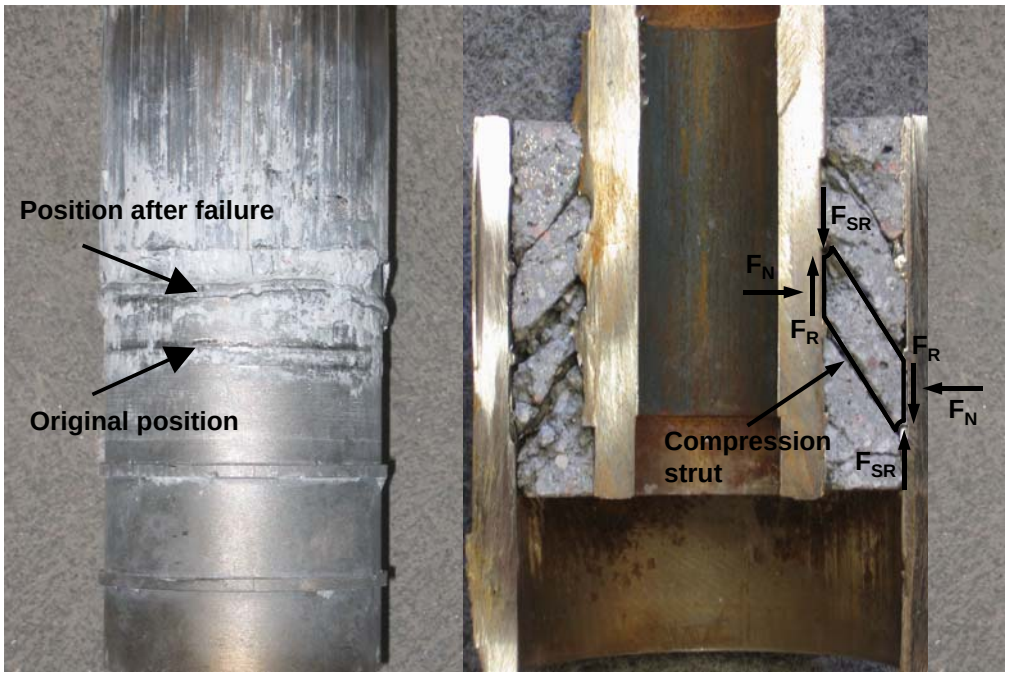

Figure 5: Failed shear key on the pile and crack pattern after fatigue testing

Figure 5 displays the cracks that developed in the grout during fatigue tests. Obviously marked compression struts develop between the shear keys on the pile and the sleeve, which are separated by cracks. According to figure 5 the forces transferred by friction (F_R) at the interface between grout and steel as well as the normal stresses acting horizontally on the pile (F_N) and the sleeve can be calculated using a model presented in 1988 by Lamport [8]. Lamport developed this model for a single compression strut and static tests. Consequently identically stressed shear keys in the whole connection are assumed, which have already been shown not to exist.

The normal forces can be calculated using the geometric properties of the grouted connection. The force transferred by friction depends on the stresses that are induced by the shear keys F_{SR} and calculate the load-deformation curve up to the pile shear strength. Lamport applied two plasticity models for concrete in order to estimate F_{SR} and calculate the load-deformation curve. A simpler approach has already been given by the American Petroleum Institute [1] using 2.5 times the compressive strength of the grout. Apart from the longitudinal forces the circumferential forces have to be taken into account. If the approach described by Lamport is combined with the approach of the API, the stresses can be calculated as follows:

$$\sigma_R = \frac{(D_P - t_P)}{2 \cdot t_P \cdot s \cdot D_P \cdot \pi} \cdot \frac{(t_g - h)}{t_g(\tan\alpha - \mu)} \cdot F_{SR} \qquad (2)$$

$$\sigma_L = \frac{F_{max}}{A_P}\left(1 - \frac{1}{n}\right) \qquad (3)$$

σ_R equals the circumferential stresses, σ_L the longitudinal stresses, D_P the outer pile diameter, t_P the wall-thickness of the pile, t_G the wall-thickness of the grout, s the spacing of the shear keys, h the shear key height, μ the coefficient of friction, F_{SR} the force applied by

the shear keys, A_P the area of the pile in the cross-section, n the number of shear keys on the pile, α the angle of the compression strut against the horizontal and finally F_{max} the ultimate load-bearing capacity.

The resulting local stresses can be estimated by the equivalent stress. The load-bearing capacity of the Grouted Connection should be estimated using the approaches by Det Norske Veritas [3,4] or the Health and Safety Executives [2]. As an example the equivalent stresses calculated for a grout with a compressive strength of about 190 MPa and an h/s-ratio of 0.056 are shown in figure 6. According to this estimation the equivalent stress will exceed the yield stress of the pile if the wall-thickness of the pile is less than about 7 mm. The specimens used in the experiments had a wall-thickness of 9.75 mm. Therefore yielding did not occur.

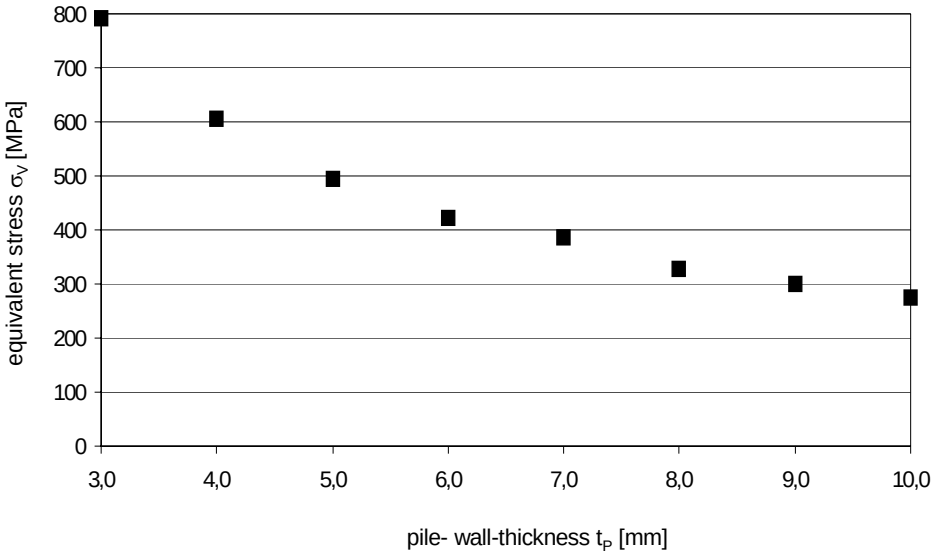

Figure 6: Equivalent stress in the pile, calculated for the specimens used, compressive strength of the grout about 190 MPa, h/s-ratio 0.056

The experiments and the estimation of the load-bearing capacity of the shear keys, pile and sleeve have shown that a separate design of the named parts of the Grouted Connections is inevitable in order to ensure the load-bearing capacity of the whole connection. This is especially true for Ultra-High Performance grouts. The outlined approaches for the estimation and design should be complemented with further instrumented tests to fix the local stresses and deformations. In addition the coefficient of friction between steel and grout with further compressive stresses should be investigated. Another aspect is a suitable estimation of the angle of the compression struts.

The technology of Grouted Connections is already applied for the rehabilitation and strengthening of aged offshore structures. Therefore the described results can be easily transferred. If one does not only think about offshore structures Grouted Connections could also be used for steel structures onshore for rehabilitation, strengthening or joining. Another aspect are double-walled concrete filled hybrid members, which could also be joined using grouting technologies. In either case, further tests are needed concerning the effects of the

radial stiffness on the load-bearing capacity if smaller or larger steel members with a bigger or smaller radial stiffness than in the offshore industry are used.

5 Summary

In this paper, the load-deformation behaviour of Grouted Connections is described. It is demonstrated that the compressive strength of the grout, fibre reinforcement and the shear key height are three independent means of increasing and adapting the load-bearing capacity of a Grouted Connection. Furthermore it is shown that the increases stated for static behaviour can be transferred to fatigue loading. Enhanced static load-bearing capacity means enhanced fatigue strength. Failure of the shear keys in static and dynamic tests has shown that a separate design of the shear keys, the pile and the sleeve are inevitable. Therefore approaches for the design and calculation of these members are briefly outlined and discussed. In some cases their suitability could be shown.

6 Acknowledgements

The financial and non-material support of the Stiftung Industrieforschung is kindly acknowledged.

7 References

[1] American Petroleum Institute (Hrsg.): Recommended Practice for Planning, Designing and Constructing Fixed Offshore Platforms – Working Stress Design. 21st edition, Washington, 2000.

[2] Health & Security Executives: Pile / Sleeve Connections. *Offshore Technology Report* 2001/016, Norwich, 2002.

[3] Det Norske Veritas: Rules for fixed Offshore Installations. Det Norske Veritas, 1998.

[4] Det Norske Veritas: DNV-OS-J101 – Design of Offshore Wind Turbine Structures. Det Norske Veritas, 2004.

[5] Department of Energy: Report of the Working Party on the Strength of Grouted Pile / Sleeve Connections for Offshore Structures. In: Offshore Technology Paper, OTP 11, 1982.

[6] Billington, C.J.: The Integrity of Jacket to Pile Connections. In: Oceanology International, p. 79-88, 1978.

[7] Billington, C.J.; Tebbett, I.E.: The Basis for new Design Formulae for Grouted Jacket to Pile Connections. In: 12th Offshore Technology Conference, OTC 3788, Houston, 1980.

[8] Lamport, W.B.: Ultimate Strength of Grouted Pile-to-Sleeve Connections. Dissertation, University of Texas at Houston, 1988.

[9] Hordyk, M.: The Static and Fatigue Strength of Grouted Pile-Sleeve Connections. In: Fatigue in Offshore Structures, Volume 2, Oxford & IBH Publishers, 1996.

[10] Lohaus, L.; Anders, S.: Static and Fatigue behaviour of High-Performance Concrete in “Grouted Joints” for hybrid structures. In: Proceedings of the 2nd Int. fib Congress, June 2006, Naples.

[11] Anders, S.: Betontechnologische Einflüsse auf das Tragverhalten von Grouted Joints. PhD-Thesis, Hannover, 2007 (in german).

Martin Schäfers
Dipl.-Ing.
University of Kassel
Kassel, Germany

Werner Seim
Prof. Dr.-Ing.
University of Kassel
Kassel, Germany

Development of adhesive-bound UHPC-Timber Composites

Summary

This report describes theoretical and experimental investigations which were carried out within the development of glued UHPC-Timber-Composites. To detect, which geometries for the cross-section and which timber-materials are reasonable for the UHPC-timber composites, calculations about the stress distribution and the bending-stiffness of the composites were conducted. Further on, shear-tests on the glued joint between timber and UHPC are described. The surface-properties of concrete and timber were varied for this investigations and five different adhesives where applied.

Keywords: *timber-concrete, hybrid structures, composites, UHPC*

1 Introduction

Until now, for timber-concrete-structures the two composites which are timber beam and concrete plate are mostly connected by steel connection of different shape. This type of connection leads to a more or less elastic bond between the two composite materials. For typical geometries (see Figure 1 (a)) slender plates of fibre-reinforced UHPC are capable to transfer life-loads without conventional reinforcement. If fibre-reinforced ultra-high-performance-concrete (UHPC) will be used, it becomes reasonable to apply adhesives to connect concrete and wood, because the surface-tensile-strength of the fibre-reinforced UHPC is much higher than that of common concrete. Continously bonding with adhesives leads to a rigid compound and therefore to high stiffness of the bending member.

By many research-projects and a lot of existing timber buildings it could already be shown, that the gluing technology is applicable to timber components. Further more the post-strengthening of concrete members with adhesive bonded FRP´s was well investigated in the last decades (Niedermeier [1], Seim [2], Schilde [3]). The high surface-tensile-strength of UHPC emphasizes the gluing technology to be most efficient for connecting UHPC-members. This could be backed up by experimental studies by Schmidt [4], Mühlbauer [5] and Teichmann [6].

To now only few research activities focused on adhesive bonding of timber and concrete. Brunner et. al. [7] studied the shear-behaviour on small specimens and the bending-behaviour of full scale members. The gluing was carried out by pouring the fresh concrete on the fresh resin (wet in wet). Brunner achieved a stiff compound between the two materials and could prove the full bond of the bending member. But the adopted technology was vulnerable to local deficiencies. Further manifestations on glued timber-concrete-composites

are to be found in a publication from Negrao [8] who focused on shear tests under variable conditions of moisture contents and bending tests in structural size.

2 Preliminary design studies

To find out which geometries and which timber-materials are most efficient for UHPC-timber composites, extensive parametric studies were carried out. In these calculations the stress distribution within the cross-section and the bending-stiffness of the bending-member are determined and compared for different dimensions of the timber-beam and for different thicknesses of the UHPC-plate as well as for different E-Modules of timber products.
The following assumptions are made:

- Bernoulli´s beam theory is adapted
- bond between timber and UHPC is modelled as a stiff connection
- 3-dimensional effects are not considered
- The bending-moment for the calculation of the stress-distribution is 60 kNm for all observed cases

Two different types of cross-sections are observed: In the first case a Typical t-beam section (Figure 1 (a)), in the second case a solid section (Figure 1 (b)). The geometries are shown in Figure 1. The E-Modules for the basic calculations are 12.600 N/mm^2 for the timber and 50.000 N/mm^2 for the UHPC.

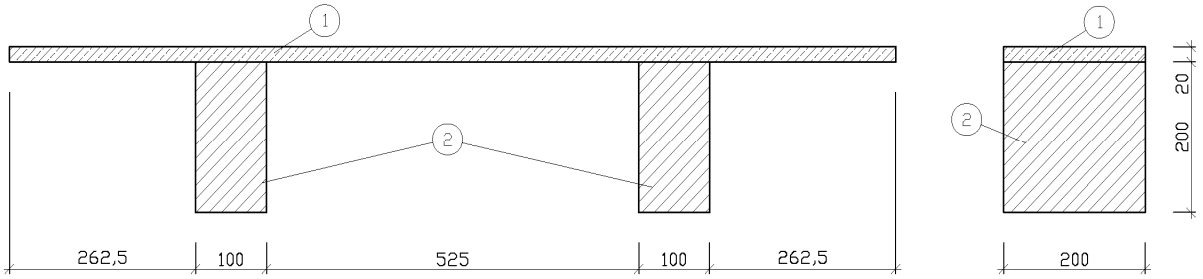

(a) (b)

Figure 1: Cross-sections of the composite-girders: (a) double t-beam section; (b) solid section

The material and geometrical parameters are shown in Table 1. The first part of the index refers to the part of the composite girder (UHPC = 1; timber = 2). The second part shows which type of cross section is observed. The UHPC-slab should be as slim as possible to create economically efficient structures. Therefore it was varied between 20 mm and 60 mm, whereas 20 mm is a lower limit, if common loads and the given geometry are considered. The E-Modulus of the timber was varied between 7.000 N/mm^2 which corresponds to low graded soft wood and 15.200 N/mm^2 which can be achieved with derived timber products or hard wood.

Two main ambitions are connected with the design of hybrid structures from timber and UHPC: The first is a high utilisation of both materials and the second is a high bending stiffness of the composite-girder. Beyond the basics of engineering mechanics the results of the calculations which are documented in Table 1 and the Figures 2 and 3 depict the following: In case of the beam stiffness the t-section is the one which is more efficient. Its stiffness is more than six times of the stiffness of the pure timber-beam for a thickness of the UHPC-slab of 60 mm. If the height of the timber beam is varied stiffness reaches values up to five times of the pure timber-beam (see Figure 3). The influence of the E-Modulus of the timber on the stress-distribution is quite small for the t-Section. For the solid section this parameter has only a small influence on the tension-stresses in timber but there is a significant decrease of compression-stress in the UHPC-slab if the E-Modulus of timber increases. To get an image of the shear stresses which occur in the adhesive joint, the bending moment of 60 kNm can be connected to a four-point bending-situation. For this case the maximum shear-stresses in the adhesive joint lay between 1,03 and 4,76 N/mm^2 if material and geometrical parameters are varied as documented in Table 1.

Table 1: Results of the parameter variation

Parameter	**Width of Variation**	**compression** [N/mm$^{2]}$]	**tension** [N/mm$^{2]}$]	**$(EI)_{ef,compl}/(EI)_{timber}$** [-]
$h_{1,t}$	20 – 60 mm	20.5 – 13.1	22.3 – 15.8	3.60 – 6.11
$h_{1,s}$		77.3 – 41.1	29.1 – 19.9	2.02 – 3.84
$h_{2,t}$	100 – 500 mm	59.3 – 11.8	75.2 – 10.6	4.78 – 3.12
$h_{2,s}$		209.7 – 41.7	94.0 – 14.3	2.92 – 1.70
$E_{2,t}$	7000 – 15200 N/mm^2	24.0 – 19.6	21.3 – 22.7	4.00 – 3.40
$E_{2,s}$		94.1 – 71.6	26.1 – 30.2	2.50 – 1.89

Concluding it can be detected, that the best utilisation of both materials can be achieved with the solid-section but the highest improvement of stiffness compared to the timber-beam can be achieved with the t-section. It should be mentioned, that there are further conditions which have to be considered, like the distribution of shear stresses or the bending-strength of the UHPC-plate in the transverse direction of the beam. Overall it can be found, that for the solid section a ratio from UHPC-slab thickness to timber-thickness of 0.13 – 0.14 is an optimum for a high capacity utilisation of both materials if timber products with higher strength are applied. For common soft wood or glued laminated timber this ratio has to be smaller. For t-sections, the cross section which is shown in Figure 1 is considerable even if the stresses are much below the compression-strength of the UHPC. This is reasonable because of the high stiffness of the slim and lightweight structure.

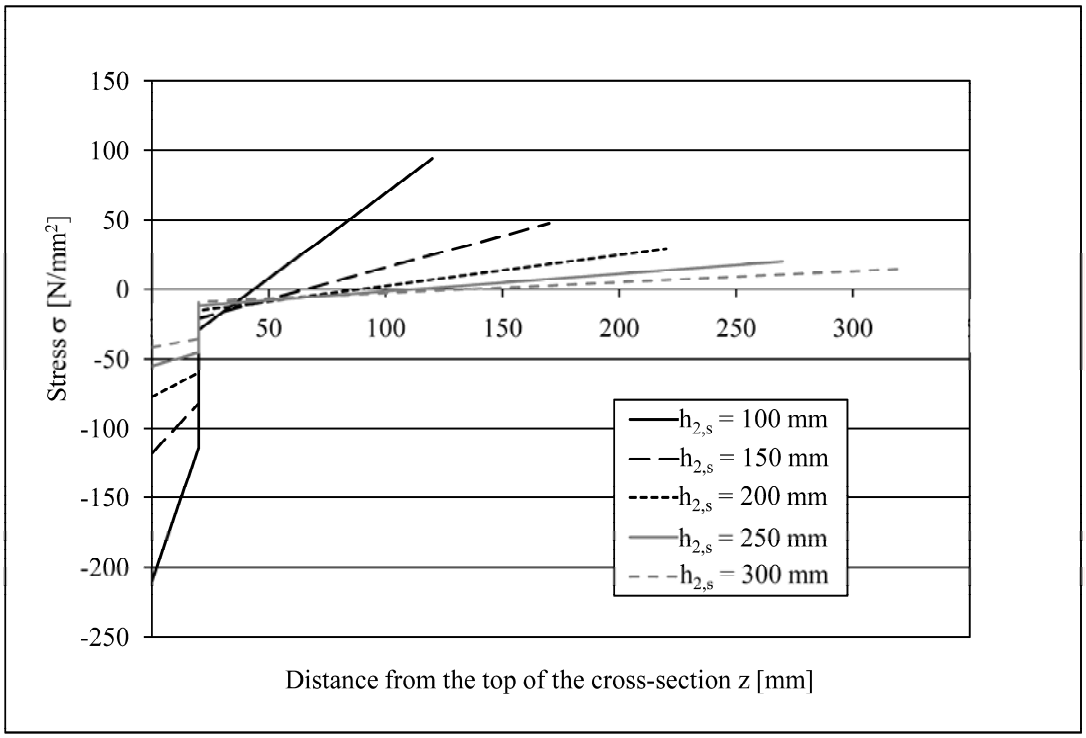

Figure 2: Bending stresses within solid section (h_1 = 20 mm)

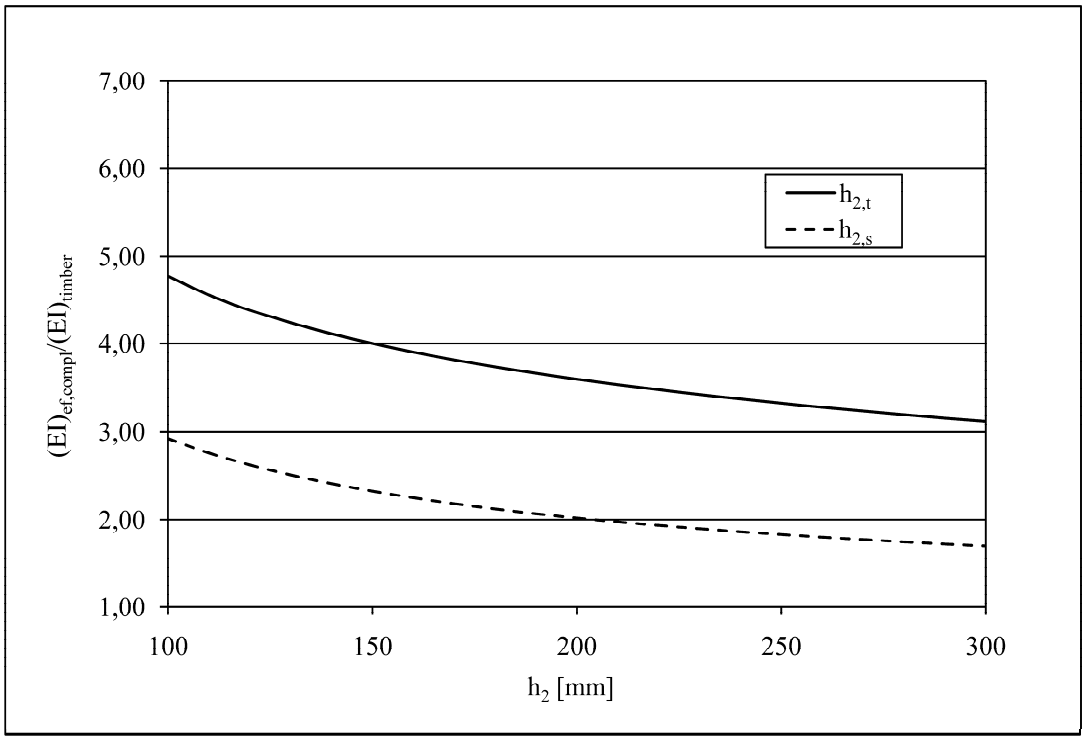

Figure 3: Stiffness ratio for solid and t-section

3 Short-time shear tests

To detect, which adhesives are applicable and to compare different forms of surface treatment of the UHPC and of the timber overall 51 shear tests have been carried out. The adhesives used for this study are documented in Table 2.

Table 2: Applied adhesives

Denotation	Adhesive	Hardening Compound	Producer	Viscosity
R1	Phenol Resorcinol Resin 1775	2575	Akzo Nobel	fluid
M1	Melamin-Urea Resin 1247	2526	Akzo Nobel	fluid
E1	Resin Epoxy 55	Komp. II	S&P	fluid
E2	Sikadur 330	Komp. II	Sika	viscous
E3	Sikadur 30	Komp. II	Sika	viscous

Table 3 depicts the combinations of surface treatment and adhesive for the shear samples. For all test specimens, the UHPC-plates were glued on the timber prisms. Three different kinds of surface-treatment were used for the UHPC: No treatment, sandblasting and steel brushing. The timber-surface was planed or raw-sawn. All bondings were produced according to the handling instructions of the producers of the adhesives. The humidity of the timber was located between 7 % and 11 % during adherence as well as during testing. For every parameter combination three samples were produced and tested.

Table 3: Shear samples

Denotation	UHPC-Surface			Timber-Suface	
	untreated	sandblasted	steel-brush	planed	raw-sawn
R1UH	•			•	
R1GH		•		•	
M1UH	•			•	
M1GH		•		•	
E1UH	•			•	
E1US	•				•
E1GH		•		•	
E1GS		•			•
E2UH	•			•	
E2US	•				•
E2GH		•		•	
E2GS		•			•
E2DS			•	•	
E3UH	•			•	
E3US	•				•
E3GH		•		•	
E3GS		•			•

The geometry of the test specimens was taken according to DIN EN 392 [9]. The side lengths of the timber-cubes was 42 mm. UHPC-prisms measured 42 mm x 42 mm x 20 mm. The timber cubes were sawn out of GL 24h laminated beams. The UHPC-mixture which was selected, has been approved for practical application [10]. The orientation of the fibre-reinforcement could not be determined experimentally. But it can be assumed, that the prevalent orientation of the fibres is parallel to the slab surface which is the bonding surface. All specimens were tested parallel to the grain.

The mean values of the shear-strength are listed and the fracture surfaces are documented in Table 4 for all specimens. For the calculation of the shear strength a constant shear-stress over the whole shear-surface was assumed. The results show, that the resorcinol-resin is well applicable for the bonding of timber and UHPC because of the high shear strength and because there is only a small percentage of failure in adhesive. The specimens which were bonded with the resorcinol-resin were the only ones which showed a significant fraction of failure in the UHPC. The melamine-resin is not adequate for connecting timber and UHPC because failure-surfaces in the resin were significant (see Figure 4). Overall the epoxy-resins performed best. Excepting the specimens whose surfaces were treated with a steel-brush all epoxy bonded specimens failed almost exclusively in timber (Figure 4, Table 4). Shear stresses reached values around of 10 N/mm^2. Among the tests with the epoxy specimens there was no significant influence of the surface-treatment on the results. The variation of the shear-strength in this group was probably caused by the variation of shear strength of the timber-specimens.

Table 4: Results of the shear tests

Den.	**$f_{v,mean}$**	**Std. Deviation**	**Percentage of the fracture surface [%]**		
	[N/mm^2]		Timber	UHPC	Adhesive
R1UH	7,29	1,13	73	22	5
R1GH	10,03	1,82	75	15	10
M1UH	6,18	3,41	80	3	17
M1GH	5,74	1,01	45	5	50
E1UH	9,95	1,02	96	1	3
E1US	11,35	1,47	97	1	2
E1GH	9,23	1,15	95	2	3
E1GS	10,96	0,89	98	1	1
E2UH	8,96	2,02	100	0	0
E2US	6,24	1,81	100	0	0
E2GH	11,22	1,47	94	4	2
E2GS	10,10	1,64	98	2	0
E2DH	5,04	1,97	48	0	52
E3UH	12,59	1,20	100	0	0
E3US	10,61	3,06	100	0	0
E3GH	9,17	0,95	100	0	0
E3GS	9,45	2,13	100	0	0

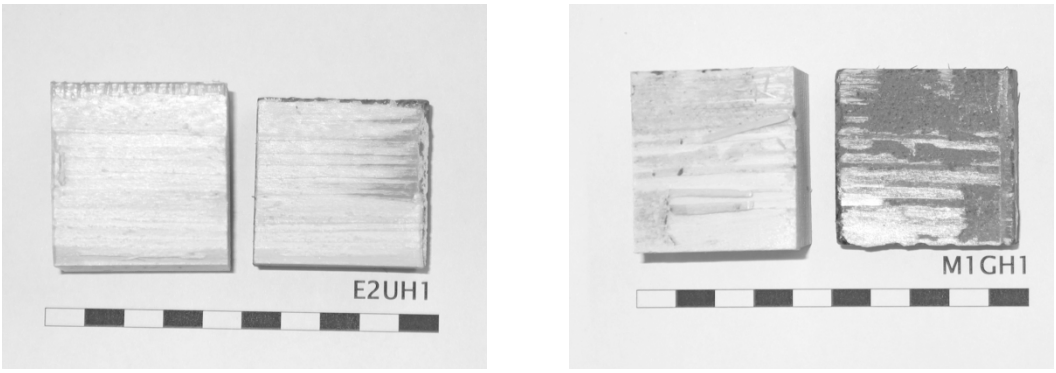

(a) (b)

Figure 4: Characteristic fracture surfaces (a) epoxy-resin, (b) melamin resin

4 Summary and Conclusions

Parameter studies showed, that the bending stiffness of timber-beams can be multiplied for about five to six times by the bonding of a thin UHPC-plate on the beams. In case of the solid-section a high utilization of both materials can be achieved but the increase in bending-stiffness is smaller, compared to the t-section. The shear-tests carried out on 51 samples displayed, that epoxy- and resorcin-resins are applicable for the connection of timber and UHPC. If these adhesives are applied, the kind of the surface-treatment has no significant influence on the shear-strength and a shear-failure in wood is decisive.

Therefore hardwood and derived timber-products will be included in further studies. Furthermore the shear stress-strain characteristics will be investigated by further testing and an analytical model for the shear-behavior of the bond will be derived. Within these studies the assumption of the rigid compound has to be verified. Finally the capability of the construction shall be demonstrated by full scale testing. Within these tests also the load bearing in transverse direction will be observed.

5 References

[1] Niedermeier, R.: Zugkraftdeckung bei klebearmierten Bauteilen. Berichte aus dem Konstruktiven Ingenieurbau. Dissertation, Technische Universität München, Lehrstuhl für Massivbau, 2001.

[2] Seim, W.; Karbhari, V.; Seible, F.: Poststrengthening of Concrete Slabs: Full-Scale Testing and Design Recommendations. ASCE Journal of Structural Engineering, S. 743 – 752, June 2003.

[3] Schilde, K.: Untersuchungen zum Verbund zwischen Beton und nachträglich aufgeklebten CFK-Lamellen am Zwischenrisselement. Dissertation, Universität Kassel, Fachgebiet Bauwerks-erhaltung und Holzbau, 2006.

[4] Schmidt, M.; Teichmann, T.: New developments in Ultra High Performance Concrete – non corrosive PVA-fibres and gluing of structural elements. Proceedings of the 2nd fib congress, Neapel, 2006

[5] Mühlbauer, C.; Zilch, K.: Joining of Ultra High Performance Concrete (UHPC) Members by gluing. In: SEMC 2007, The Third International Conference on Structural Engineering, Mechanics and Computation, Cape Town, South Africa, 2007.

[6] Teichmann, T.: Kleben auf UHPC – erste Versuchsdaten. Forschungsbericht, unveröffentlicht, Kassel, 2005.
[7] Brunner, M.; Schnüriger, M.: Holz-Beton-Elemente mit Klebeverbund. Forschungsbericht an das BBW – Bern, Bericht Nr. 2637-SB01, Hochschule für Architektur, Bau und Holz, HSB Biel, 2005.
[8] Negrao, J. H.; Oliveira, F. M.; Oliveira, C.L.: Investigation on Timber-Concrete Glued Composites. WCTE 2006, 9th World Conference on Timber Engineering, Protland, Oregon, USA, 2006.
[9] DIN EN 392: Brettschichtholz, Scherprüfung der Leimfugen, 1996-04.
[10] Schmidt, M., et. al.: Fügen von Bauteilen aus UHPC durch Kleben – Voruntersuchungen und Anwendung bei der Gärtnerplatzbrücke in Kassel. Beton und Stahlbetonbau. 102 (2007), Heft 10

Horst Peters
Dipl. Ing., Dr. rer. pol.
Sika Deutschland GmbH
Stuttgart, Germany

Heinz Bänziger
Dipl. Ing.
Sika Services AG
Pfäffikon ZH, Switzerland

Marco Poltera
Dipl. Ing.
Sika Services AG
Pfäffikon ZH, Switzerland

Durable adhesive bonding with epoxy resins in civil engineering construction

Summary

History shows that there is an interrelationship between a new material and the form of structures it is used for. Early arches were built with stones. Steel enabled trusses and long span girders. High strength wires made long span suspension bridges possible, etc. Ultra high performance concrete, with its extremely high strength and durability, is basically a new material, even though it is called concrete. Its application should not follow the path of regular concrete. It is anticipated that, with time, new structural concepts will be developed that can better utilize the superb properties of the UHPC.

Keywords: *epoxy resin, Zulassung Z-36.12-29, ETAG 013*

1 Introduction

Bonding of structural elements is a very old and traditional technology. The Romans and other ancient civilisations used mineral adhesives (mortars) for bonding and pointing natural and artificial stones. The historic buildings surviving from that era demonstrate how durable these bonds can be.

The first polymer based adhesives for producing durable high-strength adhesive bonds in “rigid” construction were investigated in the early Sixties.

One of the first major applications to attract worldwide attention was the construction of the bridge viaduct near Chillon Castle (Switzerland) in the late 1960’s. Here precast concrete segments produced on an industrial scale, were joined by high-strength epoxy adhesive bonding for the first time. This method reduced construction times and improved performance dramatically and the technology was soon in use worldwide.

Epoxy-bonded segmental concrete bridges are still ‘state of the art’ today and their economy, efficiency and durability, have been proven many times during the last 40 years.

The adhesives used as part of this technology are also used for the post-strengthening of structures with bonded strengthening elements. Steel profiles were used initially in the 1960’s, but generally these have now been superseded by carbon fibre profiles since the mid

1990's. The adhesives used for both of these applications are the same high performance epoxy resins. The durability of these materials in these applications has been demonstrated in countless trials and evaluations including: performance and endurance testing, being subjected to literally millions of dynamic load cycles and extensive and accelerated artificial and natural weathering.

This paper aims to illustrate with some striking examples, that adhesive bonding in construction provides reliable, economic and ecologically sound solutions to many problems, plus that it can extend the design possibilities and creative opportunities.

2 Long-term experience with epoxy resins

The absolute structural integrity and safety of modern reinforced concrete structures always has the top priority for engineers, architects and their clients. Yet, despite all the careful planning and painstaking workmanship during the original construction work, there are still many reasons why structural post-strengthening can prove necessary during the service life of a structure. One of the most common is a change of use, demanding higher load carrying capabilities. This has been the case with numerous bridges, largely due to the hugely increased traffic volumes and the much higher axle loads that have been introduced in recent years.

Figure 1:
Ravenna Bridge: strengthened with CFRP-Prestressingsystem *Sika Leoba CarboDur®* and final trial with with heavy load trucks.

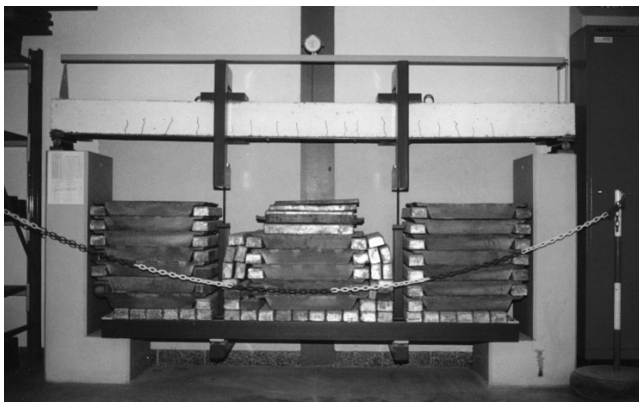

Figure 2:
EMPA beam, steel plate bonded with *Sikadur®-31* in 1970

Epoxy adhesives have been used for many years in the structural bonding of load-bearing members in construction engineering. The method using bonded steel plates for post-strengthening of reinforced concrete members was already established by the mid-60s. Thirty years later experiments began with different types of polymer plates for tensile strengthening. It soon transpired that carbon fiber (CFRP) was far superior to all other types of fiber for this purpose. A long-term test on a bonded reinforced concrete beam has been running at the EMPA Dübendorf (Switzerland) ever since 1970. It was strengthened with a steel plate, bonded with epoxy resin and it has been under constant load and monitoring since then.

3 Examples of Segmental Bridges, bonded with *Sikadur*® Epoxy Adhesive

3.1 Viaduct de Chillon, the oldest segmental bridge in Switzerland bonded with epoxy resin adhesive

In Switzerland, the first bridge built with precast concrete segments bonded together with epoxy resin, was completed in 1970. This was the Viaduct de Chillon, which was also one of the earliest Segmental Bridges to be bonded with epoxy resin adhesives anywhere in the world.

Figure 3: Viaduct de Chillon, Switzerland

The Project

As early as 1960, it was known that the section of the new Lausanne – Simplon Highway (N9), behind the Château of Chillon in Switzerland, would be one of the most problematic and challenging stretches of the road. Following a design competition between several leading Consulting Engineers, who each presented alternative project design concepts (tunnels as well as viaducts), the design for this section of the highway was awarded to the scheme of J.-Cl. Piguet, Lausanne. The detailed design (calculations and drawings) was started at the end of 1965. Tenders were invited for the construction of the viaducts and the contract was awarded to P. Chapuisat Eng. and Dentan Frères contractors. They first proposed the innovative use of bonded segmental construction on the project, without changing the Consulting Engineers design for the appearance and performance of the new viaducts.

The two parallel viaducts, each 2'150 meters long with a 12 metre wide roadway having two lanes plus a hard shoulder or emergency lane, follow an extremely sinuous route. The viaducts have a longitudinal gradient of between 1.5% and 3.0%, with a maximum camber of 6% necessitated by the relatively tight curves, having a minimum radius of 700m.

The Superstructure

The viaducts are built from hollow precast segments of varying depths, joined in the form of a post-tensioned continuous box girder beam. Each viaduct is divided into five independent sections by expansion joints and supported by 22 columns and two abutments. The stability is achieved by the abutments, and a brace support in the middle of each of the three intermediate sections. The viaducts are then formed by the juxtaposition of two balanced cantilevered sections of 92 metres or 104 metres, which are symmetrical about the axis of the supporting columns. The 92 metre sections are comprised of 26 segments 3.20 metres long and four segments 2.20 metres long. The 104 metre ones have four extra segments 3.0

metres long, but otherwise, the two are identical. The precast segments are formed in hollow rectangular section 5 metres wide and of varying depths, with hollow triangular shaped flanges 4 metres wide each side of the central section, giving an overall width of 13 metres. This somewhat unconventional shape was chosen after considerable research into its performance.

This innovative segment shape has excellent structural properties and since it is ultimately entirely enclosed in service, it creates a thermal 'blanket' under the roadway, which decreases the risk of ice formation during the long periods of the year when temperatures are around freezing point for at least some time every day.

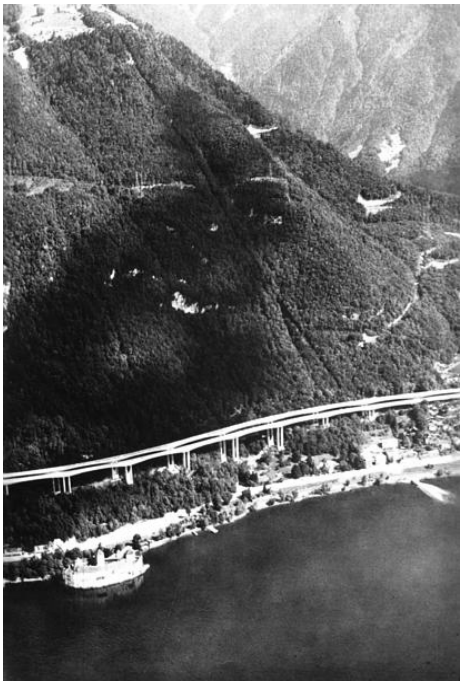

Figure 4: Viaduct de Chillon

Segment Production

The segment production and stockpiling areas were situated at the southern end of the viaduct. The production area was equipped with five segment moulding areas, which each produced one segment per day, and together had to produce 1'376 elements in two years (which represents 32'000m^3 of concrete, and 3'900 tons of steel reinforcement). The complex geometry of the viaducts demanded a very high degree of precision for that time in the production of reinforced concrete segments. This precision was achieved by the use of electronically controlled formwork, which enabled tolerances as fine as ±0.5mm to be obtained. Each segment was match cast against its future adjacent segment, which was also given its actual erected position (gradient, camber) by the use of hydraulic jacks.

Erection

The individual segments, weighing between 45 and 80 tons each, were erected by a rolling gantry (230 t) which moved along rails fixed to the bridge, maintained in a vertical position by a series of hydraulic jacks fixed to the bogies of the gantry legs. The central leg could therefore be moved sideways to facilitate the erection of the segments in the curved sections of the viaduct.

During construction the rolling gantry was extended to the next column and fixed using a temporary support on its side, the four special units were set on top of the columns and the erection of the rest of the cantilevered construction could continue at both sides.

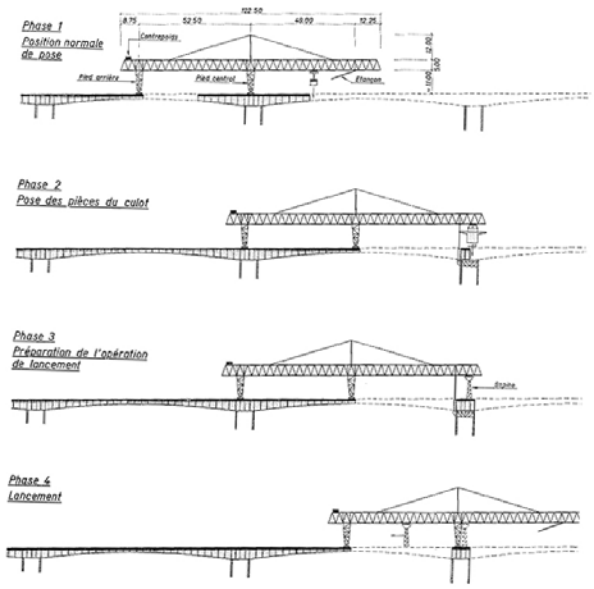

The segments were erected in pairs symmetrically placed about the columns, and the joints between them were formed from the epoxy resin adhesive. When a pair of segments had been provisionally erected, four 145 ton post-tensioning cables were installed between them. Normally, 4 pairs of segments were fixed each day. This method of construction enabled the viaduct to be built at the rate of over 300 meters per month.

The Viaducts of Chillon, 40 years after their construction, are still in continual daily use and in good condition

Figure 5: Errection of a segmental bridge

3.2 Sutong Bridge, China, the longest cable stayed bridge in the World

Figure 6: Sutong Bridge, China

The Project

The Sutong Bridge lies between Nantong City and Changshu (near Suzhou City) in the east of Jiangsu Province (Eastern China), an important route across the Changjiang River in the national key highway system for the Ministry of Communications. This project is on a massive scale and will be one of the most complex ever built in China.

The total length of the Sutong Bridge is 32.4 km. It consists of three sections: the north bank link, the main crossing and the south bank link.

The whole project requires 200’000 tons of steel, one million cubic metres of concrete for the bridge and culverts and 3 million cubic metres of earthworks. The total investment for the project is more than RMB 6 billion (about US $ 750 Mio.) and the programmed construction period is 6 years from 2003 to 2009.

Figure 7: Errection of the Sutong Bridge

The Main Crossing:

Total length is 8’206 m.

The main bridge is a double-cable-plane, double-tower steel box girder, cable-stayed bridge with sections of 100 + 100 + 300 + 1088 + 300 + 100 + 100 = 2088m. This will be the largest bridge of this type in the world. The central channel consists of a140 + 268 + 140 = 548 m

T-type steel girder bridge, which is the second largest of this type in the world. Both the north and south approach bridges to the Links are both 30 + 50 + 75 m sections of pre-stressed concrete continuous box girder bridges.

The North Bank Link:

The total length is 15.1 km and there will be two interchanges, a Tollgate on the main highway and a Service Zone.

The South Bank Link:

The total length is 9.1 km, and there will be one interchange.

4 CFRP-strengthened engineering constructions bonded with epoxy resin

Since the mid-90s, CFRP (carbon fiber reinforced plastic) -plates have been used for flexural strengthening on many structures such as bridges, which either have stability problems or need their maximum working load classification increased (ie maximum axle load).

A General Building Authority Approval (AbZ, Z-36.12-29) for the shear strengthening of load-bearing reinforced concrete members with CFRP plates has existed In Germany since November 1997. The epoxy adhesive defined here is an essential component. To utilise the high-performance CFRP plate material to the limit of its capacity, post-tensioning systems meeting

the requirements of ETAG 013 have also been developed. These high-strength tendons can only be anchored by a combination of mechanical pressure and the epoxy adhesive bond.

Figure 8:
BAB A6 Heilbronn-Bridge over River Neckar with *Sika Leoba CarboDur®, SLC II*

Figure 9:
BAB A3 Bridge ICE-Access, CFRP-Carbodurplates with *Sikadur®-30*

Approval Z-36.12-29 requires the formulation of the epoxy adhesive *Sikadur®-30* to be filed at the Deutsche Institut für Bautechnik (DIBt). With the Declaration of Conformity (Ü-mark), the manufacturer must certify this for its production and have it checked by an external quality control agency (DUE). The approval also covers all of the other important criteria and conditions such as the area of application, substrate preparation, installation, ambient environment and conditions etc. The qualifications of the contractor (proof of competence/training) are also defined.

5 Bonding of UHPC with epoxy resin

Figure 10: Toll station for the Millau Bridge

In 2004, on the approach to what is now the tallest bridge in the world, near Millau in Southern France, a 98x28m curved concrete structure was produced – the roof of the toll station spanning the new section of the A75 motorway. 54 separate curved elements made of UHPC were assembled with prestressing strands.

The high-strength bond between the elements was achieved with Sikadur® epoxy resin based adhesive.

In July 2007 a bridge was opened across the River Fulda at Kassel in Germany which is again constructed in Ultra High Strength Concrete. Following several development and trial

projects, Kassel University put its knowledge and experience into practice on the 136m long Gärtnerplatz Bridge. This pedestrian and cycle path bridge is designed for vehicles up to 5 tons. It consists of a lattice steel frame. The 2 top chords and the 5m wide bridge deck consist of precast UHPC sections containing steel fibres. For the first time in the world, these load-bearing units were only joined by bonding. It was decided to use the epoxy adhesive *Sikadur® 30 DUE* for this bonding. The reasons were its long-term experience, the Z-36 approval and naturally also the research work carried out for this project at Kassel University. The construction company already had many years of experience in bonding CFRP strengthening systems and together with the precast segment producer; they developed new methods and systems to level the precast units both longitudinally and transversely during erection with the epoxy adhesive.

Figure 11:
Gärtnerplatz-Bridge, placing the UHPC-elements and bonding with *Sikadur® 30 DUE*

Figure 12:
Opening-celebration at 11. July 2007

6 References

[1] Bänziger H.; Steiner W. Sika AG: Epoxy resins for high-strength adhesive bonds 1989

[2] Deutsches Institut für Bautechnik: General Building Authority Approval Z-36.12-29 Sika CarboDur®, 11.11.1997

[3] Bundesanstalt für Straßenwesen, Working instructions for analysis of the durability of post-tensioned reinforcement on older prestressed concrete superstructures, 1998

[4] Fehling, E.; Bunje, K.; Schmidt, M.; Schreiber, W.: UHPC bridge across the River Fulda in Kassel – Conceptual Design Calculations and Invitation to Tender. Intern. Symp. on UHPC, Schriftenreihe Baustoffe und Massivbau, Vol. 3, Kassel 2004

[5] Schmidt, M.: Kassel University Test Report
Durability of adhesive bonds on UHPC members for construction of the new Gärtnerplatz bridge across the River Fulda in Kassel, May 2005

[6] Andrä, H.P.; Maier, M.: Rehabilitation of bridges with a new generation of CFRP-prestressing - tendons. Bauingenieur Band 80, Jan. 2005

[7] Peters, H.: Experience with Sika CarboDur® plates, Beton- und Stahlbeton 101 (2006) Vol. 9

[8] Zilch, K.; Niedermeier, R.: Strengthening with prestressed CFRP –plates, International symposium: Strengthening and refurbishing of RC-structures, Innsbruck Jan. 2007; Berlin Sept. 2007

Susanne Freisinger
Dipl.-Ing.
University of Kassel
Kassel, Germany

Gregor Wisner
Dipl.-Ing.
Technical University Braunschweig
Braunschweig, Germany

Ralf Krelaus
Dr. rer. nat.
University of Kassel
Kassel, Germany

Michael Schmidt
Prof. Dr.-Ing. habil.
University of Kassel
Kassel, Germany

Stefan Boehm
Prof. Dr.-Ing.
Technical University Braunschweig
Braunschweig, Germany

Klaus Dilger
Prof. Dr.-Ing.
Technical University Braunschweig
Braunschweig, Germany

Structural and semi-structural adhesive bonding of UHPC by modifying the surface and close to surface layers

Summary

Bonding on concrete with polymer based adhesives rather than mortar is well established for decades. The significantly low tensile strength of layers close to the surface of standard concrete parts is the main limitation for optimal utilization of the concrete substrate. In contrast, the tensile and shear strength at the surface of Ultra-High-Performance Concrete (UHPC) are excellent requirements for the use of structural adhesive technology. For optimal utilization of semi-structural or even structural adhesive bonding of UHPC parts the substrate surface, the thin layer close to the surface and the adherence of appropriate polymer adhesives on it has to be investigated. The Gaertnerplatz bridge in Kassel is the first bridge, whose structural UHPC precast elements are bonded exclusively by adhesive. [3], [4]

Keywords: *surface modification, structural adhesive bonding, steel fibre reinforcement, workability, ductile cracking, two-part epoxy resin, two-part polyurethane resin, layers close to inner formwork*

1 Target

The results presented in this paper come from a research project which has the aim to investigate adequate surface treatments together with different adhesive systems in consideration of typical environmental situations. The main topic presented here is the optimization of UHPC with special remark on grain and steel fibre reinforcement and their effects on close to surface layers when bonded with suitable adhesives. The experimental should indicate the abilty of activating steel fibres for structural and ductile behaviour of bonded joints and display a possible weaker layer close to formwork in comparison to the core concrete.

2 Materials

The mixtures of investigated UHPC substrates are made of three basic compositions [1] which differ in steel fibre content and maximum grain size. The specifications of the eight investigated mixtures of UHPC are shown in Table 1.

Table 1: Mixtures of UHPC

		M1	M2	M3	M4	M5	M6	M7	M8
Steel fibre 17 mm	kg/m^3	77	134	192	77	134	192	78	136
CEM I 52,5 HS-NA	kg/m^3	733			832			650	
Water	kg/m^3	161			166			158	
Sand 0/0,5	kg/m^3	1008			975			354	
Quartz powder 1	kg/m^3	183			207			325	
Quartz powder 2	kg/m^3	0			0			131	
Micro silica	kg/m^3	230			135			177	
Basalt 2/5	kg/m^3	0			0			298,53	
Basalt 5/8	kg/m^3	0			0			298,53	
HRWRA	kg/m^3	28,5			29,4			30,4	
		M1Q			M2Q			B4Q	

Mixtures M4, M5 and M6 contain more cement and less sand than M1, M2 and M3 and the maximum grain size is the sand part with up to 0,5 mm. Mixtures M7 and M8 have additional basalt grain with a maximum grain size of up to 8 mm. Mixtures M1, M4 and M7 have a fibre content of 1,00 volume-%, M2, M5 and M8 of 1,75 volume-% and M3 and M6 of 2,50 volume-%. The specifications of steel fibres are shown in Table 2.

Table 2: Specifications of steel fibre reinforcement material [2]

	geometry		specific density	modulus of elasticity	tensile strength
steel fibre	Length = 17 mm Diameter = 0,15 mm		7,85 kg/dm^3	210.000 N/mm	2300 N/mm

The research project started with 14 different adhesives, eight two-part epoxy resin types (EP) and six two-part polyurethane resin types (PUR) to study the workability and adhesion on UHPC substrates. Some of the EP types are filled with quartz sand for a thixotrope behaviour whitch allow thick layers and bonding of vertical structures. Some specifications regarding the workability of the selcted adhesives are shown in Table 3.

Table 3: Workability of selected adhesives after material screening on UHPC (5 out of 14)

adhesive	**chemical basis**	**sand filled**	**density** kg/m³	**application temperature**	**working time** at 20 °C	**consistancy** at 20 °C
adhesive - 1	two-part EP	yes	1,6	10 – 25 °C	90 min.	thixotrope
adhesive - 2	two-part EP	no	1,65	8 – 30 °C	40 min.	viscous
adhesive - 3	two-part EP	no	1,5	5 – 35 °C	60 min.	viscous
adhesive - 4	two-part PUR	no	1,52	7 – 35 °C	60 min.	viscous
adhesive - 5	two-part EP	yes	1,65	8 – 35 °C	60 min.	thixotrope

3 Experimental

3.1 Bonded joints in 4-point bending strength test

The screening of all 14 adhesives were made by 4-point bending tests of mid-bonded UHPC prisms, see Figure 1. Concrete prisms (40 mm x 40 mm x 160 mm) were cutted in two half parts and the sawed surfaces were sandblasted with an abrasion depth of about 1mm. These prepared surfaces were adhesively bonded with a joint thickness of 3 mm. After a hardening period of seven days stored under norm climate (20°C, 65% relative humidity) the prisms were tested.

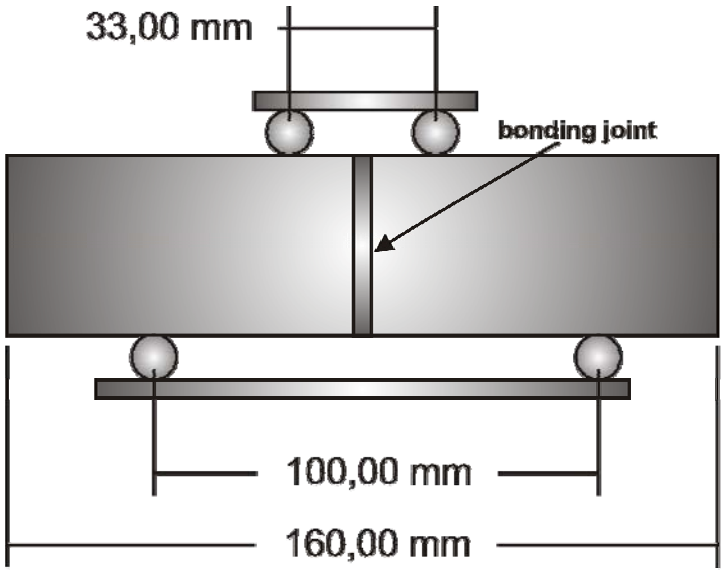

Figure 1: Bonded prism (40mm x 40mm) in 4-point bending strength test

3.2 Selection of adhesives

The selection of 5 adhesives out of 14 available were made by considering different boundery conditions and criterias. Two-part epoxy adhesives are most common for structural bonding of concrete, steel and fiber reinforcements on construction sites and a range of different types are developed for different fields of application [5]. Two-part polyurethane adhesives allow at least some semi-structural bonding and they are suitable for mechanically flexible joints. During application of PURs the substrates should not contain water on the surface because of an immediate reaction of the isocyanate component with water. The

adhesive foams immediately and can not react properly. One of the investigated PURs showed a structural bonding strength on a typical average level of some two-part epoxy adhesives. Together with acceptable workability and type of failure this PUR (adhesive - 4) were selected for further testing within the project. In addition four of the two-part epoxy adhesives were also chosen because of the highest bonding strength, good workability and a failure by cracking usually in the substrate close to the bonded joint.

The substrate of UHPC prisms was mixture M1, the surface modification was sandblasting and the prisms were bonded at the sawed area. The five adhesives where chosen according to the following rules:

- level of average bending strength
- workability (viscosity high enough and long working time)
- fracture pattern (adhesive failure is the most critical case and fractures in concrete close to adhesive layer is the desired failure because of utilisation the ductility of the compound out of concrete and steel fibers)

The fracture patterns proved to be very different [6]. Some prisms bursted in concrete only, some showed cohesive failure through the adhesive joint, most specimen failed across the joint or close to contact surface in concrete. The results of max. bonding strength in 4-point bending configuration of the five selected adhesives on UHPC substrates are displayed in Figure 2.

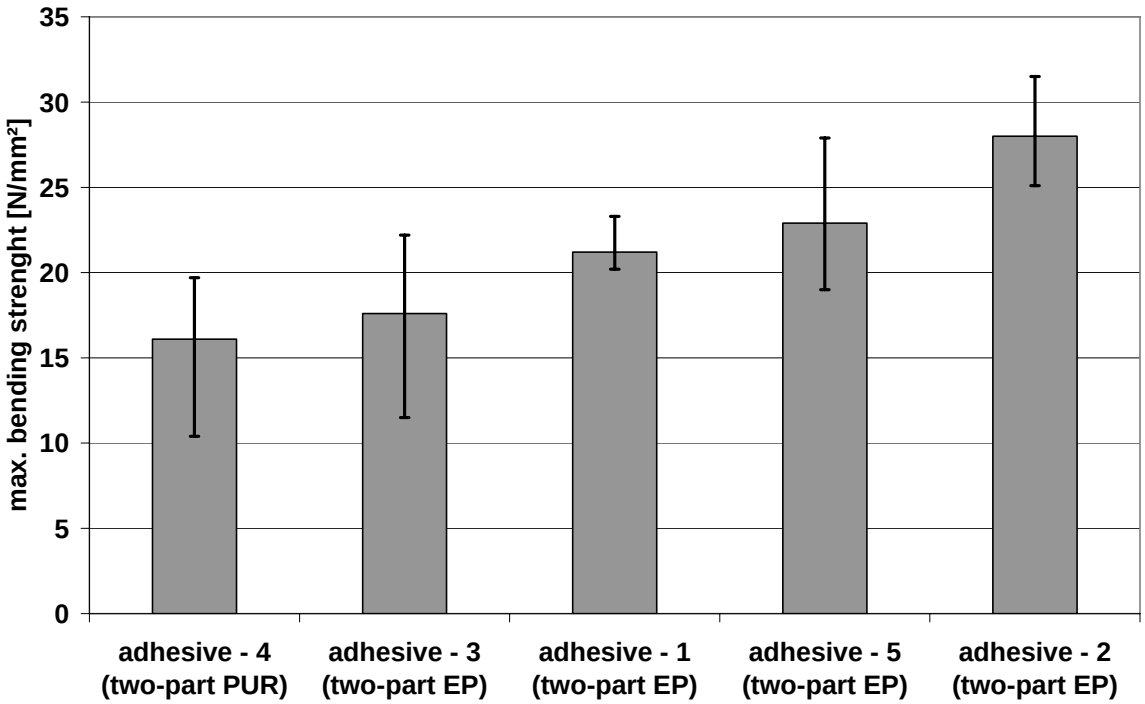

Figure 2: Results of five selected adhesives out of the 4-point bending strength test, displayed are the average out of three specimens and the range of results

3.3 Comparison of bonding on modified surfaces of formwork layers and core concrete

At construction sites or at prefabrication plants where concrete structural parts are produced it is most common that the formwork surface of the concrete is modified by sandblasting or grinding. This preparation removes weak layers and provides an excellent basis for adhesive bonding with mortars or polymer adhesives. A sawed surface displays the core concrete and there is usually no need for extra modification.

To investigate the difference on mechanical strength of UHPC substrates provided by the close to formwork layers on the one hand and the core material of UHPC on the other, some additional testing with prisms made of mixture M4 were conducted. The results are displayed in Figure 3. The values for bonding strength are always higher at the sawed surfaces than at formwork surfaces. This indicates a weaker outer surface layer in comparison with the core concrete material even on UHPC substrates but the scale of results is far beyond of results usally known from standard concrete substrates. In some cases adhesives bonded on the sawed surfaces provide a very high bonding strength so that it is in the same region as the non cutted prisms of mixture M4, where the average of the measured bending strength is displayed for comparison reasons.

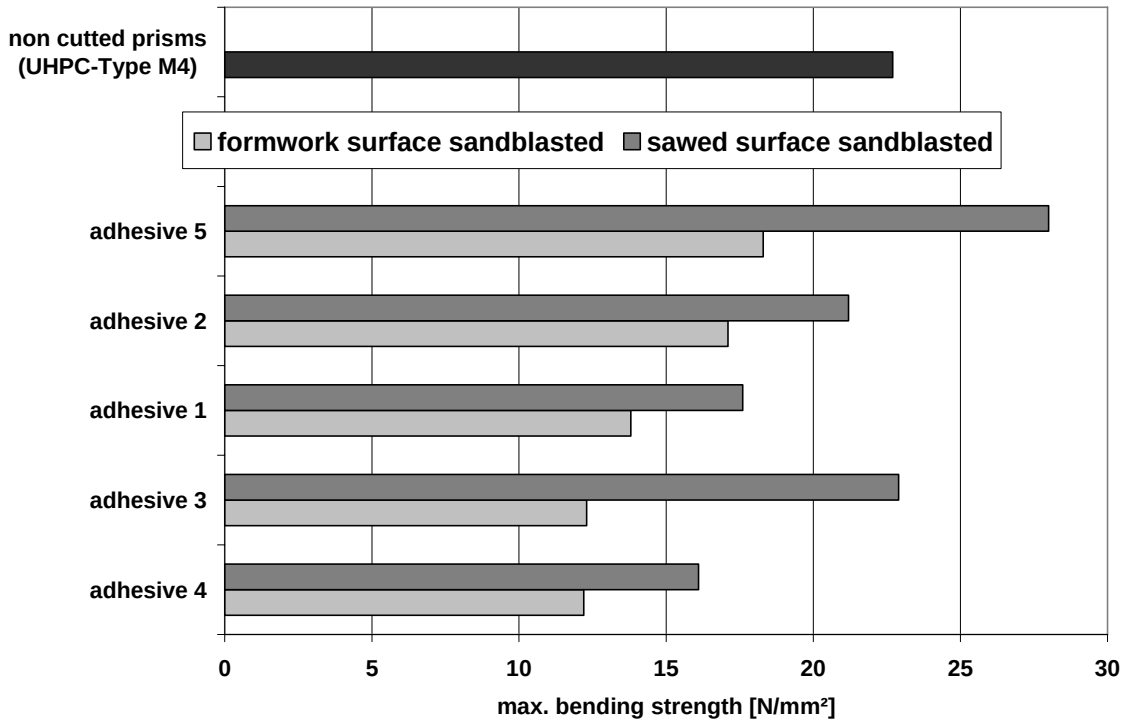

Figure 3: Comparison of bending strength on formwork surface vs. sawed surface, both sandblasted, also displayed is the average of uncutted prisms tested

3.4 Optimization of UHPC with special remark on grain and steel fibre reinforcement and their effects on close to surface layers

This research project includes three different modification methods compared with unmodified surface. These are

- sandblasting
- grinding and
- retarders at surface layer

At that time only sandblasted and unmodified surfaces are investigated, see Figure 4.

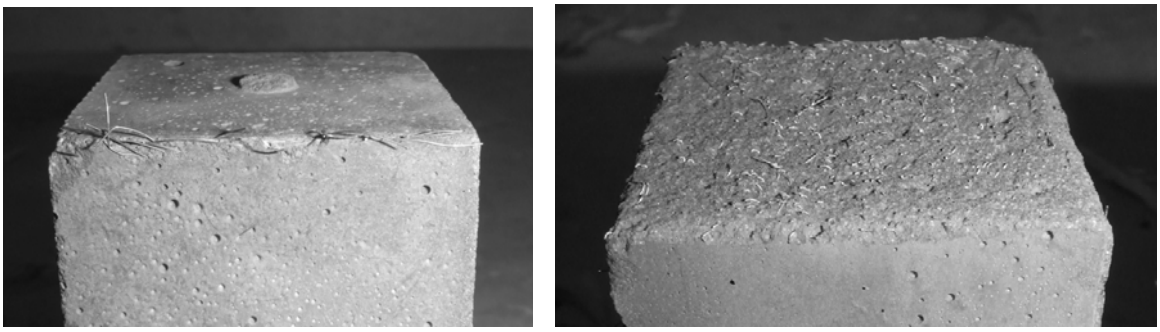

Figure 4: Unmodified formwork surface (left) and sandblasted surface (right) of UHPC prisms with the dimensions 40 mm x 40 mm of lateral cut

One aim of the research project is the optimal modification of the surfaces in that way that bonded structural members burst only in concrete because steel fiber reinforced concrete provides a ductile failure reaction, what is most important for safety reasons [7]. In the following diagram (Figure 5) the deformation behaviour of three prisms in the 4-point bending test is displayed. All three specimen showed ductile behaviour with no sudden failure.

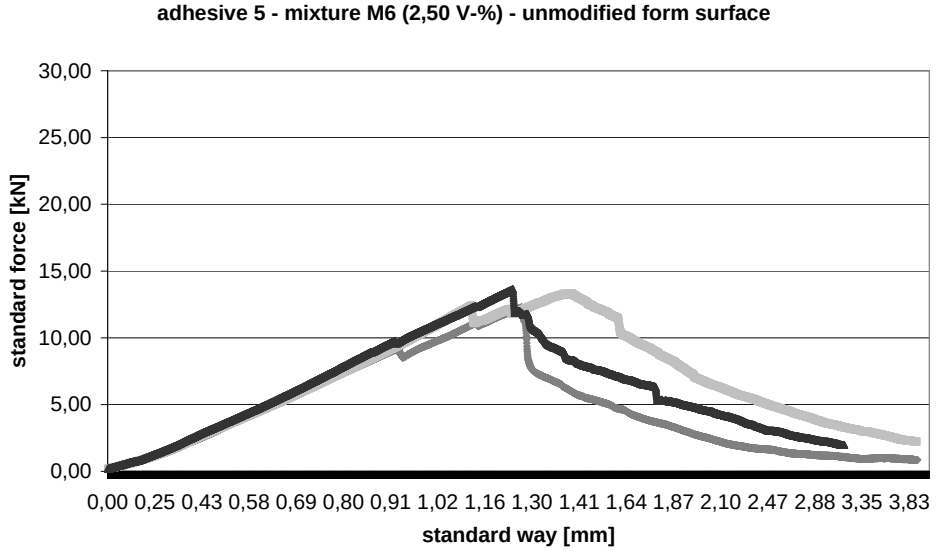

Figure 5: 4-point bending test of 3 bonded prisms (adhesive 5 on mixture M6)

In the following Figure 6 a matrix of the achieved bending strengths with the chosen five adhesives on five different mixtures are displayed. At the moment it seems to be, that mixture M6 is one of the best of all mixtures with sandblasted surface. It provides highest values for bending strength and evidences a ductile behaviour. Mixture M8 evidences a ductile behaviour in nearly all cases as well, but the achieved bending strength is lower. Mixture M8 has a maximum grain size of 8 mm, M6 of only 0.5 mm, so a macroscopic coarse-grained mixture provides not necessarily more adhesion. In comparison the bonded prisms with a sandblasted surface achieved in most cases higher mechanical values and more often ductile behaviour than bonded prisms with a non-modified surface.

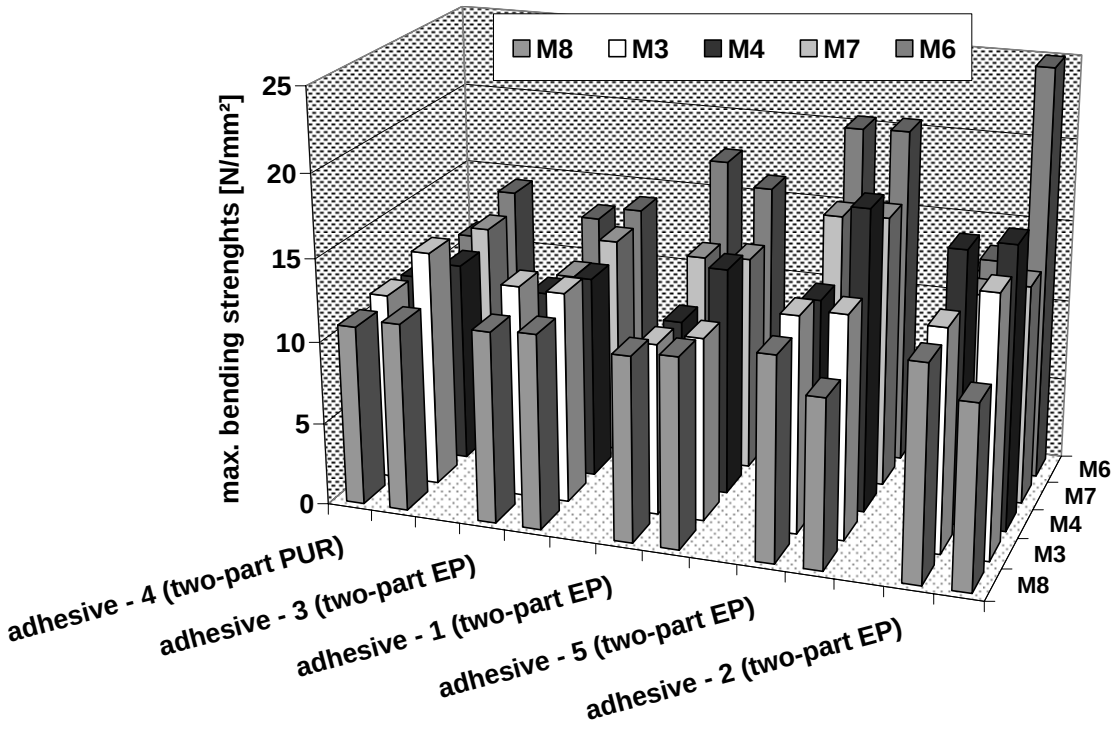

Figure 6: Comparison of achieved bending strengths with selected adhesives on different UHPC mixtures, any left column is unmodified surface, any right column is sandblasted surface (displayed are the average values of 3 prisms each)

4 Conclusions

The investigated adhesives showed appropriate bonding strenghts for bonding UHPC substrates. A modification of the thin layers close to formworks by sandblasting is a simple method to increase the bonding strength. The difference between sandblasted sawed surfaces out of the core concrete and sandblasted close to formwork surfaces amounts to 5 N/mm² in average. The bending strength of bonded prisms between sandblasted and unmodified surfaces amounts to 3 N/mm². Sandblasting the surfaces is a easy way of preparation for adhesive bonding and it showed in many cases a ductile breakdown of the joint. UHPC mixtures with a maximum grain size of 8 mm are not as strong as a mixture with

a high fibre content (2.50 V-%) and a max. grain size of 0.5 mm. Coarse grain mixtures have a similar fracture behaviour no matter if there is a high fibre content or not.

5 Acknowledgements

The investigation presented here is sponsored by budget resources of the German Federal Ministries of Economics and Labour (BMWA) and of Education and Research (BMBF), promoted by the research association AiF (Arbeitsgemeinschaft industrieller Forschung) as research project DVS 08.001/AiF 00.235 Z. The authors would like to express their thanks for this promotion and support.

6 References

[1] N. N.: DAfStb-Richtlinien für hochfesten Beton, Deutsche Ausschuss für Stahlbeton, Berlin 1995

[2] Bornemann, R.; Faber, S.: UHPC with steel- and none-corroding high-strength polymer fibres under static and cyclic loading, Proceedings 1st International Conference on Ultra High Performance Concrete, p. 673 - 682, Kassel University Press, 2004.

[3] Schmidt, M.; Krelaus, R.; Teichmann, T.; Fehling, E.; Herget, E.: Kleben von UHPC-Bauteilen bei der Gärtnerplatzbrücke in Kassel/Gluing UHPC structural members for the Gärtnerplatz Bridge in Kassel. BFT International, 73(10), p. 12–20, 2007.

[4] Schmidt, M.; Krelaus, R.; Teichmann, T.; Leutbecher, T.; Fehling, E.: Fügen von Bauteilen aus UHPC durch Kleben. Voruntersuchungen und Anwendung bei der Gärtnerplatzbrücke in Kassel. Beton- und Stahlbetonbau, 102(10), p. 681–690, 2007

[5] Swamy, R.N.; Jones, R.; Charif, A.: Shear Adhesion Properties of Epoxy Resin Adhesives, Proceedings of the International Symposium Adhesion between Polymers and Concrete, p. 741 - 755, RILEM, Chapman and Hall, London - New York, 1986.

[6] N. N.: DAFstb-Richtlinien für hochfesten Beton, Deutsche Ausschuss für Stahlbeton, Berlin 1995 Hranilovic, M.: Failure Criteria for Structural Joints, Proceedings of the International Symposium Adhesion between Polymers and Concrete, p. 650 - 660, RILEM, Chapman and Hall, London - New York, 1986.

[7] Deutschmann, K: Duktiler Hochleistungsbeton mittels geeigneter Ausgangs- und Zusatzstoffe, DAfStb-Forschungskolloquium Leipzig 1998, S. 181 - 194, Deutsche Ausschuss für Stahlbeton, Berlin 1998

Part 7:

Structural Behaviour and Testing

Hugues Vogel
Ph.D. Candidate
University of Manitoba
Winnipeg, Canada

Shahryar Davoudi
Ph.D. Candidate
University of Manitoba
Winnipeg, Canada

Martin Noël
Undergrad. Stdt.
University of Manitoba
Winnipeg, Canada

Dagmar Svecova
Associate Professor
University of Manitoba
Winnipeg, Canada

Evaluation of Properties of High Strength Concrete for Prestressed Concrete Prisms

Summary

The current project will study the use of high strength concrete in Prestressed Concrete Prisms (PCPs), which present an alternate reinforcing technique in concrete structures. The higher concrete tensile strength prevents splitting of the concrete cover upon release of prestress and also allows the elements to remain uncracked under service loads, which improves flexural rigidity with consequent reduction in deflection and crack width. Tests performed on standard cylindrical specimens have revealed a compressive strength of up to 95 MPa at 3 days and 140 MPa at 28 days, which exceeds the 120 MPa lower bound value for Ultra High Performance Concrete (UHPC). This paper will discuss the gain in both tensile and compressive strength, Poisson's ratio and stress-strain relationship for UHPC used in the research.

Keywords: *high strength concrete, tensile strength, Poisson's ratio, elastic modulus, prestressed concrete prisms, stress-strain relationship*

1 Introduction

The concrete mix used in this project was selected from the Portland Cement Association (PCA) Research and Development Bulletin RD104 [1]. The report presents engineering properties of commercially available high strength concrete obtained from six separate mixes over a period of three years. The mix with the highest strength gain was selected since the project involves prestressing of concrete elements and requires the earliest release date to minimize relaxation losses within the tendon. The mix has the highest silica fume content out of the six designs proposed by the report, which provides the lowest water absorption rate as well as the lowest permeability to chlorides. The advantages are significant when considering protection of the reinforcement to environments that are susceptible to entice deterioration.

The proportions of the mix are listed in Table 1. Aside from including the use of silica fume, the low water-cement ratio of the mix requires the use of a High Range Water Reducer

(HRWR) to achieve an acceptable level of workability during each cast. A retarder was also included in the mix to maintain workability and allow sufficient time to cast the elements before reaching the setting time. The weight of silica fume is in terms of its dry weight and the maximum size of aggregate was chosen as 12.5 mm.

Table 1: Concrete Mix Proportions

Parameters [/m^3]	**Quantity**
Cement Type I [kg]	564
Silica Fume [kg]	89
Coarse Aggs. SSD [kg]	1068
Fine Aggs. [kg]	593
HRWR Type F [l]	20.11
Retarder Type D [l]	1.46
Water [kg]	144
Water:Cementitious Ratio	0.220

2 Mechanical Properties of the High Strength Concrete Mix

Cylindrical concrete specimens with 100 mm diameter and 200 mm height were tested in accordance with ASTM Standard C39/C39M-04a [2], C496/C496M-04 [3] and C469-02 [4] for respectively determining the compressive strength, splitting tensile strength and elastic modulus. All tests were performed with a 1350 kN hydraulic testing machine. The test setup is shown in Figure 1(a) for compressive tests and in Figure 1 (b) for splitting tensile tests.

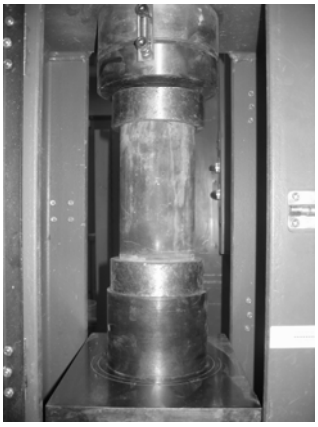

(a) Compressive Strength

(b) Tensile Strength

Figure 1: Cylindrical Concrete Test Setup

2.1 Compressive Strength

A total of 3 specimens were tested in compression at approximately 3, 7, 14 and 28 days. Compressive strengths recorded from each of these tests were averaged for each testing day and each of the three sets of 50 mm by 50 mm by 2450 mm PCPs cast in this project. Results are shown in Table 2. In order to maintain constant moisture content during all

compressive tests, specimens were taken out of the curing room 24 hours prior to testing. The curing room maintains relative humidity at 100% with temperatures averaging 20^{o}C and the procedure was considered on the basis of work presented by Li [5], which suggests that water absorbed in the pores of concrete specimens lead to transverse bursting stresses that can greatly influence the compressive strength of cylindrical specimens and therefore consistency in the results.

Table 2: Compressive Strength Development [MPa]

PCP SET #1		**PCP SET #2**		**PCP SET #3**	
Age	**Strength**	**Age**	**Strength**	**Age**	**Strength**
4	98.7	3	85.6	3	83.1
8	123.8	7	110.8	9	112.4
14	131.9	13	122.1	14	122.5
28	139.2	28	133.5	28	130.8

2.2 Splitting Tensile Strength

At each of the days selected for testing, an additional 3 specimens were set aside to determine and investigate splitting tensile strength. In order to control the effects of moisture on strength, specimens intended for tensile tests were also taken out of the curing room 24 hours prior to testing. Results in terms of age at testing are graphically illustrated in Figure 2 (a).

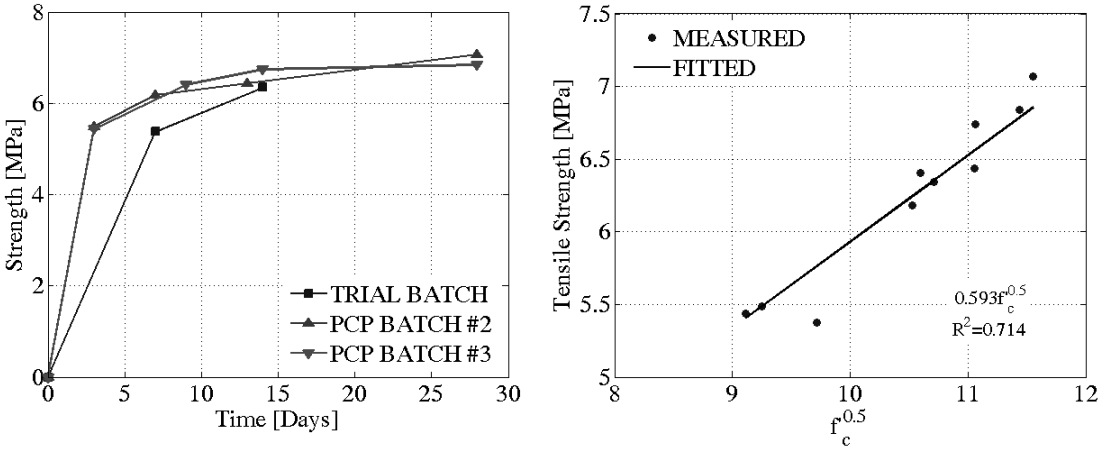

(a) with Age (b) with Compressive Strength

Figure 2: Tensile Strength Development

Tensile strength values typically display a linear trend with the square root of the compressive strength [6]. Figure 2(b) clearly demonstrates the result, which holds true at all ages since tensile and compressive strengths display similar variation over time. A relationship describing this trend was obtained by fitting a linear model to the measured data on the basis of a least squares method. It is expressed in equation (1) and has a correlation coefficient of 0.714, which suggests a strong relationship with the linear model explaining 71.4% of the variation in the measured values about the mean.

$$f_{sp} = 0.593\sqrt{f'_c} \qquad (1)$$

The splitting tensile strength is mainly used in the design of structural lightweight concrete members to evaluate shear resistance provided by concrete and to determine the development length of reinforcement [3]. Consequently, results from the splitting tensile test cannot be directly applied to determine the cracking strength of PCP reinforcement in this project. However, some approximate relationships exist that can be used to correlate values obtained from the splitting tensile test to those required for the project [7].

According to Collins and Mitchell [7], the direct cracking strength of concrete can be taken as 65% of the strength obtained from a splitting tensile test. Using test results presented for splitting tensile strength gives the following relationship for describing the strength of concrete selected for this project in direct tension. Equation (2) correlates quite well with that suggested by the reference, which relates direct tensile strength to 33% of the square root of the compressive strength.

$$f_{dt} = 0.385\sqrt{f'_c} \qquad (2)$$

3 Elastic Modulus and Poisson's Ratio

Elastic modulus and Poisson's ratio were measured during 14 and 28 day compressive tests. From each set of compression tests, two cylindrical concrete specimens were instrumented with 60 mm long 90^o cross electrical resistance strain gauges. The sensor was capable of measuring longitudinal as well as transverse strains to the nearest millionth. A 12-channel data acquisition system was used to collect stress readings from the testing machine as well as strains from the sensor. Elastic modulus values shown in Table 3 were determined by fitting a linear trend through diagrams relating the stress and longitudinal strain data. Results for Poisson's ratio displayed in

Table 4 were obtained by evaluating the relationship between transverse and longitudinal strains with an approach similar to that used for estimating elastic modulus. The linear regression analyses were performed for a longitudinal strain range extending from 50 millionths to that corresponding to a stress of 40% of ultimate.

Table 3: Elastic Modulus Development with Compressive Strength [MPa]

PCP SET #1			PCP SET #2			PCP SET #3		
Age	**Strength**	**Modulus**	**Age**	**Strength**	**Modulus**	**Age**	**Strength**	**Modulus**
7	-	-	8	112.9	38 945	9	117.3	43 293
	-	-		93.7	42 750		106.2	43 276
14	129.4	46 409	13	123.8	46 336	14	122.9	43 411
	135.1	44 897		129.7	46 423		128.8	46 595
28	142.7	44 009	28	137.3	44 134	28	129.8	46 581
	137.1	47 716		136.7	44 531		125.6	43 716

Table 4: Poisson's Ratio

PCP SET #1		PCP SET #2		PCP SET #3	
Age	**Ratio**	**Age**	**Ratio**	**Age**	**Ratio**
7	-	8	0.211	9	0.228
	-		0.190		0.215
14	0.251	13	0.248	14	0.235
	0.227		0.246		0.235
28	0.217	28	0.241	28	0.251
	0.229		0.230		0.222

While elastic modulus values for concrete appear to increase with compressive strength, those for Poisson's ratio remain consistent over the complete range of ages considered for testing. The ratios appear to fluctuate between 0.190 and 0.251 with a respective mean and standard deviation of 0.221 and 0.031. The mean of this distribution can be expected to vary within a margin of error of 0.004 at a 95% confidence level.

3.1 Stress-Strain Relationship in Compression

Thorenfeldt [8] has generalized expressions given by Popovics [9] that represent well the family of stress-strain curves for concrete of different strengths. Although more complex in form than the parabolic model, the relationship of equation (3) should offer higher potential in estimating the stress-strain behavior of high strength concrete presented in this paper.

$$\frac{f_c}{f'_c} = \frac{n\left(\varepsilon_{cf}/\varepsilon'_c\right)}{n-1+\left(\varepsilon_{cf}/\varepsilon'_c\right)^{nk}} \qquad (3)$$

In this equation, f_c is the compressive stress, ε_{cf} is the longitudinal compressive strain, ε'_c is the peak strain when stresses reach the compressive strength, n is a curve fitting factor, and k is a factor to increase the post peak decay in stress. Stress readings obtained from each of the instrumented compressive tests were plotted against longitudinal strain and compared with the estimate provided by equation (3). Results from the comparison are shown in Figure 3(a) for a 14 day compressive test performed on a cylindrical concrete specimen from the second set of PCPs. The figure also contains the progression of transverse and volumetric strains with compressive stress along with the progression of transverse strains with longitudinal strains in Figure 3(b).

The descending branch of the curve describing stress as a function of longitudinal strain is not required for estimating the behaviour of PCP reinforcement in tension for this project and therefore not captured during compressive tests. However, transverse ε_{ct} as well as volumetric ε_{cv} strains in Figure 3(a) clearly indicate the increase in volume of the sample due to excessive internal cracking when the compressive strength is approached. The root mean squared error (RMSE) values in Table 5, representing average error in stress expected at each strain value, were calculated to measure ability of equation (3) to estimate stress-strain behavior of concrete. Results in this table also contain RMSE values that arise from estimating behavior on the basis of elastic modulus measured during compressive tests. Although values in this table do not suggest a significant improvement in RMSE, they

strongly emphasize the influence of elastic modulus on the stress-strain behavior of concrete in compression.

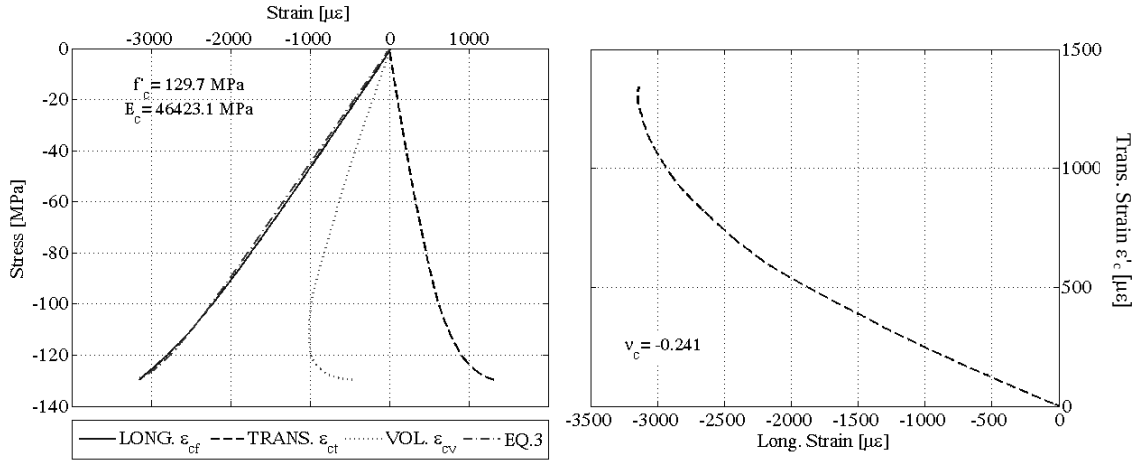

(a) Stress-Strain Behaviour (b) Poisson's Ratio

Figure 3: Testing Results at 14 Days [PCP SET #2]

Table 5: RMSE of Stress Estimation [MPa]

PCP SET #1			PCP SET #2			PCP SET #3		
Age	**EQ.3**	**Measured**	**Age**	**EQ.3**	**Measured**	**Age**	**EQ.3**	**Measured**
7	-	-	8	5.37	4.97	9	1.32	1.09
	-	-		4.77	5.10		2.33	2.73
14	2.48	2.99	13	3.17	3.66	14	1.16	0.73
	1.01	0.55		1.29	1.58		2.75	3.26
28	5.25	4.71	28	2.73	2.21	28	1.27	1.69
	1.56	2.08		1.87	1.35		1.31	0.87

The peak strain of equation (3) is usually expressed in terms of elastic modulus and is therefore a strong parameter influencing RMSE values in Table 5. The relationship was investigated as shown in Figure 4. Correlation coefficients are shown in the figure for elastic modulus values suggested by Collins & Mitchell [7] as well as for those measured during compressive tests. The results indicate that estimates of peak strain have higher correlation and therefore account for a higher level of variability in the results when using elastic modulus values obtained from compressive tests. The outcome was expected and results from lower RMSE values obtained from elastic modulus measured at some of the curing stages.

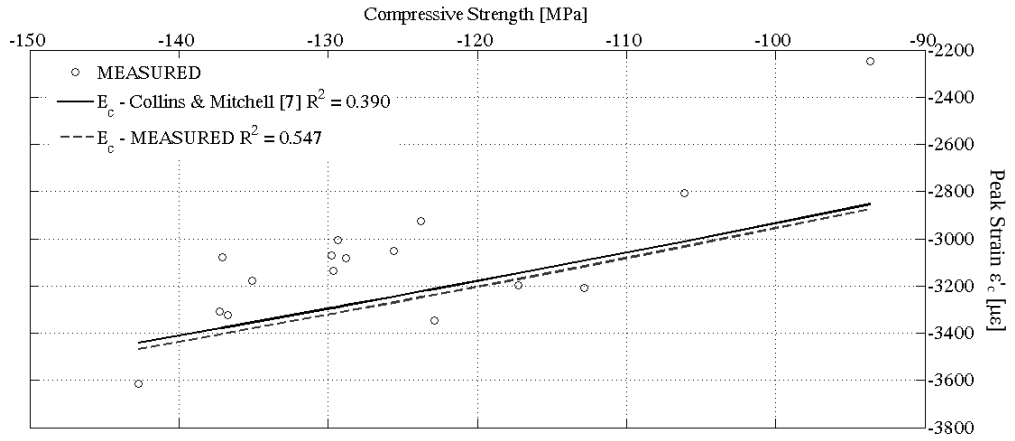

Figure 4: Trend of Peak Strain with Compressive Strength

4 Conclusions

Several conclusions can be drawn from results presented in this paper. Although a larger set of samples is required to confirm these conclusions, relationships in the literature are in close agreement with measured properties, which can be used to establish the behaviour of PCP as reinforcement in flexural members:

- The direct tensile strength obtained from splitting tensile test results presented in this paper can be written as 38.5% of the square root of compressive strength. The result agrees well with the 33% value suggested by Collins and Mitchell [7]
- The relationship for elastic modulus proposed by Collins and Mitchell [7] was modified to improve the RMSE and more adequately accounts for variability in the measured response. In order to establish a suitable comparison, adjustments were brought to the existing relationship on the basis of results obtained at 28 days of curing.
- Poisson's ratio was found to vary between 0.190 and 0.251 with an average of 0.221, which is slightly higher than the 0.15 to 0.20 range recommended for normal strength concrete in compression. The standard deviation was determined as 0.031 and the margin of error for a 95% confidence level was calculated as 0.004.
- RMSE values obtained from fitting the stress-strain relationship proposed by Thorenfeldt et al. [8] to the measured data suggests that it is reliable in estimating behavior of high strength concrete at various curing ages. The relationship can be improved by adjusting peak strain on the basis of elastic modulus measured during testing.

5 Acknowledgments

The authors would like to thank the Natural Sciences and Engineering Research Council of Canada (NSERC) for their financial support.

6 References

[1] Burg, R.G. and Ost, B.W.: Engineering Properties of Commercially Available High-Strength Concrete, Portland Cement Association Research and Development Bulletin RD104, Skokie, Illinois, USA, 1994.

[2] ASTM C39/C39M-04a: Standard Test Method for Compressive Strength of Cylindrical Concrete Specimens: Annual Book of ASTM Standards 04.02, Easton, MD, USA, S. 18-22, 2004.

[3] ASTM C496/496M-04: Standard Test Method for Splitting Tensile Strength of Cylindrical Concrete Specimens: Annual Book of ASTM Standards 04.02, Easton, MD, USA, S. 278-282, 2002.

[4] ASTM C469-02: Standard Test Method for Static Modulus of Elasticity and Poisson's Ratio of Concrete in Compression: Annual Book of ASTM Standards 04.02, Easton, MD, USA, 2004, S. 268-271, 2002.

[5] Li, G.: The effect of Moisture Content on the Tensile Strength Properties of Concrete: Masters Thesis, University of Florida, 2004.

[6] MacGregor, J.G., Bartlett, F.M.: Reinforced Concrete Mechanics and Design, First Canadian Edition., Prentice Hall, Scarborough, ON, Canada, 2000.

[7] Collins, M.P., Mitchell, D.: Prestressed Concrete Structures: Response Publications, ON, Canada, 1997.

[8] Thorenfeldt, E., Tomaszewicz, A., Jensen, J.J.: Mechanical Properties of High Strength Concrete and Application in Design. In: Proceedings of the Symposium Utilization of High Strength Concrete, Stavanger, Norway, June 1987.

[9] Popovics, S.: A Review of Stress-Strain Relationships for Concrete. In: ACI Journal 67, No. 3, 1970.

Marijan Skazlic
Dr.
University of Zagreb
Zagreb, Croatia

Marijana Serdar
University of Zagreb
Zagreb, Croatia

Dubravka Bjegovic
Dr.
Civil Engineering Institute of Croatia
University of Zagreb
Zagreb, Croatia

Influence of test specimens geometry on compressive strength of ultra high performance concrete

Summary

Existing recommendation for ultra high-performance concrete (UHPC) suggest cylinders with an aspect ratio of 2 (diameter/height) for determining compressive strength. The diameter of cylinder should not be less than 70 mm. Recommended dimension of cylinder are ϕ7×14 cm, ϕ10×20 cm and ϕ15×30 cm. None of existing recommendations for UHPC had defined conversion factors for testing compressive strength on cylinders with different geometry. This is very important for practice because UHPC is tested on different samples and there is no correlation between results.

In this paper experimental research is described in which compressive strength of different UHPC mixtures was tested on cylinders with different geometry. Furthermore, an analysis is done and conversion factors for testing compressive strength of UHPC on samples with different geometry are proposed.

Keywords: *ultra high performance concrete, compressive strength, conversion factors*

1 Introduction

Existing recommendations for UHPC suggest general rules for specimen size, such as that diameter/height ratio of cylinder should be 2 and that diameter of cylinder should be more than 70 mm. Furthermore, recommended dimensions of cylinders are ϕ7×14 cm, ϕ10×20 cm and ϕ15×30 cm (AFGC 2002, JSCE 2004). On the other hand, none of existing recommendations for UHPC has defined conversion factors for testing compressive strength on cylinders with different geometry. Since the compressive strength of concrete is the most basic and important material parameter when designing concrete structures, engineers need to have methods to test, evaluate and compare compressive strength of different concrete types measured on different specimen size in different countries (Aitcin 1994, Neville 1995, Yi et al. 2006, Yazici, Sezer 2007).

During present research different mixtures of ultra high performance concrete have been prepared and their compressive strength, tested on cylinders with different geometry (ϕ7×14 cm, ϕ10×20 cm and ϕ15×30 cm), was analysed. The aim of the research was to investigate the effect of specimen size on compressive strength of UHPC and to propose conversion factors for compressive strength of UHPC when tested on samples with different geometry.

2 Experimental program

In this research, the effect of specimen sizes on UHPC compressive strength is evaluated. During the research 10 different UHPC mixtures were prepared and tested in fresh and hardened state. After evaluating the size effect of cylinders on compressive strength, correlations between compressive strength with size of the specimen are investigated.

2.1 Mixture proportioning

UHPC mixtures were designed under the following principles (AFGC 2002, Schmidt & Fehling 2005, Skazlic 2005, Skazlic et al. 2007): compressive strength that is greater than 150 MPa, internal fiber reinforcement to ensure nonbrittle behaviour, high binder content with special aggregates and very low water content. The concrete mixture proportions are listed in Table 1. Cement type CEM II/B-M (S-V) 42,5 N is used in all mixtures. Crushed stone diabase was used as aggregate in following fractions: 0-1, 0-2, 2-4, 4-8, 8-11 mm. For reducing water demand and improve workability and consolidation of concrete superplasticizers are used in different concentrations. Water/binder ratio is between 0,16 and 0,20 in all 10 mixtures. Steel fibers (13/0,2mm, 30/0,6mm, 50/0,1mm) are added in all mixtures to improve ductility.

Table 1: Mixture proportions of UHPC

Concrete composition (kg/m^3)	**M1**	**M2**	**M3**	**M4**	**M5**	**M6**	**M7**	**M8**	**M9**	**M10**
w/b ratio	0,16	0,16	0,16	0,16	0,16	0,20	0,18	0,16	0,18	0,16
cement	1115	1115	1115	1115	1115	650	925	930	660	955
silica fume	169	169	169	169	169	65	148	140	70	171
water	204	204	204	204	204	143	193	171	131	180
superplasticizer	55,69	50	65,54	59,38	88,46	34,23	72,69	58,08	46,92	53,85
aggregate 0-1 mm	-	-	1073	1073	1073	-	-	-	-	1152
aggregate 0-2 mm	751,1	858,4	-	-	-	686,4	575,5	784,7	448,8	-
aggregate 2-4 mm	321,9	214,6	-	-	-	343,2	345,3	336,6	224,2	-
aggregate 4-8 mm	-	-	-	-	-	343,2	230,2	-	224,2	-
aggregate 8-11 mm	-	-	-	-	-	343,2	-	-	224,2	-
steel fibres 13/0,2mm	234	156	234	156	390	80	234	156	39	200
steel fibres 30/0,6mm	-	52	-	52	-	40	-	39	39	34
steel fibres 50/0,1mm	-	26	-	26	-	-	-	39	39	-

2.2 Test procedure

From every UHPC mixture 9 cylinder samples for compressive strength testing were cast: 3 cylinders size ϕ7×14 cm, 3 size ϕ10×20 cm and 3 size ϕ15×30 cm. All cylinders were demoulded after 24 h and after removal of the mould water cured for 28 days. Compression tests were carried out on Toni-technik testing press with capacity of 3000 kN. Loads were measured continuously until the specimen failed.

3 Experimental results

Compressive strengths of UHPC mixtures obtained from this experiment are shown in Table 2. Testing of compressive strength was performed on three specimens prepared from the same mixture. Mean values and standard deviation for every cylinder size and every mixture are given in Table 2.

Table 2: Compressive strength of UHPC mixtures

Mix.	Cylinder, mm	Compressive strength, MPa			Mean value, MPa	St. Dev., MPa
M1	Ø70/140	132,64	122,66	95,26	116,85	19,35
	Ø100/200	111,93	76,37	120,51	102,94	23,40
	Ø150/300	122,66	121,99	129,83	124,83	4,35
M2	Ø70/140	124,09	121,84	124,38	123,44	1,39
	Ø100/200	118,48	116,33	117,7	117,50	1,09
	Ø150/300	107,6	111,45	108,54	109,20	2,01
M3	Ø70/140	111,78	108,75	119,89	113,47	5,76
	Ø100/200	106,06	97,32	114,36	105,91	8,52
	Ø150/300	70,12	93,71	90,35	84,73	12,76
M4	Ø70/140	84,52	97,46	113,02	98,33	14,27
	Ø100/200	90,94	91,13	99,73	93,93	5,02
	Ø150/300	90,63	90,91	86	89,18	2,76
M5	Ø70/140	131,89	137,41	141,63	136,98	4,88
	Ø100/200	123,45	112,02	103,24	112,90	10,13
	Ø150/300	100,81	117,24	98,74	105,60	10,14
M6	Ø70/140	98,09	102,93	91,84	97,62	5,56
	Ø100/200	109,17	108,12	110,2	109,16	1,04
	Ø150/300	94,08	96,91	102,63	97,87	4,36
M7	Ø70/140	119,26	103,28	118,41	113,65	8,99
	Ø100/200	123,66	125,53	117,8	122,33	4,03
	Ø150/300	100,65	124,8	95,4	106,95	15,68
M8	Ø70/140	114,95	118,19	114,34	115,83	2,07
	Ø100/200	107,44	110,82	102,63	106,96	4,12
	Ø150/300	91,22	97,21	101,24	96,56	5,04
M9	Ø70/140	120,91	104,23	86,62	103,92	17,15
	Ø100/200	102,61	97,42	85,58	95,20	8,73
	Ø150/300	82,63	85,5	82,18	83,44	1,80
M10	Ø70/140	116,59	119,11	84,16	106,62	19,49
	Ø100/200	109,84	118,49	111,56	113,30	4,58
	Ø150/300	102,93	98,35	98,54	99,94	2,59

From the results of compressive strength tested on 10 UHPC mixtures, Table 2, it can be seen that the compressive strength of mixtures tested on cylinder Ø100/200 was from 93 MPa to 123 MPa. Compressive strength of tested mixtures is somewhat lower than usual compressive strength of UHPC because the specimens were cured in water and were not heat-treated which is usual procedure for UHPC curing (AFGC 2002, Tanaka et al. 2002, Skazlic et al. 2007). Compared to Ø100/200 samples, compressive strength tested on samples Ø70/140 was around 5 % higher, and was from 98 MPa to 137 MPa. On the other hand compressive strength tested on samples Ø150/300 was around 7,5 % lower than when tested on Ø100/200 and was from 83 MPa to 125 MPa. Increase and decrease of compressive strengths tested on Ø70/140 and Ø150/300 samples compared to Ø100/200 samples are shown in Table 3.

Table 3: Increase and decrease of compressive strength

Sample	**UHPC mixture**										**Mean increase**
size, mm	M1	M2	M3	M4	M5	M6	M7	M8	M9	M10	**(%)**
Ø70/140	13,51	5,05	7,14	4,68	21,32	-10,57	-7,10	8,29	9,16	-5,89	**4,56**
Ø150/300	21,26	-7,07	-20,00	-5,06	-6,47	-10,34	-12,57	-9,73	-12,36	-11,79	**-7,41**

4 Analysis of results

Figure 1 a) shows results of compressive strength when tested on Ø70/140 sample, f_{cy} (70/140 mm) as a function of the compressive strength for the same UHPC mixture when tested on Ø100/200 sample, f_{cy} (100/200 mm). Figure 1 b) shows results of compressive strength when tested on Ø150/300 sample, f_{cy} (150/300 mm) as a function of the compressive strength for the same UHPC mixture when tested on Ø100/200 sample, f_{cy} (100/200 mm).

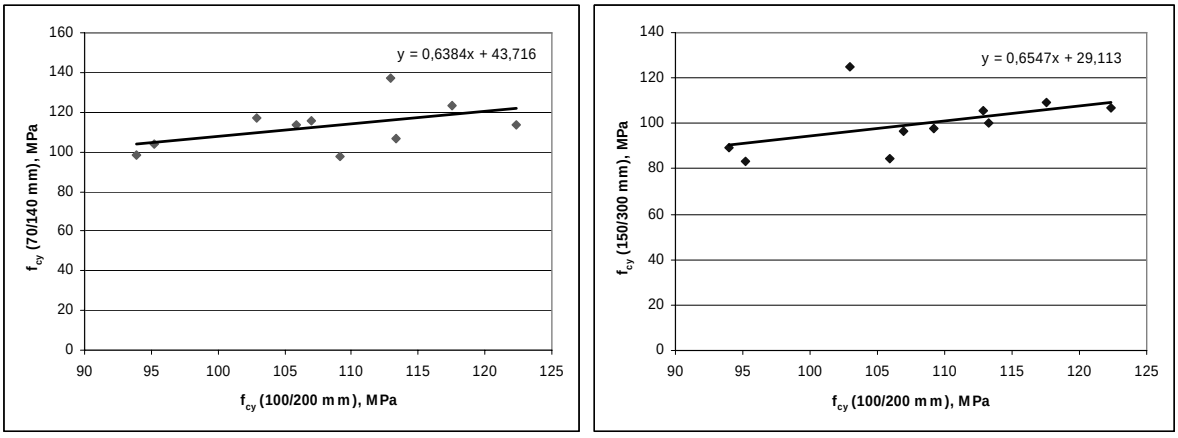

a) b)

Figure 1: a) Relationship between compressive strengths of Ø70/140 and Ø100/200 sample, b) Relationship between compressive strengths of Ø150/300 and Ø100/200 sample

From the results of the presented research conversion factors for Ø70/140 samples were calculated as ratio of compressive strength tested on Ø70/140 samples and compressive strength tested on Ø100/200 sample. Conversion factors fro Ø150/300 sample were calculated as ratio of compressive strength tested on Ø150/300 sample and Ø100/200 sample. Individual calculated conversion factors for every UHPC mixture are shown in Table 4.

Table 4: Conversion factors for compressive strength tested on samples with different geometry

Sample	**UHPC mixture**										**Mean**
size, mm	M1	M2	M3	M4	M5	M6	M7	M8	M9	M10	**value**
Ø70/140	1,14	1,05	1,07	1,05	1,21	0,89	0,93	1,08	1,09	0,94	**1,05**
Ø150/300	1,21	0,93	0,80	0,95	0,94	0,90	0,87	0,90	0,88	0,88	**0,93**

Figure 2 shows calculated conversion factors for both sample sizes (Ø70/140 mm and Ø150/300 mm) as a function of the diameter of the samples, d.

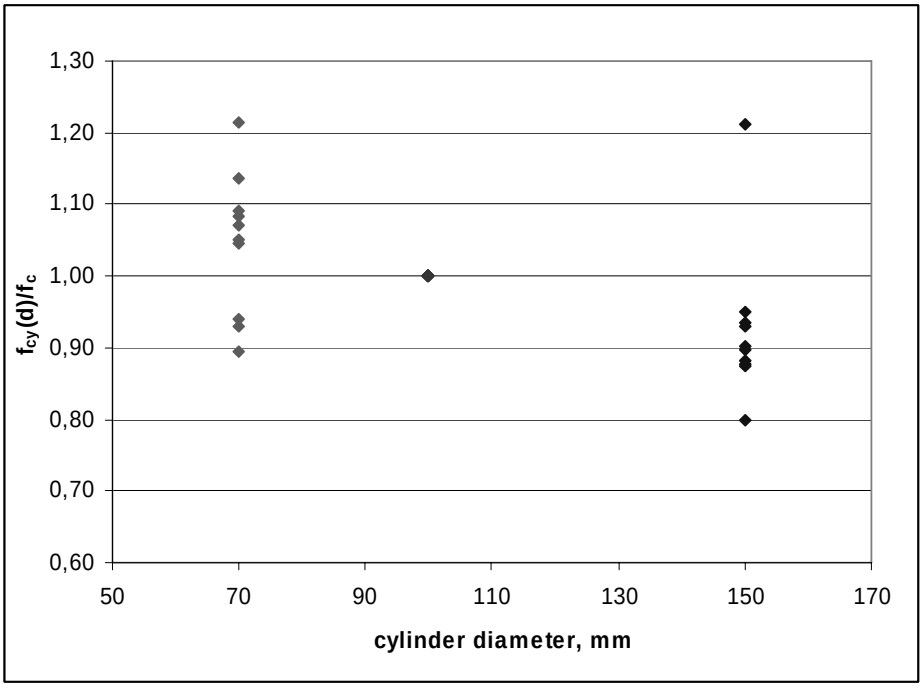

Figure 2: Effect of specimen size on compressive strength of UHPC

From Figure 2 it can be seen that that the size of specimens has influence on compressive strength and that the smaller the specimens are the larger compressive strengths are obtained. Furthermore, there is a trend in the change of compressive strength with different sample size and this trend could possible be described with adequate equation, similar to those for normal strength concrete (Yi et al. 2006). In order to perform regression analysis further research has to be performed.

Based on the results of the presented research, conversion factors for compressive strength of UHPC tested on samples with different geometry, when compared to Ø100/200, were assessed and are shown in Table 5.

Table 5: Assessed UHPC conversion factors for compressive strength

Sample size	Conversion factor for compressive strength
Ø100/200	1,0
Ø70/140	1,05-1,15
Ø150/300	0,85-0,95

5 Conclusions

In practise, it is often the case that compressive strength testing is performed on specimens with different geometry. That is why there is a need of conversion factors that would enable correlation and comparison of results gathered during testing on specimens with different size. The aim of presented research was to evaluate effect of specimen size on compressive strength of UHPC and to propose conversion factors for compressive strength of UHPC when tested on samples with different geometry.

Conversion factors were assessed comparing different specimens size to standard samples for UHPC compressive strength testing ϕ10×20 cm. Assessed compressive strength conversion factors are between 1,05 and 1,15 for specimens size ϕ7×14 cm and between 0,85 and 0,95 for specimens size ϕ15×30 cm.

In order to determine reliable and accurate values of conversion factors for compressive strength of UHPC tested on specimens with different geometry, further research is needed. It is an opinion of authors that these conversion factors should be implemented in one unique recommendation for production, design, construction and conformity assessment of UHPC.

6 Acknowledgements

This research was performed within scientific project “Modern methods of construction materials testing” (082-0822161-2996) and scientific project “The Development of New Materials and Concrete Structure Protection Systems” (082-0822161-2159) both funded by Croatian Ministry of education, science and sport.

7 References

[1] Aitcin, P. C. (1994) Effects of Size and Curing on Cylinder Compressive Strength of Normal and High-Strength Concretes, ACI Materials Journal

[2] Association Française de Génie Civil (2002), Interim Recommendations for Ultra High Performance Fibre-Reinforced Concretes

[3] JSCE (2004) Recommendations for Design and Construction of Ultra High-Strength Fiber-Reinforced Concrete Structures (UFC), Japanese Society of Civil Engineers

[4] Neville A. M. (1995) Properties of concrete, Logman Scientific & Technical, England

[5] Schimdt M., Fehling, E. (2005) Ultra-High-Performance Concrete: Research, Development and Application in Europe, Seventh International Symposium on the Utilization of High-Strength/High-Performance Concrete, Washington, D.C., USA, SP-228—4

[6] Skazlic, M. (2005) Precast Fibre Reinforced Segments of Secondary Tunnel Lining, Dissertation, Faculty of Civil Engineering, University of Zagreb (in Croatian)

[7] Skazlic, M. Jambresic, M. Dujmusic, M. (2007) Conversion Factors for Testing Strength of Ultra High Strength Concrete, Proceedings of fib symposium “Concrete Structures – Stimulators of Development”, Dubrovnik, Croatia

[8] Tanaka, Y., Musya, H., Ootake, A., Shimoyama, Y., Kaneko, O. (2002) Design and construction of sakata-mirai footbridge using reactive powder concrete, FIB 2002, Osaka-Japan, p. 417 - 426

[9] Yazici, S., Sezer, G. I. (2007) The effect of cylindrical specimen size on the compressive strength of concrete, *Building and Environment* 42 (2007) 2417-2420

[10] Yi, S., Yang, E., Choi, J. (2006) Effect of specimen sizes, specimen shapes and placement directions on compressive strength of concrete, Nuclear Engineering and Design 236 (2006) 115-127

Ana Spasojevic
PhD Candidate
EPFL
Lausanne, Switzerland

Dario Redaelli
PhD Candidate
EPFL
Lausanne, Switzerland

Miguel Fernández Ruiz
PhD, Post-Doctoral Fellow
EPFL
Lausanne, Switzerland

Aurelio Muttoni
PhD, Professor
EPFL
Lausanne, Switzerland

Influence of Tensile Properties of UHPFRC on Size Effect in Bending

Summary

Bending behaviour of members without ordinary reinforcement made of quasi-brittle materials (such as concrete or fibre-reinforced concrete) is subjected to size effect both in terms of strength and ductility. For a typical ultra-high performance fibre-reinforced concrete (UHPFRC), size effect on bending strength is less significant. In this paper, taking advantage of an analytical approach, this behaviour is confirmed if large tensile strains are developed in UHPFRC before beginning of tension softening. However, it is also shown that changes in the size of the member have a significant influence on the ductility in bending. Both results are in agreement with available experimental data. A parametric study on size effect in bending is finally performed by varying the tensile strain before beginning of tension softening and the initial slope of the tension softening law. On that basis, some considerations on the modelling and design of such members are given.

Keywords: *UHPFRC, bending, size effect, tension strain hardening, tension softening.*

1 Introduction

Ultra-high performance fibre-reinforced concrete (UHPFRC) is a new type of fibre-reinforced material, having high quantity of fibre reinforcement (usually more than 2 % in volume of metallic fibres) and a very dense matrix. UHPFRC has high compressive and tensile strengths and a ductile behaviour in tension. An interesting possibility to take advantage of UHPFRC mechanical properties in tension is to use it for thin members in bending without ordinary reinforcement. This is justified because of the significant ductility of such members and by their limited size effect on strength in bending.

Contrary to the rather ductile behaviour of UHPFRC in tension, the tensile behaviour of ordinary concrete (OC) and of fibre-reinforced concrete (FRC) is characterized by a linear elastic phase followed, after cracking, by a tension softening phase with localisation of the strains in a single crack (Figure 1a and 1b). This difference in the tensile behaviour is due to the fact that after cracking of the UHPFRC matrix, fibres can carry larger tensile forces than

the matrix itself. As a consequence, a large number of cracks develop in UHPFRC and cracking of the matrix is not directly followed by strain localisation. This phenomenon, often named multi-microcracking, results in a strain hardening behaviour characterized by a limited or no stress increase with development of large tensile strains [1] (Figure 1a). This phase will be named in this paper as *pseudo-plastic* behaviour.

The softening behaviour, characterizing the response after crack localisation, can be described in terms of the stress-crack opening relationship (Figure 1b). According to the assumptions of the Fictitious Crack Model [2], the area below the stress-crack opening relationship is the fracture energy G_F. UHPFRC is characterized by a fracture energy which is up to several hundred times that of an OC. Another significant difference between these materials is the slope of the stress-crack opening law, much larger for OC or FRC than for UHPFRC (Figure 1b).

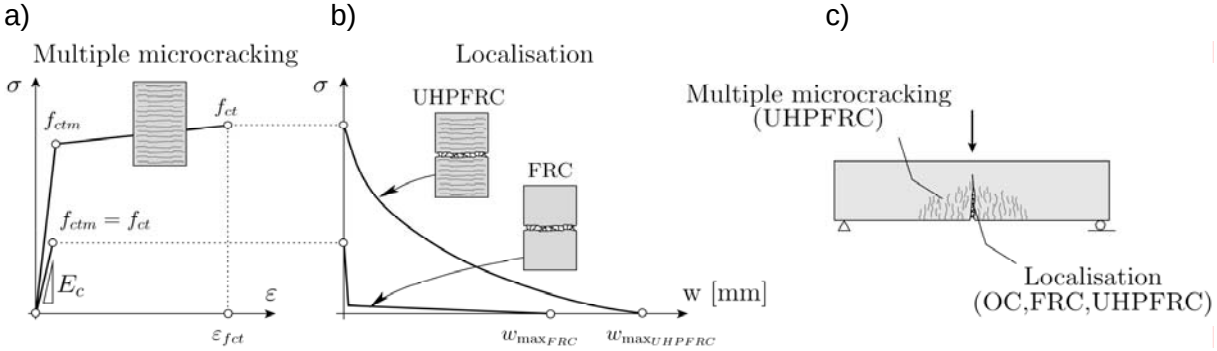

Figure 1: Qualitative comparison between the tensile behaviour of FRC and UHPFRC: a) stress-strain relationship before crack localisation; b) stress-crack opening relationship (tensile softening); c) beam in bending with crack localisation and a microcracked region.

From the point of view of fracture mechanics, both OC and FRC can be considered as quasi-brittle materials. Thus, their bending behaviour is sensitive to size effect both in terms of strength and ductility [3]. It will be shown in this paper that for quasi brittle materials that have a pseudo-plastic phase with sufficient tensile strain capacity (and for a range of thicknesses interesting for structural applications), the size effect on the bending strength is practically negligible and less significant than the scatter of test results.

This paper focuses on the behaviour of simply supported beams failing in bending. Failure is assumed to occur by the development of a discrete crack in a multi-microcracked zone (Figure 1c). The analyses presented in the paper are performed using an analytical model developed by the first author of this paper [4] based on equilibrium and energy-balance conditions. The accuracy of the analytical model has been checked against the results of a finite element model implementing the same hypotheses (fictitious crack [2] and pseudo-plastic behaviour in tension) and against experimental results on beams tested at the EPFL by the authors of this paper [4] and taken from the literature [5], Figure 2. The results shown in Figure 2 a) and b)) were obtained for beams in three-point bending with 420 mm span, whereas results in Figure 2 c) refer to beams in four-point bending with 300 and 900 mm span.

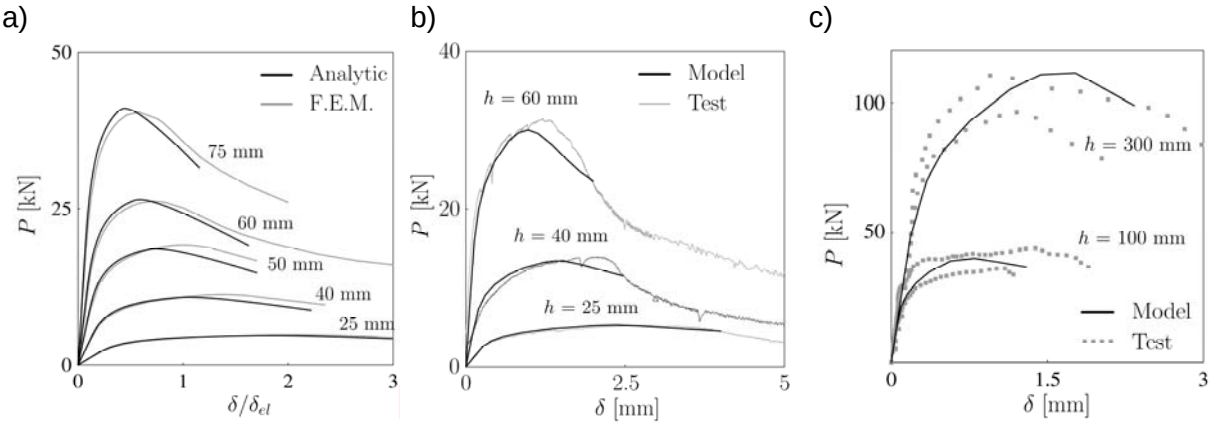

Figure 2: Comparison of theoretical and experimental behaviour for beams in bending: a) results of analytical and FEM models for UHPFRC beams; b) model and test results for UHPFRC beams taken from [4]; c) model and test results for beams made of engineered cementitious composite (ECC), [5].

To compare the bending response of beams made of different materials, the terms *equivalent bending stress* and *equivalent bending strength* are used in this paper. The equivalent bending stress is defined as:

$$\sigma_{equ} = \frac{M}{I_{z,el}} \cdot y \tag{1}$$

where M is the bending moment, $I_{z,el}$ is the moment of inertia of the elastic uncracked section and y is the distance between the centre of gravity and the outermost tensile fibre of the section. The equivalent bending strength, f_{equ}, is given by Eq. (1) with $M = M_{max}$, where M_{max} is the maximum bending moment carried by the section. Although σ_{equ} and f_{equ} have no physical meaning once tensile strength f_{ctm} is exceeded, they are used in this paper as reference values.

2 Size effect on strength and ductility of members in bending

As previously introduced, the tensile properties of a material have significant influence on its bending behaviour. This phenomenon is investigated in this section with reference to bending strength and ductility considering the case of a beam subjected to three point bending (Figure 1c). The slenderness of the beam is kept constant, with a span to depth ratio L / h equal to 8. The depth of the beams is varied from 25 to 500 mm to investigate size effect in a range of thicknesses interesting for structural applications. Three different materials are considered (Figure 3):

1. UHPFRC BSI-Céracem [6], which is characterized by a Young modulus of 60 GPa, a tensile strength of 9 MPa, a pseudo-plastic plateau extending up to a strain of 2.5 ‰ and an initial strain softening slope $F = d\sigma/dw$ equal to 6.8 MPa/mm (Figure 3a);
2. a hypothetic material with the same elastic and softening behaviour as the UHPFRC, but without the pseudo-plastic plateau;
3. an ordinary FRC with a Young modulus of 30 GPa, a tensile strength of 3 MPa and F equal to 20 MPa/mm (Figure 3b).

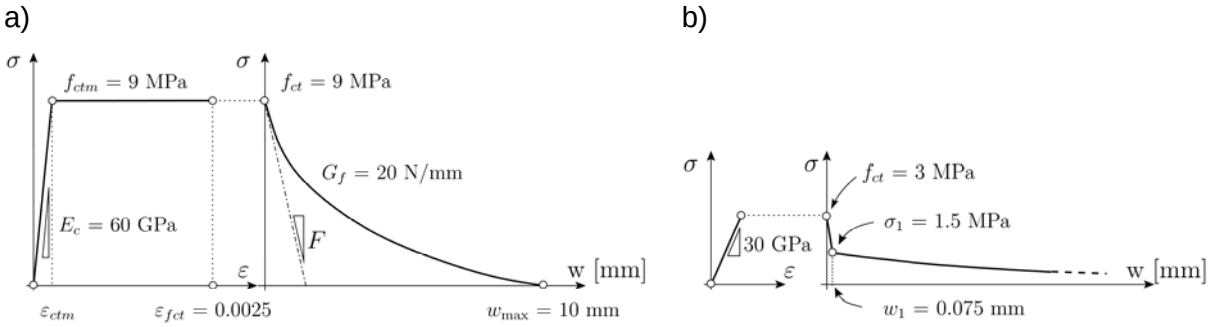

Figure 3: Tensile behaviour of: a) the UHPFRC tested at the EPFL; b) a FRC.

The results of the analyses are plotted in Figure 4 in terms of equivalent bending stress versus nominal deflection (defined as the ratio between the deflection δ at mid-span of the beam and its value δ_{el} at cracking of the matrix). Comparing the peaks of the different curves, it can be noted that for UHPFRC (Figure 4a) the equivalent bending strength depends only slightly on the size of the elements, whereas for FRC (Figure 4c) the size effect on the bending strength of the member is more significant. Figure 4 also shows that the ductility of the members strongly depends on their size and on the mechanical properties of the materials. In terms of ductility, the size effect is qualitatively similar for all materials investigated.

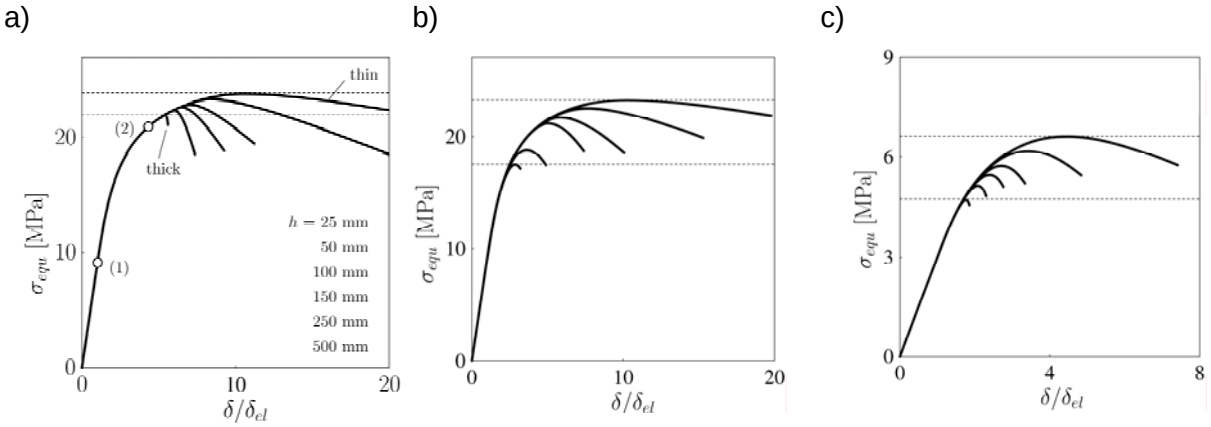

Figure 4: Bending behaviour of beams made of: a) UHPFRC with pseudo-plastic phase; b) UHPFRC without pseudo-plastic phase; c) FRC. In a), point 1 corresponds to matrix cracking and point 2 corresponds to the end of pseudo-plastic phase.

It is interesting to note that for the material with the same softening as UHPFRC but without the pseudo-plastic plateau, the behaviour is similar to that of UHPFRC for thin members (25 to 150 mm), with a limited size effect on strength. On the contrary, it is similar to that of ordinary FRC for thicker elements, for which size effect becomes more pronounced (Figure 4b, 5a).

In Figure 5a, the results of the simulations are plotted for the various materials in terms of the ratio between the equivalent bending strength and the tensile strength of the material versus the thickness of the elements. The upper value on the vertical axis ($f_{equ} / f_{ct} = 3$) corresponds to a perfectly-plastic behaviour in tension. Results are given also for an ordinary concrete

that, for significant sizes, can be considered as the limiting case of an elastic-perfectly brittle material ($\sigma_{equ} / f_{ct} \rightarrow 1$). This diagram shows that for UHPFRC size effect is clearly less significant than for FRC and OC.

Figure 5b presents the experimental results obtained at EPFL [4] for UHPFRC beams of various thicknesses. The experimental results confirm that, for thicknesses ranging from 25 to 75 mm, the size effect on the strength cannot be clearly appreciated (the scatter of the results is larger than size effect). The results of the model are also confirmed by similar experimental results presented by other authors [5, 7] who investigated materials with pseudo-plastic tensile behaviour in beams with thicknesses up to 300 mm.

a) b)

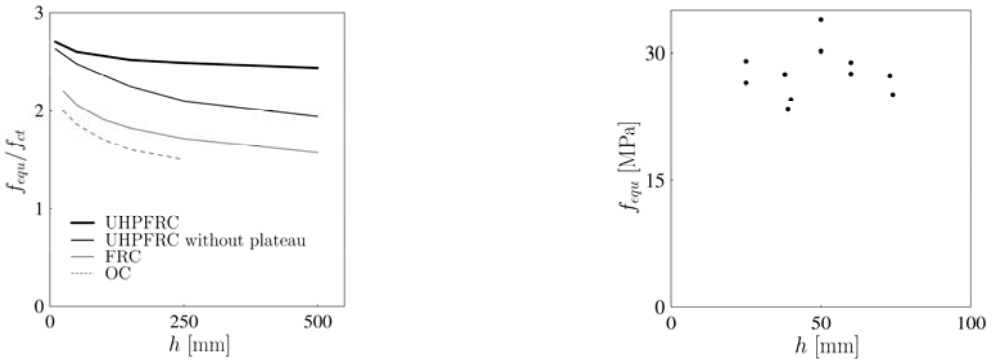

Figure 5: a) Theoretical size effect in UHPFRC, UHPFRC without pseudo-plastic plateau, FRC and OC; b) experimental size effect on bending strength for UHPFRC beam [4].

3 Influence of pseudo-plastic phase and tension softening on the bending behaviour

The limited influence of size effect on the bending strength of UHPFRC can be explained by the fact that most of the bending strength is activated during development of the pseudo-plastic phase in concrete (Figure 6a), whose behaviour is size-independent. Analytically, it can be shown that for a typical UHPFRC (ε_{fct} = 2 – 3 ‰) the equivalent bending stress attained before beginning of tension softening (Figure 6a) is between 2.2 - 2.5 times the tensile strength f_{ct}, [4]. The additional increase in strength, developed with a local tension softening (Figure 6b), is size-dependent. This increase is limited however (typically varying between 0.2 f_{ct} to 0.4 f_{ct} , corresponding to the variation of σ_{equ} between point 2 and the maximal strengths in Figure 4.a).

In addition to the strains developed prior to tension softening, the slope of the stress-crack opening law also plays a major role. For instance, considering a material with the same softening as a UHPFRC, it was shown in the previous section that size effect on the strength of thin elements is strongly reduced even without a pseudo-plastic phase. This can be understood with the help of Figure 6c: if the slope of the softening branch is small, the stress distribution in the tensile zone is similar to that obtained with a pseudo-plastic behaviour in tension (Figure 6a). As a consequence, for thin elements a pseudo-plastic behaviour or a strain softening with a small slope lead to similar results with respect to size effect.

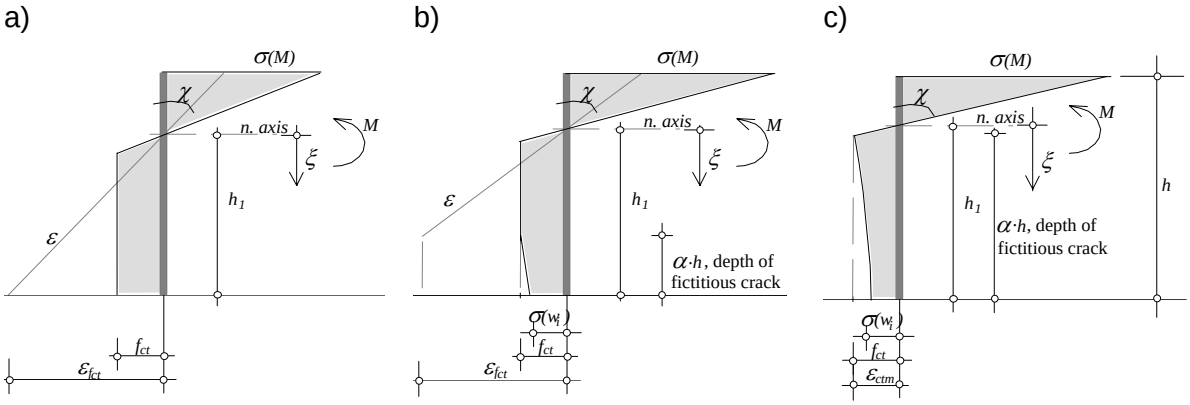

Figure 6: Stress distribution in the section developing a fictitious crack: a) development of quasi-plastic phase in tension; b) local softening due to opening of a fictitious crack (with a part of the height of the section in the quasi-plastic phase); c) softening due to opening of a fictitious crack without quasi-plastic phase in tension.

For modelling and design purposes, however, the two phenomena differ. In cases of a dominant pseudo-plastic behaviour, the sectional and the structural response can be modelled using a continuum approach based on stress-strain relationships [8]. On the contrary, when the strain softening behaviour is strong, strain localisation develops and models based on fracture mechanics theories need to be used.

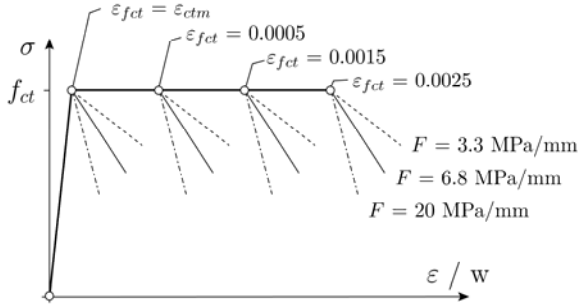

Figure 7: Variation in material properties in tension: strain ε_{fct} at the end of the pseudo-plastic phase and initial slope of the stress-crack opening law.

In order to understand the relative importance of the pseudo-plastic phase and of the softening behaviour of a material on the strength and ductility of a member, a parametric analysis has been performed. The strain ε_{fct} prior to tension softening and the initial slope of the stress-crack opening law are the main parameters for this study. The choice of the latter parameter is justified since, for most structural applications, the bending strength is reached with small crack openings and thus the initial slope of the stress crack opening relationship is more significant than the value of the fracture energy G_F [4]. The parametric study is performed considering a UHPFRC with same material properties as those detailed in Section 2. The values of ε_{fct} and of the initial softening slope are varied according to Figure 7. The values chosen for the softening slope F are: 3.3 MPa/mm, 6.8 MPa/mm, representing the

UHPFRC used in this study, and 20 MPa/mm, which reasonably approximates the initial slope for an ordinary FRC.

The results of the analyses are presented in Figure 8. The nine curves in plot a) were obtained considering a constant thickness of 50 mm. This figure shows that for increasing values of the pseudo-plastic strain prior to tension softening (black curves) the contribution of the softening slope on the structural response becomes less significant.

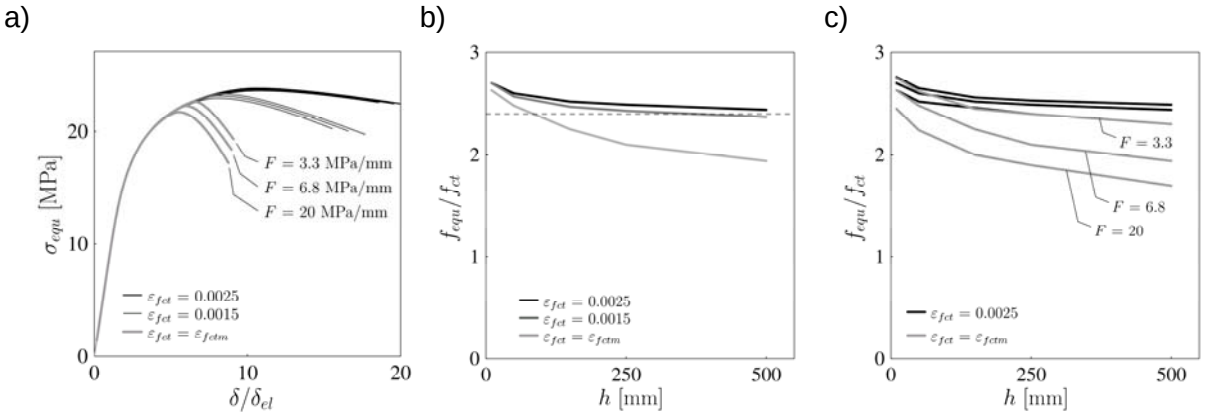

Figure 8: Influence of pseudo-plastic plateau and strain softening slope on the bending response: a) bending stress for a beam with h = 50 mm, varying ε_{fct} and F; b) influence of ε_{fct} on size effect, with constant F; c) Influence of F on size effect, for ε_{fct} = 2.5 ‰ (solid lines) and $\varepsilon_{fct} = \varepsilon_{el}$ (grey lines).

On the contrary, for small values of ε_{fct} (grey lines) variations of the softening slope have a significant influence on the bending strength (Figure 8a). In Figure 8b and 8c, the analysis is extended to thicknesses varying from 25 to 500 mm. The influence of ε_{fct} for a constant tension softening slope is shown in Figure 8-b. The results clearly show that the size effect on the bending strength is very limited in the case of a pseudo-plastic plateau with strains up to 2.5‰. The same applies for ε_{fct} = 1.5‰, whereas for smaller values of ε_{fct} the size effect is more pronounced. However, if the softening slope is small, the bending strength of elements without softening plateau (Figure 8c, grey line with F = 3.3 MPa/mm) is similar to that of elements with a pseudo-plastic plateau (black lines).

4 Conclusions

This paper investigates size effect of UHPFRC members in bending. A parametric study has been performed by varying the tensile strains prior to development of a localised crack (pseudo-plastic phase) and the initial slope of the tension softening law. The results have been compared to those obtained on members made of FRC and OC. On that basis, the following conclusions are drawn:

1 in a range of thicknesses interesting for structural applications (25 to 500 mm), size effect on bending strength is limited for a typical UHPFRC, characterized by a pseudo-plastic behaviour in tension with a deformation capacity of 2 to 3 ‰;

2 for very thin members (25 to 75 mm) it is theoretically and experimentally demonstrated that size effect on bending strength is practically negligible;

3 in presence of a significant pseudo-plastic behaviour, the influence of the post-peak tension softening on bending strength is not very significant, because most of the bending strength is developed while concrete is in the pseudo-plastic tensile phase. The post-peak tensile behaviour is however relevant to the ductility in bending;

4 in the case of limited or no pseudo-plastic phase, the bending response of UHPFRC elements is similar to that of ordinary FRC. However, for thin members the small value initial slope of the tension softening stress-crack opening law leads to a rather ductile behaviour and to a limited size effect on the strength, even if there is no pseudo-plastic phase;

5 in case of a significant pseudo-plastic behaviour, modelling and design can be performed with simple approaches based on continuum mechanics and stress-strain relationships.

5 References

[1] Naaman, A. E.; Reinhardt, H. W.: Proposed classification of HPFRC composites based on their tensile response, In: Materials and Structures, 39, pp. 547-555, 2006.

[2] Hillerborg, A.; Modéer, M.; Petersson, P.: Analysis of crack formation and crack growth in concrete by means of fracture mechanics and finite elements, In: Cement and Concrete Research, vol. 6, n°6, pp. 773-781, Lund, Sweden, 1976.

[3] Bazant, Z. P.; Cedolin, L.: Stability of structures - Elastic, Inelastic, Fracture, and Damage Theories, Oxford University Press, Dover Publications, New York, 2003.

[4] Spasojevic, A.: Structural applications of UHPFRC in bridge design, PhD Thesis, École Polytechnique Fédérale de Lausanne, Lausanne, (to be presented in January 2008).

[5] Kunieda, M.; Kamada, T.; Rokugo, K.: Size Effects on Flexural Failure Behavior of ECC Members, In: Proceedings of the JCI International Workshop on Ductile Fiber Reinforced Cementitious Composites (DFRCC) - Application and Evaluation (DRFCC-2002), Takayama, Japan, Oct. 2002, pp. 229-238, Japan, 2002.

[6] Maeder, U.; Lallemant-Gamboa, I.; Chaignon, J.; Lombard, J. P.: CERACEM a new high performance concrete: characterization and applications, In: International Symposium on UHPC, pp. 67-76, Kassel, 2004.

[7] Rossi, P.; Arca, A.; Parant, E.; Patricia, F.: Bending and compressive behaviors of a new cement composite, In: Cement and Concrete Research 35, pp. 27-33, 2005.

[8] Tailhan, J.-L.; Rossi, P.; Parant, E.; Clement, J.-L.; Arca, A. : Comportement en traction uni-axial d'un composite cimentaire à écrouissage positif à partir d'une approche inverse, Caractérisation du comportement en traction uniaxiale, In : Bulletin des Laboratoires des Ponts et Chaussées, LCPC, n° 248, pp 35-48, Paris, 2003.

Hajime Kawakane
Graduate Student
Hiroshima University
Hiroshima, Japan

Takuto Kawamoto
Engineer
Obayashi Corporation
Tokyo, Japan

Oga Takuma
Graduate Student
Hiroshima University
Hiroshima, Japan

Ryoichi Sato
Professor
Hiroshima University
Hiroshima, Japan

Effective Steel-Ratio and Size effect in Shear Sensitive HSC Beams Subjected to High-Shrinkage

Summary

The shrinkage effect on the diagonal cracking strength of reinforced high-strength concrete beams is investigated, using shear beams with the effective depth of 250mm-1000mm, made of high-shrinkage and low-shrinkage high-strength concretes. The test results show that shear strength at diagonal cracking is decreased by shrinkage 6-18%. Moreover, a new concept of equivalent tension reinforcement ratio considering strain change in tension reinforcement before and after loading is proposed. This concept shows successfully the linear relationship between shear strength at diagonal cracking and the –2/5 power of effective depth independent of the magnitude of shrinkage, and a design equation for the diagonal cracking strength is proposed.

Keywords: *reinforced high-strength concrete beams, autogenous shrinkage, shear strength, size effect, equivalent tension reinforcement ratio*

1 Introduction

High-strength concrete (HSC) is increasingly applied in order to enhance durability and decrease cross sectional area of structural members. It is well known that significant autogenous shrinkage develops in HSC. Shrinkage developed in reinforced concrete (RC) members compresses reinforcing bars, and the compression strain in tension reinforcement is released at cracking. The strain change in tension reinforcement of reinforced high-shrinkage HSC members before and after loading is larger than that of low-shrinkage HSC members. This fact should mean that the tension reinforcement ratio of RC member made of high-shrinkage HSC substantially decreases and widths of flexural and shear cracks increase, compared with those of RC members made of low-shrinkage HSC. Therefore, shrinkage of concrete may affect the shear strength at cracking, considering that the tension reinforcement ratio is one of the major factors of design equations for predicting shear strength at diagonal cracking.

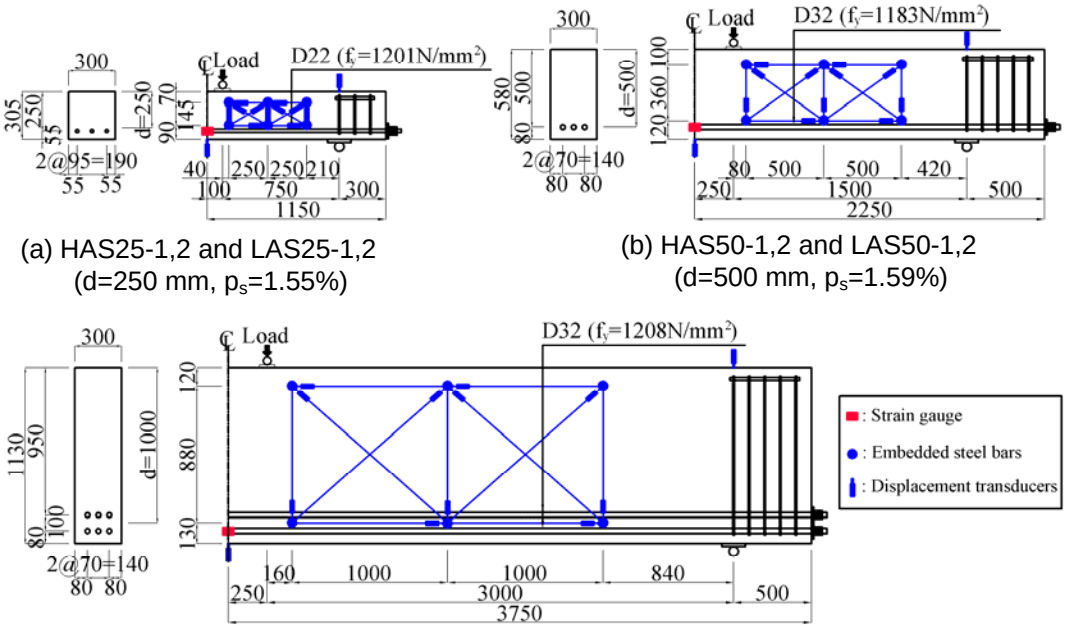

(a) HAS25-1,2 and LAS25-1,2 (d=250 mm, p_s=1.55%)

(b) HAS50-1,2 and LAS50-1,2 (d=500 mm, p_s=1.59%)

(c) HAS100-1,2 and LAS100-1,2 (d=1000 mm, p_s=1.59%)

Figure 1: Dimensions and configurations of RC beams (unit:mm)

In the present study, the shrinkage effect on the diagonal cracking strength of reinforced HSC beams is investigated experimentally. Moreover, a new design equation is proposed for the generalized evaluation of the diagonal cracking strength and size effect law of reinforced HSC beams independent of the magnitude of shrinkage.

Table 1: Mixture proportions of concretes

	Type of Cement	W/B	Unit Content (kg/m³)							
			Water	Cement	Sand	Gravel	Silica Fume	Expansive Additive	Shrinkage Reducing Agent	High-range Water-reducing Agent
			W	C	S	G	SF	EX	SRA	SP
HAS	OPC	0.23	155	607	731	894	67	0	0	12.8
LAS	LPC	0.23	155	567	740	894	67	40	6	11.1

B=C+SF+EX, B: Binder, OPC: Ordinary Portland cement, LPC: Low heat Portland cement

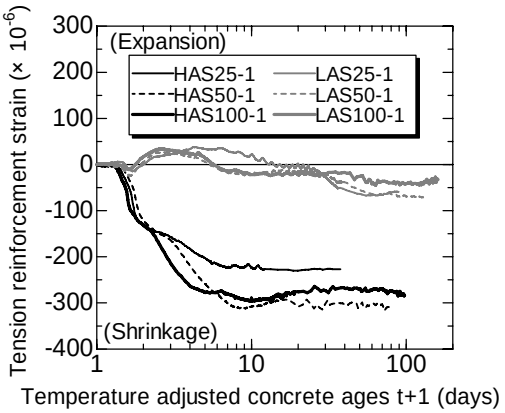

Figure 2: Development of tension reinforcement strain

2 Outline of experiment

Table 1 indicates mixture proportions of concretes. Low-autogenous-shrinkage high-strength concrete (LAS) is made of low heat Portland cement, lime type expansive additives and shrinkage reducing agent, in addition to conventional high-autogenous-shrinkage high-strength concrete (HAS) made of ordinary Portland cement in order to investigate the shrinkage effect on the shear response of RC beams, whose water-to-binder ratio is 0.23.

Dimensions and configurations of RC beams are demonstrated in Figure 1. Twelve RC beams were prepared, one-third of which had the effective depths of 250, 500 and 1000 mm, respectively. Half of them were made of HAS, and the other half was made of LAS. Two RC beams were made for the same effective depth and concrete. Two-point loading was applied

to all RC beams, as shown in Figure 1. The shear span length to effective depth ratio was fixed to 3.0.

Table 2: Results of experiment

Name of specimens	Outline of RC beams				Mechanical properties of concrete at the age of loading				Strain before loading	Shear strength				Failure mode
										Diagonal cracking		Ultimate		
	b (mm)	h (mm)	d (mm)	p_s (%)	f_c' (N/mm^2)	f_t (N/mm^2)	E_c (×10^{-3}N/mm^2)	G_f (N/mm)	$\varepsilon_{s,def}$ (×10^{-6})	V_c (kN)	τ_c (N/mm^2)	V_u (kN)	τ_u (N/mm^2)	
HAS25-1	300	305	250	1.55	121	6.9	46.4	0.201	-227	118	1.57	136	1.81	Diagonal tension
HAS25-2									-242	127	1.69	127	1.69	Diagonal tension
LAS25-1	300	305	250	1.55	117	6.7	46.5	0.211	-59	128	1.71	239	3.19	Shear compression
LAS25-2									-50	132	1.76	181	2.41	Shear compression
HAS50-1	300	580	500	1.59	117	6.7	47.3	0.231	-310	177	1.18	180	1.20	Diagonal tension
HAS50-2									-310	182	1.21	182	1.21	Diagonal tension
LAS50-1	300	580	500	1.59	124	7.4	48.0	0.225	-69	197	1.31	219	1.46	Diagonal tension
LAS50-2									-77	214	1.43	303	2.02	Shear compression
HAS100-1	300	1130	1000	1.59	123	6.6	47.3	0.216	-284	254	0.85	254	0.85	Diagonal tension
HAS100-2									-294	240	0.80	467	1.56	Shear compression
LAS100-1	300	1130	1000	1.59	126	7.4	50.7	0.209	-33	296	0.99	647	2.16	Shear compression
LAS100-2									-37	311	1.04	677	2.26	Shear compression

b: Width of beam, h: Height of beam, d: Effective depth, $p_s (=A_s/bd)$: Tension reinforcement ratio
A_s: Nominal cross sectional area of tension reinforcement, f_c': Compressive strength of concrete, f_t: Splitting tensile strength of concrete
E_c: Young's modulus of concrete, G_f: Fracture energy, $\varepsilon_{s,def}$: Tension reinforcement strain induced by early age deformation before loading
V_c: Shear force at diagonal cracking, $\tau_c (=V_c/bd)$: Shear strength at diagonal cracking
V_u: Ultimate shear force, $\tau_u (=V_u/bd)$: Ultimate shear strength

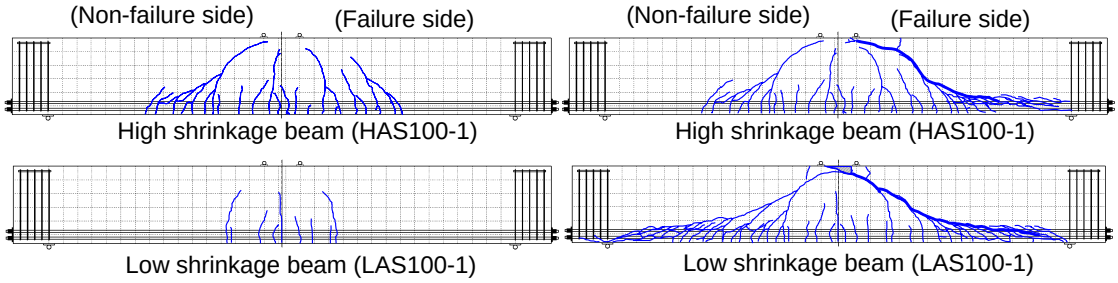

(a) Crack patterns before critical diagonal cracking (V=240kN, τ =0.80N/mm^2)

(b) Crack patterns just after failure

Figure 3: Effects of shrinkage on crack patterns of RC beams before critical diagonal cracking and just after failure (d=1000mm)

3 Results and discussion

The mechanical properties of concrete at the age of loading tests for RC beams are tabulated in Table 2. The results show that the compressive strength, splitting tensile strength, Young's modulus and fracture energy in the present program were 117-126 N/mm^2, 6.7-7.4 N/mm^2, 46-51 kN/mm^2 and 0.20-0.23 N/mm, respectively, without noticeable differences in the mechanical properties of concrete betwen HAS and LAS.

Examples of development of tension reinforcement strain in RC beams after placing concrete are shown in Figure 2. The values for tension reinforcement strain before loading induced by early age deformation are tabulated in Table 2. The differences of tension reinforcement strains between HAS and LAS beams were more than about 170×10^{-6}.

The comparison between reinforced HAS and LAS beams with effective depth of 1000mm for cracking patterns before critical diagonal cracking and just after failure is illustrated in Figure 3.

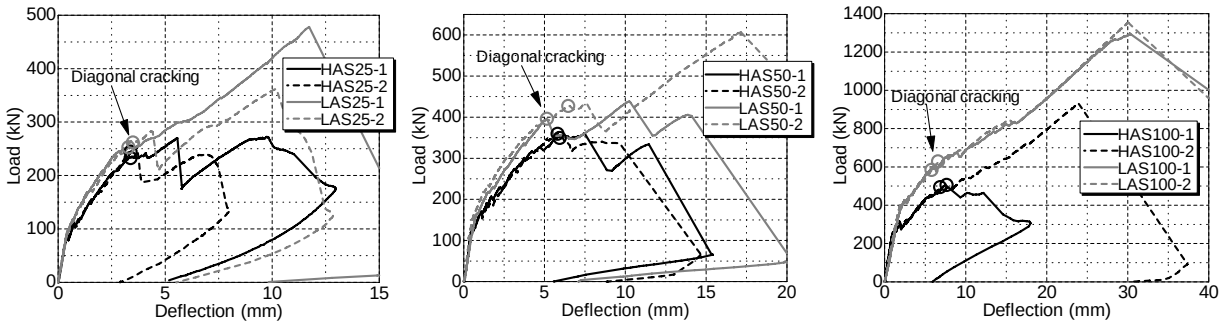

(a) d=250mm (b) d=500mm (c) d=1000mm

Figure 4: Effects of shrinkage on load-deflection relationship

According to this figure, flexural and flexural-shear cracks develop to a greater extent in HAS beam than LAS beam before critical diagonal cracking. After failure, it is found that the primary shear crack produced in HAS beam propagates toward loading point, while the primary crack in a companion LAS beam propagates below the loading point.

Figure 4 shows the comparison between all reinforced LAS and HAS beams for the load-deflection relationship. The circular marks denote the initial and primary diagonal cracking, which were determined based on the measurement of the remarkable increase of shear displacement with almost no increase or drop of load. As is shown in Figure 4, HAS beams failed in diagonal tension with decrease-slight increase of shear resisting force excluding HAS100-2, whose failure mode is defined as diagonal tension failure in the present study. LAS beams, different from the case of HAS beams, failed in shear compression after forming arch mechanism.

The diagonal cracking strength, ultimate shear strength, and failure mode of all the RC beams obtained by the loading test are listed in Table 2. These results show that the averaged shear strengths at diagonal cracking of HAS beams are decreased by 6%, 13% and 18% for d=250 mm, 500 mm and 1000 mm, compared with that of LAS beams. The differences in the averaged ultimate shear strength between the HAS and LAS beams were much more significant, and the strengths of the former were 37%, 30%, and 45% lower for d=250 mm, 500 mm, and 1000 mm than those of the latter.

4 A new generalized equation for diagonal cracking strength

Based on Eq. (1) proposed for RC beams made of normal-strength concrete by Niwa et al.[1], Fujita et al. proposed Eq. (2) for the diagonal cracking strength of reinforced HSC beams[2]. The applicability of Eq. (2) is verified for the compressive strength of concrete from 80 to 125 N/mm^2. On the other hand, Zink also proposed Eq. (3) derived mechanically and empirically, whose applicability ranges are 20-111N/mm^2 for the compressive strength [3].

$$V_c = 0.2 f_c'^{1/3} (d/1000)^{-1/4} (100 p_s)^{1/3} (0.75 + 1.4/(a/d)) bd \quad (1)$$

$$V_c = 180 f_c'^{-1/2} d^{-1/2} (100 p_s)^{1/3} (0.75 + 1.4/(a/d)) bd \quad (2)$$

$$V_c = (2/3) k_x f_{ct} (4d/a)^{1/4} (5 l_{ch}/d)^{1/4} bd \quad (3)$$

where, a: shear span length(mm), k_x: height of the flexural compression zone normalized by effective depth and given approximately by $k_x \approx 0.78(p_s \alpha_E)^{1/3} = 0.78(A_s/bd \cdot E_s/E_c)^{1/3}$, E_s: Young's

Modulus of tension reinforcement(N/mm^2), f_{ct}: axial tensile strength given by $f_{ct} = 2.12\ln(1 + f_c'/10N/mm^2)$ (N/mm^2), l_{ch} (= $E_c G_f / f_{ct}^2$): characteristic length(mm). Gustafsonn and Hillerborg gave the result based on FEM analysis that τ_c / f_t has almost a linear relation with d/l_{ch} with logarithmic scales[4]. Assuming that this linear relation is applicable to reinforced HSC beams, Eq. (2) was formulated based on the following Eqs. (4)-(6) obtained experimentally.

$$\tau_c / f_t \propto \left(d / l_{ch}\right)^{-1/2} \tag{4}$$

$$\tau^*{}_c / d^{-1/2} = 180 f_c'^{-1/2} \tag{5}$$

$$\tau^*{}_c = \tau_c / \left\{(100 p_s)^{1/3}\left(0.75 + 1.4/(a/d)\right)\right\} \tag{6}$$

Comparison of Eq. (1) with Eq. (2) shows that the size effect on the shear strength of reinforced HSC beams is noticeably sensitive compared with that of reinforced normal strength concrete beams, although the size effect of Eq. (1) is the same as that of Eq. (3). However, it should be noted that Eq. (2) include implicitly the autogenous shrinkage effect at early ages.

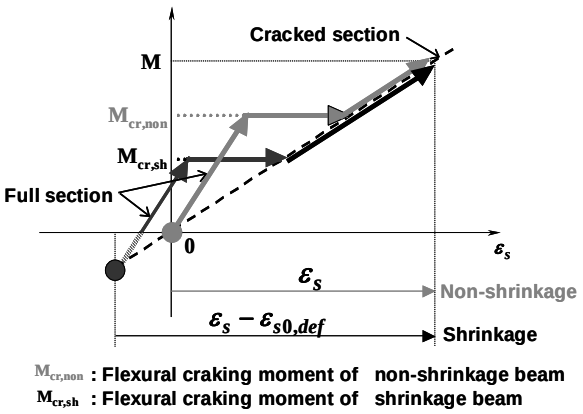

Figure 5: Concept of the effect of shrinkage on strain change in tension reinforcement

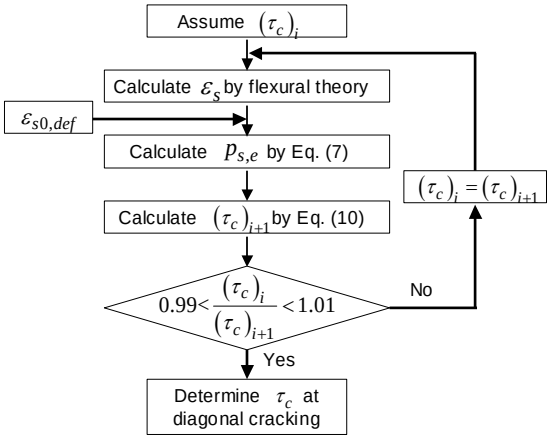

Figure 6: Flow for determining diagonal cracking strength of HAS beams

Eq. (1) and Eq. (2) contain tension reinforcement ratio as one of major factors, while the effect of tension reinforcement ratio is evaluated in height of the flexural compression zone in Eq. (3). Performance of shear transfers along cracks as well as in the concrete compression zone should be decreased when shrinkage effect is remarkable, because flexural cracking moment deteriorates due to shrinkage induced tensile stress in concrete, and flexural crack width is increased due to the strain change in tension reinforcement from compression to tension before and after loading. This fact must mean that tension reinforcement ratio is substantially decreased due to the effect of shrinkage. The following tension reinforcement ratio substantially equivalent to the decreased tension reinforcement ratio is given by considering the strain change in tension reinforcement from the condition where concrete stress at the same depth as the tension reinforcement is zero to that at diagonal cracking, whose concept is shown in Figure 5. Therefore, the equivalent tension reinforcement ratio is given by the following equation;

Table 3: Results of experiment data of specimens obtained previously

	Reseacher	number	b (mm)	h (mm)	d (mm)	p_s (%)	a/d	$\varepsilon_{s,def}$ ($\times 10^{-6}$)	Concrete f_c' (N/mm^2)	f_t (N/mm^2)	E_c (kN/mm^2)	G_f (N/mm)
HAS	Ito et al.	5	150-200	300	234-250	1.53-3.39	3.0	-192 - -360	115-127	4.9-6.2	42-43	0.22*
	Ushio et al.	5	150	600	500	1.53-2.06	3.0	-225--247	115-128	6.6-7.5	48-50	0.20-0.22
	Fujita et al.	9	150-350	300-1130	250-1000	1.36-1.53	3.0	-300*	93-103	3.9-4.9	37-41	0.22
LAS	Ito et al.	5	150-200	300	234-250	1.53-3.39	3.0	-16 - -66	101-113	4.5-5.7	40	0.22*
	Ushio et al.	5	150	600	500	1.53-2.06	3.0	-1 - -40	108-121	7.3-8.3	48-50	0.21-0.25

* Assumed value

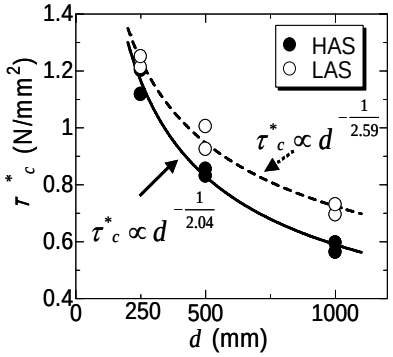

(a) Evaluation based on Nominal tension reinforcement ratio

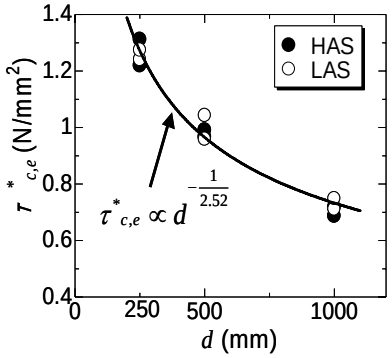

(b) Evaluation based on equivalent tension reinforcement ratio

Figure 7: Effects of effective depth and shrinkage on shear strength at diagonal cracking

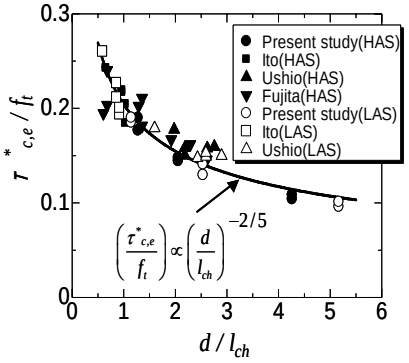

Figure 8: $\tau^*_{c,e}/f_t$ - d/l_{ch} relationship

$$p_{s,e} = \frac{\varepsilon_s}{\varepsilon_s - \varepsilon_{s0,def}} p_s \quad (7)$$

where, $p_{s,e}$: equivalent tension reinforcement ratio, ε_s : tension reinforcement strain at the section 1.5*d* distant from loading section in shear span at the diagonal cracking, $\varepsilon_{s0,def}$: tension reinforcement strain when concrete stress at the depth of reinforcement is zero, which is positive in tension and negative in compression.

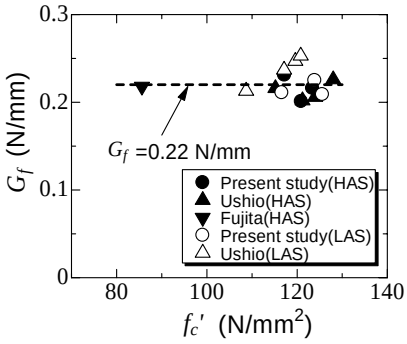

Figure 9: G_f - f_c' relationship

ε_s is obtained by iterative calculation following the flow shown in Figure 6, in which it is assumed that strain distribution is linear through the section and the section 1.5*d* distant from the loading section is critical section leading to diagonal cracking.

Figure 7(a) shows the relationship between the normalized shear strength given by Eq. (6) and the effective depth obtained from HAS and LAS beams, in which nominal tension reinforcement ratios are applied and the regression curves obtained by the method of least square are also drawn for both types of RC beams. According to this figure, the size effect is obviously different depending on shrinkage and the powers of the effective depth for HAS and LAS beams are -1/2.04 and -1/2.59, respectively. However, applying the concept of the equivalent tension reinforcement ratio given by Eq. (8), as is shown in Figure 7(b), the normalized shear strength follows approximately the effective depth to -1/2.5 power independent of shrinkage.

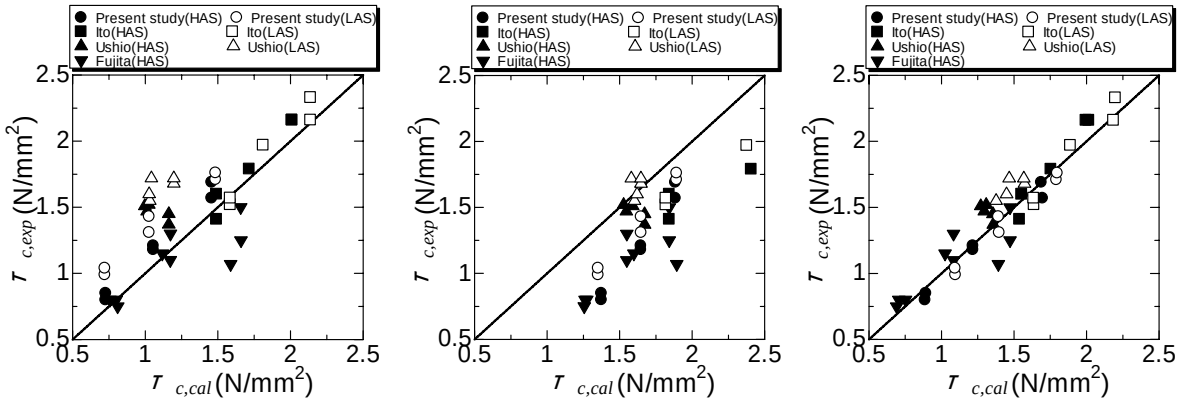

(a) Eq. (2) by Fujita et al. (b) Eq. (3) by Zink (c) Eq. (10) by authors

Figure 10: Comparison of previously proposed equations and newly proposed equation for the evaluation of shear strength at diagonal cracking

$$\tau^{*}_{c,e} = \tau_c \Big/ \left\{ \left(100\, p_{s,e}\right)^{1/3} \left(0.75 + 1.4/(a/d)\right) \right\} \tag{8}$$

The relationships between $\tau_{c,e}{}^{*} / f_t$ and $\left(d/l_{ch}\right)^{-2/5}$ obtained from all beams in the present experiment together with those from Ito et al.[5], Ushio et al.[6] and Fujita et al.[2], whose specimens' conditions are tabulated in Table 3, and the regression curve are plotted in Figure 8. Good applicability of the effective depth to -2/5 power is found from the figure for all beams. Based on the regression analysis, the following equation was obtained for predicting shear strength at diagonal cracking;

$$\tau_c = \frac{V_c}{bd} = 0.204\left(E_c G_f\right)^{2/5} f_t^{1/5} \left(100\, p_{s,e}\right)^{1/3} d^{-2/5} \left(0.75 + 1.4/(a/d)\right) \tag{9}$$

As the fracture energy of concrete, as is shown in Figure 9, is hardly varied in compressive strength from 80-130N/mm^2, Eq. (9) is simplified to Eq. (10) by using 0.22N/mm as the value of the fracture energy as follows;

$$\tau_c = \frac{V_c}{bd} = 0.11 E_c{}^{2/5} f_t^{1/5} \left(100\, p_{s,e}\right)^{1/3} d^{-2/5} \left(0.75 + 1.4/(a/d)\right) \tag{10}$$

The comparisons of the shear strengths obtained by the experiment and those calculated by the equations proposed by Fujita et al., Zink and the authors are shown in Figure 10, and the prediction accuracy of each equation is summarized in Table 4. According to these results, the equation by Fujita et al. predict tested results fairly well for HAS beams but underestimate them for LAS beams. Zink's equation tends to underestimate test results on the whole, while Heggar et al. showed that calculated results by Zink's equation agree well with experimental results[7]. One of the reasons for this discrepancy may be due to the difference in fracture energy between concrete used for the formulation of Eq. (3) and that in the present experiment. On the other

Table 4: Comparison of previously and newly proposed equations for prediction accuracy

	number	Eq. (2) by Fujita et al.			Eq. (3) by Zink			Eq. (10) by authors		
		$\tau_{c,exp}/\tau_{c,cal}$ Average	SD	CC	$\tau_{c,exp}/\tau_{c,cal}$ Average	SD	CC	$\tau_{c,exp}/\tau_{c,cal}$ Average	SD	CC
HAS	25	1.09	0.20	0.81	0.77	0.12	0.88	1.03	0.11	0.94
LAS	16	1.27	0.22	0.87	0.90	0.10	0.89	1.01	0.09	0.94
Total	41	1.16	0.22	0.80	0.82	0.13	0.86	1.02	0.10	0.95

$\tau_{c,exp}$: Shear strengt at diagonal cracking obtained by the experiment
$\tau_{c,cal}$: Shear strengt at diagonal cracking calculated by the prediction equation
SD: Standard deviation, CC: Correlation coefficient

hand, the proposed method shows the highest prediction accuracy, the smallest standard deviation and the highest correlation coefficient for the present experiment independent of the magnitude of shrinkage, compared with the results of other researchers.

5 Conclusions

The following conclusions are drawn within the limit of the present study.

(1)The shrinkage caused the deterioration of shear strength at diagonal cracking of reinforced high-strength concrete beams by 6%, 13% and 18% for the effective depth of 250mm, 500mm and 1000mm, respectively.

(2)High-shrinkage high-strength concrete (HAS) beams tended to fail in shear tension, while low-shrinkage high-strength concrete (LAS) beams tended to fail in shear compression, resulted in the remarkable difference of ultimate shear strength between HAS and LAS beams. The former was 37%, 30% and 45% for the effective depth of 250mm, 500mm and 1000mm smaller than those of the latter, respectively.

(3)The size effect on the diagonal cracking strength followed the effective depth to -1/2.04 and -1/2.59 powers for HAS beams and LAS beams prepared in the present study, respectively.

(4)A new generalized design equation independent of the magnitude of shrinkage was proposed, by applying the concept of the equivalent tension reinforcement ratio based on the strain change in tension reinforcement before and after loading. The size effect on the diagonal cracking strength was succcessfully explained by the proposed equation, which followed approximately the effective depth to -2/5 power for both HAS and LAS beams.

6 References

[1] Niwa, J.; Yamada, K.; Yokozawa, K.; Okamura, H.: Revaluation of the Equation for Shear Strength of Reinforced Concrete Beams without Web Reinforcement. In: Proceedings of JSCE, No.372, S.167-176, 1986.

[2] Fujita, M.; Sato, R.; Matsumoto, K.; Takaki, Y.: Size effect on shear strength of RC beams using HSC without shear reinforcement. In: Concrete Library International, No.41 JSCE, S.113-128, 2003.

[3] Zink, M.: Zum Biegeschubversagen schlanker Bauteile aus Hochleistungsbeton mit und ohne Vorspannung. In: Ph.D. Thesis, University of Leipzig, 1999.

[4] Gustafsson, P. J.; Hillerborg, A.: Sensitivity in Shear Strength of Longitudinally Reinforced Concrete Beams to Fracture Energy of Concrete. In: ACI Structural Journal, no.85-S30, S.286-294, 1988.

[5] Ito, Y.; Fujita, M.; Fuchiwaki, H.; Sato, R.: Effects of Shrinkage on Shear Behavior of Reinforced High Strength Concrete Members. In: Proceedings of the Japan Concrete Institute, Vol.23, No.3, S.763-768, 2001.

[6] Ushio, R.; Kawakane, H.; Maruyama, I.; Sato, R.: Studies on the Effect of Volume Change on Shear Behavior of Reinforced HSC Beams. In: Proceedings of the Japan Concrete Institute, Vol.28, No.2, S.769-774, 2006.

[7] Hegger, J.; Sherif, A.; Goertz, S.: Shear Capacity of Beams Made of High- Performance Concrete. In: Proceedings of 7th International Symposium on the Utilization of High-Strength/High-Performance Concrete, ACI SP-228, 1, Washington, D.C., USA, S.723-740, 2005.

André Glaubitt
Dipl.-Ing.
Technische Universität Dortmund
Dortmund, Germany

Bernhard Middendorf
Prof. Dr.
Technische Universität Dortmund
Dortmund, Germany

Non-destructive ultrasonic testing methods for quality control of UHPC

Summary

The use of Ultra high performance concrete (UHPC) as a high performance material for concrete constructions requires an efficient and reliable inspection process. Non-destructive tests on UHPC samples, like beams in bending or cylinders, have shown that the ultrasonic inspection can be used quickly, efficiently and in a non-destructive manner, in order to, for example, detect structural changes within the framework of quality control or material research. In the manner, compaction problems were able to be identified on UHPC beams in bending. Using highly frequent probes is possible for this fine-grained material, in comparison to ordinary concrete. This results in higher resolutions and therefore higher reliability from the inspection and quality control of UHPC.

Keywords: *UHPC, ultrasonic testing, quality control*

1 Introduction

Compared to ordinary concrete, UHPC is a very dense concrete with low porosity, which possesses high compressive strength and deformation resistance. UHPC has an excellent load capacity, as well as an enormously high resistance to the penetration of liquids and gases. As a result, it has exceptional durability qualities.

Such high performance materials inevitably require, for technical applications, very efficient and reliable test and quality control procedures, because the high loaded cross sections and are not suitable for destructive investigation.

The non-destructive ultrasonic testing method is very well suited to the investigation of UHPC, because of the fine grained components and the more homogeneous structure of UHPC compared to ordinary concrete (the aggregates of UHPC are in general 10 to 20 times smaller). Due to the dense and fine grained structure, ultrasonic frequency ranges > 1 MHz (normally used to examine steel) can be used to test UHPC. The wavelength of the impulses is at least one power of ten times smaller than for examinations of ordinary concrete. This affords a much higher resolution, and therefore a higher reliability of the examinations and quality control of UHPC, in particular using the favorable pulse-echo-method. Within a quality control system, deficiencies in material properties and production (defects) can be discovered and judged confidently and quickly.

2 Ultrasonic inspection of UHPC samples

In the following, results from inspections on UHPC samples -beams in bending and constricted cylinders- are presented, in order to make clear the necessity for a qualitative evaluation of UHPC using ultrasonic inspections which can be carried out quickly and non-destructively.

2.1 Ultrasonic inspection for quality control of two UHPC beams in bending

For these inspections, two differently composed and fabricated steel fiber reinforced UHPC beams in bending (15 x 15 x 70 cm^3) were inspected with regards to their structural formation using non-destructive ultrasonic measurements. One of the beams in bending was made from a UHPC laboratory recipe (referred to as LAB), the other was made from an industrially created mixture from a UHPC producing company, which will be referred to in the following as IND.

An ultrasonic procedure was used, in which transmitting and receiving probes are located at opposite positions of the scanned beam in bending. The beams in bending were fitted with a 2 cm spacing grid for the measurements and scanned with longitudinal wave probes (rated frequency 2.25 MHz). The measurement results were processed with the Hilbert Transformation [1] and generating the envelopes. The determination of the run time of the ultrasonic impulses is then done using the difference of the maximal peaks of the sending and receiving impulse under the consideration of the preliminary leadtimes of the probes. From the run time and the known thickness of the beams in bending, the longitudinal wave velocity was calculated and graphed (Fig. 1 and 2). Additionally, the beams in bending were scanned over their entire length (0.7 m) with the above-mentioned probes. Based on the broad frequency bandwidth of the selected probes, receiving impulses up to 1 MHz with a significant onset could be detected on a measurement of this size.

A significantly lower longitudinal wave velocity v_p (by 4600 m/s) can be seen in the results from the LAB beam in bending in the margin than in the rest of the beam (4800-4900 m/s) (Fig. 1). These differences are a result of the structural inhomogenities of UHPC, which can be traced back to non-uniform compaction of the beam in bending. Geometry effects, which sometimes can influence the measured ultrasonic signal, are not the cause of the deviations in the wave velocity in the margin, because then similar measurements would have to have been made on the IND beam in bending (Fig. 2).

The IND beam in bending showed a more homogenous structure than the LAB beam in bending with respect to the wave velocity (Fig. 2), though fluctuations of v_p were also present.

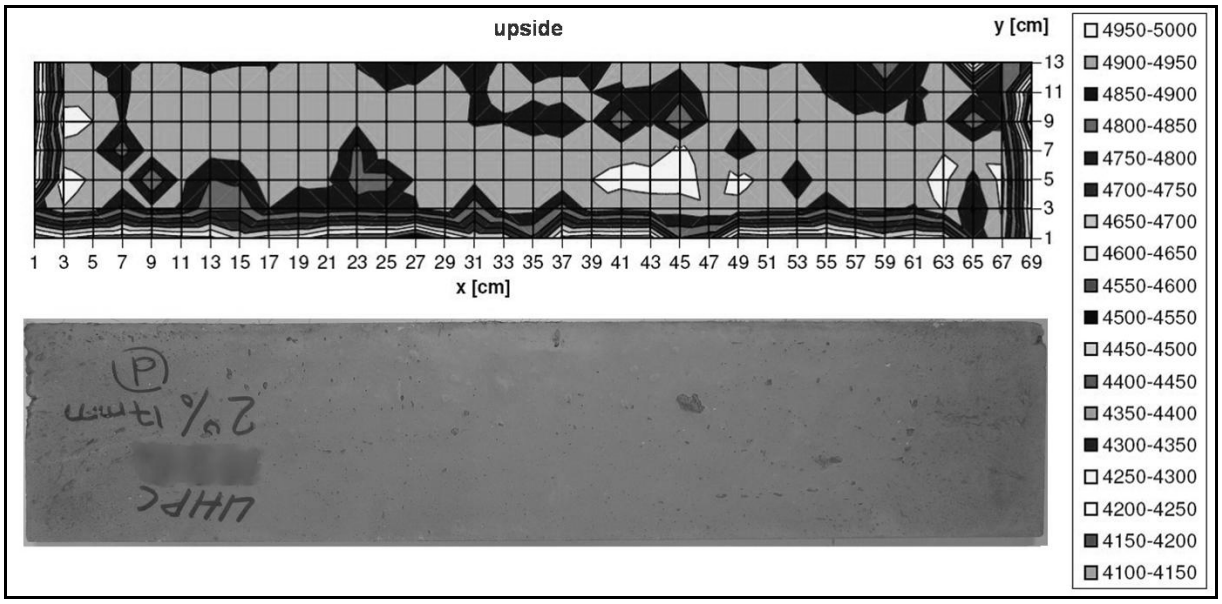

Figure 1: Longitudinal wave velocity v_p [m/s]; UHPC beam in bending LAB

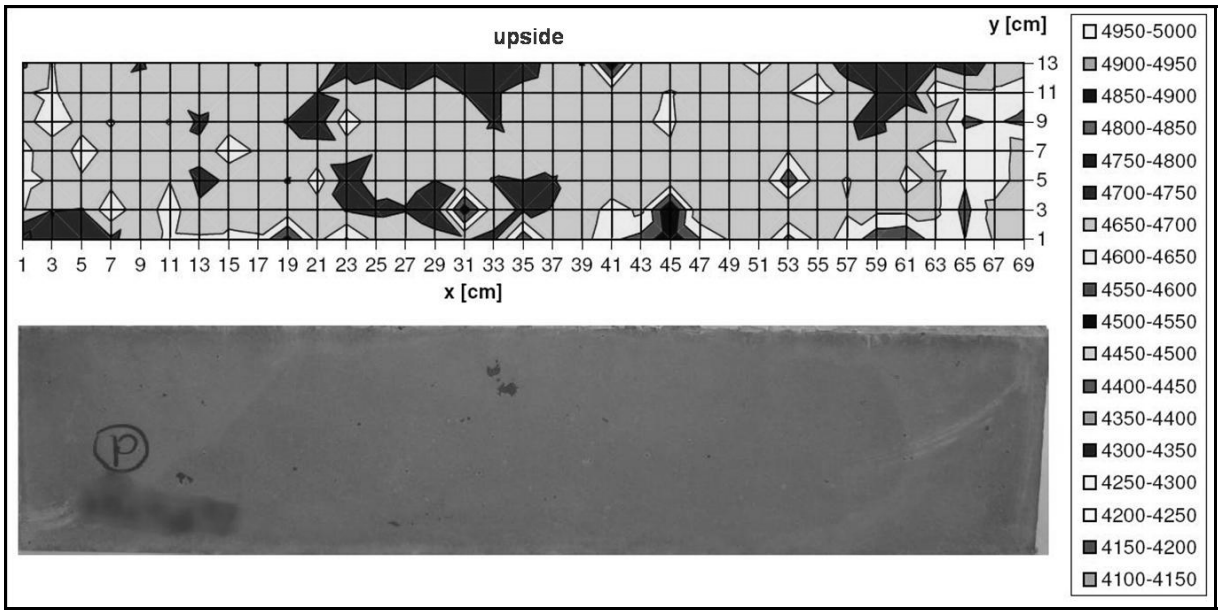

Figure 2: Longitudinal wave velocity v_p [m/s]; UHPC beam in bending IND

Looking at the obtained measurements (Table 1), one can clearly see based on the given standard deviation, that the LAB beam in bending shows a significantly higher structural inhomogenity (see also Fig. 1 and Fig. 2).

Table 1: Wave velocity v_p and standard deviation of the inspected beams in bending LAB and IND

Longitudinal Wave Velocity v_p		**LAB**	**IND**
Median	m/s	4847	4668
Standard Deviation σ	m/s	130	42

2.2 Ultrasonic Inspection for Quality Control in Materials Research on Two Constricted Cylinders

The ultrasonic run time measurement is well suited for, among other things, determining the dynamic elastic constants E_{dyn} and μ_{dyn} (see Eq. (1) and (2)). The elastic constants determined in this manner can be used both in quality assurance as well as in materials research and development, in order to, for example, show chronological (strength development) or local (workmanship) material changes [2-9]. By determining v_p, v_s and the bulk density, it is also possible to calculate the dynamic elastic constants E_{dyn} and μ_{dyn} for a material [10, 11]. Therefore, not only the wave velocity, but also the physical properties of a material are taken into account for an evaluation [12, 13].

Two constricted UHPC cylinders (Ø 15, 8, 15 cm, l ≈ 30 cm, CYL1 und CYL2) were available for inspection (Fig. 3). Their recipes were identical, but one probe was additionally reinforced with 1.5 mass % steel fibers (lf/df = 9 mm / 0.15 mm). The cylinders were scanned with longitudinal wave probes (rated frequency 2.25 MHz) and transversal wave probe arrays (rated frequency 55 kHz) and the corresponding wave velocity v_p und v_s was calculated using the run times.

In the cylinder without steel fiber reinforcement (CYL1) v_p = 4890 m/s (σ = 4 m/s) and transversal wave velocity v_s = 3183 m/s (σ = 2 m/s) were measured. By adding steel fibers, the overall velocity of the longitudinal wave impulses in the cylinder with steel fibers should have increased, due to the higher wave velocity in steel (v_p = 5900 m/s, v_s = 3230 m/s) [14, 15]. However, this is not the case in the inspected cylinder (CYL2) (v_p = 4870 m/s (σ = 26 m/s) and v_s = 3193 m/s (σ = 3 m/s)). Because the median of v_p for the steel reinforced cylinder lies below the median of v_p for the non-reinforced cylinder, this indicates different material properties of the concrete used.

For the purpose of ocular assessment of the inspected UHPCs, the cylinders were sawed through along the ultrasonic measurement range (Fig. 3). The cylinder with steel fibers shows a higher porosity – mostly air and compaction pores – than the non-reinforced cylinder. Compared to the fibre free sample, the steel fibre containing sample has a 0.05 g/cm³ higher density. If the concrete matrix of both samples would have the same porosity, the fibre containing sample must have a 0.08 g/cm³ higher porosity based on the high density of the steel fibres. It is well known, that steel fibres reduce workability of the fresh UHPC, which results in a worse compaction. Poorly compacted samples have a higher porosity, which can be easily seen in Fig 3.

A direct comparison of the mechanical properties with respect to the influence of the steel fibers is not possible at this point, because the cylinders, despite having the same composition, could not be compared on the same terms.

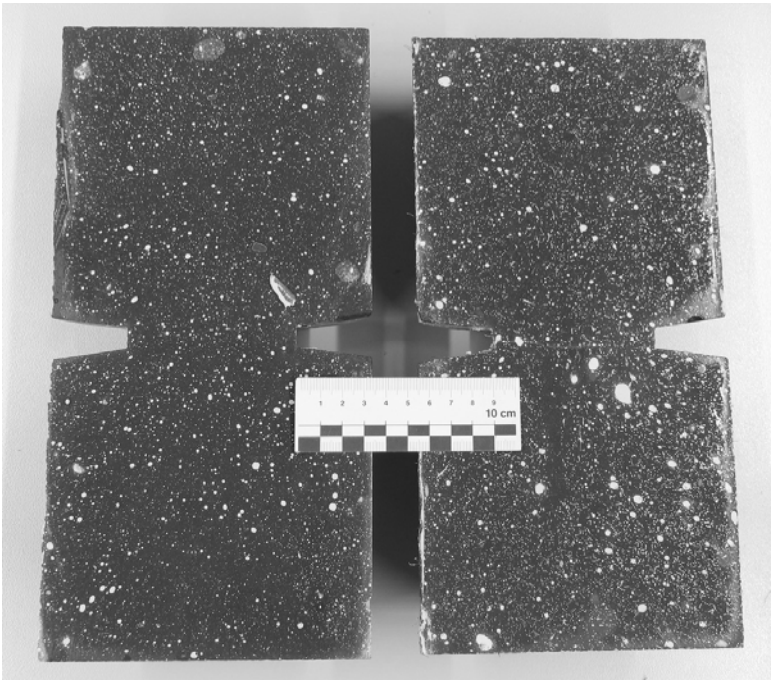

Figure 3: Photographic documentation of the structure of the inspected cylinders; left: without fibers, right: with fibers. The light specks in the UHPC are pores.

Using the determined wave velocity and the bulk density of the material, the dynamic elastic constants E_{dyn} and μ_{dyn} can be determined. This is done by solving equations (1) and (2).

$$v_s = \sqrt{\frac{E}{\rho} \cdot \frac{1}{2(1+\mu)}} \tag{1}$$

$$v_p = \sqrt{\frac{E}{\rho} \cdot \frac{(1-\mu)}{(1+\mu)(1-2\mu)}} \tag{2}$$

The material figures calculated in this manner for both cylinders are presented in Table 2.

Table 2: Wave velocity and material figures, cylinder 1 without fibers and cylinder 2 with fibers

Velocity and Material Figures		**CYL1**	**CYL2**
Longitudinal wave velocity v_p	m/s	4890	4870
Transversal wave velocity v_s	m/s	3183	3193
Bulk density ρ	g/cm²	2.26	2.31
Dynamic modulus of elasticity E_{dyn}	N/mm²	51,860	52,900
Dynamic Poisson's ratio μ_{dyn}	-	0.13	0.12

The density of cylinder 2 is, due to the steel fibers (1.5 mass %) – despite a higher porosity (see Fig. 3) – larger than in cylinder 1. As was expected, the dynamic modulus of elasticity of the steel fiber reinforced cylinder is higher than the non-reinforced cylinder. Based on the

porosity, CYL2 has a lower dynamic Poisson's ratio than CLY1. The dynamic elastic constants are in the range of statically determined values for UHPC ($E \approx 50{,}000$ N/mm², $\mu \approx$ 0.16-0.24 [16]). Dynamically determined constants are larger than the statically determined constants (secant model) due to determining them in the purely elastic state of stress of the material (tangents in the coordinate origin). Therefore, E_{dyn} and μ_{dyn} of these two cylinders are rated as being low.

3 Assessing the Inspections

The results presented here show, on the one hand, that the quality of UHPCs can be quantified using ultrasonic measurements. On the other hand, the results show the need for a qualitative assessment of UHPC samples using quickly executable, non-destructive ultrasonic measurements. It is apparent, that quality assurance of UHPC components is absolutely necessary. Both in materials research for this material, as well as in the later production of UHPC components, this quality assurance using ultrasonic inspection can be performed, but in its current state, it does not have the standard to be the only method of inspection for UHPC.

4 Pulse-Echo-Method Investigations

Using the pulse-echo-method mentioned [17] an additional monitoring of imperfections like contraction cavities, etc was also performed. For this purpose, a 3 cm deep imperfection (borehole Ø 12 mm) perpendicular to the direction of inspection was created; the geometry is illustrated in Figure 4. The imperfection was detected by a probe for longitudinal waves, (bandwidth 0.2 – 0.6 MHz), whereby due to the probe characteristics (low frequency, faulty wave bundling), the depth of the imperfection could be determined, but not the exact lateral dimensions as was desired (Fig. 5). Here, the most considerable progress is expected due to an adaption of probes from steel inspection of more coarse material (e.g. cast iron) with higher wave bundling (directivity) [18] for the inspection of UHPC. The limits of use of such probes depend on the particle maximum size of the UHPC being inspected and still require being researched. UHPCs with more coarse aggregate (up to Ø 8 mm) are, in practice, rare, but can also be inspected using ultrasonic methods that were developed for normal concrete.

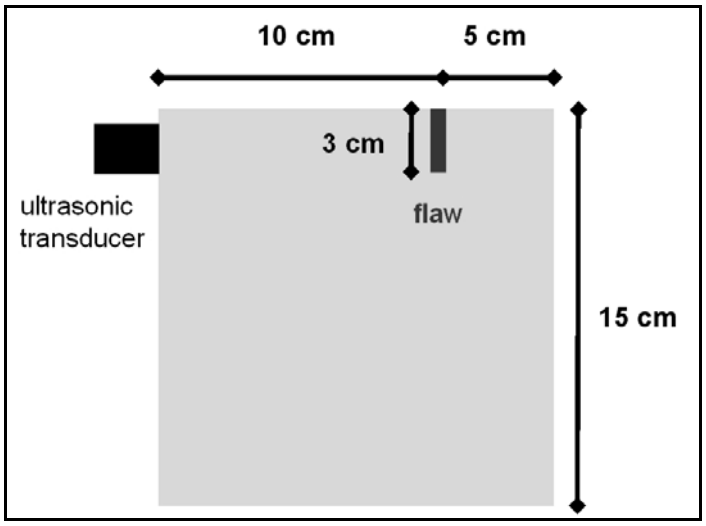

Figure 4: Measurement geometry of the UHPC probe with a fabricated imperfection

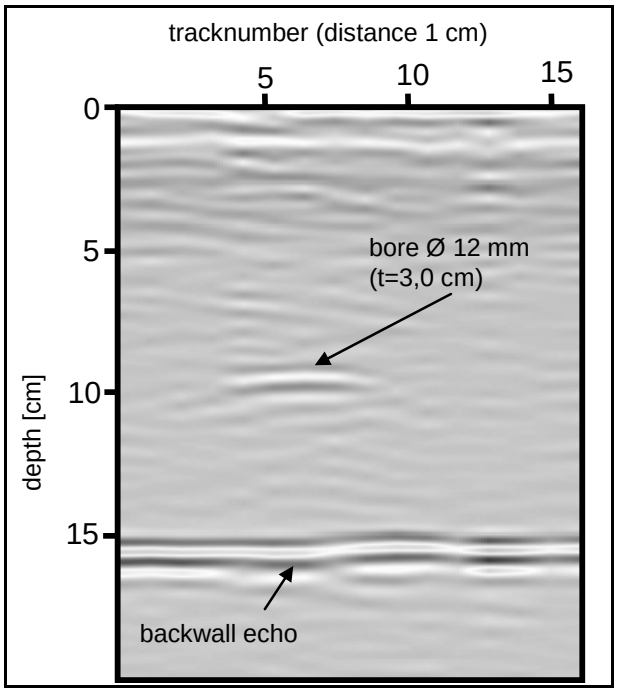

Figure 5: Detection of the imperfection with the pulse-echo-method

5 References

[1] Poularikas, A. D.: The Hilbert Transform, The Handbook of Formulas and Tables for Signal Processing, Chapter 15, CRC Press LLC, Boca Raton 1999.

[2] Rentsch, W., Krompholz, G.: Die Bestimmung der Poisson'schen Zahl durch Schallgeschwindigkeitsmessungen, Wissenschaftliche Zeitschrift der Hochschule für Bauwesen Leipzig (1963), Heft 9, S.177-181.

[3] Facaoaru, I., Stamate, G.: On the Relation between some Static and Dynamic Constants of Concrete, Report for RILEM Working Group for NDT-Meeting, Varna 1968, Bukarest, 1968.

[4] Kaplan, M.F.: Ultrasonic Pulse Velocity, Dynamic Modulus of Elasticity, Poisson's Ratio and the Strength of Concrete made with thirteen Different Coarse Aggregates, RILEM-Bulletin (1959), Nr. 1, S.58-73.

[5] Morscichin, W.N.: Bestimmung des Elastizitätsmoduls von Beton mit der Schallimpulsmethode, „Zerstörungsfreie Prüf- und Meßtechnik für Beton und Stahlbeton", Leipzig 23.-25.4.1969, S.45.

[6] Jones, R.: The Elasticity and Rupture of Concrete and Stone at Constant Rates of Loading, Nature 165 (1950), Nr. 4184, S. 49.

[7] Hennicke, H.W., Leers, K.-J.: Die Bestimmung elastischer Konstanten mit dynamischen Methoden, Tonindustrie-Zeitung 89 (1965), Heft 23/24, S. 538-543.

[8] Manns, W.: Über den Einfluss der elastischen Eigenschaften von Zementstein und Zuschlag auf die elastischen Eigenschaften von Beton, Dissertation, RWTH Aachen 1969.

[9] Neisecke, J.: Ein dreiparametriges, komplexes Ultraschall-Prüfverfahren für die zerstörungsfreie Materialprüfung im Bauwesen, Dissertation, TU-Braunschweig 1974.

[10] Lacouture, J.-Ch., Johnson, P. A., Cohen-Tenoudji, F.: Study of critical behavior in concrete during curing by application of dynamic linear and nonlinear means. J. Acoust. Soc. Am. 113 (3), March 2003, pp. 1325-1332.

[11] Glaubitt, A., Bussat, S., Neisecke, J.: Reference concrete for ultrasonic-testing and its creation by components with pre-analysed properties, Internationales Symposium "Non Destructive Testing in Civil Engineering" (NDT-CE), Berlin 09.2003, DGZfP, CD-ROM ISBN 3-931381-49-8.

[12] Glaubitt, A., Middendorf, B., Neisecke, J.: Ultrasonic tests on concrete reference samples. Beitrag: Journal of Nondestructive Evaluation Sonderheft (eingereicht).

[13] Glaubitt, A., Middendorf, B., Neisecke, J.: Ausbreitungsverhalten von Ultraschall in Referenzprobekörpern aus Beton. Abschlusskolloquium DFG-Forschergruppe FOR 384 „Moderne ZfP bei der Bauwerkserhaltung", Bergisch Gladbach, Mai 2007.

[14] Washer, G., Fuchs, P., Graybeal, B. A., Hartmann, J. L.: Ultrasonic Testing of Reactive Powder Concrete. IEEE Transactions on Ultrasonic, Ferroelectrics, and Frequency Control, Vol. 51, No. 2, February 2004, pp. 193-201.

[15] Washer, G., Fuchs, P., Graybeal, B. A.: Elastic Properties of Reactive Powder Concrete. Int. Symposium (NDT-CE 2003) Non-Destructive Testing in Civil Engineering 2003.

[16] Fehling, E., Schmidt, M., Teichmann, T., Bunje, K., Bornemann, R., Middendorf, B.: „Entwicklung, Dauerhaftigkeit und Berechnung Ultrahochfester Betone (UHPC)", Forschungsbericht DFG FE 497/1-1, Schriftenreihe Baustoffe und Massivbau, Heft 1, Kassel university press GmbH, Kassel 2005.

[17] DGZfP 1999 Deutsche Gesellschaft für zerstörungsfreie Prüfung, Merkblatt B4 für Ultraschallverfahen zur zerstörungsfreien Prüfung mineralischer Baustoffe und Bauteile; DGZfP, Unterausschuss Ultraschallprüfungen, Berlin 1999.

[18] Krautkrämer, J. und H.: Werkstoffprüfung mit Ultraschall, Springer Verlag, Berlin 1986.

Part 8:

Structural Behaviour I

Luca Sorelli
Dr.
LCPC
Paris, France

Ricardo Davila
P.Eng.
M.I.T.
Cambridge, US

Franz-Josef Ulm
Prof.
M.I.T.
Cambridge, US

Vic Perry
P.Eng.
Lafarge North America
Calgary Canada

Peter Seibert
P.Eng.
Lafarge North America
Calgary Canada

Risk Analysis of Early-Age Cracking in UHPC Structures

This work focuses on the analysis and the risk assessment of early age cracking for structures made of Ultra High Performance Concrete (UHPC) due to autogeneous and thermal shrinkages induced by the highly exothermic reaction. First, we summarize the background work on modelling of UHPC materials discussing the hypothesis at the basis of this approach of partial thermodynamics decoupling. Then, we calibrate the chemo-thermo-mechanical properties for UHPC materials. The model is employed to study the setting period and demolding sequence during the construction of an UHPC footbridge in Calgary, Canada. The comparison between the simulated and measured histories of temperature and strains is presented, while it is shown that the concept of level of loading can be employed to assess the risk of early age cracking.

Keywords: *Ultra High Performance Concretes; Early-Age Cracking; thermo-Chemo-mechanics; reaction affinity; autogeneous shrinkage.*

1 Introduction

Ultra High Performance Concrete (UHPC) is a range of new cementitious composites that exhibit remarkable properties such as ultra-high strength, enhanced toughness, high durability, and very low permeability even when cracked [1-2]. However, a recent project on UHPC bridge girders has shown that due to the low water-cement ratio, as the curing water can not be supplied externally, the chemical shrinkage, which accompanies the hydration reactions (also called autogeneous shrinkage), and the thermal shrinkage, which is due to the highly exothermic reaction due to high cement content , can lead to detrimental cracking during setting [3].

Experiments indicate that autogeneous shrinkage begins about 20 hours after casting and reaches an asymptotic value at 10 days which ranges between 400 and 800 microstrains, depending on the mix composition of the UHPC and the environmental conditions [2].

To assess the risk of early age cracking, one can consider the characteristic length governing the heat diffusion equation for hydrating concrete l_{ch} [4]. For thin structures with dimension $\mathcal{D} << l_{ch}$, the heat diffusion is sufficiently intense to dissipate the latent heat supplied by the hydration process so that temperature does not rise significantly. Figure 1.a compares the characteristic length l_{ch} for normal concrete (NC), high strength concrete (HSC), and UHPC, as a function of the hydration degree (data of UHPC are from this work).

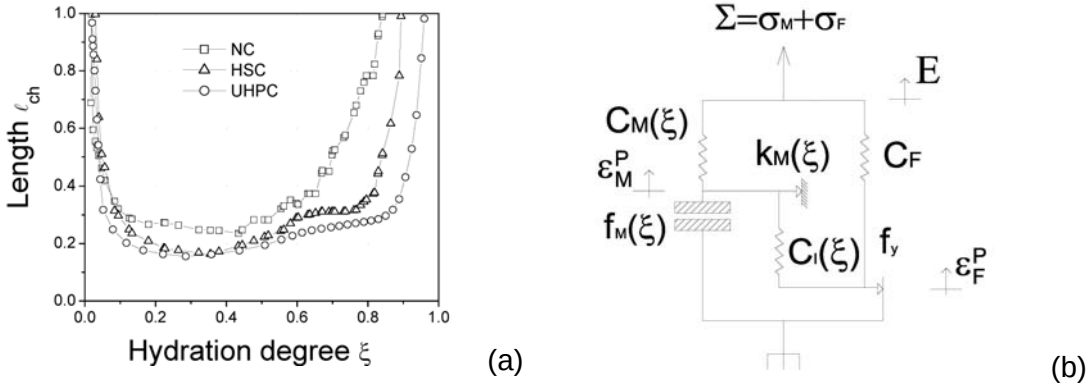

Figure 1: (a) Diffusion characteristic length vs. hydration degree; (b) 1D model for UHPC [5].

2 Background on Modelling UHPC at Early Age

2.1 Hardened model

The backbone of this model approach is the rheological model of Figue1.b proposed by Chuang and Ulm [5] to reproduce the tensile behaviour of UHPC materials. It consists of two parallel sub-devices reproducing the matrix stress σ_M and the fiber stress σ_F. The brittle-plastic behaviour of the matrix is described by an elastic spring of stiffness C_M, and a brittle crack device of strength f_t in parallel with a friction element of strength k_M. The frictional strength represents the residual stress after matrix fracture. Elasto-plastic behaviour of fibres is described by an elastic spring with stiffness C_F in series with a friction element with strength f_y. To simulate the shear transfer mechanisms at the fiber-matrix interface, an elastic spring C_I couples the matrix plastic strain ε_M^P with the fibre plastic strain ε_F^P.

As for the plasticity criteria, the elastic domains for the matrix and the fibres is described by Drucker-Prager type critera for compression-tension (CT) and compression-compression (CC) stress state and a Rankine type criterion for tensile-tensile (TT) stress state. The above mentioned loading surfaces are conveniently defined in functions of the following material parameters: the matrix tensile strength $\left(\sigma_{M,t}^0\right)$, the matrix compression strength $\left(\sigma_{M,c}^0\right)$, the

matrix biaxial compression strength $\left(\sigma_{M,b}^{0}\right)$, the fiber tensile strength $\left(\sigma_{F,t}^{0}\right)$, and the fiber compressive strength $\left(\sigma_{F,c}^{0}\right)$). At the onset of cracking, all these parameters are reduced by a constant γ to simulate the load drop.

2.2 Thermo-chemo-mechanical model

The hydration degree $\xi = m(t)/m(\infty)$ is defined as the ratio between the hydrated water $m(t)$ and the asymptotic hydrated water $m(\infty)$ [6]. The 3D thermo-chemical extension of the model is carried out within the framework of thermodynamics by replacing a second order expansion of the Helmotz free energy $\psi = \psi\left(\varepsilon, \varepsilon_M^P, \varepsilon_F^P, \xi, T\right)$ within the classical Clasius-Duhem inequality $\varphi dt = \Sigma d\varepsilon - d\psi - SdT \geq 0$, where φdt is the dissipated energy, S is the entropy and T is the temperature [7]. Under the engineering assumption that reaction affinity and entropy are not affected by external loads, the resulting incremental state equations can be decoupled in the following 2 sub-systems:

$$\begin{Bmatrix} d\underline{\underline{\Sigma}} \\ d\underline{\underline{\sigma}}_M \\ d\underline{\underline{\sigma}}_F \end{Bmatrix} = \begin{bmatrix} \underset{\sim}{C}_M(\xi) & \underset{\sim}{C}_F & -\underset{\sim}{C}_M(\xi):\underline{\underline{\alpha}}_M - \underset{\sim}{C}_F:\underline{\underline{\alpha}}_F & -\underset{\sim}{C}_M(\xi):\underline{\underline{\beta}}_M \\ \underset{\sim}{C}_M(\xi)+\underset{\sim}{C}_I(\xi) & -\underset{\sim}{C}_I(\xi) & -\underset{\sim}{C}_M(\xi):\underline{\underline{\alpha}}_M & -\underset{\sim}{C}_M(\xi):\underline{\underline{\beta}}_M \\ -\underset{\sim}{C}_I(\xi) & \underset{\sim}{C}_F(\xi)+\underset{\sim}{C}_I(\xi) & -\underset{\sim}{C}_F(\xi):\underline{\underline{\alpha}}_F & 0 \end{bmatrix} \begin{Bmatrix} d\underline{\underline{E}} - d\underline{\underline{\varepsilon}}_M^P \\ d\underline{\underline{E}} - d\underline{\underline{\varepsilon}}_F^P \\ dT \\ d\xi \end{Bmatrix} \quad (1)$$

$$\begin{Bmatrix} dS \\ d\tilde{\mathrm{A}} \end{Bmatrix} = \begin{bmatrix} -\dfrac{C}{T_0} & -\dfrac{L}{T_0} \\ 0 & -\eta \end{bmatrix} \begin{Bmatrix} dT \\ d\xi \end{Bmatrix} \quad (2)$$

2.3 Hydration kinetics

The hydration degree is obtained by integration of the normalized affinity $\tilde{\mathrm{A}}(\xi)$ from the second equation of (2). As convenient alternative, the hydration kinetics law can be written as

$$\frac{d\xi}{dt} = \exp\left(-\frac{E_a}{RT}\right)\tilde{\mathrm{A}}(\xi) \quad (3)$$

The Arrhenius's term E_a/R in Eq.(3) accounts for thermal activation behaviour of concrete hydration and was found to be about 4000K [8].

2.4 Heat Equation

A combined form of the first and second laws of thermodynamics $TdS = \delta W^{ext} - d\psi - SdT + \delta Q$ with the first equation of (2) yields the following working equation:

$$C\frac{dT}{dt} = K\nabla^2 T + L\frac{d\xi}{dt} \quad (4)$$

where ψ is Heltmotz free energy, and $\delta Q = div\underline{q}$ is the heat absorbed by the system through the boundary for a linear isotropic conduction law, $\underline{q} = -K\underline{\nabla T}$, where $\underline{\nabla T}$ is the

temperature gradient and K is the (scalar) conductivity coefficient. In energy balance Eq (4), $C\,dT/dt$ is the energy change stored in the system and $K\nabla^2 T$ is the net heat rate provided from the outside and $L\,d\xi/dt$ is the heat generated by hydration. The heat equation needs to be completed by thermal boundary conditions for the outgoing heat flux q·n through the surface ∂S oriented by outward unit vector $\underline{n}$

$$\underline{q}\cdot\underline{n} = -\lambda\left(T - T^{ext}\right) \tag{5}$$

2.5 Equilibrium Equation

From the constitutive equations of Eq.(1), the rate form of the stress reads

$$d\underline{\underline{\Sigma}} = d\underline{\underline{\sigma}}_M + d\underline{\underline{\sigma}}_F = \underset{\sim}{C}_M(\xi):\left(d\underline{\underline{\varepsilon}} - d\underline{\underline{\varepsilon}}^P_M - \alpha_M \underline{\underline{1}}dT - \beta_M \underline{\underline{1}}d\xi\right) + \underset{\sim}{C}_F(\xi):\left(d\underline{\underline{\varepsilon}} - d\underline{\underline{\varepsilon}}^P_F - \alpha_F \underline{\underline{1}}dT\right) \tag{6}$$

which explicitly shows the thermo-chemo-mechanical couplings of the physical phenomena.

3 Material Characterization

3.1 Hardened Property and Strength's and Stiffness' Evolution

The elastic properties ($\underset{\sim}{C}_M(\xi), \underset{\sim}{C}_F, \underset{\sim}{C}_I$) and strength properties ($f_M(\xi), k_y(\xi), f_y$) of the rheological model of Figure 1.b are calibrated by fitting the model response against the experimental uniaxial tensile response on specimens of dimension 70×70×280 mm [9] as shown in Figure 2. For low fiber content (~2% in Ductal®), fibers have a negligible effect on the composite elastic stiffness so that the fiber stiffness $\underset{\sim}{C}_F$ can be disregarded.

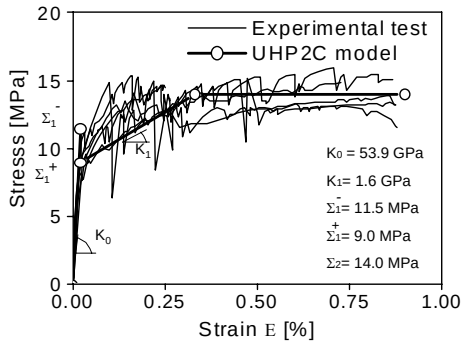

(a)

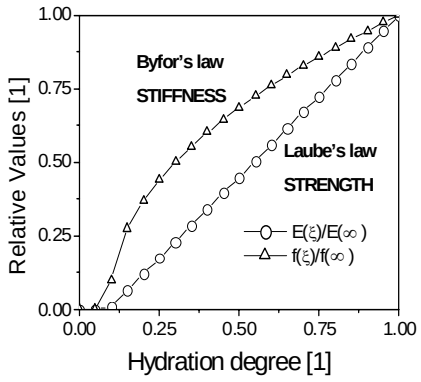

(b)

Figure 2: (a) Experimental and simulated uniaxial stress-strain response; (b) Stiffness' and strength's evolutions laws.

The strength properties of the loading functions ($\sigma^0_{M,t} = 11.5MPa$, $\sigma^0_{M,c} = 158.6MPa$, $\sigma^0_{M,b} = 190MPa$, $\sigma^0_{F,t} = 4.6MPa$, $\sigma^0_{F,c} = 9MPa$) are taken in accordance to available data in [1-2]. In a first approach, material isotropy and an unique Poisson's ratio ($\upsilon = 0.2$) are assumed.

3.2 Strength Growth and Stiffness Evolution

We assumed a single evolution law known as Laube's law (1990), for both tensile and compressive strength, which is a bi-linear relation between the strength property and the

reaction degree as shown in Figure 2.b. Note that the strength increases from 0 to f(∞) only after an initial percolation threshold ξ_o. Like the mechanical strength, the Young's modulus evolves substantially with the hardening of material and increases continuously from zero to an asymptotic value. For the stiffness evolution, the Byfors' law (1980) is assumed as showed also in Figure2.b.

3.3 Thermo-chemical properties

Owing to the high cement content in UHPC, an upper bound value of the volume heat capacity C is assumed as C=2700 kJ/(m³×K) [10]. The thermal conductivity, which mainly depends on the density of concrete, has been extrapolated from the available data for ordinary concrete as $K = 7\,kJ/(hr \times m \times K)$ [10].

The chemical dilatation coefficient $\beta_M = -450\,\mu m/m$ is taken from the asymptotic strain measured in shrinkage tests on Ductal® specimens in open air [2]. A percolation threshold ξ_o=0.1 is commonly employed in the early-age concrete literature [6].

3.4 Affinity kinetics

The increase of isothermal strength growth f_c^{iso} is found to be approximately proportional to the increase of hydration degree[10]. Thus, replacing $df_c^{iso} \propto d\xi$ in Eq.(3) yields a means to access the normalized affinity from the isothermal strength evolution tests. Figure 3.a and 3.b show the isothermal compressive strength curve interpolating the experimental tests on Ductal® [2,7] and the corresponding normalized affinity $\tilde{A}(\xi)$, respectively.

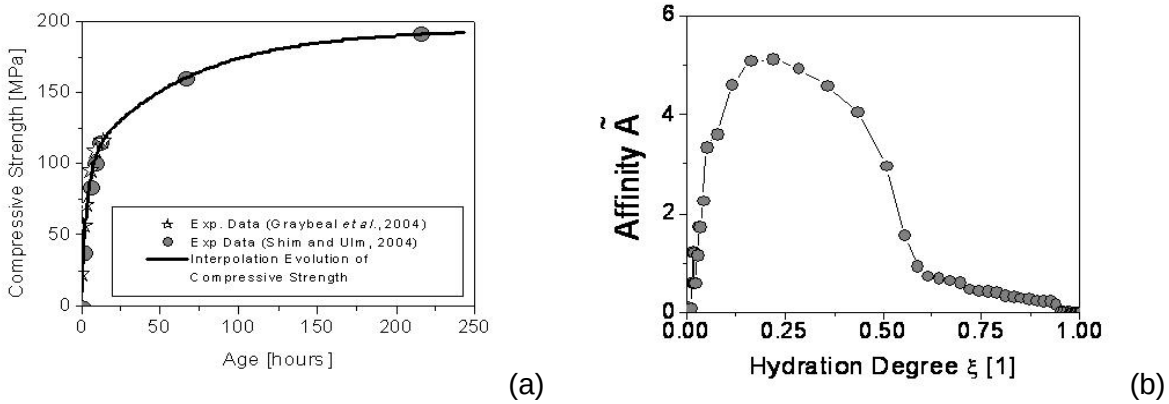

(a) (b)

Figure 3: (a) Compressive strength vs. time [2,7];(b).Employed affinity vs. hydration degree.

4 Case Study: The Glenmore Footbridge

The pedestrian bridge in Glenmore, Canada, constructed by Lafarge North America on November, 2006, consists of 37 m³ of UHPC material (Ductal®) has a length of about 33.6 m and a width of about 3.6 m. Figure 4.a shows the lateral view of the footbridge. The height of the tee-girder section varies from 1.1 m to 1.4 m so that the curved intrados is about 0.3 m higher than the ends. Bars of Glass Fiber Reinforced Polymer (GFRP) were added as

longitudinal and shear reinforcement. The prestressing cables are made of multiple strands 15 mm in diameter. Measurement equipment consisted of 8 thermocouples (TC) and the 4 strain gauges (SG) measuring both temperatures and longitudinal strains. The formwork is shown in Figure 4.b.

(a)

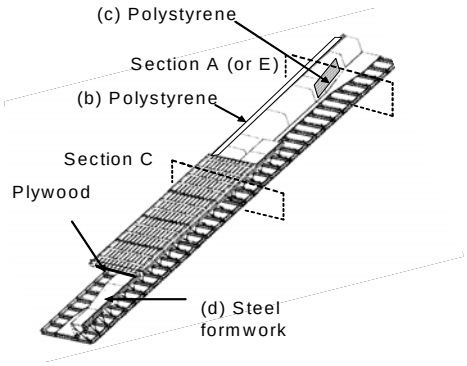

(b)

Figure 4: (a) Lateral view of the Glenmore footbridge; (b) Formwork.

Table 1 summarizes the construction phases during the first 200 hours of curing. The casting procedure lasted 8.8 hours. For the curing, the footbridge was placed in a tent equipped with a heat system.

Table 1: Construction phase.

Phase	Duration [hours]	Note
1	0-74.5	Curing before the formwork layers (c) of polystyrene is removed
2	74.5-77.8	Curing before the tendon T#1 in the deck is prestressed
3	77.8-107.0	Curing before the rest of the formwork is removed
4	107.0-131.7	Curing before the two multi-strand tendons T#2 and T#3 were prestressed
5	131.7-201.6	Curing

The decoupling hypothesis allows us to apply the early-age model in a two step manner. First, the thermo-chemical problem of Eqs. (3) and (4) is solved to predict the temperature and reaction degree within the structure; then, the thermo-chemo-mechanical problem of incremental Eq.(6) is solved to obtain the stress and strain fields. In the finite element model, the effect of the GFRP bars on the elastic behaviour of the structure is disregarded, while prestressing is modelled by equivalent loading.

4.1 Thermo-chemical analyses

The average temperature of the material at the beginning of casting was about 6^{O}C. Within the module TEXO of the finite element code CESAR-LCPC [11], the hydrating bulk material is modelled by means of solid elements, while the loss of heat through the formwork is modelled by linear exchange elements according to Eq.(5). Formwork removal is modelled by modifying the exchange coefficient taken from existing literature (Ulm and Coussy, 2001). Figure 5 shows a comparison between the simulated and measured temperatures over time for the points monitored at the midspan section. The effect of hydration heat is not negligible, since the temperature rise is slightly higher than one expected for ideal adiabatic condition.

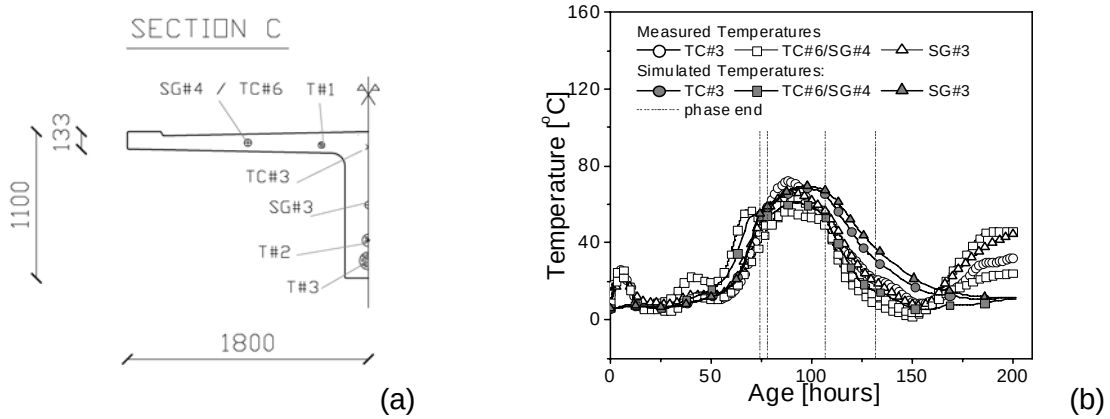

Figure 5: (a) Thermocouple (TC) and strain gauges (SG) in midpspan section; (b) Comparison between simulated and experimental temperature histories.

4.2 Mechanical analyses

Displacement boundary conditions reflect the formwork demolding: no displacement is allowed with the formwork in place, while the surface becomes stress-free once the formwork is released. Displacement in the longitudinal direction is slightly restrained as the supports are inclined upwards by 3.4%.

Figure 6.a compares the measured and simulated strain history for the monitored point of the midspan section. Finally, we employ the concept of a level of loading $\mathscr{L}$ to evaluate the risk of early age cracking (Hellmich et al., 2004) which for a Drucker-Prager and Rankine type criterion are defined respectively as

$$\mathscr{L}_j = \frac{\phi_M(\xi)\, tr\left(\underline{\underline{\sigma}}_M\right) + \left|\underline{\underline{s}}_M\right|}{c_M(\xi)} \leq 1 \quad j = CC, CT; \quad \mathscr{L}_{TT} = \frac{tr\left(\underline{\underline{\sigma}}_M\right)}{\sigma^0_{M,t}(\xi)} \leq 1 \tag{7}$$

where $\left|\underline{\underline{s}}_M\right|$ is the magnitude of the deviator stress tensor, and $\phi_M(\xi)$ and $c_M(\xi)$ are standard coefficients depending on the matrix or fibre strength values. Figure 6.b shows the levels of loading for the point in the midspan section which experienced the highest strain gradient.

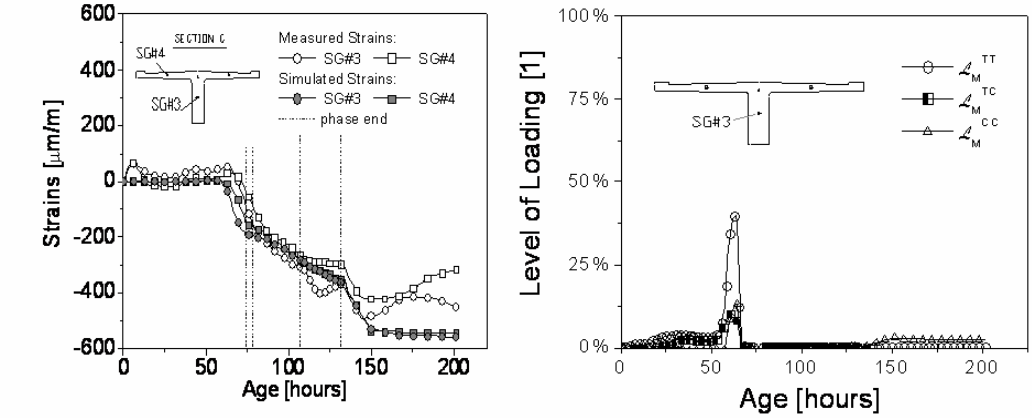

Figure 6: (a) Simulated and experimental strain histories for mid-section; (b) Level of loadings;

5 Conclusions and outlook of future works

1. The effect of hydration heat can be critical in UHPC structure with size larger than the critical diffusion length of 0.20-0.40 m, depending on the hydration degree;

2. The energy de-coupling hypothesis at the base of the presented thermo-chemo-mechanical approach facilitates the calibration of the model properties and yields an accurate prediction of temperature and strain histories (strain measurement error is about 24%± 2% for a time setting between 70 and 200 hours);

3. The concept of level of loading can be used as quantitative indicator of risk of early age cracking. In this application, the level of loading for tension-tension stress of states has reached a maximum of 39% at about 63 hours after casting, i.e., relatively limited risk of cracking.

Acknowledgements. We would like to thank the Marie Curie FP6 progarmme for supporting the mobility of the first author and Lafarge North America for making available the data of Glenmore footbridge.

6 References

[1] Association Française de Genie Civil (2002). "Ultra high performance fibre-reinforced concrete - interim recommendations." J. Resplendino and J. Petitjean eds.

[2] Federal Highway Administration (2006a). "Material Property Characterization of Ultra-High Performance Concrete" U.S. Department of Transportation, Publication No. FHWA-HRT-06-103.

[3] Park H., Ulm F.-J., and Chuang E. (2003). "Model-based optimization of ultra high performance concrete highway bridge girders," CEE Report R03-01, Massachusetts Institute of Technology, March.

[4] Loukili, A., and Richard, P, (1995) “Creep and Shrinkage of Ultra High Performance Steel fibre Reinforced Concrete” Int. Conf. Concrete Under Sever Condition Environment and Loading, Ed. KSakai, N. Banthia and O.E.Gjørv, Sapporo Japan, 2-4 August, 2, 1553-1559.

[4] Ulm, F.-J., Coussy, O., (2001). "What is a "massive" structures at early ages? Some dimensional arguments," J. Engrg. Mech., May, 512-522.

[5] Chuang, E., and Ulm, F.-J. (2002). "Two-phase composite model for high performance cementitious composites," Journal of Engineering Mechanics-ASCE, 128(12), 1314-1323.

[6] Ulm, F.J., and Coussy, O. (1996). "Strength Growth as Chemo-Plastic Hardening in Early Age Concrete," J. Engrg. Mech., ASCE, December, 1123-1132.

[7] Shim, J.M., and Ulm, F.J. (2004). "Prediction of Early-Age Cracking of UHPC Materials and Structures: A Thermo-Chemo-Mechanics Approach," MIT-CEE Report R04-03 to Lafarge, M.I.T., Cambridge, MA.

[8] Torrenti, J.M., (1992) "La résistance du béton au très jeune âge (Strength of concrete at very early ages)" Bulletin de Liason des Laboratoires des Ponts et Chaussées, Paris, France, 179, 31-41 (in French).

[9] Chanvillard, G., Rigaud, S., (2003) "Complete characterization of tensile properties of Ductal® UHPFRC according to the French recommendations," Proc. of the Fourth Int. RILEM workshop HPFRCC4, Eds. Naaman, A.E., Reinhardt, H.W., 21-34.

[10] Mindess, S., and Young J.F., (1981) "Concrete", Prentice-Hall, Englewood Cliffs, New Jersey.

[11] LCPC. (2004). "CESAR-LCPC Manual of examples: modeling of early-age UHPC," Laboratoire Central des Ponts et Chaussées, Paris, France.

Federico Bonomelli
Mako Shark
Dolzago (LC), Italy

Matteo Colombo
Assistant Professor
Politecnico di Milano
Milan, Italy

Marco di Prisco
Professor
Politecnico di Milano
Milan, Italy

Letizia Mazzoleni
Research Assistant
Politecnico di Milano
Milan, Italy

Textile cementitious composites at high temperatures

Summary

Textile materials are more and more used for special applications. This paper proposes the use of textile cementitious composites in car brakes and investigates their behaviour at high temperatures.
A high performance mortar reinforced with carbon fibre fabric is here presented.
The experimental investigation is made by two different phases: the first one is aimed to a mechanical characterization of the cementitious matrix at room condition according to national recommendation. The second phase of the experimental programme investigates the compressive behaviour of small disks (80mm diameter and 20mm thick) at high temperatures. The tests are performed at hot condition inside a furnace mounted onto a compressive machine and three different temperatures (200, 400, 600°C) were considered beside room condition taken as a reference. In the disks, 3 or 5 fabric layers were introduced and, in one case, an external carbon fibre ring was applied in order to prevent cracks related to cooling thermal shock. The stiffness variation of the specimen was investigated by means of unloading-reloading cycles performed with a frequency equal to 0.5Hz and in a stress range between 2 and 6 MPa.

Keywords: *textile cementitious material, high temperatures, stiffness variation, brakes*

1 Introduction

Modern textile technology offers a wide variety of fabrics with great flexibility in fabric design, like the control of yarn geometry and orientation. Several researchers investigated the improvement in the mechanical behaviour of cement matrixes when fabrics are introduced. Different geometry [1] and materials were considered in many investigations as, for instance, woven [2,3], glass [4] and carbon [5,6]. In this paper an unusual application of these materials is presented: the use of carbon fibre textile cementitious composite for car brakes. The main idea is to take advantage of the low thermal diffusivity of the cementitious matrix, its mechanical performance even at high temperature and the physical and mechanical properties of the carbon textile used.

In the application, here presented, a textile cementitious composite disk is kept between two spheroid-graphite cast iron disks and the brake pressure is directly applied over the iron ring. The scheme and a picture of the braking system is represented in Figure 1.

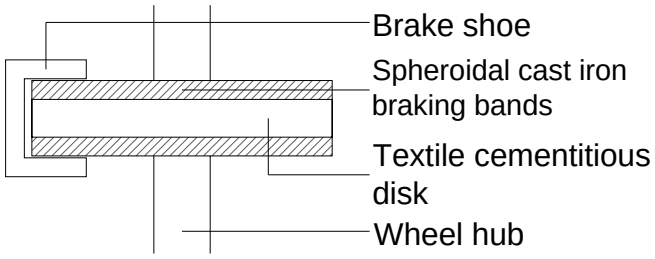

(a)

(b)

Figure 1: Braking system: (a) scheme (b) picture.

2 Material characterisation

The material characterization of the matrix was performed according to Italian Standards for mortars. First of all, three point bending tests on unnotched specimen were carried out according to UNI EN 196-1 on small beams, 160 mm long, with a 40 x 40mm cross section. The loading scheme used is presented in Figure 2, where also a picture of the test is shown. Once performed the bending tests, on each remaining half of the specimen a compressive test was carried out considering a loading area of 40 x 40 mm.

The experimental results are summarized in Table 1, by means of the indirect tensile strength ($f_{ct,fl}$) and the cubic compressive strength (R_c).

(a)

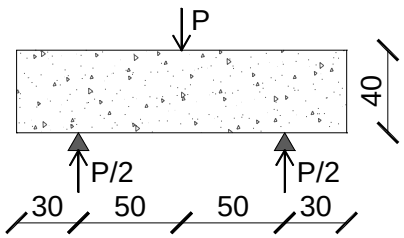

(b)

Figure 2: Three point bending test set-up: (a) picture (b) scheme.

Table 1: Three point bending test and uniaxial compressive test results.

Identification specimen	**Max load [N]**	**$f_{ct,fl}$ [MPa]**	**$f_{ctm,fl}$ [MPa] (std %)**	**R_c [MPa]**	**R_{cm} [MPa] (std %)**
E1	3884.3	9.10	9.52 (4.03%)	82.32	77.50 (8.87%)
				78.46	
E2	4206.1	9.86		76.71	
				80.30	
E3	4099.2	9.61		82.90	
				64.29	

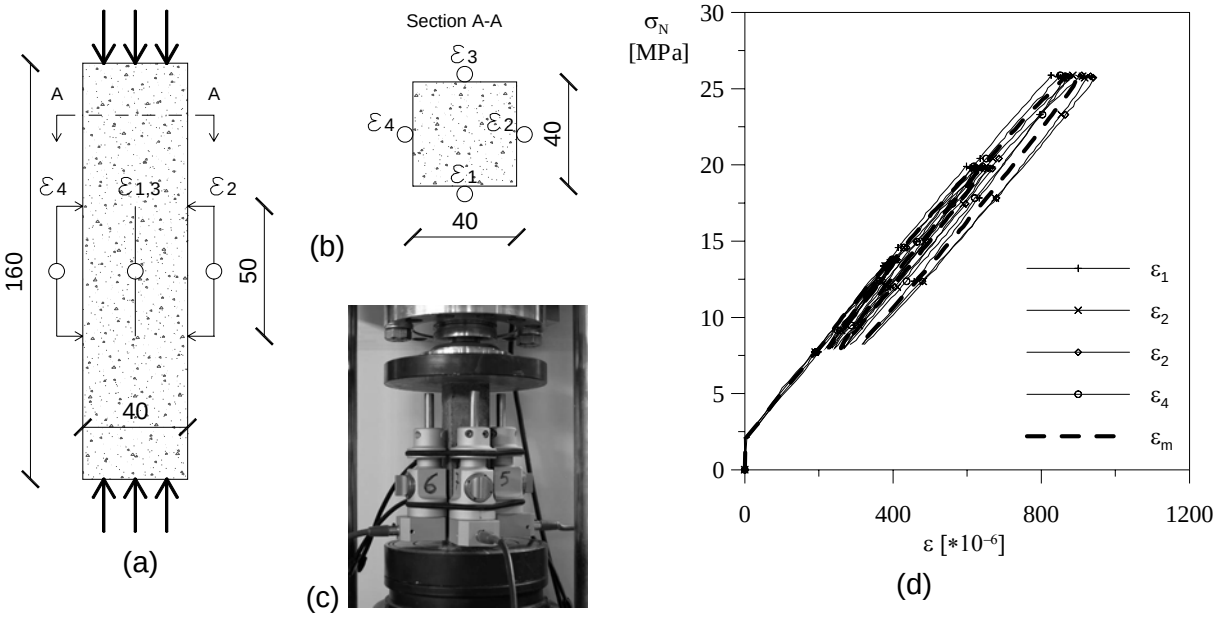

Figure 3: Elastic Modulus tests: (a,b,c) test set-up, (d) test results for specimen E1.

Table 2: Elastic modulus results.

Identification specimen	**σ_{min} [MPa]**	**σ_{max} [MPa]**	**E_{sec} [GPa]**	**E_{sec-av} [GPa] (std %)**	**R_c [MPa]**	**R_{cm}[MPa] (std %)**
E1	7.75	25.83	29.72	29.67 (0.11%)	75.84	76.50 (3.93%)
					70.91	
E2	7.75	25.83	29.64		77.57	
					81.08	
E3	7.75	25.83	29.67		76.38	
					77.24	

The elastic modulus of the mortar was evaluated by means of proper tests according to Italian standard UNI 6556. A specimen 160 mm high and a 40x40 mm cross section was adopted, four extensometers were used to measure the central displacement of the specimen by considering a gauge length equal to 50 mm; different loading cycles were applied to each specimen in the range 1/10 - 1/3 of the average compressive strength of the material, previously evaluated. The test set-up is presented in Figure 3.

Table 2 shows test results by means of the stress range used to define the elastic modulus (minimum σ_{min} and maximum σ_{max} stresses applied), the secant modulus defined for each specimen, its average value and finally the cubic compressive strength obtained on each specimen, once defined the elastic modulus according to the same provisions previously specified (UNI EN 196-1).

3 Disk tests at high temperatures

Once performed the mechanical characterization of the matrix, the behaviour of the textile material was investigated both at room and high temperatures. In order to better reproduce the brake situation, a proper experimental set-up was adopted. A 80 mm diameter disk, 20 mm thick, was uniformally supported on the lower face and loaded on the upper one by a punch acting on a small circular region, characterized by a 20 mm diameter. For each specimen the stiffness at 20, 100, 200, 400 and 600°C was evaluated.

The test set-up is shown in Figure 5a; the test region was placed inside a furnace and two quartz bars (characterized by a very low thermal dilatancy coefficient; $\alpha=5\cdot10^{-7}$) were used to take into account the steel shaft thermal elongation, when heated. During the tests, each temperature threshold was reached with the maximum heating rate allowed by the furnace (4.5°C/min), and once reached, a one hour stabilization phase at that temperature was imposed to guarantee a uniform temperature distribution into the specimen. The stiffness at each temperature was defined performing 20 unloading re-loading cycles between an average pressure of 2 and 6 MPa at a 0.5Hz frequency and the assumption shown in Figure 5b was adopted.

Three different specimens were considered: a three and a five layer carbon fibre over the thickness and a five layer fabric with an external ring made of carbon fibre were prepared.

The experimental results are summarized in Table 3 and Figure 6, where the specimen stiffnesses at different temperatures are indicated.

It's quite interesting to observe how the specimen stiffness increases with temperature for all the tests performed. This result can be related to the high homogeneity into the mortar matrix in which no differential thermal expansion was experienced. Analogue results were proposed in the literature referring to the residual compressive strength of different cement pastes at increasing temperatures (up to 600°C) by Khoury [7]: the strength in very homogeneous matrix is also in that case quite constant or even increases with temperature growths.

After the unloading-reloading cycles at maximum temperature (600°C), the furnace was opened and the disk was extracted from the oven. The two disks without the external ring experienced some cracks due to thermal shock. The crack patterns are highlighted in Figures 7a,b.

First of all, the comparison between 3 and 5 layer specimens highlights a reduced stiffness for 5 layer one: the main cause has to be searched in the more difficult compaction of the sample in the casting process.

Looking at the results, it's also possible to observe in the five layer specimens how the initial stiffness is lower when the external ring is applied even at room condition.

Two possible reasons can be found to justify this fact. The first one is that the specimen with external ring was previously subjected to a thermal shock in order to verify that no cracks occur into the specimen after a fast cooling of the structure itself. The disk was heated up to 800°C and, once reached this temperature, was extracted from the furnace. In this way the

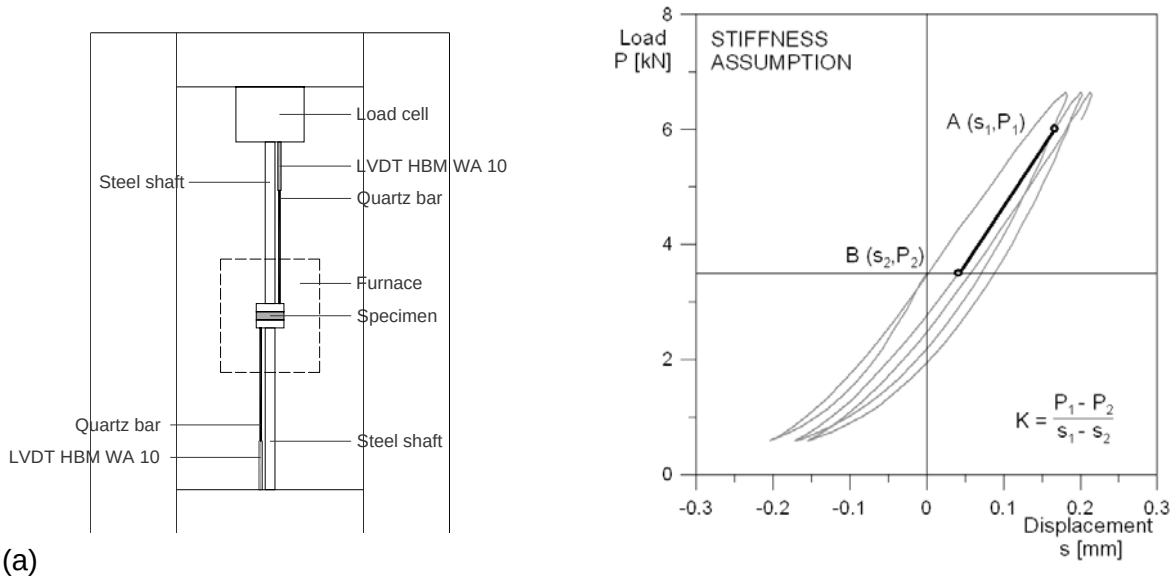

(a)

Figure 5: Test set-up (a) scheme (b) stiffness assumption.

specimen experienced a thermal damage before unloading-reloading cycles were applied. As well known, carbon fibre has a negative thermal expansion coefficient. In this way the confining action increases with temperature and allows a better crack control in fast cooling phase starting from high temperatures.

The second reason to justify the lower stiffness can be related to the rough upper surface of the disk; this occurrence caused a stress concentration during the first loading of the specimen at room condition, giving rise to the crack shown in Figure 7c.

In order to evaluate the ring contribution and the effect of the crack that covered the 2/3 of the disk thickness, some linear elastic numerical simulations of the disk were performed. The numerical stiffness of the disk are summarized in Figure 8 with the model used to reproduced the cracked specimen. In this model, the crack pattern (position, depth and opening) was taken similar to the one presented in the disk discussed (Figure 7c).

Comparing the results obtained, the confining effect of the ring at room temperature is quite negligible (less than 1%), while the crack introduction causes a stiffness reduction close to 4%, lower than the one experimentally detected. This consideration brings us to suppose that the interaction between the crack formation and the thermal damage experienced before loading (thermal shock due to fast cooling) caused the stiffness reduction shown in the results.

4 Application example

In order to verify the performance of the solution proposed in the real operating conditions, a real brake test was performed. A mortar disk 26 mm thick with an internal diameter equal to 149 mm and an external one of 305 mm was casted with 7 layers of carbon fibre fabric and with an external ring of carbon fibre. The mortar disk was closed between two spheroid-graphite cast iron disks, specifically designed. The weight of the disk, so conceived, is lighter than a common one (only 5.9 kg against 8.6 kg).

Table 3: Experimental results: stiffness and standard deviation (std) for the three samples.

T [°C]	3 layers		5 layers		5 layers + ring	
	K_m [kN/mm]	K_{std} [kN/mm] (%)	K_m [kN/mm]	K_{std} [kN/mm] (%)	K_m [kN/mm]	K_{sdt} [kN/mm] (%)
20	25.611	1.796 (7.014%)	20.362	1.360 (6.677%)	17.541	0.107 (0.612%)
100	27.022	0.563 (2.084%)	20.653	0.399 (1.930%)	-	-
200	27.785	0.360 (1.296%)	20.493	0.604 (2.947%)	18.232	0.205 (1.125%)
400	28.468	0.399 (1.401%)	23.691	0.437 (1.844%)	20.087	0.040 (0.197%)
600	27.585	0.515 (1866%)	23.560	0.472 (2.003%)	21.802	0.055 (0.251%)

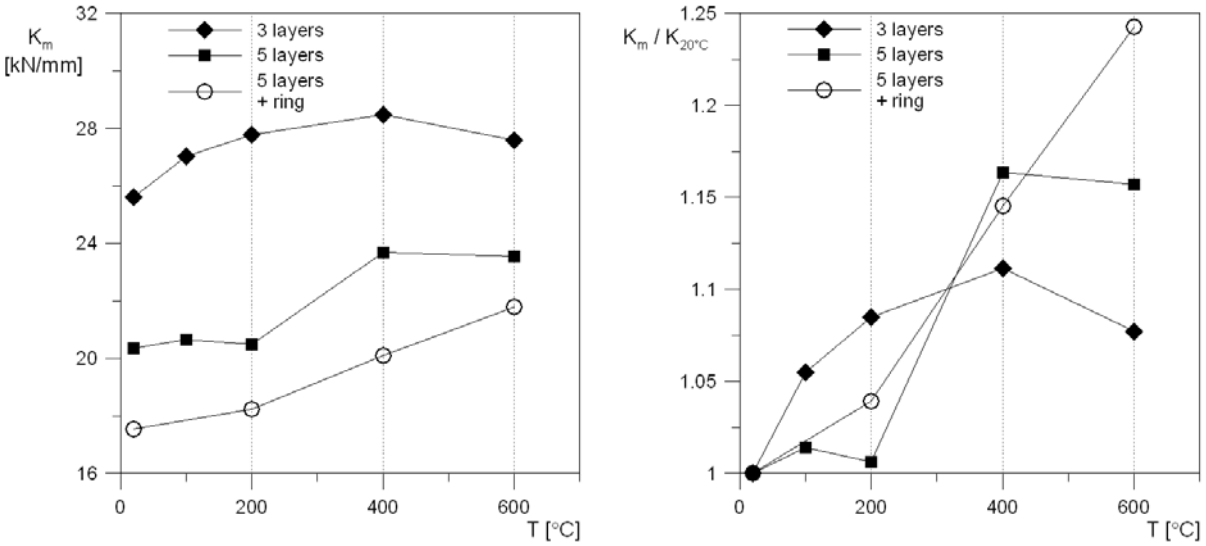

Figure 6: Experimental results: stiffness vs. temperatures and its variation for the three sample compared.

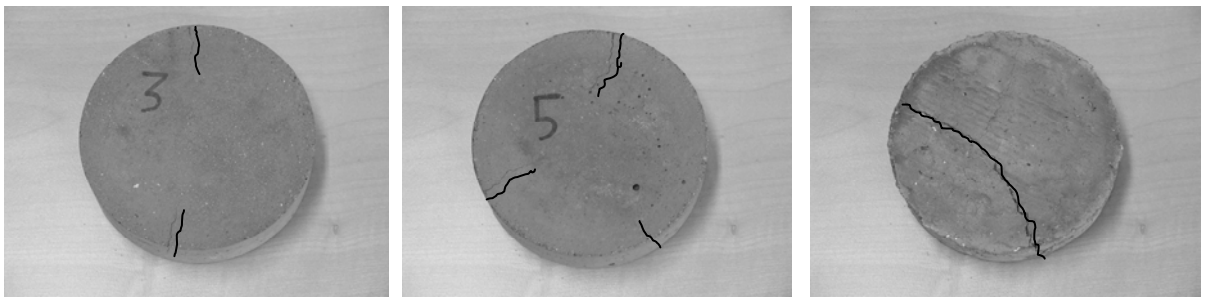

(a) (b) (c)

Figure 7: Crack pattern of the specimen after test: (a) 3 layers (b) 5 layers (c) 5 layers+ring.

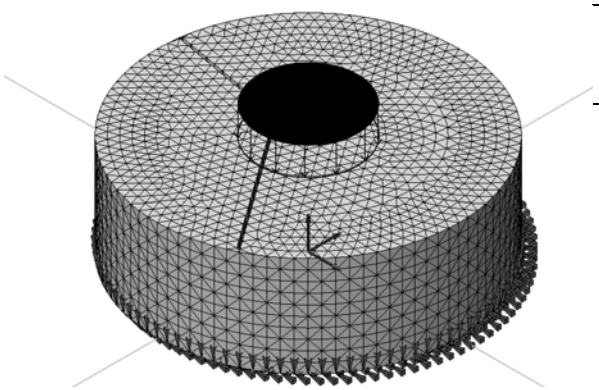

Specimen	Numerical stiffness [kN/mm]
Without ring	28.0
With ring	28.2
Cracked disk	26.9

Figure 8: Numerical model for the cracked specimen and stiffness numerically obtained.

The brake tests was performed on a proper machine made of a heavy basement with a 180kg flywheel able to simulate the speed of a vehicle balanced on a single wheel. The power of the engine was 85 hp and the breaking system used to stop the flywheel was connected to an electronic equipment devoted to control the test and measure the temperature of the brake itself. This test was aimed to reproduce the situation of the brake in a GT racing car. The set-up is shown in Figure 9a.
A series of 23 full brakings from 300 km/h was performed and the test data are summarized in Table 4.
At the 23rd braking, the un-sintered brake pads started burning and the mortar disk becomes incandescent. After the fire, as can be see from Figure 9b, the concrete disk didn't experience any serious damage.

5 Conclusions

The paper refers to a preliminary investigation on a new braking system conceived to reduce the weight and optimizing the durability by means of high performance textile mortar obtained by using a carbon fabric.
Taking advantage of the experimental results described in this paper it is quite interesting to

Figure 9: Brake test: (a) test set-up (b) textile cementitious disk after test.

Table 4: Braking test: number of consecutive braking events and final temperature of the braking band and of the disk.

Number of consecutive braking events	2	4	6	11
Final temperature of braking band [°C]	120	474	470	500
Final temperature of the disk [°C]	94	160	283	345

observe how the high homogeneity of the mortar ensures the material to have a constant or even increased stiffness at different high temperatures. The use of external carbon fibre ring ensures a confinement action increasing with temperatures also because of the negative sign of the carbon fibre thermal expansion coefficient. This contribution prevents the crack formation into the disk after a fast cooling. In order to improve the performance of the material, an addition of short fibre randomly dispersed can be supposed to reduce any possible crack into the cementitious matrix, in the direction at right angle with respect to fabric plane. As a matter of fact, some investigations in the literature show how the interaction of fibre and fabrics improves ductility and ensures to the material a strength higher than the simple cumulative behaviour of the fabrics and the fibre themselves [4].

6 References

[1] Peled, A., Bentur, A.: Geometrical characteristics and efficency of textile fabrics for reinforceing composites. In Cement and Concrete Research 30, pp. 781-790, 2000.

[2] Peled, A., Bentur, A., Yankelevsky, D.: Flexural performance of cementitious composites reinforced by woven fabrics. In Materials in Civil Engineering (ASCE), 11(4), pp. 325-330, 1999.

[3] Peled, A., Mobasher, B.: Pultruded fabric-cement composites. In ACI Materials J., 102(1), pp. 15-23, 2005.

[4] Hinzen, M., Brameshuber, W.: Influence of short fibres on strength, ductility and crack development of textile reinforced concrete. In proceding of the Fifth International RILEM Workshop HPFRCC5 PRO53, Reinhardt, H.W. and Naaman A.E. (eds.), RILEM Pubblications S.A.R.L.,pp. 105-112, Mainz, 2007.

[5] Kazuhisa, S., Noayoshi, k., Yasuo, K.: Development of Carbon Fiber Reinforced Cement. In Advanced Materials: The Big Payoff National SAMPE Technical conference, SAMPE, pp. 789-802, Covina, calf., 1998.

[6] Nishigaki, T., Suzuki, K., Matuhashi, T., Sasaki, H.. High Strength Continuous Carbon Fiber Reinforced Cement Composites (CFRC). In Proc. Of the Third International Symposium on Brittle Matrix composites, A.M. Brandt and I.H. Marshall (eds.), Elsevier Applied Science, pp. 344-355, Warsaw, 1991.

[7] Khoury, G.A.: Compressive strength of concrete at high temperatures: a reassessment. In Magazine of Concrete Research, 44, No. 2, pp. 291-309, 1992.

Ulrich Diederichs
Prof. Dr.-Ing.,
Universität Rostock
Rostock, Germany

Olaf Mertzsch
PD Dr.-Ing. habil.
Universität Rostock
Rostock, Germany

Behaviour of Ultra High Strength Concrete at High Temperatures

Summary

This paper reports results of experimental investigations concerning high temperature behaviour of four ultra high strength concrete mixtures. Two series were made with coarser diabase aggregates (max. grain size 3 mm – 6 mm), two only with fine quartz powder (max. grain size 0.125 mm - 0.6 mm). Three series were heat treated at 90 °C for 48 hours, and three series contained Polypropylene fibres (PP-fibres). Their cylinder (∅ 70 mm, h = 195 mm) strength was in between 160 and 180 N/mm^2.

The studies comprised investigations of mechanical properties, behaviour and tests like stress-strain-relations, thermal strain, transient creep strain and restraint tests. Attention was also paid to the chemical and physical background of their alterations due to heating and investigations by aid of simultaneous thermal analysis, dilatometry and Hg-porosimetry were performed.

The investigated materials showed very similar behaviour, partly it was comparable with the behaviour of high strength concrete. Specimens containing PP-fibres suffered no spalling during heating.

Keywords: *Ultra High Performance Concrete (UHPC); high temperature behaviour, thermal analysis, porosity, transient creep, thermal strain, restraint forces, σ – ε – relations.*

1 Introduction

Ultra High Strength Concrete, also called Ultra High Performance Concrete (UHPC), is a very dense material with compressive strength between 150 N/mm² and 250 N/mm². The enormous strength reveals new possibilities to build very filigree, light weight and raw material saving concrete structures.

Investigations concerning UHPC have been already conducted during the 1970ies in the USA and Scandinavia [1]. First applications in building technology followed in 1997 by the erection of a pedestrian bridge in Canada and a repair of a cooling tower in Cattenom in France [2, 3].

Concerning high temperature behaviour of UHPC up to now only a few data are at hand [3]. The aim of the study discussed hereafter was to fill some of the present gaps of knowledge [4].

2 Experimental programme

To obtain information concerning thermally induced changes of the material behaviour thermal analyses, weight loss measurements and dilatometric studies were performed during heating of the materials. The resulting structural changes were analysed by mercury porosimetry.

The main part of the study formed investigations of the mechanical behaviour and the determination of material data by following tasks:

- investigations concerning the spalling behaviour
- measurements of ♦ – ℳ– relations at high temperatures, and determination of the respective strengths, E-moduli and ultimate strains
- determination of transient creep strain and free thermal strain
- determination of the restraint forces

3 Materials

The proportions of the investigated mixes are given in the following table 1.

Table 1: Mix proportions of the specimens, related to the cement weight

Materials	**FIR/LA/PF/H Series 1**	**FIR/LA/PF Series 2**	**FIR/022/PF/H Series 3**	**FIR/022/H Series 4**
CEM I 42.5 N (SR)	1	1	1	1
Silica fume	0.2500	0.2500	0.2500	0.2500
PP fibres	0.0004	0.0004	0.0004	0
Sand (0.125mm-0.6mm)	0.8000	0.8000	0.8000	0.8000
Diabase	1.8000	1.8000		
Quartz	0.2000	0.2000	0.2000	0.2000
Super plasticiser	0.0500	0.0500	0.0400	0.0400
Water	0.2190	0.2190	0.2000	0.2000
W/B ratio	0.2600	0.2600	0.2200	0.2200
W/C ratio	0.2000	0.2000	0.1760	0.1760

The binder consists of Finnish Super Rapid Cement and 25 % silica fume. Series 1 and 2 were made with coarse crushed diabase aggregates (3 – 6 mm grain size). Series 3 and 4 contain only fine quartz sand (0.125 - 0.6 mm grain size) and series 4 was made without PP-fibres. “H” indicates heat treatment at 90 °C and saturated water vapour for 48 hours. The materials were cast in plastic pipes to produce cylindrical specimens (diameter=70 mm, length=200 mm) for the mechanical high temperature tests.

The selection of materials and production of the specimens were conducted by Prof. Vesa Penttala and Dr. Andrzej Cwirzen at Helsinki University of Technology, Dep. of Building Materials Technology [5]. At the commencement of the test the age of the specimens was more than half a year.

4 Results

4.1 Thermal stability and structural changes

The thermal stability of the materials has been investigated by simultaneous thermal analysis. Measured and determined, resp., were the weight loss, the differentiated weight loss and the DTA-curves, which give the temperature difference between an inert sample and the sample under investigation.

The series 1 sample showed a series of peaks indicating the following endothermal and exothermal reactions (see Figure 1):

- 20 °C – 120 °C evaporation of the physically bound water (about 3 % weight loss)
- 175 °C – 210 °C exothermal reaction due to the deterioration and oxidation of PP-fibres
- 120 °C – 650 °C continuous liberation of physically stronger bound water (about 3% weight loss)
- 573 °C DTA-peak due to quartz transformation ♋ ✹ ß-quartz, which is hardly visible in Figure 1, but was very small in the original curve
- 650 °C – 700 °C step in the weight loss curve, which indicates the dehydration of the CSH-phases, connected with the formation of ß-C_2S (about 0,3 % weight loss) [6]
- 700 °C–1000 °C further continuous liberation of CSH-water (again 1 % weight loss)

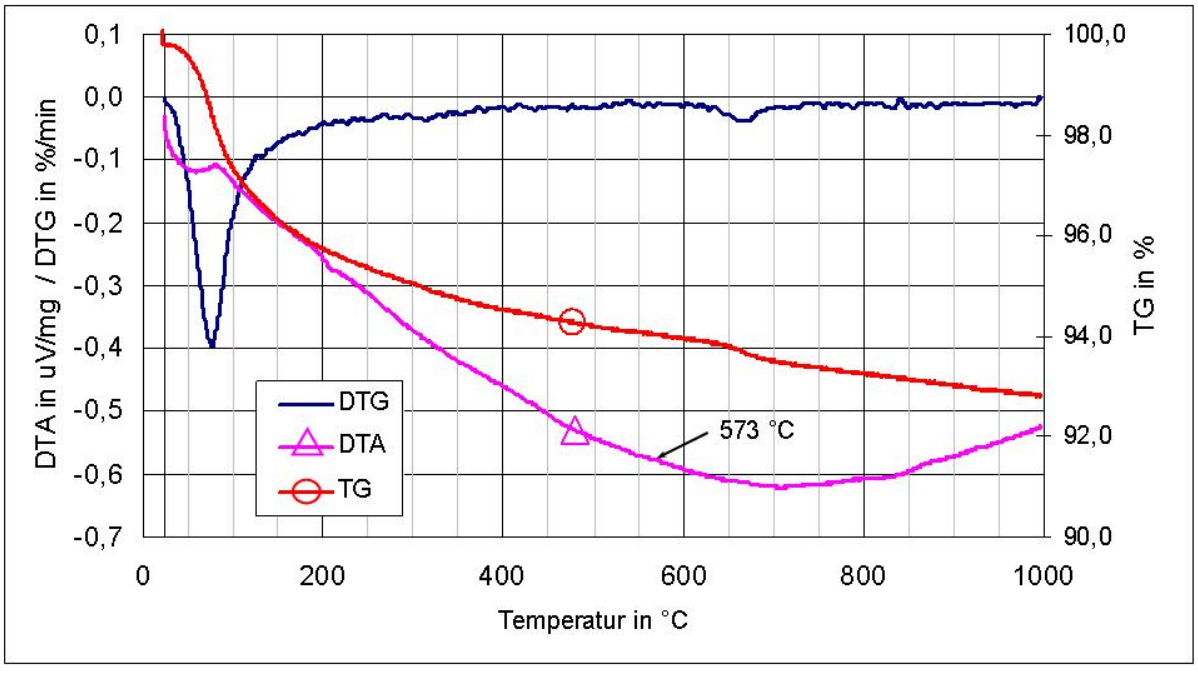

Figure 1: Results of the simultaneous thermal analyses obtained with series 1 material

The structural changes due to heating were investigated by aid of mercury porosimetry. For these tasks 10 mm thick slices were cut out of the cylindrical specimens and heated with a rate of about 5 K/min to 150 °C, 250 °C, 350 °C, 450 °C, 550 °C, 650 °C, 750 °C and 850 °C,

resp., and analysed after cooling to ambient temperature. – The 20 °C specimens were only vacuum dried at room temperature. – Figure 2 shows typical results of the measurements.

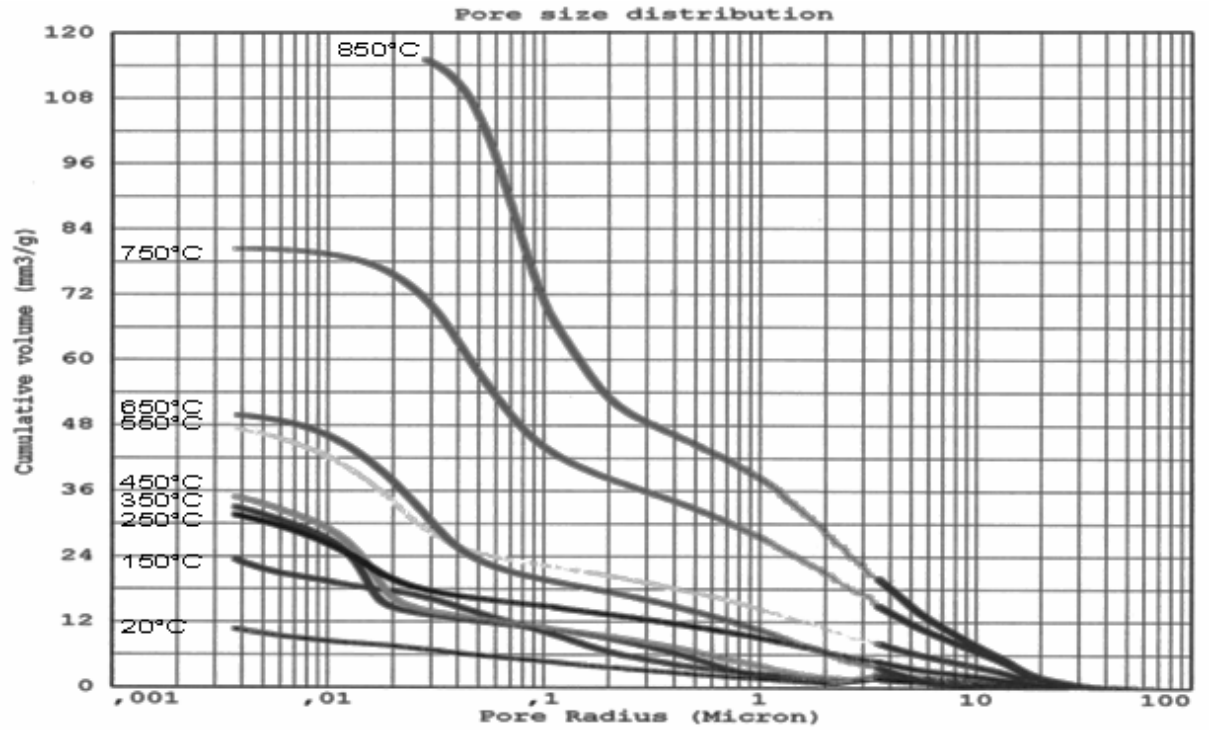

Figure 2: Cumulative pore size distributions of specimens of series 3, at ambient temperature and after heating to 150 °C, 250 °C, 350 °C, 450 °C, 550 °C, 650 °C, 750 °C and 850°C, resp.

Figure 2 indicates that the thermally unstressed material has nearly no porosity in the pore region between 30 µm and 0.4 µm. The capillary porosity in pore region 0.4 - 0.03 µm, which amounts to roughly 3 mm²/g, or about 0.8 Vol.-%, is also negligibly low. The accessible gel pore volume (0.03 - 0.00375 µm) has also a rather low volume. It reaches ≙ 4 mm³/g or 0.9 Vol.-%.

But, already a mild thermal treatment (150 °C exposure) leads to remarkable changes in the capillary pores and the gel pores. Above 250 °C growth of the gel pores radii seems to be much bigger than that of the capillary pore radii. Obviously only when heated to 450 °C or above the formation of bigger cracks seems to start, and the pore volume between 30 µm and 1 µm appears in the diagram.

From these results, it can be concluded that first after heating to 250 °C or higher temperatures cracks are formed and capillaries are opened, which enables the water vapour to escape at such low vapour pressure that spalling of the material may be avoided.

4.2 Mechanical behaviour

The stress-strain relations have been measured at 20, 150, 250, 350, 450, 550, 650, 750, and 850 °C, resp., with all four materials. Figure 3 shows the testing equipment (with oven and length measuring device). The specimens were heated to the test temperatures (with

rate of 3 K / min) and homogenized for 1 h. The homogenizing was necessary to obtain a steady state temperature distribution in the specimens. During this thermal regime none of the specimens, which were made with PP-fibres exploded or indicated spalling. The subsequent compressive tests at high temperatures have been carried out with a loading rate of 0.5 MPa/s while stress-strain-relations were measured.

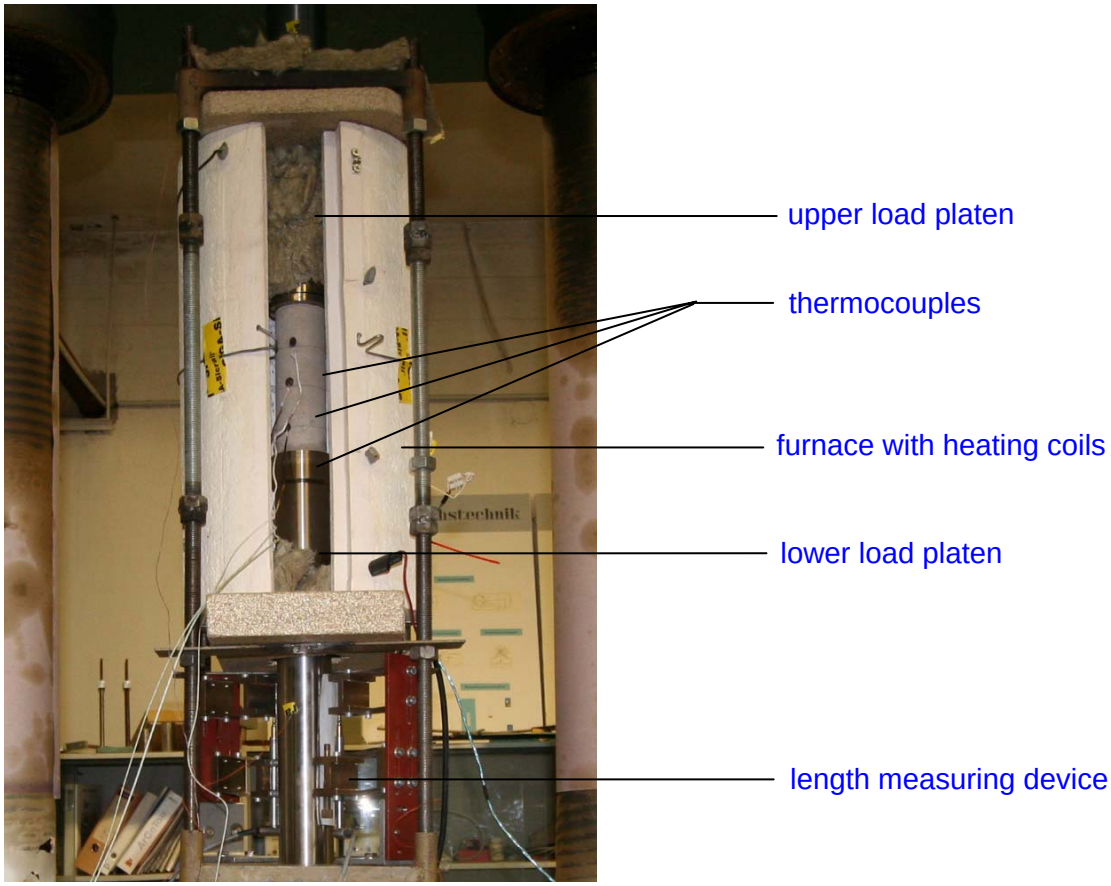

Figure 3: Test equipment (with oven and length measuring device)

Figure 4: Explosive spalling of a specimen of series 4 (without PP-fibres) after exceeding 300 °C (heating rate 3 K/min, left hand side) and preheated specimens (right and side), which indicated rupture, while heating from 180 °C (after 24 h homogenization) to 350 °C

The specimens of the series 4 (without PP fibers) had to be pretreated to avoid explosive spalling in excess of 250 °C. These specimens were heated to temperatures of 180 °C and homogenized for 24 h. After this, the specimens were heated up to 250 °C, and homogenized once more for 24 h. Without this pretreatment the specimens broke during the heating-up in a temperature area between 200 °C and 350 °C, as shown in Figure 4.

The complete set of results is given in [4]. Figure 5 summarizes the results of compression tests obtained with specimens of series 1. Up to 250 °C there is hardly a loss of strength. In the region 350 °C to 550 °C the strength is continuously descending from about 80 % to 60 % of the original strength, simultaneously the ultimate strain increases. Above this temperature region a rather steep decrease of strength occurs.

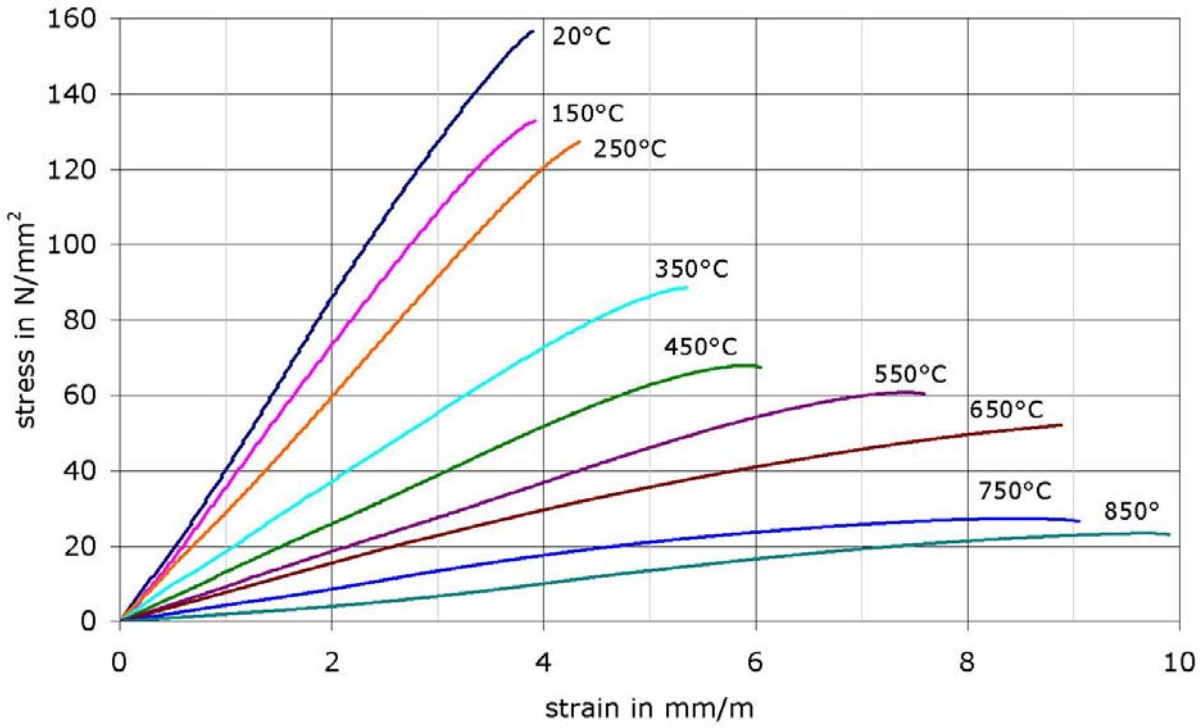

Figure 5: Stress-strain-relations obtained with cylindrical specimens of series 1 (FIR/LA/PF/H)

Some results of the thermal strain and transient strain measurements are shown in Figure 6. It can be seen that the non-loaded material expands up to 250 °C almost linearly with temperature increase. With further temperature rise shrinkage due to accelerated evaporation of the water occurs, and counteracts the thermal expansion such that the specimens keep their length almost constant. At around 570 °C again a small expansion appears, which is due to quartz inversion.

The loaded specimens show distinct transitional creep deformations, which seem to increase linearly with the load level. The temperature of rupture (also called critical temperature) for specimens, which are loaded to 30 % or less is in between 720 and 780 °C. Specimens loaded with 40 to 60 % of the ultimate load failed a little bit above 500 °C. Similar

observations have been made with the specimens of the series 1, 2 and 4, too. – None of the specimens containing PP-fibres suffered spalling when passing 250 °C to 350 °C.

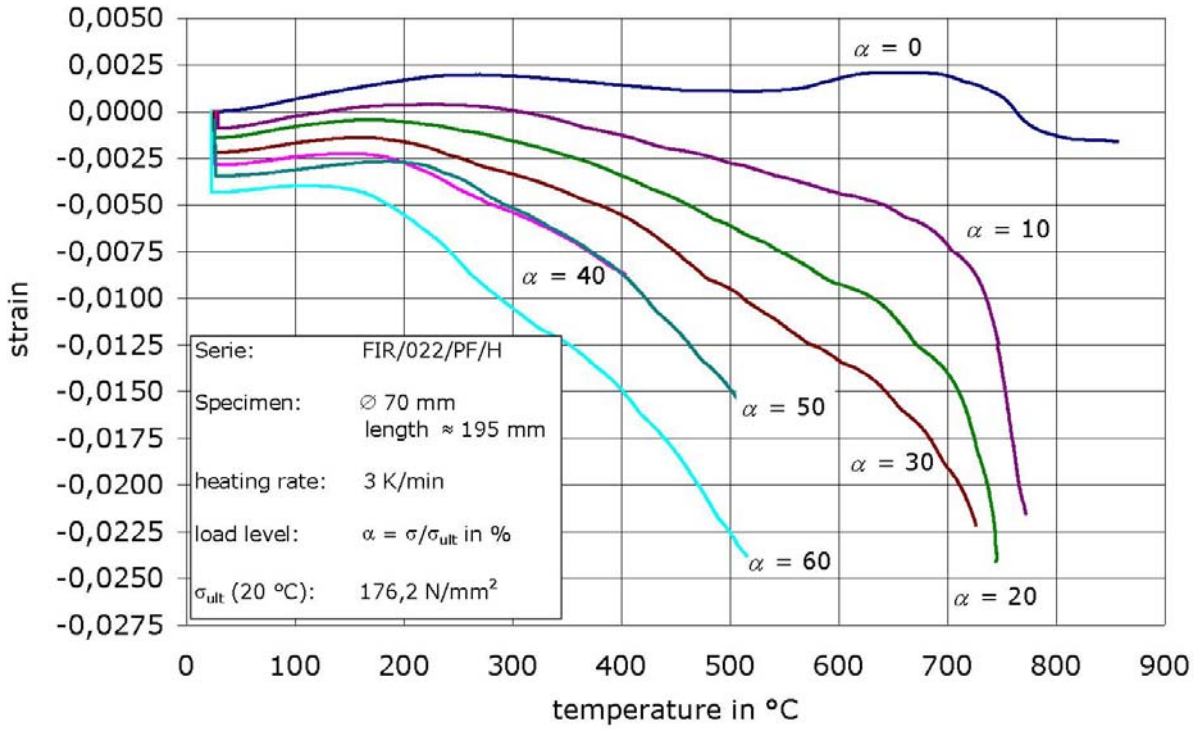

Figure 6: Thermal strain and transient strain of cylindrical specimens of series 3 (FIR/022/PF/H)

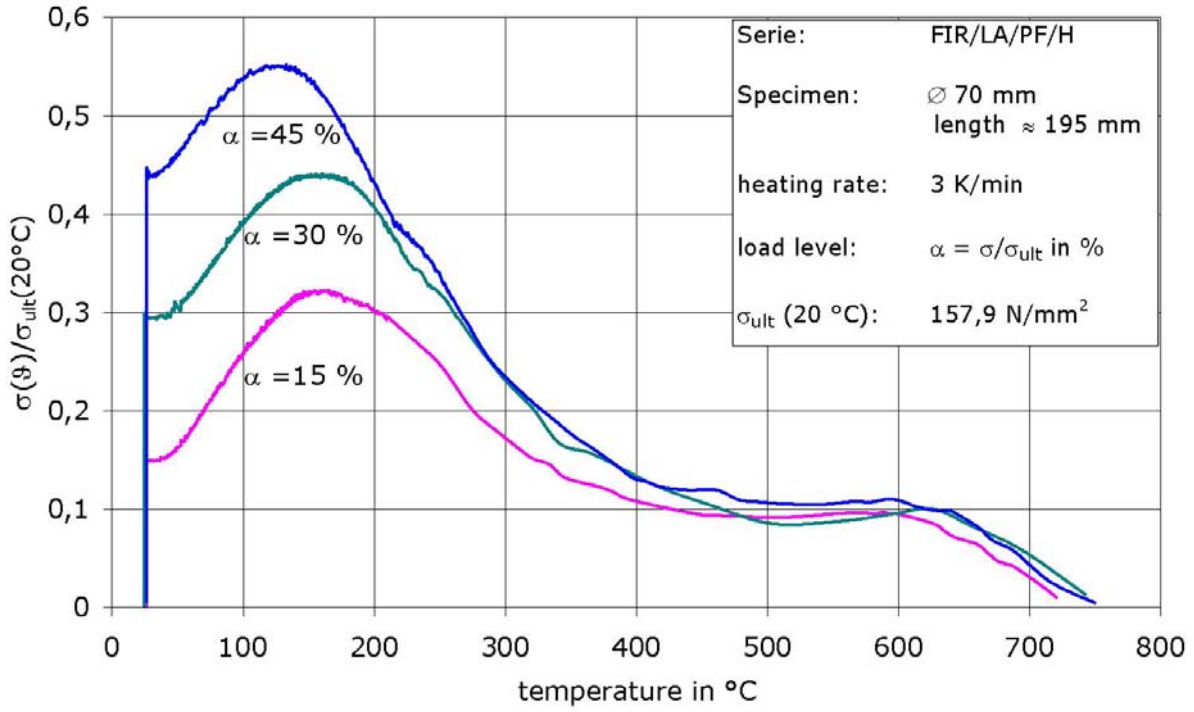

Figure 7: Development of restraint forces with cylindrical specimens of series 1 (FIR/LA/PF/H)

In Figure 7 the results of the restraining tests performed with specimens of series 1 are indicated. During the starting phase of heating the stress rises according to the restraint thermal expansion almost linearly with temperature and reaches the maximum stress with specimens of the series 1 at approx. 150 °C. The specimens which were not heat treated (series 2) reached their stress maximum already at 100 °C [4].

5 Conclusions

From the result of the investigations of four different Ultra High Strength Concretes the following conclusions may be drawn:

The studies concerning thermal stability by aid of simultaneous thermal analysis revealed that the various UHPC mixes show in the thermograms generally the same peak locations and roughly the same peak heights as conventional high strength concretes. Thus the same deteriorations reactions occur in UHPC and high strength concrete [7].

The investigations of the porous structure by means of mercury porosimetry indicated that thermally unstressed UHPC have perceptibly smaller porosity than ordinary high strength Portland cement pastes and concretes. Thermal loads alter the microstructure of the UHPC in the same way as in normal high strength pastes and concretes, but the microstructure of the UHPC is much denser then that of high strength concrete. This holds also for elevated temperatures.

The mechanical behaviour of UHPC differs distinctly from those of normal strength concrete, but not much from high strength concrete. In general the failure of UHPC is more brittle than that of high strength concrete.

6 Refenences

[1] Jumppanen, U.-M.: High Temperature Properties and Spalling Behaviour of High Strength and Ultra High Strength Concrete. Nordic Concrete Research, Publication 4, Oslo 1989

[2] Dowd, W.; Dauriac, C.; Adeline, R.: Reactive Powder Concrete for Bridge Construction, Mat Cong 5-5th Materials Engineering Congress, Cincinnati, May 1999

[3] Mindeguia, J.C.; Dhiersat, M.; Simon, A.; Piementa, P.: Behaviour of the UHPFRC BSI at high temperatures. International Workshop „Structures and Fire", Aveiro, Portugal, 2006, pp 683-695

[4] Diederichs, U.; Gratz, U.; Mertzsch, O.: Untersuchung des Hochtemperaturverhaltens von Superhochfestem Beton; Rostocker Berichte aus dem Institut für Bauingenieurwesen, Heft 16, Rostock, 2006, and Heft 17, Rostock, 2007

[5] Diederichs, U.; Gratz, U., Mertzsch, O.; Cwirzen, A.; Penttala, V.: HIGH TEMPERATURE BEHAVIOR OF ULTRA HIGH STRENGTH CONCRETE; Helsinki University of Technology, Building Materials Technology , Report 20; under preparation

[6] Schneider, U.: Zur Kinetik festigkeitsmindernder Reaktionen in Normalbeton bei hohen Temperaturen.; Dissertation, Techn. Hochschule Braunschweig, Institut für Baustoffkunde und Stahlbetonbau, Heft 27, 1973

[7] Diederichs. U., . Jumppanen, U.-M., Penttala, V.: Behaviour of high strength concrete at high temperatures, Helsinki University of Technology, Department of Structural Engineering, Report 92, Espoo 1989

P.Y. Yan
Prof. Dr.
Tsinghua University
Beijing, P. R. China

J.W. Feng
Master
Tsinghua University
Beijing, P. R. China

Mechanical Behavior of UHPC and UHPC Filled Steel Tubular Stub Columns

Summary

UHPC with the compression strength higher than 170 MPa was prepared using PO 42.5 ordinary Portland cement, silica fume, ground granulated blast-furnace slag or fly ash. Mechanical behaviors of UHPC, such as the compressive/flexural stress-strain curves and Poisson's ratio etc., are investigated. UHPC shows high strength, large compressive peak strain but brittle failure. Based on the study on mechanical behaviors of UHPC, it is also studied the interaction between steel tubes and the UHPC core as well as the interaction's influence on the bearing capacity and deformability of UHPC filled steel tubular (UHPCFT) stub columns when the columns are subjected to axial load. UHPCFT stub columns get tremendous ductility and overwhelm UHPC's disadvantage of brittle failure. Steel tubes' confinement effect on UHPC is weaker than that on normal strength concrete (NSC), thus it can be neglected in the design for convenience and safety.

Keywords: *UHPC, stub column, interaction, bearing capacity*

1 Introduction

Reactive powder concrete (RPC) is a new type of concrete with compressive strength up to 200 MPa or 800 MPa [1] (with iron aggregates and cured by steam with high pressure and high temperature). On the other side, with wide use of high efficiency water-reducing agents, the strength of concrete prepared and cured in conventional method is higher and higher. Compressive strength of this type of concrete can reach 130 MPa, even more than 150 MPa. However, there is no clear definition of UHPC. In this study, UHPC is defined as concretes with compressive strength more than 100 MPa, but regardless of whether the concrete contains coarse aggregate or steel fiber.

UHPC is a brittle material. Brittle failure may occur when it is subjected to high stress level. Its brittleness limits its application in engineering. The addition of steel fiber can enhance the tensile ductility of UHPC, but its effect on compressive performance of UHPC is limited. Here ductility is the amount of inelastic deformation which a structural member experiences before complete failure. The fluidity of fresh concrete also declines significantly when the ratio of steel fiber exceeds 2 % by volume.

Concrete filled steel tubular columns exhibit good ductility and bearing capacity because concrete encased in steel tubes can be under effective lateral confinement. So it is available to utilize steel tubes' confinement to alleviate brittle failure of UHPC.

2 Experimental description

Raw materials used for preparing UHPC are as follows: PO 42.5 Portland cement (C); silica fume (SF); ground granulated blast-furnace slag (GS); fly ash (FA); polycarboxylate superplasticizer; tidy river sand (S) with particle diameters ranging from 0.2 to 0.4 mm; copperized steel fiber (F) with the diameter of 0.2 mm and the length of 13 mm.

Six UHPC samples (C1-C6) were prepared. The mix proportions used are shown in Table 1. The samples was cured with 90 °C steam for 3 days after initial setting. After heat treatment, hydration of cementitious materials had almost completed, and the strength of UHPC did not increase obviously. Therefore, the strength of UHPC was measured on 5 day (Table 1).

It is derived from Table 1 that cement-water ratio has obvious effect on the strength of UHPC; either GS or FA can be used to prepare UHPC; adding high-volume fly ash is available.

Table 1: UHPC mix proportions (kg/m^3) and 5 day compressive strength (MPa)

Code	C	SF	GS	FA	W	S	F	f_c	f_{cu}
C1	745	132	219	0	175	1096	0	115.8	125.5
C2	745	132	219	0	175	1096	37	117.9	133.9
C3	884	221	0	0	155	1105	0	136.7	163.0
C4	884	221	0	0	155	1105	150	144.9	178.2
C5	737	184	0	184	155	1105	75	144.2	170.0
C6	553	184	0	368	155	1105	150		172.2

The experimental setup of UHPCFT specimens is shown in Fig. 1. The specimens' length is 300 mm; their diameter is about 110 mm; the wall thickness of the steel tubes is 5 to 6.5 mm. Loading was controlled by displacement. The axial load was increased at the speed of 10 με/s monotonically until the axial deformation rate of the columns reached approximately 5 %. Two displacement transducers were used to monitor the axial compressive stain of a 120 mm gauge length.

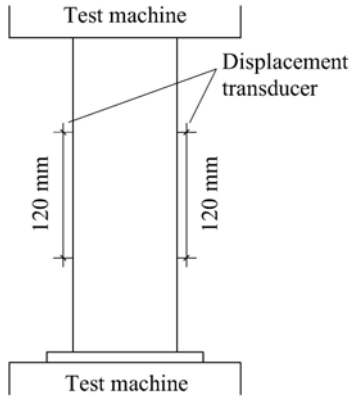

Figure 1: Experimental setup of UHPCFT specimens

3 Mechanical behaviour of UHPC

3.1 Bend and compression behavior of UHPC

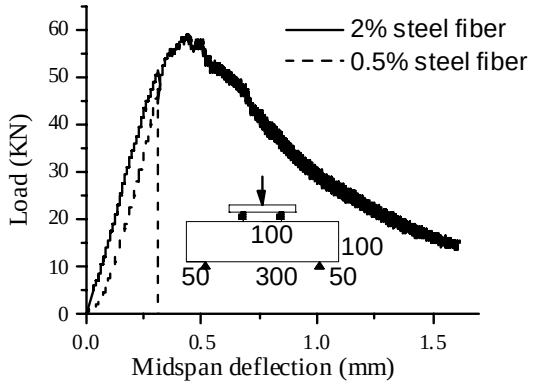

Figure 2: Bending behavior of UHPC

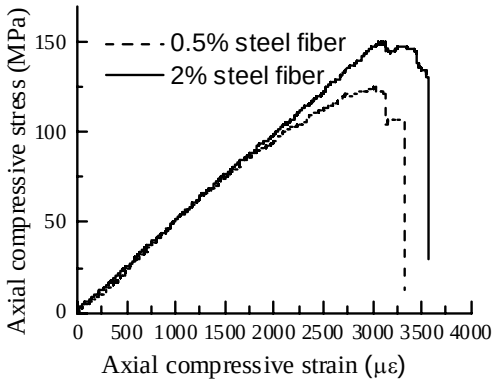

Figure 3: Compression behavior of UHPC

Four-point bending behavior and compressive bahavior of UHPC with different steel fiber content is shown in Fig. 2 and Fig. 3. Steel fiber improves bending ductility of UHPC significantly. However, when axial compressive strain of UHPC exceeds the peak strain, axial stress descends rapidly and explosive failure occurs. The descending branch of stress-strain curve can not be derived even if the loading speed is as low as 1 με/s. Steel fiber plays little act in improving compressive ductility of UHPC. So it is necessary to utilize steel tubes to alleviate brittleness of UHPC.

3.2 Interaction capacity between UHPC and steel tubes

Difference in mechanical behavior between UHPC and normal strength concrete (NSC) leads to difference in steel tube-concrete confinement effect. Here, NSC mainly refers to concretes with compressive strength below 60 MPa, interfacial zone in which is rather weak.

The classical load-strain curve of a NSC filled steel tubular (NSCFT) stub column under axial loading can be divided into three phases shown in Fig. 4:

Linear Elastic Phase (OA):

In this phase, both the steel tube and the NSC core are in the elastic stage. Initial Poisson's ratio of concrete is about 0.2 while that of steel tubes mainly ranges from 0.27 to 0.3. So the lateral deformation of the steel tube is larger than that of concrete and there is no interaction between the steel tube and NSC.

Elastic-Plastic Phase (AB):

When the steel tube enters plastic phase, its longitudinal rigidity decreases while its Poisson's ratio increases to about 0.5. However, the microcracks in the interfacial transition zone of NSC propagate when the compression strain of NSC exceeds 50 % of the compressive peak strain of NSC. The appearance and propagation of microcracks increases the lateral deformation of NSC and increases the Poisson's ratio. With the increase of compression strain, Poisson's ratio of NSC exceeds that of steel, leading to the restraint in steel-concrete interface.

Platform phase (BC):

In this phase, as NSC is under three-dimension compression, its deformability is enhanced significantly.

However, properties of UHPC rendered below limit the confinement effect between steel tubes and UHPC.

(a) Poisson's ratio

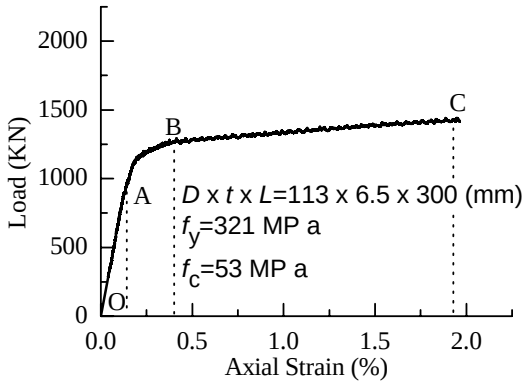

Figure 4: Typical load-strain curve of a NSCFT stub column under axial load

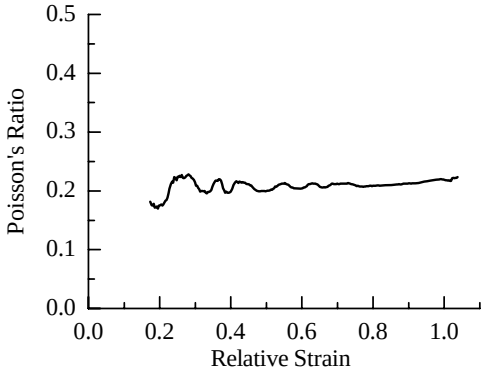

Figure 5: Poisson's ratio vs. relative compressive strain of UHPC

Fig. 5 shows the typical development of UHPC's Poisson's ratio with respect to the relative compression strain in this study. Poisson's ratio keeps constant (about 0.2) before UHPC's strain reaches the compressive peak strain and visible cracks occur.

For high strength concrete (HSC), the strength of interfacial transition zone is high, which retards the crack growth. Thus, the increase speed of Poisson's ratio is far lower than that of NSC. For HSC with compressive strength of about 100 MPa, its Poisson's ratio starts to increase only when the load exceeds 90 % of the peak strain [2].

Length of initial cracks in UHPC is reduced as its interfacial transition zone has been greatly diminished, so the strength of interfacial transition zone of UHPC is even higher than that of HSC. Therefore, the cracks in UHPC propagate later than those in HSC and Poisson's ratio of UHPC stays constant until the compressive strain of UHPC reaches the peak strain.

It is shown in Fig. 3 that the ascending branches in the strain-stress curves are almost linear. Linear strain-stress relation indicates that there is basically no propagation of microcracks. So even the steel fiber volume concentration is 2 % , there is still no obvious increasing process of Poisson's ratio.

(b) Deformability

Fig. 3 shows the stress-strain curves for UHPC subjected to axial compression. The peak strain of UHPC is 3000-3700 με, which is much larger than that of NSC (about 1500-2000 με), even larger than the yield strain of common steel (about 1500-2500 με). The Young's modulus of UHPC measured in this study is about 44 GPa. With higher strength but relatively lower Young's modulus, UHPC has larger deformability than NSC. Even if the steel tube enters plastic phase and large lateral deformation occurs, the UHPC core is still under linear

phase and its lateral deformation is tiny. The incongruity in lateral deformations limits the confinement effect between the steel tube and the UHPC core.

(c) Crack propagation

There are two possibilities for a crack in the cement-aggregate interfacial zone to propagate: propagating along the interface or penetrating into the aggregate [3].

Cracks in low strength concrete propagate along cement-aggregate interfaces. When a coarse aggregate is being extracted, the bonding between the aggregate and the cement matrix provides great bridging strength over a large scale to improve the fracture toughness of concrete. Furthermore, extraction of an aggregate forms a cave in the cement-aggregate interface which leads to the volume expansion of concrete that can promote interaction between concrete and steel tubes. Cracks in HSC penetrate into aggregates and propagate unstably and the aggregates' function of enhancing the toughness of concrete disappears. After a HSC specimen under compression fails, no obvious global lateral expansion of the specimen but a few permeable cracks occur. Therefore, the confinement effect between steel tubes and HSC is not as effective as that between steel tubes and NSC.

Table 2: Values of α prescribed by CECS 104:99

f_{cu}	<=50	55	60	65	70	75	80
α	2.00	1.95	1.90	1.85	1.80	1.75	1.70

It is derived from the analysis above that the interaction capacity between steel tubes and concrete decreases with concrete strength. The formula in Chinese code CECS 104:99 calculating axial bearing capacity of concrete filled steel tubular stub column is $N_c = A_c f_c + \alpha A_s f_y$. α, whose value is prescribed in Table 2, is a correction factor related with concrete strength, which reflects the confinement effect between steel tubes and concrete. It is also derived from Table 2 that the interaction capacity between steel tubes and concrete decreases with concrete strength.

4 Whole load-strain behavior of UHPCFT stub columns under axial compression

Despite the content of steel fiber, typical load-strain relationship of a UHPCFT stub column under axial compression is as the curve shown in Fig. 6. The whole curve can be divided into four phases:

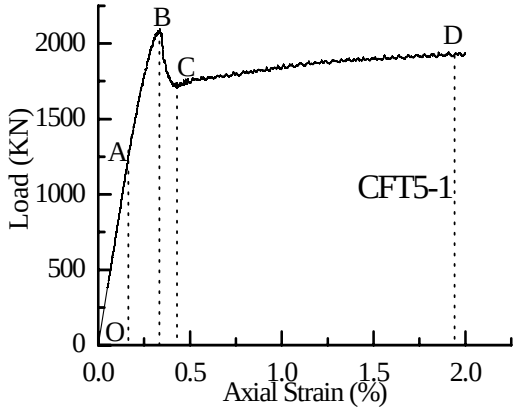

Figure 6: Typical load-strain curve of a UHPCFT stub column under axial compression

Linear Elastic Phase (OA):

In this phase, both the steel tube and the UHPC core are in elastic stage, the steel tube and the UHPC core work independently.

Elastic-Plastic Phase (AB):

In this phase, the steel tube enters plastic stage, and the UHPCFT stub column is achieved.

It is discovered in experiments that the failure mode of UHPC prismy specimens is longitudinal splitting failure while the failure mode of UHPC encased in steel tubular stub columns is shearing failure. When a UHPCFT stub column is subjected to compression, the ends of steel tube are confined by the welding plate or the end plates of the testing machine, so the steel tube wall near each end presses the UHPC core. The pressure caused by the steel tube wall will arrest longitudinal cracks in the UHPC core when they propagate to the zone near the ends of the UHPC core. However, shearing cracks will not be arrested as they do not pass the ends of the column.

Descending Phase (BC):

When the stress of the UHPC core reaches the ultimate strength, a shearing crack occurs in the middle of the UHPC core and the UHPC core was separated into two wedges. These two blocks slip and press the tube wall to generate the hoop force F_c, which impedes the slip. When the slip between wedge blocks is small, F_c is not large enough to restrict the slip. Therefore, the bearing capacity of the UHPCFT stub column declines with the development of the slip. F_c increases with the development of the slip, so if the slip researches some degree, F_c is large enough to stop wedge blocks from unstable slip and the load-strain curve enters the platform phase.

D/t in this study is 17 - 22 and all the UHPCFT specimens have descending phase. However, specimens with D/t of 13 show no obvious descending phase [4]. This is due to relatively thicker steel tube wall offering more lateral rigidity to stop the slip between wedge blocks.

Platform phase (CD):

In this phase, the Load-strain curve is horizontal. F_c is large enough to stabilize the slip. UHPCFT stub columns show excellent ductility. The platform phase of all specimens is approximately horizontal till the loading is complete. However, the part of the curve in Fig. 6 beyond the strain of 2 % is not rendered.

5 Practical formulas

It is convenient and safe to calculate axial bearing capacity of UHPC filled steel tubular stub columns by the formula $N_c = f_y A_s + f_c A_c$, in which the interaction between concrete and steel tubes is neglected.

The purpose of calculating the bearing capacity of a column is getting a solution with degree of security high enough but not getting an “accurate” solution. Columns are the most important elements in a frame so that they should keep high enough bearing capacity to avoid collapse of structures, however, beams should yield in time to consume kinetic energy when the frame is subjected to seismic effect. It is important to follow the principle of “strong column but weak beam” in structure design.

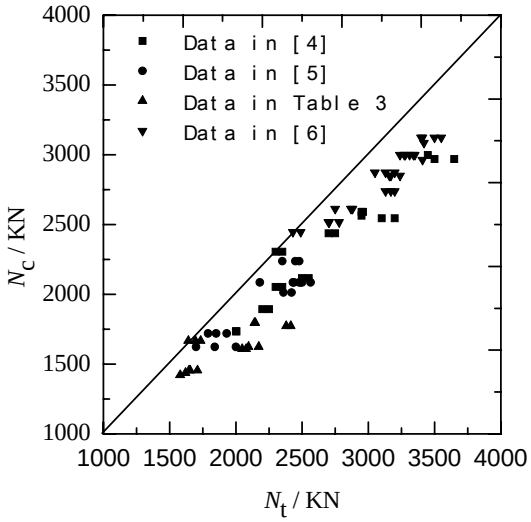

Figure 7: Comparison between calculated results and experimental results

Table 3: Parameters and Axial Bearing Capacity of Specimens

Number	***D*×*t*×*L* / mm**	**Concrete**	**f_y / MPa**	**N_t / KN**
CFT1	110×5×300	C1	310	1 580
CFT2-1	113×6.5×300	C1	321	2 076
CFT2-2				2 048
CFT3-1	110×5×300	C2	310	1 620
CFT3-2				1 621
CFT4-1	110×5×300	C2	320	1 645
CFT4-2				1 709
CFT4-3				1 655
CFT5-1	113×6.5×300	C2	321	2 096
CFT5-2				2 172
CFT6-1	113×6.5×300	C3	321	2 379
CFT6-2				2 415
CFT7-1	108×6×300	C5	391	2 141
CFT7-2				2 146
CFT8-1	110×5×300	C4	320	1 693
CFT8-2				1 641
CFT8-3				1 734

Comparison between the bearing capacity calculated by $N_c = f_y A_s + f_c A_c$ and experimental results is rendered in Fig.7. The experimental data is from this study, which is shown in Table 3, as well as data from reference [4], [5], and [6]. It is obvious that this formula is safe.

6 Conclusions

UHPC with the compressive strength of 170 MPa was prepared using ordinary Portland cement, silica fume, ground slag or fly ash, steel fiber and superplasticizer.

Adding of steel fiber shows significant influence on improving tensile ductility of UHPC but no obvious influence on improving compressive ductility of UHPC.

Steel tube confinement can increase the ductility of UHPC, eliminating the risk of collapse of structures caused by fragile failure of UHPC under high stress state.

Confinement effect on UHPC by steel tube is not as good as that on normal concrete. The interaction between UHPC and steel tube can be neglected in calculation of bearing capacity.

7 Notation

D = diameter of circular steel tube;

L = length of column;

t = thickness of steel tube wall;

f_y = tensile yield strength of steel tube;

f_c = prismy strength of concrete, specimen dimension is 100mm×100mm×300mm;

f_{cu} = cube strength of concrete, specimen dimension is 100mm×100mm×100mm;

A_s = cross section area of steel tube;

A_c = cross section area of concrete;

N_t = bearing capacity measured in experiments;

N_c = bearing capacity calculated by formulas.

8 References

[1] Richard, P.; Cheyrezy, M.: Composition of reactive powder concrete. In: Cement and Concrete Research 25, No. 7, pp.1501-1511, 1995.

[2] Tan, K.F.; Cai, S.H.; Pu, X.C.: Microstructure study on the mechanical properties of steel extra-high strength concrete encased in steel tubes. In: Journal of Building Structures 20, No. 1, pp.18-23, 1999.

[3] Zhang, J.; Liu, Q.; Wang, L.: Conditions promoting crack growth in concrete along the aggregate/matrix interface or into the aggregate. In: Journal of Tsinghua University (Science and Technology) 44, No. 3, pp.387-390, 2004.

[4] Lin, Z.Y.: Research on behavior of RPC filled circular steel stub axial columns. Master theses. Fuzhou University, Fuzhou, 2004.

[5] Zhang, J.: Experiment investigation on behavior of reactive powder concrete filled steel stub-columns. Master theses. Fuzhou University, Fuzhou, 2003.

[6] Pu, X.C.; Pu, H.J.; Wang, Y.W.: Preparation and study on kilometer compressed material. In: Concrete, No. 3, pp.3-9, 2003.

Special Part I:

DFG Priority Program – Materials

Tobias Gerlicher
Dipl.-Ing. scientific assistant
cbm centre for building materials
TU-München
Munich, Germany

Detlef Heinz
Prof. Dr.-Ing.
cbm centre for building materials
TU-München
Munich, Germany

Liudvikas Urbonas
Dr.-Ing.
cbm centre for building materials
TU-München
Munich, Germany

Effect of Finely Ground Blast Furnace Slag on the Properties of Fresh and Hardened UHPC

Summary

Ultra high performance concrete (UHPC) is a cementitious material containing a very high proportion of ordinary Portland cement which requires a high amount of energy for its production. This work aimed at systematically developing UHPC made with less Portland cement, but achieving strengths above 150 MPa at an age of 28 days under normal conditions or above 200 MPa with heat treatment. Up to 75% Portland cement was volumetrically replaced by ground blast furnace slag of different fineness. The effect of slag content on the workability of fresh concrete and compressive strength was investigated. It was found that cement replacement by finely ground blast furnace slag reduces the water and superplasticizer requirement of the mix. However, compressive strength decreases with the content of slag. This loss was partly compensated by increasing the fineness of the slag. The type and dosage of superplasticizer had a significant effect on strength development. An appropriate choice of materials enabled the achievement of 28 d strengths above 200 MPa after heat treatment of concrete made with binders containing 25% Portland cement and 75% slag.

Keywords: *UHPC, GGBS, mineral additions, binder, superplasticizer*

1 Introduction

The following investigations were performed in a project “Binder Optimisation” within the German Research Foundation (DFG) priority programme No. 1182 “Sustainable Building with Ultra High Performance Concrete”. Different UHPC compositions were designed and investigated with the aim of reducing the proportion of Portland cement in UHPC, but maintaining high strengths and good workability of the fresh concrete.

Investigations performed by Bornemann et al. [1], Ludwig et al. [4] as well as at the Centre for Building Materials of the Technical University of Munich [3] have shown that UHPC made

with Portland blast furnace cement CEM III/B has a lower strength at an age of 28 days or after heat treatment at 90°C than equivalent concrete made with Portland cement CEM I.
Yazici [7] found that the replacement of up to 40 wt.% of Portland cement by fly ash or GGBS need not lead to a reduction in strength of UHPC. Heat treatment at 90°C and autoclaving at 210°C yielded much higher strengths compared with untreated concretes. However, the heat treatment was performed over 9 to 12 days which is not acceptable for plant production. Moreover, the maximum compressive strength was at most 180 MPa after autoclaving which is rather low.
The present investigations focus on the use of finely ground blast furnace slag as an alternative binder component in UHPC.

2 Materials Used

As well as the materials in Table 1, quartz sand and two different superplasticizer based on polycarboxylate ether were used. The quartz sand grading ranged from 0.125 to 0.500 mm with d_{50} and d_{95} values of 291 µm and 412 µm, respectively. Two different finely ground blast furnace slags were used which differed in density and specific surface, see Table 1.

Table 1: Characteristic values of the materials used

Material			**Cement**	**Finely ground slag**	**Finely ground slag**	**Silica fume**	**Quarz flour**
			CEM I 52.5R -HS/NA	**Slag C (coarse)**	**Slag F (fine)**		
Density		[g/cm³]	3.21	2.94	2.91	2.53	2,67
Specific surface	Blaine	[cm²/g]	4 840	3 760	8 690	-	4 423
	BET	[cm²/g]	12 800	10 800	38 800	152 300	12 500
Slope n		-	1.21	1.59	2.86	-	1.41
Location parameter		[µm]	11.8	13.4	3.4	-	18.1
d_{95}		[µm]	37.5	35.1	6.4	0.52	55.2
d_{50}		[µm]	9.5	10	2.6	0.17	14.7
Main oxides (XFA)	SiO_2	wt.%	21.1	36.9	36.9	97.6	98.7
	Al_2O_3	wt.%	3.42	11.7	11.7	0.8	0.5
	Fe_2O_3	wt.%	5.23	0.45	0.30	0.05	0.05
	MgO	wt.%	079	6.85	7.03	0.13	0.06
	CaO	wt.%	66.4	40.6	40.9	0.37	0.15
	SO_3	wt.%	1.93	0.98	1.09	0.08	0.03
	Na_2O	wt.%	0.19	0.15	0.2	0	0
	K_2O	wt.%	0.38	0.28	0.39	0	0

3 Specimen Preparation and Investigations

The fresh concrete mixes were prepared in an intensive mixer (EIRICH R02 Vac.) which produced homogeneous mixes after short times due to the high mixing intensity and inclined drum of this mixer. A vacuum unit attached to the mixer was used to remove air from the fresh concrete so that the air content could be kept between 1.0 and 2.0 vol.%. An optimised mixing procedure was used which was based on earlier work performed at the Centre for Building Materials [5].

Besides the determination of air void content according to DIN 18555-2, the fresh concrete was characterised by its slump flow (following DIN EN 1015-3, but without jolting) and its setting behaviour with the Vicat needle based on DIN EN 196-3.
After mixing, the concrete was poured into moulds for cylindrical specimens with a diameter of 50 mm and a height of 50 mm. The specimens were kept at 20°C/95% RH before demoulding after 24 hours. They were then immersed in water at 20°C until testing. Instead of storage in water, some of the specimens were heat treated for 24 hours at 90°C after demoulding. To do this, the temperature was gradually increased from 20 to 90°C over a period of 1 hour and after the treatment at 90°C continuously cooled down to 20°C over 6 hours. During the heat treatment, the specimens were tightly enclosed in a polyethylene foil. After cooling down, the specimens were transferred to a controlled climate 20°C/95% RH were they were kept until testing.
The compressive strengths were measured at ages of 7 and 28 days.

4 Concrete Composition

The fine concrete mix M2Q investigated in the priority programme mentioned above was used as the reference concrete composition in the present investigations, see Table 2. This mix was designed in the course of earlier optimisation and research work at the University of Kassel in Germany [2]

Table 2: Composition of reference concrete mix M2Q

Component		**M2Q**
Cement	kg/m³	832
Silica fume	kg/m³	135
Water	kg/m³	166
Superplast. I	kg/m³	35
Quartz flour	kg/m³	207
Quartz sand	kg/m³	975

The characteristic values determined from the investigations performed with fresh and hardened concrete are listed in Tables 3 and 4.

Table 3: Fresh concrete properties M2Q

Property		**M2Q**
Temperature	[°C]	28
Bulk density	[kg/m³]	2,43
Air content	[%]	1,2
Spread	[cm]	24,5

Table 4: Hardened concrete properties M2Q

Compressive strength		**M2Q**
7d	[MPa]	139
28d	[MPa]	188
7d, heat treated	[MPa]	228
28d, heat treated	[MPa]	219

5 Replacement of Cement by Finely Ground Blast Furnace Slag

The effect of cement replacement was investigated by exchanging 15, 35, 55 and at most 75 vol.% of Portland cement by finely ground blast furnace slag, i.e. the volume fraction of

binder in the mix was constant. This corresponds to slag contents of 14, 33, 53 and 73 wt.% with respect to the weight of cement and slag together.

As can be seen from the particle size distributions in Figure 1, the granulometric values for the coarser finely ground blast furnace slag C were almost same as those of the cement. Figure 1 also shows distributions for the dry components of mix M2Q and the slag rich mix C-75 with 75 vol.% cement replacement. It is apparent that even this high level of cement replacement does not significantly affect the particle size distribution of the total mix.

Slag F, which is much finer than the cement and finer than slag C, was used in a further series of investigations. Figure 2 compares the particle size distributions of the reference mix M2Q without slag and the high slag content mix F-75 with the distributions for cement and slag alone. As opposed to slag C, it is apparent that the replacement of cement significantly affects the overall particle size distribution of the mixed concrete components.

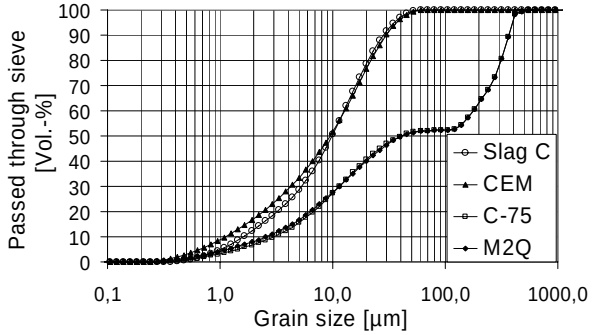

Figure 1: Particle size distributions for cement, finely ground blast furnace slag C (coarse) and the mixes M2Q and C-75

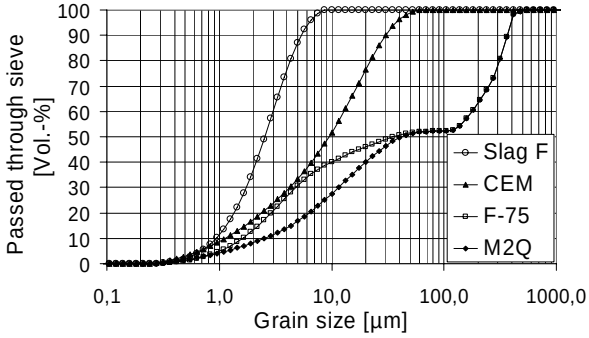

Figure 2: Particle size distributions for cement, finely ground blast furnace slag F (fine) and the mixes M2Q and F-75

The packing densities of the dry material, determined according to a method described by Schwanda [6], in Table 5 exhibit only a small decrease in density as the amount of slag C increases. In the case of the finer slag F, the packing density seems to increase slightly at first reaching a maximum value at approximately 15% before decreasing like slag F.

Table 5: Packing density according to Schwanda [6] in dependence of slag content and cement replacement level

Cement replacement, [vol.%]	**0**	**15**	**35**	**55**	**75**
with coarse slag C	0,886	0,884	0,882	0,880	0,878
with fine slag F	0,886	0,889	0,887	0,880	0,874

5.1 Cement Replacement with Finely Ground Slag C (coarse)

The concrete mixes in which 15, 35, 55 and 75 vol.% cement is replaced by slag C are denoted by C-15, C-35, C-55 and C-75 in the following.

The lower surface area of slag C compared with the cement (Table 1) and thus the smaller amount of water needed to wet the surface of the particles together with the corresponding lower reactivity of the slag resulted in an increase in slump flow at constant water content

from 24.5 cm (M2Q) to 35.7 cm (C-75). The effect of cement replacement on compressive strength at 7 and 28 days is shown in Figure 3 for concretes with and without heat treatment.

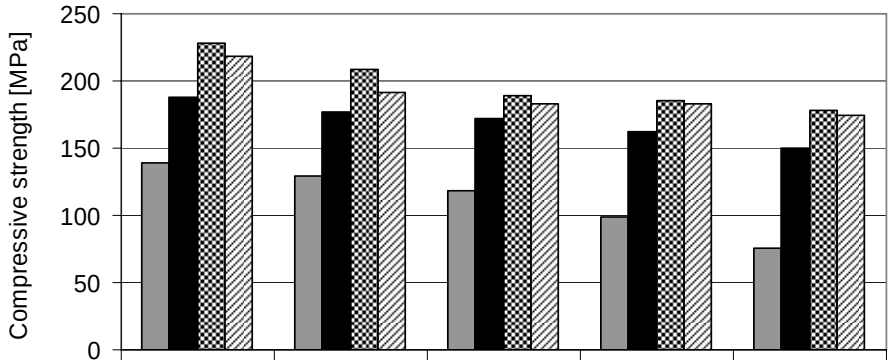

	M2Q	C-15	C-35	C-55	C-75
7d	139.1	128.7	118.9	99.1	76.1
28d	187.9	176.4	171.6	162.8	149.4
7d-HT	228.0	208.7	188.5	185.4	178.1
28d-HT	218.5	191.3	183.3	183.0	174.5

Figure 3: Compressive strength at 7 and 28 days in dependence of cement replacement by finely ground blast furnace slag C. Constant water and superplasticizer dosage. HT: heat treated concretes

In general, the compressive strength decreases as more and more cement is replaced by slag at a constant volumetric water-to-binder w/b ratio of 0.59 - the binder comprises cement, finely ground slag and silica fume. For replacement levels of 35% and higher, the strength of the heat treated concrete falls well below 200 MPa.

Table 6: Dependence of setting times on slag content

Mix		**M2Q**	**C-35**	**C-75**
Setting begins	[h:min]	09:20	18:00	41:30
Setting ends	[h:min]	09:40	18:30	43:20

The heat treatment for mixes with 55 and 75% replacement could only be performed after 48 hours because setting was delayed (Table 6) and the strength development was slower for these mixes.

To achieve comparable workability of mixes made with slag, the water content was reduced until a slump flow of approximately 25 cm was reached, i.e. the target value for M2Q. The w/b ratio decreased correspondingly. The compressive strengths are shown in Figure 4 where the water reduced mixes are denoted by W.

The loss in strength due to cement replacement could, to some extent, be compensated by reducing the amount of water. For concrete with 15% cement replacement it was possible to regain the reference 28 d strength of 188 MPa for M2Q specimens stored in water. For the heat treated specimens, the strengths were only 4 MPa, i.e. 2%, below the reference values. In the case of 55% replacement, the strengths of the water reduced concretes after heat treatment were even above 200 MPa.

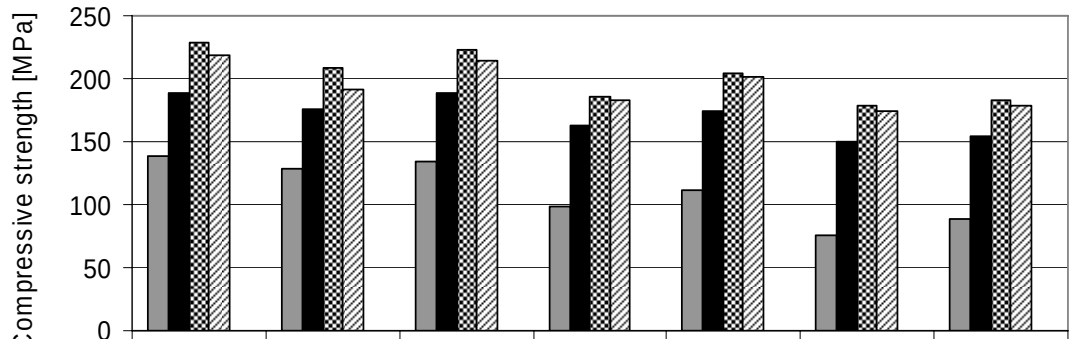

	M2Q	C-15	C-15-W	C-55	C-55-W	C-75	C-75-W
7d	139,1	128,7	133,9	99,1	111,1	76,1	88,8
28d	187,9	176,4	188,4	162,8	174,3	149,4	154,6
7d-HT	228,0	208,7	223,5	185,4	205,0	178,1	183,2
28d-HT	218,5	191,3	214,1	183,0	201,3	174,5	179,1
w/b ratio	0,19	0,19	0,18	0,20	0,17	0,20	0,17

Figure 4: Effect of water reduction on compressive strength

5.2 Cement Replacement with Finely Ground Slag F (fine)

The same levels of replacement were used for the finer slag F as for slag C above.
Like slag C, the slump flow of fresh concrete made with slag F increased as more slag was used in the mix at constant water content. However, the increase in slump flow with slag F content was less than with the coarser slag C, Figure 5.

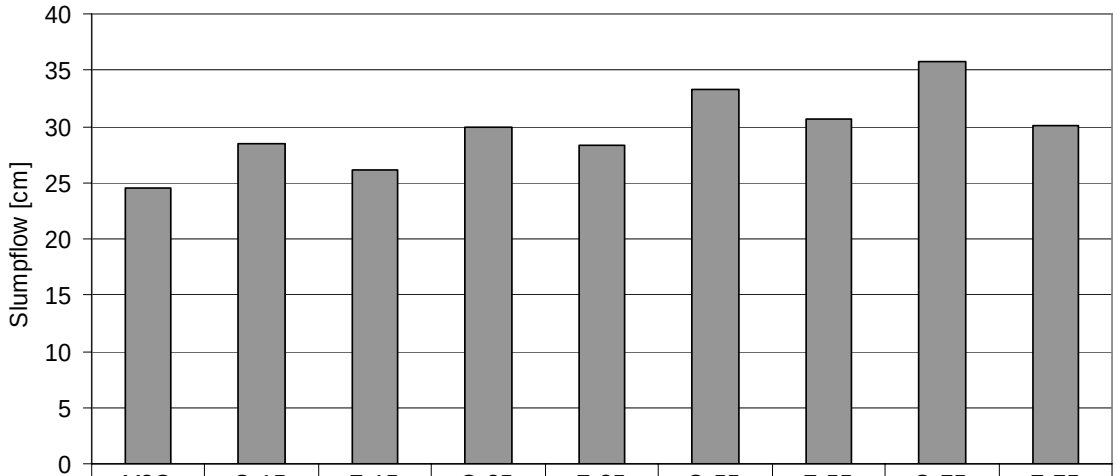

	M2Q	C-15	F-15	C-35	F-35	C-55	F-55	C-75	F-75
	24.5	28.5	26.2	29.9	28.3	33.3	30.6	35.7	30.1

Figure 5: Effect of fineness of ground blast furnace slag on slump flow for different fresh concrete compositions

The fineness of the slag also affected concrete strength. An increase in fineness led to higher compressive strengths, Figure 6. For example, the 7 d strength of concrete with 55% cement replacement by slag F (without water reduction) is higher than the equivalent concrete with the coarser slag C.

Owing to the delay in the development of sufficient strength for demoulding, the concretes made with 55 and 75 vol.% slag F were heat treated after 48 hours.

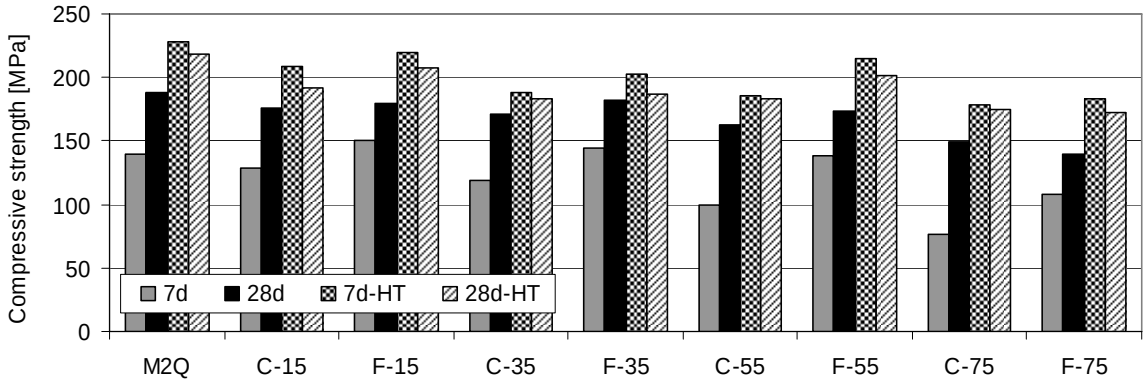

Figure 6: Effect of fineness of ground blast furnace slag on compressive strength

The reduction of water content to adjust slump flow to the reference mix value did not significantly affect strength, i.e. the decrease in strength due to cement replacement with the finer slag F cannot be compensated by lowering the water content.

6 Effect of Superplasticizer

A high dosage of superplasticizer I (4.2 wt.% with respect to cement) was required to obtain a flowable consistency of the fresh reference concrete mix M2Q. For the different binder compositions used, the superplasticizer dosage was kept constant with respect to binder content (cement, slag, silica fume) so that the superplasticizer content with respect to cement content alone increased from 4.2 to 17%. To reduce the amount of superplasticizer, the fluidising effect of a number of different superplasticizers based polycarboxylate ether was tested and a suitable superplasticizer (II) found with which the dosage could be considerably reduced. With superplasticizer II only 1.5 wt.% (with respect to cement) was necessary to obtain the target in slump flow of 25 cm for mix M2Q at constant total water content.

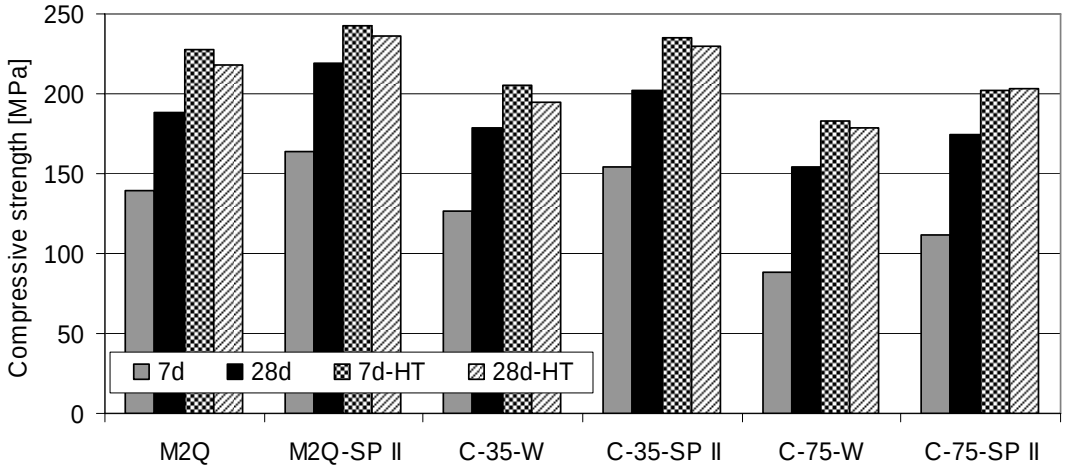

Figure 7: Comparison of the effect of superplasticizer at dosages to give the same slump flow at constant water content (with respect to binder)

The lower dosage had a decisive effect on the development of the compressive strength of the different mixes. The 28 d strength of M2Q stored in water was increased by 17%, and 8% with heat treatment. The strengths of concrete prepared with superplasticizer are denoted by SP II in Figure 7.

It was also possible to increase the strength of concrete made with the coarser slag C by using superplasticizer II. Even at a replacement level of 75%, it was possible to demould specimens after 24 hours and heat treat the concrete to achieve strengths above 200 MPa at an age of 28 days.

The mixes with high slag content were noticeably stiffer in consistency than the original mix M2Q even though they possessed the required slump flow. This indicates a future need for superplasticizers which are better adapted to the needs of UHPC, especially containing high amounts of secondary cementitious materials. Detailed investigations on the effect of cement replacement on the rheology of fresh UHPC are planned using a rotation viscometer.

7 Conclusions

Cement replacement by finely ground blast furnace slag reduces the water and superplasticizer requirement of the mix. At the same time, compressive strength decreases with slag content. This loss can be partly compensated by increasing the fineness of the slag.

The type and dosage of superplasticizer have a significant effect on strength development. An appropriate choice of materials enabled the achievement of 28 d strengths above 200 MPa after heat treatment of concrete made with binders containing 25% Portland cement and 75% slag.

8 References

[1] Bornemann, R.; Fehling, E.: Ultrahochfester Beton – Entwicklung und Verhalten. In: 10 Leipziger Massivbau-Seminar, 2000, S. 1-15.

[2] Fehling, E; Schmidt, M.; Teichmann, T.; Bunje, K.; Bornemann, R.; Middendorf, B.: Entwicklung, Dauerhaftigkeit und Berechnung Ultra-hochfester Betone (UHPC). Forschungsbericht DFG FE 497/1-1, Schriftenreihe Baustoffe und Massivbau, Heft 1, Universität Kassel, 2005.

[3] Heinz, D., Schachinger, I., Urbonas, L.: Hochleistungs-Feinkorn-Beton. Forschungsbericht F 10005/00, Bayerische Staatsministerium für Wirtschaft, Verkehr und Technologie, 2004

[4] Ludwig, M.-H., Thiel, R.: Dauerhaftigkeit von UHFB. Ultrahochfester Beton, Innovationen im Bauwesen, Beiträge aus Praxis und Wissenschaft. Universität Leipzig, 2000, S. 89-105

[5] Schachinger, I., Schubert, J., Mazanez, O.: Effect of Mixing and Placement Methods on Fresh and Hardened Ultra High Performance Concrete (UHPC). Proc. of the Int. Symp. On Ultra High Performance Concrete, September 13-15, 2004, pp. 575-586.

[6] Schwanda, F.: Das rechnerische Verfahren zur Bestimmung des Hohlraumes und Zementleimanspruches von Zuschlägen und seine Bedeutung für den Spannbetonbau, Zement und Beton, Band 37, S. 8-17, Wien, November 1966.

[7] Yazici, H.: The effect of curing conditions on compressive strength concrete with high volume mineral admixtures. Building and Environment 42, 2007, pp. 2083-2089

Dietmar Stephan
Dr. rer. nat.
University of Kassel
Kassel, Germany

Ralf Krelaus
Dr. rer. nat.
University of Kassel
Kassel, Germany

Michael Schmidt
Prof. Dr.-Ing. habil.
University of Kassel
Kassel, Germany

Direct measurement of particle-particle interactions of fines for UHPC using AFM technology

Summary

In this paper, fundamental aspects on interparticle forces like the DLVO theory will be discussed. In the experimental section, the influence of pH, composition and concentration of pore solutions and different superplasticisers are presented for glass spheres as a model substance for UHPC. Some experiments were conducted by indirect measurements of interparticle forces like zeta potential measurements and rheological tests. By using the highly sophisticated colloidal probe AFM technique (AFM = atomic force microscopy), it was possible to measure directly the forces that occur between two single particles. For these experiments, single particles were glued with a resin to the free end of an AFM cantilever. Other particles were fixed on a microscope slide. The force measurements were performed in water containing different pore solutions and polymers.

Keywords: *AFM, zeta potential, interparticle forces*

1 Introduction

The fraction of fines < 125 µm (Portland cement, ground limestone, ground quartz, rock powder, silica fume etc.) of the solid constituents of the UHPC composition amounts to much more than 50 wt.-%. Compared to “normal” concrete this high amount of fines results in an enormous increase in the total surface area. This effect is even more important if the packing density and reactivity is enhanced using colloidal particles like silica sol. In Table 1 the surface fraction of UHPC constituents are shown for a mixture either containing silica fume or silica fume and silica sol. The total surface area of the mixture is multiplied by both kinds of silica and even with only a minor mass fraction; the total surface area is dominated by silica. As a consequence, the chemical and physical behaviour of the mixture is changing and colloidal properties have to be taken into account. With finer particles the stability of a dispersion is increasing, the reactive surface area is increasing and optical properties are changing. But with increasing fineness also the interactions of the fine particles via their surfaces are more and more dominating the rheological characteristic of the dispersion.

The fundamentals of the interaction between surfaces are given in the DLVO-theory (**D**erjaguin, **L**andau, **V**erwey und **O**verbeck [1, 2]). It suggests that the interaction between charged particles depends on the total potential energy function V_T, which is the sum of the repulsive forces V_B and V_R and the attractive force V_A.

Table 1: Surface fraction in UHPC with silica fume (SF) and silica fume plus silica sol (SS)

Fine	Specific surface [m^2/kg]	Mass fraction [%]		Fraction in concrete [kg/m^3]		Surface area [m^2/m^3]		Surface fraction [%]	
		SF	SF+SS	SF	SF+SS	SF	SF+SS	SF	SF+SS
Fine sand 0/0.5	-	45.4	45.4	975	975	-		-	-
Cement	465	38.7	38.7	832	832	386880	386880	12.2	5.5
Quartz powder	417	9.6	9.6	207	207	86319	86319	2.7	1.2
Silica fume	20000	6.3	4.9	135	105	2700000	2100000	85.1	29.7
Silica sol	150000	-	1.4	-	30	-	4500000	-	63.6
Sum				**2149**	**2149**	**3173199**	**7073199**		

V_A is the long-distance attractive van der Waals force, V_B the strong but only short-distance repulsive Born-repulsion that prevents the particles to fully interlock and V_R is the long-distance electrostatic force, which is repulsive for equal charged particles and attractive for opposed charged particles. V_A and V_B are mainly dominated by constant material properties, whereas V_R is a complex function depending on the particle radius, the solvent permeability, the ionic composition and the zeta potential [3]. Opposed charged particles will coagulate. For equal charged particles, the main correlations are given in Figure 2. It is visible, that the surface charge has a considerable influence on the interparticle forces and the stability of the dispersion.

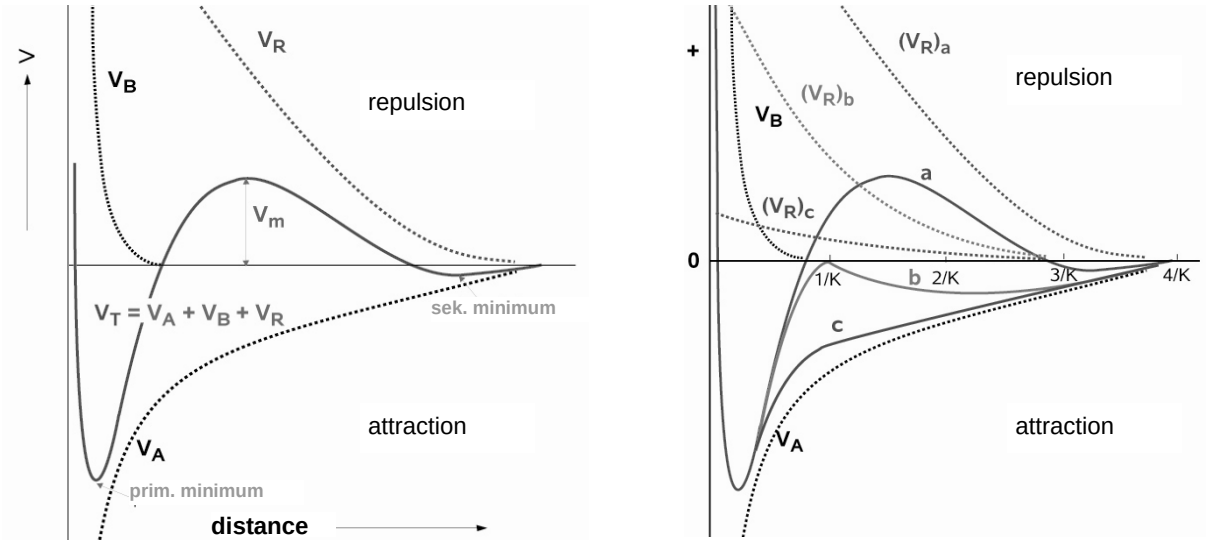

Figure 1: left: total interaction V_T of particles after DLVO-therory; V_R= electrostatic repulsion, V_B= Born-repulsion, V_A= Van der Waals attractive force; right: $(V_R)_a$= high surface charge, $(V_R)_b$= medium surface charge, $(V_R)_c$= low surface charge; according to [3]

For a given aqueous dispersion of particles, the zeta potential ζ is the main factor influencing the stability of the dispersion. The zeta potential ζ is the potential difference between the dispersion medium and the stationary layer attached to the dispersed particle; in simple terms it is the outwards effective charge of the particles. The ζ-potential is mainly influenced by surface potential, the pH value, the electrolyte concentration and the kind and valence of the ions in solution. Therefore the ζ-potential is the main factor influencing the rheological properties and packing density of particle dispersion like UHPC if only electrostatic mechanism is considered [4, 5].

Instead of an electrostatic stabilization mechanism, modern superplasticisers act via a “steric stabilization” [6], were the entropic repulsion of particles with adsorbed comb polymers on the surface is used to prevent the coagulation of particles. In this case there is no direct correlation between ζ-potential and rheology and direct measurements of interparticle forces are necessary to characterise particle interactions [7]. The principles of both mechanisms are shown in Figure 2.

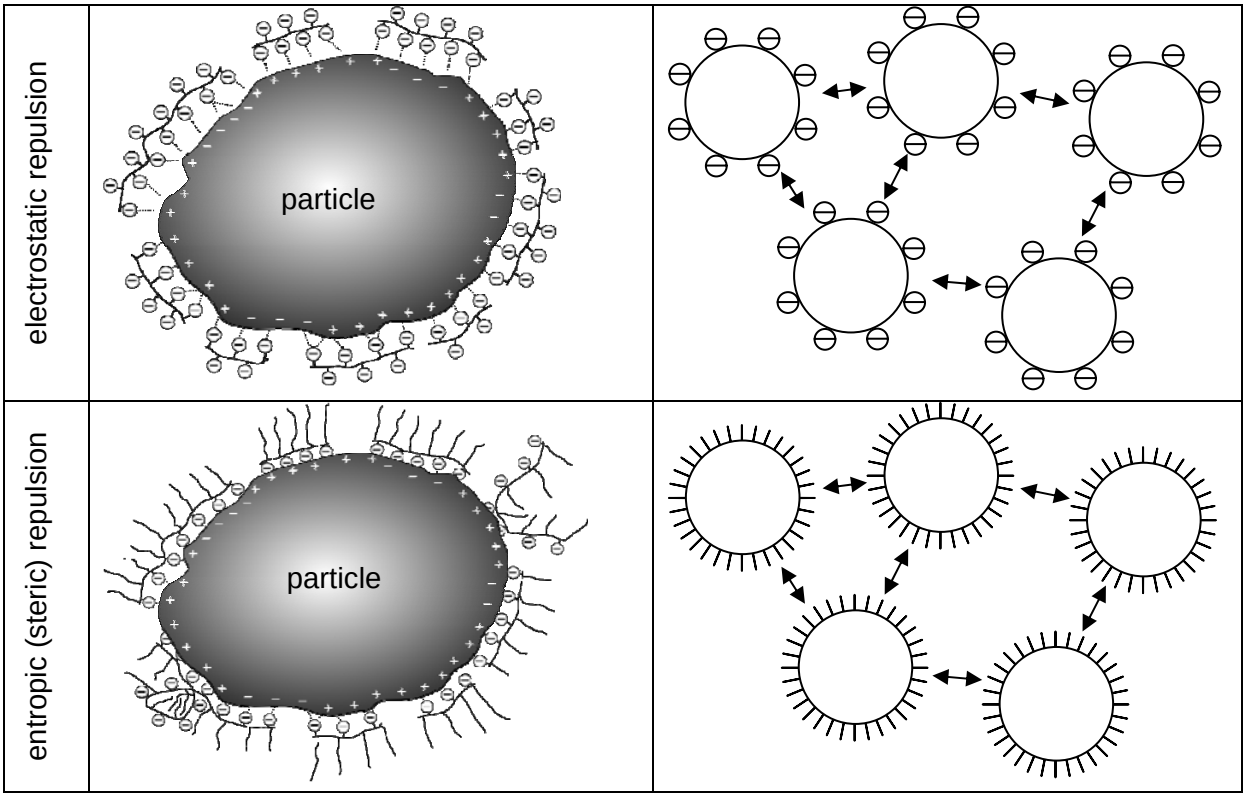

Figure 2: Principles of electrostatic and entropic stabilization of dispersions

2 Samples and Measurement

The measurement of ζ-potential was done using the ZetaProbe analyser from Colloidal Dynamics. The determination of zeta potential is done using the electro acoustic principle and therefore it is possible to measure in undiluted dispersions. Rheological properties were analysed with a rotary viscosimeter CS-50 from Bohlin. For direct measurement of interparticle forces glass spheres (app. diameter 50 µm) were glued onto an AFM cantilever

and a glass plate (see Figure 3). The colloidal probe measurements were performed in aqueous solution using a Multimode with Nanoscope IV controller from Veeco Instruments Inc. The schema of colloidal probe measurement is shown in Figure 3. The spring constant of the cantilever with the glass sphere was determined and from the colloidal probe measurement that is not influenced by the way of stabilization the interparticle forces were calculated [8].

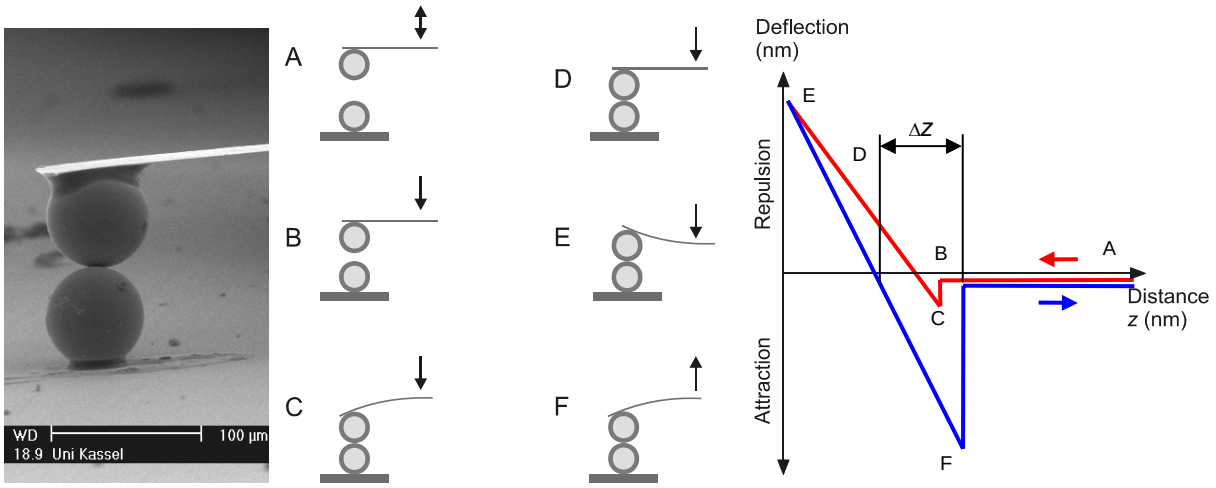

Figure 3: Left: SEM of glass spheres glued onto an AFM cantilever and a glass plate; middle: movement of cantilever with glass sphere during colloidal probe measurement; right: Schematic position sensitive detector signal vs. piezo position (z) including approaching and retracting part during colloidal probe measurement.

3 Results and discussion

Like mentioned in the introduction, for fine particles there is a strong correlation between zeta potential and the rheological behaviour [9-11]. In order to check this relation, the viscosity and zeta potential of an alumina dispersion (Al_2O_3, particle size app. 500 nm) was measured versus pH-value. The results in Figure 4 show that the zeta potential is decreasing with rising pH-value and at the same time the viscosity is increasing. At a pH-value were the zeta potential is around zero (iso electric point, IEP), the viscosity is reaching its maximum and is then decreasing again while the absolute value of zeta potential is increasing but now with the opposite sign.

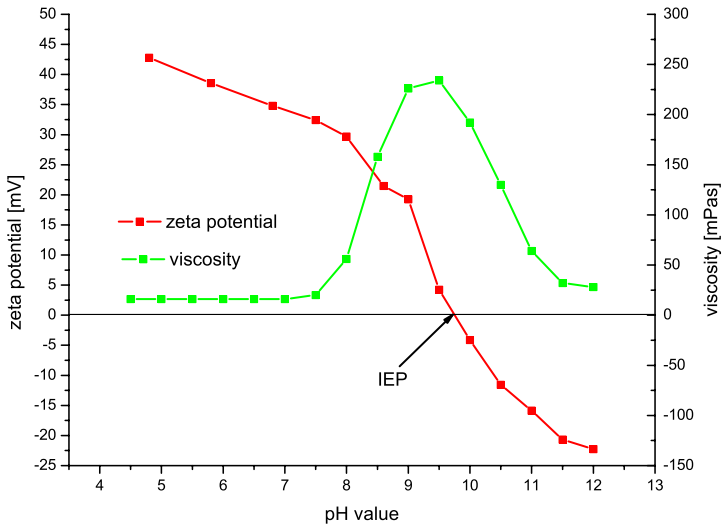

Figure 4: Principles of electrostatic (left) and entropic stabilization of dispersions (right)

In Figure 5 the correlation between zeta potential and rheology is shown for a dispersion of $CaCO_3$ that was stepwise treated with an aqueous solution of sulphonated melamine formaldehyde resin. There is a good correlation between the yield point τ_y and ζ^2 that can be derived from the DLVO theory [10, 12, 13].

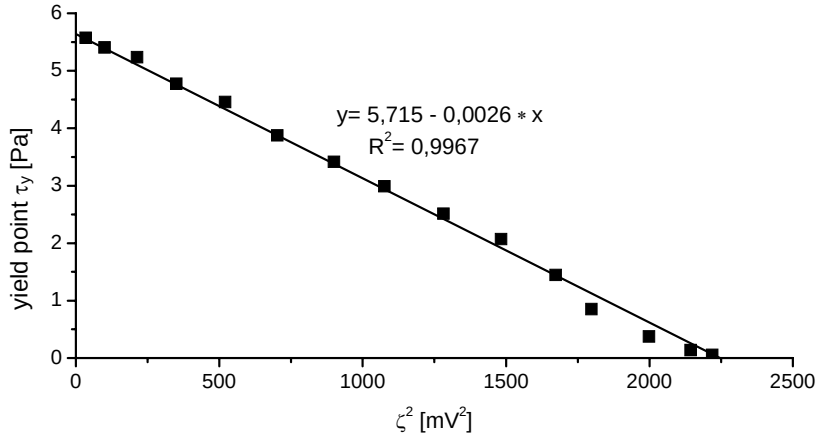

Figure 5: Linear correlation between yield point τ_y and ζ^2 for a dispersion of $CaCO_3$ with different dosages of sulphonated melamine formaldehyde resin

The measurement of zeta potential gives a good understanding for the stability and rheological behaviour of dispersions in the absence of superplasticisers or if there is an electrostatic working mechanism of the superplasticizer like in the case of naphthalene or melamine based superplasticisers.

If the superplasticizer is based on polycarboxylates or other systems with an entropic working mechanism, there is no correlation between rheology and zeta potential and a direct measurement of the interparticle forces is necessary to learn more about the working mechanism. In Figure 6 the measurement of the interactions of two glass spheres glued onto a cantilever and a glass plate is shown. The first measurement was done in pure water and the interaction force of the spheres resulted in about 20 nN. After several measurements in

pure water, the liquid was exchanged by a solution of 0.2 wt.-% of a polycarboxylate ether (PC1) in water and the measurements were repeated. The results are shown in Figure 6 b). The interaction force between the particles is decreased to 6 to 8 nN.

The tests were repeated with other kinds of superplasticisers. As shown in Figure 6 c) the interparticle force is reduced more efficiently by the use of another type of superplasticiser (PC2). Measurements were done in the same way and with PC2 it is possible to decrease interparticle forces to less than 5 nN. The spring constant of the cantilever is 0.03 nN/nm in all cases.

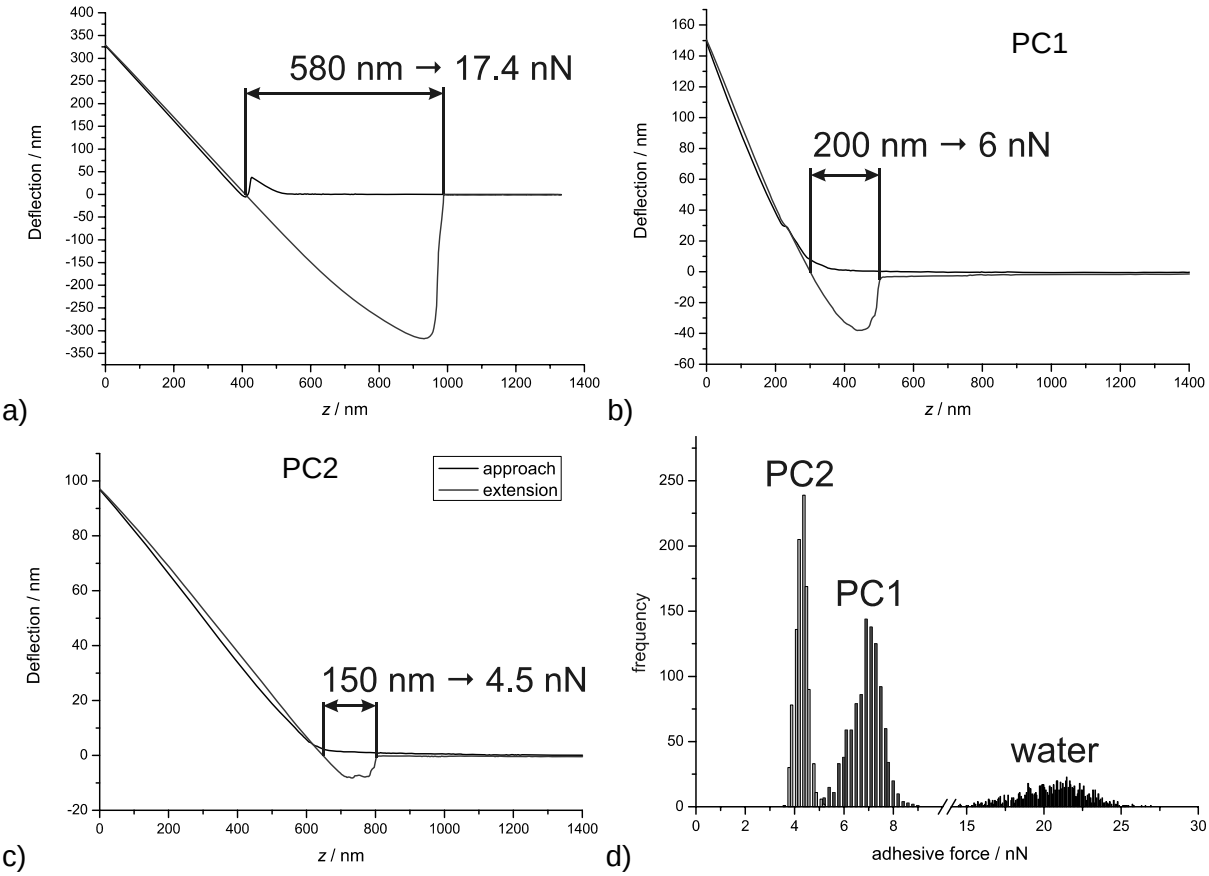

Figure 6: Force curves of glass spheres in AFM. a) pure water, b) 0.2% of PC1, c) 0.2% of PC2, d) histograms of forces. Spring constant of cantilever is 0.03 nN/nm.

Due to changing conditions during the process of measurement (i.e. changing spot of interparticle touching) the measured interparticle forces are changing more or less. Thus it is necessary to repeat AFM measurements many times. In the examples shown in Figure 6 all experiments were repeated more than 1000 times. Results are presented in histograms shown in Figure 6 d).

4 Conclusion

For superplasticisers which act via electrostatic repulsion, the experimental results show a good correlation between the rheological behaviour and the zeta potential. For other superplasticisers with an entropic working mechanism, it was necessary to measure the

particle interaction directly via colloidal probe measurement with an AFM, where the measurement is direct and independent from the working mechanism of the superplasticizer.

5 Acknowledgement

The tests are part of a comprehensive research project aiming at a rheological model for fine grained UHPC considering the influence of the composition of the fines and their particle size as well as the influence of the interparticle forces on the rheological behaviour. It shall give a basis to further optimize the composition of UHPC regarding workability, strength and cost effectiveness.

The authors would like to thank the Deutsche Forschungsgemeinschaft for financial support within the framework of SPP 1182.

6 References

[1] Derjaguin, B. V.; Landau, L.: Theory of the stability of strongly charged lyophobic sols and of the adhesion of strongly charged particles in solution of electrolytes. Acta Physicochim. URSS 14 (1941) pp. 633-662.

[2] Verwey, E. J.; Overbeek, J. T. G.: Theory of the Stability of Lyophobic Colloids. Elsevier, Amsterdam, 1948.

[3] Lagaly, G.; Schulz, O.; Zimehl, R.: Dispersionen und Emulsionen: Eine Einführung in die Kolloidik finerverteilter Stoffe einschließlich der Tonminerale. Steinkopff, Darmstadt, 1997.

[4] Dörfler, H. D.: Grenzflächen und kolloid-disperse Systeme. Springer, Berlin-Heidelberg, 2002.

[5] Hunter, R. J.: Introduction to Modern Colloid Science. Oxford Science Publications, Oxford, 1993.

[6] Uchikawa, H.; Hanehara, S.; Sawaki, D.: The role of steric repulsive force in the dispersion of cement particles in fresh paste prepared with organic admixture. Cement and Concrete Research 27 (1997) pp. 37-50.

[7] Palmqvist, L.; Lyckfeldt, O.; Carlstrom, E.; Davoust, P.; Kauppi, A.; Holmberg, K.: Dispersion mechanisms in aqueous alumina suspensions at high solids loadings. Colloids and Surfaces a-Physicochemical and Engineering Aspects 274 (2006) pp. 100-109.

[8] Butt, H. J.; Cappella, B.; Kappl, M.: Force measurements with the atomic force microscope: Technique, interpretation and applications. Surface Science Reports 59 (2005) pp. 1-152.

[9] Leong, Y. K.: Yield stress and zeta potential of nanoparticulate silica dispersions under the influence of adsorbed hydrolysis products of metal ions - Cu(II), Al(III) and Th(IV). Journal of Colloid and Interface Science 292 (2005) pp. 557-566.

[10] Leong, Y. K.; Ong, B. C.: Critical zeta potential and the Hamaker constant of oxides in water. Powder Technology 134 (2003) pp. 249-254.

[11] Scales, P. J.; Johnson, S. B.; Healy, T. W.; Kapur, P. C.: Shear yield stress of partially flocculated colloidal suspensions. Aiche Journal 44 (1998) pp. 538-544.

[12] Russel, W. B.; Saville, D. A.; Schowalter, W. R.: Colloidal Dispersions. Cambridge Univ. Press, Cambridge, 1989.

[13] Laxton, P. B.; Berg, J. C.: Relating clay yield stress to colloidal parameters. Journal of Colloid and Interface Science 296 (2006) pp. 749-755.

Christof Schröfl
Dipl.-Chem., Ph.D. stud.
TU München
Garching, Germany

Mirko Gruber
Dipl.-Chem., Ph.D. stud.
TU München
Garching, Germany

Johann Plank
Prof. Dr., Chair of Construction Chemicals
TU München
Garching, Germany

Structure performance relationship of polycarboxylate superplasticizers based on methacrylic acid esters in ultra high performance concrete

Summary

The effectiveness of various superplasticizers was studied in a simplified recipe for ultra high performance concrete (UHPC) containing only cement, microsilica and no aggregates. Water/cement (w/c) ratios were varied between 0.70 and 0.20. The target was to identify chemical compositions which are most effective at w/c 0.22, i. e. which require low dosages to minimize cement retardation and to reduce costs. Accordingly, comb-type methacrylic acid-co-(*ω*-methoxypolyethyleneglycol)-methacrylate-co-methallylsulfonic acid superplasticizers were synthesized and characterized. A polymer possessing a molar ratio of methacrylic acid to MPEG-methacrylate ester of 12 / 1, a short backbone length, a high proportion of methallylsulfonic acid and a side chain length of 45 ethylene oxide units was found to be most effective. At w/c 0.22, a dosage of 1.1 % by weight of cement is required.

Keywords: *superplasticizer, ultra high performance concrete, polycarboxylate*

1 Superplasticizers for ultra high performance concrete

Ultra high performance concrete is a demanding material due to its characteristically low water/cement ratio. Highly efficient superplasticizers are needed to obtain a workable, i. e. pumpable, paste. Traditional high range water reducing agents like BNS (*β*-naphthalene sulfonate formaldehyde condensate) or PMS (poly melamine formaldehyde sulfite condensate) cannot be used since they are not efficient enough. They disperse binder grains only by electrostatic repulsive forces [1]. However, to liquefy binder compositions containing very low amounts of water, this effect is not sufficient. To overcome this problem, comb-type molecules were developed which disperse particle suspensions by a combination of electrostatic repulsion and steric hindrance [2]. This so-called electrosteric mechanism explains why molecules causing electrostatic repulsion as well as steric hindrance can successfully be applied to UHPC with w/c ratios below 0.25. Molecules acting in an electrosteric manner usually consist of a polymeric backbone, along which anionic functional

groups such as carboxylate, phosphonate or sulfonate are situated. These enable the dispersing agent to adsorb to the grain surface. Only adsorbed molecules can act as dispersants. These functional groups are furthermore responsible for the electrostatic part of dispersing the binder particles. Additionally, water-soluble, uncharged polyoxyalyklene branches are connected to the backbone. When the molecule adsorbs to a surface, these attached branches spread into the liquid phase. Thus, the side chains act like spacers between the cement grains and prevent their agglomeration [3].

Nowadays, several types of comb-type superplasticizers are successfully used as cement dispersing agents. Methacrylic acid-co-(*ω*-methoxypolyethyleneglycol)-methacrylate on the one hand and copolymers of maleic acid anhydride and *α*-allyl- or *α*-vinyl-*ω*-methoxypolyethyleneoxide on the other hand are the most common basic molecules. Especially in the first copolymers, methallylsulfonic acid is used as an important comonomer. Furthermore, copolymers containing polyamido-amine functional groups as well as mixed polyalkyleneoxides (ethylene oxide and propylene oxide) in the side chains are available [4, 5].

The type of polycarboxylate superplasticizer used in this study was based on poly(methacrylic acid) containing polyalkyleneoxide side chains. Their structural formula is shown in Figure 1. In previous work, this type of carboxylated and sulfonated polymer has been found to disperse pure cement well at w/c ratios to 0.23 [6].

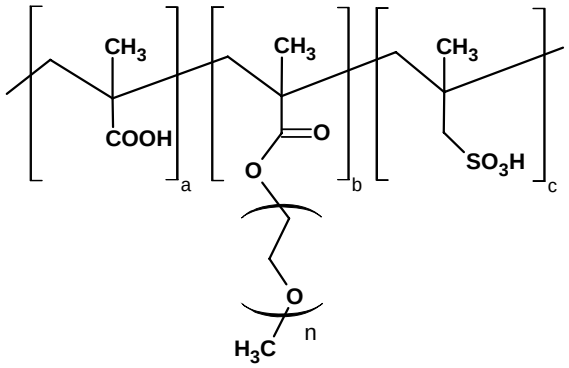

Figure 1: Chemical structure of methacrylic acid-co-(*ω*-methoxypolyethyleneglycol)-methacrylate superplasticizer containing methallylsulfonic acid; molar ratios of the comonomers are indicated by a, b and c

2 Dispersive force

To test the plasticizing effect of the superplasticizers, a mini slump test with a VICAT cone was applied. The complete recipe of UHPC type M2Q, as given in [7], was reduced to water, superplasticizer, cement and 16 mass-% by weight of cement (bwoc) microsilica (Table 1). Microsilica is hydraulically active and represents the finest powder component in the model system. Because of its huge surface area of 15.5 m^2/g (N_2 adsorption, BET method), it has a potential to influence the effectiveness of superplasticizers. The test program started at w/c 0.70 which was then stepwise reduced to 0.20. As a reference, w/c 0.22 was chosen as this is the standard w/c ratio in the Priority Program on UHPC of the German Research Foundation. For calculation of the amount of water at a certain w/c ratio, the solids content of

the aqueous superplasticizer solution was taken into account. Cement and microsilica were interspersed into the mix of deionised water and superplasticizer within one minute. After one minute of rest, the paste was stirred with a spoon by hand for three minutes. The workability of a paste was regarded to be good when a flow value of 26.0 ± 0.5 cm was obtained. The performance of a superplasticizer was judged by its dosage required to achieve this paste flow.

Table 1: Reduced UHPC recipe for mini slump test

Component	Amount [g]
Cement CEM I 52.5 R HS/NA	296.8
Microsilica Elkem Grade 983	48.2
Total water (including water from polymer solution) for w/c 0.22	65.3

3 Methacrylic acid-co-(*ω*-methoxypolyethyleneglycol)-methacrylate-co-methallylsulfonic acid

In this work, methacrylic acid-co-(*ω*-methoxypolyethyleneglycol)-methacrylate-co-methallyl-sulfonic acids as shown in Figure 1, were synthesized, characterized and tested for their effectiveness as superplasticizers in UHPC. Their chemical composition was optimized in order to most effectively disperse a UHPC paste at w/c 0.22, i. e. achieve a certain level of workability at the lowest possible dosage. The challenge was to develop polymers capable of achieving an UHPC paste flow of 26.0 ± 0.5 cm at w/c 0.22.

The three comonomers methacrylic acid, *ω*-methoxypolyethyleneglycol-methacrylate (MPEG-methacrylate) and methallylsulfonic acid were radically copolymerized in a one-pot synthesis. The density of side chains along the backbone was determined by the molar feed ratio of methacrylic acid and methallylsulfonic acid to MPEG-methacrylate. Since their reactivity ratios coincide adequately, statistic copolymerization can be assumed [8]. The main chain length can be adjusted by varying the molar ratio of all the monomers to the polymerization initiator sodium peroxodisulfate [9]. Methallylsulfonic acid can act as a chain transfer agent. Thus, the degree of backbone polymerization can be predetermined by varying its molar feed ratio. In this function, it is only copolymerized as a backbone terminating monomer. Because of the high molar feed of methallylsulfonic acid used in our synthesis, it will also incorporate into the polymer backbone to a significant degree. In an earlier work, YAMADA *et al.* described similar polymers which were able to plastify pure cement pastes (without microsilica or other aggregates) at w/c 0.23 [6]. Most effective were those polymers with longer MPEG side chains, lower degree of backbone polymerization and a higher content of sulfonic acid groups.

Molecular parameters such as side chain density, side chain length and degree of backbone polymerization were varied independently, offering a rather huge matrix of polymer structures. Side chain lengths were set by using commercial *ω*-methoxypolyethyleneglycol methacrylates as macromonomers. In preliminary tests, a side chain length of 45 ethylene glycol units proved to be most useful. None of the polymers possessing longer or shorter side chains were able to disperse this non-slump mixture of cement and microsilica at w/c ratios below 0.25. The side chain density was adjusted by the molar feed ratio of methacrylic

acid and methallylsulfonic acid to MPEG-methacrylate. Only copolymers with a molar ratio of methacrylic acid to MPEG-methacrylate higher than 6 / 1 were able to plastify below w/c 0.26. Most copolymers lost their effectiveness already below w/c 0.35. The third molecular parameter, namely the degree of backbone polymerization, was regulated independently by two means. First, the molar ratio of the sum of comonomers to initiator was varied. To be specific, the ratio of initiator to methallylsulfonic acid was kept constant and only the sum of methacrylic acid and MPEG-methacrylate to initiator was varied. The second way was to vary the molar ratio of methallylsulfonic acid to initiator while the overall ratio of the comonomers to initiator was kept constant. These polymers should incorporate different molar ratios of sulfonic acid groups along the backbone.

Backbone length and side chain density (ratio of comonomers) are the key parameters studied in detail in this paper. A molar ratio of methacrylic acid to MPEG-methacrylate of 10 / 1 and more, combined with a side chain length of 45 ethylene glycol units, turned out to be effective at w/c 0.22. Compositions of the synthesized copolymers are listed in Table 2. Size exclusion chromatography was applied to characterize the polymer batch solutions. The eluate from the chromatographic column was analyzed by refractive index and dynamic light scattering detectors. From these, molar mass and molecular radii were derived. The molecular data in Table 2 are based on the number average mass of the polymer fraction of each polymer solution. Since the molar composition of each polymer is known from the feed of the polymer synthesis and from the determination of the molecular mass, the degree of backbone polymerization was calculated. In addition, hydrodynamic radius and radius of gyration were measured. Based on this data, the shape of the molecules in aqueous solution (conformation) can be deduced. According to GAY *et al.* [10], all superplasticizers effective in our UHPC formulation are shaped as “flexible backbone worms”.

Table 2: Molar composition, backbone length and dispersing force of methacrylic acid-co-(*ω*-methoxypolyethyleneglycol)-methacrylate-co-methallylsulfonic acid superplasticizers for UHPC, side chain length 45 ethylene glycol units

Polymer	**Molar ratio methacrylic acid / MPEG-methacrylate / methallylsulfonic acid**	**Backbone length [no. of monomers]**	**Dosage for paste flow 26.0 ± 0.5 cm at w/c 0.22 [% by weight]**
PCE 1	8.0 / 1.0 / 0.5	90	3.0
PCE 2	10.0 / 1.0 / 0.5	100	2.6
PCE 3	12.0 / 1.0 / 0.6	105	2.4
PCE 4	15.0 / 1.0 / 0.8	115	2.6
PCE 5	12.0 / 1.0 / 1.4	85	1.4
PCE 6	12.0 / 1.0 / 2.5	65	1.5
PCE 7	12.0 / 1.0 / 3.0	50	1.1
PCE 8	10.0 / 1.0 / 2.6	60	1.5
PCE 9	15.0 / 1.0 / 3.8	40	1.5
PCE 10	12.0 / 1.0 / 8.0	25	no plastification

Polymers PCE 1 to 4 possess similar backbone lengths and the same methallylsulfonic acid content. Among them, the most effective superplasticizer was PCE 3 which has a molar ratio of methacrylic acid to MPEG-methacrylate of 12 / 1. Thus, the next step was fixing this molar ratio while varying the methallylsulfonic acid proportion. This led to different degrees of backbone polymerization. Within this group made up of PCE 3 and PCE 5 to 7, the copolymer possessing the highest amount of sulfonate groups (PCE 7) and consequently the shortest backbone was most effective. A copolymer with a higher content of sulfonate groups and shorter backbone length (PCE 10) was not able to disperse the UHPC paste at all. For these reasons, different comonomer compositions based on PCE 7 were investigated (PCE 8 and 9). However, these could not meet the performance of PCE 7.

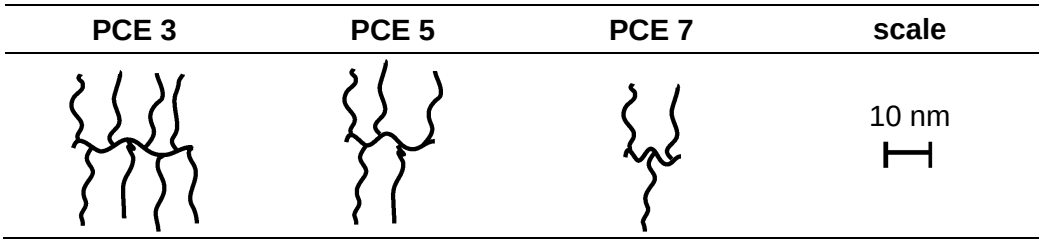

Figure 2: Schematic representation of the molecule architecture of selected methacrylic acid-co-(ω-methoxypolyethyleneglycol)-methacrylate-co-methallylsulfonic acid comb-type copolymers for UHPC

4 Structure-performance relationship

In Figures 3 to 5, the effectiveness of the copolymers PCE 1 to 9 is shown. All dosages given correspond to solid polymer. The side chain length of each polymer is 45 ethylene oxide units. As a reference, commercial superplasticizers PCE A and PCE B are included. These are used in the Priority Program on UHPC of the German Research Foundation.

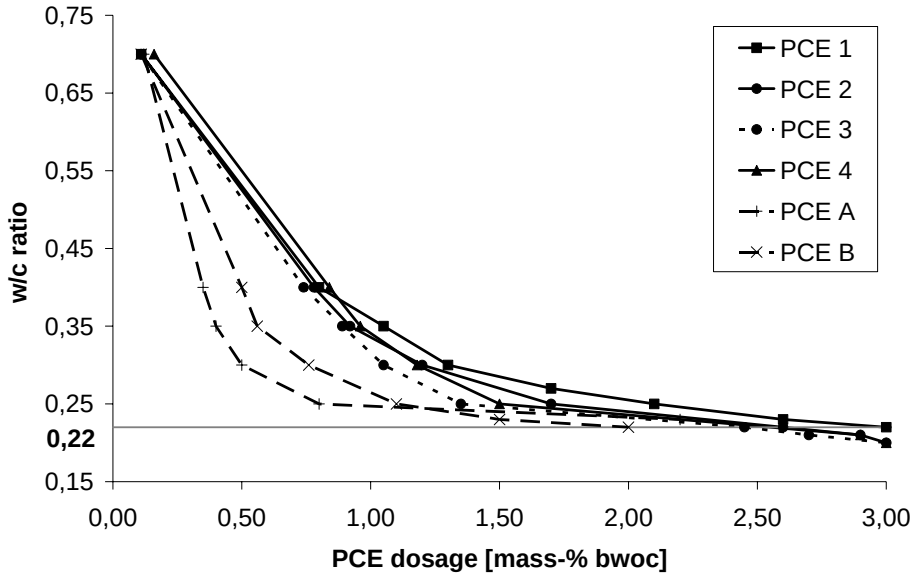

Figure 3: Influence of molar ratio of comonomers on polymer effectiveness; polymer dosages given are those required to achieve 26.0 ± 0.5 cm paste flow at w/c 0.22

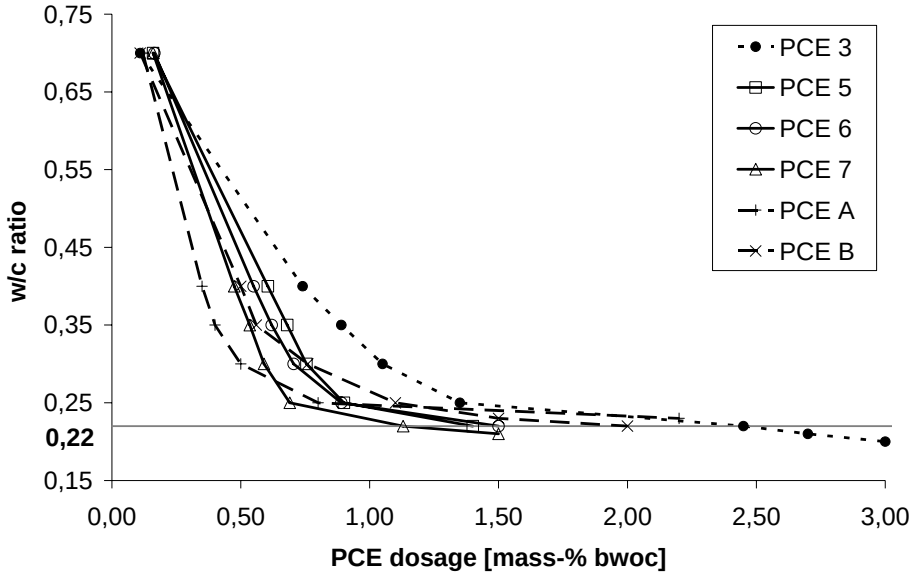

Figure 4: Influence of main chain length and sulfonate content on polymer effectiveness; polymer dosages given are those required to achieve 26.0 ± 0.5 cm paste flow at w/c 0.22

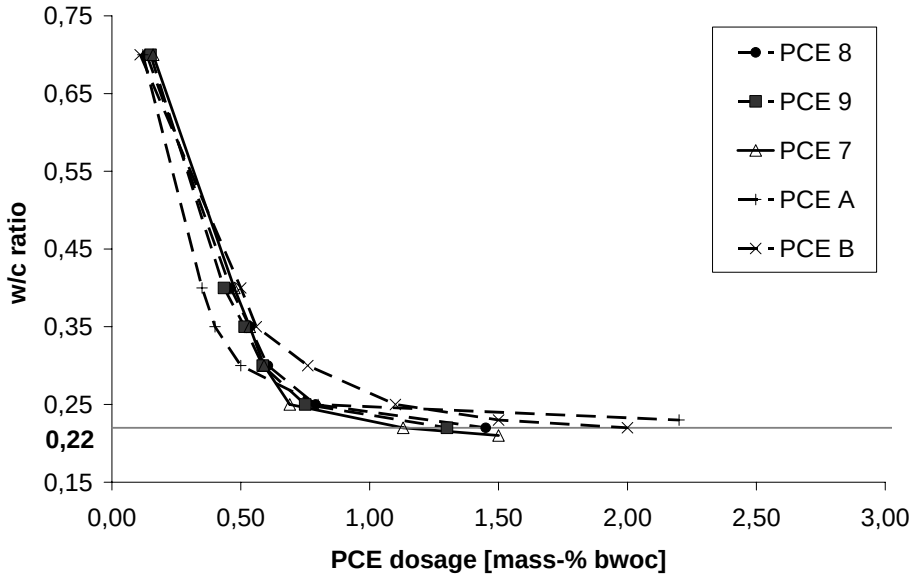

Figure 5: Influence of molar ratio of comonomers on polymer effectiveness; polymer dosages given are those required to achieve 26.0 ± 0.5 cm paste flow at w/c 0.22

The influence of the molar ratio of comonomers on the dispersing effectiveness of the polymers is presented in Figure 3. Polymers PCE 1 to 4 possess similar backbone lengths and sulfonic acid contents. Their molar compositions are shown in Table 2. Obviously, their different performance is based on different side chain densities along the backbone. The polymer possessing a molar ratio of methacrylic acid to MPEG-methacrylate of 12 / 1 (PCE 3) is most effective. Polymers of this molar ratio, but shorter backbones achieved by increased addition of methallylsulfonic acid (PCE 5 to 7), were even more effective, as can be seen in Figure 4. Among them, PCE 7, which possesses the highest content of sulfonate

groups and the shortest backbone, performed best. Figure 5 demonstrates the effectiveness of copolymers with similar sulfonate content and backbone length, but different side chain densities. Both higher and lower side chain densities than in PCE 7 resulted in decreased performance. Obviously, a certain degree of backbone polymerization accompanied by a certain comonomer composition and side chain length is responsible for optimum performance in UHPC. PCE 7 performs significantly better than the commercial products PCE A and B which are used as standard superplastizicers in the Priority Program.

5 Retardation of cement hydration

Polycarboxylate superplasticizers have the potential to retard cement hydration [11]. Carboxylic groups which are not adsorbed to a surface, can complex calcium ions [12]. This complexed calcium is not any longer available for cement hydration reactions. Calcium depletion in the pore solution is supposed to cause retardation. This effect is especially pronounced when the superplasticizer is applied at a very high dosage (above 1.0 M-% bwoc). Retardation was found to be predominantly a matter of dosage and was rather independent of copolymer structure. For this reason, development of new polymers has to focus on reducing the dosage. High dosages of more than 1.0 M-% bwoc are usually not required in conventional concretes since mixing is done under high-shear conditions which support plasticization. A cement paste or mortar mixed in a high-shear blender does not show retardation of cement hydration to a large extent, since agitation is very strong and the applied superplasticizer dosage is low [13]. Within this study, PCE 7 was the most preferred copolymer also in terms of retardation since its dosage was the lowest of all superplasticizers investigated.

6 Summary

Methacrylic acid-co-(*ω*-methoxypolyethyleneglycol)-methacrylate-co-methallylsulfonic acid polymers are effective superplasticizers for UHPC with a characteristic w/c of 0.22 and a binder composition of cement and microsilica. A comb-type copolymer with a rather short backbone length, a high molar ratio of methacrylic acid to MPEG-methacrylate (12/1), and a long side chain length of 45 ethylene glycol units is most effective. This molecular shape matches similar structures reported in an earlier publication by SUGIYAMA *et al.* They had found that these structures have a very strong dispersive force [3]. However, they did not point out the importance of sulfonic acid. Polymers synthesized with an elevated level of sulfonate groups show a better performance. However, a certain balance between the degree of backbone polymerization, side chain length and side chain density has to be accomplished to obtain the most effective polymer. Retardation of cement hydration with these superplasticizers is predominantly an effect of polymer dosage rather than molecular composition.

To understand the different performances of the synthesized copolymers, the working mechanism has to be investigated, e. g. by solubility tests in the highly electrolyte loaded pore solution of UHPC, by adsorption measurements and further molecular polymer analysis. Hopefully, this will lead to new superplasticizers with further improved properties.

7 Acknowledgements

The authors gratefully thank the German Research Foundation (DFG) for financial support of this work and for being part of the priority program 1182 “sustainable building with ultra-high performance concrete“.

8 References

[1] Uchikawa, H.; Hanehara, S.; Sawaki, D.: The role of steric repulsive force in the dispersion of cement particles in fresh paste prepared with organic admixture. In: Cement and Concrete Research 27, No. 1, p. 37-50, 1997.

[2] Yoshioka, K.; Sakai, E.; Daimon, M.; Kitahara, A.: Role of steric hindrance in the performance of superplasticizers for concrete. In: Journal of the American Ceramic Society 80, No. 10, p. 2667-2671, 1997.

[3] Sugiyama, T.; Ohta, A.; Uomoto, T.: The dispersing mechanism and applications of polycarboxylate-based superplasticizers. In: Proc. 11th International Congress on the Chemistry of Cement, Durban 2003.

[4] Plank, J.; Stephan, D.; Hirsch, C.: Bauchemie. In: Winnacker-Küchler (Hrsg.): Chemische Technik – Prozesse und Produkte, Band 7 (Industrieprodukte), Weinheim 2004.

[5] Plank, J.: Current Developments on Concrete Admixtures in Europe. In: Proc. Symposium on Chemical Admixtures in Concrete, Dalian (China) 2004.

[6] Yamada, K.; Takahashi, T.; Hanehara, S.; Matsuhisa, M.: Effects of the chemical structure on the properties of polycarboxylate-type superplasticizer. In: Cement and Concrete Research 30, No. 2, p. 197-207, 2000.

[7] Fehling, E.; Schmidt, M.; Teichmann, T.; Bunje, K.; Bornemann, R.; Middendorf, M.: Entwicklung, Dauerhaftigkeit und Berechnung Ultra-Hochfester Betone (UHPC) – Forschungsbericht. Schriftenreihe Baustoffe und Massivbau, No. 1, 2003.

[8] Borget, P.; Galmiche, L.; Le Meins, J.-F.; Lafuma, F.: Microstructural characterisation and behaviour in different salt solutions of sodium polymethacrylate-g-PEO comb polymers. In: Colloids and Surfaces A: Physicochemical Engineering Aspects 260, No. 1-3, p. 173-182, 2005.

[9] Drescher, B.; Scranton, A. B.; Klier, J.: Synthesis and characterisation of polymeric emulsifiers containing reversible hydrophobes: poly(methacrylic acid-g-ethylene glycol). In: Polymer 42, No. 1, p. 49-58, 2001.

[10] Gay, C.; Raphael, E.: Comb-like polymers inside nanoscale pores. In: Advances in Colloid and Interface Science 94, No. 1-3, p. 229-236, 2001.

[11] Morin, V.; Tenoudji, F. C.; Feylessoufi, A.; Richard, P.: Superplasticizer effects on setting and structuration mechanisms of ultrahigh-performance concrete. In: Cement and Concrete Research 31, No. 1, p. 63-71, 2001.

[12] Uchikawa, H.; Sawaki, D.; Hanehara, S.: Influence of kind and added timing of organic admixture on the composition, structure and property of fresh cement paste. In: Cement and Concrete Research 25, No. 2, p. 353-364, 1995.

[13] Farrington, S. A.: Evaluating the Effect of Mixing Method on Cement Hydration in the Presence of a Polycarboxylate High-Range Water Reducing Admixture by Isothermal Conduction Calorimetry. In: Proc. 12th International Congress on the Chemistry of Cement, Montreal 2007.

Arjan Korpa
Dr.
Consultant at technical research and consulting for cement and concrete
Wildegg, Switzerland

Reinhard Trettin
Prof. Dr.
Institute for Building and Materials Chemistry, University of Siegen,
Siegen, Germany

Ultra high performance cement-based composites with advanced properties containing nanoscale pozzolans

Summary

We present here in this paper the advantage of using nanoscale pyrogene oxides for producing ultra high performance concretes with advanced properties. The inclusion of pyrogene oxides and especially of their powder form in well optimised ultra high strength/performance concrete formulations enable the decrease of total porosity and causes pore refinement similarly as in the case when pyrogene oxide (aerosil®) dispersions are used. The strength property of the resulting specimens is further enhanced when the powder form of pyrogene oxides is involved.

Keywords: p*yrogene oxide, Ultra High Performance Concrete; advanced properties, porosity*

1 Introduction

The production of extremely dense ultra high performance concretes with advanced properties is based on the designing of systems with highly compatible well graded components. The various pozzolanic fillers used in these formulations play an essential role. Since various pozzolanic fillers that are characterised by different surface characteristics, grain sizes and different reactivity can be used, in order to optimise the packing density, they will also behave and affect differently the micro- and nanostructure development. Additionally some filler will accelerate the hydration reactions, while others may retard it [1].

Actually, the finest component that is being used in different UHPC systems is microsilica (silica fume) with grain sizes which have their lower limit at around 0.1µm. Hence, the need for extending the granulometry and optimising at the nanoscale through aimed use of nanosize particles becomes obvious. A better and denser packing can be realised by extending the size range below this limit using nanopowders (nanoscale oxides), which have specified particle sizes covering the nanometre range from 1-100nm. Their use is expected to allow the development of materials with increased durability and improved performance or new properties.

Among various existing synthetic nanopowders (1-100nm), pyrogene oxides arise a particular interest due to their very high purity, possibility of controlling the particle sizes, surface modification and to their very high reactivity. Hence, it is expected that their use alone or appropriately combined with other pozzolanic fillers in various concrete formulations will bring considerable improvements of micro- and nanostructure, strength, reduction of

porosity, hydration behaviour, durability etc [1]. The UHPC composites of this work that contain ultra fine powders are characterised by lower porosity and pore refinement, which correlate very well with scanning electron microscopy (SEM) and atomic force microscopy (AFM) investigations [2]. These results show a further structure densification at all levels and agree also with the mechanical property improvements. An acceleration of the hydration reaction has been observed for formulations containing highly reactive nanopowders. The rate of heat development measured by using isothermal conduction calorimetry is also lower and the induction period shorter (4-5h) [1]. Highly pozzolanic nanoscale powders can be used to produce high and ultra high performance cement-based composites with advanced properties.

2 Materials and processing

In this work we have used nanoscale pyrogene oxide products (aerosil® is the representative product) in their powder form. The powder form of pyrogene oxides offers the possibility to vary the water quantity, without being dependent on the water coming from dispersion. Thus, more variations of the component quantity used for the mixture formulation can be done. Also, because of differences of surface characteristics and agglomeration state, the mixing procedure together with properties of obtained concrete formulations will differ, depending on the form of the pyrogene oxide used.

The following components were chosen for the investigations of this work:

- Sand quartz 125-500µm
- Portland cement “PC I 52.5 R HS/NA,
- Elkem microsilica grade “G-983” named in this work “SF1”
- Fly ash type “FA SWF”
- Polycarboxylate-ether based superplasticizer (in dispersion form)
- Polycarboxylate-ether based superplasticizer (in powder form)
- Pyrogene oxides (aerosil®) with some of their properties depicted in table 1.

Table 1: Some properties of the pyrogene nanoscale oxides used

	Hydrophilic types				**Hydrophobic type**
Pyrogene oxide	POx 1	POx 2	POx 3	POx 4	POx 5
BET m^2/g	50±15	80±20	100±15	90±15	110±20
Primary particle size [nm]	40	30	13	20	16
pH	3.8-4.8	3.6-4.5	4.5-5.5	3.7-4.4	3.6-4.4
Oxide (s)	SiO_2	SiO_2/Al_2O_3	Al_2O_3	SiO_2	SiO_2

The nanoscale pyrogene oxide products were included in the formulation of the ternary combination microfiller (SF) - microfiller (FA) - nanofiller (pyrogene oxide, POx), as in the table 2 (no fibres were included for these formulations). The fly ash quantity was varied inside the optimal range (17-22%) depending on the nanoscale-oxide used and its specific surface area.

Table 2: The reference UHPC formulation.

Formulation components	Component ratio referring to cement
PC I 52.5R HS/NA	1
Fly ash (FA SWF)	0.17-0.22*
Silica fume SF1 G983	0.24
Quartz sand 125-500µm	1.34
SP (polycarboxylate-ether)	<0.03
Pyrogene oxide	varying
Water	<0.3
Heat treatment temperature	20°C

*The FA content was 0.22 for the UHPC specimen containing only silica fume and fly ash

Mixing and processing

The mixing process that is required for an efficient mixing of all components was found to be circa 10 minutes. After the specified mixing time, fresh concrete was filled in the mould (1.5x1.5x6 cm) in two layers and vibrated for 2 minutes. The prism-shaped specimens were demoulded after 24h of hydration time and then stored in water (20°C) for the rest of specified curing time. Investigations were carried out for the following representative specimens:

- Normal mortar specimen having a w/c = 0.45 and quartz aggregates < 2mm
- Simple RPC specimen containing 25% silica fume (SF1 G983), without quartz flour and without fibres [3]
- UHPC specimen containing both silica fume (SF1 G983) and fly ash (FA SWF), cast after table 2, but without pyrogene oxide
- UHPC specimen with SF1 (G983) - FA (SWF) - POx cast after table 2

As pyrogene oxide were used those indicated in table 1.

3 Results and discussion

3.1 Strength results for specimens of ternary combination microfiller (SF) - microfiller (FA) - pyrogene oxide (POx)

The 28 days strength values of specimens that contain small amount of pyrogene oxides, cast according to the mixture formulation given in table 2, are shown in figure 1. Here are shown only the compressive strength values for 1.5% of pyrogene oxide (POx) in powder form used in combination with silica fume (SF1) and fly ash (FA) in an optimised UHPC mixture formulation. This pyrogene oxide content was chosen inside the optimal range being circa 1-2.5% (referring to quantity of the cement used) for a considerable strength increase and appropriate rheological behaviour.

The compressive strength results indicate that in these formulations, the pyrogene oxide quantities more than 3%, referring always to cement are unfavorable for maximizing strength, even though, higher quantities realize higher volume filling effects and higher pozzolanic reaction degrees. The lower strength results are related to the observed poorer rheological behaviour, which is due to the increased water retention. There is no sufficient water available to contribute for lubrication and particles free movement. At the same time, a

poorer deairing of the fresh formulation that is related to the worsened flowing behaviour in the presence of higher pyrogene oxide contents, results in lower strength values. Here of course, the maximal pyrogene oxide quantity that can be used is depended on the specific oxide and formulation workability.

A further strength improvement results when using nano-oxides in powder form, as compared to the strength enhancement in the case when pyrogene oxide dispersions are used. From an average estimation of the compressive strength contribution by pyrogene oxide in powder form, at least 10% strength improvement results, depending on pyrogene oxide type, compared to the strength achieved by the UHPC specimen without pyrogene oxide. A trend of better strength contribution with the increase of pyrogene oxide specific surface area is also observed.

The reason for the better strength contribution of pyrogene oxide in powder form is not well understood. It is however assumed that this is due to an improved mixing and flowability of the formulations in the fresh state in the case where powdered pyogene oxides are used. In figure 2 is shown the strength improvement for the simple RPC specimen, the UHPC specimen that contains silica fume and fly ash, and the UHPC specimens that additionally contain small quantities of pyrogene oxide, both in dispersion and in powder form.

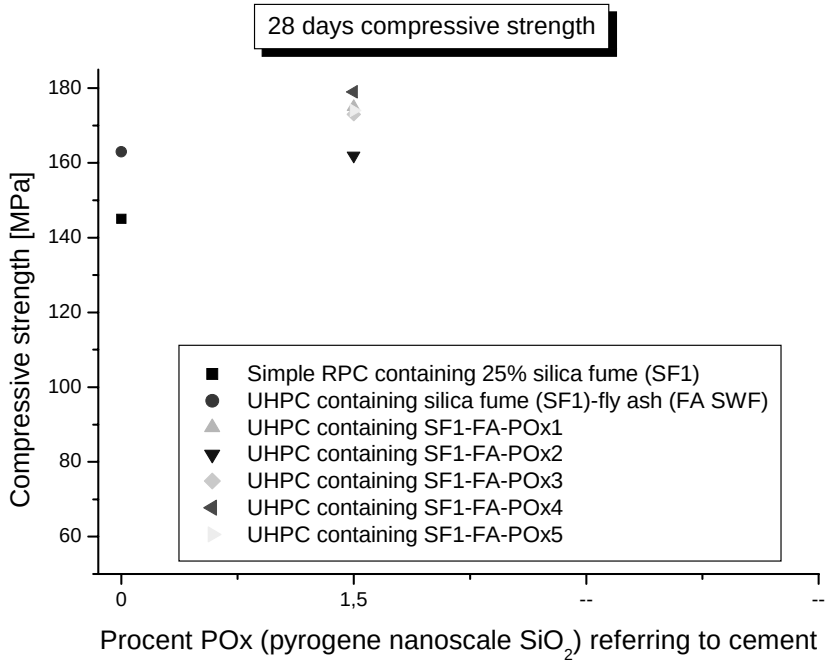

Figure 1: Compressive strengths comparison for UHPC specimens of ternary combination microfiller (SF) - microfiller (FA) - pyrogene oxide (POx)

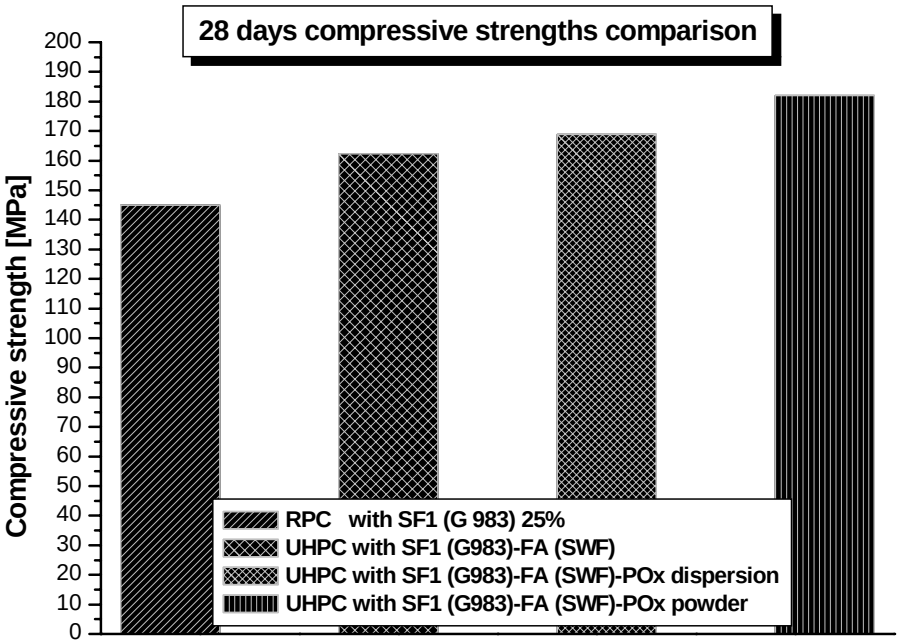

Figure 2: Strength improvement for UHPC specimens that contain pyrogene oxide in dispersion and powder form.

As previously mentioned the specimen that contains pyrogene oxide in powder form is characterised by the highest strength value.

3.2 Porosity and pore size distribution (PSD) for the UHPC specimens of ternary combination Microfiller (SF) – microfiller (FA) - pyrogene oxide (POx)

Both, the gas adsorption (GA) and mercury intrusion porosimetry (MIP) measurements were carried out for representative specimens, in order to obtain an integral picture of the whole porosity distribution. These methods can be used as complementary of each-other [4]. Measurements were done on 28 days old specimens that were dried according to the "F-drying" method of our previous work [5]. The obtained porosity distribution plots cover the porosity range from around 200μm down to 2nm. The porosity peak maximum (figure 4) corresponding to around 150μm, which is also considered as air porosity according to pores classification, might be entrapped air during the mixing process. The porosity distribution plots obtained by both methods, shown in figures 3 and 5, confirm the expected results of a much coarser and higher total porosity for the normal concrete specimen, as compared to the RPC and UHPC specimens. The normal concrete specimen represents much more porosity beyond around 10nm (has a maximum at around 50-60nm) and much lower pore volume at the fine pore range 2-10nm.

The Hg-porosimetry porosity distribution plot of the RPC specimen that contains only silica fume (figure 3) stands slightly above those of UHPC specimens at the range 30-60nm but much below that of normal concrete. The threshold values assessed from the distribution plots of figure 3 are; around 100nm for the normal concrete, 25-30nm for RPC with only silica fume, and 20nm for the UHPC specimens group. The percolation threshold values give in

this way additional evidence for a pore refinement in direction from normal concrete to RPC with only silica fume and UHPC specimens. This trend of pore refinement is in good agreement with the conclusions found on literature [6], [7], [8], [9]. Inside the UHPC specimens group there are only very small differences of pore distributions to be seen, referring to the plots assessed by Hg-porosimetry.

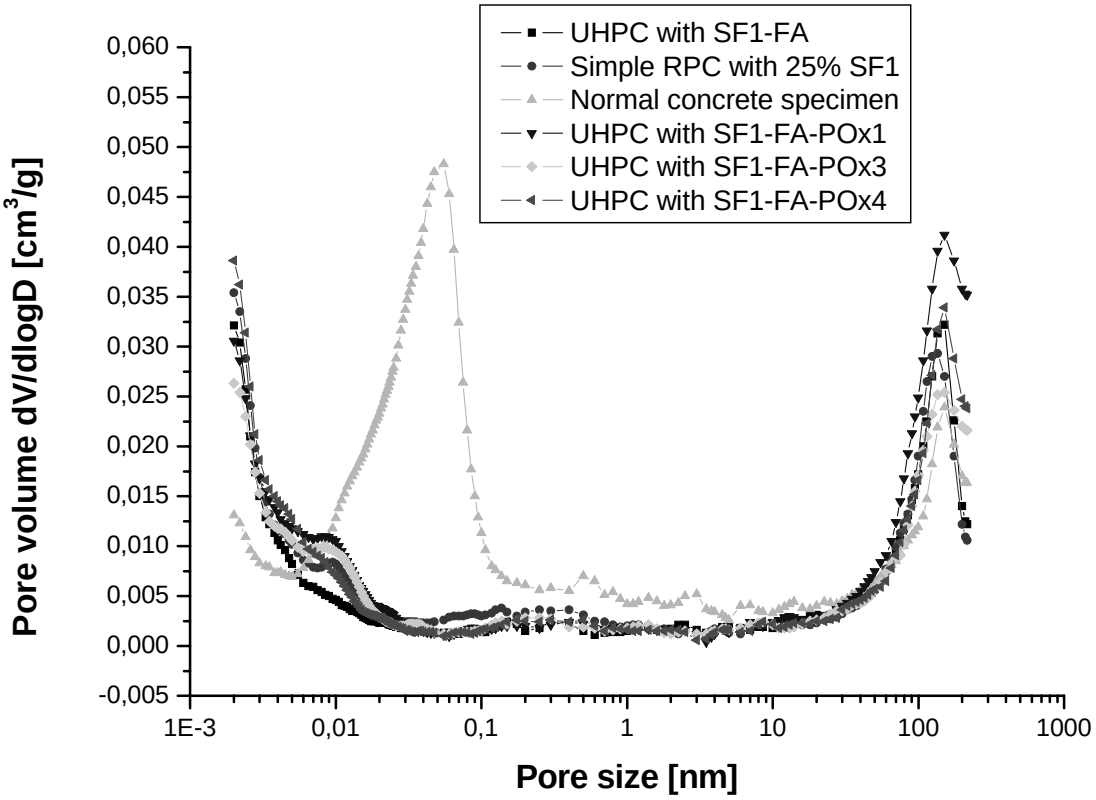

Figure 3: Pore size distribution plots assessed by mercury intrusion porosimetry (MIP) (56 days old specimens)

Capillary porosity (0.03-10 µm after Smolcyk [10]) plays the most important role for concrete durability. By a smaller capillary porosity, a lower probability for the ingress of damaging species would result, and an increased concrete durability should be expected. The differences between values of measured capillary porosity are very small (figure 4). The simple RPC specimen represents slightly higher capillary porosity than the UHPC specimens group, whereas the normal concrete is characterised by a remarkably higher capillary porosity, as it has to be expected.

The method of gas adsorption is better suited than mercury intrusion for detection in the range pore 2-10nm [11]. At the very fine pore range below 10nm (figure 5) only a very small pore sizes shifting can be observed, referring to gas adsorption plots. Both UHPC specimen cast with SF - FA and the RPC specimen have a peak maximum at around 4nm, whereas the UHPC specimens of the ternary combinations SF – FA - POx have this maximum at 3-3.5nm. At this pore maximum the last mentioned UHPC specimens have also a slightly higher pores volume. In other words, for the UHPC specimens of the ternary combinations SF – FA - POx only a very slight pore size shifting was observed by gas adsorption. The

increase of finer pores proportion for the UHPC specimens that contain pyrogene oxides can be used to explain the measured strength improvements, and is in good agreement with conclusions of others [11], [12].

For concluding it can be said that, whether a great difference results between the normal concrete, the RPC and the UHPC specimens, only very small differences could be recorded inside the UHPC group, which might also be associated to the accessibility limitations of both methods at these very fine porosity range.

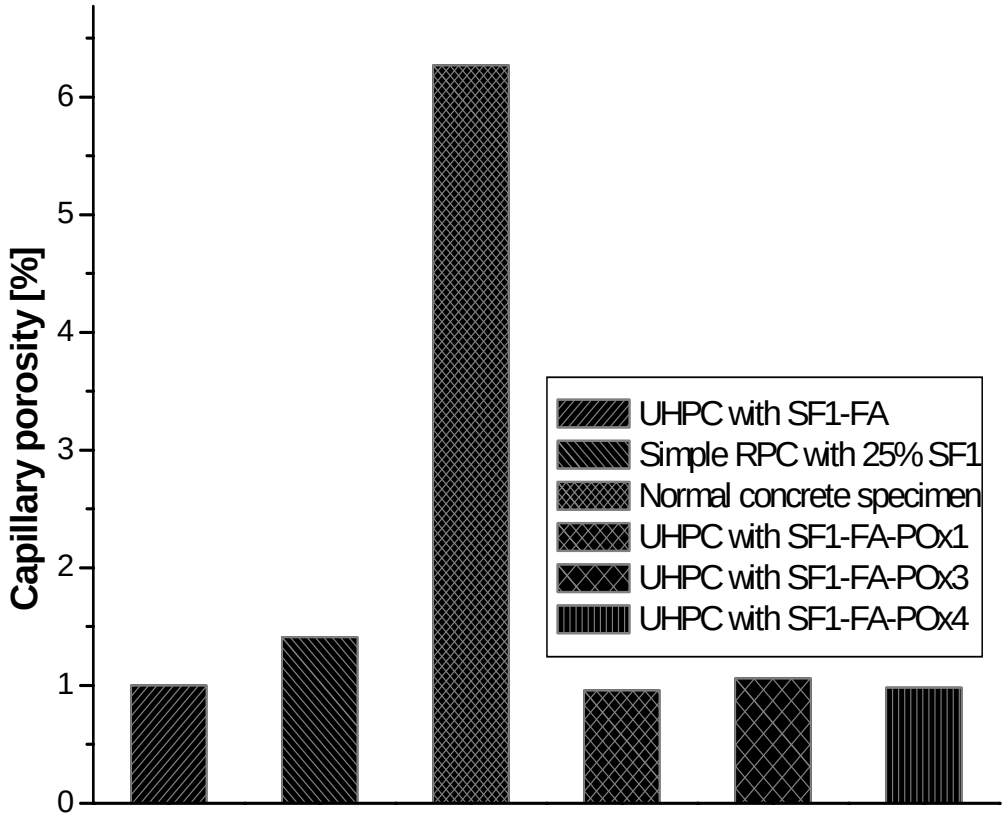

Figure 4: Capillary porosity assessed by mercury intrusion porosimetry (MIP) (56 days old specimens)

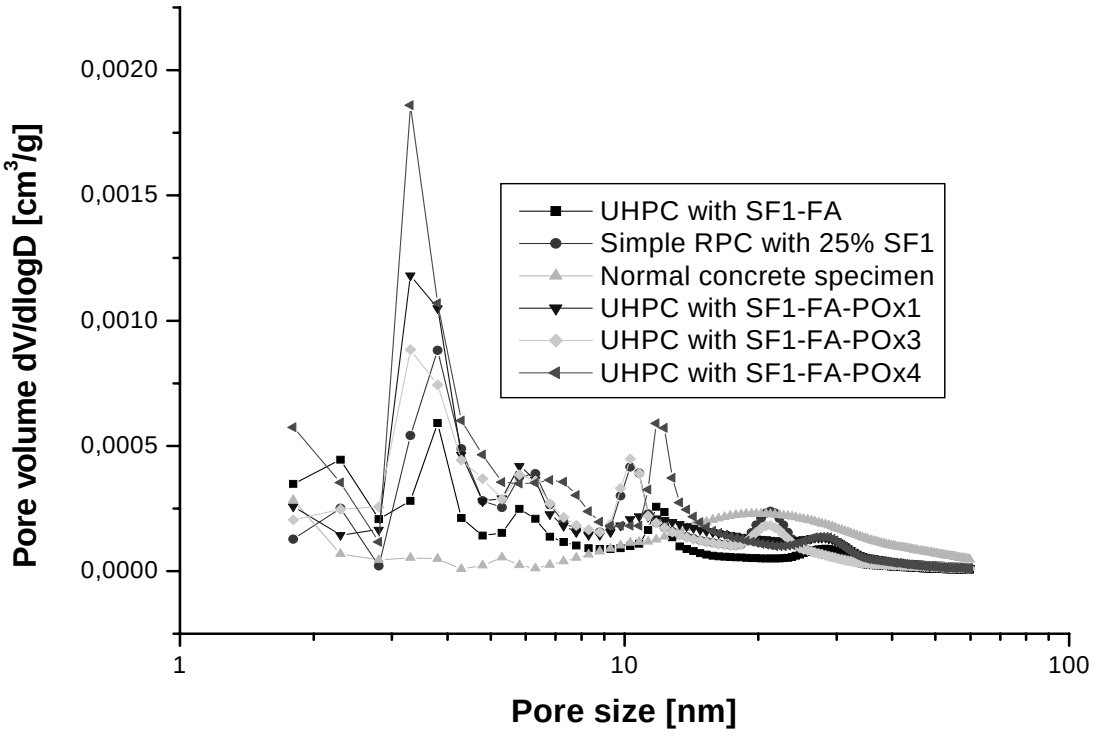

Figure 5: Pore size distribution plots assessed by gas adsorption (GA).(56 days old specimens)

3.3 Capillary water absorption behaviour for the UHPC specimens of ternary combination Microfiller (SF) – microfiller (FA) - pyrogene oxide (POx)

Since the absorptivity of a material can be inversely correlated to its degradability, absorption measurements performed on uniformly prepared concrete specimens can provide useful information concerning the quality control and the determination of which specimens are likely to have a longer service life. The measurements for estimation of the capillary water coefficients were done on prismatic specimens after the specifications of DIN 52 617 norm. In the figure 6 are given the results of capillary water absorption (water uptake) coefficients for representative specimens.

The results of water absorption coefficient are in good agreement with capillary porosity values, assessed by MIP and other previous conclusions. The normal concrete specimen is characterised by the highest coefficient of capillary water absorption, followed by the RPC specimen and the UHPC of the combination silica fume (SF) - fly ash (FA). The water absorption coefficient of the last-mentioned concrete specimen is only slightly higher than those corresponding to the UHPC specimens of the combinations silica fume (SF) - fly ash (FA) - POx. Other authors address the lower water absorption to the higher concrete compactness and increased pores tortuosity [12]. Our results confirm these conclusions, but indicate also that specific features of the oxide surface play additionally a key role for the water uptake. This is also the case for the UHPC specimen cast with POx3. The UHPC with POx3 has the highest coefficient of water absorption among all UHPC specimens of the ternary combinations, comparable to that of UHPC with silica fume and fly ash. Its water

absorption behaviour cannot be related to just the capillary porosity space, but also probably to other characteristics of the resulting micro and nanostructure.

According to these results, it can be concluded that at least theoretically an improved durability and service life has to be expected for the UHPC specimens containing additionally pyrogene oxides.

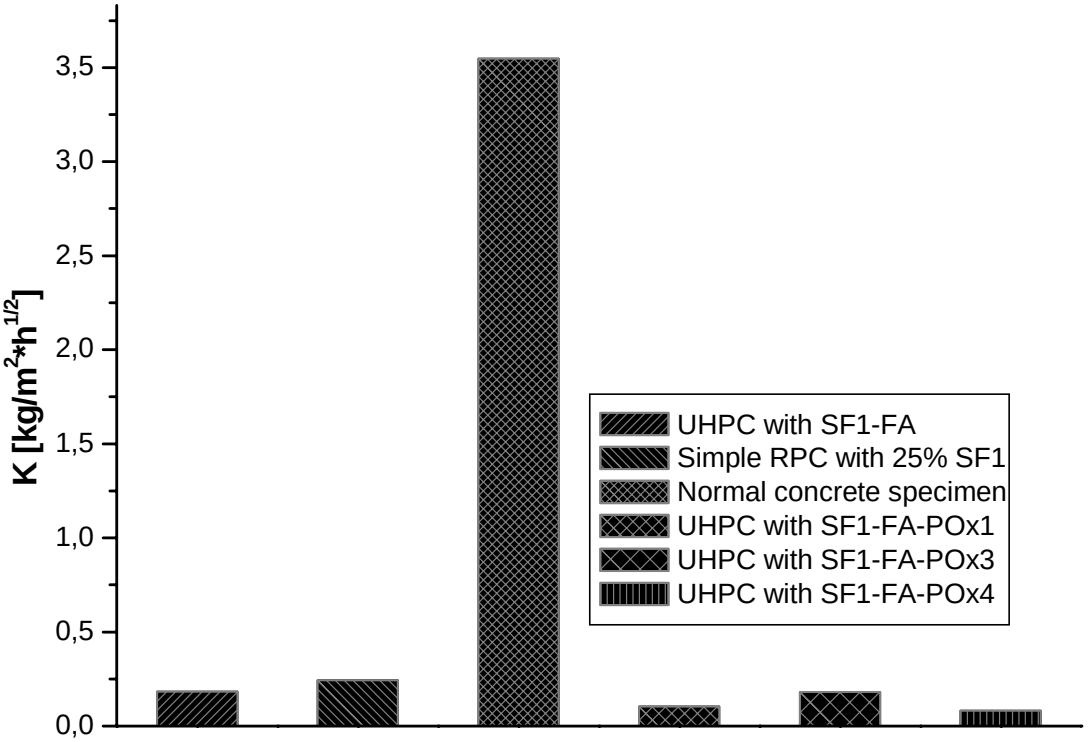

Figure 6: Coefficients of capillary water absorption values (28 days old specimens)

4 Conclusions

We have used pyrogene oxides in powder form for obtaining ultra high strength and performance concrete specimens with improved properties.

The inclusion of pyrogene oxides in powder form in combination with microfillers, as it is expected, could further improve the strength properties of the resulting UHPC specimens, even more than pyrogene oxides in dispersion form.

Around 10% compressive strength improvement results, compared to the reference UHPC system without pyrogene oxide have been calculated.

The simultaneous use of gas adsorption and mercury intrusion porosimetry techniques could give an integral picture for porosity and pore size distribution of these specimens. A pore refinement from normal concrete systems to RPC and UHPC direction in agreement with literature has been as well assessed. Measurement of porosity inside the UHPC group did not show any remarkable difference concerning the total porosity. The only difference was a pore shifting to smaller ones for the specimens that additionally contain nanoscale powders.

5 References

[1] Korpa A.; Trettin R. The use of synthetic colloidal silica dispersions for making high performance and ultra high performance systems (HPC/UHPC). International symposium on Ultra High Performance Concrete, September 13-15, Kassel, Germany, 2004, pp 155-164.

[2] Korpa A.; Trettin R. Pyrogene nano-oxides in modern cement based composites. 2nd International Symposium on Nanotechnology in construction, 13th-16th November 2005, Bilbao, Spain.

[3] Richard P. and Cheyrezy M. H. Reactive powder concretes with high ductility and 200-800 N/mm2 compressive strength. Metha, P. K. (ed), Concrete Technology: Past, Present and Future, SP144-24, pp. 507-517, 1994.

[4] Meyer K., Röhl-Kuhn B. Porosity of ceramic compacts: Gas adsorption and mercury porosimetry. Cfi. DKG 72 (1995) No 3. 108-114.

[5] Korpa A.; Trettin R. The influence of different drying methods on cement paste microstructures as reflected by gas adsorption: Comparison between freeze-drying (F-drying), D-drying, P-drying and oven-drying methods. Cement and Concrete Research, Vol 36, Issue 4, April 2004, pp. 634-649.

[6] Fidjestol P. and Lewis R. in: Lea´s chemistry of cement and concrete. Fourth edition. Edited by Hewlett P. C. Butterworth-Heinemann, 2001. pp 679-712.

[7] Könnig G., Tue N. V., Zink M. Hochleistungsbeton, Bemessung, Herstellung und Anwendung. Ernst & Sohn, A Willey Company, 2001, Germany.

[8] Rougeau P., Borys B. Ultra high performance concrete with ultrafine particles other than silica fume in; Ultra high performance concrete. International Symposium on Ultra High Performance Concrete, September 13-15, 2004, pp 213-225, edited by Schmidt M. et al.

[9] Feylessoufi A., Villieras F., Michot L. J., De Donato P., Cases J. M. and Richard P. Cement & Concrete Composites 18 (1996), 23-29.

[10] Romberg H. Zementsteinporen und Betoneigenschaften, Beton-Information, 18 (1978), S. 50-55.

[11] Zaitsev Y., in 7th International Congress on the Chemistry of Cement (Paris 1980), Vol. III, P. VI-176.

[12] Sereda P. J., Feldman R. F. and Ramachadran V. S., in 7th International Congress on the Chemistry of Cement (Paris 1980), Vol. I, P. VI-1/3.

Mazanec, Oliver
M.Sc., scientific assistant
centre for building materials, TU Munich
Munich, Germany

Schießl, Peter
Prof. Dr.-Ing. Dr.-Ing. E.h., director
centre for building materials, TU Munich
Munich, Germany

Mixing Time Optimisation for UHPC

Summary

At present the production of ultra high performance concrete (UHPC) requires mixing times which are much longer than for odinary concrete. The present work focuses on the effect of mixing technology (mixing time and tool speed) and concrete composition on the properties of fresh and hardened concrete. The composition of UHPC was systematically varied to determine the factors affecting the mixing time necessary for optimum workability (slump flow). The shortest mixing time (stabilisation time for homogenisation) was determined by monitoring the power consumption of the mixer. It is shown that the stabilisation time depends on w/c ratio and the grading of the fine material. An important new parameter is presented for the effect of concrete composition on mixing time of UHPC which takes the effect of particle sizes into account. It is known as the relative solid concentration and is the ratio of actual to maximum packing density. By dividing the mixing process into two stages with first high (6.1 m/s) and then low (1.4 m/s) tool speeds it was possible to reduce the mixing time of UHPC to only two minutes.

Keywords: *UHPC*, *mixing time, packing, grain abrasion*

1 Introduction

Since the 1990s, the development of high and ultra high performance concrete with strengths above 200 MPa and good durability has opened new possibilities in construction such as filigree load-bearing components. To exploit fully the performance of this material it is necessary to consider not just concrete composition, placement and curing technology, but also the actual process of concrete production, i.e. the mixing technology. Currently, the mixing time for ultra high strength concrete is well above that of conventional concrete. In practice, mixing times between 7 and 18 minutes are currently used for UHPC constructions [1, 2, 3]. These long mixing times are mainly due to the special composition of UHPC. Very low water/cement ratios, high superplasticizer dosages and high contents of fine mineral additions are indispensable for good workability and high compressive strength. In addition, the mixing technology used affects the time necessary to produce a homogeneous mix. It has been shown in previous investigations on self-compacting concrete [4] that mixing time can be considerably reduced by increasing mixing tool speed. The effect of mixing time, tool speed and concrete composition on the mixing process of UHPC are considered in this contribution. The main factors which lead to the long mixing times of UHPC are explained. A method is proposed for the optimisation of the mixing process for UHPC.

2 Investigations

The time necessary to achieve a sufficient degree of mixing is an important technical and economic aspect of UHPC production in practice. In the course of preliminary investigations, the effect of mixing time and mixing tool speed on the properties of fresh UHPC was investigated systematically. A 75 l intensive mixer with an inclined drum and variable tool speed was used for the investigations. It was possible to vary the tool speed continuously over a range covering 1.5 to 20 m/s. In addition, it was possible to monitor and record the electric power supplied to the mixing tool during the mixing process.

As well as tool speed, concrete composition has a considerable effect on the necessary mixing time. UHPC has a higher binder paste content, a lower w/c ratio, a higher content of mineral additions and a significantly higher amount of admixtures than ordinary concrete. Thus the effect of the UHPC composition on the mixing process was investigated by varying mix composition. Two different UHPC mixes containing silica fume and quartz flour as mineral additions were considered (Table 1). Concrete UHPC.A was a fine-grained concrete with a maximum aggregate grain size of 0.5 mm. UHPC.B was coarser, containing aggregate with a maximum size of 8 mm.

Table 1: Mix proportions and concrete properties

Reference mix			**UHPC.A**	**UHPC.B**
cement	c	kg/m³	853	682
quartz flour	qf	kg/m³	212	170
silica fume	sf	kg/m³	138	111
water	w	kg/m³	167	132
fine sand 0/0.5 mm	f_s	kg/m³	999	799
crushed basalt 2/8 mm	g	kg/m³	-	614
superplasticizer	sp	wt.%	4.1	4.5
water/cement ratio	w/c		0.23	0.23
compressive strength (28d / 20 °C)	$f_{c,20}$	[N/mm²]	130-140	125-135
compressive strength (28d / 90 °C)	$f_{c,90}$	[N/mm²]	180-195	170-180

The water/binder ratio of the reference mix UHPC.A and the grading curve of the fine material were varied systematically. The volumetric ratio of water to fine material ranged over V_W/V_f ratios between 0.36 to 0.70 while keeping the volume of fine paste (volume of cement, silica fume, and quartz flour) constant. The grading curve of the fine material was varied by changing the proportions of cement and mineral additions. The silica fume content ranged between 10 and 30 vol.-% and the content of quartz flour between 9 to 32 vol.-%, both with respect to the volume of fine material, keeping the volume ratio of water to binder constant.

The ultra high performance concrete UHPC.B differed from UHPC.A primarily by its maximum aggregate size. In an additional investigation, up to 40 vol.% coarse aggregate (crushed basalt with a maximum grain size of 8 mm) was used in concrete mixes with the same binder paste composition.

3 Results and Discussion

3.1 Mixing Time

To achieve a high packing density during mixing, all particles must take part equally in the mixing process and be blended evenly together. This requires the complete dispersion of agglomerates and the distribution of cement, aggregate and additions. Especially in the case of fine-grained UHPC.A more particles must be moved relative to each other to achieve homogenisation than in normal concrete. The effect of mixing time was studied using a fine-grained UHPC.A and a coarse-grained UHPC.B. The mixing water and all the superplasticizer were added at the beginning of mixing after which the electric power required by the mixer was observed to increase significantly, Figure 1. According to [4] water bridges form between the particles after the water has been added and distributed in the mix. The forces between the particles increase due to the surface tension of water and the Laplace pressure difference between the inside of the liquid and the surroundings, see [4]. The particles are attracted to each other owing to capillary pressure which explains the increase in mixing power observed. As mixing proceeds, water and superplasticizer are distributed more and more evenly. The superplasticizer is adsorbed on the surface of the particles and the hydration products. The slump flow of the mix increases which leads to a decrease in mixing power as shown in Figure 1. The power supplied to the mixing tool decreases asymptotically towards a plateau where it may be assumed that the concrete components are homogeneously blended and the superplasticizer fully distributed in the mix [4]. Both types of UHPC mixes investigated exhibited maximum flowability when the plateau was reached. The time taken for the mixing power to reach the asymptotic limit of the power curve is defined as the stabilisation time t_s [5]. Thus the stabilisation time is the minimum mixing time needed for complete dispersion of all the concrete components.

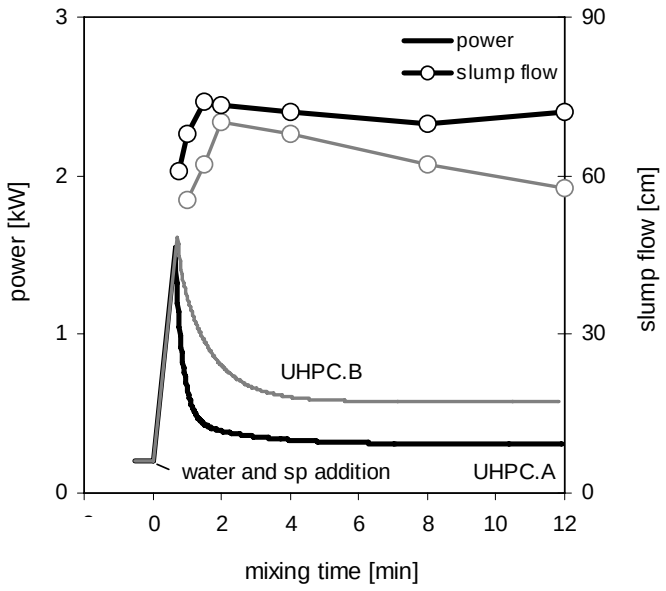

Figure 1: Effect of mixing time on power and slump flow

Whereas the slump flow for the fine-grained UHPC.A remains essentially constant having reached the optimum flow properties after 2 minutes, additional mixing energy supplied to the coarser UHPC.B results in a progressive decrease in slump flow, Figure 1. Lowke [4] observed a similar reduction while mixing self-compacting concrete and explained the loss of flowability by the ongoing dispersion of agglomerates due to the action of the mixing tool. This results in an increase in surface area and consequently water requirement of the mix. It is also possible that additional particles are produced by abrasion of the coarse aggregate [4]. Moreover, abrasion of the initial hydration products may also take place which would lead to new surfaces for reaction [6, 7].

3.2 Tool Speed

The properties of concrete can be influenced by mixing tool speed. The degree of dispersion at higher speeds was characterised by slump flow and the 28 d compressive strength of 10 cm cubes (without heat treatment). Figures 2 and 3 show the development of slump flow for the fine-grained UHPC.A and the coarse-grained UHPC.B as a function of mixing time for a number of different tool speeds. As the tool speed becomes faster the time needed to reach maximum power is shorter. Water and superplasticizer are distributed faster and the water bridges between the particles are broken up more quickly. Thus the time needed to achieve optimum flow properties is shorter. The mixing time for good flow properties is halved from 4 to 2 min by roughly doubling the tool speed from 1.4 to 2.9 m/s. Tool speeds above 2.9 m/s only led to a small additional reduction of mixing time for fine-grained UHPC.A.

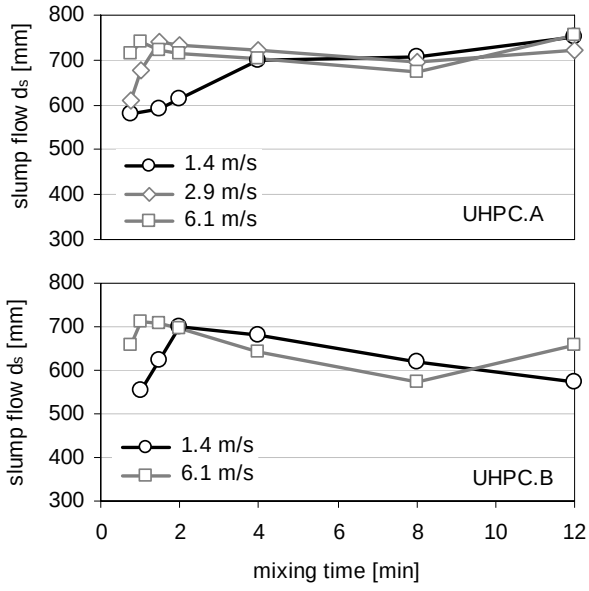

Figure 2: Effect of tool speed on slump flow

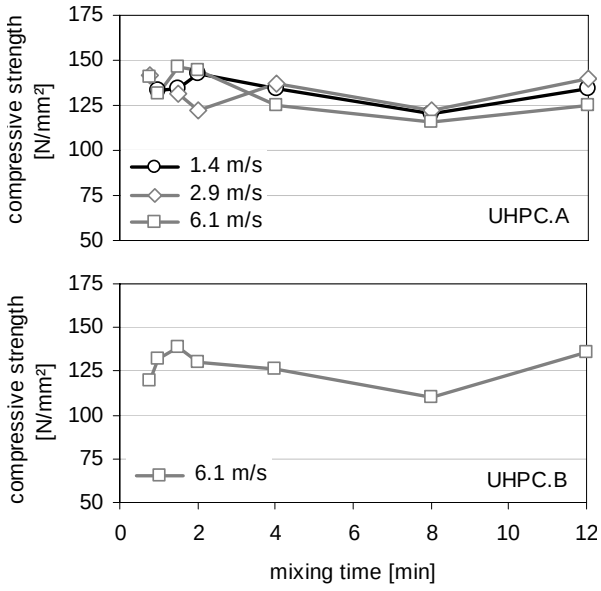

Figure 3: Effect of tool speed on compressive strength

The extent to which mixing time can be reduced by higher tool speeds depends on concrete composition. Lower tool speeds were sufficient for the coarse-grained UHPC.B compared with fine-grained UHPC.A. Consequently, optimum flow properties were already reached for UHPC.B after 2 min at 1.4 m/s. The additional action of the coarse aggregate in this concrete

enhances the mixing process speeding up the distribution of water and superplasticizer [4]. However, the maximum slump flow and the duration of the phase with optimum flow properties are smaller. Longer mixing times result in a decrease in slump flow. The investigations show that concrete made with coarser aggregate is, due to the reasons discussed above, more sensitive to mixing. In contrast, no perceptible loss in flowability was observed for the fine-grained UHPC.A as tool speed was increased in the range investigated.

The development of compressive strength reflects the behaviour of slump flow, Figure 3. However, high compressive strengths are already achieved with low tool speeds and short mixing times.

3.3 Concrete Composition

In order to compare objectively the mixing energy necessary for different concrete compositions the stabilisation time t_s was calculated from the power curves recorded during mixing. As already mentioned, the stabilisation time is defined as the time need for the power curve to reach the asymptotic value [5]. In the course of earlier investigations in [5] and earlier investigations at the Centre for Building Materials it was shown that optimum fresh concrete properties are obtained when the power supplied to the mixing tool does not significantly decrease anymore. The shortest mixing time is therefore given by the stabilisation time. To find the stabilisation time, the power curve is normalised and divided into two regions. The increase in power between the beginning of mixing and the time of maximum power was described by a linear approximation. The region following peak power was described using an exponential function, Eq. 1.

$$P = P_0 + P_1 e^{-\frac{t}{t_1}} + P_2 e^{-\frac{t}{t_2}} \tag{1}$$

The stabilisation time t_s is assumed to be the time at which the slope of the curve dP/dt reaches $-4 \cdot 10^{-4}$; i.e. the asymptotic limit has been reached to within reasonable accuracy.

The stabilisation time is strongly affected by concrete composition. Figure 4 shows the effect of silica fume content on the stabilisation time where the silica fume content was varied between 10 to 30 vol.% while keeping the content of fine material and water constant. The silica fume content in the reference UHPC.A mix was 15% with respect to the fine material, Table 1. It can be seen in Figure 4 that the addition of silica fume leads to much shorter stabilisation times. This is because the silica fume particles fill the spaces between the larger cement and quartz flour particles increasing packing density. This means that more water is effectively available for the smaller particles which therefore lowers internal friction. In addition, the friction between the particles is reduced owing to the spherical form of the silica fume particles which also reduces stabilisation time. As well as silica fume, the amount of quartz flour was varied between 9 and 32 vol.% by replacing cement and silica fume while keeping the volume of fine material constant. The addition of quartz flour resulted in longer stabilisation times, Figure 4. The longer stabilisation times are due to lower packing densities. To understand the effect of silica fume and quartz flour content on mixing time, a

general parameter was sought to describe the effect of particle packing with regard to mixing time. The results for silica fume and quartz flour have shown that the actual volumetric packing density of particles in concrete (concentration of solids) ϕ and the maximum possible packing density (maximum concentration of solids) ϕ_{max} are important parameters with regard to mixing time. The ratio of this parameters ϕ/ϕ_{max} - known as the relative solid concentration - is related to the degree or state of homogenisation and was therefore determined for the concrete mixes investigated. The values of ϕ_{max} were calculated for each mix according to Schwanda [8]. Comparison of stabilisation time with ϕ/ϕ_{max} in Figure 5 shows that stabilisation time correlates well with the relative solid concentration. The figure also includes data for UHPC.A with different ratios of water to particle volume (V_W/V_f-ratio) and UHPC.B with different amounts of coarse aggregate. The relative solid concentration is thus a useful value for characterising the mixing energy needed to produce concrete of good workability.

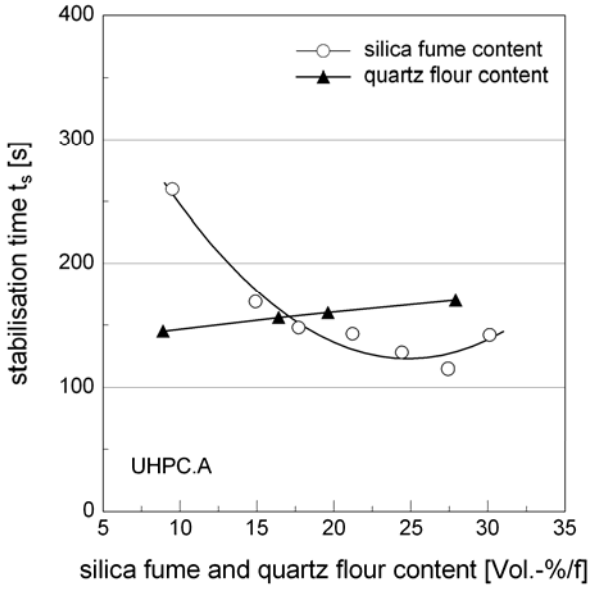

Figure 4: Relationship between stabilisation time and content of silica fume and quartz flour

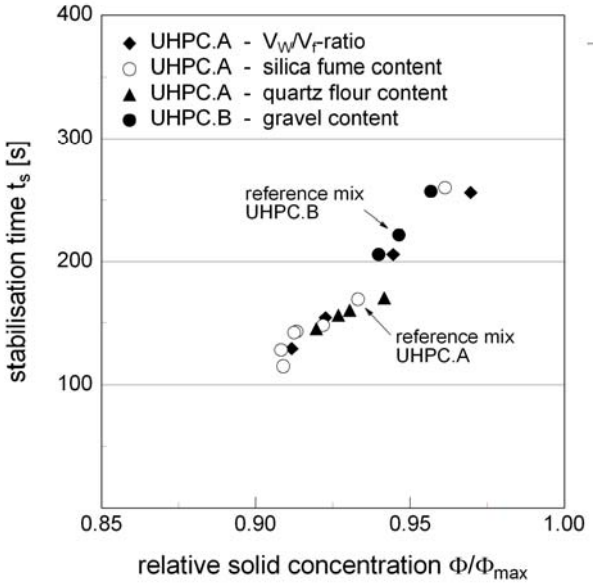

Figure 5: Relationship between stabilisation time and relative solid concentration

In particular, UHPC possesses large numbers of well-packed fine particles which affect the rheological properties of the fresh concrete. For example, a reduction in water content results in an increase in ϕ and therefore ϕ/ϕ_{max} as well. The stabilisation time is longer. In contrast, the volumetric replacement of cement by silica fume (ϕ is constant) results in a larger maximum solid concentration. Thus the relative solid concentration ϕ/ϕ_{max} is smaller and the stabilisation time shorter. This relationship is demonstrated by comparing the stabilisation time for the two reference mixes UHPC.A ($\phi/\phi_{max} = 0.93$) and UHPC.B ($\phi/\phi_{max} = 0.95$). The fresh and hardened concrete properties are similar for these mixes. Whereas UHPC.B requires a stabilisation time of 222 s for optimum mixing, UHPC.B requires only 169 s, Figure 5. When designing ultra high performance concrete, high maximum packing densities ϕ_{max} of the particles should be aimed at since this helps reduce mixing time. This has been confirmed for other concrete compositions and is described in detail in [9].

3.4 Optimisation of Mixing Process

Based on the above knowledge of the factors which affect the mixing process, the mixing procedure for UHPC was optimised. By investigating the effect of mixing tool speed, it was found that increasing tool speed to 2.9 m/s results in sufficient blending after two minutes. However, increasing tool speed can cause more air voids to enter the mix resulting in loss of strength. Moreover, the effect high tool speed on the adsorption of superplasticizer is unknown. This could adversely affect the time available for placement of UHPC which is already short. In a first intensive mixing stage, high tool speeds were used for the first distribution of water and superplasticizer [4]. Afterward, final blending was performed at a lower tool speed. This mixing procedure permitted the production of fresh UHPC.A in two minutes. Mixing for 40 s at 6.1 m/s was found to be most favourable for the first mixing stage, see Figure 6, left. In the second mixing stage, the tool speed was reduced to 1.4 m/s and mixing performed for 70 s. Prolongation of the first intensive mixing stage was not advantageous because loss of flowability occurred. Figure 6, right, shows the power recorded during the mixing stages. Optimum flowability was obtained when mixing was performed at high speed until the peak of the power curve was reached and then the tool speed switched down to the lower value for the remaining time. Shortening the intensive stage to 20 s resulted in lower slump flow values for the UHPC investigated. This occurred because at the time of speed reduction the dispersion of the mix components was incomplete - which explains why the power increased further after the speed was reduced, Figure 6, right. Prolongation of intensive mixing resulted in a reduction of slump flow, perhaps due to the abrasion of the initial hydration products on the surface of the cement particles containing adsorbed superplasticizer.

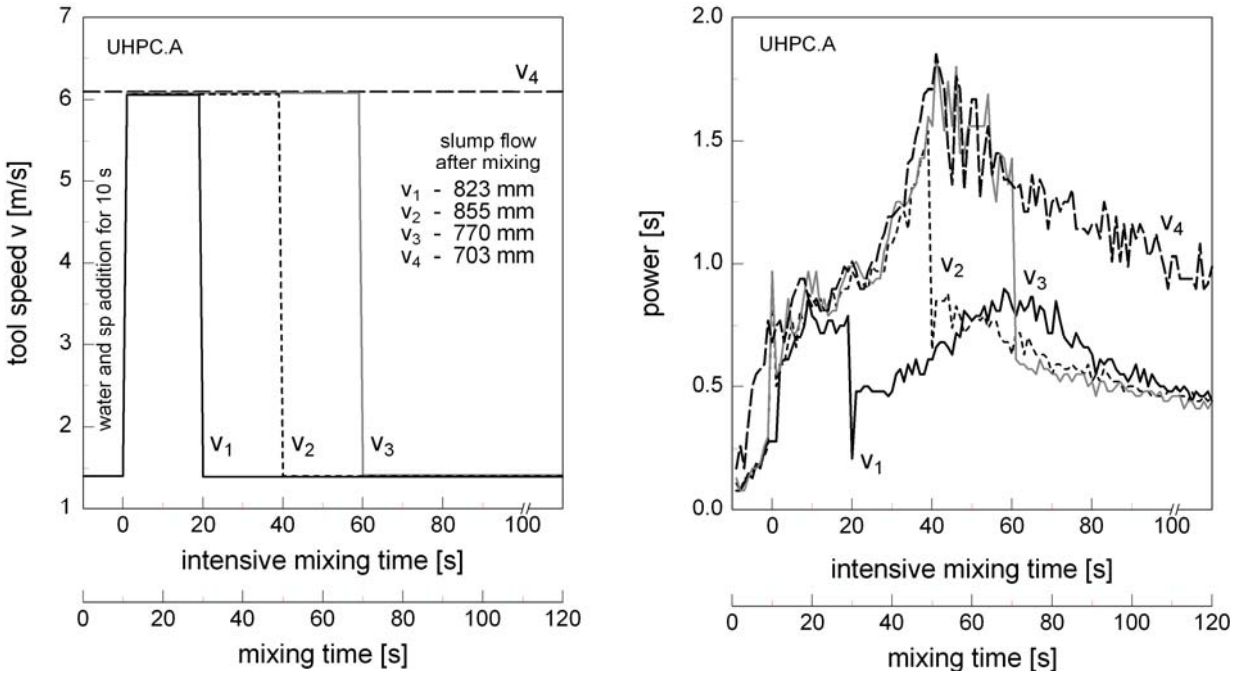

Figure 6: Slump flow and electric power of mixing tool as a function of tool speed and intensive mixing time at 6.1 m/s. Intensive mixing started 10 s after water and sp addition. v_1, v_2, v_3, v_4 intensiv mixing for 20, 40, 60, 120 s respectively.

4 Conclusions

Although the workability and strength of ultra high performance concrete is excellent, the application of UHPC in practice is currently hampered by long mixing times which impede continuous production processes and lower the capacity of concrete plants. In the present work, the main parameters governing the mixing process of UHPC are considered as exemplified by fine-grained and coarse-grained mixtures, UHPC.A and UHPC.B, respectively. At the beginning of mixing at constant tool speed, the slump flow of the mix increases. In the case of the coarse-grained concrete this was followed after 2 minutes by a steady reduction in flowability. This can be explained by the dispersion of agglomerates which increases the surface area of particles in the mix and, consequently, water requirement. In the case of the fine-grained concrete, the slump flow remained virtually constant having reached a maximum value. By increasing the mixing tool speed from 1.4 to 2.9 m/s it was possible to reduce the mixing time (including 10 s for the addition of mixing water and superplasticizer) for both fine and coarse concretes to two minutes. Continius tool speeds above 2.9 m/s did not significantly further reduce mixing time. By systematically varying concrete composition an important new parameter regarding the effect of particle sizes on the mixing time of UHPC has been found. It is known as the relative solid concentration and is the ratio of actual to maximum packing density which describes the actual degree of mixing. Based on this, optimum fresh and hardened UHPC properties were obtained by intensively mixing at high speed 6.1 m/s for 40 s followed by a low speed mixing period 1.4 m/s for 70 s.

The investigations were performed in the German Research Foundation (DFG) priority programme No. 1182 “Sustainable Building with Ultra High Performance Concrete”.

5 References

[1] Bonneau, O.; Lachemi, M.; Dallaire, E.; Dugat, J.; Aitcin, P.-C.: Mechanical Properties and Durability of Two Industrial Reactive Powder Concretes. ACI Materials Journal, pp. 286-290, Juli-August 1997

[2] Tanaka, Y.; Ootake, A.; Uzawa, T.; Tsuka, T.; Kano, K.; Shimoyama, Y.: Structual Performance of a 50 m Footbridge Applying Fiber Reinforced Reactive Powder Concrete. Proceedings of the JCI International Workshop on Ductile Fiber Reinforced Cementitious Composites (DFRCC) - Application and Evaluation - pp. 209 - 218, October 2002

[3] Borghoff, M.: Die erste europäische Verbundbrücke mit UHPC in Kassel - Herstellung der ultrahochfesten Betonfertigteile. Beton + Fertigteil-Technik, Heft 9, S. 58 - 65, 2006

[4] Lowke, D.; Schießl, P.: Effect of Mixing Energy on Fresh Properties of SCC. In: SCC 2005, Proceedings of the 4th International RILEM Symposium on Self-Compacting Concrete, Chicago. Hanley Wood Publication 2005, Addison, ISBN 0-924659-64-5

[5] Chopin, D.; de Larrard, F.; Cazacliu, B.: Why Do HPC and SCC Require a Longer Mixing Time? Cement and Concrete Research (2004), pp. 2237 - 2243

[6] Takada, K.; Walraven, J.: Influence of Mixing Efficiency on the Properties of Flowable Cement Pastes. In: Proceedings of the Second International Symposium on Self-Compacting Concrete. 2001, Tokyo, Japan

[7] Wischers, G.: Einfluß langen Mischens oder Lagerns auf die Betoneigenschaften. beton 13 (1963) 1, S. 23-30 und beton 13 (1963) 2, S. 86-90

[8] Schwanda, F.: Das rechnerische Verfahren zur Bestimmung des Hohlraums und Zementleim-anspruchs von Zuschlägen und seine Bedeutung für den Spannbetonbau. Zement und Beton (1960), pp. 8 – 17

[9] Schießl, P.; Mazanec, O.; Lowke, D.: SCC and UHPC - Effect of Mixing Technology on Fresh Concrete Properties. Advances in Constructions Materials 2007, Symposium in honour of H.W. Reinhardt, University of Stuttgart, 23-24 July 2007.

Jens Ewert
Dipl.-Ing., research assistant
iBMB, TU Braunschweig
Braunschweig, Germany

Harald Budelmann
Prof. Dr.-Ing., director of the institute
iBMB, TU Braunschweig
Braunschweig, Germany

Matias Krauß
Dr.-Ing.
GRS mbH
Cologne, Germany

Heat of Hydration and Hardening of Ultra High Performance Concrete (UHPC)

Summary

Several models exist to describe the time dependent mechanical properties of normal strength and high performance concrete. For ultra high performance concrete (UHPC) only first approaches are existing. To get durable UHPC constructions the properties of the material have to be known from casting to usage. The degree of hydration α, the maturity and the equivalent age t_e of the UHPC respectively are important criteria for a close description of the material. For the purpose of temperature stress analyses it is established to calculate the degree of hydration from the adiabatic heat release during hydration. An accurate approach of the maturity and the equivalent age for normal strength concrete was developed by Freiesleben Hansen/Pedersen [1]. In this paper it is shown that the maturity concept and the activation energy concept can be applied to a reference fine grain ultra high performance concrete (cf. chapter 2) too.

Keywords: *Ultra high performance concrete, hardening, heat release, degree of hydration*

1 Introduction and Background

UHPC is often used in combination with other building materials, in so-called “hybrid” or rangy constructions with high contents of reinforcement in combination with steel fibres. The hardening of UHPC often occurs in thermal and mechanical bond with stiffer members [2]. High cement contents provide a quick and high heat release during hydration leading to thermal restraint and cracking of young concrete, with the subsequence of reduced durability of UHPC structures. Within the framework of the Priority Program 1182 - Sustainable Building with Ultra High Performance Concrete (UHPC), supported by the Deutsche Forschungsgemeinschaft (DFG) [3], the Institute for Building Materials, Concrete Structures and Fire Protection (iBMB) is investigating the early age properties of UHPC in the normal temperature range. The main aim is the development of constitutive models to describe the degree of hydration and the mechanical properties of hardening UHPC. At iBMB constitutive models of hardening concrete have been developed before describing the time dependent

development of mechanical properties of normal strength concrete, massive concrete and high performance concrete respectively [4, 5, 6, 7]. A heat treatment in the temperature range up to 90°C, as it is widely used for pre-cast members, was not investigated here. Such treatment is leading to a nearly completed hydration and autogenous shrinkage in short time. By contrast in on-site casted constructions UHPC is hardening at ambient temperature, the hardening process becomes influential for structural behaviour. Besides the development of compression and tensile strength and Young's Modulus concrete hardening models must comprise the description of the heat release, degree of hydration, creeping and shrinkage. The main focus of this paper is on the heat release, the development of the degree of hydration α and the activation energy E_A of UHPC.

2 Mix proportions

The investigated concrete mixture M2Q is a fine grain UHPC with a cement content of 832 kg/m³ and a water cement ratio of 0.22 developed and tested by Fehling et al. [8]. The cement is an ordinary Portland cement CEM I 52.5 R HS/NA. The packing density of the concrete mixture is optimized by using the following aggregates and admixtures: quartz sand (maximum grain size 0.5 mm), a quartz flour (maximum particle size of 0.125 mm) and silica fume (maximum particle size of 0.02 µm). An acceptable workability of the fresh concrete was achieved by adding a superplasticiser based upon polycarboxilatether. The ductility of the hardened concrete was improved by adding steel fibres with a length of 9 mm and 0.15 mm diameter. Table 1 gives a general survey of the mix proportions of M2Q.

Table 1: Mix proportions of 1 m³ M2Q

		M2Q	
Cement CEM I 52.5R HS/NA	kg/m³	832	
Quartz sand	kg/m³	975	
Silica fume	kg/m³	135	
Steel fibres (2.5 Vol.-%)	kg/m³	192	
Quartz flour	kg/m³	207	
Superplasticiser	kg/m³	29.4	(60% liquid; 40% solid)
Water	kg/m³	166	
Water cement ratio	[-]	0.22	

3 Experimental procedures

Since UHPC is sensitive against variation of mixing procedure, the raw materials were weighted exactly and stored sealed at 20°C for at least 48h before the mixing process started. The sequence of the mixing procedure is shown in table 2. For measuring the heat release during hydration an adiabatic calorimeter is used. The fresh concrete is placed in a 10 dm³ bucket with a temperature sensor being placed in the middle of the specimen. The calorimeter is well insulated and temperature controlled because adiabatic conditions prohibit any heat exchange between the concrete specimen and the surroundings. All generated heat due to hydration reactions of the cement and reactive additives remains within the concrete

body. High temperatures occur due to the high cement content. Although the calorimeter shown in figure 1 is cooled by oil, the tests had to be stopped before time because temperature reached more than 110°C in less than 20 hours. This was necessary to avoid damages of the cables and the fans. All in all eight tests were carried out. To determine the degree of hydration and to verify the applicability of the maturity concept four different fresh concrete temperatures were tested (10°C, 20°C, 25°C and 35°C).

Table 2: Mixing procedure

Action	**Time [sec]**
Premixing of silica fume and quartz sand	240
Addition of quartz flour and cement	120
Addition of water and superplasticiser	60
Additional mixing time	300
Interspersing steel fibres	60
Final mixing time	120
Total mixing time	900

Figure 1: Oil cooled adiabatic calorimeter

4 Results

4.1 Degree of hydration

In temperature stress analysis the degree of hydration α is usually calculated from the heat development during hydration, directly from adiabatic calorimeter tests as shown in equation (1).

$$\alpha(t) = \frac{Q_{ad}(t)}{Q_{pot}} \tag{1}$$

with: α = degree of hydration

Q_{ad} = adiabatic heat release

Q_{pot} = maximum heat release according to equation (5)

The adiabatic heat release $Q_{ad}(t)$ is directly derived from the temperature increase in the adiabatic calorimeter. The relation between temperature rise $\Delta T_{ad}(t)$ and adiabatic heat release $Q_{ad}(t)$ can be calculated with equation (2).

$$\Delta T_{ad}(t) = \frac{Q_{ad}(t)}{c_c \cdot \rho_c} \tag{2}$$

with: c_c = specific heat capacity of the concrete

ρ_c = density of the fresh concrete

The theoretical maximum heat release ΔT_{pot} depends on the cement composition and other reactive additives of the mixture and is expressed by equation (3).

$$\Delta T_{pot} = \frac{Q_{pot}}{c_c \cdot \rho_c} \tag{3}$$

So finally the degree of hydration can be given by equation (4).

$$\alpha(t) \approx \frac{\Delta T_{ad}(t)}{\Delta T_{pot}} \tag{4}$$

The maximum heat release Q_{pot} is calculated by adding up the individual heat releases of the different clinker phases Q_i. Equation (5) by Rostásy and Krauß [6] is modified in order to include silica fume.

$$Q_{pot} = C \cdot \left[(1 - m_{SL}) \cdot \sum_{i=1}^{6} m_i \cdot Q_i + m_{SL} \cdot Q_7 \right] + FA \cdot Q_8 + SF \cdot Q_9 \tag{5}$$

with: Q_1 to Q_9 = individual heat releases of the single clinker phases (free calcium oxide, free magnesium oxide, slag, fly ash and silica fume)

Table 3 shows the values of the several heat releases Q_i [6]. The individual heat release for silica fume is taken from [9]. The mass analyses of the portland cement have been done by the Verein Deutscher Zementwerke (VDZ) [10] using x-ray diffraction.

Table 3: Individual heat release in kJ/kg

Q_1	Q_2	Q_3	Q_4	Q_5	Q_6	Q_7	Q_8	Q_9
C_3S	C_2S	C_3A	C_4AF	free CaO	free MgO	SL	FA	SF
500	250	1340	420	1150	840	290	35	565

A maximum heat release Q_{pot} of 433102 kJ/m³ can be determined for the fine grain concrete M2Q by means of equation (5). The density value of the fresh concrete used here is the average value of all M2Q-mixtures. The ultimate value of the heat capacity c_c of the M2Q-mixture can be calculated with equation (6) as shown by Krauß [7].

$$c_c = \frac{1}{\rho_c} \cdot \left[C \cdot c_c + W \cdot c_w + A \cdot c_A + FA \cdot c_{FA} + SF \cdot c_{SF} \right] \tag{6}$$

The maximum heat capacity of the M2Q-mixture is 1.10 kJ/(kg · K). This value is within the range from 1.00 to 1.10 kJ/(kg · K) for concretes with quarzitic aggregates given by Rostásy and Krauß [6]. With the maximum heat release Q_{pot} and equation (7) the limiting value $\max \Delta T_{ad}$ is calculated to 158.42°K.

$$\max \Delta T_{ad} = \frac{Q_{pot}}{c_c \cdot \rho_c} \tag{7}$$

The development of the degree of hydration is estimated with equation (8).

$$\alpha(\Delta T_{ad}(t)) = \frac{\Delta T_{ad}(t)}{\max \Delta T_{ad}} \tag{8}$$

with: $\Delta T_{ad}(t)$ = time dependent adiabatic temperature rise

$\max \Delta T_{ad}$ = see equation (7)

In figure 2 the measured degree of hydration (average value of two adiabatic tests, unset concrete temperature 20°C) is compared with the Jonasson approach, shown in equation (9). The calculation result agrees with the experimental result besides the first hours of hydration (dormant phase).

$$\alpha(t_e) = \exp\left[-\alpha\left(\ln\left(1+\frac{t_e}{t_k}\right)\right)^{c_1}\right] \tag{9}$$

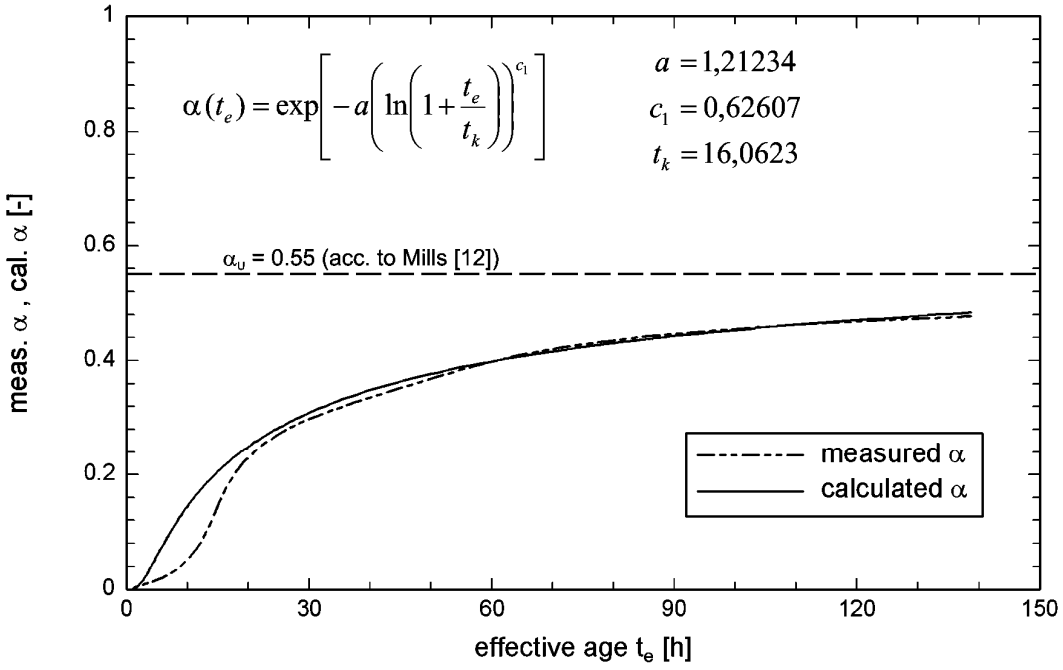

Figure 2: Measured and calculated degree of hydration α vs. effective age t_e

The effective age indicates the time span for an arbitrarily temperature history $T_j(t)$ in which the same degree of hydration is reached as for a temperature of T = 20°C = constant. This approach by Freiesleben Hansen/Pedersen [1] is expressed in equation (10) and is more specified in section 4.2.

$$\alpha_{ad}(T_{c0} + \Delta T_{ad}(t)) \equiv \alpha(20°C; t_e) \equiv \alpha(T_j(t)) \tag{10}$$

Usually models of the degree of hydration assume a complete hydration enabling a final degree of hydration of 1.0. If the water cement ratio is less than about 0.40, such as 0.22 of the tested M2Q-mixture, it can be expected that the hydration process will stop when the whole store of water is consumed. Several approaches have been developed to calculate a maximum degree of hydration α_U, taking an incomplete hydration into account [11, 12, 13]. Equation (11) developed by Mills [12] gives an example how to calculate α_U dependent on the water cement ratio. For a concrete with a water cement ratio of 0.22 the maximum degree of hydration α_U would be 0.55.

$$\alpha_U = \frac{1.031 \cdot w/c}{0.194 + w/c} \tag{11}$$

4.2 Activation energy (E_A-concept)

Concrete hardening depends on the activation energy E_A. To start the hydration the activation energy should exceed the activation barrier. The activation energy depends on the chemical composition and the particle size distribution of the binding agents. To determine the activation energy experimentally calorimetric tests with different fresh concrete temperatures (10°C, 20°C, 30°C and 35°C) were carried out. The transformation of the effective age is realized by using the maturity concept by Freiesleben Hansen/Pedersen, as shown in equation (12) [1].

$$t_{e,j} = \int_0^t \exp \frac{E_A}{R} \left[\frac{1}{293} - \frac{1}{273 + T_j(t')} \right] dt' \tag{12}$$

with: $T_j(t')$ = temperature of concrete at position j during hardening

R = gas constant, R = 8.315 [J/mol · K]

E_A = activation energy [J/mol]

E_A / R = ratio [K] (see equation (13) or (14))

Several approaches are available to determine the value of the activation energy E_A. The approach by Freiesleben Hansen/Pedersen [1] is expressed in equation (13) and (14). This approach assumes that a temperature dependency of E_A is only valid for concrete temperatures below 20°C. At higher temperatures above 20°C the value of E_A is constant.

$$\frac{E_A}{R} = 4030 = const. \qquad if\ T \geq 20°C \tag{13}$$

or rather

$$\frac{E_A}{R} = 4030 + 177 \cdot (20 - T) \qquad if\ T < 20°C \tag{14}$$

Another approach to determine the activation energy is made by Jonasson [14] (see equation (15)).

$$E_A = \Theta_{ref} \cdot \left(\frac{30}{T + 10} \right)^{\kappa} \tag{15}$$

with: Θ_{ref} = 47.39 kJ/mol

κ = 0.54

The approach of van Breugel [15] is based exclusively upon the C_3S content of the cement used (see equation (16)).

$$E_A = 30 + 0.33 \cdot m(C_3S) \tag{16}$$

Compared to the approaches of Jonasson [14] and van Breugel [15] the approach of Freiesleben Hansen/Pedersen [1] seems to be more appropriate to determine the activation energy E_A. Figure 3 shows the degree of hydration α versus the effective age t_e calculated with the model for the activation energy E_A by Freiesleben Hansen/Pedersen [1] for the four temperatures of the fresh concrete included. Ideally all values of α and t_e should be temperature independent if the approach applies. The differences between the calculation results in figure 3 can be explained with uncertainties calculating $\max \Delta T_{ad}$ (see equation (7)) and with unavoidable scattering of mixing proportions and measurement procedures.

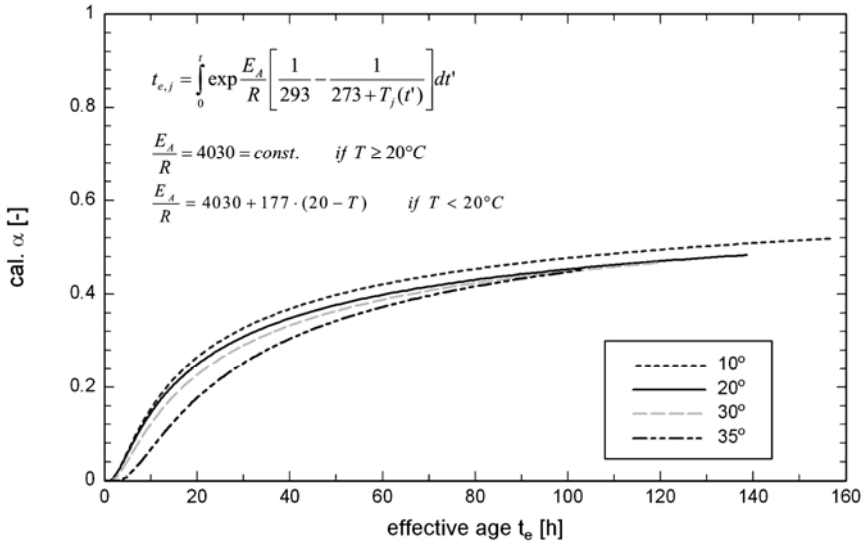

Figure 3: Calculated degree of hydration α vs. effective age t_e

5 Conclusions

The calorimetric tests carried out so far show a sufficient reproducibility. The calculation of the degree of hydration by means of the adiabatic heat release seems to be a suited

instrument for UHPC too. It should be pointed out that the water cement ratio of 0.22 of the M2Q-mixture is limiting the final degree of hydration. The end of hydration α_U can be calculated as shown in section 4.1. Another intention was to show the applicability of the maturity concept of Freiesleben Hansen/Pedersen [1] for UHPC at the example of the M2Q-mixture. It could be shown that the concept of Freiesleben Hansen/Pedersen [1] is suited to describe the activation energy dependent temperature development appropriately. This indicates that constitutive models describing the time dependent material properties of normal and high strength concrete developed at the iBMB [5, 6] can be applied also on UHPC.

6 References

[1] Freiesleben Hansen, P. and Pedersen, E. J.: Måleinstrument til kontrol af betons hærdning. Nordisk Betong 1, Stockholm, 1977.

[2] Schmidt, M. et al.: Die Gärtnerplatzbrücke in Kassel. In: Ultra High Performance Concrete (UHPC). 10 years of research and development at the University of Kassel. Structural Materials and Engineering Series No. 7, Kassel, April 2007.

[3] Deutsche Forschungsgemeinschaft [www.dfg.de]

[4] Rostásy, F. S. and Onken, P.: Konstitutives Stoffmodell für jungen Beton. DFG-Forschungsbericht (Kennwort: RO 288/25-1), May 1994.

[5] Gutsch, A.-W.: Stoffeigenschaften jungen Betons – Versuche und Modelle. Dissertation. iBMB-Schriftenreihe Heft 140, 1998.

[6] Rostásy, F. S. and Krauß, M.: Frühe Risse in massigen Betonbauteilen – Ingenieurmodelle für die Planung von Gegenmaßnahmen. Deutscher Ausschuss für Stahlbeton Heft 520, Beuth Verlag Berlin, 2001.

[7] Krauß, M.: Probabilistischer Nachweis der Wirksamkeit von Maßnahmen gegen frühe Trennrisse in massigen Betonbauteilen. Dissertation. iBMB-Schriftenreihe Heft 179, 2004.

[8] Fehling E. et al.: Entwicklung, Dauerhaftigkeit und Berechnung Ultra-Hochfester Betone (UHPC). DFG-Forschungsbericht (Kennwort: FE 497/1-1), 2005.

[9] Maruyama, I.; Suzuki, M.; Sato, R.: Prediction of Temperature in Ultra High-Strength Concrete Based on Temperature Dependent Hydration Model 1175. In: Seventh International Symposium on the Utilization of High-Strength/High-Performance Concrete, Washington D.C., USA, June 20-24, 2005.

[10] Verein Deutscher Zementwerke e.V. [www.vdz-online.de]

[11] Hansen, T.C.: Physical Composition of Hardened Portland Cement Paste. ACI-Journal, May 1970.

[12] Mills, R. H.: Factors influencing cessation of hydration in water cured cement pastes. ACI-SP60, Washington 1966.

[13] Waller, V.: Relations entre composition des bétons. Thèse de doctorat. Laboratoire Central des Ponts Chaussées (LCPC), Nantes, France, May 2000.

[14] Jonasson, J.-E.: Modelling of Temperature, Moisture and Stresses in Young Concrete. Doctoral Thesis. Luleå Universtity of Technology, Luleå, Sweden, 1994.

[15] van Breugel, K.: Heat of hydration and apparent activation energy. In: IPACS: Improved Production of Advanced Concrete Structures. Report N : 2001: 25-7. BriteEuRam Project BRPR-CT97-0437, June 1997 – May 2001.

Bernd Möser
Dr. rer. nat.
University of Weimar
Weimar, Germany

Claudia Pfeifer
Dipl.-Min.
University of Weimar
Weimar, Germany

Microstructure and Durability of Ultra-High Performance Concrete

Summary

The investigations on Ultra-High Performance Concrete (UHPC) with different High Resolution Electron Microscopy Imaging Techniques and Isothermal Heat Conduction (DCA) show a strong retardation of the hydration process caused by a high amount of superplasticizer. The C-S-H phases with a length of max. 200 nm are visible after 18 hours of hydration time. During the hardening process an extremely dense and compact UHPC microstructure is formed. For this purpose a FE-SEM with high resolution low vacuum imaging capabilities in the low voltage mode (using a helix detector) was deployed. The existing results of pre-treated UHPC (stored in water or heat treated up to 90 °C) show no significant deterioration in the microstructure and only marginal elongation after the storage in the climate chamber. In pre-damaged samples with microcracks a “secondary hydration” of unreacted clinker particles can be observed. In heat treated samples also a secondary ettringite formation can be found. Nevertheless, the elongation damage threshold value of 0.4 mm/m was not exceeded.

Keywords: *UHPC, hydration, microstructure, durability*

1 Introduction

So far only a few investigations on the hydration process, the formation of the microstructure and the durability under defined climate conditions of UHPC have been published. In this paper the hydration process and the formation of the microstructure were investigated on samples which had been stored in water or had undergone a heat treatment.

Several high resolution electron microscopy imaging techniques (ESEM-FEG and FE-SEM) were used for the imaging of the hydration process and for the characterization of the complex microstructure of UHPC. In addition DCA and quantitative X-ray phase analysis were used. These results are not presented here and can be taken from [1, 2]. Furthermore, the durability of UHPC was evaluated by means of cyclic climate storage, a procedure developed in Weimar at the Bauhaus University. This program simulates the climate conditions in Central Europe in an accelerated manner on constructions exposed to free weathering [3]. All investigations were carried out on a standardized fine grain UHPC mixture (M2Q). Furthermore, durability studies were performed on a standardized coarse grain UHPC mixture (B4Q).

2 Materials and Methods

The investigations were carried out on two UHPC reference mixtures (M2Q, B4Q) [4]. An ordinary Portland cement (OPC) CEM I 52.5 R – HS/NA and the following additives and aggregates were used: silica fume, quartz powder, quartz sand (0.125/0.5 mm), basalt (2/8 mm), and superplaticizers (SP) based on polycarboxylate ether. In order to improve the ductility of the material steel fibres (length/diameter: 9.0/0.15 mm) were used. The chemical composition and the properties of the raw materials can be taken from [1, 2].

For the investigations of the hydration process and the characterization of the very dense and complex microstructure of UHPC various **H**igh **R**esolution **S**canning **E**lectron **M**icroscopy (**HR-SEM**) imaging techniques were used such as [5, 6]:

- ESEM-FEG in a water vapour atmosphere (WET mode) – in early state of the hydration process: During the early hydration process of cementitious materials it is possible to image the microstructure in detail at high accelerating voltages and at high water vapour pressures (relative humidity near 100 %) in the sample chamber. Through crystal formation and growth during the hydration process the microstructure becomes more and more dense. In the ESEM-WET mode the high gas pressure in the sample chamber causes a significant scattering of the primary electron beam (“beam skirting“). In order to optimize the contrast conditions we have used another type of microscope - the Nova NanoSEM - for more dense and complex microstructures.
- Ultra high resolution FE-SEM (Nova NanoSEM, FEI Company): This microscope was deployed for the investigations in the low voltage mode with imaging capabilities in a water vapour pressure up to 1.3 mbar in the sample chamber. High resolution (e.g. 1.8 nm at 3 kV) without partial charge build-up can be achieved by means of a helix detector when the magnetic immersion lens technology is connected with the ESEM technology. By means of this type of microscope it becomes possible to choose excitation conditions for charging non-coated and extreme dense materials in such a way that contrast rich imaging as well as spatial resolution in the X-ray microanalysis can be optimized. This method enables us to see structures in ultra-high-resolution which are not evident using conventional SEM or ESEM.
- High resolution backscattered electron (BSE) imaging technique on highly polished microsections cut through the UHPC microstructure: The BSE image contrast is generated by the different phase compositions relative to their average atomic number and is observed by the differential brightness in the image (material contrast).

The hydration process and the development of the microstructure were studied in detail on the reference mixture M2Q. The investigations were carried out on samples stored in water (series A) and on samples which had been heat treated (series B). After the production of the concrete the samples were kept in moulds at room temperature (20°C) for 48 hours. After the de-moulding the samples of series A were stored in water until examination. Series B was heat treated in a regime of 90°C maximum temperature for 48 hours analogous to the heat treatment regime of [4] and afterwards stored under standard conditions (20°C, 65% RH).

Investigations on the durability were carried out in a climate simulation chamber (Feutron Klimasimulation GmbH, Greiz). The cyclic climate storage had been developed in Weimar.

This program can simulate weather conditions in Central Europe (such as: drying, moisturing, freezing and thawing). The cycle scheme for the climate simulation chamber is described in [1, 3, 9]. It is especially tailored for problems relating to alkali silica reaction (ASR) [3, 7]. The cement and silica fume (SF) content in UHPC mixtures is generally high. For this reason it is necessary to estimate the durability of UHPC regarding ASR. A homogenous dispersion of silica fume is an essential prerequisite to prevent ASR. In these investigations the silica fume is added as dry component, usually slurry is used, but this would exceed the required water to cement ratio. At an age of 8 days the samples were undergone the cyclic climate storage. The pre-treatment of the samples was similar to the investigations by means of electron microscopy. After the twelfth day a pre-damage due to mechanical stresses was carried out to increase the permeability of the concrete and to accelerate possible damaging potentials [8]. The pre-damage was reviewed with resonance frequency measurements. One cycle of the cyclic chamber storage lasts 21 days and simulated drying at 60°C and <10 % relative humidity [RH] (4 days), moisturizing at 45°C and 100 % RH (14 days) and freeze - thaw – alteration between +20°C and -20°C according the CDF-Test (3 days). An evaluation of the expansion by cyclic chamber storage is usually carried out after 6 – 8 cycles (Fig. 9) [3, 7, 9].

3 Results and Discussion

3.1 Hydration process and microstructure of UHPC

The aspect of extremely dense microstructures is particularly important during the investigation of UHPC by means of electron microscopy. The UHPC mixtures were optimized as to their grading. They have - when used with superplaticizers - a very low water to cement ratio (approx. 0.22). Because of the spatial limitation caused by the dense mixture it comes to an extreme obstruction of growth of the hydration products being formed. The image sequence (Fig. 1–4) shows the hydration process and the development of the UHPC microstructure under usage of ESEM in WET mode. The sequence was taken on pasty samples in the early hydration state (scratched by the micromanipulator in the sample chamber). Then, with the hydration proceeding, fresh fracture patterns were imaged. Up to a hydration time of eight hours and beyond, the microstructure of the UHPC reference mixture is dominated by spherical silica fume particles (Fig. 1). Between the silica fume spheres isolated ettringite crystals with a short prismatic habit (length up to 400 nm) are visible. The hydration of the clinker phase alite is retarded up to this point in time by the superplaticizer used, so that no C-S-H phases are observed. With the hydration process proceeding, after a time of 18 hours, C-S-H phases having a length of up to 200 nm are visible (see Fig. 2). After further six hours hydration time (1 day) a clear densification of the microstructure can be observed caused mainly by the growth and new formation of C-S-H phases. At individual points the alite phase of the clinker grains having a size of up to 1 µm has been dissolved completely and cavities (hollow shell grains) have been formed in the microstructure (Fig. 3, see arrows). The microstructure densification continues to progress, this becomes evident e.g. on the basis of Fig. 4 after a hydration time of six days at a fresh fracture surface (the crack runs through the quartz grain as well as the UHPC matrix). It is clearly visible that at an accelerating voltage -

necessary in the ESEM WET-mode - certain structure components (mainly C-S-H phases, SF and ettringite) cannot be imaged clearly although the resolution is high.

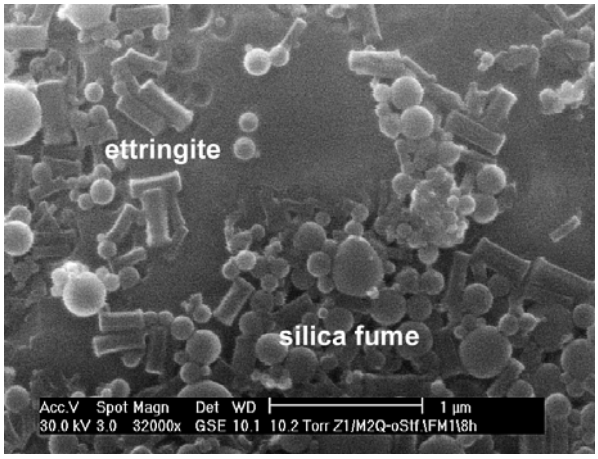

Figure 1: Hydration time 8 h: spherical silica fume particles and short prismatic (length up to 400 nm) ettringite crystals

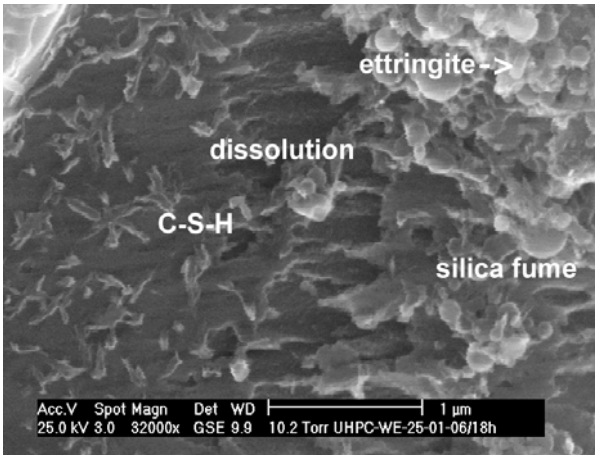

Figure 2: Hydration time 18 h: needle-like C-S-H phases (length up to 200 nm) and cavities on the surface of an alite grain

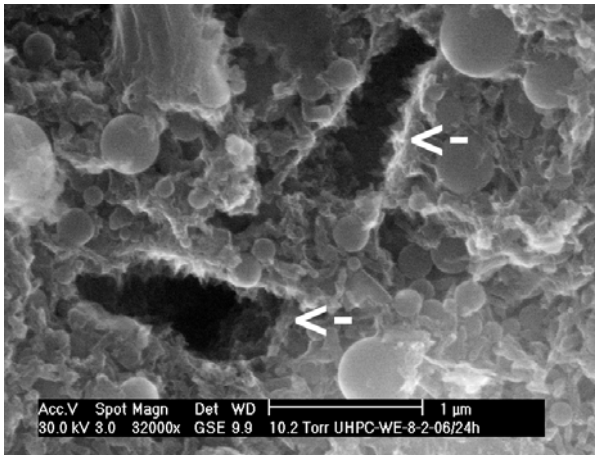

Figure 3: Hydration time 24 h: densification of the UHPC matrix, some of the clinker grains completely dissolved (see arrows)

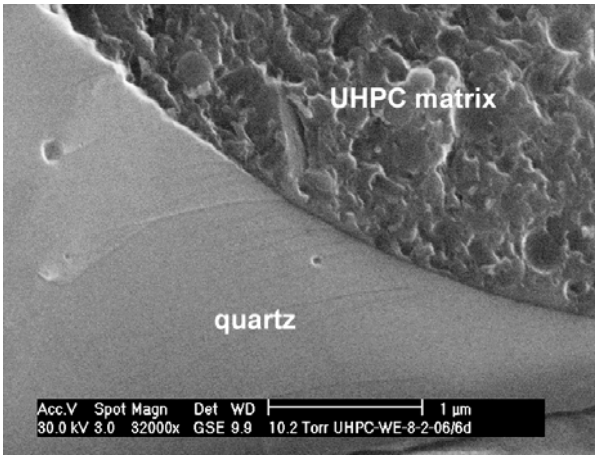

Figure 4: Hydration time 6 d: fractured surface: the crack runs through the quartz grain as well as the UHPC matrix

Only by optimizing the contrast by means of Nova NanoSEM at low accelerating voltages in a low water vapour atmosphere it becomes possible to image such extremely dense microstructures in detail at high resolution and without charge build-up artifacts. The microstructures of UHPC imaged by means of this type of microscope (with helix detector) can be looked at in Fig. 5 and 6. The several hydration and reaction products in the microstructure can now clearly be imaged at a high resolution. A further option to characterize ultra dense microstructures is the FE-SEM analysis using backscattered electron imaging in combination with X-ray microanalysis. Modern detectors permit a high-resolution BSE-imaging at polished specimens using accelerating voltages between 4 and 10 kV. The most important contrast mechanism of BSE is the dependence of the backscattering coefficient on the mean atomic

number (Z) which allows phases with differences in Z to be recognized (material contrast). Due to the comparatively small mean atomic number of the silica fume (spherical particles of glass) Z = 10.8 it can be imaged clearly in the UHPC matrix.

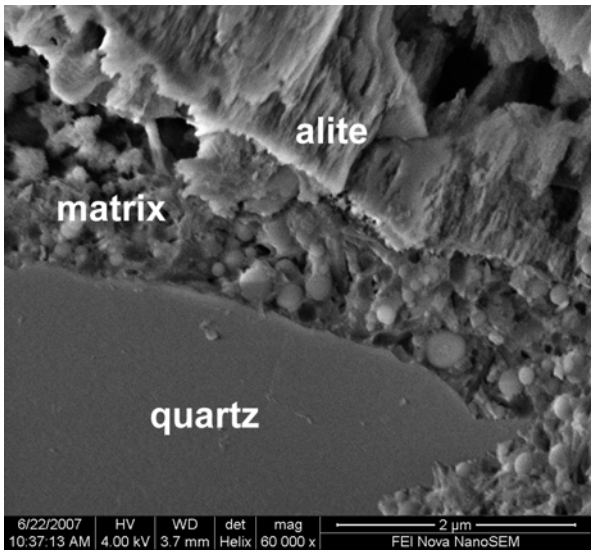

Figure 5: 2d hydration time: by optimizing the contrast even very dense microstructures can be imaged in detail

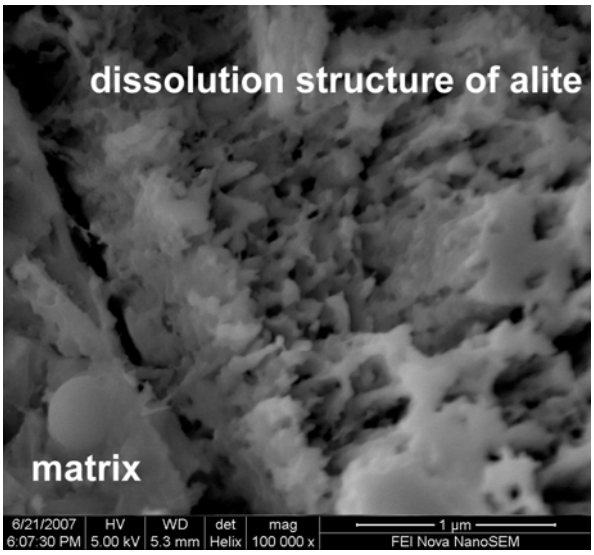

Figure 6: 8 d hydration time: interface area of the partially dissolved alite clinker grain and the dense matrix

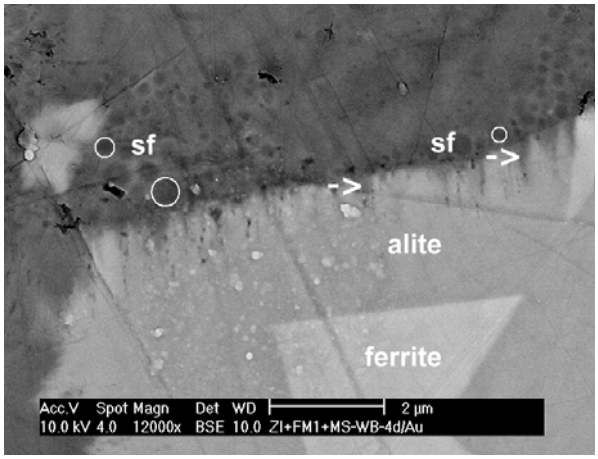

Figure 7: Heat treated sample after 4 d hydration time: marginal heterogeneous dissolution of alite (see arrows); sf – silica fume – dark spherical particles (see white circles)

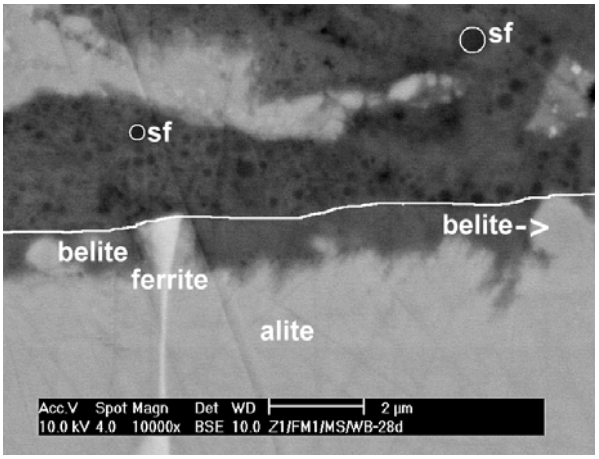

Figure 8: Heat treated sample after 28d hydration time: phases of a clinker grain with different reactivity – with line marked the former grain size

After a hydration time of 4 days (heat treated sample) the clinker grain shows only a marginal, heterogeneous dissolution structure of the alite phase (Fig. 7). On the other hand after a hydration time of 28 d (see Fig. 8) the clinker grain shows a strongly dissolved area of the alite phase (reaction zone approx. 1 µm). In contrast the weaker reactive clinker phases ferrite and belite appear in their original habit. So one can see the former clinker grain

surface (white line in Fig. 8) which is also decorated by the dark spherical silica fume particles in the matrix.

3.2 Durability

In the following paragraph the UHPC reference mixtures M2Q-SP1 and B4Q-SP2 are evaluated as to their durability. After every climate cycle the expansion was measured. At the beginning of these measurements a tempering of the concrete samples to 20°C is necessary to eliminate a temperature influence. An uncritical threshold of expansion was determined at 0.4 mm/m. After the drying period of the climate cycle the mass and the dynamic elastic modulus were routinely measured [3, 7]. Every second cycle the microstructure is studied with ESEM and SEM to investigate changes in the microstructure. In Fig. 9 the expansion of the reference mixture M2Q-SP1 is shown.

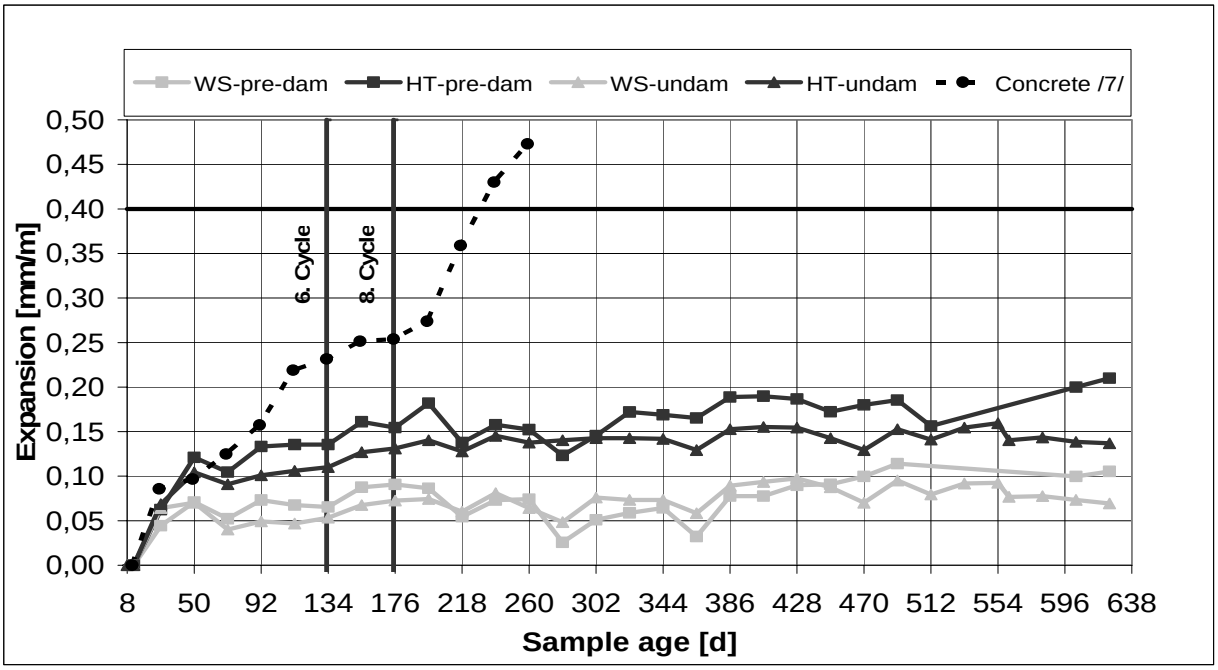

Figure 9: Expansion measurements of reference mixture M2Q-SP1 (water storage with pre-damage [WS-pre-dam], heat treatment with pre-damage [HT-pre-dam], water storage undamaged [WS-undam], heat treatment undamaged [HT-undam])

It is obvious that the expansion of the UHPC reference mixture is below the threshold of 0.4 mm/m regardless of water storage, heat treatment or pre-damaging. During the first two cycles of cyclic climate storage a minor increase in the expansion caused by a hygric expansion can be observed. For comparison purposes a normal concrete (CEM I 32,5R, greywacke, quartz sand) with a w/c-ratio of 0.45 has been integrated in Fig. 9. You can see a continuous increase of expansion. After 10 cycles of storage the threshold is trespassed. The expansion progression of the heat treated reference mixture M2Q-SP1 shows the double amount of expansion compared to water storage. A value of 0.2 mm/m is not exceeded. Only a minor difference can be observed between the undamaged and pre-damaged series. So

far after 29 cycles (603 days) no increase in expansion could be measured. For a final assessment of the samples with a highly impermeable microstructure the usual evaluation period of 6-8 cycles has to be exceeded. The measurement period has to be expanded to 24 months (after manufacturing). The durability investigations in cyclic climate storage were also carried out with a coarse grain reference mixture (B4Q-SP2: Figure is not displayed). The water stored, pre-damaged samples show an expansion value of max. 0.2 mm/m. The undamaged samples show an expansion value between 0 - 0.07 mm/m compared to the pre-damaged samples. By means of electron microscopy investigations it was found that in pre-damaged samples a 'second hydration' takes place namely in the crack areas (Fig. 10). After the 4th cycle of cyclic climate storage it can be observed that in heat treated and pre-damaged samples a delayed ettringite formation (Fig. 10) occurs in cracks having a width smaller than 10 µm. Cracks which exceeded a crack width of 10 µm show a strong carbonation effect. Furthermore, it was found that cracks near the surface were filled with calcium carbonate. Through insufficient dispersion of silica fume isolated silica fume aggregates are present in the UHPC microstructure. An ASR (Fig. 11) can take place irrespective of the storage conditions like heat treatment, water storage or cyclic climate storage. Although a cement with a low alkali content was used an ASR could not be avoided.

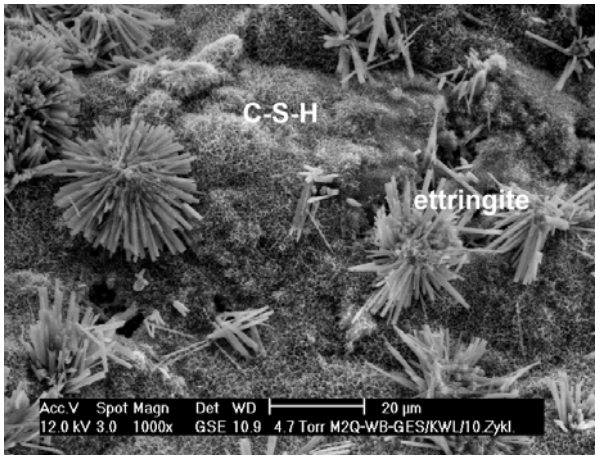

Figure 10: UHPC – reference mixture M2Q-SP1 after 10th cycle in cyclic climate storage (218 days), delayed ettringite formation and C-S-H phases (crack width ≤ 10 µm)

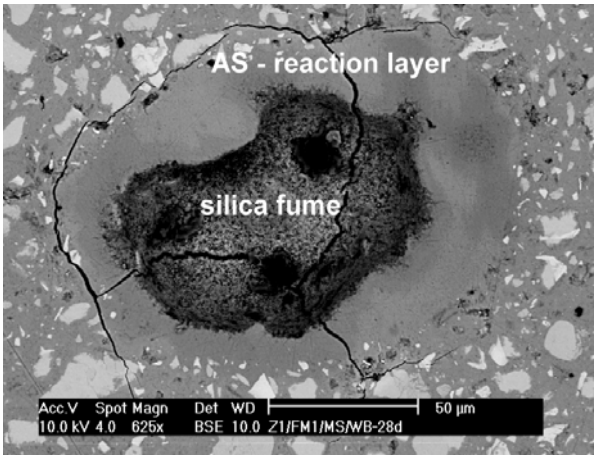

Figure 11: Cement + silica fume + SP1 after heat treatment and a hydration time of 28 days, silica fume accumulation and development of cracks caused by ASR

4 Conclusions

Different HR-SEM imaging techniques are necessary for the characterization of the hydration process and the development of the microstructure of UHPC: ESEM in WET mode for the early hydration process, NanoSEM for the examination of the extremely dense microstructures of hardened samples and BSE imaging analysis for polished microsections. A strong retardation of the hydration process caused by a high amount of superplasticizer can be observed. Furthermore, the growth of ettringite is influenced. The length of the ettringite crystals is smaller than 600 nm whereas under "normal" cement hydration conditions a length of up to 3 µm is visible. Clinker grains smaller than 2 µm had often been completely dissolved, re-

sulting in hollow shell grains in the UHPC microstructure. The bonding between the aggregates and the UHPC matrix is very strong. The interfacial region shows no gaps between these components. Individual silica fume aggregates up to a diameter of 250 µm are visible in the UHPC microstructure irrespective of the storage conditions of the samples. Locally concentrated a starting ASR can be observed but the typical crack formation occurs isolated around the silica fume aggregates. No damages due to ASR occur. Investigations on the durability in a climate simulation chamber show that the expansion of the UHPC reference mixtures is below the threshold value of 0.4 mm/m regardless of water storage, heat treatment or pre-damaging. In heat treated and pre-damaged samples a delayed ettringite formation in microcracks with a crack width smaller than 10 µm can be observed whereas in wider cracks a strong carbonation occurs. Nevertheless the expansion threshold value is not trespassed.

5 Acknowledgements

The authors would like to thank the German Research Foundation (DFG) for the funding within the framework of the priority program SPP1182.

6 References

[1] Möser, B.; Pfeifer, C.: Gefügestruktur und Dauerhaftigkeit von Ultrahochfestem Beton. In: Tagungsband 6. Baustoffkolloquium, Freiberg, Deutschland, 07-08.Februar 2007, S. 7-16

[2] Pfeifer, C.; Möser, B.; Stark, J.: Hydratation und Gefügeentwicklung von Ultrahochfestem Beton. In: Jahrestagung der Fachgruppe Bauchemie, Siegen, Deutschland, 27-28.September 2007, GDCh-Monographie Band 37, S. 47-54

[3] Seyfarth, K.; Stark, J.: Performance Testing Method for Durability of Concrete using Climate Simulation. In: Proceedings of the 7th CANMET/ACI International Conference on Durability of Concrete, Montreal, Canada, May 28 – June 3, 2006, Ed. By V.M. Malhotra, American Concrete Institute SP-234, Farmington Hills, Michigan, S. 305 – 326

[4] Fehling, E.; Schmidt, M.; Teichmann, T.; Bunje, K.; Middendorf, B.: Entwicklung, Dauerhaftigkeit und Berechnung Ultra-Hochfester Betone (UHPC). In: Forschungsbericht DFG FE 497/1-1, Schriftenreihe Baustoffe und Massivbau, Heft 1, Universität Kassel 2005

[5] Möser, B.; Stark, J.: High Resolution Imaging of WET Building Material Samles in their Natural State using Enviromental Scanning Electron Microscope. In: 11th International Congress on the Chemistry of Cement Durban, South Africa, 11-16. May 2003, CD-ROM

[6] Möser, B.; Stark, J.: Nanoscale Characterization of Hydration Processes by means of High Resolution Scanning Electron Microscopy Imaging Technique. In: 12th International Congress on the Chemistry of Cement Montreal, Canada, 8-13 July 2007, CD-ROM

[7] Giebson, C; Stark, J.: Assessing the Durability of Concrete Regarding ASR. In: Proceedings of the 7th CANMET/ACI International Conference on Durability of Concrete, Montreal, Canada, May 28 – June 3, 2006, Ed. by V.M. Malhotra, American Concrete Institute SP-234, Farmington Hills, Michigan, S. 225 – 238

[8] Meyer; T.: Auswirkungen von gezielt erzeugten Schädigungen auf die Dauerhaftigkeit von Hochleistungsbetonen, Diplomarbeit, Bauhaus – Universität Weimar, 2003

[9] Stark, J.; Freyburg, E.; Seyfarth, K.; Giebson, C.: AKR – Prüfverfahren zur Beurteilung von Gesteinskörnungen und projektspezifischen Betonen. In: Beton, 12, S. 574 – 581, 2006

Lukasz Dudziak
PhD student
TU Dresden
Dresden, Germany

Viktor Mechtcherine
Prof. Dr.-Ing.
TU Dresden
Dresden, Germany

Mitigation of volume changes of Ultra-High Performance Concrete (UHPC) by using Super Absorbent Polymers

Summary

Autogenous shrinkage is one of the major sources of volume changes in Ultra-High Performance Concrete (UHPC), which leads to the development of eigenstresses as well as stresses due to external restraints, and finally to concrete cracking. The internal curing of concrete using small, well distributed water reservoirs seems to be able to solve this problem. In this research project, the effects of the internal curing by using Super Absorbent Polymers (SAP) on autogenous shrinkage and other properties of a self-compacting UHPC were investigated. The results of the investigation display that the autogenous shrinkage after concrete setting was strongly reduced by the internal curing, while rheological properties of fresh concrete and the strength of hardened concrete did not change negatively upon adding SAP if the right amount of extra water was added for the purpose of internal curing.

Keywords: *UHPC, autogenous shrinkage, internal curing, Super Absorbent Polymers (SAP)*

1 Introduction

High Strength/High Performance Concrete (HSC/HPC) and Ultra-High Performance Concrete (UHPC) have become objects of intensive research due to their advantages: high compressive strength to density ratio, high durability, favourable workability etc., which justifies the use of the term “high performance” materials.

However, the low water to cement ratios (below 0.4), which are necessary for the enhancement of strength and durability, lead to a so-called self-desiccation of concrete as a result of the cement hydration process [1]. This causes considerable volume changes known as autogenous shrinkage, which in turn lead to the development of eigenstresses as well as stresses due to external restraints, and finally to concrete cracking. Mitigation of autogenous shrinkage using external curing is not effective due to the fact that very dense microstructure of HPC or UHPC enables only very slow water ingress into interior of concrete members.

In this research project, the effectiveness of the internal curing was investigated for UHPC, while Super Absorbent Polymers (SAP) were used as materials, which first absorb water in the fresh mix and subsequently release it when the relative humidity in the pore system decreases due to the hydration process. The particular UHPC under investigation was developed for a pavilion built in conjunction with the FIFA World Cup 2006 in Germany and situated in Kaiserslautern, one of the host cities. The pavilion was designed as a filigree, thin-

walled structure with very slender columns (minimum wall thickness of 20 mm), and without conventional reinforcement, cf. Figure 1 (structural design: Prof. Schnell, TU Kaiserslautern). Besides the requirement for reduced autogenous shrinkage, a number of specific requirements were defined with regard to concrete to be developed due to particularities of the design and production process: high durability, enhanced ductility, self-compaction as well as “perfect” surface appearance with an appealing anthracite colour. This paper reports the effects of the SAP addition on autogenous shrinkage of UHPC as well as on other properties of fresh and hardened concrete.

Figure 1: Pavilion made of UHPC with internal curing by using SAP

2 Concrete composition

A number of different compositions was developed and tested in the process of the mixture development and optimisation. Detailed information on the material design is published elsewhere [2]. Table 1 gives four of the tested UHPC compositions, which particularly met the requirements with regard to the strength and workability of concrete. The so-called reference mixtures without (Ref) and with (Ref-SAP) addition of SAP were produced without pigment, while ELBA one-wave laboratory 60 l mixer was used. In order to supply additional water for internal curing, the total amount of mixing water was increased in the mixture Ref-SAP so that an amount of entrained water was equal to the water to cement ratio increase by 0.05 compared to the reference mixture without SAP. The mixture Pav-SAP is the composition which was used for the construction of the pavilion. In comparison to the Ref-SAP, changes involved a slight decrease of water to cement ratio (including extra water), addition of the pigment and utilization of a high intensity mixer of the Eirich company. The

mixture Pav differs from Pav-SAP only by the absence of SAP and a lower addition of water which would correspond to a reduction of the total water to cement ratio by 0.03.

Table 1: Compositions of UHPC under investigation with and without addition of SAP

Components		**Ref**	**Ref-SAP**	**Pav**	**Pav-SAP**
Cement CEM I 42.5 R HS	kg/m³	800	800	800	800
Silica fume	kg/m³	120	120	120	120
Water (total)	kg/m³	171	211	179	203
SAP	% m.c.	-	0.4	-	0.4
W/c total $((w/c)_{effective} + (w/c)_{internal\ curing})$	kg/m³	0.24	0.29 (0.24+0.05)	0.25	0.28 (0.25+0.03)
Quartz powder	kg/m³	211	190	206	195
Fine sand 0.125/0.5 mm	kg/m³	234	211	229	217
Crashed basalt sand 0/2 mm	kg/m³	188	169	184	173
Basalt split 2/5 mm	kg/m³	533	481	522	493
Steel fibre 6x0.015 mm	kg/m³	144	144	144	144
Superplasticizer	% m.c.	4.3	4.3	4.3	4.3
Pigment Fe_2O_3	kg/m³	-	-	12	12

In both mixtures with SAP addition (Ref-SAP and Pav-SAP), the amount of SAP was 0.4 mass% of cement. Covalently cross linked acrylamide/acrylic acid copolymers were used as SAP. It consisted of suspension polymerised, spherical particles with an averaged particles size of approx. 200 µm, cf. Figure 2.

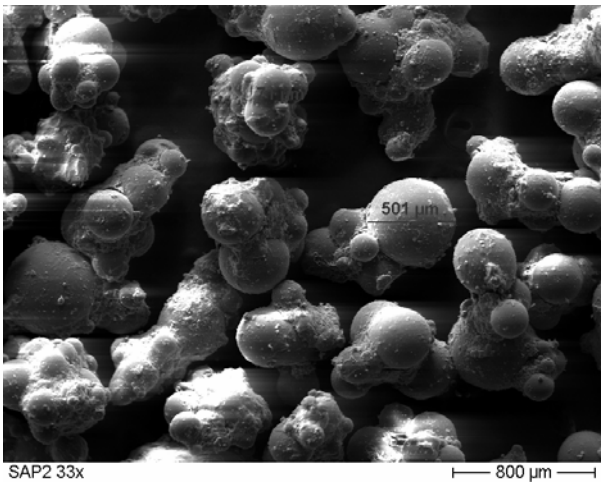

Figure 2: Dry SAP particles

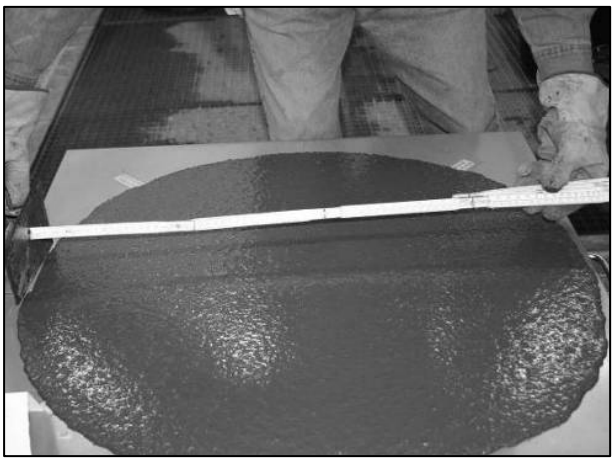

Figure 3: Slump Flow test on fresh UHPC

3 Properties of fresh concrete

Fresh concrete was subjected to the slump flow tests (Figure 3) using standard slump cones for concretes (height of 300 mm) and mortars (height of 60 mm). Additionally, V-funnel tests were performed. The measured averaged values of the slump flow diameter relate to the yield stress of concrete, while the V-funnel flow time relates to the apparent viscosity of mixtures. Table 2 gives the results obtained from these tests.

Table 2: Results of rheological measurements

Mixture	w/c (total) [-]	SAP [% m.c.]	Slump flow [mm]		V-funnel flow time [s]
			Small	Large	
Ref	0.24	0	240	675	44
Ref-SAP	0.29	0.4	265	765	14
Pav	0.25	0	270	770	5
Pav-SAP	0.28	0.4	270	780	13

With regard to the obtained slump flow values, all presented mixtures can be considered as self-compacting. However, it is obvious, that the difference in the water addition (corresponding w/c = 0.05) in the reference mixtures Ref and Ref-SAP was too high. Not all extra water in the mixture Ref-SAP was absorbed by SAP, which lead to an increase in the slump flow and a considerable decrease in the V-funnel flow time.

In the mixture Pav-SAP the amount of extra water corresponded to an increase of water to cement ratio by 0.03 in comparison to the mixture Pav (no SAP addition). As a result, identical slump flow values were measured for both mixtures. However, slight difference could be observed with regard to the V-funnel flow time: the mixture with SAP showed a higher viscosity.

From the experience collected until now, it can be pointed out that the measurement of rheological behaviour can serve as a reliable indicator of the water demand of SAP in the fresh mixture and correspondingly of the approximate amount of water available for internal curing. The investigations on this issue continue using a universal rheometer.

4 Water entrained pores in hardened concrete

Different methods were used in order to investigate the shape, sizes and spatial distribution of pores entrained by means of SAP. Micro-computer tomography images of hardened UHPC showed that such pores were regularly distributed over the concrete volume (cf. Figure 4) which is an important prerequisite with regard to the efficiency of internal curing. Figure 5 gives an SEM image of an entrained water pore: it corresponds to the spherical shape of dry SAP particle (cf. Figure 2), just like before their addition to the mixture. Due to the absorption of water, the pores are considerably bigger then the SAP particles. The investigations on the entire pore content, number of pores and pore size distribution continue.

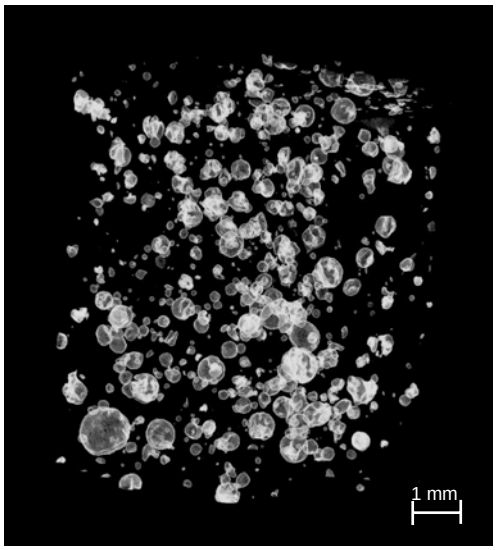

Figure 4: Micro-computer tomography image of pores entrained by using SAP

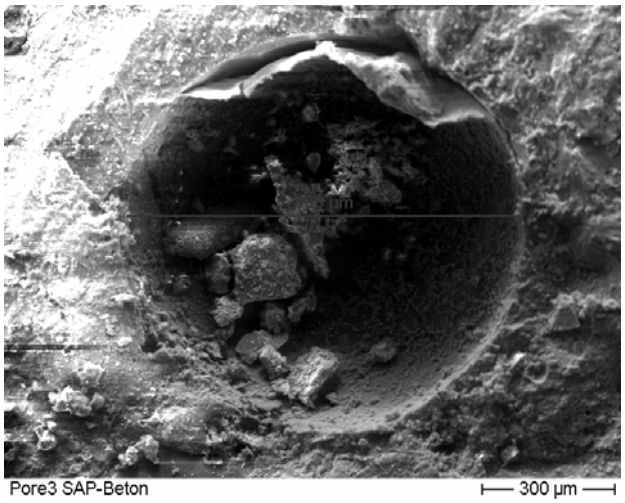

Figure 5: Entrained pore in hardened UHPC

5 Autogenous shrinkage

The measurements of autogenous shrinkage were carried out using corrugated tubes according to the method developed by Ole M. Jensen [3]. This method allows a continuous measurement of the deformation of concrete starting immediately after filling the tubes.

In order to enable the evaluation of the results with regard to the stress-inducing parts of these deformations, the setting behaviour of concrete was recorded as well. For this purpose testing procedure acc. to DIN 480-2 was used, which implies the measurement of the change in a pin penetration in mortar over time. The time of final set was chosen as ‘time zero’ as the time of the fluid-solid transition, when self-supporting skeleton is formed and the subsequent autogenous deformations lead in the hardening concrete, if hindered, to development of tensile stresses in concrete and eventually to cracking.

Figure 6 shows representative autogenous strain-time curves obtained for the first 28 days after the end of concrete setting for the compositions with and without SAP. The curves were derived from the bulk strain data by subtracting the strain value at the end of setting, so that only potential stress inducing strains were considered. The mixtures with addition of SAP (Ref-SAP and Pav-SAP) showed a dramatic decrease of the autogenous shrinkage in comparison with the corresponding mixtures without SAP (Ref and Pav). For example, at the concrete age of 3 days the autogenous shrinkage of the reference concrete Ref-SAP was in average about 50 µm/m, while the corresponding values for the reference concrete without SAP were above 400 µm/m.. Further data on autogenous shrinkage of different UHPC compositions may be found in [2].

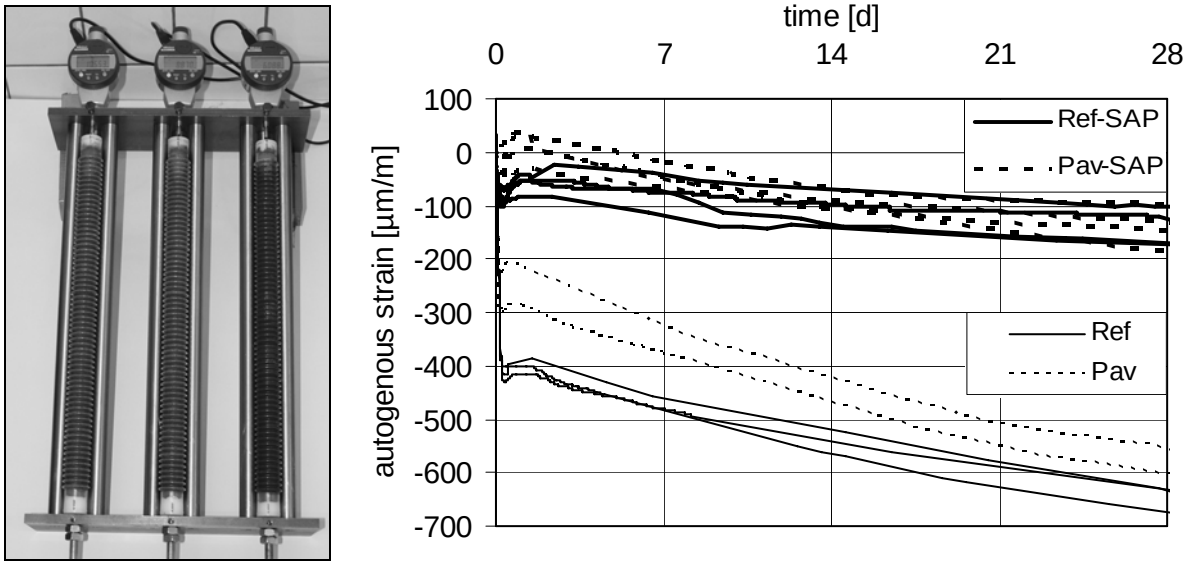

Figure 6: a) Dilatometer for autogenous shrinkage measurements; b) Development of the autogenous shrinkage of UHPC with and without internal curing versus time

6 Mechanical properties

The compression strength was measured on cubes with a side length of 150 mm as well as on the halves of small beams (cross-section equal to 40 mm by 40 mm, these specimens will be referred further as “prisms”), which were obtained from the previously performed bend tests according to EN 196-1. Two different curing conditions were applied for the specimens: storing unsealed in the standard laboratory climate and tested at the age of 28 days, and alternatively, storing sealed at a temperature of 20°C.

Table 3 gives the average values obtained from the tests as well as the corresponding standard deviations. The higher values obtained from the experiments on small prisms are commonly observed in comparison to the tests on larger cubes. This phenomenon can be traced back to the size effects and to some particularities of the test set-up.

The measurement on both reference mixtures Ref and Ref-SAP were performed on the specimens stored in the standard laboratory climate right after demoulding. In this series a slight but clear decrease of the compressive and flexural strength could be observed. This could be expected, since, as shown in the Section 3 of this paper, the addition of curing water was too high and correspondingly the effective water to cement ratio of the mixture Ref-SAP was likely higher than that of the mixture Ref.

The interpretation of the results from the test on the concretes Pav and Pav-SAP can not be that straightforward. The compression tests on cubes provided equal values for both mixtures in the case of the storing in the standard laboratory climate (unsealed). However, the compressive strength measured on sealed cubes was lower in the case of the mixture with SAP. The compressive strength from the tests on prisms at the concrete age of 28 days showed, on the contrary, equal values for both mixtures in the case of the sealed specimens, but lower values for the mixture with SAP in the case of the unsealed ones. In the bend tests on sealed specimens made of the mixture with SAP, higher flexural strength was measured

in comparison to the mixture without SAP, while for the unsealed specimens the flexural strength was higher in the case of the mixture without the SAP addition.

Table 3: Mechanical properties of investigated concretes (average values), Standard deviations are given in parentheses.

Mixture	Compressive strength [MPa]						Flexural strength [MPa]		
	Cubes			Prisms			Prisms		
	Unsealed	Sealed		Unsealed	Sealed		Unsealed	Sealed	
	28d	2d	28d	28d	2d	28d	28d	2d	28d
Ref	132 (4)	-	-	172 (3)	-	-	16.4 (0.4)	-	-
Ref-SAP	129 (4)	-	-	150 (1)	-	-	12.3 (0.8)	-	-
Pav	140 (3)	96 (-)	139 (-)	163 (6)	112 (3)	166 (2)	20.9 (2.4)	13.0 (0.6)	15.3 (1.1)
Pav-SAP	140 (6)	85 (-)	131 (-)	150 (6)	107 (2)	166 (4)	16.1 (-)	14.8 (-)	19.1 (1.2)

(-) only two specimens were tested

A number of possible mechanisms influencing the compressive and flexural strength, partly in different or even opposite ways, could be responsible for the findings. For sure the water content and moisture distribution is one of them, a very evident one. Higher water content causes generally lower strength value, so do the pronounced moisture gradients over the cross-section of the specimens (leading to eigenstresses). The geometry of the specimens and the mode of loading are decisive with regard to the effect of these factors on the strength values. Information on the moisture content and distribution in the specimens should be collected for a more precise interpretation.

Also other particular mechanisms leading to the observed effects on the mechanical properties of UHPC must still be investigated in more detail. Generally, on the one hand, a reduction of strength of the concrete matrix can be expected for the mixtures with SAP and extra water as a result of the formation of entrained pores (cf. Figure 4), which are initially filled with water. Such voids affect the strength negatively. On the other hand – due to internal water supply – the hydration process continues and the microstructure of the matrix becomes denser, which is positive with regard to the strength development. Finally, due to the reduction of the autogenous shrinkage of the cement paste, the internal stresses resulting from the hindrance of shrinkage deformations by stiff aggregates are more developed in the specimens with SAP. However, there is no quantitative information on these effects.

Comparing the tests results obtained for the concrete age of 2 days and 28 days it can be stated that the increase in strength of the mixture with SAP is more pronounced. This can be probably traced back to the more intensive continuation of the hydration process for the concrete with internal curing.

7 Conclusions and final comments

From the performed experiments on the effect of internal curing using SAP on the material behaviour of the developed UHPC, the following conclusions can be drawn:

- The addition of SAP has no negative effect on the workability of concrete if extra water for internal curing is used.
- The applied SAP material displayed a sufficient robustness in the highly alkaline concrete environment as well as in the case of a relatively high mechanical loading during mixing process in a high intensity mixer.
- The internal curing using SAP practically eliminated autogenous shrinkage of the investigated UHPC for the first week after setting. With increasing age, i.e. with continuing hydration process, water “reservoirs” gradually expired and as a result, the autogenous shrinkage increased, however, still remaining small. In contrast, a very pronounced autogenous shrinkage was observed for the UHPC mixtures without SAP.
- There are no pronounced negative effects on the compressive strength and the flexural strength of UHPC upon adding SAP if a right amount of extra water is added for the purpose of internal curing.

Based on these results, worldwide first known practical application of internal curing, a filigree pavilion in Kaiserslautern (Germany), was successfully built.

However, further intensive research is needed for a better understanding of the kinetics of water absorption by SAP in fresh concrete and the subsequent water release in the hardening concrete. With this knowledge the efficiency of internal curing using SAP could be further improved. This is the goal of an ongoing research program by the authors. The program deals with HPC and UHPC and includes the investigation of the effects of the type of SAP, particle size, absorption capacity of ionic solutions, quantity of the added SAP and other parameters.

8 References

[1] Jensen, O. M., Hansen, P. F.: Water-entrained cement-based materials – I. Principles and theoretical background. Cement and Concrete Research 31, No. 5, S. 647-654, 2001.

[2] Mechtcherine, V., Dudziak, L., Schulze, J., Staehr, H.: Internal curing by Super Absorbent Polymers – Effects of material properties of self-compacting fibre-reinforced high performance concrete. International RILEM Conference on Volume Changes of Hardening Concrete: Testing and Mitigation, O. M. Jensen et al. (eds.), RILEM Proceedings PRO 52, RILEM Publications S.A.R.L., S. 87-96, 2006.

[3] Jensen, O.M., Hansen, P.F.: Water- entrained cement-based materials – II. Experimental observations. Cement and Concrete Research 32, No. 6, S. 973-978, 2002.

Sören Eppers
Dipl.-Ing.
German Cement Works Association
Düsseldorf, Germany

Christoph Müller
Dr.-Ing.
German Cement Works Association
Düsseldorf, Germany

Autogenous Shrinkage Strain of Ultra-High-Performance Concrete (UHPC)

Summary

Very low water/cement-ratios are accompanied by high autogenous shrinkage in the early stage of hydration and strength development, potentially leading to cracks. Results of autogenous shrinkage strain of UHPC reported to date show a huge variation mainly attributable to different measurement methods and experimental setups. The values presented herein were obtained from small prisms with a mechanically coupled sensor. The initial set was taken as time-zero. The influence of cement, water/cement-ratio, content of silica fume, superplasticizer and steel fibres was focused upon. The autogenous shrinkage strain at the age of 28 days was between approx. 0.6 and 0.9 mm/m. The shrinkage rate was particularly high within the first day.

Keywords: *ultra-high-performance concrete, autogenous shrinkage*

1 Introduction

The volume of concrete diminishes as pore water is either incorporated into hydration products or evaporates to the ambient air. The volume change due to hydration of cement is called chemical shrinkage, while evaporation of water causes the known drying shrinkage. Part of the chemical shrinkage is the autogenous shrinkage. This term is widely accepted for the macroscopic volume reduction of a hardening concrete specimen which is not subjected to evaporation. Autogenous shrinkage is commonly attributed to the internal desiccation.

The autogenous shrinkage can be measured either linearly or volumetrically and vertically or horizontally [1]; values usually are given in linear strain. The autogenous shrinkage strain is considerably influenced by the way it is measured. Its rate usually reaches a maximum within the first 24 hours and decreases significantly afterwards. The concrete age, at which the measurement starts, is fundamental for the outcome of the measurement. The age, at which concrete has formed a self-supportive skeleton, sufficiently solid to transfer relevant tensile stresses, is called “time-zero” [2]. When the risk of early-age cracking is to be evaluated, it is essential to start the measurement of the autogenous shrinkage by time-zero. Time-zero needs to be determined individually for every concrete composition based on an experimental convention, for example the initial setting [3]. Like hydration, time-zero under field conditions is affected by the course of temperature.

2 Current State of Knowledge

The basic mechanisms underlying the autogenous shrinkage are known. It generally increases with decreasing water/cement-ratio. The usage of silica fume reportedly increases the autogenous shrinkage. While these correlations have been examined extensively for high-performance concrete, only few parameter studies have been undertaken for UHPC.

In [4] the linear horizontal autogenous shrinkage of UHPC (f_{c28}=156 MPa, CEM I 42,5 R, w/c=0.268, s/c=0.2, max. grain size: 0.8 mm) amounted to about 0.4 mm/m from the moment of maximum temperature (32.8 °C at the age of 45.5 hours) inside the concrete specimen (150 x 150 x 700 mm³) to the age of 28 days, taken with two mechanically coupled sensors. The thermal dilation was subtracted from the total deformation based on the approximation of a constant coefficient of thermal expansion, which was quantified at the age of 14 days (12.6 µm/m/K).

A similar method was used in [5] for UHPC (f_{c28}=155 MPa, CEM I 52,5 R, w/c=0.20, s/c=0.325). The coefficient of thermal expansion (22 µm/m/K after 3 days) was calculated from the deformations of normal (20 °C) and heat (42 °C) cured samples. The time-zero was chosen at the equivalent age of 1 day. The calculated autogenous shrinkage from time-zero to the age of 6 days was 0.4 mm/m.

Results of the autogenous shrinkage of temperature controlled, horizontal prisms (100 x 100 x 500 mm³) made of very high-strength concrete (f_{c28}=140 MPa, CEM I 52,5, w/c=0.276, s/c=0.20, steel fibres: 77 kg/m³, max. grain size: 16 mm) are presented in [6]. The isothermal measurement started at initial set. The autogenous shrinkage at the age of 28 days was approx. 0.8 mm/m.

In [7] the autogenous shrinkage of UHPC (f_{c28}=171 MPa, CEM I 42,5 R/HS, w/c=0.27, s/c=0.30) was determined on horizontal cylinders. The influence of an increase in temperature by 1.7 K inside the specimens at the beginning of the acceleration period was shown to be negligible. The steep increase of temperature at the age of 6.5 hours was taken as time-zero. Initial and final set occurred at 6.4 and 6.6 hours respectively. The autogenous shrinkage amounted to approx. 1.2 mm/m after 24 hours and 1.7 mm/m after 28 days.

In [8] again, temperature controlled, horizontal prisms (50 x 50 x 1000 mm³) were examined. Time-zero was chosen as the end of swelling, which lasted until the age of 31 hours, obviously owing to the extreme retardation effect of the superplasticizer. The autogenous shrinkage of the UHPC (f_{c28}=168 MPa, CEM I 52,5 N, w/c=0.18, s/c=0.26, c:1050 kg/m³, steel fibres: 470 kg/m³, max. grain size: 0.5 mm) from time-zero to the age of 7 days was approx. 0.325 mm/m.

In [9] the measurement of autogenous shrinkage apparently began 24 hours after mixing. Vertical cylinders (d=90mm, l=600 mm) were used. The strain resulted in approx. 0.56 mm/m after 28 days. Similar values were obtained with a similar method in [10].

Some of the aforementioned results are summarized in Figure 1. Though the investigated concrete compositions were quite similar, the results show a huge variation. This can be attributed mainly to the different measurement methods and experimental setups.

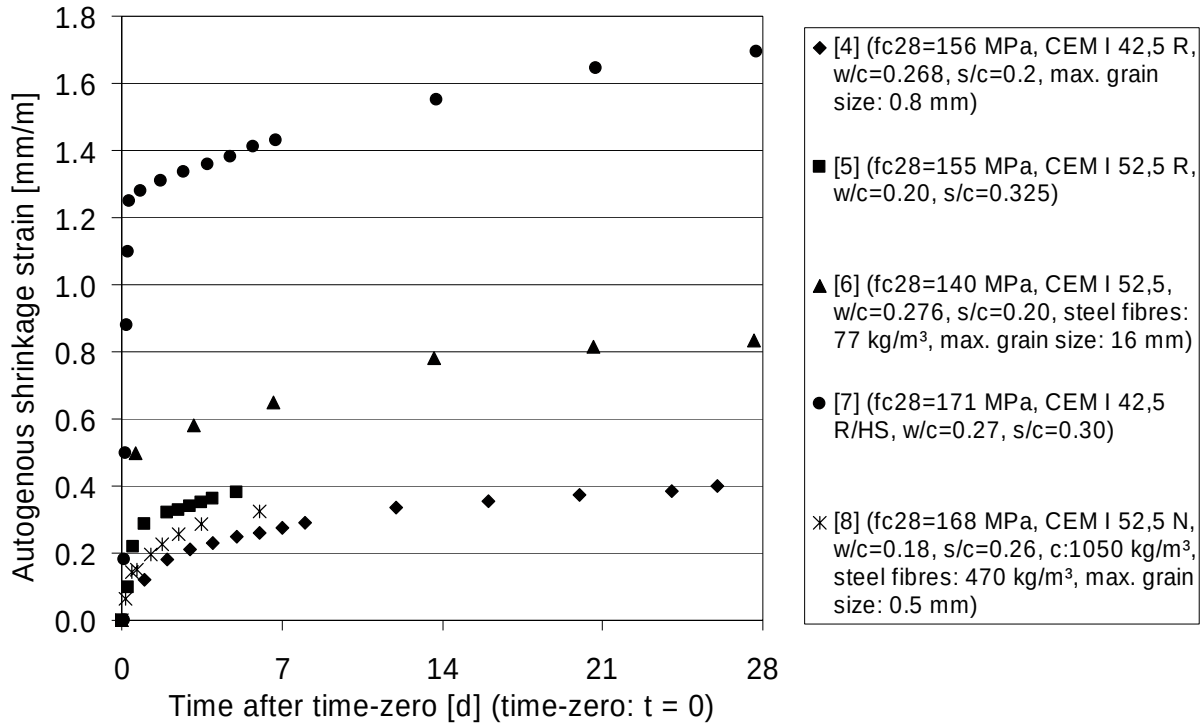

Figure 1: Results of the autogenous shrinkage of UHPC from time-zero (t = 0). Data: [4-8]

3 Measurement technique

There is no common standard for measuring the autogenous shrinkage yet. This may be due to the complexity of the task. The particular importance of determining time-zero has already been discussed above. Another problem lies in the separation of thermal dilation and autogenous shrinkage [11, 12]. While isothermal methods eliminate the influence of changing temperature histories on the autogenous shrinkage, they do not necessarily allow for realistic predictions of the behaviour of a concrete member with a large cross section or at varying ambient temperatures. However, as typical concrete members made of HPC or UHPC are rather slender, prisms with a small cross section (25 x 25 x 285 mm³) were used herein to measure the linear autogenous shrinkage under quasi-isothermal conditions (20 °C). Besides that, very low water contents prevent extreme heat development even with high cement contents. Sealed with a stainless steel foil, tape and beeswax, the heat of hydration flowed off fast and temperature changes due to hydration (max. 1.2 K) could be neglected. The continuous measurement was done with a mechanically coupled high-precision sensor (Figure 2). The influence of friction between the bottom side of the prism and the mould was minimized by means of felt covered with a thin foil. From the sixth or seventh day the length change of the prisms was measured manually in regular intervals. A minimum of two prisms per mix was tested. In addition the setting was determined by an automatic Vicat apparatus according to EN 196-3 at a constant water bath temperature of 20 °C. The initial set was taken as time-zero.

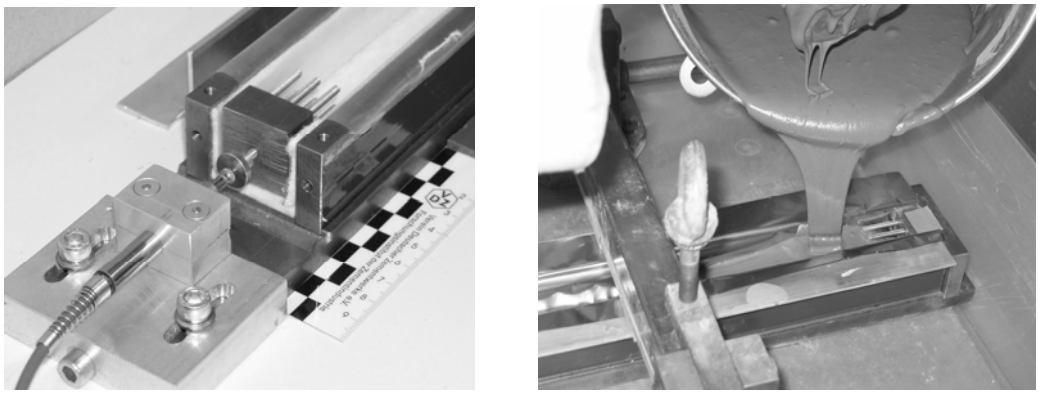

Figure 2: Experimental setup for the autogenous shrinkage and production of a prism

4 Aim and scope of the investigations

The investigations were to quantify the autogenous shrinkage of different UHPC-compositions and to identify the most important parameters influencing the autogenous shrinkage of UHPC. The results will be used for future investigations on cracking due to restrained shrinkage and on the potential impairment of durability of UHPC by cracks.

The influence of the following parameters was examined: cement, water/cement-ratio, content of silica fume, superplasticizer and steel fibres. Two cements were used; their chemical composition is given in Table 1; Table 2 contains some basic granulometric and physical parameters. The individual concrete compositions are given in Table 3. The cylinder compressive strength (150/300 mm) of the concrete compositions 1A, 4A, 5A, 1B, 4B and 5B was between 182 and 152 MPa, exceeding the lower limit of UHPC used in Germany, namely 150 MPa.

Table 1: Chemical analysis of cements A and B

Parameter		LOI	SiO_2	Al_2O_3	Fe_2O_3	CaO	SO_3	Na_2O-eq.	C_3S[1)]	C_2S[1)]	C_3A[1)]	C_4AF[1)]
Unit		mass %										
Cement	**A**[2)]	1.19	21.2	3.31	5.21	65.2	2	0.51	60.3	17.4	1.98	14.3
	B[3)]	1.08	22.3	4.1	1.39	65.7	3.5	0.52	61	18.6	8.59	4.29

1) X-ray diffractometry with Rietveld-refinement

2) CEM I 52,5 R-HS/NA (High Sulfate Resistance/Low Alkali Content)

3) CEM I 52,5 R

Table 2: Granulometric and physical parameters of cements A and B

Parameter		Density	Blaine-Value	x'	N	Water demand for standard consistency	Initial Set	Final Set	Compressive strength (2 d)	Compressive strength (28 d)	Heat of Hydration (7 d)
Unit		kg/dm³	cm²/g	µm	-	mass %	min	min	MPa	MPa	J/g
Cement	**A**[2)]	3.18	4650	15.5	0.76	28.5	140	195	30.6	61.8	320
	B[3)]	3.12	4710	12.8	0.81	30.5	155	195	39.8	64.3	357

2) CEM I 52,5 R-HS/NA (High Sulfate Resistance/Low Alkali Content)

3) CEM I 52,5 R

Table 3: Composition of the 28 tested concrete compositions, varied parameters **bold**

concrete composition	cement[1]	cement content	water	w/c-ratio	$(w/c)_{eq}$[2]	silica fume	superplasticizer	quartz sand[3]	quartz powder[4]	steel fibres[5]
	-	kg/m³	kg/m³	-	-	mass % of c	mass % of c	kg/m³	kg/m³	vol.-%
1	A/B	**800**	**168**	**0.230**	**0.198**	**16.2**	**3.0**	1019	220	-
2	A/B	800	**192**	**0.260**	**0.223**	16.2	3.0	960	215	-
3	A/B	800	**224**	**0.300**	**0.258**	16.2	3.0	890	200	-
4	A/B	**700**	168	0.260	0.223	16.2	3.0	1106	244	-
5	A/B	**600**	168	0.300	0.258	16.2	3.0	1193	268	-
6	A/B	800	168	0.230	0.191	**20.0**	3.0	993	210	-
7	A/B	800	168	0.230	0.209	**10.0**	3.0	1069	230	-
8	A/B	800	168	0.230	0.219	**5.0**	3.0	1100	245	-
9	A/B	800	173.5	0.230	0.198	16.2	**2.0**	1020	220	-
10	A/B	800	163	0.230	0.198	16.2	**4.0**	1009	220	-
11	A/B	800	158	0.230	0.198	16.2	**5.0**	1003	220	-
12	A/B	800	168	0.230	0.198	16.2	3.0	1019	220	**1.0**
13	A/B	700	168	0.260	0.223	16.2	3.0	1106	244	**1.0**
14	A/B	600	168	0.300	0.258	16.2	3.0	1193	268	**1.0**

1) cement: A: CEM I 52,5 R-HS/NA (High Sulfate Resistance/Low Alkali Content); B: CEM I 52,5 R

2) k-value for silica fume: $k_s = 1.0 \rightarrow (w/c)_{eq} = w / (c + s)$

3) grain size: 0.125 mm - 0.5 mm

4) grain size: 0 mm - 0.125 mm

5) straight, diameter d = 0.15 mm, length l = 9 mm, l/d = 60

5 Results of autogenous shrinkage measurements

5.1 Variation of w/c-ratio at constant cement content

The concrete compositions 1, 2 and 3 showed a rapid increase in the linear autogenous shrinkage strain within the first day and a second period with much lower shrinkage rate (Figure 3). The strain of concrete 1A at the age of 28 days was approx. 0.70 mm/m, those of 1B approx. 0.79 mm/m. With cement A lower w/c-ratios did lead to higher shrinkage. There was no clear correlation for cement B. The shrinkage strain was generally higher with cement B; the transition to the second period of lower shrinkage rate was smoother. Cement B contained considerably more C_3A (A: 2.0 mass %; B: 8.6 mass %).

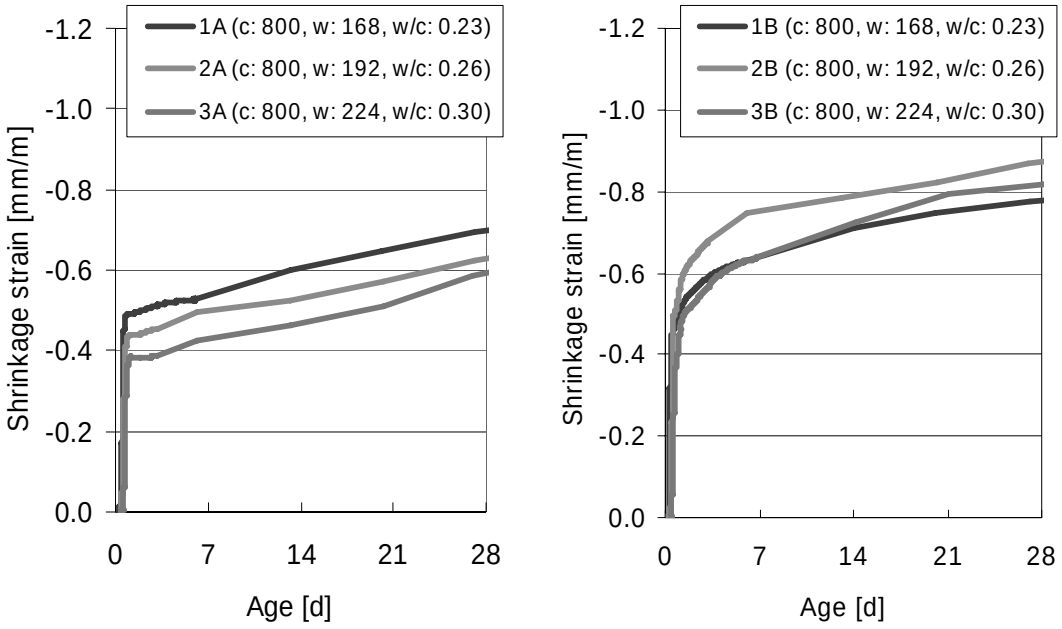

Figure 3: Autogenous shrinkage vs. age – variation of w/c-ratio at constant cement content. Left: cement A, right: cement B

5.2 Variation of water/cement-ratio at constant water content

The above variation of the water/cement-ratio at constant cement content is widely used. At low degrees of hydration, however, a change of the water/cement-ratio at the same time changes the paste volume that causes shrinkage. To account for this superimposition it would be necessary to determine the degree of hydration. Herein the water/cement-ratio at constant water content was varied instead.

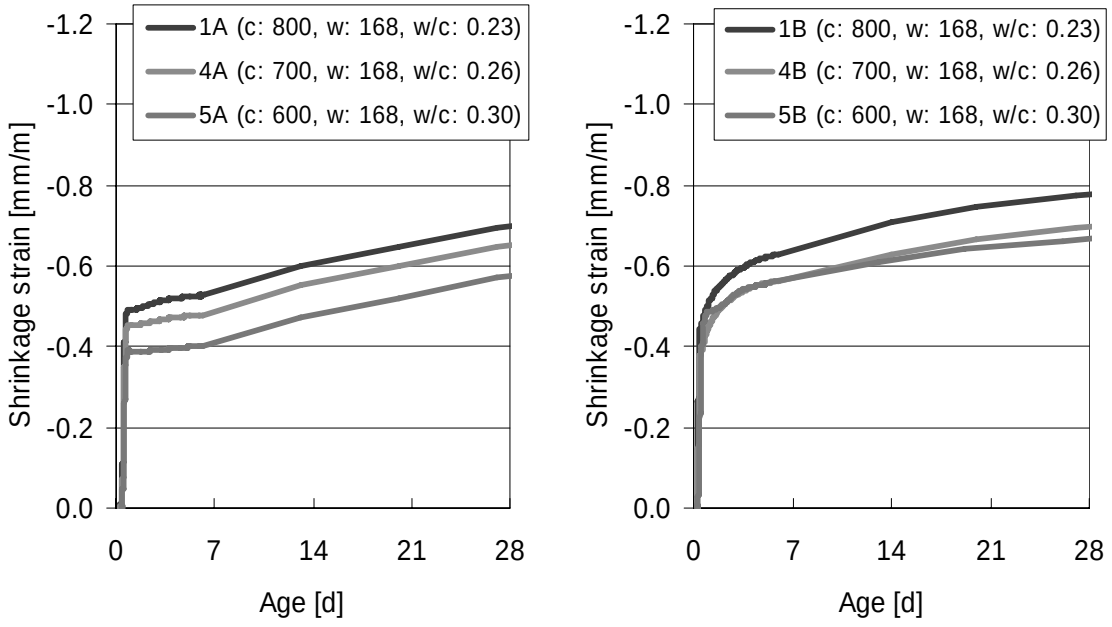

Figure 4: Autogenous shrinkage vs. age – variation of cement content at constant water content. Left: cement A, right: cement B

Due to the identical water content almost the same amount of cement hydrated in the concrete compositions 1 (c: 800 kg/m³), 4 (c: 700 kg/m³) and 5 (c: 600 kg/m³), so they varied only in the amount of unreacted cement. Tests of the evaporable water content proved this assumption right. The results for cement A (Figure 4, left) were very similar to those of concrete compositions 1, 2 and 3 (Figure 2, left). As for cement B, there was a weak correlation of water/cement-ratio and shrinkage strain at the age of 28 days.

5.3 Variation of silica fume content

The variation of the silica fume content (5 to 20 mass % of cement) led to no clear correlation (Figure 5). However, the concrete composition with cement A and the lowest silica fume content (8A, s/c=0.05) showed the lowest shrinkage. Similarly composition 6B (s/c=0.20) showed the highest shrinkage.

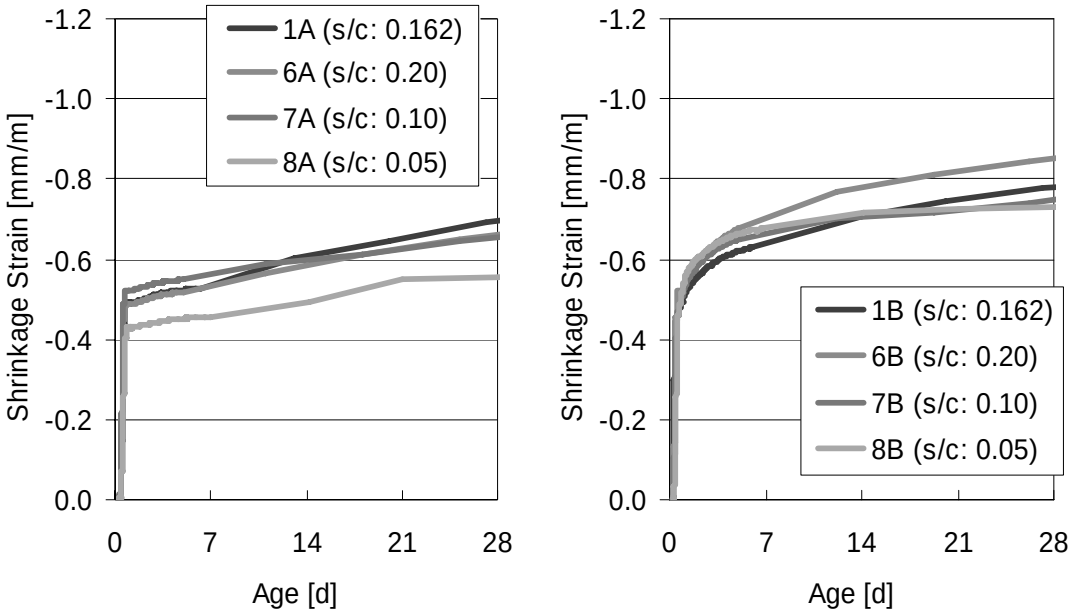

Figure 5: Autogenous shrinkage vs. age – variation of silica fume content by weight of cement (s/c); c: 800 kg/m³, w: 168 kg/m³, w/c: 0.23. Left: cement A, right: cement B

5.4 Variation of content of superplasticizer

Varying the superplasticizer content did not lead to significant changes in the autogenous shrinkage strain at the age of 28 days. However, the early development of the autogenous shrinkage clearly depended on the retardation effect caused by the superplasticizer, as shown in Figure 6. The less superplasticizer was added, the earlier did the autogenous shrinkage rise.

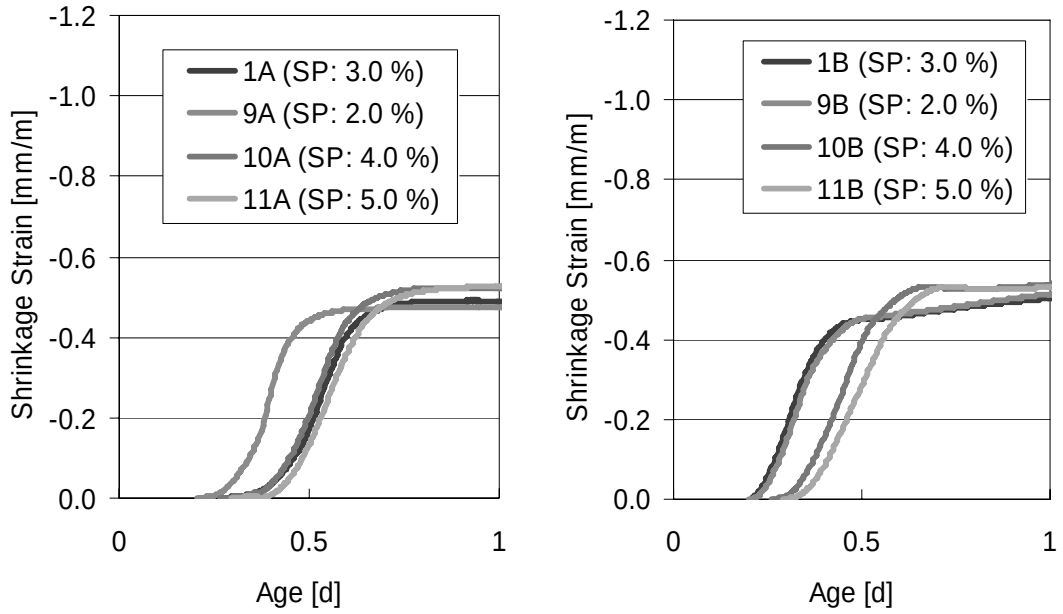

Figure 6: Autogenous shrinkage vs. age – variation of content of superplasticizer (SP) by weight of cement; c: 800 kg/m³, w: 168 kg/m³, w/c: 0.23. Left: cement A, right: cement B

5.5 Variation of steel fiber content

The addition of steel fibers (1.0 vol.-%, concrete compositions 12 - 14, s. Table 1) led to a general decrease in the autogenous shrinkage strain of between 10 and 15 % in relation to the correspondent compositions without fibers (1, 4, 5).

6 Conclusions

The autogenous shrinkage strain of the examined UHPC-compositions from time-zero to the age of 28 days was approx. 0.6 to 0.9 mm/m. These values are higher than most of those reported to date for UHPC. The differences can be due to different experimental setups. However, it is important to note that the experimental setup applied here – a mechanically coupled sensor and horizontal prisms with some residual friction between their bottom side and the mould – may lead to values lower than the true value, but not to higher ones. Therefore, the results clearly show that the autogenous shrinkage strain of UHPC can be very high and must be taken into account both for assessing the risk of cracking and for obtaining the correct dimensions of structural elements.

The most important parameters for the autogenous shrinkage strain of UHPC were the water/cement-ratio and the cement composition. The strains were higher with lower water/cement-ratios. Cement B, containing more C_3A than cement A, led to higher strains. This confirms the importance of the C_3A for the autogenous shrinkage. High silica fume contents led to high strains, whereas the correlation within the whole range of examined silica fume contents ($0.05 < s/c < 0.20$) was not clear. This may be due to different rates of hydration of the silica fume. The complex interaction of the reactive constituents needs further investigation. The superplasticizer content had no significant influence on the

shrinkage at the age of 28 days, but changed the early age behavior. Steel fibers reduced the autogenous shrinkage strain by about 10 to 15 %.

7 References

[1] Barcelo, L., Boivin, S., Rigaud, S., Acker, P., Clavaud, B., Boulay, C.: Linear vs. volumetric autogenous shrinkage measurements: material behaviour or experimental artifact. In: Self-desiccation and its importance in concrete technology. Proceedings of the international research seminar, Lund, Sweden, 1997.

[2] Weiss, J.: Experimental determination of the ‚time-zero' t0 (maturity-zero M0). In: Early Age Cracking in Cementitious Systems. RILEM Report 25 of RILEM Technical Committee TC 181-EAS, 2003.

[3] Japan Concrete Institute: Technical committee report on autogenous shrinkage of concrete, 1996. Partly translated into English in: Autogenous shrinkage of concrete. Proceedings of the international workshop organized by JCI (Japan Concrete Institute), Hiroshima June 13-14, 1998.

[4] Ma, J., Dehn, F., Koenig, G.: Autogenous shrinkage of self-compacting ultra-high performance concrete. In: Advances in Concrete and Structures, Proceedings of the International Conference ICACS, Xuzhou, China, 2003, pp. 255-262.

[5] Staquet, S., Espion, B.: Early-age autogenous shrinkage of UHPC incorporating very fine fly ash or metakaolin in replacement of silica fume. In: International Symposium on Ultra High Performance concrete September 13-15, 2004, Kassel, pp. 587-599.

[6] Bjoentegaard, O., Sellevold, E.J.: Very high strength concrete. In: In: Early Age Cracking in Cementitious Systems. RILEM Report 25 of RILEM Technical Committee TC 181-EAS, 2003, pp. 285-294.

[7] Schachinger, I., Schmidt, K., Heinz, D., Schießl, P.: Early age cracking risk and relaxation by restrained autogenous deformations of ultra high performance concrete. In: 6th International Symposium on High Strength / High Performance Concrete, Leipzig 2002, pp 1341-1354.

[8] Habel, K., Charron, J.-P., Denarie, E., Brühwiler, E.: Autogenous deformations and viscoelasticity of UHPFRC in structures. Part I: experimental results. In: Magazine of Concrete Research, 2006, No.3, pp. 135-145.

[9] Loukili, A., Khelidj, A., Richard, P.: Hydration kinetics, change of relative humidity, and autogenous shrinkage of ultra-high-strength concrete. In: Cement and Concrete Research 29 (1999), pp. 577-584.

[10] Guangcheng, L., Youjun, X., Zhengwu, J.: Volume changes of very-high-performance cement-based composites. In: Magazine of Concrete Research, 2006, No. 10, pp. 657-663.

[11] Bjoentegaard, O., Sellevold, E.J.: Thermal dilation – autogenous shrinkage: how to separate. In: Autogenous shrinkage of concrete. Proceedings of the international workshop organized by JCI (Japan Concrete Institute), Hiroshima June 13-14, 1998.

[12] Bjoentegaard, O., Sellevold, E.J.: Interaction between thermal dilation and autogenous deformation in high-performance concrete. In: Materials and Structures, 2001, Vol. 34, pp. 266-272.

Susanne Palecki
Dr.-Ing., scientific assistant
University of Duisburg-Essen,
Essen, Germany

Max J. Setzer
Prof. Dr., former head of institute
University of Duisburg-Essen,
Essen, Germany

Ultra-high-performance concrete under frost and de-icing salt attack

Summary

For ultra-high-performance concrete with its high amount of cement, additives, admixtures as well as steel fibers and maximum grain sizes of 0.50 mm, totally different damage and transport mechanisms under climatic exposures like the frost and de-icing salt attack must be considered. The previous knowledge about the behavior of UHPC under this kind of stress is at present not sufficient to assess the durability and to understand the responsible mechanisms for a wider range of UHPC mix designs. Beyond this, also different aspects like the curing conditions, after-treatment or the testing age have to be taken into account for the assessment of the durability. Under this consideration, fundamental investigations concerning the analysis of the transport and damage mechanisms of UHPC under frost and de-icing salt attack are currently carried out under the scope of the priority program SPP1182 “Sustainable Building with Ultra High Performance Concrete (UHPC)”, funded by the German Research Foundation (DFG). An extract of these new results can be found in this paper.

Keywords: *frost salt resistance, moisture uptake, damage mechanisms*

1 Introduction

During the last decades of years several damage models for normal strength concrete (NSC) under frost and de-icing salt attack have been developed by different authors. Although the knowledge of the basic deterioration process of concrete under such type of exposure is in the meantime well advanced, a deeper understanding especially for modern concrete types is still necessary. With the significant variation of the mix design by means of addition of additives and admixtures, as it is the case for HPC and UHPC, the durability cannot be longer assessed by the composition and the descriptive approach solely. Although excellent durability properties can be supposed due to their extreme dense structure, this phenomena as well as the stiffer matrix, can lead to unpredictable damage behaviour compared to normal strength concrete. With this knowledge it comes obvious that the different damage and also transport process of these special types of concrete under climatic exposures have to be better understood.

1.1 Frost and de-icing salt resistance

Frost attack with and without de-icing agent leads at first to an external damage in forms of surface scaling, but also to an internal damage, characterized by an internal micro cracking

of the concrete matrix. In the process both phenomena are not directly linked together due to the fact that they are based on different damage mechanisms.
When concrete is exposed to cyclic freeze-thaw exposure, an artificial saturation of the matrix due to the so called frost pump takes place, which finally results into a critically saturation of the concrete structure. As a result micro cracking, caused by the 9% ice expansion, and finally loss of the relative dynamic modulus of elasticity are the consequences. This process is explained by the micro-ice-lens model [3, 5]. It becomes obvious, that both mechanisms - moisture uptake and internal damage - are directly linked together. This implies that the speed, with which the concrete is saturated, is the most important parameter for the frost resistance of a concrete structure. With a more efficient frost pump, the concrete is saturated faster and internal damage starts earlier. Beyond this, the speed of saturation depends on the pore structure, which is again connected with the composition; in front the w/b ratio as well as the addition of additives and admixtures.
External damage occurs in case of a pure frost attack only secondary and does not represent the acceptance parameter. This is different in case of a combined frost and de-icing salt attack, where surface scaling is the dominant damage factor, at least for normal strength concrete. Responsible for this kind of external damage is here a superposition of different phenomena. At first phase transformations, but also chromatographic effects are relevant [7]. For the degree of damage most important factors are the chloride content and gradient, the water uptake capacity, the moisture gradient and saturation as well as the physical and chemical aggressiveness of the de-icing solution and last but not least the temperature stress.

1.2 Durability of high-performance concrete

For high-tech concrete, whereas additives and admixtures are usually incorporated and low w/b ratios are used, the pore size distribution is considerably different from normal strength concrete. Besides the shifting of coarser to smaller gelpores, also pores caused by self-desiccation play a more important role. These changes of the pore structure and the extreme dense matrix compared to normal concrete results also into different transport and damage mechanisms. In 0 this relation has been described for HPC and NSC with low w/c ratios.

In the past, extensive investigations with the frost test methods CDF/ CIF-Test have been carried out at the IBPM, in order to determine the frost and frost-salt resistance of a wide spectrum of different concrete structures with various compositions [4, 5]. Examples of results found for w/b ratios in the range between 0,42 down to 0,30 are shown in figure 1. From these CIF-test results with demineralized water as test solution, it could be concluded that with lowering the w/b ratio, the moisture uptake and accordingly the internal damage behavior differs significantly. With start of freeze-thaw testing normal strength concrete always show a linear water uptake and course of damage, due to continuous saturation of the matrix by the frost pump. When testing HPC the frost suction is often essentially delayed or even interrupted, especially when using additives like silica fume or fly ash. It can be summarized that due to the denser structure the critical saturation is reached at lower values of water content and loss of RDM runs often faster compared to concrete without silica fume.

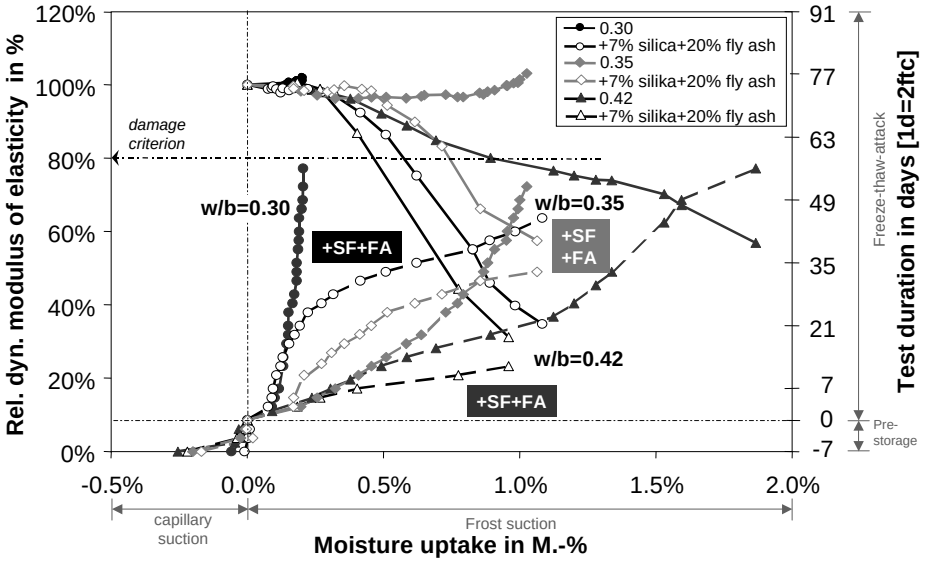

Figure 1: CIF-results of HPC mixes with w/b ratio 0.30 and 0.42 with and without additives.

Further investigations [4, 5] could also show and approve that even slight variations within the composition of HPC mixes could result into significant changes of the frost and frost salt resistance due to essential changes within the pore structure. While using e.g. a different cement and/ or superplasticizer combination the time until frost damage starts and especially the speed of saturation varies importantly. At this point, it can be concluded that in most instances a higher resistance against outdoor exposure is observed for concretes with very dense structures, but also sudden and unexpected damages could occur due to different interactions. Furthermore boundary conditions like the testing age or curing conditions have to be more considered for the assessment of the durability of HPC as well as UHPC. This could also be shown by investigations with UHPC carried out at the *Technical University of Finland (HUT)* [8].

2 Research activities

2.1 Test programm and test procedures

In order to study the transport and damage mechanisms of ultra-high-performance concrete in detail, different UHPC mixes with w/b ratios below 0,27, addition of steel fibres and different cement types have been investigated under the scope of the DFG funded SPP 1182 project at the University of Duisburg-Essen [6]. The pervious test program includes beside the variation of the mix design also different types of heat treatment, testing age as well as cyclic pre-treatment (cyclic temperature attack before frost testing (7d → +60°C/ 7d → capillary suction at 20°C/ 7d → +20°C/ -20°C)). An extract of representative UHPC mix designs with their fresh and hardened concrete parameters includes Table 1. The target flow of the UHPC mixes was fixed to be in the range of > 650 mm.

Table1: Mix design and characteristic data of the different UHPC mixes.

		M2Q	+ 2d at 90°C	M2Q-C2	+ 2d at 90°C	+2d at 90°C→8°C	+2d at 180°C	+2d at 180°C→8°C	B4Q-C2	+ 2d at 90°C	+2d at 90°C→8°C	+ 2d at 180°C	+ 2d at 180°C→8°C
cement	kg/m³	832							650				
type	-	CEM I 52,5 HS/NA		CEM I 52,5					CEM I 52,5				
w/b	-	0.19							0.21				
silica	kg/m³	135							177				
quartz I	kg/m³	207							325				
quartz II	kg/m³	-							131				
basalt 2/16	kg/m³	-							625				
sand	kg/m³	969							362				
fibres	kg/m³	192				-			-				
SP	%	3,95				3,78			5,25				
SP Type	-	PCE 1				PCE 2			PCE 2				
$f_{c,28d}$*	N/mm²	191	195	143	188	190	237	232	147	181	189	232	207
air pore cont., fresh	%	3,8**				4,3***			2,6***				
air pore cont., hardened state	%	5,6				4,8			2,8				
porosity	%	5,5	2,9	7,6	10	9	11	10,1	7,9	6,9	6,5	6,6	7,1

*tested on 4x4x8cm samples (½ of standard prism)

**determined on 8 liter air pore container

*** 1 liter air pore container

As it can be seen from the table, a higher air pore content due to the sticky consistency and the difficult compaction could be found for nearly all mixes, although the casting process had been continuously optimized. The concrete specimens were usually demoulded after 2 days and then stored under water for another 5 days. Half of the specimens were exposed to a heat treatment after demoulding with duration of 2 days at 90°C. After this procedure the specimens were placed under water until age of 7 days, when they were stored in a climate chamber as well. Start of frost testing was at specimen age of 28 days as well as 180 days, in order to determine the influence of ageing on the durability.

The frost- and de-icing salt testing was conducted with the CDF- and CIF-test [1,2]. The analysis of the pore structure by MIP and Helium pycnometer measurements as well as microscopic analysis has been carried out in addition.

2.2 Results of Frost- and de-icing salt testing

2.2.1 Scaling behaviour of UHPC

Examples of the scaling behavior of some UHPC mixes are given within the following figure. The difference between NaCl and a demineralized water test solution becomes obvious, although the maximum scaling rate after 112 ftc amounted not higher than 591g/m², independent from the type of curing or testing age. This value is far below the CDF-test limit, although the test duration has been expanded, so that an extremely high frost salt resistance for this UHPC mix M2Q can be guaranteed, despite variation of the curing conditions. It should be still considered, that the air pore content of the tested samples is conform to air entrained concretes.

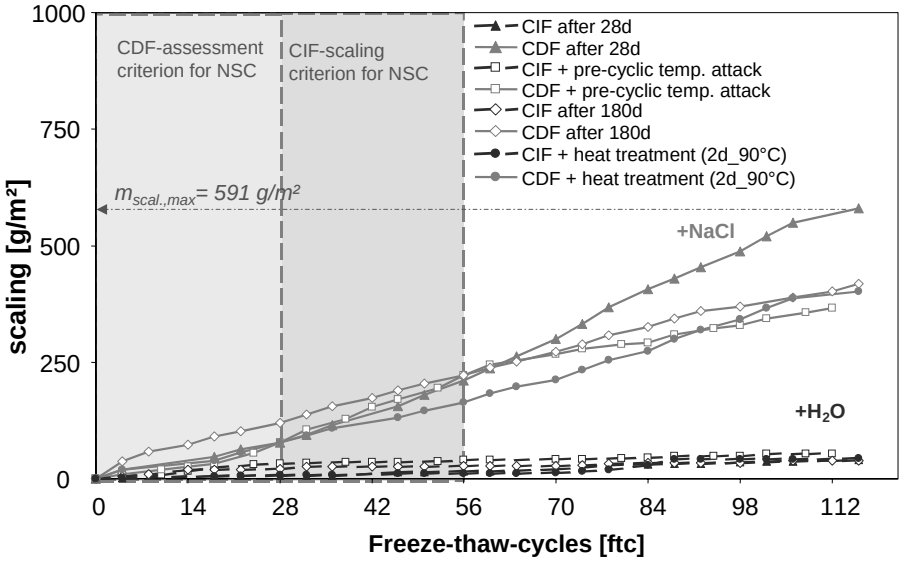

Figure 2: Scaling of mix M2Q (w/b=0.19+ fibres) and variation of after-treatment as well as testing age within the CDF/ CIF-test.

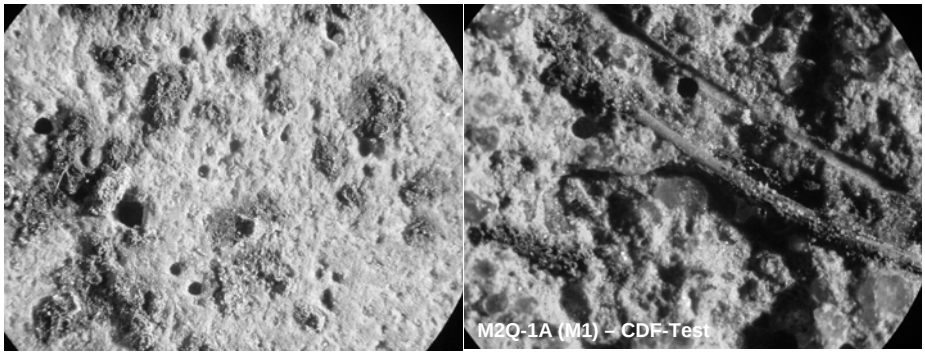

Figure 3: Microscopic pictures of the CDF-tested surface of the M2Q mix. Left photo: overview of test surface with corrosion scums, right side: corroded steel fibre in detail.

Nevertheless, in comparison to non-fiber mixes a slightly higher scaling rate could be found for mixes containing fibres [6]. From the microscopic pictures, given above, it can be seen,

that local spalling of cement particles around partly corroded fibres could be observed after end of CDF-testing. Here, it still needs to be clarified whether the corrosion of the steel fibres is responsible for the scaling of the first concrete layers or if it is a secondary effect. This means, despite low scaling rates, the corrosion of steel fibres could be problematic for practical use of UHPC, which implies aesthetic as well as functional losses.

2.2.2 Internal damage and moisture uptake

Figure 4 shows at first the course of the relative dynamic modulus of elasticity (RDM) versus the moisture uptake as well as the moisture uptake as function of time for the mix M2Q (w/b 0.19 + fibers) during the CDF/ CIF-test. Again the curing conditions i.e. after-treatment has been varied. It can be seen that a stagnation of the moisture uptake takes place, when using a demineralized test solution (CIF-test). But also for the CDF-tested specimens only a slightly higher sodium chloride uptake can be observed without any internal damage. Here an interaction between the low amount of freezable water and the high air pore content seems to be responsible for this behavior.
The same course of moisture uptake as well as internal damage could be observed for the mix with coarser aggregates (B4Q), so that the results are not presented at this point.

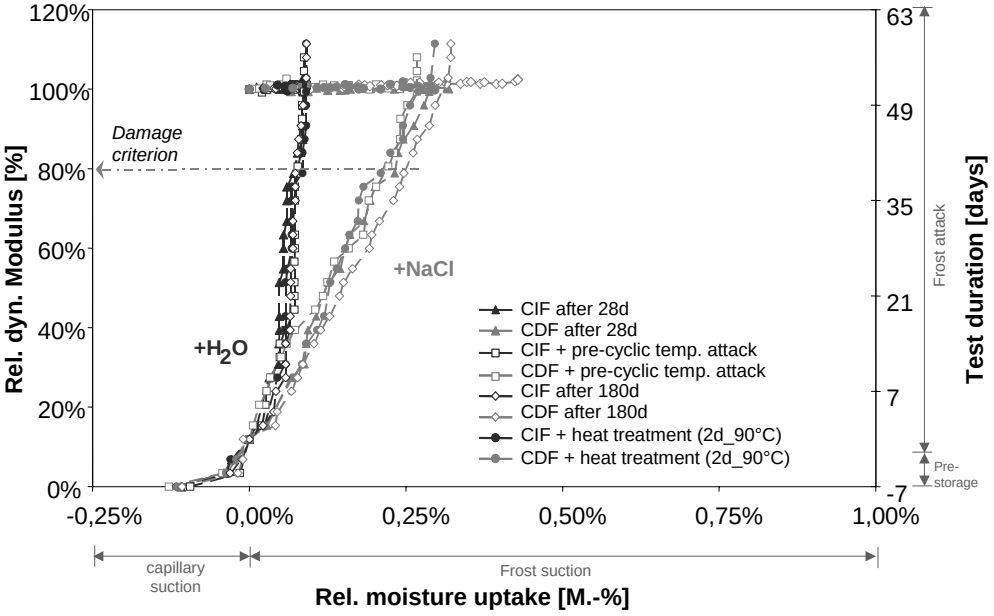

Figure 4: CIF/ CDF-results of the UHPC mix M2Q with w/b ratio 0.19 and steel fibres – Variation of after-treatment and curing. Testing until 112 ftc!

In general, when testing concrete with such a dense structure, the amount of freezable water down to temperatures around –20°C is inside the concrete drastically reduced, which can be also verified by MIP as well as DSC investigations [6]. This leads to a significant reduction of the efficiency of the micro-ice-lens pump. In case of no internal ice formation the driving force of the frost pump – the potential difference between water and ice – is missing and therefore no re-suction of moisture takes place during the thawing phase. This can be also derived from the results of continuous ultrasonic transit time measurements during different freeze-

thaw cycles of some HPC and UHPC mixes (figure 5). In contrast to a HPC mix with a w/b ratio of 0.35 and silica addition, where micro cracking starts after 85 ftc and results into complete deterioration of the matrix, the mixes with w/b=0.30 (fig. 5b) and 0.19 (fig. 5c) show nearly no changes within the course of the US transit time. That means for these two mixes on one side no loss of RDM during the testing period and on the other side no freezing and melting of ice during the separate frost and thawing phases. While the HPC mix with w/b=0.30 gets absolutely no ice formation during freezing, the UHPC sample (w/b=0.19) shows some small changes within the US transit time during the frost phases. This signifies that a small amount of ice is still generated within the UHPC mix, but does not lead to micro damages of the matrix.

Another effect is, that high air pore contents generally causes an interruption of the frost pump as well. This has been already approved by previous investigations on air entrained HPC mixes [4]. It can be pointed out that both phenomena – low amount of freezable water and high air pore content - finally lead to changes within the freezing and thawing behavior of UHPC, which influence the micro-ice lens pump as well.

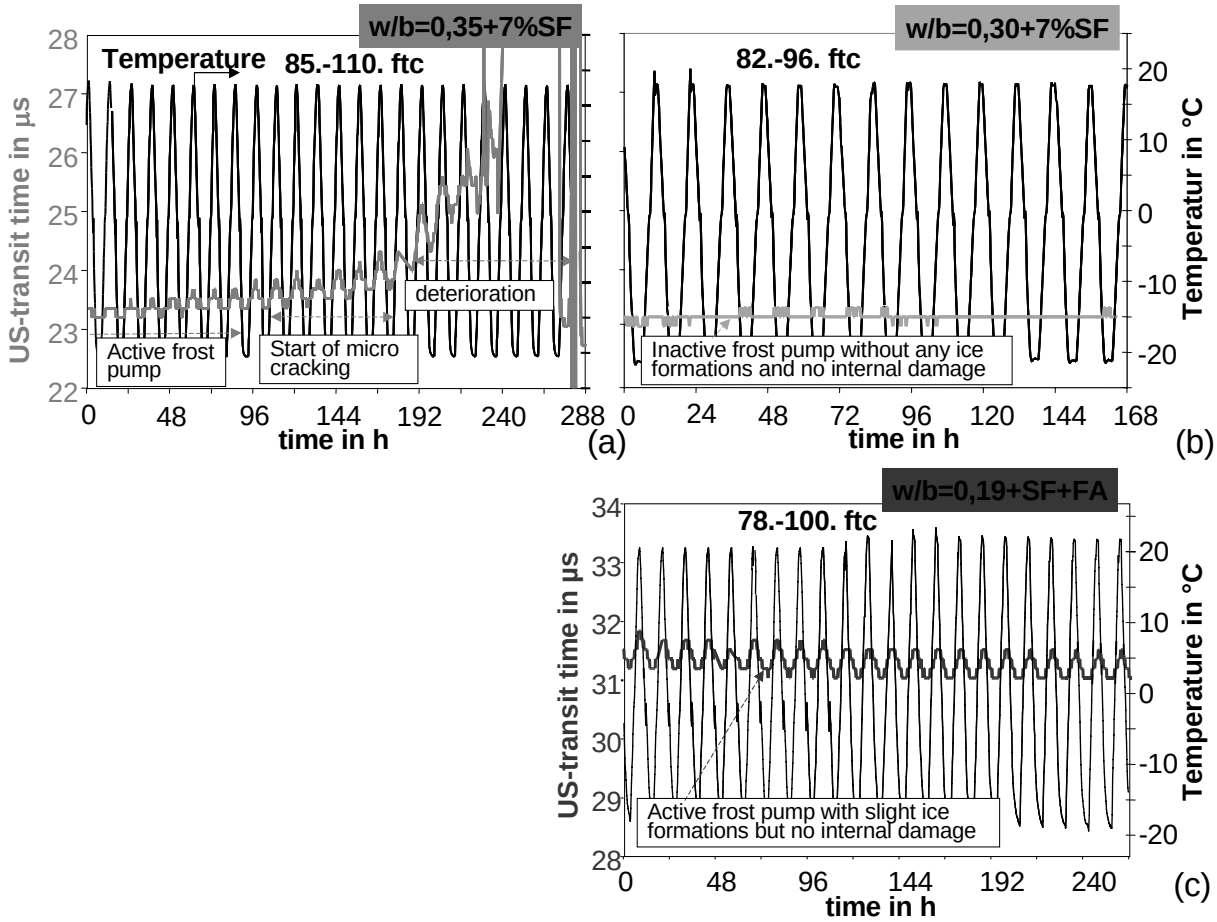

Figure 5: Continuous US transit time measurements during different freeze-thaw cycles within CDF/ CIF-testing of mixes with a) w/b ratio 0.35 + silica fume, b) w/b ratio 0.30 + silica fume, c) w/b ratio 0.19 + silica fume + fly ash (M2Q+FA).

Here it must be noticed that the high frost and frost salt resistance of UHPC mixes with respect to internal damage could be not explained by the reduced amount of freezable water

and the very dense pore structure alone. The question is, whether there is still any impetus of damage process, which provokes start of micro cracking of UHPC matrixes. One factor certainly is existing micro damages before start of frost exposure e.g. because of pre-damages by higher autogenous shrinkage or induced stress.

2.2.3 Influence of pre-damage on the durability

The influence of pre-damages is rudimentary presented in figure 6. After demoulding the specimens were exposed to different heat treatments, which differ between water storage, heat treatment (90°, 180°C) with moderate cooling down in a climate chamber (20°C, 65% RH) and heat treatment (90°, 180°C) with rapid cooling to 8°C until start of frost testing. The following results of the internal damage reflect a higher micro cracking of the special heat-treated specimens compared to the other samples. The loss of the rel. dyn. modulus starts in all cases, except the water stored samples (reference concretes), even after some few ftc and drops down to 75% i.e. 50% while continuing the test. In case of a rapid cooling of the samples a significant internal damage could be already found after 4 ftc. Also the moisture uptake is much higher for the special treated samples, which can be certainly correlated with the course of the internal damage. This is in contrast to the water stored and non-heat treated samples and also investigations with standard curing conditions of UHPC mixes.

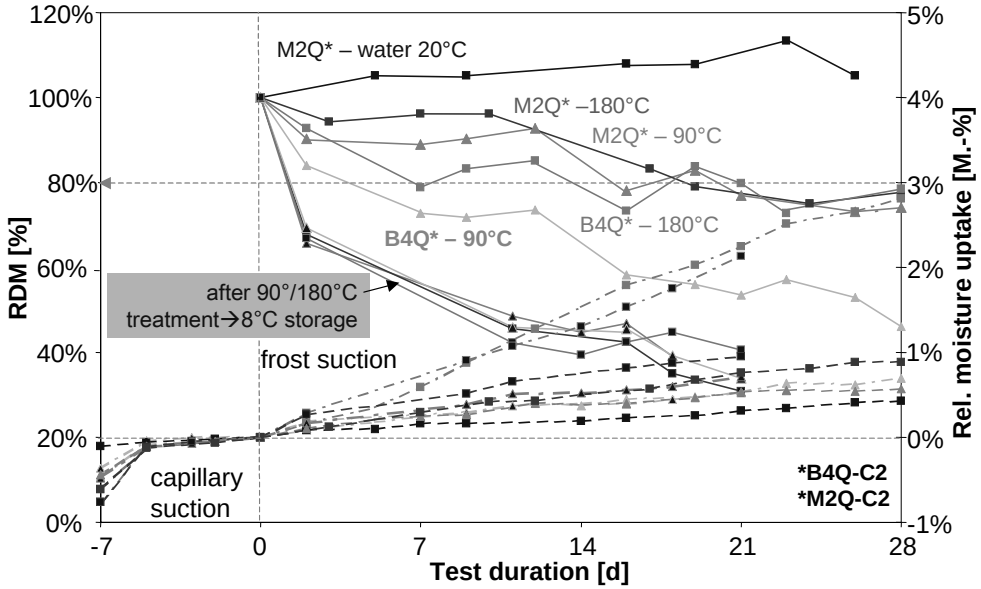

Figure 6: CDF-results of M2Q-C2, B4Q-C2 mixes with w/b ratio 0.19 and 0.21 and cement 2 (CEM I 52,5) – Variation of heat treatment and storage conditions.

3 Conclusions and Outlook

In cases of lower w/b ratios and high amounts of additives only very low amounts of scaling and no critical saturation can often be found under frost and de-icing salt attack. Regarding the scaling behavior the observed corrosion of steel fibres could be despite low scaling rates problematic for practical use of UHPC. Concerning the internal damage it could be found that

the amount of freezable water is so much reduced that no further moisture uptake according to the frost pump takes place during frost or frost salt exposure. It seems that here both effects, the low amount of freezable water as well as the high air pore content prevents the structure from re-saturation due to the micro-ice lens model. A totally different behavior can be assumed in case of an existing micro cracking at start of testing. First investigations on pre-damaged UHPC mixes, which have been exposed to harsher heat treatments after demoulding, higher moisture uptakes and following start of internal damage as well as surface scaling could be found under freeze-thaw attack. The same can be assumed for UHPC structures with higher autogenous shrinkage values, massive structures with expansion obstructions or mechanical stress. Overall, the mentioned aspects lead again to the conclusion that the behavior of HPC/ UHPC mixes is much more difficult to predict than in case of OPC. As the variation of constituents is very high for UHPC, the testing of the resistance of the mix design by accelerated test procedure before the application can be necessary. However, it should be kept in mind that the results only reflect some major parameters and not the variety of internationally available constituents and further incompatibility aspects. This latter topic is of greatest interest for safe and durable use of these special types of concrete. Further investigations are still necessary to clarify the influence of further boundary conditions and variation of mix designs on the durability.

4 References

[1] RILEM Recommendation “CIF-Test – Capillary Suction, Internal Damage and Freeze-Thaw Test; Method and alternative Methods A&B”, Materials & Structure, 2004.

[2] RILEM Recommendation “CDF-Test – Capillary Suction, Deicing agent and Freeze-Thaw Test”, Materials & Structure, No. 1996

[3] Setzer, M.J. “The micro-ice-lens pump - a new sight of frost attack and frost action” CONSEC 2001 Conference proceedings, pp.428-438

[4] Palecki, S.: Hochleistungsbeton unter Frost-Tau-Wechselbelastung – Schädigungs- und Transportmechanismen, phd thesis at the University of Duisburg-Essen, Cuvillier publisher Göttingen, 2005

[5] Palecki, S., Setzer, M.J.: Proceedings of the international conference on durability of high-performance concrete and final workshop of CONLIFE, Universität Duisburg-Essen, Aedificacio publisher 2004

[6] DFG Schwerpunktprogramm SPP1182 Nachhaltiges Bauen mit ultra-hochfestem Beton, http://www.uni-kassel.de/fb14/baustoffkunde/spp/, Rev. 2007-11-5, 1st research report of IBPM

[7] Stark, J., Ludwig, H.-M.: Frost- und Tausalz-Widerstand von Beton – ein rein physikalisches Problem? Wiss. Zeitung der Hochschule Weimar 40 (56-7), 1994

[8] Cwirzen, A., Vornanen, C., Habermehl-Cwirzen, K: Long-term mechanical properties of low-water cement ratio ultra-high strength concretes, proceedings of international concrete symposium, Australia 2007

Lutz Franke
Prof. Dr.-Ing.
TU of Hamburg-Harburg
Hamburg, Germany

Gernod Deckelmann
Dr.-Ing.
TU of Hamburg-Harburg
Hamburg, Germany

Holger Schmidt
Dipl. Ing.
TU of Hamburg-Harburg
Hamburg, Germany

Behaviour of ultra high-performance concrete with respect to chemical attack

Summary

In this document the analyses of ultra high-performance concrete with respect to chemical attack will be characterised and discussed. The possibility of using UHPC without additional external protection, e. g. coatings, in settings of higher acid and salt concentrations than XA3 is hereby of special interest. Particularly the leaching attack of dissolving acid and ammonia solution and expansion by salt water is investigated. In this context the difference in durability of an ordinary reference mortar and various optimized UHPC mortars will be examined. Some different criteria are necessary to evaluate the damage in progress. Furthermore an extrapolation of the corrosion depth will be presented. It is possible to calculate the expected corrosion depth occurring during normal exposure times. In the framework of a more extensive research project on the behaviour of durability of ultra high-performance concrete, initial results of investigations are presented.

Keywords: *chemical attack, durability, sulphuric acid, lactic acid, sulphate, ammonia*

1 Introduction

The aim of the research is to evaluate if UHPC has a defined higher resistance as an ordinary concrete or a high performance concrete with respect to the durability. In the first test series the behaviour of UHPC against sulphuric acid, lactic acid, sulphate solutions and ammonia solutions was investigated. These experiments were carried out on the optimized mixtures M2Q and B4Q without fibres, which were heat treated at 90°C for two days. In comparison to UHPC an ordinary reference mortar was also investigated. For the investigation in this research project, ultra high-performance concrete with compressive strength values of approximately 170 N/mm² to 200 N/mm² is used.

2 Composition and characterization of concrete

The ordinary reference mortar consists of ordinary Portland cement CEM I 42.5 R-HS and is produced according to Sielbau-Richtlinie [1]. In both ultra high-performance concretes the

powder was composed of ordinary Portland cement CEM I 52.5 R-HS/NA, microsilica and quartz powder. The fineness of this quartz powder is between the silica fume and the cement and was used as a micro filler to optimize the packing density of the powder mixture. Superplasticizer on the basis of polycarboxylateether ensured the flowability of the investigated compacted UHPC. Table 1 gives more details on the composition of the ordinary reference mortar and the UHPC mixtures.

Table 1: Composition of ordinary reference mortar and ultra high-performance concrete

material	unit	Ord. mortar	M2Q 90	B4Q 90
cement				
cement CEM I 52.5 R-HS/NA	kg/m³		832	650
cement CEM I 42.5 R-HS	kg/m³	512		
aggregates				
CEN sand	kg/m³	1536		
quartz sand 0.125/0.5	kg/m³		975	354
basalt split 2/8	kg/m³			597
additives				
quartz powder Q I	kg/m³		207	325
quartz powder Q II	kg/m³			131
microsilica	kg/m³		135	177
admixtures				
superplasticizer	kg/m³		29.4	15.2
water	kg/m³	230	166	158
water to cement ratio (w/c)		0.45	0.20	0.24
water to binder ratio (w/b)		0.45	0.17	0.19

The values of compressive and flexural tensile strength of the specimens (prisms 40 x 40 x 160 mm³) of the above mixtures were determined at seven and 28 days (see Table 2).

Table 2: Compressive and flexural tensile strength of the concrete

strength	unit	Ord. mortar	M2Q 90	B4Q 90
compressive strength				
after 7 days	N/mm²	-	172	201
after 28 days	N/mm²	58	167	192
flexural tensile strength				
after 7 days	N/mm²	-	16	14
after 28 days	N/mm²	8	20	16

For all mixtures the concentration of calcium hydroxide was determined via differential thermal and thermogravimetric analysis (DTA/TG). After heat treatment of ultra high-performance concrete no calcium hydroxide was detected as expected. In contrast the value measured for the ordinary reference mortar amounts to about 19 mass percent.

The total porosity of ultra high-performance concrete and ordinary reference mortar was determined by the bulk density using the dipping and weighing method and the skeletal

density using helium pycnometer. With this procedure it is possible to detect a widely spectrum of pores, particularly nano pores. Measurements of porosity were also performed by mercury intrusion porosimetry. The maximum pressure used in this method was about 420 N/mm². In this project the specimens were oven dried at 105°C.

Table 3: Results of porosity measurements

porosity	**unit**	**Ord. mortar**	**M2Q 90**	**B4Q 90**
total porosity	Vol.-%	17.4	13.1	8.9
fraction gel pores	Vol.-%	7.3	12.1	8.3
fraction capillary pores	Vol.-%	9.9	0.9	0.4
fraction raw pores	Vol.-%	0.2	0.1	0.2
Hg-porosity (420 N/mm²)	Vol.-%	14.8	6.7	2.5

The ultra high-performance concrete has a lower porosity as the ordinary reference mortar because of it's higher packing density. The difference in porosity is the fraction of the pores. UHPC consists mostly of gel pores while the reference mortar has more capillary pores.

3 Mass transfer coefficients in the building material matrix

The corrosive process in concrete is mostly caused by the transport of fluids and gases. Because of their minimum of capillary pores the ultra high-performance concrete is more resistant in corrosive environment as an ordinary mortar. In the following the water absorption and the diffusion coefficients will be presented.

3.1 Water absorption

The determination of the capillary water absorption was carried out on concrete cubes (a = 40 mm) and was determined by gravimetric weighing. The depth of immersion in water was about 3 mm.

In Figure 1 is showed the capillary water absorption of ultra high-performance concrete and the ordinary reference mortar. The water absorption coefficient w_{24} is determined after 24 hours. It equals to 0.033 kg/m²h$^{0.5}$ for the mixture M2Q and 0.044 kg/m²h$^{0.5}$ for the mixture B4Q. For the ordinary reference mortar the water absorption coefficient amounts to 1.84 kg/m²h$^{0.5}$. As expected the water absorption of ultra high-performance concrete is much lower than the ordinary reference mortar or high-performance concrete.

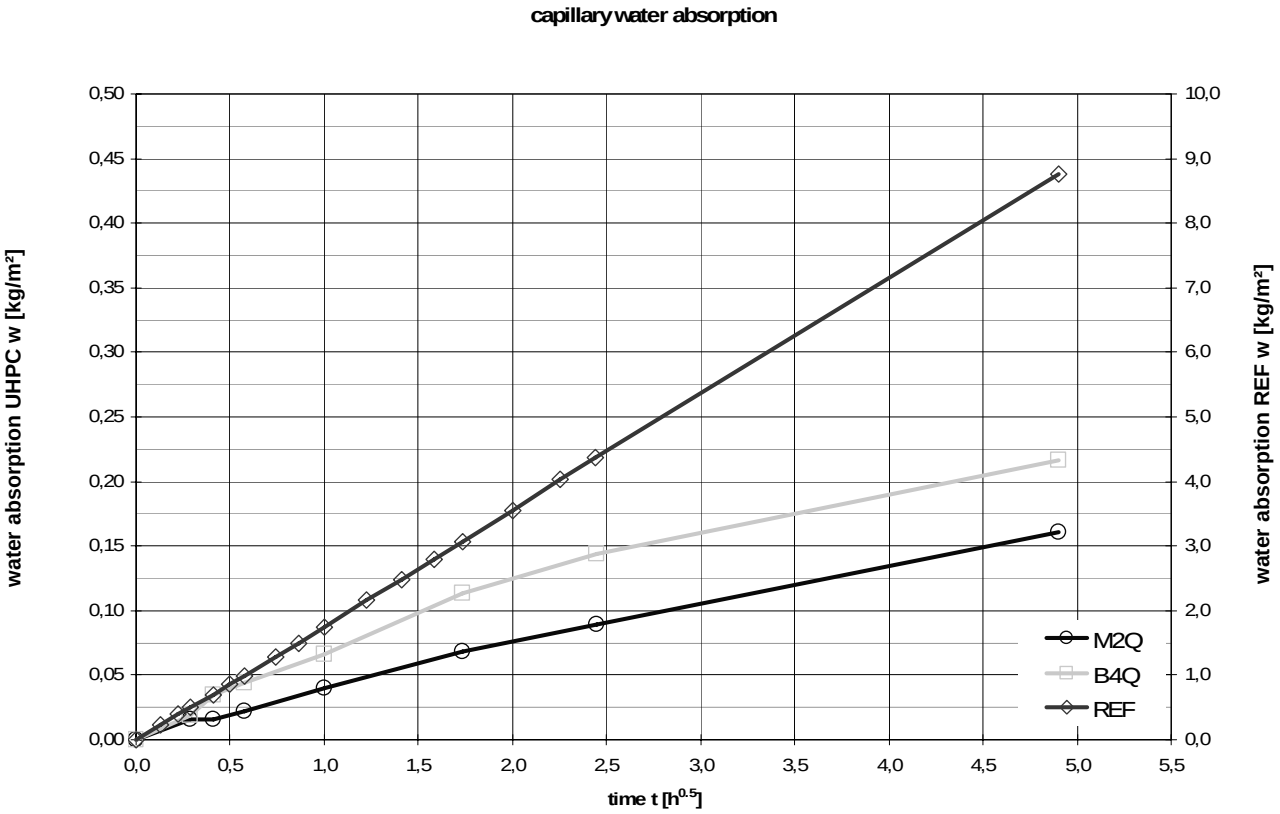

Figure 1: Water absorption of UHPC (left) and ordinary reference mortar (right)

3.2 Diffusion in an electrical field

The diffusion coefficients of concrete are determined by using an electrical field method measurement. This optimized method was developed in the institute of the authors. It will be acquired how much greater is the diffusion resistant W_{spec} of a specimen compared to the diffusion coefficient $D_{i,free}$ in free solution.

$$D_{spec} = W_{spec} \cdot D_{i,free} \quad (1)$$

In this work the cation Na^+ is used for this diffusion method. The diffusion coefficient $D_{Na,free}$ of Na^+ in free solution amounts to $1.344*10^{-9}$ m²/s. The experimental results are presented in Table 4. The diffusion resistance of UHPC is also much better than the ordinary reference mortar. Because of knowledge of the total porosity it is possible to calculate the tortuosity τ of the materials. This parameter is necessary for numerical simulation.

Table 4: Results of diffusion measurements

diffusion resistance	unit	Ord. mortar	M2Q 90	B4Q 90
W	-	40	1500	2500

4 Investigations to durability

As mentioned above, ultra high-performance concretes have a much better packing density than the ordinary reference mortar. Because of these results a higher resistance of UHPC against to chemical attack will be indicated. But also a really dense concrete is not inert against acid or salt due to soluble components in the cement paste. Depending on the kind of acid or salt attack it could be important to get a high basic buffer potential without influence on the porosity. This could be realised by adding unreacted cement with high density in the cement paste like in ultra high-performance concrete.
To characterise the resistance of UHPC against acid or salt attack, corrosion experiments with ultra high-performance concrete and ordinary reference mortar has been carried out. The ordinary reference mortar is stored in the same corrosive environment like the UHPC. The test program and the results of these experiments are shown in the following parts.

4.1 Attack of aggressive acid solutions

A important part of the investigations are experiments in aggressive acid solutions. The specimens (40 x 40 x 80 mm³) of the ultra high-performance concrete and ordinary reference mortar are stored in sulphuric acid and lactic acid. By using a dynamic multitasking titration system (MultiT) the pH value is always constant and the consumption of protons is recorded. The boundary conditions of this investigation are listed in the following.

- Exposure time ≥ 8000 h
- Chemical attack by using sulphuric acid with a pH value of 3 and 4 (M2Q, B4Q, REF)
- Chemical attack by using lactic acid with a pH value of 4 (M2Q, REF)
- Constant temperature of T = 20°C
- Constant mixing of the solution using magnetic mixers

In Figure 2 you can see the chemical laboratory of the institute with some of the measurement properties.

Figure 2: Ultra high-performance concrete in sulphuric acid pH 3, chemical laboratory

To minimize the influence of foreign ions in the solution, the aggressive water is renewed every 1000 hours during the complete exposure time. At the end of the experiment the specimens are getting of all loose particles using a wire brush. The alteration of the external dimensions is represented by the erosion depth X_A. The visual corrosion depth X_V is measured using the phenolphthalein method and by a light microscope. In addition a new method to calculate the corrosion depth X_{VR} was developed. This corrosion depth is determined on the basis of the consumption of protons (can be extrapolated) during the embedding experiments and the total consumption of protons caused by a powdered specimen. To calculate the corrosion depth X_{VR} the following parameters must be determined.

- total consumption of protons of a powdered specimen after oven drying at 105°C: $H^*_M = H_M \cdot \rho_{M,tr}$ in gH^+/dm^3
  with dry bulk density $\rho_{M,tr}$ in g/cm^3 and H_M in gH^+/kg_{mortar}
- consumption of protons of the embedded specimens in the acid solution for the interested exposure time $H_{M,t}$ in the unit gH^+/dm^2

$$X_{VR} = \frac{H_{M,t} \cdot 100}{H^*_M} \quad [mm] \tag{2}$$

The corrosion depth, the consumption of protons and the bulk density of the examined concretes in sulphuric acid are shown in Table 5 and Table 6.

Table 5: Results of the sulphuric investigations at pH3 after 8000 h

results	**unit**	**Ord. mortar**	**M2Q 90**	**B4Q 90**
consumption of protons $H_{M,t}$	gH^+/dm^2	0.257	0.253	0.249
consumption of protons H_M	gH^+/kg_{mortar}	5.83	9.33	7.43
bulk density $\rho_{M,tr}$	g/cm^3	2.115	2.19	2.34
corrosion depth X_{VR}	mm	2.08	1.23	1.43

Table 6: Results of the sulphuric investigations at pH4 after 8000 h

results	**unit**	**Ord. mortar**	**M2Q 90**	**B4Q 90**
consumption of protons $H_{M,t}$	gH^+/dm^2	0.145	0.131	0.125
consumption of protons H_M	gH^+/kg_{mortar}	5.33	8.45	5.98
bulk density $\rho_{M,tr}$	g/cm^3	2.115	2.19	2.34
corrosion depth X_{VR}	mm	1.32	0.71	0.89

The resistance of both ultra high-performance concretes in sulphuric acid environment at pH3 and pH4 is much better than the resistance of the ordinary reference mortar.
In lactic environment at pH 4 the corrosion depth of the ordinary reference mortar is determined to 3.7 mm. The corrosion depth of the UHPC mixture M2Q is much lower and amounts to 1.7 mm. The high leaching zone of the reference mortar is shown in Figure 3 on the left. Both samples on the right were treated with phenolphthalein.

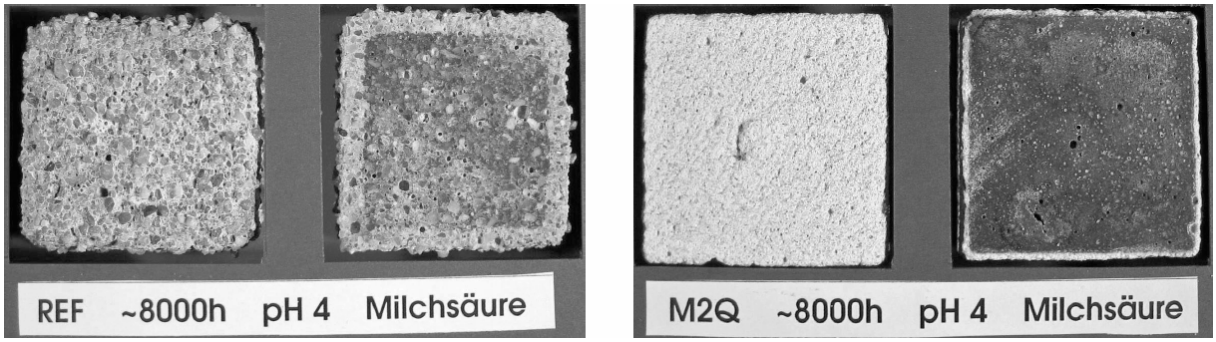

Figure 3: REF (left) and UHPC (right) in lactic acid at pH 4 after 8000 h

4.2 Attack of aggressive salt solutions

The experimental design to test the behaviour of ultra high-performance concrete in salt solutions is similar to the acid investigations. The boundary conditions are as follows.

- Exposure time ≥ 8000 h
- Chemical attack by ammonium nitrate with a concentration of NH_4^+ about 100 mg/l and 11250 mg/l (M2Q, REF)
- Chemical attack by sodium sulphate with a concentration of SO_4^{2-} about 6000 mg/l and 33800 mg/l (M2Q, REF)
- Constant temperature of T = 20°C
- Constant mixing of the solution using magnetic mixers

The solution is renewed every 500 hours to get a constant concentration and to minimize the influence of foreign ions. Every 500 hours the alteration of weight and the dissolved mass of calcium in the solution is determined. After the experiment the erosion depth X_A and the visual corrosion depth X_V is measured.

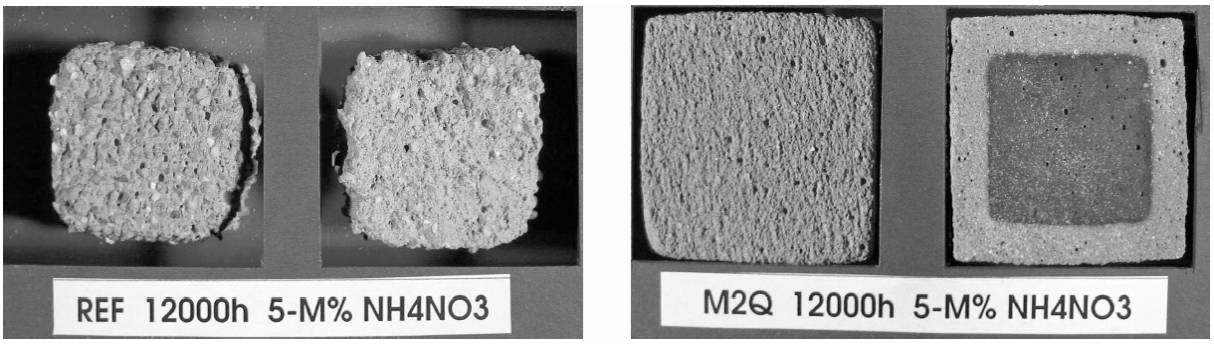

Figure 4: REF (left) and UHPC (right) in ammonium nitrate solution after 12000 h

Figure 4 shows the ordinary reference mortar and ultra high-performance concrete after 12000 hours in ammonium nitrate solution. Both samples on the right were treated with phenolphthalein, too. The results of this investigation are shown in Table 7. Even though the ultra high-performance concrete has a higher amount of calcium in cement paste, the

concentration of dissolved calcium in the solution is lower than that of the reference mortar. This indicates a much deeper leaching zone of the reference mortar and the better resistance of ultra high-performance concrete against aggressive ammonium solutions.

Table 7: Results of the ammonium investigations NH_4^+ = 11250 mg/l after 12000 h

results	**unit**	**Ord. mortar**	**M2Q 90**
loose of weight	%	9.7	8.1
concentration of dissolved calcium	g/m²	1502	1477
erosion depth	mm	3.9	0.4
visual corrosion depth X_V	mm	20.3	6.7

In sodium sulphate solution (SO_4^{2-} = 33800 mg/l) the resistance of ultra high-performance concrete is also better than the reference mortar. The corrosion depth after 12000 hours amounts to 0.9 mm for UHPC and about 1.7 mm for reference mortar.

5 Conclusions

The behaviour of ultra high-performance concrete in sulphuric acid, lactic acid, ammonium nitrate solution and sodium solution was tested in lab and was compared with an ordinary reference mortar. Furthermore a new method to calculate the corrosion depth for a long exposure time was developed and described.

It was shown that the UHPC has a better resistance against the investigated chemical attacks compared to the reference mortar. In sulphuric acid pH 3 the corrosion depth of ultra high-performance concrete is the same as the reference mortar in pH 4. Also in comparison to the leaching zone of the aggressive salt environment in the reference mortar the zone developed in UHPC was small due to its high packing density.

In the near future it will be possible to calculate the corrosion process using simulation software. For this work the simulation software ASTra [2] was developed and expanded.

6 References

[1] L. Franke, M. Oly, S. Witt: Richtlinie für die Prüfung von Mörteln von Mörteln für den Einsatz im Sielbau, Fassung 2001.

[2] L. Franke, R. Espinosa, G. Deckelmann, C. Gunstmann, D. Bandow: ASTra – Simulationsprogramm des allgemeinen Stofftransportes in porösen Baustoffen, 12. Bauklimatisches Symposium, Dresden 2007.

[3] L. Franke: Korrosion von Zementstein in sauren Wässern, Materials Science and Restoration, Vol 3, Aedificatio Publishers, IRB-Verlag 1996.

[4] L. Franke, J. Kiekbusch: Behaviour of High-Performance Concrete under Acid Attack, In: International Conference on Durability of HPC and Final Workshop of CONlife, Aedificatio Publishers, pp. 331-320, Freiburg 2004.

[5] E. Nägele, B. Hillemeier, H. K. Hilsdorf: Der Angriff von Ammoniumlösungen auf Beton, Beton + Fertigteiltechnik 11/1984 p. 742.

[6] H. Dorner: Säurewiderstand von Hochleistungsbetonen, Beitrag 38. Forschungskolloquium DAfStb, TU München 2000.

Thorsten Stengel
Dipl.-Ing.
Technische Universität München
Centre for Building Materials (cbm)
Munich, Germany

Peter Schießl
Univ.-Prof. Dr.-Ing. Dr.-Ing. E.h.
Technische Universität München
Centre for Building Materials (cbm)
Munich, Germany

Sustainable Construction with UHPC – from Life Cycle Inventory Data Collection to Environmental Impact Assessment

Summary

The results of a research project aimed at developing a scientific basis for the life cycle assessment (LCA) of ultra high performance concrete (UHPC) are presented from which the environmental impact of UHPC production is derived for the first time. The environmental impact of UHPC production is mainly due to the manufacture of micro steel fibres, cement and superplasticizer. To reduce environmental impact it is necessary to lower the quantity of these materials used in the UHPC mix. Based on the results of this study, the environmental impact of existing UHPC bridges and comparable conventional constructions is being currently analysed.

Keywords: *sustainable construction, life cycle assessment, life cycle inventory*

1 Introduction

Structures made from normal concrete with a mass to strength ratio which ranges from 40 to 120 kg / MNm usually require considerable quantities of raw materials. In the case of UHPC, the mass to strength ratio of 15 kg / MNm is lower than that of normal concrete which provides for more economical deployment of resources. However, a disadvantage of UHPC when produced according to current technology is its high cement content which is well above that of normal concrete. Moreover, the high content of high-performance superplasticizer and the use of micro steel fibres increase demands on resources and energy. These factors partially offset the advantages of UHPC. However, the evaluation of the sustainability of building materials requires consideration of many parameters – not just mass to strength ratio. The aim of the research project presented here is the development of a scientific basis for the LCA of UHPC.

2 Environmental Impact Assessment with the Help of LCA

LCA enables estimation of the potential environmental impact of production processes. The procedure is laid down in the standards DIN ISO 14040 ff.. Owing to the large amount of data, LCA is carried out using software and databases for processes and materials. In this study, the software SimaPro and the Swiss ecoinvent database were used. The impact assessment can, in principle, be performed using different methods. Depending on the

particular method, one or more impact category indicators are specified. In this study, the estimation of impact was performed using the CML method in SimaPro where results were obtained for the impact categories global warming (GWP), ozone depletion in the stratosphere (ODP), summer smog, i.e. photo chemical ozone creation (POCP), acidification (AP) and eutrophication (NP).

3 Composition of State-of-the art UHPC

The mean composition of UHPC was investigated based on the evaluation of literature covering the last 10 years. The mean cement content is roughly 750 kg/m^3. If all reactive components are included, the binder content is about 925 kg/m^3. This yields a mean water / binder ratio of 0.20 for a mean water content of 180 kg/m^3. A high content of superplasticizer on polycarboxylate ether (PCE) basis is necessary which is, on average, 30 kg/m^3, i.e. 3.4 wt.% with respect to the binder. The mean content of steel fibres used is 240 kg/m^3 or 3 vol.%. Another literature research [1] yielded similar results. To estimate the environmental impact of UHPC production in the scope of a LCA, production process data for the individual concrete components are required. Process data may be taken directly from or represented by appropriate values in the ecoinvent database for the production of cement, quartz sand and quartz flour as well as the provision of water. In this study, inert powder is represented by a dataset for inert finely ground limestone. The effect of polypropylene fibres is neglected since UHPC contains an average of only 2 kg/m^3 of this material. Process data are not available for the production of micro steel fibres and PCE so far. To obtain process data for these materials it is necessary to analyse the production method and prepare the information so that modelling using the basic ecoinvent modules is possible.

4 Production of Micro Steel Fibres

4.1 General

The production of high strength micro steel fibres can be divided into the subprocesses electric steel production, hot rolling, descaling, dry wire drawing, wet wire drawing, tempering, steel cord strand production and cutting to length, Figure 1. Ecoinvent process data are directly available for the first two subprocesses. In this study, the remaining subprocesses were modelled with the help of other ecoinvent subprocesses.

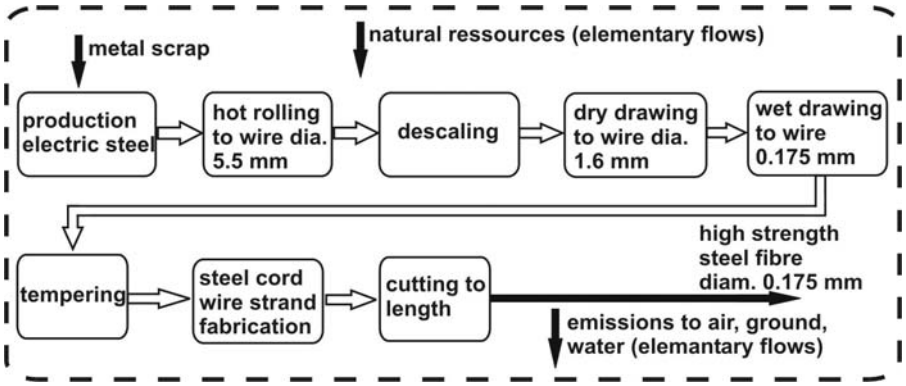

Figure 1: Process stages for the production of high strength steel fibres and system boundary (dashed line)

4.2 Descaling

When hot rolled wire cools down a hard, brittle surface oxide layer known as scale forms which must be removed before the wire can be drawn to smaller diameters. The conventional descaling method is to bend the wire in different directions in order to loosen the scale which is then removed by brushing. Based on data in [2, 3], the descaling machine was assumed to weigh 1 500 kg and operate at a feed rate of 1.25 m/s being electrically powered by 30 kW. It is assumed that 1 g scale per metre wire is removed. The service life of the machine is taken to be 25 years which, when running for 23 hours a day, means an output of 105.68×10^6 kg. The descaling process was modelled using the ecoinvent process data sets for an industrial machine and the energy mix needed for its operation.

4.3 Dry Wire Drawing

Dry wire drawing is performed to pull hot rolled wire down to a diameter of approximately 1.8 mm [4]. Mostly calcium and sodium soaps are used as a dry lubricant. Since friction can cause temperatures as high as 400 °C, the drawing dies are cooled with water and the wire with compressed air. Dry wire drawing machines have as many as 14 consecutive drawing dies each usually separately driven. In this study, it was assumed that the complete machine weighs 25 t and operates at an electric power of 164 kW to draw wire at a speed of 20 m/s. Thus assuming the same operating conditions as for the descaling machine, the total output is 181.11×10^6 kg steel wire. The dry wire drawing process was modelled with ecoinvent process data sets for an industrial machine and the energy mix necessary for its operation. The lubricant was taken into account by a data set for soaps.

4.4 Wet Wire Drawing

During wet wire drawing the wire diameter is reduced to its final value of appr. 0.175 mm. In wet wire drawing machines, a series of drawing and deformation cones are placed beside each other in a “parallel” arrangement and driven by a common electric motor [2, 3]. The wire and dies are cooled with a drawing liquid consisting of an aqueous emulsion of vegetable oils and fats (lubricant). The machine considered in this study draws wire at a speed of 24 m/s and is electrically powered at 40 kW. A machine weight of 2 t was assumed. The drawing liquid is in a bath with a capacity of 700 l and is used over a period of 3 months before renewal. Thus a total of 42 000 l liquid is used during the service life of the machine. A consumption of 2 kg lubricant per tonne of wire is assumed. Applying the same operating conditions as for dry wire drawing, the total output of the wet drawing machine is 2.05×10^6 kg steel wire. The wet wire drawing process was modelled with ecoinvent process data for an industrial machine and the energy mix necessary for its operation. Moreover, the lubricant was taken into account by a data set for lubricating oil and the drawing liquid by water.

4.5 Tempering

Although wire drawing enables tensile strength as high as 4 000 N/mm^2 ductility is lost. To improve ductility, the wire is tempered in a continuous feed method by heating to 500°C and cooling in water or oil [3]. Tempering is performed under an inert gas blanket to avoid

unwanted oxidation reactions. The tempering machine in this study weighs 2.2 t and is able to treat simultaneously 16 wires with diameters around 0.175 mm [5]. The total electrical power for heating is rated at 22 kW. The mean feed speed may be assumed to be 16 m/s so that the total output is 21.91×10^6 kg for the same operating conditions as the above machines. The tempering process was modelled with ecoinvent process data for an industrial machine and the energy mix necessary for its operation.

4.6 Steel Cord Wire Strand Fabrication

Single steel wires are laid in strands by twisting around a common central axis. Strand is easier to handle than wire thus enabling a larger output in fibre production in the last stage of manufacture. Laying is performed by so-called double-twist bunching machines. The pay-off bobbins are located outside the machine and the steel wire cord is produced and spooled inside the laying system. The weight of the stranding machine considered was appr. 15 t and the electric power 43 kW. The laying speed is 2.5 m/s if a twist length of 2 cm and 7 500 wire twists per minute are assumed. A total output of 5.78×10^6 kg results for operating conditions the same as the above machines. The laying process was modelled with ecoinvent process data for an industrial machine and the energy mix necessary for its operation.

4.7 Cutting to Length

In this last sub process the high strength steel wire strand is cut to length producing individual fibres having the required length. This is performed with a wire cutting machine where the required fibre length is set by adjusting feed speed and the speed of a rotating cutter. The wire feed and cutter are powered by an electric motor with a continuously variable rotational speed. The machine considered weighs 700 kg and has an electric power of 5 kW. The total operating time was assumed to be 30 000 h and the mean throughput 150 kg/h [6]. This results in a total output of 4.5×10^6 kg. The cutting process was modelled with ecoinvent process data for an industrial machine and the energy mix necessary for its operation.

4.8 Impact Assessment of the Production of High Strength Steel Fibres

The results of the environmental impact assessment for the production of 1 kg of micro steel fibres are presented in Table 1. Figure 2 shows the contributions of the different sub processes to each impact category.

Table 1: Results of the impact assessment for the production of 1 kg high strength steel fibres

Impact category	Result	Unit
GWP	2,68	kg CO_2-eq
ODP	$1{,}41 \times 10^{-7}$	kg CFC_{11}-eq
POCP	$6{,}86 \times 10^{-4}$	kg C_2H_4-eq
AP	$1{,}41 \times 10^{-2}$	kg SO_2-eq
NP	$1{,}02 \times 10^{-3}$	kg PO_4^{3-}-eq

The largest contribution to the impact indicators is from the wet wire drawing process which lies between approximately 35 and 52%. This is followed by the production of electric steel and steel cord wire strand fabrication which both range approximately from 14 to 32%. Hot rolling contributes about 6 to 15% and dry drawing approximately 3%. The contributions of the remaining subprocesses are all below 1%.

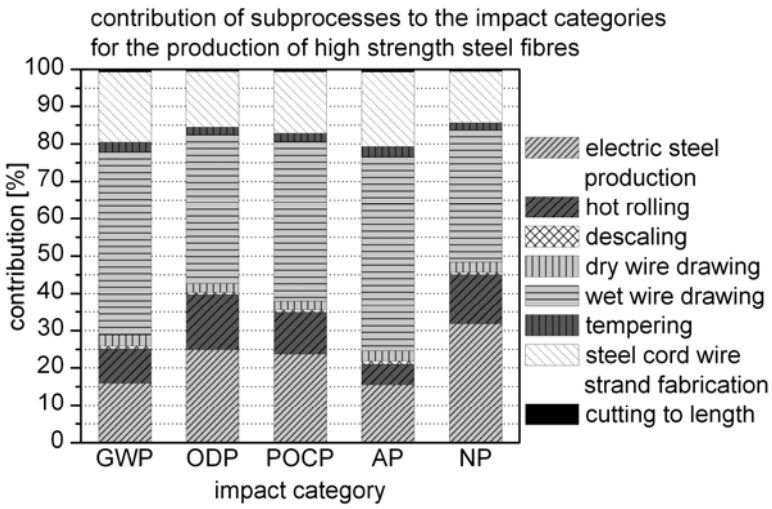

Figure 2: Results of dominance analysis for the production of micro steel fibres

5 Production of Superplasticizer Based on Polycarboxylate Ether

5.1 Raw Materials and Constituents

Polycarboxylate ethers (PCE) contains groups with polyoxyalkylene, especially polyethylene or polypropylene glycol groups as well as carboxylic acid and/or carboxylic acid anhydride monomers, e.g. acrylic acid , methacrylic acid, maleic acid and its anhydride, itonic acid and its anhydride. In addition monomers based on vinyl or acrylate can contribute to the chemistry of PCE. The raw materials and the molecular chaining hierarchy of the constituents for the synthesis of PCE are shown in Figure 3 in a schematic flow diagram. The constituents are represented by ecoinvent process data for acrylic acid, maleic acid, ethylene glycol, sodium hydroxide and hydrogen peroxide. The final product, superplasticizer based on PCE, also contains water and biocides which were also represented with the help of ecoinvent process data. The batch polymerisation process requires a polymerisation plant and suitable industrial buildings. The necessary infrastructure and energy for this was determined in this study.

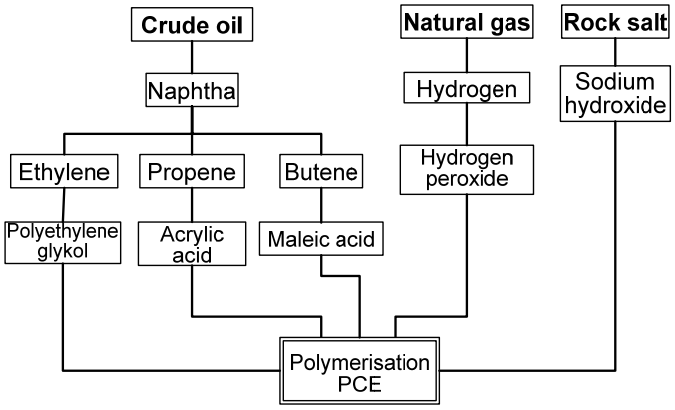

Figure 3: Flow diagram for raw material and chaining hierarchy of constituents for polymerisation of PCE

5.2 Polymerisation Plant

The following information on process engineering for the production of PCE is taken from [7, 8, 9, 10]. PCE plants comprise a number of storage and supply vessels as well a chemical reactor with a capacity usually around 20 m^3. The lid of the reactor is fitted with a cross beam stirrer complete with motor. A supply system is used to charge the reactor with the constituents from above. Beforehand, some of the monomers are transformed into macromonomers in a small agitator container and then transferred with the main charge to the reactor. The main polymerisation reaction is controlled by the dosage of initiator and a heating and cooling system. The temperature of the reactor is maintained at 60 to 80 °C during polymerisation. In this study, the reaction time was set at 5 h. After a cooling phase lasting one hour, neutralisation and the addition of substances such as defoamer and biocides, the reactor can be recharged. The plant in this study weighs 95 325 kg and has electric motors with a total power of 135 kW as well as operation and production buildings with a volume of 35 000 m^3. The service life of the plant is set at 25 years. Working in three shifts, the plant synthesises approximately three times 20 t PCE per day. This corresponds to a total production of 390 × 10^6 kg aqueous polycarboxylate solution for a total operating time of 156 000 h. The polymerisation plant was modelled with ecoinvent process data for an industrial machine, a general operating building and the energy mix necessary for operation.

5.3 Impact Assessment for the Production of PCE

The results of the impact estimation for the production of 1 kg PCE are presented in Table 2. Figure 4 shows the contributions of the different subprocesses to each impact category. The production of maleic acid contributes with 42% most to GWP. This is followed by the production of ethylene glycol, approximately 26%. Acrylic acid and sodium hydroxide each contribute between 10 and 12%, respectively. ODP is dominated by the production of maleic acid , approximately 62%. The production of sodium hydroxide, biocides and ethylene glycol also contribute with between 8 and 11% significantly to this indicator. 99% of POCP comes from the production of acrylic acid.

Table 2: Results of the impact assessment for the production of 1 kg PCE

Impact category	Result	Unit
GWP	1.11	kg CO_2-eq
ODP	6.09×10^{-8}	kg CFC_{11}-eq
POCP	1.97×10^{-2}	kg C_2H_4-eq
AP	4.81×10^{-3}	kg SO_2-eq
NP	1.75×10^{-3}	kg PO_4^{3-}-eq

With 35%, ethylene glycol production has the largest effect on AP. It is followed by the production of acrylic acid, maleic acid and sodium hydroxide which each contribute between 13 and 21% to AP. With 83%, ethylene glycol production clearly dominates NP.

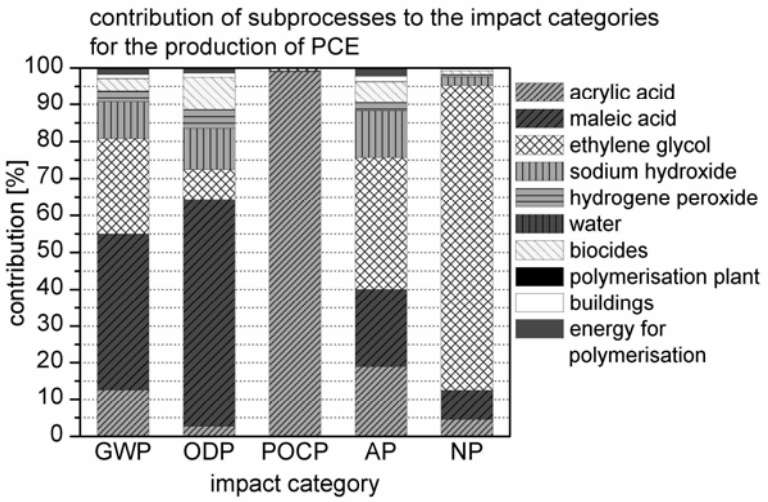

Figure 4: Results of dominance analysis for the production of PCE

6 LCA for a mean UHPC

Based on the process data derived in this study and the ecoinvent process referred to in section 3, it is now, for the first time, possible to estimate the environmental impact of UHPC. The mean UHPC composition in section 3 is used in this calculation. The results of the LCA for the production of 1 m^3 UHPC are presented in Table 3. The corresponding contributions of the subprocesses are shown in Figure 5. The manufacture of micro steel fibres dominates with 48 to 76% the categories GWP, ODP, AP and NP. The contribution from cement production, approximately 20 to 47%, is also considerable for these categories. The impact POCP is essentially due to the production of PCE, 75%, and the production of micro steel fibres, 21%.

Table 3: Results of the impact assessment for the production of 1 m³ UHPC

Impact category	Result	Unit
GWP	1.35×10^{3}	kg CO_2-eq
ODP	5.64×10^{-5}	kg CFC_{11}-eq
POCP	8.12×10^{-1}	kg C_2H_4-eq
AP	4.53	kg SO_2-eq
NP	4.45×10^{-1}	kg PO_4^{3-}eq

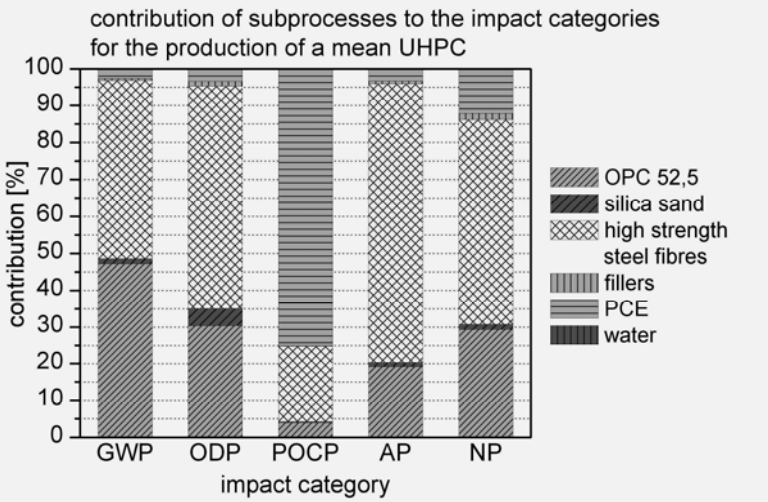

Figure 5: Results of dominance analysis for the production of state-of-the-art UHPC

7 Discussion

The main effect of UHPC production on the environment is caused by the manufacture of micro steel fibres, cement and PCE. Lowering the amount of these materials in UHPC is the easiest way of producing UHPC which is more environment friendly. The amount of fibres could be reduced to an optimum by improving the bond between the fibres and the binder matrix as well as the distribution and orientation of the fibres in UHPC. Since the contribution of wet wire drawing down to diameters around 0.175 mm to the environmental impact of steel fibre production is very large, the use of fibres with larger diameters is recommended. This would also be economically advantageous because micro steel fibre currently cost between 1 800 and 2 000 Euros per tonne and therefore present a high proportion of UHPC production costs. The production of PCE and its constituent acrylic acid cause the most part of POCP in UHPC production. This study did not consider whether use of other basic monomers for PCE production could reduce POCP.

8 Conclusions

The present research project aimed at developing a scientific basis for the LCA of UHPC. The results enabled, for the first time, the estimation of the environmental impact of UHPC production within LCA. It was found that the environmental impact of the UHPC production is mainly due to the production of micro steel fibres, cement and superplasticizer. The verification of the process data, determined in this study for the production of UHPC components, could be performed by process monitoring at the factory. This was not within the scope of the present research project. Moreover, the environmental effect of heat treatment, which is often carried out during UHPC production, was not taken into account. At present, the environmental impact of existing UHPC bridges and comparable conventional constructions is being investigated. Soon an answer could be given to the question as to whether building with UHPC is more sustainable than with conventional materials.

9 Acknowledgements

This research project is part of the German Research Foundation (DFG) priority programme 1182 “Sustainable Building with Ultra High Performance Concrete”.

10 References

[1] Dehn, F.: Ultrahochfester Beton: Technologie und Anwendung, in: Beton, Heft 5, 2004.
[2] Ruge, J.; Wohlfahrt, H.: Technologie der Werkstoffe, Vieweg Verlag, 2001.
[3] Schimpke, P.; Schropp, H.; König, R.: Technologie der Maschinenbaustoffe, Hirzel Verlag.
[4] Schruff, E.: Stahl Lexikon, Wissenschaftsverlag, Mainz, 2004.
[5] www.bongard.de; Rubrik Maschinenliste; 26.05.2006.
[6] Hrsg.: Werner Bolz GmbH: Firmenprospekt Drahtzerkleinerungsmaschinen, Teningen, 2006.
[7] Plank, J. et. al.: Bauchemie. In: Dittmeyer, R. et. al. (Hrsg): Chemische Technik – Prozesse und Produkte; WILEY-VCH Verlag, 2004.
[8] Hirsch, C. M.: Untersuchungen zur Wechselwirkung zwischen polymeren Fliessmitteln und Zementen bzw. Mineralphasen der frühen Zementhydratation; Dissertation, München, 2005.
[9] Ignatowitz, E.: Chemietechnik, Verlag Europa-Lehrmittel, 2003.
[10] Sattler, K.; Kasper, W.: Verfahrenstechnische Anlagen – Planung Bau Betrieb, WILEY-VCH Verlag, 2000.

Isabel Burkart
Dipl.-Ing.
University of Karlsruhe
Karlsruhe, Germany

Harald S. Müller
Prof. Dr.-Ing.
University of Karlsruhe
Karlsruhe, Germany

Creep and shrinkage characteristics of ultra high strength concrete (UHPC)

Summary

An essential precondition for a reliable design of UHPC constructions is a substantiated knowledge about the time-dependent stress-strain behaviour of this material. A comprehensive research programme at the University of Karlsruhe is therefore aiming at the development of suitable material laws and design methods. The related experimental programme includes various creep and shrinkage experiments on different UHPC, considering well known parameters on the deformation characteristics of concrete. As concrete generally shows a distinctive nonlinear deformation behaviour several experiments under varying stress levels will be performed also including the measurement of the creep recovery and relaxation tests.

Keywords: *UHPC, creep, shrinkage, strength limit of sustained loading*

1 Introduction

Due to the distinctive creep and shrinkage capability of concrete the consideration of the time- and load-dependent deformation behaviour is indispensable in corresponding design codes for reinforced and pre-stressed constructions. The material laws developed so far, are based on various experimental investigations performed since the 60’s of the previous century. Primarily developed for normal strength concretes ([1], [2]) they have later been adjusted to the latest developments in concrete technology as for example high-strength concretes and light weight concretes [3].

Ultra high strength concretes (UHPC) are one of the latest and most promising developments in recent years. Although several UHPC constructions have already been realised a profound experimental basis has not been available so far to describe the material and its load bearing behaviour in constructions. For that reason a priority programme was initiated by the German Research Foundation (DFG) financing numerous research projects within a period of six years [4].

Previous to the begin of the priority programme creep of UHPC had only been investigated by a few researchers, using different concrete compositions and considering parameters such as the age at loading and the storing conditions [7], [8]. Despite of the low water content a considerable deformation capability could be observed especially in the young concrete age and even a small drying creep component was measured [9]. Nevertheless the small

number of experimental results does not allow for the development of a corresponding material law and the project at the University of Karlsruhe is therefore aiming at the creation of a sufficient database enabling the development of a thermodynamically sound material law for the time- and load-dependent deformation behaviour of UHPC. The related experimental programme includes various creep and shrinkage experiments, considering well known parameters on the deformation characteristics of concrete. For the quantification of potential nonlinearities several experiments under varying stress levels will be performed also including the recording of the creep recovery and relaxation tests.

The priority programme started in fall 2005 and the experiments performed so far allow for a first estimation of the creep and shrinkage deformations as well as the strength limit of sustained loading. The comparison of these data with a prediction based on models currently used in corresponding German and European design codes revealed that especially the deformations in the young concrete age cannot adequately been predicted. An adjustment of existing creep and shrinkage models is therefore necessary.

2 Experimental programme

2.1 Reference concretes

To ensure the comparability of the experimental results within the priority programme two reference concretes have been determined which shall be investigated within all projects. The composition of the concretes which had originally been developed at the University of Kassel is given in the following Table 1.

Table 1: Composition of the reference concretes

Constituents		**M2Q**	**B4Q**
Cement, CEM I 52.5R HS/NA	kg/m³	832	650
Quartz sand, H33 0.125/0.5 mm	kg/m³	975	354
Basalt 2/8	kg/m³	-	597
Micro silica, MS Grade 983 [1)]	kg/m³	135	177
Steel fibres, Stratec, d/l = 0.15/9 mm/mm (2.5 Vol.-%)	kg/m³	192	194
Quartz powder, Millisil W3	kg/m³	207	325
Quartz powder, Millisil W12	kg/m³	-	131
Superplasticiser	kg/m³	33	30
Water	kg/m³	166	158
w/c-ratio	-	0.2	0.24

[1)] Production of this type of silica has been stopped. Adjustment of the composition is under way

Due to the long duration of the creep and shrinkage tests the experimental programme within the first years focuses on the investigation of the reference concretes. In this publication a first estimation of the deformation behaviour of UHPC is presented based on the experiments on the reactive powder concrete M2Q.

2.2 Mechanical parameters

Within this project the parameters compressive strength f_{cm} and Young‘s Modulus E are determined for the characterisation of the age-dependent mechanical behaviour and additionally f_{cm} serves as an input parameter for the calculation of the stress levels within the creep experiments. All samples were demoulded after 24 hours and stored under water at a temperature of 20 °C. At the concrete age of 7 days the specimens were exposed to a climate of 20 °C and 65 % r. h.

Table 2: Mean values of the compressive strength and the Young’s Modulus (M2Q)

Parameter [MPa]	**Specimen [mm]**	**Age at testing (average over 3 specimens)**				
		1 d	**3 d**	**28 d**	**120 d**	**180 d**
f_{cm}	Cyl. 150 x 300	51	101	166	186	194
E	Cyl. 150 x 300	30.900	40.400	47.700	55.200	55.200

The compressive strength used for the calculation of the stress levels was determined on specimens with a geometry similar to those used in the creep experiments.

2.3 Shrinkage

In combination with published shrinkage experiments the own tests provide a basis for the modelling of the load-independent deformation behaviour of UHPC. Additionally they are indispensable for separating the creep deformations from the total deformations measured in the creep experiments.

Table 3 gives a brief overview over the experimental programme considering parameters such as the specimen’s geometry, the storage conditions and the duration of moisture curing.

Table 3: Shrinkage experiments (climate conditions 20 °C / 65 % r. h.)

Concrete	**Concrete age at begin of drying [d]**	**Specimen diameter [mm]** [2)]
M2Q	1	100
	2	75 / 100 / 150
	7	100
	sealed [1)]	100

[1)] Begin of measurement at the concrete age of 1 day

[2)] Cylinder height to diameter equals 3

The shrinkage deformations measured on unsealed specimens consist of autogenous shrinkage deformations and drying shrinkage deformations resulting from moisture loss. The two components may only be separated by the investigation of both sealed (by means of aluminium tape coated with butylcaoutchouc) and unsealed specimens. The corresponding data is shown in the left diagramme of Figure 1, whereas the curves represent the mean values measured on two identical specimens (d = 100 mm). The begin of measurement coincided with the begin of drying at the concrete age of 1 day. Due to the low water content of UHPC, only marginal drying shrinkage deformations had been expected. This is confirmed

by the deformations of the sealed and unsealed specimens which hardly show any differences.

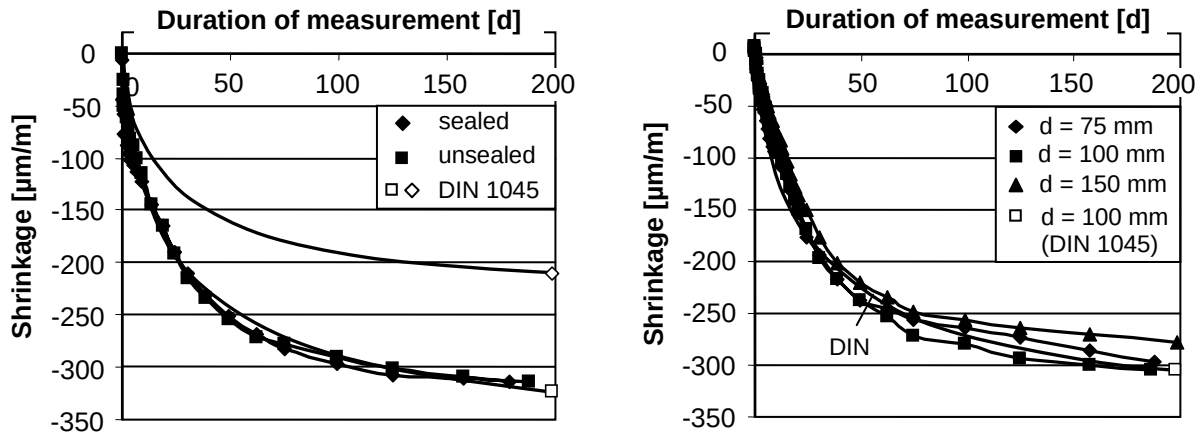

Figure 1: Shrinkage deformations of M2Q; left: Influence of storage conditions, begin of drying t_s = 1 d, d_{cyl} = 100 mm; right: Influence of specimen size, t_s = 2 d; the prediction according to German standard DIN 1045 is plotted as well

In Germany the consideration of shrinkage in the design of concrete structures (according to DIN 1045) is based on a model, which was originally developed for normal strength concretes and in the meantime has been extended to high strength concretes [3]. The comparison of the prediction according to DIN 1045 – which is not valid for UHPC – with the deformations of the sealed and unsealed specimen (see Fig. 2, left) gives first evidence, that the autogenous shrinkage is significantly underestimated in the young concrete age, whereas the drying shrinkage component is overestimated. Nevertheless the total shrinkage deformations of an unsealed specimen are well predicted.

The influence of the specimen size on the magnitude and the time-development of shrinkage has been investigated on unsealed cylinders with diameters of 75, 100 and 150 mm. The specimens were moisture cured up to the begin of measurement at the concrete age of 2 days. As also considered in the prediction according to the German standard, an increase in the specimen size has no influence on the magnitude of both autogenous and drying shrinkage but is delaying the time-development of diffusion processes. As the drying shrinkage component of this UHPC is negligibly small the differences between the curves in the right diagram of Figure 1 mainly result from scatter.

Furthermore the influence of the duration of moisture curing on the final value of drying shrinkage was investigated on unsealed cylinders with a diameter of 100 mm. The concrete age at the begin of drying was 1 d, 2 d and 7 d, which corresponded to the respective begin of measurement. Though hardly any drying shrinkage could be observed on this UHPC no final conclusions should be drawn before the investigation of further concrete mixes.

The analysis of published experimental data and a comparison with own results have shown a large scatter of the measured final shrinkage values between 0.2 and 1.0 ‰. Main parameters affecting shrinkage are the water/binder-ratio and the – compared to normal

strength concrete – considerably higher cement content which increases the total shrinkage deformation. Nevertheless the large scatter does not seem to be founded in the concrete composition but in the concrete age at begin of measurement. With measuring devices enabling a begin of measurement a few hours after casting large deformations have been observed within the first 24 hours [5].

2.4 Creep

Numerous experiments have shown that creep of normal and high strength concretes is influenced by various parameters, such as the age at loading, the storing conditions, the specimen size and geometry and the stress level. These experiences were considered in the experimental programme of this project, given in the following Table 4.

Table 4: Creep experiments (climate conditions 20 °C / 65 % r. h.)

Concrete	Age at loading [days]	Storing conditions	Specimen diameter [mm]	Stress level [-]
M2Q	1	unsealed/ sealed	100	0.30 / 0.60
	3	unsealed	75 / 100 / 150	0.30 / 0.60
		sealed	100	0.30 / 0.60
	28	unsealed/ sealed	100	0.30 / 0.60
	180	unsealed	100	0.60

The comparison of creep experiments under different stress levels (here 30 and 60 % of the compressive strength at the age at loading, respectively) gives information about the linearity of concrete creep. In each experiment the deformations of two identical specimens are recorded, the data shown in the following diagrams, however, are the calculated mean values.

Except for the creep experiments starting at the concrete age of 1 day, all unsealed specimens were moisture cured up to the age of 2 days and afterwards moved to a climate of 20 °C and 65 % r. h. which also corresponded to the test conditions. The sealed specimens were enwrapped at the age of 1 day.

The influence of the concrete age at loading on the deformation behaviour of UHPC is investigated by experiments starting at the age of 1, 3, 28 and 180 days. The left hand side of Figure 2 shows the relation between specific creep (creep per unit stress) and age at loading of 1 and 3 days under a stress level of 30 % (d = 100 mm, unsealed). As already observed in experiments on normal and high strength concretes the creep ability is decreasing with increasing concrete age.

Considering creep one usually distinguishes between basic creep (measured on sealed specimens) and the additional drying creep deformation of unsealed specimens initiated by a water loss of the concrete. Resulting from a relocation of water and sliding processes on microstructure basic creep is independent of the size of the specimen. In contrast thereto the thickness of a concrete member influences the diffusion processes and therefore the drying

creep rate. Analysing the shrinkage experiments, only marginal drying shrinkage deformations could be observed. The same could be expected for the drying creep component which is partly confirmed by the data in the right diagram of Figure 2 showing the specific creep of unsealed specimens with diameters of 75, 100 and 150 mm. The age at loading was 3 days and the stress level 30 %. No significant difference could be observed between the creep capabilities of the specimens with a diameter of 100 and 150 mm. In contrast thereto creep of the smallest specimen seemed to be larger. However, own experiences in the past have shown that the measured deformations of these specimens are not only influenced by the concrete itself, but also by the casting method and the sample preparation, especially regarding compacting and grinding of the cylinders. Therefore a final conclusion on the creep behaviour of small specimens compared to larger geometries does not seem reasonable before the analysis of further experiments.

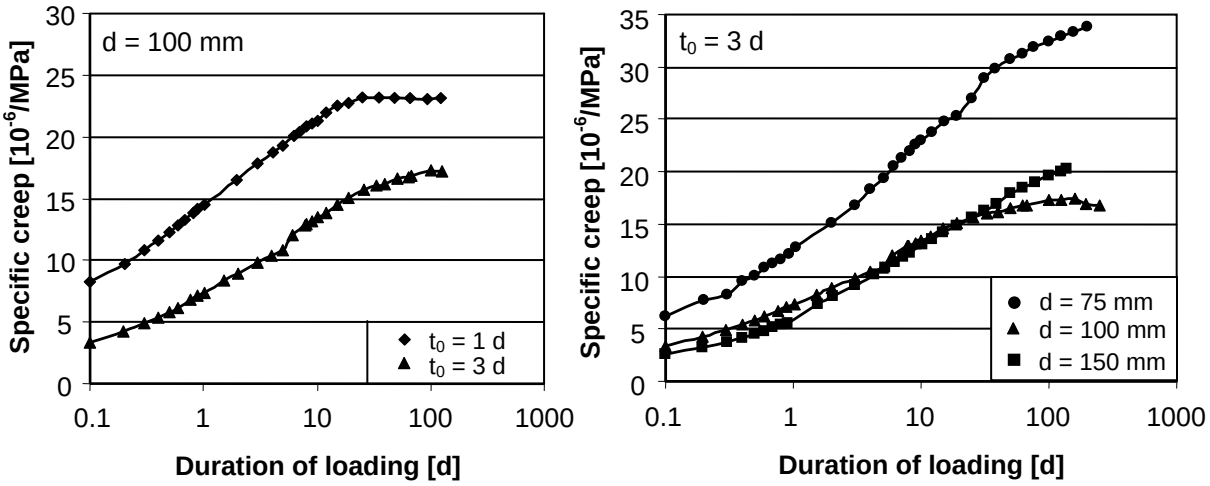

Figure 2: Specific creep of M2Q dependent on the age at loading (left) and the specimen size (right)

The distinctive time- and load-dependent deformation behaviour of concrete has been considered for decades in corresponding design codes. Main input parameter is the creep coefficient expressing the ratio between creep deformation and elastic deformation at the age of 28 days resulting from a certain stress. In Figure 3 the curves marked with filled symbols describe the time-development of the creep coefficient calculated from the experiments on unsealed cylinders (d = 100 mm) under a stress level of 30 % at an age of 1 and 3 days, respectively. The comparison of the experimental data with the prediction according to the German design code DIN 1045 – which is not valid for UHPC – shows that the deformation capability of young UHPC is underestimated considerably and the measured deformations develop much faster.

Resulting from the marginal drying of the specimens the curves given in Figures 2 and 3 mainly represent basic creep deformations. The time-development of basic creep has often been predicted by using a logarithmic function which turns into a straight line in the half logarithmic scale [10]. The given curves, however, show the trend of a hyperbolic function

which has mainly been used to model the drying creep component [6]. But before drawing final conclusions this observation will have to be confirmed by further experiments.

The creep model of DIN 1045 is valid within the range of service stresses ($\sigma \leq 0.4 \cdot f_{cm}$), where creep is assumed to be linearly related to the creep inducing stress. However, the analysis of numerous experiments on normal and high strength concretes has shown an over proportional creep capability with increasing stress levels even within the range of service stresses. As the limit between linear and nonlinear creep is increasing with the compressive strength, a limit above the originally defined range of service stresses is expected for UHPC.

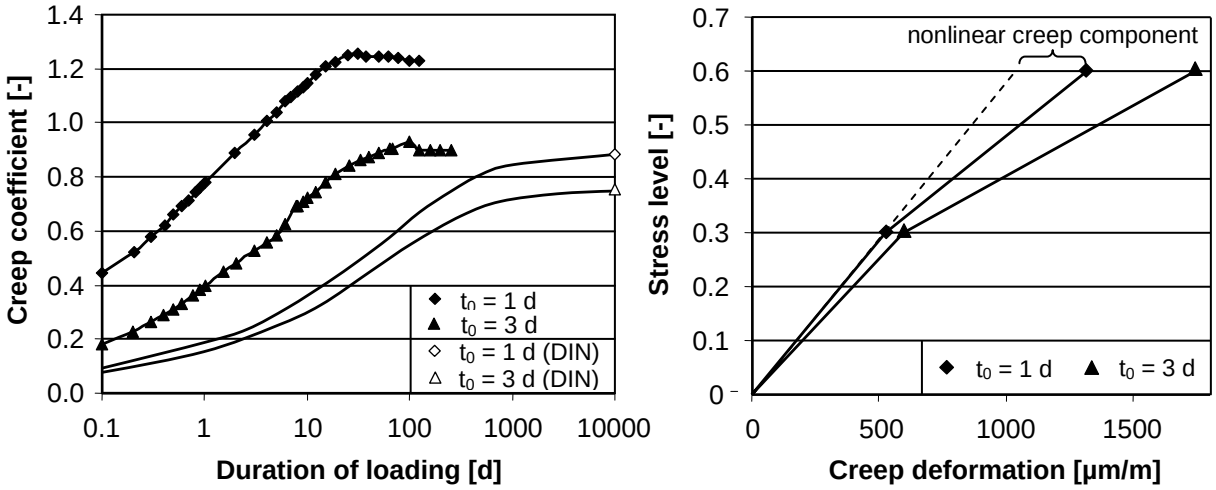

Figure 3: Measured and predicted (DIN 1045) creep coefficients dependent on the age at loading (left) and nonlinearity of creep after a duration of loading of 100 days dependent on the age at loading (right)

Within this project stress levels of 30 and 60 % of the corresponding compressive strength were applied at different ages at loading. This does not allow for the exact determination of the limit between linear and nonlinear creep, but it enables a first estimation of the nonlinear creep behaviour under high stress levels. The relation between stress level and resulting creep deformation is shown on the right side of Figure 3, exemplarily for the deformations measured after a duration of loading of 100 days. The unsealed cylinders (d = 100 mm) were loaded at the age of 1 and 3 days with stress levels of 30 and 60 %. The comparison of the curves shows an increasing nonlinearity with increasing age at loading, probably resulting from the time-development of the compressive strength. During the experiment the initial stress level is reduced all the more the younger the concrete is.

In various creep experiments on normal strength concretes a decrease of the nonlinearity with increasing duration of loading was observed [6]. As the own experiments have not shown a uniform tendency, yet, a final conclusion should not be drawn before the end of the entire experimental programme.

2.5 Strength limit of sustained loading

The strength limit of sustained loading is influenced by two contradicting processes which are on one hand the increase of the compressive strength of the cement paste due to the

ongoing hydration and on the other hand the development of micro cracks. Within this project the strength limit of sustained loading is therefore determined on young UHPC at the age of 1 day and additionally at the age of 28 days where the strength gain has almost been completed. Resulting from the rapid hydration at the age of 1 day the strength limit of sustained loading lies presumably in the range of a relatively high value of 90 % of the short-time strength. The experiments at the age of 28 d are still under way, but from first results a higher strength limit than observed on normal strength concretes can be expected.

3 Conclusions

Various experiments have shown a distinctive deformation capability of UHPC especially in the young concrete age which should not be disregarded in design codes for UHPC constructions. As UHPC is a relatively new material, the development of corresponding material laws is still at the beginning. The experimental results presented in this paper are the first part of an extensive experimental programme designed for an overall period of six years aiming at the development of a thermodynamically sound constitutive approach.

4 Acknowledgement

The authors gratefully acknowledge the financial support provided by the German Research Foundation (DFG) within the priority programme “Sustainable Building with Ultra High Performance Concrete (UHPC)” [4].

5 References

[1] Eurocode No. 2 (EC 2): ENV 1992-1, Design of Concrete Structures. Part 1: General rules and rules for buildings, European Committee for Standardization (CEN), 1991

[2] Comité Euro-International du Béton (CEB): CEB-FIP Model Code 1990. CEB Bulletin d’Information, No. 213/214, Lausanne, Schweiz, 1993

[3] DIN 1045: Tragwerke aus Beton, Stahlbeton und Spannbeton. Teil 1: Bemessung und Konstruktion, Ausgabe Juli 2001 (in German)

[4] DFG-Priority Programme SPP 1182 “Sustainable Building with Ultra High Performance Concrete (UHPC)”. URL: http://www.uni-kassel.de/fb14/baustoffkunde/spp/

[5] Müller, H. S.; Kvitsel, V.: Kriechen und Schwinden von Hochleistungsbetonen. Beton 1+2 / 2006, pp. 36-42 (in German)

[6] Müller, H. S.: Zur Vorhersage des Kriechens von Konstruktionsbeton. Dissertation, University of Karlsruhe, 1986 (in German)

[7] Fehling, E., Schmidt, M., Teichmann, T., Bunje, K., Middendorf, B.: Entwicklung, Dauerhaftigkeit und Berechnung Ultra-Hochfester Betone (UHPC). Forschungsbericht an die DFG, Projekt Nr. FE 497/1-1, University of Kassel, 2003 (in German)

[8] Acker, P., Behloul, M.: Ductal® Technology: A Large Spectrum of Properties, a Wide Range of Applications. In: Schmidt, M., Fehling, E., Geisenhanslüke, C.: Ultra High Performance Concrete. Int. Symp. on Ultra High Performance Concrete, University of Kassel, 13.-15. Sept., 2004

[9] Ma, J., Schneider, H.: Creep of ultra-high performance concrete under compressive stresses. Leipzig Annual Civil Engineering Report, No. 8, 2003

[10] Bazant, Z. P., Chern, J.-C.: Log double power law for concrete creep. ACI Journal, Sept./Oct. 1985, No. 5, pp. 665-675

Manfred Curbach
Prof. Dr.-Ing.
TU Dresden
Dresden, Germany

Kerstin Speck
Dipl.-Ing.
TU Dresden
Dresden, German

Ultra High Performance Concrete under Biaxial Compression

Summary

Ultra high performance concrete (UHPC) is characterized especially by high compressive strength up to 250 N/mm² as well as high impermeability and resistance to corrosion. These properties go along with increasing brittleness. Brittle concretes have lower scaled strength under multi-axial load compared to ductile normal strength concrete. The effective application of UHPC requires specific knowledge of load bearing behaviour under multi-axial stress conditions. This paper describes the behaviour of UHPC under biaxial compressive load in comparison to normal strength concrete. It will show that the calculation approach for EN 1992-1-1 is not transferable to UHPC unreservedly.

Keywords: *biaxial compression, stress-strain-behaviour, strut-and-tie-model, transversal isotropy*

1 Introduction

Multi-axial states of stress occur in many places of building structures. The increased strength under multi-axial compression load often is left unconsidered for the dimensioning, e.g. of columns. The core cross-section is confined by stirrups; therefore the core is under triaxial compression. The resultant strength increase is disregarded for design. In contrast to that multi-axial strength is explicitely considered by using strut-and-tie-models. Accordingly, the design strength for concrete struts should to be reduced in cracked compression zones. Under specific conditions the uni-axial design stress values for compression nodes may be increased by up to 10 % [1]. In normal strength concrete, this increase is conservative for all biaxial stress ratios, figure 1. The percental increase of strength under multi-axial compression stress decreases with increasing uni-axial strength and decreasing ductility. For high strength concrete the strength under stress ratio $\sigma_1 = \sigma_2$ is only 8 to 10 % higher than under uni-axial strength [2], [3]. Increasing the ductility by adding a fibre mix of steel- and polypropylene-fibres the load bearing behaviour develos near to the behaviour of normal strength concrete [4], [5]. As for the further embrittlement of ultra high performance concrete, a further decrease of the scaled biaxial strength may be expected.

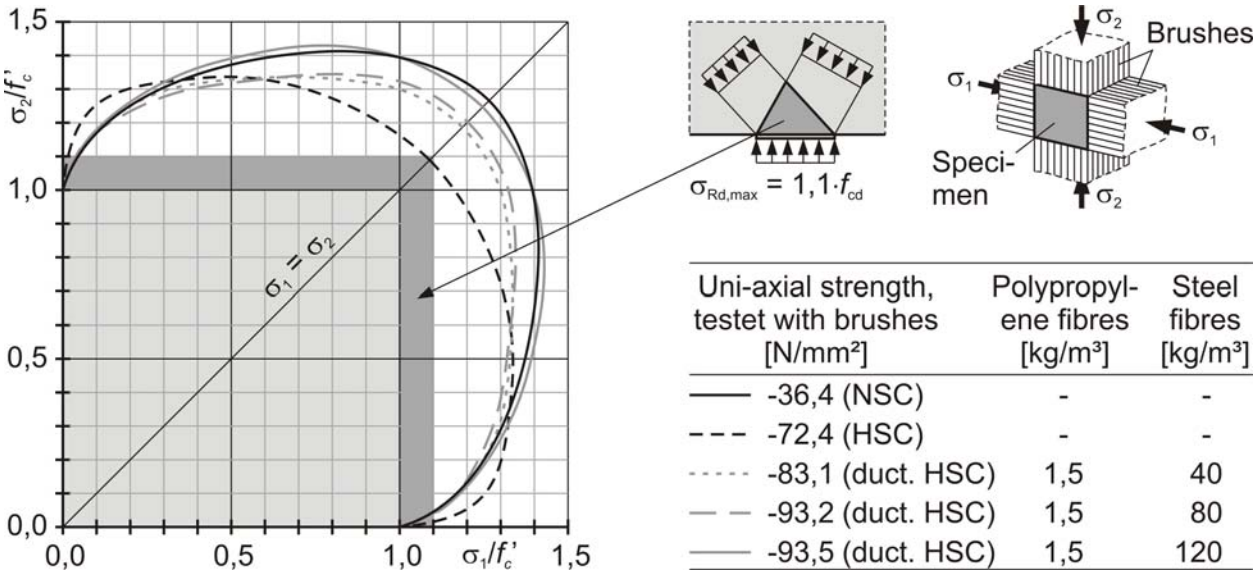

Uni-axial strength, testet with brushes [N/mm²]	Polypropyl-ene fibres [kg/m³]	Steel fibres [kg/m³]
—— -36,4 (NSC)	-	-
– – – -72,4 (HSC)	-	-
····· -83,1 (duct. HSC)	1,5	40
— — -93,2 (duct. HSC)	1,5	80
—— -93,5 (duct. HSC)	1,5	120

Figure 1: Biaxial compression strength of normal strength concrete, high strength concrete and ductile high strength concrete compared to approach for multi axial strength in compression nodes of strut-and-tie-models, EN 1992-1-1:2003 [1]

2 Experimental Program

2.1 Material Properties

The tests were carried out within the framework of the DFG-Priority Program 1182 “Sustained Constructing with Ultra High Performance Concrete (UHPC)”. In the Priority Program, two reference mixtures are examined: fine-grained mixture M2Q-2,5 (D = 0.5 mm) and coarse-grained mixture B4Q-2,5 (D = 8 mm). Both mixtures contain fibres with a length of 9 mm and a diameter of 0.15 mm. Yet, the coarse-grained mixture is also applied with longer fibres but less fibre content. For the examination of columns (Dr. Teutsch, Braunschweig), mixture B4Q-1,25 is used, whereas for the examination of shear connector (Prof. Hegger/ Prof. Tue, Leipzig/Aachen) mixture B4Q-0,9 used. In both projects, multi-axial stress states occur. Therefore, these mixtures have been incorporated into the bi-axial experimental program. The examinations are completed by a fibre-free reference mixture, table 1.

Due to the production technology, the fibres were mainly horizontally oriented in the fine-grained mixture M2Q-2,5. The resulting effect is a transversal isotropic material behaviour. The basalt supplements in the coarse-grained mixture hinder the even distribution of the fibres, figure 2. The supplements also hinder the horizontal orientation of the fibres. In contrast to fine-grained concrete, coarse-grained concrete can be regarded as isotropic material. The cylindrical compressive strength of the concrete lay between 160 and 170 N/mm² without heat treatment. Coarse-grained concretes tend to have slightly higher strengths than fine-grained concrete. The examined fibre contents do not have a significant influence on the uni-axial compressive strength. It can be deduced from the tensile tests that the tensile strength increases with increasing fibre content and increasing fibre length.

Table 1: Properties of the investigated concretes

		M2Q-2,5	**B4Q-2,5**	**B4Q-1,25**	**B4Q-0,9**	**B4Q-0,0**
Fibre content	Vol.-%	2,5	2,5	1,25	0,9	0,0
Fibre geometry						
Diameter	mm	0,15	0,15	0,38	0,15	-
Length	mm	9	9	30	17	-
Fibre orientation						
vertical	%	~20	~30	~30	~30	-
horizontal	%	~40	~35	~35	~35	-
horizontal	%	~40	~35	~35	~35	-
Compression strength						
Cylinder 30/15 cm	N/mm²	-159,7	-161,2	-	-169,3	-
Cube 10 cm[1)]	N/mm²	-156,4	-169,8	-168,4	-179,9	-172,3
Flexural strength						
Prism 4/4/16 cm	N/mm²	28,9	27,0	34,2	22,9	12,6

1) Tested with steel brushes in the triaxiale testing machine

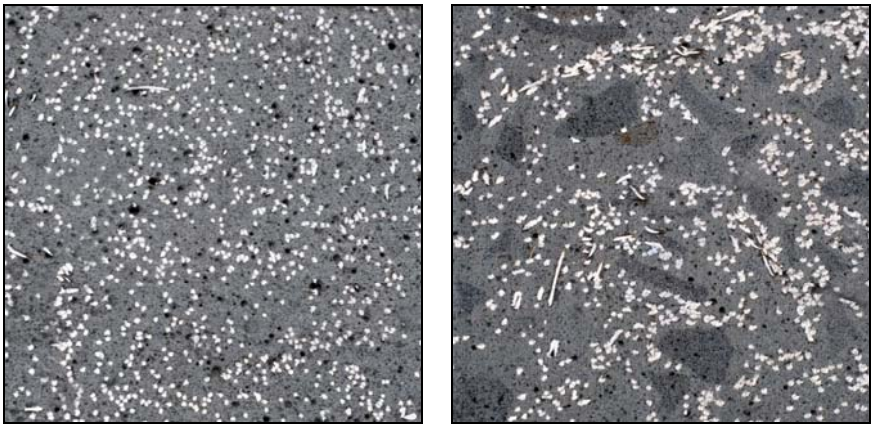

Figure 2: Fibre distribution at fine-grained concrete M2Q-2,5 (left) and coarse-grained concrete B4Q-2,5 (right)

2.2 Experimental Setup and Execution of the Tests

The tests are carried out in a one-piece tri-axial testing machine. A quite stiff steel casting frame encloses the three load axes. There is a cylinder in each axis that can produce pressure of up to 5 MN, figure 3. Cubes with an edge length of 10 cm are used as specimens. Load is applied via steel brushes. These steel brushes follow the deformation of the specimen and do not hinder it. Moreover, they prevent parts of the load being introduced through friction into the load application system of the lateral direction. Therefore, the complete load is ablated parallel through the specimen.

The load components in both directions are increased proportionally. The larger compression component is strain-controlled and is increased with 0.004 mm/s and with 0.002 mm/s respectively close to the peak load. Depending on the force in this direction and the examined stress rate, the lateral direction is stress-controlled. For each stress rate, three to six single tests are carried out.

Strain is measured directly at the specimen with the help of strain gauges and a snap gauge. The deformation of the stress brushes is additionally measured with the help of displacement transducers and then converted to the deformation of the specimens.

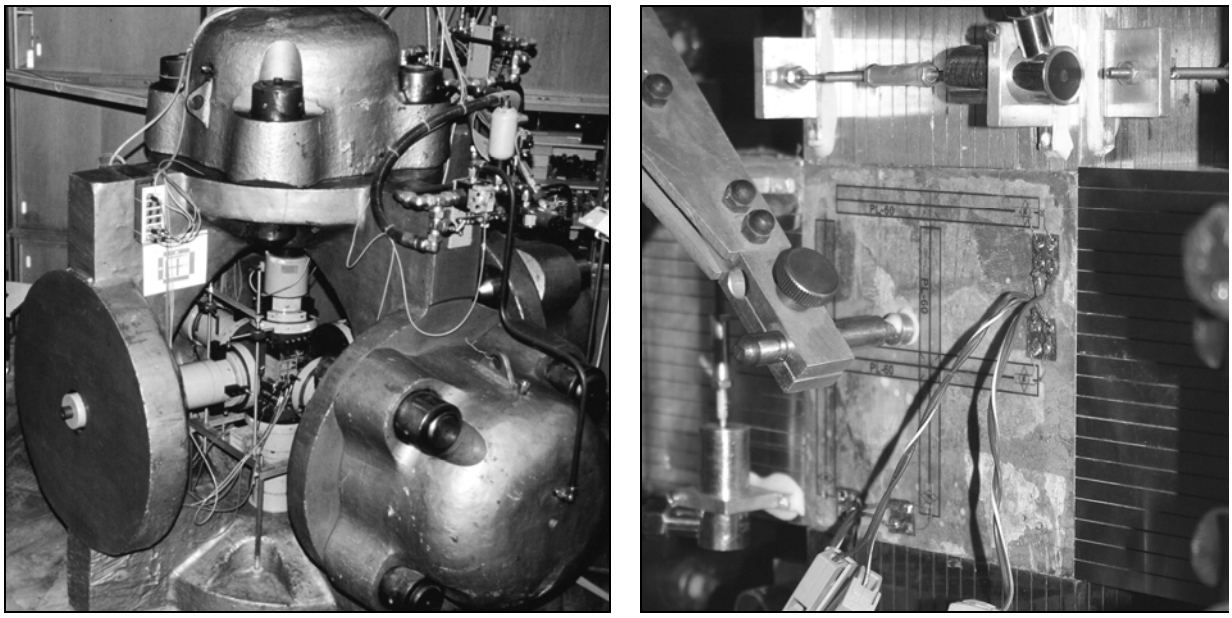

Figure 3: Experimental setup; left: triaxiale testing machine; right: testing space during a biaxial compressive test

3 Behaviour under Biaxial Compressive Stress

3.1 Influence of Grain Size

Under all stress ratios, the bi-axial compressive strength of coarse-grained concrete is higher than the one of fine-grained concrete, figure 4 left side. The single values of the measured strengths as well as the details concerning dispersion can be extracted from the [6] and the [7]. The uni-axial strength in concreting direction (f'_{c2}) is higher than in the directions lateral to it ($f'_{c1} = f'_{c3}$), as for load in concreting direction more fibres lie in the direction of lateral expansion. With 2 %, the difference is within the range of the test dispersions for coarse-grained concrete, an indication for nearly isotropic behaviour. Because of the anisotropic fibre distribution, fine-grained concrete has an 11 % higher strength in concreting direction than in the direction lateral to it. To evaluate the strength increase under bi-axial stress ratios, an averaged uni-axial compressive strength is used.

$$\overline{f}'_c = \left(f'_{c1} + f'_{c2} + f'_{c3}\right)/3 \qquad \text{with} \quad f'_{c3} = f'_{c1} \tag{1}$$

The scaled bi-axial compressive strengths do not show significant differences between fine-grained and coarse-grained concrete as long as the concretes do have the same fibre content, figure 4 right side.

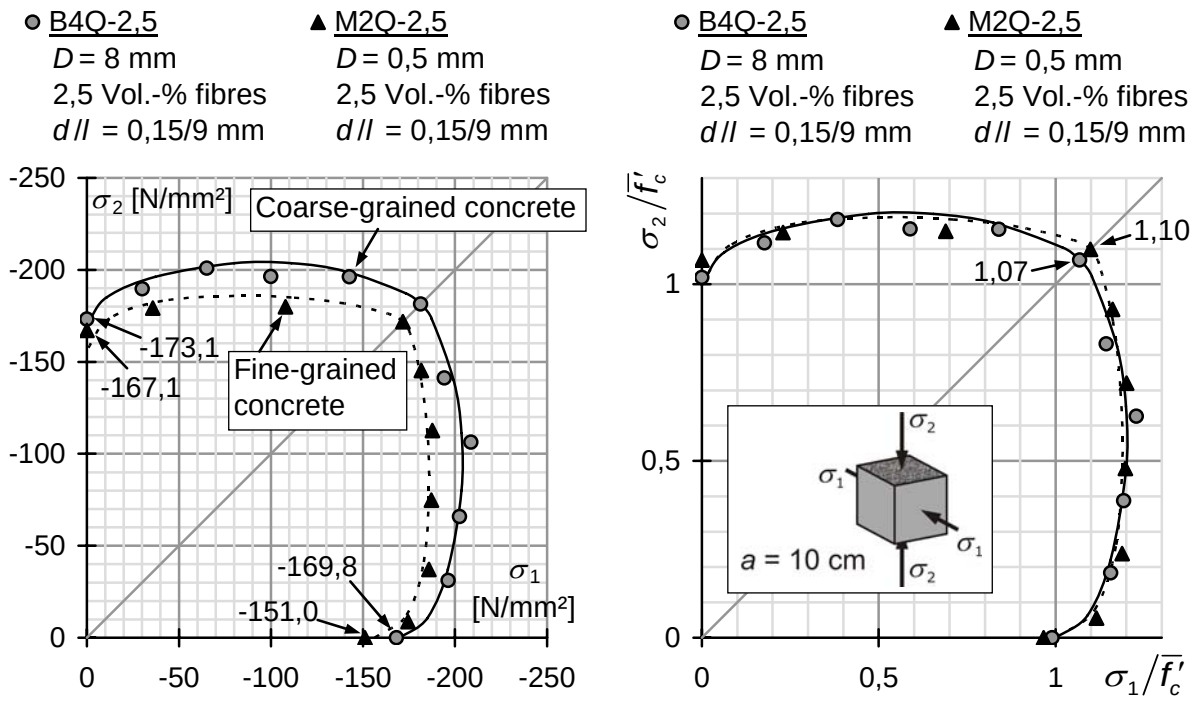

Figure 4: Strength under biaxial compressive stress depending on grain size; left: absolute values; right: scaled values

In contrast, significant differences can be seen in the stress-strain-behaviour. In figure 5, the strains under uni-axial (σ_1 = 0) and bi-axial compressive strains ($\sigma_1 = \sigma_2$) are compared. Negative strains are strains in load direction; positive strains are lateral strains. Both concretes behave less brittle under bi-axial compressive load than under uni-axial stress. This behaviour is known from normal concrete and High Performance Concrete. Under bi-axial stress, the influence of the coarse supplement basalt is clearly displayed. The high-strength basalt grains are able to stop or deflect the development of cracks. Cracking is slowed down, the crack surfaces are partly interlocked and several finely distributed cracks develop. For this crack growth, 2.5 Vol.-% fibres are able to minimise emerging cracks. This behaviour is reflected in the stress-strain-curves by a flattening of the curve before fracture and by a slow drop after the fracture. Whereas coarse-grained concrete B4Q-2,5 shows hardly detectable cracks after load relieving, the fibres of fine-grained concrete M2Q-2,5 are not able to control crack width, figure 6. Thus, the necessary minimum fibre content for Ultra High Performance Concretes of this strength ranges around 2,5 Vol.-%.

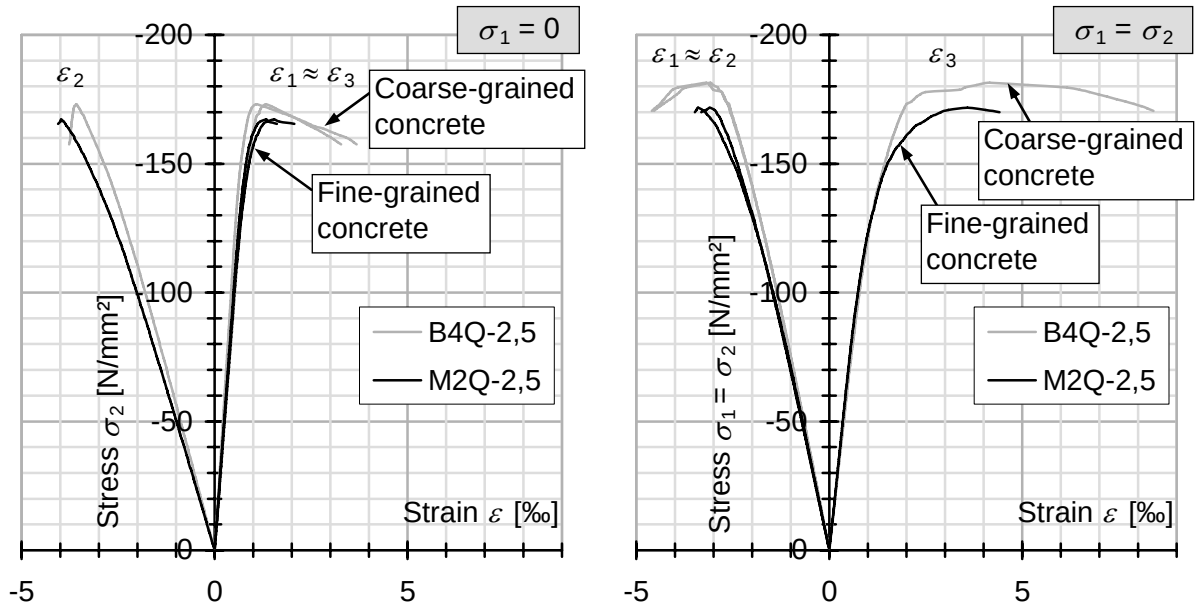

Figure 5: Stress-strain-behaviour depending on grain size under uni-axial load (left) and biaxial load (right)

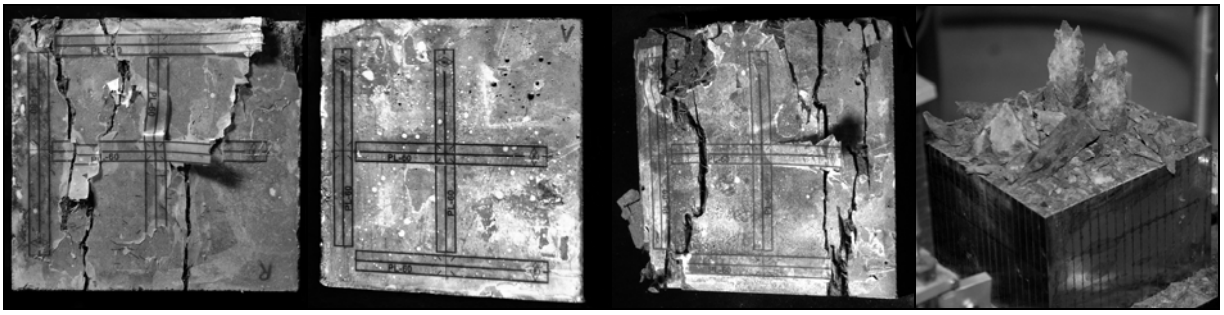

Figure 6: Crack pattern under uni-axial load (M2Q-2,5, B4Q-2,5, B4Q-0,9, B4Q-0,0, from left)

3.2 Influence of Fibre Content

According to a comparison between the coarse-grained concretes, figure 7, the percental increase of strength under bi-axial compression increases with increasing fibre content. The bi-axial strength in case of a fibre content of 2,5 Vol.-% lies above the uni-axial strength, irrespective of the examined stress ratio. For lower fibre contents, it is merely the uni-axial strength that is reached at a stress ratio of $\sigma_1 = \sigma_2$. The bi-axial strengths of fibre-free concrete exceeds the uni-axial strength only inconsiderably and only under few stress ratios.

The differences in the scaled bi-axial strength in turn correlate with the ductility of the concretes. The lowest scaled strength is noticed at the brittle, fibre-free concrete B4Q-0,0. Figure 8 illustrates the linear-elastic slope of the stress-strain-curve until fracture which occurs without advance notice and under a sudden release of energy. With increasing fibre contents, failure is signalised by a disproportionally soaring increase of the strains. In this process, the lateral strains are growing more than the negative strains in load direction.

This behaviour is also reflected by the fracture patterns, figure 6. Whereas concrete B4Q-2,5 with 2.5 Vol.-% fibres shows hardly any cracks after load relieving, concretes B4Q-1,25 and B4Q-0,9 with roughly 1 Vol.-% fibres show very wide cracks which do not close after load relieving. Fibre-free concrete B4Q-0,0 partly collapses fully at fracture, particularly under uni-axial load ratios with a low lateral compressive stress.

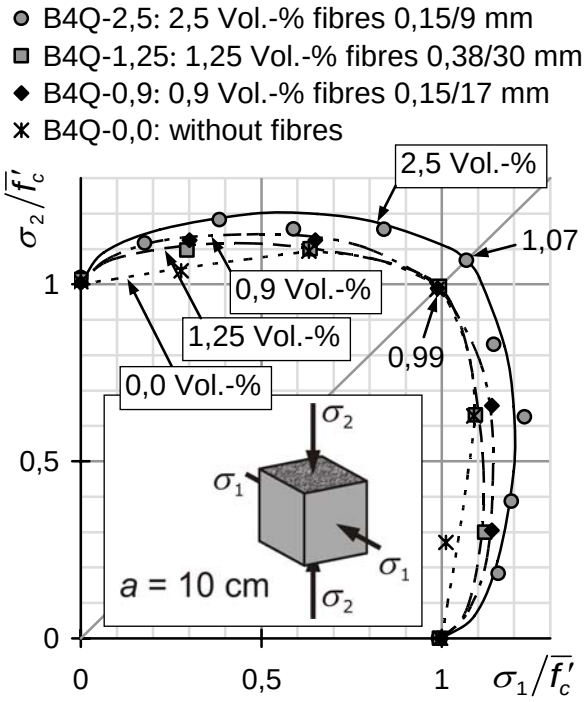

Figure 7: Strength under biaxial compressive stress depending on fibre content, scaled values

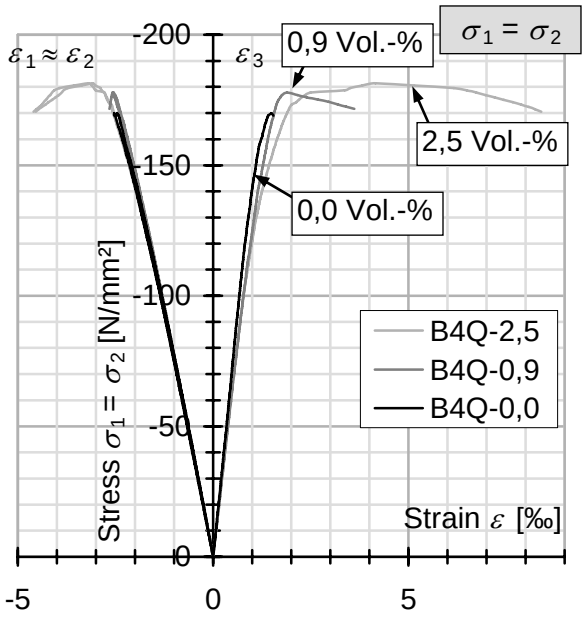

Figure 8: Stress-strain-behaviour depending on fibre content under biaxial load

4 Conclusions

UHPC is a highly innovative building material lending itself to various fields of application. However, some properties of UHPC clearly differ from those of normal concrete and have to be taken into account for calculations and for the construction of components made out of UHPC. In order to perform equivalently to High Performance Concrete, UHPC requires at least 2.5 Vol.-% fibres. For smaller fibre contents, a strength increase should not be taken into account for, e.g., pure bi-axial compression nodes. Some preliminary tests in the tri-axial compression area indicate that the strength increase under partial area compression is also smaller for UHPC than for normal strength concrete. Therefore, elaborate tests on this subject will be carried out in the near future. On the basis of the results, a failure criterion will be set up which will enable the examination of other calculation approaches concerning their validity for UHPC, too.

The strength of UHPC then depends on the fibre content, but also on the distribution of the fibres. Anisotropies in the behaviour of the material that result from an uneven distribution of fibres have to be considered in the calculation. Coarse supplements may even the orientation of the fibres and increase the strength. Moreover, high strength supplements are able to retard cracking and thereby allow for an advance notice of the failure. For the usage of coarse supplements, the cement content is also smaller, a fact that highlights the usage of coarse supplement concerning sustainability, too.

5 Acknowledgement

The authors gratefully acknowledge financial support from the Deutsche Forschungsgemeinschaft (DFG).

6 References

[1] Comité Euro-International du Béton (Hrsg.): CEB-FIP Model Code 1990. Lausanne, 1991, (CEB Bulletin d'Information No. 203-205).

[2] Curbach, M.; Hampel, T.; Speck, K.; Scheerer, S.: Versuchstechnische Ermittlung und mathematische Beschreibung der mehraxialen Festigkeit von Hochleistungsbeton. Abschlussbericht Forschungsvorhaben CU 37/1-2 der Deutschen Forschungsgemeinschaft (DFG), TU Dresden, 2000.

[3] Hampel, T.: Experimentelle Analyse des Tragverhaltens von Hochleistungsbeton unter mehraxialer Beanspruchung. Dissertation, Dresden: Technische Universität Dresden, Fakultät Bauingenieurwesen, 2006 – urn:nbn:de:swb:14-1168424399352-63668.

[4] König, G., Deutschmann, K., Friedrich, P., Kützing, L., Sicker, A.: Entwicklung zäher zementgebundener Hochleistungswerkstoffe, die in neuartigen Anwendungen im Bereich des Bauwesens eingesetzt werden können. Abschlussbericht LIK - Forschungsvorhaben, Leipzig, 1999.

[5] Curbach, M.; Speck, K.: Mehraxiale Festigkeit von duktilem Hochleistungsbeton. DAfStb-Deutscher Ausschuss für Stahlbeton, Schriftenreihe des DAfStb, Heft 524, Beuth-Verlag, 2002.

[6] Curbach, M.; Speck, K.: Versuchstechnische Ermittlung und mathematische Beschreibung der mehraxialen Festigkeit von Ultra-Hochfestem Beton – Zweiaxiale Druckfestigkeit. Arbeitsbericht zum Forschungsvorhaben CU 37/6-1 der Deutschen Forschungsgemeinschaft (DFG), TU Dresden, Eigenverlag, 2007 - urn:nbn:de:swb:14-1188817107167-18408.

[7] Curbach, M.; Speck, K.: Zweiaxiale Druckfestigkeit von ultrahochfestem Beton. Beton- und Stahlbetonbau 102 (2007), Heft 10, S. 664-673 - doi:10.1002/best.200700573.

Jürgen Grünberg
Prof. Dr.-Ing.
Institute of Concrete Construction
University of Hannover
Hannover, Germany

Ludger Lohaus
Prof. Dr.-Ing.
Institute of Building Materials
University of Hannover
Hannover, Germany

Christian Ertel
Dipl.-Ing.
Institute of Concrete Construction
University of Hannover
Hannover, Germany

Maik Wefer
Dipl.-Ing.
Institute of Building Materials
University of Hannover
Hannover, Germany

Multi-Axial and Fatigue Behaviour of ultra–high–performance concrete (UHPC)

Summary

The development of a multiaxial mechanical model for ultra-high performance concrete for numerical investigations is reported in this paper. The parameters for calibrating the three phases model for UHPC shall be determined in uni- and multiaxial experimental investigations. The uniaxial fatigue tests indicate that UHPC under fatigue loading is different from normal-strength concrete. The gradient of the second phase of strain development can be used to estimate the number of cycles until failure.

Experimental investigations of rotation-symmetric lateral pressure have been carried out. The results of low peripheral pressure show that the failure of UHPC is significantly more ductile in comparison to uniaxial failure. The parameters for an anisotropic damage model shall be determined for multiaxial fatigue loading in further dynamic investigations.

Keywords: *multiaxial mechanical model; fatigue; damage development*

1 Introduction

The outstanding characteristics of ultra-high-performance concrete (UHPC) require the development of a multiaxial mechanical model for numerical investigations. The three phases model allows for describing the behaviour of concrete in range from extremely brittle to more ductile by using the characteristic developments of the principal meridians of the fracture surface in particular the compressive meridian. Furthermore, the anisotropic damage due to fatigue is considered in the principal-stress area by different grades of damage in relation to the tensile and the compressive meridian.

The necessary parameters are determined in experimental investigations in order to calibrate the three phases model for UHPC by specifying the failure curve of static loading on the principal meridians.

Uniaxial investigations have been carried out under static as well as under compression fatigue conditions. Actually, multiaxial investigations are focussed only on static loading

along the compressive meridian, i.e. under longitudinal compression combined with transversal compression or tension.

2 Three phases model for ultra-high-performance concrete

The general shape of a failure surface in the three-dimensional stress space can be described by its failure curves in the principal meridians sections and its cross-sectional shapes in the deviator sections (Figure 1). The surface in the 60 degree sectors between the principal meridians are generated by means of elliptic interpolation. There are a lot of mutiaxial failure models (e.g. Drucker-Prager or Willam-Warnke) in literature to be used for normal-strength concrete (see [1]). But these traditional failure criteria are not applicable for UHPC. The failure of UHPC under uniaxial loading is brittle, in both, tension and compression. Therefore the three phases model [2] has been modified to take into account these characteristic material properties of UHPC. The change-over range is wider and probably moves to higher hydrostatic pressure.

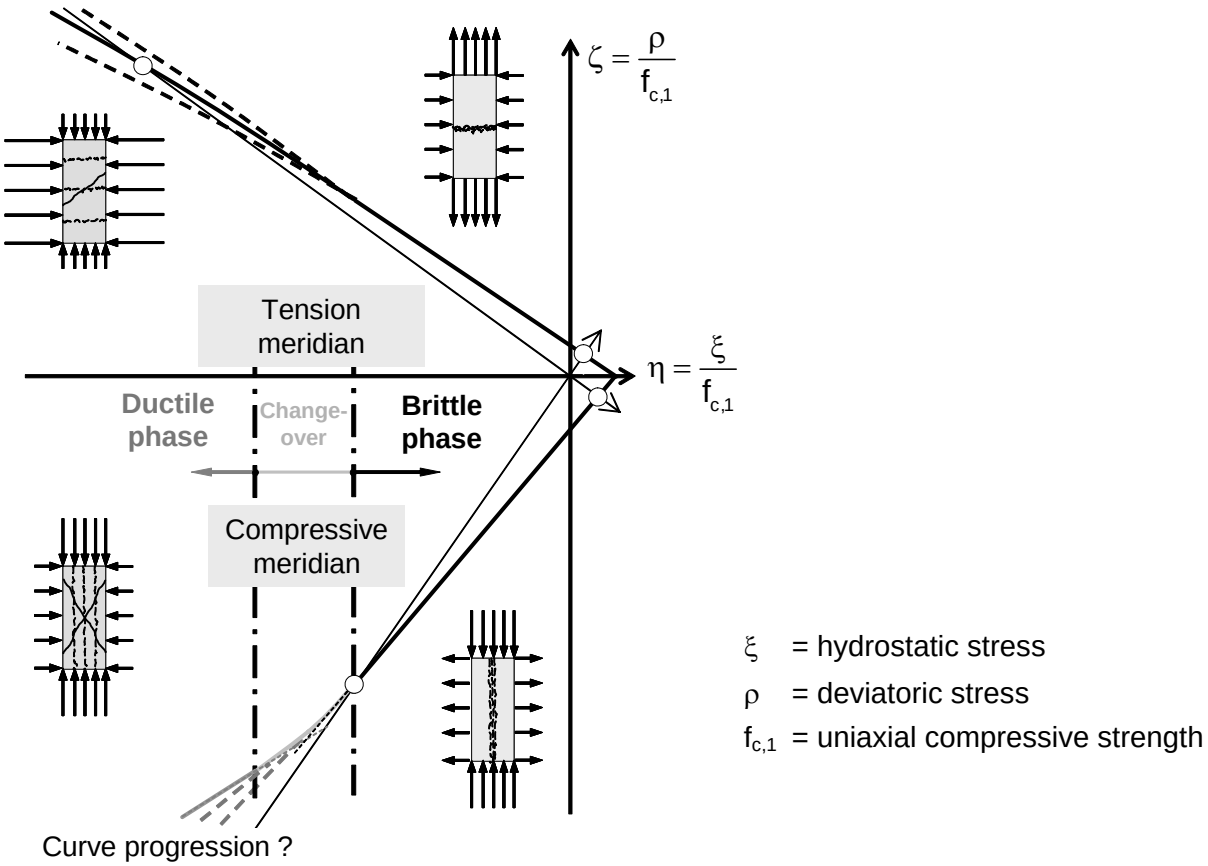

Figure 1: Principal meridians section of the failure surface due to three phases model for ultra high performance concrete

The compressive meridian is described by two straight lines with different slope which are connected by a parabolic curve. The cross section on the deviatoric plane changes from nearly triangular (brittle phase) to nearly circular with increasing hydrostatic pressure.

3 Experimental Investigations

Information about the concrete mixtures examined in the Priority Programme 1182 “Building Suitable with Ultra-High Performance Concrete”, the test specimens and the test-setup can be found in [3]. The results of the uni- and multiaxial investigations are presented in the following.

3.1 Uniaxial Investigations

The fatigue behaviour of normal-strength or high-strength concrete has been documented in several articles e. g. [4], [5] or [6]. Figure 2 shows the fatigue tests on ultra-high performance concrete examined at the Leibniz University of Hannover. The investigations were carried out with a constant lower-stress level of 5% of the static strength and varying upper-stress levels.

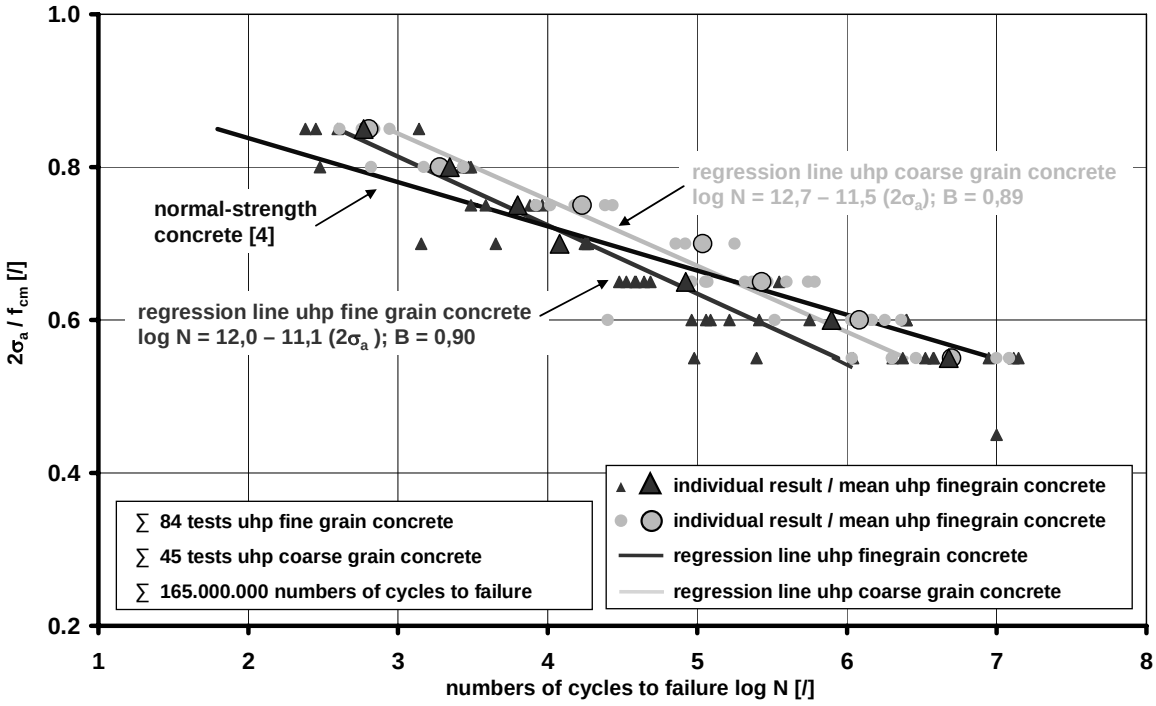

Figure 2: Wöhler-curves for ultra-high performance fine and coarse grained concrete

Until now more than 125 specimens have been tested with up to $1.5 \cdot 10^7$ load cycles subjected to uniaxial compression fatigue tests with a total number of more than 165.000.000 cycles. The regression lines for the S/N-average-value curves of the ultra-high performance concrete mixtures display scopes above and below the Wöhler-line for normal-strength concrete derived by Klausen [4]. With a coefficient of determination of B = 90% for the fine grain concrete and B = 89% for the coarse grain concrete, linear regression lines seem to be expedient for a first approximation. Further tests have to show the reliability of this approach.

Various indicators for the damage development can be found in literature, e. g. the strain, the stiffness or the consumed energy per load-cycle [4], [5]. Figure 3 displays the development of

strain and of secant stiffness against the normalized numbers of cycles of a fibre-reinforced ultrahigh-performance fine grain concrete. The fatigue test has been carried out with an upper stress level of 80% f_{cm}, a lower stress level of 5% f_{cm} and a load frequency of 10 Hz, where f_{cm} means the main value of uniaxial compressive strength.

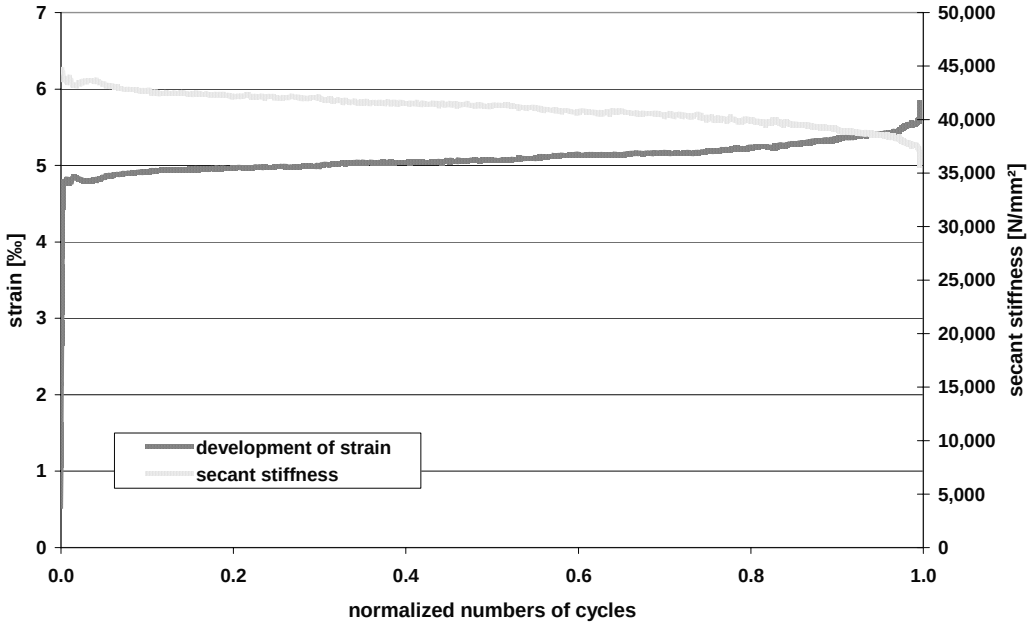

Figure 3: Development of strain and secant stiffness of a fine grain fibre-reinforced ultra-high performance concrete during fatigue loading

The characteristic three-phase damage development known from normal-strength concrete [4], [7] can be verified also for ultra-high performance concrete. The development of strain increase indeed non-linearly only up to about 3 % to 5 % of the number of cycles to failure. Between 5 % and 95 % a distinct linear increase in strain is found, followed by a third phase where the damage increases exponentially till the fracture of the sample. This fact is in contrast to normal-strength concrete, where the boundaries can be found at 20% and 80% of the normalized numbers of cycles. It seems as if there is a shortening of phase I and phase III caused by the brittleness of UHPC reported for static loading [3].

Investigations carried out by Cornelissen [8] indicate that the gradient of the second phase presented in a logarithmic scale is an indicator for the number of cycles until failure. Because of the linear increase between 25 % and 75 % of the number of cycles until failure, these points were chosen to calculate the gradient in the second phase and normalized using the total loss in strain (1).

$$\log(\dot{\bar{S}}_{II}) = \log\left(\frac{S_{0.75\cdot N} - S_{0.25\cdot N}}{\left(n_{0.75\cdot N} - n_{0.25\cdot N}\right)\cdot\left(S_{1.0\cdot N} - S_{0.0\cdot N}\right)}\right) \quad (1)$$

Figure 4 presents the single values of the gradient of phase II plotted against the numbers of cycles until failure in a logarithmic scale for the ultra-high performance concrete mixture examined in the Priority Program 1182 [3].

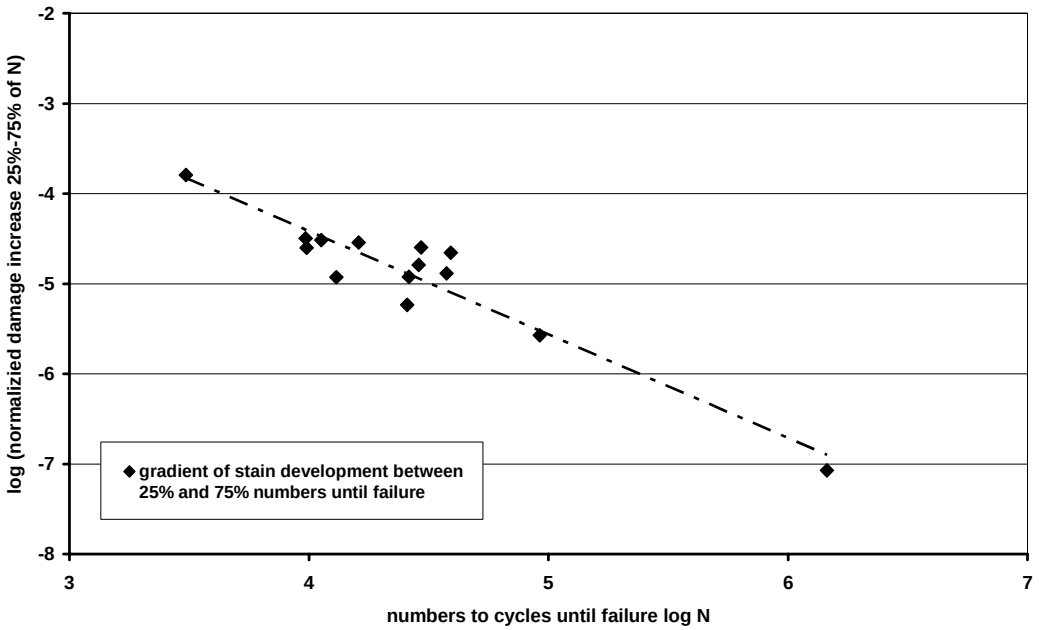

Figure 4: Correlation between the gradient in phase II and the number of cycles until failure

Figure 4 indicates that a linear regression seems to be possible with respect to the correlation between the gradient of phase II and the ultimate numbers of cycle to failure for ultra-high performance concrete. But because of the scatter of the measurement, more data points are required for a reliable conclusion.

3.2 Multiaxial loading

3.2.1 Compressive Meridian

The failure curve on the compressive meridian is characterized by specific loading conditions. These are states of stress composed of predominantly axial compression and rotationally symmetrical transversal stress, either tension or compression.

One point on the compressive meridian – the uniaxial compressive strength – is already known and can be found on σ_{33}-axis ($\sigma_{11} = \sigma_{22} = 0$). The uniaxial compressive strength divides the failure curves into two parts, uniaxial compression below compressive strength combined with transverse tension and uniaxial compression above compressive strength combined with transverse compression.

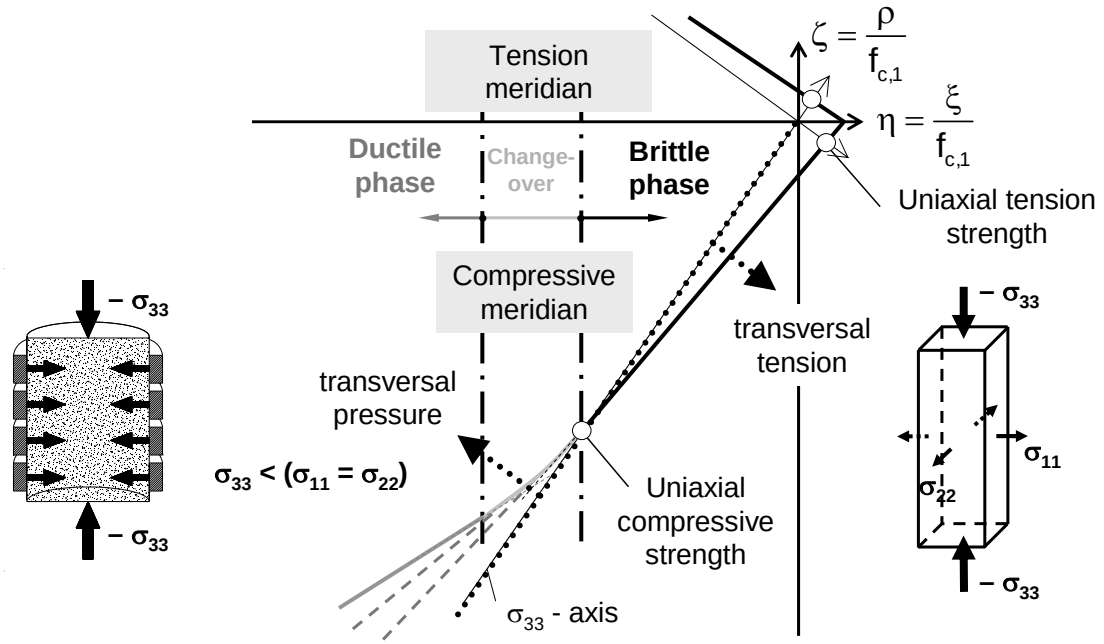

Figure 5: Loading conditions of compressive meridian

3.2.2 Uniaxial Compression combined with Transverse pressure

The design of the experimental set-up for these loading conditions should be as simple as possible especially for later following dynamic investigations. Therefore, cylindrical specimens (∅ 60mm, h=180mm) were tested under longitudinal compression and restrained transverse extension. The idea was to generate passive transverse compression by means of circular reinforcement. Different loading paths were to be realized by varying the thickness of reinforcement. Different test arrangements (e.g. rings, coil) have been developed [3]. But all these experiments did not produce suitable results.

Finally a triaxial compression testing device was used. This experimental setup allows controlling different rotation-symmetric transverse compression states in combination with longitudinal compression. The specimen geometry (cylinder d/h 60/180 [mm]) is the same used for uniaxial fatigue loading (see 3.1). First results up to a lateral pressure of -45 MPa are shown in Table 1.

Table 1: Experimental results of triaxial testing

Lateral pressure [MPa]	Axial failure load [MPa]	$\eta = \xi / f_{cm}$ [-]	$\zeta = \rho / f_{cm}$ [-]	Series
-2	-215.8	-0.641	-0.882	B
-5	-249.5	-0.757	-1.009	B
-10	-280.1	-0.876	-1.115	B
-20	-305.1	-0.991	-1.158	A
-30	-326.3	-1.121	-1.216	A
-40	-367.9	-1.307	-1.353	B
-50	-354.0	-1.325	-1.255	B

The uniaxial strengths are $f_{cm,1}$ = 199 MPa (Series A) and $f_{cm,1}$ = 198 MPa (Series B), respectively. Figure 6 shows these results transformed into the Haigh-Westergaard-Coordinate System and compared to some possible failure curves produced by the three phase model. The array of these curves is generated by different parameters. Currently, the EN 1992-1-1 approach seems to be most convenient. But a von-Mises approach combined with a wide change over range also could be possible.

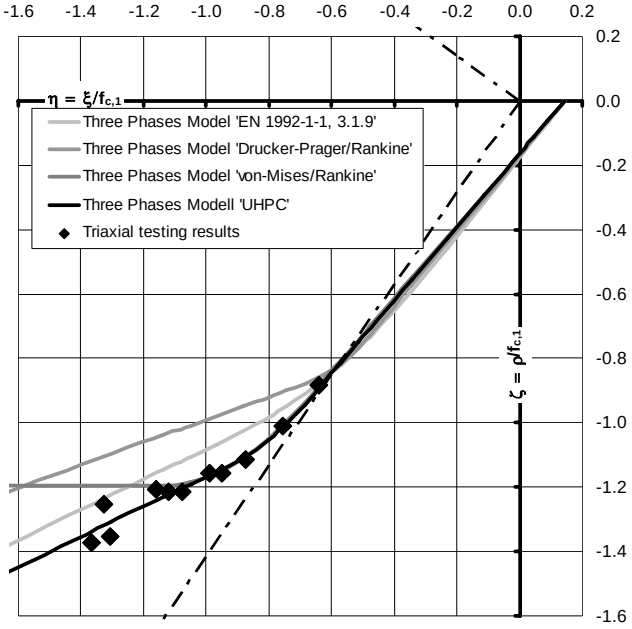

Figure 6: Experimental results of triaxial testing

In case of low transverse pressure the failure behaviour of UHPC is significantly more ductile in comparison to brittle failure behaviour due to uniaxial compression. The maximum axial elongation at fracture was up to 15 $^{o}/_{oo}$.

4 Outlook and Conclusion

4.1 Uniaxial Fatigue Investigations

Ultra-high performance concrete under fatigue loading shows a different behaviour in comparison to normal-strength concrete. First results indicate that the correlation between the gradient of phase II of the damage development and the ultimate numbers of cycle until failure is quite strong not only for normal-strength concrete but also for ultra-high performance concrete. Further investigations are needed to examine the different factors of influence, e.g. the load frequency.

4.2 Extension of Three phases model with respect to fatigue loading

The ultimate numbers of stress cycles until failure according to the uniaxial S-N-curve are attached to the σ_{33}-axis (see triangular symbols in Figure 7). Further S-N-curves shall be developed according to specific ratios of deviatoric versus hydrostatic stresses (e.g. ρ/ξ = 0,10; 0,20; 0,30; …). Attaching ultimate numbers of stress cycles until failure (see rhombic symbols) to the straight lines defined by these ratios, affine curves connecting equal cycle

numbers can be derived. Thereby, the three phases failure model is extended to a three phases fatigue model (see Figure 7).

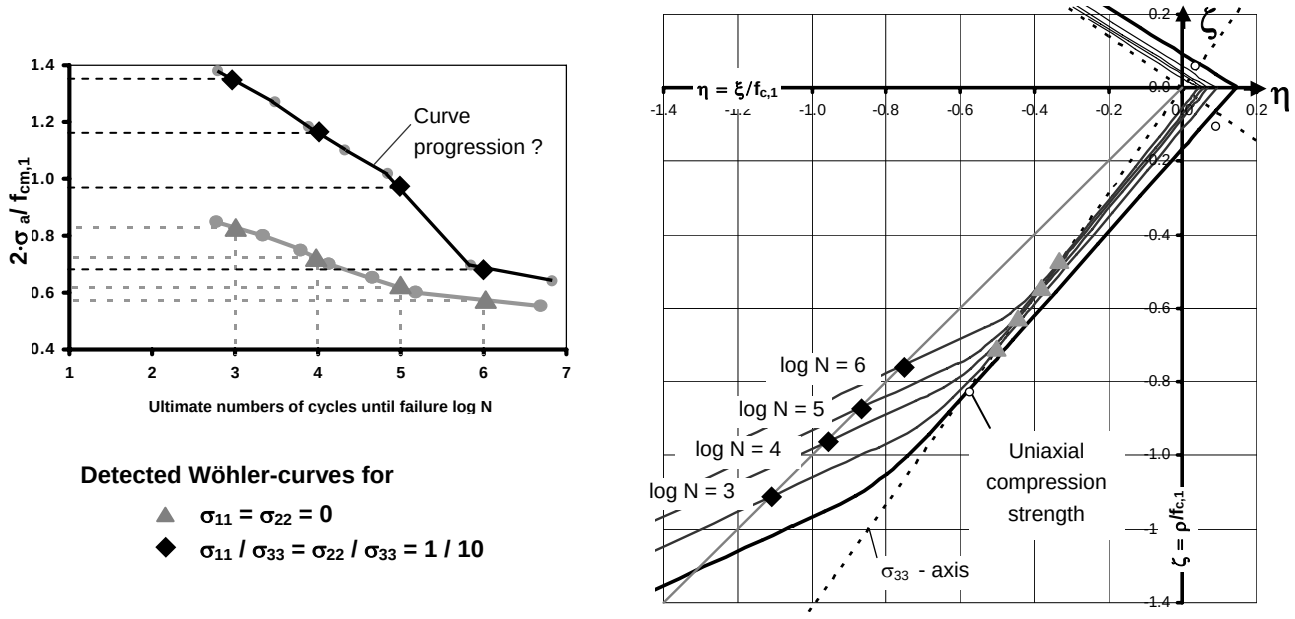

Figure 7: Three phases modell extension for fatigue loading

5 Acknowledgement

The authors thank the “Deutsche Forschungsgemeinschaft (DFG)” for the financial support of this research work.

6 References

[1] Chen, W. F.: Plastitity in reinforced concrete, McGraw-Hill Book Company, New York, 1982

[2] Grünberg, J.; Funke, G.; Göhlmann, J.; Stavesand, J.: Fernmeldetürme und Windenergieanlagen in Massivbauweise.In: Beton-Kalender 2006, Teil 1, Seite 103 – 223. Ernst & Sohn.

[3] Grünberg, J.; Lohaus, L.; Ertel, C.; Wefer, M.: Mehraxiales mechanisches Ermüdungsmodell von Ultra-Hochfestem Beton – Experimentelle und analytische Untersuchungen. In: Beton- und Stahlbetonbau 102, Heft 6, S. 388-398, 2007.

[4] Klausen, D. 1978. Festigkeit und Schädigung von Beton bei häufig wiederholter Beanspruchung. PhD-Thesis

[5] Hohberg, R. 2004. Zum Ermüdungsverhalten von Beton. PhD-Thesis, TU Berlin.

[6] Lohaus, L. & Anders, S. 2006. High-Cycle Fatigue of Ultra-High Performance Concrete – Fatigue Strength and Damage Development. 2nd International fib Congress, 5.-8. June 2006, Naples.

[7] Reinhardt, H.W. & Stroeven, P. & den Uijl, J.A. & Kooistra, T.R. & Vernecken, J.H.A.M. 1978. Einfluss von Schwingbreite, Belastungshöhe und Frequenz auf die Schwingfestigkeit von Beton bei niedrigen Bruchlastwechselzahlen. Betonwerk+Fertigteil Technik.

[8] Cornelissen, H.A.W. & Reinhardt, H.W. 1984. Uniaxial tensile fatigue failure of concrete under constant amplitude and programme loading. Magazine of Concrete Research, Vol. 36, p. 216-226.

Special Part II:

DFG Priority Program – Construction

Torsten Leutbecher
Dr.-Ing.
IBB Fehling + Jungmann
Kassel, Germany

Ekkehard Fehling
Prof. Dr.-Ing.
Institute of Structural Engineering
University of Kassel
Kassel, Germany

Crack Formation and Tensile Behaviour of UHPC Reinforced with a Combination of Rebars and Fibres

Summary

To carry tensile loads beyond the tensile strength of fibre reinforced UHPC in beams or tensile members, fibres can be combined with conventional bar reinforcement or prestressing steel. Thereby, the structural and deformation behaviour in serviceability as well as in ultimate limit state is affected significantly. Based on equilibrium and compatibility, the introduced mechanical model enables to predict both the integral load-deformation-behaviour and the width of discrete cracks of UHPC-tensile members reinforced with rebars and fibres. Fundamentals are the well-known mechanical principles for cracked reinforced concrete and the stress-crack-opening-relationship of fibre concrete. The application of the proposed model to an extensive test series with numerous varied parameters shows a very good agreement even for fibre-reinforced UHPC with strain softening behaviour.

Keywords: *tensile behaviour, combined reinforcement, crack width, durability, economic mix design*

1 Introduction

To achieve ductile post failure behaviour in compression and to increase tensile strength and ductility of UHPC, often fibres, normally high strength steel fibres, are added. Thus very high flexural strengths can be achieved, particularly for thin structural members. However, to realise long-span structures (i. e. bridges) under systematic utilisation of the high compressive strength of concrete, additional untensioned or prestressed reinforcement in the tensile area is needed.

Thereby, differences in the load bearing and the deformation behaviour compared to common reinforced concrete and prestressed concrete result from the interaction of continuous reinforcement elements and discontinuously distributed short fibres. In particular stiffness and cracking, but also bearing capacity and ductility, are significantly affected by the reinforcement configuration.

The calculation of UHPC structures therefore requires methods and models, which describe the mechanical processes of cracking well and thus enable a material suited structural design. In order to ensure durability, a secure limitation of crack width in serviceability state plays an important role.

2 Bond between UHPC and bar reinforcement

Within a test series, the bond between rebars (BSt 500, high strength ribbed prestressing steel St 1420/1570 and St 1470/1620) with different diameters (d_s = 8, 10 and 12 mm) and fine-aggregate UHPC of mixture M1Q (table 1) was investigated experimentally. Depending on the fibre content the compressive strengths of the UHPC-mixture lie between 160 and 190 N/mm².

Table 1: UHPC-mixture [1]

UHPC-mixture		**M1Q**	**M2Q**
cement	kg/m³	733	832
sand 0.125/0.50	kg/m³	1008	975
silica fume	kg/m³	230	135
fine quartz	kg/m³	183	207
finest particles < 0.125 mm	l/m³	405	403
superplasticiser	kg/m³	28.6	29.4
water	l/m³	161	166
water-cement-ratio		0.24	0.22
water-binder-ratio		0.19	0.19

Differing from the recommendations of RILEM [2], for the pull-out-tests' specimens the bond length was reduced to 1.5 d_s, to avoid yielding of reinforcing steel. Besides concrete cubes with edge lengths of 10 d_s specimens with reduced concrete cover (2.5 and 1.0 d_s) were tested. Furthermore, the influence of steel fibres (l/d = 17 mm/0.15 mm) was investigated.

The highest bond strength was reached for BSt 500 with a concrete cover of 4.5 d_s at comparatively small relative displacements of about 0.1 to 0.2 mm (figure 1). High strength steel with indentation showed definitely softer bond behaviour. For reduced concrete cover of 2.5 d_s longitudinal cracks along the reinforcing steel bar caused a reduction of bond strength. This could not be avoided even by adding fibres of 1.0 vol.-%.

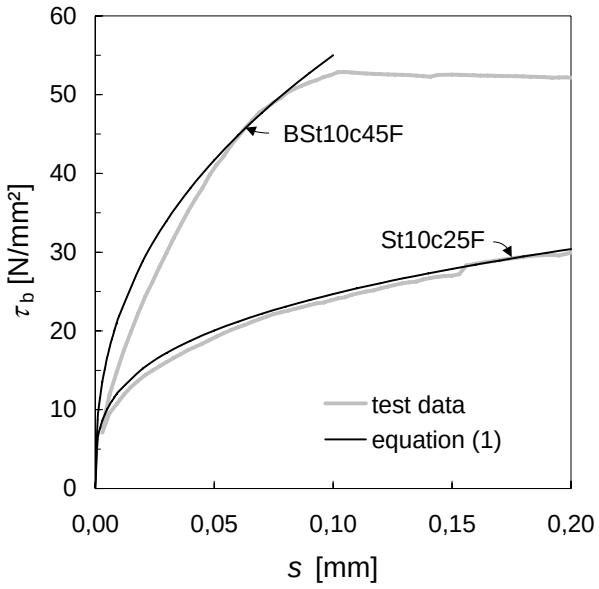

BSt10c45F = BSt 500, Ø 10 mm, concrete cover: 45 mm, 1.0 vol.-% steel fibres

St10c25F = St 1420/1570, Ø 10 mm, concrete cover: 25 mm, 1.0 vol.-% steel fibres

Figure 1: Bond behaviour of reinforcing steel (BSt 500) and high strength ribbed prestressing steel (St 1420/1670) in fibre reinforced fine-aggregated UHPC (grey) and approximation by equation (1) (black)

As bond law for reinforced NSC equation (1) is used frequently. Fitting the input parameters, the bond behaviour of UHPC can be approximated by equation (1) as well (figure 1). Table 2 represents the parameters based on the results of the conducted pull-out-tests.

$$\tau_b = \tau_{b\,max} \cdot \left(\frac{s}{s_1}\right)^{\alpha} \leq \tau_{b\,max} \qquad (1)$$

with $\tau_{b\,max}$ bond strength
s slip
s_1 slip at reaching the bond strength
α constant, depending on the bond quality of the reinforcing steel

Table 2: Parameters to describe the bond behaviour of UHPC by equation (1)

type of reinforcement		**BSt 500**	**St 1420/1670**
$\tau_{b\,max}$	N/mm²	55	40
s_1	mm	0.1	0.5
α	-	0.40	0.30

3 Stress-crack-opening-relationship of fibre reinforced UHPC

For fine-aggregate UHPC of mixture M2Q (table 1), the stress-crack-opening-behaviour was investigated experimentally within a test series on notched prisms. Smooth high strength steel fibres with a diameter of 0.15 mm and a length of 9 mm or 17 mm were added to the concrete in different volume fractions (0.9 up to 2.5 vol.-%). The prisms had a cross section of 40 x 40 mm² with 5 mm x 5 mm sawn notches at two opposite sides (figure 2).

To avoid failure outside the notch and to enable the measurement of very small values of crack opening, thin steel plates, which reached directly to the notch edge, were glued to the lateral surface of the test specimens. The chosen load application per threaded bars without hinges led to an elastic restraint of the specimens (figure 3).

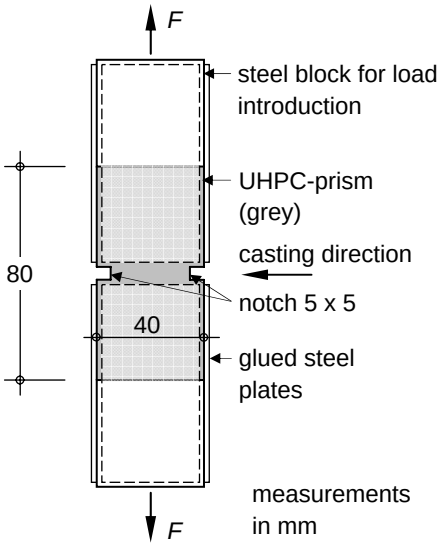

Figure 2: Test specimen

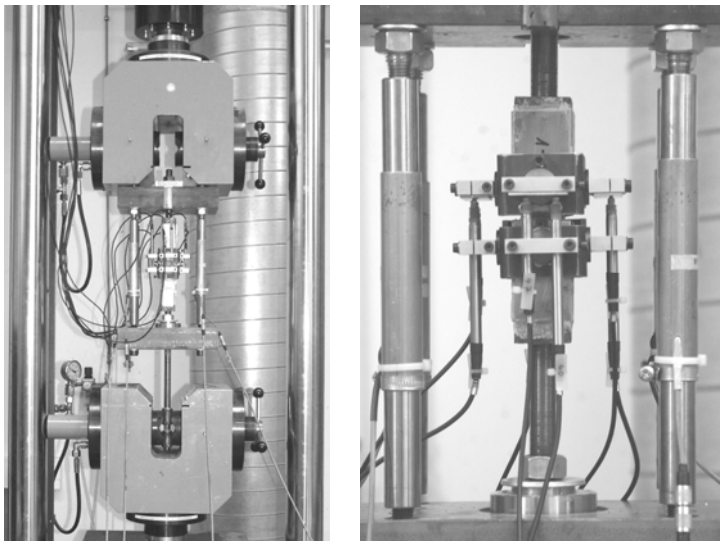

Figure 3: Test set-up (left) and instrumentation (right)

The deformations were measured by LVDT's, which were fastened at the steel plates by a device near to the notch edge. Figure 4 shows the obtained stress-crack opening-relationships. They can be approximated very well in the phase of both, fibre activation (figure 4a) and fibre pull-out (figure 4b) by the following equations, as given among others by Pfyl [3].

fibre activation: $\sigma_{cf} = \sigma_{cf0} \cdot \left(2\sqrt{\frac{w}{w_0}} - \frac{w}{w_0} \right)$ (2a) fibre pull-out: $\sigma_{cf} = \sigma_{cf0} \cdot \left(1 - \frac{2w}{l_f} \right)^2$ (2b)

with σ_{cf0} maximum stress of fibre concrete (post-cracking phase)
w_0 crack width at reaching the maximum stress of fibre concrete
l_f fibre length

To consider the influence of shrinkage and of matrix-softening in the state of micro cracking, the equations (2a) and (2b) can be extended as shown in [4].

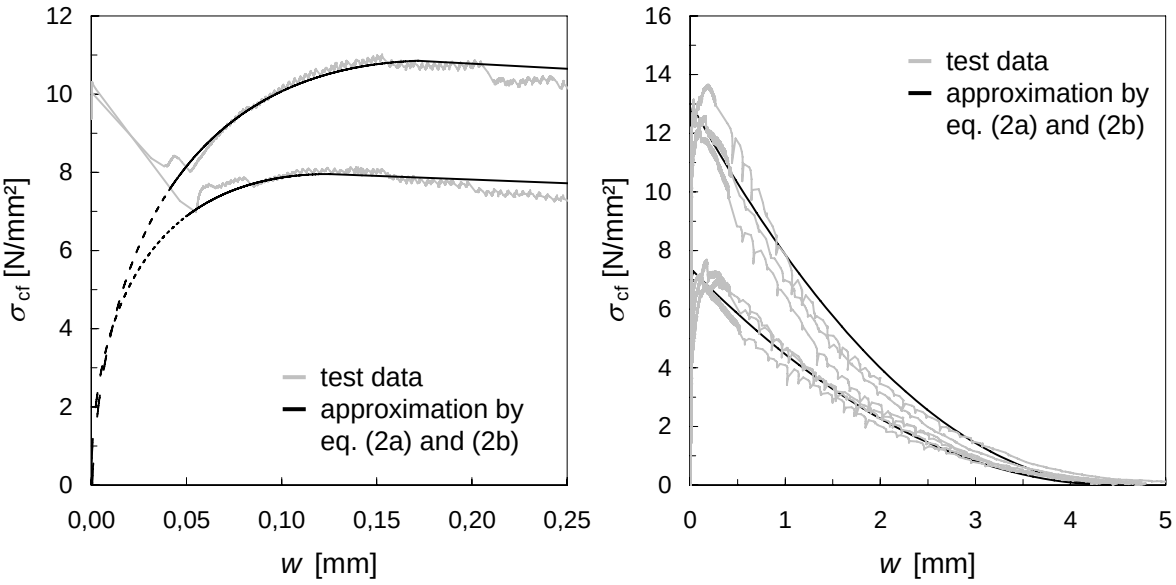

Figure 4: Stress-crack opening-relationship in the fibre activation phase (left, 17 mm long steel fibres) and until complete pull-out of all fibres (right, 9 mm long steel fibres)

4 Tensile behaviour of UHPC reinforced with rebars and fibres

4.1 Mechanical model

To describe the tensile behaviour of tensile members with a combination of bar and fibre reinforcement, the mechanical relationships valid for fibre concrete and reinforced concrete have to be linked. For balance reasons, within the crack equation (3) is true. In the state of micro cracking, equation (3) may be extended by the contribution of the UHPC-matrix F_c.

$F = F_s + F_f$ (equilibrium condition) (3)

with F external tensile force
F_s tensile force of reinforcing bars
F_f tensile force of fibres

Implying plane cross sections, the relative displacement between bar reinforcement and matrix on one hand and the stress-crack-opening-relationship of fibre concrete on the other hand must lead to identical crack widths (compatibility condition). Considering the equilibrium condition and the compatibility condition, the tensile forces of bar and fibre reinforcement and therewith the local as well as the integral strain of an UHPC-tensile member with combined reinforcement can be determined definitely.

As shown in [4], with increasing bond stress between concrete and reinforcement acc. to figure 1 and with further fibre activation (figure 2a) new cracks can arise up to high elastic tensile strain. At this, the fibre concrete itself does not need to show a strain hardening behaviour.

Because of the quite complex mechanical relationships, the iterative evaluation of the equilibrium and compatibility conditions has to be done numerically. In the proposed model the tensile member is divided into a finite number of “crack elements” of discrete lengths. These elements differ in the fibre content effective in tensile direction (considering the scatter of fibre distribution and orientation) and in their length. The lengths of the elements measure the single up to the twice of the load transition length of the bar reinforcement (possible crack spacings in the state of single cracking), which shows a more unfavourable bond behaviour compared to the fibres.

The calculation of the load-deformation-behaviour of the different elements is conducted force-controlled. Therefore, the external load is increased incrementally, starting with the smallest cracking strength of all considered crack elements. On each load level, the internal forces, the crack width, the average tensile strain etc. are determined by iteration for all crack elements. It is checked, if in the middle of two existing cracks the cracking strength of fibre concrete is reached again. In this case for the next load level the crack spacing is halved and the number of cracks of the corresponding element is doubled. Subsequently, for each load level a statistical evaluation (frequency distribution of the crack spacings and crack widths, extreme and mean values etc.) and the superposition of the average steel strain values is done. Thereby the results of the elements are weighed according to their distribution density.

4.2 Experimental verification of the proposed mechanical model

4.2.1 Test programme and test execution

To analyse the interaction of bar and fibre reinforcement, tensile tests on panel-shaped UHPC-members (mixture M2Q acc. to table 1) have been carried out. Within the test series the influence of the fibre length (9 and 17 mm), of the fibre content (0.9 up to 2.5 vol.-%), of the type of bar reinforcement (BSt 500, high strength steel, see figure 1), of the bar diameter (8 and 12 mm) and of the content of bar reinforcement (1.3 and 3.0 %) on the load and deformation behaviour under short-term monotonic loading was investigated.

The panels had a cross section of 70 x 220 mm² and a length of 1300 mm (figure 5). They were reinforced in tension direction concentrically with one layer of 4 steel bars each. Some specimens had an additional lateral reinforcement. The panels were implemented by clamp jaws in a servo-hydraulic test device (figure 6). The loading was conducted path controlled.

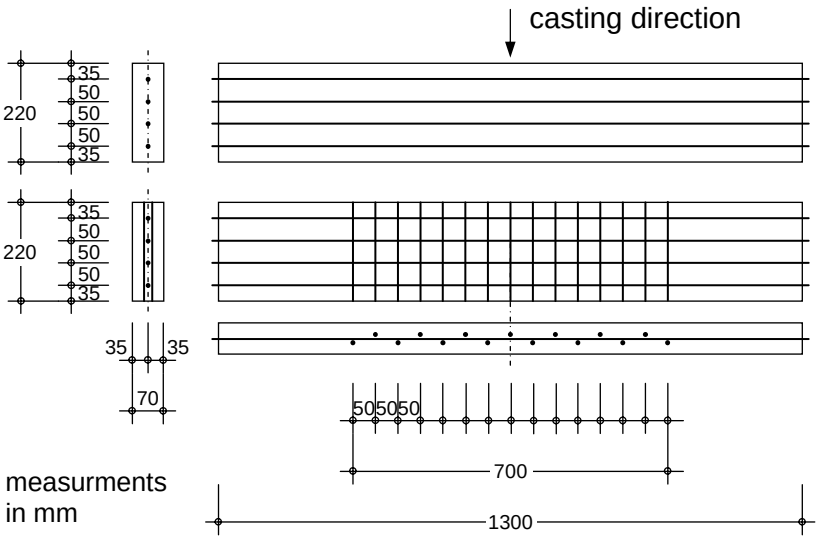

Figure 5: Dimensions and reinforcement of UHPC-panels

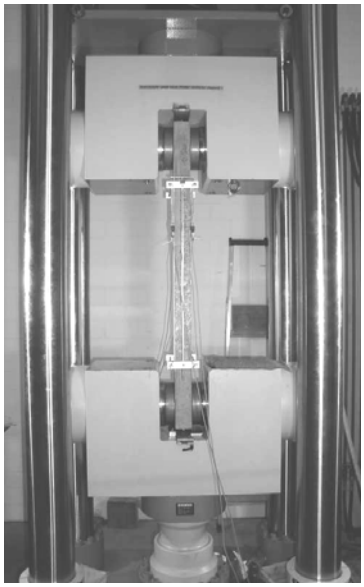

Figure 6: Test setup

The deformations were measured integrally by 4 LVDT's over a measuring range of 750 mm. Crack formation and development of crack width were observed visually via crack loupe at discrete strain states. Furthermore, results about the crack width distribution should be gained indirectly through the correlation between crack width and crack spacing. Therefore, the crack spacings were measured on the front and back side along 3 measuring ranges each.

4.2.2 Shortening due to shrinkage

Due to the high cement content and the low water-binder-ratio of UHPC the autogenous shrinkage exceeds the drying shrinkage. According to tests done by Fehling et al. [1] with mixture M1Q, the autogenous shrinkage strain ε_{cas} amounts to about 0.9 ‰. Considering the minor drying shrinkage strain ε_{cds} the total degree of total shrinkage $\varepsilon_{cs\infty}$ sums up to approximately 1 ‰.

Within the test series, the shortening due to shrinkage $\varepsilon_{s,shr}$ was determined experimentally. For that purpose the length of the reinforcement bars, which stick out at the ends of the panels, were measured before being implemented in the formwork and another time several days after finishing the heat treatment of the hardened specimens. Figure 7 shows the measured shrinkage shortening as a function of the total reinforcement ratio ρ_{tot}. The fibre content is considered by half in comparison to the bar reinforcement ratio.

Equation (4) describes the theoretical $\varepsilon_{s,shr}$ - ρ_{tot} -relationship. The unknown parameters can be determined via regression analysis using the measured values (broken line in figure 7).

$$\varepsilon_{s,shr} = \frac{\varepsilon_{cs\infty}}{1+\alpha_E \cdot \rho_{tot} \cdot (1+\rho \cdot \varphi)} \tag{4}$$

with φ creep coefficient

ρ relaxation coefficient

$\alpha_E = E_s / E_c$

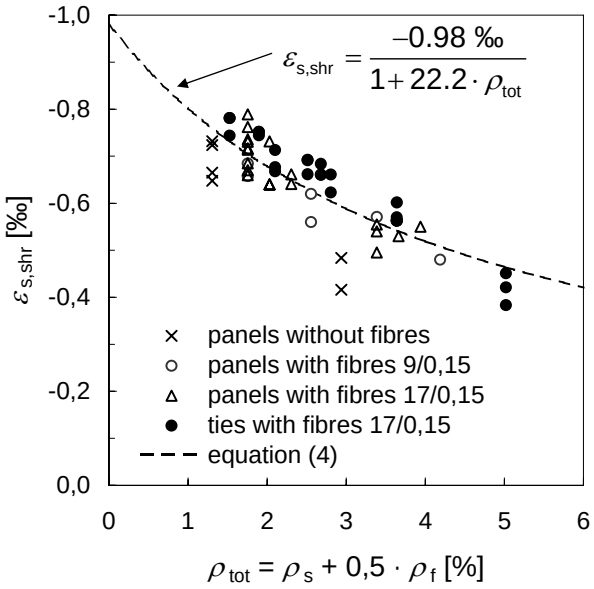

Figure 7: Shortening of tensile members due to shrinkage

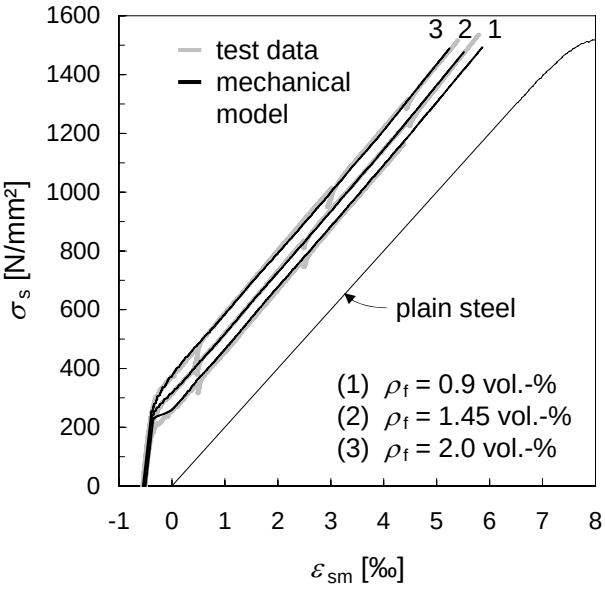

Figure 8: Load-deformation-behaviour of tensile members (high strength steel, d_s = 12 mm and 17 mm long fibres)

4.2.3 Load-deformation-behaviour and crack formation

Figure 8 shows the stress-strain-relationships obtained by the tensile tests. The average strain ε_{sm} was calculated from the displacements measured by the 4 LVDT's and the shrinkage shortening acc. to figure 7. A very good agreement with the proposed model is achieved.

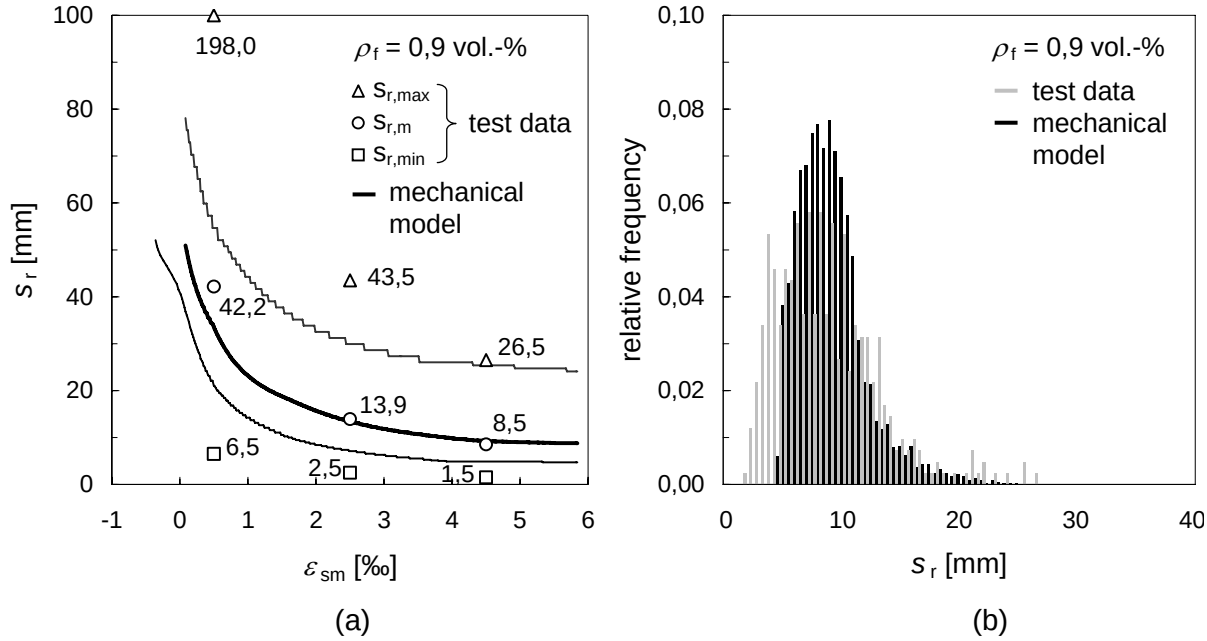

Figure 9: Development of crack spacings during tests (a) and relative frequency distribution of the crack spacings at the end of tests (b) in comparison to the mechanical model (high strength steel, d_s = 12 mm and 17 mm long fibres)

In figure 9a, the maximum, minimum and mean values of crack spacings are depicted numerically and by symbols. They were obtained by the analysis of recorded test data for the specimens with a fibre content of 0.9 vol.-%. Figure 9b shows the relative frequency distribution of crack spacing at the end of tests as histogram (grey bars).

The calculation by the mechanical model is based on the same material parameters as the calculation of the load-deformation-behaviour. Again, an overall very good agreement between test data and mechanical model could be obtained. Due to the assumption of plain cross sections (Bernoulli's hypothesis), the minimum crack spacings, measured in the tests, which may emerge near to crack splittings, are overestimated by the model.

5 Conclusions

The load-deformation-behaviour as well as the development of crack spacings and crack widths observed in the tests can be represented very well by the suggested mechanical model [4]. The calculations are based on the bond-stress-slip-relationships of bar reinforcement and on the stress-crack-opening-relationships of ultra high strength fibre concrete. Thus, the introduced model enables both calculations of stiffness and of crack widths of non-prestressed reinforced as well as prestressed UHPC-tensile members.

Experimental and theoretical studies show, that the tension stiffening effect increases strongly with increasing fibre, but crack spacings and crack widths do not decrease in the same manner. The maximum contribution of fibres is reached at high strain levels, which frequently lie above the elastic range of bar reinforcement. The results, obtained for a fibre content of only 0.9 vol.-%, confirm that in combination with bar reinforcement, the fibre concrete itself does not need to show strain hardening behaviour to achieve progressive crack formation with very small crack spacings and crack widths, which enables very durable structures. Since the costs of the fibres mainly determine the costs of UHPC, this finding is of high economical importance.

Model ideas developed so far, which primarily suggest a superposition of the load-deformation-behaviour of fibre concrete and stress-strain-relationship of plain steel without considering compatibility (e.g. [5]) are not able to reproduce this observation.

6 References

[1] Fehling, E.; Schmidt, M.; Teichmann, Th.; Bunje, K.; Bornemann, R.; Middendorf, B.: Entwicklung, Dauerhaftigkeit und Berechnung Ultra-Hochfester Betone (UHPC). In: Forschungsbericht DFG FE 497/1-1, Structural Materials and Engineering Series, no. 1, Kassel University, 2005.

[2] RILEM 1970, Technical Recommendations for the Testing and Use of Construction Materials: RC 6, Bond Test for Reinforcement Steel, 2. Pull-out Test, 1970.

[3] Pfyl, Th.: Tragverhalten von Stahlfaserbeton. PhD Thesis, ETH Zürich, 2003.

[4] Leutbecher, T.: Rissbildung und Zugtragverhalten von mit Stabstahl und Fasern bewehrtem Ultrahochfesten Beton (UHPC). PhD Thesis, Kassel University, 2007.

[5] Jungwirth, J.: Zum Zugtragverhalten von zugbeanspruchten Bauteilen aus Ultra-Hochleistungs-Faserbeton. PhD Thesis No 3429 (2006), École Polytechnique Fédérale de Lausanne, 2006.

Nguyen Viet Tue
Prof. Dr.-Ing. habil.
Leipzig University
Leipzig, Germany

Stefan Henze
Dipl.-Ing.
Leipzig University
Leipzig, Germany

Determination of the distribution and orientation of fibres in steel fibre reinforced UHPC by photographic method

Summary

Micro steel fibres are often used to improve the ductility as well as to increase the tensile and bending strength of Ultra High Performance Concrete. An improved photographic presented in this paper enables users a significant and simple determination of the distribution and orientation of micro steel fibres in UHPC. This contribution describes the main features of the method.

Keywords: *fibre distribution, fibre orientation, photographic method, surface preparation, image analysis*

1 Introduction

An appropriate characterisation of the material properties is needed for the application of steel fibre reinforced Ultra High Performance Concrete (UHPC) in structures. The knowledge of the distribution and orientation of fibres is important to predict the load capacity of structures. They are also relevant from an economic and ecological point of view. Due to the multiple influence factors, such as geometry, concrete properties and manufacturing technology, it is necessary to investigate the distribution and orientation of fibres for individual application. Therefore, suitable testing methods are required to determine these parameters. In this case some specifics must be considered for UHPC reinforced with micro steel fibres.

2 Theoretical approach

The spatial fibre alignment is described by the fibre distribution and fibre orientation. The fibre distribution describes the number of fibres N_F within a volume unit V or a cross-sectional area A (figure 1a). The fibre orientation is characterised by the orientation coefficient η_F (figure 1b). The coefficient η_F is defined as the average ratio of the fibre length $l_{F,proj.}$ in tensile stress direction to the actual fibre length l_F of all fibres in the examined volume unit or cross section (equation 1).

$$\eta_F = \frac{1}{N_F} \sum_{i=1}^{N_F} \frac{l_{F,proje.,i}}{l_{F,i}} \qquad 0 \le \eta_F \le 1{,}0 \tag{1}$$

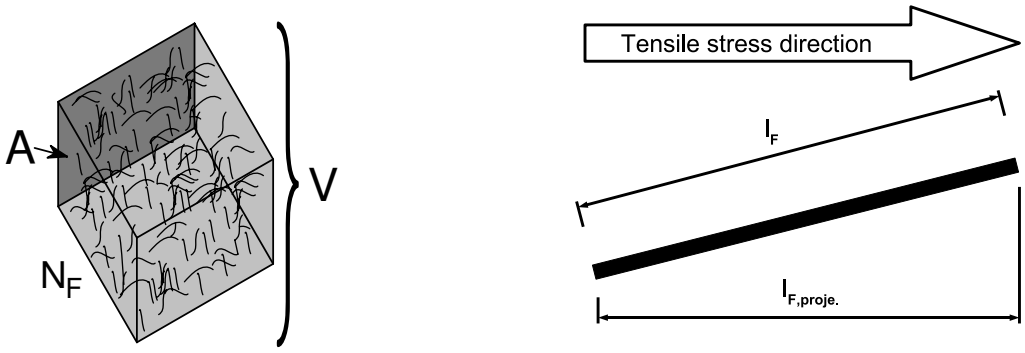

(a) fibre distribution (b) fibre orientation

Figure 1: Definition of the fibre distribution and orientation

Four methods are mostly used for the experimental determination of the fibre distribution and orientation:

- Counting the fibres in the cross-section [1]
- Radiography (X-ray) [2] / computer-tomography (CT) [3]
- Magnetic induction [4]
- Photographic method [5]

Equation 2 is often used for the investigation of the fibre orientation by counting the fibres in an section of a specimen.

$$\eta_F = 25 \cdot \frac{N_F \cdot \pi \cdot d_F^2}{A_P \cdot v_F} \qquad (2)$$

with	η_F	Orientation coefficient	[-]
	N_F	Number of fibres	[-]
	d_F	Fibre diameter	[mm]
	v_F	Nominal fibre content	[vol.-%]
	A_P	Cross-sectional area	[mm²]

In this case only the number of fibres in the section must be counted to determine the orientation coefficient. However, this approach offers only correct results if the actual fibre content in the section corresponds to the nominal fibre content. In other cases, e.g. in fracture zones the orientation coefficient is estimated too high or too low [6]. Then X-ray, CT, magnetic induction or photographic methods are better suitable.
The photographic method used at the Leipzig University is based on the work of *Schönlin* [5] and *Markovic* [7]. The fibre orientation is determined on the basis of the elliptical-shaped fibre cross sections which appear in the section of the specimen.
The fibre orientation for a spatial oriented fibre can be determined with equation 3 if the tensile stress direction is identical to the y-direction (figure 2).

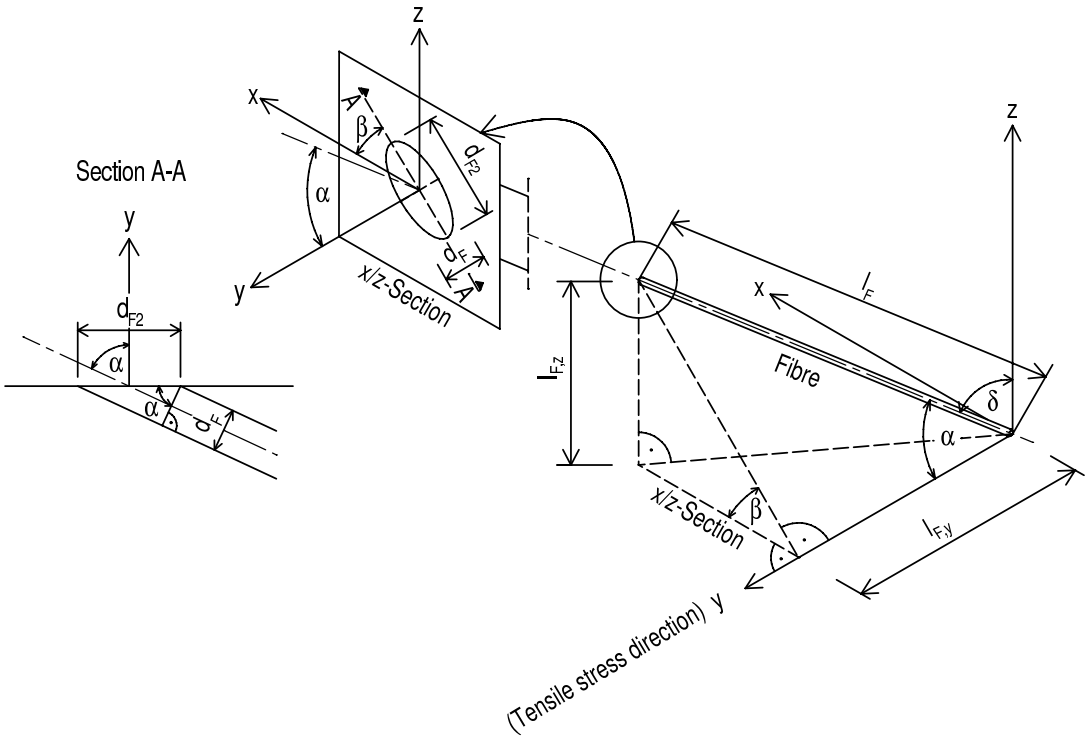

Figure 2: Geometric relations for the determination of the fibre orientation

$$\eta_{F,y} = \frac{l_{F,y}}{l_F} = \frac{l_F \cdot \cos\alpha}{l_F} = \cos\alpha = \frac{d_F}{d_{F2}} \tag{3}$$

The average orientation coefficient of the examined can be calculated as:

$$\eta_{F,y} = \frac{1}{N_F} \cdot \sum_{i=1}^{N_F} \frac{l_{F,y,i}}{l_{F,i}} = \frac{1}{N_F} \cdot \sum_{i=1}^{N_F} \frac{d_{F,i}}{d_{F2,i}} \tag{4}$$

with	$d_{F,i}$	Length of the short principal axis of the ellipse (fibre diameter)	[mm]
	$d_{F2,i}$	Length of the long principal axis of the ellipse	[mm]
	N_F	Number of fibres	[-]

Furthermore, the fibre orientation for other directions orthogonal to the examined direction (y-direction) can be calculated if the angle β between the principal axis of the ellipse and one axis of the examined section is known. The fibre orientation of a single fibre in relation to the z-direction can determinate with equation 5.

$$\eta_{F,z} = \frac{l_{F,z}}{l_F} = \frac{l_F \cdot \cos\delta}{l_F} = \frac{l_F \cdot \sin\alpha \cdot \sin\beta}{l_F} = \sin\alpha \cdot \sin\beta = \sin\left(\arccos\frac{d_F}{d_{F2}}\right) \cdot \sin\beta \tag{5}$$

The average orientation coefficient is:

$$\eta_{F,z} = \frac{1}{N_F} \sum_{i=1}^{N_F} \sin\left(\arccos\frac{d_{F,i}}{d_{F2,i}}\right) \cdot \sin\beta_i \tag{6}$$

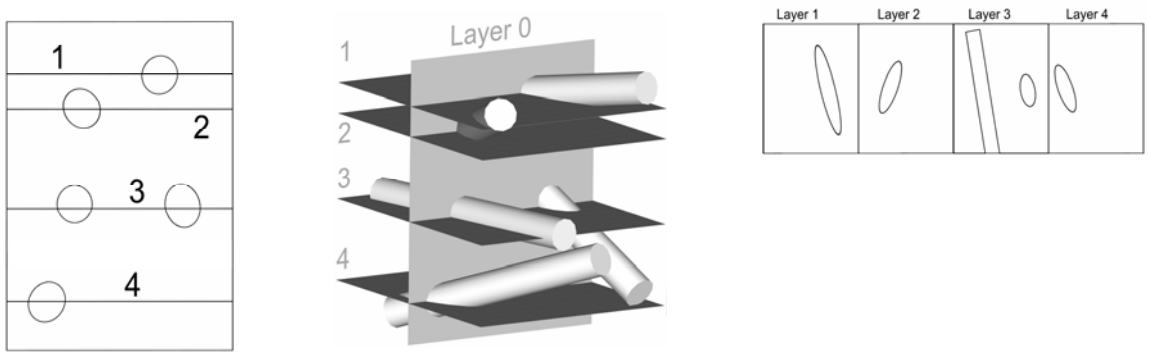

(a) Fibre cross sections in the examined section

(b) Spatial position of the fibres

(c) Fibre cross sections in the calculated sections

Figure 3: Mathematic determination of the fibre orientation

For the mathematic determination of the fibre orientation the spatial position of the fibres (figure 3b) is calculated based on the experimentally found values of d_F, d_{F2} and β in the examined section (figure 3a). In this process the "duality-orientation problem" [8] (figure 4) is not considered because it has no influence on the calculated sections (layer 1 until 4 in figure 3c) which are orthogonal to the examined section (layer 0). Afterwards, for each fibre the coefficient $\eta_{F,i}$ is determined based on the fibre cross sections in the calculated section. The average value of the coefficients gives a good estimate of the fibre orientation in the direction orthogonal to the examined direction. The validity is limited to an area of $l_F/2$ perpendicular to layer 0.

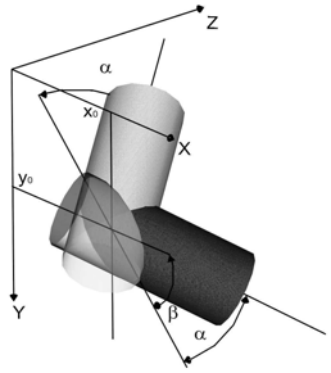

Figure 4: Graphic illustration of the „duality-orientation-problem“

3 Determination of the distribution and orientation of micro steel fibres in UHPC

The photographic method developed at the Leipzig University stands out thanks to an improved photography and analysis of the sections in comparison to the method from *Schönlin* [5]. The image analysis software FiDiOr (Fibre Distribution and Orientation) was developed to that end. Furthermore, the preparation of the section was adapted on the

requirements of UHPC reinforced with micro steel fibres. Three factors are important for an accurate determination of the fibre distribution and orientation:

- Preparation of the sections
- Photography of the sections
- Computer-assisted image analysis

3.1 Preparation of the intersections

High thermal and mechanical stresses occur during cutting the specimens and the fibre cross sections melt in the section. The melting effect is especially significant for the micro steel fibres (diameter about 0.16 mm) usually used in UHPC (figure 5a). So the sections must be prepared after cutting to restore the original elliptical geometry of the fibre cross sections (figure 5b). Furthermore, fibres can be separated which are melt to clusters before preparation. The preparation of the sections begin with a levelling of the rough unevenness, e.g. from lurching of the saw blade. After that a wet grinding procedure is applied to restore the original fibre cross sections.

(a) Before preparation

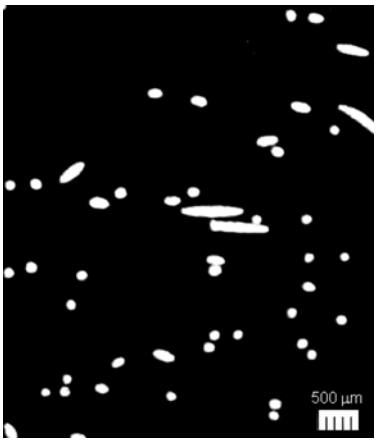

(b) After preparation

Figure 5: Light-optical microscope view of a section

3.2 Photography of the sections

The images of the sections should be taken with a high resolution digital camera because the pictures must be available in a digital format for the analysis. The following requirements are made on the pictures of the sections:

- Good contrast between fibre and concrete
- Uniform lightening
- High resolution
- Avoidance perspective distortions

The fibre diameter should correspond to a minimum of 9 pixels in the image. Therefore a camera with a resolution of 9 million pixels is required to take a picture with a size of 50 x 50

mm and a fibre diameter of 0.16 mm. A lower resolution limits the precision of the logging of the geometry of the ellipses and thus also the determination of the fibre orientation. Perspective distortions by camera shake can be avoided by the use of a tripod. Other perspective distortion, e.g. barrel, pincushion or complex distortions can be compensated by the use of high quality lens and camera with full frame senor or with software applications.

3.3 Computer-assisted image analysis

The computer-assisted image analysis is carried out with the self-developed software FiDiOr in 3 steps:

- Step 1: Image analysis
- Step 2: Post-editing
- Step 3: Data interpretation

An automatic image analysis is executed in the step 1. The differentiation between fibres and concrete is carried out by a threshold limit value on a grey scale with 256 brightness graduations. Pixels with a grey tone above the threshold value are interpreted as fibre parts. Afterwards groups of pixels are assigned to fibres using a recursive algorithm. The fibre geometry is subsequently idealized by substitute ellipses for groups of pixels.
In step 2 the ellipses from step 1 are transmitted to a CAD-unit and marked in the picture of the section. Through this a visual control is possible. The ellipses are plotted in four different colours (green, red, magenta, blue) (figure 6). The colours have following meanings:

- Green: Correct fibre - length of the short principal axis of the ellipse is equal with the nominal fibre diameter
- Red: Failure 1 - length of the short principal axis of the ellipse is larger than the nominal fibre diameter (e.g. overexposed fibres)
- Magenta: Failure 2 - length of the short principal axis of the ellipse is smaller than the nominal fibre diameter (e.g. fibre fragments)
- Blue: Failure 3 - fibre cluster

The program FiDiOr allows not only identifying incorrect fibres but also the manual post-editing of incorrect fibres. It is possible to change the measurements of the ellipses, add new ellipses or erase incorrect ellipses. The combination of automatic fibre detection with additional post-editing remarkably reduces the effort for the image analysis. At the same time a convincing database for the determination of the fibre distribution and orientation is created.

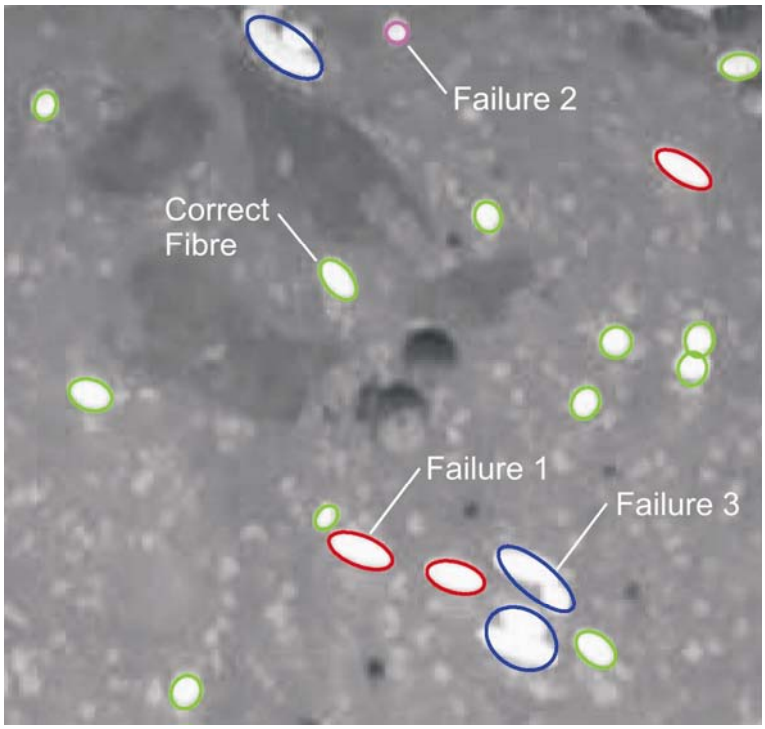

Figure 6: Illustration of the equivalent ellipses in the section

In step 3 the data of the substitute ellipses is transmitted from the CAD-unit to a calculation unit. The calculation-unit determines following results:

- Number of fibres N_F [-]
- Experimental fibre content v_{exp} according to *Hilsdorf* [9] [vol.-%]
- Fibre orientation η_F according to equation (2) [-]
- Fibre orientation η_F according to equation (4) [-]

Because fibre orientation is determined according to equation (2) and (4) it is possible to check the results if the experimental (actual) fibre content correspond to the nominal fibre content.

4 Conclusion

For the application of fibre reinforced UHPC the knowledge about the fibre distribution and orientation is important from structural, economic and ecologic point of view. However, some specifics must be considered for UHPC reinforced with micro steel fibres. The preparation, photography and analysis of the specimens are similarly important for a accurate determination of the fibre distribution and orientation. With the suggested photographic method a suitable technique is presented to determine these parameters.

5 References

[1] Erdem, E.: Probabilistisch basierte Auslegung stahlfasermodifizierter Betonbauteile auf experimenteller Grundlage, Dissertation, Ruhr-Universität Bochum, 2002

[2] Stroeven, P., Shah, S.P.: Use of radiography-image analysis for steel fibre reinforced concrete. Proceedings, RILEM Symposium on Testing and Test Methods for Fibre Cement Composites, Construction Press Ltd, 1978, pp. 275-288

[3] Linsel, S., Dehn, F.: Determination of fibre distribution in self-compacting steel fibre concrete (SCSFC) by computer tomography (CT), Sixth Int. Symposium on High Strength/High performance concrete, Edited by König, Dehn, Faust, University of Leipzig, pp. 1129-1137

[4] Wichmann, H.-J.; Niemann, P.; Droese, S.: Messung des Stahlfasergehaltes auf elektromagnetischer Basis, Forschungsarbeiten aus dem Institut für Baustoffe, Massivbau und Brandschutz der Universität Braunschweig, Heft 144, Braunschweig 1999

[5] Schönlin, K.: Ermittlung der Orientierung, Meng und Verteilung der Fasern in faserbewehrtem Beton, Beton- und Stahlbetonbau 83, Heft 6, Verlag Ernst und Sohn, Berlin 1988

[6] Tue, N. V., Henze, S., Küchler, M., Schenck, G., Wille, K.: Ein optoanalytisches Verfahren zur Bestimmung der Faserverteilung und -orientierung in stahlfaserverstärktem UHFB, Beton- und Stahlbetonbau 102 (2007), Heft 10, S. 674-841

[7] Markovic, Ivan: High-Performance Hybrid-Fibre Concrete - Development and Utilisation -, Dissertation, TU Delft, Delft University Press, 2006.

[8] Zak, G., Park,C. B., Benhabib, B.: Estimation of Three-Dimensional Fibre-Orientation Distribution in Short-Fibre Composites By a Two-Section Method. Journal of Composite Materials, No 4, 2000

[9] Hilsdorf, H. K., Brameshuber, W., Kottas, R.: Abschlußbericht zum Forschungsvorhaben „Weiterentwicklung und Optimierung der Materialeigenschaften faserbewehrten Betons und Spritzfaserbetons als Stabilisierungselemente der Felssicherung“, Universität Karlsruhe, 1985

Josef Hegger
Prof. Dr.-Ing,
RWTH Aachen University
Aachen, Germany

Guido Bertram
Research Engineer
RWTH Aachen University
Aachen, Germany

Shear carrying capacity of steel fiber reinforced UHPC

Summary

Ultra-High Performance Concrete (UHPC) is a high-tech material opening new opportunities especially for slender constructions as for example pretensioned beams. Within a priority program [1] supported by the German Research Foundation (DFG) the shear carrying capacity of beams is in vestigated at the Institute of Structural Concrete at RWTH Aachen University. Several tests on beams with and without openings were carried out. Due to the steel fibers added to the concrete, no shear reinforcement is required. The shear carrying capacity of UHPC beams is significantly increased compared to normal strength or even high strength concrete. The parameters varied were the fiber content, the prestressing grade, the shear slenderness as well as the position and amount of web openings in the beams.

Keywords: *ultra-high performance concrete, steel fibers, shear carrying capacity, prestressing*

1 Field of application and research significance

It is well known that the compressive strength of UHPC is about five times the strength of conventional normal strength concrete. Therefore, a high degree of prestressing can be applied and thus, more slender structures are feasible. This leads to significant savings in dead load, which is an important issue especially for prefabrication. The essential savings of the new construction material are the low consumption, lower transport costs and dead load.
The production requirements for UHPC restrict the main field of application to prefabricated members, e.g. roof girders of large storages. For the building service systems web openings are arranged in the girders, which effects the flow of the shear stresses. Also, the ultimate shear carrying capacity is considerably reduced. The steel fibers contribute to the shear resistance and thus the fibers also improve the post-cracking behavior. The load bearing behavior becomes nearly ductile after crack initiation. To take into account the fibers, constitutive design rules for the shear carrying capacity of UHPC are essential for both, beams with and without web openings.

2 Specimen design and fabrication

The concrete composition is based on the mix design of the priority program [1] (M0 with 2.5% p.v.). With respect of the sustainability, the fiber content was varied. Table 1 summarizes the concrete mixes used for the beam tests. The steel fibers of 0.15 mm diameter had a length between 9 mm and 17.5 mm. The reference composition MR

contained no fibers. The concrete showed nearly self consolidating properties and could be cast without compacting.

Table 1: concrete composition

material [kg/m³]	M0 (2.5% p.v.)	M1 (0.9% p.v.)	MR (w/out fibers)
cement CEM I	650	660	666
silica fume	177	180	181
quartz powder	456	463	467
sand 0.125-0.5 mm	354	360	363
basalt 2-8	598	606	612
steel fiber 9.0/0.15	194	-	-
steel fiber 17.5/0.15	-	70	-
water	158	161	162
superplasticizer	31	32	32

An overview of the conducted shear test program is given in table 2. So far, four beams have been fabricated. Due to the specific loading (Figure 1) two tests with different prestressing grades could be performed on one beam. The first test is indicated with “a” and the second with “b”. To avoid an anchorage failure, two stirrups Ø6 were arranged behind the support. A considerable enhancement of the overhang is not expedient because the rising arch action influences the shear carrying capacity more than in common practice. A size of 15 cm was appointed for all shear tests. The specific concrete cover was $c/d_p = 2{,}5$ according to preceding tests [2].

Table 2: parameters of the shear tests

test	concrete			slender-ness	support overhang	strands with bond / total
	M1	M0	MR	a/d [-]	[m]	units 0.5’’
T1a	x			3.8	0.15	7 / 9
T1b	x			3.8		9 / 9
T2a			x	3.8		7 / 9
T2b			x	3.8		9 / 9
T3a		x		3.8		7 / 9
T3b		x		3.8		9 / 9
T4a	x			3.8		9 / 9
T4b	x			4.4		9 / 9

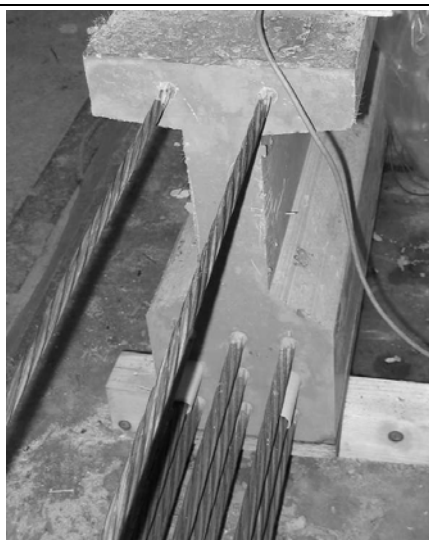

The lower chord was pretensioned with nine 0.5’’ strands, each with a prestressing of 125 kN (figure 1). Two of the middle strands were debonded on one side of the beam. This way, two different ratios or prestressing could be tested. All other parameters as the effective depth maintained the same. To check out the influence of the shear slenderness, the forth beam was tested with a/d = 3.8 (T4a) and 4.4 (T4b).

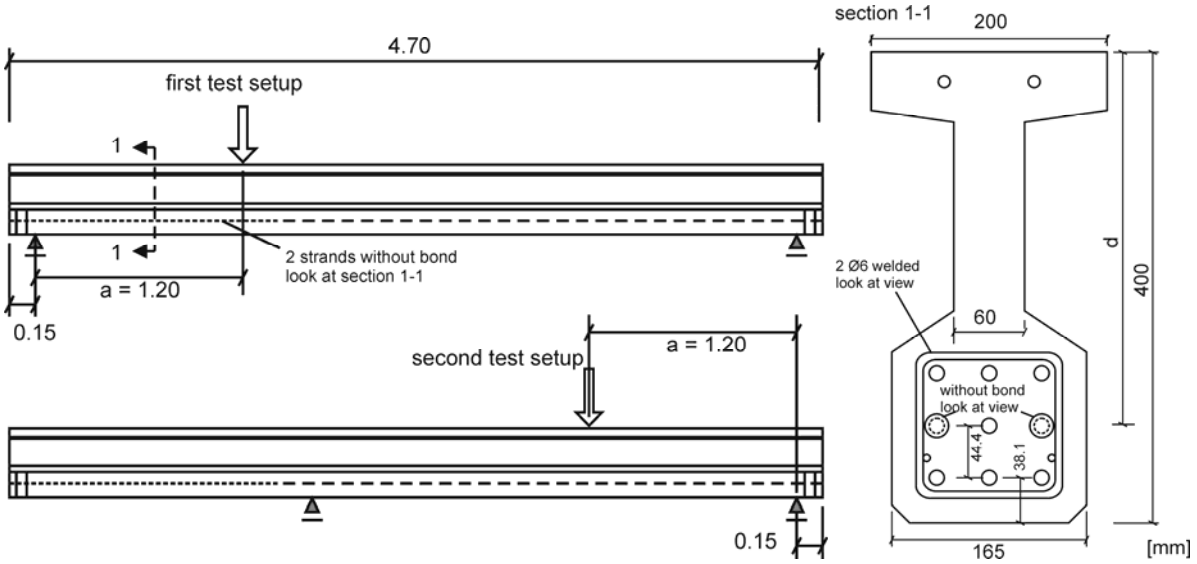

Figure 1: view and section of the specimens and the test set-ups

3 Prestressing

The prestressing force was induced in steps of 20 % three days after concreting. The concrete compression strength at that time was about β_{cube} = 100 to 110 N/mm². As shown in figure 2, the longitudinal concrete strain due to prestressing was about -0.8 ‰ (T1a with seven strands) and -1.0 ‰ (T1b with nine strands). Due to creep and shrinkage the concrete strain increased up to -1.25 ‰ and -1.6 ‰ until the day of the first shear test.

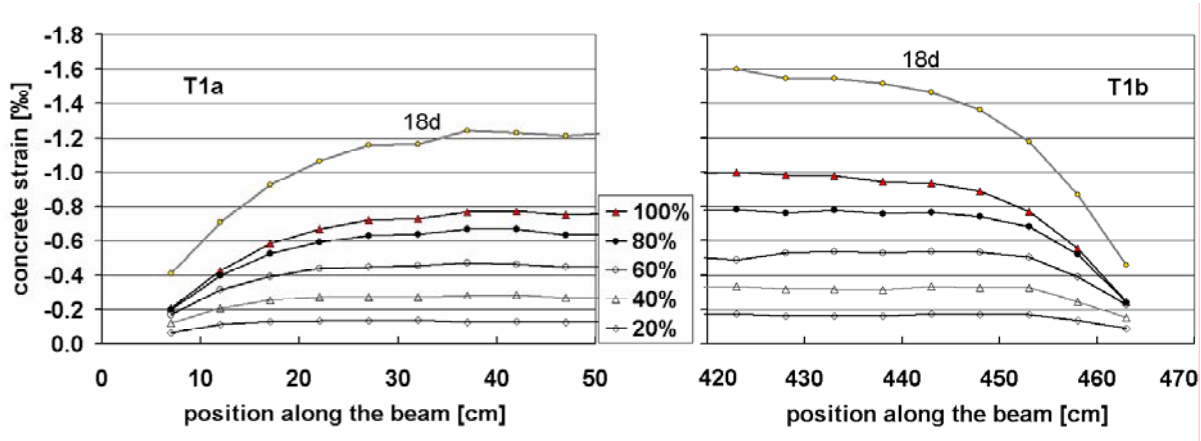

Figure 2: longitudinal concrete strain along the lower strands of T1

The simultaneous loss of prestressing directly influences the shear carrying capacity since the arch action is decreased. At the time of the shear tests of beam T1 the losses of prestressing were 18 % (T1a) and 24 % (T1b) with regard to the initial state in the prestressing bed.

Furthermore, the concrete strains indicated, that the transfer length is appr. 25 cm to 30 cm. This means, that the transfer length is longer than the support overhang, which influences also the arch action [2]. The beams T2, T3 and T4 showed comparable results, but the missing fibers in T2 led to horizontal hairline cracks lateral to the middle strands and the

transfer length was increased.

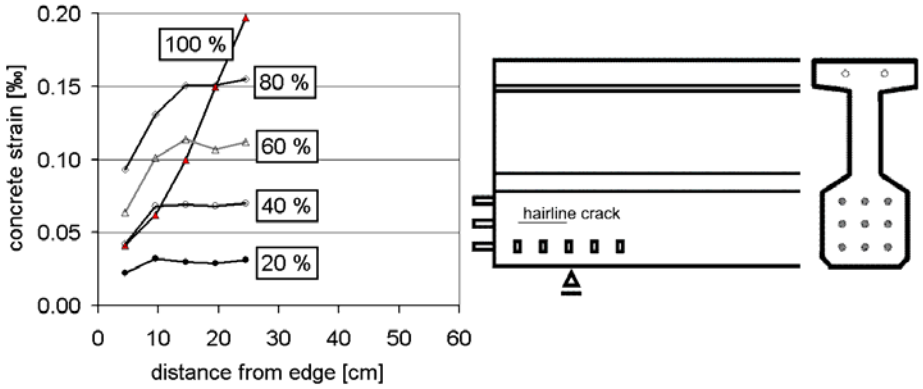

Figure 3: vertical concrete strain in the anchorage zone lateral to the middle strands of T2

At the end of the member the so-called hoyer-effect leads to lateral tension in the concrete, which may arise till tension failure of the concrete. When the prestressing was induced, the lateral strain has been measured in five measuring points with strain gauges (figure 3). They were arranged in the height of the lower strands (detail view in figure 3). The first three steps of prestressing led to a lateral strain of about 0.035 ‰ in each step, that means about 0.105 ‰ after 60 %. After that, the increase of lateral strain became nonlinear and at the end of the prestressing, the failure strain of about 0.2 ‰ was exceeded. Hairline cracks lateral to the middle strands appeared on the front as well as on the back side. These cracks developed in a distance of appr. 10-15 cm from the end of the beam, but did not reach the edge (detail view in figure 3). An increase of the end slip of the strands has not occurred. In almost the same manner as T1b, the end slip ranged between 0.8 mm and 1.0 mm. On the other side of the beam, where seven strand were arranged, the maximum lateral strain was 0.17 ‰ with no cracks visible.

4 Shear tests

Generally, the shear tests showed a very stiff load bearing behavior due to the high prestressing. In figure 4 the load-deflection diagrams for all four beams are presented. In the left diagram the shear tests with different fiber ratios are compared. In test T1b (0.9 % p.v.) first shear cracks developed at a shear load of 245 kN which led to a decrease in initial stiffness. Further cracks appeared continuously while loading. The ultimate shear load of 267 kN was reached at a deflection of 9 mm. The main failure cracks were declined between 20° and 24° (figure 8) with spacings from 2 to 3 cm. As expected, the ultimate shear force of T1b was superior to T1a due to the higher prestressing (table 3). Two main failure cracks in T1a were declined 20° and 22°. Entirely different, the second beam without steel fibers failed without any indication. The crack pattern of the failure cracks was similar but there was a sudden failure after the first crack developed. When 2.5 % steel fibers were added to the concrete there was a significant increase in ultimate load. The load deflection curve indicates first cracks at approximate 220 kN, however, at this time no cracks were visible. Only at a higher load level capillary cracks with a spacing of appr. 3 mm appeared. About 90 % of all

cracks showed a width less than 0.05 mm and after failure these cracks were completely closed again and no longer visible.

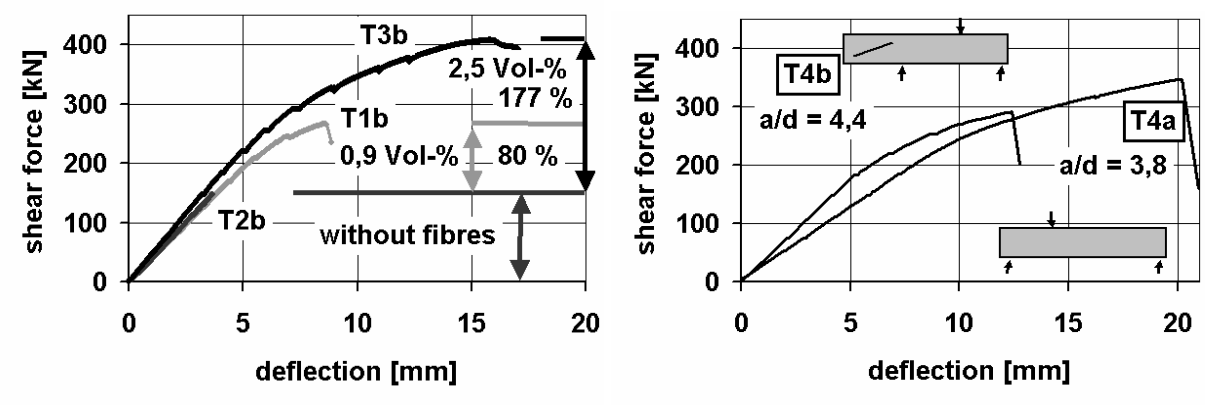

Figure 4: load deflection behavior depending on the fiber ratio and the shear slenderness

The comparison of the load deflection curves of T1b, T2b and T3b in figure 4 as well as the ultimate shear forces in table 3 indicate the effectiveness of the steel fibers as shear reinforcement. Even 0.9 % p.v. of steel fibers led to an increase of 80 % and an amount of 2.5 Vol-% even of 177 % in comparison to T2b without fibers. The shear bearing capacity of T3a was even higher than the bending resistance. To prevent bending failure, the test was aborted. The flexural strength R_f of the concrete compositions with 0.9 % fiber content (T1, T4) and 2.5 % (T3) were almost in the same range. But the flexural strength without fibers (T2) was considerably reduced. The flexural strength was determined with three point bending tests (prism dimension: 4cm x 4cm x 16cm).

Table 3: material properties and ultimate shear forces of the shear tests

	test	T1a	T1b	T2a	T2b	T3a	T3b	T4a	T4b
$f_{c,W100}$	[N/mm²]	151	174	134	134	162	170	176	183
R_f	[N/mm²]	22.7	21.2	12.3	12.3	23.1	24.1	19.1	20.2
V_u	[N/mm²]	234	267	134	147	abort	408	344	291

The ultimate shear force of T4b with an enlarged shear slenderness of a/d = 4.4 was about 15 % lower compared to T4a with a/d = 3.8 as presented in the right diagram of figure 4. This leads to the assumption, that a higher arch action is still present even when a/d = 3.8. The different stiffness is not caused by the slenderness but the different spans of the first and second test set-ups. A comparison of T1b and T4a is not possible without restrictions, because they were fabricated with different casting methods. The fiber orientation, which is influenced by the casting method, will be investigated within the project.

Apart from T2 most of the shear cracks started at the bottom of the web (A in figure 5). Some of these cracks developed slowly upwards the web and were decisive for the later failure (B). When shear failure occurred, the cracks grew suddenly towards the anchorage zone of the strands (C). However, a significant strand slip before shear failure was not observed and anchorage failure may be excluded.

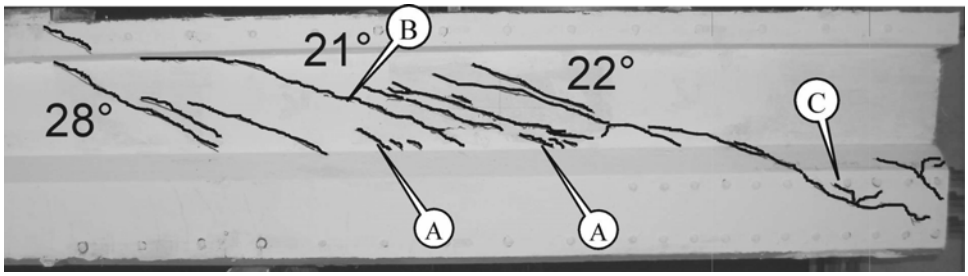

Figure 5: crack pattern and characteristic stages of crack formation of T4b

5 Girders with web openings

Former shear tests with multiple openings in the web [2] showed that the remaining shear resistance was about 60 to 65 % compared to solid beams. Within the current research project the influence of single and multiple openings will be investigated systematically. In the first step, single openings are arranged with different spacings to the support and varying diameters. Girders with openings and additional shear reinforcement will complete the experimental program of this research project.

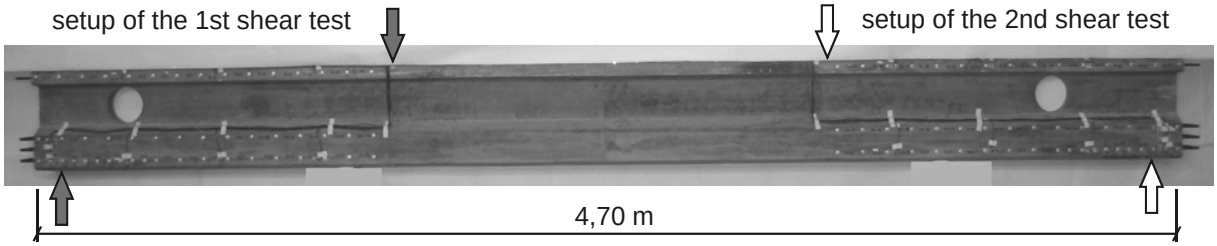

Figure 6: pretensioned girder with single web openings and different spacings to the support

To predict the load bearing behavior and the crack formation, nonlinear numerical simulations were conducted. The simulations were carried out with the program LIMFES, which includes the micro plane model [7-10]. This material model is appropriate to describe the distinctive fracture energy of UHPC with steel fibers. As presented in figure 7 the finite element model has been calibrated amongst others with test T1b. The experimental and calculative results agree in stiffness as well as the ultimate load very well. At a load stage of about 70 % the stiffness decreases, in the test as well as in the simulation.

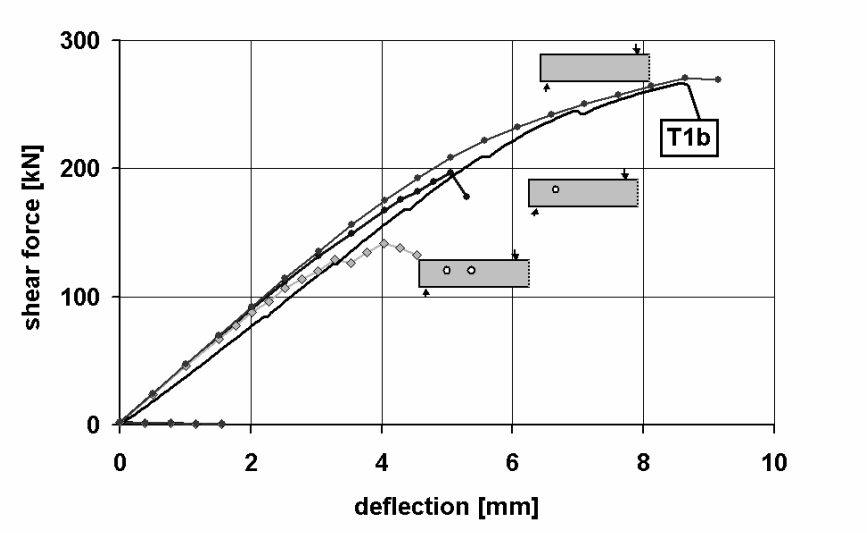

Figure 7: preliminary simulations with web openings – load deflection curves

One opening led to a theoretical decrease of the shear carrying capacity of 27 %, when the opening was arranged 30 cm (effective depth d = 30 cm) from the support. The spacing was varied as well, but the influence was barely noticeable. The high prestressing and the crack angle accounts for this behavior. Adding a second opening, the shear resistance decreases to 50 % compared to the solid beam. In each case, the crack development initiated lateral to the openings and led finally to shear-tension failure as presented in figure 8. These results are used to attach the measurement equipment like displacement transducers as well as other devices (e.g. Aramis [5, 6]) to the most effective position. Furthermore, the simulations indicate, that a vertical reinforcement adjacent to the openings is an effective enhancement.

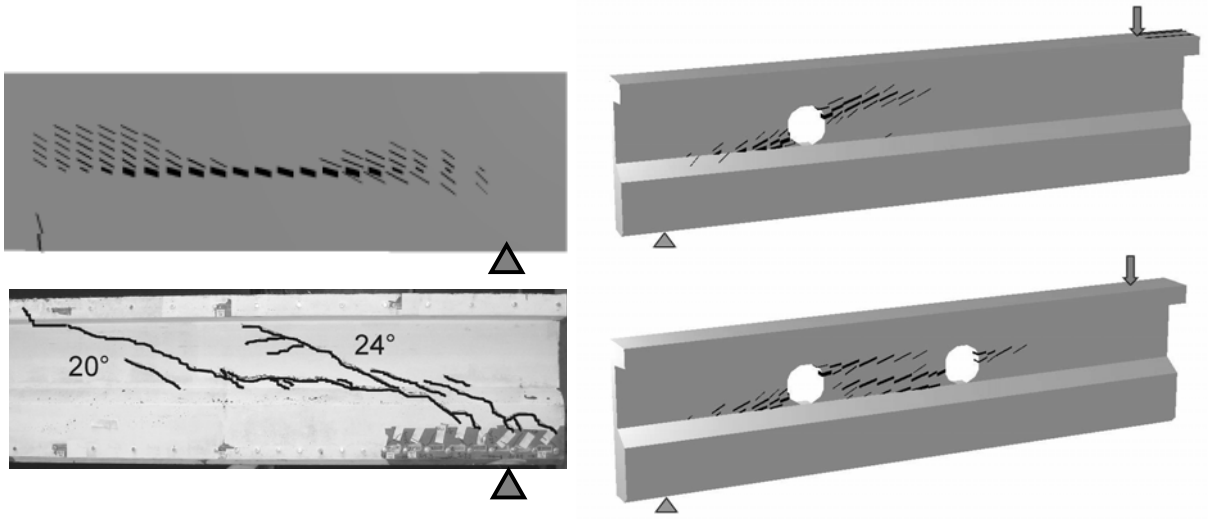

Figure 8: simulated crack formation of T1b compared to the test result (left) and preliminary simulations with one and two web openings

6 Summary and conclusions

Shear tests with pretensioned girders made of UHPC were carried out. The main test parameters were the fiber content, the prestressing grade and the shear slenderness. In advance, the following beam tests with openings were simulated.

The results can be summarized as follows:

- The amount of steel fibers has a significant influence on the shear carrying capacity. With increasing the fiber ratio the failure becomes more and more ductile.
- The specific concrete cover $c/d_p = 2{,}5$ seems to be adequate for this strand arrangement when steel fibers are added. Without fibers, single hairline cracks in the anchorage zone were observed.
- Higher prestressing forces led to approximate proportional higher shear resistance.
- One test with a shear slenderness a/d = 4.4 leads to the assumption, that a higher fraction of arch action seems to be present when a/d = 3.8.

7 Acknowledgement

This research project is part of the SPP 1182 which is founded by the DFG (German Research Foundation). The authors acknowledge the support.

8 References

[1] German Research Foundation, Collaborative research project (DFG SPP 1182), Nachhaltig Bauen mit UHPC (Sustainable Building with UHPC).

[2] Hegger, J.; Bertram, G.: „Anchorage behavior of pretensioned strands in steel fiber reinforced UHPC", Proceedings, 2nd International Symposium on UHPC, Kassel, Germany in 2008.

[3] Hegger, J.; Rauscher, S.; Voss, S.: Shear Carrying Capacity of Fiber-Reinforced UHPC, CCC°2005, 11.-13. Juli 2005, Lyon/Frankreich, pp. 1173-1180.

[4] Hegger, J.; Kommer, B.; Tuchlinski, D.: Untersuchungen an Spannbetonträgern aus UHPC. Betonwerk + Fertigteil-Technik, BFT-China 2006, S. 3-8.

[5] Görtz, S.: Schubrissverhalten von Stahlbeton- und Spannbetonbauteilen aus Normal- und Hochleistungsbeton, Dissertation, RWTH Aachen; 2004.

[6] Hegger, J.; Görtz, S.; Schwermann, R.: Analyse des Schubrissverhaltens unter Einsatz der Photogrammetrie. Bautechnik 79, 2002, Heft 3, S. 135–142.

[7] Hegger, J.; Beutel, R.; Karakas, A.; Häusler, F.: Ersatz oder Teilersatz von Querkraftversuchen durch Finite-Elemente-Berechnungen. DiBt-Forschungsvorhaben des Instituts für Massivbau der RWTH Aachen. ZP 52-5-7.237-1121/04, Final Report August 2006.

[8] N. Kerkeni: LIMFES documentation. Hegger+Partner Aachen (not published).

[9] Bažant, Z.P; Caner, F.C; Carol,I; Adley, M.D; Akers, S.A.: ''Microplane model M4 for concrete.I : Formulation with work-conjugate deviatoric stress.'' J. Eng. Mech.,1269,944–953 (2000).

[10] Caner,F.C; Bažant, Z.P.: ''Microplane model M4 for concrete. II: Algorithm and calibration.'', J. Eng. Mech.,1269,954–961 (2000).

Martin Empelmann
Prof. Dr.-Ing.
Technical University Brunswick, (iBMB)
Brunswick, Germany

Manfred Teutsch
Dr.-Ing. Academic Director
Technical University Brunswick, (iBMB)
Brunswick, Germany

Guido Steven
Dipl.-Ing. Research Assistant
Technical University Brunswick, (iBMB)
Brunswick, Germany

Load-Bearing Behaviour of Centrically Loaded UHPFRC-Columns

Summary

Ultra High Performance Concrete (UHPC) shows a very brittle material behaviour, both in compression and in tension. This can result in a sudden, unannounced failure of UHPC columns. Experimental research [4] carried out at the iBMB of the Technical University of Brunswick, Germany, shows that the load-bearing behaviour of UHPC can be improved considerably by the addition of steel fibres, leading to Ultra High Performance Fibre Reinforced Concrete (UHPFRC), as well as by a longitudinal reinforcement of high-strength rebars and a core confinement by reinforcement stirrups. These UHPFRC-Columns are able to produce a similar robustness and ductility compared to HPC and NPC columns. As a result of the tests carried out in this context, a design model for the load-carrying and post-peak behaviour of centrically loaded UHPFRC-Columns was developed, which takes these mechanical measures into account.

Keywords: *UHPFRC-Columns, confinement, steel fibre, ductility, robustness*

1 Introduction

Due to architectural reasons and for the optimisation of the rentable floor space, the current structural layouts of high rise buildings often demand very small column cross-sections. These requirements cannot be achieved with the presently available and used concrete qualities and with still economical reinforcement ratios. Very often highly loaded columns in high rise buildings have been constructed as composite steel columns, although - in comparison to concrete columns - there is still the need for an additional fire protection but the need for difficult connection details remains. With the development of UHPC the achievable compression strength can be increased in such a way, that UHPC-Columns with a high load-bearing capacity and very small cross sections become possible. However, in order to use UHPC for these structural members, it is necessary to improve the fracture behaviour by appropriate measures in such a way that a comparable robustness to normal strength concrete columns, can be achieved. The following paper describes the possible

measures able to improve the robustness of these columns and presents the result of a series of tests carried out at the iBMB in order to investigate the load-bearing behaviour of centrically loaded UHPFRC-Columns.

2 Post Peak Behaviour and Ductility

The margin between the design load and the ultimate load-bearing capacity of a column is a function of the structural vulnerability and, if a sudden, brittle failure can occur, appropriate additional safety precautions have to be provided. Non-reinforced UHPC columns show a brittle failure, which occurs without prior warning. Therefore, the strength potential of UHPC cannot fully be utilised without additional measures, which ensure a much more ductile behaviour and robustness. In principle the following measures or their combinations are possible:

- Addition of high strength steel fibres to improve the post fracture behaviour,
- Core confinement reinforcement by stirrups,
- Confinement provided by a steel jacket pipe,
- High-strength longitudinal reinforcement.

3 Test Lay-Out

The ultimate stress level and the post-peak deformation behaviour of UHPFRC-Columns was tested with a set of six short columns (20 x 20 x 60 cm). Figure 1 shows the principle test set-up and one of the test specimens prior to testing. The lateral strain was measured with four strain gauges in the middle of the columns. The longitudinal deformation was derived from the piston lift of the testing machine and two linear variable differential transducers (LVDT), arranged at the opposite sides of the test specimens. The longitudinal strain was measured by four vertical strain gauges, placed on the four column sides, as indicated in Figure 1.
The concrete mix was chosen in accordance with the investigations carried out in context with „Improvement of Post Fracture Behaviour of UHPC by Fibres“ [2]. The mix design is given in Table 1.

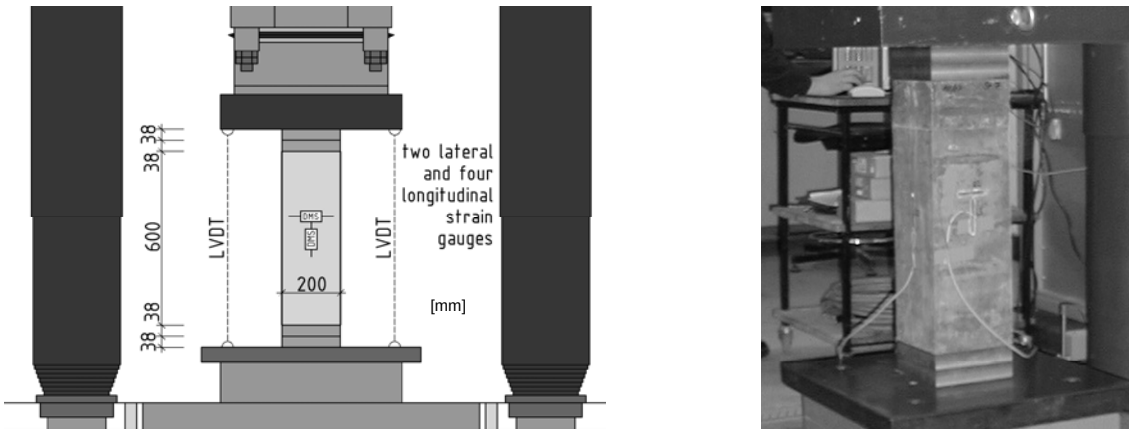

Figure 1: Test set-up for the short columns and installation in a 10 MN testing machine

With reference to the measures already mentioned in Chapter 2 of this paper, a core confinement reinforcement by stirrups was chosen. The possible effect of a confinement by a

steel jacket pipe was not further investigated. The influence of steel fibres and high strength reinforcement was determined by a variation of these test parameters.

Table 1: Concrete Mix (B4Q-3) for Columns S1 to S5, S6 (B4Q without steel fibre)

UHPFRC 160 (B4Q-3)	[kg/m³]		[kg/m³]		[kg/m³]
CEM-I 52,5 R HS-NA	650.0	Quartz flour II	131.0	Superplasticizer Glenium 51	30.4
ELKEM Microsilica Grade 983	177.0	Basalt 2/5	298.5	SF RC 80/30 BP (1.25 Vol.-%)	98.1
Quartz sand 0,125/0,50 mm	354.0	Basalt 5/8	298.5		
Quartz flour I	325.0	Water	158.0		

The design details of the test specimens are summarised in Table 2.

Table 2: Test column details

Column:	S 1	S 2	S 3	S 4	S 5	S 6
Concrete:	B4Q-3 (UHPFRC 145)					B4Q w/o SF UHPC 145
Steel fibre:	$\Sigma v_f \times l_f/d_f$ = 1.25 Vol.-% x 30 / 0.38 = 1.0					0
b / d / l:	20 • 20 • 60 cm					
Arrangement:	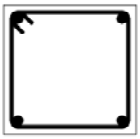		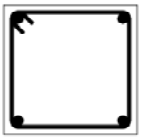	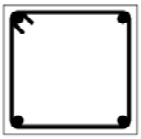	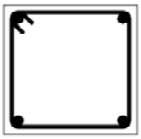	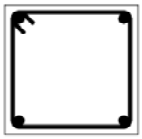
A_{sl}:	4 Ø 28	8 Ø 28	4 Ø 14	4 Ø 28	4 Ø 28	4 Ø 28
Grade A_{sl}:	S 670/800		BSt 500	S 670/800		BSt 500
ρ_l :	6.16%	12.32%	1.54%	6.16%	6.16%	6.16%
Stirrups	1 x Ø 8 / 8.4 cm	2 x Ø 8 / 8.4 cm	1 x Ø 8 / 8.4 cm	1 x Ø 8 / 6.0 cm	1 x Ø 8 / 4.1 cm	1 x Ø 8 / 4.1 cm
Grade A_{sq}:	BSt 500 S					
ρ_s :	1.48 Vol.-%	2.74 Vol.-%	1.48 Vol.-%	2.20 Vol.-%	3.31 Vol.-%	3.31 Vol.-%
Σv_f : fibre volumetric ratio, l_f / d_f : fibre length and Ø, ρ_l :longitudinal reinf. ratio, ρ_s :lateral reinf. volumetric ratio						

4 Test Results

The ultimate load level and the corresponding concrete strains are given in Table 3, showing column S2 with the highest and column S3 with the lowest load-bearing capacity.

Table 3: Ultimate load-bearing capacity and related strain of tested columns S1 to S6.

	S 1	S 2	S 3	S 4	S 5	S 6
N_u	6.516 kN	7.358 kN	5.612 kN	6.057 kN	6.224 kN	6.297 kN
ε_u	3.1 ‰	2.8 ‰	2.9 ‰	3.1 ‰	3.0 ‰	3.0 ‰

Figure 2 shows the load-strain relationship of the six tested columns. It can be seen from these curves, that all columns show a more or less elastic load increase until the maximum load level is reached. Then, depending on the column design, a certain load decrease occurs, followed by a post peak-deformation behaviour, which can differ considerably.

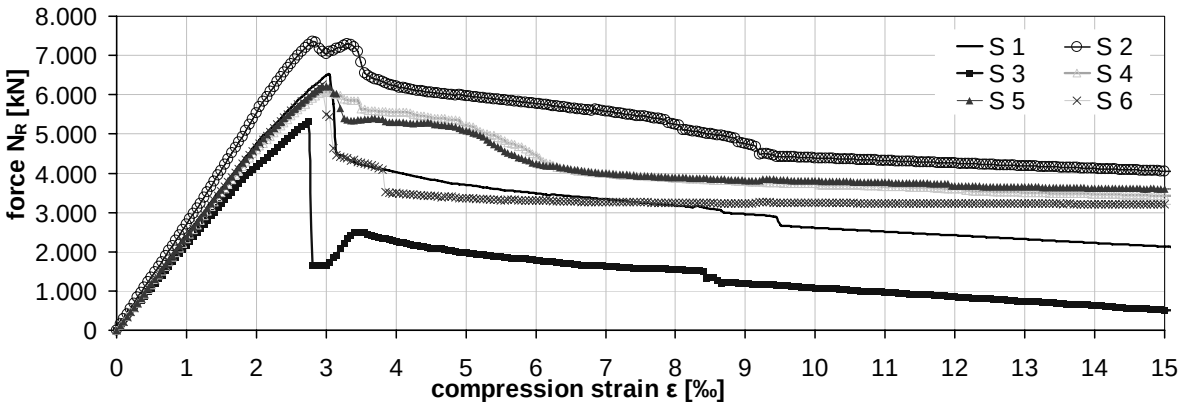

Figure 2: Load - strain relationship of UHPFRC columns S1 to S6

5 Test Analysis

In order to analyse the test results and to evaluate the column ductility, a performance index, based on the proposal in [5], was determined, which compares the area under the force-strain relationship with the internal elastic work, resulting into a ductility index I_{10}. A ductility index I_{10} = 1 means ideal brittle behaviour and I_{10} = 10 indicates an elastic ideal plastic behaviour. The relationship is given in Figure 3.

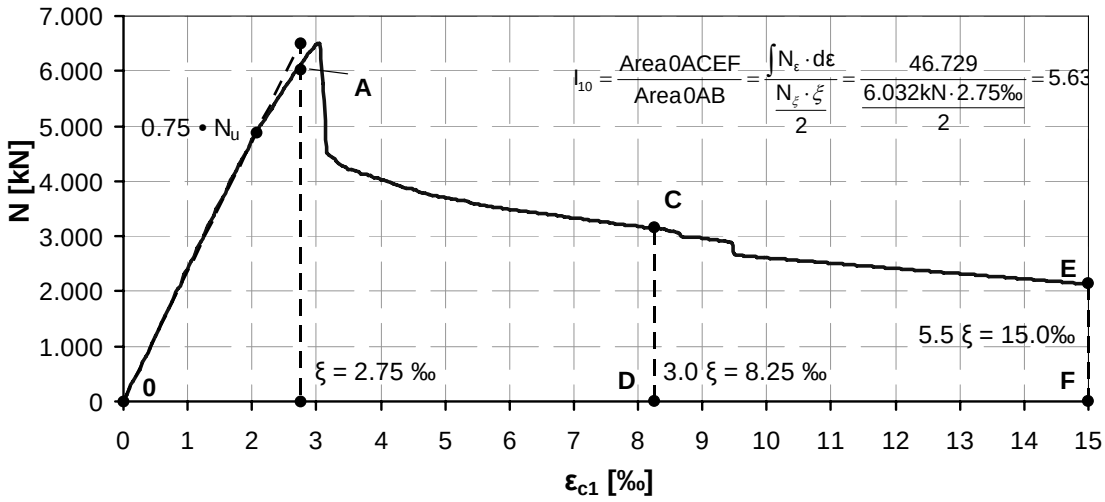

Figure 3: Ductility index I_{10} = 5.63 for column S1, ξ = 2.75 ‰, N_u = 6.512 kN

Figure 4 shows the ductility indices I_{10} according to [5] for the tested columns S1 to S6 [4].

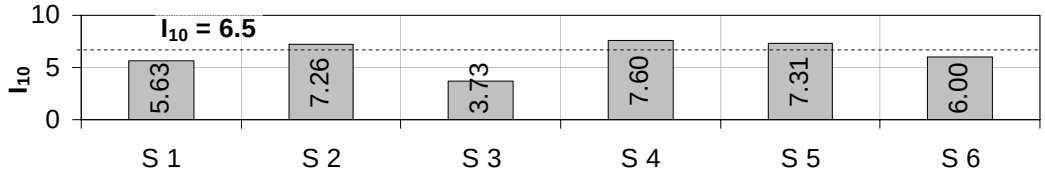

Figure 4: Ductility index I_{10} of columns S1 to S6

Experimental and numerical analysis described in [4] and [5] show, that conventionally constructed RC-columns with compression strengths up to 40 MPa reach a ductility index of I_{10} = 6.5 [5] and this value is reduced to I_{10} = 4 for a column with a compression strength of

100 MPa and minimal lateral and longitudinal reinforcement [4,5]. The question of a required or necessary ductility index has to be determined for the respective application.

It can be concluded from these tests, that the UHPFRC-columns S2, S4 and S5 show a robustness which is comparably to conventional RC-Columns ($I_{10} \geq 6.5$). These columns are constructed with a combination of steel fibres with v_f = 1.25 Vol.% and l_f / d_f = 30 / 0.38 mm, lateral reinforcement ratio of ρ_s > 2,0 Vol.-% and a high strength longitudinal reinforcement which is able to carry approx. 15 % of the ultimate axial load N_u ($N_{Asl} \geq 15$ % N_u).

Furthermore, the different load-strain relationships were normalised to their maximum load level. Figure 5 shows the normalised curves of column S1, S4 and S5, consisting of the same concrete mix (B4Q-3) and longitudinal reinforcement (4 Ø 28, S 670/800), but have a different lateral confinement. Firstly, it can be seen that the post peak deformation behaviour can be improved by increasing the ratio of the lateral confinement reinforcement from 1.48 Vol.-% for column S1 up to 2.20 Vol.-% for column S4. Secondly, a further increase of confinement reinforcement as in column S5 up to 3.31 Vol.-% does not result in an additional improvement of the post-peak behaviour.

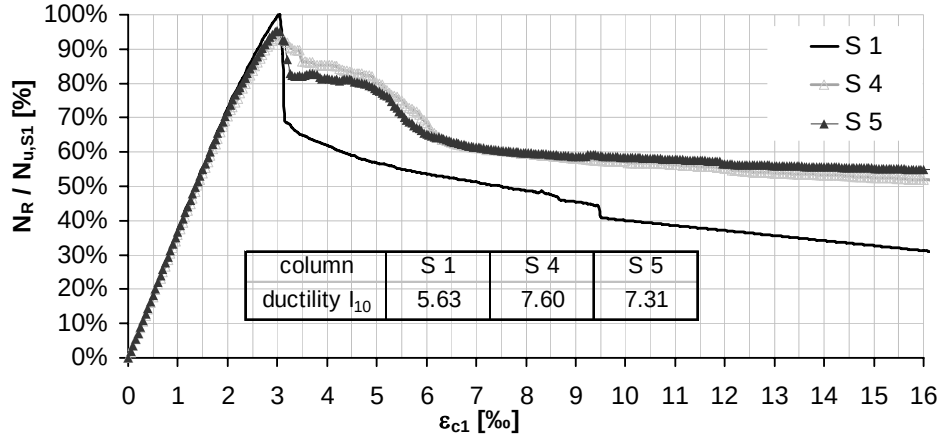

Figure 5: Normalised compression-strain relationships of columns S1, S4 and S5

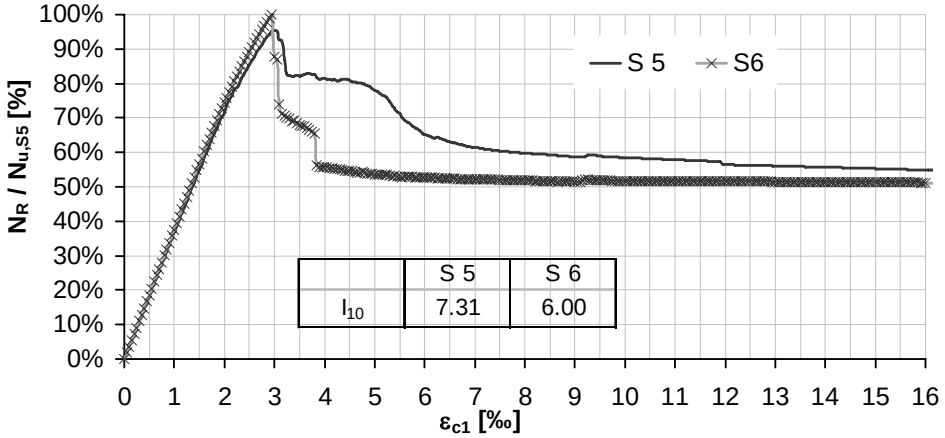

Figure 6: Normalised compression-strain relationship of columns S5 and S6

Figure 6 shows the influence of the steel fibre content. Column S6 consists of B4Q without steel fibres, whereas column S5 has a steel fibre content of v_f = 1.25 Vol.-%. Both columns are reinforced with stirrups Ø 8 mm / e = 4,1 cm, ρ_s = 3.31 Vol.-%. The difference in the steel

grades of the longitudinal reinforcement (S5: S670/800 and S6: BSt 500S) was considered in the normalised curve. Figure 6 show, that the ultimate load-bearing capacity cannot be increased by additional steel fibres, but the post-peak behaviour / robustness is improved considerably from I_{10} = 6.00 without fibres to I_{10} = 7.31 with fibres.

6 Analytical Model

The load carried by a centrically loaded short UHPFRC-column can be described as the sum of the load carried by the unconfined concrete, the confined concrete and the longitudinal reinforcement at each load step. For an analytical description of the load-deformation behaviour in the pre- and post-peak-range the modification of the concrete stress-strain curve of the confined concrete due to a confinement provided by stirrups and steel fibres and the load of the partially spalling unconfined concrete cover have to be considered. In this paper a "smeared" approach is chosen, which idealizes the aforementioned bearing behaviour of unconfined and confined concrete only by a modification of the concrete load-bearing cross section $A_{c,eff}$.

The assumption of an ideal and full bond between reinforcement steel and concrete allows the superposition of the concrete- and steel - loads. For levels with a concrete strain $\varepsilon_c < \varepsilon_{c,u}$, indicating the load-bearing capacity of short columns, the following equation (1) can be used:

$$N_{R,\varepsilon} = N_{c,\varepsilon} + N_{s,\varepsilon} = 0.9 \cdot \sigma_{c,\varepsilon} \cdot A_{c,eff} + \sigma_{s,\varepsilon} \cdot A_s \quad (1)$$

$$A_{c,eff} = A_c - A_s \quad (2)$$

$A_{c,eff}$: net concrete cross-section, A_s : cross section of the longitudinal reinforcement,
$\sigma_{c,\varepsilon}$: uniaxial compressive stress of the concrete, $\sigma_{s,\varepsilon}$: stress of longitudinal reinforcement

For force levels in the post peak range, i.e. $\varepsilon_c > \varepsilon_{c,u}$ indicating the ductility and robustness of short columns, the effective load bearing concrete cross section has to be adopted, due to the spalling of the concrete cover. In order to study different failure possibilities, the following approaches A to C were investigated (Figure 7 and 8).

Approach A: $$A_{c,eff} = \left(b_c \cdot d_c - \frac{\sum (w_i)^2}{6} \right) \cdot \left(1 - \frac{s'_1}{2 \cdot b_c} \right) \cdot \left(1 - \frac{s'_1}{2 \cdot d_c} \right) \quad (3)$$

Approach A (Figure 7) is based on the research work of Held3 on NPC- and HPC-columns with the participation of steel fibres considered according to an approach of Campione et. al. [1] with the steel fibre modified vertical stirrup spacing s_1' according to equation (4).

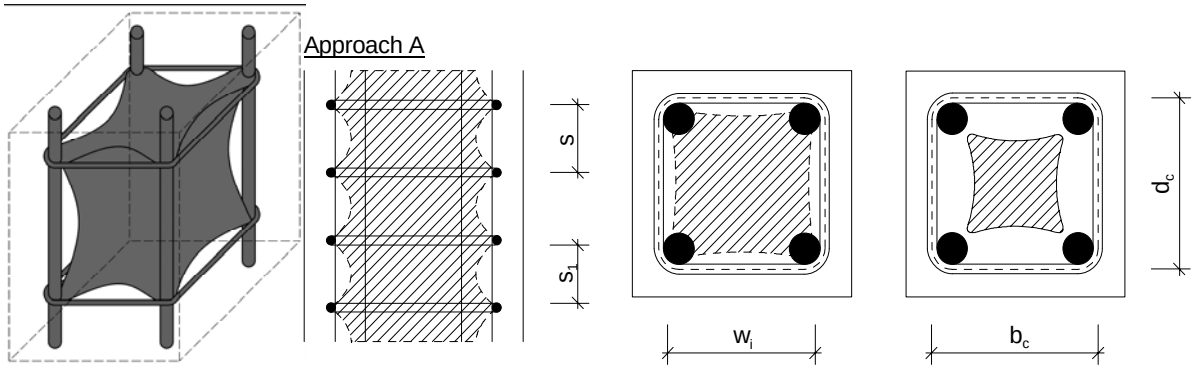

Figure 7: Approach A for the effective post peak load bearing concrete cross section

$$s'_1 = s_1 - \frac{v_f \cdot l_f}{d_f} \quad (4)$$

s_1 : clear vertical spacing between the stirrup [cm]; v_f : volumetric ratio [Vol.-%]; l_f: fibre length and d_f : diameter [mm] of steel fibre

Approach B assumes the complete inner concrete core within the confinement stirrups as still able to carry the compression stresses.

Approach B: $A_{c,eff} = b_c \cdot d_c \quad (5)$

Approach C is based on approach B and assumes that, due to the steel fibre reinforcement, a part of the outer concrete cover is still connected to the inner concrete core. The activation of the outer concrete cover is limited to a quarter of the steel fibre length l_f.

Approach C: $A_{c,eff} = \left(b_c + \frac{2 \cdot l_f}{4}\right) \cdot \left(d_c + \frac{2 \cdot l_f}{4}\right) \quad (6)$

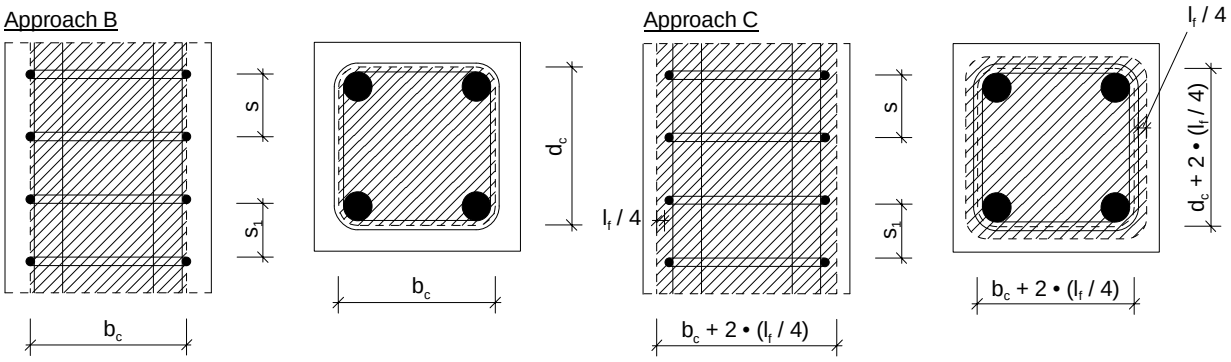

Figure 8: Approach B and C for effective post peak load bearing concrete cross section

The comparison of the load deformation behaviour of the column S1 derived from the tests with the three design approaches is given in Figure 9. For column S1 approach B shows a good correlation over the whole load-strain-range.

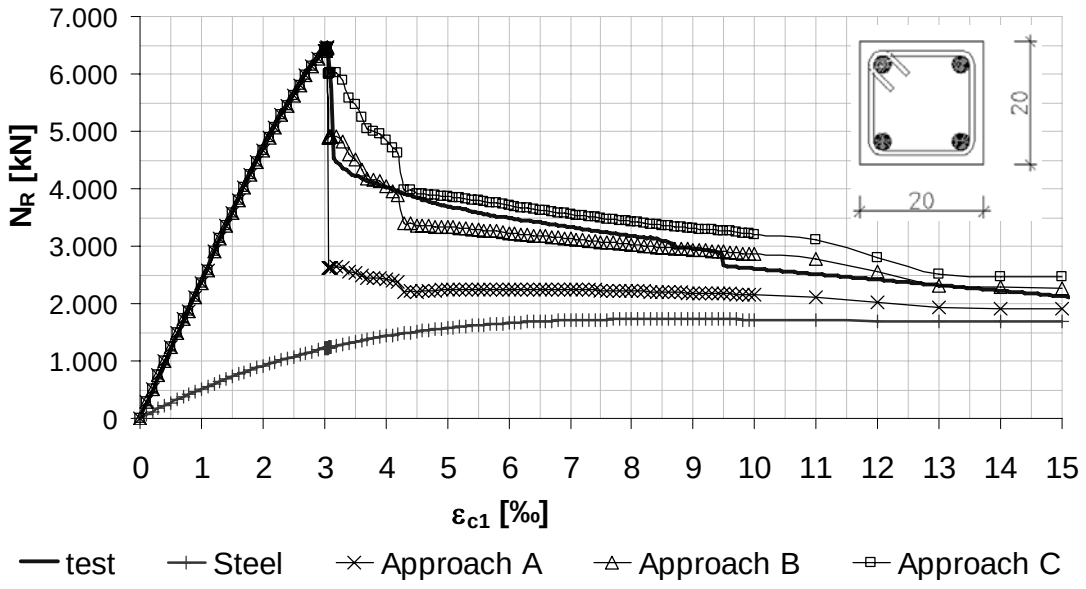

Figure 9: Comparison of column S1 with design approaches A to C

7 Parametric Study of UHPFRC-Columns

In order to define minimum requirements which are able to provide a robust post-peak behaviour of centrically loaded UHPFRC-Columns with square cross sections and a compression strength up to 160 MPa a parametric study was carried out [4]. Herein the parameters concrete dimensions, volumetric steel fibre ratio v_f and aspect ratio l_f / d_f, lateral reinforcement volumetric ratio ρ_s and longitudinal reinforcement ratio ρ_l was changed. The load-strain curve was calculated using the material model for the compression stress-strain relationship of UHPFRC developed in [2] and the idealized load-bearing areas of concrete according to equation (3) (Approach A). This parametric study showed that centrically loaded UHPFRC-Columns are able to show a robust load carrying behaviour when the following parameters are observed.

Minimal steel fibre content:	$\Sigma\, v_f \times l_f / d_f \geq 100$	(7)
Minimal lateral reinforcement volumetric ratio d:	$\rho_s \geq 2.0$ Vol.%	(8)
Minimal load supported by the longitudinal reinforcement:	$N_{Asl} \geq 15\ \%\ N_u$	(9)

8 Conclusion

A series of tests was carried out in order to determine the load bearing behaviour of six centrically loaded UHPFRC - columns. The test results can be summarised as follows:

- A robustness which is comparably to conventional RC-columns can be achieved by the combination of steel fibres and a reinforcement cage composed by longitudinal bars made of high-strength steel and a comparatively moderate confinement by stirrups.
- Columns without steel fibre addition do not show a sufficient robustness for still executale reinforcement ratios.

9 Acknowledgement

The authors thank the “Deutsche Forschungsgemeinschaft (DFG)“ for their financial support in the context of DFG Priority Program (SPP) 1182 “Sustainable Building with Ultra-High-Performance Concrete (UHPC)”.

10 References

1. Campione, G., Scibilia, N., Zingone, G.: Influence of Concrete Cover on the Compressive Strength of FRC Columns, in: 6th Int. RILEM Symposium FRC, 2004., Vol. 2: 935-944.
2. Empelmann, M.; Teutsch, M.; Steven, G.: Improvement of Post Fracture Behaviour of UHPC by Fibres, Proceedings of 2nd Int. Symposium on UHPC, Kassel 2008.
3. Held, M.: Ein Beitrag zur Herstellung und Bemessung von Druckgliedern aus hochfestem Normalbeton, 1992.
4. Teutsch, M.; Steven, G.: DFG-SPP 1182-Arbeitsbericht UHPFRC-Druckglieder. (Not published).
5. Zaina, M., Foster, S.J.: Modelling of fibre-reinforced HSC columns, UNICIV Report R 439, 2005.

Birol Fitik
Dipl.-Ing., Research Assistant
Department of Concrete Structures
Technische Universität München
Munich, Germany

Roland Niedermeier
Dr.-Ing., Research Assistant
Department of Concrete Structures
Technische Universität München
Munich, Germany

Konrad Zilch
Univ.-Prof. Dr.-Ing. habil. Dr.-Ing. E.h.
Department of Concrete Structures
Technische Universität München
Munich, Germany

Fatigue Behaviour of Ultra High-Performance Concrete under Cyclic Stress Reversal Loading

Summary

Structures designed economically by taking advantage of the material properties of Ultra High-Performance Concrete (UHPC) feature reduced self weight. Compared to its high compressive strength UHPC is characterised by low tensile strength. Hence structural members made of UHPC should be prestressed appropriately. Due to economic design alternating live load may cause cyclic stress reversal loading. For diversified application of UHPC the examination of cyclic loading in tension-compression is of considerable practical relevance.

Representing this kind of loading 120 single-level fatigue tests were performed on UHPC specimens without reinforcement. This contribution presents the effect of important parameters like stress level, stress range and fibre addition on the fatigue behaviour of UHPC in classical S-N-diagrams.

Keywords: *ultra high performance concrete, fatigue, cyclic stress reversal loading*

1 Introduction

The high strength of Ultra High-Performance Concrete enables the economical design of slender stuctures with reduced self weight. Compared to structures made of normal strength concrete (NSC) structures made of UHPC show a diverging ratio of dead load to live load. An auspicious design principle for the utilisation of the specific material properties of UHPC is its application combined with prestressing. Economic design of prestressed members made of UHPC may cause cyclic stress reversal loading.

It is well known that NSC shows a reduced fatigue strength under cyclic reversal stress loading compared to threshold loading. Further the stiffness of structures is reduced gradually by the occurring damage progress under cyclic loading.

For the first time comprehensive experimental research was performed on the fatigue behaviour of UHPC under cyclic reversal stress loading in tension-compression. In the first stage of the research project the fatigue strength and the reduction of the uniaxial stiffness due to cyclic loading were examined in 120 force controlled fatigue tests on bone-shaped non-reinforced UHPC-specimens. The lower and upper stress level were defined with respect to practical conditions and material properties such as the prestress level and the assumed long term behaviour under tension loading. Compared to similar previous examinations the fatigue tests were not restricted to 2 million load cycles. Testing an adequate number of tension-compression combinations in this first stage and an additional second stage the indication of approximately linearised limiting curves for defined number of load cycles in terms of Goodman diagrams is the long term objective of the research project.
During the first stage the effect of important parameters like stress range and stress level, fibre addition, fibre orientation and heat treatment on the fatigue behaviour have been investigated in different experimental series.

2 Material

2.1 Concrete composition

The bone-shaped UHPC-specimens were composed according to [1]. The ingredients for the mixture M2Q are listed below in table 1.

Table 1: Composition of the Mixture M2Q

resource		description	addition
cement	kg/m³	CEM I 52,5 R - HS/NA	832
water	kg/m³	water	169
additive	kg/m³	silica fume grade 983	135
	kg/m³	silica dust (QM1) W12	207
	kg/m³	superplasticizer glenium 51	24
fine aggregate	kg/m³	glass sand H33	975
steel fibres	kg/m³	steel fibres stratec 0,9/0,15	192

2.2 Concrete properties

The consistency of fresh UHPC was determined by a slump flow test, executed immediately after mixing. The slump flow for UHPC with and without steel fibres was about 750 - 800 mm.
In figure 1 the development of the compressive strength of UHPC with steel fibres and heat treatment (mSF mWB), with steel fibres and without heat treatment (mSF oWB) and without steel fibres and with heat treatment is shown (oSF mWB). As expected the addition of steel fibres and heat treatment led to an increase of the compressive strength. Even after 90 days of curing the compressive strength of UHPC without heat treatment is far below the compressive strength of UHPC with heat treatment. The testing load levels for cyclic testing were appointed in relation to the static strength values. The static compressive and tensile strength were determined in tests on reference specimens manufactured of the same

concrete batch as the bone-shaped UHPC-specimens for the cyclic tests. The compressive strength was determined on cubes with a edge length of 100 mm.

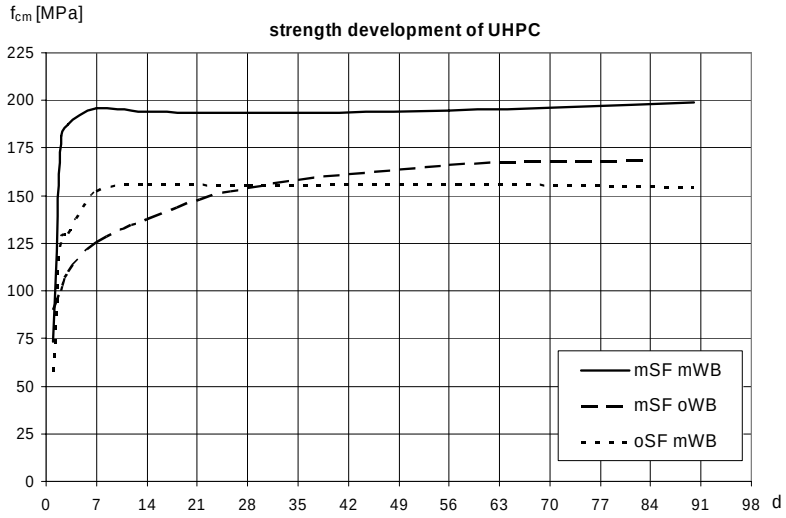

Figure 1: Strength development of UHPC

Due to the limitation of the capacity of the concrete mixer the reference specimens for static tensile testing had a small cubature. To devise an equation for the uniaxial tensile strength of the bone-shaped UHPC-specimens at the beginning of the research programm some investigations on the correlation of the static tensile strength determined in different kind of tests on variant specimens were carried out. For a few concrete batches the uniaxial tensile strength ($f_{ctm,gr}$) was acquired in tests on specimens (figure 2a) equal to the specimens for cyclic testing. For these concrete batches the uniaxial tensile strength ($f_{ctm,kl}$) was also determined in tests on small bone-shaped UHPC-specimens bonded to the testing gadget at their top and bottom with the solvent-free epoxy resin-based two-component adhesive MC-DUR 1280 (figure 2b). Additionally the bending tensile strength ($f_{ctm,fl}$) was determined in flexural tests on prisms of 40/40/160 mm The tensile testing loads for the further cyclic tests were appointed in relation to the static tensile strength (f_{ctm} = $f_{ctm,gr}$) calculated from the results of the tests on the reference specimens for each concrete batch [2].

a) b)

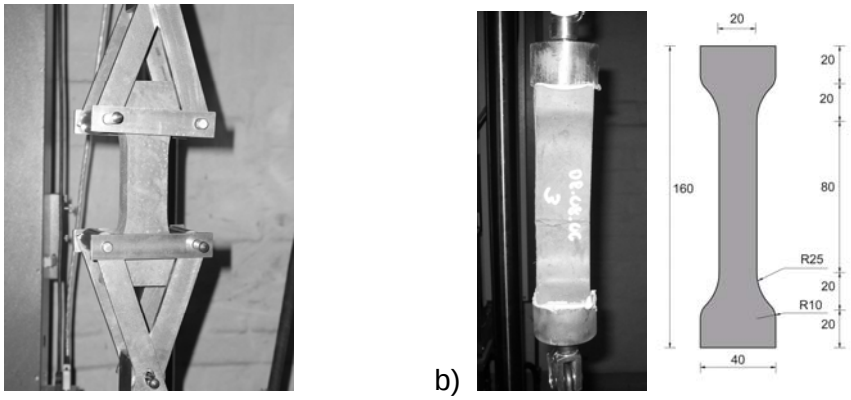

Figure 2: Uniaxial tensile strength test ($f_{ctm,gr}$) and ($f_{ctm,kl}$)

3 Test program

3.1 Production of test specimens

The bone-shaped UHPC-specimens were cast in the concrete laboratory. The formwork for six specimens consisted of plastic (polyoxymethylen). The dimensions of the bone-shaped UHPC-specimens are shown in figure 3a. The concrete was poured into the mould and compacted with an external vibrator. Simultaneously the reference specimens (cylinder, small bone-shaped UHPC-specimens and bending tensile prisms) were cast. One day after casting the specimens were stripped off and all cured under water till the 7th day (only for series WB) or were subjected to a heat treatment for two days at 90°C (series OF, FO and HV). Then the bone-shaped UHPC-specimens and the reference specimens were moved into the testing laboratory and stored under laboratory conditions until testing.

3.2 Test arrangement

The test rig for the main tests is shown in figure 3b. The top and the bottom of the bone-shaped UHPC-specimens were bonded with the epoxy resin-based two-component adhesive MC-DUR 1280 to the testing machines adapters. Between the adapter and the ends of the specimen the adhesive was applied to compensate the uneven concrete surface and for bonding. Above the lower crosshead, a load cell with reference to the testing machines maximum load was arranged. Three different testing machines were used depending on required stress range.

After bonding the specimen to the adapter a curing period of 24 hours followed up. Then the gauges were prepared, the instrumentation applied and the first zero readings taken.

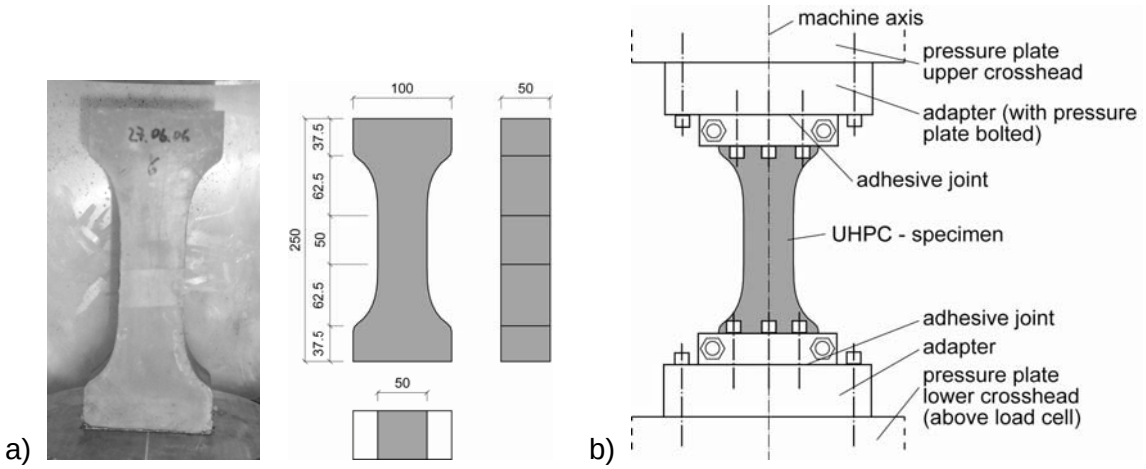

Figure 3: a) Dimensions of bone-shaped UHPC-specimens
b) Test arrangement

3.3 Test procedure

In four test series of cyclic fatigue test the following parameters were investigated:

- Influence of stress level and stress range
- Influence of fibres
- Influence of heat treatment

The direction of casting was supposed to influence the fibre orientation and will be checked with random controls on the tested specimens. With the background of the expected test

duration and in combination with the necessary number of at least five specimens for a statistical analysis some parameter of influence were examined restrictedly. In figure 4 the intended load combinations are marked. The four test series are divided as follows:

- Series 1 (OF): tests on specimens without fibres
- Series 2 (HV): main tests on specimens with fibres, horizontally casted, with heat treatment
- Series 3 (FO): tests on specimens with fibres, vertically casted, with heat treatment
- Series 4 (WB): tests on specimens with fibres, horizontally casted, without heat treatment

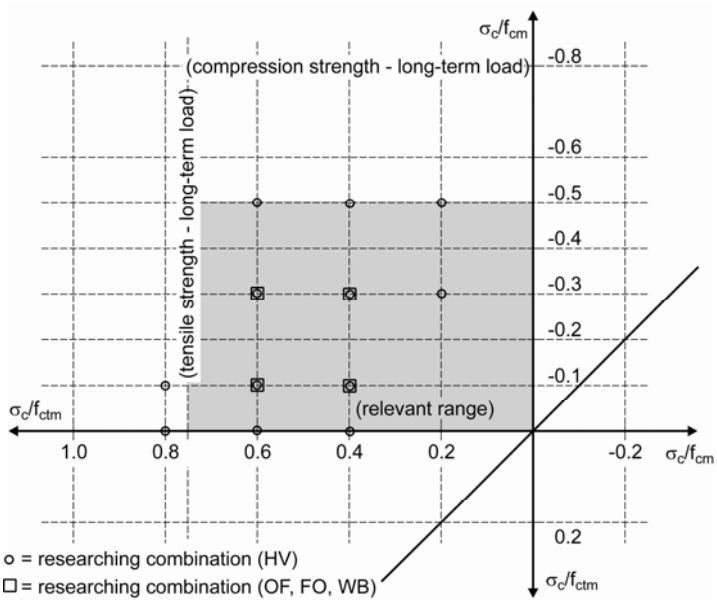

Figure 4: Goodman diagram, researching combinations marked

The relevant range for the experimental investigations is limited by the strengths under permanent load. For UHPC neither the compressive nor the tensile strength subjected to permanent load is known so far. In [3] the limit value for the tensile strength of High Strength Concrete (HSC) under permanent load was investigated to be 75% of the static tensile strength under short-term loading. At an average the limit value for compression strength under permanent load of HSC amounts to 80%. Tensile members of UHPC at economic design do not fall below a lower stress of $|\sigma_c| \approx 0{,}5 \cdot f_{cm}$. With these boundary conditions the relevant range in figure 4 was designed. The experimental tests included in the main series (HV) 60 tests and the three additional test series (OF, FO, WB) consisted of 20 tests in each case.

3.4 Instrumentation

In addition to the load the elongation of some specimens at a basic length of 50 mm on selected tests (range of constant cross section) was measured. To measure the strain, four inductive displacement transducers were used. The measurement were recorded with digital measurement amplifiers and a sampling rate of 100 Hz. The strain measurement were only performed at some specimens of each series. The frequency of the testing machines varied between 8 and 10 Hz.

4 Test results

4.1 Survey on test results

The whole test program comprised 60 tests with heat treatment and fibre addition (HV) as well as 60 additional tests without heat treatment (WB), without addition of fibres (OF) and direction of casting (FO). In autumn 2007 the test series HV and the test series OF have been appraised.

The linearised S-N-curves for the tests on specimens with heat treatment are represented in the semi logarithmic diagrams of figure 5 showing the number of load cycles to failure (logN) against the specific compression strength (σ_c/f_{cm}). Figure 5a shows the results of tests either on specimens without fibres (OF) whereas figure 5b exemplifies the results of tests on specimens with fibres (HV). Remarkable is the large spread of the number of load cycles. As a reason for these variations local faults which initiate and accelerate the failure progress can be assumed.

Additionally in figure 5a the average number of load cycles to failure of normal strength concrete (NSC) is shown [4]. The number of load cycles found in the tests on UHPC exceeds the results of tests on NSC by far.

The complete evaluation of the test results for the main tests is shown in figure 5b. The number of load cycles reached depends on the upper stress level as well as on the stress range. Remarkable is that some tests failed under compression (marked with filled symbols). A couple of tests have been stopped after 10 million load cycles without failure as the research program could not be realised in the scheduled period otherwise.

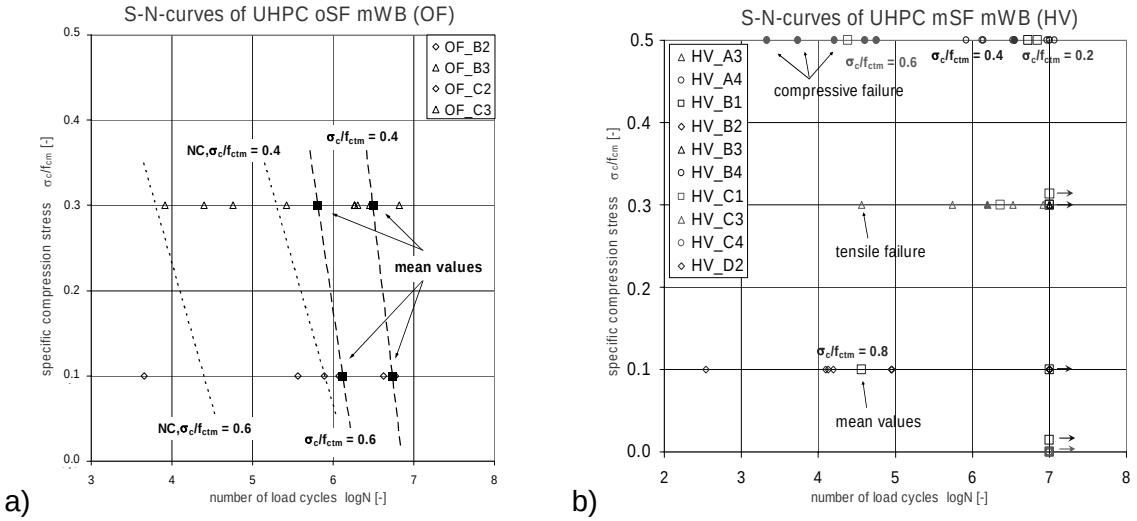

Figure 5: a) S-N-curves of UHPC oSF mWB (OF)
b) S-N-curves of UHPC mSF mWB (HV)

4.2 Results of deformation measurements

The measurement of deformation performed on selected specimens showed damage progress similar to normal strength concrete (NSC) and high-strength concrete (HSC) subjected to cyclic loading. As known for normal concrete and high strength concrete, the increase of deformation to be observed in tests on UHPC can also be divided into three phases reffered to as crack formation (phase I), constant crack propagation (phase II) and

instable crack growth (phase III). Exemplifying the damage progress figure 6 shows the increase of deformation of a bone-shaped UHPC-specimen without fibres subjected to tensile threshold loading. Especially phase III is shorter as known for normal concrete. Figure 6 also shows the failure behaviour of normal concrete and high strength concrete of [5]. Due to the addition of fibres the damage progress may be decelerated and proceed less brittle.

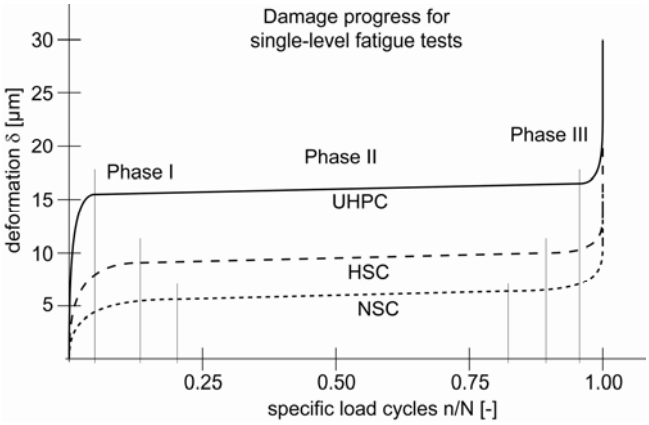

Figure 6: Failure behaviour of UHPC-specimen without fibres under tensile threshold loading

4.3 Fracture pattern

Depending on the compression stress level different fracture patterns occurred as shown in the next figures. Figure 7a shows a bone-shaped UHPC-specimen after tension failure occurring at low compressive stress levels. The UHPC-specimen was without steel fibres and with heat treatment (OF series). The fracture was plain at the basic length. Local faults constituted by air voids can also be seen in the figure 7a.

UHPC-specimens with steel fibres and with heat treatment (HV series) subjected to cyclic loading at a high compressive stress level showed compression failure and appropriate fracture pattern as shown in figure 7b.

a) 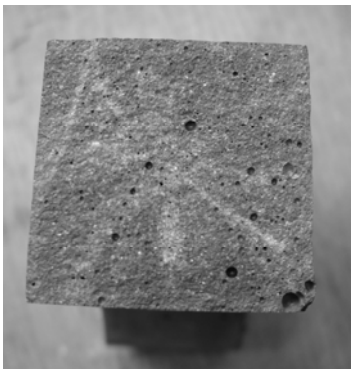

b) 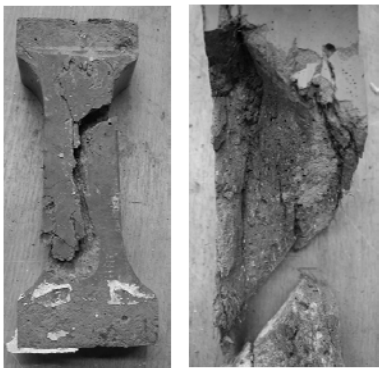

Figure 7: a) Fracture pattern of UHPC-specimen without fibres and with heat treatment (OF series) under tension failure
b) Fracture pattern of UHPC-specimesn (HV series) under compression failure

Figure 8 shows an UHPC-specimen with steel fibres after tension failure. UHPC with fibres is characterised by a more ductile behaviour then UHPC without fibres. The fracture surface was not plain like in figure 7a. The fibres and air voids can also be seen in the figure 8.

Figure 8: Fracture pattern of UHPC-specimen with fibres and heat treatment (HV series) under tension

5 Conclusions

As expected the number of load cycles found in the tests on UHPC exceeds the results of tests on NSC by far. Remarkable is also the large spread of the number of load cycles. Local faults which initiate and accelerate the failure progress can be assumed to be a reason for these large spread. Due to the addition of fibres the damage progress may be decelerated and proceed less brittle. Considering these test results economic design of UHPC structures under cyclic loading is possible.

For the next research phase additional tests with more than 10 million load cycles are planned. Furthermore, the damage behaviour of UHPC under cyclic loading will be investigated by deformation measurement. Other stress ranges will also be investigated to get the correlation between the specimens with and without failure.

6 Acknowledgement

The research project was funded by the Deutsche Forschungsgemeinschaft (German Research Foundation).

7 References

[1] Fehling, E.; Schmidt, M.; Teichmann, T.; Bunje, K.; Bornemann, R.; Middendorf, B.: Entwicklung, Dauerhaftigkeit und Berechnung Ultrahochfester Betone (UHPC). Forschungsbericht Universität Kassel DFG FE 497/1-1 (2005)

[2] AFGC 2002: Betons fibres á ultra-hautes performances. Recommandations provisoires (Jan .2002)

[3] Rinder, T.: Hochfester Beton unter Dauerzuglast. In DAfStb Heft 544, Beuth Verlag Berlin (2003)

[4] Cornelissen, H.; Reinhardt, H.: Uniaxial tensile fatigue failure of concrete under constant-amplitude and programme loading. In: Magazine of Concrete Research 36 (1984), Nr. 129, p. 216-226

[5] Kessler-Kramer, C.: Zugtragverhalten von Beton unter Ermüdungsbeanspruchung. Diss., Universität Karlsruhe (2002)

Josef Hegger
Prof. Dr.-Ing,
RWTH Aachen University
Aachen, Germany

Guido Bertram
Research Engineer
RWTH Aachen University
Aachen, Germany

Anchorage behavior of pretensioned strands in steel fiber reinforced UHPC

Summary

Ultra-High Performance Concrete (UHPC) is an appropriate construction material for pretensioned girders. To ensure an economic and safe design a detailed knowledge of the behavior of pretensioned strands in the anchorage zone is essential. The dimension of the bond anchorage zone favors the cost-effective design of pretensioned girders, especially when the shear resistance is decisive. However, a minimum concrete cover has to be maintained to avoid splitting cracks in the transmission zone, since they lead to an uncontrolled increase in transfer length and may cause a premature anchorage failure.

Within a priority program [1] supported by the German Research Foundation (DFG) experimental and theoretical investigations on the bond behavior of strands in UHPC are carried out at the Institute of Structural Concrete at RWTH Aachen University. The influence of the hoyer-effect and the concrete cover was systematically investigated by pull-out-tests. The results indicate a reduction in anchorage and transfer length. Tests on the transfer of prestressing forces were performed to verify the coherence between local bond stress and transfer size.

Keywords: *ultra-high performance concrete, steel fibers, anchorage, prestressing*

1 Influence of the anchorage behavior on shear resistance

Generally, the number of strands in pretensioned girders results from the bending design. In addition, the prestressing force above the support is essential to calculate the shear resistance. A decisive part of the shear carrying capacity arises from arch action as presented in figure 1. When the anchorage length is shorter than the support overhang, the full prestressing force is available to intensify arch action. The vertical support reaction corresponds with the prestressing and the arch action. Prestressing forces, which have to be transferred in front of the support line, do not contribute to the arch action.

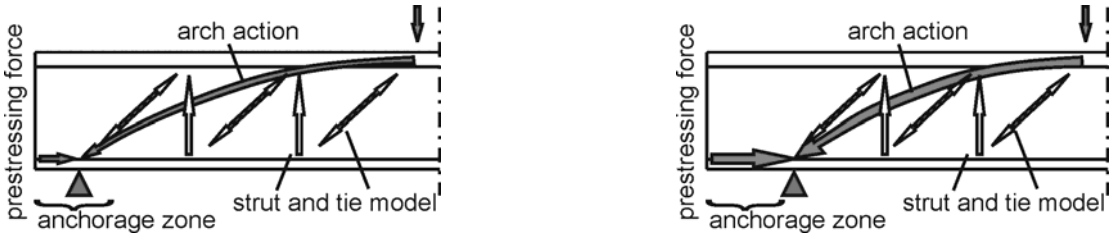

Figure 1: principle of arch action with corresponding prestressing force

The higher the bond stresses between strands and concrete the shorter is the anchorage length. The compressive strength of UHPC is about five times higher than normal strength concrete. The bond strength and the compressive strength, however, show no linear coherence. To ensure a safe design, constitutive design rules to calculate the anchorage and transfer length of strands in UHPC are required. In addition, the gradient of the bond forces is important as the topic of shear resistance points out. The bond slip behavior is important for the design of the beam tests [2], which followed these investigations.

2 Anchorage behavior of strands

So far, several investigations have been performed on the anchorage behavior of strands [3-6]. Generally, the bond stresses can be divided into three parts (figure 2):

- a constant part caused by the basic friction, also called the rigid-plastic bond behavior.
- a stress dependent part which is based on the hoyer-effect and which increases with the transfer of pretensioning.
- and a slip dependent part which is also independent of the prestressing. This effect can be explained by the “lack of fit” which results from the geometry of the strands which is not completely uniform.

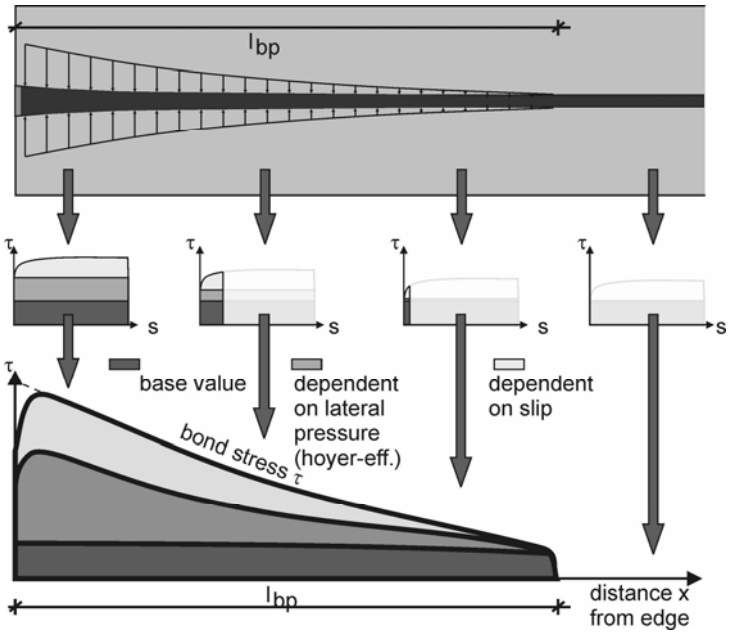

Figure 2: schematical stress distribution along the transfer length of strands

Furthermore, the bond stress is not constant along the transfer length. The slip as well as the lateral stress arises from the difference between steel and concrete strain while the pretensioning is released. Close to the concrete edge, almost the full pretensioning has to be transferred which leads to high lateral pressure between steel and concrete. All three bond parts are fully activated. The prestressing of the concrete increases along the transfer length. Thus, the stress which has to be transferred decreases. At the end of the transfer length, most stresses already have been transferred from steel to concrete. Here the lateral stresses and the slip are very low the bond is mainly established by the base value of the bond. Outside the transfer length there are neither bond nor lateral stresses nor slip due to prestressing.
To determine the bond stresses along the transfer length and to investigate the anchorage behavior, pull-out tests with different pretensioning, what means different lateral strain, were performed.

3 Pull-out tests

The concrete composition is based on the mix design of the priority program [1] (M0 with 2.5% p.v. fibers). With respect of the sustainability, the fiber content was varied. Table 1 summarizes the concrete mixes used for the beam tests. The steel fibers of 0.15 mm diameter had a length between 9 mm and 17.5 mm. The reference composition MR was made completely without fibers. The concrete showed nearly self consolidating properties. It was cast without compacting.

Table 1: concrete composition

material [kg/m³]	M0 (2.5% p.v.)	M1 (0.9% p.v.)	M7 (1.04% p.v.)	MR (w/out fibers)
cement CEM I	650	660	660	666
silica fume	177	180	180	181
quartz powder	456	463	463	467
sand 0.125-0.5 mm	354	360	359	363
basalt 2-8	598	606	606	612
steel fiber 9.0/0,15	194	-	-	-
steel fiber 17.5/0,15	-	70	-	-
steel fiber 13.0/0.16	-	-	39	-
steel fiber 6.0/0.15	-	-	42	-
water	158	161	160	162
superplasticizer	31	32	32	32

In table 2 an overview of the pull-out tests is given. A total of 72 tests were performed. The main test parameters were the fiber ratio, the specific concrete cover, the concrete strength (age) and the strand diameter. Because of the high bond stresses, short embedment lengths between 25 and 50 mm were chosen. Each batch contains three tests with three different

lateral strain stages (0 %, 50 %, 100 %). Figure 3 shows the sequences of the pull-out tests. Three strands have been prestressed inside a testing rig. Then, the specimens were concreted. After a hardening period of three days the first three tests have been conducted. Afterwards, the prestressing force was decreased about 50% and further three tests were preformed. Finally, the last tests were accomplished with full release (100 %), which means full lateral strain of the strand.

Table 2: parameters of the pull-out tests (72 tests)

test batch	concrete				concrete cover	bond length	age of concrete	strands		number
	M1	M0	M7	MR	c/d_p [-]	[cm]	[d]	0.5''	0.6''	[-]
PO1-3	x				4.4	3.0	3		x	3 x 3
PO4-6		x			4.4	3.0	3		x	3 x 3
PO7-9			x		4.4	3.0	3		x	3 x 3
PO10-12	x				1.5-2.5	3.0	3		x	3 x 3
PO13-15	x				1.5-2.5	5.0	3		x	3 x 3
PO16-18	x				5.5	2.5	3	x		3 x 3
PO19-21	x				4.4	3.0	14		x	3 x 3
PO22-24				x	4.4	3.0	3		x	3 x 3

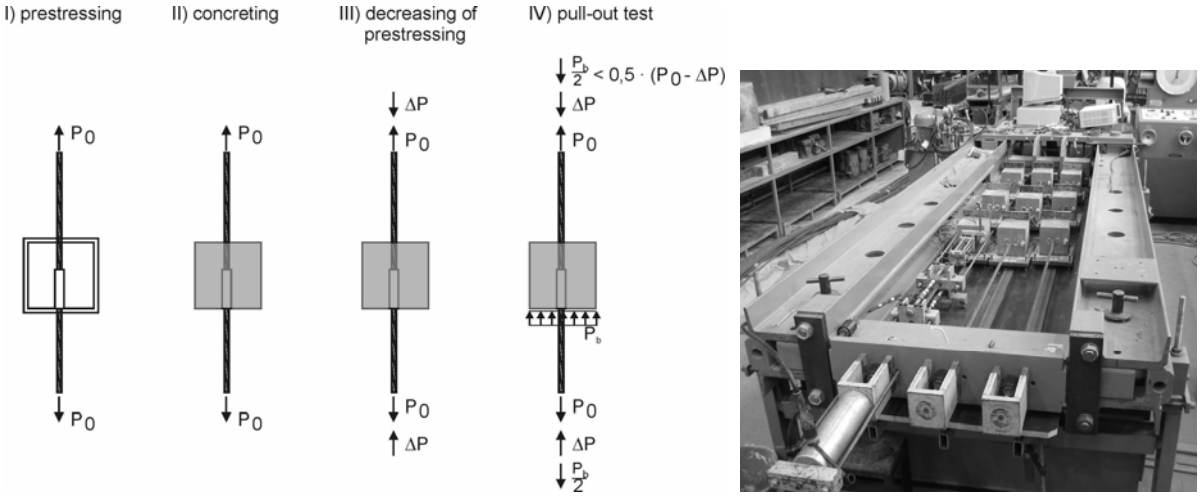

Figure 3: fabrication and test sequences of pull-out tests

The diagrams in figure 4 indicate, that the fiber ratio has no significant influence within the tested range. With a concrete compressive strength of 100 N/mm² at an age of three days a bond strength of 30 N/mm² was achieved with full lateral strain (100 % release of prestressing), 20 N/mm² with 50 % release and about 12 to 14 % without a change of the prestressing force.

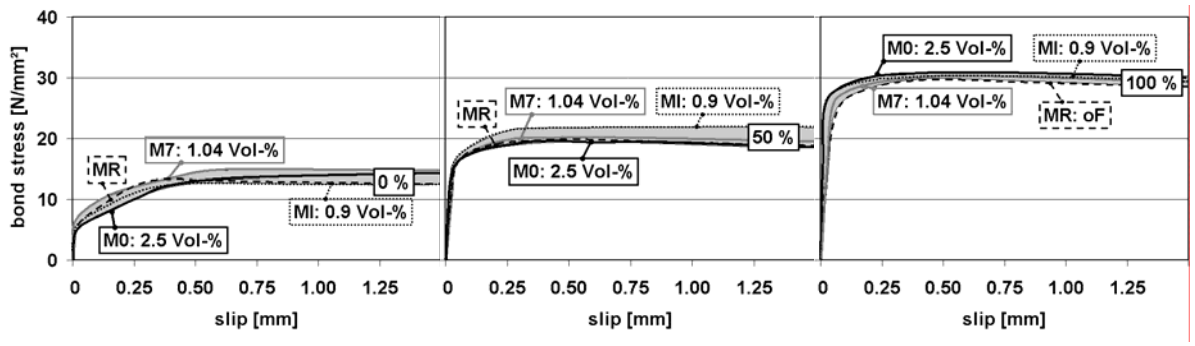

Figure 4: Influence of the fiber ratio and the prestressing (0%, 50%, 100%) on the bond slip behavior of the test batches PO1 to PO9, PO22-PO24

The variation of the concrete cover showed no effect on the bond strength when the prestressing remains unchanged as presented in figure 5. A release of 50 %, however, led to a reduction of the bond stresses of about 10 to 15 %. When the full lateral strain was preset, visible splitting cracks appeared below a specific concrete cover of $c/d_p = 2.5$. This means, the transferred bond stresses were reduced for 10 to 30 % according to the existing concrete cover.

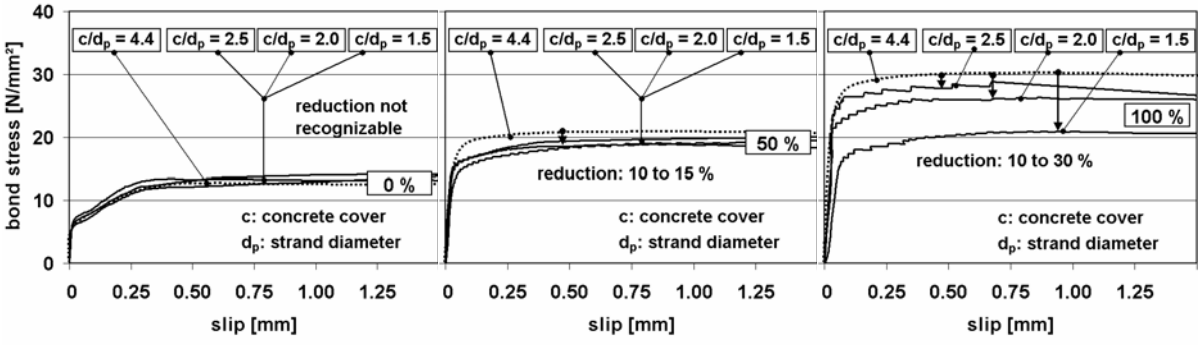

Figure 5: Influence of the concrete cover, test batches PO10 to PO12

By varying the strand diameter (0.5'' and 0.6'') no differences in bond behavior were observed. The higher concrete strength of the 14 days old specimens led to higher bond stresses. However, the increase of the bond strength was disproportionately low compared to the compressive strength.

4 Tests to investigate the transfer length

The main targets of these 10 tests were to determine the minimum dimensions of the concrete cross section to avoid splitting cracks and to investigate the transfer length of the specimens which remained uncracked. Specimens with two strands were chosen to investigate the minimum concrete cover (figure 6). Four strands were required to test the minimum spacing between the strands. The test parameters are listed in table 3. The concrete mix M1 with 0.9 % p.v. was used for all beams and the concrete age at the day of the tests was always three days.

Similar to the pull-out tests, the specimens were fabricated in a rig. The strands were already prestressed at the time of concreting. After the hardening period the prestressing was

released in steps of 20 %. At each load stage the concrete strains were measured along the longitudinal axis of the specimen. This way, the transfer of prestressing can be derived from the strain differences. In addition, the slip at the end of the specimen was measured continuously with displacement transducers.

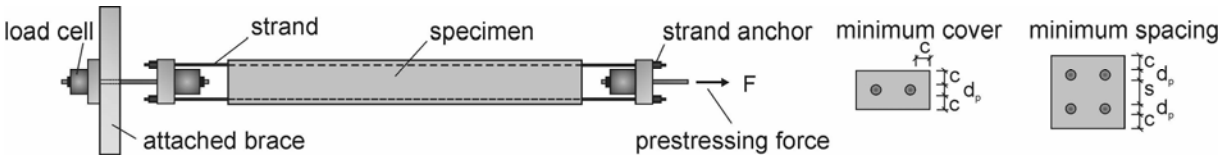

Figure 6: test setup to determine the transfer length as well as the minimum dimensions

Table 3: parameters of the small beam tests

test	concrete cover c/d_p [-]				spacing s/d_p [-]		age of concrete	number of 0.5'' strands	
	1.5	2.0	2.25	2.5	hor.	vert.	[d]	2	4
SE1	x				3.0		3	x	
SE2		x			3.0		3	x	
SE3				x	2.5	2.5	3		x
SE4				x	3.0	3.0	3		x
SE5				x	3.0		3	x	
SE6				x	3.0		3	x	
SE7		x			2.5	2.5	3		x
SE8		x			2.5	2.0	3		x
SE9		x			3.5	3.5	3		x
SE10		x	x		3.0	3.0	3		x

Splitting cracks in the area of the transfer zone are hardly visible, especially when steel fibers are added to the concrete. However, the development of splitting cracks can be spotted by a sudden slip increase. As charted on the left side of figure 7 the specimen SE1 with a specific concrete cover of $c/d_p = 1.5$ started cracking when 70 % of the prestressing was induced. Due to the splitting crack the stress depending part (hoyer-effect) diminished leading to a higher slip. SE2 with $c/d_p = 2.0$ cracked at 95 %. Only when the specific concrete cover amounts at least $c/d_p = 2.5$ the full prestressing was feasible without visible cracks as indicated by the continuous load-slip behavior in the middle diagram. Compared to HSC a reduction of the minimum concrete cover cannot be accomplished. Most likely, the splitting stresses arose simultaneously due to the higher bond stresses.

Nevertheless, the transfer length becomes shorter compared to HSC or even NSC when cracks were avoided as shown in the right diagram of figure 7. In these cases the measured transfer length amounts to 25 cm on average. The transfer length was extended when splitting cracks appeared, anyhow the strands have been anchored after 40 to 50 cm (SE1).

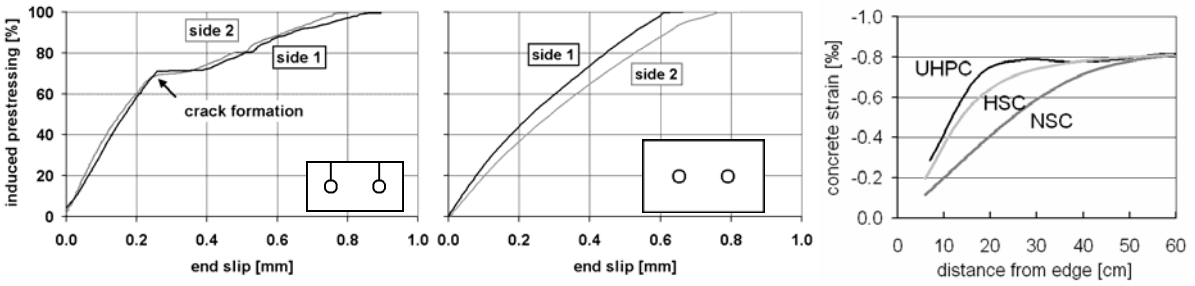

Figure 7: end slip of the strands, SE1 with cracks, SE5 without visible cracks – concrete strain at the end of the test compared to HSC and NSC

5 Calculative bond model

On the basis of the results from the pull-out tests a stress-slip relation can be derived, which takes into account the lateral strain and the slip. As demonstrated in [7] the local bond strength can be translated to components by using the bond differential equation system. Therefore, the differential equation for steel bars [6] has been upgraded to a formulation for strands prestressed with pretensioning:

$$\frac{d^2 s_p(x)}{dx^2} = \frac{1}{E_p} \cdot \left(f(s_p;\sigma_p) \cdot \frac{U_p}{A_p} \left(1 + \alpha_p \cdot \rho_p\right) \right) \tag{1}$$

Using any stress-slip relation the stresses as well as the slip in the transfer zone can be calculated. The resulting theoretical transfer length can be checked by the measured one in the beam tests. The test SE3 without visible cracks was used to check the applicability of the bond law according to [6]. The theoretical transfer length was calculated by using the local bond stresses of the pull-out tests. The theoretical transfer length $l_{bp,cal}$ = 12.2 cm (figure 8, left) as well as the theoretical slip s_{cal} = 0.37 mm (figure 8, right) fall below the experimental values ($l_{bp,exp}$ » 20 cm / s_{exp} » 0.48 mm).

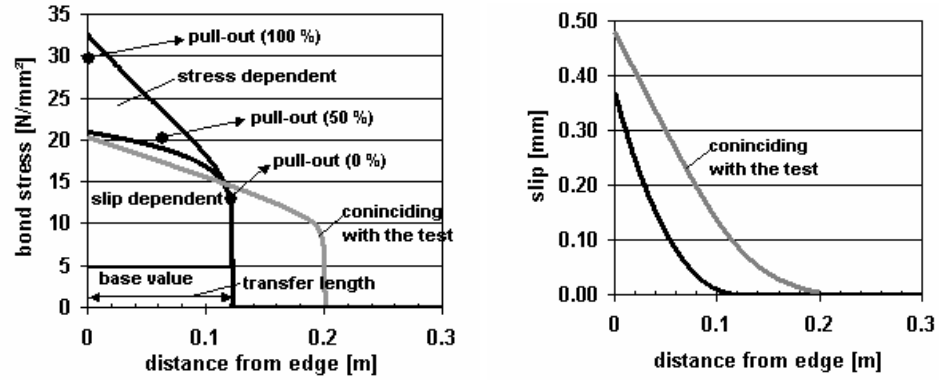

Figure 8: comparison of theoretical and experimental transfer length and slip for SE3

In principle, these differences may have the following reasons:

- The bond law, which was derived for normal and high strength concrete, cannot be transferred without adequate modification. Especially the proportion between compressive strength and bond strength may have an influence.

- A damage of the specimen may have occurred, even though it was not visible. This means, that micro-cracks developed but the steel fibers avoided the crack growth. Nevertheless, the stress dependent part of the bond stresses was decreased. The cracks in the other specimen with smaller concrete cover were hardly visible, too.

In the left diagram of figure 8 the results of the pull-out tests are marked. The bond stresses are insignificantly lower than the theoretical values of the curve, i.e. the approached bond law according to [6] leads to results in the right range. Furthermore, the experimental transfer length is too long compared to high strength concrete. Invisible crack development seems to be the main reason. Therefore, further tests with enlarged concrete cover will be added on.

6 Summary and conclusions

Pull-out test to determine the local bond stresses as well as beam tests to investigate the transfer length were performed. The results can be summarized as follows:

- Bond stresses about 30 N/mm² (100% release of prestressing), 20 N/mm² (50%) and 12-14 N/mm² (0%) result from the pull-out tests.
- An influence of the fiber ratio on the bond stresses was not observed inside the investigated range.
- A specific concrete cover less than $c/d_p = 2{,}5$ led to a significant decrease of bond stresses and splitting cracks.
- The experimental transfer length seems to be too long and further tests are required.

7 Acknowledgement

This research project is part of the SPP 1182 which is founded by the DFG (German Research Foundation). The authors acknowledge the support.

8 References

[1] German Research Foundation, priority project (DFG SPP 1182), Nachhaltig Bauen mit UHPC (Sustainable Building with UHPC)

[2] Hegger, J.; Bertram, G.: „Shear carrying capacity of steel fiber reinforced UHPC", Proceedings, 2nd International Symposium on UHPC, Kassel, Germany in 2008

[3] Hoyer, E.: Der Stahlsaitenbeton. Otto Elsner Verlagsgesellschaft, Berlin Wien Leipzig, 1939

[4] Stocker, M.F., Sozen, M.A.: Bond characteristics of prestressed strand. Investigations of prestressed reinforced concrete of Highway bridges, University Illinois, Structural Research, Series No. 344, 1969

[5] den Uijl, J.: Bond and splitting action of prestressing strand. Proceedings, Bond in Concrete, Riga, Oktober 1992. S. 2/79-2/88

[6] Nitsch, A.: Spannbetonfertigteile mit teilweiser Vorspannung aus hochfestem Beton. Dissertation, Schriftenreihe des Lehrstuhls und Instituts für Massivbau der RWTH Aachen, Heft 13, ISBN 3-9807302-0, 2001

[7] Bülte, S.: Zum Verbundverhalten von Spannstahllitzen unter Betriebsbeanspruchung. Institut für Massivbau der RWTH Aachen, Dissertation in Vorbereitung

Josef Hegger
Prof. Dr.-Ing.
RWTH Aachen University
Aachen, Germany

Sabine Rauscher
Dipl.-Ing., Research Engineer
RWTH Aachen University
Aachen, Germany

UHPC in Composite Construction

Summary

The paper summarizes the results of a research program (DFG priority program SPP 1182 [1]) involving the testing of push-out specimens and composite beams with innovative continuous shear connectors in ultra-high performance concrete. In the push-out tests the load-slip behavior of the shear connectors was evaluated and compared for various parameters. The parameters included the steel fiber content, the transverse reinforcement ratio and the thickness of the puzzle strip. The test results indicate that the steel fiber reinforcement ratio has only a minor influence on the load carrying capacity whereas the transverse reinforcement ratio is more vital. The beam tests are focused on the moment carrying capacity and the transition of the shear forces across the joint between steel and concrete. The results of one of the tests with an innovative cross section are presented as an outlook.

Keywords: *composite structures, high strength steel, UHPC, steel fibers, shear connectors*

1 Introduction

Composite structures combine the favorable features of structural steel and concrete. Taking into account the mechanical properties, the steel carries the tensile forces and the concrete is arranged in the compression zone of a composite beam. Due to the composite action a significant increase in load carrying capacity and stiffness is achieved, resulting in savings in dead load, construction depth and construction time. Further savings can be accomplished when high strength steel and high performance concrete are used [2] [3]. Within a priority program [1] ultra-high performance concrete (UHPC) with steel fibers is applied for hybrid structures. Due to its high compressive strength of up to 200 MPa, even more slender and attractive structures are feasible. In addition, ultra high performance concrete features a high tensile strength under considerable tensile strains which is primarily caused by the steel fibers added to the concrete mainly for ductility reasons.

The increase in load carrying capacity of a composite beam also leads to higher stresses in the composite joint. So far, the shear connection is commonly accomplished by headed studs, however, in high strength concrete they are suitable only to a limited extend [2]. Due to their high load carrying capacity and high initial stiffness continuous shear connectors, e.g. the puzzle strip described in [2] [3], are very appropriate. The shear connectors are expected to withstand high loads with sufficient ductility. In the paper the results from push-out tests and one beam test are presented.

2 Ultra-high performance concrete

The ultra-high performance concrete (UHPC) used in the tests is based on the concrete mix B4Q which is one of the reference mixes in the priority program. The fiber content was varied between 0.9 and 2.5 % of the concrete volume. In addition, an UHPC without steel fibers was tested (Table 1). For comparison reasons all specimens were cast the same way with flow direction parallel to the shear connector's axis.

Table 1: Concrete Composition

material [kg/m³]		**M0 (2.5 % p.v.)**	**M1 (0.9 % p.v.)**	**MR (w/out fibers)**
cement CEM I	[kg/m³]	650	660	666
silica fume	[kg/m³]	177	180	181
quartz powder	[kg/m³]	456	463	467
Coarse aggregates	[kg/m³]	952	966	975
steel fiber	[kg/m³]	194	70	-
w/cm	[-]	158	161	162

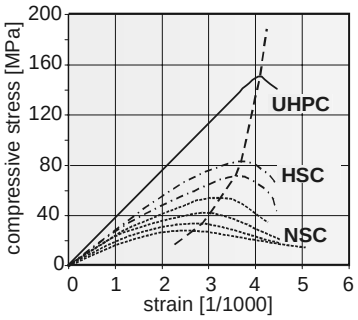

Due to the steel fibers, UHPC not only features a high compressive strength but also a linear-elastic behavior until about 90 % of its compressive strength at a strain rate of about 4.5 ‰ (see graph in Table 1). Conventional concrete (NSC and HSC) shows a distinctive nonlinear behavior due to the micro-cracks which develop at a stress level of about 40 % of the compressive strength.

3 Continuous Shear connectors

Continuous shear connectors have been used for about 20 years. The most common one is the perfobond strip [4], where the shear forces between the steel beam and the concrete slab are transferred by vertical steel plates with holes. In [5] [6] the so-called puzzle-strip is introduced. Its main advantage is the symmetrical geometry (Figure 1). This way it is possible to receive two shear connector strips with one cut and no material is wasted. If the cut is performed in the web of a steel I-beam, two composite beams can be produced.

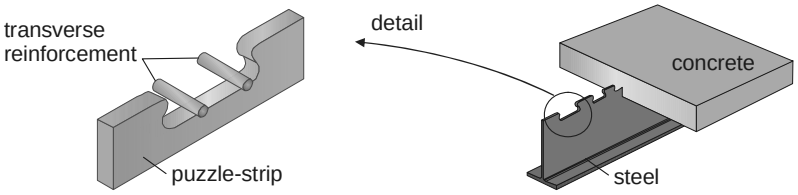

Figure 1: Puzzle-strip shear connectors (left) and filigree composite beam (right)

Since the neutral axis of a composite beam under positive bending moments is in the region of the upper flange the strains are usually relatively low. Thus, there is little loss in load carrying capacity compared to a conventional composite beam with equal height. However, there are significant savings in production costs. The load bearing behavior of continuous shear connectors has been investigated by several researchers [2] [4] [6] [7]. Four failure modes have to be considered (Figure 2, left): local concrete failure in front of the shear connector, concrete pry-out failure, shear failure of the concrete and steel failure due to the moment stress of the puzzle profile which is described in [3].

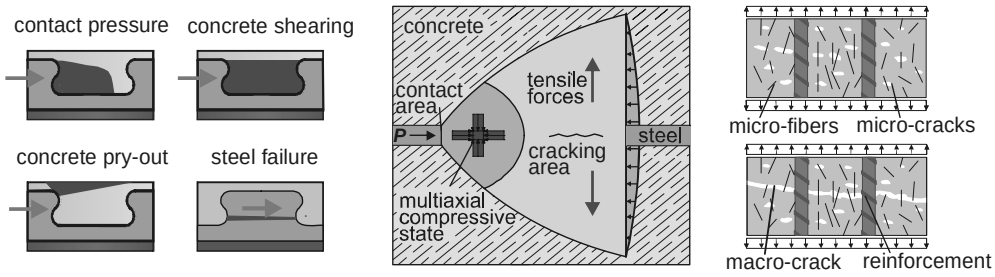

Figure 2: Failure modes (left), load carrying model according to [7] (middle), crack behavior (right)

According to the model described in [7] there are lateral tensile forces between the steel teeth resulting from the concentrated load introduction of the steel profile (Figure 2, middle).
In the early state of testing fine micro-cracks begin to form in the concrete. The steel fibers are capable to bridge the micro-cracks and thus the formation of macro-cracks is deferred (Figure 2, upper right). However, as the micro-cracks grow the tensile forces have to be sustained by additional reinforcement and the fibers fail due to the missing anchorage (Figure 2, lower right).

4 Push-Out Tests

4.1 Test Set-up

The specimens were designed for both, concrete and steel failure. Concrete failure is mainly governed by the concrete cover between shear connector and concrete surface and the ratio of transverse reinforcement by means of steel fibers and steel rebar, respectively.
The tests were performed using two different set-ups, the Push-Out Test (POT) and the Single Push-Out Test (SPOT). The POT according to [8] simulates the shear transfer in the composite joint of composite girders (Figure 3).

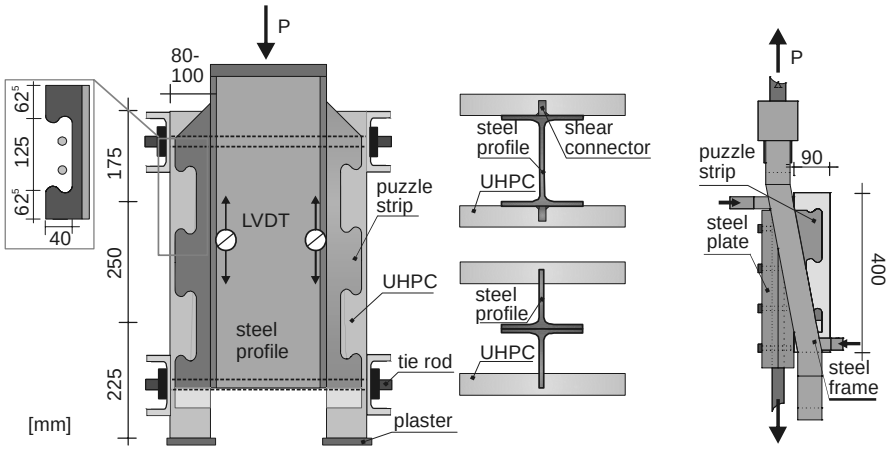

Figure 3: Push-Out Test POT (left) and Single Push-Out Test SPOT (right)

The standard POT (Figure 3, left) consists of a steel I-beam where the shear connectors are welded on the outer side of the flange. In slender composite beams as shown in Figure 1, there is no upper flange and thus there is less confinement of the concrete in this area. For this reason, push-out tests were performed on steel profiles where the geometry is cut in the web (lower cross section in Figure 3) [5]. In this case the thickness of the shear connector

equals the thickness of the web. The Single Push-Out Test (SPOT, Figure 3, right) consists of a steel frame embracing the UHPC block. Due to its compactness it is an appropriate test set-up to pre-select shear connectors effectively under nearly pure shear load. In all tests, LVDTs were applied to measure the slip between the steel profile and the concrete slab.

4.2 Test parameters

The tested parameters are summarized in Table 2. As a reference, the puzzle strip with a thickness t_w of 20 mm and a concrete cover c_o between puzzle and concrete surface of 10 mm was tested (Series A) in which the effects of the amount of steel fibers were determined. For the following tests the concrete cover c_o was 20 mm and the fiber content 0.9 %. The influence of the transverse reinforcement was investigated in Series B. In Series C the thickness of the shear connector t_w was varied. Series D consisted of a steel beam without a confinement through a flange and served as a basis for the beam tests with equal shear connection.

Table 2: Test program

Series	# of Tests	Test Set-up	Description	$f_{c,cube100}$ N/mm²	$f_{y,connector}$ N/mm²	$P_{max,mean}$ kN	P_{Rk} kN	δ_{uk} mm
A1	2	POT	2.5 Vol.-%	191.0	499	426.0	372.4	2.2
A2	3	POT	0.9 Vol.-%,	177.9	499	389.1	340.7	1.4
A3	2	POT	0 Vol.-%,	134.2	499	268.3	200.2	0.18
B1	1	POT	Reinf. 2 Ø 12	177.9	499	492.7	443.4	5.1
B2	2	POT	Reinf. 2 Ø 12 + Ø 8/5	179.5	499	562.5	493.5	7.1
B3	2	POT	-	194.4	499	432.8	369.5	4.0
C1	2	SPOT	t_w = 10 mm	182.6	441	326.2	282.1	15.1
C2	2	SPOT	t_w = 15 mm	178.0	521	375.2	327.0	11.8
C3	2	SPOT	t_w = 20 mm	179.5	499	412.6	330.5	5.2
D	3	POT	t_w = 12 mm,c_o = 30 mm	179.1	472	587.0	495.0	8.4

5 Test Results

For each test series the load-slip diagrams were evaluated according to the procedure of EC 4 [8]. The characteristic slip δ_{uk} describes the deformation measured in the tests during the plastic period when the characteristic load P_{Rk} was maintained. The concrete compressive strength for a 100-mm-cube $f_{c,cube100}$, the yield strength of the shear connector, the mean maximum loads $P_{max,mean}$, the characteristic loads for one recess of the shear connector and corresponding slip δ_{uk} are presented in Table 2. In almost all tests failure of the concrete due to pry-out occurred. Only in the specimens with thin shear connectors (Series C1 and D), the yielding of the steel determined the ultimate load. In the following the results are discussed in detail.

5.1 Load-slip behavior

As a result of the push-out tests the load-slip diagrams are plotted for each series. In the evaluation not only the ultimate load but also the initial stiffness and the ductility, which is the slip after reaching the characteristic load P_{Rk}, were examined.

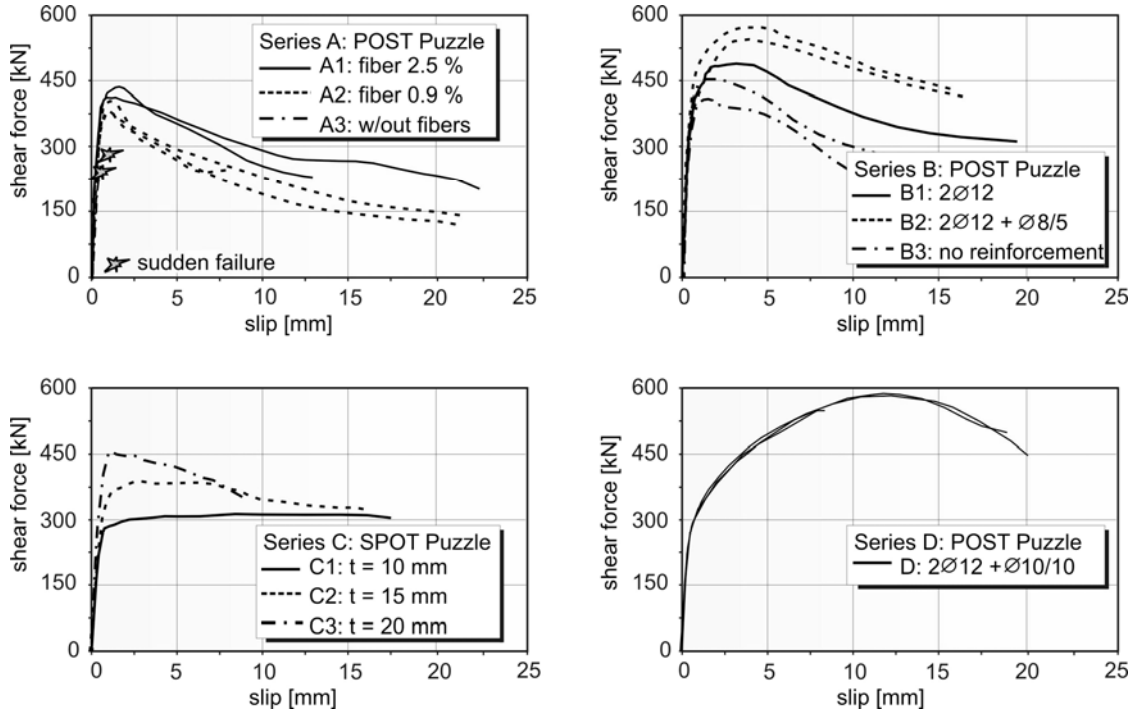

Figure 4: Load-slip diagrams

5.2 Effect of steel fibers

The first load-slip diagram in Figure 4 shows that the amount of steel fibers added to the concrete influences the load carrying capacity of the puzzle-strip. When there are no fibers added to the concrete there was a sudden failure after the ultimate load was reached. With 0.9 % steel fibers there was an increase in ultimate load of appr. 33 %. In addition, the steel fibers had a positive effect on the descending branch after reaching the maximum load. Adding 2.5 % of steel fibers led to a further increase of appr. 10 %. However, an increase in the maximum load of 10 % with about 2.7 times more steel fibers cannot be recommended for practical use in terms of cost effectiveness since the steel fibers are the most cost-intensive factor in UHPC.

5.3 Effect of transverse reinforcement

In Series B the effect of transverse reinforcement in the puzzle recesses and above the shear connector was investigated (Figure 4, upper right). The transverse reinforcement increased the confinement of the concrete in front of the puzzle and thus led to higher ultimate loads and an increase in ductility in case of concrete failure.

5.4 Effect of the shear connector thickness

The influence of the shear connector's thickness was investigated in the SPOT. There was a slight difference in initial stiffness. With increased thickness of the shear connector higher ultimate loads were achieved (Figure 4, lower left). The specimens of Series C1 with a thickness of 10 mm failed due to the yielding of the puzzle. After the test, the puzzles were deformed noticeably and a horizontal crack was observed. In Series C2 with a connector thickness of 15 mm a combined steel and concrete pry-out failure was observed. Due to the larger thickness pure concrete pry-out failure occurred in Series C3 with no visible

deformation of the steel. With increasing thickness and predominating concrete failure the ductility was significantly reduced compared to pure steel failure. However, even for concrete failure the behavior was not brittle due to the steel fibers.

5.5 Reference test

The shear connector in Series D results from a cut in the web of an IPE 600 profile with a web thickness of 12 mm. Even though the thickness of the web was only 60 % of the one in series B (20 mm) there was no difference in the ultimate load. However, the thinner shear connector was more flexible and its ultimate load was reached after a slip of 10 mm. The failure mode in Series D was steel failure with a horizontal crack in the puzzle strip. On the outer surface there were signs of concrete pry-out failure, however, on the inside of the concrete surface no cracks were visible.

6 Beam Test

6.1 Test Set-up

Under positive bending moments it has to be verified that the yield-line theory is applicable, i.e. the steel profile plasticizes before the concrete compression zone fails. Using high performance materials this becomes even more vital since the high strength steel requires a higher yield strain to plasticize and for concrete the strain at failure generally decreases with increasing concrete strength. This effect was investigated in beam tests. One of the four tests performed with UHPC and high strength steel S460 is introduced. The puzzle strip was directly cut into the steel web. Figure 5 presents the test set-up and the cross section of the tested beam. Taking into account the load-slip behavior achieved in push-out tests (Figure 4, Series D) the beam was fully shear connected. Along the shear joint between the steel profile and the concrete slab, LVDT's were attached to measure the slip. At midspan, strain gauges were fixed across the cross section to investigate the strain distribution.

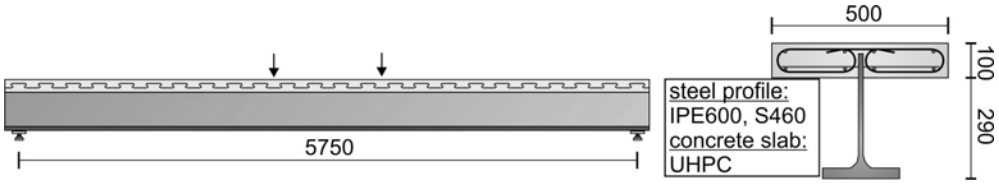

Figure 5: Beam test under positive bending

6.2 Test results

In the beam test a failure of the compression zone was observed when the ultimate strain of the concrete slab was exceeded. Figure 6 shows the moment-rotation curve of the tested beam with the angle φ representing the rotation of the beams cross section at midspan, which is determined by the tangent angles of the rotation at the supports. The EC 4 [8] regulation ($M_{pl,calc}$) for composite beams was reached under consideration of the actual material properties with the safety factors γ_i set to unity.

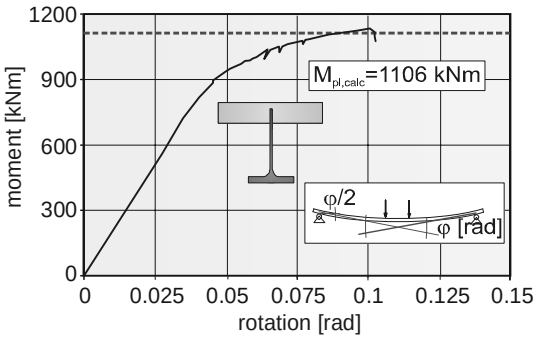

Characteristic	unit	
f_y	N/mm²	468
$f_{c,cyl}$	N/mm²	180
M_{test}	kNm	1156
$M_{pl,calc}$	kNm	1106
M_{test}/M_{calc}	kNm	1.05

Figure 6: Moment-rotation behavior

For full and rigid shear connection between steel and concrete there is a continuous strain distribution with no slip between the two components. However, due to the flexible puzzle strip there is a step in the strain distribution in the composite joint. Figure 7 shows the strain distribution at distinct load levels for the cross section at midspan. With increasing load the neutral axis moves upwards in the composite cross section. At about 80% of the maximum load the lower flange started to yield (ε_y = 2.3 ‰). In the ultimate limit state the neutral axis was in the concrete slab and the steel profile was almost completely under tension. The offset in the composite joint, which corresponds to the slip, becomes apparent (see enlargement in Figure 7, left).

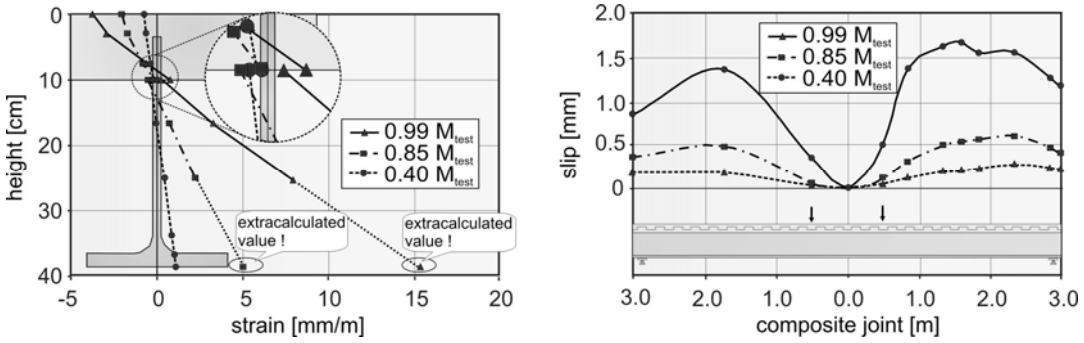

Figure 7: Strain distribution (left), slip along the interface (right)

In Figure 7, right, the slip along the interface is presented. In the linear-elastic range, there is only a minor increase in slip and the shear connectors are equally stressed. After the yield strength was exceeded, the slip increased non-linearly and the slip distribution became more and more uneven. After removing the concrete slab, the shear connectors in the composite joint were investigated. No cracks were found in the puzzle strip even though there was measurable slip.

7 Summary and conclusions

Experiments with Push-Out Test (POT) and Single Push-Out Test specimens on continuous shear connectors in UHPC were carried out. The parameters of the tests were the fiber content, the transverse reinforcement ratio and the thickness of the shear connector.

The results can be summarized as follows:

- The influence of the amount of steel fibers added to the UHPC is of minor importance. With almost 3 times more steel fibers only an increase of 10 % in ultimate load could be

achieved. Independent of the fiber content concrete failure occurred. Nevertheless, a minimum fiber ratio has to be maintained to guarantee a ductile behavior.

- Arranging transverse reinforcement in the puzzle recesses and between the shear connectors and the concrete surface leads to an increase in ultimate load of up to 30 %. Also the ductility was improved.
- Different failure modes were observed depending on the thickness of the shear connector. For thin puzzles (10 mm) steel failure occurred with a very ductile behavior. Concrete failure (pry-out and local concrete compression failure) was achieved at a thickness of 20 mm. A combined steel and pry-out failure occurred at a thickness of 15 mm.
- In the beam test the plastic moment according to EC 4 was reached. Due to the characteristic load carrying behavior of the puzzle strip the composite joint was rather flexible despite theoretical full shear connection. However, no cracks could be found in the puzzles after removing the concrete slab.
- The puzzle strip is capable of transferring high shear forces. Especially with thick steel webs, as for example at HEM profiles, a rigid shear connection can be established.

8 Acknowledgement

This research project is part of the SPP 1182 which is founded by the DFG (German Research Foundation). The authors acknowledge the funding through the DFG and express their thanks for the support of Arcelor S.A. and Schmitt Stumpf Frühauf, Munich.

9 References

[1] Priority Program SPP 1182: Nachhaltiges Bauen mit UHPC, German research foundation, 2007.

[2] Hegger, J., Sedlacek, G., Döinghaus, P., Trumpf, H. 2001. Testing of Shear Connectors in High Strength Concrete. Proc. RILEM – Symposium on Connections between Steel and Concrete, Stuttgart, Germany, Sept. 9-12, 2001.

[3] Hegger, J., Feldmann, M., Rauscher, S., Hechler, O. 2006. Load-Deformation Behavior of Shear Connectors in High Strength Concrete subjected to Static and Fatigue Loading. Proc. IABSE Symposium on Responding to tomorrow's challenges in structural engineering, Budapest, Hungary, Sept 13-15, 2006.

[4] Leonhardt, F., Andrä, W., Harre, W. 1987. Neues, vorteilhaftes Verbundmittel für Stahlverbund-Tragwerke mit hoher Dauerhaftigkeit. Beton- und Stahlbetonbau, 82(12), pp. 325-331.

[5] J. Hegger, S. Rauscher: Shear Connectors in Steel Fibre Reinforced Ultra High Performance Concrete. 3rd Int'l Conference on Steel and Composite Structures (ICSCS 07), Taylor & Francis/ Balkema, ISBN: 978-0-415-45141-3. pp. 403-409.

[6] Schmitt, V., Seidl, G., Hever, M. 2005. Composite Bridges with VFT-WIB-Construction Method. Proc. Eurosteel 2005, Maastricht, Netherlands, June 8-10, 2005.

[7] Wurzer, O. 1997. Zur Tragfähigkeit von Betondübel, PhD thesis. Institut für Konstruktiven Ingenieurbau, Universität der Bundeswehr, München, Juni 1997.

[8] EC 4, prEN 1994-1-1, 2004. Design of composite steel and concrete structures Part 1.1 – General rules and rules for buildings. Brussels.

Nguyen Viet Tue
Prof. Dr.-Ing. habil.
Leipzig University
Leipzig, Germany

Michael Küchler
Dipl.-Ing.
Leipzig University
Leipzig, Germany

Load and deformation behaviour of confined ultra high performance concrete dowels

Summary

In this paper the application of UHPC dowel in truss construction made of steel tubes is presented. The innovative connector is characterized by high bearing capacity and adequate ductility, in which the main parameter are the confinement and the roughness of the cracking surface of the dowels. Based on the experimental results and theoretical analysis a model for the design of nodal joints using UHPC dowels should be developed.

Keywords: *UHPC, hybrid nodal joint, confined UHPC dowel, truss construction*

1 Introduction

Since about 10 years Ultra High Performace Concrte (UHPC) is investigated in Germany. Priviously results show that UHPC has excellent mechanical and durability properties. But, it is also very expensive and highly sensitive to the quality of its components, as well as to flutuation in the production technology. An use in the same maner as with normal strength reinforced concrete seems not to be reasonable [1]. Therefore, it is necessary to develop new construction in order to use UHPC efficiently in the future.

In this contribution a new idea to simplify the nodal joints of truss constructions made of steel tubes is presented. For this purpose, steel tubes will be filled with UHPC. Instead of usually welded connections confined UHPC dowels are arranged in nodal joints (see Fig. 1). The equilibrium in nodal joints is reached by carring compression force by concrete and transfer tension force by concrete dowels.

Experimental and theoretical investigation with FE simulation show very high bearing cappacitiy and adequate ductility of confined UHPC dowels. The main influence parameters for load capacity of the UHPC dowels have been determined.

2 The Construction Principle

Truss constructions made of steel tubes are generally architectural sophisticated constructions. They are used in representative buildings e.g. sport or city halls and bridges with large spans. An important element in this construction is the nodal joint. Nowadays, welded or cast steel joints are usually used. Both joint types have disadvantages. For the welded joints the wall thickness in the region of nodal joints is generally higher than the thickness of the truss members because the design of the joints is often controlled by the shape stability and not by the stress analysis. Furthermore, the verification of the fatigue strength is necessary for dynamic loads. Structural problems may be caused by the

connection of truss members with fillet welds because the allowable stress is considerably reduced. Cast steel joints avoid this disadvantage because the welds are located into the truss members. Furthermore, other types of welds, which are more adequate for the fatigue strength, can be used. However, a load transmission area in the nodal joints has to be considered to compensate the different material strength between the joint and the truss members. Other problem is the high requirement on the erection accuracy between cast steel joints and truss members. If the erection accuracy is not sufficient expensive reworking is necessary. Additionally, complex FEM-calculations are necessary for an economic design of the joints. Figure 1 shows both types of the nodal joints

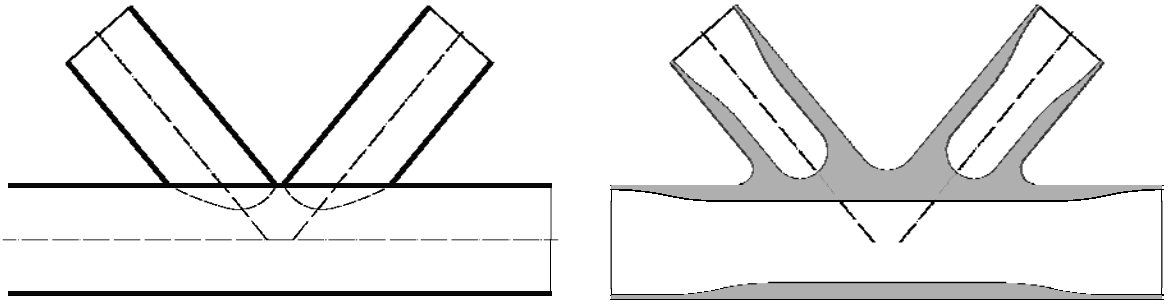

welded Steel joint

Cast-Steel joint

Figure 1: usually types of nodal joint in truss construction made of steel tubes

A new solution with UHPC for the nodal joints is shown in Fig 2. Two concepts are developed. The first one is the “cast in site” joint (Fig. 2a). In this case, steel construction including perforated steel plate in the nodal joints is assembled. Then, the steel tubes are filled with UHPC. In this process, the UHPC mus be able to flow through the joint without any blockage. The dowel effect is reached by concrete in the hollows of steel plate. The transfer of the compressive force from compressive diagonale into the chord is only realised by the concrete at the pressure-tension-joint shown in figure 2a. This means that in the whole structure the compressive force remains in concrete. The welds in the joint have only a sealing function. Only the load transfer between steel plate and tensile diagonale must be ensured by weldes. In this location HV-welds with good fatigue properties according to the Eurocode can be used.

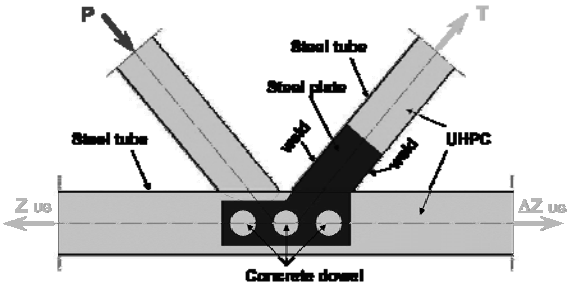

Figure 2a: Hybrid joint “cast in site” solution

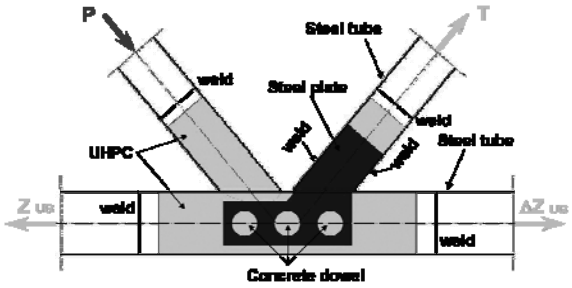

Figure 2b: hybrid joint “prefabricated“ solution

The second concept is the “prefabricated UHPC” joint (Fig. 2b). It is similar as the cast steel joints accoding to Fig. 1b. Outside the nodal joint the load is carried only by the tubes, both tensile and compressive force. However, in the region of the joints the compressive force is carried by concrete and the tensile force by tubes. The equilibrium in the joints is achieved by a perforated steel-plate placed in the joint and welded to the tubes. The perforated steel-plate isl completely be surrounded by UHPC. The load can be transfered by friction forces activated in the dowel cracking surfaces.

To determine the bearing capacity of the concrete dowels static and dynamic tests were performed. It can be shown that no reinforcement is required in the dowel as presented in [2] for the composite beams if the confinement of the joint is sufficient.

The manufacturing cost of truss construction made of steel tubes can be reduced with the suggested hybrid joint without affecting the durability or the robustness. A comparison between the hybrid joint and conventional joints shows, that more than 20% of the steel could be saved [3], [4]. This results in lower building costs.

3 Bearing Capacitity of the Confined Conrete Dowels

The load and deformation behaviour of the hybrid joint depend strongly on the behaviour of the UHPC dowels. An extensive test program focusing on the UHPC dowels was carried out at the institut for concrete structure and building material of the University Leipzig. The test program included the influence parameters on the bearing capacitiy of confined dowels als shown in Figure 3.

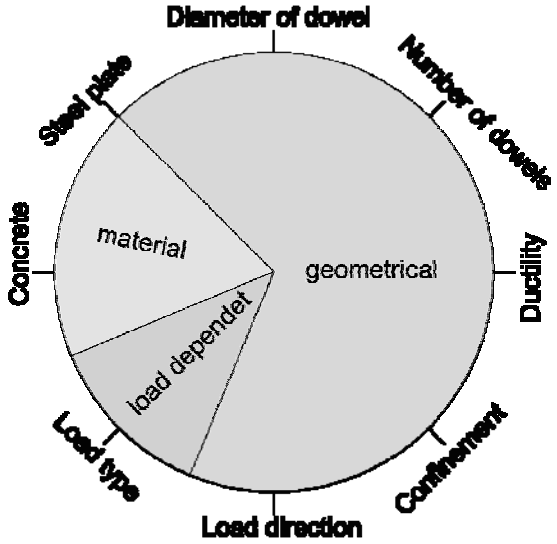

Figure 3: Influence parameters on the bearing capacity of confined UHPC dowels

A non fibre reinforced selfcompacting UHPC with coarse aggragat with a grain size of 5 mm was used in all tests. Its mechanical properties are shown in Table 1.

Table 1: mechanical properties of UHPC used in test program

compressive strength :	150 MPa
tensile strength :	8 MPa
Modulus of elasticity :	56 GPa

According to Figure 3 the influence parameters can be classified in three groups

- Influence of geometries
- influence of the concrete strength
- influence of load history
-

Two specimen types are choosen in order to consider different confinement condition in real structures, in which the specimen type N° 1 represents the best and the specimen type N° 2 the worst confinement condition. Totally 38 tests have been carried out. Table 2 shows the details and the variations in the test program. All tests are displacement controlled.

Table 2: Test program

Nr.	Specimen Type	Material	Test	Variation
1	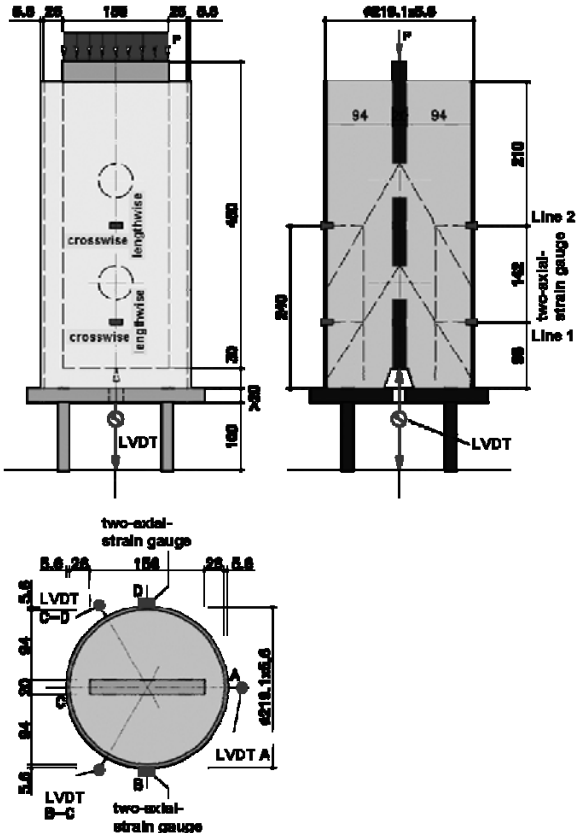	tube: S355 J0 Ø219,1x5,6 mm Ø355,1x5,6 mm Ø219,1x4,2 mm Ø219,1x7,8 mm steel plate: S355 J2 G3 t= 15mm concrete: UHPC G7 Without fibres C70/85 C30/37	9 test-series with 35 single tests	diameter of dowel single dowel double dowel ductility ring confinement load direction and load type material
2	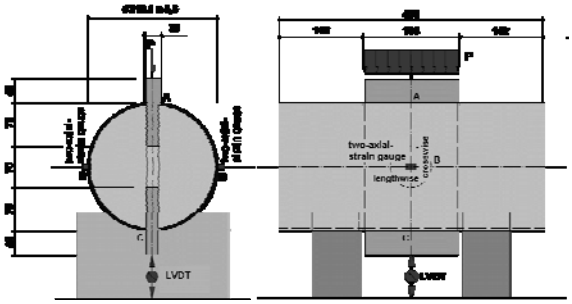	tube: S355 J0 Ø219,1x5,6 mm steel plate: S355 J2 G3 concrete: UHPC G7 without fibres	1 test series-with 3 single tests	single dowel

Figure 4 illustrates the general behaviour of the confined UHPC dowels. Due to the vertical displacement of the steel plate the UHPC dowel is subjected to shear stress. If the shear strength of UHPC is reached cracks occurred in the dowel. After crack formation the behaviour of the dowel depends strongly on the characteristic of the crack surface and the confinement by concrete-tension-ring and by the tube. If the crack surface is smooth the load drops down to zero without any reaction in horizontal direction. In the case of a rough crack surface the vertical displacement leads also to a displacement in horizontal direction. Due to the stiffness in horizontal direction (concrete-tension-ring and steel tube) a horizontal force is activated. Therefore, it can be assumed, that the bearing capacity of confined UHPC dowels is mainly caused by the friction. The roughness of the surface is higher, the greater the displacement in horizontal direction. Furthermore, the modulus of elasticity and the plastic deformation capacity of the concrete play in this relation an important roll.

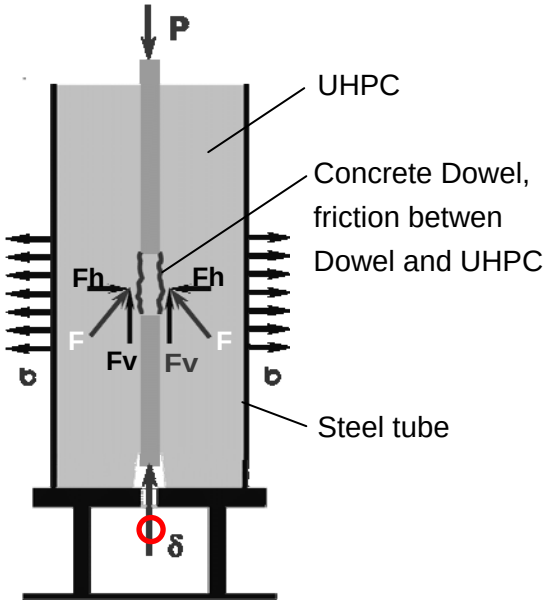

Figure 4: Illustration of the general behaviour of the UHPC dowel

The influence of the main geometric parameters is illustrated in figure 5. In details the variation of the dowel diameter (figure 5a), the influence of the number of dowels in a steel plate (figure 5b), the confinement by concrete-tension-ring (figure 5c) and the type of the specimen (figure 5d) can be seen.

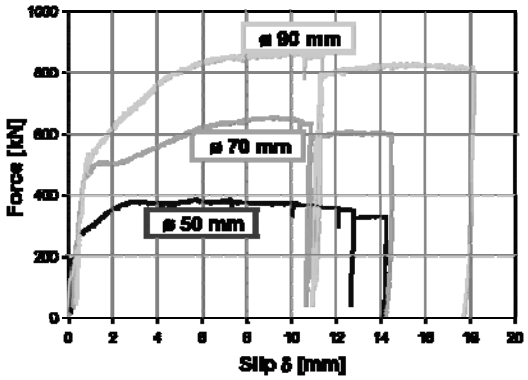

a) diameter of the dowels

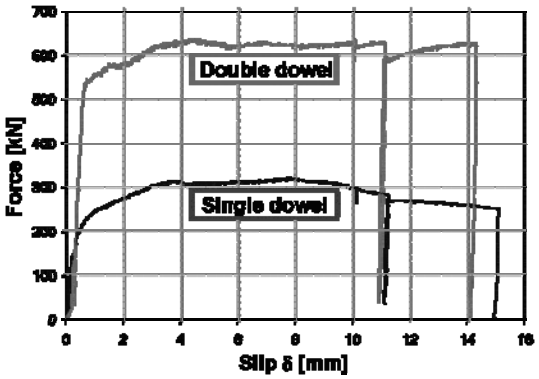

b) number of dowels Ø 50 mm

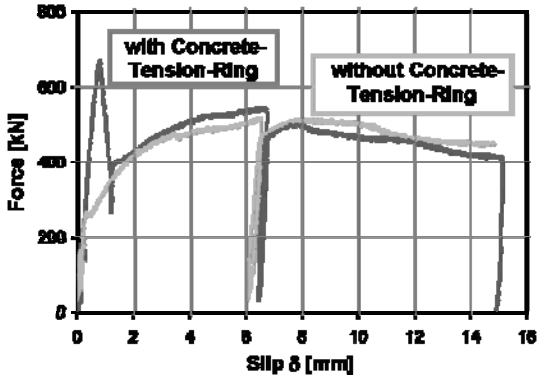

c) confinement concrete-tension-ring Ø 70 mm

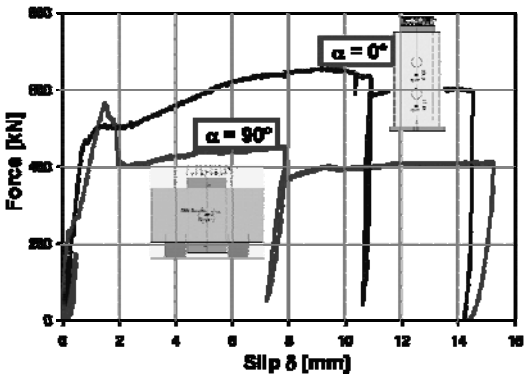

d) load direction Ø 70 mm

Figure 5: choosen test results

In the case of single dowel the increase of the dowel diameter leads to an increase in the bearing capacity. The increase is overproportional with the dowel diameter, however, unterproportional with the dowel area (figure 5a). In other words the bearing capacity per unit area decreases with the increase of dowel diameter. A double of the number of the dowels leads also to twice bearing capacity. A reduction of the bearing capacity due to interaction within a group of dowels seems not to be avaiable (figure 5b). The confinement of the dowels consists of two parts. The first is the concrete-tension-ring and the second the tube itsself. The capacity of the concrete-tension-ring dependends on its dimensions, length of the test speciment and the shortest distance between the steel plate and the tube, and on the tensile strength of the UHPC. For a similar thickness of the wall of the tube, the influence of the concrete-tension-ring on the load-displacement-curve is shown in figure 5c. Prior to the cracking the specimen with concrete-tension-ring exhibits a higher stiffness. After cracking the bearing capacity of the specimen with concrete-tension-ring drops down on the level of the speciment without concrete-tension-ring. The confinement is also dependent on the variation of the load direction (5d). In case of the specimen type N°2 the confinement is somewhat lower than that of the specimen type N° 1. This can explain with the slit in the tube for the implementation of the steel plate.

4 FEM-Simulation and Parameter Study

Finite element modeling is used in order to study more detailed the bearing and deformation behaviour of confined UHPC dowels, especially the interaction between the confinement and the carring load. Fig 6 shows the calculated 3D-model. The friction on the crack surface of the dowels is modeled using the interface element with nonlinear behaviour. The main object of the FE-modelling is toe investigate the relationship beween the vertical and horizontal forces. This informations is very important for designing of the hybrid nodal joints.

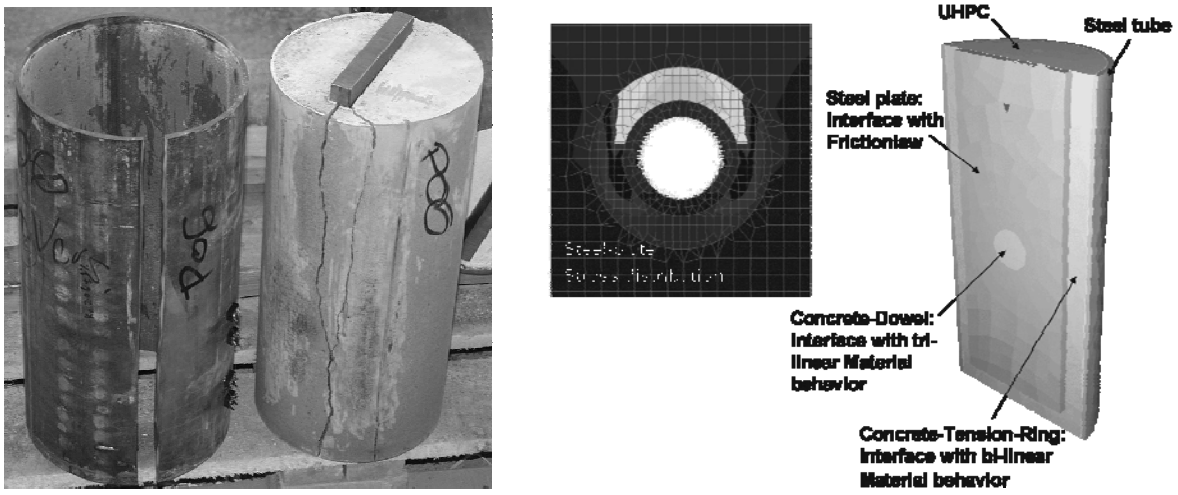

Figure 6: Implementation of the Specimen Type No. 1 into the 3D-FEM-Model [5]

Up to date the 3D-FEM-model have been calibrated with selected test data in order to verify the material law for the interface elements. The calculated results are in good agreement with the test results. In the next step a parameter study will be started. The experimental and theoretical results are background for the development of a calculation model for the design of nodal joints using UHPC dowels.

5 Summary and Conclusion

Confined UHPC dowels are a connector with high bearing capacity and adequate ductility. Its application in truss constructions made of steel tubes is an innovative application of UHPC.The main parameters of the bearing and deformation capacity are number and size of the dowels as well as the confinement attributes of steel and UHPC. A design model is currently being generated on the basis of experimental and theoretical studies [5].

The authors thank the DFG for the financial support of our research work in the context of the SPP 1182.

6 References

[1] Tue N. V.; et al.: Das Verbundrohr als Innovationsmotor für hybrides Bauen, Abschlußbericht 2004, Universität Leipzig, Leipzig, 2004

[2] Zapfe C.: Trag- und Verformungsverhalten von Verbundträgern mit Betondübeln zur Übertragung der Längsschubkräfte, Dissertation, Universität der Bundeswehr München, München 2001

[3] Tue N. V.; et al.: Konkretisierung der Tragsysteme des mit UHFB gefüllten Verbundrohres, Abschlußbericht 2005, Universität Leipzig, Leipzig, 2006

[4] Tue N. V.; Küchler M.: Betondübel als kraftübertragen des Element in hybriden Fachwerkkonstruktionen, LACER 9, Universität Leipzig, Leipzig, 2004

[5] Küchler M.: Zum Tragverhalten von Verbundmitteln für Hybridkonstruktionen aus Ultrahochleistungsbeton, Dissertation in Vorbereitung, Universität Leipzig, Leipzig, 2008

Christian Muehlbauer
Dipl.-Ing., Research Assistant
Department of Concrete Structures
TU Muenchen
Munich, Germany

Konrad Zilch
Univ.-Prof. Dr.-Ing. habil. Dr.-Ing. E.h.
Department of Concrete Structures
TU Muenchen
Munich, Germany

Experimental investigation of the long-term behaviour of glued UHPC joints

Summary

Within this article a very significant part of the research work of joining UHPC members by gluing with epoxy resin adhesive and reactive powder concrete adhesive, which is done at the Department of Concrete Structures at the Technische Universitaet Muenchen, is described.

One of the most important aspects with glued UHPC joints is the investigation of their long-term behaviour under service conditions. Therefore glued shear-compression specimens were stored at different load levels, different temperature levels and under moisture. The intention of the tests is to get a long-term model of the material for the different glued UHPC joints, i.e. UHPC joints that are glued with epoxy resin adhesive and reactive powder concrete adhesive. The knowledge of a long-term material model for the different joints is the background for a long-term design model for glued UHPC joints.

Keywords: *Ultra High Performance Concrete (UHPC), joining, gluing, Epoxy ResinAdhesive, Reactive Powder Concrete (RPC) adhesive, time dependent strength, long-term strength under permanent load, long-term strength under moisture*

1 Introduction

For most applications of UHPC a fabrication of UHPC in factories is necessary. Therefore a basic aspect with building UHPC structures is the development of elementary joints, which can be realized at the construction site. A perfect method of joining UHPC units is gluing the structural elements with appropriate high performance adhesives. These are epoxy resin adhesive and a special reactive powder concrete (RPC) adhesive. Within the priority programme SPP1182 of the German Research Foundation research work on (UHPC) is done since a while. At the department of concrete structures at the Technische Universitaet Muenchen there is a project about gluing UHPC units with these above mentioned high performance adhesives. One significant part of this research project is the investigation of the long-term behaviour of glued UHPC joints. Therefore tests were done to determine the time dependent strength at different temperature and load levels, the long-term strength under permanent load and the long-term strength under moisture.

2 Materials

2.1 UHPC

Within the research work a fine-grained UHPC with steel fibres was used. After stripping the forms heat treatment was carried out to the UHPC specimens for two days at 90°C. Afterwards the UHPC specimens were stored under laboratory conditions until they were glued together. The ingredients of the used UHPC mixture, called M2Q, are presented in Muehlbauer and Zilch [4] and Zilch and Muehlbauer [6].

2.2 Epoxy Resin Adhesive

Cold curing epoxy resin adhesives, i.e. epoxy resin curing at room temperature, exist of the two components resin and hardener. Epoxy resin adhesives have proofed on value in construction for the last decades. They are mainly used for strengthening concrete and prestressed concrete structures with CFRP strips, which are bonded externally or glued into slits. In this research work a cold curing two component epoxy resin adhesive called MC DUR 1280 was used. Epoxy resins exhibit a high cohesion and a very good adhesion to the adherends[1]. They also offer a high compression, tensile and shear strength. However, the mechanical properties highly depend on the temperature [3]. By reaching a limit temperature area, called glass transition area, these epoxy resins change their mechanical and physical properties. Therefore the glass transition area marks the critical temperature area for a UHPC construction, which is glued with epoxy resin adhesives. The glass transition temperature of common cold cured epoxy resin adhesives that are used in civil engineering is round about 60°C. For this reason research work was done to determine the strength of glued joints at temperatures, i.e. at 50°C, tight under the glass transition temperature of the epoxy resin adhesive.

2.3 Reactive Powder Concrete Adhesive

For applications that inhibit the use of epoxy resin adhesives due to elevated requirements a reactive powder concrete adhesive was developed. This adhesive bases on the M2Q UHPC mixture. Substantially there were changed just two ingredients: Finer aggregate and applicable cement were used. Also another superplasticizer was applied. The RPC adhesive was not heat treated. The processing time of this mineral adhesive is about 40 minutes. The ingredients of the used reactive powder concrete adhesive and details of the mixing process and the mixing time are presented and described in Muehlbauer and Zilch [4] and Zilch and Muehlbauer [6].

3 Specimen, Gluing and Test Setup

3.1 Specimen

For the tests shear-compression specimens as described in Muehlbauer and Zilch [4] and Zilch and Muehlbauer[6]. The adhesive joint had an inclination of 60° to the horizontal. The specimens were cast in a formwork consisting of plastic (polyoxymethylen) with an inclined stainless steel sheet of 1 mm thickness, so that there were two parts belonging together to be glued. Each series one mixture of adhesive was used. The adhesive joint area was 30 mm x 40 mm, i.e. the edges of the “raw specimens” were cut with a saw before the two parts

of the specimens were glued together. The adhesive layer had a thickness of about 1 mm for all specimens. The joint surfaces were sandblasted before gluing.

3.2 Gluing

3.2.1 Gluing with Epoxy Resin Adhesive

The sandblasted joint surfaces were glued with epoxy resin adhesive (thickness of adhesive layer 1 mm) – whereas the adherends were dry – and cured for seven days at room temperature.

3.2.2 Gluing with Reactive Powder Concrete Adhesive

Before the specimens were glued, they were stored for two days under water. The RPC adhesive was applied to the moist joint surface with a thickness of the adhesive layer of about 1 mm. After gluing the specimens were covered with a wet jute cloth and one day after gluing they were stored under water until they were installed to the test equipment two weeks after gluing.

3.3 Test Setup

The specimens that were applied to long-term load were installed to a long-term testing equipment. The load was applied with a testing machine and retained with disc clamps. The displacement of the spring deflection was measured with two displacement transducers and in case of displacement the spring deflection was adjusted by screwing the nuts. For each load level certain testing equipment was used, which generally differed in the size and arrangement of the disc clamps.

4 Time dependent strength of the adhesive joint at different temperature and load levels

4.1 Epoxy Resin Adhesive

The specimens glued with epoxy resin adhesive were loaded to 70%, 60%, 50% and 40% of the short term shear-compression strength in dependence of the ambient temperature. The tests were done at room temperature and at 50°C. The specimens were installed to the long-term testing equipment after seven days curing time. After seven days curing the specimens that were tested at 50°C were stored for one day at 50°C before they were installed to the long-term testing equipment at 50°C and then stored at 50°C until failure or in case of no failure until determination of the residual strength. The residual strength was tested according to former investigations of gluing in concrete structures [5] after two months. Each series three specimens were tested. The short term shear-compression strength at 50°C was determined to 70% of the short-term shear-compression strength at room temperature. The specimens that were loaded to 70% of the short-term shear-compression strength at room temperature had a life time of round about ten minutes, the ones loaded to 60% had a life time of half an hour and the ones loaded to 50% had a life time of round about 48 hours. The specimens loaded to 40% of the short-term shear-compression strength obtained a life time of two months and for those the residual shear-compression strength was determined. The

residual shear-compression strength did not differ from the short-term shear-compression strength at room conditions. The specimens that were loaded to 70% of the short-term shear-compression strength at 50°C had a life time of round about 2 hours, the ones loaded to 60% had a life time of round about three hours and the ones loaded to 50% had a life time of round about seven hours. Note that the load levels were determined from the short-term shear-compression strength at 50°C, which again was investigated to 70% of the short-term shear-compression strength at room conditions. The specimens loaded to 40% of the short-term shear-compression strength at 50°C obtained a life time of two months and for those the residual shear-compression strength was determined. The residual shear-compression strength did not differ from the short-term shear-compression strength at 50°C. Independent of the temperature and load level the failure in the joint was always a cohesion failure of the adhesive.

4.2 Reactive Powder Concrete Adhesive

In comparison to the long-term strength of joints glued with epoxy resin adhesive the long-term strength of joints glued with reactive powder concrete adhesive was experimentally investigated. Fourteen days after being glued the specimens were installed to the long-term equipment. The specimens were loaded to 70%, 60%, 50%, 40%, and 30% of the short-term shear-compression strength. The investigations were only carried out at room temperature, because for this mineral high strength adhesive no influence of high temperatures to the strength is expected. With a load level of 70% of the short-term shear-compression strength the specimens broke after some minutes. The specimens loaded to 60%, 50%, 40%, and 30% of the short-term shear-compression strength did not fail within the two months. Figure 1 represents the residual shear-compression strength of the specimens after two months. Each series three specimens were tested and the result of each single specimen is presented in Figure 1. The average short-term compression strength was determined to about 45 MPa. As you can see from Figure 1 there is no loss of strength after two months independent from the load level. The fracture pattern was always an adhesion failure as it was detected in the short-term tests.

5 Long-term strength of the adhesive joint under permanent load

5.1 Epoxy Resin Adhesive

Franke and Deckelmann [2] suggested for the long-term strength of joints glued with epoxy resin adhesive a value of 25% of the short-term strength. This reduction is due to long-term and environmental influences as moisture, temperature, permanent load and dynamic load.
For testing the long-term strength of UHPC joints glued with epoxy resin adhesive the glued specimens were permanently loaded with 25% of the short-term shear-compression strength under room conditions for one week, three months, six months and one year. The specimens were installed to the long-term testing equipment one week after gluing. To compare the long-term strength under permanent load to the long-term strength without load, specimens free from tension were stored at same conditions. The residual shear-compression strengths of the glued specimens were determined after dismounting them of the long-term testing

equipment. Figure 2 shows the residual shear-compression strength of the glued specimens after a certain time with and without permanent loading. Each series three specimens were tested. Figure 2 presents the experimental results of all single specimens. As you can see from Figure 2 a permanent load of 25% of the short-term shear-compression strength, which was determined to be round about 35 MPa, has no influence to the residual strength of the glued joint.

5.2 Reactive Powder Concrete Adhesive

To compare the performance of the new developed RPC adhesive to the one of the epoxy resin adhesive under permanent load the specimens glued with RPC adhesive were permanently loaded with 25% of their short-term shear-compression strength, which was determined to be round about 45 MPa. The glued specimens were installed to the long-term testing equipment after a curing time of two weeks and then permanently loaded with 25% of their short-term shear-compression strength under room conditions for one week, three months, six months and one year. In addition specimens were stored free from tension at same conditions as the permanently loaded specimens. The residual shear-compression strengths of the glued specimens were determined after dismounting them of the long-term equipment. Figure 3 shows the residual shear-compression strength of the glued specimens after a certain time with and without permanent loading. Each series three specimens were tested. In Figure 3 the experimental results of all single specimens are presented. The experimental results do not show an influence of a permanent load of 25% of the short-term shear-compression strength to the residual shear-compression strength. However, Figure 3 shows big deviations of the average shear-compression strength especially for the specimens stored for long time. Although this effect can not be explained yet, it may indicate an increase of strength with longer curing times (post-curing effect).

6 Long-term strength under moisture

6.1 Epoxy Resin Adhesive

The influence of moisture to joints glued with epoxy resin adhesive was investigated. Therefore the specimens were stored at 20°C under water after seven days curing time for seven days, three months, six months and one year. After storing the specimens under water for a certain time the residual shear-compression strength was determined. Each series three specimens were tested. Figure 4 shows the residual shear-compression strength of every single specimen after a certain time of storing under water. The fracture pattern for specimens stored for 7 days and three months under water was a cohesion failure. For the specimens stored for six months and one year the fracture pattern was not only a cohesion failure but also in parts an adhesion failure. However, as you can see in Figure 4 the residual shear-compression strength decreases with increasing storing time under water. After one year of storing the specimens under water the residual shear-compression strength decreases to round about 85% of the short-term shear compression strength. Franke and Deckelmann [2] proposed a long-term reduction factor of 0.8 to consider the influence of the

moisture to joints glued with epoxy resin adhesives. This seems to be in accordance with the results got from the above described tests.

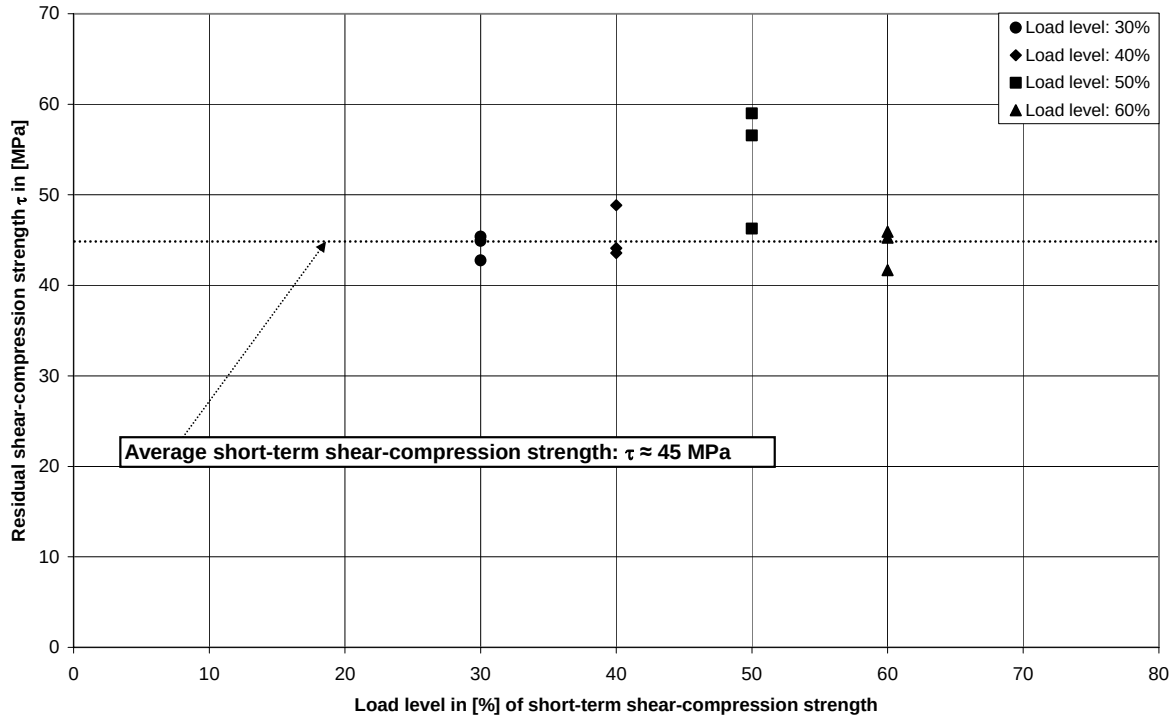

Figure 1: Residual shear-compression strength of specimens glued with RPC adhesive after two months of loading the specimens with different load levels

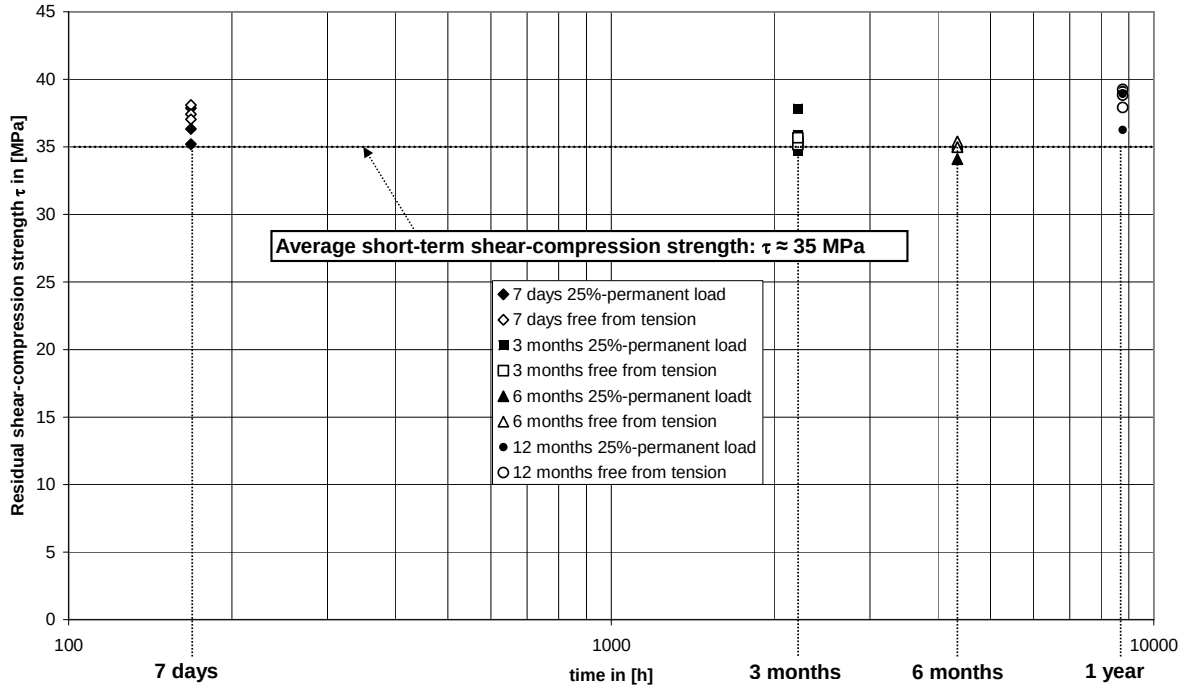

Figure 2: Residual strength of specimens glued with epoxy resin adhesive after certain time of permanent loading of 25% of short-term strength and of storing free from tension (gluing, storing and testing at room conditions)

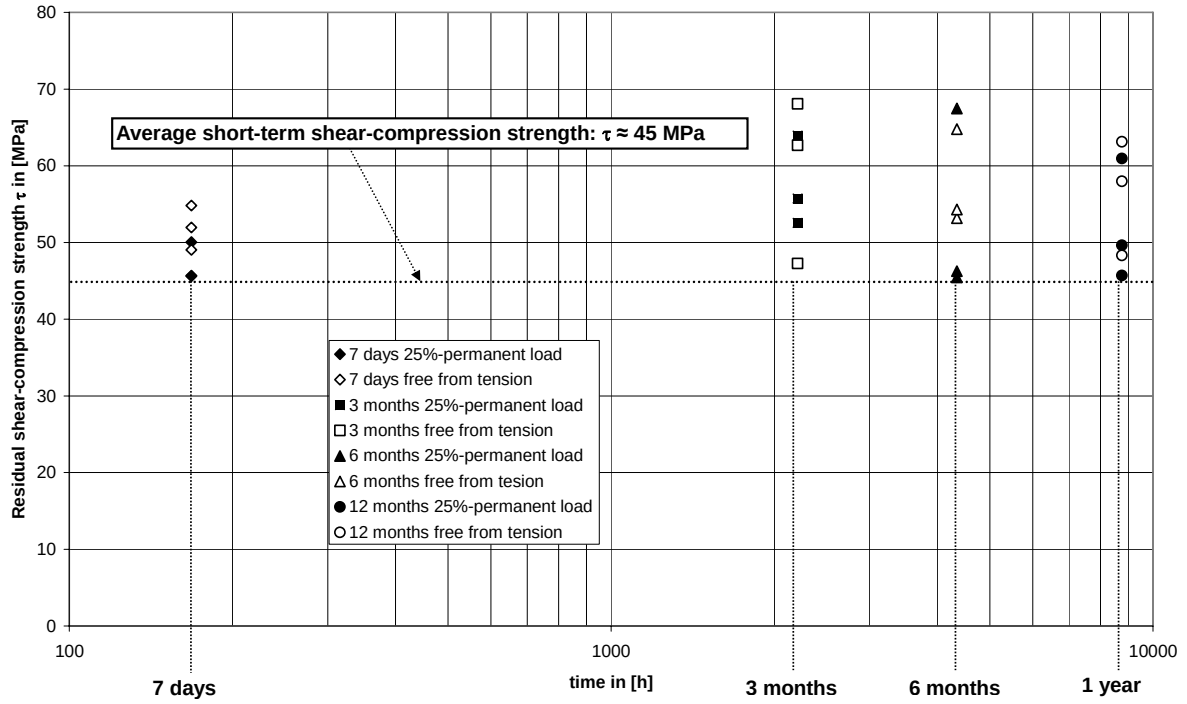

Figure 3: Residual strength of specimens glued with RPC adhesive after certain time of permanent loading of 25% of short-term strength and of storing free from tension (gluing, storing and testing at room conditions)

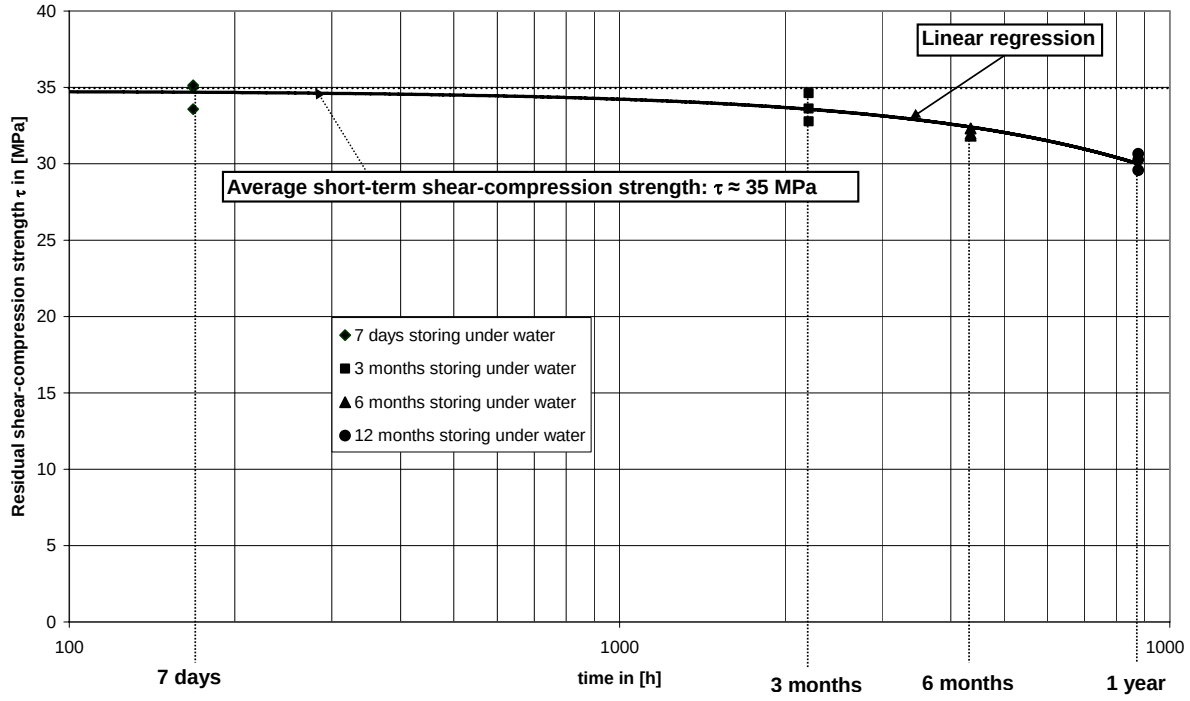

Figure 4: Residual strength of specimens glued with epoxy resin adhesive after certain time of storing free from tension under water
(gluing, storing and testing at room temperature)

7 Conclusion

The investigations demonstrated that a long-term strength for joints glued with epoxy resin adhesive can be achieved for 40% of the short-term strength. The short-term strength at 50°C is reduced to 70% of the short-term strength at room conditions. For joints glued with RPC adhesive a long-term strength for a load level of 60% of the short-term strength could be detected. An influence of the temperature to the strength of joints glued with RPC adhesive is not expected. A permanent load of 25% of the short-term strength of the joint did not show any influence to the residual strength whether for joints glued neither with epoxy resin adhesive nor for joints glued with reactive powder concrete adhesive. For joints glued with epoxy resin adhesive an influence of moisture to the residual strength was detected.

8 Acknowledgement

This research project was funded by the German Research Foundation within the priority programme 1182. The epoxy resin adhesive was committed by MC-Bauchemie Müller Gmbh & Co, Germany.

9 References

[1] Ehrenstein, G.W.: Polymer – Werkstoffe: Struktur, Eigenschaften, Anwendung, 2. Auflage, München. Carl-Hanser-Verlag, 1999

[2] Franke, L.; Deckelmann, G.: Die Biegebemessung von Stahlbetonbauteilen mit nachträglich aufgeklebter Bewehrung unter Gesichtspunkten einer ausreichenden Dauerhaftigkeit. In: Festschrift zum 60. Geburtstag Peter Schießl. TU München: Schriftenreihe Baustoffe des Centrums Baustoffe und Materialprüfung, 2003

[3] Habenicht, G.: Kleben, Grundlagen, Technologie, Anwendungen, 5. erweiterte und aktualisierte Auflage, Springer-Verlag, Berlin, Heidelberg, 2006

[4] Muehlbauer, C.; Zilch, K.: Joining of Ultra High Performance Concrete (UHPC) Members by Gluing, In: Proceedings of the Third international Conference on Structural Engineering, Mechanics and Computation, 10-12 September 2007, Cape Town, South Africa, Recent Developments in Structural Engineering, Mechanics and Computation, edited by Alphose Zingoni, Millpress, 2007

[5] Rehm, G.; Franke, L.: Kleben im Konstruktiven Betonbau. Ernst & Sohn, Berlin, 1982 (DAfStb-Heft 331)

[6] Zilch, K.; Muehlbauer, C.: Zum Fügen von Ultra-Hochfestem Beton (UHPC) durch Verkleben, Grundlegende Untersuchungen, In: Bauen mit innovativen Werkstoffen, VDI-Gesellschaft Bautechnik, VDI-Berichte 1970, VDI Verlag GmbH, Düsseldorf, 2007

Ekkehard Fehling
Prof. Dr.-Ing.
University of Kassel
Kassel, Germany

Torsten Leutbecher
Dr.-Ing.
IBB Fehling + Jungmann,
Consulting Engineers,
Kassel, Germany

Friedrich-Karl Röder
Dr.-Ing.
University of Kassel
Kassel, Germany

Simone Stürwald
Dipl.-Ing.
University of Kassel
Kassel, Germany

Structural behavior of UHPC under biaxial loading

Summary

Within a research program, reinforced ultra high performance concrete (UHPC) panels have been investigated experimentally under biaxial compression-tension loading. The effects of transverse tensile stress and the cracking as a result of the compressive strength have been studied. Based on the experimental results and those of an earlier research program on normal strength concrete (NSC) panels, a proposal for the reduction of the compressive strength of cracked reinforced non-fiberd and steel fiber concrete against the applied tensile strain, could be developed.

Keywords: *UHPC, bar reinforcement, steel fibers, panel, compression, tension, biaxial test, reduction factor, material model*

1 Introduction

Over the past 40 years tests on the bearing capacity of cracked concrete panels have been carried out, e.g. by Vecchio/Collins [1], Belarbi/Hsu [2], Eibl/Neuroth [3], Mehlhorn/Kollegger [4] and Schlaich/Schäfer [5].

The results of particular tests vary significantly and lead to contradictory conclusions because of the partly different objectives and due to the highly differing execution of tests (test setup, order of load application etc.), the dimensions of test specimens and the reinforcement configurations. This was the motivation to start a research program on normal strength concrete (NSC) panels at first [7] and subsequently for the current research program on UHPC-panels [8].

This paper describes the investigations on UHPC-panels. The experimental results are used to develop a proposal for the reduction of the compressive strength in dependence of the applied tensile strain. Furthermore, the results of the UHPC-panels and of the NSC-panels are compared.

2 Test Program

In the test program a total number of 47 plain, fiber and/or bar reinforced UHPC-panels were tested. A general overview of the test program on UHPC-panels is given in table 1.

Table 1: Overview of the test series

reinforcement:	plain	steel fibers	steel bars	bars and fibers
series 1	3 (3c)	3 (3c)	3	3
series 2	-	-	6	6
series 3	1 (1c)	-	9 (2c)	-
series 4	-	1 (1c)	-	1 (1c)

(c) specimens that were tested with compression load only

Except for the panels loaded only by compression, the specimens were loaded sequentially, i. e. at first the tensile loading and afterwards the compressive loading was applied.
The influence of the magnitude of applied average tensile strain (between approx. 0.5 ‰ and 8 ‰), of the addition of steel fibers and of the interfering effect of the reinforcement on the reduction of the compressive strength at simultaneously acting lateral tension have been studied.

3 Test Specimens

The dimensions of the UHPC-panels were 350 mm in compressive direction, 500 mm and 1000 mm respectively in tensile direction. The thickness was 70 mm. The panels were reinforced orthogonally in two layers in tensile and compressive direction with high-strength reinforcing steel bars d_s = 8 mm, St 1420/1570. The high-strength steel was selected to enable high elastic strains (> 6 ‰). For the panels with a length of 500 mm the dimensions and the configuration of reinforcement are shown in figure 1.

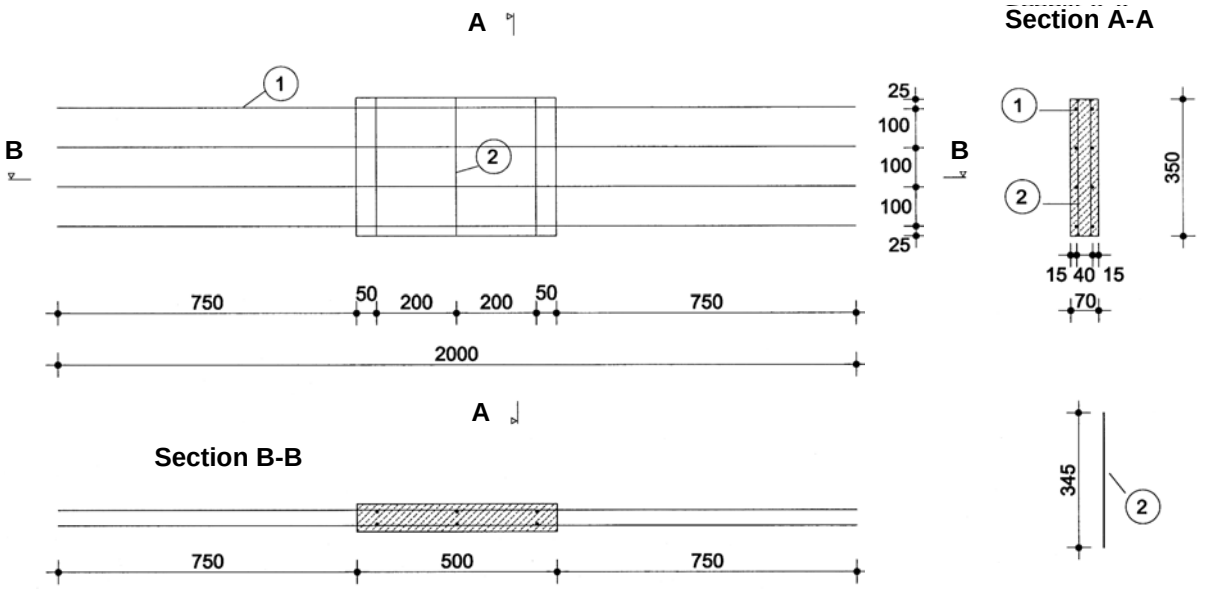

Figure 1: Reinforcement dimensions of the concrete panels

The spacing of the reinforcing bars was 100 mm in tensile direction (reinforcement ratio ρ_s = 1.64 %) and 200 mm in compression direction (reinforcement ratio ρ_s = 0.86 %).
The concrete mixture of the fine-aggregate UHPC was M1Q with a fiber content of 1.0 vol.- %. The high strength steel fibers had a length of 17 mm and a diameter of 0.15 mm. Further details of the concrete mixture are given in the research report ”Entwicklung, Dauerhaftigkeit und Berechnung Ultra-Hochfester Betone (UHPC)” [6].
Standard concrete cylinders with a diameter of 150 mm and a height of 300 mm were fabricated accompanyingly with the panels. They were cured under the same conditions and were tested on the same day as the panel. The compressive strengths of the cylinders served as reference values.

4 Execution of the tests

The compression tension tests were carried out at the Strong Floor of the Central Laboratory of the Institute of Structural Engineering of Kassel University. The test setup is shown in figure 2.

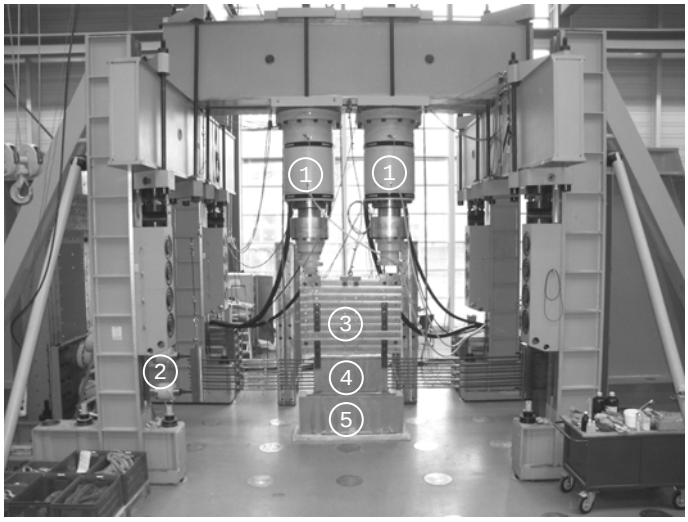

(1) 2.5 MN-hydraulic jacks for compressive forces
(2) 2 x 400 kN-hydraulic jacks for tensile forces
(3) load distribution
(4) specimen
(5) UHPC-bearing block

Figure 2: Testing frame for the compression-tension tests

The horizontal tension force was applied by two hydraulic jacks, each with a nominal capacity of 400 kN. This force was routed by a crosshead as well as by interposed threaded bars and sleeves to the rebars of the reinforced concrete panel. The vertical compression forces were applied by two hydraulic jacks, each with a nominal loading capacity of 2.5 MN, and were routed by two roller bearings in two load distributing steel panels and into the specimen. The steel panels were protected against a deviation from the loading plane by horizontal guidance struts. A block of reinforced UHPC acted as the bearing for the specimens.
The vertical compression forces were measured by load cells at the two hydraulic jacks. The measurement of the horizontal tension forces was performed by load cells at the hydraulic jacks and by further load cells on the abutment side, to check the balance of the forces. The tension forces in the continuous reinforcing bars were measured additionally by load cells to check the constancy of the load application distribution across the panel height.

Three inductive displacement transducers were fixed in vertical and horizontal direction respectively on the front and on the back of the panel to measure the displacements. For the panels the gauge lengths were 270 mm in vertical and 420 mm in horizontal direction.
The recording of the forces and displacements was carried out continuously (one measured value per second) with a multi-channel-measuring-system. The measured values were routed to a PC, registered there with a software package for monitoring the measurement reading and were stored on the hard disk.
The loading of the specimens was performed under displacement control using a process monitoring unit and a control software. For this purpose, displacements were measured at the panel and were read by the monitoring unit with a clock rate of 1000 Hz. The software-based processing and the output of the control commands to regulate the hydraulic jacks followed subsequently.
A drop of the displacement transducers fixed at the panel directly could not be avoided, because of the cracking. Therefore the displacement values used for the control were collected with separate measuring mechanisms in vertical (compression) and horizontal (tension) direction respectively outside the specimens.
The specimens were placed in the testing device in such a way that the compression loading could be carried out centrically after applying the respective tensile strain. The loading of the panels was carried out sequentially. At first the tensile loading was applied in horizontal direction and then the vertical compression loading was carried out until the specimen failed.

5 Experimental results

There is a significant difference between the behavior of the UHPC-panels with fiber reinforcement and the panels without fibers.
The different crack patterns are shown in figure 3. After tensile loading up to a tensile strain of 4.5 ‰, the fiber reinforced panels showed smaller crack spacings and smaller crack widths than the panels reinforced only with rebars.

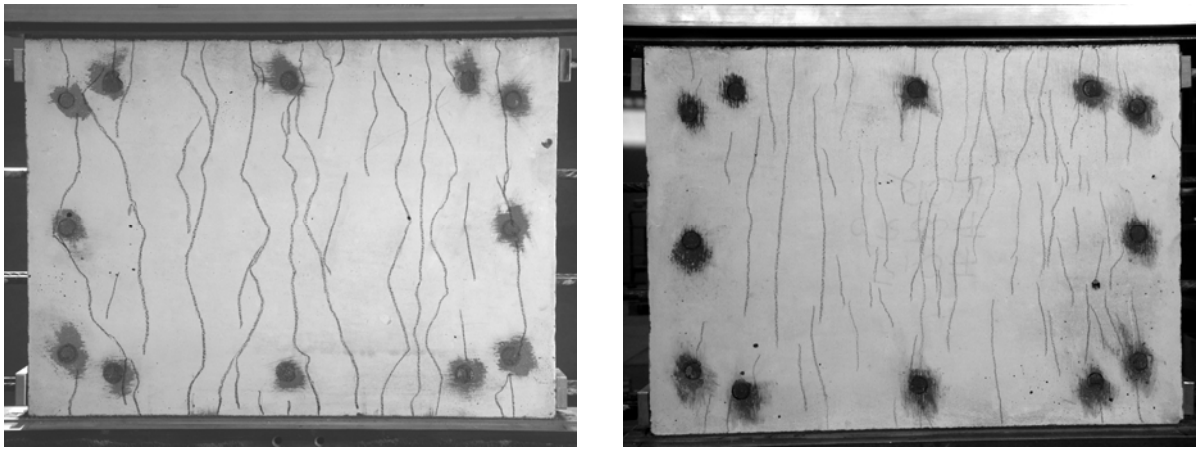

a) specimen with rebars only b) specimen with rebar and fibers

Figure 3: Crack pattern of the UHPC-specimens at an applied tensile strain of 4.5 ‰ in horizontal direction.

At the end of the compressive loading a different failure pattern of the panels could be observed. As shown in figure 4, the failure pattern of the non-fiberd UHPC-panels was very brittle in contrast to the panels reinforced with a small fiber content of 1.0 vol.-%. The panels with fiber reinforcement also reached higher compressive strengths.

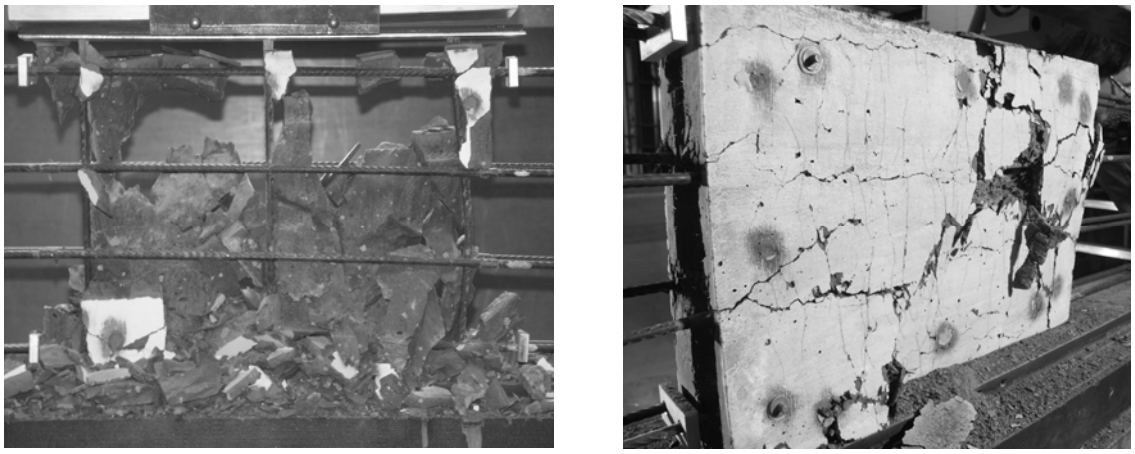

a) specimen with rebars only (applied tensile strain is 1.5 ‰)

b) specimen with rebars and fibers (applied tensile strain is 3.5 ‰)

Figure 4: Failure pattern of the UHPC specimens.

Selected results of the tests on UHPC-panels are shown in figure 5. Further details are summarized in a research report by Fehling et. al. [8].

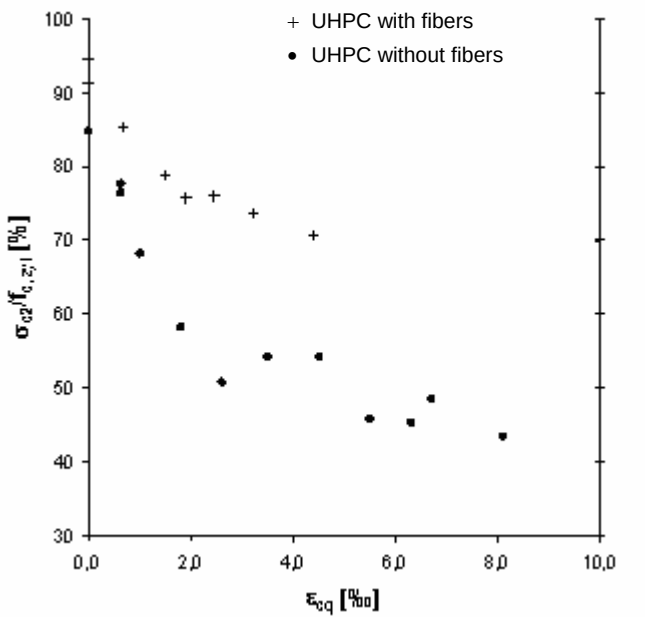

The ordinate represents the normalized compressive strength $\sigma_{c2}/ f_{c,zyl}$. At this, σ_{c2} is the compressive stress referring to the concrete gross cross-section and $f_{c,zyl}$ is the compressive strength of the standard concrete cylinders.

The absissa shows the transverse tensile strain ε_{cq}.

Figure 5: Test results of the UHPC-panels

6 Proposal for the reduction of the compressive strength due to applied transverse tensile strain

The development of the compressive strength of the panels in dependence on the applied tensile strain clarifies some characteristics. The compressive strength of the UHPC-panels decreases significantly and almost linearly already at small tensile strains. The normalized compressive strength stabilizes for average tensile strains of more than approx. 2.5 ‰. For higher tensile strains, an influence of the applied tensile strain is hardly noticeable.

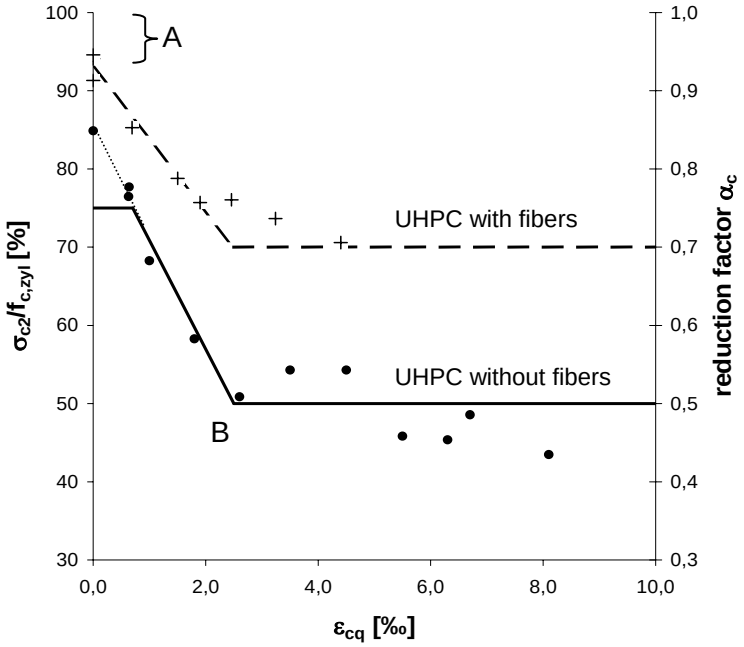

(A) reduction, caused by the interfering effect of the bar reinforcement
(B) complete loss of aggregate interlock

Figure 6: Proposal for the reduction of the compressive strength of reinforced UHPC against the applied tensile strain

Figure 6 shows the proposal for the reduction of the compressive strength of cracked reinforced fiberd and non-fiberd UHPC.
Because of the interfering effect of the bar reinforcement (A in figure 6), the compressive strength decreases even for the non-tensioned specimens. This effect is more distinctive for the non-fiberd panels, due to the ability of the fibers to transfer tensile forces effectively already in the state of micro cracking. The initial reduction caused by the bar reinforcement depends on the geometry of the concrete member and on the reinforcement ratio.

The biaxial tension compressive strength of reinforced UHPC is significantly affected by the crack width and the crack spacings. To consider the reduction of the concrete compressive strength due to transverse tensile strain $\varepsilon_{c,q}$, a simple bilinear approach is suggested.
The linear descending for small tensile strains considers the decrease of the aggregate interlock effect due to the increasing crack width. Conservatively, for non-fiberd UHPC a reduction factor of 0.75 according to the valid German code 1045-1 [9] can be introduced.
After complete loss of aggregate interlock (B in figure 6), the load has to be beared by small compressive struts. Because of the crack formation up to high elastic strains (small crack

spacings and crack widths) this effect is less distinctive for fiber reinforced UHPC. For the non-fiberd specimens a minimum reduction factor of 0.5 has been obtained. With 1.0 vol.-% of steel fibers a limit value of 0.7 could be achieved.

7 Comparison of UHPC and NSC under biaxial loading

UHPC and NSC show a similar behavior under biaxial loading (figure 7).

Due to the smaller aggregate size (aggregate interlock!), the decrease of the compressive strength is steeper for UHPC. Furthermore, the maximum reduction of the compressive strength of the non-fiberd concrete is higher for UHPC, because of the lower ductility and the smaller resisting compressive struts.

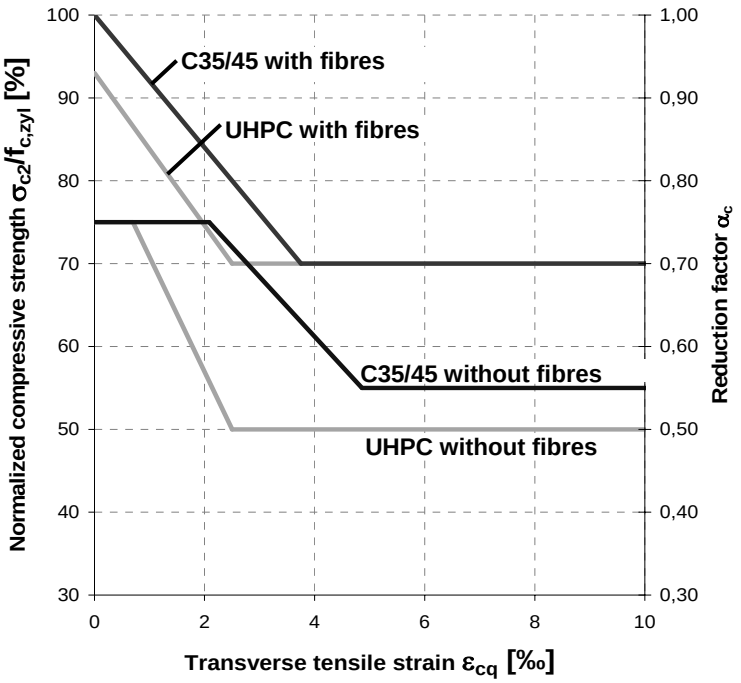

Figure 7: Proposal for the reduction of the compressive strength of NSC (C 35/45) and UHPC against the applied tensile strain

8 Conclusion

On the basis of experimental results, a proposal for the reduction of the compressive strength of cracked reinforced UHPC-panels with and without steel fibers has been presented. The experimental investigations show, that the aggregate size, the crack spacing and the crack width have an important influence on the decrease of the compressive strength. In contrast, the yield point of the reinforcement shows obviously no effects. Over all, reinforced UHPC and NSC behave similar under biaxial compression-tension loading.

Acknowledgement

This research project is supported by the German Research Foundation (DFG) within the priority program 1182: “Sustainable Building with ultra high performance concrete (UHPC)”. The authors would like to express their gratitude for the financial support.

9 References

[1] Vecchio, F. J., Collins, M. P. 1986. The modified Compression Field Theory for Reinforced Concrete Elements Sub-jected to Shear. ACI Structural Journal, Vol. 83, 1986: 219-231.

[2] Belarbi, A., Hsu, TH. T. C. 1995. Constitutive Laws of Softened Concrete in Biaxial Tension-Compression. ACI Structural Journal, Vol. 92, 1995: 562-573.

[3] Eibl, J., Neuroth, U. 1988. Untersuchungen zur Druckfestig-keit von bewehrtem Beton bei gleichzeitig wirkendem Querzug; Forschungsbericht T2024, Stuttgart: IRB Verlag.

[4] Kollegger, J., Mehlhorn, G. 1988. Biaxiale Zug-Druck-Versuche an Stahlbetonscheiben. Research report of the Chair of Structural Concrete, no. 6, University of Kassel, 1988.

[5] Schlaich, J., Schäfer, K. 1983. Zur Druck-Querzug-Festigkeit des Stahlbetons. Beton- und Stahlbetonbau 78, Ernst & Sohn Verlag, Berlin, 1983: 73-78.

[6] Fehling, E.; Schmidt, M.; Teichmann, T.; Bunje, K.; Bornemann, R.; Midendorf, B.; 2005. Entwicklung, Dauerhaftigkeit und Berechnung Ultra-Hochfester Betone (UHPC)

[7] Fehling, E., Leutbecher, T., Röder, F.-K. 2008a. Compression-tension-strength of reinforced concrete and reinforced steel fiber concrete in panel-shaped structural members. Research report of the Chair of Structural Concrete, Faculty of Civil Engineering, University of Kassel, 2008.

[8] Fehling, E., Leutbecher, T., Stürwald, S. 2008b. Compression-tension-strength of ultra high performance concrete (UHPC) and ultra high performance fiber reinforced concrete (UHPFRC) in panel-shaped structural members. Research report of the Chair of Structural Concrete, Faculty of Civil Engineering, University of Kassel, 2008.

[9] DIN 1045-1: Tragwerke aus Beton, Stahlbeton und Spannbeton; Teil 1: Bemessung und Konstruktion, Juli 2001

Special Part III:

Gärtnerplatz Bridge

Ekkehard Fehling
Prof. Dr.-Ing.
University of Kassel
Kassel, Germany

Kai Bunje
Dipl.-Ing.
IBB Fehling – Jungmann GmbH
Kassel, Germany

Michael Schmidt
Prof. Dr.-Ing. habil.
University of Kassel
Kassel, Germany

Walter Schreiber
Dipl.-Ing.
IBB Fehling – Jungmann GmbH
Kassel, Germany

The "Gärtnerplatzbrücke" Design of First Hybrid UHPC-Steel Bridge across the River Fulda in Kassel, Germany

Summary

A 132 m long hybrid UHPC-steel bridge with 6 spans has been built across the river Fulda in Kassel, Germany. UHPC offers supreme durability characteristics and, hence, has been selected for the replacement of an existing, damaged timber structure. The novel structural concept consists of a hybrid steel – UHPC truss structure and precast UHPC plates for the bridge deck. The deck plates are glued to the upper chords of the truss structure. For the transfer of shear forces from the truss diagonals (steel tubes) to the UHPC chords, prestressed bolted friction connections are used. The paper describes the final design, accompanying tests, finite element calculations and the erection of the bridge structure. A monitoring system will be installed in order to gather practical experience with the new materials and the novel structural concept.

Keywords: *Ultra-High-Performance Concrete (UHPC), durability, hybrid UHPC-steel structure, bridge design, glued connections, prestressed bolted connections, monitoring, precast elements, prestressing, posttensioning*

1 Introduction

Ultra High Performance Concrete (UHPC) not only offers very high strength but also superior durability characteristics due to the low permeability for liquids and gases. Both, the very high strength as well as the significantly improved durability in comparison to normal and high strength concrete are a consequence of the extreme packing density of the cement matrix. At the University of Kassel, the mix design and optimization as well as the investigation of the characteristics of the hardened UHPC with values of the compression strength between 150 and 400 MPa have been in the focus of research since 1998. Furthermore, the behaviour of UHPC elements in bending and shear has been studied intensively [1]. This research, mainly founded by the DFG (Deutsche Forschungs-Gemeinschaft / German Research Foundation),

has encouraged the authors to start with some UHPC-projects for bicycle and pedestrian bridges. Some major results are as follows:

- For elements subject to bending or bending and normal force, the tensile strength of UHPC with fibres can be used, since due to the fibres, a ductile behaviour in tension can be ensured. Reduction factors accounting for the inhomogeneity of the spatial distribution of the fibres and their orientation should be introduced. For thin elements, the dominating fibre orientation can be observed to be parallel to the formwork.
- For rectangular cross sections, failure due to shear forces could only be observed for very low or no fibre contents. For UHPC without fibres, the shear force resistance can be calculated well by the model according to Zink [4] which is mainly based on the bearing capacity of the compression zone.
- Bar reinforcement and fibres as reinforcement can be combined effectively.
- UHPC can develop very high bond stresses (about 50 MPa) leading to short anchorage lengths or splice lengths. However, in order to avoid or control longitudinal cracks due to bond, a minimum fibre content should be provided.
- The fatigue strength of UHPC with fibres under cyclic compression amounts to about 40 % of the static compressive strength. This means that UHPC behaves similar as normal strength concrete in that respect.
- Precasting may be recommended in order to obtain structural elements with high quality. The relatively high, mainly autogenous shrinkage can be eliminated for the final product if heat treatment (70 – 90°C) is applied. The residual shrinkage then is very low and the creep coefficient is decreased drastically, from φ= 0.8 … 1.2 to φ= 0.2 … 0.3.
- Prestressing and posttensioning can effectively be used in order to exploit the high strength of UHPC. Also, serviceability characteristics can be influenced in a positive way (e.g. minimization or avoidance of cracking due to shrinkage, reduction of deflections due to creep and shrinkage).
- Due to the relatively high tensile strength (around 10 MPa) and the dense structure, also at the surface, UHPC is very well suited for gluing. This holds true for the application of e.g. glued carbon fibre laminates as well as for gluing UHPC elements amongst each other.

2 First UHPC bridge projects in Germany

Following these observations, the first UHPC bridges in Germany have been built in Niestetal near Kassel [5]. These bridges consist of precast, prestressed UHPC elements with spans of 7, 9, and 12 m. The 12 m bridge, which was the first one to be mounted, has an inverted U-shape. The two webs have been posttensioned each by a tendon with 1.2 MN prestressing force. No bar reinforcement has been used except for the anchoring regions of the tendons and for the integrated transverse girder at the supports. The other bridges have been prestressed. The geometry of the cross section is a π-shape. The curved geometry of the lower side of the webs leads to a variable position of the centre of gravity of the cross section. As a consequence, the variation of the prestressing moment along the bridge

becomes curvilinear although the prestressing strands are straight. Thus, it suits the distribution of moments due to external loads quite well. Two additional bridges of the π-shape typ have been build in 2007. One near the town of Friedberg with 12 m span and one in the City of Weinheim with 18 m span.

Figure 1: Mounting of the 12 m UHPC footbridge in Niestetal

Figure 2: 18 m bridge with TT-shaped cross section

3 Design requirements of the Gärtnerplatzbrücke

The timber bridge existing until 2005 had been built for the 1981 federal garden show (Bundesgartenschau) in Kassel to provide a connection for pedestrians and for bicycles across the river Fulda. It had been severely damaged due to fungus attack. Thus, the city of Kassel as the owner of the bridge was searching for a durable, lightweight structure to replace the old bridge. UHPC, as an innovative material being investigated at the University of Kassel, promised superior durability in comparison to timber, steel or conventional concrete. Since the bridge is part of a regional bicycle trail, the state of Hessen would

financially support the new bridge. However, the budget for a bridge using an innovative material had to be oriented to the costs of a conventional solution. For the design of the new bridge, the city of Kassel commissioned IBB Fehling+Jungmann consulting engineers in Kassel.

- The existing pillar foundations had to be used also for the new bridge. Otherwise the old foundations would have to be demolished since they should not obstruct the ship traffic on the river. Although larger spans could have been conceived, this requirement would have increased the cost of the whole project substantially.
- Since the old foundation had to be re-used, the new superstructure could not be much heavier than the old timber structure. A conventional prestressed concrete solution would have disadvantages in that respect, but a filigree UHPC structure could easily overcome this problem.
- The new bridge should have a deck width of 5 m. The loads to be assumed are those for pedestrian and bicycle traffic (5 KN/m²) and, in addition, a 6 tons rescue or service vehicle.
- For the ship traffic, a usable height of 5.50 m and a width of 30 m were required. With respect to disabled persons, the maximum slope of the deck should not exceed 5 %.
- Loads from ice and ship impact on the pillars had to be considered.

Different design concepts have been evaluated. Mainly, systems with two or three UHPC girders, including truss systems have been discussed. In addition, cable stayed bridge solutions have been conceived. The required supervision and maintenance of the cables, however, has been regarded as a disadvantage.
In order to avoid vibration problems, a continuous girder system was preferable rather than a system of independent single span girders.

4 Final design and execution

The continuity of the multi span system is provided by bolted connections of the steel plates which are attached at the ends of the UHPC chords and the lower (steel) chord. The precise deck plates (dimensions 2.00 m * 5.00 m) are glued to the upper chords and amongst each other. Gluing has been selected since mechanical (steel) connectors would be difficult to put into the filigree UHPC elements.

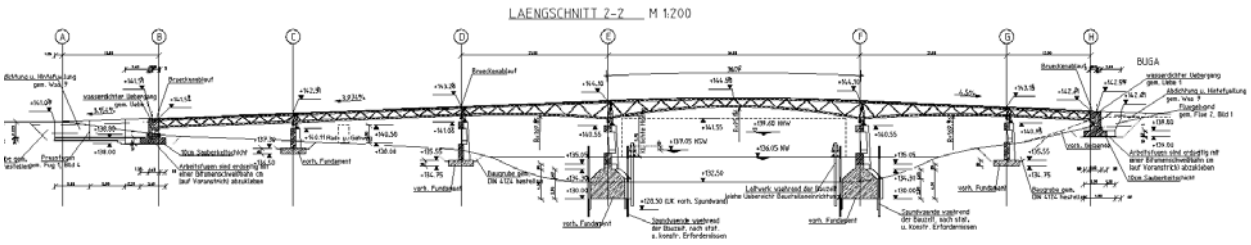

Figure 3: Superstructure in longitudinal direction

The precast deck plates are prestressed with strands in transverse direction in order to ensure the required bending resistance. The selected UHPC mix uses 0.9 percent by volume of high strength steel fibres (diameter 0.15 mm, length 17 mm). For drainage of the bridge, a 2 % gradient in transversal direction down to the middle is provided. In longitudinal direction it is made use of the gradient towards the abutments in order to avoid additional joints for drainage in the deck.

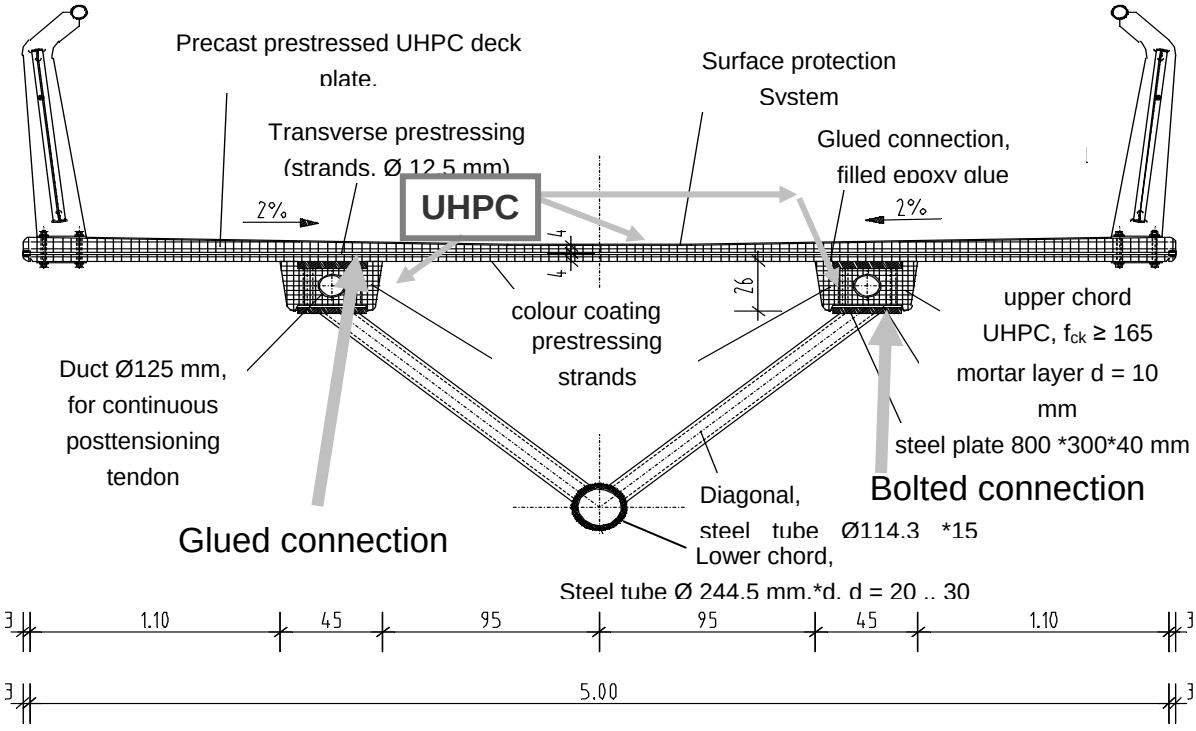

Figure 4: Cross section of hybrid three chord truss at midspan

Although the upper chord in the 36 m field is curved, it was produced as a straight precast prestressed beam. The high strength and the corresponding large strains enable to bend a slender prestressed UHPC beam without cracking (see figure. 5) .

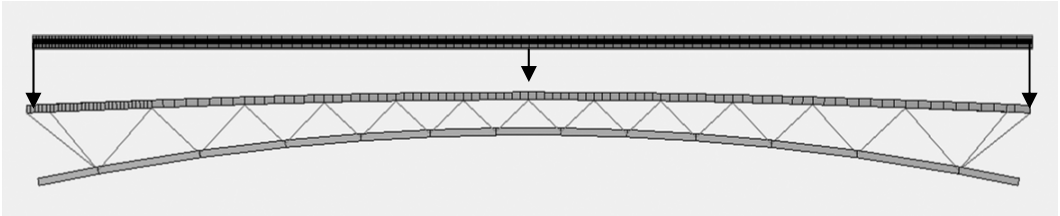

Figure 5: Bending of the straight precasted chord of the 36m field

The UHPC-chords are prestressed with strands in the factory. The strands are bondless in order to enable a wedge anchoring in the end plates made of steel. For the production phase as well as for transport and mounting, the chords are sufficiently prestressed. For the final state, a continuous posttensioning is applied in order to provide enough compression for the serviceability limit state in the bridge deck, especially in the joints between the deck plates.

For this reason, a duct with 125 mm diameter is provided, where a 2 MN tendon can be placed. The selected tendon type is one which normally would be used for external prestressing (SUSPA Type EX 6-12). The tendons are to be anchored in the transverse girders (made from in situ-concrete) at the abutments.
Until October 2006, the truss system has been completely mounted and the deck plates have been placed. The total dead load of the deck plates, hence, is already in effect. For gluing, the plates had to be lifted one by the other and glued to the upper chord and to the previous plate. This procedure has become necessary in order to reduce additional tensile stresses in the plates due to the construction process as well as additional shear stresses at the interface to the chords. Finally, the continuous posttensioning in the chords will provide sufficient compression stresses in the deck. The continuously glued connection of the plates to the chords enables to activate both the chords and the deck plates for the live loads or traffic load cases.

5 Finite element analasys

Since the slender bridge konstruction reacts very sensitive to all external and internal forces a 3-D finite-element model, using the Sofistik software has been used for the structural analysis. The system was build up, considering every step of the erection procedure and the load cases according to DIN Fachbericht 101 (see figure 7). In this model, also all effects due to creep and shrinkage have been accounted for.

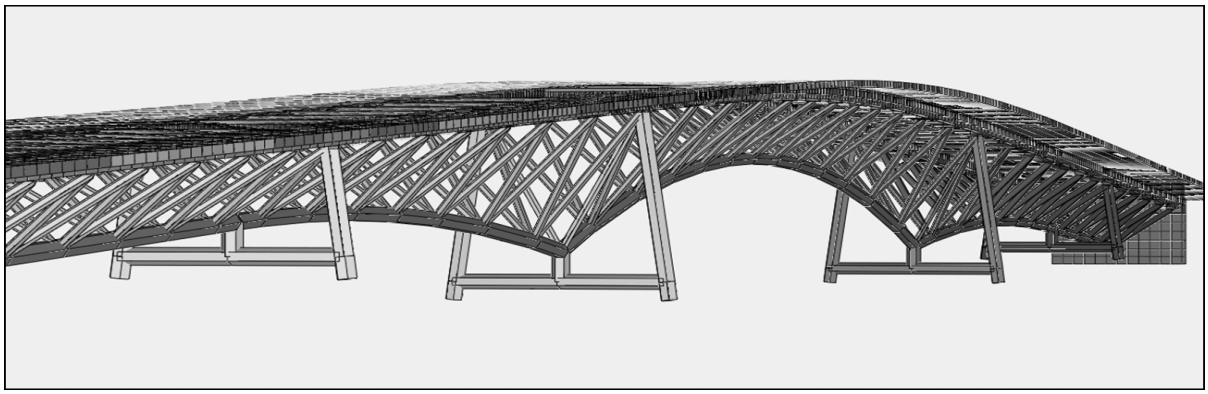

Figure 6: 3 - D finite element modell

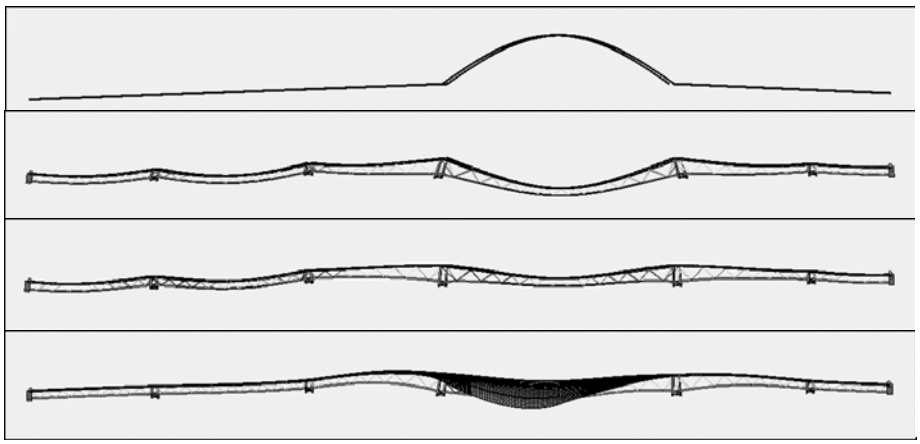

Figure 7: Differrent stepps of the 3-D finite-element model

6 Additional Investigations for the special case approval

Since for UHPC not yet any commonly accepted regulations exist, a special case approval by the authorities has been necessary in addition to the verification of the design by an independent checking engineer. For the special case approval, an expert report on the design concept and the required additional experimental investigations has been prepared by Prof. Tue at the University of Leipzig.

According to the report by Prof. Tue, the following investigations had to be performed:

- Characteristics and quality control of the UHPC,
- Experimental validation of the bearing capacity of the deck plates in bending and shear and for the anchoring of the posts for the railing,
- Friction coefficient for the bolted connection between a steel plate und the UHPC girder,
- Tensile and shear strength of the glued connections as well as durability for thermal / hygral action.

All tests have shown sufficient resistance of the UHPC elements (see figure. 8). For the epoxy glue (SIKA), it could be shown that the tensile and the shear strength are practically identical with the tensile strength of the UHPC itself. The measured friction coefficient between UHPC and steel (sand blasted) amounted to $\mu > 0.80$.

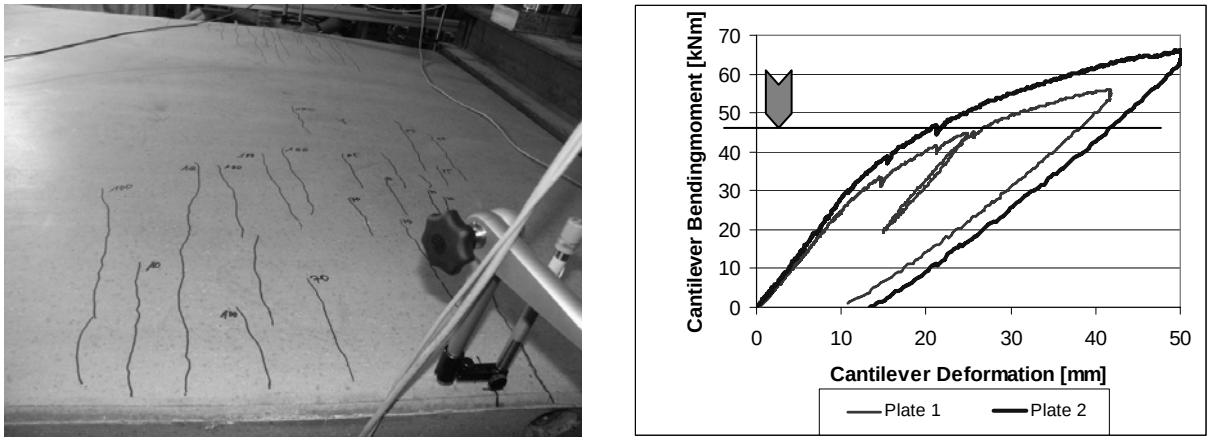

Figure 8: Behaviour of deck plate in bending

For the durability of the glued connection, additional tests have been made with combined mechanical and thermal / hygral loading. As a result, it could be stated, that sandblasted UHPC-surfaces provide a good connection and a durable strength.

7 Discussion, Conclusions and Acknowledgements

As a pilot application for UHPC in bridge construction, the Gärtnerplatz-bridge across the river Fulda in Kassel is the first larger bridge project using UHPC in Germany. It also is the first time to erect a bridge as hybrid UHPC-steel structure. Besides the application of UHPC, further innovations are the use of structural gluing for the connection between the truss chords and the deck plate and the use of prestressed bolted friction connections between UHPC and steel.

The project of the Gärtnerplatzbrücke transfers some of the research results obtained at the University of Kassel and at other places and follows some smaller bridge projects in Niestetal, which is situated nearby. A special case approval has been obtained since the project comprises several of innovative aspects outside the commonly accepted technical rules. Experimental investigations have been performed in order to validate the proposed design and the design checks.

Figure 9: Gärtnerplatzbrücke in the Summer of 2007

Since several new technologies are applied in the Gärtnerplatz-bridge, a continuous survey of the behaviour of the structure and its elements is desirable. For this reason, a monitoring programme will enable to identify possible changes in the structural behaviour of the superstructure. Thus, experience on the service life behaviour of UHPC as well as about glued connections will be gathered.

The authors like to thank the responsible persons at the city of Kassel and at the state of Hessen authorities who made it possible to apply UHPC for this innovative bridge project.

8 References

[1] Fehling, E.; Schmidt, M.; Teichmann, T.; Bunje, K.: Entwicklung, Dauerhaftigkeit und Berechnung Ultra-Hochfester Betone (UHPC), Heft 1, Schriftenreihe Baustoffe und Massivbau, Kassel university press, Kassel 2005

[2] AFGC / SETRA (2002): Bétons fibrés à ultra-hautes performances. Recommendations provisoires. Documents scientifiques et techniques. Association Française de Génie Civil, Setra, Bagneux Cedex, Janvier 2002, 152 pp.

[3] Sachstandsbericht Ultrahochfester Beton – Betontechnik und Bemessung, Publication under preparation, Deutscher Ausschuss für Stahlbeton, (2007).

[4] Zink, M.: Zum Biegeschubversagen schlanker Bauteile aus Hochleistungsbeton mit und ohne Vorspannung. Dissertation, University Leipzig, 1999.

[5] Schmidt, M.; Bunje, K.; Fehling, E.; Teichmann, Th.: Brückenfamilie aus Ultrahochfestem Beton in Niestetal und Kassel, Beton- und Stahlbetonbau, Vol. 101, Nr. 3 (2006), S. 198-204, Verlag Ernst & Sohn, Berlin.

Urban Goldbach
Concrete technologist
ELO Beton
Eichenzell, Germany

Steffanie Stehling
Assistent
ELO Beton
Eichenzell, Germany

Precasting of UHPC Elements

Summary

UHPC in practice stands for an extensive challenge for the personnel and the technical equipment. The batching and mixing of the components by the available installation requires a demanding supervision. The UHPC casting and compacting compared with normal concrete is very distinctive, especially regarding the complex processing, due to its ductile consistency.

Keywords: *UHPC, precast plant, experiences and applications*

1 Introduction

UHPC means a challenge and a chance for the future. The outstanding opportunities of this new technology enable specialised companies to break new grounds on the market. In recent years ELO Beton has pursued this way. Therefore it was possible to realise new projects and to cope emerging challenges. Continuous development and tests permit to deal with increasingly sophisticated geometries and to meet the customers' requests.

2 Prerequisites

The manufacture of UHPC of constant quality and on an industrial scale requires state-of-the-art, technically sound machinery and equipment. At ELO Beton, a 1.5 m³ forced-action mixer is in operation and a second system for the manufacture of high-performance concretes according to specifications is under construction. Continuous measurement of all parameters as well as precise knowledge and control of the initial constituents are absolutely necessary. A concrete laboratory with all customary equipment is available for concrete-technological tasks. Organization and quality assurance is subject to factory production control (FPC). AMPA Kassel and PÜZ Bau (quality control) accompany the various projects and perform external quality control.

The concrete and its constituent materials are monitored by two qualified concrete technologists and specifically skilled personnel. All work steps are precisely thought out and planned in advance in order to pinpoint and eliminate potential sources of error. Instructing and sensitizing the personnel to the challenges, possibilities and opportunities of the new construction material is an important part of the production process.

3 Development

In collaboration with Prof. Dr.-Ing. habil. M. Schmidt, Chair of Structural Materials Prof. Dr.-Ing. E. Fehling, Chair of Structural Concrete at Kassel University, the mix designs for UHPC concrete were developed, tested and brought to series-production maturity in January 2004. Following successful laboratory results, several mixes were then manufactured in a large-scale test. Within the test series, experimental slabs were cast, cut to beams suitable for testing and tested in accordance with the code of practice for testing steel-fiber concrete. A controlled addition of the steel fibers to the mix and the dimensions of the selected fibers turned out to be conducive to a uniform distribution and to prevent from balling. For strength development, energy supply in the form of heat is required. The slab had been cut into shapes that made the test specimens suitable for testing in longitudinal and transverse direction. The flexural tensile strengths of the test specimens were 21.5 N/mm² +/- 3 N/mm². The compressive strength was determined using cylinders ∅ 150 mm and test cubes of various dimensions. The cylinders attained a strength of between 165 and 190 N/mm². In the laboratory it was not possible to compress the customary cubes of 150-mm edge length to the point of failure. For this reason, cubes of 100-mm edge length were manufactured in order to gather experience and for rapid determination of strength. The strength values of these experimental cubes of up to 240 N/mm² are to be compared with the results of the compressive cylinder strengths. Technical approval on an individual basis must be obtained for every new construction project.

4 Casting

4.1 Mixing and production process

The UHPC is mixed and cast at ELO Beton early in the morning. This is necessary due to the rising temperatures over the course of the day; otherwise the intense development of hydration heat will cause the concrete to set prematurely.
Furthermore, this time of day was selected so as not to interfere with the other ongoing concrete mixing operations.

Table 1: Mix design of the UHPC

		aggregates
cement	kg/m³	750
basalt or quarz sand	kg/m³	1.100
microsilica	kg/m³	250
quarz powder	kg/m³	200
water	l/m³	150
superplatiziser	kg/m³	30
steel fibers	kg/m³	75

Mixing of the fresh concrete takes place only partly via the weigh unit of the mixing plant; some of the constituents, due to the high fineness of the aggregate and the high measuring precision required, must be pre-measured in batches. The steel fibers, for example, are

weighed, put in bags and placed next to the mixer, ready to be used. This process is followed for every mix in order to be able to guarantee the correct quantities of all the constituents for a mix.

The dry mixing period lasts for about two to three minutes, followed by the addition of the water and the superplasticizer. The subsequent mixing process takes place for about three to four minutes. Following determination of the slump, more superplasticizer is added if required. The steel fibers are added slowly in a controlled manner via chute and are “vibrated in” This prevents so-called “balling” from occurring. The concrete is mixed once more for about three minutes before being further processed. As a final step and prior to further processing, the slump is once more determined for the fresh concrete.

A noteworthy phenomenon that occurs during the mixing process is the sudden “reversal” of the mix: if it seems at first that the mix is much too dry, an abrupt change in the consistency occurs and the batch once more becomes flowable. The temperature development in the concrete is closely tested during the mixing process. During dry mixing of the constituents, a temperature of < 25 °C is reached; following the addition of water and superplasticizer and renewed mixing, the temperature increases once more up to 27 °C. Following the addition of the steel fibers, the temperature then once more rises up to 30 °C upon reaching the final consistency.

Following production, the concrete is transported via chute in the 2.0-m³ bucket that is also used for other casting processes to the casting station and filled into the form, thus minimizing air ingression. At ELO Beton, the precast elements are cast into hydraulic formworks. Of special importance are the stability and the tightness of the formwork, since the concrete is highly flowable and the casting pressure accordingly high. But of yet greater importance is a rapid work process. The processing window for casting is very small; it is important to place the concrete in the form before viscosity impairs the casting process. This is a good example of the importance of well-coordinated teamwork. Even minor delays might cause the effect that the fresh concrete was not processed quickly enough, rendering it useless.

Upon completion of the casting process, the elements are compacted as usual by internal and external vibrators.

5 Curing

The elements are covered with plastic sheets immediately after casting and remain in the form for three days. During the first 24 hours, a temperature of approx. 50 °C is reached; three days later the temperature drops once again to 35 °C. After 72 hours, the precast elements are stretch-wrapped and subjected to three additional days of heat curing. For this purpose, the elements are encapsulated and heated; during this stage, the concrete elements attain a maximum temperature of 83 °C.

During the curing process, the temperature is continuously controlled, since correct heat treatment is requisite for the component to attain the required strengths. For this purpose, sensors are built into the fresh concrete that enable an appropriate measuring device to continuously test the temperature.
In general, UHPC can be exposed to heat curing of up to 90 °C. These temperatures thus considerably exceed the limit values for normal concrete. Heat treatment is typically administered following at least one to two days of prestorage so that ettringite formation – which is prevented when heat-curing at excessive temperatures – has already taken place.
Following the necessary heat treatment, the UHPC elements are transported to external storage; within one day, the elements have cooled down to outdoor temperature.

6 Projects and Applications

In the following a couple of projects carried out by the company Elo Beton are shown. The first bridge for pedestrians and cyclists was erected in Niestetal-Sandershausen with a span length of 12 m and a weight of the precast element of 12 tons (see figure 1). The cross-section of the bridge consists of a U-shape which is prestressed. The track slab of the bridge has a thickness of 10 cm and is built of UHPFRC.
The elements poured of UHPC were installed without treating the surface. A base seal surface coating was not necessary either. Two further bridges with 7 m and 9 m followed (see figure 2)

Figure 1: Bridge for pedestrians and cyclists in Niestetal-Sandershausen

Figure 2: Pedestrian bridge in Sandershausen

The next food bridge built of UHPC was erected in Weinheim (see figure 3). The bridge is manufactured of two precast t-beam elements with a thickness of the plate of 8 cm and a span length of 21 m. The Weinheim pedestrian bridge has an approval for ambulance vehicles to cross over the bridge. The surface of this bridge is uncoated, too.
Another food bridge similar in design to the one in Weinheim was built in Friedberg with a span length of 12 m.

Figure 3: Pedestrian bridge in Weinheim

The Gärtnerplatz bridge in Kassel (see figure 4) was finalized in 2007 and replaced a removed timber bridge. The bridge is built of steel and UHPC elements and has an overall length of 135 m. The truss structure is manufactured of steel-elements except the upper chord which is made of UHPC. The transport of this upper chord from Elo Beton factory to the company which built the steel framework and joined both parts with each other is shown in figure 5. The UHPC precast and prestressed plates (see figure 6) with a thickness from 8 cm up to 12 cm were glued to the upper chord of the truss giders.

Figure 4: View of the Gärtnerplatz bridge in Kassel

Figure 5: UHPC upper chord of the Gärtnerplatz bridge

Figure 6: UHPC precast plates of the Gärtnerplatz bridge

7 References

[1] Orgass M., Dehn F.: Ultrahochfester Beton (UHFB) – Ein Überblick. BetonWerk International, Dezember 2004

[2] Prof. Dr.-Ing. habil. M.Schmidt, Prof. Dr-Ing. E.Fehling: Ultra-Hochfester Beton – Planung und Bau der ersten Brücke mit UHPC in Europa; Heft 2 Sep. 2003

[3] Teichmann T., Goldbach U.: Influence of the precasting process on the material properties of fibre reinforced UHPC. Internationales UHPC Symposium, Kassel 2004

[4] ARCONIS Spezial; Ultrahochfester Beton – Forschungsergebnisse, Entwicklungen, Projekte, Band 2 (Fraunhofer IBR Verlag)

Ralf Krelaus
Dr. rer. nat.
University of Kassel
Kassel, Germany

Susanne Freisinger
Dipl.-Ing.
University of Kassel
Kassel, Germany

Michael Schmidt
Prof. Dr.-Ing. habil.
University of Kassel
Kassel, Germany

Adhesive Bonding of UHPC Structural Members at the Gaertnerplatz bridge in Kassel

Summary

In many industries, e.g. automotive engineering and aircraft construction, the assembling of structural members by gluing with epoxy based or other resins proved itself for many years. The advantages of gluing are e.g. that resins can easily be applied and that shear or tension stresses can be transmitted very homogeneously. The mechanical properties of Ultra High Performance Fibre Reinforced Concrete (UHPFRC), especially its superior tensile and shear strength at the surface give an opportunity to use the adhesive-technology for the assembling of load-bearing structural elements in civil engineering as well. The first prototype of a glued UHPC-structure without any additional mechanical bonding devices is the Gaertnerplatz bridge in Kassel built in 2007. The upper girders and the slabs of the bridge deck (both prefabricated and both consisting of prestressed fibre reinforced UHPC) are connected with an epoxy mortar. The paper presents the results of the pre-tests done for the Gaertnerplatz bridge and the experiences gained from the practical application.

Keywords: *UHPC, gluing*

1 Introduction

In gluing technology assembly parts are joined by the use of plastic or liquid adhesives that harden by chemical or physical processes. The strength of an adhesive joint is caused by two major types of forces, the adhesive and the cohesive forces.

Based on a molecular view the cohesive forces cause the stability of the adhesive layer itself due to chemical bonds and attraction between the molecules of the adhesive. The adhesive forces result in the adhesive strength which is the strength of bonding between the adhesive and the assembly parts. The cause of Adhesive forces originated in interactions of the molecules of the adhesive with the surface of the assembly parts, which is divided into electrostatic and van der Waals interactions.

While the cohesive forces only depend on the properties of the adhesive, e.g. chemical composition, the adhesive force depends on the properties of both, the type and composition of the adhesive and the material properties of the structural members. [1]

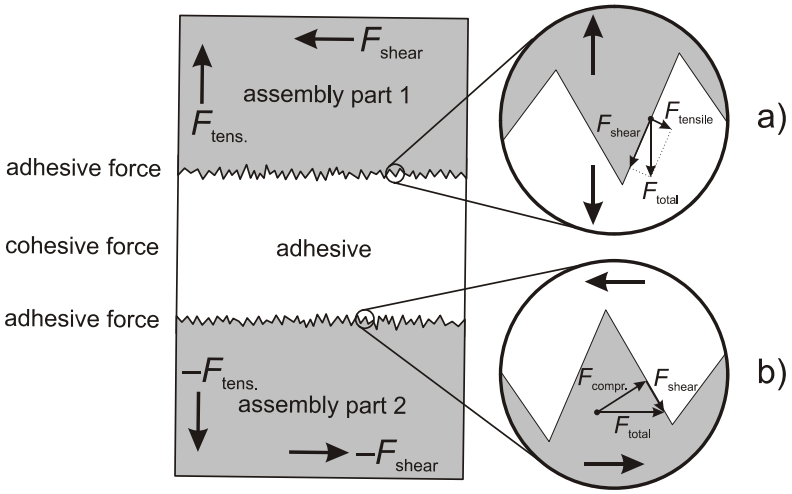

Figure 1: Adhesive joint of a rough surface in detail; a) tensile load, b) shear stress.

To obtain optimal results in the application of gluing technology the surface properties of the assembly part are most important. This implies the roughness of the surfaces and removal of non-sustainable surface layers and impurities. As shown in figure 1 a) the in case of a tensile load total force which affects one single point of a rough surface is divided into a shear component and a tensile component. In case of shear stress force is divided into a shear component and a compressive component (figure 1 b). By using assembly parts of high roughness the transmission of forces between adhesive and the structural member occurs mainly by shear forces. Thus the pretreatment of surfaces is essential for reliable adhesive bondings.

2 Gluing of concrete

The application of adhesives to concrete surfaces is known for years. Improvement of the bearing capacity by reinforcing of existing structures by CFK lamellas and steel straps fixed by epoxy resins is a common method in civil engineering.[2-5] Epoxy resins are used in the construction of segmental bridges, where prefabricated sections of concrete are temporarily fixed by adhesives and finally fastened with conventional mechanical measures.[6] In this construction method. The adhesive there acts more or less as a sealant.

In all these conventional applications the adhesive joint never had to be capable of bearing the constructional loading for the whole life service. Adhesive joints used on normal concretes are additional reinforcements or sealings.

Ultra high performance concrete (UHPC) has got superior properties compared to normal concretes. With compressive strengths of more than 150 N/mm² and, if reinforced with steel fibres, high tensile and surface tensile strengths UHPC differs significantly from standard concretes and even high performance concretes (HPCs). Table 1 shows the mechanical

properties of UHPC. The high compressive strength of UHPC is achieved by an optimised composition of the fine particles.[7]

The microstructure of UHPC is very dense with practically no capillary pores. Figure 2 shows a SEM image of the contact area between UHPC and a quartz-filled epoxy resin which illustrates the narrow interconnection of both materials.

A very important aspect for gluing of UHPC is the fact that strength of the bulk material is the same as of the surface regions. This makes UHPC a very homogeneous material with respect to its mechanical properties. Especially the high tensile strengths of about 9 N/mm² and surface tensile strengths of 6 to 8 N/mm² qualify UHPC to apply the modern method of gluing to this material.

Table 1: Mechanical properties of the UHPC mixture M1BS.

UHPC	**unit**	**M1BS**
Compressive strength 7/90 with 0.99 vol.-% steel fibres	N/mm²	179
Tensile strength	N/mm²	9
Flexural tensile strength	N/mm²	19.6
Surface tensile strength	N/mm²	6–8

UHPC by itself is a very brittle material to avoid sudden failure steel fibres as an essential component of UHPC are added in an amount of 0.5 to 2.5 vol.-% to reach a sufficient ductility and load-bearing capacity even after rupture of the matrix.

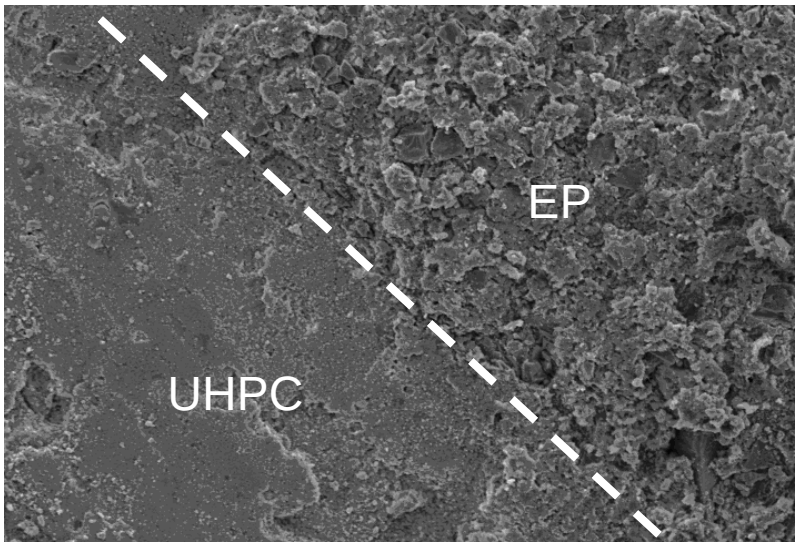

Figure 2: SEM image of the contact area between UHPC and epoxy resin.

3 Gluing of UHPC at the Gaertnerplatz bridge in Kassel

The Gaertnerplatz bridge in Kassel spans the river Fulda over a length of about 140 m. It is the first larger bridge in Germany which was built from precast UHPC and the first bridge in the world with structural UHPC elements connected exclusively by gluing.[8, 9] Figure 3 d) shows the bridge after completion.

The application of adhesive to the structural members at the Gaertnerplatz bridge required the use of special equipment and methods. The precast bridge deck slabs had to be raised by the use of mobile lifting equipment as illustrated in figure 3 a). The surfaces to be glued had to be roughened manually by using a needle apparatus. After removal of dust and loose particles the epoxy resins was applied as shown in figure 3 b). The slabs were subsequently laid in place and worked with a hand-guided vibration plate until the target thickness of the joint was reached. Excessive epoxy resin was pressed out as shown in figure 3 c).[10, 11]

Figure 3: Application of epoxy resin at the Gaertnerplatz bridge in 2007. a) mobile lifting equipment, b) upper chord before laying the deck slab, c) underside of the bridge with freshly laid slab, d) bridge after completion.

Due to the fact that a bridge is exposed to weather and climatic conditions, resulting in high humidity and change of temperatures over long (seasonal) and short (night/day) cycles caused by sun, rain and ice, a series of tests were done to ensure the stability of glued UHPC joints.

With these conditions in mind a testing program was established in which test specimens were made from UHPC and an epoxy resin from Sika, Sikadur-30. The properties of Sikadur-30 are listed in table 2.

Figure 4 shows the types of specimens that were used. Prisms (40 x 40 x 160 mm) bonded by gluing of their end faces that were used for flexural tensile strength tests and for tensile

strength test. A second type of specimen is used for eccentric tensile-shear strength tests and for centric shear strength tests is illustrated in figure 4.

Table 2: Properties of epoxy resin Sikadur-30.

Type of adhesive	**unit**	**epoxy resin, two components**
Part of filler material[1)]	M.-%	75 to 80
Colour		light grey
Density	kg/dm³	1.65
Glass transition temperature	°C	53
Tensile strength (DIN 43455)	N/mm²	33 (bond on steel)
Compressive strength		
(DIN 1164-7) after 24 h	at 35°C	ca. 95
	at 10°C	ca. 55
Tension-shear strength[2)]	N/mm²	ca. 20
Static E-modulus	N/mm²	12800
Thermal expansion coefficient	K–1	$9 \cdot 10^{-5}$ (–10°C to +40°C)
Shrinkage	%	0.04

[1)] tested in laboratory experiment

[2)] tested on small cylinders, 20 mm diameter

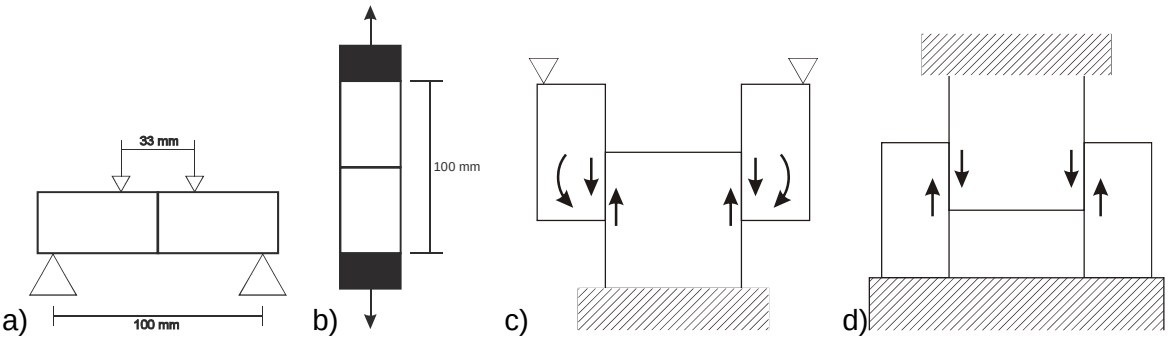

Figure 4: Glued test specimens used for mechanical strength tests. a) Flexural tensile strength, b) tensile strength, c) tensile-shear strength, eccentric, d) shear strength, centric.

4 Testing results

Parameters changed during the testing program are:

- preconditioning of UHPC surfaces (smooth, sandblasting, brushed)
- use of a low viscosity epoxy primer
- temperature conditions in the curing process of the epoxy resin (10/20/30 °C)
- temperature and humidity during long-term shear strength tests (20/35 °C, 65/95% rel. humidity)
- thickness of the epoxy layer (3/6 mm)
- 14 freeze-thaw cycles in NaCl solution (CDF)

- curing with and without heat treatment of UHPC (90 °C, 24 h/curing under water, 28 d)

The epoxy resin was cured for 10 days before testing, testing speed was set to 0.01 mm/s. Tensile strengths and flexural tensile strength of glued prisms were measured with variation of thickness of the epoxy resin layer, different surface preconditions, temperature in the curing process, curing conditions of UHPC and freeze-thaw cycles. Results of these experiments are shown in table 3. The glued specimens were

Table 3: Results of testing with prisms.

	Flexural tensile strength [N/mm²]	**tensile strength [N/mm²]**
Test setup	see fig. 4 a)	see fig. 4 b)
Curing of UHPC (90 °C/water)	10.0/10.3	6.6/5.9
Surface roughness (smooth, sandblasted, brushed)	10.0/10.1/10.2	6.6/7.1/6.1
Gluing temperature (10/20/30 °C)	11.0/10.0/11.1	6.0/6.1/5.8
Thickness of epoxy resin (3/6 mm)	10.0/10.1	6.9/6.5
14 freeze-thaw cycles in NaCl solution	13.1	–

Tensile strengths of glued prisms were between 6 and 7 N/mm² and were independent of the tested parameters. The strengths of flexural tensile specimens was in the range of 10 to 13 N/mm². Specimens failed within the concrete structure adjacent to the epoxy layer.
Long-term stability tests were done by fixing specimens in a frame shown in figure 5 a) with application of a constant force of 20 kN. These frames are stored under thermal and climatic conditions shown in table 4 for 56 days. Figure 5 b) shows a typical failure in the concrete matrix after a strength test done at the end of a long-term stability test. The shear stress in the epoxy layer during these tests was 2 N/mm² which was similar to the shear stress in the bridge structure. Sandblasted UHPC specimens with and without epoxy primers were used. Table 4 shows the conditions and results of these tests.

Table 4: Results and conditions of long-term stability tests.

Specimen no.	**Glued area [mm²]**	**surface pretreatment**	**climate [°C/% r.H.]**	**permanent load stress [N/mm²]**	**strength after 56 d [N/mm²]**	**rupture**
H 1	2 x 4875	sandblasting, EP-primer	35/95	2.0	12.4	concrete
H 2					14.7	
H 3			20/65	2.0	16.1	adhesion
H 4					14.5	
H 5	2 x 2880	sandblasting	35/95	3.5	14.9	concrete
H 6					13.3	
H 7					14.0	

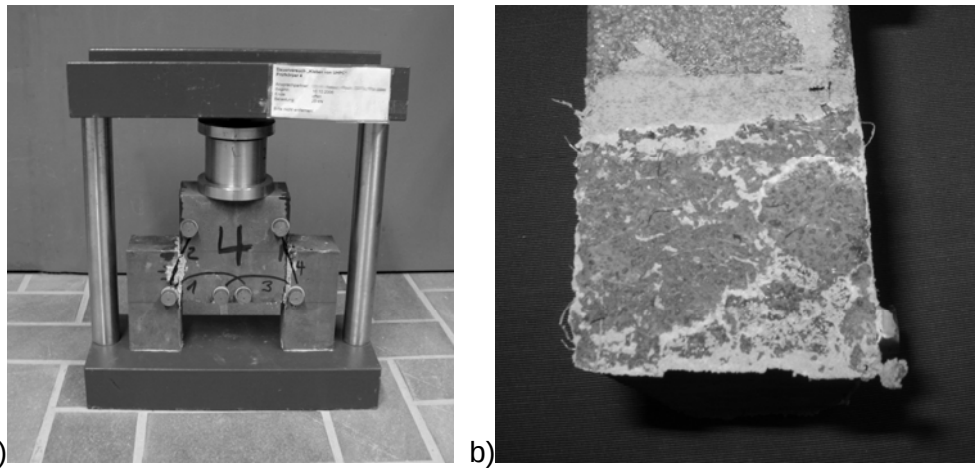

a) b)

Figure 5: a) Test frame for long-term stability tests, b) typical failure in the concrete matrix.

The deformation was measured during the long-term stability tests was about 0.2 ‰ and is illustrated in figure 6.
In most of the tests shown in table 4 the failure occurred in the concrete matrix. When an EP-primer was used, the failure of the glued joint cannot be predicted. Without the use of a primer it was reliably possible to get the failure only in the concrete.

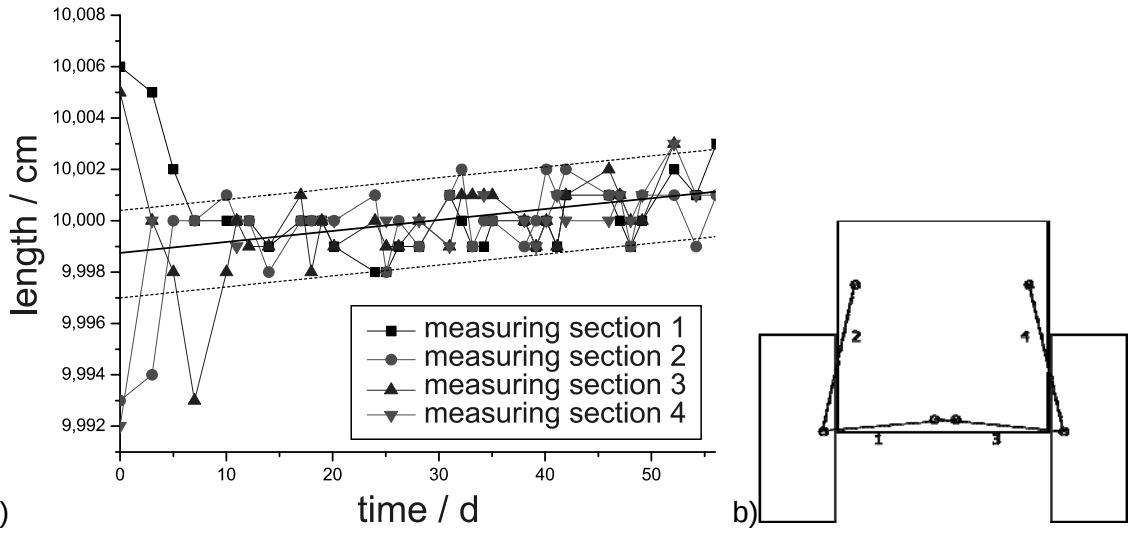

a) b)

Figure 6: a) deformation of specimens during permanent static load, b) assignment of measuring sections.

5 Conclusions and outlook

Preliminary experiments on the durability and strength of glued UHPC joints have been accomplished for the Gaertnerplatz bridge in Kassel, the first bridge being assembled by gluing only. These experiments have shown that it is important to carefully look for a number of parameters in the gluing process. Pretreatment of the UHPC surfaces to be glued is of enormous importance. The surface has to be rough to ensure a firm mechanical bonding of the adhesive to the UHPC surface. Steel fibres in the UHPC have to get in well contact with the epoxy resins to get an optimal transmission of forces into the concrete.

The testing program has also shown that there are a number of open questions left. These issues have to be solved to make adhesive joining of UHPC a general method in building industry and civil engineering.

Based on the comprehensive experiments done at the University of Kassel for the bridge and to extend the technical and the scientific knowledge for this innovative technology an extensive research project, funded by AiF (German Federation of Industrial Research Associations) started in 2007. Investigations are made considering the influence of the strength, the texture and the activation of the surface, the influence of the fibre reinforcement and especially of the fibre orientation, the microstructure of the concrete, the kind and performance of different adhesives (polymers or mineral based) as well as the application of the adhesives and the long-term durability of the glued joints over time at different climatic conditions with and without static and dynamic loads.

6 References

[1] Habenicht, G.: Kleben – Grundlagen, Technologien, Anwendungen. 5. ed, Springer, 2006.

[2] De Hesselle, J.: Bauwerksverstärkung mit CFK-Lamellen. beton, 48, p. 406–408, 1998.

[3] Bergmeister, K.: Verstärkung mit Kohlenstofffaser-Lamellen – Teil 1: Verstärkung von Biegeträgern. Beton- und Stahlbetonbau, 100 Spezial, p. 62–68, 2005.

[4] Bergmeister, K.: Verstärkung mit Kohlenstofffaser-Lamellen – Teil 2: Verstärkung von Stützen. Beton- und Stahlbetonbau, 100 Spezial, p. 69–73, 2005.

[5] Letsch, R.: Kleben von Beton. Straßen- und Tiefbau, 33, p. 17–18, 1979.

[6] Rombach, G.: Brücken in Segmentbauweise. Internationale Beispiele und Anwendungsgebiete in Deutschland. 50. Betontage, Neu-Ulm, 2006.

[7] Schmidt, M.; Fehling, E.; Geisenhanslüke, C.: Ultra High Performance Concrete (UHPC). International Symposium on Ultra High Performance Concrete, ed. Schmidt, M.; Fehling, E.; Geisenhanslüke, C., Vol. 3, Kassel University Press, 2004.

[8] Schmidt, M.; Fehling, E.; Geisenhanslüke, C.: Ultra-Hochfester Beton – Planung und Bau der ersten Brücke mit UHPC in Europa. 3. Kasseler Baustoff- und Massivbautage, ed. Schmidt, M.; Fehling, E.; Geisenhanslüke, C., Vol. 2, Kassel University Press, 2003.

[9] Schmidt, M.; Bunje, K.; Fehling, E.; Teichmann, T.: Brückenfamilie aus Ultrahochfestem Beton in Niestetal und Kassel. Beton- und Stahlbetonbau, 101(3), p. 198–204, 2006.

[10] Schmidt, M.; Krelaus, R.; Teichmann, T.; Fehling, E.; Herget, E.: Kleben von UHPC-Bauteilen bei der Gärtnerplatzbrücke in Kassel/Gluing UHPC structural members for the Gärtnerplatz Bridge in Kassel. BFT International, 73(10), p. 12–20, 2007.

[11] Schmidt, M.; Krelaus, R.; Teichmann, T.; Leutbecher, T.; Fehling, E.: Fügen von Bauteilen aus UHPC durch Kleben. Voruntersuchungen und Anwendung bei der Gärtnerplatzbrücke in Kassel. Beton- und Stahlbetonbau, 102(10), p. 681–690, 2007.

Michael Link
Prof. Dr.-Ing.
University of Kassel
Kassel, Germany

Matthias Weiland
Dr.-Ing.
University of Kassel
Kassel, Germany

Thomas Hahn
Dr.-Ing.
University of Kassel
Kassel, Germany

Structural Health Monitoring of the Gaertnerplatz Bridge over the Fulda River in Kassel

Summary

Structural monitoring is aimed at evaluating the structural performance and safety upon completion of the construction. Natural frequencies and mode shapes extracted from the dynamic response resulting from artificial or ambient excitation are commonly used as indicators of changes of the structural performance. Before the monitoring measurements are started it is necessary to analyse the structural behaviour including possible damage scenarios by numerical Finite Element analysis. Despite the high quality of the numerical tools prediction errors, e.g. caused by erroneous modelling and parameter assumptions, are unavoidable in practical applications. It is therefore advisable to conduct pre-monitoring tests permitting to establish a reference model calibrated to real test data by computational model updating techniques. The generation of such a reference model based on experimental eigenfrequencies and mode shapes obtained from artificial impact excitation of the Gaertnerplatz Bridge in Kassel is described in the paper.

The construction of the bridge is characterised by the first time application of Ultra High Performance Concrete (UHPC) for bridges of this size and by the application of adhesive bonded connections between the UHPC parts of the bridge.

In particular we will present the concept of damage detection taking account of the effect of temperature dependent modal data. This concept leads to a signature function of the healthy structure which might be the result of monitoring the state of the bridge over typically one year. It is expected that any significant deviation of the healthy state signature from the signature of the actual monitoring state shall indicate the onset of structural degradation. This would initiate another modal test and subsequent updating of the initial reference model to be used to assess the type and the severity of the degradation.

In addition to dynamic data static strain and displacement data and also physical data like temperature and humidity are also used for monitoring permitting to relate the experimental modal data to environmental conditions and to directly monitor the state of the adhesive bonded connections.

Keywords: *structural health monitoring, damage detection, model updating, system identification*

1 Introduction

The generally accepted procedure for structural health monitoring comprises the steps summarized in table 1 which have bee extracted from the national and international guidelines in refs.[1] and [2]. In the present paper we will concentrate on the highlighted boxes of this table referring to the life cycle phases (1) design, (2) completion of the bridge construction and phase (3) in service inspection. It is important to note that all monitoring tests shall be planned based on the finite element model used in the design phase. Very often the features to be monitored are not covered by the design model in which case it is necessary to modify the design model appropriately. In the case of the Gaertnerplatz Bridge presented later in this paper it was necessary to supplement the design model by special elements for modelling the adhesive bonded connection between the upper cord and the bridge deck since the long term structural behaviour of this connection is of primary interest for long term monitoring.

After completion of the bridge construction the experimental analysis of the structure served for estimating the healthy reference state of the structure. Experimental modal analysis using artificial impact excitation tests as well as quasi statically moving load tests were used for this purpose. The identified modal parameters were used to update the physical parameters of the design finite element model by minimizing numerically an objective function which contains the differences between analytical predictions and experimental results. This updated model parameters present the reference state which are subsequently compared with the actual parameters extracted from the monitoring data at given inspection intervals. The parameter changes between the reference and the actual state are assumed to indicate not only the location but also the type and the extent of a possible structural modification (damage). It should be noted that in practice the updating parameters must not only reflect the structural properties due to damage but also due to other modelling uncertainties. In the ideal case test data are available for the healthy initial state and the actual monitoring state. For monitoring purposes the actual state may be recorded continuously or periodically so that the differences of the structure responses between the two states are available at any time.

For monitoring purposes it is not advisable to rely solely on model based monitoring parameters. Due to unavoidable uncertainties related to the modelling simplifications and the experiments these parameters might indicate false alarm, for example, when the variation of eigenfrequencies over time is not caused by structural modifications but by unmodeled environmental effects. Therefore, it is necessary to use other features as well. The dynamic monitoring concept for the Gaertnerplatz Bridge therefore requires to record temperature and humidity which are needed to correlate the experimental modal data to environmental effects.

It is well known that low frequency vibration test data or static response data are not very well suited for detecting and quantifying localized small size damage. Exploitable results can only be expected if high spatial resolution of the response data is available. Data acquired with scanning laser vibrometers may be used but also test data from static tests. In particular for bridge structures static influence lines can be measured with high spatial resolution when

static responses (deflections, deflection slopes, strains) are nearly continuously measured when a vehicle is slowly crossing the bridge [3]. Examples for high resolution modal data of the Gaertnerplatz Bridge are presented later in this paper.

2 Vibration monitoring concept for the Gaertnerplatz Bridge

The most important steps of vibration monitoring are summarized in table 1 (refs.[1], [2]).

Table 1: Objectives and measures for bridge monitoring (based on ISO 18649:2004(E))

Life cycle of a bridge	Objectives of vibration monitoring	Required actions	
		Analysis	**Test**
(1) design	Anticipation of structural performance	Modelling: • Finite element model of structure • environment (traffic, wind) • damage scenarios	Test planning: • transducers (type and location) • data recording and analysis system for initial, temporary and continuous states (strains, accelerations, traffic, wind, temperature, humidity ...)
(2) Completed Construction	• Control of construction accuracy, • confirmation of structural performance • Establishment of a reference model representing the healthy initial state	• test/ analysis correlation • model updating (calibration)	Test performance and evaluation related to initial state: • Static/ dynamic response • environment • Identification of vibration characteristics
(3) In service inspection and maintenance	• Ensure bridge safety and serviceability • Anticipate remaining life time	• test/ analysis correlation • model updating • comparison with reference model => indication for actual structural state => proposal for maintenance actions	Test performance and evaluation related to actual state: • Static/ dynamic response • environment • Identification of vibration characteristics (real time evaluation)
(4) Structural modifications	confirmation of effect of structural modifications potentially due • to changed operation requirements • to retrofit actions	• test/ analysis correlation • model updating • comparison with reference model	Test performance and evaluation related to modified state: • Static/ dynamic response • Identification of vibration characteristics

The steps in phase 1 as applied to the Gaertnerplatz Bridge were characterized by:

(a) Structural analysis and test planning.

In this phase a detailed Finite Element (FE) was generated permitting to:

- to study the efficiency of different damage indicators for different damage scenarions under varying ambient temperatures.
- to select optimal sensor and exciter locations for the vibration tests

Figure 1 shows the bridge design and the FE- model and the selected measured degrees of freedom (MDOFs). The model is composed of about 200 plane shell elements for the bridge deck and the abutments and 650 beam elements for the truss and the inner columns resulting in about 3500 DOFs. Special attention was given to the adhesive bonded connection of the UHPC cord and the deck and the eccentric connections between deck and cord and cord and truss members (fig.2a). The bonded connection was modelled with special shear elements. The shear modulus of these elements represent important monitoring parameters.

(b) Test performance and experimental modal analysis (EMA)

The modal test was performed by artificial impact excitation using an impact hammer instrumented by a force sensor. The impacts were applied at the 96 locations shown in figure 1(c). For each impact the acceleration response was measured simultaneously at 5 reference locations. These data permitted to acquire 96 frequency response functions (FRF) for each reference. In figure 3 a typical example is shown of the acceleration FRFs identified at reference R2 in the range between 2 and 11 Hz where six well separated resonance peaks could be observed.

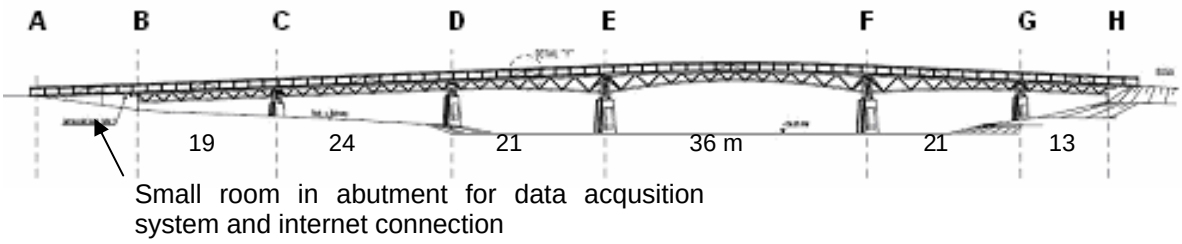

Figure 1(a): bridge design [4]

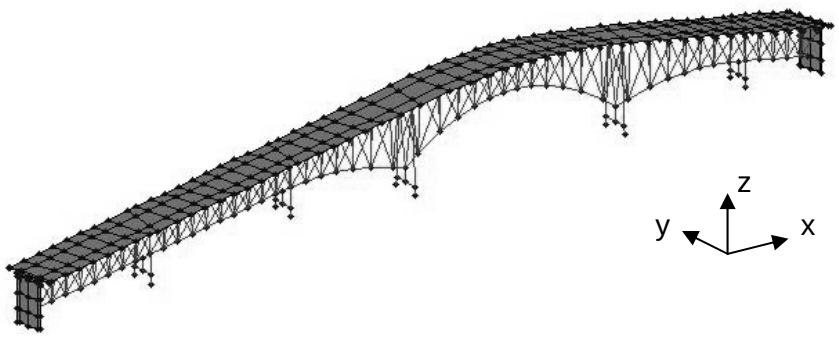

Figure 1(b): Finite Element model

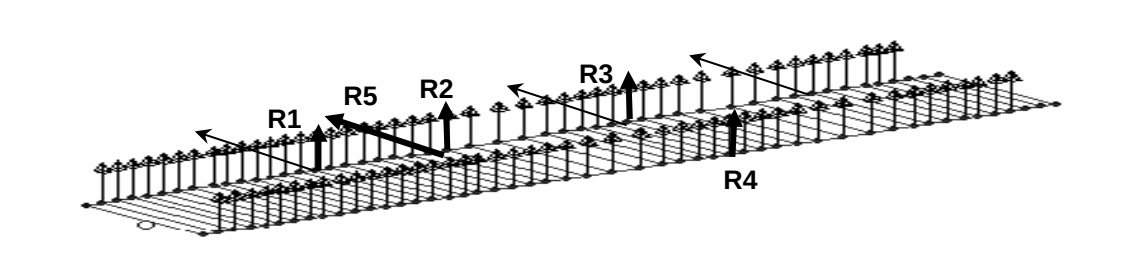

Figure 1(c): 96 measured FE- DOFs and 5 reference DOFs R1- R5 on bridge deck

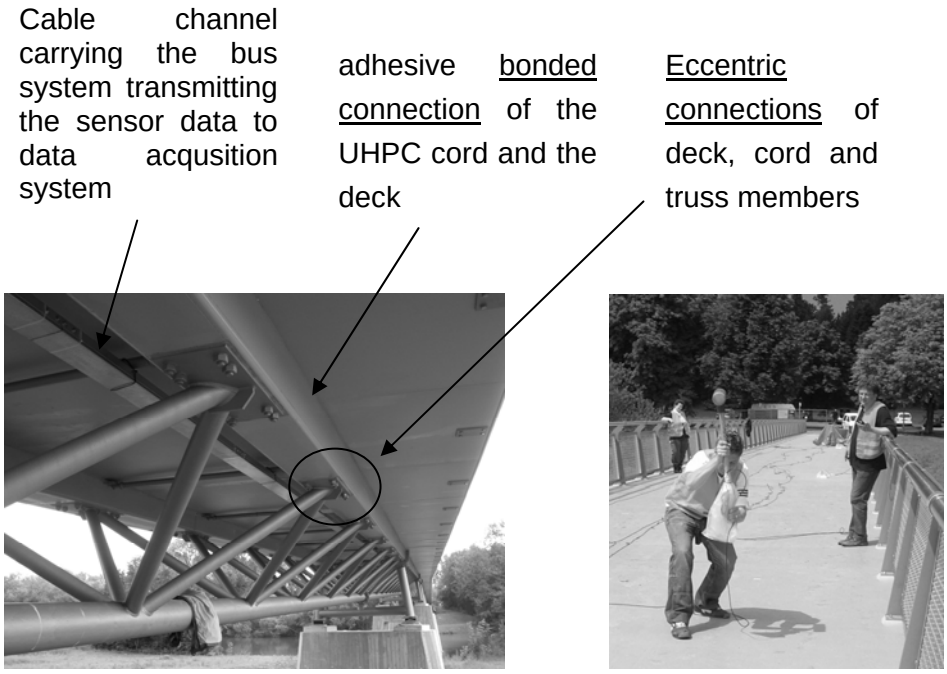

(a) (b)

Figure 2: View on the bridge underside (a), impact testing (b)

The modal data (eigenfrequencies, mode shapes and modal damping values) were extracted from these FRFs for each reference using our in-house EMA code ISSPA [5]. In principle the modal data should be identical and should not dependent on which reference was used for modal data extraction. However, since the magnitude of the response depends on the location of the impact and might result in low signal to noise ratios, it is not advisable to extract modal data from FRFs in low response ranges were modes are weakly excited. Therefore, the most reliable modal data were selected from different references based on indicator functions (e.g. ref.[6]) and engineering experience.

(c) Comparison of FE- predictions and experimental modal data

The comparison of the experimental and analytical eigenfrequencies depicted in table 2 reveals quite a satisfactory agreement. The experimental frequencies are in average a bit higher than the analytical frequencies with the maximum error not higher than 4,4%. The modal assurance criterion MAC was used to compare the corresponding mode shapes (MAC = 100 % indicates perfect correlation. The MAC value is calculated from the square of the

cosine of the angle between the experimental and the analytical eigenvector). In practical applications any value beyond 80% must be considered as a satisfactory agreement. An excellent agreement of the fundamental mode no.1 (MAC = 95,9%) can be observed from the spike plot in figure 4(a) where the measured and analytical eigenvectors are plotted over the impact locations shown in figure 1(c) . The correlation is still good for a higher mode like the torsional mode no. 10 with MAC = 76,5% in figure 5.

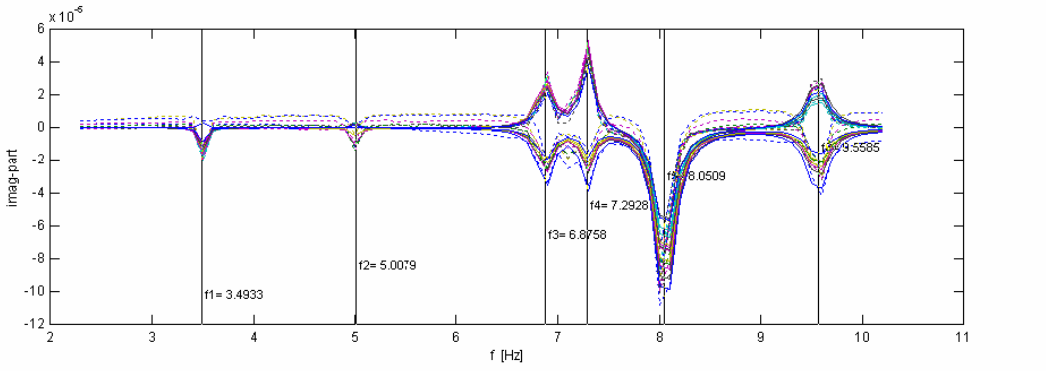

Figure 3: Experimental acceleration frequency response functions (FRFs imaginary parts) at 15 DOFs

Table 2: Comparison of modal data test/analysis

1	2	3	4	5	6	7	8	9	10	11	12	13
Reference No. used for experimental modal analysis												
R1	R2	R3	R4	R5	R6	R7	R8	R9	R10	R11	R12	R13
Experimental eigenfrequencies [Hz]												
3.49	5.01	7.32	8.05	9.40	9.56	10.92	12.92	15.16	18.36	20.34	22.44	22.93
Initial analytical eigenfrequencies [Hz] before parameter updating												
3.36	4.84	7.10	7.93	9.05	9.45	10.60	12.38	14.86	18.00	20.19	21.52	23.05
Initial Prediction error test/analysis [%] before parameter updating												
3.34	3.55	3.10	1.55	3.88	1.11	3.02	4.36	2.05	2.02	0.75	4.27	-049
Prediction error test/analysis [%] after parameter updating												
-1.69	-1.38	-0.41	-0.86	-0.53	-0.52	0.55	1.25	1.34	0.33	-0.44	2.14	-1.38
MAC [%] test/ initial model before parameter updating												
95.9	94.8	95.7	98.2	87.5	93.2	85.8	91.8	97.2	76.5	73.1	93.4	62.6
MAC [%] after parameter updating												
97.0	95.7	95.7	98.9	82.6	98.1	82.5	91.9	97.1	83.7	71.7	94.0	62.4
Experimental viscous modal damping values [%]												
0.91	0.84	1.13	1.41	0.80	1.32	0.64	0.65	1.30	0.54	0.73	2.15	0.68

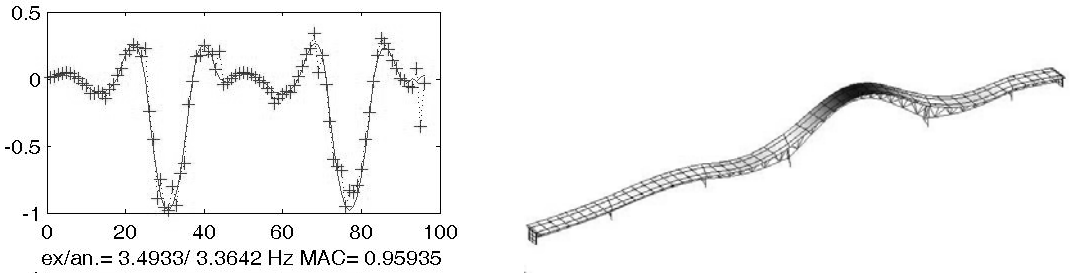

(a) (b)

Figure 4: Mode no. 1: (a) spike plot of test (+++) and FE on measured DOFs, (b) FE

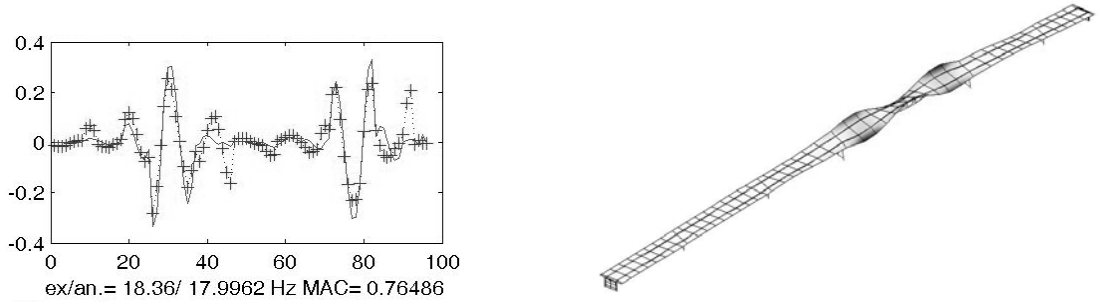

(a) (b)

Figure 5: Mode no. 10: (a) spike plot of test (+++) and FE on measured DOFs, (b) FE

(e) Generation of a reference FE- model by computational model updating

The reference FE- model represents the structure in its initial healthy state and should include all the parameters which are likely to change over the time either due to damage or due to changing environmental conditions. The initial FE- model of the Gaertnerplatz Bridge was therefore supplemented with parameters related

- to the shear stiffness of the bonding elements connecting the deck and the upper cord,
- to the stiffness of the bearings and to
- the bending stiffness of the deck.

To find optimal reference values for these parameters our in-house parameter identification software UDATE_X which is based on the theory described in [7] was applied. This software permits the minimisation of an objective function

$$J = \boldsymbol{\varepsilon}_{\mathrm{w}}^{T} \boldsymbol{\varepsilon}_{\mathrm{w}} \rightarrow \min \tag{1}$$

where the residual vector

$$\boldsymbol{\varepsilon}_{\mathrm{w}} = \mathbf{W}_{v} \boldsymbol{\varepsilon} = \mathbf{v}_{\mathrm{m}} - \mathbf{v}(\mathbf{p}) , \tag{2}$$

defines the weighted differences between the measured quantities $\mathbf{v}_m$ (in the present application we used eigenfrequencies und mode shapes, $\mathbf{W}_v$ denotes a weighting matrix) and their analytical counterparts $\mathbf{v}(\mathbf{p})$ which are a function of the parameters **p** to be updated. The comparision of the results of the initial model and the results after numerical parameter updating in table 2 show that the eigenfrequency predictions have been improved and now are centered around zero between -1.7 % and 2.1 % wheras the MAC values have not changed very much so that this updated model can be considered suitable for the simulation of different damage scenarios.

3 Analysis of damage scenarios

For long term monitoring about 15 permanent acceleration sensors were installed on the bridge for recording data from ambient excitation as well as temperatures. The time domain response data will be analysed after data decimation based on triggering to specified treshold values, to day time and ambient temperature. The evaluation of these data will focus on a number of resonance peaks selected according to the results of the reference data in table 2. Continuous recording of this data will permit to correlate the resonance frequencies to ambient temperature similar to the results obtained from long term monitoring of the Westend Bridge in Berlin reported in [8] and presented in figure 6. The two data clouds for two resonance frequencies show not only the systematic decrease of the resonance frequencies with temperature but also their variation in a given temperature interval. For the Gaertnerplatz Bridge we have simulated such data by letting three material parameters vary within a temperature range beteen -20°C and 30°C (shear modulus of the bonding elements and the Young's modulus of UHPC and steel) and adding normally distributed artificial measurement noise on the eigenfrequencies calculated with the initial FE – model. To simulate a partial degradation of the bonded connection between the deck and the upper cord we have reduced the shear modulus of the bonding elements in the inner three spans by a factor of 0.1. A similar temperature dependence like for the Westend Bridge can be observed in figures 7(a) and 7(b) where the data for the healthy structure (upper data clouds) as well as for the degradated structure (lower data clouds) are plotted. It should be noted that the two data clouds for the healthy and the degradated structure can visually be well distinguished for the first frequency whereas this distinction is not possible for the second frequency in figure 7(b) where both clouds merge.

In order to assess the onset of structural degradation which in practice might happen at any time and temperature we will use a special damage indicator which is calculated continuously over time and the corresponding temperature. The indicator is based on the assumption that the structure will keep its healthy state unitil it has experienced the typical temperature range of one year. The temperature dependent indicator thus forms the reference indicator of the healthy structure. The indicator is calculated in three steps. In the first step the frequencies recorded in each temperature interval are averaged which results in n_f mean frequencies $\bar{f}_k$ (k= 1,...n_f) per temperature interval where n_f represents the number of monitored resonance frequencies (n_f = 6 was used in the present simulation). In the next step the mean frequencies are further condensed to just one number per temperature interval by calculating the root mean square (rms) value of the frequency means by

$$\mathrm{rms}(t_i) = \sqrt{1/n_f \sum_{k=1}^{n_f} \bar{f}_k^2(t_i)} \qquad (3)$$

For the simulated test case of the Gaertnerplatz Bridge the evolution of the rms values versus temperature is shown in figure 8 together with a linear regression line. The upper curve forms the signature of the healty structure over temperature which might be the result of monitoring the state over typically one year. It is expected that any structural degradation

will modify this signature as is shown by the lower curve in figure 8 for a temperature range between 5°C and 20°C. Any significant deviation of the healthy state signature from the signature of the actual monitoring state would indicate the onset of structural degradation and could necessitate another modal test with subsequent updating of the initial reference model to be used for an assessment of the type and the severity of the degradation.

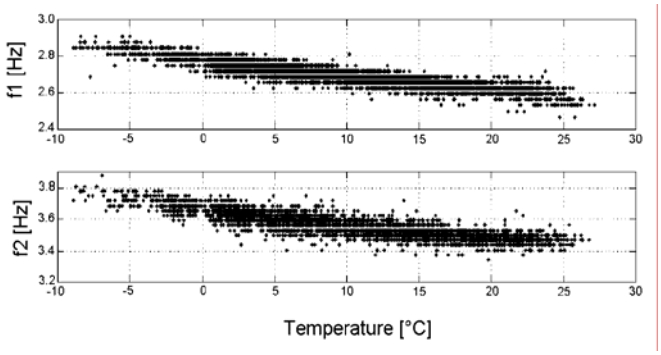

Figure 6: Westend Bridge in Berlin: measured resonance frequencies vs. ambient temperature (taken from ref.[8])

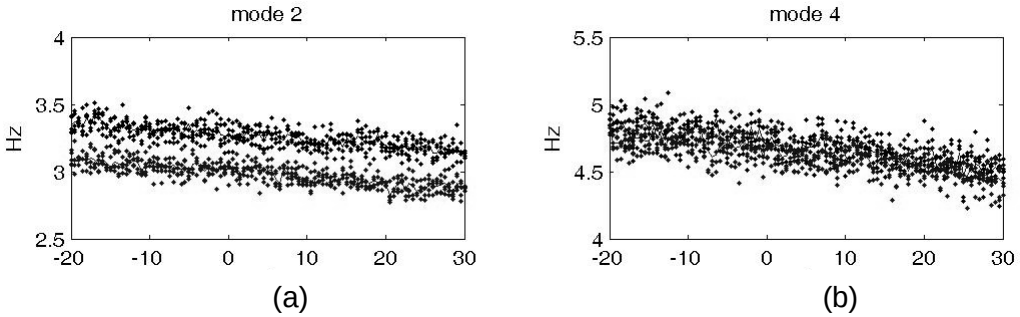

Figure 7: Gaertnerplatz Bridge eigenfrequencies with simulated measurement error versus ambient temperature, upper data cloud without damage, lower with damage

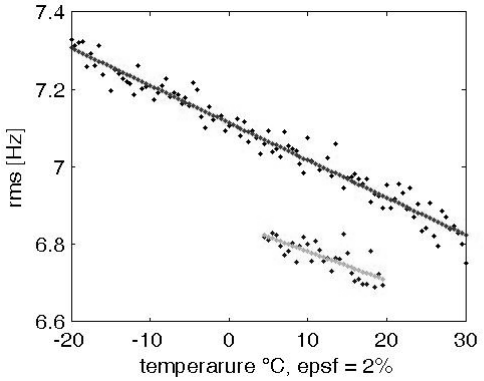

Figure 8: Simulated signature of the Gaertnerplatz Bridge Kassel versus ambient temperature (2% measurement error), upper curve without damage, lower with damage

4. Long term monitoring of static and physical data

In addition to vibration monitoring static and physical data are also measured and used for monitoring. The first part includes the measurement of strain gradients at different measuring locations which are obtained from displacement transducers and strain gauges (DMS). The second part includes temperature and humidity data measured by sensors embedded in the constructional concrete parts of the bridge together with the ambient temperature and humidity data.

4.1 Static data (strain and displacements)

For direct monitoring of the state of the adhesive bonded connection between the bridge deck and the upper cords made of UHPC strain gradients are measured at some representative locations. At these locations potential local damage should be detected by the following procedures:

- Installation of displacement transducers for direct determination of the relative displacement between the bridge deck and the upper cords. The arrangement **L** of the displacement transducers is shown in figure 9. This arrangement was installed at altogether six locations. Two of them 2 are located in the middle of the longest field of the bridge between axes E and F and four at the adjoining columns. If the measured values of the displacement are bigger than an established threshold value this would indicate a local failure in the adhesive bonded connections.

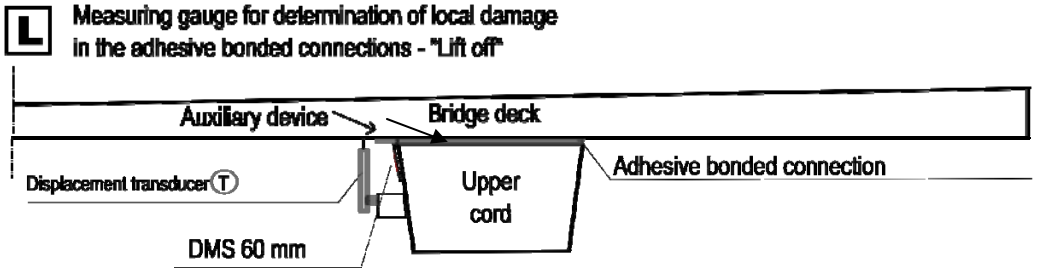

Figure 9: Arrangement **L** of displacement transducers and strain gauges

- Application of strain gauges (DMS) at representative locations on the upper cords and the bridge deck according to the arrangement **D** shown in figure 10 . These gauges are situated in immediate vicinity so that a direct comparison of the measured strain values is possible. A clear difference between these strains would also indicate a local damage in the adhesive bonded connections. Altogether six such arrangements are used. Two of them are situated in the middle of the longest field of the bridge (axes E to F in fig.1a) and the other four at the adjoining columns.

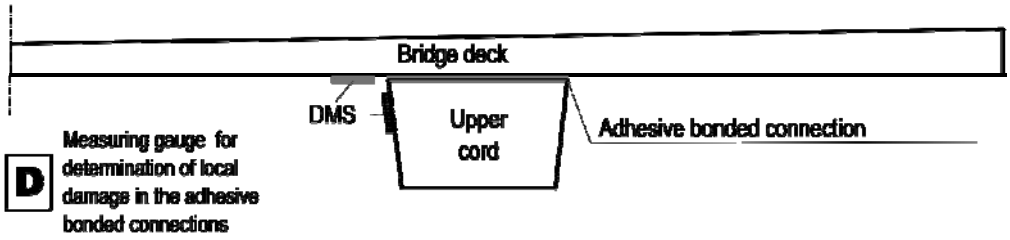

Figure 10 Arrangement **D** of strain gauges

- A special small auxiliary construction for direct measuring of the relative displacement between the bridge deck and the upper cord was build. This auxiliary construction consists of two aluminium plates, one of which is bonded on the upper cord and the other in immediate vicinity at the bridge deck, so that there is only a small joint between these plates. Above these joints strain gauges are directly applied (see arrangement **L** in figure 9). With this method both horizontal and vertical displacements can be detected. These values when exceeding a predefined treshold value would also indicate local damage. There are altogether six such measurement arrangements from which two are situated in the middle of the longest field of the bridge (axes E to F) and four at the adjoining columns.
- Strain gauges are also used for determining possible local damage in the adhesive bonded connections between the individual panels of the bridge deck. At four points at the adjoining columns of the longest field of the bridge between axes E and F strain gauges have been applied directly above the joints between the beams of the bridge deck (see arrangement **J** in figure 11). This arrangement allows for the direct determination of both horizontal and vertical displacement between the two bonded panels. Increased values of the relative displacement indicate the onset of local damage.

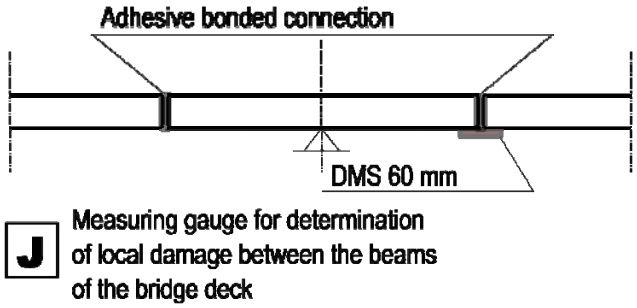

Figure 11: Arrangement J of strain gauges between deck panels

4.2 Physical data

At representative locations of the construction digital combined temperature and humidity sensors habe been embedded in the UHPC parts to determine these physical parameters in different depths of the cross sections both in the panels of the bridge deck and in the upper cords (see arrangement in figure 12). With this procedure profiles over the cross section for temperature and humidity can be determined. In the middle of the longest field of the bridge between axes E and F there are two measuring arrangements in one panel of the bridge deck: One in the diagonal direction at the middle of the panel (sensors 1, 2 and 3) and the other one with sensors 4, 5 and 6 is located directly at the upper cord (see arrangement in figure 12). Within this upper cord there are located two further measuring points: One at the top of the cord (sensor 7) and the other one at the bottom (sensor 8). Therefore the number of measuring points at these measuring arrangements is eight. In the middle of the adjoining next field of the bridge between axes D and E the corresponding measuring equipment (altogether eight sensors) has been installed. In addition to the sensors mentioned above three more sensors have been installed in different depths of the upper cord near the abutment of the bridge in axis B. The ambient temperatures and humidities are also measured.

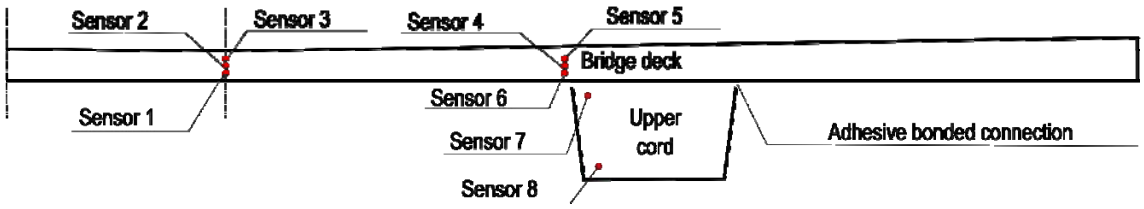

Figure 12: Location of temperature and humidity sensors between axes D – E and E - F

4.3 Extracts of measurement results

The long term monitoring of the Gaertnerplatz Bridge has meanwhile been carried out since about half a year. In comparison with the planned duration of the monitoring (at least five years) this period of time is very short. In accordance with this short measuring time the measured values can not yet give comprehensive insights. At present there is no indication at all for any local damage in the adhesive bonded connections. The temperature and humidity values don´t show unexpected results. In Figures 13 and 14 examples of temperature and humidity profiles are shown at the measuring points between axes D and E and axes E and F, determined on the warmest day (August 24, 2007) in the measuring period. Figure 13 shows the temperature profile in longitudinal axis of the bridge in the area of one upper cord, Fig. 14 shows the corresponding values in the middle-axis of the bridge. It can be seen, that the highest temperature in the bridge deck 2 centimeters or rather 3,8 centimeters under the surface has increased to over 50 degrees centigrade while the ambient temperature is about 25°C. The corresponding temperature directly at the surface of the bridge deck has to be expected a little bit higher. The measurement campaign will be continued over the next five years.

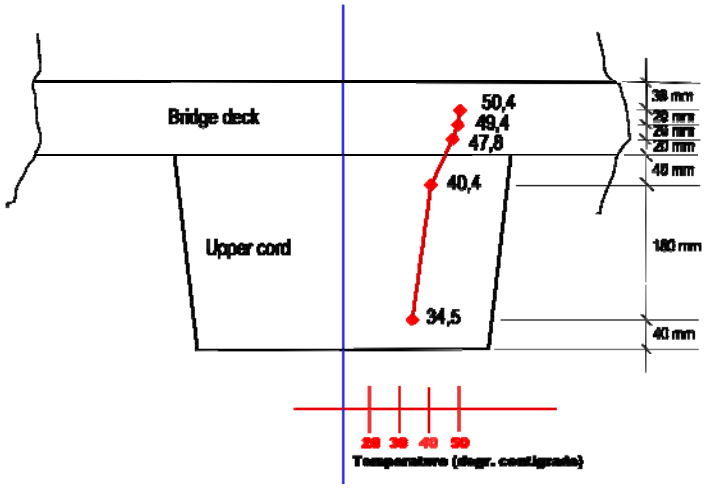

Figure 13: Temperature profile of the bridge deck and the upper cord in the field between axes D and E

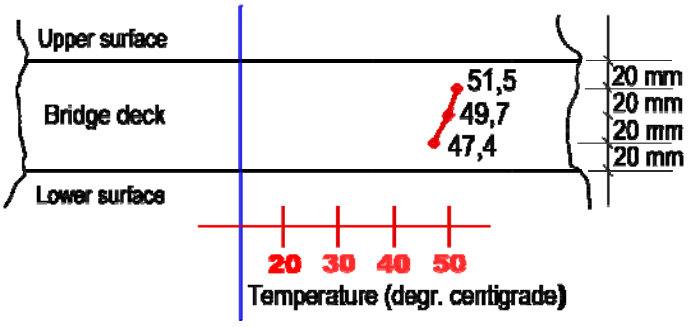

Figure 14: Temperature profile of the bridge deck in the field between the axes E and F

5 Summary and conclusions

In the paper we first presented the methodology of vibration monitoring applied to the Gaertnerplatz Bridge in Kassel which is characterised by the following steps:

(1) Establishment of a reference FE- model representing the healthy structure in its initial state. This model was generated by computational model updating using experimental modal data obtained by artificial impact excitation of the bridge after completion of the construction. The updated model results show very good agreement with the experimental data.

(2) Simulation of a data base to be established in the future from continuous recording of the bridge resonance frequencies from ambient excitation. This simulation included the analysis of structural degradation scenarios based on temperature dependent material properties and on an assumed degradation of the bonded connection between deck and upper cord.

(3) Establishment of a signature function of the healthy structure which might be the result of monitoring the state of the bridge over typically one year.

It is expected that any significant deviation of the healthy state signature from the signature of the actual monitoring state indicates the onset of structural degradation. This could initiate another modal test and subsequent updating of the initial reference model to be used to assess the type and the severity of the degradation.

In addition to the dynamic test data static strains and displacements are measured for direct monitoring of the state of the adhesive bonded connections between bridge deck and upper cords and the bonded connections between the deck panels. Physical data (temperature and humidity) are also recorded permitting to relate the static and dynamic test data to the environmental conditions.

6 References

[1] Automatisierte Dauerüberwachung im Ingenieurbau, Merkblatt B9, Deutsche Gesellschaft für zerstörungsfreie Prüfung (DGZfP), Okt. 2000

[2] Mechanical vibration – Evaluation of measurement results from dynamic tests and investigations on bridges. International Standard ISO 18649:2004(E), 2004

[3] Link M., Stöhr St. and Weiland M.: *Identification of Structural Property Degradations by Computational Model Updating*. Key Engineering Materials Vol. 347, pp.19-34, Trans Tech Publications, Switzerland, 2007

[4] Fehling E., Schreiber W., Bunje K., Schmidt M.: Brücke aus Ultahochfestem Beton in Kassel über die Fulda. Bauingenieur, Bd. 79, Juli/August 2004

[5] ISSPA Manual, University of Kassel, Instiute of Statics and Dynamics, 2005

[6] Ewins D.J.: *Modal Testing, Theory, Practice and Application*, 2nd. Ed., Research Studies Press Ltd. Baldock, UK, 2000

[7] Link, M., ”Updating of Analytical Models – Basic Procedures and Extensions”. Proc. of NATO Advanced Study Institute, Sesimbra, Portugal, May 1998 in "Modal Analysis and Testing"(J.M.M. Silva and N.M.M. Maia (Eds.), Kluwer Acad. Publ., London , 1999

[8] Rohrmann R.G., Matthias M., Said S., Schmid W. and Ruecker W.F.:Structural Causes of Temperature Affected Modal Data of Civil Structures Obtained by Long Time Monitoring. Proc. of the International Modal Analysis Conference IMAC XVIII, San Antonio, USA, 2000

Michael Schmidt
Prof. Dr.-Ing.
University of Kassel
Kassel, Germany

Dagmar Jerebic
Dipl.-Ing.
University of Kassel
Kassel, Germany

UHPC: Basis for Sustainable Structures - the Gaertnerplatz Bridge in Kassel

Summary

Ultra-High Performance Concrete (UHPC) is a very dense and corrosion resistant concrete with a compressive strength of about 150 to 200 MPa. It allows for material saving filigree but nevertheless highly loadable and durable constructions. One actual example is the Gaertnerplatz bridge in Kassel. The 136 long hybrid structure consists of a light 3-D steel truss being combined with two upper chords and a min. 85 mm thin bridge deck - both made of UHPC. For the first time in the world the load bearing concrete elements are connected by an epoxy resin only. Due to the filigree structural layout the mass of the bridge is 370 tons only compared to about 880 tons for a conventional bridge made of prestressed concrete. In correlation with the reduced mass the amount of raw materials, of energy and of emissions is significantly reduced and the impact on the environment is lowered. Considering the fact that the costs of the bridge did not exceed those for a “traditional” construction and that UHPC has a much longer service live, one can state that the use of UHPC is a very effective way to further improve the sustainability of concrete structures.

Keywords: *Gaertnerplatz Bridge, Ultra-High-Performance Concrete, ecological impact, sustainability, energy, raw materials, greenhouse effect.*

1 Introduction

Ultra-High Performance Concrete is characterized by an extremely dense structure free of capillary pores, an increased corrosion resistance and a compressive strength of about 150 to 200 MPa. Reinforced by a sufficient amount of steel or other high performance fibres the tensile strength can be increased up 15 MPa and the bending tensile strength up to about 35 to 45 MPa. The high compressive strength especially allows to apply very high prestressing forces. The material and its application is extensively described in [1,2]. The 136 m long Gaertnerplatz bridge in Kassel is the first application of UHPC for a wide span pedestrian bridge in Germany and the first bridge in the world whose load bearing concrete elements are connected by epoxy resin only [3 6]. Figure 1 gives an impression of the hybrid bridge structure. Figure 2 shows its load bearing members and figure 3 gives the cross section together with an alternative “traditional” structure having the same load bearing capacity

Figure 1: View of the Gaertnerplatz Bridge in Kassel.

Figure 2: Bridge structure: Steel truss; upper chords and bridge deck made of UHPC

based on prestressed ordinary concrete C 35/45 acc. to EN 206. The upper chords of the 3D-truss structure of the Gaertnerplatz bridge consist of spaghetti-like filigree prefabricated and prestressed elements with a length of 12 to 36 m and a cross section of 300 x 400 mm only. They were fitted to the steel framework using high strength screws. Thereafter, the 5 m wide and 8.5 to 12 cm thin deck slabs were glued onto the chords and finally the chords were internally post-tensioned over the whole length of the bridge.

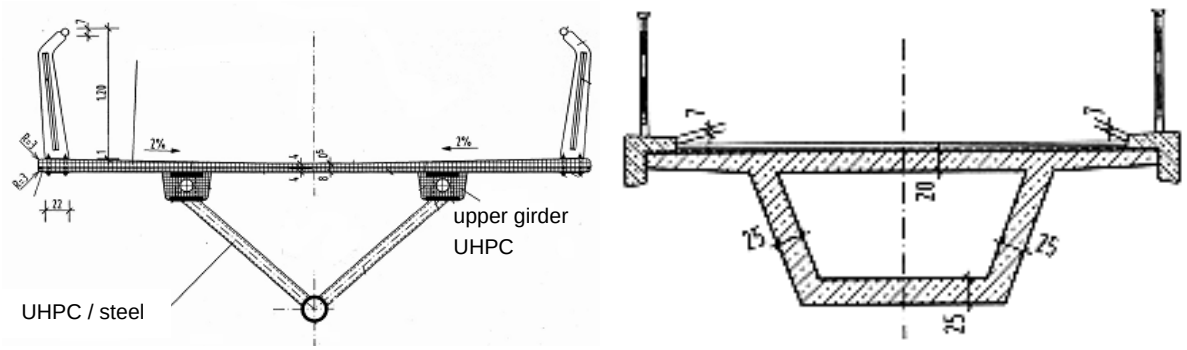

Figure 3: Comparison of the cross sections evaluated. Left: existing design with UHPC and a steel truss (version 1 in table 2) or with a truss made of UHPC (version 2 in table 2). Right: Conventional design consisting of prestressed ordinary concrete (version 3 in table 2).

The composition of the UHPC used for the Gaertnerplatz bridge is given in table 1. It is characterized by a comparatively high amount of cement and silica fume, a very low w/c-ratio of about 0.20 and the use of one or more fine grained mineral powders, primarily quartz to achieve an optimum of the packing density of the fine components of the matrix [2, 4, 5]. Table 1 shows as well that due to the high amount of cement especially the energy “burden” of one m^3 of UHPC is about double as high as for ordinary concrete. Corresponding to that the greenhouse effect is doubled as well.

Table 1: UHPC used for the Gaertnerplatz Bridge and “alternative” ordinary concrete

Concrete		**C35/45**	**UHPC**
Cement	kg/m³	350	733
Quartz powder		-	183
Quartz sand/gravel	kg/m³	1802	1008
Water	kg/m³	175	161
Silica fume	kg/m³	-	230
Steel fibres	kg/m^3	-	75
Primary energy demand 1)	MJ/m³	1702	3440
Greenhouse effect	kg/m³	282	571

1)Calculated using commonly accepted impact data given in [7,8,9,10]

However, the material itself is not the appropriate measure to rate the sustainability of a building. One has to relate it to the total mass of concrete, reinforcing steel etc. being used

Table 2: Demand of raw materials and energy of 3 alternative bridge designs

Material	**UHPC + Steel** (Version 1) (truss structure of steel)		**UHPC+UHPC** (Version 2) (truss made of UHPC)		**Ordinary concrete** (Version 3) (presstressed massive)	
	Raw material	Energy	Raw material	Energy	Raw material	Energy t
	to	MJ	to	MJ	to	MJ
Cement	87	31.000	98	35.199	120	43.080
Silica fume	16	-	18	-	-	-
Aggregates	151	2.200	170	2.518	620	9.176
Water	19	-	21	-	60	-
Steel fibres	7.2	171.000	10	242.800	-	-
Reinforcing steel (incl. foundation, abutment, pillars)	22	541.000	22	541.000	70	1.720.000
Prestressing steel	8	223.000	12	327.000	10	278.000
Steel truss incl. connectors	51 62	1.441.000	-	-	-	-
Sum	-	2.409.200	-	1.148.517	-	2.050.256

for a certain object. Table 2 and figure 5 elucidate the differences between three alternative bridge designs for the Gaertnerplatz Bridge. Their cross sections correspond to figure 3. Version 1 in table 2 is the structure already build und version 3 “traditional” solution made of prestressed ordinary concrete C35/40 as shown in figure 3. Due to the larger sizes of all structural members the total mass of the conventional concrete structure (version 3) adds up to about 880 tons compared to about 370 tons only for the actual hybrid bridge (version 1).

.

The content of primary energy of the structural members is considered as well. The total energy content – including the energy being used for the production and the transportation of the steel and the concrete elements– is by far dominated by the steel being used for the truss, the steel fibre reinforcement and the prestressing steel within the UHPC elements as well as by the conventional reinforcement of the foundations, the abutments and the pillars. Regarding the energetic aspect the actual hybrid structure is not really an ecologically optimized solution because of the high energy content of the steel for the truss structure and the elements fitting the UHPC girders to the framework. Replacing the tubes of the steel truss by prestressed massive UHPC elements of the same size would lead to a further reduction of the weight by another 20 tons (version 2 in table 2) to 350 tons and of the energy content by about 50% compared to version 3. This structure is technically feasible. As an example figure 4 shows a model of the Gaertnerplatz bridge scaled 1:2 purely made of UHPC.

Figure 4: Model of the Gaertnerplatz bridge, scale 1:2 made of UHPC only (Design: Bögel, Neumarkt)

Figure 5 shows the “burden” of primary energy of all three versions covering the constructions phase as well as the whole life-cycle of the bridge [10].

To be able to compare and to summarize different ecological criteria – raw materials, energy and emissions – impact factors has been established which are commonly accepted weighing the different “burdens” with regard to their individual impact on the environment. They have been adopted from [7-10]. In figure 6 as an example the contribution to the greenhouse effect (a global value) are compared. It is obvious that the lightweight filigree structure totally made of ultra-high performance concrete is ecologically superior again.

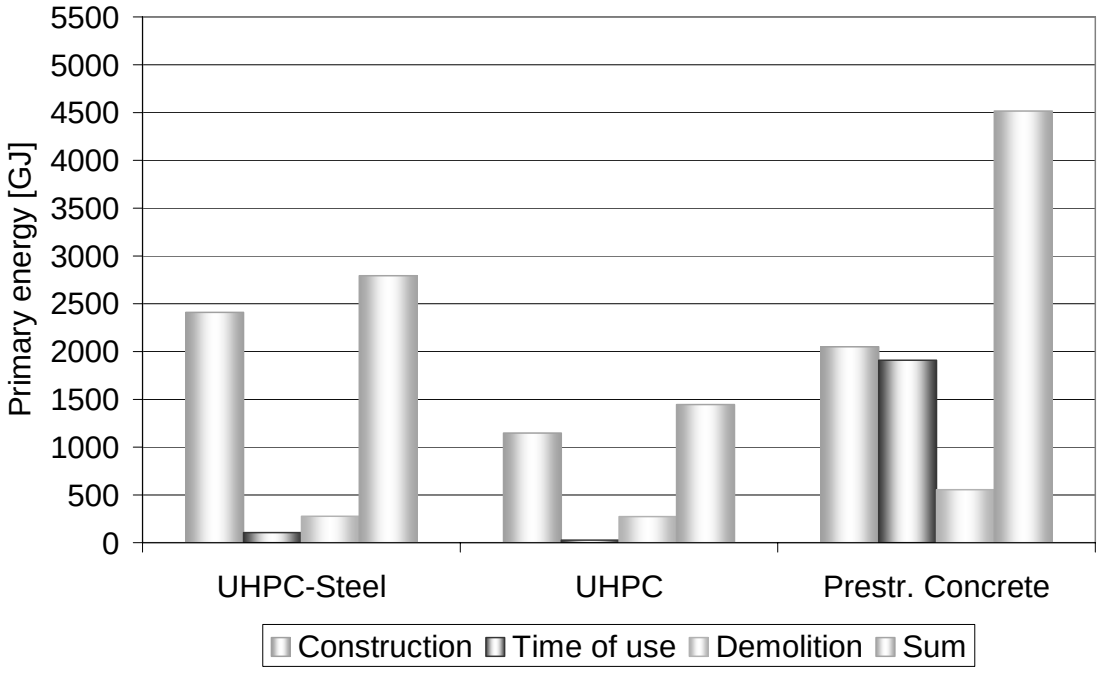

Figure 5: Content of primary energy of three alternative designs for the Gaertnerplatz Bridge

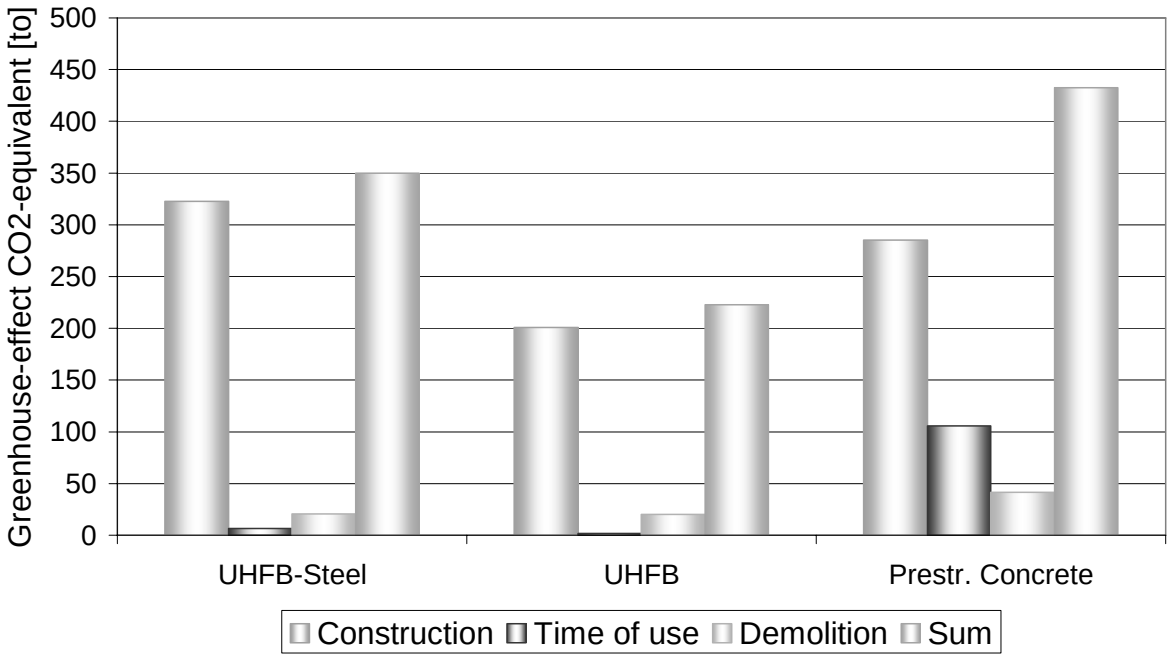

Figure 6: Contribution to the Greenhouse-effect

Despite of the ecological aspects one has to consider that UHPC due to its dense structure free of capillary pores is much more resistant to harmful gases or liquids than ordinary concrete or even high-performance concrete. Its durability is increased and thus the service life is significantly prolonged without or even with a reduced need of protection or repair of the structure. The practical experiences gained with the Gaertnerplatz bridge proved that the costs for such an innovative structure are adequate to a conventional concrete or steel bridge with the same load bearing capacity.

Considering all three aspects – ecological impact, durability and costs – one can summarize that structures made of UHPC which are adequately designed to really exploit the very special performance of this high strength, highly durable material are of superiour sustainability compared to common concrete or steel structures.

2 References

[1] Schmidt,M., Fehling, E., Geidenhanslüke, C (Ed.): Ultra High Performance Concrete (UHPC). Proc. International Symposium on UHPC, Kassel, Sept. 13-15, 2004, 868pp. Structural Materials and Engineering Series No.3. Kassel University Press. ISBN:3-89958-086-9.

[2] Fehling, E., SCHMIDT, M., TEICHMANN,T.,BUNJE,K.,BORNEMANN,R. and B. MIDDENDORF: Entwicklung, Dauerhaftigkeit und Berechnung Ultra-Hochfester Betone (UHPC). Forschungsbericht DFG FE 497/1-1. Structural Matrials and Engineering Series, No. 1. Kassel University Press 2005. ISBN 3-89958-108-3.

[3] Fehling, E., Bunje, K., Schmidt, M., Tue, N.V., Schreiber ,W., Humburg, E.: Design of first UHPC-Steel Bridge across the River Fulda in Kassel, Germany. Paper IABSE Conference, Weimar 2007.

[4] Teichmann,T., Sschmidt, M.: Influence of the packing density of fine particles on structure, strength and durability of UHPC. Proc. Int. Symp. on UHPC, Kassel 2004, pp 313-323 (see [1]).

[5] Schmidt, M., Geisenhanslüke, C.: Optimierung der Zusammensetzung des Feinstkorns von Ultra-Hochleistungs- und selbstverdichtendem Beton, beton, Heft 5, 2005.

[6] Schmidt, M., Teichmann, T.: New Developments in Ultra-High Performance Concrete - non corrosive PVA-fibres and glueing of structural elements. Proc. fib-Congress, Naples, June 2006.

[7] Verein Deutscher Zementwerke e.V.: Umweltdaten der Deutschen Zementindustrie 2001, Verlag Bau + Technik, Düsseldorf, 2001

[8] Hrsg.: Gesamtverband des deutschen Steinkohlenbergbaus, Essen, Rohstoffeinsatz in hochindustrialisierten Volkswirtschaften – ein strukturprägender Faktor, Forschungsvorhaben des Herausgebers, Endbericht 2005, http//www.gvst.de

[9] Löckener, R.; Timmer, B.: Nachhaltigkeit und Zementindustrie – Dokumentation von Beiträgen und Handlungsoptionen; Düsseldorf: Verlag Bau + Technik, 2002

[10] Jerbic, D.: Eine vergleichende Ökobilanzierung zur Gärtnerplatzbrücke aus UHPC; Diploma thesis, University of Kassel, 2005.

Part 9:

Structural Behaviour II

Udo Wiens
Dr.-Ing.
German Committee for Structural Concrete at DIN German Institute for Standardisation
Berlin, Germany

Michael Schmidt
Prof. Dr.-Ing. habil.
University of Kassel
Kassel, Germany

State of the Art Report on Ultra High Performance Concrete of the German Committee for Structural Concrete (DAfStb)

Summary
Within the last years in several countries technical guidelines for UHPC have been released, e.g. in France and in Japan [1, 2]. They mainly deal with the materials adequate design of structural members and whole constructions made of UHPC. As a rule for design of the material itself, processing of UHPC and other aspects not directly being relevant for the structural design have not been dealt with in these papers. In another activity a fib-guideline on UHPC is currently elaborated covering materials aspects in detail as well. In Germany a couple of measures have been started to develop a technically sound, scientifically proven basis to produce individually designed UHPC for specific applications and to design and construct durable and economic structures. One important step is a "State of the Art Report" covering all aspects from the raw materials, the mix design and the production to the materials adequate design and construction [3].
Keywords: *UHPC, state of the art report, concrete properties, design values, construction*

1 Introduction

The specific German philosophy to enhance the development of new technologies such as UHPC technically and economically is to establish comprehensive knowledge based technical rules, that enables concrete producers, precast concrete companies and/or constructors to design individual UHPC-mixtures for their specific application using raw materials being regionally available. The knowledge data base is founded on

- a state of the art report elaborated by a group of experts under the responsibility of the German Committee for Structural Concrete (DAfStb) [3];
- a comprehensive 9 Mio. € Priority Research Project initiated and financed by the German Research Foundation (DFG) covering all aspects from the appropriate raw materials to the structural design and the assembling of UHPC members. About 20 projects are in progress performed by 15 research groups under the coordination of the University of Kassel [4];
- the practical experiences gained with different applications e.g. several smaller bridges up to 20 m length and primarily resulting from the "Gärtnerplatz Bridge" in Kassel [5, 6].

The state of the art report of the DAfStb deals with the following aspects:

- Examples of application;
- raw materials (cement, additions, admixtures, aggregates);
- fresh and young concrete characteristics;
- hardened concrete properties (strength, deformation behaviour, durability, fire resistance);
- design and construction;
- research activities.

The approaches regarding the design and the design relevant mechanical behaviour of (fibre) reinforced UHPC is given in more detail in chapter 3. The material related content of the state of the art report is based on the literature being available worldwide starting with the fundamental ideas published e.g. by Bache and others in the 1960s. First UHPC-products were already produced by Aalborg Portland Cement (Densit) at these times. About 1990 the basis for a wider application for structural concrete members and for a large scale technical production has been laid – e.g. by the efforts of DUCTAL® and other companies developing different kinds of pre-mixes resulting in a first spectacular structure: the "Sheerbrook Bridge" in Canada. To a great extend this progress became possible because of the development of new high performance superplastizisers based on polycarboxylate ethers (PCE) and – of coarse – great research efforts by the producers.

2 Materials aspects

Table 1 gives a survey of the material related content of the state of the art report. It starts with physically and chemically based evaluation criteria for the raw materials, the scientific and practical background of an optimized design e.g. concerning the influence of the packing density of the fine particles and it gives numerous mixtures which have already been studied scientificly or which has been applied practically. The Report as well deals with the mechanical behaviour of UHPC with and without fibres including the influence of the kind and amount, the diameter and the orientation of the fibres within the concrete. And last not least the main durability aspects are extensively discussed – e.g. the resistance to frost in combination with deicing salts, the carbonation behaviour, the permeability to chloride ions etc. and its susceptibility for late ettringite formation.

Table 1: Material related content of the state of the art report [3]

Raw Materials and Mixtures	Aggregates, cement, reactive and inert mineral additions (silica-fume, stone powders, fly ash etc), chemical additives, fibres
Mix optimization	Packing density (distribution and shape of grains), rheology, test procedures, reference mixtures
Curing and heat treatment	Influence on microstructure, strength and durability
Hardened UHPC	Shrinkage (drying and autogenous), mineral phases, microstructure, strength and deformation behaviour (with and without fibres), porosity, permeability to gases and liquids, chloride penetration, alkalinity, durability (frost, frost and deicing salt, alkali-silica-reaction, late ettringite formation), creep
Application	Reference mixtures, mixing, placing, reference projects

The material related aspects will be further discussed during the Symposium. Thus, this paper focuses on the design and construction related aspects.

3 Design and Construction

3.1 Introduction

Unlike in France or Japan, for example, there are no design specifications for ultra high performance concrete (UHPC) structures in Germany at the present time. However, a number of research projects have been started in Germany in recent years which aim not only to expand our fundamental understanding of the mechanical behaviour of UHPC [4] but also to derive material laws and parameters. The initial results of the German investigations were first published in the state of the art report in the form of recommendations for design parameters and approaches. The description of those design approaches is essentially based on the design specifications for high strength concretes in DIN 1045-1 [7] which in turn is largely based on Eurocode 2 (EN 1992-1-1). Furthermore, national provisions laid down in the "Recommendations of the German Association for Concrete and Construction Technology for Steel Fibre Reinforced Concrete" (DBV-Merkblatt Stahlfaserbeton) [8] and the draft "Guideline on Steel Fibre Reinforced Concrete", published by DAfStb, the German Committee for Structural Concrete at DIN (DAfStb-Richtlinie Stahlfaserbeton) [9] are cited in the state of the art report. Another important source is the French guideline published by AFGC/SETRA [1] in which the design of fibre reinforced ultra high performance concrete components is dealt with for the first time. Reference is also made to the Japanese guideline "Recommendations for Design and Construction of Ultra-High Strength Fiber-Reinforced Concrete Structures" (USC) [2] published by JSCE.

The most important design parameters and approaches given in the various specifications are presented and compared below and constitute an extract from the state of the art report. As the French and Japanese specifications are well known, this chapter will focus on the recommendations for the design of UHPC components which have been derived from existing or draft German specifications and are included in the state of the art report.

3.2 Design values for UHPC

Table 2 is a summary of some relevant design values extracted from literature.

Compressive strength

There are only minor variations in the approaches to the design compressive strength. Apart from the coefficient θ for transient loads given in the AFGC/SETRA-guideline [1] the design compressive strength of UHPC is defined in the same way in each of the three guidelines considered here, being based on the characteristic value f_{ck} (5% fractile). It can be seen that the partial safety factor based on DIN 1045-1 [7] which is proposed in Table 1 is considerably higher than the factors given in the French and Japanese guideline. This is due to the additional partial safety factor γ_c' specified in DIN 1045-1 for high strength concrete.

Tensile strength

The design tensile strength of fibre reinforced UHPC based on the fib-Recommendations [10] and on the AFGC/SETRA publication [1] is also shown in Table 2. The coefficient of 0.85 aims to take account of the reduction due to permanent loading and is initially the same as that used for high performance concrete (see the studies by Rinder [11]). The characteristic tensile strength f_{ctk} should generally be determined by tests on specimens cut out of components with approximately proportional dimensions, taking into consideration the concreting, loading and compacting direction (particularly on the vibrating table). Axial tensile tests or flexural tests are suitable for this purpose. A standard test specimen as used in the four-point flexural tensile test with the dimensions 150 x 150 x 700 mm³ (see Figure 1) is specified in the DBV-Merkblatt Stahlfaserbeton [8] and in the DAfStb-Richtlinie Stahlfaserbeton [9] for the determination of the tensile strength.

Table 2: Design values for UHPC according to different sources

Equation	Parameters in equation	Source
	Design values for Compressive strength	
$\sigma_{bc} = \frac{0{,}85}{\theta\,\gamma_b} f_{cj}$	γ_b = Partial safety factor (1.5 for normal cases, 1.3 for special cases) θ = Coefficient representing the period of load action: θ = 1.0 for a period of load action > 24 h θ = 0.9 for a period of load action between 1 h and 24 h θ = 0.85 for a period of load action < 1 h) f_{cj} = Characteristic value of compressive strength at j days	AFGC/SETRA [1]
$f_{cd} = 0{,}85 \cdot \frac{f_{ck}}{\gamma_c}$	f_{ck} = Characteristic value of compressive strength γ_c = 1.3	Japanese Guideline (JSCE) for USC [2]
$f_{cd} = 0{,}85 \cdot \frac{f_{ck}}{\gamma_c \cdot \gamma_c'}$	f_{ck} = Characteristic value of compressive strength for UHPC at 28 days γ_c = 1.5 for cast insitu normal strength concrete and 1.35 for precast normal strength concrete with $f_{ck} \geq 150$ MPa for UHPC: $\gamma_c \cdot \gamma_c'$ = 1.885 for cast insitu UHPC without fibres $\gamma_c \cdot \gamma_c'$ = 1.665 for cast insitu UHPC with fibres $\gamma_c \cdot \gamma_c'$ = 1.688 for precast UHPC without fibres $\gamma_c \cdot \gamma_c'$ = 1.499 for precast UHPC with fibres	Recommendation based on DIN 1045-1 for high strength concrete [7]
	Design values for tensile strength	
$f_{ctd} = \frac{0{,}85\, f_{ctk}}{\gamma_{ct} \cdot \gamma_f}$	f_{ctk} = 5 % - Quantile of the tensile strength (maximum value of the σ–ε-curve) γ_{ct} = Partial safety factor for the tensile strength of fibre reiniforced concrete: γ_{ct} = 1.3 for ultimate limit states (ULS) γ_{ct} = 1.0 for serviceability limit states (SLS) γ_f = Partial safety factor taking into account irregularities in fibre orientation: = 1.25 in general, except for local effects (deficiencies) = 1.75 when taking local defeciencies into account	Derived from fib-Recommendation [10] and AFGC/SETRA [1]
	Design values for creep	
creep coefficient φ	0.8 for UHPC without heat curing 0.2 for UHPC after heat curing	AFGC/SETRA [1]

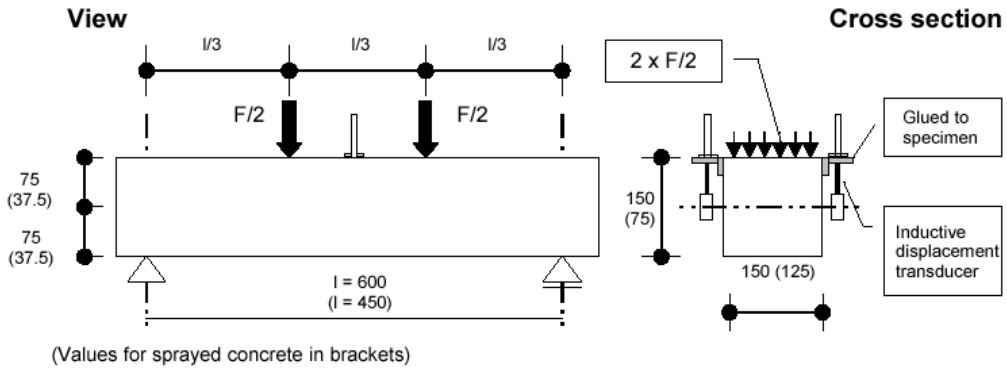

Figure 1: Four-point flexural tensile test to determine the load-deflection curves for beams in accordance with [8, 9]

The tensile strength and what is known as the characteristic post-cracking flexural tensile strength for crack openings of around 3.5 mm can be derived from the load-deformation relationships for such test specimens. The stress-strain curve required for design and which is shown in Figure 3 has been derived from this type of tests. The stress values are defined as follows:

- $f_{ct,fl,L1}$ when the flexural tensile strength is achieved;
- $f_{ct,fl,L2}$ when a deflection of 3.5 mm is reached (corresponding to a crack opening of 3.5 mm).

The tensile stresses in deformation zones 1 und 2 of the design curve are determined as follows on the basis of the flexural tensile test:

$$f_{ctk,L1} = 0.4 \cdot f_{ctk,fl,L1} \text{ (deformation zone 1)} \quad (1)$$

$$f_{ctk,L2} = \beta \cdot f_{ctk,fl,L2} \text{ (deformation zone 2)} \quad (2)$$

The coefficients 0.4 in equation (1) and β in equation (2) were determined by verification calculations performed after the tests. As for normal weight concrete with a compressive strength of up to C50/60 in [9], the coefficient β for UHPC depends on the ratio $f_{ctk,fl,L2}/f_{ctk,fl,L1}$ and can be seen in Figure 2.

Modulus of elasticity

The value E_c = 50 GPa can be used in preliminary designs although it must be taken into account that the modulus of elasticity of UHPC is influenced by a number of factors just as it is in the case of normal weight concrete. As UHPC members are generally thin and thus susceptible to deformation, the modulus of elasticity should be determined by testing on a case-to-case basis.

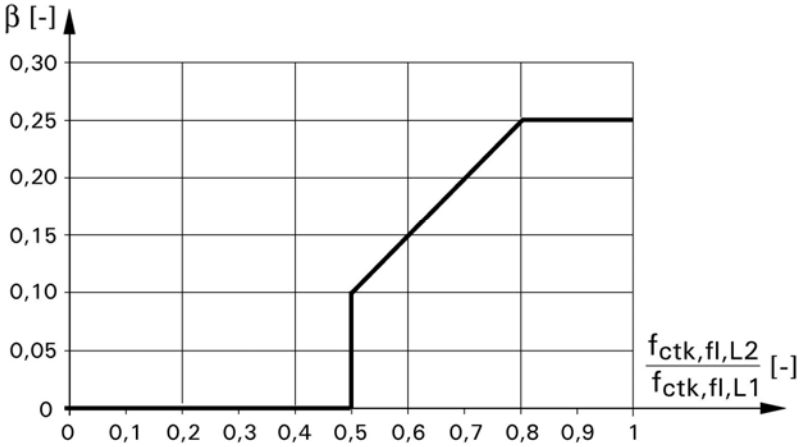

Figure 2: Values of β in equation (7-2), based on [12]

Poisson's ratio

Poisson's ratio, μ, can be taken as equal to 0.2.

Coefficient of thermal expansion

The coefficient of thermal expansion, α_T, can be taken as equal to $1.1 \cdot 10^{-5}$·1/K unless more exact values are available.

Shrinkage and creep

Autogenous shrinkage and drying shrinkage must both be taken into account when designing UHPC members, although autogenous shrinkage generally predominates.

According to current findings, autogenous shrinkage depends to a very high degree on the composition of the concrete. As for drying shrinkage, a value of 250 µm/m can generally be taken for UHPC which has not been heat cured while a value of 0 µm/m can be taken for UHPC after heat curing.

According to the AFGF/SETRA guideline [1] the creep coefficient can be taken as follows:

- φ = 0.8 without heat curing;
- φ = 0.2 after heat curing.

These values only apply to UHPC subjected to loading at an age of 28 days. If loading is commenced earlier than at 28 days, higher values must be expected for non heat-cured UHPC.

Tensile stress-strain relation for non-linear structural analysis and deformation calculations

A stress-strain relationship is derived from a stress-crack opening relation in the AFGC/SETRA-guideline [1] in order to simplify the calculations. The strain at the relevant points depends on the crack width and height of the members. However, the ultimate strain is not a fixed value but depends on the length of the fibres and the height of the member.

Based on theoretical estimates of the tensile strength of UHPC according to Behloul [13] or with a knowledge of the tensile strength and the geometry of the fibres, a theoretical method

of determining the stress, σ(w), in cracked cross-sections as a function of the crack width, w, and the length of the fibres, l_f, can be established in the same way as for steel fibre reinforced concrete (cf. Pfyl [14], for example).

In order to be able to continue applying the usual design approach, a stress-strain relation for the tension zone is also derived from the tests in [8] and [9] instead of the tensile stress-crack opening relation. This provision is also suitable for estimates or the preliminary design of UHPC. Teutsch and Grunert [12] have obtained a good level of agreement during verification calculations performed after tests conducted with coarse aggregate UHPC. However, for UHPC with a low maximum aggregate size, there were considerable differences between the results of the tests and those obtained by calculation. For exact verifications it must be considered in particular that the flexural tensile strength includes a scale effect. An example is shown in Figure 3 that illustrates how the stress-strain curve in the tension zone is obtained for UHPC on the basis of the DAfStb-Richtlinie Stahlfaserbeton [9] for a certain set of assumptions.

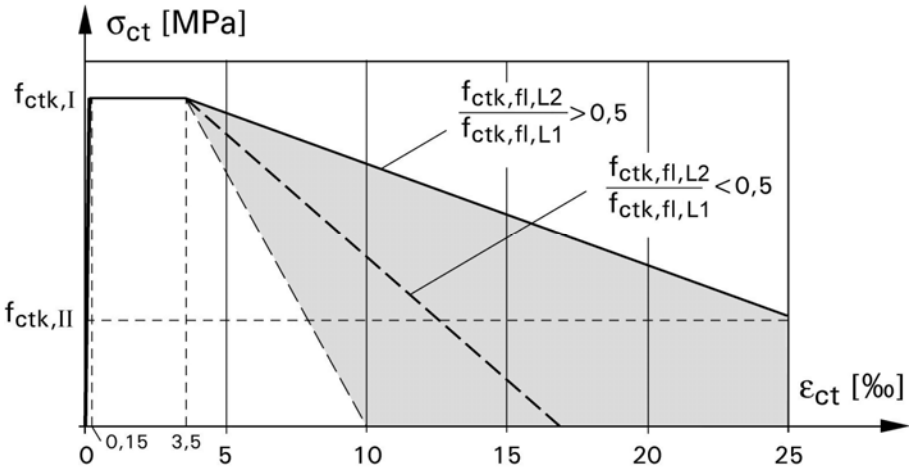

Figure 3: Stress-strain curve for UHPC in the tension zone derived on the basis of [12]

The 0.15 ‰ strain given in Figure 3 represents the elastic limit and is obtained for a tensile strength of 8.25 MPa and a modulus of elasticity of 55 GPa, for example. Generally speaking, an ultimate strain, ε_{ct}, of 25 ‰ can be assumed for design purposes. However, verification calculations performed after tests on fibre reinforced normal weight concrete have shown that designs performed with $f_{ctk,fl,L2}/f_{ctk,fl,L1} < 0.5$ could be unconservative. A relationship for the ultimate strain $\varepsilon_{ct,ult.}$ is given in Figure 4 for that reason. The shaded area shown in Figure 3 indicates the reduction in strain for the relation $f_{ctk,fl,L2}/f_{ctk,fl,L1} \leq 0.5$.

Both of the methods of describing the stress-strain relation on the tension side of flexural members described in the DAfStb-Richtlinie Stahlfaserbeton [9] and in the AFGC/SETRA publication [1] are empirical, with the AFGC/SETRA approach taking the scale effect (influence of the specimen height) into account. While the method described by the DAfStb [9] and the DBV [8] is mainly intended for members designed with a combination of steel fibres and reinforcing steel, the proposal put forward by AFGC/SETRA [1] can be used in particular for steel fibre reinforced members without additional steel reinforcement.

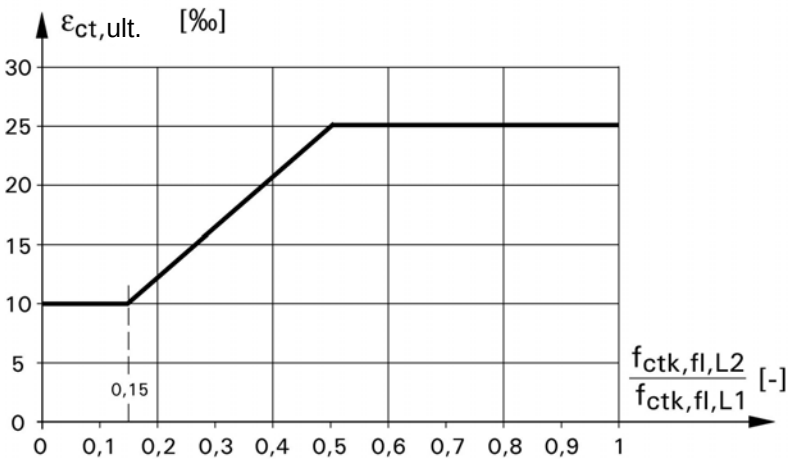

Figure 4: Values of the ultimate strain $\varepsilon_{ct,ult.}$

The two proposals also differ in the specification of the ultimate tensile strain. While the DAfStb [9] specifies a fixed ultimate strain, variable values which depend on the length of the fibres and the height of the components are given in the AFGC/SETRA publication [1].

It must be considered for both proposals that the stress-strain curve should not be applied without taking account of the thickness of the member being designed and the direction of the fibres as in both cases the former determines the correlation between the stress-crack opening relation and the stress-strain relation. Further research in this field is urgently needed and part of the Priority Research Program [3].

3.3 Ultimate limit state (ULS) design and serviceability limit state (SLS) design

The state of the art report also contains recommendations for ultimate limit state (ULS) and serviceability limit state (SLS) design based on [1, 2, 7, 8, 9].

4 References

[1] AFGC/SETRA: Bétons fibrés à ultra-hautes performances. Recommandations provisoires. Documents scientifiques et techniques. Association Française de Génie Civil, Setra, Bagneux Cedex, janvier 2002, S. 1-152.

[2] JSCE-USC Guideline for Concrete No. 9: Recommendations for Design and Construction of Ultra-High Strength Fiber-Reinforced Concrete Structures, 2006

[3] Sachstandbericht "Ultrahochfester Beton". Berlin. Beuth Verlag. In: Schriftenreihe des Deutschen Ausschusses für Stahlbeton, Nr. 561, 2008.

[4] Nachhaltiges Bauen mit ultra-hochfestem Beton (*sustainable building with UHPC*). Schwerpunktprogramm SPP 1182 der Deutschen Forschungsgemeinschaft (DFG).

[5] Schmidt, M.; Krelaus, R.; Teichmann, T.; Fehling, E.; Herget, E.: Glueing UHPC structural members for the Gärtnerplatzbridge in Kassel. Concrete Plant + Precast Technology (Betonwerk + Fertigteil-Technik) 73 (2007), No. 10, pp. 12-20.

[6] Schmidt, M.: Einsatz von UHPC beim Bau der Gärtnerplatzbrücke in Kassel. In: Beton 57 (2007), H. 6, S. 252-255.

[7] DIN 1045-1: Deutsche Norm: Tragwerke aus Beton, Stahlbeton und Spannbeton - Teil 1: Bemessung und Konstruktion (Concrete, reinforced and prestressed concrete strutures - Part 1:

Design), S. 1-148, Normenausschuss Bauwesen (NABau) im DIN Deutsches Institut für Normung e.V. Beuth Verlag Berlin, Juli 2001.

[8] DBV-Merkblatt Stahlfaserbeton. Deutscher Beton- und Bautechnik Verein E.V., Berlin, Wiesbaden, Oktober 2001.

[9] DAfStb-Richtlinie Stahlfaserbeton. Ergänzungen zu DIN 1045, Teile 1 bis 4 (07/2001). 21. Entwurf. DAfStb im DIN Deutsches Institut für Normung e.V., Berlin, April 2005.

[10] fib-Recommendations: Practical Design of Structural Concrete. FIP-Commission 3 "Practical Design", Sept. 1996. Publ.: SETO, London, Sept. 1999. (Distributed by: fib, Lausanne, email: fib@epfl.ch).

[11] Rinder, T.: Hochfester Beton unter Dauerzuglast. Berlin. Beuth Verlag. In: Schriftenreihe des Deutschen Ausschusses für Stahlbeton, Nr. 544, 2003.

[12] Teutsch, M.; Grunert, J.P. (2004): Biegebemessung von Bauteilen aus Ultrahochfestem Beton. Beston- und Stahlbetonbau 99 (2004), H. 8, S. 657 – 661.

[13] Behloul, M.: Les micro-bétons renforcés de fibres. De l'éprouvette aux structures. XIVèmes Journées de l'AUGC, Clermont-Ferrand. Prix Jeunes Chercheurs «René Houpert», 1996.

[14] Pfyl, T. (2003): Tragverhalten von Stahlfaserbeton. Dissertation. Institut für Baustatik und Konstruktion, ETH Zürich. Februar 2003

Yang Yuguang
Msc.
Delft University of Technology
Delft, The Netherlands

Joost Walraven
Prof. Dr. Ir.
Delft University of Technology
Delft, The Netherlands

Joop den Uijl
Ass. Prof.Ir.
Delft University of Technology
Delft, The Netherlands

Study on bending behavior of an UHPC overlay on a steel orthotropic deck

Summary

The approach of strengthening a steel bridge deck with reinforced UHPC (Ultra High Performance Concrete) is studied in this work. The bending behavior of the composite deck plate is modeled by the so called multi-layer model with a simplified stress-strain relation derived from direct tensile tests, and checked by bending test results. Based on the results of the simulation, some suggestions have been derived for future design. Reference is made to the redesign of the Caland Bridge which has been provided with a new UHPFC bridge deck in 2003.

Keywords: *UHPC, overlay, multi-layer model, bending behavior*

1 Introduction

Conventional orthotropic steel decks are widely used in bridge structures around the world. The advantage of this type of decks lies in its considerably reduced self weight. However, with the increase of traffic loads, it turns out, that the bearing capacity, especially under fatigue loading of those orthotropic bridge decks is not satisfactory. Fatigue cracks have been observed in a number of Dutch bridge decks [1]. Those cracks might endanger the bearing capacity, so upgrading is necessary, especially for the bridges in highways. It is believed that local stress concentrations are the main reason for this phenomenon [1, 2]. To that aim several measures are developed in order to reduce the stress level. A promising solution among them is to place a concrete overlay on the existing bridge deck [1, 3, 4]. This approach has been applied in several projects world widely such as the Mihara Ohashi Bridge in Japan, and the Caland Bridge in the Netherlands.

As a reference the deck configuration of the Caland Bridge is plotted in Figure 1. The 56 mm thick concrete overlay and the 12 mm thick steel deck plate are connected by an epoxy layer with sprinkled-in bauxite aggregate. After the hardening of this epoxy layer, the concrete overlay was cast on top of it. It is reinforced by two rebar mesh layers (Ø8 mm spaced at 50 mm) as well as steel fibers. For further information reference is made to [1]. The overlay was

heavily reinforced: approximately 24 kg/m² traditional rebar and 5 kg/m² steel fibers were applied, which corresponds to 580 kg/m^3 reinforcement and 1.2 Vol.% fibers [5]. However the effectivity of this heavy reinforcement on the behavior of the composite plate is still under discussion.

For that reason, the bending behavior of the reinforced UHPFRC overlay on the steel plate, especially when it is under negative bending, was studied. A semi-analytical method, denoted as the multi-layer model, is used in that process for which a stress-strain relationship based on direct tensile tests can be used.

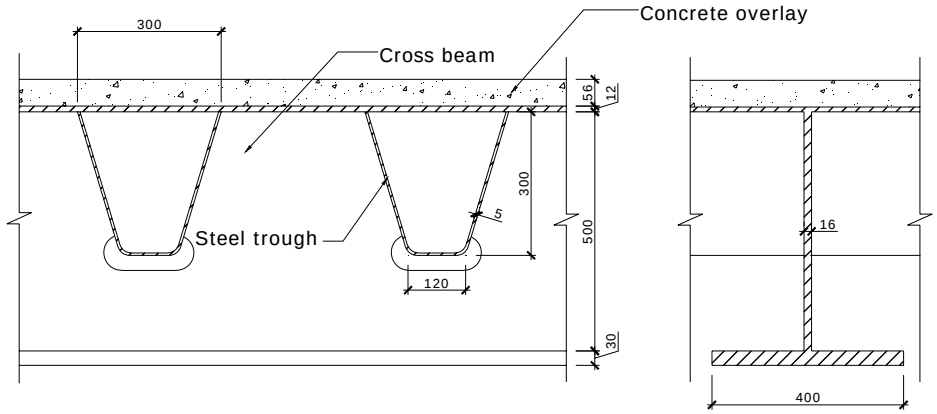

Figure 1: Cross-section of the deck plate of the Caland Bridge

2 Material properties

2.1 UHPC (Ultra High Performance Concrete)

Because of its favourable behavior in tension, especially with regard to crack distribution, heavily reinforced UHPC is an attractive material to be applied in a deck overlay. In order to apply this material in the design of the overlay, simplified material characteristics are defined on the basis of a number of direct tensile tests (dog-bone test) carried out at TU Delft. The mixtures of those tests were designed to achieve mechanical properties comparable to those used in the Caland Bridge. They had strengths of 130 MPa and 180 MPa. Each strength group contained specimen with 0 Vol.%, 0.8 Vol.% and 1.6 Vol.% of steel fibers 13x0.16 mm. Further details of the mixture are given in [10].

In Figure 2, some of the test results are shown. It can be seen that the material behaves as a tensile softening material. When the deformation increases, crack localization can be observed. The steel fibers can transfer a tensile force even if the crack width is relatively large (2 mm). On the other hand, the post-cracking behavior of UHPC is also depending on the fiber distribution across the cracks. In some cases one can even expect strain hardening after cracks have been initiated. This is reported e.g. by Marković [7]. According to his study this uncertainty might be amplified if the casting process is taken into account.

In this study, the tensile behavior of UHPC is modeled in a relatively conservative way. First of all, the load-COD curve is translated into an equivalent stress-strain relationship by: $\sigma = F / A$, $\varepsilon = \text{COD} / l_c$. Here l_c is the so called characteristic length. A = 70×70 mm² and l_c = 100 mm follow from the dimensions of the test specimen and the calculation target. After that, the stress-strain curve is further simplified by replacing the possible strain hardening part of the

load-COD curve by a yield plateau, which means that the tensile stress in UHPC jumps directly from its cracking strength f_t to a constant value αf_t as shown in Figure 3. At a certain position, a linear strain softening part is included after the yield plateau. The value α varies according to the fiber volume percentage and fiber property in the concrete matrix. In [8, 9], several theoretical models have been developed to explain the influence of steel fibers in a brittle matrix like concrete. This will not be discussed further in this paper. The value of α in this study is adjusted according to the dog-bone tensile test results.

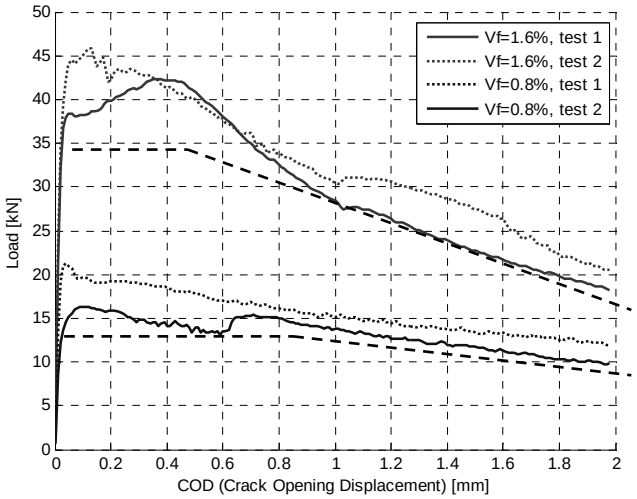

Figure 2: Result of dog-bone tensile test

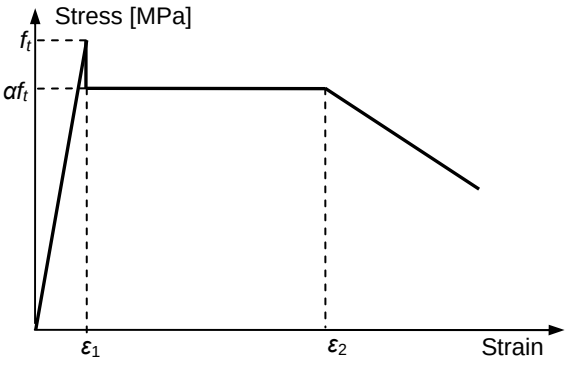

Figure 3: Schematic tensile stress-strain relation for HPC

In Figure 3, ε_1 is the cracking strain of UHPC, ε_2 is the end of the yield plateau, and ε_3 is the ultimate tensile strain, where no more stress can be transmitted across the cracks. The curve is defined with the following values: f_t = 8.5 MPa, α = 0.8, ε_2 = 4 ‰, E = 40 GPa. These values will be assessed further by the 4 point bending test results described in [10].

2.2 Epoxy interface

The interface between UHPC overlay and steel deck plate was tested by Braam [5]. The tensile strength of the interface reached 4.81 MPa, and in the bending test, the bonding stress reached 12.5 MPa. The interface between UHPC and the steel plate of the orthogonal steel deck turned out to be stronger than the plain concrete (without steel fibers). According to the study carried out in [3], the interface bond between concrete overlay and the steel plate can be improved significantly if the ductility of the concrete overlay is increased. Thus, before the crack in the overlay reaches the steel deck plate, these two materials can be seen as perfectly bonded.

3 Multi-layer model

In this study, the cross section of the target element cross section is simulated with the so called multi-layer model. This method was proposed by Kooiman in [11] to simulate the bending behavior of a steel fiber reinforced concrete beam. Because of its simplicity this method can be easily applied for the case considered here and is more user-friendly and

faster than a non-linear FEM analysis. With this model, the constitutive relation, assumed for UHPC, is optimized by comparing the computer generated results with test results from experiments. The procedure of this method is presented in the sequel:

First of all it is assumed that the strain over the height of the cross section is linearly distributed. After that, the cross section is divided into a number of layers along its height. One can get a strain value at the end of each layer. With that value the predefined stress-strain relationship is implemented, yielding the stress at certain levels in the cross section. This procedure is demonstrated in Figure 4.

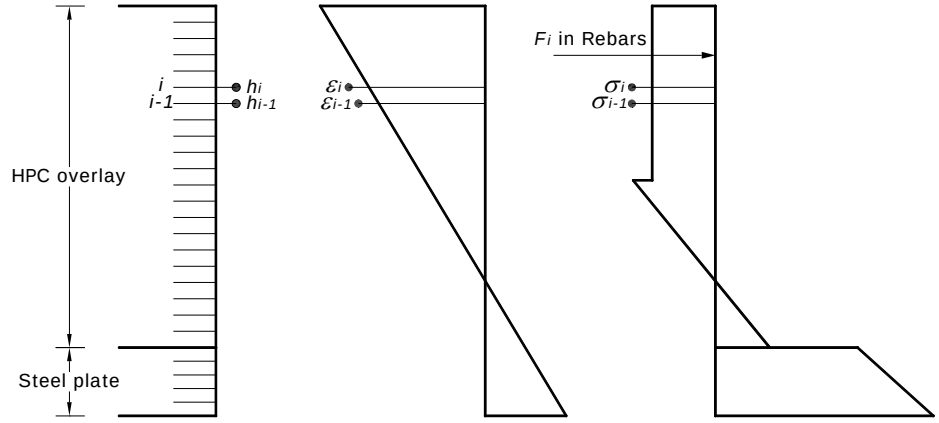

Figure 4: Procedure of multi-layer simulation

Along the whole cross section, the horizontal forces in each layer shall be in equilibrium, so:

$$F = \sum \frac{1}{2}(\sigma_i + \sigma_{i-1})(h_i - h_{i-1}) + \sum F_i = 0 \qquad (1)$$

The total bending moment of the cross section is formulated as:

$$M = \sum \frac{1}{4} t(\sigma_i + \sigma_{i-1})(h_i - h_{i-1})(h_i + h_{i-1} - 2x) + \sum F_i h_i \qquad (2)$$

in which:

- h_i is the position of node *i* in the cross section
- σ_i is the stress at given node *i*
- F_i is the horizontal force of rebar *i* in the cross section
- ε_i is the strain of a given node *i*, $\varepsilon_i = \kappa\ (h_i - x)$
- κ is the curvature of the cross section.

For a given cross sectional curvature κ, the position of the neutral axis *x* is calculated first from the equilibrium equation by an iteration process. For a given *x*, the bending moment of the section *M* under a certain curvature can be determined, and the moment-curvature relationship of the cross section is plotted.

4 Assessment with four-point bending test

Shionaga [10] has carried out a number of four-point bending tests on UHPC plate elements with various fiber volumes and reinforcement, Fig. 5. The dimensions of the specimens, the content of fibers and the reinforcement are in the same order of magnitude as the concrete overlay of the composite deck plate. Thus, it is believed that the test results are

representative enough to assess the assumed UHPC constitutive relationship with the multi-layered model presented in this study. Furthermore, this proved design method can be applied in estimating the negative bending performance of the composite deck plate, since one can find comparable stress distributions in both conditions.

In general 3 configurations are involved in the test program, with different number of rebars. With each configuration, specimens of 3 fiber volume percentages are tested, namely Vol% = 0%, Vol = 0.8% and Vol = 1.6%. In order to check the influence of the fiber distribution, the specimens with no reinforcing rebar are divided into two groups, according to their casting directions. For more detailed information reference is made to [10].

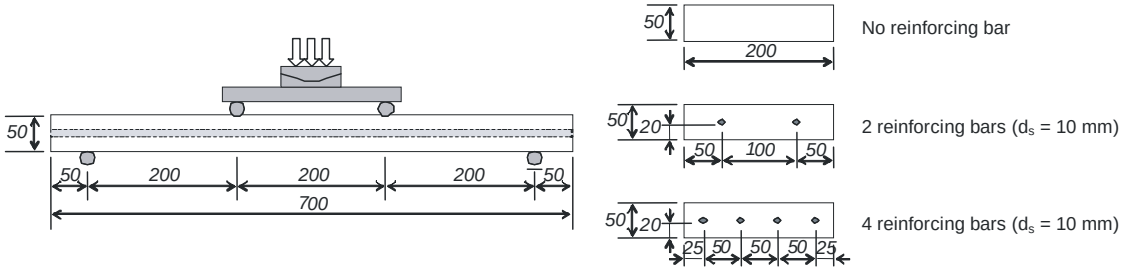

Figure 5: 4 point bending test configurations according to Shionaga [10]

The moment-curvature relationship computed from the multi-layer model is first translated into moment-deflection relationship with:

$$W = \iint \kappa \mathrm{d}x = \frac{5}{8}\kappa l^2 \tag{3}$$

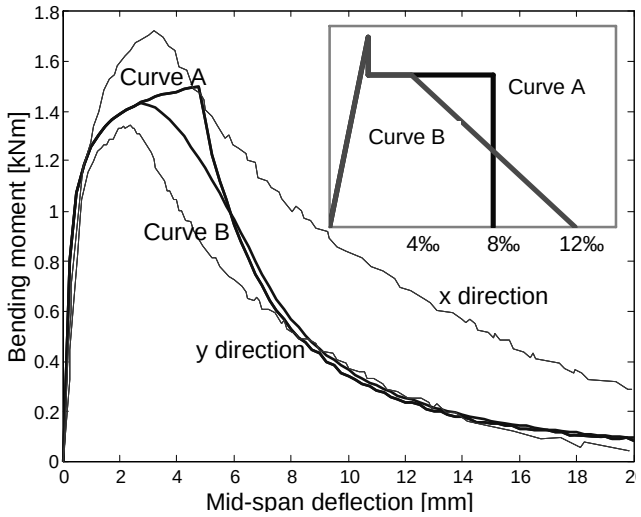

Figure 6: 4 point bending test result (no rebars) and multi-layer simulation

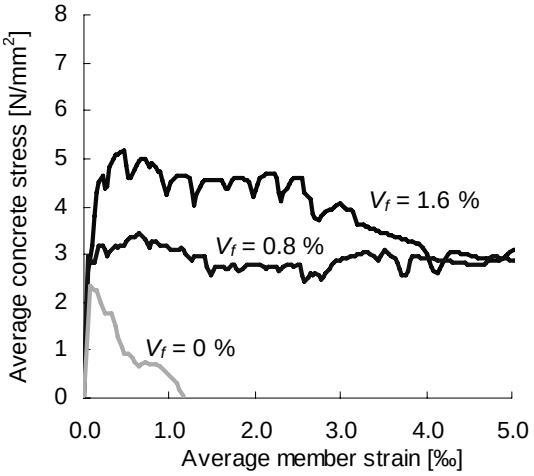

Figure 7: Average stress in fiber concrete component in tension [10]

The calculated result from the multi-layer model is plotted in Figure6 together with the test result from the four-point bending tests with V_f = 1.6 vol%. The curve named ‘x direction’ means the response of the specimen cast along the longitudinal direction of the beam, while ‘y direction’ means the specimen cast along its transverse direction. In order to check the influence of the softening branch in the stress-strain relation, another extreme condition is

considered in which $\varepsilon_3 = \varepsilon_2 = 8$ ‰ (curve A), while as was introduced before, in curve B, $\varepsilon_2 =$ 4 ‰, $\varepsilon_3 = 12$ ‰. So, the energy dissipated according to both curves is the same.

The result makes clear that both curves offer a reasonable prediction for the moment-deflection relationship of the target plate, especially before the load capacity has been reached. This comparison actually shows that a simple constitutive relation such as a perfect yielding curve might be accurate enough for designing an UHPC element. In this respect it should be noted that usually the designers are more interested in the behavior of a structural element until its load capacity is reached. Moreover, in a reinforced UHPC element, because the crack width in UHPC-element is limited by the steel rebars, the stress level in the UHPC stays at a high level even when a relatively large equivalent strain is reached. This phenomenon was observed in [10], in which uniaxial tensile tests were carried out on long centrically reinforced UHPC prismatic elements. The stress-strain response of the fiber concrete component is derived and plotted in Figure 7, where an obvious plastic plateau can be distinguished. For that reason, the constitutive relationship of UHPC is modeled as a perfectly elastic-plastic material when it is reinforced by steel rebars.

5 Implementation in the deck plate

Based on the stress-strain relationship defined before, it is possible to model the moment-curvature relationship of the steel plate with the UHPC overlay with the multi-layer model. The dimension of the target deck plate is based on the original design of the Caland Bridge as is shown in Figure. In order to check the influence of the rebar to the composite deck, three configurations have modeled in this study, being: a deck plate without rebar, a deck plate with one rebar mesh at the top, and a deck plate with two rebar meshes as the original design. The moment-curvature relationship for each case is plotted in Figure 8.

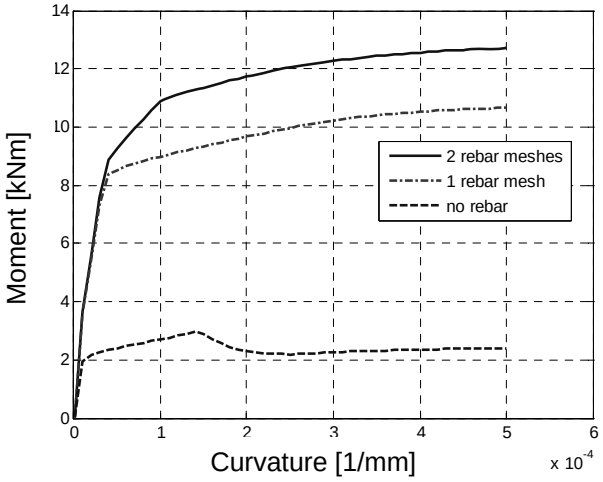

Figure 8: Comparison of different reinforce ment configurations

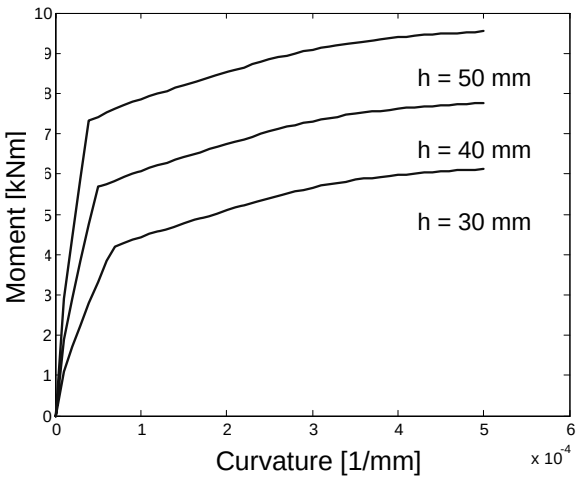

Figure 9: Influence of overlay thickness on the bending behavior

To compare these curves with the design load on the bridge, Load Model 1, defined in Eurocode 1 is used to estimate the maximum negative moment in the deck plate. Under the maximum axial load applied on the deck (300 kN, 400 × 400 mm), the maximum bending

moment at the joint of the deck plate, trough and the cross beam is 1.4 kNm. The capacity of the UHPC overlay without reinforcement is sufficient to withstand the maximum traffic load.

In Figure 8, one can also find that a rebar mesh at the top side of the UHPC overlay can increase the bending capacity of the composite plate greatly. Clearly, this is because the mentioned rebar mesh is within the tensile zone of the composite element. That also explains why the second reinforcement mesh is less effective to the bending capacity. Also, the increased ductility of the UHPC due to the reinforcement results in an increase of the bending capacity. The reinforcement in the UHPC delays the softening effect of the UHPC, by distributing the cracks in a more optimized way. Based on that, one can conclude that rebars in a UHPC overlay can increase the load capacity of the whole element by two means, namely transferring the tensile stress across the cracks and uniformly distributing the cracks.

The previous conclusions offer several improvement suggestions for the original design of the deck system of Caland Bridge. First of all, the second rebar mesh close to the steel plate seems to be unnecessary. Because of the good connection between concrete overlay and the steel plate reported before, it is reasonable to treat the steel plate as reinforcement during the calculation. On the other hand, as explained before, the rebar mesh at the top side of the overlay is essential, even though the load capacity of the whole element becomes very conservative compared to the design traffic load. Thus, a positive option to optimize the overlay design is to reduce the thickness of the concrete topping. In Figure 9, the influence of the overlay thickness on the bending behavior of the composite deck plate is plotted, where an UHPC overlay of 30 mm thick seems to be still sufficient to withstand the design traffic load. With the classic beam theory, the cracking moment of this composite beam can be easily formulated as:

$$M_{cr} = \frac{(h_c^2 + 2nh_s h_c + nh_s^2)^2}{6(h_c + nh_s)^2} tf \tag{4}$$

For a UHPC overlay with thickness of 30 mm and 40 mm, the cracking moment is 1.4 kNm and 0.9 kNm respectively. Thus an UHPC overlay of 30 mm is supposed to be sufficient, including the safety factor corresponding.

6 Conclusions

In this paper, a relatively new system to strengthen an existing bridge deck plate with reinforced UHPC is investigated. A simplified equivalent stress-strain relationship is introduced based on direct tensile test results.

The newly derived constitutive relation is then implemented in a so called multi-layer model and validated by four-point bending test results. Different softening curves are used during that process: the result turns out that they do not influence the bending behavior before the maximum load is reached, although a linear softening curve offers more accuracy in simulating the post-peak behavior of the specimen. Furthermore, the UHPC is suggested to be a plastic material when the influence of the rebars is included.

The proven multi-layer model is then employed in modeling the bending behavior of the composite deck plate. The original configuration of the Caland Bridge is proven to be

conservative according to this model. To improve the material efficiency of the deck design, one rebar mesh with reduced overlay thickness is suggested. Further study is still needed to check the suggestions for optimization.

7 References

[1] Jong, F.B.P.d., Renovation technique for fatigue cracked orthotropic steel bridge decks. 2007, delft. 457.

[2] Petitjean, J. and J. Resplendino. French recommendations for Ultra-Hihg Performance Fiber-Reinforced Concrete. In 6th International Sympsium on High Performance Concrete: 485-496.

[3] Walter, R., Cement-Based Overlay for Othotropic Steel Bridge Decks: A Multi-Scale Modelling Approach, in Department of civil engineering. 2005, Technical Univercity of Denmark.

[4] Li, V.C., On Engineered Cementitious Composites (ECC): A Review of the Matrtial and Its Applications. Juornal of Advanced Concrete Technology, 2003. 1(3): p. 215-230.

[5] Braam, C.R., P. Buitelaar, and N. Kaptijn, Reinforced high performance concrete overlay system for steel bridges, in 5th Int. CROW-workshop, on Fundimental Modelling of the Design and performance of Concrete Pavement. 2003.

[6] Naaman, A.E. and H.W. Reinhardt, Proposed classification of HPFRC composites based on their tensile response. Materials and Structures, 2006(39): p. 547-555.

[7] Marković, I., High-Performance Hybrid-Fibre Concrete. 2006, Technische Universiteit Delft: Delft. p. 103-159.

[8] Aveston, J., G.A. Cooper, and A. Kelly. Single and multiple fracture. in The properties of fibre composites. 1971. National Physical Laboratory.

[9] Li, V.C. and C.K.Y. Leung, Steady-State Multiple Cracking of Short Random Fiber Composites. Journal of Engineering Mechanics, 1992. 118(11): p. 2246-2264.

[10] Shionaga, R., et al., Combined effect of steel fibers and steel reinforcing bars in High Performance Fiber Reinforced Concrete.

[11] Kooiman, A.G., C.v.d. Veen, and J.C. Walraven, Modelling the Post-Cracking Behaviour of Steel Fibre Reinforced Concrete for Structural Design Purposes. Heron, 2000. 45(4): p. 275-307.

Cornelius Oesterlee
Dipl. Ing., Civil Engineer
EPFL
Lausanne, Switzerland

Hamid Sadouki
Senior Scientist, Dr., Material Science
EPFL
Lausanne, Switzerland

Eugen Brühwiler
Prof., Dr., Civil Engineer
EPFL
Lausanne, Switzerland

Structural analysis of a composite bridge girder combining UHPFRC and reinforced concrete

Summary

Reinforced concrete being the most applied construction material today performs very well in most applications but still lacks durability under severe environmental conditions. Especially existing structures built decades ago show degradation. Using Ultra-High Performance Fiber Reinforced Concrete (UHPFRC) to improve durability is a promising option seeing the extraordinary performance of this material when applied in a composite section. Restrained shrinkage of the overlay plays an important role in this type of application.

A conceptual bridge cross section combining UHPFRC and reinforced concrete has been numerically analysed. Two main parameters, tensile strength and strain hardening capacity, were varied. The analysis indicates the importance of strain hardening of UHPFRC and the influence of its tensile strength on the structural response under restrained shrinkage (deformation controlled loading) and traffic loads (force controlled loading). The results validate the concept of using a UHPFRC layer to improve the structural durability of concrete constructions.

Keywords: *UHPFRC, composite structure, variability, strain hardening, FE-Analysis*

1 Introduction

Ultra-High Performance Fiber Reinforced Concrete (UHPFRC) defines a class of strain hardening – softening cementitious composites with outstanding performance in terms of mechanical properties and durability. High fiber dosage and high quantities of reactive powders make these materials rather expensive compared to normal reinforced concrete, and therefore besides other reasons not appropriate for mass applications in massive structural elements. Applications turn out to be efficient only if several of the outstanding properties of UHPFRC are exploited to a maximum, especially its high compressive and tensile strength, its capacity for strain hardening and softening and its very low permeability towards water and aggressive substances. This requires new ways of design and construction leading to structural elements combining different types of concrete. At the

same time it has the potential to solve the major problem of reinforced concrete structures: durability. Applying UHPFRC locally to “harden” the most severely exposed zones of a structure helps to improve durability and load bearing capacity. This scheme replies effectively to the above pointed out issues.

The present paper shows findings of a FE-analysis of a conceptual bridge girder design combining a thin UHPFRC overlay with a reinforced concrete substructure (Figure 1) [1]. Besides its load carrying contribution, the UHPFRC overlay replaces conventional waterproofing membrane. Therefore it has to remain in an impermeable state under service conditions and during the whole service life in order to protect effectively the conventional reinforced concrete structure below. The present structural analysis focuses thus on the serviceability limit state of the structure.

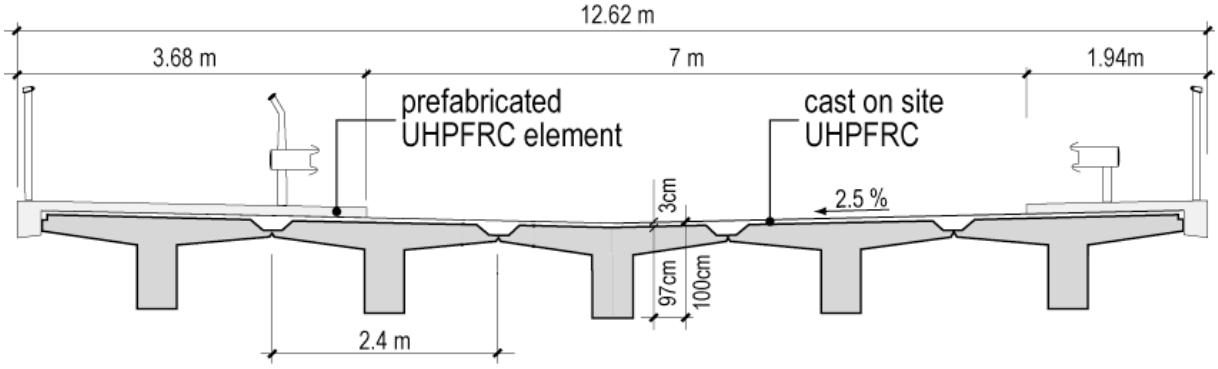

Figure 1: Cross section of the composite bridge girder [1]

2 Constitutive material modelling of UHPFRC

2.1 Requirements

The UHPFRC designed for this application responds to the following general requirements:

- high compressive and tensile strengths
- strain hardening and softening in tension
- very low permeability
- self-compacting fresh mix with the ability to be cast with a slope of 3%
- low variability of mechanical properties

Details about UHPFRC mixes fulfilling these requirements can be found in [2, 3, 5].

2.2 Tensile behaviour

High tensile strength as well as strain hardening and softening are characterising properties of UHPFRC. The uniaxial tensile behaviour was determined using dogbone specimens. The results of several experiments were averaged (Figure 2a) and transformed into the constitutive material law for tension (Figure 2b) as input for the FE-program.

2.3 Viscoelastic behaviour

UHPFRC develops important shrinkage (mostly autogenous shrinkage) which leads to Eigenstresses in the composite element due to the restrained deformation conditions. Free shrinkage under drying conditions reaches up to 590 µm/m after 1 year with an evolution of 2/3 of the value after 35 days [2]. Induced stresses are partly balanced as a function of time

by an important creep and relaxation capacity. The high dosage of fibers (9%) prevents micoracking of the matrix and provides a high deformation capacity. Both effects are crucial for the proper working of the UHPFRC-layer regarding mechanical and physical requirements. Input data for the FE-analysis were deduced from comprehensive laboratory tests on the evolution of mechanical and physical properties depending on maturity [2, 3, 5].

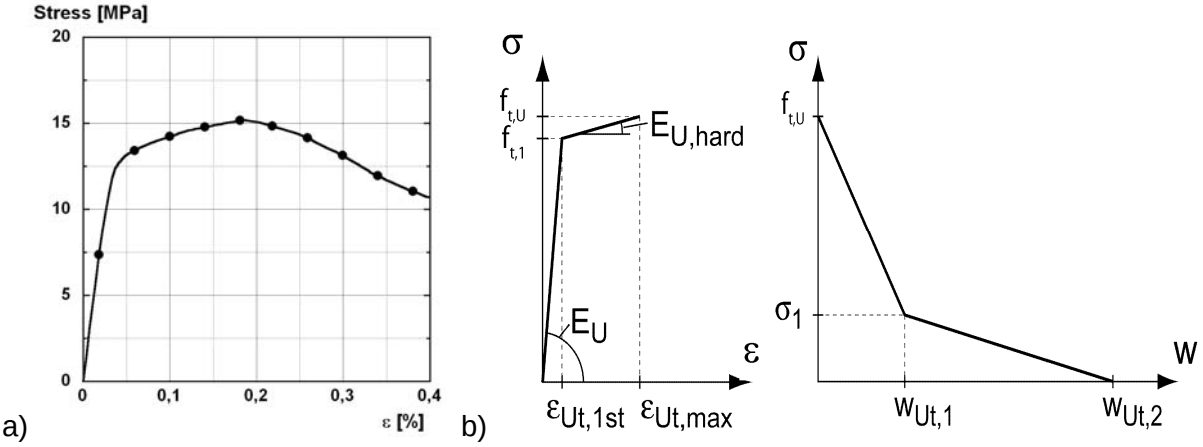

Figure 2: a) Stress-strain diagram from experiments [3] and b) corresponding constitutive tensile law for FE-analysis input

2.4 Variability of mechanical properties

An inherent property of fiber reinforced composites is the non-uniform fiber orientation and distribution depending on the mixing process, casting method and formwork boundaries [3]. This was taken into account in the FE-analysis by varying the values of tensile strength and deformation capacity (Figure 3).

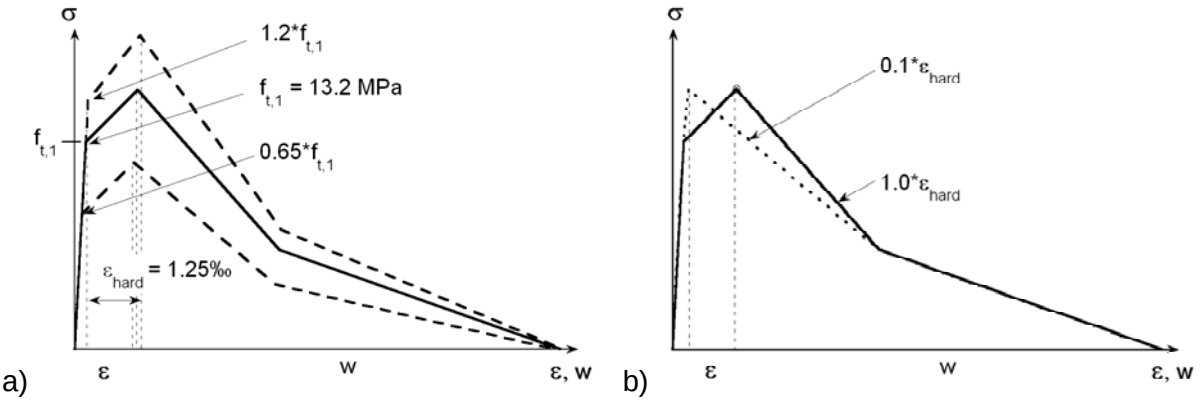

Figure 3: Variation of a) tensile strength f_t and b) deformation capacity ε_{hard}

The tensile strength, defined as elastic limit of the material, was modified to 65% and 120% of the reference value $f_{t,1}$=13.2MPa (Figure 3a), while the strain hardening, defined as the deformation between $f_{t,1}$ and the ultimate tensile strength $f_{t,U}$, was modified between 10% and 100% of the reference value $\varepsilon_{hard} = \varepsilon_{Ut,max}-\varepsilon_{Ut,1st}$=1.25‰, (Figure 3b). The ultimate tensile strength $f_{t,U}$ is considered to evolve with a constant factor of 1.25*$f_{t,1}$ in relation to the elastic limit.

3 FE-Analysis

3.1 Description of the numerical tool

The FE-analysis was done with FEMASSE MLS [4]. This numerical tool allows to conduct comprehensive analyses including the coupling of age dependent thermal, hygral, chemical and mechanical properties.

In the given 2-D model the deformation in z direction (longitudinal sense of the bridge girder) was not restrained. The UHPFRC layer was applied to inert concrete, cured for 7 days and afterwards exposed to environmental conditions described by constant values at a temperature of 20°C. The numerical analysis starts at the instant of the UHPFRC overlay casting (time 0).

The structural analysis can be considered as representative regarding the observations made concerning the age-dependent variation of stresses and mechanical properties in the present structural element.

3.2 Cross sectional model

The model represents an exemplary transversal cross section of the bridge girder near the support, showing 5 (prefabricated) T-beams in conventional prestressed concrete with the UHPFRC overlay (Figure 4). The bottoms of the beams are vertically and horizontally fixed limiting the flexional deformability of the bridge deck to a minimum and increasing the degree of restraint to a maximum.

The loads are transferred laterally by the UHPFRC that also connects the longitudinal beams. The thickness of the layer is increased at the longitudinal joints to 15 cm instead of 3 cm on top of the T-beams.

In general, viscoelastic behaviour of the T-beams is beneficial for the stress evolution in the UHPFRC since it indirectly reduces the degree of restraint but this effect was not considered in the analysis.

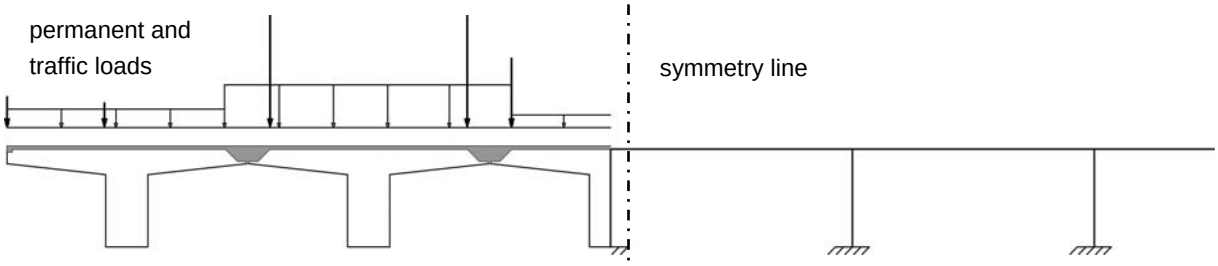

Figure 4: Transversal bridge section with UHPFRC layer, exemplary loading scheme and static system

3.3 Load cases

The following load cases were considered in the modelling:

- Permanent loads due to self weight of the structure and the UHPFRC layer
- Permanent loads due to self weight of non-load bearing elements such as the curbs, crash barriers, railings and the asphalt layer, applied at 28 days

- Traffic loads at serviceability limit state including two traffic lanes according to EC 1 [6], applied at the most unfavourable position regarding stresses in the UHPFRC layer in the transversal sense

All external loads are superimposed to the continuous evolution of the mechanical and physical properties of UHPFRC such as Young's modulus, compressive and tensile strength, shrinkage and viscoelasticity.

4 Results

The results of the numerical simulation are presented exemplarily for a typical reference point showing highest stresses:

4.1 Restrained shrinkage

Restrained shrinkage is the load case the UHPFRC overlay is subjected to from the very beginning (after casting) and also the one that consumes an important part of the resistance capacity of the material. It is a deformation controlled loading process, and consequently, it is the deformation capacity of the material that predominantly replies to this load case (Figure 5). The absolute value of the tensile strength is not of great importance here. Depending on the level of the evolving tensile strength, shrinkage causes Eigenstresses that almost reach the elastic tensile strength $f_{t,1}$ before the external loads are applied. If the UHPFRC overlay is stressed beyond its elastic limit due to restrained shrinkage it enters into the hardening domain where it possesses an important deformation capacity, i.e. the stress increase at this stage will be very small. In this way, the strain hardening behaviour represents a significant stress release potential which is essential for the structural response of the overlay in terms of avoidance of macrocrack localisation and maintaining the low permeability of the UHPFRC layer.

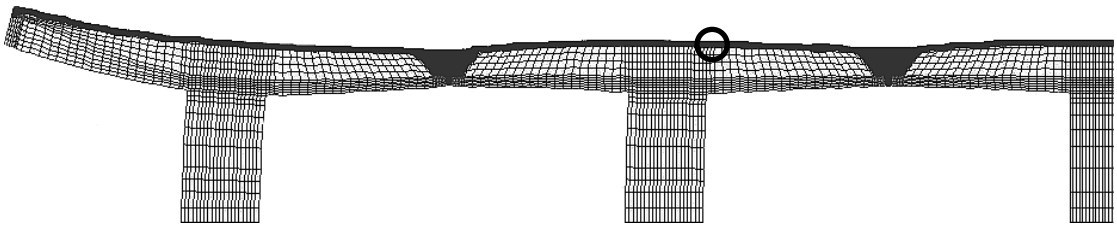

Figure 5: Deformed shape (not in scale) due to shrinkage of UHPFRC (without external loads) and location of the reference point

4.2 Permanent and traffic loads

Permanent and traffic loads are applied 28 days (672 h) after the application of UHPFRC. They represent a force controlled load case. The UHPFRC layer is subjected to an immediate stress increase which is superimposed to the stresses induced by restrained shrinkage.

Figure 7 shows the stress and strength evolution in the UHPFRC layer on the time axis until 42 days (1000 h) for three cases. The lower dotted lines represent the elastic strength evolution $f_{t,1}$ whereas the upper dotted lines show the evolution of the ultimate strength $f_{t,U}$.

The solid lines describe the stress evolution at the reference point. The step in the solid lines marks the point in time of external load application.

- In case of $f_{t,1}=0.65*f_{t,1,ref}$ (Figure 6a) the stresses due to restrained shrinkage reach the elastic limit before the external loads are applied. The application of these creates an inelastic response in the hardening domain. The important deformability of the strain hardening domain keeps the stress level in the UHPFRC layer very close to its elastic limit. The ongoing shrinkage does not significantly raise the stresses. The stress evolution closely follows the elastic strength evolution.
- In case of $f_{t,1,ref}$ (Figure 6b) the stress increase due to the external loads at 28 days is balanced partly by an elastic response and partly by the strain hardening of UHPFRC. The global behaviour is again similar. Once the stress level exceeds the elastic limit further stress increase is very small.
- In case of $f_{t,1}=1.2*f_{t,1,\,ref}$ (Figure 6c) external loads lead to a purely elastic response of the overlay. The loads induce a principal tensile stress of approximately 3 MPa at the reference point. Further stress increase is then induced by the continuing shrinkage until the stress level reaches the elastic limit and subsequently follows it.

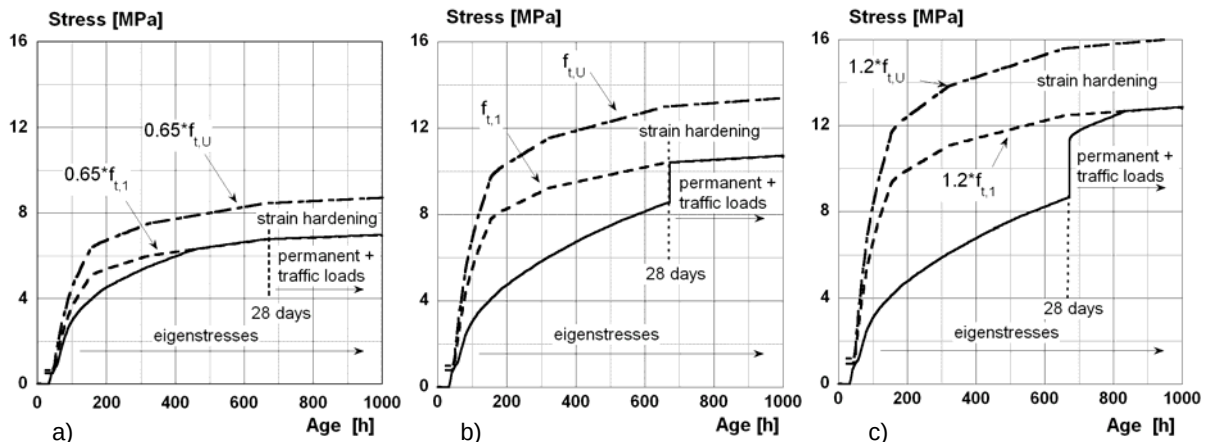

Figure 6: Evolution of stress and strength for a) $0.65*f_{t,1}$; b) $1*f_{t,1}$ and c) $1.2*f_{t,1}$

In all the cases, it can be seen that once the material exceeds its elastic limit strength external loads and continuing shrinkage do not cause a significant further stress increase. The redistribution of loads and increased deformability due to the pronounced strain hardening behaviour and loss of stiffness prevent further stress increase in the UHPFRC layer. Therefore, it is unlikely that the ultimate tensile strength $f_{t,U}$ of the UHPFRC is reached. The UHPFRC layer thus remains at the initial stage of multiple microcracking without developing localised macrocracks. The material enters merely very little into the hardening domain, thus keeping its low permeability. It is not subjected to softening within the considered period of 1000 h.

An exemplary simulation with traffic loads increased by a hypothetical factor of 3 shows that in fact the stress step continues significantly into the hardening domain if the level of loading is sufficiently high (Figure 7a). Then the stresses evolve parallel to the elastic tensile strength

but at a higher level. UHPFRC seems to possess enormous reserves in a setup as described above to resist localised cracking even if its elastic tensile strength is exceeded.
In case the strain hardening capacity is reduced significantly the UHPFRC overlay obviously enters far into the hardening domain, (Figure 7b). The two lines with markers show the stress evolution at a reference point for two materials with $0.1*\varepsilon_{hard,ref}$ (upper line with square markers) and full strain hardening capacity (lower line with round markers).

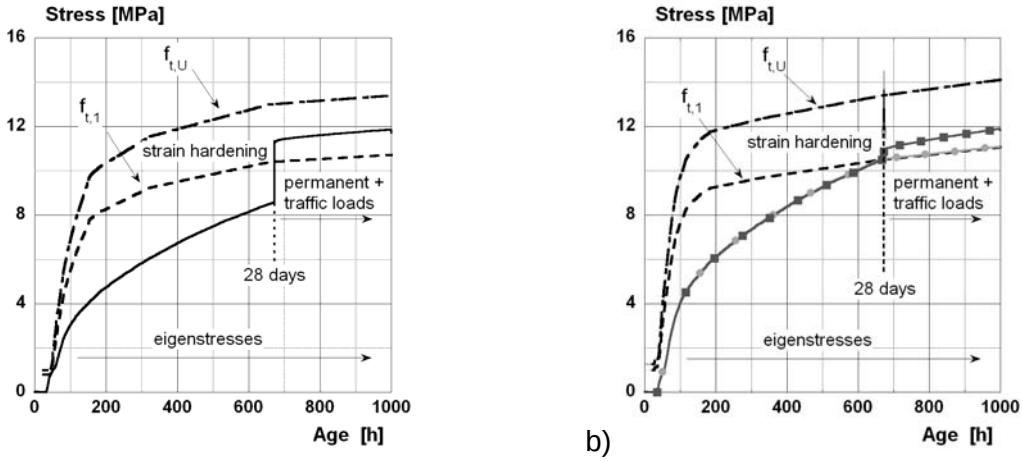

Figure 7: a) Evolution of stress and strength for $1.0*f_{t,1}$ and three times the external loads; b) influence of ε_{hard} on the stress level for $\varepsilon_{hard}=0.1*\varepsilon_{hard,ref}$

4.3 Serviceability and waterproofing

Charron et al. [7] have shown for a UHPFRC respecting the requirements given in 2.1 that the water permeability of UHPFRC remains low ($K_{w\ equiv} < 2 \times 10^{-8}$ cm/s) until a tensile deformation of 1.3‰. This threshold deformation corresponds to a cumulated crack opening equal to 0.13 mm as compared to 0.05 mm for normal concrete. Since the numerical results show that at all levels of tensile strength the principal stresses in the UHPFRC overlay do not significantly enter into the strain hardening domain, the proposed concept of an "impermeable" and waterproof UHPFRC layer is validated.

5 Conclusions

A structural analysis of a composite bridge girder combining reinforced concrete and UHPFRC at the serviceability limit state was performed. The structural response of the UHPFRC layer under combined loading due to restrained shrinkage and traffic loads was investigated. The obtained results show:

- Restrained shrinkage and external loads may generate stresses close to the elastic tensile strength in the UHPFRC overlay of the composite element with a high degree of restraint. The stresses then follow the age-dependent elastic strength evolution of UHPFRC.
- The evolution of applied stresses in the strain hardening domain is independent of the level of the elastic tensile strength. The loss of stiffness of the UHPFRC layer as it enters into the hardening domain causes a stress release and redistribution.

- The risk of transverse cracking of the UHPFRC layer in the presented structural configuration is unlikely due to the increased deformation capacity and significantly lower stiffness at strain hardening.
- Strain hardening is an essential property for the described type of application since it allows maintaining the low permeability of UHPFRC in its function as waterproofing layer.

6 References

[1] Brühwiler, E., Fehling, E., Bunje, K., Pelke, E. 2007., Design of an innovative composite road bridge combining reinforced concrete with Ultra-High Performance Fibre Reinforced Concrete. Proceedings, IABSE Symposium “Improving Infrastructure Worldwide”, Weimar, September 2007.

[2] Kamen A. (2007) Comportement au jeune âge et différé d’un BFUP écrouissant sous les effets thermomécaniques. Doctoral thesis n° 3827, Swiss Federal Institute of Technology Lausanne (EPFL), Switzerland.

[3] Wuest J. (2007) Comportement structural des bétons de fibres ultra performant en traction dans des éléments composés. Doctoral thesis in press, Swiss Federal Institute of Technology Lausanne (EPFL), Switzerland.

[4] Roelfstra P. E., Salet A. M., Kuiks J. E. (1994) Defining and application of stress-analysis-based temperature difference limits to prevent early-age cracking in concrete structures. Proceedings n 25 of the International RILEM Symposium: Thermal cracking in concrete at early age, pp. 273-280. Munich, Germany.

[5] Habel, K. (2004) Structural behaviour of elements combining ultra-high performance fibre reinforced concretes (UHPFRC) and reinforced concrete. Doctoral thesis n° 3036, Swiss Federal Institute of Technology Lausanne (EPFL), Switzerland.

[6] Eurocode 1: Einwirkungen auf Tragwerke - Teil 2: Verkehrslasten auf Brücken; Deutsche Fassung EN 1991-2:2003

[7] Charron, J.-P., Denarié, E., Brühwiler, E. (2007) Permeability of Ultra High Performance Fiber Reinforced Concretes (UHPFRC) under high stresses. Materials and Structures, 40, n°3, pp 269-277.

Cornelia Schmidt
Referat III A2
Ministerium für Bauen und Verkehr NRW
Düsseldorf, Germany

Dr. Steffen Riedl
FG Bau und Erhaltung von Verkehrswegen
Universität Kassel
Kassel, Germany

Carsten Geisenhanslüke
FG Werkstoffe des Bauwesens
Universität Kassel
Kassel, Germany

Prof. Michael Schmidt
FG Werkstoffe des Bauwesens
Universität Kassel
Kassel, Germany

Strengthening and Rehabilitation of Pavements Applying Thin Layers of Reinforced Ultra-High-Performance Concrete (UHPC-White topping)

Summary

“White topping” means the improvement or the rehabilitation of fatigued bituminous or concrete road pavements by applying a new concrete layer using the existing structure as base course. This method is known since the 1920th when it was firstly performed in the USA. Up to now as a rule, ordinary concrete is used and the thickness so far is equivalent to those of newly paved structures depending e.g. on the intensity of the traffic and the load bearing capacity of the base. Only in a few cases even thinner overlays were applied [1].

A new technology is white topping of heavily trafficed pavements with thin layers of only 60 to 80 mm consisting of continuously reinforced High- (HPC) or Ultra-High-Performance (UHPC) concretes. The method is appropriate to strengthen the load bearing capacity of existing pavements preventively to enable it to withstand the increasing intensity of the traffic or to restore fatigued structures already showing structural damages. Due to the high quality of the concretes used the system is assumed to be very durable and long lasting. The technology is both economic and sustainable because of the facts that no material from the existing pavement has to be removed and to be replaced and only a minimum of material is needed for the overlay. The thin overlay can be applied within a short time so that the obstruction of traffic is minimized. A small test section has already be performed [2].

In a comprehensive research project coordinated by the Federal Highway Research Institute (BAST), supported by the State of Nordrhein-Westfalen (NRW) and primarily performed by the University of Kassel the technical and economic aspects of the new technique are studied covering the development of adequate concretes as well as the design of the pavement structure and its long time load bearing behaviour under dynamic traffic loads. The economic efficiency will be compared to traditional rehabilitation measures considering the whole life-cycle.

1 High- an Ultra-High-Performance concrete

High Performance Concrete is already part of the European Concrete Standard EN 206 and of the German Standard DIN 1045-2 [3]. It is defined by its compressive strength ranging from strength class C55/67 to C100/115. It has already been applied for structural concrete members e.g. for bridges and sky scrapers and in a few case for pavement layers. From strength class C80/95 upwards usually silica fume is used as concrete additive to further increasing both the strength and the structural density.

Ultra-High-Performance Concrete is primarily characterized by a compressive strength of 150 to 220 N/mm^2 and by a very dense and non permeable microstructure free of capillary pores. The very low porosity of the matrix originates from both a low w/c-ratio of about 0.20 and a very dense packing of the fine particles due to the use of different mineral additions like silica fume and quartz or other finely ground stone powders [4].

Table 1: Raw materials and mix design of the UHPC and the HPC

Raw Materials	**Amount in kg per m^3 Concrete**		
	UHPC [4]	**UHPC- WT [1)]**	**HPC-WT**
CEM I 52,5R HS-NA	650	725	400
Quartz W12 (Blaine 4,200 cm²/g)	325	223	-
Quartz W3 (Blaine 1,300 cm²/g)	131	146	-
Silica fume MS 971	177	123	80
Amount of fines < 0.125 mm	1283	1217	480
Sand 0/0.5	354	395	-
Sand 0/2	-	-	710
Basalt 2/5	299	333	598
Basalt 5/8	299	333	598
Steel fibres 0.15/9 mm	195 (2.5 vol.-%)	87 (1 vol.-%)	87 (1 vol.-%)
Water	158	160	140
Superplasticizer (PCE based)	30.4	16.7	6
w/(c + ms) – ratio	0.19	0.19	0.29
Standard test			
Spread (DIN EN 12350-5) [cm]	55	45	45
Compressive strength 7 d [MPa]	188	168	75
28d [MPa]	205	190	112
Modulus of Elasticity 28 days [MPa]		49.000	44.000

[1)] further rheological optimization in progress

Concretes used for pavement layers have to be adequately workable to be placed, compacted and finished by a customary concrete paver. They had to fulfil the strength levels of HPC (min. 85 N/mm^2) or UHPC (min. 150 N/mm^2) and have to be sufficiently ductile to be able to withstand the high traffic loads despite of the low thickness of the layer of 60 – 80 mm

only. In addition the microstructure must be sufficiently dense to withstand attacks of frost and de-icing salts and to prevent the reinforcement from corrosion caused by chloride ions.
The raw materials used and the mixes developed are given in table 1 together with the spread of the fresh concretes and their 7 and 28-days compressive strength. The tests performed to evaluate the workability, the mechanical behaviour and the durability are listed in table 2. At the time being most of them are still under progress. The results will be presented at the Symposium.

Table 2: Laboratory Tests and Test Procedures[1)]

Criteria	**Test Procedure**
Workability and stiffening	Spread acc. to DIN EN 12350-5; 10,20,30,60 min after mixing
Compressive strength (1, 2, 7, 28, 59 days)	Cylinders 150x300 mm, cubes 150 mm Acc. to DIN EN 12390-3:2000-04
Bending tensile strength (1, 2, 7, 28, 56 days)	Beams 150x150x700 mm, 4-point loading, strain controlled Acc. to [9]
Mod. Of Elasticity	Ultrasonic device
Porosity and pore size	Mercury Intrusion (at 28 days)
Frost resistance with salt	CDF-procedure acc. to [10] (3% NaCl-solution)
Cloride diffusion (28 days)	Procedure acc. to [11]
Shrinkage	Cyl. 150/300 mm, unrestrained, 20°C/65% r. hum.
Carbonation	20°C, 65% r. hum.

[1)] partly in progress

The UHPC developed principally based upon a coarse grained and nearly self compacting concrete with a maximum grain size of 8 mm and 2.5 vol.-% of steel fibres, that had already been designed for prefabricated concrete members [4]. Primarily the consistency of the concrete had to be modified to become more stable when being placed and finished. In a first step the amounts of superplasticizer, silica fume and steel fibres were reduced and thus the spread was reduced from about 55 to 45 cm. Actions are in progress to further reduce the stickiness of the mixture to ease the mixing and handling of the concrete on site. The HPC-WT corresponds to strength class C100/115 of DIN EN 206. The compressive strength of the UHPC-WT exceeded the limit of 150 N/mm^2 by about 25%.

2 Design of the pavement structure

The design of the reinforced overlay primarily covers the determination of its adequate thickness in relation to the traffic loads expected and the load bearing capacity of the existing structure. In addition the minimum amount of reinforcement being necessary to limit the crack width to less than 0.1 mm to protect the reinforcement from corrosion due to chloride penetration has to be calculated. Full bond between the overlay and the concrete slabs underneath was assumed.

To minimize the crack width in the HPC layer the procedure described in DIN 1045-1 [3] for structural members made of reinforced concrete up to strength class C100/115 was used. UHPC however is more brittle and its post cracking behavior is usually modified by the addition of steel fibers. In [5] an appropriate model was developed considering the effect of both the conventional reinforcement and the steel fibers. 7.75 cm²/m of steel is adequate to limit the crack width to 0.1 mm, if 8 mm steel bars are used.
For concrete up to strength class C 100/115 the minimum concrete cover protecting the steel bars resulting from DIN 1045-1 would have been 55 mm. As a rule High Strength Concrete shows a slightly and UHPC a significantly denser microstructure and thus a substantially reduced permeability to e.g. chloride ions. That allows for a reduction to about 25 mm (UHPC) to 30 mm (HPC) covered by the practical experiences gained with HPC-overlays on bridge decks [6].
For the design of continuously reinforced concrete “white topping” layers on top of an inhomogeneous fatigued concrete pavement an FE-model commonly used for the design of conventional pavement structures was modified. In a first step it was applied to design an appropriate laboratory model structure to test the behavior of the structure under dynamic wheel loads. The material properties considered are as given in table 1. The “base-course” system (see chapter 4) was characterized by an E-modulus of 20.000 N/mm^2.

The model structure tests confirmed the assumptions made for the pre-design in so far as the white topping layers after 1 Mio. load cycles did not show any structural degradation. The deformations and the stresses measured during the tests were used to calibrate the FE-model. The calculations resulted in a maximum tensile stress of 1,68 N/mm² at the bottom and 0.60 N/mm^2 at the surface of the HPC/UHPC-layer both being much smaller than the direct tensile strength of e.g. 4-8 N/mm^2 of fiber reinforced HPC and UHPC [4].

3 Tests on model scale structures

The model scale pavement structure tested in the laboratory had an extension of 5.00 x 2.50 m. It consisted of 8 prefabricated concrete slabs (each 1.25 x 1.25 x 0.26 m) based on an elastic mat representing cracked slabs of an fatigued and instable concrete pavement with a reduced load bearing capacity, see fig. 1. The joints were undoweled. According to the pre-design the HPC/UHPC overlay was 60 mm thick. They were reinforced with steel fabric mats (D = 8 mm) as calculated in chapter 2. To simulate the load situation under a truck’s wheel 1 Mio. cycles of a sinusoidal load (upper load level 60 kN (test 1, UHPC) resp. 70 kN (Test 2, HPC), lower level 15 kN, frequency 2 Hz) were applied on the white topping layer right above (test 1) or directly beneath the joint-crossing of the 4 center slabs, see fig. 2. At this position the load is assumed to induce the maximum stresses and strains in the HPC/UHPC layer due to the minimum load bearing capacity of the concrete slabs underneath. The loads represented a 120 or 140 kN single wheel axel of a lorry. The load was generated by one (test 1) or 2 (test 2) hydraulic pulsating cylinders installed in a stiff test frame as shown in fig.2. The loading plates had a diameter of 300 mm. In the second test (test 2, HPC) the loads alternated among the two cylinders. The conditions were further aggravated by

implementing a hollow space between the “base“ elements and the HPC layer under one of the loads see fig. 1.

Subsequently after placing the “base“ elements and the reinforcement the concrete was mixed in a 500 l laboratory drum mixer for about 6-8 minutes and then placed in a thickness of 60 mm +/- 5 mm. Both concretes were compacted by vibration and finally finished with a static bar. The surface was immediately covered with a plastic foil. To measure the deflections occurring during the test strain gauges and extensometers were installed and 14 days after placing the concrete the loading began.

In fig. 3 the deflections at the point of loading are plotted for the first 500.000 cycles. During the first 200.000 load cycles the deformation increased. This is typical for dynamic fatigue tests due to the stabilization and rearrangement of the whole system. Thereafter a cyclic stabilization could be observed. The difference between the deformations at maximum and minimum load remained constant over the whole range of 1 Mio. cycles. That means only elastic deformations occurred indicating that the microstructure was not affected.

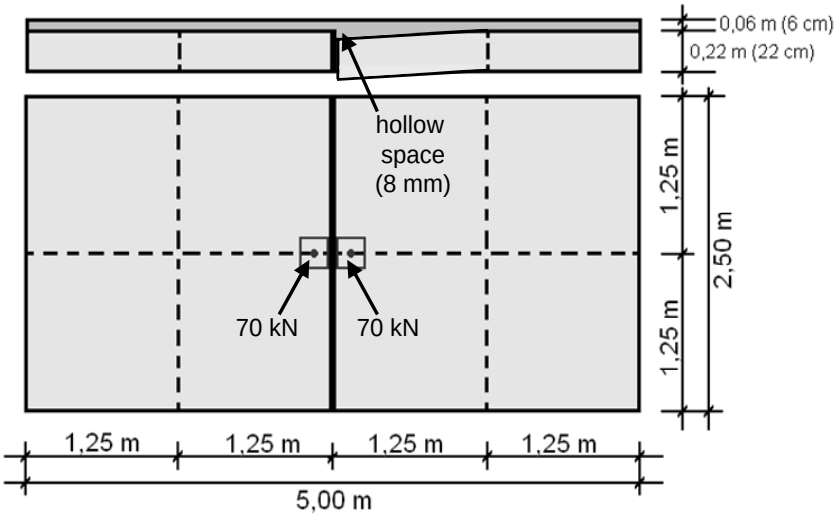

Figure 1: Details of the model test structure (test 2)

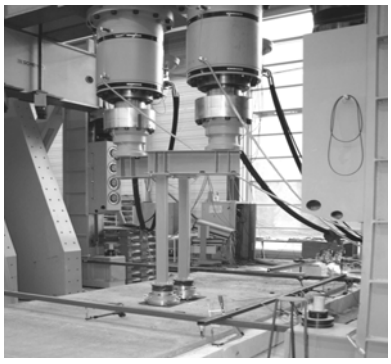

Figure 2: Model structure test installation

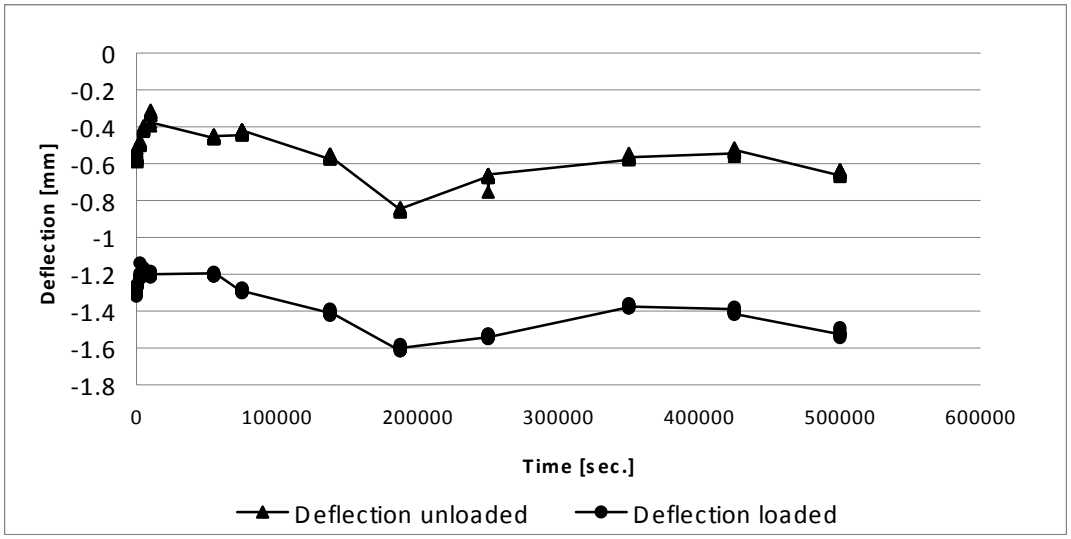

Figure 3: Deflections at the load center during the first test (1 cyclic load)

In accordance with [4] one can conclude that under the specific circumstances of the tests performed on model pavements the UHPC as well as the HPC were not stressed exceeding their pulsating fatigue strength defined as about 50% of the strength under static loads.

4 Economic feasibility study

When the technical aspects will completely be clarified an economical evaluation will follow, covering all criteria influencing costs, equivalency to alternative solutions, durability and service life. Thereto belong e.g. the reliability (**R**), the availability (**A**), the maintainability (**M**) and the safety (**S**) of the pavement system.

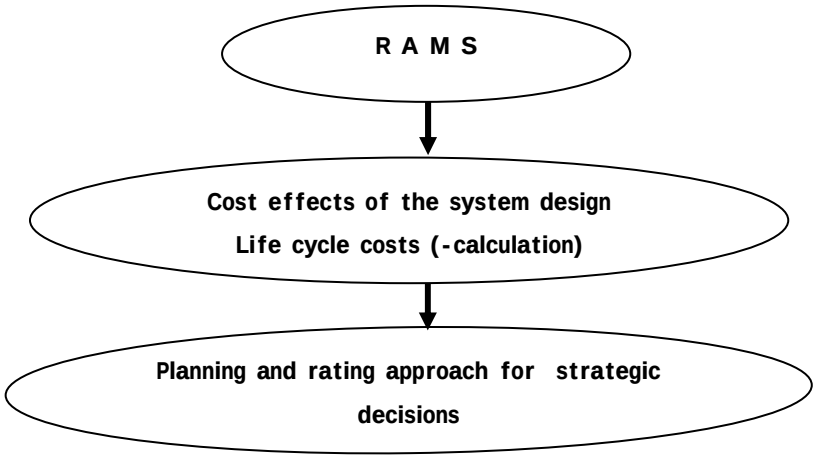

Decisive for the public road authorities acting as investor and operator are especially the avoidance of all danger of accidents resulting from an insufficient pavement condition, an acceptable travel comfort, the economical conservation of the capital assets and the environmental compatibility e.g. a low noise emission. These aims can be put into praxis by

defining both a user-oriented utility value (regarding capability and safety) and an asset value respecting the interests of the investor and the operator (conformity with requirements and quality of the existing constructional substance).

To rate the **reliability** of the system data are needed indicating how often one has to expect defects (also methodical) and defect related interruptions if the system has to be maintained or repaired (service maintenance, constructional maintenance or constructional repair) or has to be replaced (replacement). Reliable data are available for conventional pavements investigated by [7, 8]. Data for overlays consisting of HPC and UHPC will be deduced from the theoretical, laboratory and practical investigations performed in this project.

The **availability** describes the periods of time the system is in service. In addition those periods are determined where the road system is not available or the availability is restricted. These data can be used to calculate the user's costs as well. To establish the **maintainability** the amount and the kind of measures being appropriate to maintain the structure have to be documented. To be able to compare the new white topping system with alternative (traditional) solutions appropriate methods have to be developed. The maintainability has an important influence on the costs caused by repair and on the capitalized costs of maintenance. Comparable criteria will be investigated and described regarding the **safety,** e.g. concerning the durability of the surface texture once established.

The pre-mentioned criteria will be used to calculate the costs being relevant to rate the single measures as well as to rate and to compare the costs of whole pavement systems. This includes the construction, the maintenance and the user's costs as well as the costs caused by repair, rehabilitation and replacement. These costs again serve as a basis to evaluate the capitalized maintenance costs and at least of the total costs for the period of time regarded.

Within the frame of the evaluation additional parameter are of interest, e.g. the sustainability of the structure and the possible rate of recycling of the materials. The intention is to consider, whether a higher investment in the construction itself in the long term may result in lower maintenance costs and in how far costs might be reduced by improving the availability of the system and thus avoiding construction zones. These considerations all together aim at a reduction of construction costs, costs of traffic congestions and costs of accidents.

5 Practical applications

The State of Nordrhein-Westfalen has the intention to construct a test area at a parking site of the federal highway A 2 near Porta Westfalica. By midyear 2008 a lane with a length of 280 m and a width of 4.50 m exclusively used by heavy lorries will be added to an existing asphalt structure. It will consist of a base course made of ordinary concrete C 25/30 and a 60 to 80 mm HPC respectively UHPC overlay. The long time performance will be evaluated. The experiences gained with the parking lane will then be the basis for another test section on a highway lane being scheduled for 2009.

6 Summary and Perspectives

In a comprehensive research project the technical and economic feasibility of a new “white topping” technique applying thin overlays consisting of continuously reinforced High- or Ultra-High-Performance Concretes is evaluated. Theoretical design in combination with fatigue tests on a model pavement structure in the laboratory indicate a sufficient load bearing behaviour even if the thickness of the overlay is 60-80 mm only. The research is still under progress. A prototype application on a parking site used by heavy lorries is schedule for mid 2008. When the technical aspects are clarified an economical evaluation will enable to rate the life-cycle advantages of the new strengthening or rehabilitation technique.

7 References

[1] Great Falls Experimental Annual Evaluation, 2001-2003, Final Report Iowa Highway Research Board, 1996.

[2] Riffel, S.: Whitetopping - eine unkonventionelle Sanierungsmethode für Asphaltstraßen? Erste Erfahrungen und Ergebnisse vom Pilotversuch im Zementwerk Wetzlar. In: Betonzement, pp 40-44, 2005.

[3] DIN 1045-1: Tragwerke aus Beton, Stahlbeton und Spannbeton Teil 1: Bemessung und Konstruktion Ausgabe Juli 2001 mit Berichtigung Juli 2002. Beuth Verlag, Berlin.

[4] Fehling, E.; Schmidt, M.; Teichmann, T.; Bunje, K.; Bornemann, R.; Middendorf, B.: Entwicklung, Dauerhaftigkeit und Berechnung Ultra-Hochfester Betone UHPC, Schriftenreihe Baustoffe und Massivbau (Structural Materials and Engineering Series) No. 1, Kassel, 2005, ISBN 3-89958-108-3.

[5] Leutbecher, T.: Rissbildung und Tragverhalten von Ultrahochfestem Beton mit gemischter Bewehrung aus Stabstahl und Fasern unter Zugbeanspruchung; Dissertation (noch unveröffentlicht), Universität Kassel, 2007.

[6] Denkinger, M. D.; Buitelaar, P.: Ertüchtigung orthotroper Fahrbahnplatten von Stahlbrücken. In: Stahlbau, Heft 7, pp. 602-604, 2006.

[7] Rübensam, J.; Hellmann, L.; Staroste, D.; Stoltz, J.: Untersuchungen zur Wirtschaftlichkeit und bautechnischen Bewährung von Fahrbahnbefestigungen aus Asphalt und Beton auf bestehenden Bundesautobahnen. Forschung Straßenbau und Straßenverkehrstechnik, Heft 914, 2005.

[8] SEP Maerschalk: Anwenderhandbuch zum Inhalt des Pavement Management System (PMS). Hrsg. Der Bundesminister für Verkehr, Berlin 2001.

[9] Richtlinie Stahlfaserbeton, 22. Entwurf der Richtlinie für Stahlfaserbeton des DAfStb, 2005-02-18.

[10] Setzer, M. J.; Fagerlund, G.; Janssen, D. J.: CDF-Test – Prüfverfahren des Frost-Tau-Widerstands von Beton – Prüfung mit Taumittel-Lösung (CDF). Rilem recommendation.

[11] Tang, L. und Nilsson, L.O.: Rapid determination of the chloride diffusivity in concrete by applying an electrical field. In: ACI Materials Journal, pp. 49-53, 1992.

Thanh T. Le
PhD student
The University of Liverpool
Liverpool, UK

Marios N. Soutsos
Reader, Dr.
The University of Liverpool
Liverpool, UK

Steve G. Millard
Professor
The University of Liverpool
Liverpool, UK

Kang K. Tang
PhD student
The University of Liverpool
Liverpool, UK

Structural Behaviour of a UHPFRC Flag Pavement

Summary

Roadside pavements are normally designed for use by pedestrians but overrun by vehicles leads to cracking. The possible use of UHPFRC flags for pedestrian pavements to reduce the risk of cracking has been investigated. The experimental results as well as finite element analysis modelling have shown that the pavement made with UHPFRC flags was over three times stronger than the pavement made with conventional factory flags. Therefore not even overrun by a truck would crack the UHPFRC flag pavement.

Keywords: *crack, failure load, paving flag, pedestrian pavement, Ultra High Performance Fibre Reinforced Concrete (UHPFRC).*

1 Introduction

Previous studies at the University of Liverpool [1, 2, 3] indicated that UHPFRC can be produced using (a) a very low water-cementitious ratio of 0.15, achieved by using a high cement content (657 kg/m^3) together with silica fume (119 kg/m^3) and Ground Granulated Blast-Furnace Slag (GGBS) (418 kg/m^3) and a high dosage of a superplasticiser (12.5 kg/m^3), (b) fine (150-600 mm) quartz sand (1050 kg/m^3) as the only aggregate, (c) high percentages (1.0 to 6.0 % by volume) of steel fibres (13 mm length and 0.2 mm in diameter) for improved flexural strength. The experimental studies achieved compressive strength of 160 - 210 MPa and flexural strength of 15 - 45 MPa. This concrete can be used for the production of improved performance UHPFRC paving flags.

Roadside pavements are normally designed and built to carry pedestrian traffic, but overrun by vehicles often causes cracking. Cracked and uneven pavements cause slips, trips and falls. A report from The Pedestrians Association in 1998 entitled “Enjoy Your Trip” stated that the claims culture in the UK was costing local authorities around £500m each year [4]. The development of high performance pedestrian pavements may therefore reduce accidents and consequential compensation claims.

The manufacture of a UHPFRC flag is costly in material terms but it has very high flexural strength and fracture energy. Life-cycle costing analysis may favour UHPFRC flags, especially if the following factors are considered: (1) UHPFRC paving flags can be made thinner and lighter, resulting in the reduction of health and safety concerns during handling and placing and also the reduction in transportation costs; (2) increase of pavement service life due to the reduced maintenance cost; (3) reduction of liability claims arising from uneven pavements.

In this study, UHPFRC was used to fabricate 200x400x30 mm paving flags comprising two layers, each with a 15 mm thickness. The bottom layer comprised UHPFRC with 2.0% fibres and the top layer comprised UHPFRC without fibres. This fabrication procedure was developed to optimise the use of expensive steel fibres by only providing a high flexural tensile strength on the underside where tensile sagging stresses are anticipated. In addition, the use of a fibre-free upper layer prevented the possible hazard of fibres projecting accidentally from the pedestrian surface. The experimental results indicated that the flexural strength of a UHPFRC paving flag was around 20 MPa while current factory produced paving flags had a flexural strength of only 6 MPa. These UHPFRC paving flags were laid and tested in a section of a pavement created in the laboratory. The results were compared with another section of pavement which used currently produced factory flags. Both pavements were then modelled using finite element analysis software ABAQUS. The structural behaviour of the pedestrian pavement made with UHPFRC paving flags is discussed in this paper.

2 Setting up pavement tests and finite element models

A section of a pavement was laid in a rigid frame-box. This section comprised a 250 mm thick sub-base layer, using material Type 1 (0.075 – 37.5 mm granite aggregate), and a 40 mm thick sand bedding layer. Both layers were placed following the recommendations of BS 7533-4:1998 [5]. Factory flags and UHPFRC flags were then laid in turn on the sand layer and tested. Strain gauges were attached at the central underside of several flags to measure the tensile strains while displacement transducers were also set up to detect the deformation of the pavement upper surface. All strains and displacements were recorded using a data acquisition system. Initially a single paving flag was positioned at the centre of the sand bedding layer and tested with a central 100 mm square loading plate. This test was carried out for both flag types to ensure that the finite element analysis modelling could be successfully validated against experimental results before full pavements were investigated experimentally and numerically modelled. The full pavement test arrangement comprised six 200x400x30 mm paving flags (F1 to F6) and four half-flags (F7 to F10), i.e. 200x200x30 mm laid on the sand bedding and tested with a central load. This was applied using a 250 mm circular plate to represent a vehicle wheel loading [6, 7]. The load position was chosen so that flags were loaded at the centre of a flag edge and also at flag corners. These load positions have been recommended as critical positions for a pedestrian pavement [8]. The loading was applied using a hydraulic jack at a rate of approximately 15 kN/minute. The experimental arrangements are shown in Figure 1.

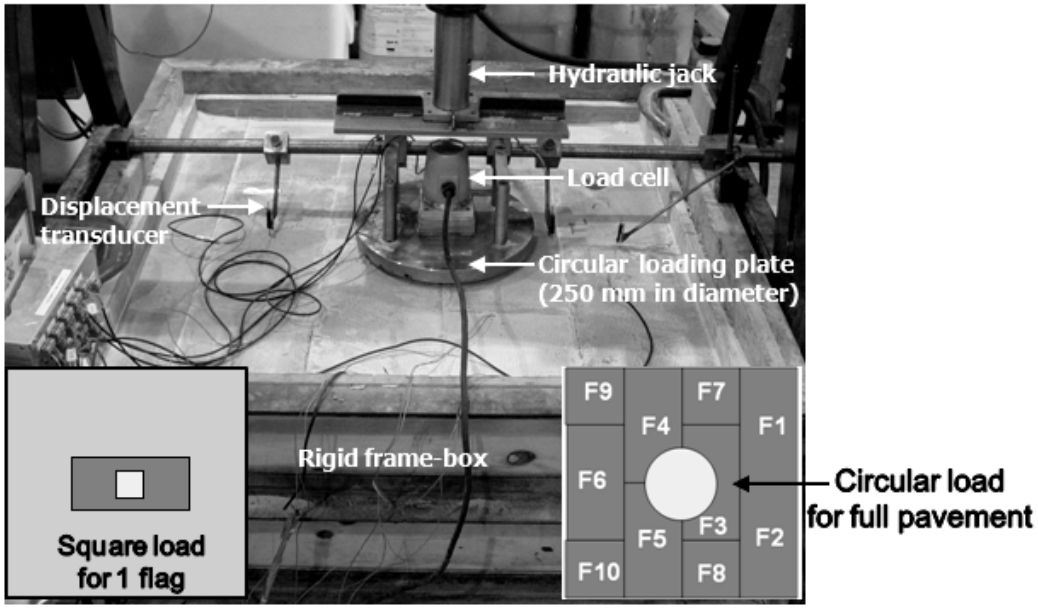

Figure 1: Experimental test arrangements

The pavement tests were then modelled using a commercial finite element analysis software package, ABAQUS. The material properties shown in Table 1 were first determined in the laboratory and then used in the finite element analysis model.

Table 1: Material properties used for finite element modelling

Part (dimension, mm)	**Properties**						
	Density (kg/m^3)	Elastic modulus (MPa)	Poisson ratio	Compressive strength (MPa)	Plastic strain	Failure tensile stress (MPa)	Ultimate displacement (mm)
Sub-base (800x800x250 mm)	2,000	200	0.25	N/A	N/A	N/A	N/A
Sand bedding (800x800x40mm)	1,800	50	0.25	N/A	N/A	N/A	N/A
Square and circular loading plate	7,850	210,000	0.3	N/A	N/A	N/A	N/A
Factory flag (200x400x30 and 200x200x30)	2,400	29,000	0.2	45 0	0 0.002	3.6	0.5
UHPFRC flag (200x400x30 and 200x200x30)	2,500	55,000	0.2	150 170 120 50	0 0.002 0.004 0.005	13.6	10.0

Ordinary concrete and UHPFRC were both modelled using a “concrete smeared cracking” material, using fracture energy as an input property. The fracture energy is defined as the

area under the tensile stress versus ultimate displacement curve of concrete [9], see Figure 2. The ultimate displacement of ordinary concrete input was very small, i.e. 0.5 mm, modelling brittle failure while that of UHPFRC was 10 mm modelling a ductile material. Although tensile stress versus displacement model for UHPFRC used in ABAQUS does not match perfectly with the experimental behaviour, the most important criteria, i.e. failure tensile stress and approximate fracture energy, were an acceptable fit.

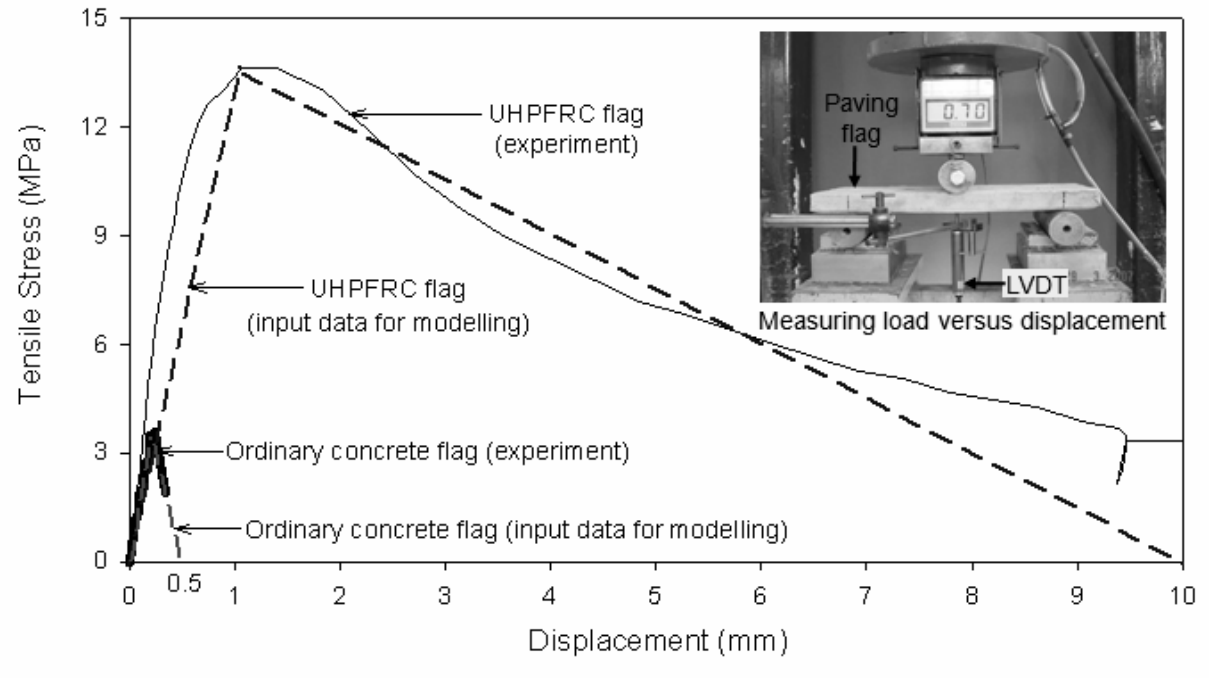

Figure 2: Tensile stress versus displacement relationships used to model ordinary concrete flags and UHPFRC flags

3 Experimental and modelling results on the structural behaviour of pavement

- Single paving flag loaded centrally

The different behaviour of UHPFRC and factory ordinary concrete flags is shown in Figure 3. The single paving flag failed in bending under a concentrated load applied at the centre. The factory concrete flag appeared to behave in a linear elastic manner until brittle failure occurred, see Figures 3 and 4. The failure load and failure strain were 6 kN and 1.9×10^{-4} respectively. Although the pavement containing a failed concrete flag was still able to carry higher load, the displacement of the broken pieces increased rapidly. This post-failure behaviour of a conventional concrete flag pavement causes an unacceptable uneven surface for pedestrian usage. In contrast the UHPFRC flag failed in ductile manner as shown in Figure 5. The cracking strain of the UHPFRC flag was larger than that of the factory flag, i.e 2.4×10^{-4} compared with 1.9×10^{-4} of factory flag. The load causing first cracking of the UHPFRC flag was 14 kN and the failure load was approximately 19 kN. After failure, the pavement with a centrally-loaded UHPFRC flag still carried load up to 24 kN but the flag was not broken into separate pieces. This is because when the UHPFRC flag cracked the steel fibres held the two broken parts together and the pull-out behaviour of the fibres was still

active. The failure load of the pavement using UHPFRC flag was observed to be over three times that of the pavement with factory flag, as shown in Figure 3. Strain hardening of UHPFRC was seen clearly in this experiment and the flag continued to perform up to a strain of nearly 6 x10^{-4}, see Figure 3.

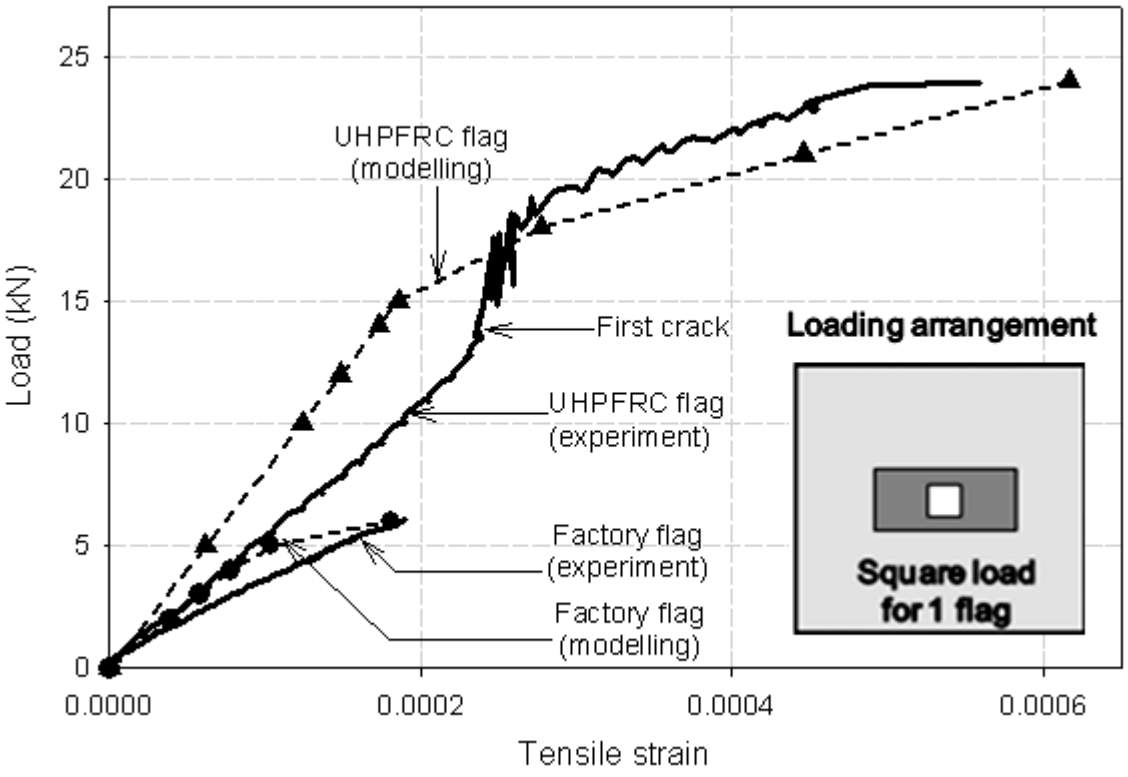

Figure 3: Load versus tensile strain at the central underside of single paving flag

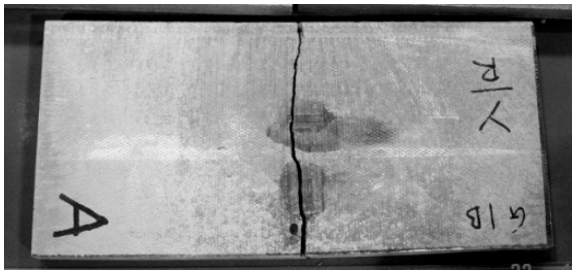

Figure 4: Brittle failure of factory paving flag

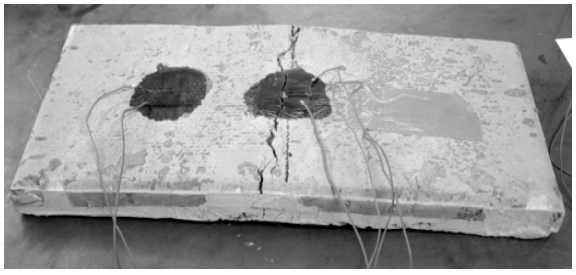

Figure 5: Ductile failure of UHPFRC paving flag

Finite element modelling predicted the experimental behaviour relatively well for both factory and UHPFRC flags in this single paving flag test, as shown in Figure 3. The failure load of both flags was predicted very closely but the predicted tensile strains appeared to be slightly smaller than experimental values.

This was very encouraging and indicated that finite element analysis could be used reliably to predict the behaviour of full pavements in the next stage.

- Section of a pavement loaded with a circular plate

In this experiment, the factory flag pavement continued to show brittle cracking failure behaviour, Figure 6, while the UHPFRC pavement failed in a ductile manner. Both the modelling and experimental results indicated that the maximum tensile stress and initiation of cracking first occurred directly beneath the circular loading plate at positions F and K, on the undersides of flags F4 and F5 as seen in Figures 6 and 7. Paving flag F3 subsequently cracked at position I and H. The load causing failure of flags F4 and F5 was approximately 10 kN for the factory flag and 30 kN for the UHPFRC flag. The failure of flag F3 occurred at a higher load of 15 kN for factory flag and over 40 kN for UHPFRC flag. The maximum load capacity of the test frame was 40 kN and had insufficient capacity to crack flag F3 made with UHPFRC. Nevertheless, the modelling predicted that the load causing failure of UHPFRC flag F3 was 45 kN. The modelling results also indicated that the tensile stresses in both axis directions X and Z on the underside of flag F3 at positions H and I, were very close to each other. As a result the factory concrete flag F3 could crack in either direction, as shown in Figure 7.

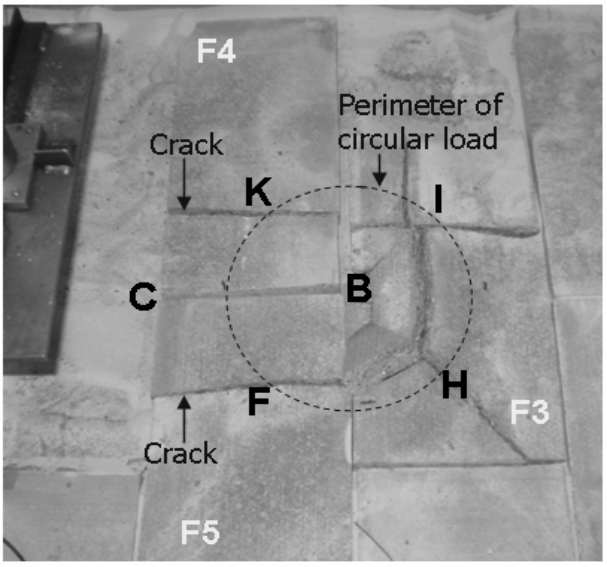

Figure 6: Failure of factory flag pavement – topside

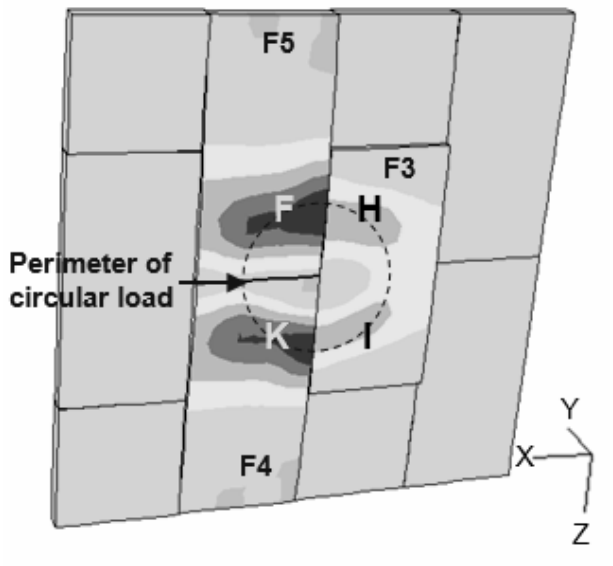

Figure 7: Tensile stress distribution in the pavement - underside

When applying circular load the three flags F3, F4 and F5 moved downwards and rotated around the circular loading plate. These movements lead to a concentration of the vertical load transferred from the circular plate to the pavement through only four points, i.e. F, H, I and K, as shown in Figure 8. Finite element analysis modelling also showed an understanding of how the flags get displaced by increasing load. The displacement changes the way the load transferring from the circular plate to the concrete flags and therefore to the supporting sand bedding. Figure 9 shows that the corners B, C of the flag F5 get displaced

downwards but not by the same magnitude. Corner A and point D (75 mm far from corner D) have approximately zero vertical displacement. Corner E is displaced upwards and loses contact with the soil. This means that the underside of flag F5 only remains contact with the sand layer in the area of (ABCD). The load being applied eccentrically on the flag F5 therefore causes the flag to rotate which about both the X and Z axes. The only contact point on flag F5, above a certain load, is at point F shown in Figure 8. It is because of this point load and the support reaction offered by the soil shown in Figure 10 that flag F5 cracks as shown in Figure 6.

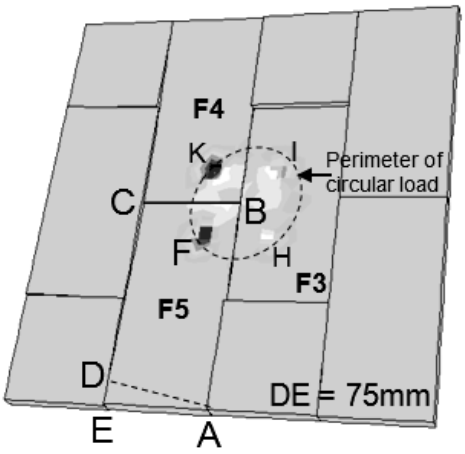

Figure 8: Vertical stress distribution at the topside of pavement

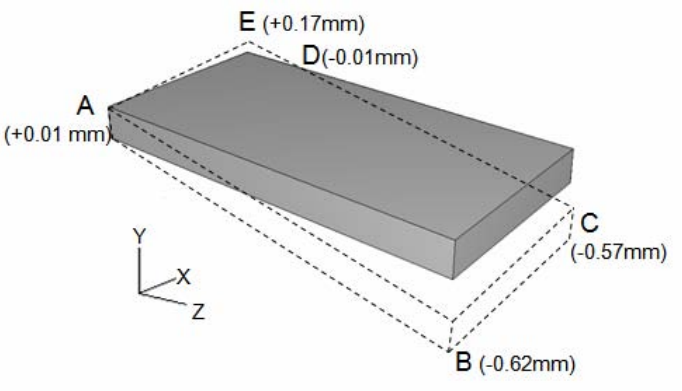

Figure 9: The movement of flag F5 under a load of 30 kN

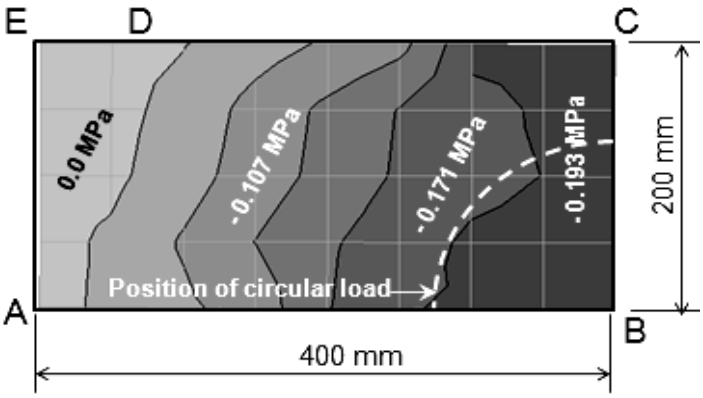

Figure 10: Load transfer to the soil from UHPFRC flag F5 for a load of 30 kN

4 Conclusions

- UHPFRC can be used to fabricate very high performance crack-resistant paving flags to resolve the poor cracking behaviour of conventional concrete pavements and therefore achieve a reduction in the number of slip, trip and fall compensation claims.

- The results from experimental testing and finite element analysis modelling of a UHPFRC flag pavement showed that a failure load of over three times higher than that of a factory flag

pavement could be achieved. The failure load of a factory flag pavement was approximately 10 kN while that of a UHPFRC flag pavement was approximately 30 kN. This means that while a UHPFRC flag pavement can carry vehicles having a wheel load up to 3 tonnes, e.g. a truck, the factory flag pavement can only carry a wheel load around 1 tonne. However, the prediction of structural behaviour of UHPFRC pavement using finite element analysis modelling could be improved if more realistic properties of materials are inputted, i.e. the sand bedding and sub-base are input as nonlinear-behaviour materials and the stress versus displacement relationship for UHPFRC is input as the experimental curve.

5 Acknowledgements

The principal author would like to express gratefulness for the PhD scholarship sponsored by The Vietnamese Government. The supply of materials from BEKAERT, ELKEM Materials, APPLEBY GROUP Ltd. (Civil and Marine) and FOSROC Ltd. for this project is highly appreciated. The authors would also like to thank Mr P. Farrell and Mr J. Wilkinson, for their assistance with casting paving flags and developing the software used for data acquisition during the experimental work.

6 References

[1] Soutsos, M. N.; Millard, S. G. and Karaiskos, K.: Mix Design, Mechanical Properties and Impact Resistance of Reactive Powder Concrete (RPC), In: Proc. International Workshop on High Performance Fiber Reinforced Cementitious Composites in Structural Applications, Hawaii, 2005.

[2] Le, T. T.; Soutsos, M. N.; Millard, S. G. and Barnett S. J: UHPFRC – Optimisation of Mix Proportions. In: Proc. of CONCRETE PLATFORM International Conference, Belfast, Northern Ireland, pp 339-348, 2007.

[3] Barnett, S. J.; Millard, S. G.; Soutsos, M. N.; Schleyer, G.; Tyas, A. and Le, T. T.: Ultra High Performance Fibre Reinforced Concrete for Explosion Resistant Structures. In: Proc. of CONCRETE PLATFORM International Conference, Belfast, Northern Ireland, pp 565-573, 2007.

[4] BBC News Online: Pavement Injuries 'Similar to Car Crashes', In: http://news.bbc.co.uk/2/low/health/147195.stm, Published at 00:54 GMT 01:54 UK, Monday, August 10, 1998.

[5] BS 7533-4:1998, Code of Practice for the Construction of Pavements of Precast Concrete Flags or Natural Stone Slabs, UK, 1998.

[6] Croney, D. and Croney, P.: The Design and Performance of Road Pavements. McGraw-Hill Book Company, Second Edition, UK, 1991.

[7] Silwerbrand, J. L.: Test on Load Carrying Capacity of Concrete Flags. In: Proc. of the 7th International Conference on Concrete Block Paving, South Africa, 2003.

[8] Al-Khalid, H. and Bull, J.W.: Finite Element Analysis of Precast Concrete Flag Pavements with Reference to Wheel Load Configuration and the Implications on Their Design. In: Res. Mechanica: International Journal of Structural Mechanics and Materials Science, 28(1-4): p. 295-305, 1989.

[9] ABAQUS / Standard – User's Manual. Hibbitt, Karlsson & Sorensen Inc., USA, 2002.

Part 10:

Applications – Thin Elements

Marco di Prisco
Professor
Politecnico di Milano
Milan, Italy

Marco Lamperti
M.S. Civil Engineer
Politecnico di Milano
Milan, Italy

Simone Lapolla
Research Assistant
Politecnico di Milano
Milan, Italy

Rabinder S. Khurana
Technology Director
BASF Construction Chemicals
Italy

HPFRCC thin plates for precast roofing

Summary

The use of High Performance Fibre Reinforced Cementitious Composites allows the designer to reduce the dead weight of roofing keeping concrete covering structures still more competitive in relation to steel structures in terms of costs, thermal and acoustic insulation and fire resistance.Thin plates can be used as tertiary elements in roof floors beside the border beams and the simply supported prestressed precast roof elements. The high performances are mainly used for bending along the 1.2m span width of the plates and in order to drastically simplify the detailing of the support zones. A wide experimental investigation is in progress to mechanically characterize the material in uniaxial tension and to identify all the data available for design like toughness, bending resistance, fire resistance and durability. After the preliminary tests carried out on the material, bending tests on 2.5 long and 1.2 m wide plate specimens are presented. The goal is to understand if the ductility calculated with the Italian Recommendations fits the experimental results. A modelling of the tests performed by means of beam theory is also discussed.

Keywords: *cast procedures, crack opening displacement, hardening in bending, mechanical characterization tests, plane section model, steel fibres*.

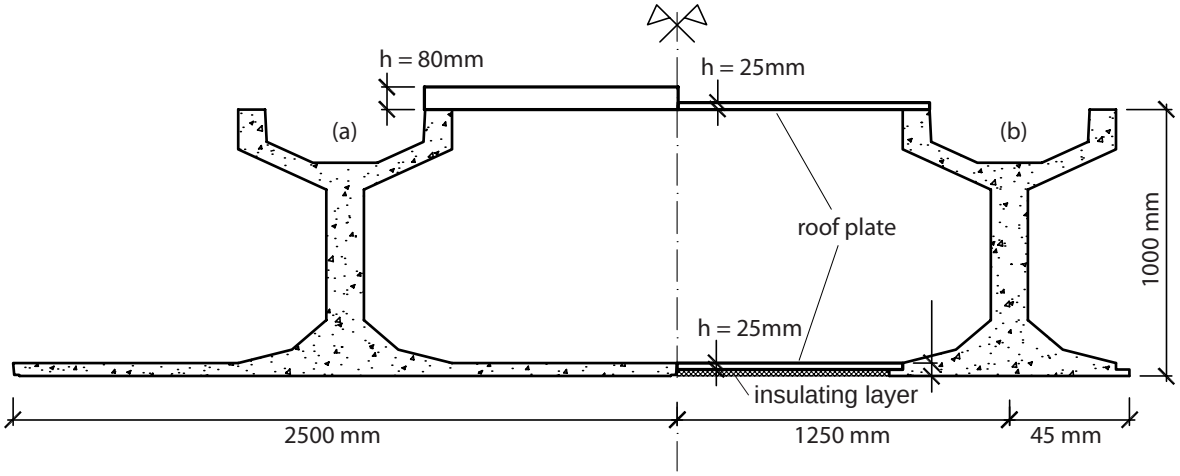

Figure 1: roofing system selected: (a) actual solution and (b) new design scheme.

1 Introduction

Precast concrete roofing is often disadvantaged by an average dead weight close to 2kN/m^2, that can be regarded as quite large if compared to the snow load (close to 1.5 kN/m^2). A reasonable compromise in terms of costs and weight can be searched by adopting ultra High performance materials [1,2] which are more expensive, but can be much more lighter. Preliminary results from bending are here presented.

2 Material mix design and preliminary tests

The composite (n. 7; Tab.1) was selected by comparing different solutions starting from the aggregates generally used by the precast producer and limiting their maximum size to 2 mm. Preliminary tests on shrinkage, free and constrained (Fig.2), allow us to estimate the quite large strain that was expected due to the significantly large fraction of fine aggregates used in the mix. Unnotched specimens were tested according to a three point bending set-up (Fig.3): two span lengths were investigated. The related results highlight the influence of the span length that seems to reduce the peak nominal strength and to increase ductility (Figs. 4a,b; Tab.2). It is also very interesting to observe as in the post peak branch the relation between crack-opening w and deflection (Fig.3) is linear and respects the rigid block-kinematics. The uniaxial compressive behaviour is resumed in Table 3 and Fig.5: a cubic compressive strength of 143 MPa and an elastic modulus close to 40 GPa characterize the material in the preliminary qualification.

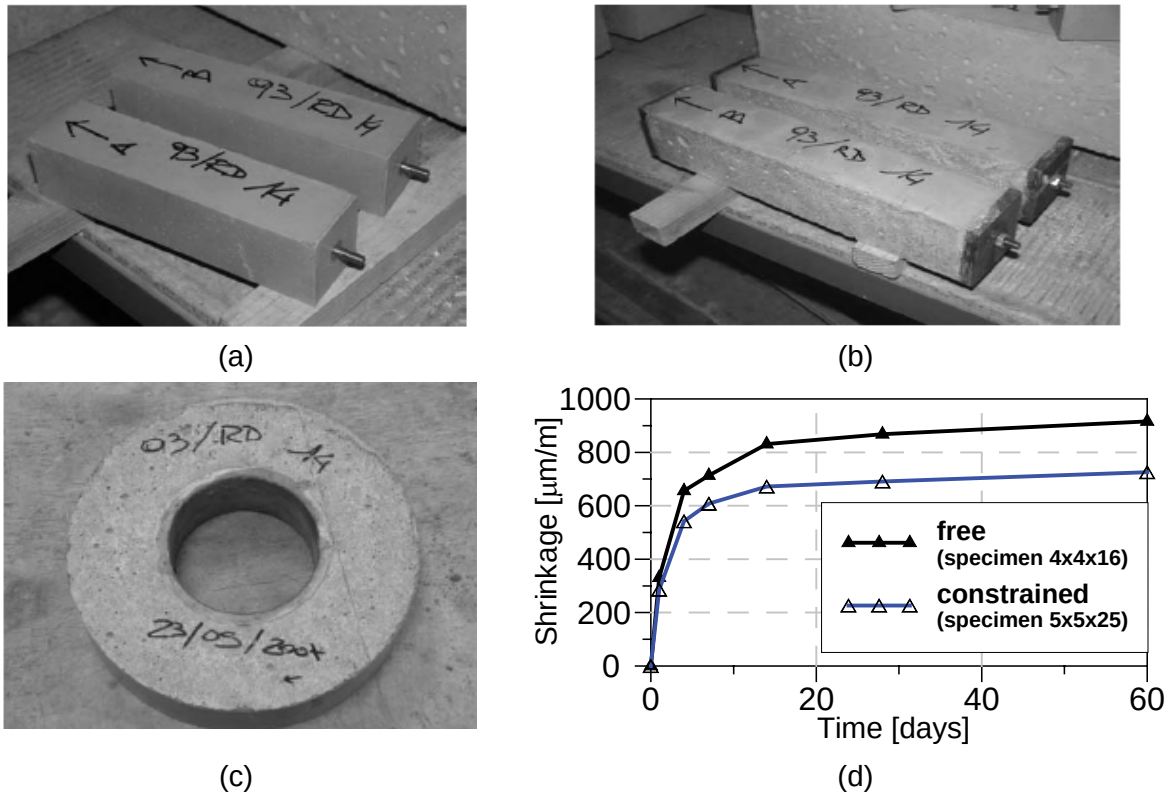

Figure 2: Shrinkage tests: (a) free, (b) constrained, (c) O-ring tests and (d) strain vs. time.

Table 1: Mix design attempts and related compressive and bending peak strengths.

N°	Cement 52,5 I class [kg/m^3]	Slag [kg/m^3]	Sand 0/2 [kg/m^3]	Fiber [kg/m^3]	Additive [l/m^3]	Water [l/m^3]	Compressive strength [Mpa]			Bending strength [Mpa]	
							1d	7dd	28dd	1d	28dd
4	600	500	983	100	33	210	46.1	124.9	136.9	12.7	23.5
5	600	400	1015	100	33	210	67.4	127.7	142.1	25.4	39.2
6	600	500	983	100	33	210	63.1	121.5	141.0	13.1	44.2
7	600	500	983	100	33	200	79.3	133.0	146.0	24.0	37.8
8	600	500	983	100	33	200	72.4	127.0	139.0	23.2	35.4

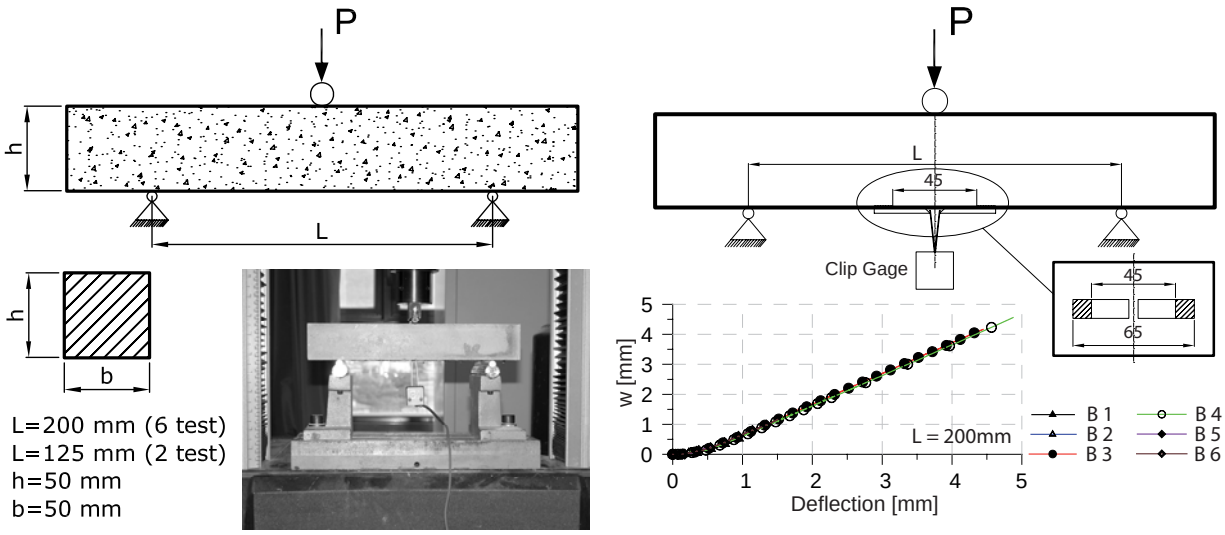

Figure 3: preliminary tests in bending on unnotched specimens with different span lengths.

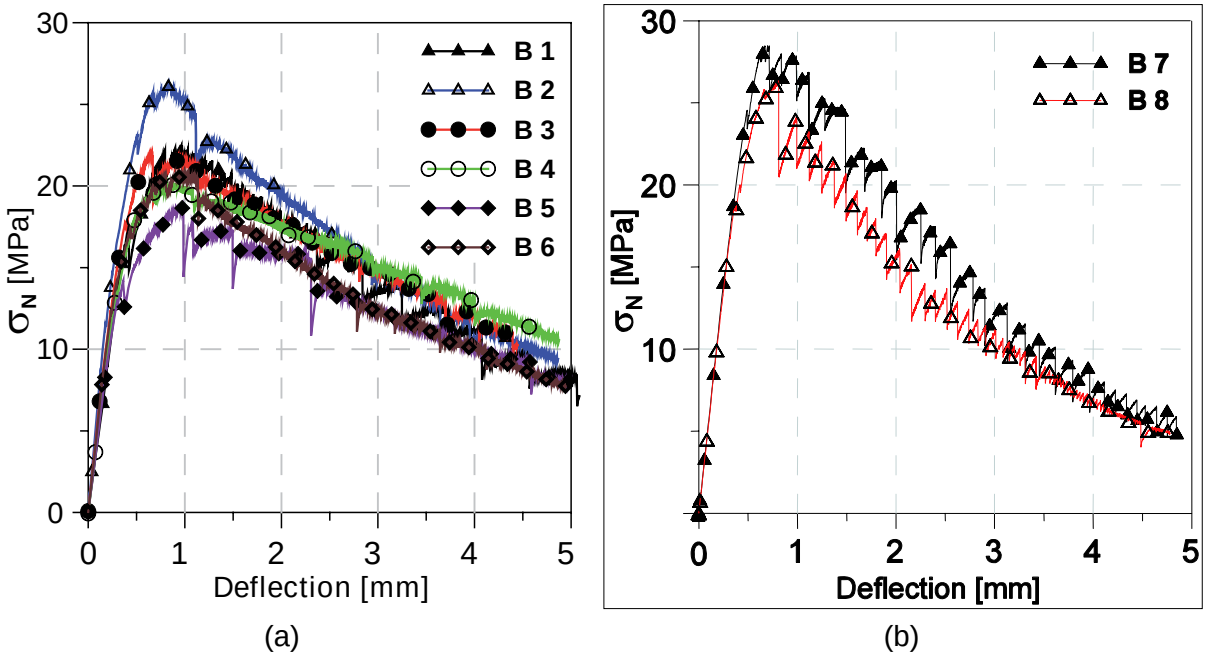

Figure 4: Nominal stress vs. deflection for the different test carried out: (a) span length L=200mm and (b) span length L=125mm.

Table 2: Bending tests: peak strength and energy dissipated up to a deflection/span length ratio equal to 2%.

Specimen	Age [days]	Span length [mm]	Max load [kN]	Energy dissipated [kNmm]	$f_{ct,fl}$ [MPa]	$f_{ctav,fl}$ [MPa] (std)
B 1	14	200	9.36	26.49	22.47	21.71 (2.57)
B 2	14	200	10.92	29.63	26.22	
B 3	14	200	9.13	27.18	21.91	
B 4	14	200	8.40	26.73	20.15	
B 5	14	200	7.82	22.84	18.77	
B 6	14	200	8.64	24.44	20.72	
B 7	14	125	18.98	34.24	28.47	27.4 (1.51)
B 8	14	125	17.55	29.38	26.33	

Table 3: Compressive behaviour: cylindrical peak strengths and elastic modulus measures.

Spec.	Age [days]	Diameter [mm]	Depth [mm]	Mass [g]	Density [kg/m^3]	Max load [kN]	f_c [MPa]	$f_{c,av}$ [MPa] (std)	E_c [GPa]	$E_{c,av}$ [GPa]
C 1	14	99.8	194.4	3766	2480	1148.54	146.24	143.52 (3.69)	39.98	39.68
C 2	14	100.0	193.7	3773	2481	1138.79	145.00		40.01	
C 3	14	99.7	196.0	3798	2482	1094.22	139.32		39.05	

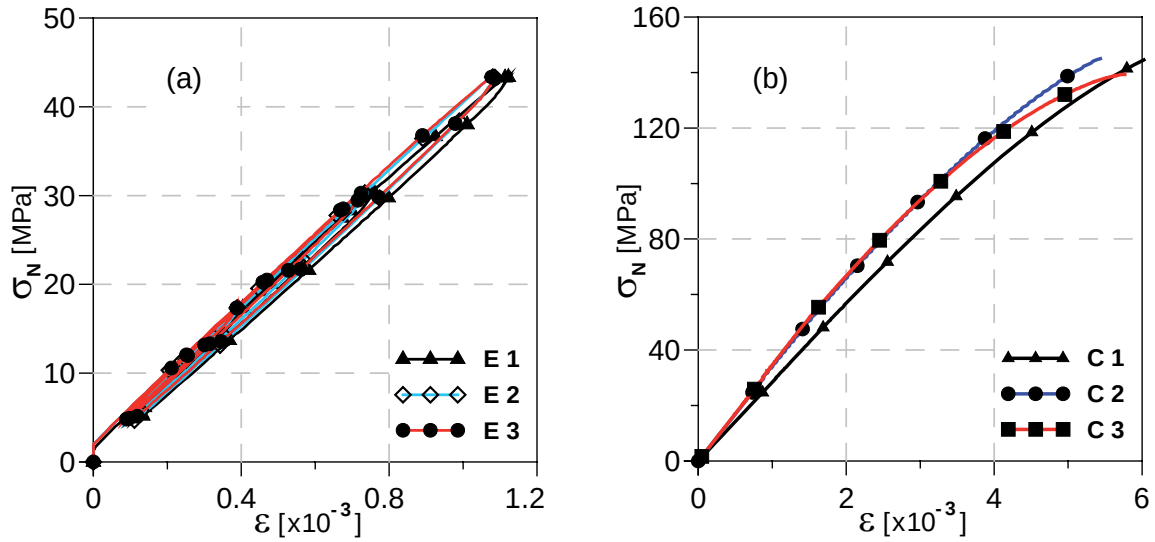

Figure 5: Uniaxial compression tests: (a) elastic modulus and (b) behaviour up to failure.

3 Prefabrication factory cast: fresh behaviour and mechanical characterization by means of nominal and structural specimens

The same mix design was used to cast three prototypes of thin slabs in the prefabrication implant. The fresh behaviour tests confirmed a SCC consistency (Fig.6). Cubic compression tests (Table 4) and 4 point bending tests on notched specimens gave first cracking and residual strengths (Fig.7, Table 5) significantly smaller than those obtained in the preliminary tests.

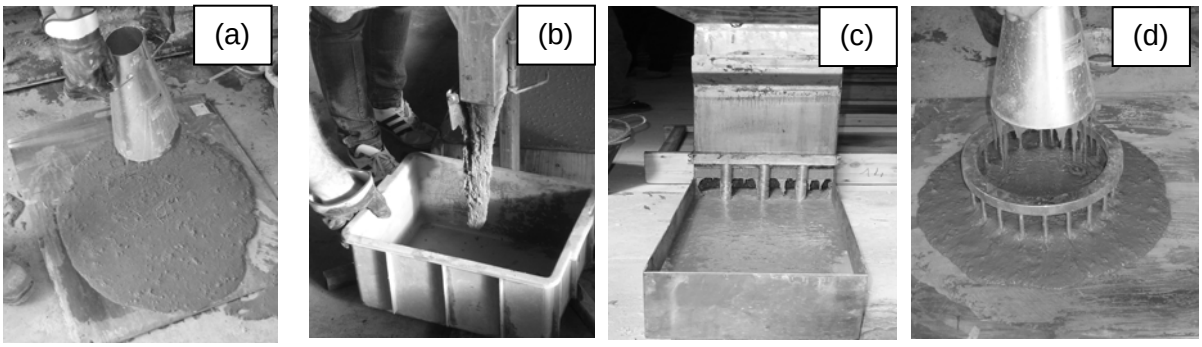

Figure 6: Fresh behaviour tests: (a) Slump Flow; (b) V –Funnel; (c) L-shape Box; (d) J-ring.

Table 4: Cubic compressive strengths.

Age [days]	1	7	28
$R_{c,m}$ / std / Density [MPa]/ [%] / [kg/m^3]	66.31/ 7.44/ 2480	99.13/ 5.96 / 2452	116.49 / 8.78 / 2474

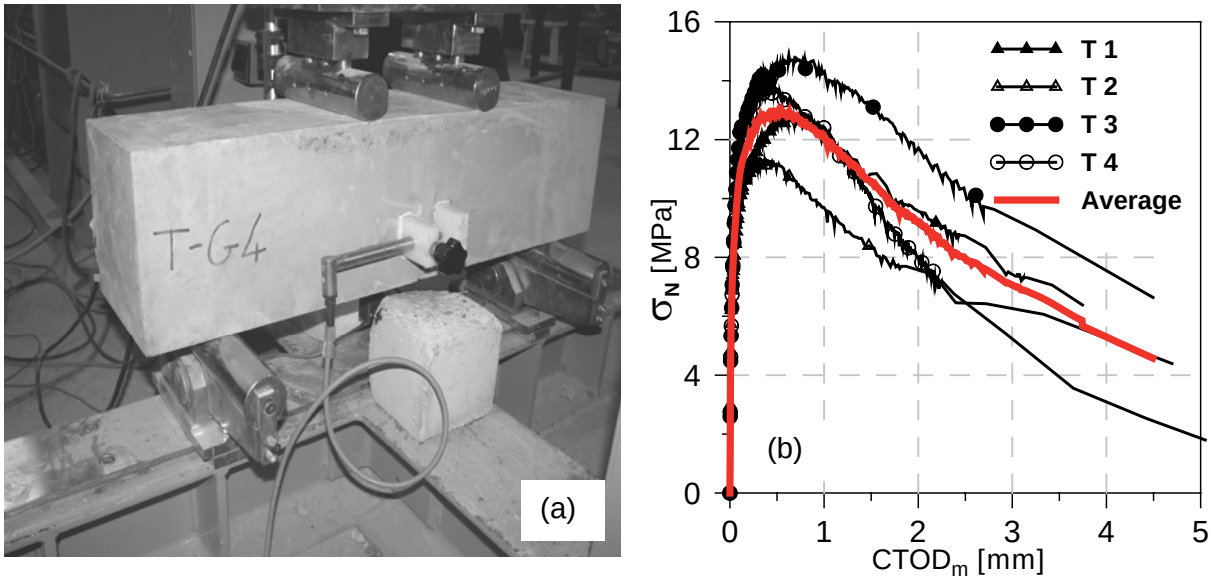

Figure 7: Notched tests according to UNI 11188: (a) test set-up and (b) nominal stress vs. CTOD

Table 5: Bending strengths from nominal tests according to UNI 11039.

Specimen	**f_{IF} [MPa]**	**$f_{IF,av}$ [MPa] (std [%])***	**f_{eq1} [MPa]**	**$f_{eq1,av}$ [MPa] (std [%])***	**f_{eq2} [MPa]**	**$f_{eq2,av}$ [MPa] (std [%])***
T1	6.96		11.43		10.09	
T2	7.29	7.10	10.70	12.06	7.94	9.77
T3	7.21	(1.97 %)	13.37	(11.28 %)	12.09	(18.73 %)
T4	6.96		12.76		8.94	

4 Full size plate structural tests

Three tests were carried out on full size plates to verify the predicted design performances and to reproduce the real behaviour at serviceability and ultimate limit states Four-point bending tests were carried out using a servo-controlled hydraulic jack, equipped with a distribution frame able to impose a constant bending moment on the middle share of the specimen. Data acquisition system was designed both to match parameters from flexural characterization and to record the structural response of loaded plates (Fig.8). The first ones

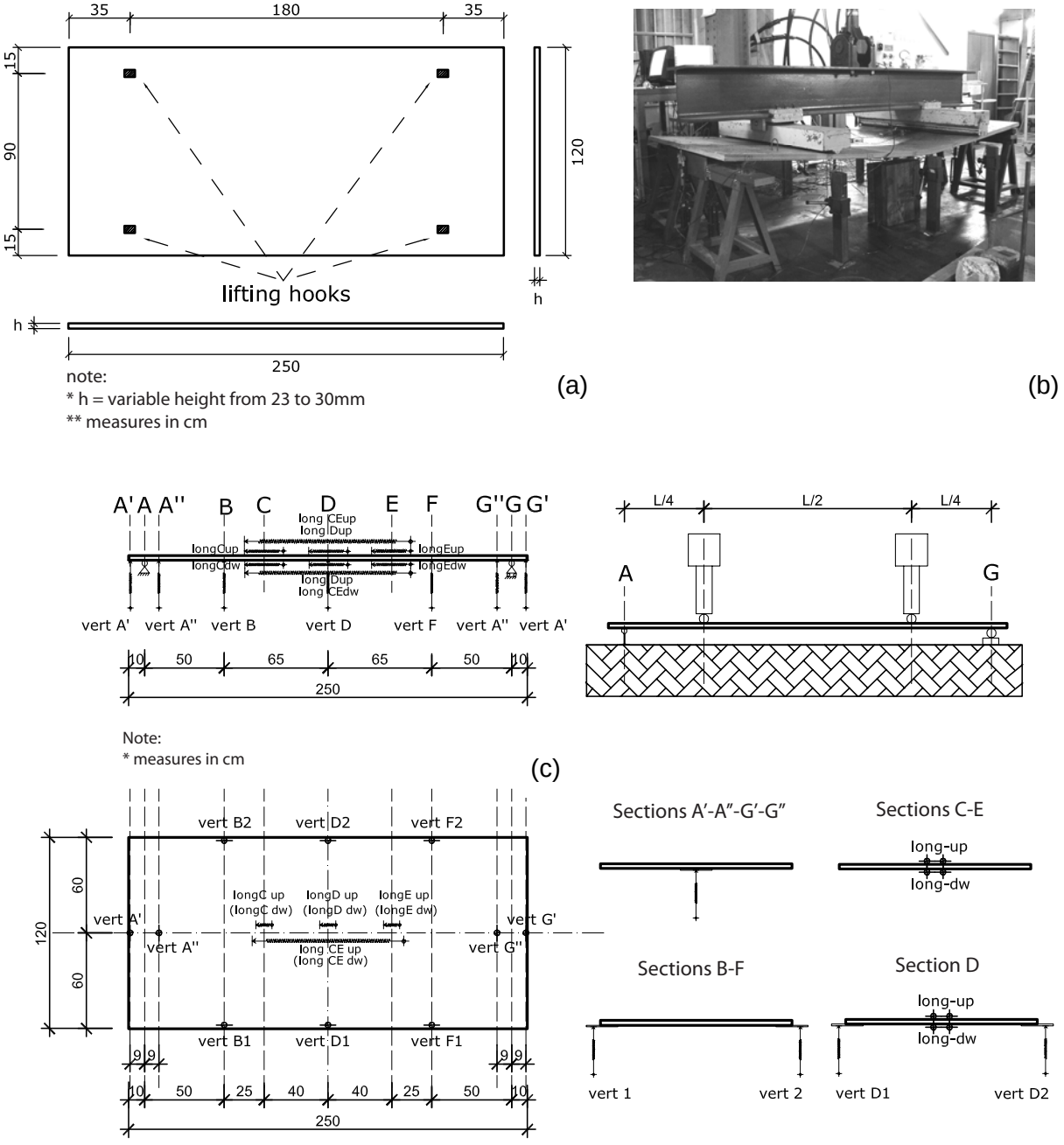

Figure 8: Full-size tests: (a) specimen geometry, (b) test set-up and deformed shape; (c) measuring equipment

were measured by LVDT with 10 mm stroke and the last ones by resistive transducers with 75 mm stroke. Eighteen instruments were used, together with the jack displacement and the applied load (measured by a 25 kN load cell).

Each specimen was subjected to three different load conditions. Two cycling loads for one-hundred times, from zero to 1.0 kN and from zero to 3.0 kN. Finally the last cycle to the maximum load. The test displacement control allows us to follow the specimen behaviour beyond the peak-load until the 50% of residual bearing capacity.

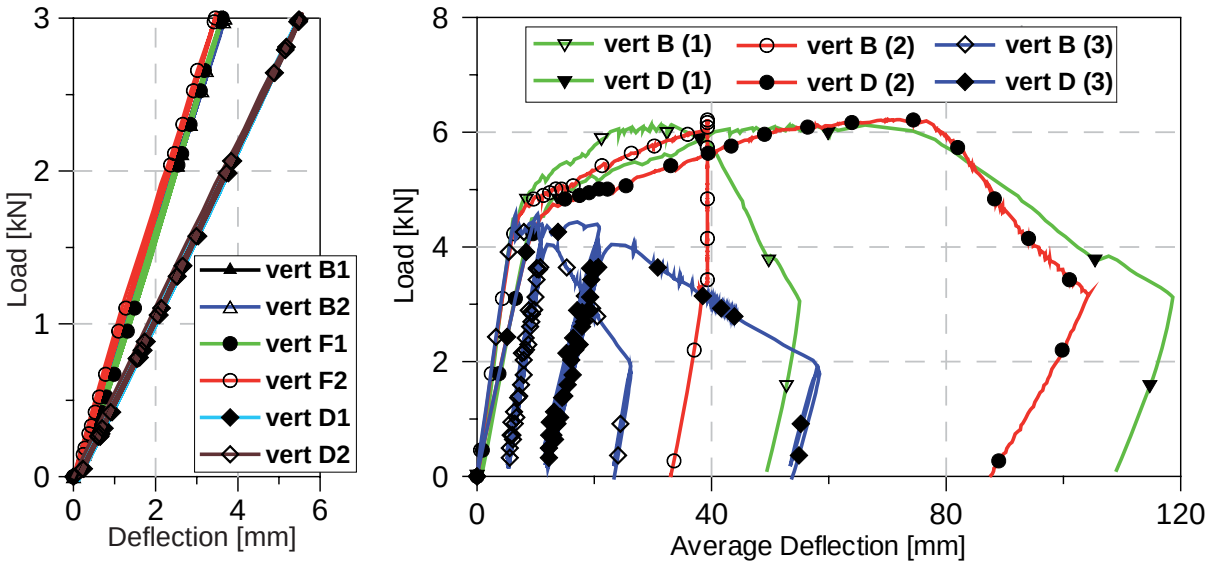

Figure 9: Load vs. deflection: (a) elastic loading-unloading cycles; (b) load vs. deflection curves for three nominally identical plates.

5 Bending behaviour prediction by means of plane section approach

On the basis of the constitutive law in uniaxial tension identified according to Italian Guidelines CNR DT-204 ([3]; Fig.10b) starting from the strengths measured in the notched 4 point bending tests, the average generalized constitutive relationship bending moment vs. curvature was predicted (Fig.10a). It is interesting to notice how this prevision is strongly on the safe side with respect to bearing capacity, but it fits quite well the real ductility which is expressed by CE gauge measures which can be regarded as average values on a gauge length equal to 95 cm.

The characteristic structural length l_{cs} assumed in the computation was equal to the plate thickness (t = 26 mm) and therefore the ultimate crack opening w_u defined in the Italian guidelines is equal to 0.02 l_{cs} = 0.52 mm. For such threshold, the bending behaviour of the plate is hardening.

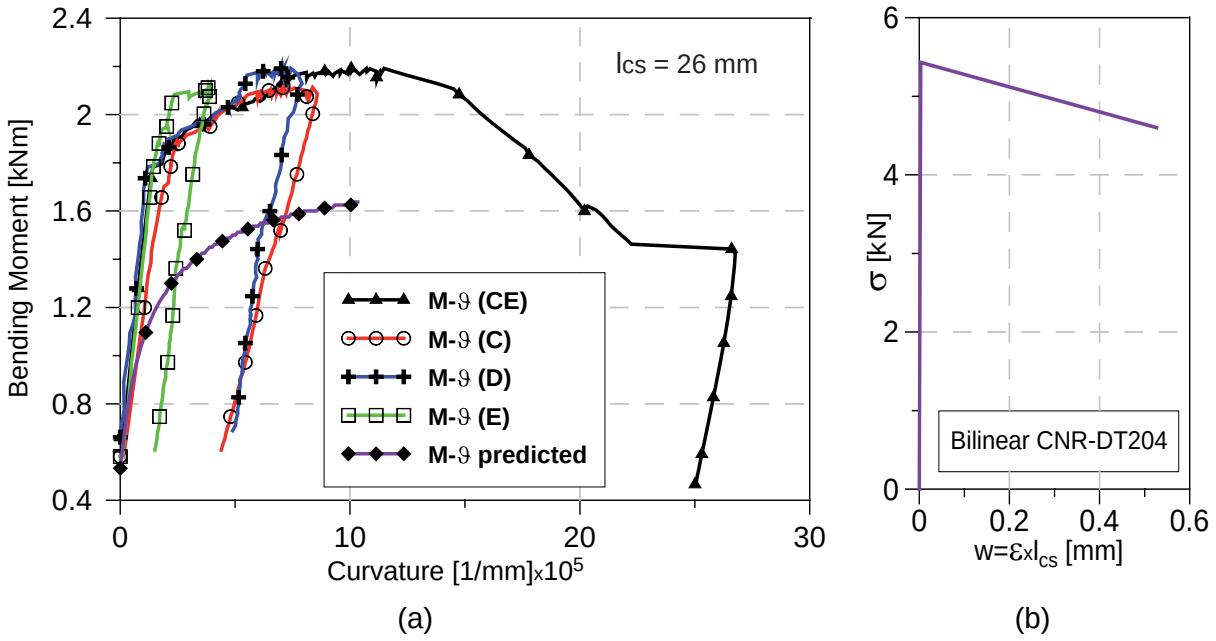

Figure 10: (a) Prediction reliability: Bending Moment vs. Curvature according to plane section vs experimental results in different sections and (b) Constitutive law identified in uniaxial tension

and this means that a multicracking occurs after this threshold, characterized by very small crack-openings (w < 30 μm). It is also important to observe how even the average behaviour is well reproduced, the curvature is not homogeneous in the gauge length as proved by curvatures measured in gauges C,D,E (Fig.10a).

6 Conclusions

The preliminary tests carried out on thin plates made of a UHPCC satisfy the acceptance design criteria established in the Italian guidelines. Significant difference were observed in the bending tests between notched and unnotched specimens and even in unnotched specimens with the same cross section when the span length is increased. The small thickness requires a very careful casting procedure, because with the same SCC mix is possible to obtain very different bending behaviour either in terms of maximum bearing capacity and in terms of ductility.

7 References

[1] Naaman, A.E., Reinhardt, H.W., Eds. (2003), High Performance Fiber Reinforced Cement Composites (HPFRCC4), PRO 30, Rilem publication S.A.R.L..

[2] Reinhardt, H.W., Naaman, A.E., Eds. (2007), High Performance Fiber Reinforced Cement Composites (HPFRCC5), PRO 53, Rilem publication S.A.R.L..

[3] CNR-DT 204: Instruction for design, execution and control of fibre reinforced concrete structures, Italian Standards, 2006.

Martin Kobler
Dipl.-Ing.
ILEK, University of Stuttgart
Stuttgart, Germany

Werner Sobek
Prof. Dr.-Ing.
ILEK, University of Stuttgart
Stuttgart, Germany

The Introduction of High Forces into Thin-Walled UHPC Elements by the Use of Implants

Summary

Given its high compressive strength, its relatively low specific weight and its formability, UHPC offers a lot of new possibilities for the building sector. However, in order to make the material competitive for widespread use, structural elements made of UHPC have to be prefabricated. The main objective of using the high performance material UHPC both economically and efficiently is a homogeneous and maximal utilization of the structural elements exposed to compression. The assembly of thin precast UHPC elements to such structures which also need to be high-temperature or fire-resistant requires point connections that lead to the introduction of high local compression forces. The implant developed by the authors introduces a high compression force that serves exactly this purpose; it thus allows utilizing precast elements almost to the compressive strength of UHPC.

Keywords: *UHPC structures, thin elements, prefabrication, point connection, load introduction, maximal utilization, homogeneous stress distribution, competitiveness*

1 Preliminaries

The development of ultra-high performance concrete (UHPC) offers a variety of new possibilities. Having the compressive strength of regular steel but only 1/3 of its specific weight, UHPC can be considered as a very efficient lightweight material. In addition to its low weight combined with a high compressive strength, UHPC has another key advantage: just as regular concrete it can be used to build structures in almost any shape. UHPC has the disadvantage of very low tensile strength; but the use of steel fibers instead of regular reinforcement makes it possible to reduce the thickness of structural elements significantly. These specifications predestine UHPC as material for thin compression members.

2 Principles and Possibilities of Thin-Walled UHPC Construction Members

2.1 UHPC – A High Performance Material?

High performance materials offer the possibility to construct highly efficient structures with significantly reduced cross-sectional areas. Given its high compressive strength of 150 – 250 N/mm² (800 N/mm² were reached under laboratory conditions [1]), there is very good reason to consider UHPC as such a high performance material. This is particularly the case when UHPC is used to build construction members that carry mainly compressive forces; such construction members are for example required for efficient lightweight structures [2].

As regular reinforcement is no longer necessary, achieving a thickness of only 20 mm is possible [3]. Almost all high performance materials are usually also high tech materials, and so is UHPC. Compared to normal or high-strength concrete, a lot more effort is necessary: This starts with strict requirements for the ingredients, a very stringent mixing process, heightened attention that is necessary during concreting, and finally various steps of sealing [4]. These specific requirements for the production of UHPC elements make prefabrication highly advisable. Only stationary production can make UHPC elements economically speaking competitive.

2.2 Structures of UHPC Elements

However, only individual components of a structure can be prefabricated; the structure itself still has to be assembled on-site. This leads necessarily to element connections that require special attention. There are two ways of connecting precast UHPC elements that differ substantially from each other: continuous connections and point connections. In the context of a load path, continuous joints are optimal: stresses are transferred directly from one structural element to the other. But, unfortunately, it is very difficult to produce continuous joints for UHPC elements in the homogenous quality needed (see 3.2).

Point connections, on the other hand, are easy to handle during on-site assembly. But point connections logically cause a concentration of stresses in the connection area which will govern the design of the UHPC element. The usual way of dealing with this concentration of stresses is to enlarge the cross-section (at least in the relevant areas); this leads to a thickness that is no longer economic. The avoidance of stress concentrations and the complete elimination of the resulting stress peaks by a specially designed implant will prepare the ground for highly efficient and optimized UHPC structures.

3 Joints of Structural Elements

3.1 Principles of Connections of Structural Elements

A multiplicity of parameters has to be considered whenever structural elements are connected [5]. The most important parameters are load transmission and interconnection of deformations, assembling, disassembling and recycling, thermal and acoustic interconnection as well as corrosion. [6] assembles the resulting requirements as follows:

- Distribution of forces has to be as simple as possible
- There are to be as few connections as possible
- The connection has to be functional in every occurring condition
- There has to be a possibility to adjust construction tolerances

According to [6] these basic requirements cause the following problems. They are the central issue in point connections for prefabricated elements:

- Introduction of concentrated forces into neighbouring structural elements
- The connection and the connected structural elements have different properties

3.2 Connecting Precast Concrete Elements

3.2.1 Precast Elements of Normal Strength Concrete

Precast concrete elements usually are connected either by starter bars and concreting or by steel parts bolted or welded together after assembly. The main disadvantage of the starter bars is related to the concreting of the gap between the precast elements: formwork has to be put in place; often the gap is difficult to reach; there is no suitable way to verify the quality of the concreted gap; it takes some time before the concrete has set; and, finally, the concreted gap remains visible. The big advantage is the possibility to handle tolerances of almost any magnitude; moreover there is no need for further measures to ensure the material's resistance against corrosion and fire. Most of the disadvantages mentioned above can be avoided by steel mounting parts, which – in turn – require significantly reduced construction tolerances. However, the connecting area has to be protected against fire and corrosion.

3.2.2 Precast UHPC Elements

There is a huge variety of possibilities to connect precast UHPC elements. The most important are [7]:

- Combining the elements with continuous prestressing cables
- Bolting the elements with high strength prestressed bolts [8]
- Glued connection of the UHPC elements [8]
- Bridging the gap with thin bars or steel fibers and concreting the gap with UHPC [9]
- Butt joint of UHPC elements fixed by carbon fiber composite plates glued on both sides
- Steel mounting parts bolted, welded or glued together

Adhesive joints are increasingly used in the construction industry and allow hitherto unknown structures [10]; but gluing is only of limited use for joints of UHPC elements since only the resistance of the matrix (which is only about 1/3 of the tensile strength [11]) can be activated. Furthermore, the continuous adhesion is difficult to ensure, construction tolerances are difficult to handle, and the temperature range in which this technique can be used is quite small. Already in general concreting a gap between elements is not advantageous for connections (see 3.2.1). It is completely unsuitable for the high performance material UHPC. Connections by prestressing are only applicable in the case of some beam structures as the continuous cables require a minimum thickness of the UHPC element.

The only remaining solution for easy connections between UHPC elements are steel mounting parts connected after assembly of the elements. The stricter requirements of construction tolerances for this solution can be met by increasing the number of industrial processes in the production of these elements. The use of steel mounting parts leads to point connections. Such connections cause concentrated compression forces that have to be introduced locally; in its turn, this again causes stress peaks.

4 Application of High Local Forces on Plate Elements

4.1 Principles

At a certain distance from the point of load application, the compressive stresses reach an equal distribution. The application of local forces thus creates singularities; these singularities cause stresses in the area of load application that are much higher than in areas of homogeneous utilization. For an efficient lightweight structure, a homogeneous distribution of stresses is necessary in order to avoid stress peaks that may cause early failure [12]. Only such a homogeneous distribution of stresses allows an optimal utilization of the structural components: the failure load is reached at any point at the same time. Trying to reach maximum utilization in an uninfluenced area of the element leads necessarily to problems in the singularity area as there is no high margin for increased stresses. The problems that have to be solved in the context of load introduction are:

- Statically indeterminate problems of disturbance
- Geometrical construction problem: interaction of dimensions
- Contact problems between different materials

Figure 1a shows the principal stresses in a thin UHPC plate that is exposed to a local compressive force. The compressive trajectories spread out from the point of load application causing orthogonal tensile stresses. For the load introduction zone of a normal strength concrete plate the usual approach by strut-and-tie models (fig. 1b) merges these tensile stresses on one single tie (T), which will be represented by the reinforcement bars.

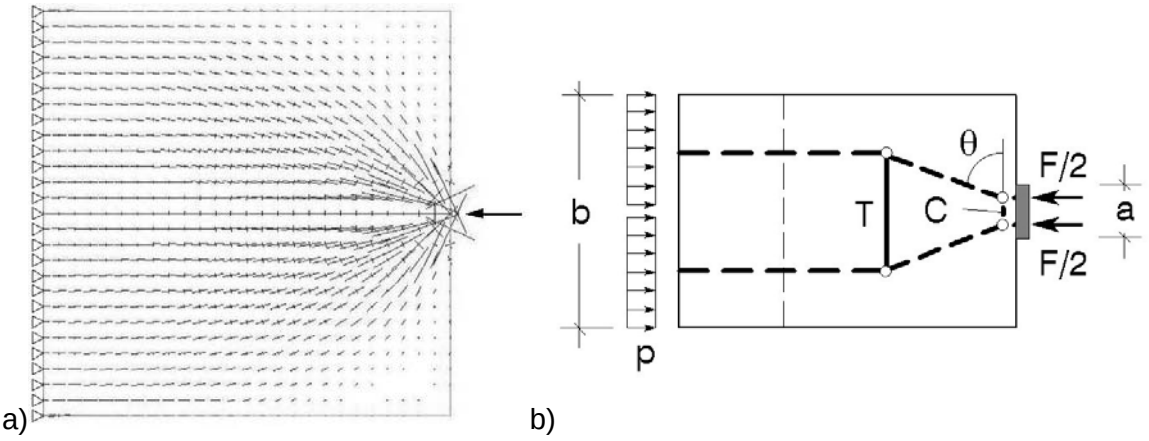

a) b)

Figure 1: Local load application:
a) principle stresses in UHPC plate; b) strut-and-tie model for concrete plate [13]

The pressure in the contact zone defines the dimensions of the surface of the load inducing plate (fig. 1b). The more the concrete element is utilized, the wider it has to be. As the cross-section in the point of load introduction has to be reduced significantly – compared to the concrete cross-section – the load has to be introduced along a certain length in the line of action of the force (see fig. 2a and 3b).

4.2 Adjusting the Stiffness of the Load-Inducing Component

The central objective of an improved load application is to dampen the singularities and to homogenise the stress fields. At best the load-inducing component transfers only as much stresses per length unit to the thin plate as this can carry without exceeding the ultimate strength. In the final consequence this leads to the fully stressed design of both the thin plate and the load inducing component.

Such a design can be achieved by adjusting the stiffness of the load-inducing component as shown in figure 2a. Compared to a load-inducing component with constant stiffness (as shown in the upper part of figure 2b), this adjustment of the stiffness leads to a shortened length of load introduction (as shown in the lower part of figure 2b): On the right end the complete force is transferred from the load-inducing component to the plate; the plate is utilized more than in the upper part, where, in addition, the force has not yet been transferred completely.

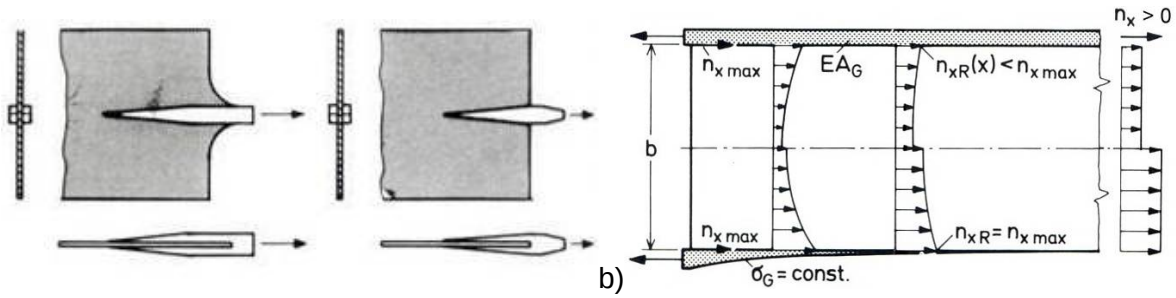

Figure 2: Adjustment of stiffness along the length of load transmission [12]:
a) examples for thin lightweight elements; b) influence on stresses and forces

5 Implants for Introduction of High Forces

5.1 Basic Requirements

The implant that introduces concentrated and high forces into thin-walled UHPC elements has to meet the following basic requirements:

- Complete introduction of force on a minimum length for efficient utilization of the element
- Following the flow of forces
- Preferably full and homogeneous utilization of all members: fully stressed design
- Complete avoidance of stress peaks
- Solution of contact problems between the different materials and the environment
- Integral element: no assembling of different parts necessary
- Visualization of the distribution of forces by the visible components
- Producibility of the implant
- Integration of the implant in the manufacturing process of the UHPC element
- Concretability of the UHPC element and bonding of the implant in the cross-section

The objective of connecting thin UHPC elements by implants makes it necessary to reduce the cross-section in the connection point significantly. The high compressive strength of UHPC together with the designated utmost utilization requires implant materials with a much greater strength than regular steel, i.e. high strength steel with a yield stress of almost 900 N/mm². An alternative material is titanium, which seems appropriate for this purpose with a yield stress of about 1.000 N/mm² and a modulus of elasticity of 110.000 N/mm². However, the costs of this material are up to 6 times that of high strength steel. This high price allows the use of titanium only in small quantities (if at all).

5.2 The Problem

The core of the problem lies in the section of a thin UHPC plate as shown in figure 3a. The compressive stresses σ_x in section 1-1 – which is located at a distance L as close to the point of load application as possible – have to be constant. This means $\sigma_{x,1\text{-}1}$ = const. A thickness of 20 mm, a compressive strength of 180 N/mm² for the UHPC, and a maximum compressive stress $\sigma_{x,1\text{-}1}$ of 160 N/mm² (which equals approx. 90 % of the compressive strength) form the basis of the following research. With a width h (fig. 3a) of 250 mm, the resulting compression force F is already 800 kN. This requires a high strength steel cross-section of the implant in the point of load application of 20 x 45 mm.

5.3 Development of the Implant Geometry

As requested above, the geometry of the implant is developed by accurate observation of the load bearing behavior in the load introduction zone. The extreme utilization of the precast element generates tensile stresses orthogonal to the compressive trajectories (fig. 1a) which already exceed the tensile strength of UHPC at only 14 % of the required force F. The implant has to carry not only these tensile stresses by suitable tension elements adhering to the directions of the principle tensile stresses; the implant also has to carry the compressive stresses.

The best solution for the latter is an adaptation of the saw-tooth-connections developed for normal strength concrete [14] to the needs of UHPC and the special requirements of the implant (fig. 3b). A simple bond is not sufficient for the load transmission between the UHPC element and the tension elements: the loading is too high, and the small thickness favors splitting. Therefore, suitable tension elements support the UHPC cross-section along its whole thickness as shown in fig. 3b. The interlocking component is of major influence for the homogenization of stresses discussed in the next chapter. This interlocking component is shown in fig. 3b with a linear decreasing stiffness.

5.4 Homogenization of Stresses

The importance of a homogenized stress distribution for an efficient use of structural members has been explained above (2.1). Figure 4 shows the deviation of stresses σ_x in section 1-1 from the ideal constant stress distribution for different materials and designs of the interlocking component. The stresses are shown in one symmetric half of figure 3a for a width of the UHPC plate of h = 250 mm (h/2 = 125 mm).

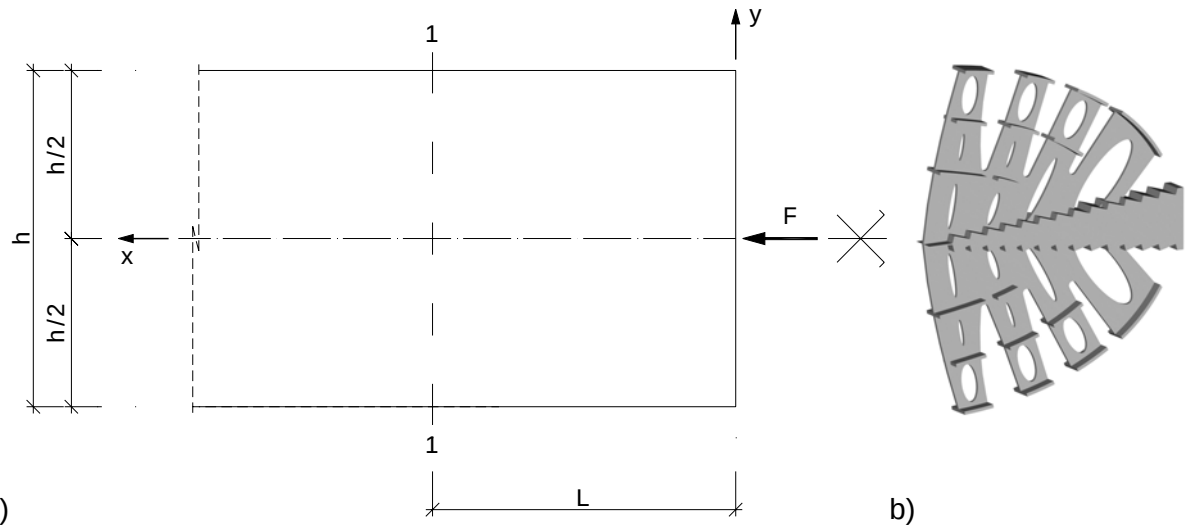

Figure 3: Problem statement and final solution:
a) analyzed detail of the UHPC plate; b) final implant

Starting with high strength steel and a constant cross-section (“steel, EA=const.” in fig. 4), the maximum stresses $\sigma_{x,1\text{-}1}$ reach about ± 40 % of the designated value. By simply adjusting the cross-section of the interlocking component following the rule of fully stressed design like explained in 4.2 (“steel, EA=opt.”), these stress deviations can be reduced to ± 30 %. For the investigated problem, the fully stressed design leads to an almost linear decrease of the cross-section of the interlocking component. Further reduction of the stiffness is only possible by using less stiff materials like titanium – with an adjusted cross-section (“titanium, EA=opt.”) this leads to significantly reduced stress deviations of only ± 15 %. This reduction already allows the application of a considerably increased compression force.

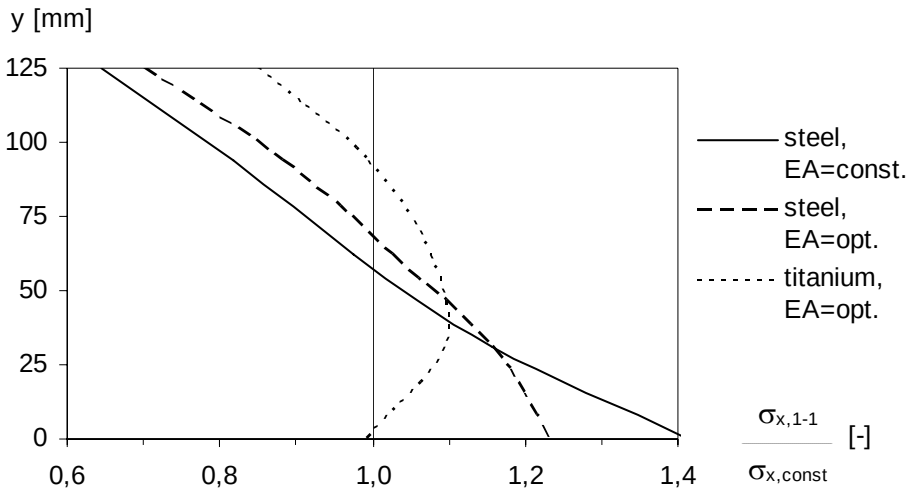

Figure 4: Distribution of stresses σ_x in section 1-1 in relation to constant stresses

Further reduction of the stress deviations can be reached by adding defined elasticity to the area of connection between the interlocking element and the UHPC plate, for example by the application of plastics in certain thicknesses on the teeth flanks. These measures allow a constant stress distribution at only L = 220 mm (fig. 3a) from the point of load application,

which is only about 90 % of the width h. Finally, only this constant stress distribution allows the maximal utilization of the thin structural compression member made of UHPC.

6 Conclusion

The maximum loading that is possible on structural elements is normally defined by the concentrated stresses in the area of load application. Stress peaks usually cause failure in this area long before the load bearing capacity of the whole element is reached. The implant developed by the authors introduces high compression forces into thin-walled UHPC elements without creating such stress peaks. This allows a maximum utilization of the UHPC element up to almost 90 % of its compressive strength. This is a fundamental prerequisite for an economic and competitive application of the high performance material UHPC in the construction industry.

7 References

[1] Holschemacher, K.; Dehn, F. (2003): Ultrahochfester Beton – Stand der Technik und Entwicklungsmöglichkeiten. S. 1-12 in: Ultrahochfester Beton. Innovationen im Bauwesen. König, G.; Holschemacher, K.; Dehn, F. (Hrsg.). Berlin, Bauwerk Verlag, 2003.

[2] Sobek, W. (1995): Zum Entwerfen im Leichtbau. Bauingenieur 70 (1995), S. 323-329.

[3] Vincenzino, E.; Culham, G.; Perry, V.H.; Zakariasen, D.; Chow, T.S. (2005): First Use of UHPFRC in Thin Precast Concrete Roof Shell for Canadian LRT Station. PCI Journal, Vol. 50 (2005), No. 5 (September-October), S. 50-67.

[4] Dehn, F. (2005): Qualitätsgerechte Herstellung, Verarbeitung und Nachbehandlung von Ultra-Hochleistungsbeton. Betonwerk + Fertigteil-Technik 71 (2005), Heft 2, S. 22-23.

[5] Sobek, W.; Schäfer, S. (1996): An der Nahtstelle – Fügen von Bauteilen aus unterschiedlichen Werkstoffen. deutsche bauzeitung 130 (1996), Heft 1, S. 106-114.

[6] Witta, E. (1975): Kraftschlüssige Verbindungen und ihre Rückwirkungen auf das Bauwerk. Betonwerk + Fertigteil-Technik 41 (1975), Heft 11, S. 527-530.

[7] Greiner, S. (2006): Zum Tragverhalten von dünnen Bauteilen aus ultrahochfestem Faserfeinkornbeton. Göttingen, Cuvillier Verlag, 2006.

[8] Fehling, E. (2005): Konstruieren von Tragwerken aus Ultra-Hochleistungsbeton – eine Herausforderung. Betonwerk + Fertigteil-Technik 71 (2005), Heft 2, S. 26-27.

[9] Reineck, K.-H.; Greiner, S. (2004a): Dichte Heißwasser-Wärmespeicher aus ultrahochfestem Faserfeinkornbeton. Forschungsbericht zum BMBF-Vorhaben 0329606 V. Institut für Leichtbau Entwerfen und Konstruieren, Universität Stuttgart, 2004.

[10] Blandini, L. (2005): Structural Use of Adhesives in Glass Shells. Stuttgart, Verlag Grauer, 2005.

[11] Behloul, M. (1996): Les micro-bétons renforcés de fibres. De l'éprouvette aux structures. XIVième Journées de l'AUGC, Clermont-Ferrand. Prix Jeunes Chercheurs „René Houpert", 1996.

[12] Wiedemann, J. (1989): Leichtbau – Band 2: Konstruktionen. Berlin, Springer Verlag, 1989.

[13] Schlaich, J.; Schäfer, K. (1998): Konstruieren im Stahlbetonbau. S. 721-895 in: Beton-Kalender 1998, Teil II. Berlin, Ernst & Sohn, 1998.

[14] Schmid, V. (2001): Geometry, Behaviour and Design of High Capacity Saw-Tooth Connections. S. 1119-1128 in: Proceedings of the International Symposium on Connections between Steel and Concrete, Vol. 2. Eligehausen, R. (Hrsg.). Cachan, RILEM Publications s.a.r.l., 2001.

Olivier Remy
Vrije Universiteit Brussel (VUB)
Brussel, Belgium

Jan Wastiels
Vrije Universiteit Brussel (VUB)
Brussel, Belgium

Niki Cauberg
BBRI: Belgian Building Research Institute
Sint-Stevens-Woluwe, Belgium

Julie Piérard
BBRI: Belgian Building Research Institute
Sint-Stevens-Woluwe, Belgium

Flexural Behaviour of Fibre Reinforced Ultra High Performance Concrete and the Application in Cladding Panels

Summary

Developments in admixture technology have been a tremendous boost last years for developing advanced concrete types. With the last generation of superplasticizers for instance, water-cement-ratio can be decreased dramatically, allowing among others self-compactability of concrete. Addition of (ultra)fine materials increases furthermore packing densities. The combination of these techniques results in concrete types with extra-ordinary mechanical properties and durability, usually referred to as Ultra High Performance Concrete (UHPC). A BBRI and VUB research evaluated the mix design of this type of concrete, the shrinkage at early age, the flexural behaviour of the (fibre/textile) reinforced concrete and its applications. As a case study, the use of UHPC for cladding panels has been detailed.

As far as mix design concerns, the research focused on the choice of admixtures and (micro)fillers, aggregate grading and fibre cocktail. A mortar-like UHPC with a compressive strength between 150 and 200 N/mm², a high powder content up to 1000 kg/m³ and a maximum aggregate diameter of 3 mm has been used for characterizing the flexural behaviour of UHPC with micro and macro fibres. For a number of tests, the steel fibres have been combined with textile reinforcement. Besides a number of bending tests on small specimens, several real-scale cladding panels have been casted and tested. Alternative anchorage systems have been studied as well, possibly allowing the use of large panels.

Keywords: U*ltra High Performance Concrete, fibre reinforced concrete, textile reinforced concrete, cladding, anchorage systems, flexural behaviour, shrinkage*

1 Ultra High Performance Concrete: General Principles and objectives

The main objective in the development of Ultra High Performance Concrete (UHPC) is to obtain superior mechanical behaviour compared to standard concrete. Concrete with a compressive strength of about 150 N/mm² or more is usually labelled as UHPC. Extensive research has been done in this field, resulting in the development of “Reactive Powder

Concrete". The development of this concept continued in France and Canada during the nineties.

The basic principles of this concept are:

- An increased homogeneity by excluding coarse aggregates, increasing the powder content and restricting the maximum particle size to 1 mm, sometimes even less;
- An improved aggregate packing by selecting appropriate particle size distribution;
- A decrease of water-cement-ratio (W/C-ratio) using large quantities of third generation superplasticizers.

Taking these three principles into account, a matrix with superior properties can be obtained. Addition of fibres counteracts the brittle behaviour, improving the ductility and, possibly, the tensile strength of the concrete. The optimized packing results furthermore in a very dense matrix, with a high durability. This does not compromise the workability, and even self-compacting UHPC is possible.

Over the last decade, the impact of this material in the building industry is growing and, considering the ever growing demand of performance, will continue to gain importance. Therefore, an increasing amount of examples can be given where Ultra High Performance Concrete is used, sometimes as an alternative for steel. For instance, the pedestrian bridges in both Sherbrooke (Canada, 1997) and Kassel (Germany 2004-2005), a roof with a helicoidal shape covering the toll plaza of the Millau bridge (France 2004), …all of them illustrating the potential of the material.

Nowadays, UHPC usually requires precast production and thermal curing. The goal of this research was to obtain a mixture for ready-mix concrete and on-site placing. Furthermore, only locally produced and available constituents have been used rather than dry premixed compositions.

2 Ultra High Performance Concrete: composition

The mentioned basic principles for reactive powder concrete have been applied for the development of different concrete types: an important increase of the powder content and a limitation of the particle size (with an upper limit of 3 mm). This mortar-like concrete is composed of ultra reactive powders (cement, silica fume) and inert fillers (quartz sand and porphyry). Without special treatment, a compressive strength of 180 N/mm² has been achieved. Silica fume in suspension slurry (1 : 1 in mass) was used. The total W/C ratio is 0.21. The powder content is 1000 kg/m³. To improve flexural behaviour and ductility, four different types of fibre reinforcement have been selected: two types of steel microfibres[*] and one type of longer steel fibres[**] plus one continuous PVC coated glass fibre grid[***].

[*] 160 µm diameter microfibres with a length of 6mm (l/d = 38) or 13mm (l/d= 81)

[**] 380 µm diameter fibres with a length of 30mm (l/d = 79) with hooked ends

Table 1: Composition of the reference mixture

Composition	Material Density [g/cm³]	[kg/m³]	vol. [%]
Porphyry 1/3	2.70	789	29
Quartz sand 0/0.5	2.65	363	13
CEM I 42,5 R HSR LA	3.10	833	26
Superplasticizer (polycarboxylate based)	1.06	20	2
Silica Fume (dry)	1.40	167	12
Water	1.00	179	18

3 Basic material tests

3.1 Compressive strength of fibre reinforced UHPC

The compressive strength (6 specimens) has been measured at 2, 7, 28 and 91 days using 100x100x100 mm³ cubes preserved in moist conditions (RH > 95%) at 20°C. The results for the reference mixture (Table 1) with 2% vol. microfibres of 6 mm length are mentioned in Table 2.

Table 2: Compression strength of reference mixture

2 days		7 days		28 days		91 days	
AVG [MPa]	stDEV [MPa]	AVG [MPa]	stDEV [MPa]	AVG [MPa]	stDEV [MPa]	AVG [MPa]	stDEV [MPa]
99	1.2	138	0.5	172	3.5	188	3.8

3.2 Flexural behaviour of UHPC

The flexural behaviour of the reference mixture with different types of reinforcement was determined by means of a four-point bending test specified in the Belgian standard NBN B15-238 (similar to ASTM C1018) on 150x150x600 mm³ prisms. The results (3 to 6 specimens) for the reference mixture (Table 1) with 0%, 2% and 4% vol. microfibres are mentioned in Table 3.

Table 3 and Figure 1 both show an increase in ductility. The values B150 and B300 quantify this ductile behaviour by calculation of the area beneath the displacement-force curve until a displacement of 1/500 (B150) or 1/300 (B300) of the span is reached. An addition of 4% fibres (in volume) leads to a limited hardening in flexure (Figure 1), but a strain hardening in tension is not expected. Howerver, it seems that a higher dosage would affect strongly the workability of the concrete.

*** 108 g/m² 1 x 1 544tex glass fibre grid with EVA coating

Table 3: Flexural behaviour of fibre reinforced UHPC

Fibres [%]	Fr [kN]	fr [N/mm²]	Fu [kN]	fu [N/mm²]	B150 [kNmm]	B300 [kNmm]
0%	97	13	97	13	4	4
2%	95	13	107	14	8	104
4%	123	16	136	18	13	144

Fr: force at first crack
fr: tension at first crack
Fu: ultimate force
fu: ultimate tension

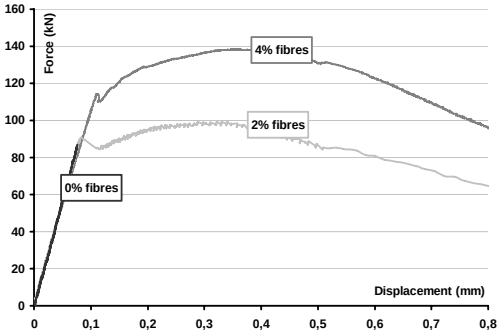

Figure 1: Displacement vs. force curves for fibre reinforced UHPC

3.3 Shrinkage of UHPC

Immediately after the end of binding (10-13 hours after casting), 70x70x280 mm³ samples are demoulded and drying shrinkage measurements are started. The shrinkage of the UHPC is measured vertically using a device attached to the samples, which are exposed to ambient conditions (20±2°C; 65±5% RH). Figure 2 shows the results of drying shrinkage measurements for the reference mixture (Table 1). Furthermore, the effect of admixtures, fibres and reduced powder content has been evaluated as well.

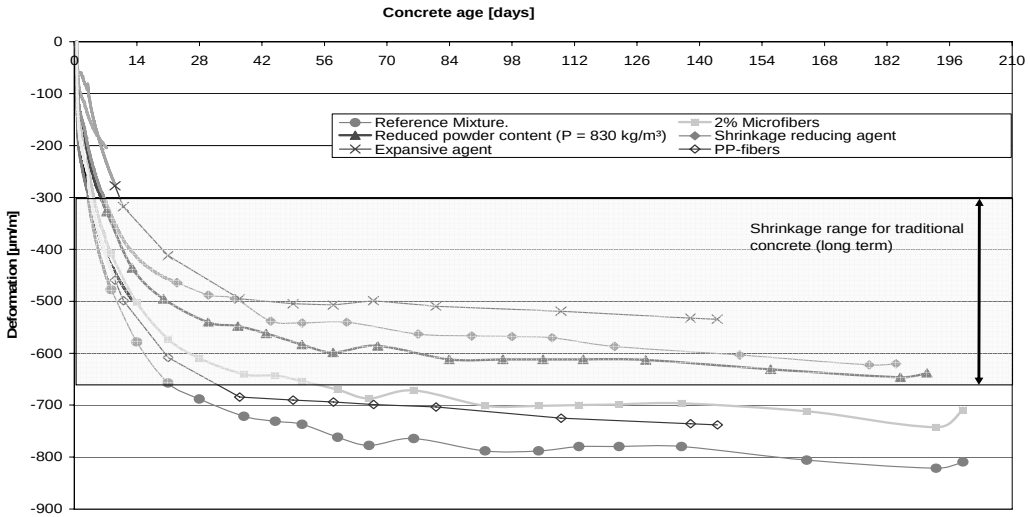

Figure 2: Long term drying shrinkage for the reference mixture with different type of admixtures.

4 Case study: Thin panels in fibre reinforced UHPC

As an example of a small-scale application of UHPC, thin panels have been proposed for a first case study. Main loads for these thin plate-elements, for instance when used as cladding panels for facades, are wind and self-weight. Two aspects are important when increasing the dimensions of these elements: the flexural behaviour and the anchoring to the supporting structure.

Wind-pressure for instance will introduce well distributed stress; compressive as well as tensile. The forces introduced due to this wind load have to be transferred from the cladding to the structure by anchorage. In this anchorage zone, a local stress concentration exists. The two mentioned aspects, flexural behaviour and anchorage, are linked: the anchorage choice will affect the flexural behaviour of the thin plate-element.

4.1 Flexural behaviour of thin plates in UHPC

The reinforcement should give the thin plate sufficient flexural strength and should increase the ductility of the brittle UHPC material. Therefore, a hybrid reinforcement was engineered using a PVC coated glass fibre scrim and 6 mm steel microfibres. The scrim was positioned near to the tensile surface, while the micro steel fibres were added to the concrete mixture and were assumed as equally three dimensionally distributed. Three point flexural tests over a 120mm support span have been performed on prisms with dimensions of 40x60x160 mm³ (h x w x l) to determine the influence of the textile reinforcement. Figure 3 plots the displacement-force curve for the textile reinforcement, using three different densities of longitudinal fibres (54, 108 or 162 g/m²). The results show a gradual increase in post cracking behaviour.

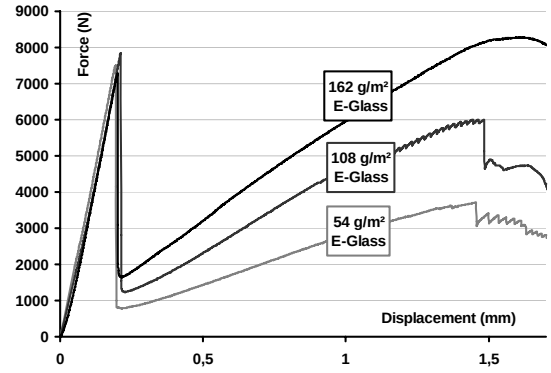

Figure 3: Displacement-force curves using only textile reinforcement

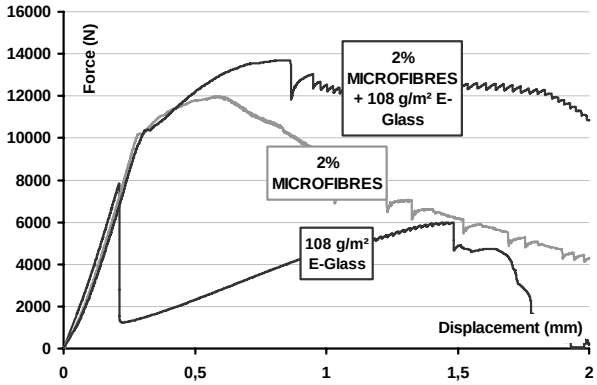

Figure 4: Comparison of displacement-force curves to evaluate the influence of textile reinforcement.

Figure 4 illustrates the effect of a combination of steel microfibres with a PVC coated glass fibre grid. A clear ductility increase can be seen from the moment the microfibres are pulled out of the UHPC: the effect of microfibres and of glass grid on the post cracking behaviour can be superimposed, leading to a ductile behaviour at constant maximum load.

The standardised four–point bending test on 150 x 150 x 600 mm³ prisms shows a fairly low degree of ductility. To further increase this degree of ductility, mixes of short and longer fibres have been tested. Real scale cladding elements with a length of 2 m and thickness of 0.04 m have been realized on which a 4 point bending test has been performed (span L = 1800 mm,Figure 5).

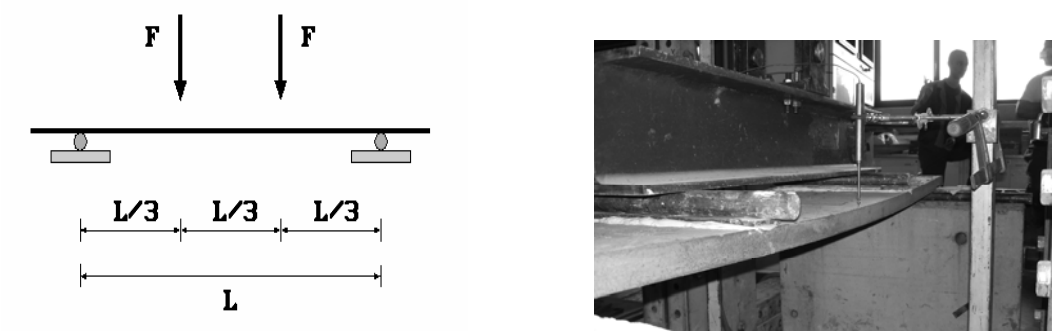

Figure 5: Four-point bending test on cladding elements.

Three different combinations of fibres have been used:

- 2 % vol. microfibres of 6 mm
- 1.3 % vol. microfibres of 6 mm and 0.7% vol. microfibres of 13 mm (microfibre mix)
- 1.3 % vol. microfibres of 6 mm and 0.7% vol. macrofibres of 30 mm (macrofibre mix)

The combination of 6 mm and 13 mm fibres does not improve noticeably the ductility. Addition of longer fibres however introduces strain hardening: the element resists an increased load after the appearance of the first cracks (Figure 6).

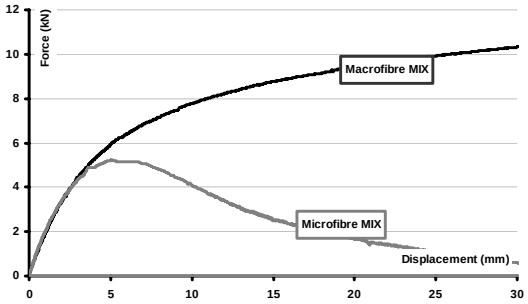

Figure 6: Displacement vs. force curves for cladding elements

A partial explanation for this strain hardening behaviour is that the 30 mm fibres get a better orientation due to the limited thickness of the cladding element: most of the fibres near the surface are (partially) aligned due to the "wall effect". Moreover, the anchorage of the hooked-end fibres enhances their crack bridging load bearing behaviour, compared to the straight microfibres. It can be mentioned that all tests performed using steel fibres as reinforcement show pull out as the cause of failure.

4.2 Anchorage

Traditionally the anchoring of claddings is made by dowels on the border side of the cladding, lying in the plane of the cladding. This usually is the best option for cladding panels made from natural stone, but concrete-made panels offer new possibilities for anchorage, for instance integrated in the concrete and perpendicular to the surface of the cladding. In this way, both the span between the anchorages and the local stress could be decreased.

Based on numerous tests, the performance of dowels embedded in (6 mm microfibre reinforced) UHPC has been compared to the performance of natural stone (Figure 7). A dowel is placed in a stone with specified dimensions and is loaded perpendicular to the length. Table 4 indicates the average breaking force in N and the average width of the damaged zone (bA).

Figure 7: Determination of the breaking load at dowel hole (NBN EN 13364)

An increase in fibre volume fraction results in a higher breaking load, and a much increased toughness. Comparison with most natural stones, which roughly have an ultimate load varying in between 2000 and 2500 N, illustrates that anchorages in fibre reinforced UHPC transfer higher loads which could lead to larger dimensions of the cladding elements. It can be seen on the displacement vs. force curve (Figure 8) that an increase of reinforcement increases the safety of the anchorage.

Table 4: Determination of the breaking load at dowel hole

Test Sample	Avg bA (mm)	Fu (N)
UHPC 0% fibres	54	2150
UHPC 1% fibres	58	2700
UHPC 2% fibres	52	3800
UHPC 3% fibres	47	4350

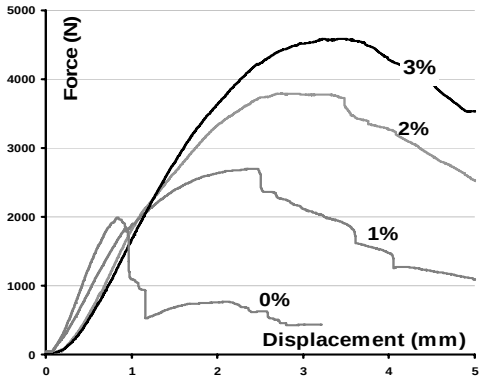

Figure 8: breaking load at dowel hole

Concrete claddings offer furthermore the possibility to insert an anchorage system while cast-ing, which could result in a more performant system. Connected to a reinforcement, a durable and safe anchorage could be guaranteed. For preliminary testing, a simple system connecting the anchorage to a PVC coated glass fibre grid (Figure 9) has been developed. Three different thicknesses of panels were produced and tested (20-30-40 mm). The scrim was placed in the centre of the panel (Figure 9).

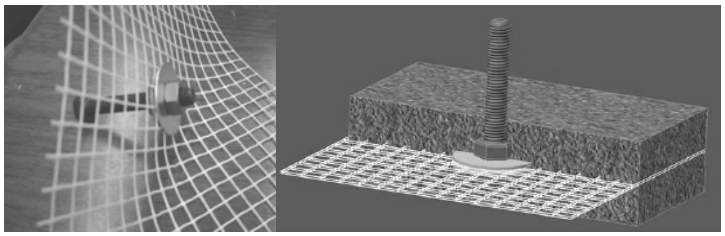

Figure 9: Anchorage

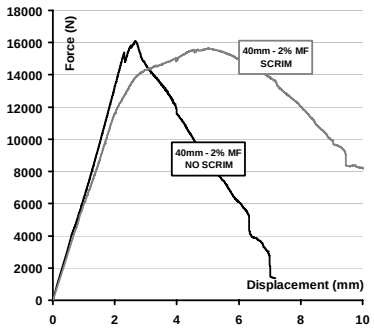

Figure 10: Anchorage Pull-Out

Table 5: Pull-out force of an (anchorate) dowel

Average Force (N)	20mm	30mm	40mm
2% MF - NO SCRIM	6431	11342	16505
2% MF - SCRIM	6163	10664	15530

Comparing between this anchorage to the conventional system, it appears that three times higher loads can be safely transmitted to the supporting structure. Connecting the anchorage to the grid does not lead to an increased strength, but a gain in ductility was clearly noticeable (Figure 10).

5 General conclusions

A BBRI and VUB research evaluated the mix design and production of UHPC using standard materials and equipment. Basic properties such as the shrinkage at early age and the flexural behaviour of the UHPC have been tested, with promising results. The acceptable shrinkage results do not limit the application possibilities, and the choice of an adapted reinforcing system results in high ductility and tenacity, high flexural strength and even strain hardening behaviour for some fibre mixes. Evaluation of the properties of thin plate elements (e.g. claddings) in fibre reinforced UHPC, indicates the possibility to manufacture strong and ductile building elements with a high durability. The obtained strain hardening behaviour, using a combination of long and short fibres, allows the designer to engineer thinner/larger plates while the increase of strength of the integrated anchorages still ensures the transfer of wind loads to the supporting structure.

Financial support of IWT through contract VIS/CO-040763 is gratefully acknowledged

6 References

[1] Richard P. en Cheyrezi M. Composition of reactive powder concrete. New York, Elsevier Science, Cement and Concrete Research, Vol. 25, nr. 7, pp.1501-1511, 1995.

[2] NBN B15-238: four point bending test on fibre reinforced concrete.

[3] NBN EN 13364: Determination of the breaking load of a dowel hole.

Tommy Cousins
Prof.,
Via Department of Civil Engineering
Virginia Tech
Blacksburg, USA

Carin Roberts-Wollmann
Prof.,
Via Department of Civil Engineering
Virginia Tech
Blacksburg, USA

Elisa Sotelino
Prof.,
Via Department of Civil Engineering
Virginia Tech
Blacksburg, USA

UHPC Deck Panels for Rapid Bridge Construction and Long Term Durability

Summary

This paper will report the authors' vision and research plan for developing a ultra high performance concrete (UHPC) bridge deck system for short, medium and long spans bridges This development is being funded by the Virginia Department of Transportation (DOT) and coordinated with the Federal Highway Administration. Use of the UHPC bridge deck system on steel or prestressed concrete girders is anticipated. There is significant potential for development of a bridge deck system that will be much lighter, easier to install, and longer lasting than the recently developed alternatives to the conventional cast-in-place reinforced concrete bridge deck system. The proposed bridge deck system will include UHPC precast, prestressed (waffle or ribbed) deck panels with a target compressive strength of from 172 to 193 MPa. The research plan includes modeling and optimization of section geometry as well as static and fatigue testing of deck configurations.

Keywords: *bridge decks, prestressing, high performance concrete*

1 Introduction

Bridge decks are essential components of the national transportation infrastructure lifeline and represent a significant financial investment. For many years, conventional cast-in-place reinforced concrete decks have been the technology of choice for these components even though their performance has been under continuous scrutiny. Of particular concern is their short lifecycle (ranging from 35 to 40 years depending on location in the USA), which requires frequent overlays and/or replacement. These repairs result in traffic disruption and a threat to public safety. An evidence of this concern is the level of funding dedicated by federal and state agencies to seek alternative technologies to these conventional systems. However, to date a single solution has not become the de facto answer.

Two concretes, which have been labeled "ultra-high performance concrete" (UHPC), have been developed by Bouygues Construction and Eiffage Group. The concretes have the

brand names Ductal and BSI (Beton Special Industriel), respectively. UHPC has very high compressive strengths (159 to 345 MPa) combined with other desirable properties such as improved workability, reduced labor for installation, superior durability and long term cost savings as compared to normal concrete [1][2]. Steel fibers can be added to UHPC to further improve performance. The fibers, in the very fine and dense cementitious matrix, allow tensile stresses of 6.9 to 8.3 MPa to be carried across open cracks. This tensile capacity can allow the elimination of mild reinforcement in many applications. These products have been used in a few structures internationally, and in a handful of demonstration projects in North America.

The objective of this research is to provide an effective alternative solution for the bridge deck dilemma by investigating the applicability of UHPC to bridge deck panels. The proposed bridge deck system includes UHPC precast, prestressed deck panels with a target compressive strength of from 172 to 193 MPa that are connected together and made composite with the supporting girders. The proposed deck cross section is a waffle or ribbed slab configuration with the panels bolted together on site and made composite with supporting the girders. The development of the bridge deck system is being accomplished through a comprehensive experimental and analytical program. The research program includes the following critical steps:

- the proper characterization of this material's properties,
- the development and testing of critical structural details,
- the development of analytical models to optimize deck sections and to predict the long term behavior of these systems,
- the casting and testing of the most promising deck sections,
- the implementation and monitoring of a precast, prestressed deck panel system with UHPC concrete,
- the development of design guidelines for these systems, and recommendations for future research.

The main advantages of using UHPC in bridge decks are:

- Significant super-structure weight savings.
- Improved durability and life span of the bridge deck.
- Significant reduction if not elimination of cast-in-place concrete in bridge decks which speeds up construction.

1.1 Comparison to other systems

The proposed UHPC deck panels offer added benefits when compared with other similar ideas being investigated as replacements to the conventional reinforced concrete cast-in-place bridge deck system. Following is a brief comparative description of other technologies to the proposed UHPC deck system:

Full depth precast, prestressed panels: In the United States, the Federal Highway Administration (FHWA) through National Cooperative for Highway Research Program (NCHRP) and several state DOTs have funded the development of this alternative. The advantages to this system are similar to those of the present proposal. The precast panels

should be more durable than conventional cast-in-place concrete because the panels are prestressed in both directions and the quality control of the concrete should be improved through precasting. Even though the cost of these systems is only a little higher than conventional systems, UHPC decks have a major advantage over this system because of its nearly impermeable nature, which will produce a longer lasting system and eliminate the need for longitudinal post-tensioning.

SPS (steel sandwich panel system) deck panels: These steel plate/composite sandwich systems are prefabricated and bolted and welded together in the field which speeds up construction. Unlike UHPC deck panels, the SPS system requires field welding, a slow and difficult process which can lead to fatigue issues and thus affect the long term performance of the system. In addition, the per square foot cost of an SPS bridge deck system is higher than the anticipated cost of the proposed UHPC bridge deck system.

FRP (fiber reinforced polymer) deck systems: Pre-fabricated FRP panels are adhesively bonded, grouted, or bolted together in the field. Besides its high cost, due to low modulus, FRP decks are mainly suitable for short span bridge applications. UHPC deck panel sections can be designed to have higher stiffness and thus have the potential for applicability to virtually any span length.

The proposed bridge deck system is superior to the above mentioned alternatives in many ways. It is lighter weight than conventional precast bridge deck panels, it is far more durable than any alternate and it is more rapidly constructed. The system being developed will enable bridge decks to be replaced very quickly and the new deck should have a far longer maintenance-free life than any current option. Older bridges will be given new life and will be able to carry heavier live loads due to the reduction in dead load.

1.2 Background

UHPC is a reactive powder concrete that can be produced with compressive strengths up to 759 MPa [1], although typical strengths are between 159 and 345 MPa [3]. The mixture consists of cement, silica fume, crushed quartz, sand, superplasticizer, water, and steel fibers. The steel fibers, approximately 2.5% by volume, add ductility to the otherwise very brittle material. The underlying principle in the design of UHPC mixtures is that a material with minimum defects, such as microcracks and pore spaces, will have the ability to achieve a larger percentage of the ultimate strength of its constituent materials, and will obtain enhanced durability properties.

The high compressive strength is derived primarily from the exclusion of coarse aggregate, a very low water-cement ratio, and the optimized compact grading which results in a very dense matrix with minimal voids. The largest granular material in the mix is the fine sand, typically between 150 and 600 μm. UHPC's tensile strength originates from small steel fibers, 0.18 mm diameter by 12.7 mm long, randomly distributed throughout the matrix, which act as reinforcement similar to rebar, but on a smaller scale. In addition, the permeability of UHPC is very low as a result of the dense matrix, making the material highly resistant to the corrosion and deterioration often associated with reinforced concrete and steel structures. This resistance should result in a long service life for UHPC, making it an ideal material for a number of structural applications, particularly bridge structures. Graybeal [4] reported results

of extensive durability testing conducted at FHWA. His testing program included freeze-thaw resistance, Alkali-Silica reaction, rapid chloride ion penetration, chloride penetration, scaling resistance, and abrasion resistance tests. His results showed that “UHPC displays durability properties that are significantly beyond those normally associated with concrete”.

The improved material properties, which result in significant weight savings, come at a cost. Presently, it is more costly than typical concrete, with prices quoted from $785 to $1700 per cubic meter [1][5][6]. More recent estimates place the per cubic meter price of UHPC between $1829 to $2222. However, because of its improved material properties it is expected that the lifecycle cost of a structural system built with UHPC may not ultimately differ that much than a conventional system. Furthermore, if the downtime, inconvenience, and risks to the public associated with the replacement of a deteriorated bridge are factored in, the use of this initially more expensive material will be fully justifiable.

2 Proposed Bridge Deck System

The researchers’ vision is the development of a lightweight, precast, durable, concrete bridge deck system for short, medium and long spans bridges. Figure 1 shows a schematic representation of the concept. Use of the UHPC bridge deck system on steel or prestressed concrete girders is anticipated. However, steel girders are shown in Figure 1 for simplicity. The researchers view this as a important step in the development of bridge deck systems for the future. There is significant potential for development of a bridge deck system that will be much lighter, easier to install, and longer lasting than the recently developed alternatives to the conventional cast-in-place reinforced concrete bridge deck system. In this research project the technical barriers to full implementation of these systems are being identified. This is a first step towards the development of a fully implementable system, which eventually will lead to the application of this new technology for long span bridges.The vision for the future is, therefore, UHPC bridge deck panels that can be very reliably modeled and designed, easily and rapidly installed, and that will last far longer than any currently available alternative. UHPC is impermeable and is not degraded by environmental stresses. In addition, tests have shown that it is highly impervious to impact and blast loads. Science fiction novels have coined the term “perma-crete”, and UHPC is the closest that current technology can come to this vision. So, with UHPC the life span of the bridge decks may be beyond our ability to imagine, but will certainly be far greater than current conventional reinforced concrete or orthotropic steel decks. New life can be given to old structures through the replacement of a deteriorated deck with a UHPC full-depth deck panel system.

UHPC has material properties that are very different from normal or even high performance concrete. The compressive strength can range from 159 and 345 MPa, and a tensile stress of 6.9 to 8.3 Mpa can be carried across an open crack. However, for this project compressive strengths in the 172 to 193 MPa range are targeted. The first step of the research plan is to optimize the deck panel configuration in order to take the greatest advantage of these properties. Aspects of the panel geometry to be optimized include the web spacing, the web width, top slab depth, web taper, amount of prestress and others. The investigators are at the forefront of the research in the use of UHPC in bridge infrastructure. They have gained

significant experience identifying the challenges associated with the modeling of UHPC for structural applications as part of a current effort to optimize I-girder shapes for bridge applications (Project titled “Modification of existing Prestressed Girder Cross Sections for the Optimal Use of Ultra-High Performance Concrete (UHPC)” which is funded by FHWA through a contract with PSI is in progress). They are using this knowledge to develop bridge deck panel concepts which make the best use of the UHPC material properties.

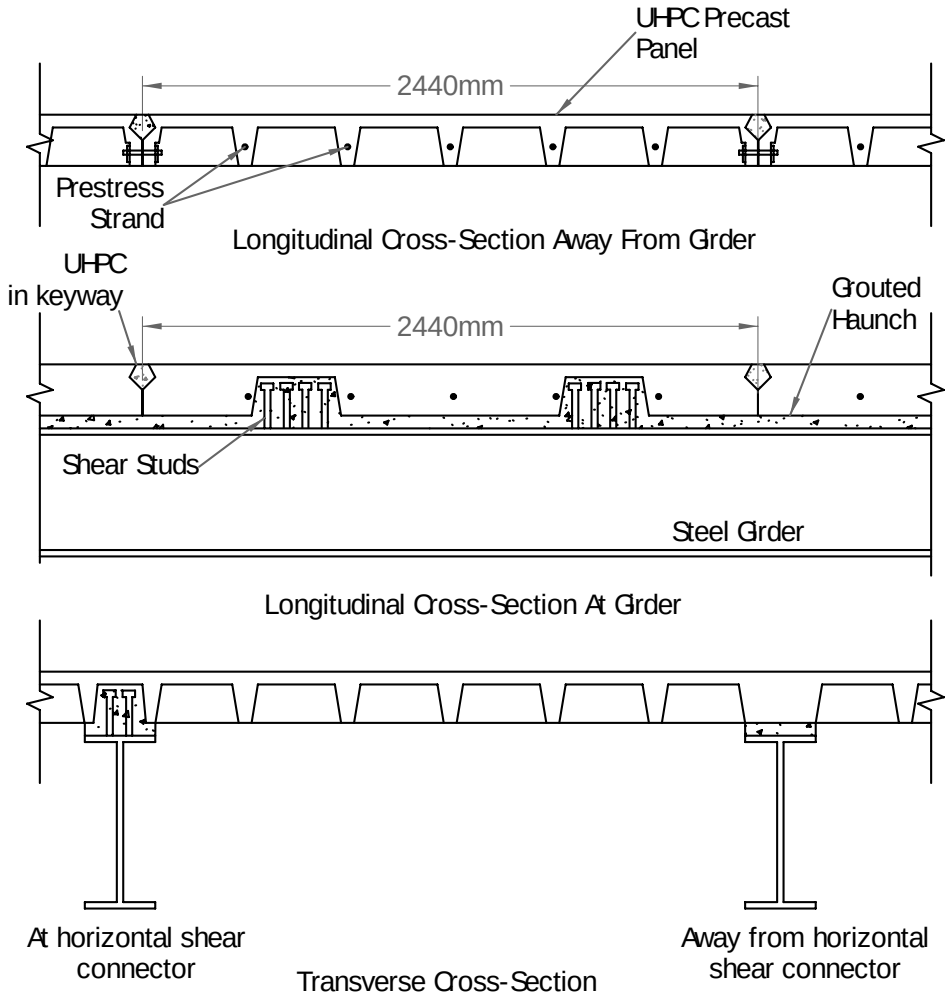

Figure 1: UHPC Deck Panel Concept

The overall research program includes two major fully integrated and interdependent components. The experimental component is intended to provide the necessary material fundamental properties and detailed connection behavior. With the full understanding of these basic behaviors and data, reliable analytical models are developed. These models are then used for the optimization of the deck panel configuration. Once optimal configurations are developed, further experimental testing will be carried out on a prototype deck system, which will be used to further validate the analytical models. Once fully validated the analytical models will be used in the development of practical design guidelines.

2.1 Experimental program

The first phase of the experimental program consists of basic tests to characterize UHPC material constitutive behavior, which is imperative for the success of the analytical program. In addition to typical one-dimensional compression and tension tests, two-dimensional tests are necessary in order to accurately characterize the shear behavior of the material.

Additionally, two critical connection details will be developed and tested: the panel-to-panel connection and the panel-to-girder connection. Issues being addressed in the development of these connections include the need for them to be easy to install and to not be highly affected by typical construction tolerances. They also need to be durable under cyclic loads and environmental stresses. Finally, they need to exhibit the required strength. Two important characteristics of the panel-to-girder connection that will be investigated in addition to those listed above are: 1) amount of composite action it develops and 2) the effective flange width within the UHPC deck.

2.2 Analytical Program

A major goal of the analytical study is to determine the optimal structural configuration for using UHPC as bridge deck panels. This analysis will focus on shear and flexural efficiency.

Preliminary studies have revealed that existing reinforced concrete (RC) models implemented in commercial software, such as ABAQUS, are not able to capture the true behavior of UHPC, and in particular its shear behavior. This is because of how parameters that characterize reinforced concrete material post-cracking behavior, such as tension stiffening, aggregate interlock, and dowel action, are modeled. Typically, the two last effects are modeled together and a shear retention factor is used to capture the post-cracking shear stiffness of the material. However, in UHPC there is no aggreagate intelocking and the effect of the embedded steel fibers must be captured. To characterize the later it is proposed that a scheme similar to the dowel action model be developed in conjunction with the smeared crack approach. The smeared crack approach is selected because it does not track individual “macro” cracks. Instead the calculations of the material behavior for each element in the finite element mesh are performed independently at each integration point of the finite element model. The representation of cracks in this approach is done by capturing how they affect both the stress and material stiffness associated at specific integration points. It is thus crucial that an accurate representation of the stress-strain relationship be selected. The available material stress-strain curves for UHPC such as those developed by Park et al. [7], AFGC [8], JSCE [9] and Hajar et al. [10] are being considered and the best candidate curve will be incorporated with the proposed model. The laboratory tests such as uniaxial compression, uniaxial tension (using notched prism), and biaxial tests will be used to obtain the material constants necessary in the developed material model.

A second goal of the analytical program, is to develop structural finite element models using the developed material model. More specifically, these high-fidelity models will be used in the development of practical design guidelines for UHPC bridge decks.

3 Summary

A two-pronged research program for developing a new bridge system technology for slab-girder bridges has been presented. The research program includes both experimental investigation of materila properties and behavior od structural connections as well as an analytical study aimed at optimizing the UHPC deck cross section dimensions.

4 References

[1] Semioli, W.J. (2001). "The New Concrete Technology", Concrete International, Nov. 2001, pp. 75-79.

[2] Cheyrezy, M. (1999). "Structural Applications of RPC", Concrete, 33(1), pp. 20-23. Dick, J.S. (2002). "Precast technology and bridge design", Structural Engineer, May 2002, pp. 24-29. Gowripalan, N. and Gilbert, G.I. (2000). "Design Guidelines for RPC Prestressed Concrete Beams", VSL Australia Pty Ltd.

[3] VSL (2002). "'Ultra' High Performance Concrete", notes from presentation at VSL Symposium II, Baltimore, MD, Feb. 7 and 8, 2002.

[4] Graybeal, B.A. (2005). "Characterization of the Behavior of Ultra-High Performance Concrete", PhD Dissertation, Civil Engineering, University of Maryland, College Park.

[5] Blaise, P.Y, and Couture, M. (1999). "Precast, Prestressed Pedestrian Bridge – World's First Reactive Powder Concrete Structure", PCI Journal, 44(5), pp. 60-71.

[6] Bonneau, O., Poulin, C., Dugat, J., Richard, P., and Aitcin, P-C (1996). "Reactive powder concretes: from theory to practice", Concrete International, April 1996, pp. 47-49.

[7] Park, H., Ulm, F-J., Chuang, E. (2003). "Model-Based Optimization of Ultra High Performance Concrete Highway Bridge Girders", CEE Report R03-01 – Massachusetts Institute of Technology.

[8] Association Française de Génie Civil (2002) – Interim Recommendations for Ultra High Performance Fibre-Reinforced Concretes, Association Française de Génie Civil Scientific and Technical Documents.

[9] JSCE (Japan Society of Civil Engineers) (2004). "Recommendations for Design and Construction of Ultra High Strength Fiber Reinforced Concrete Structures, Draft.

[10] Hajar, Z., Simon, A., Lecointre, D. and Petitjean, J. (2003). "Construction of the First Road Bridges Made of Ultra-High-Performance Concrete", Proceedings of the International Symposium on High Performance Concrete, Orlando, FL, 2003

Ivailo Terzijski
Associated professor
vice head of the department
Brno University of Technology
Brno, Czech Republic

Optimization of UHPC for the Model of a Pedestrian Bridge

Summary

The paper describes an area concerning development of UHPC used for a physical model of an arch shell structure. There are described specifications of required UHPC properties, development program, and finally reached parameters. Shortly specified is the structure, which serves as the role model, too. The last part of the paper describes manufacturing of the physical model and final test of its load bearing capacity.

Keywords: *UHPC, strength, flow ability, shrinkage, creep, setting time, load-deflection curves, arch shell structure, physical model, manufacturing, load bearing capacity, crash test.*

1 Lead-in

At the Brno University of Technology, Department of Concrete and Masonry Structures, we decided to test the behaviour of a modern type of an arch shell structure. There were two main courses of this study:

1. Development and tests of the proposed main structural material – the UHPC.
2. Test of the behaviour of the structure at ultimate limit state (based on the structural model).

While information concerning point 2 are mostly in the writings [1] and [2], information about the development of the relevant UHPC is concentrated in this paper.

2 The structure

The arch shell structure was originally designed for a design competition for a pedestrian bridge in Jersey, UK by professor Strasky (BUT Brno) with Cezary Bednarski, London. The proposed span of the shell was 62m on which a slender composite deck was suspended. The shell, formed by projection of two cylindrical shells, creates a diagonal arch shell – see figures 1 and 2. The arch shell diagonally crosses the deck that serves as a tied girder. The shell was primarily designed from aluminium, but very detailed static and dynamic analysis made at the Faculty of Civil Engineering of Brno University of Technology has proved that the shell and deck can be made from a high strength or better from an ultra high strength concrete. The diagonal arrangement of both the arch shell and tied girder calls for suspending the deck at mid-span only. To reduce the bending stresses in the shell, the suspenders' top anchors are distributed at the length of 10m and the shape of the arch shell follows the bending moment diagram.

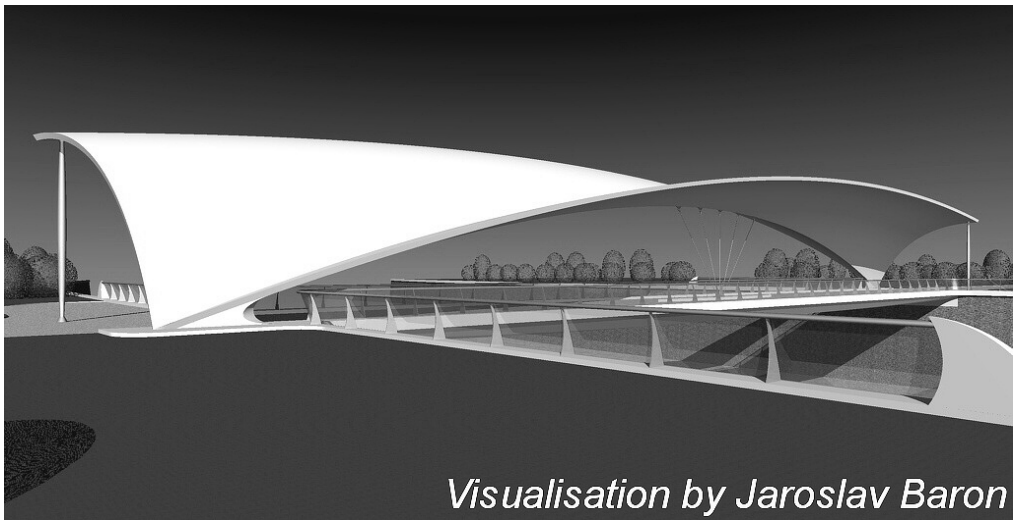

Figure 1: Visualization of the shell structure concept

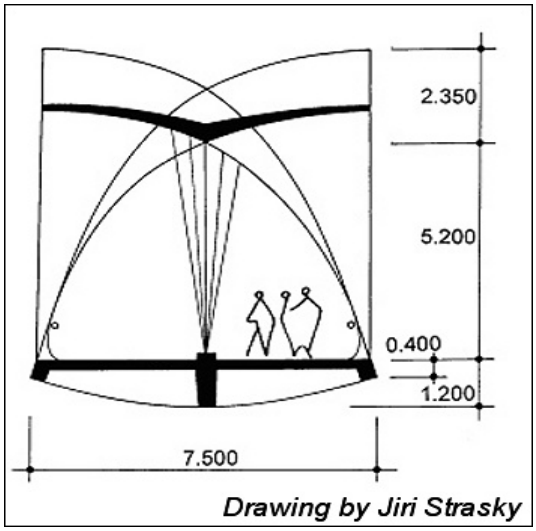

Figure 2: Shape of the structure in a cross section

3 The model – part I.

The scale of 1:21.5 was chosen for the structure itself, and the scale of 1:12.5 was used for the shell thickness [2]. At the first step, special formwork for the model was designed and built – see figure 3. Character of the formwork and chosen technique of its filling with an UHPC has important impact on desired properties of used UHPC - see following caption.

4 The UHPC

From side of the designer [1], [2] following basic demands on the UHPC were formulated:

- Compressive strength of the UHPC after 28 days of curing should be in the region of 150 MPa.
- Tensile strength by bending after 28 days of curing should be in the region of 22 MPa.

- The fresh UHPC should be very flow-able and non-stiffening, to fill correctly the tilted formwork without any air voids. Even the ability to power inject the high-stressed marginal parts of the shell should be assured.
- Due to proposed time for complete formwork refill, the desired flow-ability should be assured at least one hour after mixing.

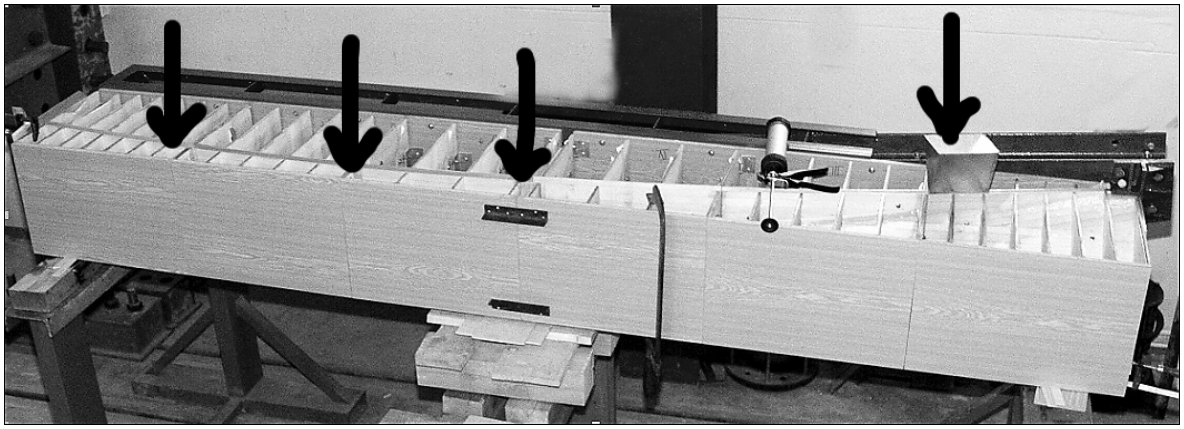

Figure 3: Tilted formwork with marked fill direction

4.1 Materials used for UHPC design

Basically, the materials regularly placed on the Czech market were used. In the following text specifications that are more detailed are given.

Cement – By two manufacturers regularly produced Portland cements of the class CEM I 52.5 R were used. For detailed characteristics, see www.cmcem.cz and www.cement.cz.

Ground blast furnace slag – This fine ground slag (Blaine value of 420m^2/kg) was tested, but finally not used for the physical model due to increased stickiness of the relevant UHPC.

Silica fume (micro filler) – As by cements, two brands of silica fume were used. The first one was regular "Elkem origin" silica fume supplied in 50% water suspension. The second one was very fine and very pure (the SiO_2 content is of about 98 %.) silica fume from Iran, sold on the Czech market as Sioxid IR.

Plasticizers – More plasticizers on the polycarboxylate or polycarboxylate-ether basis (stabilizing or not stabilizing, with fast or slow setting when mixed with cement) were tested.

Retarder – One retarder on the phosphate basis was tested and used.

Filler – There was used one type of siliceous filler, only.

Aggregate – There were combined two types of washed siliceous sand with gradation of 0/1mm and 0/2mm respectively in the UHPC.

Fibres – Two types of Fe-fibres (0.15/6mm and 0.15/12mm) were used.

4.2 Optimization procedure of UHPC composition

Task of the optimization was clear – to reach the desired properties defined at the beginning of the caption 4. During the development works different composition of UHPC with and without fibres of the length 6mm or 12mm were tested. Other variables were kind of the silica fume, type of used plasticizer (all of a PCE basis), presence (or absence) of ground blast furnace slag, content of the retarder and gradation of used sand and filler – see table 1.

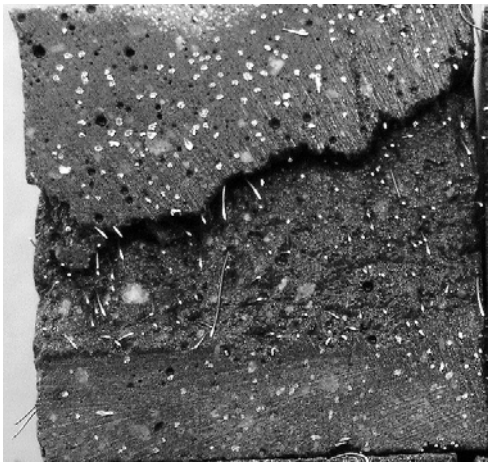

Figure 4a: UHPC with large voids of air

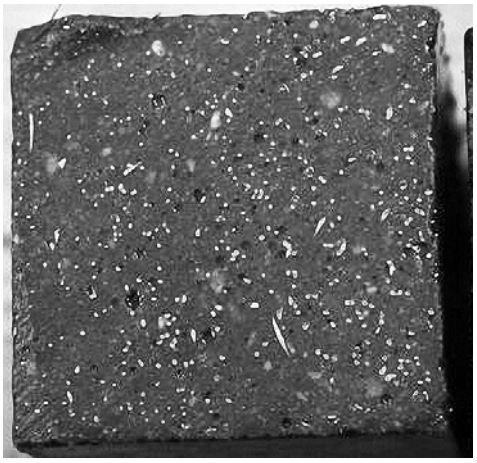

Figure 4b: UHPC without large voids of air

Table 1: Composition of the main variants of tested UHPC

Component	**Unit**	**1**	**2**	**3**	**4**	**5**	**5F**	**6**
CEM I 52,5 R (A)	kg/m³	805	815					2
CEM I 52,5 R (B)	kg/m³			805	830	815	815	850
Silica fume 1 (dry c.)	kg/m³	121	125	71	-	-	-	85
Sioxid IR powder	kg/m³	-	-	-	120	120	130	60
Grinded slag	kg/m³	-	-	-	81	81	81	-
PCE-1 (dry content)	kg/m³	7,6	7,8	4,2	3,4	-	-	-
PCE-2 (dry content)	kg/m³	-	-	4,2	-	3,8	3,8	3,8
PCE-3 (dry content)	kg/m³	-	-	-	3,4	4	4	4
Siliceous filler	kg/m³	380	310	245	280	350	250	250
Retarder	kg/m³	-	3,0	5,0	5,8	6,5	6,5	6,7
Sand 0/1 mm	kg/m³	760	520	510	810	500	500	505
Sand 0/2 mm	kg/m³		250	310	-	280	280	300
Water (total content)	kg/m³	248	248	244	245	242	242	230
MF 0,15/6 mm	kg/m³	-	70	45	44	-	44	39
MF 0,15/12 mm	kg/m³	-	-	26	30	-	32	39

There were three main problems present there:

1. The first one – to reach desired strength properties - was rapidly solved.
2. The second problem – to reach very good flow ability combined with the ability to release entrapped air (see figure 4) together with sufficient stability - was the most difficult one. First, it was necessary to select carefully the type of used PCE plasticizer (finally, a mix of two was used). The usage of ground blast furnace slag should be abandoned due to not acceptable stickiness of the relevant fresh UHPC. From the same reason the content of very effective (from the final strength point of view) Silica fume Sioxid IR had to be limited (as it proves as a “plasticizer eater”) and the mix of fibres of different length were used.

3. The third main problem was the necessity to keep desired flow ability of fresh UHPC at least one hour. The basic solution for that was usage of a retarder. However, there were other, earlier mentioned, precautions, which helped to keep desired flow ability: careful selection of PCE plasticizers and type of the silica fume. For more details, see tables 1 and 2.

Table 2: Basic properties of the main variants of tested UHPC

Parameter	**Unit**	**1**	**2**	**3**	**4**	**5**	**5F**	**6**
Spread of the UHPC	mm	195	265	245	180	300	265	285
Spread after 1 hour	mm	100	165	185	120	260	205	265
Stickiness	-	o	Ɵ	o	Ɵ	o	o	+
Strength in flexure								
7 days	MPa	16,3	11,1	17,6	21,1	18,2	20,8	19,3
28 days	MPa	17,0	19,6	19,0	26,8	19,7	24,6	25,0
90 days	MPa	19,2	20,3	19,5	26,2	20,1	25,8	25,2
Compressive strength								
7 days	MPa	83,3	93,5	103,9	121	102,5	113,8	116,1
28 days	MPa	94,0	122,9	140,2	152,7	113,9	138,1	151,7
90 days	MPa	96,8	129,5	156,6	165,3	143,6	163,5	157,3
Temperature 30 min	°C	38	34	28	26	22	23,5	24

Legend: Stickiness: **Ɵ** - not good (sticky), **o** – average, **+** - good (not sticky)
Spread: the value 100mm means without measurable spread.

In the above presented tables 1 and 2 the composition and principal properties of main variants of tested UHPC are documented. By the fresh UHPC flow-table, spread according to Haegermann was measured and by hardened UHPC flexural and compressive strength were tested. Besides above-mentioned “usual” tests of UHPC, other - extended tests of selected variants of UHPC were executed. First of all, the shrinkage and creep of the UHPC without fibres and with 6 and 12mm fibres were tested. For both quantities a measurement based on the usage of strain gauge units has been applied. Shortly the technique of specimen preparation and measurement:

1. In related mould, four anchoring pins (2 + 2 on each side) were fixed.
2. The mould (moulds) was filled with UHPC (in the self-compacting way) and covered with a PE foil.
3. After 3 hours were the moulds with the fresh UHPC submerged into 20°C water, where they remained for 5 days.
4. 24 hour after mixing were (under water level) the moulds removed and prepared anchoring pins were fitted with waterproof strain gouges. From this point, the volume changes measurements (shrinkage or creep) were started and related data was continually (one reading per a minute) recorded in a data logger unit.
5. The specimens for shrinkage measurement were kept in the water during first 5 days and then they were laid loose in the conditioned room with the air temperature of 20 +/-1°C and the relative humidity of 50 to 60%. (Simulation of a real structure curing).

6. The specimens for creep measurement were prepared and cured in the same manner. The only difference was that related specimens were after 28 days of curing fastened into spring press units. Then they were loaded with the force, which causes in the specimens stress level equal to 40% of the expected ultimate stress. In this case it was 150x0.4 = 60 MPa.
7. Both the shrinkage and creep measurement last in this experiment 320 days. For relevant results see figure 5a, and figure 5b.

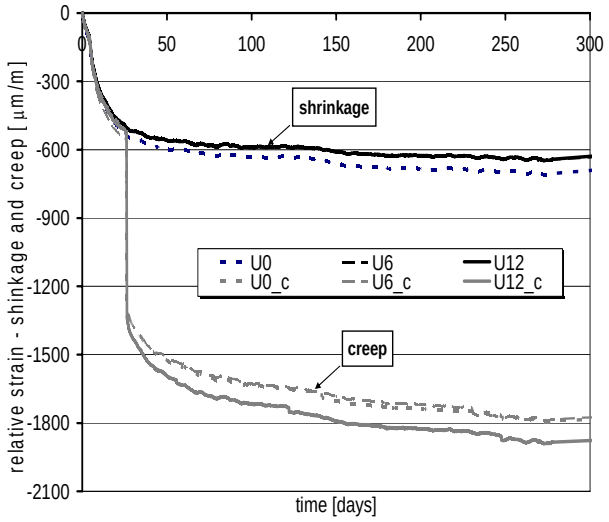

Figure 5a: Shrinkage and creep of different variants of UHPC

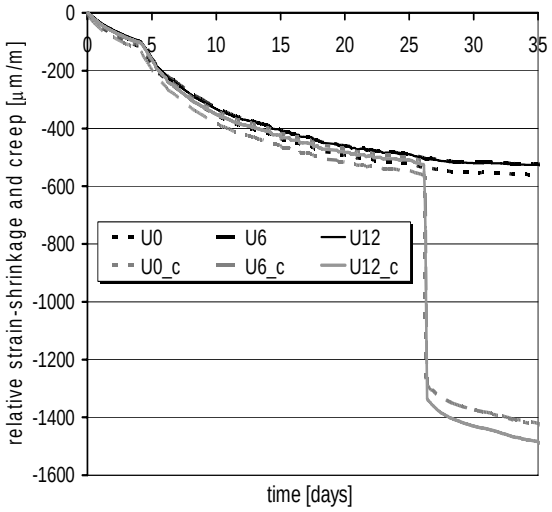

Figure 5b: Shrinkage and creep of UHPC detail of the first 35 days

Legend: The number in specimens marking indicates kind of used fibres (0=without f.)
The “c” in specimens marking indicates creep measurement

As can be seen in the figures 5a and 5b, there are no significant differences among specimen with different kind of fibres (or without them). The initial rate of **shrinkage** of tested variants of UHPC was relatively high (e.g. when compared to HPC). Even the autogenous shrinkage in the water imposition was distinct – see time interval 0 to 5 days in the figure 5b. On the other hand, after of about 60 to 80 days, shrinkage has practically stopped. Recorded small variations in the strain after this age were probably caused mostly due to small changes of the temperature and relative humidity in the deposit. The **creep** after distinct immediate value of strain was relatively low, too. Notice: We have to realize, that the real creep is in fact the difference between related top curve in the figures (free shrinkage) and the bottom one (the addition of free shrinkage and creep). Finally, it can be deduced, that the presence or absence of fibres has no significant impact on free shrinkage and creep. Of course, this is not a big surprise, as the positive impact of fibres presence is demonstrated in other way – see following text.

By strength tests, it has been obvious; that there is relatively small difference between strength in flexure for the same composition of the UHPC with and without fibres (sees table 2 and variants 5 and 5F). It is caused by the fact that standard testing equipment detects already small decrease of load as reaching of ultimate limit state. To clarify this, we made a

set of test based on the methodology and equipment used for testing of fracture properties. Due to limited space of this paper it can be presented the basic fracture parameter-measured load-deflection curves, only- see fig. 6.

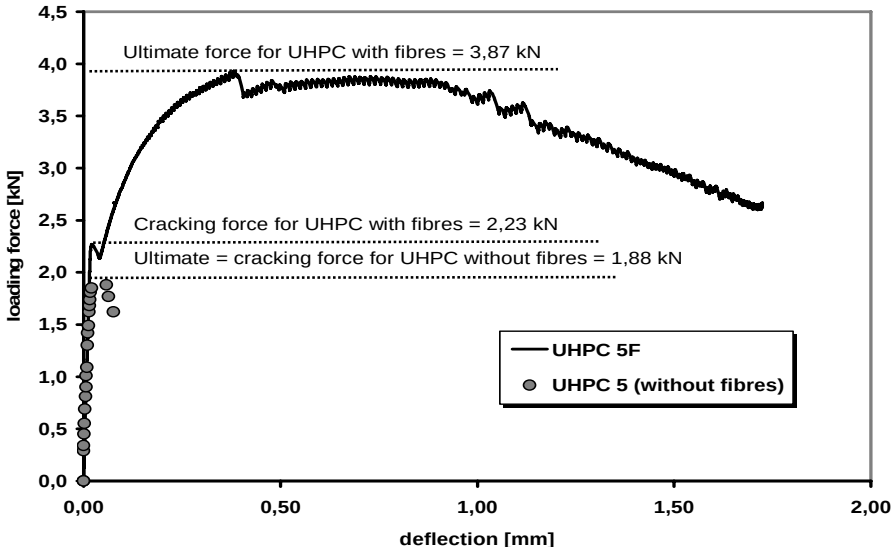

Figure 6: Load-deflection curves of the UHPC with (5F) and without (5) fibres

In the figure 6 can be clearly observed that by the UHPC without fibres the ultimate force is equal to the cracking one. By the UHPC with fibres is the magnitude of ultimate load in case of variant “5F” 74% above the cracking one. This demonstrates the real increase of the load-bearing capacity of regular UHPC with fibres. Of course, the deflection or maximal allowed deflection is the fact, which should be respected.

5 The Model – part two

5.1 Manufacturing of the physical model

Manufacturing of the physical model can be divided into two major stages: preparation of the formwork and casting of the UHPC itself.

Preparation of the formwork was very challenging activity (similar to the design of an airplane wing), but it is not the topic of this paper. On the other side, the final mixing and casting of the UHPC was surprisingly trouble-free, probably thanks to the detailed preparation. Finally, after removing the formwork, very nice and clean corpus of the model arch shell has occurred – see figure 7.

5.2 Load bearing and crash test of the physical model

During this test variable load was simulated with the usage of a hydraulic press unit, which has induced equivalent vertical single force acting at the top of the arch shell. The shell was loaded in steps with the magnitude of 5kN. After each loading step and strain equalisation the “variable” load was completely released. Then (after 5-minute break) the next loading step started. Finally, the collapse of the model structure was reached by the force of the magnitude of 21.3kN. (Proposed value was 20kN.) The first crack had developed by the left support and by overshooting the loading force of 20kN it had opened significantly, the fibres ruptured, which was followed by complete crash of the model – see Fig. 8.

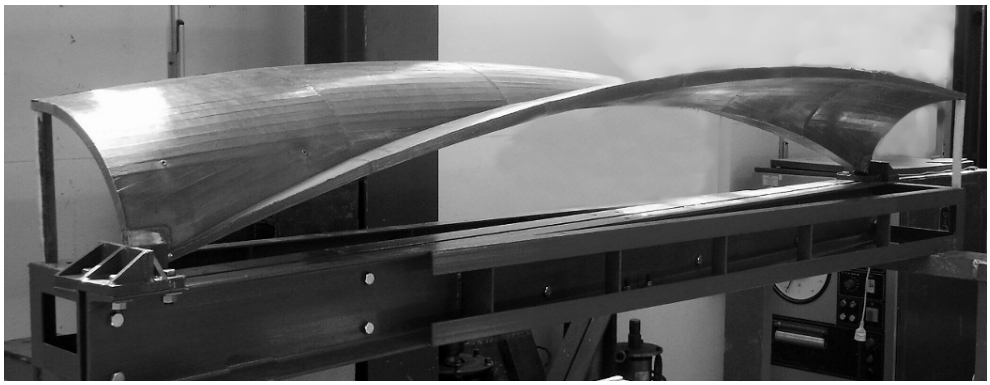

Figure 7: Finished model of arch shell from UHPC

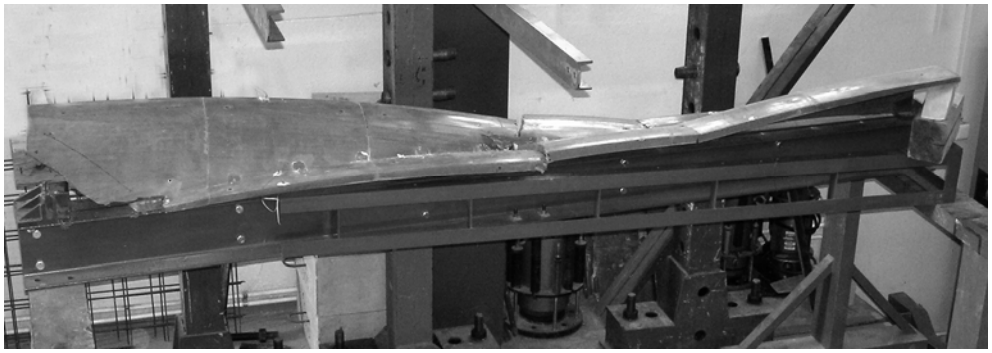

Figure 8: Model of arch shell from UHPC after crash test (testing equipment removed)

6 Conclusions

- Arch shell and similar structures can be successfully designed on the UHPC basis.
- Behaviour of such structures can be with a good accuracy predicted with help of numerical and physical models.
- UHPC can be designed to have workability (flow ability) good enough for vibration-free casting into relative complicated formwork.
- In the UHPC contained steel fibres have significant effect on its mechanical properties what partially cannot be recorded with help of standard (regular concrete) tests.
- Shrinkage of the UHPC is relatively high at early age, but stops after certain time.

7 Acknowledgement

This outcome has been achieved with the financial support of the Ministry of Education, Youth and Sports, project No. 1M0579 – CIDEAS research centre and the financial support of the Ministry of Industry and Trade, project No. FI-IM/185.

8 References

[1] Stráský, J.: Pedestrian Bridges Utilizing High strength concrete. Footbridge 2005. In: 2nd International Conference. Venice, Italy, 2005

[2] Vítek, J., Stráský, J.: Návrh skořepinové mostní konstrukce lávky pro pěší a cyklisty. In: Proceedings of the Conference Concrete Days 2006, Hradec Králové, 2006, 425–429 (in Czech).

Part 11:

Impact and Blast Effects

Changbin Joh
Ph.D., Senior Researcher
Korea Institute of Construction Technology
Goyang, Korea

Hoonhee Hwang
Ph.D., Postdoctoral Researcher
Korea Institute of Construction Technology
Goyang, Korea

Eunsuk Choi
Researcher
Korea Institute of Construction Technology
Goyang, Korea

Jungjun Park
Researcher
Korea Institute of Construction Technology
Goyang, Korea

Byung-Suk Kim
Ph.D., Research Fellow
Korea Institute of Construction Technology
Goyang, Korea

Punching Shear Strength Estimation of UHPC Slabs

Summary

The improved mechanical properties of UHPC make it possible to design slenderer, lighter, and more durable structures. However, insufficient established design formulas have been obstacles to the application of UHPC to structural design. The design formula for punching shear is one of them. This paper reports the result of punching shear test of 6 slab specimens made of UHPC developed by Korea Institute of Construction Technology (KICT). The test result implies the punching strength of UHPC slabs depends not only on tensile strength but also on local composition and fabrication method. The test result also indicate that ACI punching formula for RC slabs predicts reasonably the punching strength of an UHPC slab considering its prediction for RC slabs, and the general formula with 38˚ failure angle gives good prediction of punching strength of UHPC slabs with the boundary condition used in the test.

Keywords: *UHPC, slab, punching shear, design formula*

1 Introduction

Together with flexural strength, in general, the design of a slab requires punching strength of the slab. The punching shear formula for conventional RC slabs has developed based on numerous test results, but since UHPC is relatively new building material, more test results are required developing a practical design formula.

This paper reports the result of punching shear tests of UHPC slabs. A total of 6 slabs are made of UHPC developed by Korea Institute of Construction Technology (KICT), and the aspect ratio of a loading plate and slab thickness are chosen as test parameters. To recommend the reliable punching shear formula for the design of UHPC slabs, the test results are compared to the punching shear formula for UHPC (Ductal®) proposed by Harris

and Robert-Wollmann [1], ACI punching shear formula [2] for RC slabs, and the general formula for prestressed concrete slabs proposed by Graddy et al. [3].

2 Punching Shear Formulas for Normal Concrete and UHPC slabs

Basic approach to calculate the punching shear strength is to find the equilibrium of forces acting on assumed diagonal failure plane. The angles of failure plane are assumed to be about 45° for RC slabs [2].

Graddy et al. [3] proposed the general formula (Equation 1) to explain the change in the angle of failure plane due to prestressing. They proposed θ = 38° for a prestressed concrete slab and this formula reduced to ACI punching shear formula [2] when θ = 45° (Equation 2).

$$V_{General} = 2\left(a + b + 2d/\tan\theta\right)\left(d/\tan\theta\right) f_t, \text{ Newton} \quad (1)$$

$$V_{ACI} = \left(0.17 + 0.33/\beta_c\right)\sqrt{f_c'}\, b_0 d \le 0.33\sqrt{f_c'}\, b_o d, \text{ Newton} \quad (2)$$

In these equations, a = the length of loaded area (mm); b = the width of loaded area (mm); β_c = the ratio of long side to short side of loaded area (the aspect ratio of a loading plate); d = effective depth of a slab (mm); f'_c = the compressive strength of concrete (MPa); f_t = the tensile strength of concrete (MPa); b_0 = the perimeter of critical section (mm); θ = the angle between the assumed failure and horizontal planes.

Harris and Robert-Wollmann [1] proposed punching shear formula (Equation 3) for UHPC slabs based on punching shear tests of 12 UHPC (Ductal®) slabs. Their equation is the modification of the ACI equation for concrete breakout strength. Their loading plates are all squares. In this equation, k_1 = empirical constant (determined to be 0.38); c = the loading plate dimension (inch); d = effective depth of a slab (inch); f_t = the tensile strength of UHPC (ksi).

$$V_{VT} = k_1 f_t \frac{(3d + c)^2 - c^2}{\sqrt{d}}, \text{ kips} \quad (3)$$

3 UHPC Slab Specimens and Test Setup

UHPC slab specimens are fabricated using UHPC composition developed by KICT (Table 1). The UHPC slab specimen is a 1600 mm x 1600 mm plate with block-outs (Figure 1). The specimens are steam cured at the 90℃ for 72 hrs after 24 hr- curing at room temperature.

Table 1: UHPC Composition developed by KICT (by weight)

W/B	Cement	Silica fume	Sand	Filling powder	Superplasticizer	Steel Fiber(V_f)
0.2	1	0.25	1.1	0.3	0.016	2%

The average compressive strength, Young's modulus and Poisson's ratio of UHPC out of 4 cylinder tests are 194 MPa, 42.9 GPa, and 0.163 respectively, and the average tensile strength of UHPC from 3 split tests is 10.5 MPa.

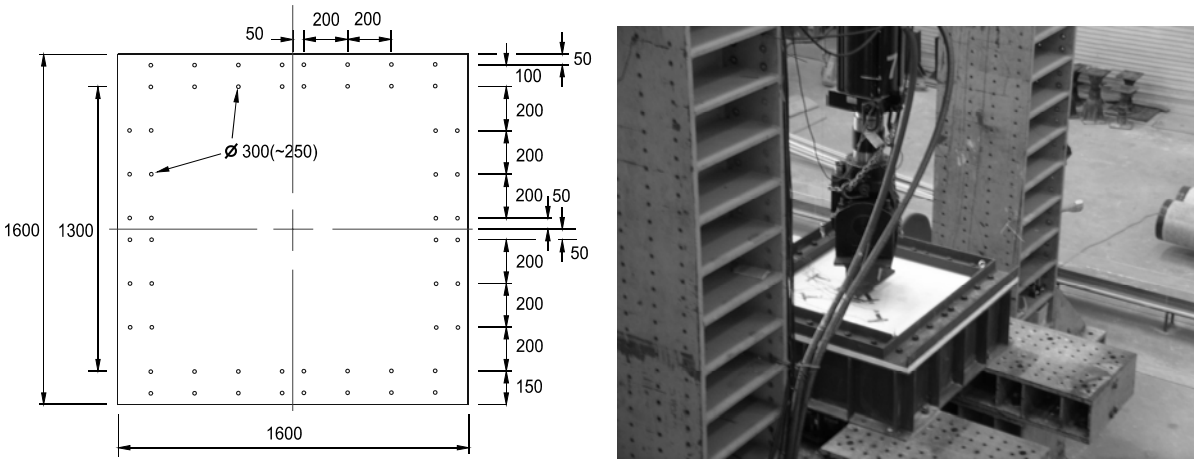

Figure 1: UHPC slab specimen and test setup

The tested portion of the specimen is 1200 mm x 1200 mm, and the block-out (200 mm) from each side is used to bolt the edges of the slab down to the test frame to simulate fixed boundary conditions along all edges (Figure 2). The fixed edges on all 4 sides are necessary to the test because a simply supported slab requires a much smaller load to cause a flexural failure. The decrease in flexural failure load would lower the possibility of a punching shear failure.

Loading is applied using a 100 ton hydraulic actuator which is attached to the portal loading frame (Figure 1). Up to 50% of the estimated failure load, the load is applied in a load-controlled mode. Beyond that the load is applied up to failure in a displacement-controlled mode.

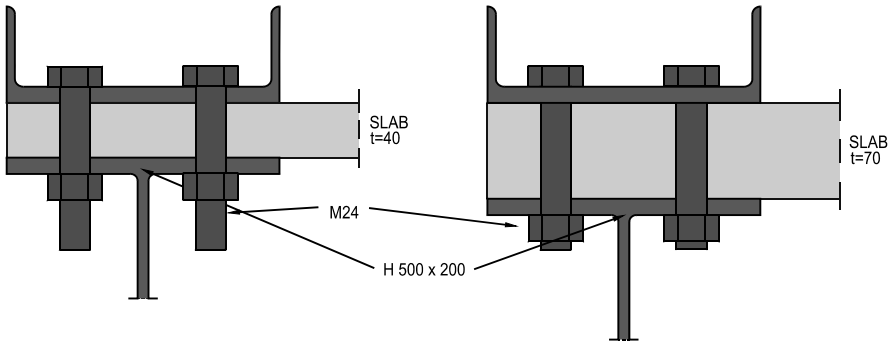

Figure 2: Details of restraint system to simulate fixed boundary conditions

Table 2 shows the details of the specimens, loading plates and predicted failure mode. The major test parameters are the thickness of the slab and the aspect ratio of a loading plate. To increase the possibility of a punching shear failure, relatively small loading plates are used. The limiting strain criterion proposed in the MIT report [4] is used to calculate flexural capacity of the cross section of the slab.

Table 2: Details of UHPC slab specimens and Loading Plates

Specimen	Thickness (mm)	Loading Plate			Predicted Failure Strength (N)			Predicted Failure Mode
		a (mm)	*b* (mm)	β_c	Flexural (Yield L.)	Punching (ACI)	Flexural/ Punching	
PT4-50	40	50	50	1	112501	66856	1.68	Punching
PT4-75	40	50	75	1.5	123862	76142	1.62	Punching
PT4-100	40	50	100	2	125285	85427	1.46	Punching
PT7-75	70	50	75	1.5	359501	155998	2.30	Punching
PT7-100	70	50	100	2	367672	188498	1.95	Punching
PT7-125	70	50	125	2.5	372042	204747	1.81	Punching

4 Test Results

Figure 3 shows load-deflection curves from punching shear tests. The load-deflection curves can be divided into two groups according to the failure mode. The specimens with 70 mm thickness (hereafter PT7 series) are failed by typical punching at the center of the slab. On the other hand, the specimens with 40 mm thickness (hereafter PT4 series) show considerable ductile behavior after reaching flexural strength of the specimen with the given boundary condition, although ultimate failure is punching.

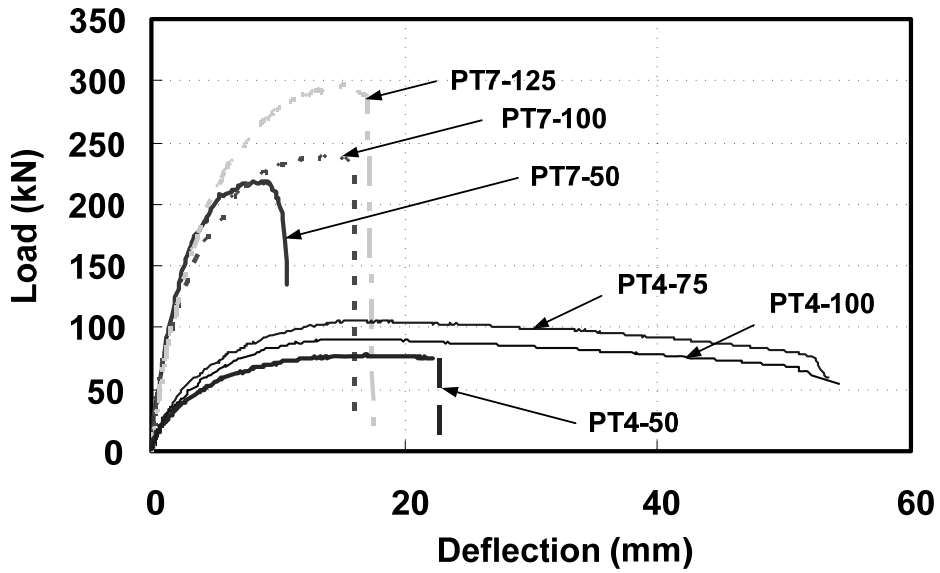

Figure 3: Load-deflection curve for UHPC specimen (at the center of the specimen)

The Load-deflection curves for PT7 series show that the displacement is increased with the load approaching a flexural failure, but punching failure (Figure 4) is occurred first. In general, punching strength is known to proportional to the area of a loading plate and the results of PT7 series show similar trend.

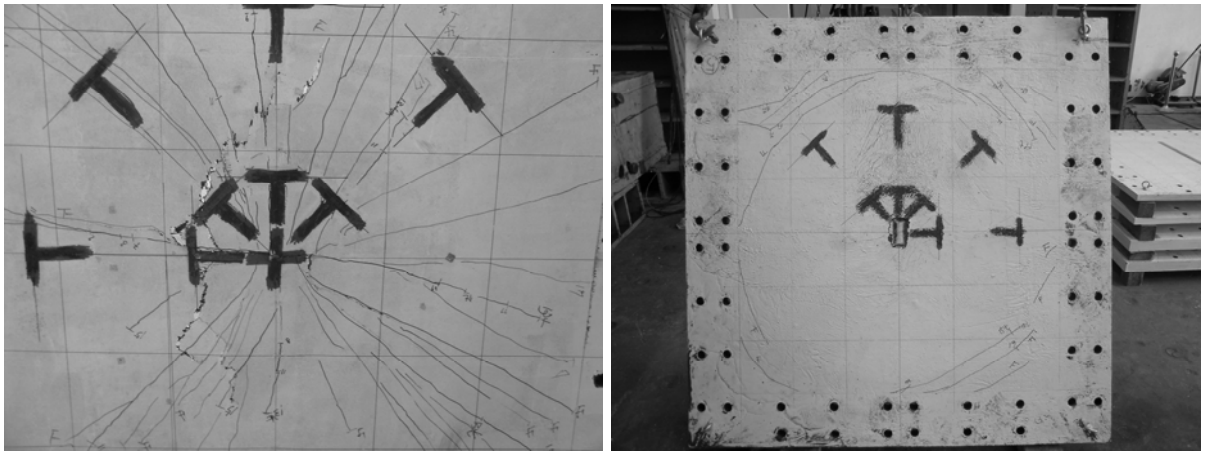

Figure 4: PT7-100 Tension (left) and Compression (right) Side

The cracks on the tensile face begin near the center and radiate out to the edges (Figure 4 left). The cracks are relatively well distributed and the width of the crack is limited, which means that the steel fiber are holding the crack opening and the clear tensile yield lines are not formed yet. The radiating cracks from the center in every direction imply the steel fibers are well distributed. In the compression side, as the load is increased after initial cracking at the center of the tension side, the cracks begin near the corner and propagate along the edges (Figure 4 right).

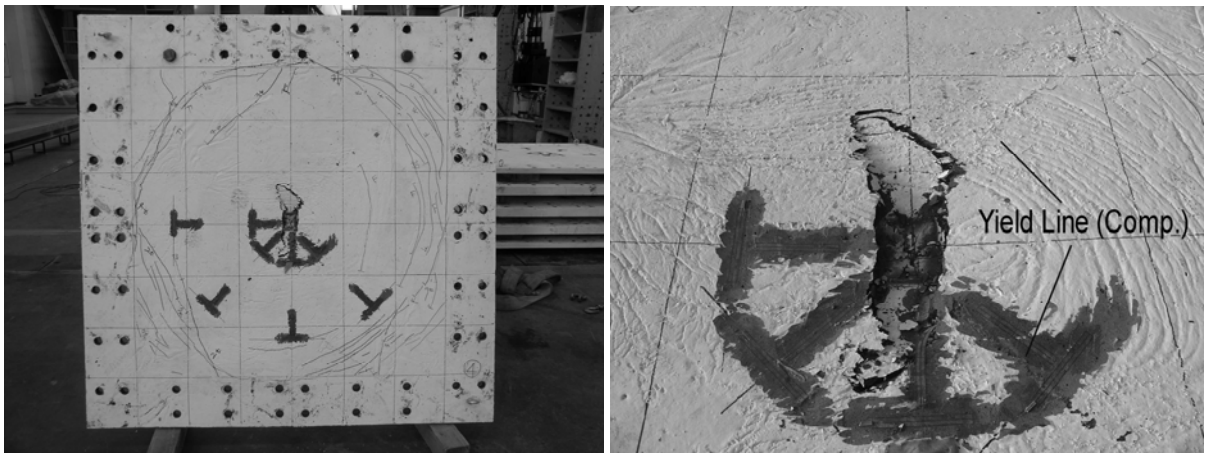

Figure 5: PT4-75 Compression Side (over view (left) and enlarged (right))

In the load-deflection curves, PT4 series are able to sustain a reduced load while continuing to deform after the peak load. Although the ultimate failures of 3 specimens are brittle punching (Figure 5), the behavior of PT4 series is different from that of PT7 series.

Only PT4-75 shows yield lines on the compression side as shown in Figure 5. But, for all PT4 series, clear yield line cracks on the tension side of the specimen (Figure 6) are formed during the descending curve before punching failure with the cone shaped UHPC block at ultimate state. The failure of PT4 series is primarily affected by the flexural behavior.

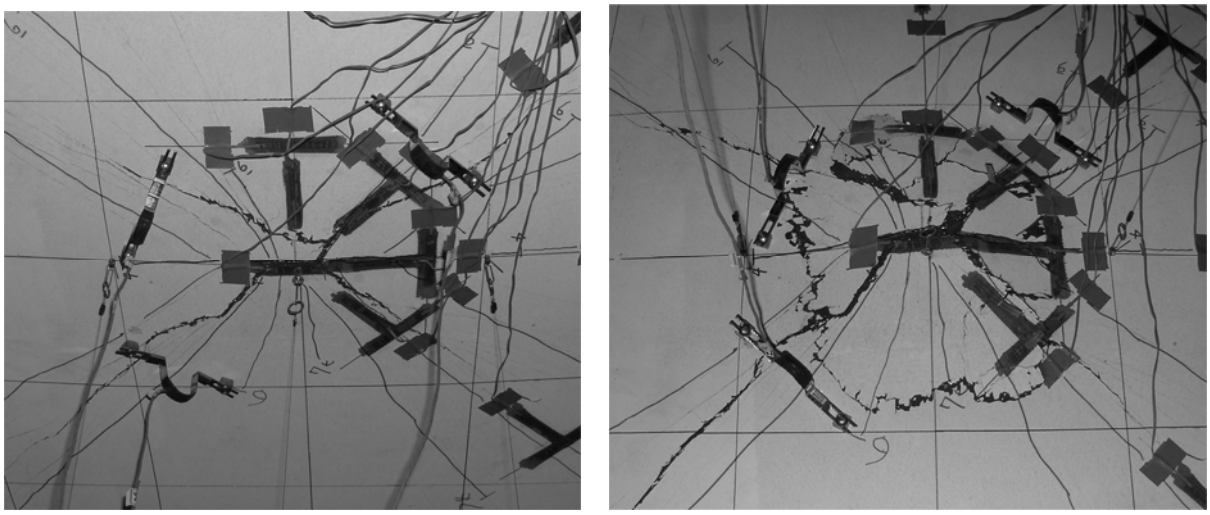

Figure 6: PT4-75 Tension Side (just before failure (left) and after failure (right))

To obtain clear indicative results in a punching test, the estimated flexural strength should be sufficiently high to exclude the possibility of flexural failure prior to punching [5]. Current test results imply the ratio of flexural to punching strength should be greater than 1.8 to guarantee punching prior to flexural failure.

5 Punching Strength Estimation of UHPC Slabs

Table 3 shows the peak loads of the tested specimens, the estimated punching strength and the flexural strength by yield line theory. For the comparison of punching shear formulas, only results from PT7 series are used, because PT4 series are primarily failed by flexure. The results from PT4 series are compared with the estimated flexural strength of the slab.

ACI punching formula [2] gives 73 % of actual punching strength in average, which is relatively good prediction considering that this formula is for practical design and also gives approximately 70 % of actual punching strength for conventional RC slabs.

The general formula [3] with the failure angle of 38˚ gives 106 % of actual punching strength in average. This formula slightly over estimated the actual strength but very close to the actual value. The failure angle lower than 45˚ can be explained by the arching action from the fixed boundary. More test results with different conditions are needed to find reliable failure angle for practical use.

Modified ACI318-02 breakout strength with k_1 = 0.38 gives 71 % of actual strength in average, which is similar to the result of ACI punching formula. However, this formula gave 101% of actual strength for UHPC (Ductal®) slabs test by Harris and Robert-Wollmann

[1]. This might imply the punching strength of UHPC slabs depends not only on tensile strength but also on local composition and fabrication method.

Table 3: Test results and comparison

MODEL	V_{exp}	V_{ACI}	V_{Gen}	V_{VT}	P_{YL}	Predicted/Test			
(kN)	(1)	(2)	(3)	(4)	(5)	(2)/(1)	(3)/(1)	(4)/(1)	(5)/(1)
PT4-50	78.0	66.9	96.2	84.0	122.5	-	-	-	1.57
PT4-75	106.2	76.1	108.1	93.6	123.9	-	-	-	1.17
PT4-100	91.3	85.4	120.0	103.1	125.3	-	-	-	1.37
PT7-50	218.7	156.0	232.3	156.6	359.5	0.71	1.06	0.72	-
PT7-100	239.5	188.5	273.9	181.9	367.7	0.79	1.14	0.76	-
PT7-125	296.7	204.7	294.7	194.5	372.0	0.69	0.99	0.66	-
					Average :	0.73	1.06	0.71	1.37

(1) Experimental strength
(2) ACI Punching Formula (Equation 2)
(3) General Formula (Equation 1)
(4) Modified ACI318-02 breakout strength (Equation 3)
(5) Flexural Strength by Yield Line Theory: $P_{YL} = 8M\left[\frac{l}{w-a}+\frac{w}{l-b}\right]$, where, M is flexural capacity of the section per unit length, and w and l are width and length of the plates, respectively.

Overestimation of flexural strength by yield line theory is probably due to the error in calculation of flexural capacity of the section and wrong assumption of failure mechanism. Since the post-cracking constitutive law of UHPC largely affects the flexural capacity of an UHPC section, more analytical studies will be done to find better the estimation of flexural strength of the UHPC slab with the completion of additional tests in progress.

In this paper, the effect of β_c is not discussed, because the β_c of tested specimens are not large enough to affect the stress distribution along the loading plate. Additional tests are in progress using narrow loading plates (β_c = 2.5, 4 and 10).

6 Summary and Future Research

Based on the limited test results and analyses, following comments can be made;

- Considering uncertainty of the estimation of flexural and punching strength, to guarantee punching prior to flexural failure in the test, the estimated flexural strength by yield line theory should be at least 180% of the estimated punching strength by ACI punching shear formula.
- ACI punching shear formula for RC slabs predicts the punching strength of UHPC slabs reasonably compared to its prediction for RC slabs

- The general formula with 38° failure angle gives good prediction of punching strength of UHPC slabs with the boundary condition used in the test. But more test results with different conditions are needed to find reliable failure angle for practical use.
- The punching strength of UHPC slabs depends not only on tensile strength but also on local composition and fabrication method.
- Overestimation of flexural strength by yield line theory is probably due to the error in calculation of flexural capacity of the section and wrong assumption of failure mechanism.

7 Acknowledgements

This research was developed in the context of the research project “Hybrid Cable Stayed Bridge 2020” financed by KICT. The support for this project is gratefully acknowledged.

8 References

[1] Harris, D. K.; Robert-Wollmann, C. L.: Characterization of the Punching Shear Capacity of Thin Ultra-High Performance Concrete Slabs, Report No. VTCR 05-CR26, Virginia Polytechnic Institute & State University, 2005.

[2] ACI; Building Code Requirements for Structural Concrete and Commentary (ACI318M-05). 2005.

[3] Graddy J. C.; Kim, J.; Whitt, J. H.; Burns, N. H.; Klingner, R. E.: Punching-Shear Behavior of Bridge Decks under Fatigue Loading. In: ACI Structural Journal, Vol 99, No. 3, pp.257-266, 2002.

[4] Park, H.; Ulm, F-J.; Chuang, E.: Model-Based Optimization of Ultra High Performance Concrete Highway Bridge Girders, CEE Report R03-01, Massachusetts Institute of Technology, Cambridge, MA, 2003.

[5] Stein T.; Ghali, A.; Dilger, W.: Distinction between Punching and Flexural Failure Modes of Flat Plates. In: ACI Structural Journal, Vol 104, No. 3, pp.357-365, 2007.

Devin K. Harris
Assistant Professor
Michigan Tech
Houghton, U.S.A

Carin L. Roberts-Wollmann
Associate Professor
Virginia Tech
Blacksburg, U.S.A.

Characterization of Punching Shear Capacity of Thin Ultra-High Performance Concrete Slabs

Summary

Twelve small, (1140 mm x 1140 m), fiber reinforced ultra-high performance concrete (UHPC) slabs were tested to failure to characterize the punching shear strength. The variables were slab thickness and loading plate dimensions. All edges of the slabs were fully restrained to yield the highest probability of a punching shear failure prior to a flexural failure. The test results were compared to the ACI 318-05 punching shear model, empirical models from other researchers, and the ACI 318-05 concrete break-out model for anchoring to concrete. Results of the testing program indicated that a modified version of the ACI 318-05 punching shear equation best predicts the punching shear capacity of UHPC slabs.

Keywords: *UHPC, Punching shear, fiber reinforced concrete, Ductal®*

1 Introduction

The Federal Highway Administration and Virginia Department of Transportation have spearheaded research on Ultra-High Performance Concrete (UHPC) for bridge applications in the United States. One research objective has been the development of a girder section for use in bridges which takes advantage of the high compressive and tensile strengths of UHPC while minimizing material use. The optimized double bulb-T section (Figure 1) developed by Park *et al.* [1] served as the impetus for the research effort reported in this paper. The resulting double bulb-T section has very thin webs, large bulbs at the bottom of each stem to accommodate the prestressing strand, and a thin top flange which serves as the riding surface. In a bridge application, the double-Ts would be set adjacent to one another, a flange connection created, and a thin overlay would be placed. With the top flange acting as the riding surface, transverse bending and punching shear must also be considered in the determination of the flange thickness. The goal of this research is to quantify the punching shear capacity of UHPC and provide design recommendations for the punching shear strength based on an experimental program.

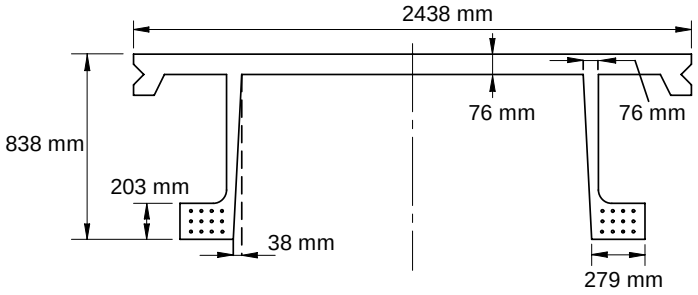

Figure 1: Optimized UHPC Double Bulb-T

2 Preliminary Analytical Investigation

With slab systems, the two most common mechanisms of failure are flexure and punching shear. In order to quantify the punching shear capacity of UHPC, it was necessary to design specimens that had a high probability of failing in punching shear prior to failing in flexure. Yield-line analysis served as the foundation for predicting the flexural capacity of a UHPC slab system, whereas a modification of the ACI [2] design equation (Eqn. *[1]*) served as the foundation of the preliminary model for predicting punching shear capacity.

$$V_c = 0.33\sqrt{f_c'}\,b_o d \qquad [1]$$

The limiting strain criterion, Equation *[2]*, and a simplification of the stress-strain relationship proposed by Park et al. [1] were used in the initial investigation to determine the flexural capacity (Figure 2). The simplification neglects a small post-cracking region and assumes the initial tensile strength, σ_{Mt}, to be constant from the cracking strain, ε_{tc}, to the limiting tensile strain, ε_{lim}. This also differs from the model proposed by the Association Française de Génie Civil (AFGC) [3] in which a gradual softening occurs from immediately after the peak tensile stress is reached to the limiting strain. To estimate the punching shear capacity, the term $0.33\sqrt{f_c'}$ was replaced with the initial tensile strength of UHPC. Also, the effective depth term, *d*, was replaced with the slab thickness, *h,* as there was no reinforcing steel.

$$\varepsilon_{\lim} = \frac{3\omega_{\lim}}{2h} \qquad [2]$$

The preliminary estimates were used to aid in the sizing of the test specimens; the specimens had to be small due to limited material availability, but not so small that their behavior would be influenced by the boundary conditions. Slab thicknesses of 51 mm, 64 mm and 76 mm thick were chosen and deemed representative of potential UHPC bridge deck thicknesses. The slab dimensions were selected to be 1143 mm square, with all edges fixed against rotation, and a clear span of 914 mm. The loading plate sizes needed to be quite small, between 25-51 mm square, to allow for punching shear failures to occur.

3 Punching Shear Models

A number of models were considered for predicting the punching shear capacity of UHPC, but only those proposed by Shaaban and Gesund [4] and Narayanan and Darwish [5] were determined to be appropriated for UHPC. The ACI [2] model for basic concrete

breakout strength for anchors in tension was also considered due to the similarities between a punching shear failure surface and the failure surface of an anchor pulling out of a shallow concrete member. The models considered herein do not represent all of the models available for the prediction of punching shear capacity, but were deemed representative of models that could be applicable to UHPC.

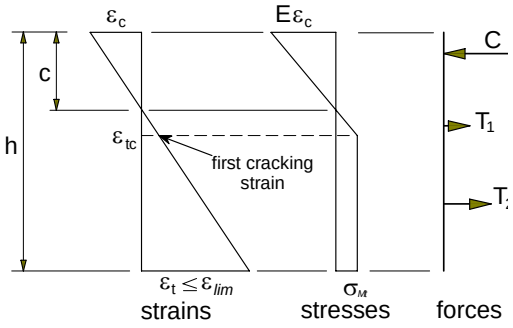

Figure 2: Simplfied Stress-Strain and Force Relationship for UHPC Section

3.1 Shaaban and Gesund Model

Shaaban and Gesund [4] studied the effects of steel fiber volume on the punching shear strength of reinforced concrete slabs. In their study, thirteen slabs of varying strength and fiber volume were tested to failure to determine if the punching shear capacity could be improved through the addition of fibers. The foundation of their research was earlier findings, which indicated that the addition of fibers increased the tensile capacity, in turn increasing the punching shear capacity. The proposed equation, Equation *[3]*, for predicting punching shear capacity was deemed acceptable for comparison in the UHPC research program because it was of a similar form as the ACI design equations and considered the fiber contribution.

$$V_c = \left[0.025W_f + 0.56\right]\sqrt{f_c'}\,b_o d \qquad [3]$$

3.2 Narayanan and Darwish Model

Narayanan and Darwish [5] studied the effects of steel fiber reinforcement on the punching shear capacity of concrete without coarse aggregate. The test parameters considered were volume fraction of fibers, reinforcement ratio, and concrete compressive strength. In their study, a total of twelve slabs were tested to failure and an improvement in punching shear capacity with the addition of steel fibers was achieved. Equation *[4]*, based on a semi-empirical model for the punching shear strength of fiber-reinforced concrete slabs, was developed. To compare this equation to the UHPC specimens, the term for the depth to the tension reinforcement was replaced with the slab thickness. The proposed equation considered the contribution of concrete, steel fibers, and tension reinforcement separately. The separate consideration of each term allowed for the punching shear capacity of UHPC slabs to be compared by neglecting the contribution of the tension reinforcement.

$$V_c = \xi_s b_{pf} h\left(0.24\, f_{sp} + 0.41\tau_u \rho_f d_f \frac{L}{D}\right) \qquad [4]$$

3.3 ACI Basic Concrete Breakout Strength Model

The concrete breakout failure mechanism that results from an anchor pulled out of a concrete surface, particularly thin slabs, was also considered to be similar to the punching shear failure mechanism in UHPC slabs (Figure 3). The concrete breakout model was originally proposed by Fuchs *et al.* [6], and was developed based on fracture mechanics concepts and results from a large database of tests in Europe and America. The model is presented in Appendix D of ACI 318-05 [2]. For the evaluation of UHPC punching shear capacity, the form of the equation was modified to account for the difference between the loading edges and also the tensile capacity of UHPC. The general form of the model is presented in Equation *[5]*; additional details of the modification are presented by Harris [7].

$$V_c = k_1 f_{sp}\left(9h + 6c\right)\Big/\sqrt{h} \qquad [5]$$

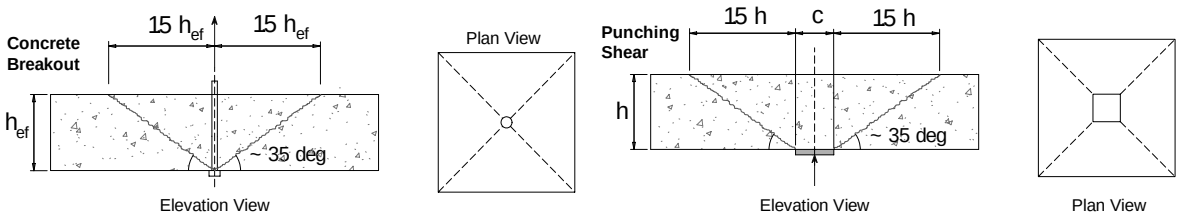

Figure 3: Concrete Breakout and Punching Shear Failure Surfaces

4 Experimental Investigation

4.1 Specimens

A total of twelve small slabs with nominal thicknesses of 51 mm [series 1], 64 mm [series 2], and 76 mm [series 3] with varying loading plate areas were tested to failure. The slabs were 1143 mm square with block-outs (voids) for tie-down bolts on the perimeter (Figure 5).

The UHPC material used in this research was Ductal® provided by Lafarge North America and cast at Prestress Services in Lexington, KY. A representative composition for Ductal® can be found in Graybeal [8], but the material will continue to be referred to as UHPC. The 0.2 mm diameter by 13 mm length fibers were added at a ratio of 2% by volume. The specimens were cast using a specially fabricated V-shaped trough which was the same width as the slabs (1143 mm) and could be moved along the side forms for the slabs. The trough was filled with UHPC, then the bottom of the trough was opened and the trough was slowly moved along the specimen length and the formwork was filled.

After initial steam curing, the specimens were removed from the forms. The slabs were then subjected to a 48 hour heat treatment to improve strength characteristics as demonstrated by Graybeal and Hartmann [9]. UHPC cylinders poured with the slab were tested and yielded average properties as shown in Table 1.

4.2 Test set-up and Test Procedures

The slabs were supported around the perimeter by steel I-beams connected to column pedestals. The deflection and rotation restraint at the slab edges was provided by channels

bolted through the block-out holes to the I-beams and angles bolted along the perimeter. An 1800 kN ram/667kN load cell combination was used to apply and measure the load during

Table 1: Average Mechanical Properties

Property		
Compressive Strength (No Modulus Test)	MPa	221
Compressive Strength (Modulus Test)	MPa	218
Split Cylinder Tensile Strength	MPa	11
Elastic Modulus	MPa	54

testing. Square steel plates of varying edge length were placed on top of the ram and used to transfer the load over the desired area.

After restraining the specimen in the loading frame, each specimen was loaded in 13 to 22 kN increments. At each load step, visible cracks were marked to record the slab failure pattern. The applied load, midspan deflections, and strains were recorded continuously during testing by a data acquisition system. Loading continued until a punching shear or flexural failure occurred.

5 Results and Discussion

5.1 Punching Shear Failures

A punching shear failure is typically a brittle failure that occurs with limited warning. For the UHPC slabs this occurred when the slab failed to support additional load followed by a conical punching failure. An example of a typical punching shear failure for UHPC is shown in Figure 4 (tension/compression faces). Cracking on the tensile face originated near the center and radiated out to one of the edges, and as the load was increased the cracking migrated to the opposite face. For all of the slabs that failed in punching shear, the widest cracks tended to be oriented in one direction (Figure 5Figure). There was cracking in the orthogonal direction, but these cracks tended to be much narrower and more closely spaced. This predominantly unidirectional cracking could be attributed to uneven bending on the support frame or uneven seating of the panels on the frame. However, visual inspection of the failed specimens led to the hypothesis that the fibers were not as randomly oriented as expected, and could be oriented primarily in one direction. The possible unidirectional fiber orientation was attributed to the casting technique, possibly resulting in alignment of the fibers parallel to the direction of pour. Slabs with this unidirectional fiber orientation would allow cracks to form between the fibers (Figure 5). This is in agreement with the trend described by the AFGC [3] that the fibers tend to align with the direction of the pour and along the formwork.

Table 2 presents a summary of the measured strength for each of the specimens tested. A comparison of predicted vs. actual punching shear capacity for all of the models discussed previously is presented in Figure 6aFigure. All models provided a reasonably consistent prediction of the response. However, a comparison of the mean of the ratio of measured load to predicted load, and its corresponding coefficient of variation, suggests that the ACI

318-05 punching shear equation provided the best prediction of punching shear capacity of UHPC. ACI 318-05 uses a constant relationship between the effective shear strength and

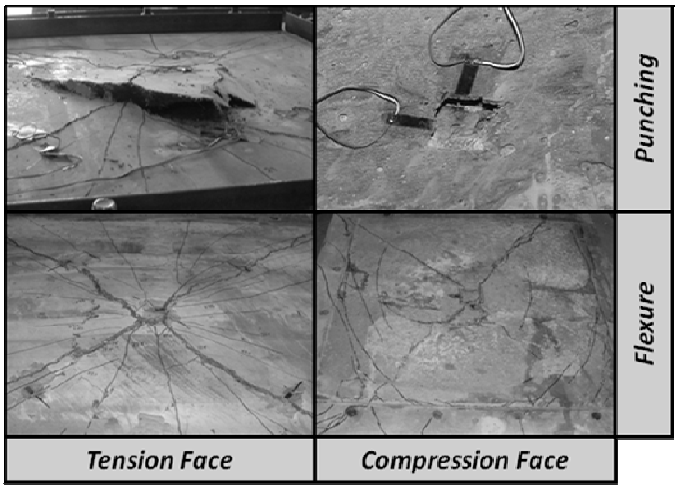

Figure 4: Failure Surfaces for Punching Shear and Flexural Failures

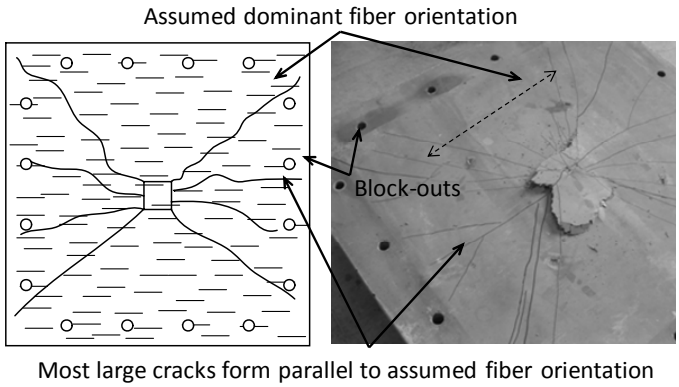

Figure 5: Fiber Orientation vs. Crack Pattern and Typical Punching Shear Crack Pattern

compressive strength ($0.33\sqrt{f_c'}$). The constant relationship appears to be reasonable for UHPC so long as the fiber volume remains constant. For the UHPC in this test program, $0.33\sqrt{f_c'}$ equates to 4.8 MPa, which is 0.44 of the measured splitting tensile strength. It is possible that a UHPC mix with a different volumetric ratio of fibers would have a different relationship between the effective shear strength and compressive strength. The modified breakout equation also provides an excellent prediction, but the coefficient, k_1=1.9, is based on a curve fit of a limited data population.

5.2 Flexural Failures

Five of the twelve specimens tested failed in shear as illustrated in Figure 6b. These flexural failures were characterized by cracks initially forming near the center of the slab on the tensile face and radiating to the edges. As loading continued, the cracks along the diagonals on the tensile face widened and extended through the slab thickness to the loading face with additional cracks forming at the fixed support on the loading face (Figure 4).

Table 2: Predicted Punching Shear vs. Measured Results for UHPC Test Specimens

Thickness (mm)	Load Plate (mm)	Measured (kN)	Failure Mode
55.1	38	104	Punching
58.9	51	121	Punching
53.8	25	101	Punching
66.2	51	147	Punching
65.5	76	160	Flexure
64.5	38	136	Punching
70.1	64	152	Flexure
78.7	64	173	Flexure
71.8	38	157	Punching
76.9	25	178	Punching
72.3	51	171	Flexure
83.1	44.4	175	Flexure

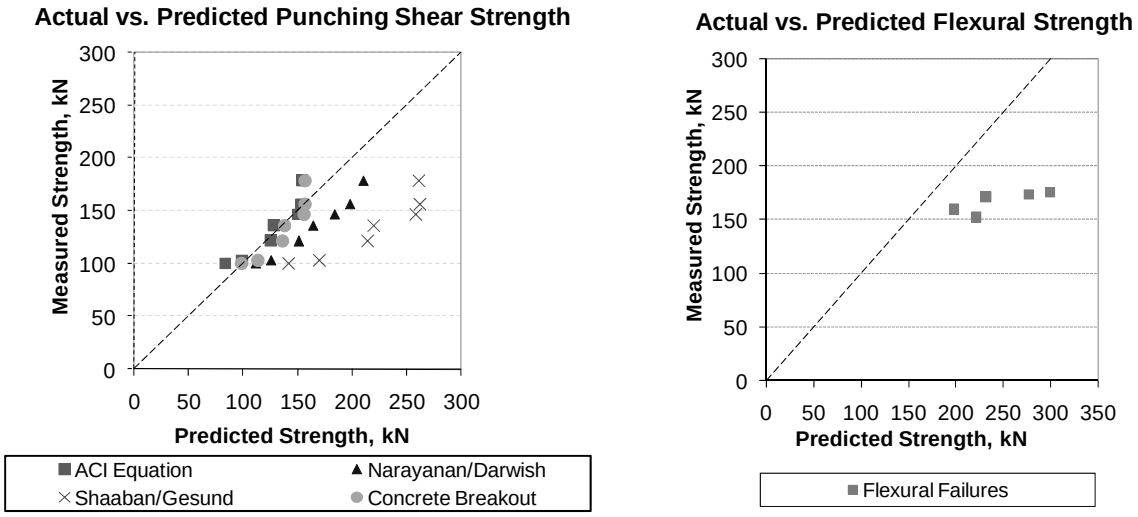

(a) *(b)*

Figure 6: Failure Predictions vs. Actual

These results indicate that the full tensile capacity of UHPC is not developed on the failure surface. This could be attributed to an overestimation of the post-cracking tensile strength and the lack of random fiber orientation resulting from the unidirectional casting technique. Also, the thinness of the slabs most likely resulted in an orientation of the fibers primarily parallel to the formed surface, rather than perpendicular to it. This is a significantly different fiber distribution than that in the tensile test specimens in which the fibers were randomly oriented.

6 Conclusions

Based on the results of the experimental program the following conclusions can be made.

- The current ACI 318-05 Code equation, with modifications for the lack of tensile reinforcement (Eqn. *[1]*), provides the best prediction of punching shear strength of UHPC.
- Based on the magnitude of the failure loads and the small loading areas required to cause failure, the probability of punching shear failures occurring as a result of tire loadings is unlikely. Slabs as thin as 2 in. would provide adequate strength in typical bridge applications, but consideration should be given to serviceability requirements and transverse flexure.

7 Notation

D – diameter of fibers (mm)

L – length of fibers (mm)

W_f – percent of fibers by weight of concrete

V_c – punching shear capacity (N)

b_o = critical perimeter (h/2 for UHPC) (mm)

b_{pf} – critical perimeter = $\left(1 - 0.55\frac{\rho_f d_f L}{D}\right)(4a + 3\pi h)$

c – loading plate length (mm)

d – effective depth of tensile steel (mm)

d_f – fiber factor = 0.5 (round), 0.75 (crimped)

f'_c – compressive strength (MPa)

f_{sp} – split cylinder strength (MPa)

h – slab thickness (mm)

h_{ef} – effective anchor embedment depth

k_1 – UHPC breakout constant = 1.9

ξ_s – empirical depth factor = 1.6 – 0.051h

ε_c – UHPC extreme compression strain

ε_{lim} – limiting strain criterion

ε_t – UHPC extremen tension strain

ε_{tc} – UHPC cracking tensile strain

ω_{lim} – max. permissible crack = 0.3 mm

ρ – percent tensile steel reinforcement

ρ_f – steel fiber volume fraction

σ_{Mt} – initial tensile strength = 7.6 MPa

τ_u – fiber-matrix bond stress = 4.15 MPa

8 References

[1] Park, H., E. Chuang, and F.-J. Ulm, Model-based optimization of ultra high performance concrete highway bridge girders. 2003, Massachusetts Institute of Technology.

[2] Building code requirements for structural concrete (ACI 318-05) and commentary (ACI 318R-05). 2005, Farmington Hills, MI: American Concrete Institute.

[3] Association Française de Génie Civil (AFGC), Interim Recommendations for Ultra High Performance Fibre-Reinforced Concretes. 2002, AFGC Scientific and Technical Documents.

[4] Shaaban, A.M. and H. Gesund, Punching shear strength of steel fiber reinforced concrete flat plates. ACI Structural Journal, 1994. 91(4): p. 406-414.

[5] Narayanan, R. and I.Y.S. Darwish, Punching shear tests on steel fibre reinforced micro-concrete slabs. Magazine of Concrete Research, 1987. 39(138): p. 42-50.

[6] Fuchs, W., R. Eligehausen, and J.E. Breen, Concrete capacity design (CCD) approach for fastening to concrete. ACI Structural Journal, 1995. 92(1): p. 73-94.

[7] Harris, D.K., Characterization of the punching shear capacity of thin UHPC plates. 2004, Department of Civil and Environmental Engineering Virginia Tech: Blacksburg, VA.

[8] Graybeal, B.A., Characterization of the behavior of ultra-high performance concrete, in Civil Engineering. 2005, University of Maryland: College Park, MD.

[9] Graybeal, B.A. and J.L. Hartmann, Strength and durability of ultra-high performance concrete, in 2003 PCI National Bridge Conference. 2003: Orlando, FL.

Dr Mark Rebentrost
General Manager - Ductal®
VSL Australia Pty Ltd
Sydney, Australia

Dr Gavin Wight
Technical Manager - Ductal®
VSL Australia Pty Ltd
Sydney, Australia

Behaviour and Resistance of Ultra High Performance Concrete to Blast Effects

Summary

Ultra High Performance Concrete such as reactive powder concrete (RPC), with compressive strength 4 to 5 times stronger than ordinary concrete, exhibit exceptional energy absorption capacity and resistance to fragmentation, making it ideal for panels and components that need to perform under explosive, impact or shock loads. The flexural toughness of RPCs enhanced with fine steel fibres is greater than 200 times that of conventional fibre reinforced concrete.

This paper provides an overview of projectile and blast effects testing undertaken in Australia with panels made from reactive powder concrete reinforced with high-strength steel fibres and additional reinforcement. The results of the tests are described and discussed. The paper will also make mention of a project where a custom designed protection solution has been deployed for an important structure in a high risk international location.

Keywords: *reactive powder concrete, projectile resistance, blast effects*

1 Introduction

Reactive Powder Concrete (RPC) is a cementitious material consisting of cement, sand, silica fume, silica flour, superplastizer, water and high strength steel fibres. The material was first described in the literature in [1] and further developed by Bouygues, the parent company of VSL, Lafarge and Rhodia and is marketed under the brand name of Ductal®.

RPC is almost self-placing, has a compressive strength of 160-200 MPa and a flexural strength of 30-40 MPa. It has exceptionally high-energy absorption capacity and resistance to fragmentation, making it ideal for panels and components that need to perform under explosive, impact or shock loads. The flexural toughness is greater than 200 times that of conventional fiber reinforced concrete. Further details of the typical quasi-static mechanical properties are well documented; refer to [2,3] for example. RPC has also been shown to exhibit extraordinary durability properties in comparison to ordinary concretes [4].

While engineering structures constructed from RPC are not a replacement for ordinary reinforced concrete applications, the use of RPC around the world has increased in recent years particularly for pedestrian and road bridges [5,6,7,8], architectural applications [9,10]

and other structural engineering applications that explore the mechanical and durability properties. Design guidelines for RPC limit analysis are now widely available [11,12]

In May 2004, the performance of seven panels was evaluated in two large explosive trials performed at Woomera (South Australia). The panels performed remarkably well, exhibiting high levels of ductility and no signs of fragmentation. In further tests, 100mm thick optimized RPC panels effectively resisted explosions from close charge blasts, projectile impacts from ballistic tests, and impacts caused by blast produced fragments using fragment simulated projectile tests. The most recent tests were in April 2006, when a building fabricated from precast panels, including a panel with a window, was subjected to large explosive trials at Woomera.

In June 2005, the first RPC panels were manufactured to provide resistance to blast and were supplied to the Australian Government to be installed on a building in a high risk international location.

2 Compression Strength at High-Strain Rates

The response of concrete to very high strain rates needs to be known in order to properly design structures subjected to blast or impact effects. At high strain rates, the strength of concrete can increase significantly. The response for RPC was determined by a series of impact tests carried out using the Split Hopkinson Pressure bar setup on large-diameter test cylinders. A range of loading rates and pressures were used.

Figure 1 shows the stress-strain curves at different strain rates of 50mm diameter RPC cylinders. Table 1 summarises the test results of the three RPC specimens. It can be seen that the compressive strength increases up to 1.5 times for a strain rate of 267.4/sec, compared with a static test (low strain rate). This corresponds to a strength Dynamic Increase Factor (DIF) of 1.5. It was found that RPC is less rate sensitive compared to both NSC and HSC [13].

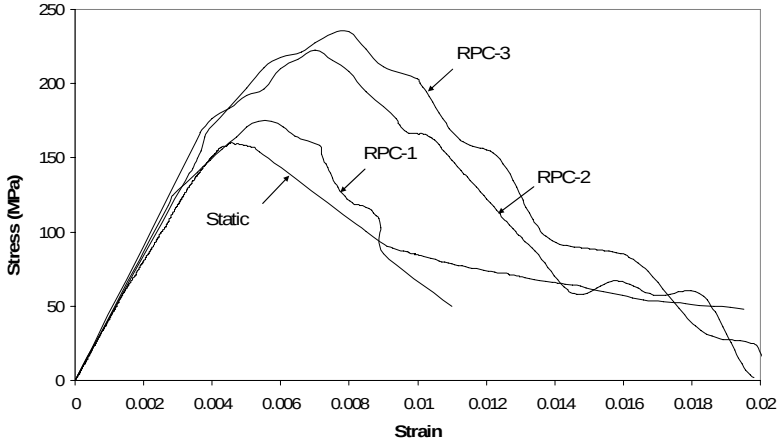

Figure 1: Stress-strain curves of RPC at different strain-rates

Table 1: Dynamic Compressive Strength of RPC

Concrete Specimen	Impact Velocity	Average Strain Rate (1/sec)	Ultimate Strength	DIF
Static Test	-	-	159.8 MPa	-
RPC-1	11.6 m/s	80.7	187.2 MPa	1.17
RPC-2	16 m/s	187.3	226.1 MPa	1.41
RPC-3	20 m/s	267.4	240.9 MPa	1.5

Based on the results of the experimental program using the Hopkinson Bar apparatus and through a rigorous calibration process, a new strain-rate dependent constitutive model has been proposed by the Advanced Protective Technologies for Engineering Structures (APTES) group at the University of Melbourne, for concrete under dynamic load. The model can take into account the strain-rate effect by incorporating multiplying factors for increases in the peak stress and strain at peak strength. This model is applicable to concrete strengths varying from 32 MPa to 160MPa with a strain rate up to 300 s-1. A detailed report is given in [13]

3 Response to Large-Scale Blast Effects

In a joint project between VSL Australia Pty Ltd and the APTES group at the University of Melbourne, reinforced RPC panels were tested under extreme explosions at blast trials performed at Woomera in South Australia. The Woomera trial in May 2004 consisted of two separate blasts equivalent to six (6) tonnes of TNT. Each detonation consisted of a bare charge of 5 tonnes of the explosive Hexolite.

A total of seven panels were tested at 30m, 40m and 50m from the blast. One conventional, reinforced concrete panel was tested at 40m from the blast. Calculated reflective blast pressures were 2000, 800 and 400kPa, respectively, for these distances. The panels had a span of 2m and were 1m wide, with a thickness of 50mm, 75mm and 100mm. Five panels contained an identical arrangement of high strength steel reinforcing. The other two panels were unreinforced. Deflections were recorded on five of the panels using a simple pen on paper apparatus. The other two panels had a laser system installed with the intent of recording the deflection and time history. However, this instrumentation failed to record accurate data.

The test data and observations showed that the panels performed remarkably well, displaying high ductility and no signs of fragmentation. The stressed panels were able to absorb substantial energy through their ability to sustain considerable deflection up to span/28 without fracture. The fact that the RPC panels displayed no fragmentation in any of the tests, even at fracture, is a major advantage compared to conventional concrete. Fragmentation poses great danger to both people and infrastructure.

Figure 2 shows a summary of the tests including installation of the panels, blast, crater and two of the RPC panels post explosion. For additional information refer to [14].

Installing panels into concrete frames

Panels ready for blast

Blast (Equivalent to 6t of TNT)

Crater (17m Diameter) caused by the blast

100mm panel at R=30m after the blast; undamaged

50mm panel at R=50m after the blast, shallow crack, no spalling or fragmentation

Figure 2: RPC panel tests, Woomera blast trial

4 Resistance to Projectile Impact

In September 2005, three 100mm thick panels were tested at a NATA registered laboratory in Melbourne, Australia, for resistance to attack by NATO standard 7.62/9.3g full metal case bullets at 850m/s. All panels were reinforced with high-strength steel. Testing procedure followed AS/NZ 2343 [15] and consisted of firing projectiles at the target piece with an intended speed. Each test piece was mounted in a frame and a witness card (paper) was placed behind it to record fragmentation impacts. A test pass was awarded if no fragment

penetrated through the witness paper. All panels passed the test, with no fragments being dislodged from the back face or penetrating the witness paper, and achieved an R2 ballistic rating. Figure 3 shows two panels following the test. Subsequent tests using armor piercing 7.62mm bullets were conducted and the same 100mm thick RPC panel configuration passed and was awarded certification against this threat level.

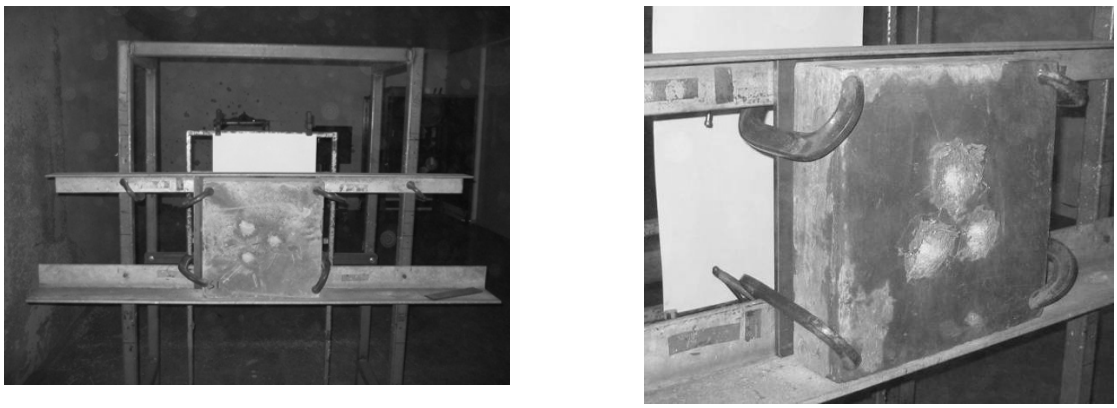

Figure 3: Test specimen after 3 impacts from 7.62mm full metal case NATO ball at 850m/s

Further tests were conducted to evaluate the resistance of 100mm thick RPC panels against the impact of typical fragments from mortars and rockets. Two types of steel projectiles were used to simulate the fragments: a 50 caliber (13mm diameter) and 20mm diameter FSP (fragment simulated projectile). The projectiles were fired at the test panels with target speeds ranging from 715 to 1120 m/s. Figure 4 shows the projectiles before and after impact with the RPC panel. The 100mm thick RPC panels sucessfully defeated 20mm FSP at 1120m/s and 50 caliber at 850m/s. The results compare favourably with impact data for 81mm mortar, general purpose (GP) and US 4.2 inch mortar fragments. For additional information refer to [16].

Figure 4: 50 caliber (13mm) and 20mm FSP, before and after impact

5 Close-charge Effects

A series of tests against close-charge effects were conducted in 2005, comparing the performance of 100mm thick RPC and ordinary concrete panels with the same flexural capacity. All test panels had plan dimensions of 1.3 x 1.0m and were simply supported along the short edge. The ordinary reinforced concrete panels were cast from Grade 50 MPa

concrete and reinforced with N20 (500 MPa yield) steel bars at 75mm spacing on the back face, and at 150mm spacing on the front face.

Testing frame and mounted panel.

Back face of concrete panels after first exposure to 0.5kg comp B charge at 100mm.

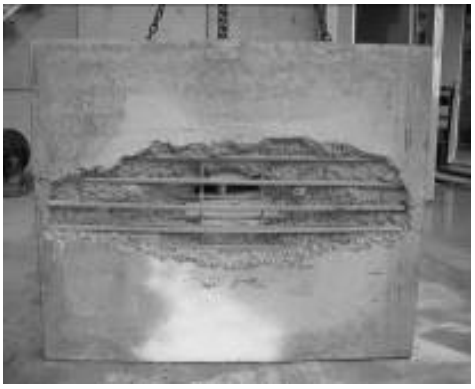

Back face of concrete panels after second exposure to 0.5kg comp B charge at 100mm.

Back face of RPC panel after exposure to 0.5kg Comp B charge at 100mm

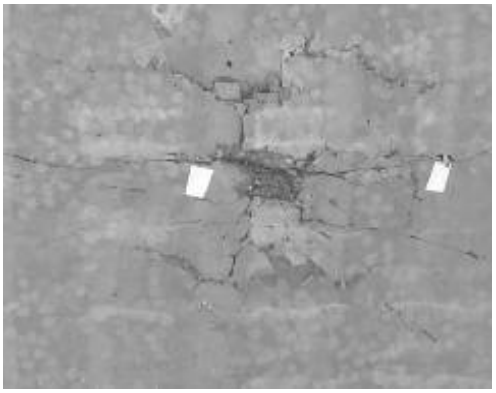

Back face of RPC panel after second exposure to 0.5kg Comp B at 100mm.

Figure 5: Test panels after close charge explosion

The panels were exposed to 0.5kg cylindrical Composition B, Powergel and other types of charges placed at 100mm from the top face of the panel. All tests were carried out by an independent government testing facility.

Visual inspection of the back panel face showed the RPC panels resisted a first exposure to the CompB charge without any scabbing and very minor damage. After a repeated exposure of the same charge, the same panel showed minimal small particle scabbing and remained structurally intact. In comparison, the ordinary reinforced concrete panel showed significant signs of high-velocity scabbing after the first exposure and was breached on the second exposure. Photos and observations of typical panels are shown in Figure 5. For additional information refer to [17].

6 Application Example

Panels for the first structure to utilize blast resistant optimised RPC panels were manufactured in March 2005 at the VSL plant in Melbourne. The client was the Department of Foreign Affairs and Trade of the Australian Government. The panels are part of a blast protection system designed by VSL Australia and APTES. Panels are up to 4.5m long x 2.0m wide x 100mm thick. They are being used to provide blast resistance to an existing building in a high risk international location. The panels were installed on site in July 2005. Photos of the panels prior to shipment from the VSL factory and as installed on site are shown in Figure 6.

Optimised blast resisting RPC panels

Installed RPC panels

Figure 6: RPC panels for protection of government facility

7 Concluding Remarks

Large-scale blast tests, close charge blast tests, fragment simulation tests, and ballistic tests have confirmed that RPC panels optimised for blast resistance are an effective solution for mitigating the risks of such threats. Panels can be much thinner than those made from conventional concrete, and the risk of injury or damage caused by concrete fragments is virtually eliminated. The application of RPC panels to protect a facility in a high risk location demonstrates the future potential for RPC in the field of infrastructure protection.

8 References

[1] Richard, P.; Cheyrezy, M.: Composition of reactive powder concrete. In: Cement and Concrete Research, Vol. 25, No. 7, S.1501-1511, 1995.

[2] Gowripalan, N.; Watters, R.; Gilbert, I.; Cavill, B.: Reactive Powder Concrete for Precast Structural Concrete – Research and Development in Australia. In: Proc. 21st Biennial Conference of the Concrete Institute of Australia, Brisbane, Australia, 2003.

[3] Acker, P.; Behloul, M.: Ductal Technology: A Large Spectrum of Properties, A Wide Range of Applications. In: Proc fib Symposium, Avignon, France, 2004.

[4] Roux, N.; Andrade, C.; Sanjuan, M. A.: Experimental Study of Durability of Reactive Powder Concretes. In: Journal of Materials in Civil Engineering, Vol. 8, No. 1, S. 1-6, 1996.

[5] Rebentrost, M; Cavill, B.: Reactive Powder Concrete Bridges. In: Proc. AustRoads 6th Bridge Conference, Perth, Australia, 2006.

[6] Rebentrost M. Design and Construction of the First Ductal Bridge in New Zealand, New Zealand Concrete Industry Conference, Auckland, New Zealand, September 2005.

[7] Blais PY and Couture M. Precast, Prestressed Pedestrian Bridge – World's First Reactive Powder Concrete Structure. PCI Journal, Sept.-Oct. 1999, pp. 61-71.

[8] Editors Schmidt and Fehling, Ultra-Hochfester Beton - Planung und Bau der ersten Bruecke mit UHPC in Europe, Tagungsbeitraege zu den 3. Kasseler Baustoff- und Massivbautagen, Heft 2.

[9] Ricciotti, Bridge to the Future. ASCE Civil Engineering Magazine, Vol 71 No 1, November 2001.

[10] Perry, V., Zakariasen, D., Chow, T., Vincenzino, E., and Culham, G, First Use of UHPFRC in Thin Precast Concrete Roof Shell for Canadian LRT Station, PCI Journal, October 2005, USA.

[11] Gowripalan, N.; Gilbert, R. I.: Design Guidelines for Ductal Prestressed Concrete Beams. Design Guide, Civil & Environmental Engineering School, University of NSW, Sydney, Australia, 2000.

[12] AFGC / SETRA Working Group: Ultra High Performance Fibre-Reinforced Concrete – Interim Recommendations. Report, Association Française de Génie Civil, Paris, France, 2002.

[13] Ngo, T. (2005). "Behaviour of High Strength Concrete subjected to Impulsive Loading", PhD Thesis, Department of Civil & Env. Engineering, University of Melbourne, Australia, 2005.

[14] Ngo, T., Mendis, P., Lam, N. and Cavill, B. "Performance of Ultra-High Strength Concrete Panels subjected to Blast Loading", The 2005 Science, Engineering and Technology Summit, Canberra, July 2005.

[15] Australian Standard for Bullet Resistant Panels and Elements AS/NZS 2343. Australia,1997.

[16] Gupta, Mendis, Ngo and Rebentrost, Modelling Localised Response of Steel Fibre Reinforced Ultra High-strength Concrete Panels under High Velocity Impact, Australasian Conference of Materials and Structural Mechanics, Christchurch, New Zealand, 2006.

[17] Kuznetsov V., Rebentrost M., and Wasch J. Strength and Toughness of Steel Fibre Reinforced Reactive Powder Concrete under Blast Loading", 1st International Conference on Analysis and Design of Structures against Explosive and Impact Loads, Tianjin, China, Sept. 2006.

Ezio Cadoni
Professor
University of Applied Sciences of Southern Switzerland
Lugano, Switzerland

Alessio Caverzan
Research Assistant
Politecnico di Milano
Milan, Italy

Marco di Prisco
Professor
Politecnico di Milano
Milan, Italy

Dynamic behaviour of HPFR cementitious composites

Summary

The use of fibres in High Performance Cementitious Composites is often justified by means of the improvement of impact and blast resistance due to their ability in energy absorption. In order to understand and appreciate the effective increase in uniaxial tension behaviour at increasing strain rates, an experimental investigation is in progress by using a Modified Hopkinson Bar for dynamic loadings available at the University of Applied Sciences of Southern Switzerland of Lugano and a conventional closed loop electromechanical press for statical tests available at the Politecnico di Milano - Polo Regionale di Lecco. The geometry of the specimens is kept exactly the same and due to limitations imposed by dynamic loadings, small size specimens are only considered; nevertheless in statics also conventional bending on notched specimens are carried out to highlight the role of reduced sizes. The material investigated is steel fibre reinforced mortar used for the production of precast roofing elements. The main aim is the comprehension of the high strain rate role on the constitutive relationship in uniaxial tension and the estimation of the improvement in terms of strength and toughness achievable by means of steel fibre addition.

Keywords: *blast, crack opening displacement, dynamic increasing factor, fibre reinforced cementitious composite, impact, sensitivity, strain-rate.*

1 Introduction

In Civil structures, the mechanical behaviour of the materials when subjected to high strain rates is mainly oriented to the investigation of impact and blasting phenomena (Fig.1). In the framework of a research focused on the possible use of Ultra High Performance mortars in tunnel linings to improve fire and blasting resistance, the present paper investigates some preliminary results obtained by comparing uniaxial tension stress-crack opening curves, characterized by strain rates in the range over 10^0 s^{-1}, with quasi-static tests characterized by a strain rate in the range of 10^{-6} s^{-1}. The high strain-rate tests are carried out by means of a modified Hopkinson bar technique first developed by Albertini et al. [1,2]. Several techniques have been developed to identify high strain-rate mechanical behaviour of FRC (Fig.2): as

highlighted by V. Bindiganavile and Banthia [3] in Split Hopkinson Pressure Bar (SHPB) Test (Figure 2a,b) the specimen is sandwiched between two elastic bars and high stress-rates are generated by propagating a pulse through one of the elastic bars. This technique has an advantage over the others like drop-weight (Fig. 2c) and swinging pendulum machines, because very large drop-heights are required in order to achieve high strain rates. However, most SHPB machines allow for very small specimen sizes and this is particularly unfavourable for FRC, given the typical length of most fibres. Recently at British University of Columbia also a dynamic fibre pull-out test machine was constructed specifically for dynamic pull-out testing of individual fibres embedded in a cement-based matrix (Fig.2d; [4]). The specimen is held in the machine such that the top half is stationary, while the bottom half is pulled down rapidly by an air-gun. The air-gun can operate at a peak pressure of 0.35 MPa, which generates a pull-out displacement rate of 3 m/s.

The main open questions related to this material are the increase due to high-strain rate of the peak both in terms of strength and strain, and above all on pull-out strength after matrix cracking. Strain rate sensitivity of concrete is found to be maximum in tension according to literature: even though one of the highest dynamic strength data reported is due to McVay [5], who observed an increase over 700% at strain rates of 102/s during spalling of a concrete slab due to blast from a conventional weapon, in FRCs the increase in pull-out strength ranges between 1.3 to 6 by using straight steel fibres [6,7], with a crack opening varying between 1 to 500 mm/s. The following research is strongly recommended by several recent indications [8] and is aimed to confirm the results presented by Cadoni et al. [9].

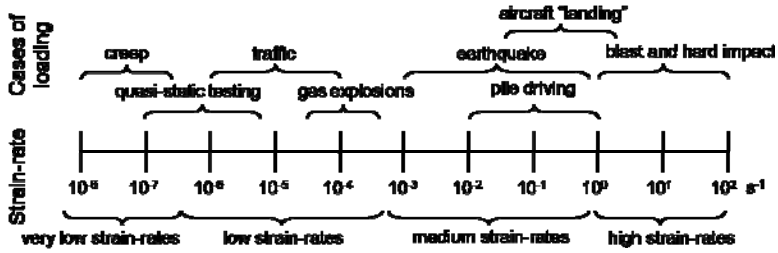

Figure 1: strain rates and related phenomena in the framework of civil engineering

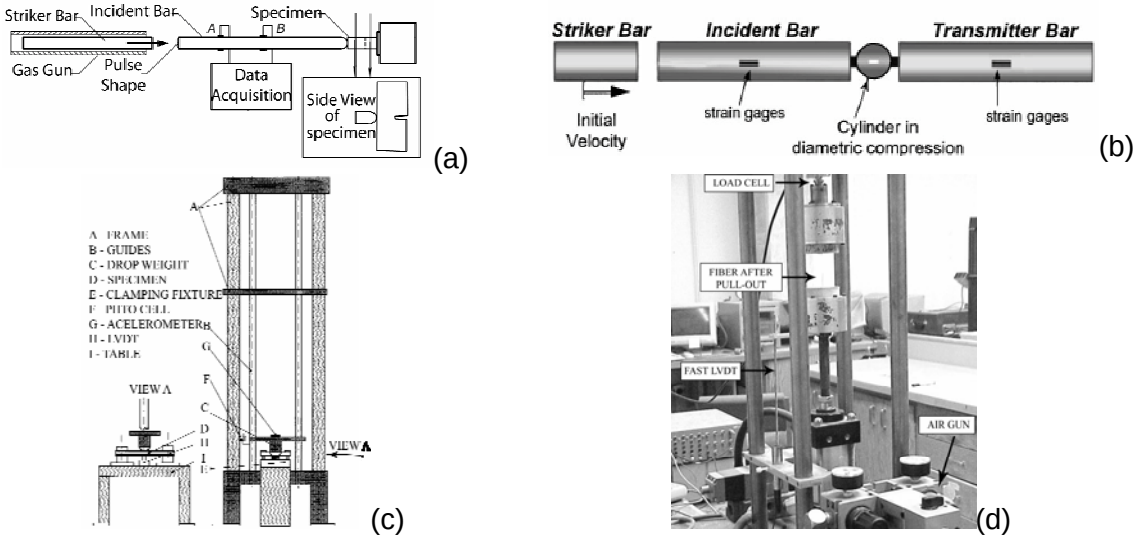

Figure 2: Dynamic uniaxial tension set-ups: Hopkinson bars for (a) bending on notched tests, (b) splitting; (c) drop-weight; (d) pull-out dynamic [3].

2 Material mix design and mechanical characterization

The mix design of the UHPFRCC material is specified in Table 1. Steel fibres are high carbon straight fibres 13 mm long, with a 0,16 mm diameter; their content is equal to 100 kg/m^3. The mechanical characteristics of the material are first identified by means of a 4 point bending test on notched specimen according to UNI 11039 Italian Standard [10], because the expected uniaxial tension behaviour after cracking was softening and not hardening. The cubic compressive strength R_c as well as the first-cracking f_{IF} and residual equivalent strengths $f_{eq0\text{-}0.6}$ and $f_{eq0.6\text{-}3}$ for crack opening ranging between 0-0.6mm and 0.6-3 mm are reported in Table 2. According to Model Code 90 before cracking and to Italian Guidelines CNR-DT 204/06 [11] to describe the post-cracking pull-out branch, as suggested by di Prisco et al. [12,13], the uniaxial tension constitutive relationship is also identified starting from the average results obtained by 4 point bending notched tests. From the bent specimens, several small cylinders were cored in the direction of tensile stresses in order to be tested in uniaxial tension at different loading rates.

Table 1: Mix design

Mix propositions of steel fiber reinforced concrete			
Cement CE 52,5 I	600 kg/m^3	Superplasticizer	33 l/m^3
Slag	500 kg/m^3	Water	200 l/m^3
Sand	983 kg/m^3	Fiber	100 kg/m^3

Table 2: SFRCC mechanical characteristics: (a) compressive strength, (b) first cracking and residual strength according to UNI 11039 ($^*\Delta=(f_{cm}-f_{cmin})/f_{cm}$).

(a)

Identification specimen	**Max load [kN]**	**Rc [MPa]**	**Rc,av [MPa] (%)***	**Age [days]**
G1/3	2460	109.33		28
G2/3	2880	126.32	116.49 (6.58 %)	28
G3/3	2715	121.48		28
G4/3	2465	108.83		28

(b)

Identification specimen	**f_{Ft} [MPa]**	**$f_{Ft,av}$ [MPa] (Δ %)***	**f_{eq1} [MPa]**	**$f_{eq1,av}$ [MPa] (Δ %)***	**f_{eq2} [MPa]**	**$f_{eq2,av}$ [MPa] (Δ %)***
T-G1_1	6.26		11.43		10.09	
T-G2_1	6.56	6.39 (2.03 %)	10.70	12.06 (11.28 %)	7.94	9.77 (18.73 %)
T-G3_1	6.49		13.37		12.09	
T-G4_1	6.26		12.76		8.94	

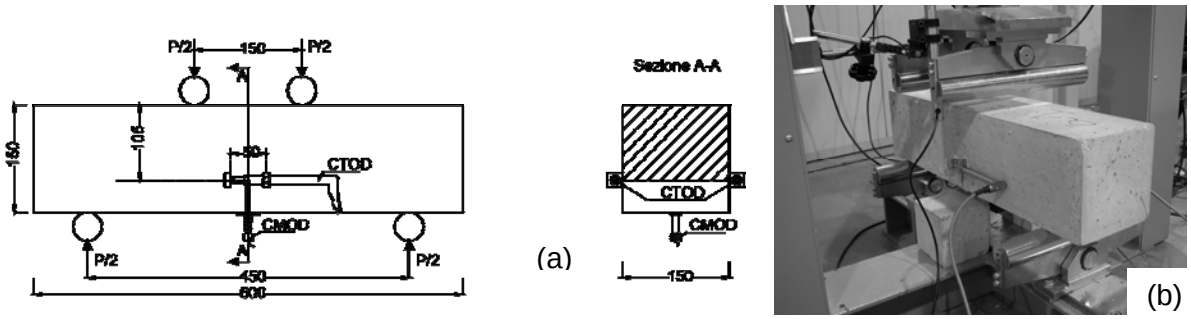

(a) (b)

Figure 3: Four point bending test: (a) set-up; (b)specimen during the test.

3 Static tensile loading

Uniaxial tension tests were carried out on notched 20 mm high cylinders with a 20 mm diameter (Fig. 4b; notch depth = 1.5 mm), glued to the press platens by means of an epoxy. Due to the small length of the specimen, the specimen was instrumented by only four LVDTs placed between the two steel end platens (Fig. 4a). The displacement rate imposed during the tests was equal to 2.7 10^{-4} mm/s up to 1.5 mm and after progressively increased to 10^{-3} mm/s. The stress vs. crack opening is plotted in Fig. 5 b,c. Some results were discarded because the small size of the specimen asked for a strict respect of the maximum aggregate size, and this condition sometime was not respected. The number of fibres quantified in the failed cross section was 106 and 54 respectively for specimens 1A and 2A. The expected value computed according to [14] ($N_f = \alpha * V_f/A_f * A_0$; with α = 0.431 according to a 3D random fibre distribution) is 65. The small size of the cross section specimen involves a quite large scattering. The results are reasonably well fitted by the tensile constitutive law identified through bending tests despite the significant scattering connected with the fibre number. The experimental measure of the initial slope is not reliable, because it corresponds to stroke measure.

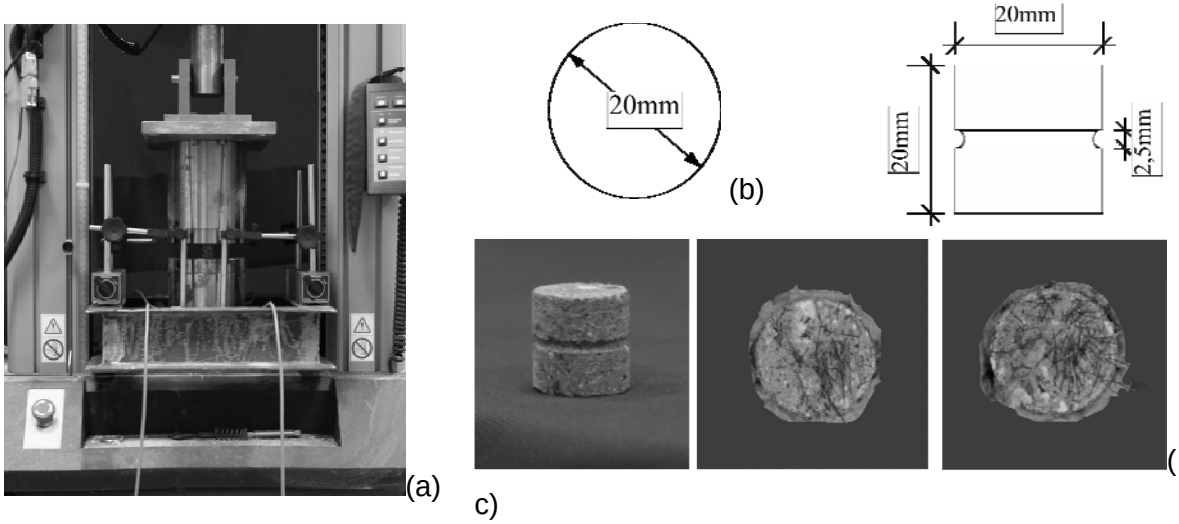

(a) (b) (c)

Figure 4: (a) Test set-up; (b) specimen geometry; (c) cross section detail.

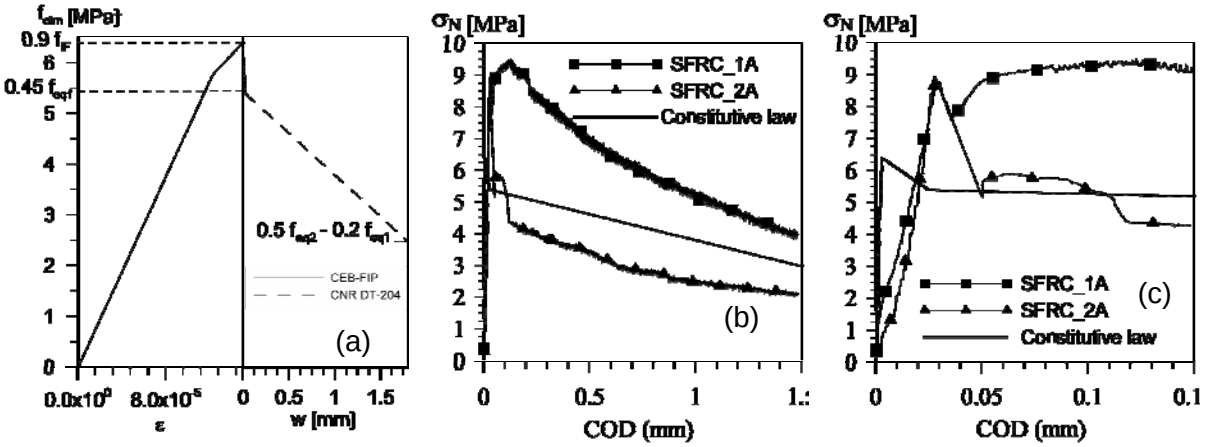

Figure 5: (a) stress- crack opening constitutive law predicted according to DT-204 Italian Standards ; (b) stress vs. crack-opening; (c) stress vs. crack-opening zoom.

4 Dynamic tensile loading

The dynamic tensile tests were carried out on specimens, having the same geometry used in the static tests, by means of a Modified Hopkinson Bar (MHB) installed in the DynaMat laboratory of the University of Applied Sciences of Southern Switzerland (Fig. 6a).

The MHB consists of a pre-stressed bar (substituting the projectile of the classic Hopkinson bar) (high strength steel bar with ϕ=12mm and L=6m) which has connected with the input bar (aluminium bar with ϕ=20mm and L=3m), followed by the output bar (aluminium bar with ϕ=20mm and L=6m), and the specimen inserted between the two last bars. Its functioning is based on storing a certain amount of elastic energy in the pre-stressed bar length by statically tensioning this bar up to a stress value lower than its yield strength; to achieve this the end section of the pre-stressed bar contiguous to the input bar is blocked by a brittle intermediate piece and the other end is pulled by means of a hydraulic actuator.

Once the necessary elastic energy is stored in the pre-stressed bar length and the specimen inserted between the input and output bars, the brittle intermediate piece is ruptured giving rise to the contemporaneous generation of two elastic plane waves:

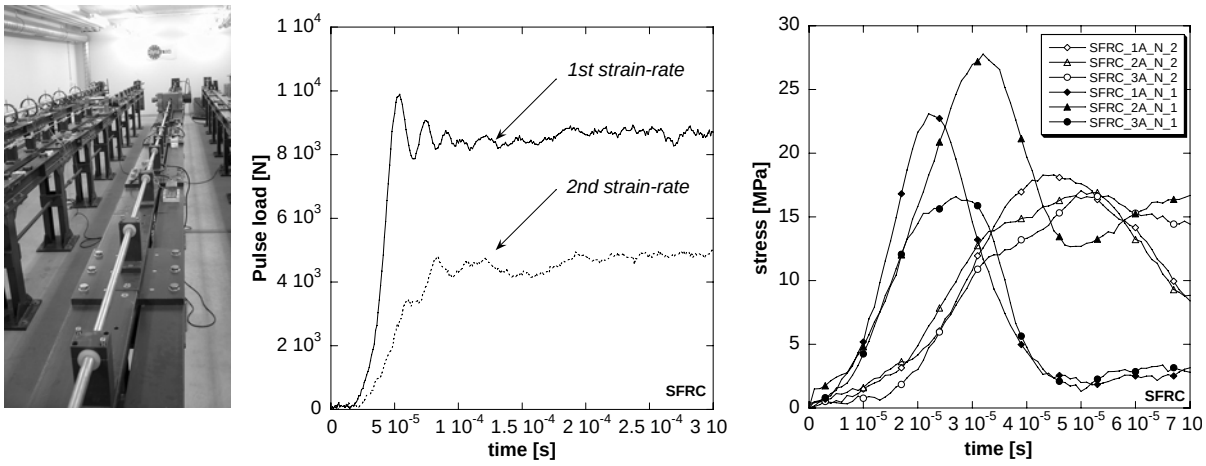

(a) (b) (c)

Figure 6: Testing set up for dynamic tensile tests; (b) pulse load versus time curves; (c) stress vs. time curves of the elastic specimens.

- a plane elastic unloading wave starts from the bar section liberated by the rupture of the brittle intermediate piece and propagates along the pre-stressed bar unloading it (compression wave).
- a plane elastic tension wave starts from the same bar section and propagates along the input bar, loading it in tension; it reaches and loads the specimen until fracture, and propagates loading in tension the output bar.

The duration of the tension pulse loading the specimen corresponds to the travel time of the unloading wave from the unblocked bar section to the hydraulic actuator and back. The amplitude of this almost rectangular pulse is half that of the static pre-tension value established in the pre-stressed bar by the hydraulic actuator. In Fig. 6b two input load versus time curves are shown, measured in the input bar that produces a loading rate of 1200 GPa/s and of 700 GPa/s corresponding to two strain-rate levels: 27 and 65 s^{-1}. The strain gauge station on the input bar measures the incident pulses ε_I and the reflected pulses ε_R. The strain gauge station on the output bar measures the pulses ε_T transmitted through the specimen. By the measure of the reflected and transmitted pulse the stress and the strain history is obtained by using the formulation of the Hopkinson bar theory, as shown by equations 1a,b,c [2].

Table 3: dynamic test results

Identification specimen	**f_t [MPa]**	**$f_{t,av}$ [MPa]**	**COD [mm]**	**n° fibre [nr. of fibres]**	**$N_f = \alpha * A_0 * V_f / A_f$ [nr. of fibres]**
SFRC_1A_N_1	23.1		0.0093	39	
SFRC_2A_N_1	27.8	22.5±5.6	0.0325	93	65
SFRC_3A_N_1	16.6		0.0207	53	
SFRC_1A_N_2	18.3		0.0334	85	
SFRC_2A_N_2	17.1	17.3±0.9	0.0391	60	65
SFRC_3A_N_2	16.6		0.0194	18	

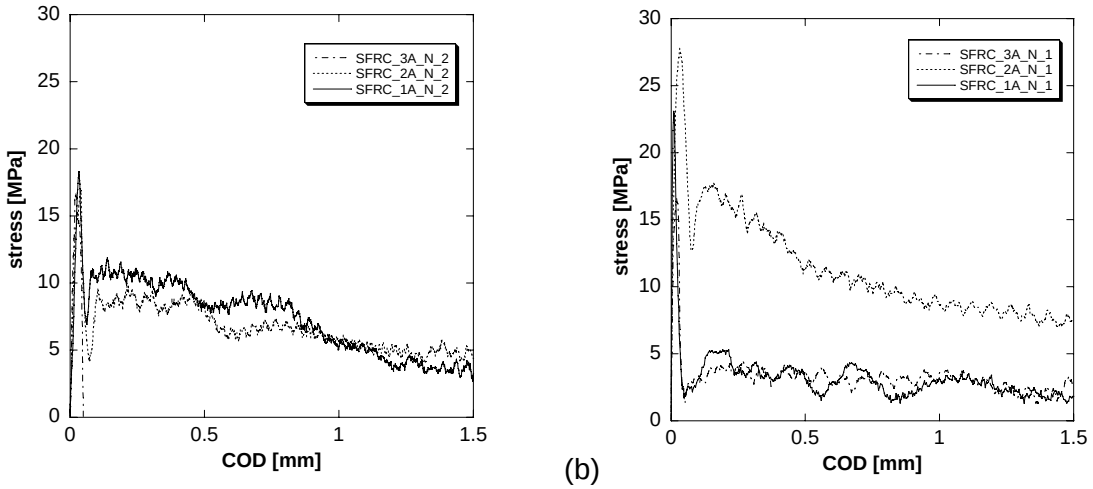

(a) (b)

Figure 7: Stress vs. Crack Opening Displacement for (a) 27 s^{-1}; (b) 65 s^{-1}.

$$\sigma(t) = E_0 \frac{A_0}{A} \varepsilon_T(t); \qquad \varepsilon(t) = -\frac{2 \cdot C_0}{L} \int_0^t \varepsilon_R(t)\, dt; \qquad \dot{\varepsilon}(t) = -\frac{2C_0}{L} \varepsilon_R(t); \qquad (1a,b,c)$$

where E_0 is the elastic modulus of the bars, A_0 their cross-sectional area, A is the specimen cross section area, L is the specimen length, C_0 is the sound velocity through bar material and t is the time. In Table 4 the results of the dynamic tensile tests carried out on SFRCC specimens are shown. Figs. 7a,b show the behaviour of the SFRCC specimens subjected to two strain-rates as stress vs. crack opening displacement. In Figs. 8b,c the photos of a SFRCC specimen after failure and its fracture surface are shown.

5 Discussion

On the basis of the presented results, the ratio between dynamic and static strength (DIF; dynamic increasing factor) can be analyzed. In literature several formulation have been developed for plain concrete. Unfortunately, no expressions are available for SFRCC. In order to verify if the most used expressions are useful also for SFRCC the obtained data have been compared with the CEB expression [15] and Malvar expression [16]. In Fig. 10a the results of this analysis are reported. The CEB formulation seems to describe better than Malvar's formula, but a new expression should be developed for SFRCC both in tension and compression.

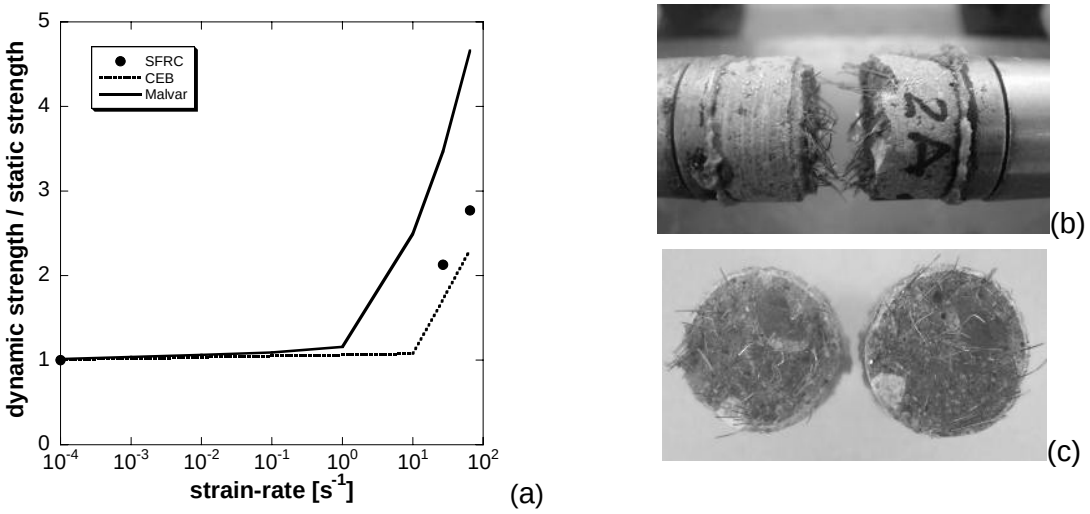

Figure 8: (a) Dynamic Increase Factor (DIF) for strength vs. strain-rate of SFRCC; (b) specimen after failure; (c) fracture surface.

6 Conclusions

Despite the relative quite small fibre content (100kg/m^3), the material investigated shows a uniaxial tensile behaviour with a very weak softening in quasi static tests, well predicted by means of identification procedure suggested in Italian guidelines CNR DT-204. The increase of strain rate significantly affects the tensile behaviour in the range considered (20-65 s^{-1}), by increasing more the peak than the residual strength. The Dynamic increasing factor is in the range 2-3 for the strain rates investigated.

7 References

[1] Albertini, C.; Montagnani, M.: Testing techniques based on the split Hopkinson bar. In: Int. Conf. on “The mechanical properties at high strain-rates”, Oxford University, Institute of Physics Conference Series, 21, 22-32, 1974.

[2] Albertini, C.; Cadoni, E.; Labibes, K.: Study of the mechanical properties of plain concrete under dynamic loading. In: Experimental Mechanics, 39 (2), 137-141, 1999.

[3] Bindiganavile, V.; Banthia, N.: Impact and blast resistance of fiber reinforced concrete. In: Draft report circulated in ACI 544 Technical Commission, 2007.

[4] Bindiganavile, V.; Banthia, N.; Aarup, B.: Impact response of ultra-high strength fiber reinforced cement composite. In: ACI Materials Journal, 99 (6), 543-548, 2002.

[5] McVay, M. K.: Spall damage of concrete structures. In: Technical Report SL-88-22,Waterways Experiment, Corps of Eng., Vicksbury, MS, 1998.

[6] Gray, R. J.; Johnston C. D.: The measurement of fiber-matrix interfacial bond strength in steel-fiber reinforced cementitious composites. In: Testing and Test Methods of Fiber Cement Composites, RILEM Symposium, 1978.

[7] Pacios, A., Ouyang, C.; Shah, S. P.: Rate effect on interfacial response between fibers and matrix. In: Materials and Structures, RILEM, 28, 83-91, 1995.

[8] Ahmad, A.; di Prisco, M.; Meyer, C.; Plizzari, G.A.; Shah, S. (Eds.): Fiber Reinforced Concrete: From theory to practice, Starrylink Editrice, 1-222, 2004.

[9] Cadoni, E.; Dotta, M.; Meda, A.; Plizzari, G.A.: Analysis of Fiber Reinforced Concrete under impact loading. In: Proc. of 1st workshop on Performance, protection & strengthening of structures under extreme loading, PROTECT 2007, Whistler, Canada. CD-ROM, 2007.

[10] UNI 11039: Concrete reinforced with steel fibres. Part II Test method for the determination of first cracking strength and ductility indexes, Italian Standards, 2003.

[11] CNR-DT 204: Instruction for design, execution and control of fibre reinforced concrete structures, Italian Standards, 2006.

[12] di Prisco, M.; Felicetti, R.; Lamperti, M.; Menotti, G.: On size effect in tension of SFRC thin plates. In: Fracture Mechanics of Concrete Structures, V.C. Li C.K.Y. Leung, K.J. Willam, S.L. Billington, (Eds.), 2, B.L.Schmick and A.D.Pollington, USA, 1075-1082, 2004.

[13] di Prisco, M.; Ferrara, L.; Colombo, M.; Mauri, M.: On the identification of SFRC constitutive law in uniaxial tension. In: Fibre Reinforced Concretes, M. di Prisco, R. Felicetti, G.A. Plizzari (Eds),RILEM Publications S.A.R.L.C, Bagneux, France, 1, 827-836, 2004.

[14] Soroushian, P.; Cha-Don, L.: Distribution and orientation of fibers in steel fiber reinforced concrete In: ACI Materials J., 87 (5), 433-439, 1990.

[15] Comité Euro-International du Béton: Concrete structures under impact and impulsive loading. In: CEB Bulletin 187, Lausanne, Switzerland, 1988.

[16] Malvar, L.J.; Ross, C.A.: Review of strain-rate effects for concrete in tension. In: ACI Materials Journal, 95(6), 735-739, 1998.

Yaghoob Farnam
MSc. Student
Construction Material Institute (CMI),
University of Tehran
Tehran, Iran

Mohammad Shekarchi
Assistant Professor
Construction Material Institute (CMI),
University of Tehran
Tehran, Iran

Alireza Mirdamadi
MSc. Student
Construction Material Institute (CMI),
University of Tehran
Tehran, Iran

Experimental investigation of impact behaviour of high strength fiber reinforced concrete panels

Summary

High strength fiber reinforced concrete (HSFRC) is being used in several structural applications where fibers are used to increase the concrete toughness, ductility, tensile and flexural strength in order to enhance the construction resistance under static and dynamic loading and to reduce crack propagation and spalling phenomena.

In this research, a qualitative impact test was performed and the HSFRC panels were subjected to impact by an 8.5 kg cylindrical steel projectile; 50 mm diameter and 550 mm height, which drop periodically from a one meter height until failure moment. In addition, panels rest on a fine sand bed in order to smooth unwanted noises and oscillations.

These HSFRC panels are prepared by a new method, slurry-infiltrated fiber concrete, known as a SIFCON, for producing high strength FRC with high amount of fibers.

The effect of thickness, different fiber types, fiber content, fiber length and fiber combinations on the impact strength of HSFRC panels have been studied. HSFRCs prepared by SIFCON method and using metakaolin show ultra performance characteristics on impact behaviour.

Keywords: *impact, fiber, penetration, HSFRC, SIFCON*

1 Introduction

The ultra high performance concrete, so called RPCs have been first developed during the early 1990's by researchers at the laboratories of Bouygues in Paris. RPCs represent a new generation of concretes with cube strengths between 200 and 800 MPa, tensile strengths between 25 and 150 MPa, and specific gravity of 2500 – 3000 kg/m3. The fracture energy of these materials can reach to 40000 J/m2, as compared to 100-150 J/m2 for ordinary concretes [1-4]. The fracture energies of RPCs, thus, are about 300 times that of normal strength concrete or even 1350 times for Slurry Infiltrated Fiber Reinforced Concrete (SIFCON) [5].

Since fibre reinforced ultra-high strength concretes (FRUHPCs) have excellent impact resistance properties, they can be employed for; i) strategic structures against earthquake damage, ii) retrofitting of reinforced concrete structures and, iii) structures exposed to sudden loading, Figure 1. They are also used for small or medium size prefabricated elements, like components of bridges, built by means of FRUHPC as pilot projects, like the well-known precast, prestressed pedestrian bridge in Sherbrooke (Canada), erected in 1997 and the Seonyu Pedestrian Bridge in Korea [7-10].

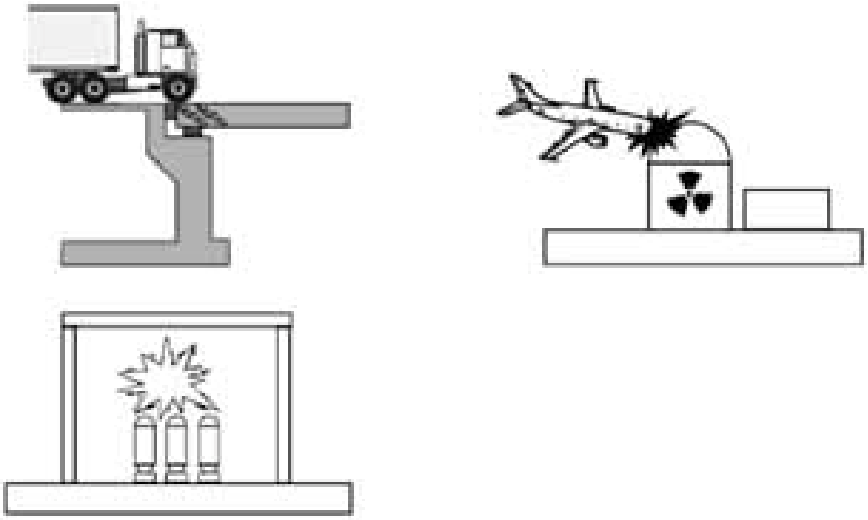

Figure 1: Impact loads on various structures [10]

Current understanding of the impact resistance of concrete, and especially of high-strength concrete, is very limited. There is some research on impact behaviour of UHPCs by Bindiganavile et al. [11], Luo et al. [12], Parant et al. [13], and Marar et al. [14]. At the heart of the problem is the absence of a standardized test technique for testing concrete under impact. Various investigators have used different impact machines, specimen configurations, specimen sizes, and instrumentation, and they have also adopted differing analysis schemes. Much still remains to be done both, towards the development of a standardized technique and towards generating fundamental understanding of concrete performance under impact loading. Some research on RPC, UHPC, FRUHPC and SIFCON has been performed at the Construction Material Institute (CMI), University of Tehran, since 2001. These investigations suggest to this study the use of the SIFCON method and of Metakaolin pozzolan to produce high strength fiber reinforced concrete samples [15-16]. For the impact test, a method which is similar to the recommendations of ACI 544-2R was used [17].

2 Experimental program

2.1 Materials and mixture proportions

The cementitious materials used in this study were Portland cement (PC) equivalent to ASTM Type II and metakaolin as pozzolan material. The chemical and physical properties of materials are given in Table 1. The aggregates used were crushed limestone with 1mm maximum size. These fine aggregates had specific gravity and absorption values of 2.50-

3.2%, respectively. Polycarboxylate superplasticizer was used for the mixes in order to improve the workability of fresh mortar. One matrix mix, used for all samples, which was achieved by trying several mixtures to obtain a compressive strength of more than 110 MPa, is shown in Table 2. This matrix was reinforced by three types of fibers (Table 3) a) steel b) alloy and c) polypropylene. Impact tests were carried out on 8 series of different sample types shown in Table 4.

Table 1: Chemical and physical properties of portland cement and metakolin

Table		**Cement**	**Metakaolin**
Physical tests			
Specific surface, Blaine, [m^2/kg]		290	—
Initial setting time, [min]		145	—
Final setting time, [min]		210	—
Compressive strength of 50 mm cubes, [MPa]	3-day	18	—
	7-day	29	—
	28-day	40	—
Autoclave expansion, [%]		0.2	—
Chemical analyses, [%]			
SiO2		20.03	51.85
Al2O3		4.53	43.87
Fe2O3		3.63	0.99
CaO		60.25	0.2
MgO		3.42	0.18
Na2O		—	0.01
K2O		—	0.12
SO3		2.23	—
LOI (Loss of Ignition)		1.37	0.57

Table 2: Matrix mix proportion

Items	**Type**	**kg/m3**
Cement	Type II	1020
Pozzolan	Metakaolin	180
Aggregate	Sand (0-1 mm)	850
Water	-	385
W/B	-	0.32
Superplasticizer	Polycarboxylate	18 (1.5% of cementitious material)

Table 3: General characteristics of fibers

Fiber type	Steel	Alloy	Polypropylen
Cross-Section shape	Circle	Square	Circle
Length (mm)	30, 50	30	12
Diameter (mm)	0.25	0.03*1.6	0.02
l/d (aspect ratio)	100, 200	100	600
Tensile strength (MPa)	2200	1700	350

Table 4: Specimen's types

Code		A	B	C	E	F	H	P	T
Kind of fiber		S*	S	S	S	A**	S+P***	P	-
Fraction of fiber	%	2	2	4	2	0.4	2+0.4	0.4	-
Length of fiber	mm	30	30	30	50	30	30+36	36	-
Panel thickness	mm	23	40	23	23	23	23	23	23

* Steel
** Alloy
*** Polypropylene

2.2 Specimen preparation, casting and curing

In mixing, cement, metakaolin and aggregates were blended first in dry condition then water with superplasticizer was gradually added to the mixture to provide a homogenous mortar according to ASTM C309 . Prepared mortar was poured in steel moulds of dimension 300×300mm with different thicknesses (23 and 40 mm) in three layers.

For steel fiber panels after the first layer was poured, the fibers were dispersed randomly in a horizontal direction. The mould was vibrated softly to insure that the matrix would completely surround the fibers. Same three steps were repeated until the panel was completely cast. This way for preparing fiber reinforced concrete is a new method, in order to use for concretes with high volume fraction of randomly oriented fibers; which is called SIFCON [6]. For other types of specimen containing polypropylene and alloy fibers, after preparing the mortar was finished, fibers were gradually added to mixture and mixed for 1:30 min. The specimens were allowed to set for 1 day, then mould were removed. The specimens were cured in water saturated with calcium hydroxide at 22 °C for 28 days.

2.3 Test method

For the impact tests, an instrumented drop-weight impact-testing machine was used (Figure 2). An 8.5 kg cylindrical steel projectile; 50 mm diameter and 550 mm height; drops freely from a one meter height, periodically until the failure moment. The projectile strikes the midpoint of the panel with a velocity of 4.23 m/s and after every five hits, the deflection of lowest point was recorded and some photos were taken by a fixed accurate photography setup from front and backside of the panel in order to document the crack propagation on the surface of the specimens. In addition, panels are laid on a fine sand bed, in order to smooth unwanted noise and oscillations.

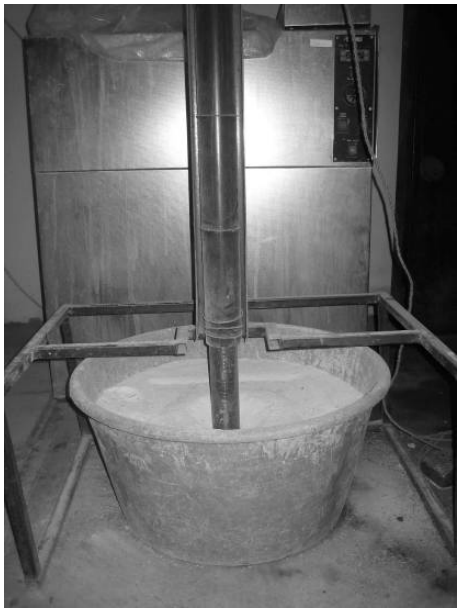

Figure 2: Drop-weight impact test device

3 Results and discussion

3.1 Failure pattern

Failure pattern, crack development and crack width in both, front- and backside as well as lateral surfaces were evaluated for all specimens by various photographs which are taken during the experiments. This evaluation presents that:

- For A, C and E samples punching failure is the governing pattern at the position of first flexural cracks which were generated during the first impacts.
- For B panels, because of greater thickness, flexural failure occurred, and also in front surface, crippling was observed.
- For F, P and T cases tensile failure was governing because of lack of tensile strength, and panels were divided into four blocks.

Figure 3 a, b, c and d show failure patterns which occurred during experiments.

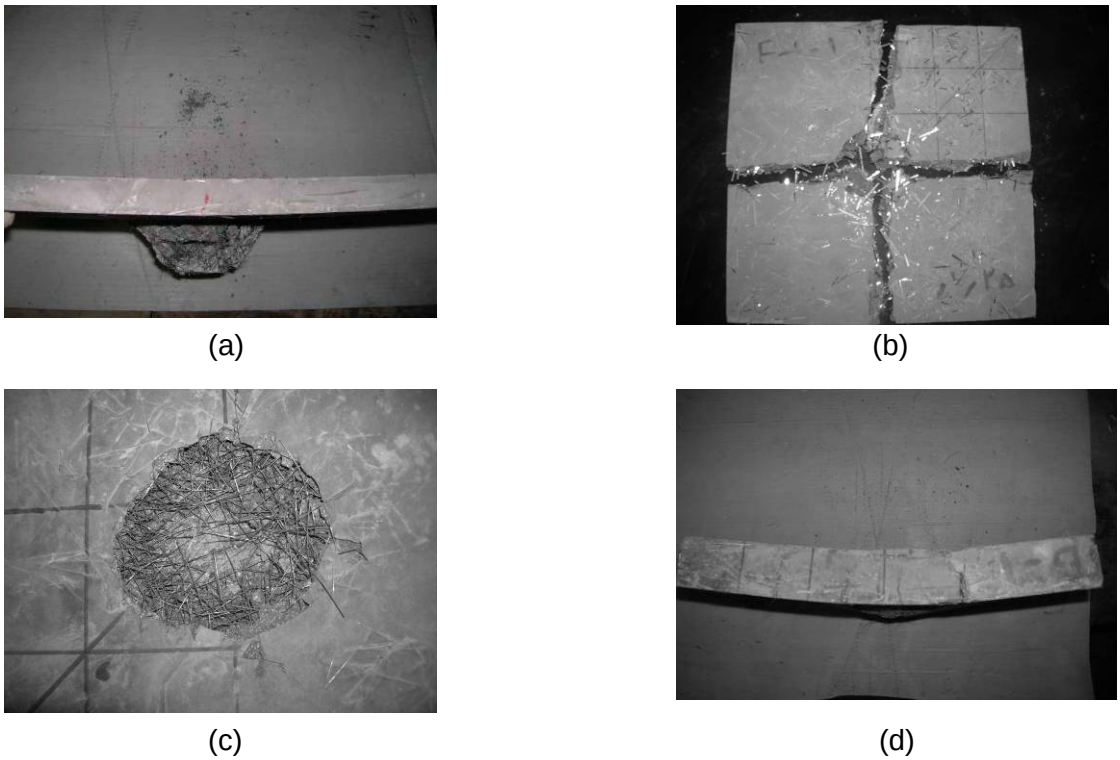

(a) (b)

(c) (d)

Figure 3: Failure patterns a) punching failure in A, C and E specimens b) tensile failure for F specimens c) crippling in B specimens d) flexural failure for B specimens

3.2 Number of applied impact loads

All of impact loads were applied until the ultimate failure. Table 5 presents the number of strikes for all types of specimens. The result shows, that the panel thickness, fiber length and fiber proportion, respectively are important effective influences on the impact resistance, and also the panels containing steel fiber have best resistance of all tested types.

Table 5: Number of strikes on panels

Code	A		B		C		E		F		H		P		T	
	A-1	A-2	B-1	B-2	C-1	C-2	E-1	E-2	F-1	F-2	H-1	H-2	P-1	P-2	T-1	T-2
First effect	5	5	10	15	10	10	10	15	1	1	10	10	1	1	1	1
Failure	15	15	60	65	25	30	30	35	2	2	30	25	1	1	1	1

3.3 Generated deflection

After performing every five hits, the average of vertical distance between the center point of the panel and the four midpoints of the edges on the front- and backside was measured and shown as deflection in table 6. This table indicates that the panels which are thicker and have longer length fibers show less deflection than other types with the same number of hits.

Table 6: Maximum deflection on the midpoint of the panel

Table		Maximum deflection at midpoint of the panel after every five strikes [mm]											
		5	**10**	**15**	**20**	**25**	**30**	**35**	**40**	**45**	**50**	**55**	**60**
A	**A-1**	7.5	15.5	33.0	-								
	A-2	7.0	16.0	39.0	-								
B	**B-1**	3.5	4.0	5.0	7.0	8.0	9.0	12.0	18.5	19.0	21.0	27.0	29.0
	B-2	2.5	4.0	6.5	7.5	9.5	11.5	14.0	21.0	23.0	24.0	32.0	34.0
C	**C-1**	3.5	6.5	14.0	30.0	37.0	-						
	C-2	3.5	5.5	10.0	29.0	35.0	39.0	-					
E	**E-1**	1.5	3.0	4.5	8.5	18.0	37.0	-					
	E-2	1.5	3.5	6.0	10.5	18.0	38.0	55.0	-				
F	**F-1**	16.0	-										
	F-2	14.0	-										
H	**H-1**	4.5	7.0	10.0	15.0	28.0	39.0	-					
	H-2	5.0	8.5	14.0	17.0	34.0	-						
P	**P-1**	-											
	P-2	-											

4 Conclusion

From the results of this study, the following conclusion can be drawn:

1. HSFRC, prepared by SIFCON method, and using metakaolin shows ultra performance characteristics such as non-brittle damage, high resistance under impact loading, and flexible behaviour.
2. Alloy and polypropylene fibers have little effect on impact resistance compared with steel fiber.
3. By increasing specimen thickness punching failure pattern converted to flexible failure pattern, so it caused they bear more hits.
4. Respectively, thickness, fiber length and fiber proportion are effective parameters in impact resistance performance.

5 References

[1] Richard, P.; Cheyrezy, M.: Reactive Powder Concrete, Bouygues Corporation, France, 1994.

[2] Richard, P.; Cheyrezy, M.: Composition of reactive powder concrete. In: Cement and Concrete Research 25, No. 7, pp.1501-1511, 1995.

[3] Dugat, J.; Roux, N.; Bernier, G.: Mechanical properties of Reactive Powder Concretes. In: Materials and Structures 29, pp.233-240, 1996.

[4] Walraven, J.: Evolution of Concrete. In: Structural Concrete: Journal of fib, Vol. P1, No.1, pp.3-11, 1999.

[5] Fritz, C.: Tensile testing of SIFCON. In: Proc. 1st International Workshop on HPFRCCs, June 23-26, Mainz, RILEM, Eds. H.W. Reinhardt and A.E. Naaman, pp. 518-528, 1991.

[6] Naaman, A.E.; Otter, D. ; Najm, H.: Elastic modulus of SIFCON in tension and Compression. In: ACI Materials Journal 88, No. 6, pp.603-612, 1992.

[7] Tang, M.C.: High performance concrete – past, present and future. In: Proc. 1st International Symposium on Ultra High Performance Concrete (UHPC), Kassel, Germany 2004, pp.3-9.
[8] Guvensoy, G.; Bayramov, F.; Ilki, A.; Sengul, C.; Tasdemir, M.A; Kocaturk, A.N.; Yerlikaya, M.: Mechanical behavior of high performance steel fiber reinforced cementitious composites under cyclic loading condition. In: Proc. 1st International Symposium on Ultra High Performance Concrete (UHPC), Kassel, Germany 2004, pp. 649-660.
[9] Orgass, M.; Klug, Y.: Fiber reinforced ultra-high strength concrete. In: Proc. 1st International Symposium on Ultra High Performance Concrete (UHPC), Kassel, Germany 2004, pp. 637-647.
[10] Ortlepp, S.; Curbach, M.: Research into high-strength concrete at high rates of loadings. In: Proc. 1st International Symposium on Ultra High Performance Concrete (UHPC), Kassel, Germany 2004, pp. 461-469.
[11] Bindiganavile, V.; Banthia, N.; Aarup, B.: Impact response of ultra-high-strength fiber-reinforced cement composite. In: ACI Materials Journal 99, No. 6, pp.543-548, 2002.
[12] Luo, X.; Sun, W.; Chan, S.Y.N.: Characteristics of high-performance steel fiber-reinforced concrete subject to high velocity impact. In: Cement and Concrete Research, Vol. 30, pp.907-914, 2000.
[13] Parant, E.; Rossi, P.; Jacquelin, E.; Boulay, C.: Strain rate effect on bending behavior of new ultra-high-performance cement-based composite. In: ACI Materials Journal 104, No. 5, pp.458-463, 2007.
[14] Marar, K.; Eren, O.; Celik, T.: Relationship between impact energy and compression toughness energy of high-strength fiber-reinforced concrete. In: Materials Letters, Vol. 47, pp.297-304, 2001.
[15] Talebinejad, I.; Bassam, S.A.; Iranmanesh, A.; Shekarchi, M.: Optimizing mix proportions of normal weight reactive powder concrete with strengths of 200-350 MPa. In: Proc. 1st International Symposium on Ultra High Performance Concrete (UHPC), Kassel, Germany 2004, pp. 133-141.
[16] Taghaddos, H.; Mahmoudzadeh, F.; Pourmoghaddam, A.; Shekarchi, M: Prediction of compressive strength behaviour in RPC with applying an adaptive network-based fuzzy interface system. In: Proc. 1st International Symposium on Ultra High Performance Concrete (UHPC), Kassel, Germany 2004, pp. 273-284.
[17] Bonakdar, A.: Impact behaviour of high strength fiber reinforced concrete panels. In: Thesis of MSc. Degree, Construction Material Institute (CMI), University of Tehran, Iran 2006.

Markus Nöldgen
Dipl.-Ing.
Schüssler-Plan Eng. ltd.
Düsseldorf, Germany

Werner Riedel
Dr.-Ing.
Fraunhofer Institute for high-speed dynamics
Ernst-Mach-Institut (EMI)
Freiburg, Germany

Ekkehard Fehling
Professor Dr.-Ing.
University of Kassel
Kassel, Germany

Klaus Thoma
Professor Dr. rer.nat.
Fraunhofer Institute for high-speed dynamics
Ernst-Mach-Institut (EMI)
Freiburg, Germany

Impact on structural Ultra High Performance Concrete (UHPC) elements in high-rise buildings

Summary

The submitted paper identifies the predominant load situations for impact on UHPC structural members in high rise building structures by means of a simulative approach. A numerical simulation of a representative impact by explicit time integration in wave propagation codes, so called hydrocodes, leads to the determination of transient stresses, strain rates and failure modes. Material parameters are derived to describe UHPC by triaxial continuum models for fibre reinforced high strength materials. The configuration of scaled impact tests is proposed.

Keywords: *aircraft impact, UHPC under dynamic loading conditions, impact safety of structural members, high strain rates, hydrocodes, RHT-Concrete-Model, fracture energy*

1 Predominant load situations in case of aircraft impact on high-rise buildings

An impact of a civil aircraft on a comparatively heavy, stiff and inert building structure can be separated into a short-time local impact and a global structural response, as the period of oscillation of a high rise building (T≅6s-12s) is more than one order of magnitude longer than the impact duration (t_{impact}<0.5s).

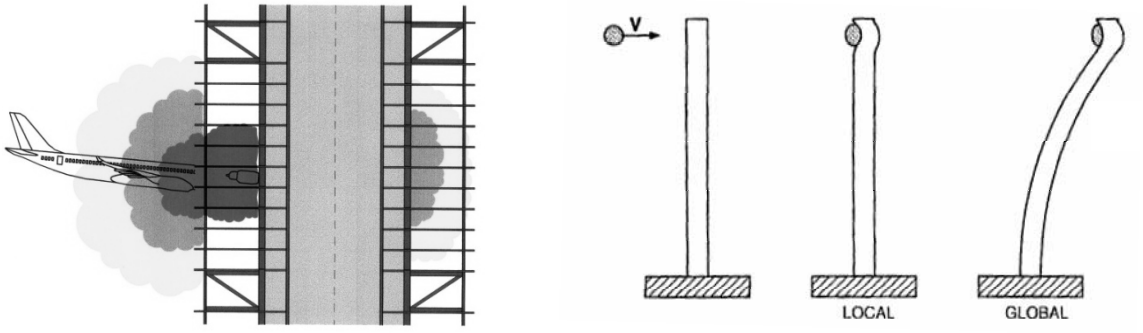

Figure 1: Separation of local and global structural response [12]

A force-time history for the aircraft is assumed from numerical simulations of civilian aircraft on rigid targets [1]. The resulting momentum input of the aircraft at maximum speed does not cause significantly higher stresses than wind loads and the global structure can be designed to resist the impact load history (example see figure 2 right). Furthermore preliminary standards [6] claim to include the influence of local damages on the overall building stiffness as well as alternate load paths for failed structural elements in the building design.

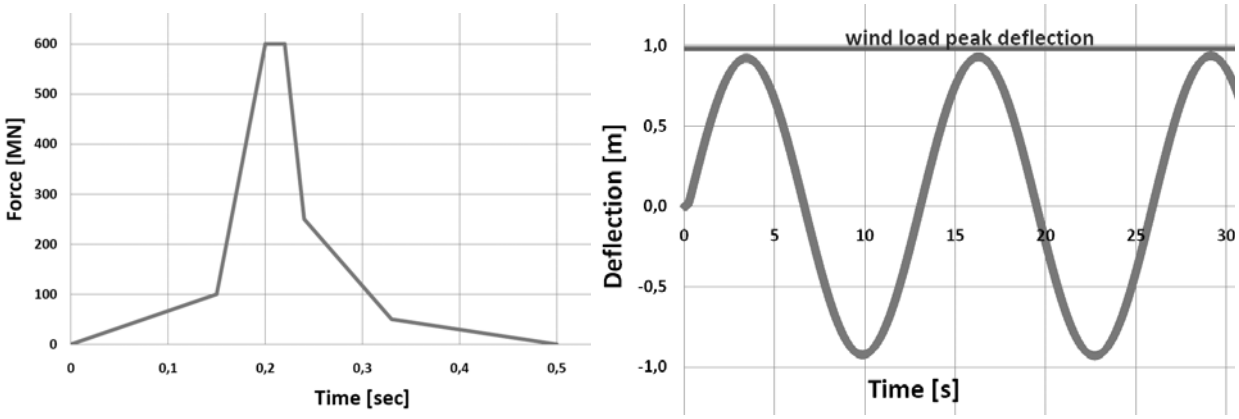

Figure 2: Force-time history (Boeing 747) [1], Impact and wind load peak deflection in a simplified example [3]: h=500m, b/h~1/8, w~2.5KN/m², I~28,000m^4, m~3.75 KN/m³

The vertical escape and rescue routes are the most sensitive part in a high-rise building in case of an emergency so that the protection of this area from penetration of rigid components, smoke and fire becomes a major demand in impact safety design (see figure 2 right). The following numerical simulation investigates a security wall of fiber reinforced UHPC as a structural element and an impact resistant outer shell of the vertical escape and rescue routes. Prior to the numerical simulation of the local impact on the UHPC wall a sophisticated model of the engine is developed with respect to the appropriate dynamic properties (impedance, material strength and stiffness). Figure 3 illustrates the projectile model as well as the target model represented by a one storey UHPC wall which was preliminary designed under static loads.

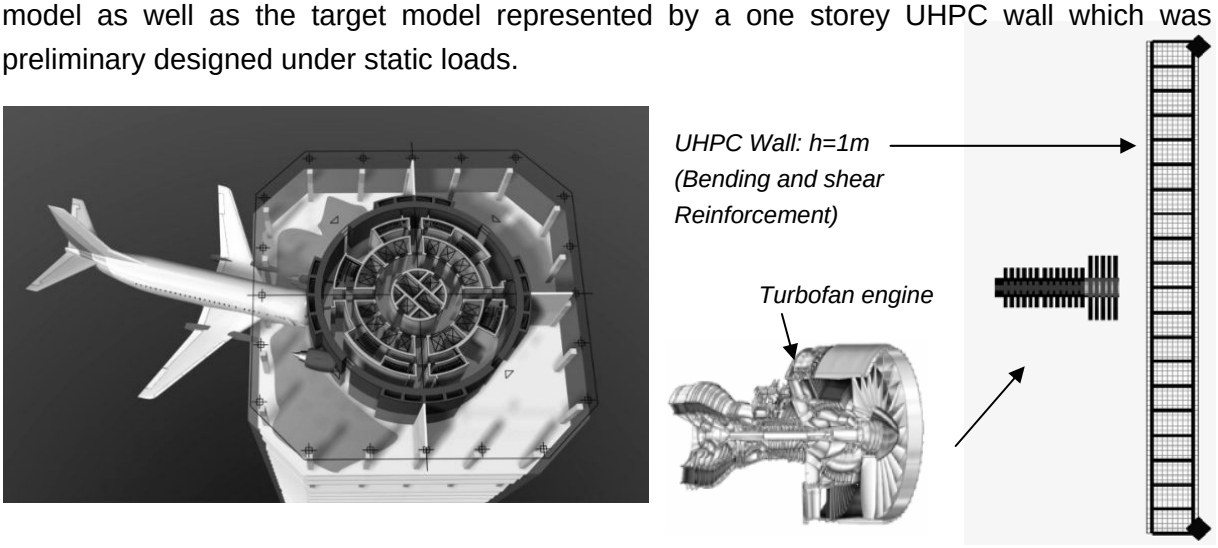

Figure 3: Local impact of an aircraft engine on a reinforced UHPC wall (left), Numerical impact simulation, engine model and reinforced UHPC wall (right)

2 Preliminary material parameters

The material behavior of UHPC in the numerical simulation of the aircraft engine impact is described by a modified data set for the RHT-Concrete-Model [9] and implemented in the hydrocode AUTODYN. The modifications described in this chapter were derived in a preliminary study of experiments with comparable high-strength materials under dynamic conditions and experiments with UHPC under static conditions. The UHPC implemented in the numerical simulation refers to a B3Q mixture [2]. The statical properties of this material are shown in table 2.

Table 1: Material Properties of B3Q (derived from experimental conditions under static loads)

Material parameter	**Unit**	**RHT 35 MPa**	**B3Q**
Compressive strength	MPa	35	158
Tensile Strength	MPa	3,5	7-15
Steel Fibers (9/0,15mm)	Vol-%	-	2,5
Fracture Energy	N/m	120	12900-19800
Pore Volume (total)	[%]	15	6
Density	[g/cm³]	2,3	2,5

2.1 Equation of State and Compressive Failure Strength

Under high velocity impact conditions hydrostatic stresses often reach values several times higher than the uniaxial compressive strength. Net density and porosity determine the material behavior as soon as the materials´ compressive strength is exceeded. This behavior beyond elastic conditions is nonlinear as shown in figure 4. An **E**quation **o**f **S**tate (EOS) is derived for UHPC from experimental data [8], [3]. Determined by a higher porous density ρ_0 and a compact matrix the UHPC-porous-compaction curve has a higher compaction stiffness compared to a conventional 35 MPa concrete (see figure 4 left).

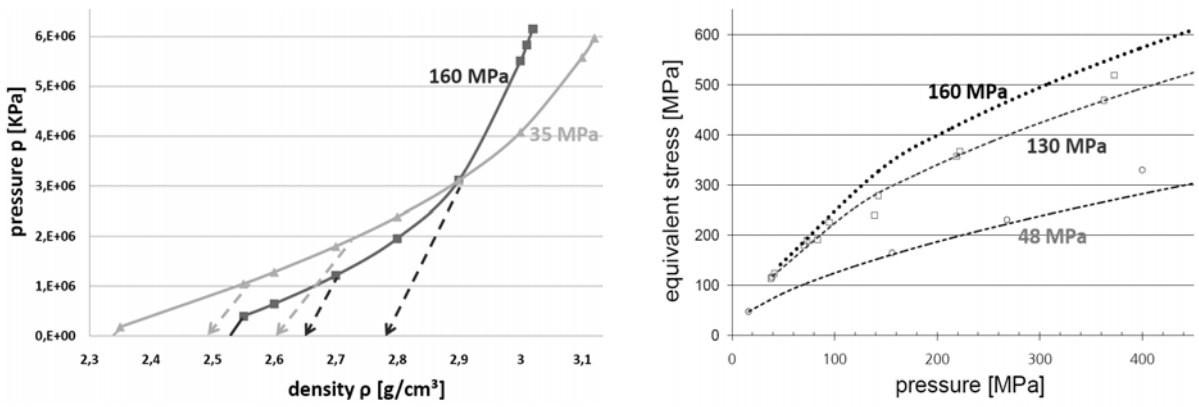

Figure 4: UHPC-EOS (left) and normalized failure strength (right) derivated from experimental data [8], [10]

The deviatoric strength of UHPC is derived analogously from the experimental data and implemented in a modified Y_{TXC} failure description in the RHT-model (see figure 4 right). Y_{TXC} determines subsequent parameters (shear and tensile strength) in the continuum model while additional parameters (third invariant R_3, the strain rate effects F_{Rate} and the damage description D) have been retained unchanged.

$$f\left(p,\sigma_{eq},\theta,\dot{\varepsilon}\right)=\sigma_{eq}-Y_{fail}\left(p,\theta,\dot{\varepsilon}\right)=\sigma_{eq}-Y_{TXC}(p)\,R_3(\theta)\,F_{Rate}\left(\dot{\varepsilon}\right)=0 \tag{1}$$

$$Y_{fail}\left(p,\theta,\dot{\varepsilon}\right)=Y_{TXC}(p)\,R_3(\theta)\,F_{Rate}\left(\dot{\varepsilon}\right) \tag{2}$$

$$Y_{el}(p,\theta,\dot{\varepsilon})=Y_{Fail}(p,\theta,\dot{\varepsilon})\cdot Y_{OF}\cdot F_{CAP} \tag{3}$$

$$Y=Y_{Fail}-D\cdot\left(Y_{Fail}-Y_{Fric}\right) \tag{4}$$

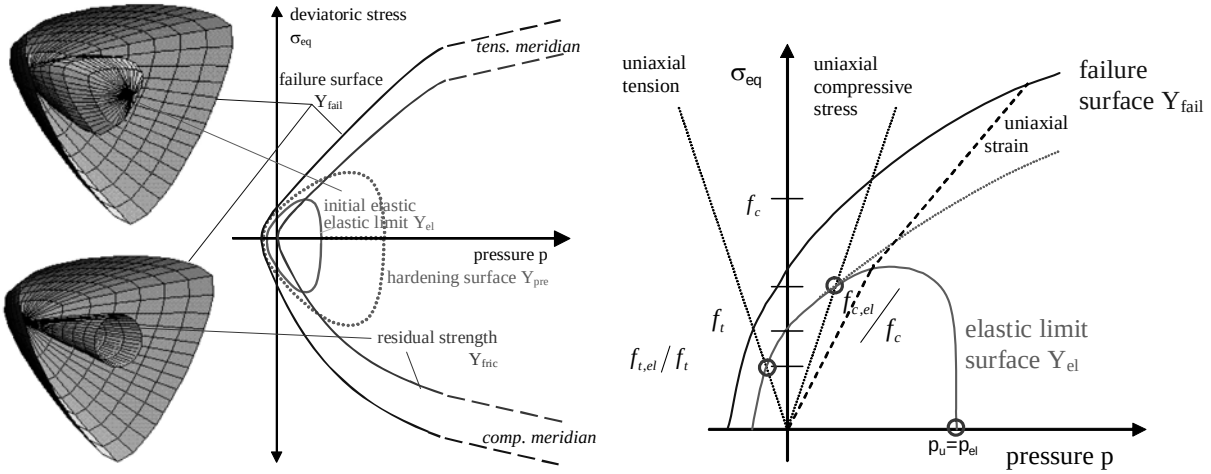

Figure 5: Three surface concept for the concrete strength with hardening, failure and residual friction resistance [9]

2.2 Strain rate effect on tensile strength and fracture energy, Dynamic increase factor (DIF)

With increasing strain rates the tensile strength of concrete increases exponentially because of velocity effects on stress, failure mechanism and crack opening [2] (see figure 6 left [11], [7]). The CEB-FIP Model Code 90 in a modified formulation by Malvar et al [7] offers an appropriate fit for the experimental data including the effect of increasing compressive strength on the DIF. Increasing compressive strength leads to a lower DIF increase as shown in figure 6. As the DIF reaches values of 2 up to 8 the importance of the strain rate effect becomes very obvious especially as tensile stresses are the major failure mode in engine impact simulation. The contribution of steel fibers to the DIF for tensile strength has been experimentally studied for strain rates up to 10^1 [4]. Optimized fiber l/d-ratio and fiber-content lead to a further exponential increase. To describe this contribution in a model code formulation more experimental data for higher strain rates and high strength material in combination with fibers is needed.

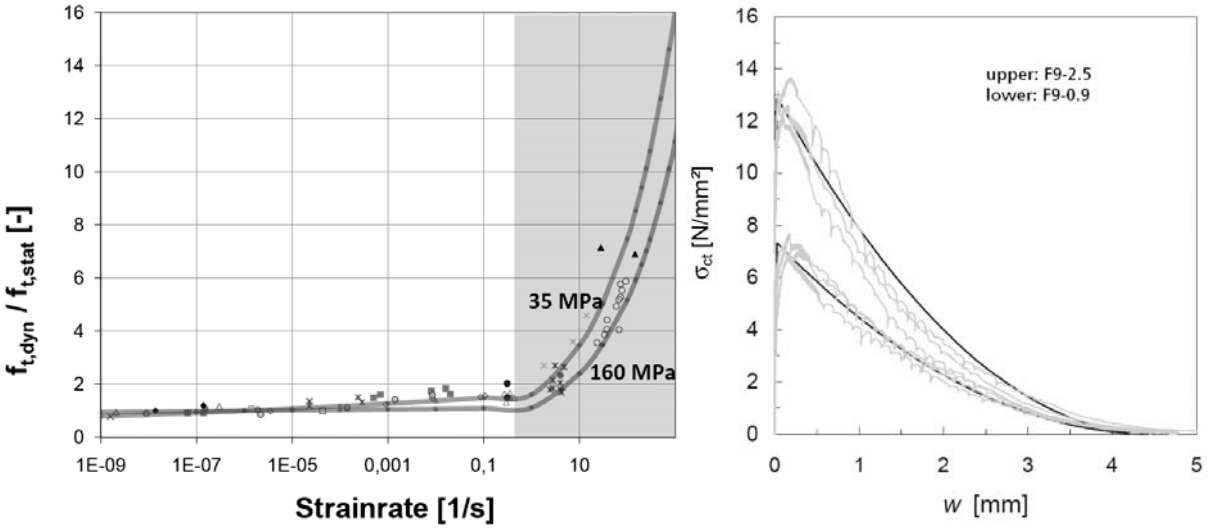

Figure 6: Influence of strain rate effects on tensile strength of UHPC [11], [7] Stress-Crack-opening relation in tensile tests on fiber reinforced UHPC [5]

When the tensile failure limit of UHPC is exceeded macroscopic cracks open while the stress decreases rapidly in the brittle material. The addition of fibers leads to further crack softening until the fibers are finally pulled out or fail in strength. Experimental Data under static loading conditions of UHPC have been presented by the University of Kassel recently. A tensile-stress-crack-opening relation is used to compare with the experimental results (figure 6, right). The fracture energy of fiber reinforced UHPC is more than a hundred times higher in comparison to non fibered concrete. In addition strain rate effects have lead to a DIF ranging from value 1.5 to 3 in conventional strength concrete [11]. Energy dissipation capacity and tensile strength of UHPC will be determined in Split Hopkinson Bar experiments and implemented in the strength and damage description of the material code.

3 Numerical Simulation

The impact has been numerically analyzed using the hydrocode AUTODYN with the preliminary triaxial material description of UHPC. The following parameters were focused

- Prediction of the ballistic limit v_{50}
- Analysis of the predominant failure modes and failure history
- Contribution and behavior of bending and shear reinforcement
- Relevant hydrostatic and deviatoric stresses and relevant strain rates
- Definition of an experimental configuration for validation purpose

Figure 7 (left) illustrates the failure mode of the wall near the ballistic limit of v_{50}=375 m/s: The membrane effect of the rear side reinforcement prevents the projectile penetration after failure of front reinforcement and UHPC. The ballistic limit is approximated by a semi-probabilistic function of Lambert/Jonas to describe the state of just non-penetration.

Exceeding the ballistic limit, a discrete increase of energy transfer occurs and leads to the steep inclination of the function.

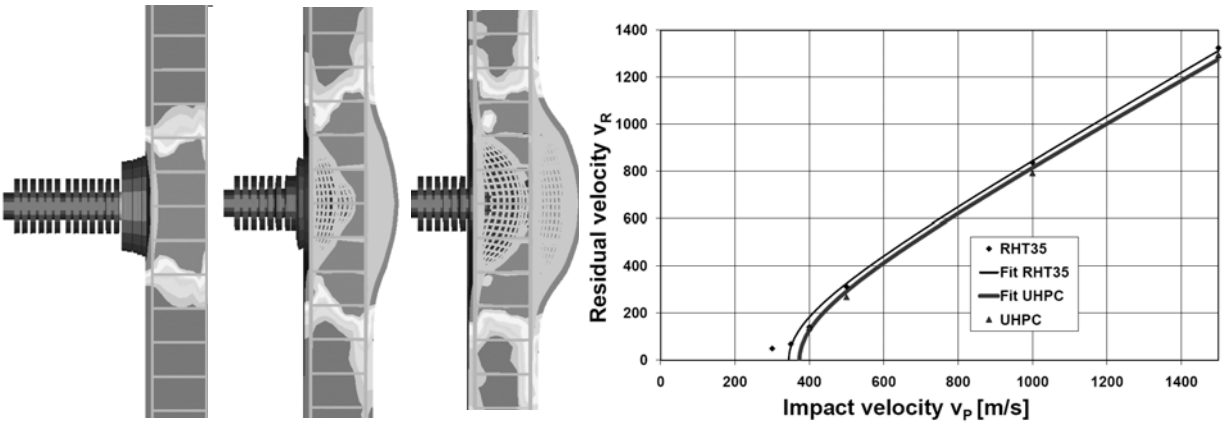

Figure 7: Comparison of failure modes (left) and Ballistic Limit in numerical simulation with 160 MPa and 35 MPa Concrete (right)

The result is compared to a 35 MPa concrete without fibers simulated in the same configuration. The result is shown in figure 7 right with the ballistic limit predicted at around 10 percent lower velocities.

Considering the failure history, the initial failure of UHPC occurs in a punching cone closely located around the impact zone and rear side tension (see figure 8 left). In the following phase shear reinforcement is activated until further deflection activates the membrane effect of bending reinforcement. Increasing reinforcement ratio leads to the same failure modes while failure stages are shifted. The results in figure 8 show a bending reinforcement ratio of 0.63% and a shear reinforcement ratio of 0.12%.

To identify the predominant influences in failure modes, stresses and strain rates have to be considered in detail. The RHT-model in AUTODYN provides an analysis of the triaxial stress state and its time-dependent development. Figure 8 shows two diagrams depicting stress-time and strain rate-time relations in comparison to the damage-time relation.

On the left side of figure 8 the diagram depicts the relations on the impact axis (rear side of the target). Strain rates up to 140 [1/s] and biaxial tensile stresses of more than (20 MPa) are noted while damage occurs. Hydrostatic compression does not exceed the order of magnitude of the uniaxial strength with value ranging from 50-90 MPa. However deviatoric stresses reach values up to 160 MPa on the compressive meridian.

The diagram on the right shows the same relations at about 1m distance of the impact axis. Strain rates reach values up to 150 [1/s] while damage occurs. Hydrostatic compression of less than 30 MPa can be neglected whereas deviatoric stresses lead to damage as they exceed the failure strength of UHPC reaching values up to 60 MPa on the shear meridian.

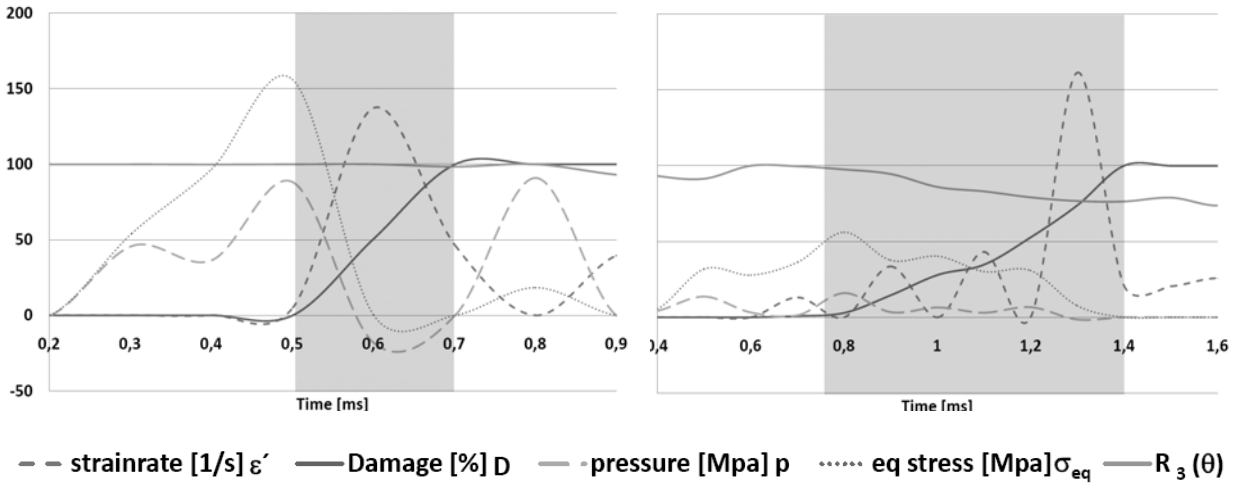

Figure 8: Damage evolution (grey array) on rear side of the concrete target and the related graphs for stresses, pressures and strain rates (y-axis, see legend below figure). Left figure: impact axis array; right figure: punching cone array

The two representative diagrams show the major damage processes and lead to the following results:

- Damage occurs in tension near the impact axis on the target´s rear side. Damaged concrete is thrown away on the rear side (scabbing)
- Hydrostatic compression does not exceed the material compressive strength by order of magnitude – the nonlinear porous compaction is hardly reached
- Deviatoric shear stresses cause damage in the outer punching area
- Relevant strain rates reach values up to 150 [1/s] during damage accumulation

The major failure modes of the reinforced UHPC wall under impact conditions have been determined in the numerical simulation using a wave propagation code with explicit time integration. To validate the assumptions and results scaled experiments have to be conducted. A proposed configuration is illustrated in figure 9.

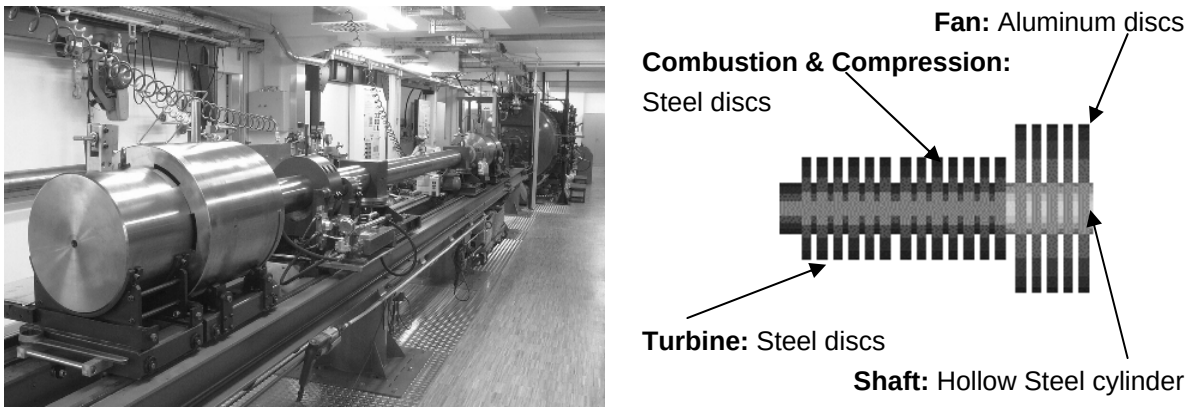

Figure 9: Medium two stage acceleration facility at the EMI (left) and scaled model of projectile and target by factor 1:10

4 Discussion

The analysis of an aircraft impact on high-rise buildings leads to the definition of the engine impact as the most endangering load situation for safe escape and rescue routes. Fiber reinforced UHPC shells which can both provide structural integrity and impact resistance have been investigated in numerical simulations. The results predict a significantly improved performance in comparison to conventional concrete. In a preliminary material parameter study an equation of state and a triaxial deviatoric failure expression for UHPC were derived from experimental data of comparable high strength material under dynamic conditions and UHPC experimental data under static conditions. The resulting parameters were implemented in the RHT-Concrete Model. The numerical simulation of an UHPC wall under aircraft engine impact conditions revealed the detailed failure procedure and the relevant stresses and strain rates. As damage occurs predominantly under shear and tensile stresses with relevant strain rates up to 150 [1/s] further research has to be made in the appropriate description of fiber reinforced UHPC under high strain rates concerning tension and fracture energy. Experimental data from Hopkinson Bar spallation tests is needed to define these important material parameters for an implementation in triaxial hydrocode formulation. Furthermore the numerical simulations have to be validated in scaled experimental impacts. A test configuration is presented including a sophisticated engine model and a UHPC target model which will be used in 1:10 impact tests at the Ernst-Mach-Institute in Efringen-Kirchen.

5 References

[1] Arros, J.; Doumbalski, N: Analysis of Aircraft impact to concrete structures, Nuclear Engineering and Design 237, 2007, pp 1241-1249

[2] Curbach, M.: Festigkeitssteigerungen von Beton unter hohen Belastungsgeschwindigkeiten, Dissertation Universität Karlsruhe, 1987

[3] Fehling, E.; Schmidt, M.: Entwicklung, Dauerhaftigkeit und Berechnung Ultra hochfester Betone DFG-Forschungsbericht DFG FE 497/1-1, Schriftenreihe Heft 1, Universität Kassel, 2005

[4] Gopalaratnam, V.S., Shah, S.P.: Properties of steel fiber reinforced concrete subjected to impact loading, ACI Journal, Title no. 83-14, Jan-Feb 1986

[5] Leutbecher, T: Rissbildung und Zugtragverhalten von mit Stabstahl und Fasern bewehrtem Ultrahochfesten Beton (UHPC), Dissertation Universität Kassel, Mai 2007

[6] National Institute of standards and technology: Final Report on the collapse of the World Trade Center Towers, US Department of commerce, Sept 2005

[7] Malvar, L.J.; Ross, C.A.: Review of strain rate effects for concrete in tension, ACI Materials Journal, Title No. 95-M73, Nov-Dec 1998

[8] Riedel, W.; Wicklein, M.; Thoma, K.: Shock properties of conventional and high strength concrete: Experimental and mesomechanical analysis, Int. Journal of the impact engineering, 2007

[9] Riedel, W: Beton unter dynamischen Lasten: Meso- und makromechanische Modelle und ihre Parameter, Fraunhofer IRB Verlag 2004, ISBN 3-8167-6340-5,

[10] Riedel, W, Kawai, N.: Numerical Simulation of Mortar Strength Measurements at highest strain rates, ISIEMS Conference, Orlando, Sept. 2007

[11] Schuler, H.: Experimentelle und numerische Untersuchungen zur Schädigung von stoßbeanspruchtem Beton, Fraunhofer Institut für Kurzzeitdynamik Schriftenreihe ε - Heft 6, 2004

[12] Zukas, J. A.: Introduction to hydrocodes, Studies in applied mechanics, 49, Elsevier, 2004

Part 12:

Applications – Bridges

François Toutlemonde
Ph.D., Head of FDOA division
Université Paris-Est, LCPC
Paris, France

Jean-Claude Renaud
Senior technician, FDOA, Structures Laboratory
Université Paris-Est, LCPC
Paris, France

Ludovic Lauvin
Senior technician, FDOA, Structures Laboratory
Université Paris-Est, LCPC
Paris, France

Alain Simon
Civil Engineer
Eiffage TP
Neuilly sur Marne, France

Mouloud Behloul
Ph.D., Head of ®Ductal development
Lafarge
Paris, France

Sébastien Bouteille
Senior technician, Bridges Division
CETE de Lyon
L'Isle d'Abeau, France

Jacques Resplendino
Chief Engineer
DIRMED
Marseille, France

Experimental validation of a ribbed UHPFRC bridge deck

Summary

Within the French R & D project MIKTI focusing on innovative steel-concrete composite bridges, an exhaustive experimental program was carried out at LCPC Structures Laboratory to provide an experimental validation of a new ultra-high performance fibre reinforced concrete (UHPFRC) ribbed slab made of segments assembled by post-tensioning. The experimental program included critical issues for which the design based on classical beam analysis requires validation. Details of the experimental program are presented in this paper, in connection with the design situations. Critical load levels corresponding to the limit of linearity, cracking development and the onset of failure mechanisms are indicated and compared to the design using AFGC-SETRA provisions. Recommendations are drawn regarding the possible application of this bridge slab concept.

Keywords: *UHPFRC, ribbed slab, bridge deck, SLS, ULS, design, punching shear, bending tests, push-out, safety barrier, Eurocodes.*

1 Context of the innovative UHPFRC deck design and validation

Extending the economic span range of composite bridge decks, classically applied for road bridges from 50 to 100 m-spans, represents an important challenge. For longer spans, the concrete slab is too heavy, and thinner slabs made of pre-cast high performance concrete (HPC) segments tend to be developed. This could provide an alternative to steel orthotropic

decks, for which fatigue degradations are a major concern. Pursuing this trend of lightness, durability, and savings of natural resources with the use of materials with optimized performance, a preliminary design of a UHPFRC ribbed slab, connected to twin longitudinal steel beams, has been studied within the frame of MIKTI French R & D national project aimed at favoring innovative steel-concrete composite applications [1]. The context of application consists in a 3-span 90 + 130 + 90 m-long, 9 m-wide road bridge (two 3.5 m-wide lanes + 1 m-side strips) with two 1 m-wide sidewalks. The overall design, determination of required pre-stressing tendons and detailing, was carried out applying French Recommendations relative to UHPFRC [2] in addition to French Bridge design codes for composite and pre-stressed concrete bridges.

Definition of the slab thickness and of the transverse ribs and pre-tensioning was first determined considering the local and transverse bending. Then longitudinal bending was considered, as well as specific design and connection aspects. The length of successive segments was limited to 2.50 m for possible truck delivery. Regular spacing and similar height of the ribs was searched, except at the ends for anchoring safety barriers. The resulting transverse profile of the deck is represented in Fig. 1 (depth of the steel girders is 4 m), and the transverse cross-section of one segment in Fig. 2. The slab thickness is 0.05 m, the total thickness with the ribs is 0.38 m, and the rib spacing is 0.6 m from axis to axis in both directions. The average resulting weight of the slab is 3.9 kN/m². Transverse pre-stressing is realized by 2 rectilinear T15S (223 kN usable capacity) tendons along the vertical axis of the ribs. The upper one is anchored from one end to the other; the lower one is sheathed along the corbels and on supports. The resisting bending moment for a current T-shaped 0.6 m-cross-section is 115 kN m, limited by the tendons capacity. Longitudinal post-tensioning ensures a minimum compressive stress of 4 MPa at the serviceability limit state (SLS) - frequent combination. Low creep of UHPFRC helps keeping the benefit of this post-tensioning as well as compressive stress due to support lowering very efficiently. An important effort has been carried out to define the anchorage detail of the safety barrier and the connection to the steel main girders. This finally demonstrated the feasibility of realizing a complete bridge design on the basis of AFGC-SETRA UHPFRC Interim Recommendations [2].

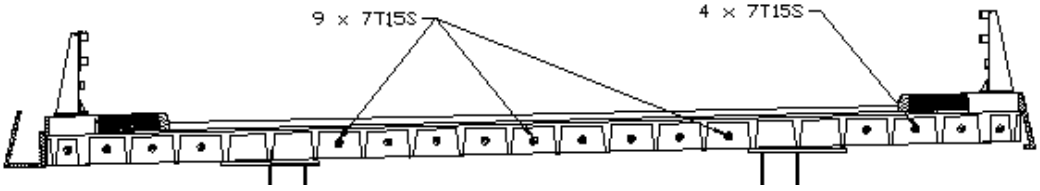

Figure 1: Transverse 12 m-wide cross-section including longitudinal post-tensioning.

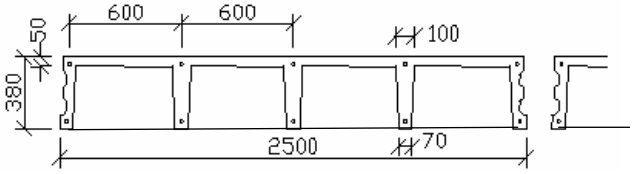

Lengths in mm

Figure 2: Longit. cross-section of a pre-cast segment incl. transverse pre-stressing tendons.

Before this project can be built, some critical aspects require validation, since the assumptions of beams theory used at preliminary design stage may be questionable when 3D efforts are concentrated on intensely loaded thin elements. Experimental validation was thus undertaken on a 6.1 m-wide model slab made of two ribbed segments, one made of ®Ductal and the other of ®BSI-Ceracem, at a scale of 1 to 1 for the length and thickness, connected realistically with a UHPFRC cast in place cold joint and longitudinal post-tensioning [3]. The transverse span was reduced to 3.98 m (clear span between longitudinal beams used as simple supports) for bending tests aimed at representing the effects of wheel loads, and the cantilever side was used for tests of anchoring of the safety barrier. The bridge edge beam for the anchorage of the safety barrier was also realistically reproduced on one side. The experimental program included critical issues for the validation of the safety margin regarding ultimate limit states (ULS), on which the present paper focuses: fatigue under transverse bending due to axle loadings, local bending of “box cells” with possible punching shear failure, ultimate load-bearing capacity under transverse bending, appropriate resistance of the safety barrier anchoring, sufficient strength of the slab connection to the steel girders.

2 Fatigue resistance

The thin deck may be critical with respect to fatigue, which is hardly documented for UHPFRC structures. For a safe validation, transverse location of the loads derived from the ribs spacing, see Fig. 3. The 1.2 m-axial distance between loaded zones also refers to the axle spacing of Eurocode 1 Part 2 fatigue load models 1 and 3 [4]. First, loads corresponding to SLS (rare combination), with an intensity varying from 5 to 155 kN under each “wheel”, were applied 10,000 times on 0.4 x 0.4 m surfaces (Fig. 4). Then, 2 million cycles were applied with a load intensity from 5 to 105 kN. Finally, loads were applied on the same locations but through 0.19 x 0.26 m plates corresponding to reduced “type A“ wheels (Fig. 5). In this “narrow wheels” configuration, 100,000 cycles were applied with an intensity varying from 5 to 85 kN, then 100,000 cycles from 5 to 125 kN, and finally 100,000 cycles from 5 to 155 kN per wheel. The same program was applied in a current part of one segment, and on box cells close to the joint (Fig. 6). Margin assessment is based on following assumptions regarding 100 years heavy traffic [4]: 100 million trucks x 50 % (proportion of type C axles) x 3 (tridem axles) x 2/3 (reduced influence length due to the ribs spacing) x 45 kN (load of C-type wheel) result in 100 million cycles with 45 kN load amplitude variation for each wheel.

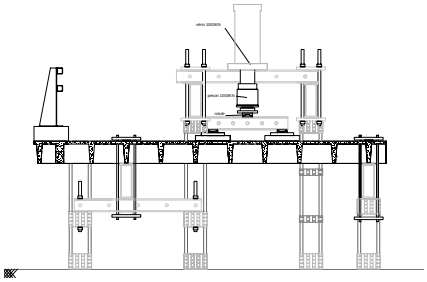

Figure 3: Fatigue test setup

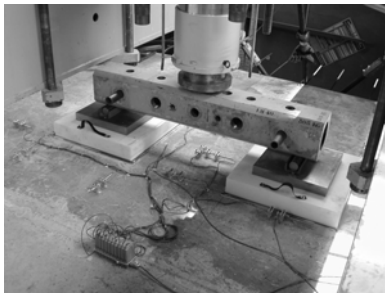

Figure 4: standard “wheels“

Figure 5: narrow “wheels“

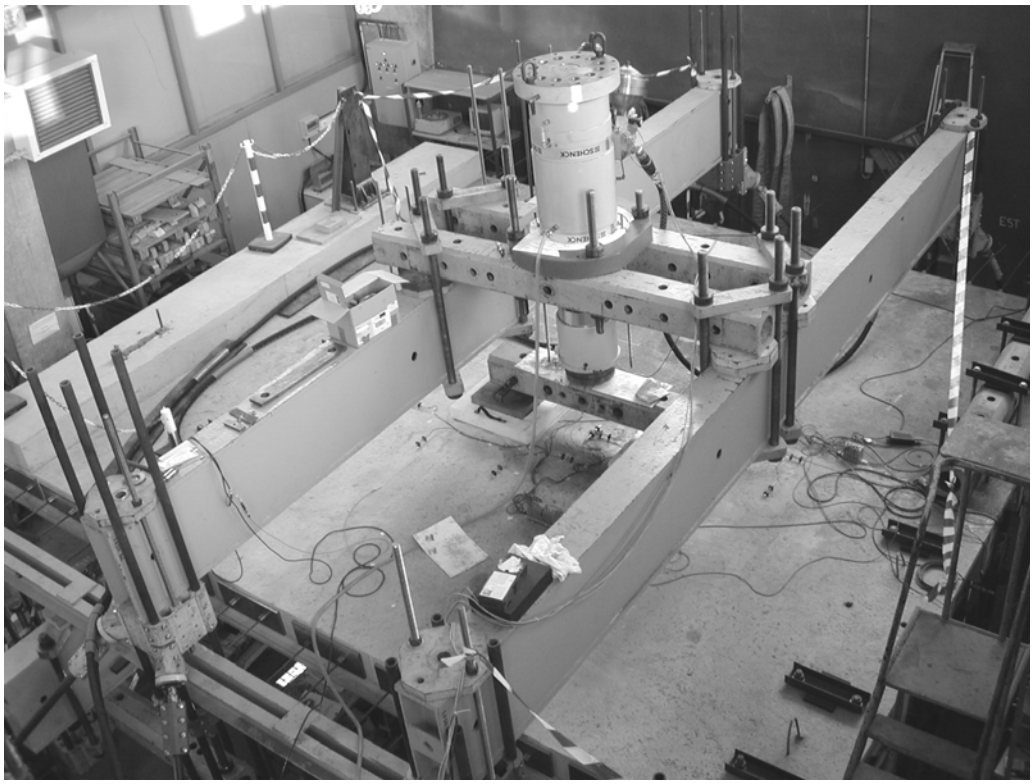

Figure 6: Fatigue loading configuration, close to the joint. The model is 6.1 m wide.

Extrapolation of this 100 years-equivalent loading is based on a conservative slope of UHPFRC SN curve, equal to – 0.14 (i.e. – 1/7). This leads to 79 kN load amplitude per wheel for 2 million cycles, or 120 kN load amplitude per wheel for 100,000 cycles. For widely distributed loadings, no stiffness evolution was observed during the whole loading process [5]. Consistently, estimated maximal stresses under the peak loads keep below the probable tensile stress [2]:

- transverse strains within the ribs reach 305 10^{-6}, the pre-stressing effect is superimposed (+ 17.5 MPa compression) thus tension is kept below 2 MPa
- longitudinal strains within the deck reach 230 10^{-6}, the post-tensioning effect is superimposed (+ 4 MPa compression) thus tension is kept below 10 MPa
- transverse strains within the deck reach 270 10^{-6}, the pre-stressing effect is superimposed (+ 4.9 MPa compression) thus tension is just below 12 MPa, which is critical.

Given this, the safety margin in terms of load applied experimentally without fatigue initiation, over the 100 years-equivalent load is larger than 1.25. For narrow wheels, a slight stiffness decrease was observed only below one wheel after 50,000 cycles with a 150 kN amplitude. During these cycles transverse strains within the deck reached 290 10^{-6}, the pre-stressing effect is superimposed (+ 4.9 MPa compression) thus tension may have exceeded 14.5 MPa, which is surely beyond the limit of linear behavior under tension [2]. Neglecting the safety margin due to the over-concentrated loading, the ratio of load applied experimentally up to fatigue initiation, over the 100 years-equivalent load is still 1.15.

3 Safety with respect to local bending and possible punching shear

Diffusion of local heavy loads appears as critical for the (only 50 mm) deck thickness determination [6]. It had thus to be verified experimentally. Loads were applied either through a B-type wheel (0.4 x 0.4 m) or through a “reduced A-type wheel” represented by a 0.19 x 0.26 m steel plate. Moreover, the diffusion through pavement layers was represented, or not, by a 90 mm-thick polymer layer with 3 GPa Young’s modulus similar to the average stiffness of bituminous concrete. Loading was applied in the mid-surface of a “box cell” simply supported on the four corners of the ribs along it (Fig. 7). Provided diffusion is ensured with a direct enough force transmission from the “wheel” to the ribs, no failure was observed up to a 700 kN loading, non-linearity with fine bending cracks only appeared for a 300 kN load, with a reference 150 kN design load (SLS, rare combination).

Quantification of the safety margin required to reduce the diffusion of the loads using a “narrow wheel” configuration (Fig. 8). Under these conditions only, failure could be obtained. Due to the compressive stresses within the slab, preventing from yield lines mechanism occurrence, failure took place in a punching shear mechanism (Fig. 9). The maximum corresponding load ranged from 350 to 420 kN [7]. No effect of previous fatigue loading was noticed. The average shear stress along the perimeter of the load equals 9.8 and 9.2 MPa for failures obtained on the ®Ductal segment, respectively 8.6 and 8.3 MPa for failures obtained on the ®BSI-Ceracem segment. These values are close to the ultimate tensile strengths f_{tu} obtained in the “thin plates” characterization process on companion specimens with the same 50 mm thickness as the deck. Namely f_{tj} = 9,8 MPa and f_{tu} = 9,5 MPa for ®Ductal, while for ®BSI-Ceracem f_{tj} = 9,3 MPa and f_{tu} = 8,3 MPa. Still neglecting the safety margin due to the over-concentrated loading experimentally applied, the following ratios are established :

- Experimental failure load / design SLS load (150 kN: rare combination) = 2.4 to 2.7
- Average experimental max. pressure / max. wheel pressure (1125 kN) = about 6
- Experimental average shear stress / max. design shear (105 kN/m) [4] = about 4.5

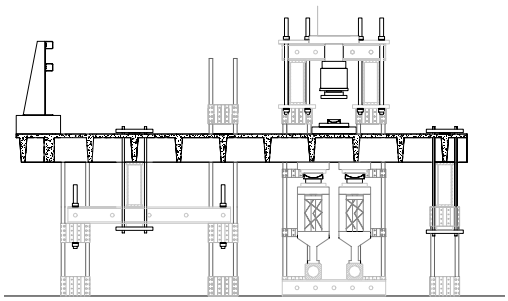

Fig. 7: Loading setup (punching test)

Fig. 8: “narrow wheel“

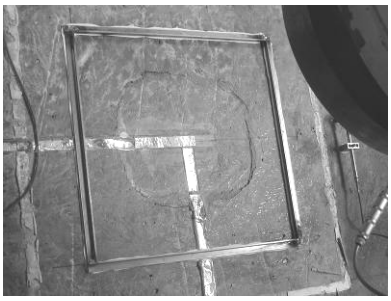

Fig. 9: Punching shear failure

4 Transverse bending – ultimate limit state verification

The transverse bending calculation at SLS (rare combination) determines the ribs height and spacing and the pre-stressing quantities [6]. It was first carried out considering the slab as successive Tee-shaped 0.6 m-wide beams. Using classical UHPFRC material parameters, especially a maximum 15 MPa-bending tensile strength at SLS, the moment corresponding

to the onset of non-linear behavior is 95 kN m (UHPFRC cracking at mid-span in the lower chord of ribs). Shear is not critical and the ULS corresponds to yielding of the lower pre-stressing steel when reaching the factored pre-stressing limit f_{prg}/γ_c, at 115 kN m. Given the 1.39 m-lever arm in the 4 point-bending test carried out, the corresponding total loads are:

- 273 kN (SLS, diffusion over 2 ribs) 331 kN (ULS, diffusion over 2 ribs)
- 410 kN (SLS, diffusion over 3 ribs) 496 kN (ULS, diffusion over 3 ribs)

Quantitatively, the loading close to the joint may be assumed as distributed over 3 ribs, while the loading in the centre of the segment is only directly taken by 2 ribs. The transverse bending configuration illustrated in Fig. 3, with a 1000 kN actuator, was used for monotonic loading, first close to the joint between both segments, then on the box cells row one row after the edge of the model. In the central zone close to the joint, non-linearity (first cracks) was observed only for a 800 kN total load. After loading up to 995 kN, the maximum residual crack opening is limited to 0.3 mm, which is the sign of probably very limited pre-stressing steel yielding. The twin ribs corresponding to the joint appear as behaving as one stiffer rib, with transverse cracks over the whole width (Fig.10).

Figure 10: Tensile cracking of the joint transverse rib after bending test up to 995 kN.

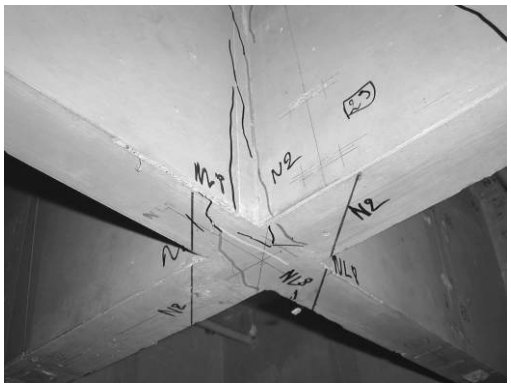

Figure 11: Cracks at corner of loaded box cell

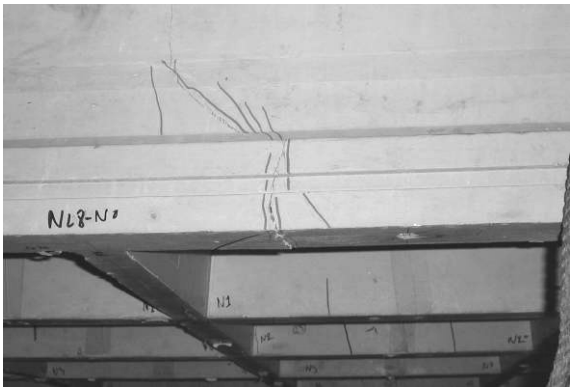

Figure 12: Major crack at end rib

For the loading applied in the central zone of the segment, nonlinearity (first cracks at the bottom of transverse ribs below the loaded zone) was observed under a total load of 500 kN.

From then on, cracks developed within the ribs upwards to the slab. The first major ones concentrated in the corners of the loaded box cells towards mid-span (Fig. 11). At 750 kN a major crack occurred in the end rib. Until 1000 kN it developed upwards in a combined bending-shear mode due to the complex diffusion within the orthogonal ribs net and reached 10 mm-opening, which is the sign of tendon yielding. However noticeable recovery was observed when unloading (Fig. 12). Such a crack developed in the end rib testifies the fact that diffusion of the transverse bending significantly takes place over more than the 2 ribs directly below the loaded box cells. Quantitatively, the safety factor identified experimentally with respect to the limit states computed with the assumption of a simplified distribution over the directly loaded ribs, is 1.83 to 1.95 for the SLS, and at least 2 for ULS.

5 Anchorage of the safety barrier: safety of the provisions

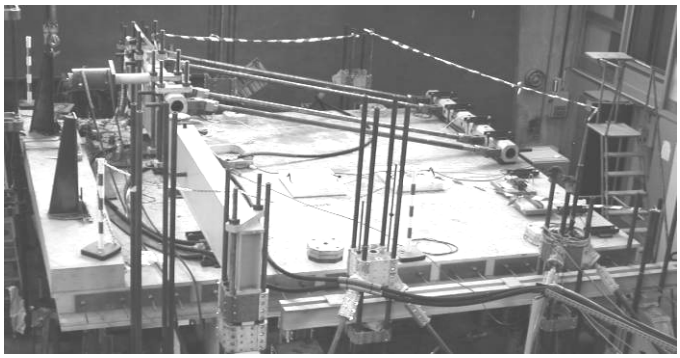

Figure 13: Test setup

Figure 14: Failure of the fuse screws

Monotonic quasi-static horizontal loading (Fig. 13) was applied twice on the post supporting the safety barrier. The load configuration is assumed as equivalent to the normal thrust of a truck accidentally driving out of its lane. Fuse screws help fixing the post to the bridge edge beam and shall control the maximum load, so that the deck itself keeps undamaged. Failure effectively took place by yielding of these fuse screws (Fig. 14) so that a second test was possible after repair of fixation inserts only. Maximum loads reached 254 kN (resp. 244 kN). A simple calculation of the bending moment with respect to a rotation axis at the rear of the post, equilibrated by the forces in the screws when yielding, leads to an expected resisting moment of 163 kN m, while experimentally determined maximum bending moments reached 165 kN m (resp. 159 kN m). Efficiency of this safety-related detail is thus demonstrated.

6 Connection of the ribbed deck to the steel girders

Provisions concerning the realization of connection between the ribbed deck and steel profiles, which are critical for ensuring the composite behavior of the full structure, have been tested after sawing undamaged parts of the model, and realizing the connection in filling box cells with a self-compacting C80/95 concrete, encasing 4 studs 22 mm in diameter, so that a symmetrical specimen is prepared for push-out test. Design values are computed with respect to studs yielding in case of excessive shear, leading to maximal forces of 430 kN (SLS, French provisions) 710 kN (ULS, French provisions) and 900 kN (ULS, Eurocode). Nonlinearity in the force-vertical slippage response was observed only for a 1200 kN-force,

and effective (yet stable) yielding beyond 1500 kN. Load was increased up to 1800 kN without reaching the bearing capacity, thus the safety margin turns out higher than 2.

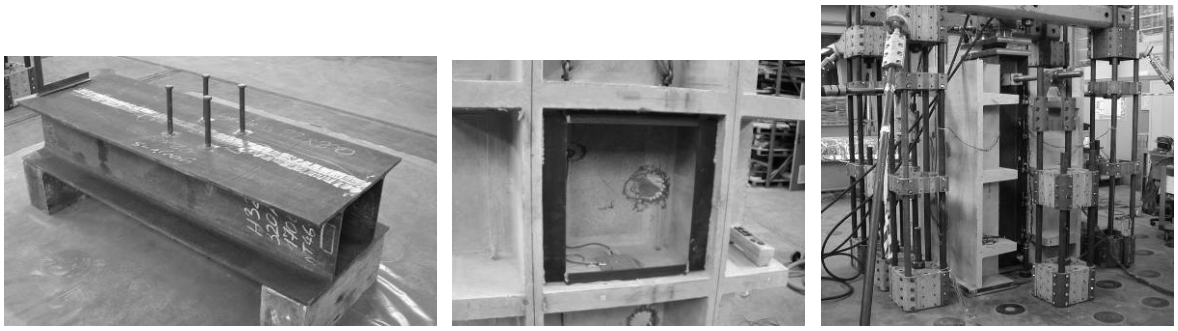

Figure 15: Connection provisions: studs, box cell to be filled, push-out test configuration

7 Concluding comments

Besides having demonstrated the industrial prototype feasibility of scale 1 UHPFRC ribbed slab segments assembled by post-tension for realization of a bridge deck, the experimental program has provided satisfactory safety quantification of critical failure mechanisms considered, with satisfactory margins with respect to SLS and ULS design estimates. The safe application of UHPFRC design Recommendations [2] has been enforced and additional validation of detail provisions has been obtained. A possible effective application is currently under study where lightweight of the slab is critical for launching due to operational constraints in the crossed lane.

8 References

[1] Bouteille S., Resplendino: J.: Derniers développements dans l'utilisation des bétons fibrés ultra-performants en France. In: Proc. GC'2005, Paris (France), 2005.

[2] Resplendino J., Petitjean J. *et al.*: Ultra-high Performance Fiber-Reinforced Concretes. Interim Recommendations, AFGC-SETRA, Bagneux, France (152 p., both in French and English). 2002.

[3] Toutlemonde F.*et al.*: Innovative design of Ultra-high Performance Fiber–reinforced Concrete ribbed slab : experimental validation and preliminary detailed analyses. In: ACI SP-228, 2005.

[4] Eurocode 1 – Partie 2: Actions sur les ponts, dues au trafic, NF EN 1991-2:2004

[5] Toutlemonde F.*et al.*: Fatigue performance of UHPFRC ribbed slab applied as a road bridge deck verified according to Eurocodes, In: Proc. CONSEC'07, Tours (France), 2007.

[6] Resplendino J., Bouteille S.: PN MIKTI. Etude d'un pont mixte à dalle BFUP nervurée, CETE de Lyon, technical report, 46 p., 2003.

[7] Toutlemonde F.*et al.*: Local bending tests and punching failure of a ribbed UHPFRC bridge deck. In: Proc. FRAMCOS-6, Catania (Italy), 2007.

Michael Reichel
Dipl.-Ing.
Graz University of Technology
Institut for Structural Concrete
Graz, Austria

Lutz Sparowitz
Dr.techn. Univ.-Prof.
Graz University of Technology
Institut for Structural Concrete
Graz, Austria

Bernhard Freytag
Dr.techn. Dipl.-Ing.
Graz University of Technology
Laboratory for Structural Engineering
Graz, Austria

UHPC-Segmental Bridges
Material-based design principles and adapted construction methods

Summary

Due to the advantageous weight/strength ratio of UHPC new and extremely fast erection-methods in the field of bridge construction are possible. Furthermore, UHPC has a very dense micro structure, which leads to strongly improved properties regarding durability aspects. Hence, durable and maintenance friendly bridge structures can be economically built with the use of UHPC and the application of segmental method of construction. The higher material costs of UHPC are compensated by a significantly longer life-time and lower effort of maintenance. Such buildings consist of very light and thin-walled precast segments which are jointed by the use of prestressing cabels in longitudinal or even additionally in transverse direction. If necessary normal cast in place concrete can be added in such a way, that the more robust UHPC serves as a protective layer according to the principle “hard skin and weak core”. Due to the low dead load of the single segments as well as of the final construction, many of the already known construction methods can be enhanced. For example, the relatively unknown swivel-in method for erecting arch bridges will get a revival in the near future in Austria. This method will be applied in the pilot project Wild Brücke, which is an UHPC-segmental-arch-bridge for traffic loads. The performance of full-scale laboratory tests covers open questions in the designing process.

Keywords: *UHPC, precast segments, construction methods, pilot project, full-scale test*

1 Introduction and idea - Why UHPC in bridge structures

The combination of high packing density of the granular skeleton up to the range of ultrafines and the low volume-rated water-ultrafines value leads to a very low porosity compared to Normal Strength Concrete (NSC) and High Strength Concrete (HSC). That brings an advantageous effect on durability. An additional heat treatment with 90°C not only enhances

the compression strength and anticipates the drying shrinkage, but also leads to a decrease of the porosity about nearly 50% [1]. Hence, the resistance against penetration of corrosive fluids and gases, against chloride penetration and mass losses due to freeze-thaw cycles is much higher compared to NSC or HSC [2]. Furthermore, UHPC is highly resistant against acid waters, mechanical abrasion and erosion. All of the properties mentioned above allow the conclusion that UHPC is very durable and will cause long lifetimes of structures, even if the long-term behaviour under service life conditions is not sufficiently known so far. Against the background of a constant increase in maintenance costs for the civil infrastructure, this outstanding durability potential has a very important macroeconomic impact.

Due to the fast decline of autogenous shrinkage and the almost inexistent drying shrinkage after heat treating, a very high level of accuracy of the prefabricated elements can be reached with finishing by means of a CNC-machine trough mechanical grinding and milling, which is very easy to handle because of the dense microstructur of UHPC.

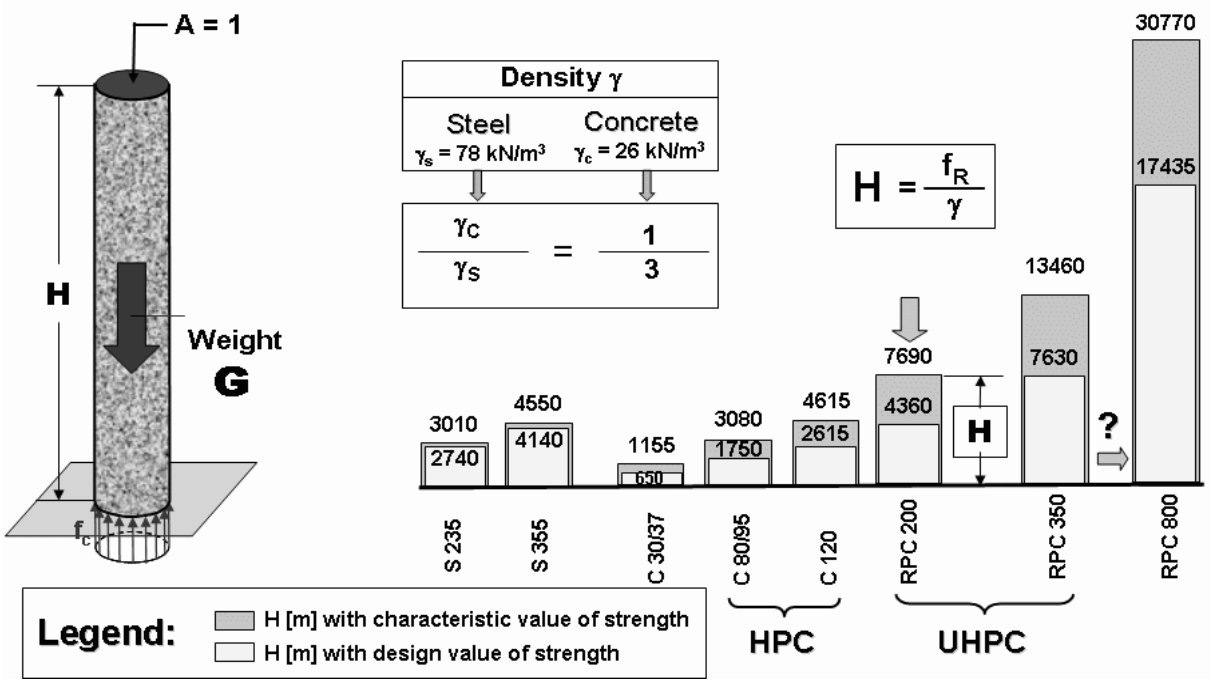

Figure 1: The predominant compression strength to weight ratio

The compression strength of Ultra High Performance Concrete (UHPC) is approximately five to ten times higher compared to conventional NSC, however the weight of these two materials is nearly the same. Therefore new possibilities for the design in bridge construction and civil engineering arise. Fig. 1 shows so-called compression-failure-heights of concrete and structural steel with different strengths without consideration of the theory of stability. The maximum height of each column is reached if the compression failure will occure at the bottom level. Fig. 1 clearly shows the advantage of concrete with a characteristic compression strength of 200 MPa compared to structural steel S 355. The lower tensile strength in relation to compression strength can be compensated by prestressing. Solely, the low increase of the modulus of elasticity from NSC compared to UHPC limits the possible slenderness of bridge superstructures. Generally, each type of structure has its typical compression strength which is being well utilized. For instance, the high compression

strength is better utilized in arched structures than in beams, because of the higher stiffness due to the shape of the arch.

2 UHPC–Segmental Bridges

2.1 Material based design principles

Given the mentioned material properties, at the time the benefits of this construction material can primarily be found in the prefabricated construction - a fact that can also change within the next few years. Industrial standard factory production with a high quality control before the final placing has a positive influence on the construction progress as well as on durability. Because of the high material costs, it is obvious to design thin walled and material saving cross sections, which will shape specify the final section of the superstructure in combination with cast in situ concrete. The geometrical dimensions of these precast segments are usually limited through permitted maximum measurements for road traffic and the elevating equipment provided. All these considerations lead to a segmental construction method like a modular construction system, whereas precast segments are not only assembled by the use of external tendons in the longitudinal direction of the superstructure (Fig. 2a), but they can also be jointed lengthwise, if beams, plates or panels will become a folded structure (Fig. 2b). The external unbonded tendons are exchangeable, restressable and inspectable, so the level of quality of the tendons can be kept equivalent to the high durability and lifetime of UHPC. The advantages of such a segmental construction method are the possible standardization and the extremely fast construction progress. In order to use the outstanding durability properties of UHPC, the principle “hard skin and weak core” will consequently be applied in forming the cross section of the bridge superstructures. Accordingly, the subsequent cast-in-situ completion is arranged in such a way, that the more robust and load bearing protective layer, made of UHPC envelopes the “inferior” HSC or NSC core, as illustrated in Fig. 2.

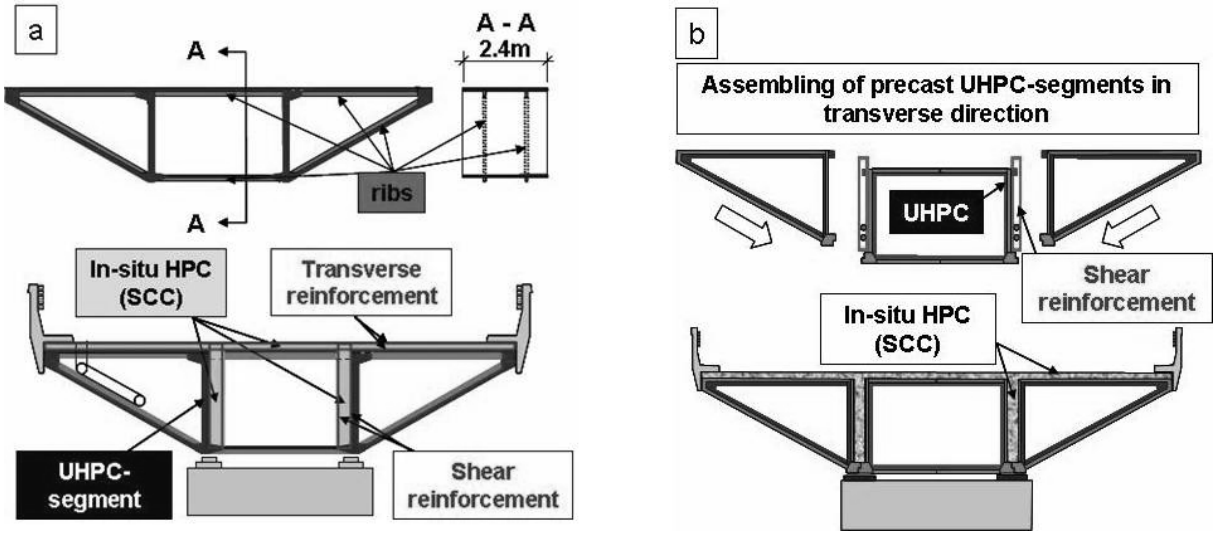

Figure 2: Cross sections for UHPC-segmental bridges

In the case of flexural members the benefits regarding the strength of UHPC cannot be found in the span/depth ratio of the construction but in light, thin-walled and sufficiently stiff

structures. Hence, the light and thin-walled UHPC-cross sections should gain its bending stiffness from high moments of inertia. Therefore, the main dimensions of some proposed cross sections, shown in Fig. 2, do not much differ from cross sections of present conventional bridge superstructures. During construction stiffening ribs in transverse direction with a spacing of 0,50 – 0,75m are necessary. The load carrying capacity as well as the required stiffness for the final loads is achieved by subsequent completions with cast-in-situ reinforced NSC or HPC continuing across the joints between the segments and additional shear reinforcement in the interior of the webs. If transversal prestressing is required, it will be realised with unbonded tendons or by pretensioning of the precast elements.

The design of the segmental joints has a very high influence on the load bearing capacity, durability and also the economy of the construction method. For this reason the Institute for Structural Concrete at Graz University of Technology is currently conducting experimental and numerical investigations concerning the surface detailing (e.g. shear keys, keyed or smooth surface) of UHPC joints on the one hand and the benefits of dry joints, mortar joints and epoxy joints on the other hand. Because of the disadvantages resulting from mortar and epoxy joints [3] such as the additional and weather-depending expense during assembling, a dry segmental joint in connection with external tendons is aimed at - primarily in order to keep the advantage of fast assembling.

2.2 Adapted construction methods

2.2.1 Segmental erection by the balanced cantilever method

The conventional erection by the balanced cantilever method can be modified in such a way, that the thin-walled and transportable precast UHPC-segments substitute the common cantilever segments, as illustrated in Fig. 3a. During construction the very light UHPC-segments require only little prestressing steel and light erection equipment. The construction progress is extremely fast with a cycle time of 2 days per 50 m [4]. For middle and large spans, haunched beams are usually built with this method. Bridges with parallel chords have required additional pylons and stayings in the past. As a consequence, balanced cantilevering with parallel chords has not been applied until now, because of the economical considerations. With the use of light precast UHPC-segments, this construction method can get a revival and will become a competitive alternative to the incremental launching method and self launching gantry systems.

2.2.2 Construction, span by span

Currently the span by span construction method with self launching gantry systems is economical for very long bridges. However the achievable spans are limited to approximately 50 m by the deflections of the launching gantry. If the launching gantry is used as assembling equipment for the UHPC-segmental construction method as shown in Fig. 3b, the load of the formwork is dropped. The launching gantry only needs to carry the relatively light UHPC-segments. Consequently larger spans and again a faster construction progress can be achieved.

2.2.3 Modified incremental launching construction method

Precast UHPC-segments are adjusted and assembled by the use of external tendons behind the abutment as shown in Fig. 3c. After prestressing one increment with a length of 20 to 30 m, the superstructure is launched forward and the construction seqence can start again. Due to the low dead load during launching the launch prestress averages approximately 30 % compared to the conventional method. One cycle lasts only between 1 and 2 days compared to typically 7 days. Larger spans are possible and as a result temporary piers or pylons with ties are not necessary anymore.

2.2.4 Swivel-in-method of arch construction

This relatively unknown construction method has two steps: Firstly, the two halves of the arch are vertically built up above the springing as shown in Fig. 3d; secondly, the two halves of the arch are swivelled in around a temporary hinge at the springing. For anchoring the horizontal forces during the swivelling process, also temporary ties are necessary. Consequently, the swivel-in-method is economical for light structures, because of the little effort for the hinges and the ties.

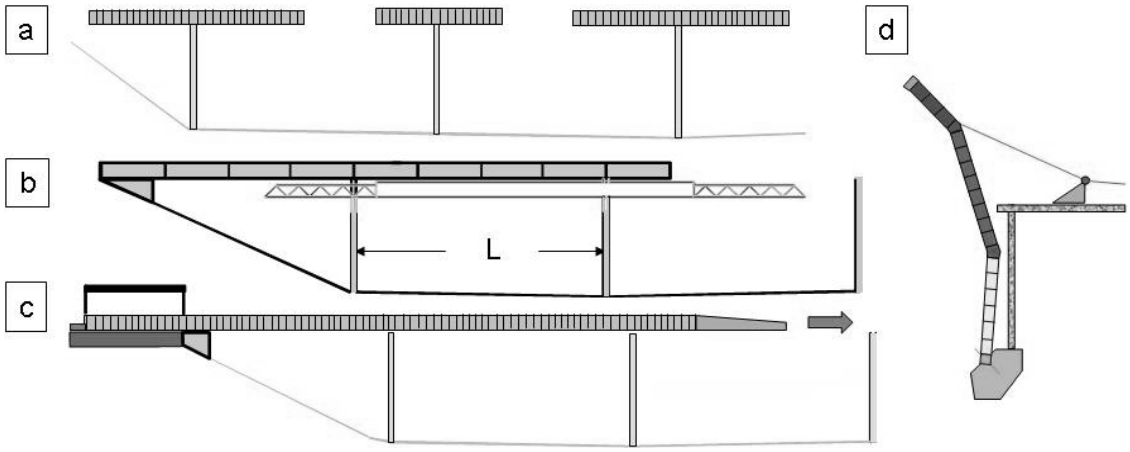

Figure 3: Construction methods for UHPC-segmental bridges

3 Application – Wildbrücke Völkermarkt

3.1 Structure

The pilot project in Carinthia/Austria for an UHPC-segmental-arch-bridge for traffic loads, is an example for the swivel-in-method that will be applied. The polygonal arranged UHPC-segmental-arches as shown in Fig. 4 consist of individual 6 cm thin-walled and for this reason very light precast UHPC-segmental-box-girders made of C 165/185, which are assembled by the use of external tendons running inside of the arches. Because the actual shear force in the arches is very low, the thin-walled webs made of UHPFRC need not any shear reinforcement for carrying the loads. Assumed that the dead load of the arches is low compared to the further loadings from columns, deck construction and traffic, the thrust line of the arch is polygonal. The additional prestressing by external tendons reduces the eccentricity of the loads and causes an important increase of the bending stiffness of the arch. These tendons are unbonded monostrands which are easy to assemble and exchange.

At the bends of the arches so called “knee-elements” are arranged. They work as deviator and anchor block for the external tendons. The columns have a rigid connection to the “knee-element” as well as to the deck.

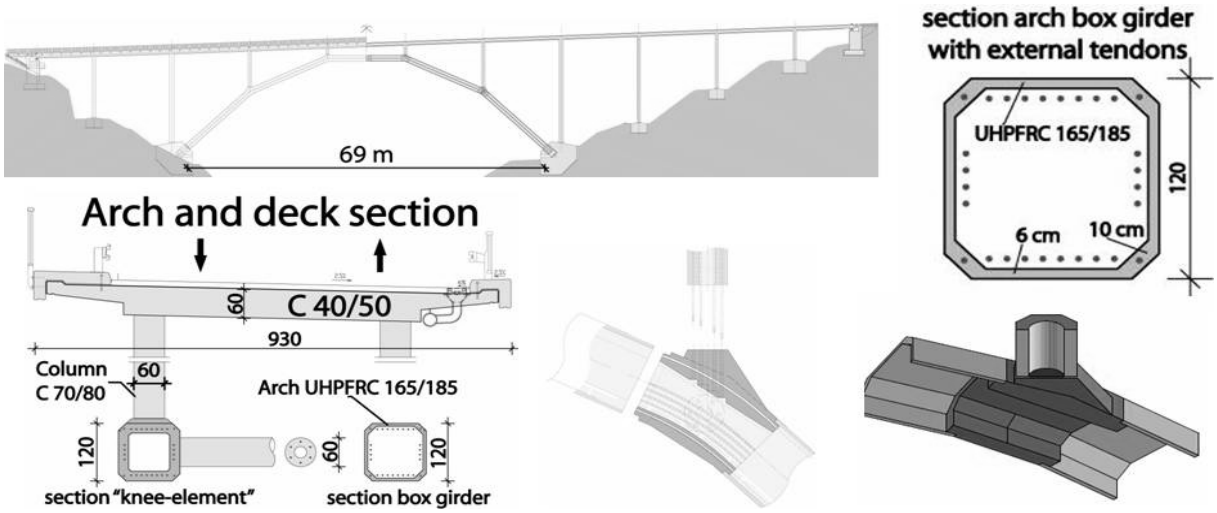

Figure 4: Construction details of the „Wildbrücke Völkermarkt“

3.2 Assembling of the arches

After completion of the foreland bridges, the several arch-segments are assembled in a vertical position using external tendons. The only equipment necessary are a mobil crane for the manipulation and temporary ties for fixing the arch’s position.The very light arch halves can easily be swivelled in and are jointed at the crown. The hinge for swivelling is a simple steel bolt with a diameter of merely 80 mm. The maximum force in the swivelling cable is about 2x450 kN, which can be beared by 2x3 Monostrands. After joining of the arch halves further tendons are installed which overlap at the arch’s crown. Due to pouring the hinge between the arch and the springing, the arch becomes a rigid restraint. Too large production tolerances of the precast arch segments have far-reaching consequences on the erection work and lately on the final arch shape. For this reason project-oriented considerations have already been made and the permitted deviations of the single segments and in addition for the final arch shape have already been declared in the bidding procedure.

3.3 Analysis and design

In order to analyse and design the arch, the material laws and the associated partial safety factors for UHPC were gathered from [5]. For the global structural design calculations of the arch in longitudinal direction under ULS conditions the gaping of the segmental joints is limited by one third of the height of the section [6]. Considering a friction coefficient of 0,20, the shear forces are very easily transferred in the remaining compression zone of the segmental joints. For the assessment of the shear carrying capacity the given design rules from [7] are used. In order to focus on the aims of the construction method proposed, a high durability of the arch should be reached. Therefore decompression in the arch under the characteristic combination of loads is specified as a design criterion. The analytical model considering each construction stage is given in Fig. 5.

Figure 5: Construction stages of the „Wildbrücke Völkermarkt“

The only steel fibre reinforced „knee-elements“ with its complex shape at the bends of the segmental arch are sensitive discontinuity regions. Several actions such as anchoring and deviation of the prestressing tendons, bending moments induced from the columns as well as the shear and axial force in the compression zone over the segmental joint stress these elements. Investigations by means of a nonlinear and linear 3D-FE Analysis (Fig. 6) deliver information about the stress distribution in the “knee-element”. As illustrated in Fig. 6, mainly the change of the cross section from the thin-walled segmental-box-girder to the thicker wall of the knee-element in the compression zone of the joint causes tensile stresses in longitudinal direction at the inside of the upper chord. Considering the large scatter of properties like the distribution and orientation of the fibres in such a complex geometrical construction element, wrapping with carbon fibre reinforced polymer (CFRP) sheets as shown in Fig. 6 is necessary in order to avoid a brittle failure in this region.

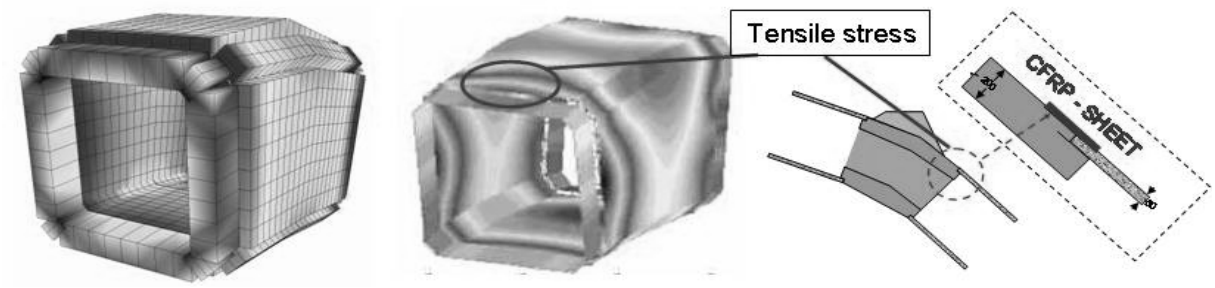

Figure 6: FE-Analysis and conclusions for design of the “knee-elements”

3.4 Tests

Present design codes and guidelines do not completely cover the use of UHPC in relation to the structure presented. Experimental tests will answer open questions in designing and construction. In addition to many other experiments, full-scale laboratory tests within the scope of the pilot project are carried out. The focus of the full-scale test is the load carrying behaviour in the region of the springing, as shown in Fig. 7. The elements involved are fixed to the testing-wall by the use of external tendons having the same type and position as in the real arch-bridge. The necessary loads are performed in two complementary ways: firstly by means of Dywidag Steel Threadbars (axial force and bending moment) and secondly by servo-hydraulic testing-jack (bending moment and shear force). So the total load path as shown in Fig. 7 is performed according to the design calculation and afterwards until failure.

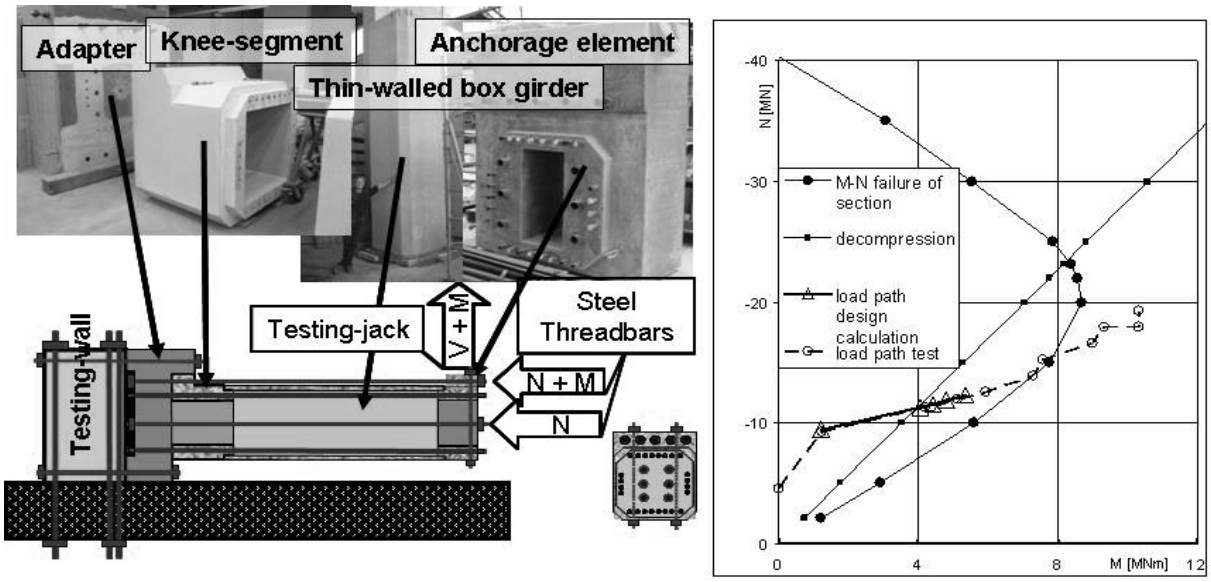

Figure 7: Arrangement of the full-scale tests

4 Conclusions

The most important principles of design can be seen in the two maxims: "*light-weight during erection – massive and robust under service"*, and "*hard skin and weak core".* The depth/span ratio of bridge structures may not be reduced significantly in order to hold a sufficient resistance against vibrations and deflection. Second order load bearing problems like lateral bending and buckling are solved by the arrangement of ribs as known from steel engineering. UHPC-segmental bridges combined with construction methods proposed offer a wide field for good applications. They bring economical advantages in comparison to common concrete bridges, because they will be built faster, are easier to maintain and will have a longer life-time.

5 References

[1] Müller, H.S., Haist, M., Scheydt, J., Burkart, I.: Neuartige Konstruktionsbetone – Eine Chance für Innovationen im Massivbau. 11. Dresdner Baustatik Seminar - Innovative Materialien und Tragwerke. Technische Universität Dresden 2007.

[2] Fehling, E., Schmidt, M., Teichmann, T., Bunje, K., Bornemann, R., Middendorf, M.: Entwicklung, Dauerhaftigkeit und Berechnung Ultrahochfester Betone (UHPC). Schriftenreihe Baustoffe und Massivbau, Heft 1. Universität Kassel 2005.

[3] Rombach, G.A., Specker, A.: Segmentbrücken. Betonkalender 2004. Ernst & Sohn, Berlin 2004.

[4] Hewson, N.R.: Prestressed concrete bridges: design and construction. Thomas Telford, London 2003.

[5] Sachstandsbericht Ultrahochfester Beton - Betontechnik und Bemessung – in preparation, Deutscher Ausschuss für Stahlbeton im DIN Deutsches Institut für Normung e. V., 2005.

[6] Bundesministerium für Verkehr: Empfehlungen für Segmentfertigteilbrücken mit externen Spanngliedern, Ausgabe 1999.

[7] Deutscher Ausschuss für Stahlbeton (DAfStb): Richtlinie „Stahlfaserbeton" (23. Entwurf). Ergänzung zur DIN 1045, Teile 1-4

Noriaki Matsubara
Research Engineer
Kajima Technical Research Institute
Tokyo, Japan

Toshio Ohno
Supervisory Research Engineer
Kajima Technical Research Institute
Tokyo, Japan

Goro Sakai
Senior Research Engineer
Kajima Technical Research Institute
Tokyo, Japan

Yuji Watanabe
Research Engineer
Kajima Technical Research Institute
Tokyo, Japan

Seiichi Ishii
Senior Structural Engineer
Sumitomo Mitsui Construction Co., Ltd.
Tokyo, Japan

Masanobu Ashida
Research Manager
Denki Kagaku Kogyo Co., Ltd.
Tokyo, Japan

Application of a New Type of Ultra High Strength Fiber Reinforced Concrete to a Prestressed Concrete Bridge

Summary

Ultra high performance fiber reinforced concrete (UHPFRC), which has a compressive strength of 200 MPa and excellent durability, was first developed in 1990's and has been applied to many structures all over the world. Meanwhile, new types of UHPFRC have been developed and are called ultra high strength fiber reinforced concrete (UFC) in Japan. One of them has the same properties as European UHPFRC due to the reduction of pores by generating ettringite in the cementitious matrix. Recently, it was applied to a prestressed concrete footbridge in Japan which was constructed with the post-tensioning system. The footbridge was divided into five segments, which were manufactured at a factory, transported to the construction site, and then connected with wet joints of UFC. This paper describes the process of manufacturing the segments and constructing the footbridge.

Keywords: *ultra high performance fiber reinforced concrete, ultra high strength fiber reinforced concrete, post-tensioning, wet joint, footbridge*

1 Introduction

There are two types of UFC in Japan. One is based on the techniques of European UHPFRC, and the other (called AFt-UFC [1]) is based on Japanese techniques of generating ettringite. AFt-UFC needs to be cured at the lower temperature of 85°C and shorter time of 20-24 hours than the other type. Properties of hardened AFt-UFC are shown in Tables 1 and 2. A draft of recommendations for the design and construction of UFC was published by the Japan Society of Civil Engineering in 2004 [2]. AFt-UFC was applied to three prestressed concrete bridges in accordance with the draft. Two of them are road bridges which were constructed with the pre-tensioning system and the other is a footbridge which was

constructed with the post-tensioning system. This paper describes the process of constructing the footbridge.

2 Outline of the Footbridge

An outline of the bridge is given in Table 3. The layout and cross section of the bridge are shown in Figure 1. The slab thickness is 70 mm and ribs of 70 mm (height) × 100 mm (width) are arranged every 1 m under the slab. The three main girders are 500 mm high and 100-200 mm wide. The bridge was divided into five segments as shown in Figure 2 and connected by four external cables of 19S15.2 after placing in-situ AFt-UFC between the segments.

3 Manufacture of the Segments

3.1 Materials and Mix Proportion

The materials and mix proportion of AFt-UFC are shown in Table 4. The pre-mixed binder gives AFt-UFC high strength and excellent durability by reducing the pores due to generating

Table 1: Mechanical Properties of AFt-UFC

Measurement Item	Test Method	Test Specimen	Test Value
Compressive strength	JIS A 1108 (ISO 4012)	Φ100×200 mm cylinder	200 MPa
Static modulus of elasticity	JIS A 1149 (ASTM C 469)	Φ100×200 mm cylinder	45 GPa
Poisson's ratio	(ASTM C 469)	Φ100×200 mm cylinder	0.2
Bending strength	JIS A 1106 (ISO 4013)	40×40×160 mm prism	40 MPa
Tensile strength	-	10×50×300 mm plate	12.5 MPa

Table 2: Durability, and Properties that Affect Durability

Measurement Item	Test Method	Test Value
Pore volume	Mercury porosimetry	4%
Coefficient of air permeability	RIREM TC116-PCD	4.5×10^{-20} m^2
Diffusion coefficient of chloride ion	JSCE-G 572 (soaked in 10% NaCl aqueous solution)	0.0032 cm^2/year (at 0.5 years)
Carbonation	JIS A 1153 (exposed to 5% carbon dioxide)	not carbonated at six months
Resistance of concrete to rapid freezing/thawing	JIS A 1148 (cycles of -18°C and 5°C in water)	not deteriorated after 3,200 cycles

Table 3: Outline of the Bridge

Name	Riverside Senshu Footbridge (tentative name)
Location	Nagaoka City, Niigata, Japan
Structural style	Three-span continuous prestressed concrete structure
Length	30.5 m
Width	4.1 m
Design strength	180 MPa

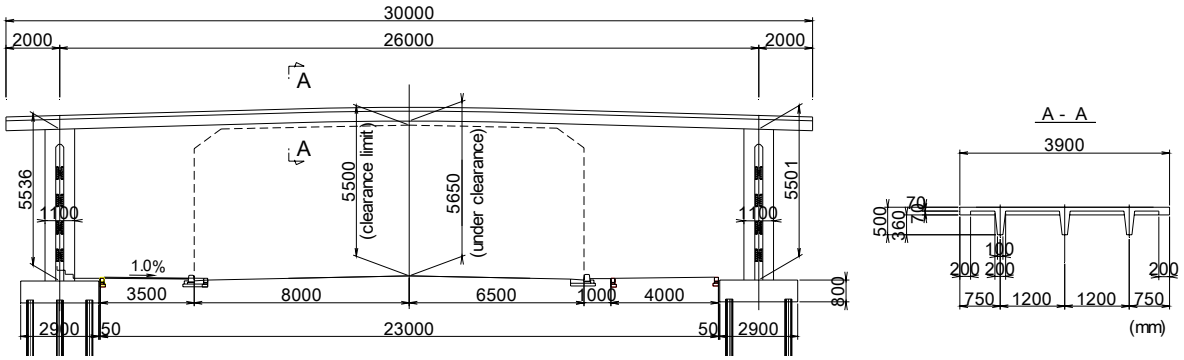

Figure 1: Layout and Cross Section of the Bridge

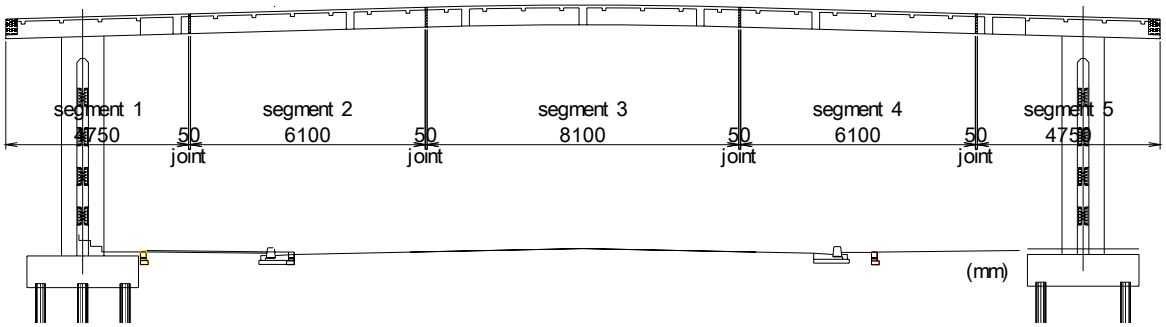

Figure 2: Pattern of Segmentation of the Bridge

ettringite in the cementitious matrix. Conventional aggregate, which was graded to prevent segregation of steel fiber in fresh AFt-UFC, was used. The superplasticizer is polycarbonate type and its amount was determined by trial-mixing before manufacturing segments. The defoaming agent was used to expel the air which reduces the strength of hardened AFt-UFC. All steel fibers have a diameter of 0.2 mm, and have two lengths of 15 mm and 22 mm. The blend ratio of the two types of fiber is a special value to keep both the bending strength and fluidity of AFt-UFC high. The mixing ratio of steel fiber is 1.75 vol% and steel fiber is not included in the unit quantity.

Table 4: Materials and Mix Proportion of AFt-UFC

Material	**Unit Quantity (kg/m^3)**
Water	195*
Pre-mixed binder (C)	1287
Aggregate	905
Superplasticizer	32.2 (CX2.5%)
Defoaming agent	6.4
steel fiber	137.4

*contains water in superplasticizer

3.2 Mixing of AFt-UFC

The segments were manufactured in a prevailing factory for concrete products. Amounts of AFt-UFC for segments 1 to 5 were 5.6 m^3, 4.7 m^3, 3.3 m^3, 4.7 m^3, and 5.6 m^3, respectively. Two forced mixing type mixers having double shafts were used for mixing AFt-UFC to place into forms continuously. The mixer is shown in Figure 3. The maximum mixing volume of the mixers was 1 m^3 and AFt-UFC of 0.8 m^3 was mixed for every batch. The time taken for mixing was about 15 minutes. Manufacture of the segments was carried out on two days in winter: segments 1, 3 and 5 on the first day, and segments 2 and 4 on the second day one week later.

3.3 Placing of AFt-UFC

AFt-UFC was placed into a form of segment continuously with buckets of 2.0 m^3 and 2.5 m^3 one after the other without stopping until the form was filled with AFt-UFC. The good quality of fresh AFt-UFC was maintained by checking samples from the outlet of the first bucket to place into the form of each segment before starting placing. Measurement items for quality control and quality standard values are shown in Table 5 and the results of measurement of fresh AFt-UFC are shown in Table 6.

Main girders and ribs were first filled with AFt-UFC before placing into the slab. Temporary barrages were set in the girders to prevent fresh AFt-UFC flowing too far from the outlet of the bucket because it would have caused surface desiccation and segregation of AFt-UFC at the front of the flow. Fresh AFt-UFC at intersections of the main girders and ribs and interface of the main girders and the slab was stirred with rods to keep fiber continuity. Times taken for mixing and placing for segments 1, 3 and 5 and segments 2 and 4 were about 100 minutes and 80 minutes, respectively. Figure 4 and 5 shows the placing of AFt-UFC. Leveling and the first surface finishing with a square bar to which a vibrator was attached were carried out immediately after finishing placing, and final surface finishing with trowels was carried out two hours after first surface finishing. Leveling and the first surface finishing are shown in Figure 6.

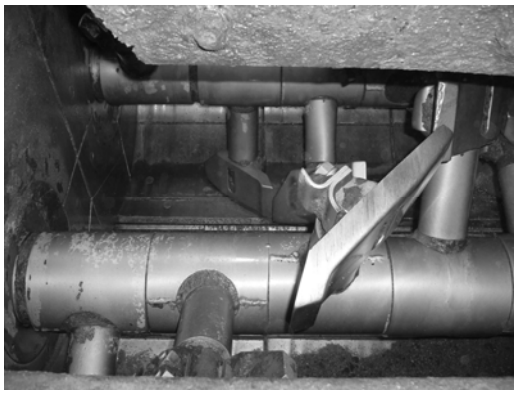

Figure 3: The Inside of the Mixer

Table 5: Measurement Items and Standard Values

Item	Method	Standard Value
Mortar Flow	ASTM C 124	250±20mm
Air		under 5.0%
Temperature of Concrete	-	5°C-40°C
Compressive Strength	ISO 4012	180Mpa
Cracking Strength	JSCE-G552*	8.0Mpa
Tensile Strength	JSCE-G552*	8.8Mpa

*Calculated from measurement value of bending test with specimens of 100X100X400mm

Table 6: Results of Measurement of Fresh AFt-UFC

Segment No.		Mortar Flow (mm)	Air (%)	Temp. of Concrete (°C)
First day	seg. 1	246	3.6	19.0
	seg. 3	249	3.9	20.1
	seg. 5	268	4.0	16.6
Second day	seg. 2	254	4.1	13.3
	seg. 4	241	3.8	16.6
Quality standard		250±20	<5.0	5-40

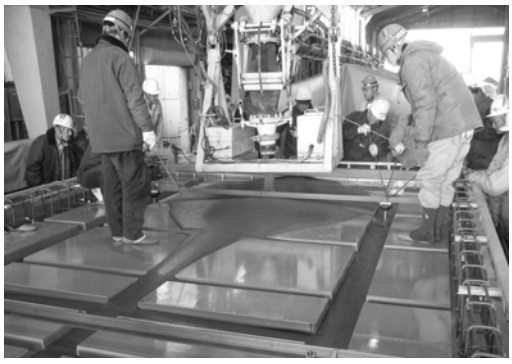

Figure 4: Placing AFt-UFC

Figure 5: Placing AFt-UFC

Figure 6: Leveling and the First Finishing

Table 7: Values of Thermal Properties Used in the Analysis

Item			**Value**
Thermal conductivity		W/m°C	1.77
Specific heat		kJ/kg°C	1.01
Initial temperature of concrete		°C	19
Heat transfer coefficient	forms	$W/m^2°C$	8
	surface	$W/m^2°C$	12
	adiabatic interface	$W/m^2°C$	0
Equation of adiabatic temperature rise $T = K(1-\exp(-\alpha(t-t_0)^{\beta}))$ T: temperature, t: age	K, α, β, t_0		96, 3.3, 1, 0.45

3.4 Heat Treatment for the Segments

The standard curing for AFt-UFC is divided into two steps: the first step is to keep it at room temperature for about 24 hours and the second is to keep it at a temperature of 85°C for 20-24 hours by heat treatment. When manufacturing thin members, all parts inside the member will receive sufficient heat treatment under the standard heat treatment. However, when manufacturing massive members, histories of temperature of the parts inside the member will differ under standard heat treatment because of the adiabatic temperature rise during the first step and the delay of rising of temperature at the center of the member during the second step. Because segments 1 and 5 of the bridge, which are anchorages for external cables, had massive members, thermal analysis was needed to check whether all parts inside the members would receive sufficient heat treatment. Values of thermal properties used in the analysis and the model of the massive members of segments 1 and 5 are shown in Table 7 and Figure 7, respectively. In this analysis, heat treatments of 30 hours and 48 hours were tried. The analysis results are shown in Figure 8. The temperature at C reached

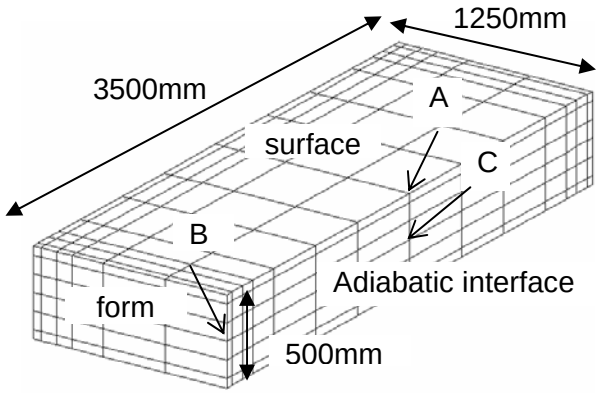

Figure 7: The Model of Massive Member

almost 85°C because of the adiabatic temperature rise when the first step was over, therefore the length of time the temperature was kept at 85°C at point A in the second step was longer than at the other points. The lengths of time the temperature was kept at 85°C of each point are shown in Table 8. In the case of 30 hours, the length of time the temperature was kept at 85°C at point B was 18.0 hours which is not sufficient for AFt-UFC. In the case of 48 hours, all the points received sufficient heat treatment. Analyses for segments 2, 3 and 4 were also carried out for confirmation, and it was shown to be sufficient to keep the temperature at 85°C for 30 hours. The results of measurement of hardened AFt-UFC are shown in Table 9.

4 Conveyance and Erection of Segments

Segments 1 and 5 weighed 141 kN, segments 2 and 4 weighed 83 kN, and segment 3 weighed 118 kN. They were transported by trailer and set on the staging by truck crane.

5 Unifying with Wet Joints

5.1 AFt-UFC for Wet Joints

Mechanical properties of AFt-UFC were needed for the joints of the bridge the same as for the segments because the whole bridge was designed based on the properties of AFt-UFC. However, there was concern that AFt-UFC in joints would crack because of autogeneous shrinkage. Therefore, AFt-UFC whose shrinkage was lessened by including expansive admixture and shrinkage reducing agent was applied. The mix proportion of AFt-UFC for the joints was the same as that of normal AFt-UFC as shown in Table 4. Expansive admixture was added to the pre-mixed binder, shrinkage reducing agent replaced water, and the amount of superplasticizer of CX3.0% was determined by trial-mixing before placing. AFt-UFC was mixed with two forced mixing type mixers having double shafts whose maximum mixing volume was 0.1 m^3 and AFt-UFC of 0.08 m^3 was mixed for every batch. The results of measurement of fresh AFt-UFC for the joints are shown in Table 10.

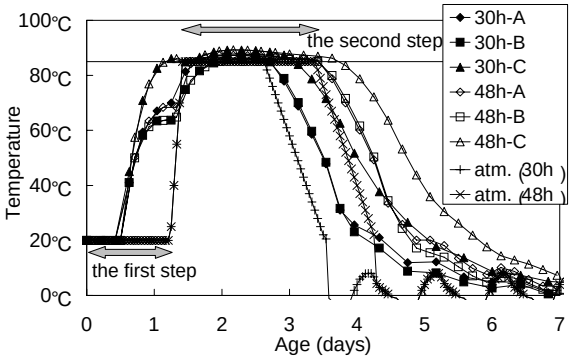

Figure 8: Results of Analysis

Table 8: Length of Time Kept at 85°C

Point of Segment	Length of Time (hours)	
	30	48
A	26.6	43.7
B	18.0	35.5
C	40.0	53.5

Table 9: Results of Measurement of Hardened AFt-UFC

Segment No.		Compressive Strength (MPa)	Cracking Strength (MPa)	Tensile Strength (MPa)
First day	seg. 1	209.7	11.1	12.6
	seg. 3	201.1	9.7	11.4
	seg. 5	207.9	10.4	13.3
Second day	seg. 2	194.4	9.8	11.2
	seg. 4	197.2	10.8	12.5
Quality standard		180	8.0	8.8

5.2 Heat Treatment for Wet Joints

The development of strength of AFt-UFC under lower curing temperature than the standard curing condition was checked in the laboratory before construction because it was difficult to keep the high temperature of 85°C at the construction site. Heat treatment of 60°C was applied for AFt-UFC for the joints after it was confirmed by the test that keeping the temperature at 60°C for seven days produced AFt-UFC with strength exceeding 180 MPa.

Table 10: Results of Measurement of Fresh AFt-UFC for Joints

Joint	Mortar Flow (mm)	Air (%)	Temp. of Concrete (°C)
seg.1-2	262	3.3	18.4
seg.2-3	259	3.5	19.4
seg.3-4	268	3.6	19.7
seg.4-5	264	3.4	20.4
Quality Standard	250±20	under 5.0	5-40

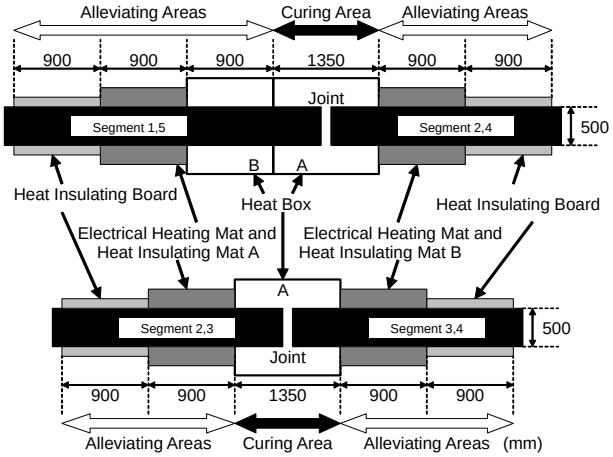

Figure 9: Curing Method for Joints

On the other hand, there was concern that the segments would crack because of thermal stress caused by heating around the joints intensively during heat treatment. Therefore, thermal alleviating areas shown in Figure 9 and Table 11 were set to prevent thermal cracks after being checked by temperature stress analysis. Hot air of 60°C was flowed within the heat box made of heat-insulating board covering the joints and alleviating areas were made of heat boxes, electric heating mats and heat insulting mats. Curing around a joint is shown in Figure 10.

Test pieces for quality control were set in the heat boxes covering the respective joints. It was also necessary to check the development of strength of AFt-UFC placed into the joints to decide when to finish curing. A curing tank permitting the temperature of its water to be controlled to equal that of placed concrete was used to check the development of strength of AFt-UFC placed into the joint. The system of curing tank is shown in Figure 11. The

Table 11: Curing Temperature for Joints

Joint	Alleviating Areas		Curing Area	
	Electrical Heating Mat and Heat-Insulating Mat		Heat Box B	Heat Box A
	A	B		
Seg. 1-2, Seg. 4-5	20°C	30°C	40°C	60°C
Seg. 2-3, Seg. 3-4	30°C	30°C	-	60°C

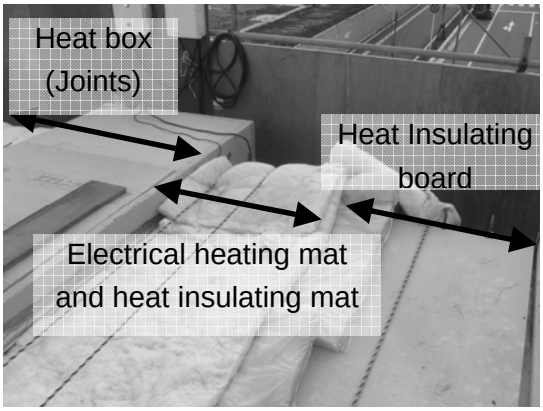

Figure 10: Curing around a joint

temperature of AFt-UFC in the joint of segments 1-2 which was placed the last was measured with a thermocouple and the temperature of the water in the tank containing test pieces was controlled to be synchronously at the same temperature as the measured one. The measured temperature and development of strength of AFt-UFC in the joint of segments 1-2 are shown in Figure 12. The strength developed faster than in the laboratory but the curing period was extended to the day permitted in the construction schedule.

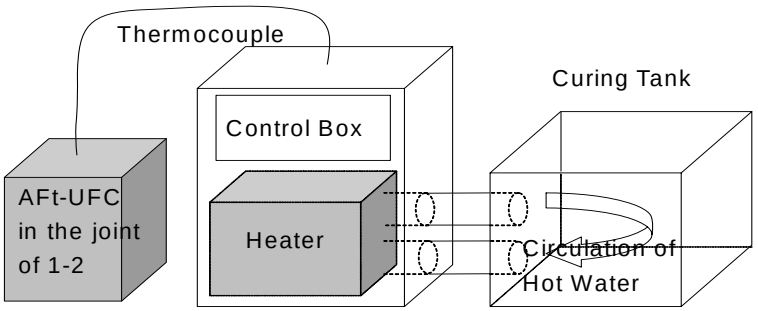

Figure 11: The system of the Curing Tank

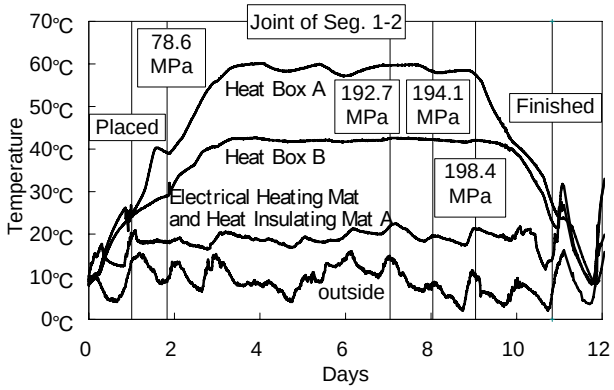

Figure 12: History of Temperature

6 Prestressing

Prestressing was carried out at 11 days after placing AFt-UFC into the joints. It was carried out from one side to prevent much loss of strength of prestress. The completed bridge is shown in Figure 13.

Figure 13: The Completed Bridge

7 Conclusions

AFt-UFC was applied to a prestressed concrete footbridge constructed with the post-tensioning system. Sufficient curing for AFt-UFC of all parts of the segments was carried out by checking the history of temperature of the parts by thermal analysis before manufacturing. Segments were jointed without cracking on whole the bridge through temperature stress analysis and setting alleviating areas.

8 References

[1] Matsubara, N.; Ohno, T.; Sakai, G.; Yanai, S.; Ashida, M.: Properties of new ultra high performance fiber reinforced concrete. In: Advances In Cement and Concrete X: Sustainability, pp. 78-81, 2006

[2] Japan Society of Civil Engineers: Recommendations for Design and Construction of Ultra High Strength Fiber Reinforced Concrete Structures (Draft), 2004

Daniel de Matteis
Technical Director
Sétra (large bridges department)
Bagneux, France

Marco Novarin
Project Manager
Eiffage TP
Neuilly-sur-Marne, France

Pierre Marchand
CTOA
Paris, France

Nicolas Fabry
Eiffage TP
Neuilly-sur-Marne, France

Aude Petel
DGO
France

Sandrine Chanut
Eiffage TP
Neuilly-sur-Marne, France

A fifth French bridge including UHPFRC components, the widening of the Pinel bridge, in Rouen (France)

Summary

This paper describes the design and the building, in 2007, of the Pinel bridge, in France. Located in the west suburb of Rouen, this little bridge has a single 27m long span and is 14m wide. It will increase the traffic capacity of an existing bridge over three railway tracks from two lanes to four. The deck of this bridge combines a classical upper slab in current reinforced concrete and seventeen beams in UHPFRC placed edge to edge prestressed by 28 strands disposed in a large lower flange.

Keywords: *bridge, design, durability, UHPFRC, prestressing, construction*

1 General description of the bridge

The Pinel bridge is a 27 m long bridge located in Le petit Quevilly, south of Rouen. It is used by the vehicles going from the roads deserving Rouen Harbour to the south bank expressways. It crosses, with an important skew, three railway tracks serving a marshalling yard (see figure 1).

The existing bridge is a two lanes bridge with a filler beam deck, with two spans of 12,20 and 14,80 m and with concrete supports on superficial foundations. Built during the seventies, it has been enlarged in 1996. Its deck is therefore composed by two parallel filler beam decks, only connected by a longitudinal expansion joint (see figure 2).

Figure 1: General view of the existing bridge

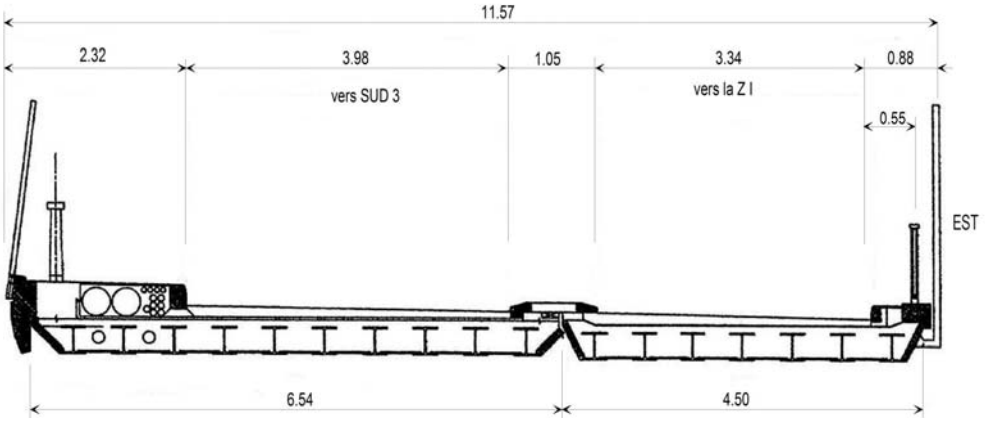

Figure 2: Deck cross section of the existing bridge

In 2008, the "la Motte" roundabout, located south of the Pinel bridge, will become the provisory end of a new expressway joining the A150 highway and the South expressway number III and crossing the new Gustave Flaubert mobile bridge. Due to this situation, the local authorities have decided to widen the existing Pinel bridge from two lanes to five (see figure 3).

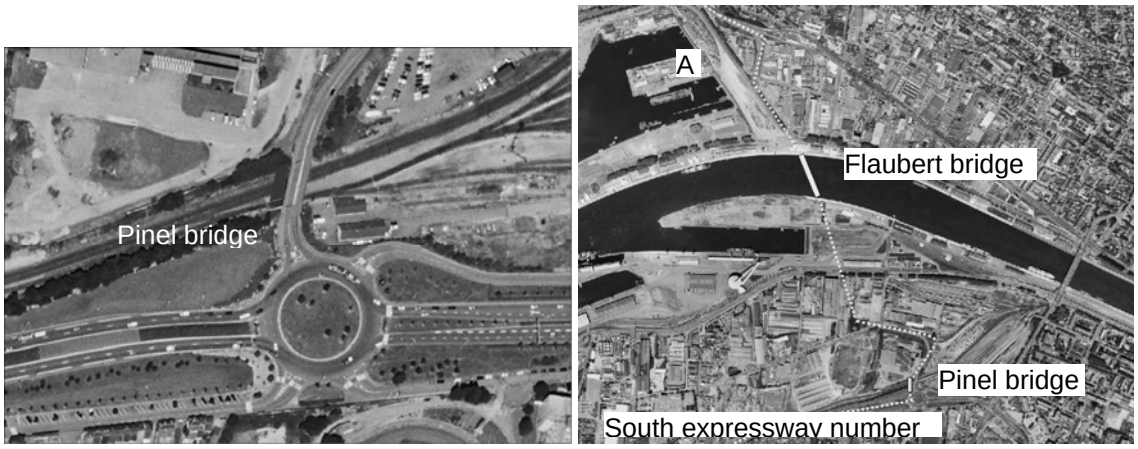

Figure 3: Location map of the Pinel bridge

The following paper describes briefly the common solution initially designed for the widening of this bridge then details the design and the building of the more innovative solution

proposed by the French contractor Eiffage TP. This latter solution combines UHPFRC beams, placed edge to edge, connected to a normal concrete slab (C35/45).
This bridge is the fifth French road-bridge including structural UHPFRC components. The first four ones are the two bridges of Bourg-lès-Valence, south of Lyon, The Saint-Pierre-la-Cour bridge in Mayenne, and the n°34 bridge on the A51 motorway (Grenoble-Marseille).

1.1 General data of the initial solution

The new Pinel bridge has the following geometrical characteristics (see figure 4):

- Single span of 27 m, 14 m wide, transversal slope of 2.5%
- Large skew : 64 centesimal degree (57°)
- Circular longitudinal section with the upper point at the mid span of the bridge
- Road cross-section : a 0,50 m left hard strip, three 3,50 m wide traffic lanes and a 2 m large pavement

As designed by the construction manager, the deck was supposed to be a filler beam deck including 17 steel beams HEB700 type.

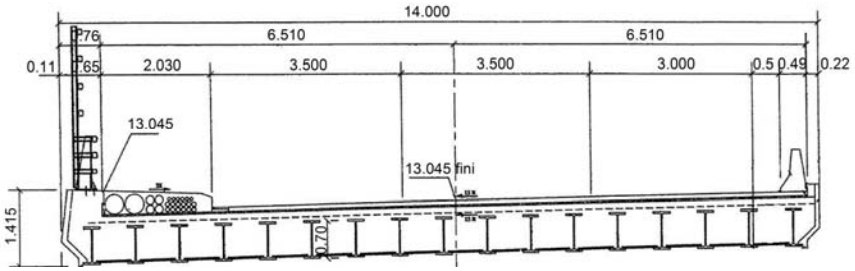

Figure 4: Cross section of the deck designed by the construction manager

1.2 General data of the Eiffage TP variant tender

The variant tender submitted by Eiffage TP proposed to erect a deck composed of seventeen UHPFRC beams, placed edge to edge, connected to a normal concrete slab (see figure 5), instead of the initial filler beam deck.

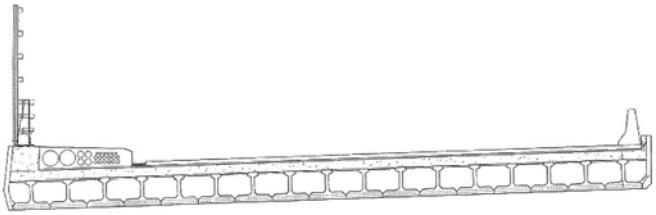

Figure 5: Cross section of the variant deck proposed by Eiffage TP

As designed in this variant tender, the seventeen beams are all identical and have the same inclination as the upper deck. Their main characteristics are the following (see figure 6) :

- Height: 62 cm
- Lower flange: 0,80 m x 0,15 m plus gussets
- Web: thickness varies between 7 cm in the common area and 12 cm close to the ends
- Upper flange: 0,25 m x 0,05 m plus gussets

- Prestressing: 28 T15,7/1860 MPa strands, all placed in the lower flange, progressively anchored thanks to the ducting of some of them
- Beam-slab connexion: steel reinforcement placed in the upper flange.

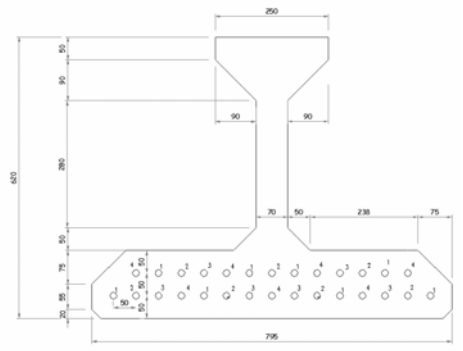

Figure 6: Cross section of a common Pinel UHPFRC beam

At the ends of the UHPFRC beams, two transversal beams are cast simultaneously with the upper slab, to link the beams together. The upper slab, whose thickness varies from 21 to 32 cm to respect the circular longitudinal section, is built using pre-slabs and cast in situ concrete with a normal strength (C35/45).
Considering the Eiffage TP variant was a little bit cheaper than the other tenders and satisfactory on the technical point of view, the owner of the bridge has decided to choose this tender.

2 The construction design

2.1 General data

Construction design has been made by Eiffage TP and checked by the Sétra large bridges division. French classical rules (BPEL, BAEL) have been used for general calculations. The guide "Bétons fibrés à ultra-hautes performances – Recommandations provisoires" edited by Sétra and AFGC has also been used to check UHPFRC beams design. Besides classical road loads, the Pinel bridge is also designed to bear a 120 tonnes military vehicule.

2.2 Deck Design

Numerical models

Calculations have been made in parallel by Eiffage TP and by Sétra. Both models are based on the same principle, i.e. a girder grill for the concrete slab, rigidly linked to beam elements modelling UHPFRC beams.
As the beams are prestressed by pre-tensioning, the prestressing force introduced in the numerical model takes into account elastic shortening losses and thermal losses. The latter are induced by concrete warming while concrete setting. Shrinkage and creep of UHPFRC are different from shrinkage and creep of classical concrete: total shrinkage is 6 to 7.10-4 instead of 2 to 2.5.10-4, and creep coefficient is 1 in place of 2. In the numerical model, shrinkage and creep are modelled with laws used for classical concrete, but with parameters modified to fit the UHPFRC behaviour.

Normal stresses

Beams can bear easily normal stress. The most critical step for the beam is the force transfer to concrete while detensionning the strands, as for a classical pre-tensioned beam.

Shear stresses

The beams design proved to be a little bit weak considering shear forces. Indeed, the two numerical models have shown that the maximum shear stress – including effects due to torsion and prestressing force distribution - was very important on the two external beams (left beam and right beam on the deck cross-section) and slightly superior to admissible shear stress. As a result, it was finally decided to adopt two kinds of beams: the common beams already described and the external beams with 3 cm wider web and upper flange.

Table 1: Web thickness

Distance to the end	**Web thickness**	
	Beams 2 to 16	Beams 1 and 17
from 0 to 2 m	0.12 m	0.15 m
from 2 m to 5 m	0.07 à 0.12 m	0.10 à 0.15 m
from 5 m to crown section	0.07 m	0.10 m

On external beams, strands have been anchored as close as possible from extremities to increase the mean compressive stress. To limit traction at the upper fibre, a strand was added in the upper flange (see figure 7).

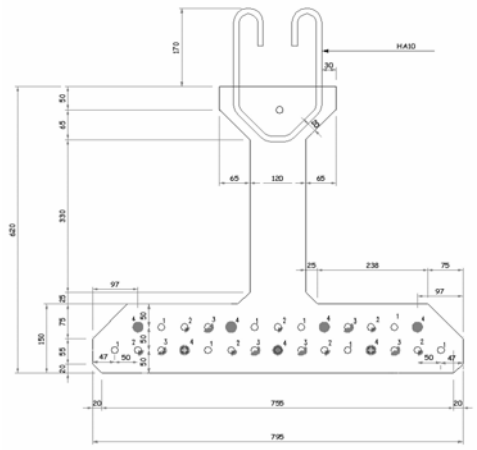

Figure 7: Cross section of the two external beams

Connexion beam-slab

As the interface between beam and upper slab was not judged rough enough, it has been considered for calculation as a slick interface through which reinforcement must resist only by shear. As a consequence, this reinforcement has been dimensioned like common composite bridges studs. This hypothesis is probably a little bit pessimistic and it would be interesting to make laboratory tests to appreciate the participation of the interface between normal concrete and UHPFRC in shear resistance.

Beams orientation

In order to facilitate laying and to limit torsion, beams have finally been laid vertically, with a vertical difference of 17 mm between each beam and its neighbour in order to give to upper slab the expected transversal slope.

Others points

The new Pinel bridge combines a classical slab with UHPFRC beams. The reason of this is both economical and technical. Economically speaking, the slab thickness must be contained between 20 an 30 cm because of the longitudinal profil. As a consequence, normal stresses in the slab are low and it is not necessary to constitute this slab with a sophisticated and expansive material such as UHPFRC. On a technical view, it was also difficult to adopt an UHPFRC slab on this bridge: the transversal slope was significant and the possible differential shrinkage between prefabricated beams and cast *in situ* slab very important.

3 Construction

Construction has been realised during year 2007, by the Haute Normandie Agency of Eiffage TP.

3.1 UHPFRC beams prefabrication

General considerations

The beams have been prefabricated in Veldhoven, close to Eindhoven (Nederland's), by the Dutch contractor Hurks Beton, which is the usual Eiffage TP partner for UHPFRC structures.

Ultra high performance fibre-reinforced concrete

The UHPFRC used for Pinel bridge beams is identical to the one used for the Millau viaduct tollgate roof. It is a 165 MPa UHPFRC whose formulation combines 2360 kg of Premix (*) Ceracem BFM-Millau from Sika, 45 kg of super plasticizer, 195 kg of water and 195 kg of steel fibres (* Premix is a dry component, manufactured in big bags, made with cement and aggregate).

The construction methodology of the UHPFRC beams

The construction methodology of the UHPFRC beams is very close to those of classical prestressed beams and is done using a tensioning unit. Considering the big difference between the lower flange width and the web thickness, contractors have decided to concrete them in two stages:

- First, the lower flange, using only the lower part of the formwork
- Then the web and the small upper flange, once added the upper part of the formwork and the reinforcement for connexion (see figure 8).

Considering the 30 to 60 minutes time needed to prepare the second phase after the end of the lower flange concreting, it is necessary to break a kind of skin which can appear on the top of concrete - and already meet on others structures – to ensure the correct mixing of the concrete and fibres of the two stages. For that purpose, a steel device was set in the lower part of the formwork before the lower flange concreting and was laid off after the setting of the formwork upper part.

The formwork was laid off as soon as maturometry indicates a concrete resistance higher than 101 MPa, a situation usually reached after about 24 hours.

The suitability test

Before the beginning of beams prefabrication and as recommended by French AFGC/Sétra recommendations relative to UHPFRC structures, a suitability test must be performed on concrete. On Pinel bridge, this test has consisted of a 5m long piece of beam built with one of the two extremities of the formwork and with the concrete and strands used for the definitive beams (see figure n°9). Of course, this production prototype has been concreted in the same conditions than those expected for the definitive beams: same factory, same mixer, same two parts formwork, same light vibration during the concreting, same way of introducing the reinforcement inside the UHPFRC, etc…

Figure 8: Putting up of the upper part of the formwork

Figure 9: Production prototype used for suitability test

Eighteen cores have been extracted of this production prototype by Hurks Beton: six horizontal, six vertical and six inclined. Their location, shown by figure n°10, can appears strange but we have to remind that they can be extracted only in the area where the web thickness is constant. Cores have been notched then tested in "3 points flexion" in the Sika laboratory of Gournay-en-Bray (Sika is the Premix supplier).

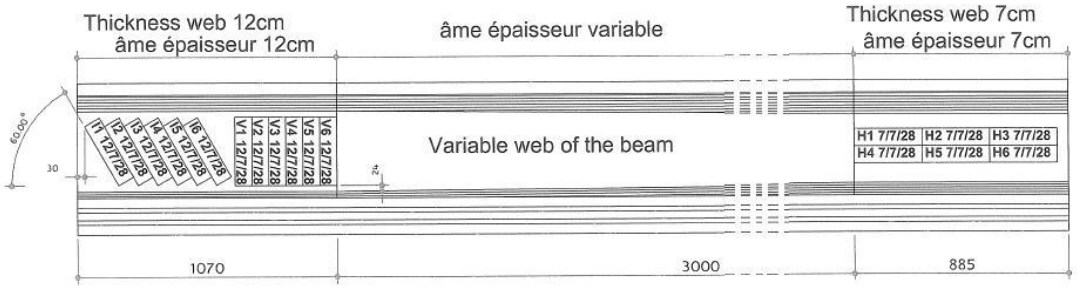

Figure 10: Coring of the suitability test

As observed on some others UHPFRC projects, the results of the first tests were not immediately satisfying:

- the first test has been destroyed immediately after form removal because the web surfaces presented a lot of bug holes, which could affect the result of the flexion tests on the extracted cores ;
- the second test was no more satisfying and showed a imperfect orientation of the fibres (according to Eiffage TP, this was probably the result of bad conservations conditions of the fibres and probably of a too small batch).

3.2 Laying of the UHPFRC beams

The seventeen beams have been lifted under railway traffic interruption the 9 June 2007, with a 300 tonnes mobile crane.

Figure 11: Laying of the beams

Figure 12: Deck underface

3.3 Concreting of the upper slab

The upper slab has been formed with 36 mm thin Duripanel sacrificial precast slabs and executed with a C35/45 common concrete. Concreting lasted about five hours, the slab parts used as transversal beams being concreted lastly to limit torsion effects in the beams.

4 Advantages of Eiffage TP variant tender

The UHPFRC beams used on this site have been developed as the main component of a new deck structure, which can be an economic alternative to filler beam decks, particularly when spans are greater than 20 m and are going over roads or railway tracks.

Considering design, the main advantages of this structure are the very important durability of UHPFRC beams and the opportunity to design very thin decks (on Pinel bridge, height of beams and deck are respectively 1/43 and 1/31 of the span length). The proposed structure is also lighter than a filler beam deck (approximatively 40% less in case of Pinel bridge), which can reduce the cost of foundations under certain soil conditions.

During the construction, the main advantages of these beams are, in one hand, their great stability and, in the other hand, quickness and safety of what is to be executed after the beams laying. Since the beams are placed edged to edge, sacrificial precast slabs can be settled very quickly and almost without traffic perturbations. Reinforcement and concreting of the upper slab are also quicker than those of a filler beam deck (low volume of concrete, no transversal bars through the beams, etc…).

The erection of the Pinel Bridge has confirmed the advantages of this innovative solution. Although some perfectible points have to be improved, such as excessive duration of preliminary concreting test, intrados and extrados surfacing quality, etc..., it shows that UHPFRC can be a very interesting material for bridges.

Yoshihiro Tanaka
Distinguished research engineer
Taisei corporation
Tokyo, Japan

Masayuki Ishido
Director
Tokyo Monorail corporation
Tokyo, Japan

Takashi Kobayashi
Director
Tokyo Monorail corporation
Tokyo, Japan

Masami Ohkawa
Construction manager
Taisei corporation
Tokyo, Japan

Technical development of a long span monorail girder applying ultra high strength fiber reinforced concrete

Summary

The authors have been challenging the technical development on the pre-stressed concrete structures applying Ductal® and have accomplished a 40m long monorail girder which must be the longest span monorail girder made of concrete material in the world. The developed 40 m in length, 0.8m in width and 2.0m in height girder is consisted of six pre-cast segments and all the segments were jointed together on the construction site. Two different kinds of joint were developed. One of the important aspects for those joints performance is to offer the accurate finishing configurations because the monorail girder is a rail. The construction and structural safety performance have been verified before the actual construction of the 40m long monorail girder, through FEM analyses and a series of experiments such as the fundamental joints tests, the fabrication tests and the loading tests using a 10m long prototype monorail girder.

Keywords: *ultra high strength fiber reinforced concrete, pre-cast segment, wet-joint, dry-joint*

1 Introduction

In 2002, a 50m span "Sakata-Mirai footbridge" [1] has been constructed in Sakata city applying ultra high strength fiber reinforced concrete Ductal® for the first time in Japan. Based on this achievement and laboratory test data, "Recommendations for Design and Construction of Ultra High Strength Fiber Reinforced Concrete Structures, -Draft" [2] was published in 2004 by Japan Society of Civil Engineers. The design and construction records of footbridges, highway bridges and architectural structures made of Ductal have been increasing for recent five years in Japan, except the railway structures.

Tokyo Monorail and Taisei corporations have been carrying out the corporative development of a long span monorail girder applying Ductal. Pre-stressed ordinary concrete monorail girders 20m in length have been generally used for the most spans of the Haneda line operated by Tokyo Monorail Corporation. One of the main reasons why the concrete material is applied for monorail girder is to keep the friction between the rubber running

wheel and the top surface of the girder, but the longest span was limited to 20m for the ordinary concrete girder because of the heavy dead weight. On the other hand, the composite structures consisting of steel girder and concrete slab have been applied for long span requests.

In this paper, the technical development of a 40m long monorail girder, the fundamental experiments for wet and dry joints which must be the key of the newly developed pre-cast segment method and the structural verification experiments using a 10m long proto-type monorail girder are described and discussed.

2 Mechanical properties of Ductal®

The basic mix proportion of Ductal is shown in Tab. 1. The self-leveling performance of this material is achieved that a flow value is around 250mm for the material temperature of 20 ~ 25°C even for including the steel fiber by 2 % in volume in the matrix. This fluid performance can be much more enhanced than the original RPC200 developed in France.

Table 1: Mix proportion of Ductal®

	cement	grain (quarts, sand, etc)	fiber	super plasticizer	water	total water
kg/m³	774	1523	157	7 (solid)	162	180

The tension softening behavior plays an important role of the design verification of the structures for ultimate limit state (ULS). The first initial cracking stress mainly depends on the tensile toughness of cementitious matrix and the ultimate tensile strength depends on the bridging effect of steel fiber, which is due to the fiber-matrix bond as well as the tensile strength of fiber. The steel fiber is 0.2mm in diameter, 15mm in length and 2800 N/mm^2 in tensile strength.

It is difficult to conduct the direct tensile test to obtain the tension softening curve without data scattering. Tanaka et al. [3] proposed a practical design oriented modeling of tension softening curve from the inverse FEM analysis proposed by Uchida et al. [4] applying the data obtained by the four-point bending test. Figure 1 shows the tension softening curves calculated by the inverse analysis using deflection data without notched specimen of the four-point bending test and crack opening width data with notched

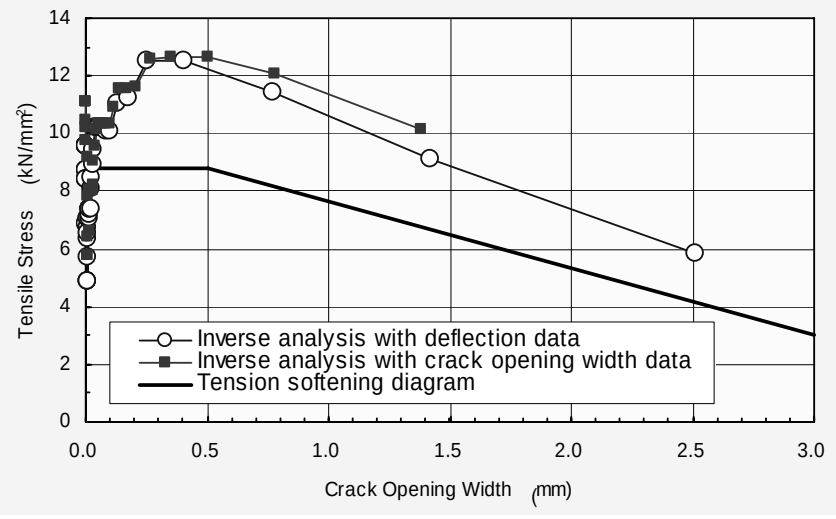

Figure 1: Tension softening curve for Ductal

specimen. Through statistical process for such bending test data and inverse analyses, the simplified design tension softening diagram was obtained for Ductal as illustrated in Fig. 1. The average value of tensile strength f_t = 11.3 N/mm^2 and the characteristic value of tensile strength f_{tk} = 8.8 N/mm^2.

3 Structural key points of long span monorail girder

3.1 Arrangement of pre-cast segments

The transportation of the final monorail girder by trailer or track usually has some limitations for dimensions or weight of the structures. Because of length restriction for the case of the 40 m long monorail girder, three reversed U-shaped girder (hereafter it is expressed "rU girder") segments and three bottom slab segments were separately manufactured in the factory, conveyed to the construction site and jointed together by wet-joint and dry-joint. The final completion of the 40m long monorail girder applying Ductal is shown in Fig.2. It was settled in the train shed line and the conventional 20m PC monorail girders were lined in front and behind.

Figure 2: 40 m long monorail girder

The composition of three rU girder segments and three bottom slab segments are illustrated in Fig. 3. Three rU girder segments are connected by dry-joint, on the other hand

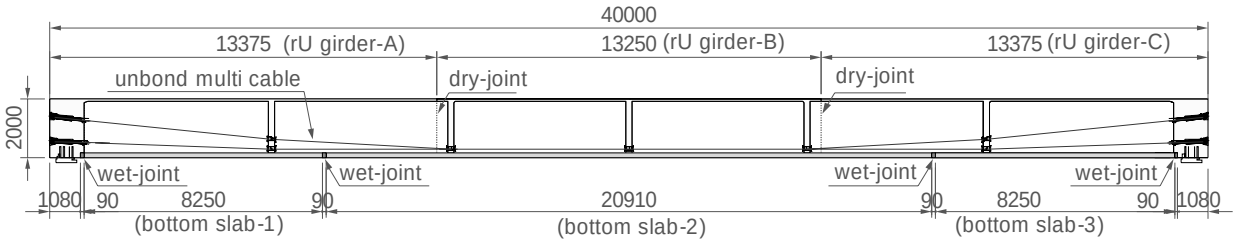

Figure 3: Structural composition of pre-cast segment

three bottom slab segments and rU girders are connected by wet-joint, as shown in Fig. 4, applying the Perfobond Strip (hereafter PBL=PerfoBod Leisten) which was originally developed by Leonhardt [5].

It should be noted that the dry-joints for rU girders are located in inner side of the span but the wet-joints for bottom slabs are located outside of the dry-joint. The tensile stress for the design load of service limit state (SLS) should be less than the first cracking strength (f_{cr} = 8 N/mm^2) except the joint section, however the tensile stress for SLS

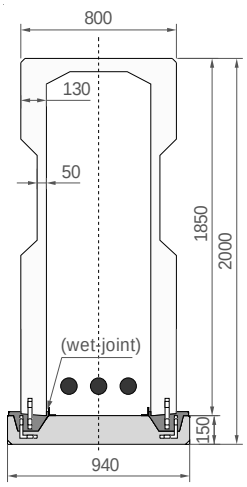

Figure 4: Wet-joint

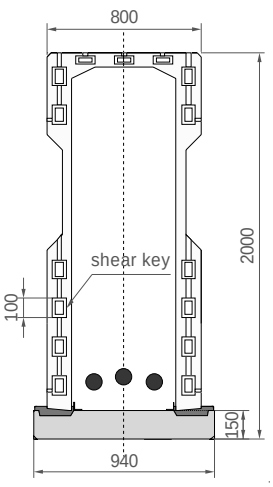

Figure 5: Dry-joint

can not be allowed on both types of joint; i.e. it should be full pre-stressing for those joints. It is therefore possible to reduce the pre-stressing cables compared with the case the locations of both joints coincide. Another reasons why rU girders and bottom slabs are separately manufactured, are 1) inner molds need to resist for enormous uplift force due to fluid like Ductal if the closed form box sectioned girders are employed, 2) the closed box section requires all pre-stressing cables to be inner cable and it makes web and slab thickness thicker as well as difficult form works.

3.2 Dry-joint

The fundamental concept of our dry-joint is same as the conventional match cast joint usually applying for PC bridges so called pre-cast segment method. The different aspect from the conventional method is how to fabricate the match casting. Shrinkage of Ductal is primarily autogenous shrinkage that is much larger than conventional concrete. Autogenous shrinkage of Ductal is affected by various factors such as initial curing temperature.

The match cast face of the new segment is usually fabricated by arranging the match cast concrete face of the old segment as a mold. However, the match cast face of the old segment must already have had some autogenous shrinkage in case of Ductal and this sequentially causes unmatched segments. Our new fabrication method of segments is that a steel end plate mold is set on the old segment to keep constant the sectional dimensions. The mold of the new segments is set on the old segment remaining the steel end plate mold on the old segment. As the steel end plate is constant thickness, the match cast faces result in the mirror image.

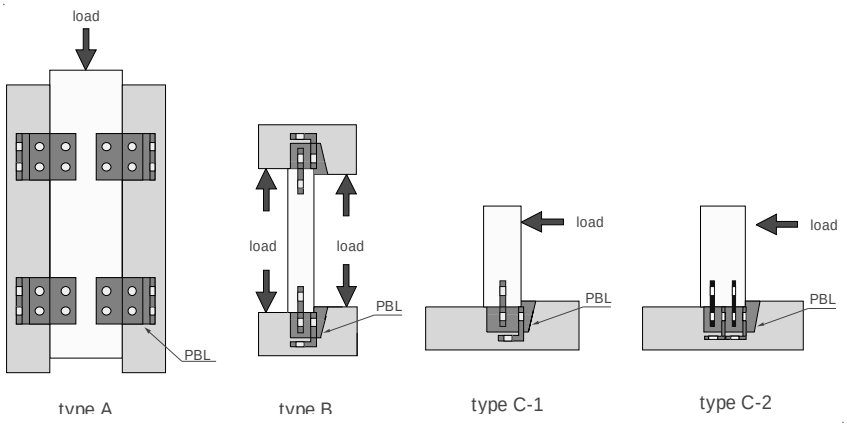

Figure 6: Loading type of PBL wet-joint

Another unique point is that all shear keys on both sides of the matching face, as illustrated in Fig. 5, are couples of concave shapes where non-shrinkage cementitious material is poured after dry-joint is completed. It is noted cracking risks usually generated around the shear keys of conventional match cast faces will not happen for this case.

3.3 Wet-joint

Wet-joint applying PBL of which main role is the shear transfer in longitudinal direction between web and flange, has been already achieved in

Table 2: Experimental parameters and results

name of EXP	loading type	numb. of PBL	web width (mm)	design load (kN) SLS L1EQ	design load (kN) ULS L2EQ	Exp. Result (kN) first cracking	Exp. Result (kN) Max. load
A-1-90	A	1	90	166	393	570	1600
A-2-155	A	2	155	166	393	1200	3356
B-1-90	B	1	90	18.9	28.6	64.0	159.4
C-1-90	C	1	90	14.3	47.0	9.2	41.3
C-1-130	C	1	130	14.3	47.0	20.0	59.0
C-2-155	C	2	155	14.3	47.0	17.2	91.6

Horikoshi Highway Bridge [6]. For this time, wet-joint should work for 1) the bending moment transfer between web and bottom slab, 2) the tension transfer between bottom slabs. Advantages of wet-joint with PBL compared with dry-joint are 1) no piercing reinforced bar needed through PBL hole because Ductal poured in the wet-joint room resists shear force, 2) size accuracy of pre-cast segments is not necessarily required, hence disadvantages are 1) heat curing after casting Ductal is required, 2) construction period is longer than dry-joint on site.

4 Structural verification experiments

4.1 Fundamental experiments of wet-joint with PBL

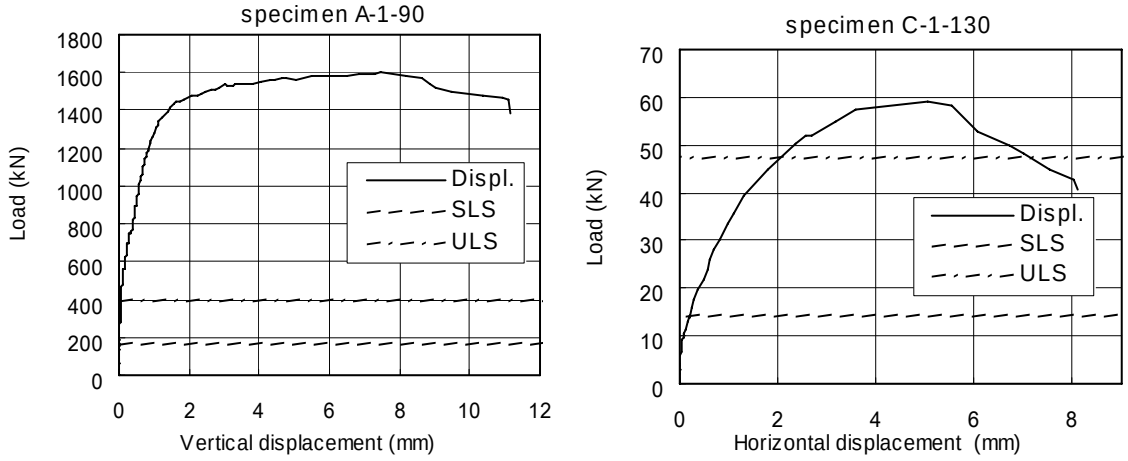

Figure 7: Load-displecement relationships for type-A and C

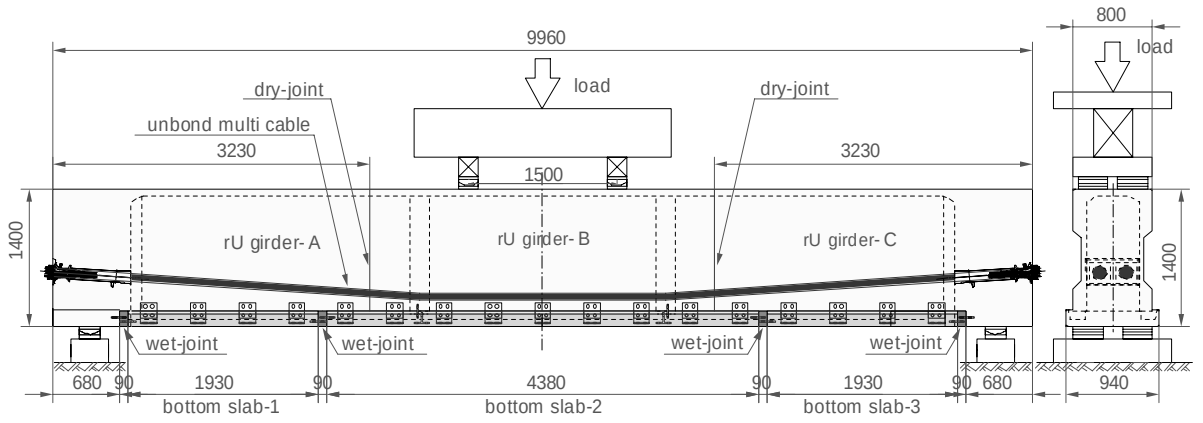

Figure 8: Structural composition and loading set up of a proto-type girder

A series of fundamental experiments of wet-joint was conducted to verify the design method of hole size, thickness and number of PBL. The loading type-A, B, C are assigned for shear force (-A), tension force (-B) and bending moment (-C), respectively as shown in Fig. 6. The modeling for each wet-joint is full scaling for the 40m span monorail girder. Based on the design of PBL, thickness and hole diameter of PBL are determined 19mm and 30mm, respectively. The parameters such as loading type, numbers of PBL and web width and the

corresponding test results are listed on Tab. 2. The design loads for SLS (Level-1 earthquake) and ULS (Level-2 earthquake) on PBL were derived from the results of elastic 3D elastic analysis. The typical load-displacement relationships for loading type-A and C are illustrated in Fig. 7. It is noted that one single PBL with web width 90mm is good enough for loading type-A and B, however web width should be 130mm for loading type-C.

4.2 Fabrication and loading experiment for a 10 m long monorail girder

Most of the modeling parameters of the proto-type 10m long monorail girder such as girder width, combination of joints and pre-cast segments, surface finishing of top slab and sizes of PBL are coincided with the 40m long girder except the total length and the height as shown in Fig. 8. The fabrication process such as production of segments, match casting, dry-joint and wet-joint was conducted and confirmed through the fabrication test using the proto-type girder.

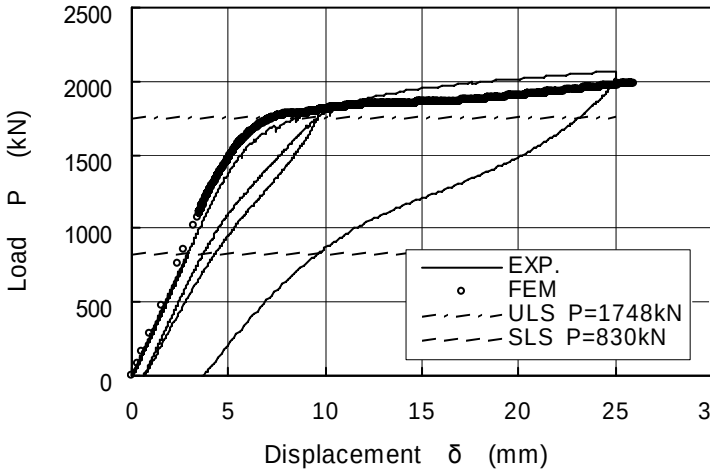

Figure 9: Result of exp. and FEM analysis

The loading set up for the completed proto-type girder was arranged so that both joints could have both bending moment and shear force. The experimental result and 3D-FEM analyses modeling material nonlinearity are indicated in Fig. 9. As the proto-type 10m long girder instead of 40m girder was tested to prove the structural safety, the equivalent loading values were calculated so as to have equivalent forces at joints for SLS and ULS. The loading value P for SLS and ULS became 830 kN and 1748 kN, respectively. It was proved that no initial cracking was observed for SLS and no serious damage for ULS.

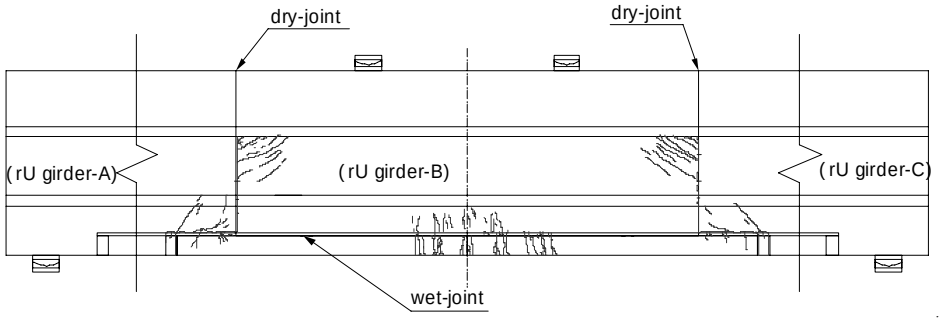

Figure 10: Cracking distribution of a proto-type girder

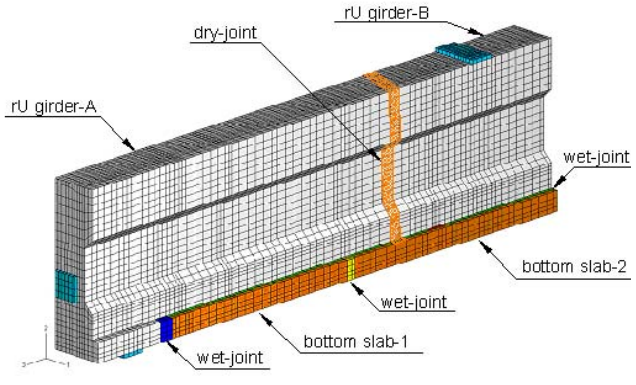

Figure 11: 1/4 axis-symmetric 3D FEM model

The first cracking was observed at the bottom slab of mid-span for the loading value P=1200-1300 kN. At the same time, the first cracking at wet-joint of bottom slab was found. For the loading value P=1700 kN, the diagonal cracks were observed on web. Those diagonal cracks were spreading out both sides around the dry-joint as illustrated in Fig.10. After reaching the ULS loading value P=1748 kN, the load was released and the residual deformation was checked, then it was reloaded up to the maximum load P=2067 kN,

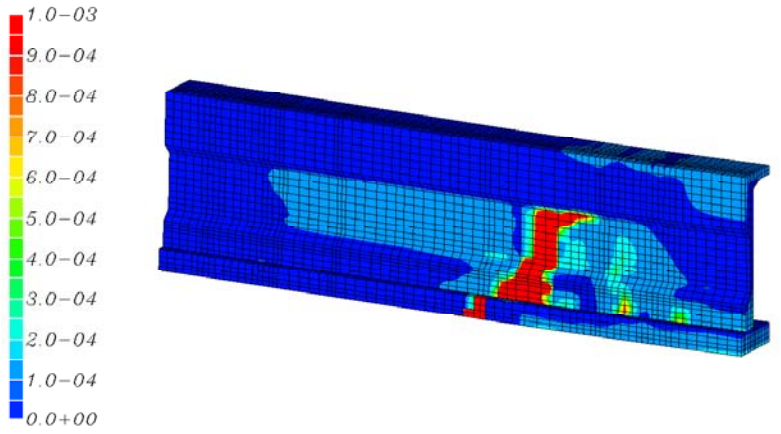

Figure 12: Max. principal strain distribution

The 1/4 axis-symmetric 3 dimensional FEM model of proto-type girder considering the nonlinear behavior such as tension softening shown in Fig. 1 for both Ductal material and joints was made as shown in Fig. 11. The modeling elements are solid element for Ductal, spring element for PBL joints and truss element for exterior cables. The dry-joint was modeled to be non-tension solid elements. The spring stiffness for PBL joints was derived from the fundamental experimental data of the wet-joint. The maximum principal strain distribution for P=1776 kN is illustrated in Fig. 12. It should be noted that the tension strain distribution around the dry-joint is similar to that of cracking observation and the simulation result of load-deformation agrees quite well with the experimental result.

5 Prefabrication of 40 m long monorail girder

Three rU girder segments and three bottom slab segments were manufactured and conveyed to the construction site. Some couples of PBL for wet-joint were in advance set on the form works before casting Ductal. Three bottom segments with PBL were settled on the leveled supporting beams as shown in Fig.13. Three rU girder segments with four adjustable legs were erected on the bottom

Figure 13:
Set up of bottom slabs

Figure 14:
Erection of rU girder segment

segments at 10cm above the final level as illustrated in Fig. 14. After giving a coat of epoxy resin on the matching surface, each rU girder segment was close and contacted firmly each other by traction equipment. The temporary contact pressure on the matching surface was 0.3 N/mm^2 and those dry-jointed segments were set down about 10cm ready to the subsequent wet-joint step. As a wet-joint step, 1) Ductal was placed into the gaps between the web and the bottom slab and the gaps between bottom slabs one and another, 2) heat curing was carried out keeping temperature 60 ^{o}C for 48 hours. After the compressive strength of wet-joint Ductal reaching up to at least 160 N/mm^2, the pre-stressing process has been proceeded supplying the design stresses not only on the dry-joint but also on wet-joint. It should be noted that no gaps were observed on the top slab surface or the side web surface of the dry-joint.

6 Conclusions

This project could have achieved for the first time the railway structure applying Ductal. This monorail girder was successfully completed as a result of structural verification of a series of experiments as well as the functional verification such as accurate configuration of the top slab surface for the rubber wheel running, surface finishing of the top slab to keep designed friction coefficient and receiving and transmission ability of signal loop lines installed inside the girder. Furthermore, the span of this girder is 40m that must be the longest span monorail girder made of concrete material in the world. What we have to step forward as a next step of the project is to develop the transversely connected monorail girders consist of a up line and a down line in order to efficiently resist the severely strong earthquake such as level-2 earthquake.

7 References

[1] Tanaka, Y.; Musya, H.; Ootake, A.; Shimoyama, Y.; Kaneko, O.: Design and Construction of Sakata-Mirai Footbridge using Reactive Powder Concrete. Proc. of 1st fib Congress 2002, Oosaka 2002.

[2] JSCE (Japan Society of Civil Engineers): Recommendations for Design and Construction of Ultra High Strength Fiber Reinforced Concrete Structures-Draft. Sept. 2004.

[3] Tanaka, Y.; Fukuura, N.; Uzawa, T.; Sakamoto, J.; Maehori, S.; Katagiri, M.: Tensile Characteristics and Modeling of Tension Softening Behavior for Ultra High Performance Fiber Reinforced Concrete. Journal of Materials, Concrete Structures and Pavements, JSCE, N0.788/V-67, 159-173, 2005.

[4] Uchida, Y.; Rokugou, K.; Koyanagi, H,: Fracture Mechanical Study of Size Effects of Concrete Flexure Strength. Journal of Materials, Concrete Structures and Pavements, JSCE, No. 442/V-16, 101-107, 1992.

[5] Leonhardt, F.; Andra, W.; Andra, HP.; Harre, W.: Neues, vorteilhaftes Verbundmitted fur Stahlverbund–Trabwerke mit hoher Dauerfestigkeit. Beton und Stahlbetonbau, 325-331,1987.

[6] Tanaka, Y.; Musya, H.; Fukuura, N.; Ooshima, K.: Design of Perfobond Strip Applied for Reactive Powder Concrete Bridge. Proc. of 2nd fib Congress 2006, Naples 2006.

Part 13:

Applications

Vic H. Perry
Vice President & General Manager - Ductal®
Lafarge North America Inc.
Calgary, AB, Canada

Peter J. Seibert
Technical Director - Ductal®
Lafarge North America Inc.
Calgary, AB, Canada

The use of UHPFRC (Ductal®) for bridges in North America: The technology, applications and challenges facing commercialization

Summary

Ductal® is an Ultra-High Performance Fiber Reinforced Concrete (UHPFRC) technology that offers a unique combination of characteristics including ductility, strength and durability, while providing highly moldable products with a quality surface. Compressive strengths reach up to 200 MPa and equivalent flexural strengths reach up to 40 MPa. Use of this technology enables the designer to create thinner sections and longer spans that are lighter, more graceful and innovative in geometry and form, with improved durability and impermeability against corrosion, abrasion and impact.

This paper presents the material, research, design assumptions, prototyping, manufacturing, and erection procedures for specific precast bridge systems and projects. The North American projects covered include precast girders, integral precast beam-deck systems, full-depth precast deck panel systems and others.

Keywords: *abrasion, aesthetics, composite, ductile, durability, fiber-reinforced, impermeability, UHPC, UHPFRC, usage-life, Ductal®.*

1 Introduction

According to the Federal Highway Administration (FHWA) National Bridge Inventory (NBI) Study, approximately 156,000 bridges in the USA are structurally deficient or functionally obsolete(1). State, provincial and municipal engineers are seeking new ways to build better bridges, thereby reducing maintenance costs that are diverted from capital budgets required for building much needed highways and bridges. Therefore, the FHWA launched a program, "The Bridge of the Future", to help drive new solutions for building bridges.

A technology being commercialized to address the problem of deteriorating bridges is a UHPFRC composite ("Ductal®"), which offers superior technical characteristics including ductility, strength, and durability while providing highly moldable products with a high quality surface aspect.

This innovative, unique combination of properties enables designers to create thinner sections and longer spans that are lighter, more graceful and innovative in geometry and form while providing improved durability and impermeability against corrosion, abrasion and impact. Many of the economies gained are a result of engineering new solutions to old problems. The material technology permits it to be used without passive reinforcing (rebar)

and reductions in formwork, labor and maintenance further add to economy. The elimination of rebar improves safety, the reduction of weight speeds construction, and the improved durability reduces maintenance and extends the usage-life.

2 Material Characteristics

This high-strength, ductile material is a formulation of constituent components including portland cement, silica fume, quartz flour, fine silica sand, high-range water reducer, water, and steel or organic fibers. The technology is covered by one of many patents in a range of ultra-high performance concrete, all under the material's trademark[(2)]. Compressive strength for bridge applications ranges up to 200 MPa and equivalent flexural strength ranges up to 40 MPa (see Figure 1).

The high mechanical properties are a result of proportioning the constituent materials to produce a modified compact grading and the fiber geometry (12mm x 0.2mm diameter) to nominal maximum coarse aggregate size of 400 µm. [(3)] Its ductile behavior is a first for concrete, with the capacity to deform and support flexural and tensile loads, even after initial cracking (Figure 1). These performance characteristics are the result of improved micro-structural properties of the mineral matrix, especially toughness and control of the bond between the matrix and the fiber.

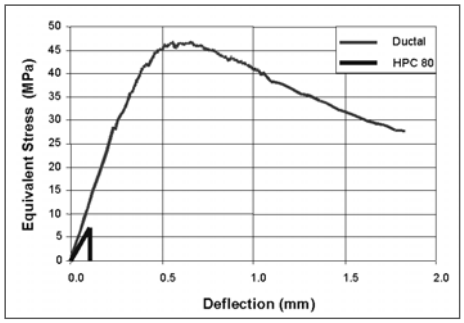

Figure 1: Load-deflection curve for ASTM prisms loaded in 4-point bending.

Table 1: Example of the range of material characteristics for a formulation with steel fibers[(4)]

Strength	Mean Values	Durability	Mean Values
Compressive	150 – 200 MPa	Freeze/thaw (after 300 cycles)	100%
Flexural (equivalent)	25 – 40 MPa	Salt-scaling (loss of residue)	<10 g/m^2
Youngs Modulus (E)	50 – 55 GPa	Abrasion(relative volume loss index)	1.2
Direct Tension	10-15 MPa	Oxygen permeability	<10^{-20}m^2
		CI permeability (total load)	<10
		Carbonation depth	<0.5 mm

The materials are normally supplied to the precaster in three components; premix (pre-blended in bulk-bags), superplasticizer and fibers. It is primarily used in precast applications however it was recently used for a cast-in-place bridge joint application (see "3.2.3").

3 Examples of Bridge Projects Completed

The implementation of new technologies in the bridge sector has proven to be a long journey due to the conservative nature of this segment. Highway bridge engineers, bestowed with guardianship of the public money and safety, have always demonstrated the technology

before using it. One way to introduce a new technology into bridges is to first validate the technology in the pedestrian bridge market where architecture is more of a driver.

3.1 Pedestrian Bridges

3.1.1 Sherbrooke Pedestrian Bridge

The Sherbrooke Pedestrian Bridge (Figure 2) in Quebec, Canada was constructed in 1997 and spans 60 m across the Magog River with a space truss, precasted in 6 segments (10 m each). The top deck is 30 mm thick and the diagonals are formed with leave-in-place stainless steel tubes containing tri-axially confined UHPFRC with post-tensioning.[5] To date, this project has received many accolades and awards, providing an excellent reference for UHPFRC and helping validate the capabilities and performances.

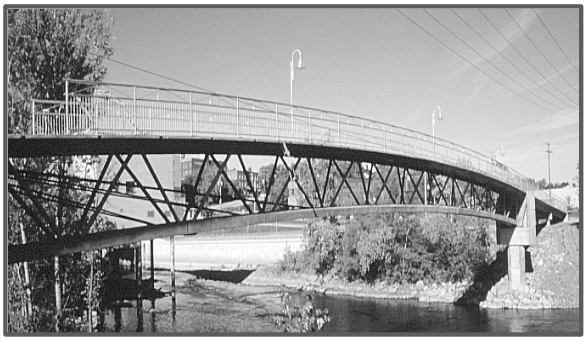

Figure 2: Sherbrooke Bridge

3.1.2 Glenmore/Legsby Pedestrian Bridge

The Glenmore/Legsby Pedestrian Overpass in Calgary, Alberta, Canada (Figure 3), is a single span, 53 m bridge that stretches across 8 lanes of traffic. It consists of two cantilevered, high performance concrete abutments and a drop-in, “T-section” UHPFRC (Ductal®) girder with an arch. The girder is 33.6m long, 1.1m deep at mid-span with a 3.6m wide deck and weighs approximately 100 tons. It is constructed with 13 mm steel fibers and post-tensioned with 42 – 15 mm strands. GFRP (Glass fiber-reinforced plastic) bars were also utilized as a redundant, passive reinforcing system.

Figure 3: Glenmore/Legsby Pedestrian Bridge

The girder required 40 m^3 of material, resulting in the largest, single monolithic pour of Ductal® in the world to date. To ensure proper, efficient mixing, a high shear mixer is recommended. Since the precast facility was only able to mix 1.25 m^3 per batch in a high shear mixer, the entire UHPFRC amount was prepared over a 16 hour batch cycle and poured into 4 ready mix trucks. A specific filling order ensured the same average pot life across the prepared material. The UHPFRC was kept agitated in the trucks, at a low revolution, until ready for casting. The material’s workability and plastic behavior remained consistent throughout the entire agitation and casting period.

This unprecedented, monolithic girder pour was achieved by filling up the stem of the T-section from one end. Random fiber orientation in the deck was ensured by using a concrete bucket the same width as the top flange of the girder. After filling the mould, the top surface was completely enclosed due to the longitudinal curvature and transversal drainage slopes.

After the girder reached an initial strength of 35 MPa, form restraints were released to allow uniform shrinkage and prevent potential cracking during its initial curing process. A detailed study about the shrinkage behavior of this particular girder shape (during initial set) was performed prior casting to ensure uniform setting of the UHPFRC within the controlled curing environment. After the required transfer strength of 100 MPa was reached, the girder was stripped and post-tensioned. Thermal treatment of 90^0C for 48 hours ensured the required design strength and durability.

Before the girder was placed into service, the owner (The City of Calgary) required completion of two simply-supported tests. In these tests, 0.9* 1.7* (service load) was first concentrically and uniformly applied over the entire girder slab and then eccentrically applied over half of the slab. The test results indicated displacements smaller than predicted and the girder fully recovered upon load removal, indicating no inelastic behavior[6]. The increased stiffness was attributed to an actual higher E-Modulus compared to theoretical. Finally, the girder was installed using two cranes at both abutment ends and lifted into position during the night to minimize traffic disruption (Figure 4).

Figure 4: Girder during night erection.

3.2 Highway Bridges

While the introduction of this technology has proceeded much faster in pedestrian bridges compared to highway bridges, there have been highway-bridge projects constructed.

3.2.1 Wapello County Bridge

In 2006, after more than 4 years of collaborative R&D between the FHWA, the Iowa Department of Transportation, Iowa State University and Lafarge North America, the first UHPFRC highway bridge in North America was completed in Wapello County, Iowa. Although a simple, single-span bridge with a 3-beam cross section, this project provides a significant step towards "*The Bridge of the Future*", utilizing three 33.5 m UHPFRC girders that do not have any rebar for shear stirrups (Figure 5). The beams were cast at a Lafarge precast plant in Winnipeg, Canada and then transported to the site in Iowa.

Full scale laboratory and in-situ load testing was conducted by Iowa State University, Ames, IA, USA. Laboratory testing covered load-deflection testing of the 23 m girder for both bending and shear. In-situ testing utilized a moving truck train to simulate traffic live loads. All tests validated a load deflection result better than the design values. (7)

Figure 5: Transportation and erection of girders.

3.2.2 Pi-Girders

Ongoing R & D at FHWA demonstrates the use of UHPFRC for bridges, generates comparative case studies, validates designs without rebar and gives confidence to state/provincial transportation engineers. The ultimate goal is to build highway bridges utilizing shapes that are optimized for the material characteristics, such as the pi-girder (at FHWA's lab). The girder includes a UHPFRC deck without rebar, thereby removing the source of problems (corroding rebar) with today's highway bridges. Collaborative work at MIT led to development of a pi-girder profile for a typical 2-lane, 2-span highway bridge, which represents nearly 75% of bridges built on the USA interstate highways (Figure 6).

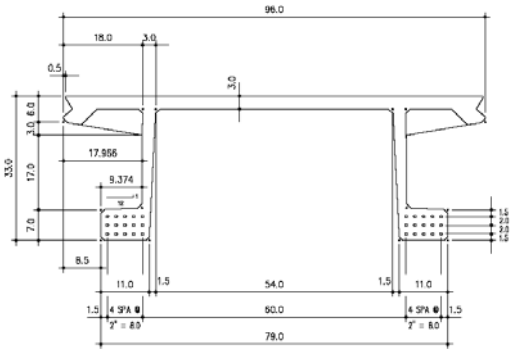

Figure 6: Pi-Girder Shape

This pi-girder was designed based on the AASHTO LRFD Bridge design specifications to carry the HL-93 load configurations. This 0.84 m overall deep pi-girder section is designed to span up to 33 m, with a 75 mm thick unreinforced integral deck. (8) In 2003, the FHWA initiated the manufacture of pi-girders (Figure 7) to be installed in a test track for long-term testing and full destructive testing at the FHWA Turner-Fairbank laboratory.

Next steps in the development of the optimized pi-girder involve installation of the girders in a demonstration project in Buchanan County, Iowa, USA. The project is currently in final design stages with a planned 2008 construction.

Figure 7: Manufactured pi-girder.

3.2.3 Rainy Lake – CN Rail Overhead Bridge

The original CN Overhead Bridge was constructed in 1962 on Ontario Highway 11 over the Canadian National rail lines near Rainy Lake, Ontario, Canada. The existing bridge deck had reached its useful life and in need of major reconstruction. A staged method of construction was utilized to maintain one lane of traffic during deck reconstruction.

The material supplier, consultant and owner worked together to develop an innovative solution for reconstructing the bridge deck.[9] The existing deck was removed transversely, one half at a time, while maintaining full traffic volume and replaced with a new precast deck panel system (one lane at a time). The new, reinforced deck panels were manufactured with 35 MPa concrete. GFRP bars were selected as top slab reinforcing to eliminate corrosion of rebar when exposed to deicing salts.

A challenge facing highway authorities is durability of the joints due to constant flexing from truckloads and corrosion from salt of the rebar crossing the joints. Design for this project focused on balancing a joint detail that provided deck continuity for loads, minimized traffic disruption, speed of construction and long-term durability. Regardless of materials used, shrinkage across the joint is a potential problem that results in a joint interface between the panel and joint fill; an area for the ingress of salts. To minimize corrosion potential, a non-corrosive rebar (GFRP) was used in the top mat and joint size was minimized to provide the least possible shrinkage across the joint. Minimizing joint size also reduced the quantity of jointing material required and simplified precast panel manufacturing (Figure 8).

The JS1000 Ductal® joint fill material utilized has superior freeze/thaw resistance, extremely low porosity, improved flexural strength and superior toughness, which provides improved resistance to climatic conditions and continuous flexing from truck loadings across the joints.

Once all panels were installed, leveled and tested for water tightness, the joints were filled with the UHPFRC material. Two in-field mixers were used in parallel, alternating to provide for batching and placing in a continuous basis. The self-leveling material was then covered with form grade plywood to protect against moisture loss. After a 4-day field cure, the UHPFRC material was ground smooth in the area of any high spots. Traffic was transferred onto the new precast deck and the second phase was reconstructed with the same system. Then, a waterproof membrane and asphalt overlay were placed on the entire new deck surface.

Figure 8: Joints ready for filling

4 4 Other Potential Uses For Bridges

To date, the use of this technology in bridges has introduced the material to engineers and enabled officials to visualize some of the benefits. The removal of passive reinforcing steel provides significant flexibility for designing innovative, more refined shapes and eliminates the basic weakness with reinforced concrete decks that eventually leads to failure of the deck. This technology can significantly alter the way bridge decks are constructed.

For pedestrian bridges, this technology provides architects and engineers with significant freedom to design new, innovative shapes that were not possible before. For highway bridges, two other promising uses of this technology include full depth precast deck panels and; leave-in-place thin deck forms in steel-free bridge decks.

Several academic and commercial groups in the USA and Canada are currently developing a full-depth, waffle precast deck panel that integrates the concepts from the Rainy Lake UHPFRC joint fill project. A 200 mm thick waffle panel, with 2-way ribs at 600 mm c/c, reinforced with GFRP and tied together with 200 mm x 200 mm field-cast joints of Ductal® JS1000, provides a full continuity of the deck slab.

5 Codes, Standards and Design Guides

One challenge facing highway bridge engineers today is how to design bridges with this technology when the current North American design codes/standards do not provide design guidance for materials with ultra-high mechanical properties. However, there has been progress by several groups in recent years to develop interim design guides to assist engineers. Working groups in France [10], Japan and Australia[11] have developed Interim Design Guidelines for UHPFRC.

In the USA, R&D started at MIT in 1999, in parallel with work at the FHWA in 2000 has supported the potential use of UHPFRC for bridges. In 2002 the FHWA engaged MIT to prepare a study on the optimization of UHPFRC for highway bridges. This collaboration lead to the release of a civil engineering report CEE Report R03-01 entitled “Model-Based Optimization of Ultra-High Performance Concrete Highway Bridge Girders.[12] In 2006, the FHWA published reports on the material property characterization of UHPFRC[13] and the structural behavior of UHPFRC prestressed I-Girders[14]. In Canada, the newly published design manual by CPCI (Canadian Precast/Prestressed Concrete Institute) discusses the uses and properties of UHPFRC[15].

6 Challenges

The applications and projects completed with this technology to date demonstrate that the manner in which the material is used is different than current uses of concrete, steel and other materials. The challenge ahead is to have adopted local design codes and find the optimized shapes for each use. When these shapes are determined, precasters, manufacturers and contractors can invest in the formworks required and the true economics (of these systems) will eventually bring value to the highway users in the standard mass production of optimized shapes.

7 Conclusion

The material's combination of properties (strength, durability, ductility, aesthetics and design flexibility) facilitates architects' and engineers' abilities to create new optimized shapes for bridge construction. It offers solutions with advantages including speed of construction, improved aesthetics, superior durability and impermeability against corrosion, abrasion and impact -- which translates to reduced maintenance and a longer life span for the structure.

Several projects presented are the first use of this material technology for bridges. While these examples demonstrate many potential benefits, it is apparent that the true benefits are not yet fully recognized or realized. The optimized profiles and use of the material technology is still in the early stages of commercialization and, in the next few years, much progress is anticipated in the area of optimized solutions and design standards. Further project developments with this technology in other market segments will demonstrate and validate its value.

8 References

[1] FHWA, National Bridge Inventory Study, 2005, http://www.tfhrc.gov/structur/ltbp.htm

[2] U.S. Patent Office: 5, 503, 670 and 5, 522, 926.

[3] Acker, P., and Behloul, M., 'Ductal® Technology: A Large Spectrum of Properties, A Wide Range of Applications', FIB Symposium, Avignon, France, April 2004.

[4] Lafarge North America Inc., "Technical Characteristics: UHPC with Metallic Fibers", www.imagineductal.com.

[5] Behloul, M., et al. 'The Sherbrooke Footbridge: The First Reactive Powder Concrete Structure', Structural Engineering International February 1998, 140-144.

[6] Parsekian, G.A., et, al, "Full-Scale Testing of a Ductal UHPFRP Footbridge" – in progress; to be published.

[7] Moore, B., and Bierwagen, D., "Ultra-High Performance Concrete Highway Bridge", PCA, 2006.

[8] Graybeal, B. A., 'Fabrication of An Optimized UHPC Bridge', PCI National Bridge Conference, Atlanta, GA, USA, October 2004.

[9] Perry, V.H., P. Scalzo and Gary Weiss, Innovative Field Cast UHPC Joints for Precast Deck Panel Bridge Superstructures - CN Overhead Bridge at Rainy Lake, Ontario

[10] AFGC (Association Francaise de Genie Civil) Interim Recommendations 'Ultra-High performance, Fiber-Reinforced Concretes', AFGC Publication, France, January 2002.

[11] Gowripalan, N., and Gilbert, R.I., "Design Guidelines for RPC Prestressed Concrete Beams".

[12] CEE Report R03-01, 'Model-Based Optimization of Ultra-High Performance Concrete Highway Bridge Girders' (MIT/FHWA), March 2003.

[13] "Material Property Characterization of Ultra-High Performance Concrete Prestressed I-Girders", U.S. Dept. of Transportation - Federal Highways Administration (Publication No. FHWA-HRT-06-103), August, 2006

[14] Structural Behaviour of Ultra-High Performance Concrete Prestressed I-Girders", U.S. Dept. of Transportation - Federal Highways Administration (Publication No. FHWA-HRT-06-115), August, 2006.

[15] CPCI Design Manual, 4th Edition, 2007.

Husham Almansour
Research Associate
Institute for Research in Construction
National Research Council Canada
Ottawa, Ontario, Canada

Zoubir Lounis
Senior Research Officer & Group Leader
Institute for Research in Construction
National Research Council Canada
Ottawa, Ontario, Canada

Structural Performance of Precast Prestressed Bridge Girders Built with Ultra High Performance Concrete

Summary

With its very high strength, high modulus and very low permeability, ultra high performance concrete (UHPC) can provide major improvements over conventional high performance concrete (HPC) in terms of structural efficiency, durability and cost-effectiveness if used in the construction of slab-on-precast prestressed girder bridges. In this study, the optimum use of UHPC is evaluated for the case of simply supported cast in place concrete slab on precast/prestressed UHPC girder bridges. These bridges are designed according to the Canadian Highway Bridge Design Code requirements, including no cracking at the serviceability limit state. The design of superstructure is achieved through an iterative procedure. The stress distributions and stress concentration zones in the girders under dead loads and traffic loads are investigated. The required number of girders, girder size, and area of prestressing steel are optimized to achieve minimum weight of superstructure. The results show that the use of UHPC enables a significant reduction in the volume of concrete girders from 49% to 65% and a significant reduction in the overall superstructure weight by 32% when compared to HPC bridges.

Keywords: *Ultra-high performance concrete, precast/prestressed bridge girder, finite element modeling, limit states design*

1 Introduction

In the last four decades, there was a considerable growth in the use of high strength/high performance concrete (HSC/HPC) in highway bridges. Simply supported slab-on-precast bridge girders is one the most common forms of structural systems used for the construction of highway bridges in North America. However, the benefits of using HSC/HSC to extend the span length or reduce the weight of simply supported precast girder bridge systems reach a limit at about 50 MPa, beyond which there is only marginal improvement as the governing design criterion is the condition of no cracking at service, (i.e. fully prestressed girders) [1,2]. Ultra high performance concrete (UHPC) represents a major development step over HPC, through the achievement of very high strength and very low permeability. The compressive strength of UHPC varies from 120 to 400 MPa, its tensile strength varies from 10 to 30 MPa, and the modulus of elasticity is in the range of 60 – 100 GPa [3,4].

A growing number of bridges are being designed and built using UHPC in Europe [5] and United States [6] and opened to traffic recently. However, no comprehensive structural evaluation or design methodology for this type of construction has been developed yet. The first UHPC highway bridge [5] was designed and constructed in France and opened to traffic in 2001 with two simply supported spans of 22 m each. At the same time, another UHPC bridge [6] was constructed in Italy with a span of 11.8 m. More recently, a 33.8 m span UHPC bridge was designed and constructed in Iowa and opened to traffic in late 2005 [7].

The only available design guidelines for UHPC structures are the French recommendations, AFGC-IR-02 [8]. These recommendations provide modifications to the existing French design standards for reinforced and prestressed concrete structures. However, it does not provide detailed design recommendations for highway bridge structures. Hence, there is an urgent need to develop a procedure for the design of UHPC bridges according to the Canadian Highway Bridge Design Code (CHBDC-06) [10] and using the available standard Canadian Prestressed Concrete Institute (CPCI) [9] precast/prestressed I-girder sections.
The objective of this paper is to evaluate the structural efficiency of UHPC when used in precast/prestressed girder bridges in terms of reducing the number of required girders and/or size of girders when compared to conventional HPC precast bridge girders.

2 Design of Slab-on- UHPC Girder Bridge Superstructure

In order to illustrate the benefits and efficiency of UHPC bridge girders, a comparative study of the design UHPC and HPC girder bridges is undertaken. Two simply supported bridge superstructures are considered in this study, namely: (i) a typical cast in place concrete slab on precast/prestressed (PC) HPC girders bridge; and (ii) a typical cast in place concrete slab on PC UHPC girders. The total width of the bridge including the barrier walls is 12.45 m and its span length is 45 m. The slab thickness for both bridges is 175 mm, which corresponds to the minimum slab thickness allowed in the Canadian Highway Bridge Design Code.

The traffic load and bridge design comply with all Serviceability and Ultimate Limit States (SLS and ULS) requirements of CHBDC-06. Two types of live loads are applied on the deck surface, the lane loading and a single moving truck. The direction of the movement is reversed between different design lanes. For multi-lane loading, modification factors of 0.9 and 0.8 are applied for two lanes and three lanes, respectively. For the Ultimate Limit States (ULS), the magnification factors for the dead and traffic loads are 1.2 and 1.7, respectively. The material reduction factors are 0.75 and 0.95 for precast concrete and prestressing steel, respectively. At each section, it is ensured that the factored moment and shear force are less or equal to the factored flexural resistance and shear resistance, respectively.

2.1 Design requirements and procedure

In this study, the bridge is designed in accordance with CHBDC-06 regarding the live load model and load factors, however, the resistance factors for UHPC at ULS are conservatively adjusted by referring the AFGC-IR-02 recommendations. The iterative design procedure for the UHPC bridge used in this study is illustrated in Fig.1. As indicated in Fig.1, once the initial

feasible superstructure design is determined, a refined analysis is performed using a linear elastic finite element model to check its adequacy. At this stage, the detailed stress distribution is examined to identify the zones of maximum stresses to optimize the girder section and prestressing steel area and layout.

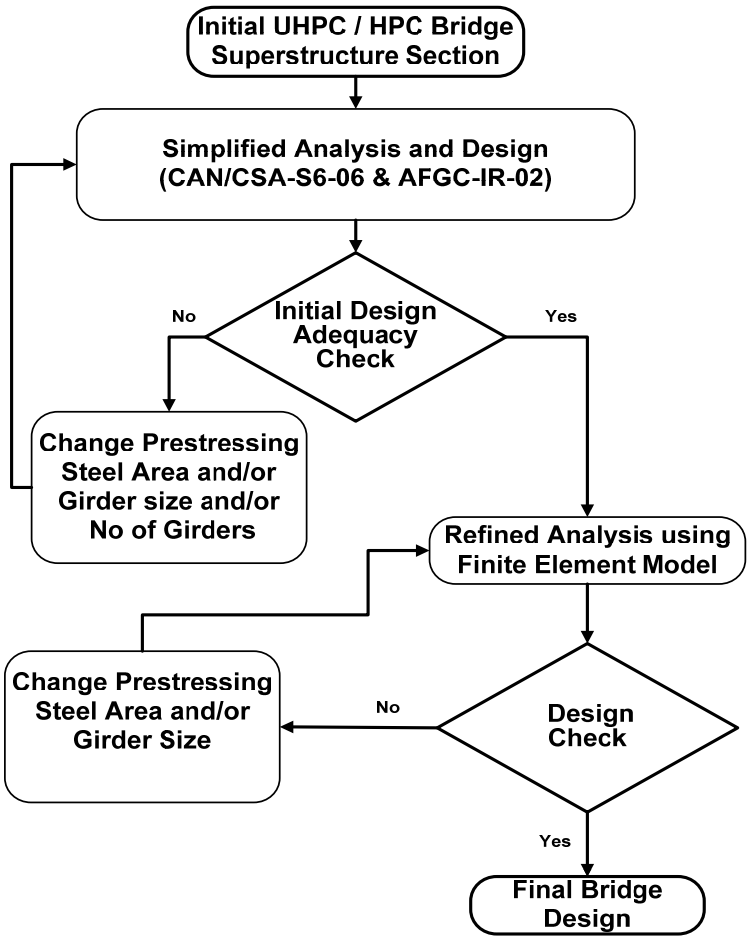

Figure 1: Design Procedure for UHPC and HPC Bridges

2.2 Prestressing system for HPC and UHPC girders

The selected prestressing are low-relaxation strands, size 13, Grade 1860, with nominal diameter of 12.7 mm and nominal area of 98.7 mm^2 and tensile strength (f_{pu}) of 1860 MPa. CHBDC-06 limits the minimum effective stress in tendons to 0.45 f_{pu}, the maximum stress at jacking is limited to 0.78 f_{pu}; the maximum tensile stress at transfer to 0.74 f_{pu}; and the maximum stress at ultimate to 0.95 f_{pu} The total prestress losses are estimated to be 16.9% of the tendon strength. The tendons for the HPC and UHPC girders are arranged in straight and conventional deflected strand pattern groups. The straight tendons provide 50% to 60% of the total prestressing steel area, depending on the maximum stresses in the girder. There was no need to debond the strands near supports as the tensile stresses remained below the allowable value.

2.3 HPC Bridge girder design

It is found that five CPCI-1600 girders are adequate for the 45 m span length (Fig. 2-a). The corresponding girder spacing is 2.5 m and the length of the cantilever slab is 1.225 m on each side. The HPC used for the girders has a compressive strength ($f_c^{'}$) of 40 MPa; initial compressive strength ($f_{ci}^{'}$) of 30 MPa, and a modulus of elasticity of 29.3 GPa. The slab is made of normal concrete with ($f_c^{'}$) of 30 MPa and a modulus of elasticity of 25.6 GPa. The cracking strength of HPC is $0.4\sqrt{f_c^{'}}$. At transfer and during construction, the allowable compression stress is $0.6f_{ci}^{'}$ and the limit for tensile stress is $0.5\,f_{cri}$, where f_{cri} is equal to $0.4\sqrt{f_{ci}^{'}}$ [10]. In the present study, the bridge is designed for no cracking at SLS. The deflection of the bridge for superstructure vibration control is checked in accordance to Cl. 3.4.4 of CHBDC-06 [10]. The main properties of all investigated CPCI sections are summarized in Table 1.

Table 1: Properties of Investigated Standard CPCI I-Sections [9]

CPCI Girder	A (m^2)	I (m^4)	S_t (m^3)	S_b (m^3)	A: cross sectional area, I : moment of inertia, S_t and S_b: section modulus with regard to top and bottom fibers, respectively
900	0.218	0.0193	0.0384	0.0486	
1200	0.320	0.0539	0.0800	0.1023	
1600	0.499	0.1747	0.2166	0.2202	

2.4 UHPC Bridge girder design

It is found that only four girders are needed for the UHPC bridge design (Fig. 2-b). The two smallest CPCI girders are the CPCI 900 and CPCI 1200, which are selected in order to investigate their structural efficiency for use with UHPC. Accordingly, the girder spacing is 3.3 m and the side cantilever slabs of the deck are 1.275 m each. The UHPC used has a compressive strength (f'_c) of 175 MPa and a modulus of elasticity of 64.0 GPa. The slab is made of normal concrete with a compressive strength of 30 MPa and a modulus of elasticity of 25.6 GPa. The allowable tensile strength of UHPC at (SLS) is taken conservatively as $f_t = 0.4\sqrt{f_c^{'}}$ [13].

At transfer and during construction, the compressive strength is taken as $f_{ci}^{'} = 105\,MPa$. The allowable compressive stress is $0.6f_{ci}^{'}$. The limit for tensile stress is $0.6f_{cri}$, where f_{cri} is taken conservatively as $f_{cri} = 0.4\sqrt{f_{ci}^{'}}$. In the present study, the bridge is designed for no cracking at SLS. The deflection of the bridge for superstructure vibration is also checked in accordance with CHBDC-06. On the other hand, the ultimate compressive strength is given as $f_{cu} = 0.64\,f_c^{'}$ and the ultimate strain in 3% [8,13].

At each section, it is ensured that the factored moment and shear are less or equal to the factored flexural and shear resistances, respectively. To ensure a ductile failure at ultimate limit state (ULS), the compressive stresses in the concrete and the tensile stresses in the

prestressing steel are kept below the ultimate limit values, respectively, while the strain in prestressing steel is well beyond the yield strain.

The ultimate shear strength V_u consists of three major components: (i) the concrete contribution, V_c; (ii) the shear reinforcement contribution, V_s; and (iii) the prestressing reinforcement contribution through the effective prestressing force component in the direction of applied shear, V_p. For UHPC, the concrete contribution is calculated using AFGC-IR-02 Cl 7.3,21, which consists of two components: (a) the concrete contribution, $V_{Rc} = 0.16\sqrt{f_{cj}}b_0 z$, where b_0 is the web width and z is the effective depth, and (b) the fiber contribution V_f, which is given in [8]. The shear strength of the UHPC girder is found to be sufficient to resist the applied shear force, however, minimum shear reinforcement should be provided in the critical shear zones to increase the safety against shear failure.

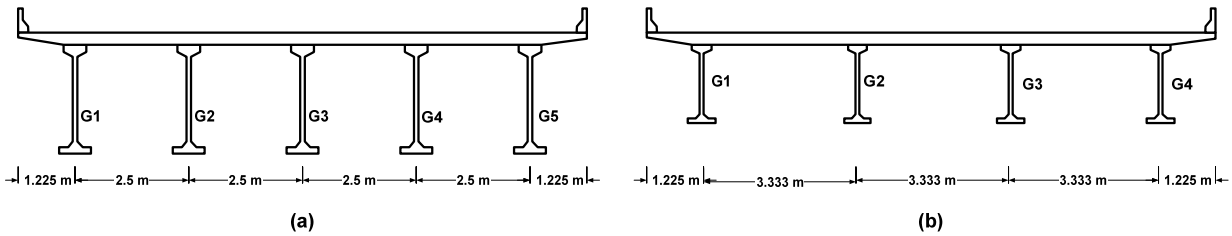

Figure 2: Slab-on Precast/Prestressed Girders Bridge: (a) HPC, (b) UHPC

3 Refined analysis using finite element method

3.1 Three dimensional finite element modeling

A linear elastic three-dimensional (3-D) finite element model (FEM) is used to determine the stress distribution in all girders that make up the two investigated bridges. This 3-D FEM model enabled a more accurate prediction of the stresses in all girders than the simplified analysis approach of the code used in the initial step. Both the deck slab and girders are modeled using shell elements, while the prestressing tendons are modeled using cable elements. The prestressing losses, deformations and relaxation are accounted in the model.

3.2 Results and discussions

The FEM results indicate that the maximum stresses are found in the central girders for both HPC and UHPC for the case of two lanes loading. On the other hand, the maximum stresses are found in the external girders for the case of three-lanes loading. In general, the results show that the maximum stresses for the three-lane loading case are less critical than those of the two lane loading case.

The FEM model enables predicting the stresses in every girder of the bridge and then optimize the prestressing steel ratio, R_{ps}, which represents the ratio of the prestressing steel area to the concrete area of the girder. Figure 3 shows the variations of the stresses at the top fiber of different girders centerline cross-section of HPC and UHPC bridges with R_{ps} at SLS. Five CPCI-1600 girders are used for the HPC bridge, while only four CPCI-1200 are used for the UHPC. Figure 3 shows that the most critical girders are the central girder (G3)

for the HPC bridge and the internal girder (G2 or G3) for the UHPC bridge. The optimum R_{ps} is found when the critical stresses are equal to the SLS limit for the tensile stresses in concrete. Figure 4 shows that the compressive stresses at ULS in the top fibers of the critical girders identified above are well below the ultimate stress level for both HPC and UHPC girders, while the strain in prestressing steel is well beyond the yield strain. The static deflection at SLS is found to be below (L/400) for CPCI-900 and below (L/500). Figures 3 and 4 demonstrate that the SLS requirements are controlling the design, while the strain in prestressing steel is well beyond the yield strain.

For all loading cases and all girders, the maximum stress zones had been identified, which are similar to HPC (for the four conventional zones at the support and mid-span sections) in addition to a zone that appears near the bottom transition area from the girder web and bottom flange near the support, which is not captured by the simplified analysis approach. In most of the cases, the concrete in this zone is subjected to compressive stresses that are higher than those at the support.. Experimental tests [11] have identified a crushing failure mode in the same zone. The stresses at the top of the support zone of the HPC bridge fluctuate between compression and tension following a slight change in the prestressing steel ratio. For the UHPC bridge, the compressive stresses in all maximum stress zones vary quasi-linearly with the prestressing steel ratio. The maximum tensile stresses at the bottom of the midspan zone exhibit linear relationships with R_{ps}. The preliminary bridge design and stress analysis show that the maximum feasible eccentricity of the conventional deflected tendons at the support section is needed for the UHPC girders.

A comparison of the results for CPCI 1200 and CPCI 900 shows that the stresses in the CPCI 1200 girder are relatively low and this section represents a conservative choice. On the other hand, all compressive stresses in the CPCI 900 girder are below $0.45f_c^{'}$ at SLS and below $0.64f_c^{'}$ at ULS, while the tensile stress at the bottom fiber of the mid-span is at its allowable limit and thus controls the design. Consequently, the prestressing area ratio needed to satisfy the non-cracking requirement is relatively high. A comparison between the two sections indicates that a more efficient section could be developed that falls between CPCI-900 and CPCI 1200.

4 Comparison of materials consumption in UHPC and HPC Bridges

As mentioned earlier, the use of UHPC enables a considerable reduction in the concrete volume of up to 49% for the CPCI 1200 and 65% for CPCI 900.The weight of the girders per unit area of the bridge deck are 0.481 tons/m^2 for HPC bridge, 0.196 tons/m^2 for UHPC – CPCI 900 girders, and 0.288 tons/m^2 for UHPC –CPCI 1200 girders. The total weight per unit area of the superstructure, including the deck slab are 0.901 tons/m^2 for HPC, 0.616 tons/m^2 for UHPC–CPCI 900 girders. Consequently, UHPC results in 32% reduction in the total weight of the superstructure and 59.3% reduction in the girders weight. The prestressing steel area required for CPCI 900 section is 39% higher than that for CPCI 1600, which is only

14% higher than that for the UHPC-CPCI 1200. It is clear that a reduction in the weight of the superstructure will lead to a reduced size of the substructure (piers and abutments) and foundations and reduced overall cost of the bridge. Furthermore, a reduction in the concrete consumption will have considerable environmental benefits through the reduction of energy consumption and greenhouse gas emission (GHG) associated with the production of cement, extraction and transportation to the construction site of raw materials [12].

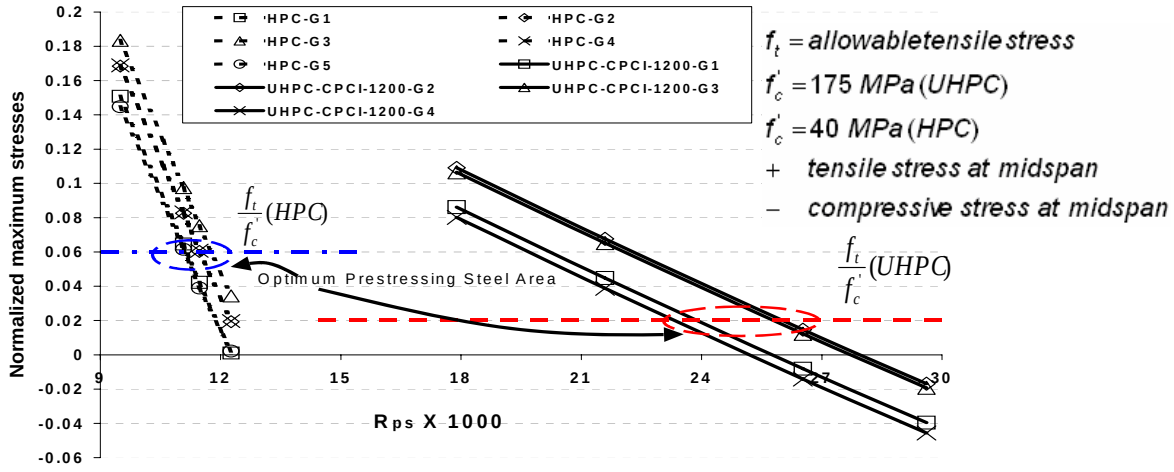

Figure 3: Variation of maximum SLS stresses with prestressing steel ratio for all girders

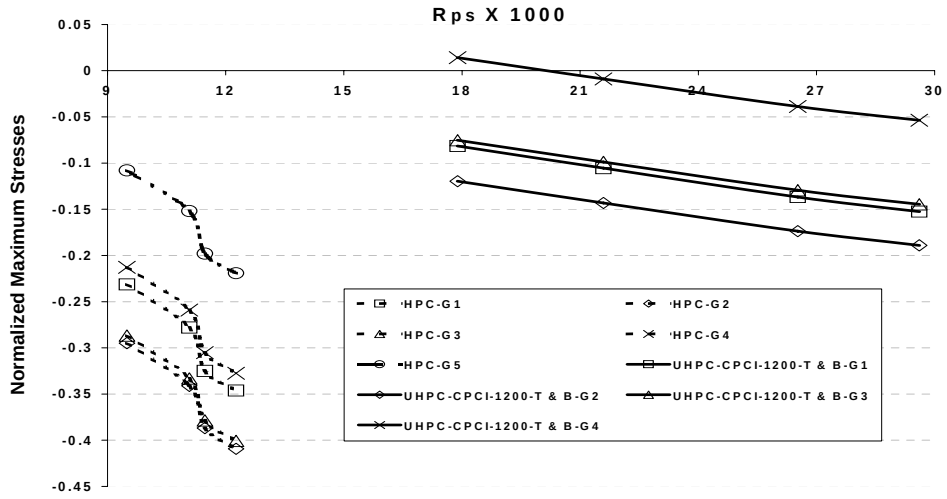

Figure 4: Variation of maximum ULS stresses with prestressing steel ratio for all girders

5 Conclusions

The use of UHPC in precast/prestressed concrete girders enables significant reductions in the number of girders and girder size when compared to conventional HPC bridge girders. It can also enable longer spans without further increase in the girder size. This study shows that UHPC yields a considerable reduction in the concrete volume from 48.7% to 65%. The finite element model shows that the stress distributions in the UHPC bridge girders yield

patterns similar to those of the HPC bridge girders. The stress distribution in the girder and the regions of stress concentration do not agree perfectly with the results obtained using the simplified load distribution method of CHBDC-06. Further investigations are needed to develop a simplified approach capable to accurately capture the extreme stresses in UHPC bridges.

A comparison between the two UHPC examined sections shows that an optimum section can be developed that is between CPCI-900 and CPCI 1200 can be achieved by increasing the section modulus. This would improve the girder capacity without adding higher concrete weight.

6 References

[1] Lounis, Z., and Cohn, M.Z., “Optimization of Precast Prestressed Bridge Girder Systems”, PCI Journal, V. 38, No. 4, 1993, pp 60-77.

[2] Lounis, Z., and Mirza, M.S., “High Strength Concrete in Spliced Prestressed Concrete Bridge girders.” Proc. of PCI/FHWA Int. Symp. on High Performance Concrete, 1997, pp.39-59.

[3] Acker, P., and Behloul, M., “ Ductal® Technology: A Large Spectrum of Properties, A Wide Range of Application”, Proc. of the Int. Symp. on UHPC Kassel, Germany, 2004, pp.11-23.

[4] Buitelaar, P., “Heavy Reinforced Ultra High Performance Concrete”, Proceedings of the Int. Symp. on UHPC, Kassel, Germany, September 13-15, 2004, pp.25-35.

[5] Hajar, Z., Lecointre, D., Simon, A., and Petitjean, J. “Design and Construction of the World First Ultra-High Performance Concrete Road Bridges”, Proceedings of the Int. Symp. on UHPC, Kassel, Germany, September 13-15, 2004, pp.39-48.

[6] Meda, A., Rosati, G., “Design and Construction of a Bridge in Very High Performance Fiber Reinforced Concrete”, Journal of Bridge Engineering, Vol. 8, No. 5, 2003, pp.281-287.

[7] Bierwagen, D., and Abu-Hawash, A., “Ultra High Performance Concrete Highway Bridge”, Proc. of the 2005 Mid-Continent Transportation Research Symposium, Ames, Iowa, 2005, pp.1-14.

[8] AFGC Groupe de travail BFFUP, “Ultra High Performance Fiber-Reinforced Concretes: Interim Recommendations”, Scientific and Technical Committee, Association Française de Genie Civil, 2002.

[9] Canadian Prestressed Concrete Institute, “Design Manual, Precast and Prestressed Concrete”, Third Edition, 1996.

[10] Canadian Standards Association, CAN/CSA-S6-06, “ Canadian Highway Bridge Design Code”, 2006.

[11] U.S. Department of Transportation, Federal Highway Administration, “ Structural Behavior of UHPC Prestressed I-Girders”, Publication No. FHWA-HRT-06-115, 2006.

[12] Daigle, L., and Lounis, Z., “Life Cycle Cost Analysis of HPC Bridges Considering their Environmental Impact”, Proc. of INFRA 2006, Quebec City, pp. 1-17.

[13] Almansour,H, Lounis, Z., “ Innovative Precast Bridge Superstructure Using Ultra High Performance Concrete Girders“, Proc. of PCI 53rd National Bridge Conference, 2007.

Bendt Aarup
manager
CRC Technology
Hjallerup, Denmark

CRC – Structural Applications of Ultra High Performance Fibre Reinforced Concrete

Summary

CRC (Compact Reinforced Composite) is the designation for a special type of fibre reinforced concrete with high strength (150-400 MPa) developed in 1986. CRC is used with a combination of steel fibres and conventional rebars. CRC structural elements are typically quite slender and some of the properties necessary to achieve this are briefly discussed. Since 1993 CRC has been used in a number of structural applications in Denmark - typically for precast elements such as balcony slabs and staircases, however, applications are still limited in other countries. A few examples of applications are presented and some of the difficulties in starting up a new product in the market are discussed.

Keywords: *ultra high performance, steel fibres, applications*

1 Introduction

High Strength or High Performance Concretes (HSC or HPC) have been in use for a number of years now for a range of structural applications, and standards in a number of countries are being revised to accommodate these improved materials. The use of these materials is not without problems, however, as HSC – in addition to the higher strength - is often also more brittle than conventional concrete. This problem of brittleness can be solved in various ways, e.g. improvement in ductility can be provided by fibre reinforcement.

Fibre Reinforced Concretes (FRC) have mostly been used in non-structural applications such as slabs-on-grade, floors and architectural concrete, but recently a new generation of concretes has been developed that combines fibre reinforcement and ultra high performance. CRC was the first of these concretes [1], but others include Ductal and BSI [2,3].

Compact Reinforced Composite (CRC), which was developed at the Cement & Concrete Laboratory of Aalborg Portland in 1986, combines large contents of fibres (2-6 vol.%) and conventional reinforcing bars. An example of a typical application – cantilevered balcony slabs – is shown in fig. 1.

Figure 1: Cantilevered balcony slabs in CRC.

2 CRC properties

CRC is the designation for a special type of Fibre Reinforced High Performance Concrete (FRHPC) with high strength (140-400 MPa). The matrix has a very large content of microsilica and water/binder ratios of 0.16 or lower. Because of a large content of steel fibres the matrix is very ductile and that makes it possible to utilise rebars much more effectively without having large cracks under service conditions. Properties vary with fibre content and the type of aggregate used. For most applications a typical quartz sand and curing at ambient temperatures is used giving a compressive strength around 150 MPa and making it possible to produce CRC with conventional production methods. For higher strength it is necessary to use special aggregates such as bauxite and if combined with heat curing strength can be as high as 400 MPa. The size of the fibres and the largest grains of the matrix dictate the distance between reinforcing bars and the cover layer to the reinforcement, both of which have to be optimised in the slender structures, which can be produced with CRC. This is the reason for typically using a mortar composition for CRC and for using fibres with a length of 12 mm and a diameter of 0.4 mm. In most applications a cover layer of 15 mm is used.

With the high fibre contents, CRC is especially suitable for precast applications, but in-situ cast concrete with 6% by volume of fibres has also been produced - for joints between

elements made in conventional concrete - using a poker vibrator for compaction [4,5]. In most precast applications fibre contents will be from 2 to 4 vol.% (from 150 to 300 kg/m^3).

Figure 2: Spiral staircase in CRC.

As recommendations that take the properties of FRHPC into account have only recently been introduced [6] – and were certanly not around in the late 1980's when CRC was developed - it has been necessary to provide extensive documentation on the properties of CRC before the material could be considered for structural applications, and the material has been the subject of a number of research projects. These projects have investigated mechanical properties as well as durability and fire resistance – properties that become increasingly important for the slender structures designed in CRC [7-11].

3 Structural applications

Based on the high strength and ductility of CRC the material was originally designed for applications in heavily loaded structures such as long span bridges, structures exposed to seismic loads or columns in high rise buildings. However, most of the appplications of CRC in the last 15 years have been for smaller structural elements. The first CRC application – in 1993 – was more than 40,000 drain covers for the Great Belt Link in Denmark, where the covers replaced a similar design made in cast iron. Other applications have been staircases, balcony slabs, beams and columns. An example of a staircase design where CRC properties

such as high compressive and flexural strength, crack control and high bond strength are utilised is shown in fig. 2.

The use of CRC is encouraged in relatively simple products that utilize some of the properties of CRC so that contractors, architects and engineers can see applications in a range of projects and get used to the material. With this large exposure ideas are generated from a wide range of users and a number of new types of applications are developing.

CRC was used for 2500 tons of structural elements in 2003 and in 2006 this figure had increased to 8000 tons. The bulk of applications are in balcony slabs and staircases – a type of product that was introduced 10 years ago, but new products are developed and tested as well as variations of the older products. The balcony slabs in fig.1 are a popular cantilevered system where “flaps” on the slabs extend into the building and are bolted onto the hollow core slab. In this case the thickness of the “flaps” has to be 80-100 mm so that insulation can be placed above and below the “flap” to avoid a cold bridge. Another system is shown in fig. 3 where the balcony slabs are bolted to the wall.

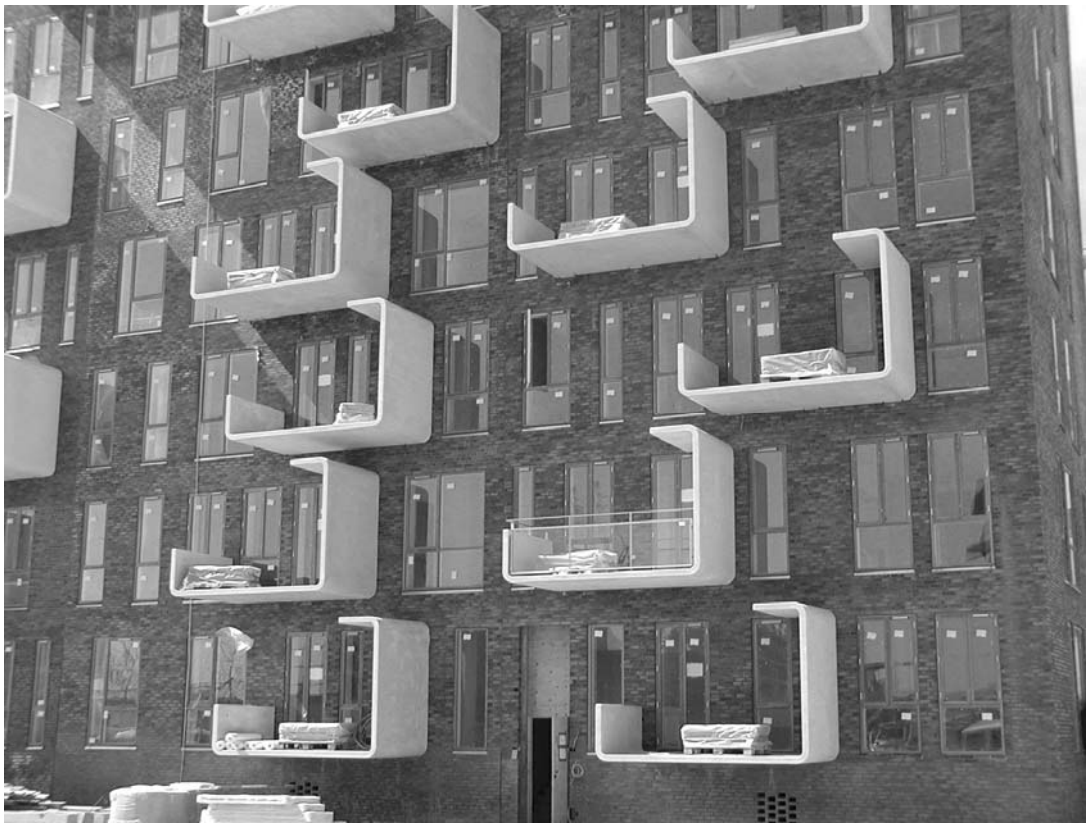

Figure 3: Balcony slabs in white CRC.

4 Production

In Denmark there are 4 precast producers making CRC and all 4 producers have a similar mix for CRC. The small mix variations make it easier to maintain a good quality control:

CRC binder	920-940 kg
Sand 0-5 mm	1300-1350 kg
Water	145-155 kg
Steel fibres	150-300 kg

In each case the producer uses a type of sand that is available locally and the variation in content of steel fibres is based on the type of application the mix is used for. The CRC binder is a premix containing cement, micro silica and a dry super plasticizer. None of the producers use special curing or mixing techniques. While the mix is almost self-levelling – at least with fibre contents of 2-3% - vibrations are always used in compacting CRC.

Figure 4: Staircase in white CRC.

With the slender products that can be produced using CRC architects have played around with the different types of design for the first few years, but recently there have been more and more requests to produce coloured CRC in addition to the normal grey CRC shown in fig. 1. The dark CRC is relatively easy to produce as a pigment is just added to the mix, but for the white CRC it has been necessary to replace the normal micro silica used in CRC with white micro silica in order to produce a white CRC with the same properties as the “grey” CRC. Examples of white CRC are shown in figs. 3 and 4. In both cases normal quartz sand

has been used so the end product is very light rather than white. The spiral staircase in fig. 2 is produced with a grey CRC and painted white afterwards.

For about 85% of the production of CRC elements regular steel fibres are used, which means they corrode at the very surface of the elements and will in some cases appear as withered pine needles on the surface of a balcony slab. For the white elements – which are more expensive than the grey anyway, due to the need for making a special mix with white micro silica – stainless steel fibres are typically used. Corrosion of the steel fibres on the surface has no effect on durability or strength of the element.

5 Discussion

For the first few applications a rather extensive documentation had to be provided for the building authorities, but as CRC has now been used on a number of projects, a simple overview of properties is usually sufficient. One reason for this is that – as described in the section on production - a standard matrix is invariably used, where only the content of steel fibres is changed from one project to another, providing a good quality control. Another reason is that the design of CRC structures is modelled after conventional design methods, so that any engineer can do the design. The tensile strength of the matrix is not taken into account in the design, but the fibres ensure ductility, control cracking, allow a very short anchorage length and closely spaced reinforcement and if shear stresses are below typically 10 MPa they are carried by the fibres so that shear reinforcement is not needed. Other modifications that have been made are to allow for: a higher compressive strength and a cover to the reinforcement of 10 to 15 mm in an aggressive environment.

This way of design is a rather conservative approach, but in most applications it is relatively easy to achieve the strength needed, even without taking the tensile strength of the matrix into account, so often the most important factors in determining the design of the typically slender structures are deformations under service loads and fire resistance. While the failure load of balcony slabs as those shown in figs. 1 and 3 may be much higher than actually needed, it is also important to achieve sufficient stiffness to avoid large long term deformations or uncomfortable vibrations, something not so easily achieved with long spans and small thickness.

While CRC has been used extensively in Denmark there is still a reluctance to use CRC in other countries. A few projects have been carried out in England, Ireland, Sweden and Spain but it is still a significant step for producers, engineers and building authorities to accept test results and case stories from other European countries, whereas architects are much more open to new influences. There is currently work under way to produce international guidelines and recommendations for using these types of materials in the ***fib*** group TG 8.6 “Ultra high performance fibre reinforced concrete”. The first meeting in the group was held in Delft in May of 2004.

CRC was invented in 1986 and as such is a relatively old concept, but new applications and new markets are still being developed and it appears that with the relatively "low-tech" production requirements for CRC compared to others of the new Hybrid FRC's there will still be a niche in the market for CRC for years to come.

6 References

[1] Bache, H.H., "Compact Reinforced Composite, Basic Principles". CBL Report No. 41, Aalborg Portland, 1987, 87 pp.

[2] Richard, P & Cheyrezy, M.H., "Reactive Powder Concretes with High Ductility and 200-800 MPa Compressive Strength". Concrete Technology: Past, Present and Future, SP-144, American Concrete Institute, Detroit, 1994, pp. 507-518.

[3] Resplendino, J., "First Recommendations for Ultra-High-Performance Concretes and Examples of Application". Proceedings of the International Symposium on Ultra High Performance Concrete, Kassel University Press, Kassel, Germany, 2004, pp 79-90.

[4] Aarup, B, "CRC JointCast", a technical note that can be downloaded from the documentation page at www.crc-tech.com.

[5] Aarup, B. & Jensen, B.C.,"Bond Properties of High-Strength Fibre Reinforced Concrete". ACI-publication SP-180, Bond and Development of Reinforcement, 1998.

[6] "Ultra High Performance Fibre-Reinforced Concretes, Interim Recommendations", January 2002, AFGC/SETRA, France.

[7] Aarup, B, "CRC – a description", a technical note that can be downloaded from the documentation page at www.crc-tech.com.

[8] Andrade, M.C. & Frias, M. & Aarup, B, "Durability of Ultra-High Strength Concrete: Compact Reinforced Composite". BHP96 Fourth International Symposium on Utilization of High-Strength/High-Performance Concrete, 29-31 May 1996, Paris, France.

[9] Jensen, B.C. & Aarup, B., "Fire resistance of fibre reinforced silica fume based concrete". BHP96 Fourth International Symposium on Utilization of High-Strength/High-Performance Concrete, 29-31 May, 1996, Paris, France.

[10] Juvas, K. & Jumppanen, U.-M. & Aarup, B.,"High Performance Concrete at High Temperatures". Proceedings of Nordic Concrete Research Meeting, 3-6 August 1999, Reykjavik, Iceland.

[11] Rom, L. & Ellegaard, P. & Aarup, B, "Slender CRC Columns", Nordic Concrete Research, also available for download at the documentation page of www.crc-tech.com.

Bernhard Monai
Dipl.-Ing.
SW Umwelttechnik, der Wasserwirt
Klagenfurt / Straßburg, Austria

Heinz Schnabl
Ing.
SW Umwelttechnik
Klagenfurt, Austria

Practice of UHPC in Austria

Summary

For the Company SW Umwelttechnik a Ultra high performance concrete (UHPC) which is called “RESCON”, made of local materials, was developed by the University of Kassel. The UHPC will assume some tasks and application range for the future in Austria.
A special part of application will take place in bridge building. Costum - built units for the bridge, used to protect the structure, are developed. The practice of this special kind of custom unit is shown, to reduce the weight and dimensions of the bridge-side layers.
A further example of application is the “monolith” concrete bridge for pedestrians. A new pre-cast concrete bridge made of UHPC was developed. The Construction is based on the bridges, which was built in Kassel already.

1 Objective / Goal

In the course of a national research project in Austria, the company SW Umwelttechnik together with its project partners Forschungsförderungsgemeinschaft Austria (FFG), University Kassel and Graz University of Technology has developed an ultra high performance concrete named “Rescon” and have tested its characteristics.
It was the main focus of the University Kassel to develop an in-house UHPC with Austrian raw materials. Another goal was to produce a concrete that is also economic.
First experimental components were produced together with Graz University of Technology in order to obtain relevant characteristics of the new building material. So-called I-panels were manufactured in order to obtain any indications for shear forces effecting thin building components.

Another goal was to find application areas for products made from UHPC. The application areas therefore pertain to construction engineering, in particular bridge construction, and architecture.

Characteristics of RESCON UHPC

- The median compressive strength is 195 N/mm²,
- The median bending tensile strength is between 17 N/mm² and 20 N/mm²

Following tables illustrates the compressive strength and the E-moduli of Heat cured specimen.

Table 1: Comparison of the mean compressive strength

components	Date of production	specimen and size [mm]	spezimen age [d]	number [-]	maximum density [kg/dm³]	compressive strength [N/mm²]
I-panel	06.07.2007	Cube 100	28	3	**2,476**	**190,8**
	06.07.2007	Cylinder 150/300	28	3	**2,495**	**174,6**

Table 2: Comparison of E modulus

components	Date of production	specimen and size [mm]	spezimen age [d]	number [-]	E $Modul_{30,Ö}$ [N/mm²]	E-$Modul_{30,D}$ [N/mm²]	E-$Modul_{70}$ [N/mm²]
I-panel	06.07.2007	Prism 40/40/160	95	3	**50587**	**n.v.**	**48204**
	06.07.2007	Cylinder 150/300	95	3	**49404**	**49466**	**47916**

Table 3: Some components of the UHPC

components	content SiO_2	Maximum grit size	Maximum density	spec. Surface (Blaine)	grit size < 0,125 mm	grit size < 0,09 mm
	[M.-%]	[µm]	[kg/dm³]	[cm²/g]	[M.-%]	[M.-%]
sand 0,125/0,5	99,5	500	2,65	100	1	0,3
Basalt	-	2500	3,06	-	-	-
Concrete CEM I 42,5 R HS	-					
Microsilica	98,3	1	2,20	20 $x10^4$	100	100
silica	99	60	2,65	3800 [1)]	99,9	99
fibres	-	-	7,85	-	-	-
binder	-	-	1,05	-	-	-

1.1 Production and tests

During the course of the research project, the company's production equipment and infrastructure was adjusted to the future production of ultra high performance concrete.
The key component of the production – the mixing system - was recently adapted. Two new Harrup mixers and a new computer control make it possible to achieve a high quality of UHPC building components.

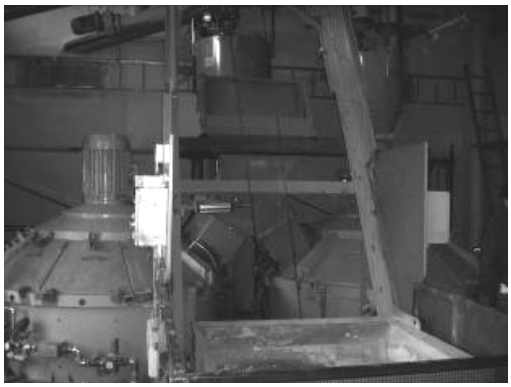

Figure 1: The new mixer.

The first experimental pieces have already been produced with the new mixing system. The building component has the capacity to hold 1.4 m³ and has been manufactured with two mixed batch capacities. This building component serves as end plate for a large-scale test project conducted at the Graz Technology University. Further, it was necessary to make experiments for the confirmation of shear forces effecting. The tests were made on so-called I-pannels.
The following tables and figures illustrate the I-pannels and the results o f the experiments.

Table 4: Shear carrying capacity

		no pre-tension [kN]	half pre-tension [kN]	full pre-tension [kN]
FE	short	457	532	570
	long	417	440	471
Test	short	367	596	338
	long	357	361	357

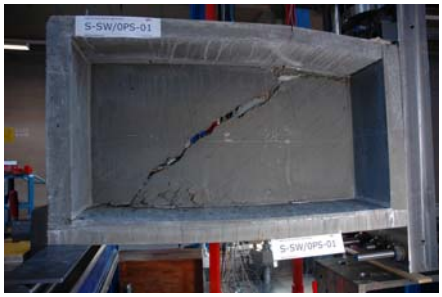

Figure 2: I-pannel

Results of shear tests performed at Graz University of Technology
Smaller concreting was produced with a smaller mixer. It has a capacity of app. 400 liters. This unit is used for little series of system components.

A total of 6 m³ UHPC concrete have currently been processed. This includes experimental building components as well as building components for bridge construction and architecture.

2 Application of UHPC in Austria

There are currently envisions areas of application and opportunities for the “building material of the future” in bridge construction (serial production of small bridges) and for the architectural field. Additionally, areas like container construction are being explored and tested for its application.

2.1 Bridge construction

Bridge-side layers

In Austria the interest in ultra high performance concrete is increasing. The implementation and/or the production of bridge-side layers made of ultra high performance concrete were made possible collectively with the Salzburg provincial government.

This pertains to the termination elements of vehicle bridges of any type. It is the purpose of the side layers to form a compact termination for the width of the bridge as well as to divert the road sewage over a drip cap in such a manner that it is does not come into contact with the bridge support system.

Common side layers are massive, heavy and bulky.

The new construction of the side layers has the following improvements:

- The side layers are light weight and easy to install
- High resistance against aggressive road sewage (chloride)
- High lifespan (reusable)
- The position and height of the side layers can be adjusted. The “alignment” of the side layers is therefore assured.
- The side layers serve as forming material for the subsequently installed cast-in-place concrete for the road shoulder.

The figure 3 illustrates the bridge construction with common side layers. (Source: Manual Asfinag)

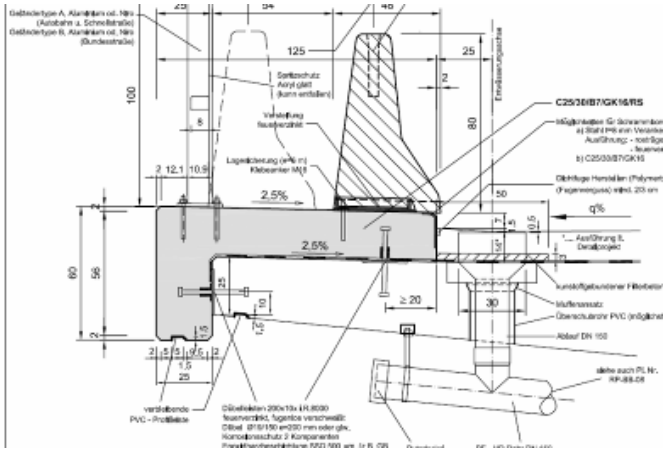

Figure 3: Common bridge side layers

The heavy and bulky building component (gray) can be clearly seen.

These building components are mostly manufactured with cast-in-place concrete producers and therefore are subject to a relatively high expense for forming work.

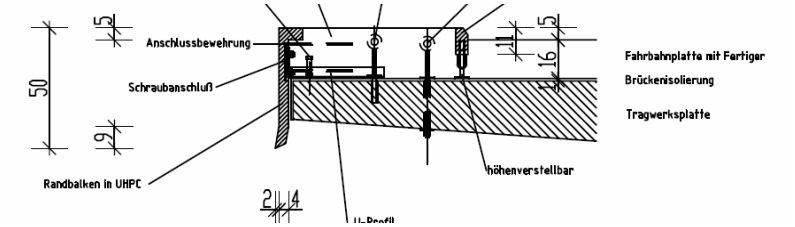

Figure 4: Thin bridge side layers

Figure 4 shows the bridge-side layer system by the extremely thin construction of the elements can be clearly seen. The installation is quick and the side layer serves as form for the concreting of the shoulder. As an option, the side layer can also be installed as a UHPC ready-made component.

The light construction of the side layers can be clearly seen here. The system offers the best possible workability of the side layer elements in combination with cast-in-place concrete.

Figure 5 and 6: Side layers made from UHPC

Pedestrian bridges

Therefore it was developed a system, which permits the economical serial production of small bridges. These are pedestrian bridges, which are calculated for the loading condition “emergency vehicle”.

A special form is used in this case, where its geometry can be completely adjusted and tailored to the specific application. This also permits a simple modification of the form and makes it very economical.

The manufacturing process permits bridge spans of up to 20 meters and bridge widths of up to 3.5 meters. The plate thickness of the bridge is app. 6 to 10 cm.

In the following, the bridge construction is illustrated schematically. The dimensions (particularly the joists) will be optimized.

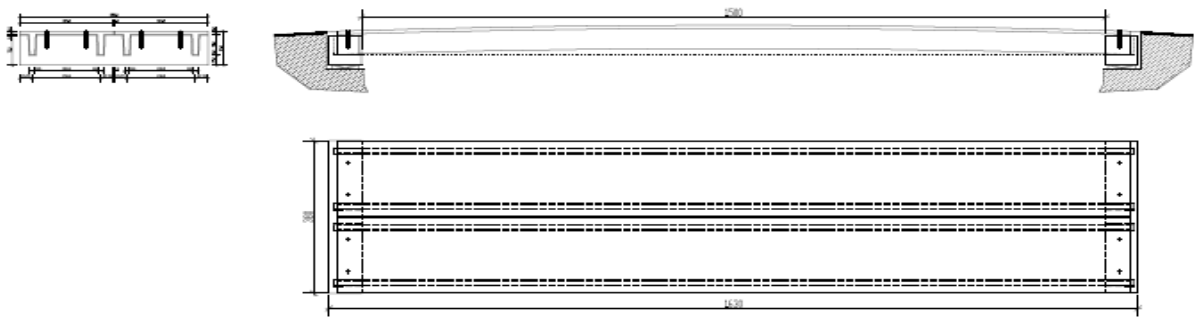

Figure 7: Draft of Plate bridge

Figure 8: Plate bridge 15 meters long and 3 meters wide

Figure 9: Plate bridge 15 meters long and 3 meters wide

The UHPC building components are illustrated below:

Wall elements for small buildings

The figure 10 and 11 illustrates a small pavilion. The wall thickness of the UHPC wall elements is 3 cm. High demands are placed on the visible concrete surface at the inside.

Figure 10a: Construction of the pavilion

Figure 10b: Interior surface of the walls

Figure 11: illustrates the fixed UHPC walls

3 Architectural applications

There also was produced designer furniture pieces for an architectural show in Carinthia already. The furniture was designed by a student group and the University of Applied Sciences Spittal.

Figure 12: furniture I

Figure 13: furniture II

Figure 14: furniture III

4 Discussion

At the beginning, the processing of UHPC presented a great challenge. First, the production team had to be sensitized for the new material. Precise time management as well as an exact operation scheduling are the prerequisite for a perfect UHPC.

The processing is now automatic. That means that the team knows what is important. It is basically important to work fast and with extremely precision. The window of opportunity during the mixing process is very precise. The window of opportunity between final mixing and pouring is also very small. The infrastructure of the company SW Umwelttechnik will in the future also be adjusted to the UHPC production.

5 Conclusion

We are convinced that UHPC is “the building material of the future”. This allows for building methods in the field of engineering as well as architecture that have not been considered until today.

We believe that the acceptance of the decision makers can be basically obtained in order to quickly implement the building materials within the industry. This can be expedited with constant testing, research and implementation. Even if in the beginning they are only small things.

6 References

[1] Schmidt, M.; Teichmann, T.: Development of an ultra high performance concrete for the company SW Umwelttechnik, final report. Kassel 2007

[2] Juhart, J: testing report on properties of hardened UHPC, Carinthian University of applied sciences. Spittal 2007

Mélanie Shink
PhD, R&D Project Manager
CTG - Italcementi Group
Guerville, France

Jean-Philippe Vacher
Chief Innovation Officer
Ciments Calcia - Italcementi Group
Guerville, France

EFFIX Design®
Properties and applications of a creative concrete

Summary

Based on the recent technology of ultra high performance concrete, CTG – Italcementi Group has developed a new cost effective and highly aesthetic product allowing the industrial manufacturing of thin lightweight elements for the production of alternative furniture or shaped elements for other architectural purposes and landscaping. This new product has been marketed in France by Ciments Calcia, a subsidiary company of the Italcementi Group, under the name EFFIX Design®.

This paper describes the main properties of EFFIX Design® and presents some of its applications.

Keywords: *ultra high performance concrete, aesthetic quality, photocatalytic properties*

1 Introduction

EFFIX Design® is a new highly aesthetic product specially designed for the industrial manufacturing of thin lightweight elements (plates, shells …) for the production of alternative furniture or shaped elements for other architectural and decorative purposes. It is also well suited for interior or exterior landscaping.

This new product has been developed according to the technology of ultra high performance concrete (UHPC). The main guidelines for its development were of course strength, durability and aesthetic quality but also cost and workability, which represent determinant factors for the widespread use of UHPC. Performances of EFFIX Design® were ensured by an appropriate selection of its components and proportioning; very expensive additions such as white silica fume produced from the zirconium industry were avoided, even to produce the white version of the product. Moreover, the fibre reinforcement and volume fraction of fibres were selected to prevent early age cracking, which proved to be sufficient to meet the requirements of the target (non structural applications). EFFIX Design® aims to provide one of the best compromises between mechanical properties, durability, aesthetic quality and costs. It is not intended to outdo the performance at any price. Workability of EFFIX Design® is self-compacting for improved manufacturing and handling. This character is among others obtained by the use of fine grain sizes and appropriate superplasticizer. It enables to produce more or less complex shapes and its fineness allows reproducing the smallest details and textures of moulds and formworks.

For uses aiming at an external exposure, photocatalytic mixes, which are known as self-cleaning and de-polluting products then having an active and beneficial impact on environment, are also available.
This paper describes the main properties of the industrially produced premix EFFIX Design® and presents some of its applications.

2 Premix

EFFIX Design® is a premix mortar containing all dry components such as cement, sand, addition, superplasticizer, defoaming agent and non-metallic fibres, in which the users only need to add water. The premix is available in white or grey basic colours according to the cement used, but pigments can be added easily to obtain various coloured effects.
EFFIX Design® has the advantage of being easy to prepare since its mixing only takes 5 minutes in a normal industrial concrete mixer; the premix solution simplifies the batching process and mixing time. The fresh mortar is simply poured into moulds or formworks and requires normal curing to develop its properties.

3 Properties

3.1 Fresh state

EFFIX Design ® is a self-compacting product with controlled viscosity. It doesn't suffer from any segregation or bleeding. Its flowability is characterized using a modified cone designed using half dimensions of the Abrams cone [1]. Figure 1 shows the filling of the cone and the resulting slump flow. Figure 2 shows a typical result of the slump flow evolution at a constant temperature of 20°C. Mortars are self-compacting when slump flow values are greater than 350 mm, which means that no vibration is needed to fill moulds and formworks.

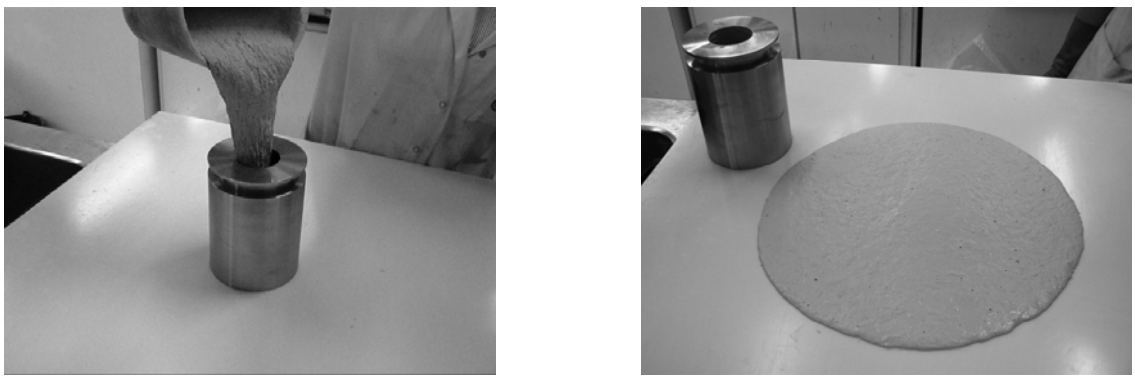

Figure 1: EFFIX Design® characterized by measuring the slump flow

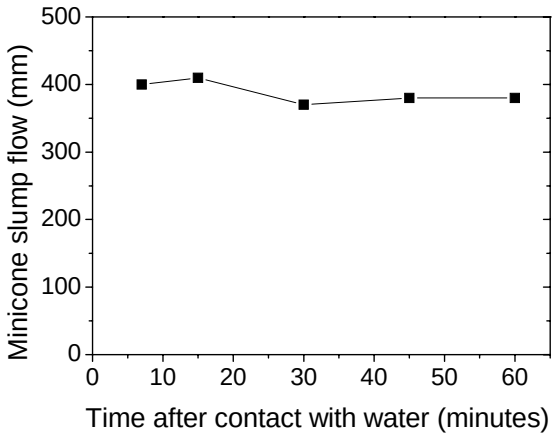

Figure 2: Slump flow according to time

The air content is less than 3.0% and density is about 2340 kg/m^3. Time of initial setting vary according to the cement used from about 215 minutes for white cement to about 280 minutes for grey cement. Such fast initial setting time helps the product to be less sensitive to ambient conditions and desiccation. Moreover, it allows demoulding and handling of hardened elements after 24 hours.

3.2 Mechanical properties

Mechanical properties have been characterized using 40x40x160 mm prisms. All prisms were cured after casting in a climatic chamber at 20°C and 95% HR, demoulded after 24 hours then cured in water at 20°C until testing. Three-point bending tests and compressive tests results shown in table 1 and represented in figure 3 are averages of the industrial premix mechanical properties.

Table 1: Mechanical properties of EFFIX Design®; flexural strength (3-pts bending test) and compressive strength on 40x40x160 mm prisms after water curing at 20°C

Testing age (days)		**Flexural strength**	**Compressive strength**
1	MPa	9.0	76
7	MPa	16.7	115
28	MPa	17.2	129
90	MPa	18.6	138

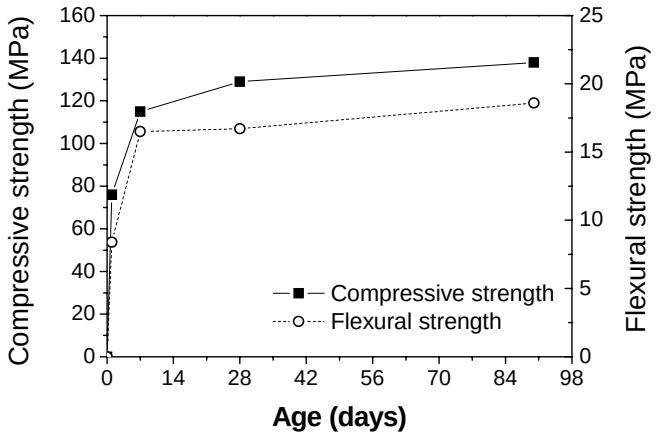

Figure 3: Compressive strength and flexural strength (3-pts bending test) on 40x40x160 mm prisms after water curing at 20°C

3.3 Shrinkage

Ultra-high performance concrete are obtained by reducing significantly the water to cement ratio while increasing the cement content and particle packing density of solids components by using fine additions and high-range water reducing admixtures. These designing rules have important consequences such as the reduction of the porosity but also the increase of chemical shrinkage due to the high quantity of cement used.

Autogenous shrinkage, which is a consequence of the cement paste self-desiccation, begins as soon as cement is in contact with water. After setting, the stiffness of the material increases and the autogenous shrinkage begins to be restrained. When manufacturing precast elements, internal or external restraints can develop from the aggregate skeleton, reinforcement or sharp angles and complex shapes of moulds and formworks. Tensile stresses may be induced, generating cracks if greater than the tensile strength of the material.

The autogenous shrinkage development of EFFIX Design® was analysed at the early age under standard isothermal conditions (20°C). Its evaluation was carried out using a test rig designed to start the measurements just after casting, as the one proposed by Boulay and described in [2, 3]. The initialization time of the deformations t0, after which shrinkage is considered as effective, was determined by the combined analysis of the temperature variations within the core of the specimen, measured using a PT100 sensor, and conductivity variations. Time t0 then refers to the time when the temperature starts to increase linearly and to the first inflection point of the conductivity curve (270 minutes). Figures 4 and 5 present typical results measured on the white version of the product. Under these experimental conditions, the magnitude of the autogenous shrinkage is about 500µm/m after 24 hours and 560µm/m after 96 hours (ceiling).

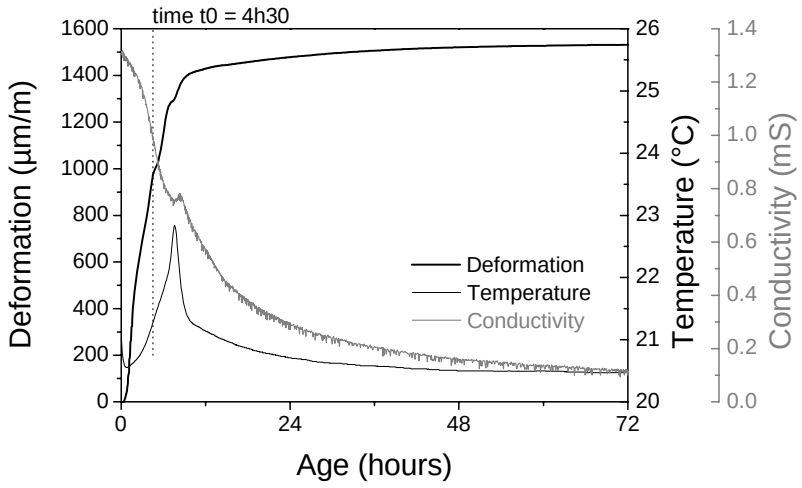

Figure 4: Deformations, temperature and conductivity of EFFIX Design®

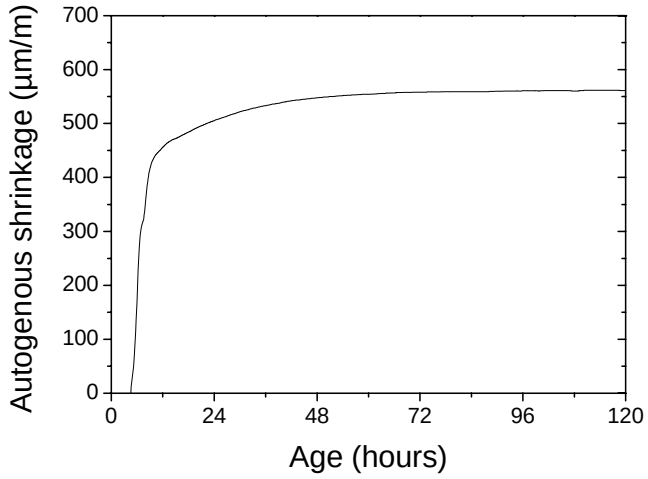

Figure 5: Autogenous shrinkage evolution of EFFIX Design® at the early age

Shrinkage was also evaluated by measuring total, autogenous and drying shrinkage according to time and under standard conditions. Tests were performed on 40x40x160mm prisms. All prisms were cured after casting in a climatic chamber at 20°C and 95% HR and demoulded after 24 hours. Total shrinkage was measured on 3 prisms cured at 20°C and 50 % HR after demoulding and autogenous shrinkage was measured on 3 prisms sealed by a single layer of adhesive aluminium foil and kept in the same conditions. Drying shrinkage is calculated as the difference between both total and autogenous shrinkage. Results obtained up to 90 days are shown in figure 6. Measured shrinkages according to time are quite low and almost achieved after 28 days.

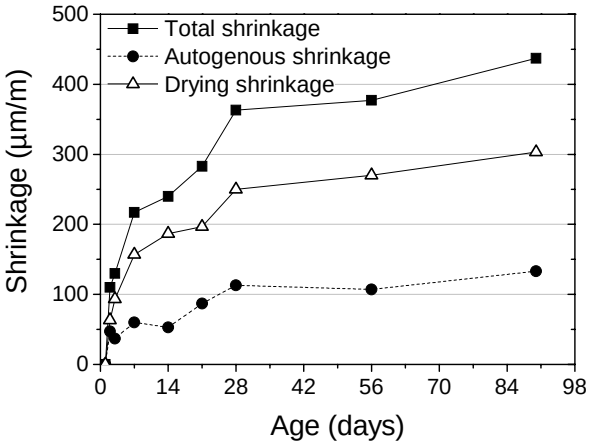

Figure 6: Total, autogenous and drying shrinkage according to time

3.4 Durability indicators

EFFIX Design® benefits of a high durability thank to its low water to cement ratio, cement content and particle packing density. Table 2 presents some of its properties, which are ranging from very high to ultra high performance when mixed in a traditional planetary mixer.

Table 2: Durability properties of EFFIX Design®

Properties		
Water porosity	%	2.3
Oxygen permeability	m^2	$< 2.5 \times 10^{-17}$
Chloride-ion diffusion factor	m^2/s	3.6×10^{-13}
Portlandite content	kg/m^3	80

3.5 Photocatalytic premixes

For uses aiming at an external exposure, EFFIX Design® is also available with photocatalytic properties through the TX Active® concept, an Italcementi Group trademark which grants self-cleaning or de-polluting abilities, meaning having an active and beneficial impact on the environment.

The self-cleaning and de-polluting abilities arise from the photocatalytic properties of titanium dioxide mainly in anatase form which can be introduced in the premix. Tests using an organic dye [4] have proved that such a mix recovers more than 50% of its initial color within 30 hours when placed under UV-light. Using a photocatalytic test chamber [5], elimination of NOx from the air was found to be more than 35 % after 40 minutes.

4 Applications

EFFIX Design® provides a total creative freedom for non-structural applications. Its self-compacting properties and aesthetic qualities allow to develop complex shapes and to reproduce the smallest details. Figures 7 to 9 show some types of furniture for indoor uses but also a landscaping project already developed by some architects and designers.

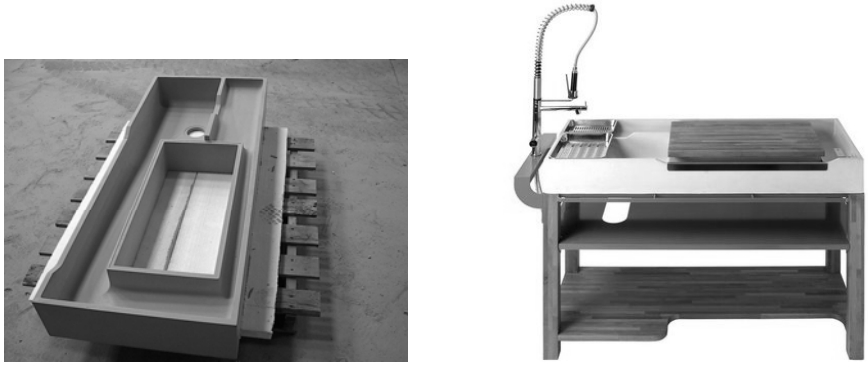

Figure 7: Happicius, kitchen sink designed by Benjamin Lignel

Figure 8: Furniture, prototypes designed by E. De Senneville

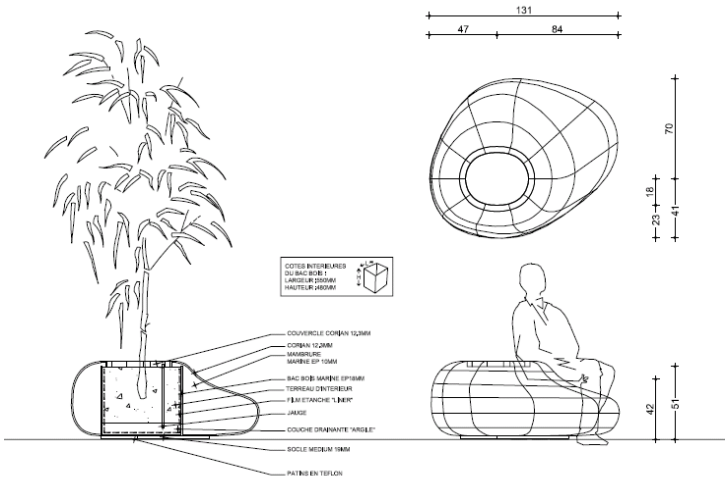

Figure 9: Landscaping project, Palais du Hanovre, Paris (France), designed by SAVI

5 Conclusion

Based on the recent technology of ultra high performance concrete, EFFIX Design® is a new highly aesthetic product offering a total creative freedom for non-structural applications.

Aiming to provide one of the best compromises between workability, mechanical properties, durability, aesthetic quality and costs, EFFIX Design® is well suited for the industrial manufacturing of thin lightweight elements, or more complex shaped elements, for architectural and decorative purposes or landscaping. For uses aiming at an external exposure, photocatalytic mixes, which are known as self-cleaning and de-polluting products, are also available.

This new product has been marketed in France by Ciments Calcia, a subsidiary company of the Italcementi Group.

6 References

[1] Schwartzentruber, A.; Catherine C.: La méthode du mortier de béton equivalent (MBE) – Un nouvel outil d'aide à la formulation des bétons adjuvantés. In: Materials & Structures 33, p. 475-482, October 2000.

[2] Boulay C.: Développement d'un dispositif de mesure du retrait endogène d'un béton au jeune âge. In: Proc. 8th Journées scientifiques du Regroupement francophone pour le recherché et la formation sur le béton $(RF)^2B$, Montréal (Canada), 5-6 juillet 2007.

[3] Staquet S.; Boulay C.; D'Aloïa L.; Toutlemonde F.: Autogenous shrinkage of a self-compacting VHPC in isothermal and realistic temperature conditions. In: Proc. 2nd International Symposium on Advances in Concrete through Science and Engineering, Quebec (Canada), 11-13 September 2006.

[4] Vallée F.; Ruot B.; Bonafous L.; Guillot L.; Pimpinelli N.; Cassar L.; Strini A.; Mapelli E.; Schiavi L.; Gobin C.; André H.; Moussiopoulos N.; Papadopoulos A.; Bartzis J.G.; Maggos T.; McIntyre R.; Lehaut-Burnouf C.; Henrichsen A.; Laugesen P.; Amadelli R.; Kotzias D.; Pichat P.: Cementitious materials for self-cleaning and depolluting facade surfaces. In: Proc. RILEM International Symposium on Environmental Conscious Materials and Systems for Sustainable Development, Koriyama (Japan), 6-7 September 2004.

[5] Amadelli, R.; Samiolo, L.: Concrete containing TiO2: An overview of photocatalytic NOx Abatement. In: Proc. Rilem Symposium on Photocatalysis, Environment and Construction Materials, Florence (Italy), 8-9 October 2007.

Mouloud Behloul
Ductal® Development manager for France
Lafarge
Paris, France

Jean-François Batoz
Vice President - Ductal
Lafarge
Paris, France

Ductal® applications over the last Olympiad

Summary

Ductal® is a new material with a combination of superior technical characteristics of strength, ductility and durability, whilst providing high quality surface aspect on mouldable products.
This material allowed to explore new construction approach in light structures: first UHPFRC used for a footbridge in Sherbrooke (1997), providing outstanding durability in drastic operating conditions (internal structure of cooling towers : Cattenom power plant) and unexpected freedom in architectural and aesthetic design by architects as well as designers in non-traditional applications such as urban furniture.
An important number of applications followed these 'firsts'. This paper gathers the references completed since the last Kassel symposium in 2004 covering the domains of bridges and footbridges, structural applications, durability and aesthetic oriented applications.

Keywords: *UHPC, FRC, aesthetics, durability, Ductal®*

1 Introduction

Ductal®, the outcome of the research over the last 10 years in the area of concrete, is a new construction material technology belonging to UHPFRC family, with very high durability, compressive strength, flexural resistance with ductility and aesthetics [1]. Through the development period, several prototypes have been produced, prior to make an extensive use in civil works, structural and architectural various applications [2].
In France, new recommendations for the use of ultrahigh strength concretes reinforced with fibres have been issued in May 2002 [3]. These recommendations were established by a BFUP working group (Béton Fibré Ultra Performant) coordinated by SETRA (Road and traffic govern-mental agency) and with representatives of construction industries (contractors, control agencies, suppliers, certification authorities).

2 Ductal® Technology

Ductal® is based on the principle that a material with a minimum of defects such as micro-cracks and pore spaces will achieve a greater percentage of the potential ultimate load carrying capacity defined by its component materials, and it will also have greater durability.
By applying this principle as a guideline, a concrete has been proportioned to provide a very dense mixture that will minimize voids and a very high compressive strength, but with not enough ductility compared to a conventional mortar. The inclusion of adequate fibres improves drastically tensile strength and provides a substantial level of ductility.

The various Ductal® formulations are all based on an optimized composition combining homogeneity and adequate granular compactness.
To enhance and to stabilize the performances, especially mechanical ones, the option of heat treatment can be chosen. For each application according to technical and economical challenges, adequate adjustments are made within Ductal® technology in order to achieve the most adapted product to the customer requirements.
As described above, Ductal® is an Ultra-High Performance Concrete reinforced with fibres.
These fibres can be made of steel (Ductal®-FM), made of organic material (Ductal®-FO) or combination of both steel and organic material (Ductal® AF).
The fresh mix of all these ranges of material has very useful properties in term of fluidity and self placing. Most of the standard industrial batching facilities are able to mix Ductal® requiring only minor adjustments.

Ductal®-FM, used for structural applications, includes small steel fibres at a dosage of 2% per volume, and of 0.20 mm in diameter and 12 mm in length. In a typical load deflection graph of a sample under three-point loading, the material exhibits linear behaviour up to its first crack stress, a post-first-crack strain hardening phase up to its ultimate flexural load, and a post-ultimate-load strain softening phase. It has an ultimate bending stress that is over twice its first crack stress and more than ten times the ultimate stress of conventional concrete.

Table 1: Main properties of the material with steel fibres or organic fibres

		Ductal®-FM or Ductal®-AF With Thermal Treatment	**Ductal®-FO without Thermal Treatment**
Density		2500 kg /m3	2350 kg/m3
Compressive Strength	Characteristical value	150 – 180 MPa	100 – 140 MPa
Tensile Strength	Characteristical value	8 MPa	5 MPa
Residual tensile strength (0.3mm)	Characteristical value	7,5 MPa	3 MPa
Young Modulus (E)		50 GPa	45 GPa
Shrinkage		< 10 µm/m	550 µm/m
Creep factor		0.3	0.8
Thermal expansion coefficient		11.8 µm/m/°C	11.8 µm/m/°C

The Ductal® microstructure is completely closed, making it resistant to abrasion, corrosion or chemical attacks. Such superior characteristics give the material ultra-high performance durability properties. The table 2 hereafter shows some durability properties of heat treated Ductal®-FM and a comparison with ordinary concrete and high performance concrete properties.

Table 2: Ductal® main durability properties

Durability indicator	Ordinary concrete	HPC	Ductal®-FM
Water porosity (%)	12-16	9-12	2-6
Oxygen permeability(m²)	10^{-15} – 10^{-16}	10^{-17}	$<10^{-19}$
Carbonation depth (mm) after one month of accelerated tests	10	2	< 0.1
Abrasion test $I=V/V_{glass}$	4	2.8	1.3-1.7

3 Ductal® recent references

The ultra high performance of Ductal® opens applications in following different domains:

- Structural applications
- Durability oriented applications
- Architectural applications

3.1 Structural applications

A material with such high ultimate compressive and flexural-tensile strength offers interesting opportunities in the field of prestressed concrete. The elimination of passive reinforcement makes it possible to use thinner sections and a wider variety of innovative and acceptable cross-sectional shapes. The current structural precast shapes used for prestressed beams in bridges and buildings have been shaped for concretes with much lower strength properties. In order to make the best use of the higher mechanical properties, there is several opportunities to introduce new shapes in prestressed beam design. Through such re-design approach of the elements the beam dead load can be reduced by a factor of three.

Among these kind of applications we can list 3 traffic bridges: the Shepherds Bridge erected in Australia [4], the Wapello bridge in Iowa-US and the Kuyshu expressway bridge erected in Japan [5]; 5 footbridges: Sherbrooke footbridge in Canada – Seonyu footbridge in Korea [6] – Sermaises footbridge in France- Sakata Mirai and Akakura footbridges in Japan. Recently a footbridge was erected in Calgary, the Glenmore footbridge and a traffic bridge completed in France, the Saint-Pierre-La-Cour bridge. This bridge is presented hereafter.

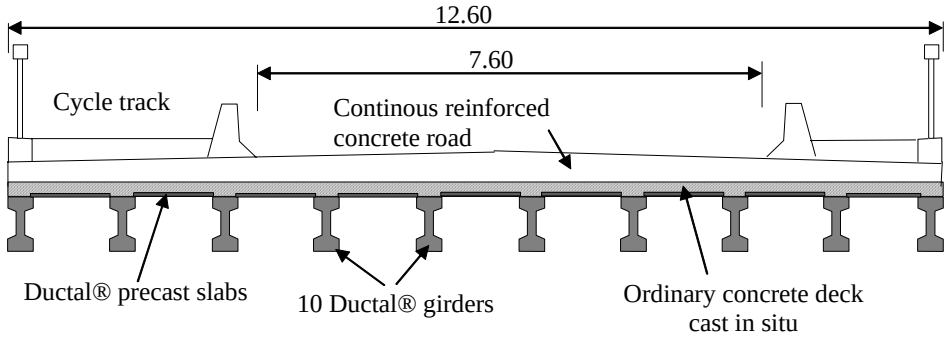

Figure 1: Transversal section of the bridge

The "Conseil Général" of the Mayenne ordered a bypass from the town of Saint-Pierre-la-Cour. It was in this context that the first bridge in France made of Ductal® was built to cross a railway line. This bridge, with a span of 19 m and 12.6 m wide, supports a continuous reinforced concrete road of 7.6 m, a pavement and a cycle track (Figure 1).

The ten 20-meters length prestressed girders without re-bars and 83 precast slabs they support are all made of Ductal® (Figure 2). Although not exceeding 25 mm thick, the precast slabs support a conventional 20-cm concrete apron. All the girders and precast slabs were laid in two days, thanks to the speed this technique affords.

A comparison with a traditional solution indicates a reduction of the weight of the bridge deck by a factor 2.2. The characteristics of the structure are enhanced by the fact that the underside of the concrete deck and its reinforcements are protected against any damage thanks to Ductal ultra high durability performances. Durability that limits maintenance budgets and provides a more globally economic solution.

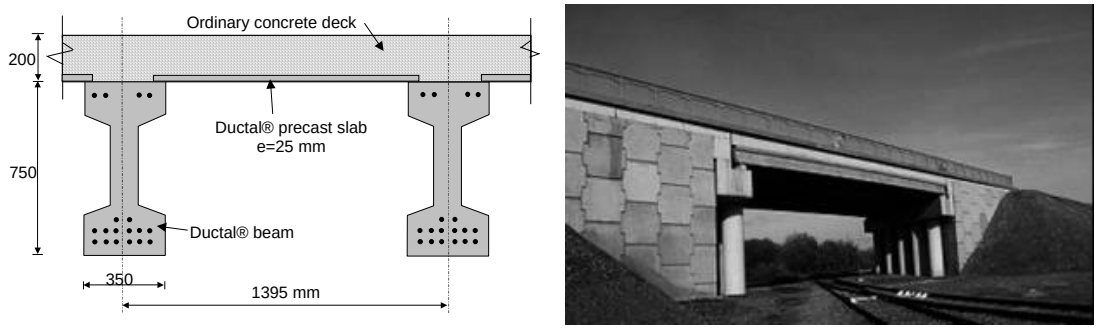

Description of the composite solution After completion

Figure 2: Saint-Pierre-La-Cour bridge description and construction

Ductal® can also be used in structural applications without any passive reinforcement or, prestressing, like the case of stairs. The material was used in several projects: stairs at Roissy airport in Paris, stairs at new Lafarge office in Birmingham (Figure 4), and a new helicoidal stair solution developed by an industrial partner, Escaliers Decors (Figure 3).

Stairs at Birmingham Escalier Decors's stairs

Figure 3: Stairs made of Ductal

The material was also used in the Ungerer Museum in Strasbourg for the construction of a "flying carpet" of 45mm in thickness to connect the entrance to the main building. The structure of 49 m length and 1,8m width, designed by the architects Dominique Marrec and Emmanuel Combarel, doesn't contain any traditional re-bars or prestressing (figure 4).

Figure 4: Flying carpet, Ungerer Museum, Strasbourg

3.2 Durability Oriented Applications

The durability of Ductal® is as important as the mechanical strength. Combining strength and durability, Ductal® can be an ideal solution for structures in severe environment. Also the durability of the material lowers the maintenance costs and makes the solution very competitive.

Ductal® was used in several durability /fire resistance oriented applications like the beams and girders (more than 2000) used for the Cattenom power plant cooling tower-France, the retained earth anchorages (more than 6000) used in Reunion Island –France- and the Ductal®-AF used for the construction of composite columns in the Reina Sofia Museum in Madrid (Spain). Recently Ductal® was used for the fabrication of the troughs of Gold Bar waste water treatment (Figure 5).

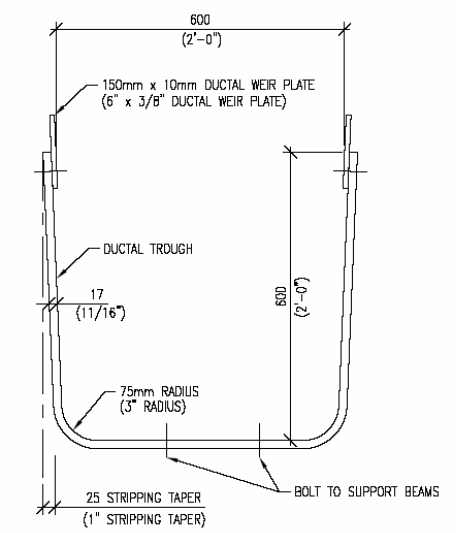

Transversal section Troughs after installation

Figure 5: Gold Bar troughs

3.3 Architectural Applications

The use of a concrete-like material but with almost unlimited possibilities of appearance, texture and colour has excited the architects by giving them access to unexpected new world of shapes and volumes. Ductal® was used in several architecturally oriented applications like the bus shelters in Tucson (USA), sun shades in France, façade panels in Monaco, Kyoto clock tower in Japan and the canopies of LRT station of Shawnessy in Canada. Recently, Ductal® was used for the construction of several projects: cladding at Thiais, sunshades at Clichy, Badia Berger mantialla at Paris and Navarra roof house at Muy; these projects are presented hereafter.

Cladding at Thiais

The RATP administrative centre in Thiais is responsible for the traffic management of 300 buses and provision of 24-hour facilities for 800 drivers. Located in an industrial zone on the outskirts of Paris, this project was designed by Dominique Marrec and Emmanuel Combarel. Mirroring the variety of coatings within the bus depot, a double skin first follows and then lifts the pavement. The result is a non-directive setting in which users are free to determine what they want to conceal and what they want to leave open to view (Figure 6).

The architects wanted to focus on the mineral nature of the site and propose a building that acts as a continuation of the ground surface and emerges like a deformation of that surface.

Figure 6: Thiais bus station – By D.Marrec and E.Combarel

It was this approach that gave the idea of a skin that would blur distinctions between traffic flows and building while giving the site a strong visual identity.

Two implementation techniques come together here: heavy prefabrication and siding, as the 3cm thick skin provides a pavement that is partly open to traffic and rises up, sweeping away any thickness, to lose itself in the sky.

The Lego-like framework offers anti-slip properties, gives colour-stippling effects that break up the play of lights and mirrors from the tinted external exterior bonded glass bays (Figure 8). This skin uses Ductal® not only for its structural properties but also for its visual aspect, its depth of colour and quality of finish.

Sunscreens at Clichy

The Clichy municipal swimming pool was built in 1968 and required extensive work. The Town Hall opted for refurbishing including reconstruction of the south-facing, fully glazed main facade.

ENIA Architects suggested the installation of outside sunscreens to control the solar impact and, accordingly, the thermal ambiance in the pool. This new double skin is made up of a grid of horizontal and vertical slats of Ductal®, of 4cm in thickness, forming rectangular modules (L. 2.50 x H. 1 m) mounted to the existing metal structure (Figure 7).

Figure 7: Sun shades for Clichy swimming pool.

Not only were the architects able to take advantage of specific technical features in order to construct a long-lasting facade with thin and slender shapes, they were attracted by the luminous color range offered by Ductal®. The top surfaces of some horizontal slats are lined in red, reflected on the outside module. The colors are never perceived directly but simply by their reflection which varies according to the brightness. The asymmetrical reflections set off the extreme regularity of the sunscreen.

Badia Berger's mantillas

The architect Badia Berger has designed an amazing green mantilla. This cladding was installed in Zac Rive Gauche (Figure 8).

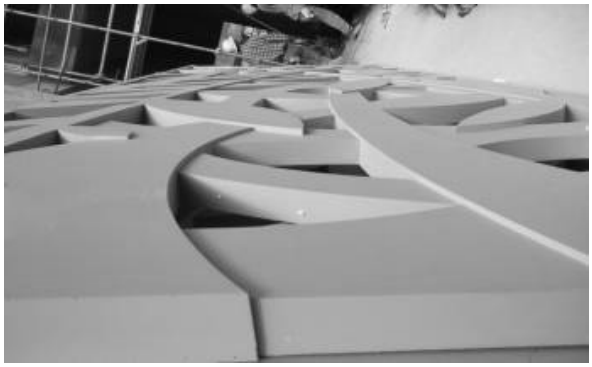

Figure 8: Green mantillas in Paris

Navarra roof house

Dreamt up by Rudy Ricciotti for art dealer Enrico Navarra, the roof over the art gallery in Muy en Provence represents a new technological achievement for Ductal®. Large dark panels with a "stealth" look will soon cover the entire gallery with a 7.7 m overhang. Each segment of Ductal® weighs in at 3 tons and has been given heat treatment at 90°. The roof is a world-first, only 3 cm thick at the edge of the overhang and 40 m wide, providing an extreme visual contribution to the landscape (Figure 9).

Figure 9: Ductal® roof of Navarra house

4 Conclusion

Ductal® is a new technology of ultra high strength concretes that constitutes a breakthrough in concrete mix design. This family of products is characterised by a very dense microstructure and very high compressive strength achieving and possibly exceeding 200 MPa. Steel and organic fibres or combination of both are one of the major components of the material enhancing the bending strength, the ductility and fire resistance.

The three main categories of applications are:

- Structural applications: The very high mechanical properties combined with prestressing technology offer to engineers and architects lot of opportunities to design elegant structures by avoiding heavy steel reinforcement. Ductal® technology gives access to very thin slender and elegant structures like footbridges. Also Ductal can be used without any re-bars to design stairs and slender structures.
- Durability oriented applications: the very dense microstructure of the Ductal® matrix offers a material which resists to very aggressive media and opens therefore a very wide range of applications.
- Architectural applications: a very wide range of textures and colours effects are accessible to Ductal®. Such properties provide architects with very high potential of innovative design in all elements that build up new architecture.

5 References

[1] Orange, G.; Dugat, J.; Acker, P.; “A new generation of UHP concrete: Ductal®. Damage resistance and micromechanical analysis”; Proc. of the 3d Internat. RILEM Workshop, HPFRCC3-1999, 101-111.

[2] Behloul, M.; Durukal, A.; Batoz, J.-F.; Chanvillard, G.; “Ductal® : Ultra High-Performance Concrete Technology with Ductility”; International Rilem Symposium on Fibre Reinforced Concretes BEFIB’2004, September 22-24 – Varenna, 2004.

[3] BFUP-AFGC; “Ultra High Performance Fibre-Reinforced Concretes, Interim Recommendations”. AFGC publication, France, 2002.

[4] Cavill, B. and Chirgwin, G; “The worlds first Ductal road bridge Shepherds gully creek bridge, NSW”; 21st Biennial Conference of the Concrete Institute of Australia, Brisbane, 2003.

[5] Okuma, H et al; “The first highway bridge applying ultra high strength fibre reinforced concrete in Japan”; 7th International Conference on short and medium span bridges. Montreal, Canada, 2006.

[6] Behloul, M.; Lee, KC. “Ductal® Seonyu footbridge”. Structural Concrete. 4 (4), 2003, 195-201.

Anders Moeller
Senior Project Manager
Densit a/s
Aalborg, Denmark

Use of UHPC in offshore wind turbine foundations

Summary

The uses of UHPC are today playing an important role in the construction of offshore wind turbine foundations. Offshore wind speeds are more than 30% higher than speeds onshore, and the offshore construction of wind turbines is planned to play an important role in the European goal of decreasing CO_2 emissions.

Keywords: UHPC in the construction of offshore wind turbine foundations

1 The driven Monopile

For most of the offshore wind farms installed in Europe, the preferred solution has been driven Monopile foundations. Part of the reason for the success of the driven Monopile is the method introduced in 2000 whereby the bottom tower section (the Transition Piece) is connected to the driven Monopile with a pumpable self compacting UHPC.

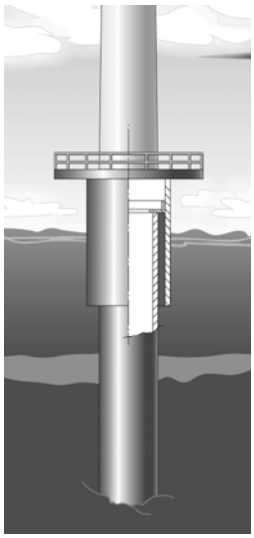

The solution accommodates the possibility of adjusting for out of verticality of the Monopile after driving, by tilting the Transition Piece to the vertical before filling the gap with UHPC. In addition, the Transition Piece can be prepared with installation of accessories onshore in order to save expensive offshore work (Figure 1).
To date, Densit has installed more than 320 units and over the next 12 months will be installing more than 250 additional units, representing altogether approximately 6000 tonnes of UHPC Densit material.

Figure 1: Driven Monopile with Transition Piece mounted

2 The Transition Piece (TP)

In order to install the UHPC offshore and under water, a number of things have to be in place.

First of all, a sealing system has to seal the bottom of the annuli between the TP and the Monopile in order to keep the UHPC from flowing out into the sea. Different seals have been developed for this purpose.

For an outside mounted TP, a wiper seal has mainly been used. The wiper seal is a rubber seal bolted onto the bottom of the TP, which has an opening diameter smaller than the Monopile. When the TP is lowered over the Monopile, the seal is forced to open by the weight of the TP, thereby tightening against the Monopile. The UHPC is then pumped through a pre-installed 75 mm steel pipe with an inlet just above the seal. Figure 2 shows a TP with a seal and a U profile ring channel.

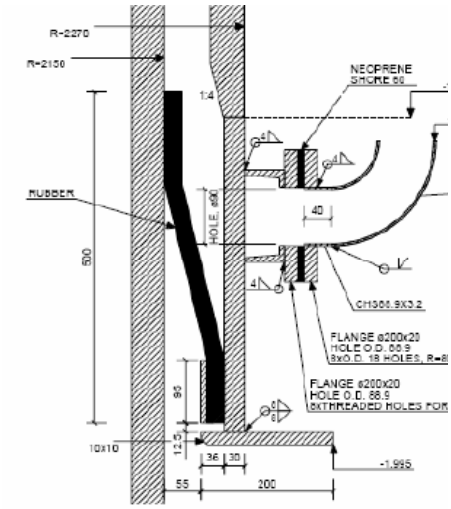

Figure 2: Wiper type seal

For an inside mounted TP, inflatable seals have mainly been used. This type of seal has been used in the offshore industry for years (Figure 3).

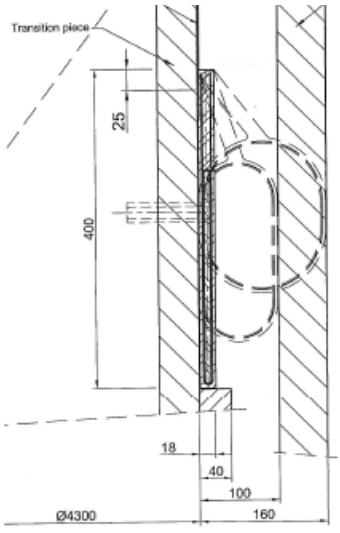

Figure 3: Inflatable Seal

3 The Development of Densit UHPC self compacting concrete

- In 1972, Aalborg Portland launched a development project “New Concrete”.
- The Densit® technology or the DSP-technology was invented and developed (DSP – Densified Systems with ultra-fine Particles).
- In 1978, the Densit technology was patented.
- In 1983, Densit a/s was established as an independent company
- In 1995, Densit made a full-scale test, pumping and filling a large pipe with UHPC named “Ducorit®” under offshore conditions. Densit was awarded its first contract for reinforcing a number of Jacket platforms for Philips Petroleum, and the offshore activities started growing.
- Over more than 3 decades, Densit has refined its methods and has a thorough understanding of how to control the process of industrial manufacturing of Ducorit® UHPC.

4 Keeping the promises

As most installations are done under water in dynamic loaded structures, knowledge about installation and the quality of the installed product is very important.
The costs of making mistakes in this kind of applications are unacceptable. Furthermore, no efficient or realistic test methods of checking the installation exist, apart from observing overflow of material.
Therefore, the key performance factors for the the supplier are:

- A thorough documentation of the product’s characteristics under extreme chemical and mechanical conditions. See bellow (Figure 4:Mechanical Properties of Ducorit®), (Figure 5: SN curve for Ducorit® D4), (Figure 6: Densit vs. good concrete)
- A well-documented QA system which includes tests of the material before it is delivered for installation.
- Thorough knowledge of the behaviour of the material in order to advise the customer how the material can be installed for best results to ensure that the material acts as an integrated part of the structure.
- Expertise in making efficient Method Statements to ensure that all elements of the installation are described with contingency procedures, in an efficient and safe way as well as prescribing safe QA and health and safety. Over the years, the Method Statement and QA have been approved and certified by DNV and GL.
- Having highly efficient and reliable mixing and pumping equipment with adequate redundancy to ensure uninterrupted installations. A breakdown during installation is not an option.
- Having a number of qualified supervisors with offshore certificates to handle all phases of the installation, including QA.

5 Material Properties

In order to be pre-qualified for deliveries and installations of UHPC as a structural element in an offshore structure, it is important to have a long proven record, showing that the material properties are constant and reliable. The key properties of the material are shown below. In addition, figures for Workability (ASTM flow), Air content, Setting time, Strength development for different temperatures, and Shrinkage are important factors.

	D4W Mean	S5W Mean	S1W Mean
Compressive strength f_c [MPa/psi]	210 / 30,400	130 / 18,850	110 / 16,000
Static modulus of elasticity E_c [GPa/ksi]	70 / 10,000	55 / 8,000	35 / 5,000
Dynamic modulus of elasticity E_d [GPa/ksi]	88 / 12,800	60 / 8,700	37 / 5,400
Tension strength f_t [MPa/psi]	10 / 1,500	7 / 1,000	5 / 725
Flexural strength f_{bt}* [MPa/psi]	23.5 / 3,400	18 / 2,600	13.5 / 2,000
Density ρ [kg/m³]	2740	2440	2250
Poisson's ratio ν	0.19	0.19	0.19
Fracture energy G_F* [kN/m]	12	5.6	4.0
Static coefficient of friction μ	0.6	0.6	0.6

(minimum 28 days curing at 20°C)
** with 1.9% by volumen of steel fibres*

Figure 4: Mechanical properties of Ducorit® UHPC

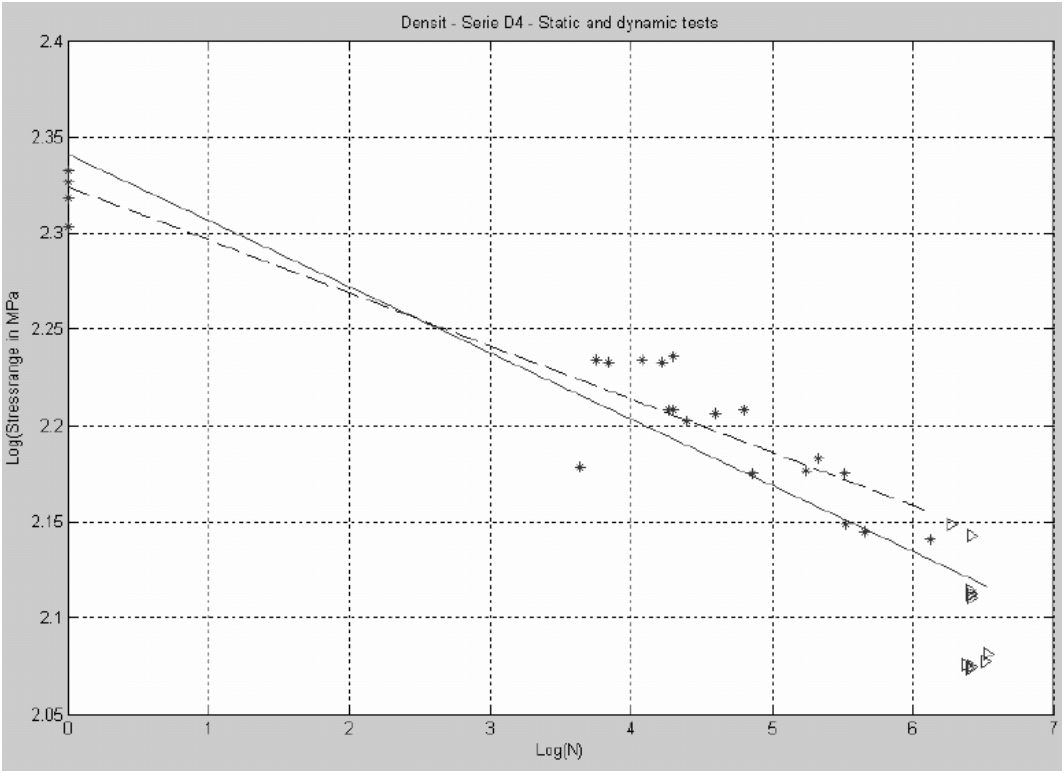

Figure 5: Ducorit® D4 SN curve, mean compressive strength 210 MPa. [1]

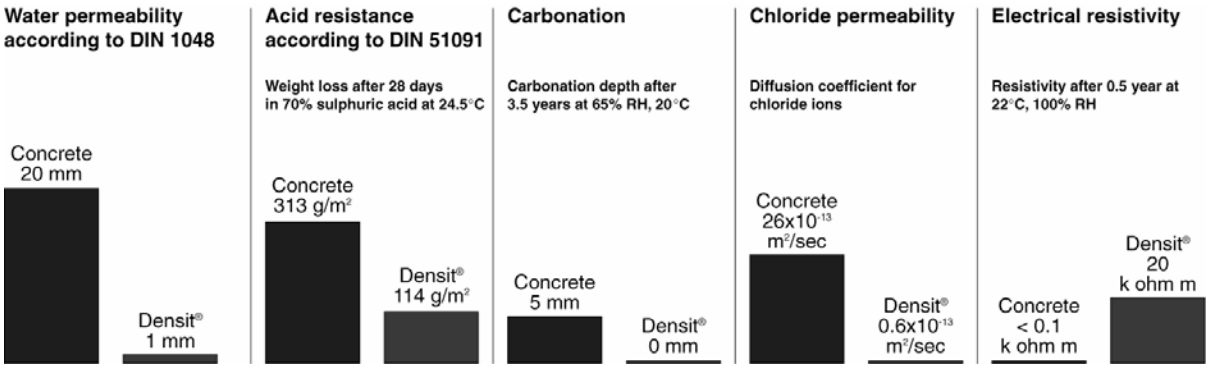

Figure 6: Densit versus good concrete

6 Manufacturing QA

Densit is ISO 9001 certified and is in the process of obtaining certification to OHSAS 18001 (occupational health and safety management system) and ISO 14001 (which covers the top environmental performance requested in the offshore sector).

Two important parts of our manufacturing QA are:

1. All products are tested prior to delivery to our customers as described below :

   A representative sample of Ducorit® is taken for each 30 tonnes produced. The sample is mixed with prescribed water, and the following properties are measured:

   - "Wetting" time
   - Workability (ASTM flow)
   - Air content/density
   - Setting time
   - Compressive strength (23 hours 80°C, ø45 x 90 mm cylinders)

2. Full traceability of all manufactured material is ensured through unique numbering of the bags.

7 Equipment

For offshore installations, there have to be incorporated redundancy for all elements in the installation in order to prevent any installation delays. The cost of delays is so high that any delays are unacceptable. Furthermore, castings done in more than one stage cannot be accepted due to the risk of non-performance.

All materials are batch mixed to avoid separation during transport and also to get acceptance to minimum QC offshore. Densit has developed its own heavy duty mixing plants with a semiautomatic water dosage system. The equipment is mounted in a 20’ half-height container for easy transport and handling.

For pumping, standard UHPC Putzmeister concrete pumps are used.

A standard set-up is shown below. The skid has a capacity of 12 tonnes per hour for mixing and pumping. On a typical wind turbine Monopile with TP, an average of 20 tonnes of UHPC Ducorit® material are used (Figure 7 shows a standard set-up for mixing and pumping Ducorit® UHPC).

Figure 7: Standard set-up for mixing and pumping UHPC

8 New structures for foundations in deeper water

In the oil and gas sector, structures for deeper water have been used for decades. Among these are Jacket and tripod structures, which could also be designed to carry wind turbine loads as well. These structures are, however, very expensive and if they are going to be economical for wind turbine foundations, they will need to be optimized.

9 Concrete Tripod

Figure 8 shows a tripod structure made in concrete where the piles and shaft are connected with UHPC. The design is by Grontmij/Carl Bro, who also designed the gravity foundations for the Middelgrunden offshore wind park and the concept design for Nysted and Lillgrund. Further information: www.grontmij-carlbro.com.

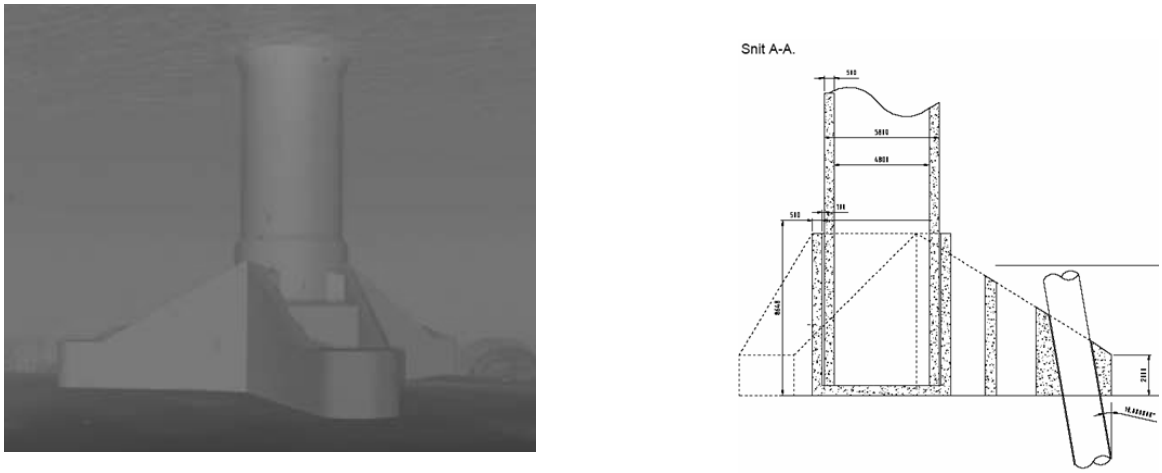

Figure 8: Concrete Tripod structure

9.1 Multi Pile Foundation

New patented concept developed by the German company Bard Engineering. The three Monopiles are connected to the centre structure with UHPC. The structure is designed for a 5 MW wind turbine. Further information: www.bard-engineering.de.

Figure 9: Multi Pile Foundation

10 Closing Remarks

The offshore wind turbine part of the market is still only a fraction of the size of the onshore wind turbine installation. To date, approximately 1600 MW has been built or is under construction. Looking at the forecast for Europe, this figure will increase dramatically during the next decade.

For water depths greater than 30 metres where new structures will be needed, it is important, that all parts of the structures are made more cost-effective. Alternatively, new, cost-efficient methods nedd to be developed for deeper water in order to make the offshore installations competitive. We expect that UHPC will play an important role in this new development as it has in the past for oil and gas structures as well as for offshore wind turbine foundations.

11 References

[1] Fatigue test with Densit “D4” UHPD, Aalborg Research Laboratory 2005, Aalborg University.

Gregor Zimmermann
Dr.-Ing.
G.tecz
Kassel, Germany

Manfred Grohmann
Prof. Dipl- Ing.
University of Kassel
Kassel, Germany

UHPC free form design with pneumatic formwork

Summary

Since Neff developed in the 1940s the pneumatic formwork the technologies didn't change significantly or are well established. Nowadays, those systems are known as airforms and the structures as monolithic domes. After a big boom in the 50s and 60s the pneumatic formworks and the shells lost ground because of their low architectural and design potentials. Today, new materials for membranes but also for concrete are available. So the idea is: combining traditional well known technologies -pneumatic formwork- with new high-tec materials -ultra high performance concrete- to enhance and develop a new pneumatic formwork as well as freeform structures to feature new architectural qualities. The result of this idea is the -Membrane Concrete Grid Shell-.

The paper will give an insight to the invention of the pneumatic formwork and theoretical descriptions of how MCGS structures could be designed, engineered and pre-dimensioned with tools like Rhino, ANSYS and RSTAB. The theory of optimizing respective reducing membrane wrinkling with ANSYS will be described and compared with prototypes. Also the question of the steel fibre orientation will be shown and solved with a very simple method for a fast pre-dimensioning. The “bending” test runs of 1:1 prototypes will show how strong a UHPC concrete grid shell with small cross sections could be. In this context it will be discussed, if it's possible to automate the design process for details e.g. by using Generative Design.

Keywords: *Membrane Concrete Grid Shells, UHPC - ultra high performance concrete, membrane formwork, pneumatic formwork, topology optimization, form finding, steel fibre orientation, generative Design, Finite Elements, fluid dynamics, FEM.*

1 Introduction

The main idea was to combine well known but different construction or assembly types in combination with new materials to get a new structure and construction method. Thus, the focus was to point out the technical advantages as well as the development of cost-effective construction systems. Secondarily an architectural appealing system respective structure should be the result of the new construction system.

In the last decade, some new technologies in the building industry had been developed but not often used. As there are new concrete types like UHPC (Ultra High Performance Concrete) that could take large pressure, flexural and tension forces or Membranes with new surface coatings that are more resistant against environmental influences.

In addition, the idea of combining pneumatic formwork and concrete shell structures is not new. Innovative is the use of UHPC that includes the reinforcement in combination with inflated double-layered membrane structures, which are directly connected to each other or joint with membrane flaps. Those membranes are arranged in a special configuration that continuous chambers could be created and filled with UHPC or another self-hardening material. The result is a thin Membrane Concrete Grid Shell, particularly a thin wide spanning concrete grid shell with nearly any user-defined concrete grid respective mesh with a curved even double curved shape.

2 Functional principle

2.1 Principal of Membrane formwork

The principle of the membrane formwork is very straightforward. One membrane layer (Fig. 1 (1)) - the first and inner layer - acts as airhall and thus as supporting structure for the second membrane layer (Fig. 1 (2)) that defines a chamber system. The airhall layer is based on the usual rules for air-supported structures: membranes must be confectioned and details dimensioned respective inner pressure and loads; the author recommends the Lufthallenhandbuch IL15. The second layer is subjected to different requirements. First and foremost, the membrane must be confectioned for the geometrical demands of the final concrete grid shell. Considered must be the inner pressure respective dead load of the fluid concrete and thus the shearing stress of the welded seams. Another aspect is avoiding wrinkling and due this a cutback of the final concrete section. Those criteria could be fulfilled, as shown in paragraph 3.

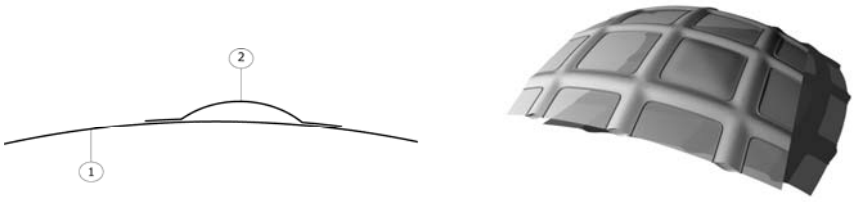

Figure 1: Left: Schematic section with pneumatic supported airhall layer (1) and secondary membrane (2). Right: Visualization of cruciformed membrane formwork.

2.2 Material – Ultra High Performance Concrete

The reduction of weight respective dead load of the reinforcement as well as dead load of concrete during the assembly of the MCGS inflated system and the minimization of concrete for structural, architectural and design aspects are the main ideas. Besides this, there is one boundary condition: no constructive steel reinforcement could be insert into the membrane chamber formwork. To obtain this, the new ultra high performance concrete (UHPC) was chosen. The institution “Structural Materials” at the University of Kassel was involved in the development of this special UHPC. It is a self-compacting concrete with a high Young's module of about 55000 N/mm², a compressive strength of between 110 N/mm² and 250 N/mm², the tensile strength is up to 17 N/mm² and bending stiffness is about 39 N/mm².

Further values are w/b=0.2 and w/z=0.28. Small steel fibres with a length of 20 mm and a thickness of 0.1 mm are added and will affect the high ductility.

2.3 Erection of the MCGS

The erection of a Membrane Concrete Grid Shells could be done in 6 steps. 1) Fixing the prefabricated membrane at the base. 2) Inflating the airhall. 3) Inflating the membrane chamber system. 4) Gradual pumping the concrete bottom-up while regulating the inner airhall pressure. 5) Repetition of step 4 till the concrete structure is complete. 6) Deflating the airhall and removing the membrane after the concrete structure is hardened. Optionally the membrane could be left and used as façade. Finally a second façade e.g. glazing could be installed.

Figure 2: Erection and concreting steps of a hemisphere shaped MCGS

3 Formwork – Chamber system

The membrane formwork is subjected to several conditions like: shape of the airform, inner pressure of the airform, geometry of the final concrete grid shell, dead load of the fluid concrete while pumping and especially cut-out concerning the reduction of wrinkles.

3.1 Dependency: Pressure – Shape - Moment of inertia

Fig. 3 shows the typical section of the membrane formwork and the deformation under inner pressure. Due to the first membrane layer is prestressed, the chamber respective formwork could not shape an ideal circular geometry. So the upper and the lower part of the section are segments with different centres. While the perimeter of the formwork section will always be the same, the area (Fig. 3) and thus the moment of inertia (Table 1) could change depending on the inner pressure.

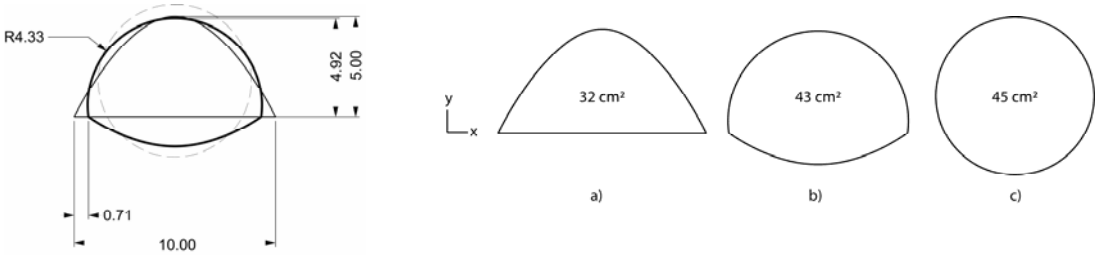

Figure 3: Left: Comparison: initial membrane formwork section, pneumatic deformed section and idealized circular section. Right: Section areas with constant perimeter.

A further boundary condition for the dimension of the final concrete section is the shearing stress of the welded seam. Thru pulling the second layer from the first layer under an angle between 0 and 180 degree, the membranes will peel off. So another constant is the

maximum feasible shear stress for the seam. Experimental tests with membranes TYPE III showed, that welded and stitched seams could take loads up to 12.5 kN/m under an angle of 180 degree.

Table 1: Shaping effect regarding the moment of inertia.

Moment of inertia	**a)**	**b)**	**c)**
I_x	55.6 cm^4	109.6 cm^4	163.7 cm^4
I_y	162.7 cm^4	200.3 cm^4	163.7 cm^4

Based on the fact, that the sections will be circular, the tangential stress of the cylindrical membrane chamber could be calculated with the “Kesselformel” (1).

$$\sigma_t = \frac{p * D}{2 * s} \quad (1)$$

Via reverse calculation, it’s now possible to determine the potential concrete section diameter subjected to the pumping height of the UHPC. For example: with a section diameter of 0.15 m, the concrete could be pumped to a height of 6 m. If the final construction will be higher then 6 m, the erection of the construction must be done in several concreting steps.
In summary, the geometry change of the membrane formwork caused by the inner pressure of the fluid UHPC will generate different concrete sections with non-continuous static properties. This must be considered for the dimensioning of the final concrete grid shell. By the use of modern Finite Element Software, this problem could be solved, but with an enormous calculation time. To simplify a pre-dimensioning of a Membrane Concrete Grid Shell, the author recommends the following approach: the simplified calculations for the grid shell could be done with an inscribed circular profile. For instance: a circular profile should be inscribed into Fig. 2 section b). Thus the static properties are reduced and are including a safety factor.

3.2 Optimizing the geometry of the formwork

Beyond the static properties of the membranes and seams, the wrinkling of the membranes is an important topic for the static properties of the final concrete grid shell. Every wrinkle will reduce the concrete section and causes a weak spot. The complexity for the cut-outs is very high, because a double curved membrane must be confectioned and welded to a double curved airhall – wrinkles are foreknown.
The reduction of wrinkles is possible. In these studies, it’s done by the parameterization of the formworks geometry. Fig. 4 shows the geometry of the prototype with the cruciform formwork layer in the middle (left). The lower left symmetric quarter is shown with a spline that defines the geometry of the formwork. By changing the splines parameters, the geometry of the final “cross” will change.
With generative design, which means the automatic and iterative generation, calculation and evaluation of the symmetric detail, it is possible to develop an optimized second formwork layer. Calculating wrinkles with FEM software is very complex and computationally intensive.
Thus the author used fast ascertainable attribute of the Finite Elements: the rotation in every direction. Optimizing the formwork under inner pressure means reducing the rotation sum of

the Finite Elements. Fig. 5 shows the rotation sum of the initial geometry. The red areas are representing the wrinkles, which will occur. The right image shows the optimized geometry. Red areas are nearly vanished.

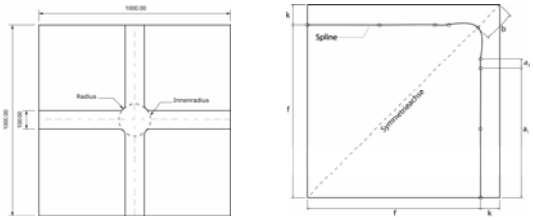

Figure 4: Left: cruciform formwork geometry and parameter.

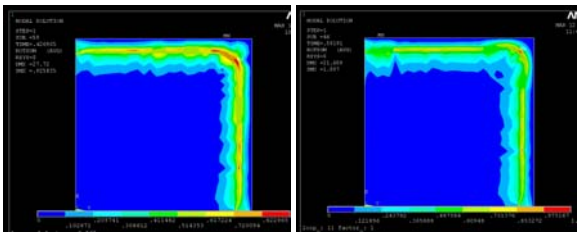

Figure 5: Finite Element rotation sum; initial and optimized.

This works not only with simple geometries. A further test series was done with more complex circular formwork geometries. Wrinkles could be avoided.

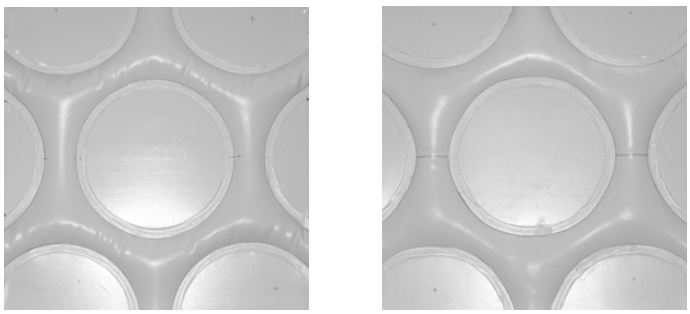

Figure 6: Prototypes Left: Initial shape with wrinkls. Right: Optimized shape.

4 Prototypes

Beside the verification of the geometrical formwork parameters, the static properties of specimens must be proofed. As the following paragraphs will show, the geometry of the formwork respectively the final concrete grid shape and the load-carrying capacity are directly correlating. Cause is the fluid dynamic property of the steel fibre reinforced concrete.

4.1 Cylindrical formwork

The main question is: Are the UHPC material properties equal along a structural-member? Therefore a simple cylindrical, vertical orientated membrane formwork was filled with UHPC from bottom-up. UHPC M1Q with 1.5 vol.% steel fibres (D/l = 0.19/9 mm) was pumped with an pressure of only 3 bar. After 7 days of hardening the membrane formwork was removed. 28 days later, the specimen was fragmented into 16 cylindrical peaces and tested on compression strength, flexural strength, density, fibre share and fibre orientation

The results showed, that the material properties are not homogeneous but changing along the specimen. While the compressive strength parallel the fibre orientation is between 140 N/mm2 and 160 N/mm^2, the perpendicular compressive strength is between 190 N/mm^2 and 218 N/mm^2. Also the flexural strength of the material varies between 17 N/mm^2 and 38 N/mm^2.

Particle flow simulations with ANSYS showed and approved, that the fibre orientation and the fibre allocation is mainly responsible for those results. At the filler neck, the fibres are orientated in any angle what leads to a low compressive strength. At the middle and the top of the specimen, the fibres are orientated parallel to the flow direction and thus leads to a higher compressive strength. Because of the different fibre allocation at the top and bottom, the flexural strength is reduced compared to the middle part.
This means for the dimensioning of the MCGS construction: The material properties of the UHPC must be attenuated for calculations. The dimensioning of the final concrete grid shell must be done with simplified assumptions.

4.2 Cruciform formwork

In further test series more complex cruciform geometries were proved. The focus was to get information about the wrinkling of the formwork with non-optimized geometries and those effects on the sections and the load-bearing behaviour. Coeval the fibre orientation, as shown before, takes effect and was determined analogue and with the FE software ANSYS.

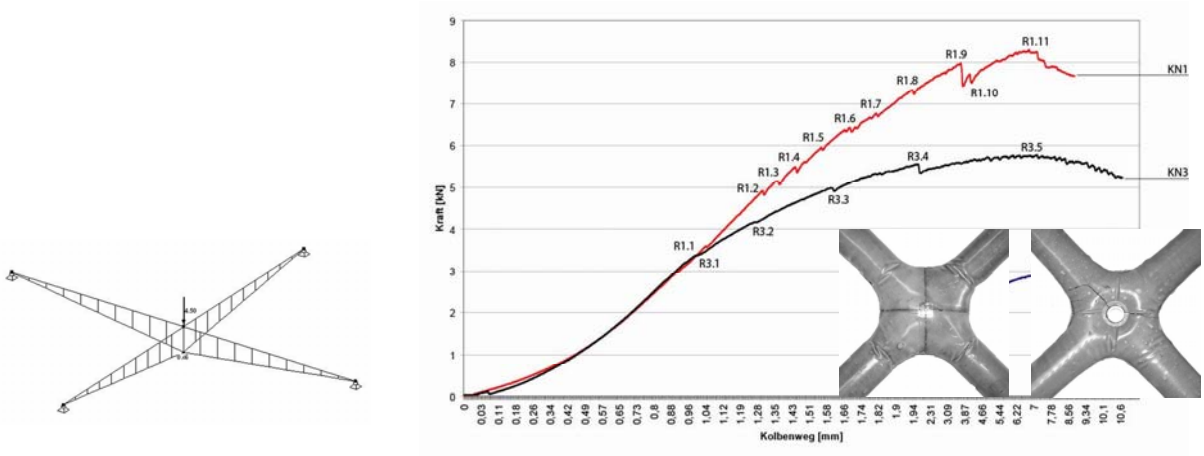

Figure 7: Left: Load bearing test series for cruciform UHPC structural members: Supports at the ends, load located in the centre.

Load-bearing tests (Fig. 7) were done by supporting the cruciform specimens at those ends and increasing loads stepwise at the centre. If you think of double curved grid shells, this load configuration is not usual but represents the worst case: high local forces that results in extreme moments at the weaken (wrinkled) sections. Fig. 7 shows also the load-bearing diagram of the details KN1 and KN2. Both are produced with a non-optimized geometry. KN2 features an opening in the centre for reducing the volume and fixing a secondary façade.
The curves are visualizing the ductility of the details KN1 and KN2. The second specimen KN2 could take a load of about 5.8 kN but with smaller sections and a lower dead load which makes it more effective, compared with KN1.
Besides those results, the failure behaviour respective the layout of the cracks was interesting. As foreseen, the first cracks at specimen KN1 appeared at the notches caused by the wrinkled formwork. Whereas KN2 showed a different crack pattern. The first crack (R3.1) appeared at the centre, increased parallel to one arm and spitted up to a Y (Fig. 8). The particle flow simulations were clarifying the causation. The fluid UHPC was pumped from

bottom-up, streamed to the left and right arms and finally up. Behind the circular formwork a ‘slipstream’ appeared where the fibres were orientated parallel and thus reduced the materials strength respective the sections resistance. Further ANSYS simulations with coupled fibre orientation and material strength resulted in similar crack patterns and failure behaviours.

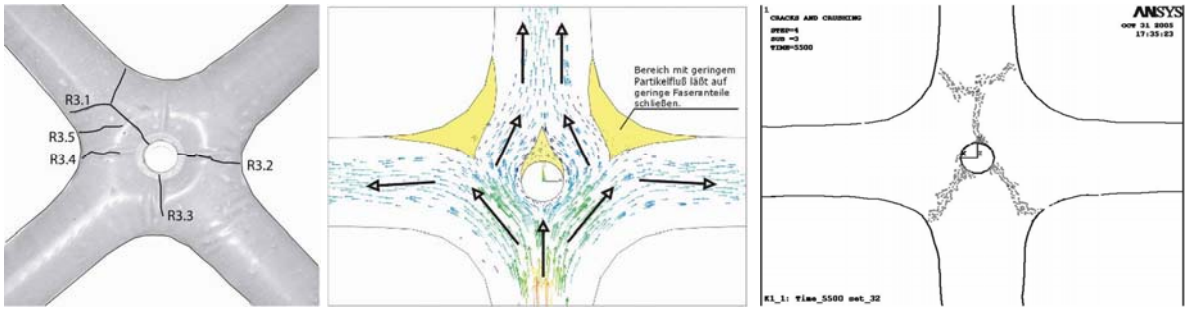

Figure 8: Left: Crack pattern of KN2. Right: Particle flow simulation and crack analysis.

With those coupled simulations it is possible to analyse the weak points and dimension the structural details. A complete simulation of a MCGS structure is hard to realize because of the enormous computational effort. With the results of the scientific research, the author developed a simplified 3D framework pre-dimensioning method for *membrane concrete grid shells*.

5 Membrane Concrete Grid Shells

5.1 Pre-dimensioning

Material properties must be attenuated for calculating and dimensioning. Regarding the specimen test series, the permissible compressive stress should be reduced to 150 N/mm^2 and tension stress to 13 N/mm^2. According to the German DIN 1055 and DIN 1045 the safety factors must be considered. For dimensioning MCGS constructions, the software RSTAB (Dlubal) was used and extended with specially written software. A tool for regular, triangular meshed hemisphere-MCGS constructions was developed, which could automatically generate and dimension the structures including analysis of dynamic behaviour and buckling.

After dimensioning the ideal circular sections of the structure, the geometry transformation for the formwork follows. Therefore a transformation code was developed, that allows the direct geometry transfer into the formworks geometry. This new formwork section must be positioned and extruded along the system lines of the grid shell. The knots then are an automatically generated freeform surface between the current ends. The airform membranes must be developed as a freeform surface between the system lines. Further dimensioning and machining of the membranes is conforming to the known techniques from airhalls and textile architecture: unrolling, compensation, cut out, seam allowance. Membrane calculations could be done e.g. with ANSYS or EASY. Thereby another technical component must be recognised: The deformation of the airhall caused by the dead load of

the fluent UHPC before hardening. To prevent deviations from the ideal geometry, the inner pressure must be conditioned.

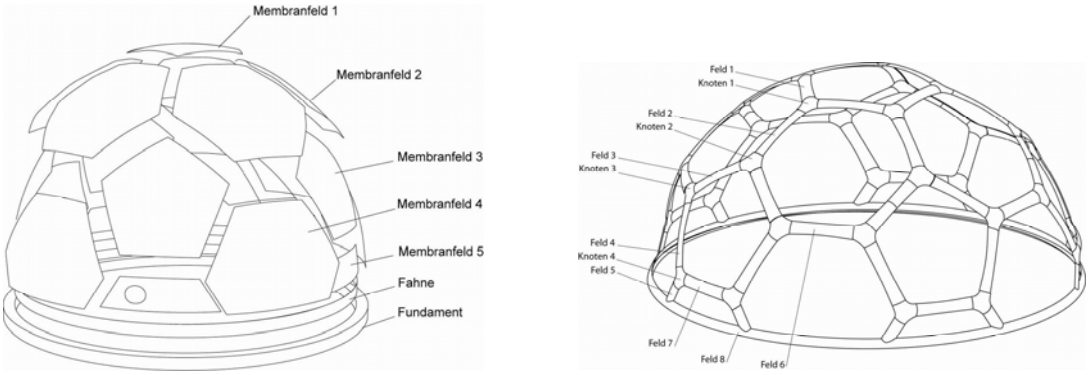

Figure 9: 3D membrane geometry for a small MCGS dome (diameter 6m). Left: Airhall membranes. Right: Formwork layer.

6 Conclusion

The idea of combining well-known construction systems with new building materials to upgrade or advance those is very simple. In this case, it's the new steel fibre reinforced ultra high performance concrete, which allows the pumping into small membrane formworks without the use of additional rebar. UHPC allows a minimal dimensioning of sections and enables large spans for thin shells. Airforms and membrane formwork could be form-fined and patterned with software like ANSYS, EASY or RHINO. The technologies to manufacture and build those structures are given and well known.

The technical coherences between airform, membrane formwork and final structure are complex. For example: The Load-bearing behaviour is dependent on fibre orientation and section respective wrinkling of the membrane formwork. Wrinkling depends on an optimized formwork geometry that again depends on the structural design. Parameters are recursively linked to each other. At all, details could be developed, analysed and dimensioned as shown in this paper. Necessary are simplifications for the handling of complete concrete grid shells. Those are leading to a constriction of material properties and the slight oversizing of sections.

Architects and designers are getting a new and simple method to build shapely structures. The challenge consists in the calculation and dimensioning of optimal respective minimal structures and their adaptation to the airform.

7 References

This paper is an abstract of the dissertation 'Membran Beton Gitterschalen Tragwerke' from Gregor Zimmermann at the University of Kassel, department architecture, division structural design in November 2006.

[1] Zimmermann, Gregor: Membran Beton Gitterschalen Tragwerke – Entwicklung und Vorbemessung; Books on Demand, Norderstedt. 2006, ISBN 9783833491153

Petr Hájek
Prof. C.Eng. CSc.
CTU in Prague
Prague, Czech Republic

Ctislav Fiala
C.Eng., researcher
CTU in Prague
Prague, Czech Republic

Environmentally optimized floor slabs using UHPC - contribution to sustainable building

Summary

Optimization of material consumption is one of the basic approaches applied in the development process of new types of structures, respecting requirements of sustainable construction. New composite high performance silicate materials could be used for construction of stronger, more durable and at the same time slender structures. The optimized lightened shape of structural elements demands less material and consequently it can lead to the improvement of environmental parameters of the entire structure. The application of HPC and UHPC is more frequent in engineering structures, such as bridges. However, in building structures there is also a good chance to reduce environmental impacts and simultaneously to increase structural reliability and safety by the use of new types of high performance concretes.

Keywords: *environmental impact, optimization, RC floor structure, UHPC, recycled materials*

1 Background

During the twenty years from 1974 to 1994 the world population increased by 40 %. Cement and steel production, municipal waste generation are increasing even faster [1] (Fig. 1).

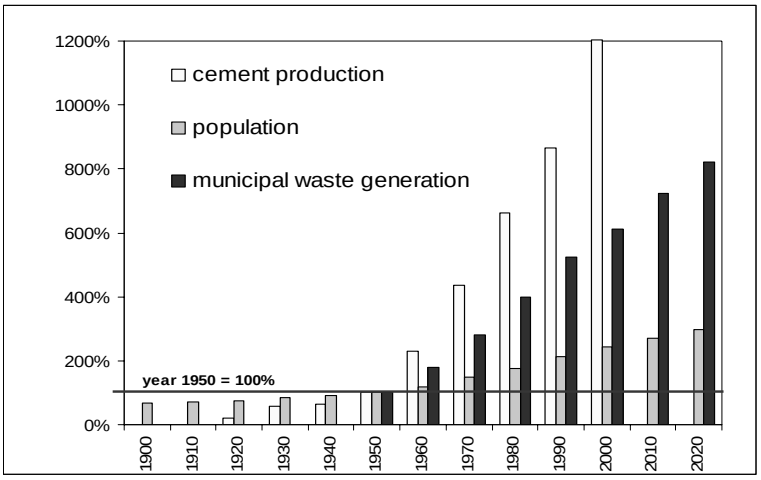

Figure 1: Tendencies in cement production and generation of municipal waste (OECD data) are compared with the population growth and its expected development up to the year 2020

The need for material saving was clearly specified in general Rio Agenda 21 (Changing Consumption Patterns) published in 1992: "To promote efficiency in production processes and reduce wasteful consumption in the process of economic growth".
Buildings in EU and other developed countries are responsible for more than 40 % of the total energy consumption, and the construction sector generates approx. 40 % of all man-made wastes [2]. The extraction of raw materials for construction of buildings, manufacturing of building products and waste landfill or incineration are associated with corresponding environmental impacts, including greenhouse gas emissions. Buildings are thus consequently responsible for more than 30 % of released CO_2 emissions.
Development of new materials, structures and construction technologies for construction of buildings should be thus based on the struggle for the reduction of primary non-renewable material and energy resources, while keeping performance quality, safety and durability on a high performance level.
Structural safety of the construction in all its life cycle stages, including exceptional situations (natural disasters, explosions, fires, etc.) comes to prominence in the hierarchy of the design criterion importance. This is also due to the increasing risk level resulting from the rise of exceptional load situations caused by global climatic changes, as well as terrorist attacks.
Both the requirements, (i) the reduction of material consumption (leading to more slender structures) and (ii) the increase of structural reliability, durability and safety can be at first sight considered as being in contradiction – the search for the optimum assuming one criterion often causes the decrease of the other criteria value. Using traditional construction materials and technologies, the typical result of the effort to ensure a higher level of structural reliability and safety is the robust structure (which needs more construction materials).
However, using high performance concrete it is possible to design more slender structures, while structural reliability and safety are kept at the required high level. Consequently environmental parameters could be improved due to primary material savings. All these aspects represent significant contribution to sustainable construction.

2 Application of UHPC in building construction

The most significant feature of UHPC is high compressive strength which allows the design of more slender structural elements. Such filigree structures could be at the same time more strong and durable. It is due to the very dense material structure and increased resistance to corrosion. Thus, UHPC offers new solutions for innovative construction in harsher conditions like aggressive environment or exceptional loads (earthquakes, floods, strong winds, blasts, etc.). Moreover, environmental impacts can be due to primary material savings reduced.
The application of UHPC is currently more frequent in engineering structures like roads and bridges [3]. However, there is a big potential for the use of UHPC also in building structures.
The advantages of application of HPC and UHPC in building construction are as follows:

- higher compressive strength permits construction of slender and lighter structural members with reduced use of primary material,
- UHPC can be used for large span structures and imposed to heavier loads,

- due to higher density the material is more durable (it requires less maintenance and repairs); it can be used also in some types of aggressive environments,
- lower loads from slender (lighter) structural members on supporting members (walls, columns, foundations) lead to reduction of their dimensions,
- structural members from UHPC are stronger and can be more ductile (e.g. if fibres are used) – the structure is more resistant in case of earthquakes or other exceptional load cases – like natural disasters, terrorist attacks, etc.,
- slender structure = less material consumption = less demolition waste = less demands on transportation = lower environmental impacts.

Several examples from abroad show that new composite fibre silicate materials and corresponding technologies can be used for thin "shell" elements with the thickness less than 30 mm (e.g. Ductal® – France). For more than two decades, high strength concretes with compressive strength 50 – 130 MPa have been used in construction of tall buildings. Due to higher compressive strength of HPC in vertical load bearing structures, it is possible to design smaller cross sections with a reduced amount of material.

The first known use of UHPC (with more than 150 MPa) in building construction dates to 2001, when in Joppa (USA Illinois) a clinker silo was built with the roof from Ductal® concrete with compressive strength up to 220 MPa and flexural strength 50 MPa. The ultra light, thin precast panels were designed without any conventional reinforcement by steel bars.

3 Environmental impact of concrete and concrete structures

Considering the volume of produced concrete and the number of concrete structures, the problem of their environmental impact forms a significant part of the whole global problem of sustainable development. The specific amount of harmful impacts embodied in a concrete unit is, in comparison with other building materials, relatively small. However, due to the high production of concrete (Fig. 1), the total negative impact of concrete structures is significant. Every improvement of concrete design principles, production, construction and demolition technologies, methodologies of assessment and management of operation of concrete structures thus provides a very significant contribution on the way towards sustainable development.

3.1 Potential for reduction of environmental impact by the use of UHPC

Using UHPC it is possible to design slender shell structures with reduced use of materials. This leads to reduction of environmental impacts connected with the use of primary natural sources and reduction of deposition of waste from demolished structures.

Potential reductions of environmental loads are:

- savings in natural resources (especially non-renewable ones),
- savings in transport environmental loads (less material, lighter structural elements, less demolition waste),
- savings in maintenance and repair demands due to higher durability,
- reduction of the volume of waste material at the end of the life cycle of the structure.

3.2 Use of recycled waste materials

The reduction of primary non-renewable resources and consequent reduction of waste amounts can also be supported by the use of secondary recycled materials originating from the waste from construction, as well as other industries. Some secondary materials (such as fly-ash, silica fume, slag, etc.) are commonly used in production of new types of concrete.
The main attention should be paid to those waste materials which are produced in large amounts and are not recycled or just a small amount is recycled. Such waste materials are e.g. non-sorted plastics and laminated carton drink boxes from municipal waste.
Several alternatives of RC floor structures lightened by fillers from recycled municipal waste have been developed, optimized and experimentally tested within the previous research at CTU in Prague.
Two types of lightening fillers from recycled waste plastic and one type from structural boards from recycled laminated cartons were developed [4]. The shapes of fillers were determined as a result of integrated environmental design and optimization considering environmental criterions, as well as structural parameters of the resulting composite RC structure.

3.3 Environmental parameters of concrete

Evaluation of environmental impact of any structure is highly determined by the quality of available data. There is no standard data set of unit embodied values for all components used in the concrete mix. One of the often used data source is Ökologisher Bauteilkatalog [5] in which the data are based on UCPTE electricity mix. These data were used in the following study for plain concrete, steel reinforcement and thin-coat plaster. Unit embodied values for recycled non-sorted plastic were calculated using energy and production statistical data provided by the producer – recycling company Transform Lazne Bohdanec. The data used for UHPC were taken from [3] (Teichmann and Schmidt). The composition of both types of concretes (C30/37 and UHPC) used in the study is presented in Table 1, environmental parameters are in Table 2.

Table 1: Composition of two types of concrete

Type of concrete		**C30/37**	**UHPC**
cement	kg/m^3	370	733
quartz powder	kg/m^3	-	183
quartz sand/gravel	kg/m^3	1800	1008
water	kg/m^3	170	161
silica fume	kg/m^3	-	230
steel fibres	kg/m^3	-	75

It is evident that UHPC have unit embodied values higher in comparison with plain concrete. This is due to the fact that steel and plastic fibres have higher values of embodied environmental parameters than plain concrete itself. An inclusion of fibres in the concrete mix represents an additional increase of embodied parameters. However, UHPC can be used for

more slender structures with significantly lower concrete content and without conventional reinforcement in thin parts of element cross sections.

Table 2: Embodied environmental parameters of different types of materials, using data from [3] and [5]

Type of material	**embodied energy** MJ/kg	**embodied emissions CO_2** kg $CO_{2,equiv.}$/kg
ordinary concrete C30/37 [5]	0.80	0.130
ultra high performance concrete - UHPC [3]	1.44	0.239
reinforcement (steel) [5]	13.00	0.800
recycled non-sorted plastic	7.36	0.492
thin-coat plaster [5]	1.40	0.140

4 Environmental assessment of selected alternatives of RC floor structures – case study

Several previously performed LCA (Life Cycle Assessment) analyses of RC floor structures showed that using the optimized shape and recycled waste materials it was possible to reduce environmental impacts, such as consumption of non-renewable silicate materials, the resulting level of embodied CO_2, embodied SO_x and embodied energy. Some results of previous LCA analyses have already been presented in [1] and [4]. The goal of the current analysis is to show if and how the use of UHPC in an optimized shape of an RC floor slab can contribute to the reduction of environmental impacts.

In total, three alternatives of RC floor structures have been analyzed. Alternative A is a reference full RC slab from ordinary concrete C30/37. Alternatives B and C are optimized hollow core pracast panels with lightening installation fillers from recycled non-sorted plastic [1], [4]. Alternative B is cast from ordinary concrete C30/37, alternative C from UHPC (composition and environmental data used from [3]). All alternatives were designed for the same performance – live load 2.0 kN/m^2, span 4.5 m and final flat ceiling finish. The overview of all the analyzed alternatives is presented in Table 3. The shape of fillers from recycled plastic is based on previous environmentally based optimization with the goal to reduce the amount of used concrete and reduce associated environmental impacts.

Alternative B (Figure 2): The lower ceiling and the top slab are 50 mm thick. In ribs (axial distance 600 mm), lattice reinforcement is inbuilt. Sides of the ribs are formed by installation fillers from recycled non-sorted plastic. Ordinary concrete C30/37 has been used for casting.

Alternative C: The lower ceiling and the top slab are 30 mm thick from UHPC without conventional reinforcement. In ribs (axial distance 450 mm), lattice reinforcement is inbuilt. Sides of the ribs are formed by installation fillers from recycled non-sorted plastic.

Table 3: Floor slab alternatives used in the environmental analysis

Floor slab alternative			Thickness mm	Self-weight kg/m^2
A	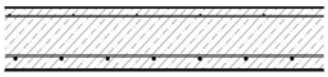	full RC slab from ordinary concrete C30/37	200	491
B		precast RC panel with lightening shell elements from recycled non-sorted plastic	200	310
C		precast UHPC panel with lightening shell elements from recycled non-sorted plastic	200	223

Figure 2: Precast filligran panel with installation shell elements – during experimental manufacturing in ŽPSV Company, 2006

The resulting relative comparison of environmental profiles of analyzed alternatives of RC floor structures is shown in Figure 3. The reference level 100 % is represented by the RC full slab.

The graph shows that the embodied energy in the UHPC alternative (Alt. C) is even higher by 4.1 % in comparison with the reference RC full slab. This is due to very high unit embodied values of UHPC (see Tab 2). However, very important is the reduction of the primary material use (for UHPC 62 %) and self weight (for UHPC 56 %) due to the optimized slender hollow core cross section. This has a positive effect on a level of environmental impacts associated with transport of materials and with the deposition/recycling of waste materials at the end of the life cycle. Consequently, lighter floor structures load less

supporting columns, walls and foundations – this can lead to the reduction of their dimensions, and additional material and environmental savings.

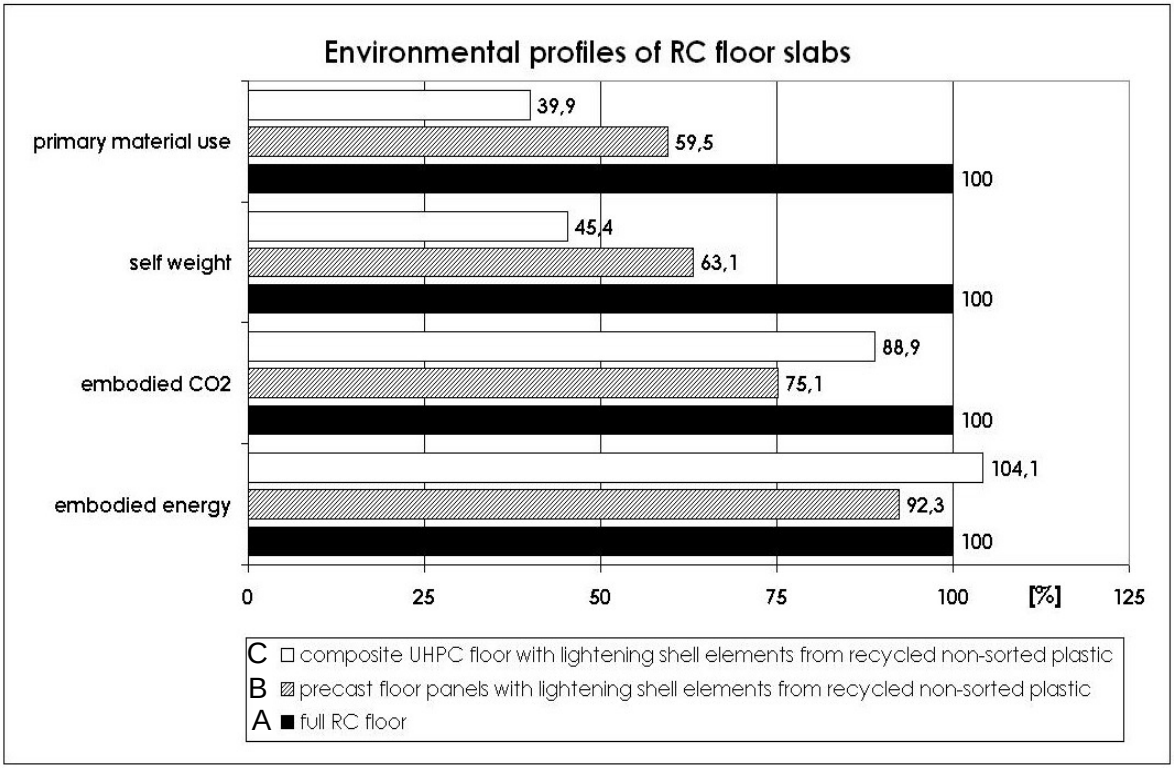

Figure 3: Environmental profiles of RC floor slab alternatives. Reference level 100 % is represented by a full RC floor slab

Figure 4 shows comparisons of input material flows (the construction phase) and output material flows (the demolition phase). Again a significant reduction of the total amount of the used material in the construction and demolition life cycle stages is evident. The proportion of used recycled materials and fully recycleable materials is based on the current construction practice and available recycling technologies, and is still rather small.

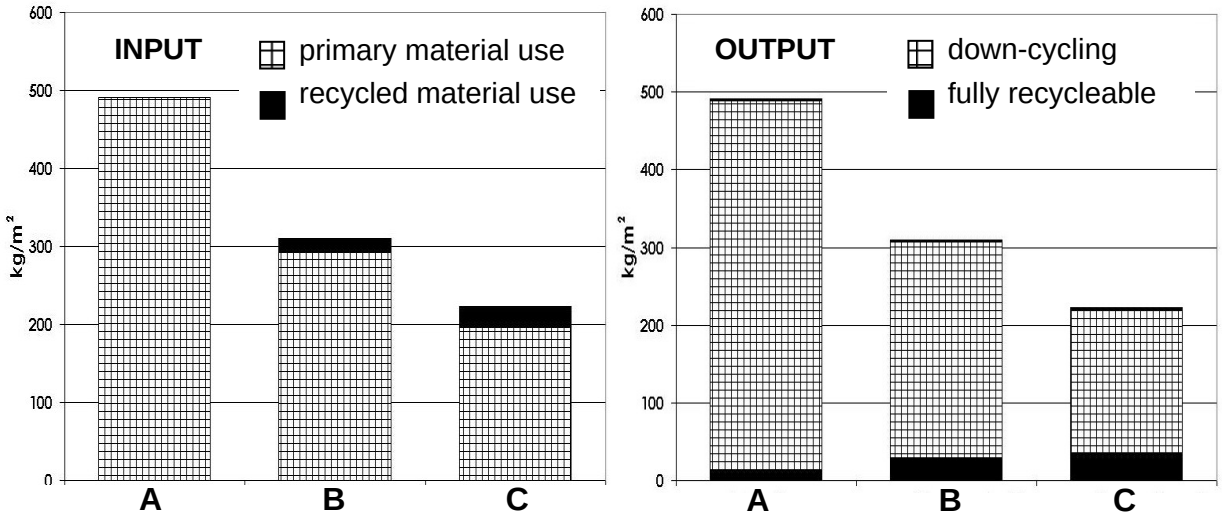

Figure 4: Input and output material flows for analyzed RC floor slab alternatives

5 Conclusion

The aim of the presented study was to show the potential of the use of UHPC in the building construction. The results are very dependent on the quality of available and used data. However, it is quite clear that although UHPC has higher unit embodied environmental values, there are environmental advantages achieved when using the optimized slender shape of the slab cross section.

The case used in the study (precast panel optimized for a 4.5 m span) is not very typical for the UHPC use. The reason for the selection of this case was to analyze an already developed precast panel for specific use in the construction of a large building near Brno and to check if the application of UHPC would bring some more environmental profits. However, the use of UHPC in large span floor structures will probably show more positive results.

A more complex assessment of the entire building considering the whole life cycle (including demolition and recycling) would show other associated environmental benefits. Moreover, high performance material properties (fire safety, water tightness, frost resistance, etc.) make structures more durable and more resistant against climatic effects and also safer in case of exceptional loads (like climatic disasters or terrorist attacks).

This all creates the potential for a wider application of UHPC for construction of sustainable buildings in the future.

6 Acknowledgements

This outcome has been achieved with the financial support of the Grant Agency of the Czech Republic Grant Project No. 103/07/0400. All support is gratefully acknowledged.

7 References

[1] Hajek, P.: The Way towards Sustainable Construction by the Use of Recycled Municipal Waste. In. Proc. Rethinking Sustainable Construction 2006, CD, RSC06 Sarasota, 2006.

[2] CIB: Agenda 21 on Sustainable Construction, CIB Report Publication 237, Rotterdam,1999.

[3] Schmidt, M, Teichmann, T.: Ultra-High Performance Concrete: Basis for Sustainable Structures. In. Proc. Central Europe towards Sustainable Building, CESB07, pp. 83-88, Prague, 2007.

[4] Hajek, P, Fiala, C.: Savings in Primary Material Use through Optimized RC or FRC Structures in Building Construction. In: CD, Sustainable Building 2007, SB07, HongKong, 2007.

[5] Waltjen, T et al.: Ökologisher Bauteilkatalog. Bewertete gängige Konstruktionen, Springer, 1999.

[6] Stengel, T., Schießl, P: Der kumulierte Energieaufwand (KEA) ausgewählter Baustoffe für die ökologische Bewertung von Betonbauteilen, Wissenschaftlicher Kurzbericht Nr. 13 (2007), cbm Centrum Baustoffe und Materialprüfung, TU München, 2007.

Jörg Jungwirth
Dr.–Ing., Structural Engineer R&D
SSF Engineering Consultancy
Munich, Germany

Günter Seidl
Dipl.-Ing., R&D Department
SSF Engineering Consultancy
Munich, Germany

Victor Schmitt
Dipl.–Ing., Director
SSF Engineering Consultancy
Munich, Germany

Dieter Ungermann
Prof., Dr.-Ing.
University Dortmund – Civil Engineering
Dortmund, Germany

Utilization of UHPC in Composite Structures – Lightweight Composite Structures (LCS) –

Summary

In the scope to optimize material utilization of the innovative material UHPC adapted composite structures - UHPC under compression and steel in tension - are assessed. A conjoint development project of the structural engineering firm Schmitt Stumpf Frühauf and the chair of steel construction at Dortmund University has been initiated in order to develop system solutions directly applicable in constructions. To take advantage of the special characteristics of UHPC classical detailing of composite construction has been modified. The utilized amount of material and hence the weight of the system has been reduced to a minimum leading to Lightweight Composite Structures (LCS).

The LCS-development project presented in this paper includes structural design of UHPC composite bridges, development and testing of new structural details and the implementation of the acquired knowledge in the design of a pilot bridge. UHPC has yet only been applied in structural concrete structures, UHPC composite structures are an innovative design.

Keywords: *UHPC, composite structure, shear connection, bridge structure; bond; composite / concrete dowel; external reinforcement*

1 Introduction

New materials provide possibilities for new structural concepts. After a period of material optimization in the 1990s the current interest in UHPC research and development mainly focuses on the adequate use of this innovative material. In a conjoint development project of the structural engineering firm Schmitt Stumpf Frühauf (SSF) and the chair of steel construction at Dortmund University system solutions are developed directly applicable in construction practice. The R&D project is financed by FOSTA “Forschungsvereinigung Stahlanwendung e.V.” and for its practical relevance conducted in cooperation with industrial partners.

The development is based on SSF competences in composite structures and presents a further development of so called VFT®-girders (Verbundfertigteilträger = prefabricated

composite girder). VFT® is a technology optimizing the quality and construction time of short and middle span bridges. Prefabricated composite bridge girders are assembled on site and finalized only with a layer of in-situ concrete [1]. Combining the VFT® technology with the high performance of UHPC very light and efficient structures - Lightweight Composite Structures (LCS) - can be designed. LCS can be applied comparable to VFT® for bridge structures. In addition, due to its low weight utilization is also intended for slabs of multi-storey buildings or industrial construction. The main aspects of the LCS technology presented in this paper are:

- Structural design of UHPC composite girder
- Adapted shear joints between UHPC and steel
- Creep and shrinkage effects in UHPC - steel composite
- Pilot project

2 Cross Section

In order to take advantage of the high performance of UHPC's and equally compensate its 'asymmetrical' material characteristics -about 200MPa in compression and 10MPa in tension [2]- the combination of UHPC with steel for taking tension stresses is an efficient design solution. Internal rebars in potential slender UHPC elements can only provide a small static height. Using steel profiles as 'external reinforcement' in a composite section is from the static point of view highly efficient. Further, steel adds high ductility to the minor ductile UHPC.

Different composite cross-sections have been analyzed in order to determine efficient longitudinal load-bearing structures (Figure 1 a-f). The shear connection is assured by the innovative system of composite dowels (Chapter 3). Among classical designs where the steel profile is situated mainly outside the concrete section, designs with partly imbedded steel profiles or UHPC webs were considered. This provides considerable advantages for the structural stability of the web (bugling), profound anchorage of the composite dowels as well as higher fire safety.

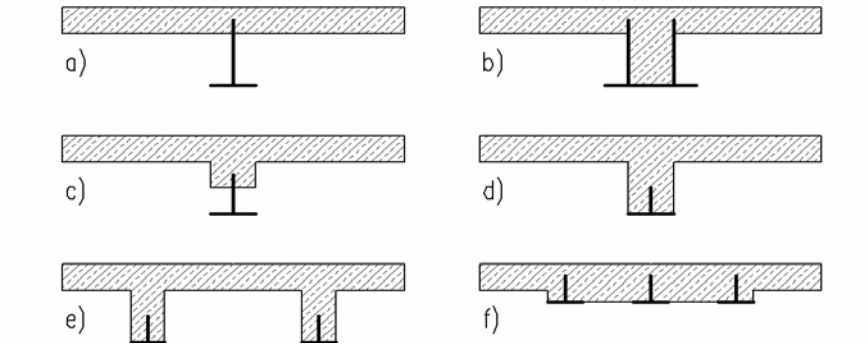

Figure 1 a-f: Study of different cross sections considering external and imbedded steel profiles.

LCS could be employed either as totally prefabricated elements or as filigree slabs with cast in-situ complement. A ready-to-use LSC girder is prefabricated in the workshop under controlled conditions, transported on site and connected locally with grouting compound.

Prefabricated filigree slabs are lighter for transport and handling but demand concreting on site. As cast in situ concrete could be applied normal concrete or UHPC when assuring adequate quality and curing conditions. The UHPC surface could be used directly as carriageway surface without adding any additional surface sealing or pavement.
In transversal sense load bearing is assured by the fibers alone or in combination with reinforcement. Transversal rips could be implemented to optimize the static efficiency. These rips are to be reinforced by pre-stressing or with rebars.

3 Shear Connection

Adapted shear joint between UHPC and steel are to be developed. UHPC provides high shear resistance due to the high tensile resistance of the matrix and the embedded fibers enabling a reduced and simplified shear connection [3]. Commonly used headed studs tend for high resistance concretes to transfer shear forces only by the stud bottom and show hence a brittle failure by shearing off the welding seam. Furthermore the fatigue resistance is not sufficient in dynamic loaded structures. Hence new long lasting and robust shear connections become necessary for LSC structures using UHPC. Two shear connection systems are considered: adhesion connections and mechanical connections with composite dowels.

3.1 Adhesion Shear Connections

Gravel is scattered in reactive adhesive and after a period of curing concrete can be added to complete the composite element (Figure 2). When loaded in shear compression struts in the concrete do prop on the gravel comparable to ribs of rebars. In the LCS development project this type of connection is developed and optimized using UHPC and optionally high tensile steel. To avoid brittle collapse the steel plate has to be designed as the weakest part of the construction since all other construction-parts do not provide ductile material behavior.

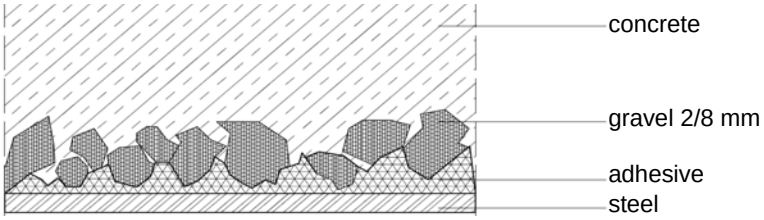

Figure 2: Composite with adhesion connection.

3.2 Mechanical Shear Connection using Composite Dowels

The composite dowel is a shear connection element where the load transfer is assured by steel tooth emerging in the concrete. This construction provides ductile failure behavior and is high durable under dynamic loading [1]. The application in composite bridges is economical as discussed in [4,5].

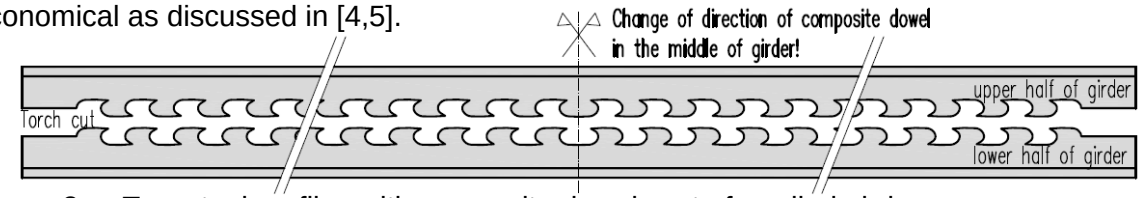

Figure 3: Two steel profiles with composite dowels cut of a rolled girder.

Composite dowels have already been applied in several bridge projects using normal strength concrete (NSC). The example shows a cross-section designed with a symmetrically cut steel profile place in the center of the concrete web of a pre-cast composite girder, so-called VFT-WIB® girder with external reinforcement (see Figure 3, Figure 4).

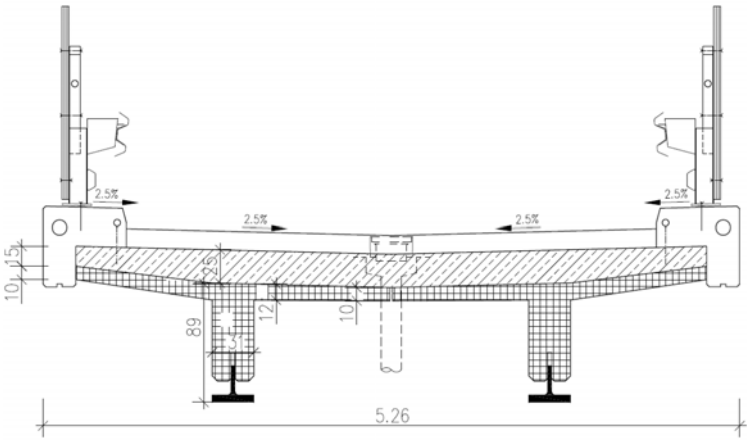

Figure 4: Cross-section of a road bridge in C70/85 in the pre-cast VFT-WIB element using external reinforcement.

3.3 Experimental Investigations

Preliminary experimental investigations (push-out tests) have been carried out considering both types of shear connections.

The adhesion connections have been investigated on small scale specimens ($A_{shear} = 2 \cdot 300cm^2$). Using NSC (C50/60) and UHPC (Figure 5). The tested elements in UHPC and NSC show a longitudinal shear force of about 240 MPa respective 260 MPa. Thus, there is almost no difference in strength. In contrast the structural behavior of UHPC is, as expected, initially considerable stiffer. Further examination of the tested specimens has shown that the UHPC hadn't penetrated the graveled surface completely and less than 50% of the space between the gavels was filled. Optimization of the workability and the casting process will lead to a better compound and the shear resistance is expected to double, providing shear strength of up to 10 MPa. Future investigation will provide detailed results.

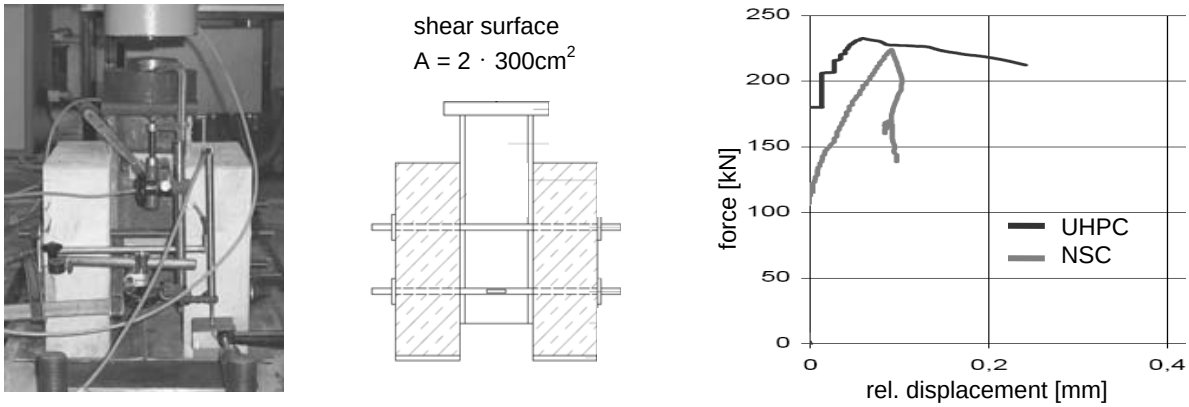

Figure 5: Push-out tests comparing the structural behavior of adhesion shear connections in NSC and UHPC.

In order to investigate the shear transmission behavior of composite dowels push-out tests were carried out (Figure 6). A bond length of two times 1 m has been provided including 3 composite dowels. The width of the concrete web has been varied from 20 to 40 cm. A first series using NSC has been tested for the VFT-WIB bridge project mentioned above (b, c). Based on this push-out tests further test were carried out to investigate the influence of the fibers in UHPC (d). To increase the stiffness of the connection in service a bond enhancement by applying adhesive and gravel on the surfaces between steel and UHPC has additionally been tested (e,f).

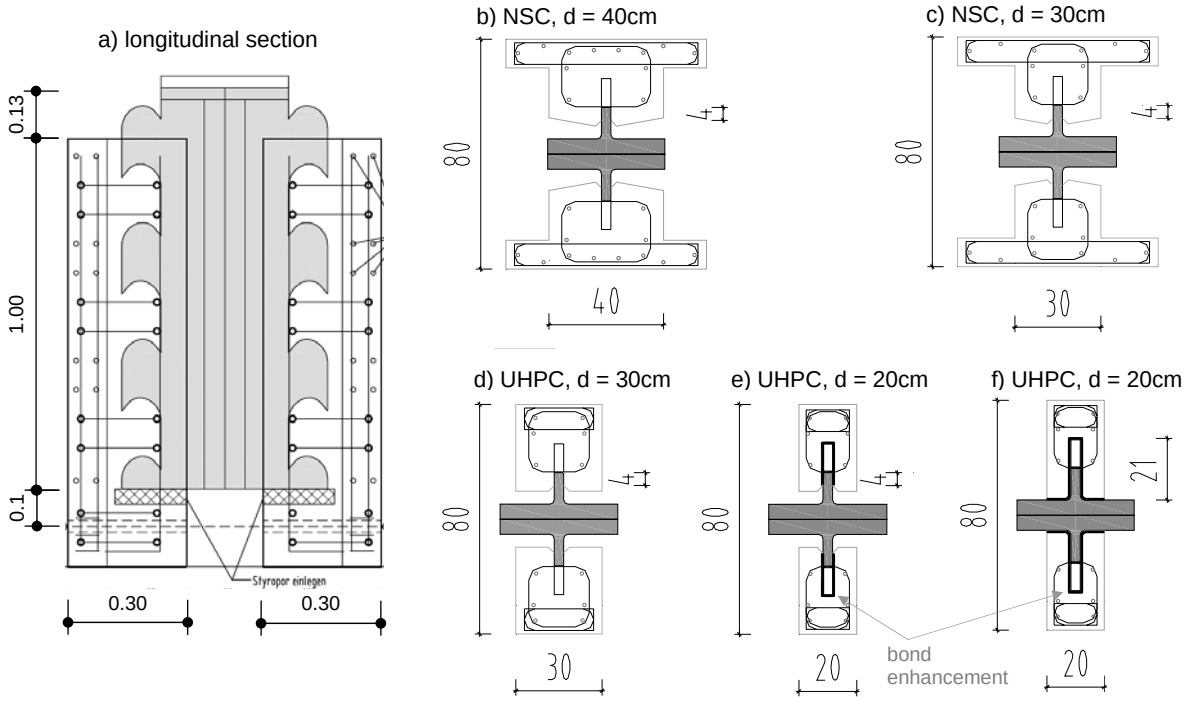

Figure 6 a-f: Longitudinal and cross section of specimens (various configurations).

The capacity of the fiber reinforced concrete increases up to 1/3 in comparison to normal strength concrete C 50/60 (Figure 7). The added bond enhancement only showed a stiffer connection in sls but a non significant uls-strength increase.

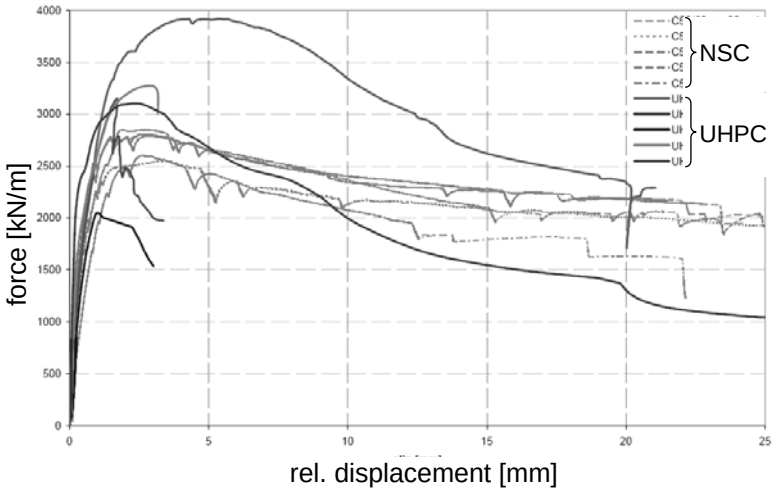

Figure 7: Specimens with fiber reinforced concrete.

4 Creep and Shrinkage

In case of UHPC relatively high shrinkage (typically ε_{cs} = 0.4 to 1.0 mm/m) has to be considered, but in contrast only little creep (typically φ_0 = 0.5 to 0.8) will occur [6]. In a composite girder shrinkage leads to primary and in case of hyper static structures also secondary internal stresses. Creeping reduces internal constraint stresses as well as long term external induced stresses. Hence, these time dependent deformations influence the deformations (dilatation and deflection) of the composite girder in a mayor way and can, in case of shrinkage, cause important cracking of the UHPC due to the restraining by rigid steel profiles. In comparison to traditional composite girders, LSC girders require in general only a very slim concrete slab. Thus, the restraining effect induced by the steel profiles and in consequence the shrinkage stresses become more important.

As a first approach, the creep and shrinkage behavior of a LSC girder can be analyzed by the 'total section method' [7] where an adapted (reduced) concrete section is considered (Figure 8). Concrete sections are adapted to steel (Ac becomes Ac,i), considering the differences of the Young's modulus ($n_0 = E_c/E_{cm}$). Shrinking causes a shortening of the concrete slap which is restrained by the steel girder. An internal force $N_{s,int}$ (Eq. 1) is provoked in the slap which leads to an internal bending moment $M_{s,int}$ (Eq. 2) in the composite girder.

$$N_{s,\mathrm{int}} = \varepsilon_s \cdot \frac{n_0}{n_{F,s}} \cdot E_{c,m} \cdot A_c \;;\; M_{s,\mathrm{int}} = N_{s,\mathrm{int}} \cdot z_{i,o} \qquad \text{(Eq. 1 und 2)}$$

These primary internal stresses lead simultaneously to creeping effects which in return reduce the internal stresses. The formulation of the 'total section method' implements these time dependent effects by adopting reduction factors for the concrete ($n_{F,s}$). By means of this method the LSC composite section can be analyzed and subsequently internal forces (M, N_c, M_c, N_s, M_s) and stresses (σ_c, σ_s) as well as the deflection (w) of the girder can be derived.

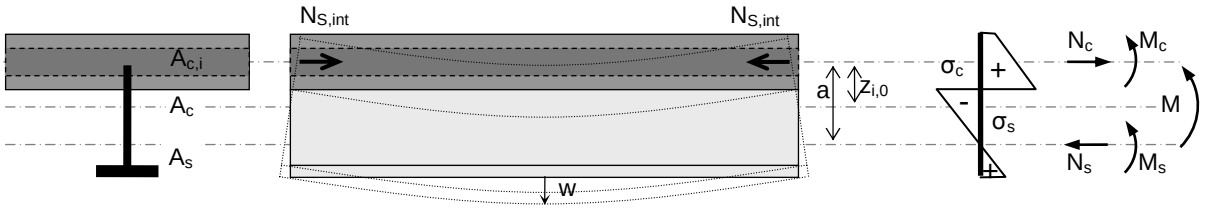

Figure 8: Total section method: adapted concrete section to analyze internal stresses, internal forces and deflection.

To assess shrinkage effects and evaluate potential cracking in early age, a limit value analysis has been performed. The investigation considers typical LSC sections with small A_c / A_s ratio. A parameter study using the total section method has shown a reduction of the restraining effect due to creep and elastic deformation of the steel profile of less than 10%. Hence, a strain range ε_{cs} for the restrained shrinkage of ε_s = 0,4 to 1‰ has to be considered (Figure 9).

The limit value analysis considering a typical UHPC with bi-linear material characteristics [8] shows that even when considering only a reduced shrinkage cracking will occur due to exceedance of the matrix strain limit $\varepsilon_{ct,m}$. By means of the fibers the cracks are bridged and

a well distributed crack pattern with uncritical micro cracks will appear (case A) in the strain hardening phase. The ultimate strain ε_{ct} = 2 to 4 ‰, where macro cracking will occur, will generally not be reached. When using an UHPC without strain hardening behavior (e.g. insufficient fiber content) macro cracks will occur instantly at matrix failure, localized in the tension zone of the composite dowel (case B) [9]. To absorb the tension stresses in these cracks by applying rebars (crack distributing reinforcement), very high reinforcement ratios have to be considered, as the cracking strength of the UHPC matrix is already on a high level.

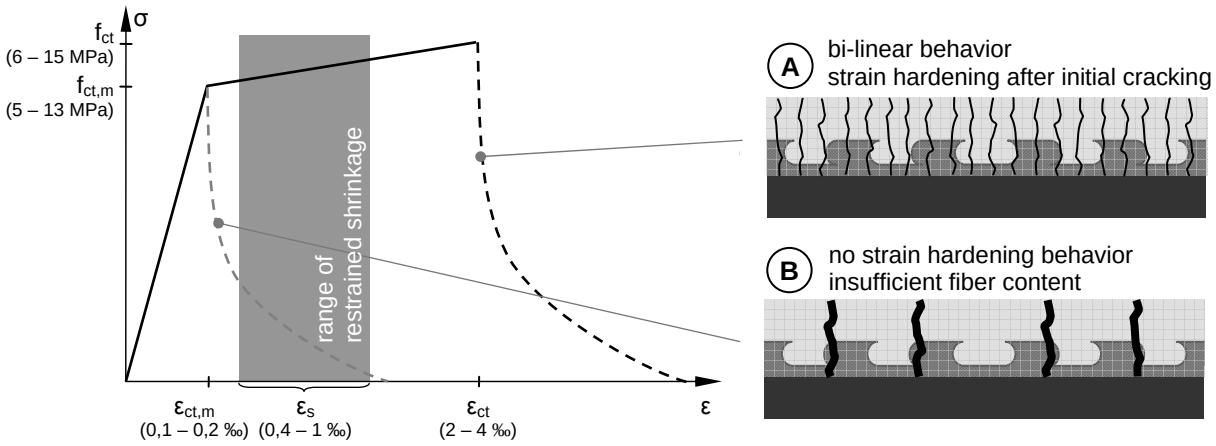

Figure 9: Restrained shrinkage in comparison to the bi-linear material behavior of UHPC; resulting crack pattern.

Future experimental investigations will be carried out to support this theoretical approach and adequate detailing to optimize the shear connection will be established. Further finite element simulations will be conducted, considering the bi-linear material behavior of UHPC which cannot be taken into account in the total section method.

5 Pilot Project

In order to proof the design a pilot project is carried out on a small span bridge connecting two parts of an industrial park where fork-lift trucks are crossing a small river. The single span beam (12 m) is designed with a composite cross section where steel profiles are imbedded in a sort of longitudinal UHPC rips. The slab is narrowed between the rips. In transversal direction rebars are added for additional safety. The traffic will run directly on the UHPC surface without any additional sealing or pavement. UHPC with its low porosity and high abrasion resistance is predestinated to resist those severe impacts.

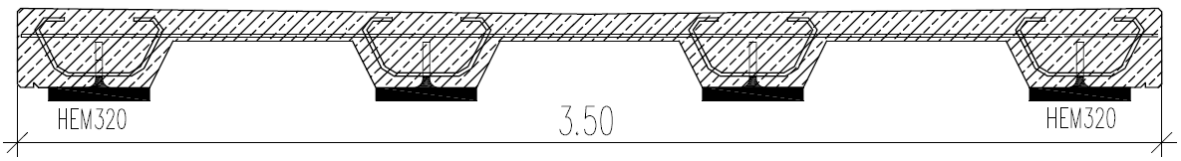

Figure 10: Cross- and longitudinal section of the pilot bridge.

Besides the technical feasibility an applicable approval process with German construction authorities is a major focus of the pilot project. As UHPC is a none standardized technology it

is to be proven not only to the proofing engineer but also by German administration that the slender LSC design is conform to safety requirements without being obliged to change the slender design and implement extra security margins. This will also affect economic considerations when comparing LSC to traditional composite structures and could be decisive if UHPC structures will be competitive under German building regulations.

6 Conclusion

A new design concept combining the VFT® composite concept with UHPC decks has been presented. Lightweight Composite Structures (LCS) are promising for an application in building design as well as for small to middle span bridges. Through design considerations of adapted cross-sections and the analysis of the time dependent behavior the theoretical feasibility of LCS has been proven. By means of experimental investigations of the shear joint first practical tests have been carried out successfully. With the design of a pilot project the high potential of this innovative marriage of steel and UHPC will be tested in day-to-day utilization.

7 References

[1] Seidl, G.; VFT-WIB-Construction Method; Compendium 5th Japanese-German Joint Symposium for Composite Bridges, Munich, 2005.

[2] Setra; AFGC; Béton fibrés à ultra-hautes performances, recommandations provisoires, documents scientifiques et techniques, 2002.

[3] Jungwirth J., Muttoni A., Versuche zum Tragverhalten von ultra hochfestem Beton - Kurzfassung , IS-BETON Bericht 00.02.R8, p. 27, Lausanne, 2005.

[4] Schmitt V., Seidl G., Hever M., Zapfe C.; Verbundbrücke Pöcking – Innovative VFT®-Träger mit Betondübeln, Composite bridge Pöcking – Innovative VFT®-girder with steel dowels, Stahlbau, 06/2004.

[5] Schmitt V., Seidl G., Hever M.; Composite bridges with the VFT-WIB construction method – robust and long lasting, Compendium Eurosteel, 2005.

[6] Fehling, E., et al.; Entwicklung, Dauerhaftigkeit und Berechnung Ultrahochfester Betone (UHPC), Forschungsbericht DFG FE 497/1-1, p. 130, 2005.

[7] Roik K. et al.; Verbundkonstruktionen, Bemessung auf der Grundlage des EC4, in Betonkalender 1999, Ernst & Sohn, 1999.

[8] Jungwirth, J.; Zum Tragverhalten von zugbeanspruchten Bauteilen aus Ultra-Hochleistungs-Faserbeton, Doktorarbeit EPFL Nr. 3429, p. 158, Lausanne, 2005.

[9] Jungwirth, J., Structural Behavior of Tension Members in Ultra High Performance Concrete, International Symposium on UHPC 2004, Kassel, 2004.

Eugen Brühwiler
Professor, Dr. Civil Engineer ETH
Ecole Polytechnique Fédérale (EPFL)
Lausanne, Switzerland

Emmanuel Denarié
Senior Scientist, Dr. Civil Engineer EPFL
Ecole Polytechnique Fédérale (EPFL)
Lausanne, Switzerland

Rehabilitation of concrete structures using Ultra-High Performance Fibre Reinforced Concrete

Summary

An original concept is presented for the rehabilitation of concrete structures. The main idea is to use Ultra-High Performance Fibre Reinforced Concrete (UHPFRC) to “harden” those zones of the structure that are exposed to severe environment and high mechanical loading. All other parts of the structure remain in conventional structural concrete as these parts are subjected to relatively moderate exposure. This conceptual idea combines efficiently protection and resistance properties of UHPFRC and significantly improves the structural performance of the rehabilitated concrete structure in terms of durability and life-cycle costs. The concept is validated by means of four applications demonstrating that the technology of UHPFRC is mature for cast in-situ and prefabrication using standard equipment for concrete manufacturing.

Keywords: *Ultra-High Performance Fibre Reinforced Concrete; durability; composite concrete construction, rehabilitation of concrete structures.*

1 Introduction

Concrete structures show excellent performance in terms of structural behaviour and durability except for those zones that are exposed to severe environmental and mechanical loading. Rehabilitation of deteriorated concrete structures is a heavy burden also from the socio-economic viewpoint since it also leads to significant user costs. As a consequence, novel concepts for the rehabilitation of concrete structures must be developed. Sustainable concrete structures of the future will be those requiring just minimum interventions of only preventative maintenance with no or only little service disruptions.

Over the last 10 years, considerable efforts to improve the behaviour of cementitious materials by incorporating fibres have led to the emergence of Ultra-High Performance Fibre Reinforced Concretes (UHPFRC). These novel building materials provide the structural engineer with an unique combination of (1) extremely low permeability which largely prevents the ingress of detrimental substances such as water and chlorides and (2) very high strength, i.e., compressive strength higher than 150 MPa, tensile strength higher than 10 MPa and with considerable tensile strain hardening (up to more than 1‰ of strain) and softening behaviour (with fracture energy of more than 15’000 J/m^2). In addition, UHPFRC have excellent rheological properties in the fresh state allowing for easy casting of the self-

compacting fresh material with conventional concreting equipment. Consequently, UHPFRC clearly have an improved resistance against severe environmental and mechanical loading thus providing significantly improved structural resistance and durability to concrete structures.
This paper presents an original concept for the rehabilitation of concrete structures. The concept is described and validated by means of four applications.

2 Conceptual idea

The basic conceptual idea is to use UHPFRC only in those zones of the structure where the outstanding UHPFRC properties in terms of durability and strength are fully exploited; i.e. UHPFRC is used to "harden" the zones where the structure is exposed to severe environmental and high mechanical loading. All other parts of the structure remain in conventional structural concrete as these parts are subjected to relatively moderate exposure. This concept (which is also applicable to new construction) necessarily leads to composite structural elements combining conventional reinforced concrete and UHPFRC.
The combination of the UHPFRC protective and load carrying properties with the mechanical performance of reinforcement bars provides a simple and efficient way of increasing the stiffness and load-carrying capacity keeping compact cross sections (Fig. 1). Depending on the structural and material properties of the composite system, more or less pronounced built-in tensile stresses are induced in the UHPFRC due to restrained deformations at early age. This stress state needs to be analysed and evaluated [1].

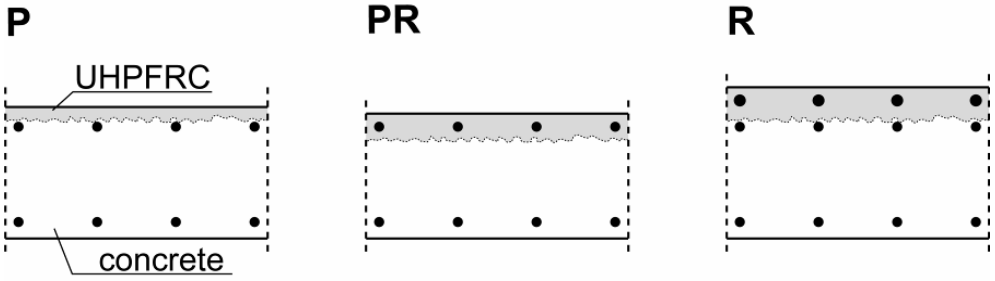

Figure 1: Basic configurations for composite structural elements combining UHPFRC and conventional structural concrete

UHPFRC is applied on existing reinforced concrete elements as thin watertight overlays (in replacement of currently used waterproofing membranes), as reinforcement layers combined with reinforcement bars, or as prefabricated elements such as kerb elements in the case of bridges. The relatively high cost of these materials imposes to use them only where they are "worth their money" and it is possible to take the maximum benefit of their outstanding mechanical properties.
The original conceptual idea (developed in 1999) has been investigated by means of extensive researches (see scientific papers under [2]) aimed at characterizing UHPFRC materials and the structural behaviour of composite structural members. The concept is well-suited for bridges and can also be implemented for buildings, galleries, tunnels or retaining walls. Validation by means of four applications will be described in the following.

3 Rehabilitation and widening of a road bridge

A short span road bridge with busy traffic has been rehabilitated and widened using UHPFRC [3,4]. The entire deck surface of the bridge with a span of 10 m was rehabilitated in three steps during autumn 2004 (Fig. 2). Firstly, the downstream kerb was replaced by a new prefabricated UHPFRC kerb on a new reinforced concrete beam which was necessary for the widening. Secondly, the chloride contaminated concrete of the upper surface of the bridge deck was replaced by 3 cm of UHPFRC in two consecutive steps such that one traffic lane could be maintained open. Thirdly, the concrete surface of the upstream kerb was replaced with 3 cm of UHPFRC.

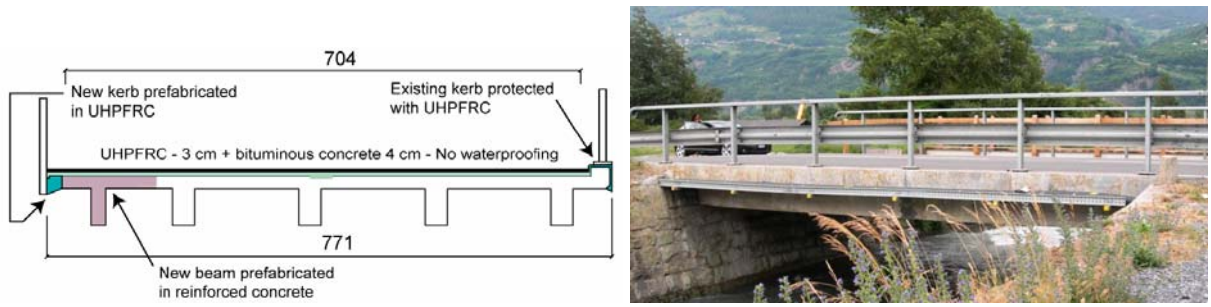

Figure 2: Bridge cross section after rehabilitation (dimensions in cm) and photo taken in 2006.

The UHPFRC mix contained 1430 kg/m^3 Cement, Microsilica, fine quartz sand with a maximum grain size of 0.5 mm; the Microsilica/Cement and Water/Binder ratio were 0.26 and 0.125 respectiveley. The reinforcement of this ultra compact matrix was provided by a mix of microfibers (steel wool of 2 to 3 mm length) and macrofibers of 10 mm length and an aspect ratio of 50, with a total dosage of 706 kg/m^3 (or 9 vol.%).

Figure 3: UHPFRC casting and handling of UHPFRC using simple tools.

The fresh self-compacting UHPFRC material was prepared at a local concrete prefabrication plant with a standard mixer, brought to the site by a truck and then poured on the hydrojetted deck surface (Fig. 3). The UHPFRC was easy to produce and place with standard tools and very robust and tolerant to the unavoidable particular site conditions [4]. The bituminous pavement was applied on a bituminous emulsion placed on the UHPFRC surfaces after 8 days of moist curing, and the corresponding lane was reopened to traffic the next day. The bridge was fully reopened to traffic one month after the beginning of the construction work.

The protective function of the UHPFRC layer was verified by air permeability tests according to the Torrent method [5]. These tests confirmed the extremely low permeability kT of the UHPFRC layer; i.e. about 30 times lower than for excellent conventional concretes. The average compressive strength and modulus of elasticity at 28 days were respectively 182 MPa and 47 GPa. Uniaxial tensile tests performed at 28 days in the laboratory on unnotched dogbone specimens cast on site showed the expected remarkable average properties: tensile strength of 13.3 MPa and maximum tensile deformation in the strain-hardening domain of 1.5 ‰ (Fig. 4).

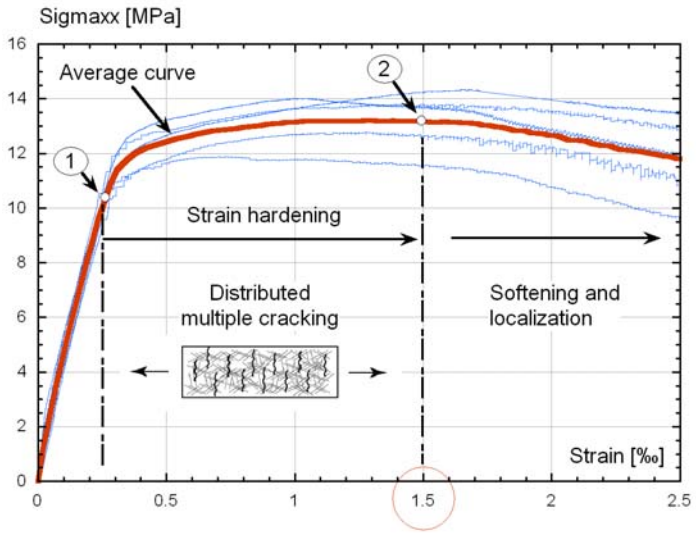

Figure 4: Uniaxial tensile test results on the UHPFRC used on site.

The analysis of the construction costs showed that the rehabilitation realised with UHPFRC was about 10% more expensive than the conventional solution (providing lower quality in terms of durability and life-cycle costs) with waterproofing membrane and repair mortar. However, in the latter case the duration of the construction site would have been largely increased by the required drying period of the mortar, prior to the application of the waterproofing membrane. It can be expected that with a wider use, application of UHPFRC for the rehabilitation of bridges, this technique will become less costly than traditional ones, not to mention its outstanding advantages of long term durability and reduction of traffic disruptions (and subsequent user costs) due to multiple interventions.

4 UHPFRC protection layer on a crash barrier wall

Specific parts of reinforced concrete structures such as crash barrier walls on highway bridges suffer from severe exposure to concrete aggressive substances such as de-icing salts and impact like action. Such elements often show insufficient durability when built using conventional reinforced concrete. Moreover, UHPFRC have very low permeability as well as high strength and deformability, it is suitable to significantly improve the durability and mechanical performance of such structural elements.

A layer of UHPFRC has been applied in September 2006 to the concrete crash barrier walls of a highway bridge [6]. The main design requirement was to obtain long-term durable crash barrier walls since traffic interruption for future rehabilitation interventions are prohibitive due

to the very high traffic volume on this highway. Long-term durability is obtained when transverse macro-cracks in the UHPFRC layer are absent and the permeability of UHPFRC layer to ingress of water and chloride ions is extremely low.

Figure 5 shows the crash barrier wall with a UHPFRC layer covering the areas subjected to splash exposure (Class XD3: reinforcement corrosion induced by chlorides). Previous research [2] indicated that a 3 cm thick UHPFRC layer would provide the required mechanical performance (tensile strength higher than 10 MPa) and extremely low permeability (20 times lower than for conventional concrete of good quality, absence of macrocracks). The used recipe contained 1100 kg/m³ cement, 26% silica fume related to the cement content, quartz-sand, 6% steel fibres by volume, superplasticiser and a w/c-ratio of 0.17. The rheological properties of UHPFRC were adapted for easy pouring into the 3 cm wide formwork to fill a height of 120 cm including a small horizontal part at the bottom of the wall that provides continuity with the conventional bridge deck with a waterproofing membrane.

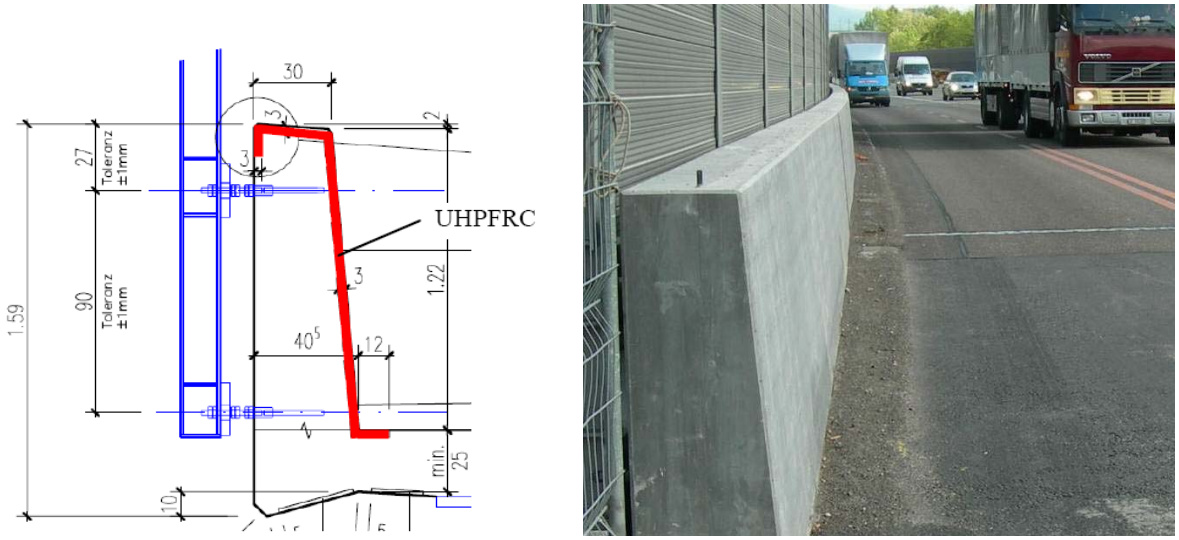

Figure 5: Typical cross section of the crash barrier wall and view after rehabilitation.

Due to restrained early age deformation of the UHPFRC (mostly due to thermal and autogenous shrinkage) bonded to the existing reinforced concrete wall, an internal stress state is built up in the composite element including, in particular, tensile stresses in the UHPFRC layer. These tensile stresses, which can cause macrocrack formation, and the capacity of the UHPFRC to resist to these stresses were investigated by means of numerical analyses prior to the intervention [6].

The fresh self-compacting UHPFRC was fabricated in a conventional ready mix concrete plant, transported to the site by a truck and successfully filled into the thin slot to realize the UHPFRC coating (Fig. 5). The (above mentioned) required mechanical properties and the protective function of the UHPFRC layer have been confirmed by in-situ air permeability tests and laboratory tests on specimens cast on site.

The aesthetic aspect was very appealing showing a smooth surface with very few voids. Four months after application no crack could be found confirming the predictions made by the numerical simulations.

5 Rehabilitation of a bridge pier using prefabricated UHPFRC shell elements

Bridge piers and retaining walls in the splash zone of highway traffic suffer from severe exposure to de-icing salts and impact like action. Such elements usually show premature deterioration when built in conventional reinforced concrete. In order to significantly improve durability and mechanical strength of such elements, UHPFRC is used following again the concept of locally “harden” the zones of severe exposure.

In this application, 4cm thick UHPFRC shell elements have been prefabricated to form an outer protection shield for the existing 40 year-old reinforced concrete bridge pier which is located very close to a busy highway which makes it virtually not accessible for future maintenance interventions (Fig. 6).

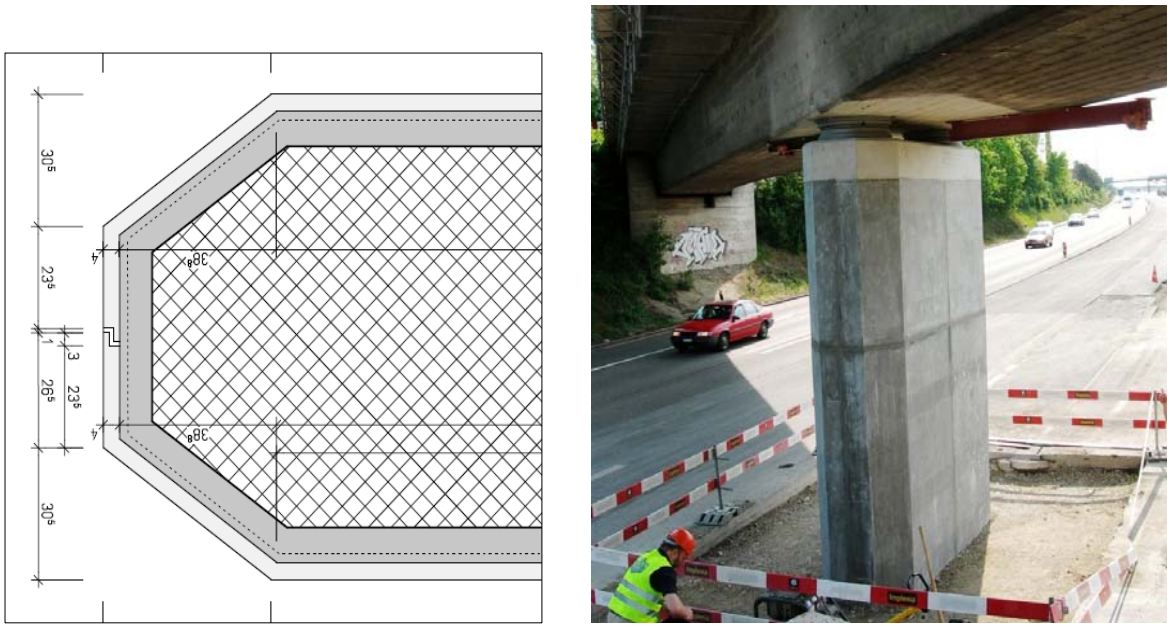

Figure 6: Cross section and general view of the rehabilitated bridge pier.

In spring 2007, the UHPFRC elements (maximum element height of 4m) were cast in a prefabrication plant, transported to the construction site and mounted, after removing of up to 10cm of chloride contaminated concrete by hydrojetting. The joints between the different UHPFRC shell elements were glued using an epoxy resin. The remaining space between the UHPFRC elements and the existing reinforced concrete was filled with self-compacting mortar.

The used UHPFRC recipe contained about 1300 kg/m³ of cement, a rather small amount of silica fume related to the cement content, quartz-sand, 3.5% of steel fibres by volume, superplasticiser and a W/C-ratio of 0.155. Long-term durability is expected since transverse cracks in the UHPFRC protection shield are absent and the permeability of UHPFRC for ingress of water and chloride ions is extremely low as confirmed by permeability tests.

6 Strengthening of an industrial floor

The 50 year-old drivable reinforced concrete floor of a fire brigade building had insufficient load carrying capacity in view of heavier future fire engines. The concept was to increase the load carrying capacity of the existing slab of 720m^2 area by pouring a 4cm thick UHPFRC layer on top of the existing RC slab, as a replacement of the existing cementitious non-load carrying overlay (Fig. 7). The UHPFRC layer leads to a thicker load carrying slab which provides (1) a better distribution of local wheel loads, (2) an increase in static height and (3) a layer of high strength material capable of resisting both compression and tension stresses.

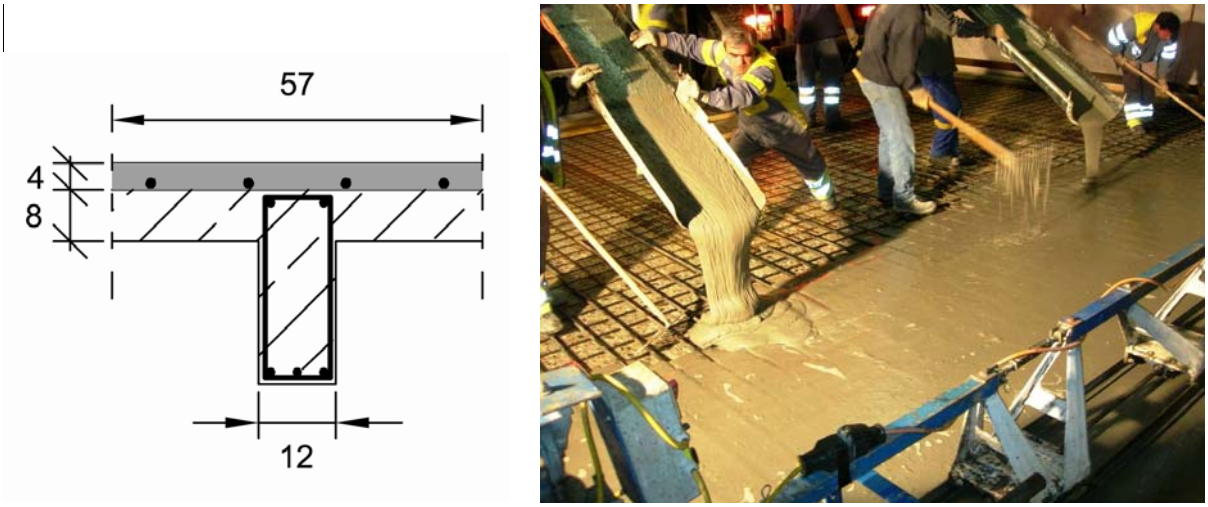

Figure 7: Cross section (dimensions in cm) with UHPFRC layer (in grey) and view of UHPFRC casting performed in autumn 2007.

The UHPFRC recipe, similar to that shown in Section 5, was again fabricated in a local ready mix concrete plant and transported to the site by trucks. The excellent workability of the fresh self-compacting material allowed for easy casting. The use of the UHPFRC solution turned out to be very economic (compared to the conventional solution of slab demolition and reconstruction), also because the utilization of the fire workers building was only slightly restricted during the intervention, holding user costs down.

7 Conclusions

An original concept using Ultra-High Performance Fibre Reinforced Concrete (UHPFRC) for the rehabilitation of concrete structures has been presented and validated by means of four applications.

This conceptual idea combines efficiently the protection and resistance properties of UHPFRC with conventional structural concrete. The rehabilitated structures have significantly improved structural resistance and durability.

The full scale realizations of the concept under realistic site conditions demonstrate the potential of these applications, proving that the technology of UHPFRC is mature for cast in-situ and prefabrication using standard equipment for concrete manufacturing.

Acknowledgments
The support of the Swiss National Science Fund, The Swiss Secretary of Education and Research, The Committee of Technology and Innovation, Cemsuisse, Holcim, Swiss Steel AG and the Swiss Federal Roads Office is gratefully acknowledged. The applications were possible thanks to the Road Administrations of the Swiss Cantons of Wallis and Aargau as well as the Town of Geneva.
The UHPFRC Group at MCS-EPFL consists of the following current and former members: Dr Katrin Habel, Prof. Jean-Philippe Charron, Dr Hamid Sadouki, Prof. Minoru Kunieda, Dr Aicha Kamen, Dr John Wuest, Dr Andrin Herwig, Cornelius Oesterlee, Agnieska Switek and Talayeh Noshiravani.

8 References

[1] Oesterlee, C., Sadouki, H., Brühwiler, E., Structural analysis of a composite bridge girder combining UHPFRC and reinforced concrete, Proceedings, UHPC-2008: The Second International Symposium on Ultra High Performance Concrete, March 2008, Kassel, Germany.

[2] mcs.epfl.ch 2007, http://mcs.epfl.ch/ see under reviewed journal papers.

[3] Denarié, E., Brühwiler, E., Structural rehabilitations with Ultra High Performance Fibre Reinforced Concretes, International Journal for Restoration of Buildings and Monuments, Aedificatio, Vol. 12, No. 5 and 6, 2006, pp. 453-467.

[4] SAMARIS 2005, Report D22, *Full scale application of UHPFRC for the rehabilitation of bridges – from the lab to the field,* European project 5th FWP / SAMARIS – Sustainable and Advanced MAterials for Road Infrastructures – WP 14: HPFRCC, http://samaris.zag.si/.

[5] Torrent R., Fernandez Luco L., Non-destructive Evaluation of the Penetrability and Thickness of the Concrete Cover, State of the Art Report, RILEM TC 189-NEC, 2007.

[6] Oesterlee, C., Denarié, E., Brühwiler, E. 2007. In-situ casting of UHPFRC protection layer on crash barrier walls. Proceedings, Advances in Construction Materials – Symposium in honour of Hans W. Reinhardt, July 2007, University of Stuttgart, Germany.